TUD | Technische Petrologie | Schnittspahnstraße 9 | 64287 Darmstadt

TUD | Technische Petrologie | Schnittspahnstraße 9 | 64287 Darmstadt

Final Report

Thermal Integrity of Clay and Claystones - Experiment and Coupled THMC – Simulations

Sub-project: ***Analysen_THMC-Sim***

Ferreiro Mählmann Rafael	TU-Darmstadt
Hoang-Minh Thao	VNU, Hanoi University of Sciences
Kasbohm Jörn	Jörn-Kasbohm-Consulting, Greifswald
Nguyen-Thanh Lan	TU-Darmstadt
Van Bui Dong	VNU, Hanoi University of Sciences
Scheuvens Dirk	TU-Darmstadt
Ukrainczyk Neven	TU-Darmstadt

June, 2024

Content

List of Symbols and Abbreviations

%S	proportion of smectitic layer in mixed layer phases
1w-smectite	Monovalent interlayer cation smectite (Na-smectite
2w-smectite	Divalent interlayer cation smectite (Ca-smectite)
BET	Brunauer–Emmett–Teller surface area
BM	beidellite-montmorillonite intergrowth
BMI-ml	beidellite-montmorillonite-illite interstratification
calc.	calculation
CEC	Cation exchange capacity
diVS-ml	K- and/or charge deficit dioctahedral vermiculite-smectite interstratification
DTA	differential thermal analysis
FTIR	Fourier Transform Infrared
IS-ml	normal charged illite-smectite interstratification
IV	tetrahedral layer
KS GLY R0	kaolinite- one water layer smectite mixed layer
KSS GL R0	kaolinite – one water layer smectite – two water layer smectite mixed layer
KSV-ml	kaolinite-smectite-dioctahedral vermiculite interstratification
meas.	measurement
SEM-EDX	Scanning Electron Microscopy linked with energy dispersive X-ray spectroscopy
SSA	specific surface area
TA	Thermal analysis
TEM-EDX	Transmission Electron Microscropy linked with energy dispersive X-ray spectroscopy
TG	thermogravimetric
Tmean	thickness of particles
VI	octahedral layer
XII	interlayer charge
XRD	X-ray diffraction
XRF	X-ray Fluoresence
Δ%S	Specific Dissolution Potential

Part I. INITIAL MATERIALS

1. Introduction

This report presents results from a joint research project on smectite-rich clay minerals with respect to their use as buffer and backfill materials in a repository for high-level radioactive waste. The project "Thermal Integrity of Clay and Claystones - Experiment and Coupled THMC Simulations" is initiated and funded by the Bundesgesellschaft für Endlagerung (BGE). The Gesellschaft für Anlagen- und Reaktorsicherheit (GRS) was commissioned with its realisation.

In this report, a clay-rich rock of a commercial high-quality bentonite from Bavaria in Germany (B25 bentonite), Opalinus clay from the Opalinus deposit, and Friedland clay are characterized from a mineralogical perspective as starting materials in THMC experiments. Different methods are used, including geochemical composition analysis via X-ray Fluorescence (XRF) for whole rocks (<40 µm fraction) of initial materials. Additionally, whole rocks are characterized by X-ray Diffraction (XRD), Infrared Spectroscopy (IR), and Thermal Analysis (TA), as well as cation exchange capacity (CEC) and specific surface area (SSA). Surface charge for powder materials and scanning electron microscopy (SEM-EDX) for claystone and compacted clay specimens are also investigated. The < 2 µm fractions are carefully examined by additional methods, including Transmission Electron Microscopy linked with Energy Dispersive X-ray Spectroscopy (TEM-EDX) and oriented mount specimens from XRD.

The application of above-mentioned analytical methods follows the principle of differential diagnostics. Differential diagnostics is a typical methodology to investigate clay minerals. Different analytical methods are combined to verify, validate and complete results of the main analytics. X-ray diffraction of bulk powder is a typical commonly applied mineralogical method. This analysis offers an overview of mineral matter (qualitative and quantitative) and describes additionally selected parameters of certain clay minerals (e.g. polytype of mica, differentiation between di- or trioctahedral clay minerals). X-ray diffraction on oriented specimen of fraction < 2 µm gives information about degree of expandability, e.g. to distinguish between smectite and mixed layer phases. Differential thermogravimetric analysis (DTA/TG) let recognize the possible occurrence of amorphous phases, which are mostly not to detect by XRD. The particle-by-particle determination of chemistry of phases by transmission electron microscopy (TEM-EDX) visualizes possible alteration processes in the composition of certain mineral phases (e.g. smectite), which are not to recognize by XRD. The verification of clustered chemical TEM-EDX-results with expandability detected by oriented XRD is to consider as further validation of TEM-data clustering and additionally an indicator to distinguish between montmorillonite and beidellite. Fourier transform infrared spectroscopy (FTIR) offers even indications to distinguish between montmorillonite and beidellite and to characterize the Al/Fe-ratio in octahedral layer of smectite (confirming the results by TEM-EDX).

Meleshyn et al. (2024) offer a description of applied samples: The solids analysed are Bavarian bentonite (Calcigel), Opalinus clay from the clayey facies and Friedland clay. The Bavarian bentonite, which has already been successfully used in the Salzdetfurth shaft seal at a density of 1.6 g/cm^3 and at a fluid pressure load of up to 70 bar (Breidung, 2002; Sitz et al., 2003), was provided by Stephan Kaufhold (BGR) and comes from batch sample B25. The Opalinus clay was obtained in the Mont Terri rock laboratory (Switzerland) (borehole BLT-A7 from 2013 (Laurich et al., 2019) and borehole BFS-B12 from 31 October 2022; the sample material from borehole BLT-A7 was used for the development of the method and the first tests, while the results documented below were obtained with the sample material from borehole BFS-B12). The Friedland clay comes from the Siedlungsscholle clay pit near Friedland in Mecklenburg-Western Pomerania (sample material extracted in the 'Ost-Feld' in September/October 2022, sampling in the external storage facility on 12 January 2023). For the main tests, cylindrical test specimens with a height of 20 mm and a diameter of 22 mm were produced from the three materials. A slightly different sample preparation procedure was required for each material.

The results revealed that the three starting materials are composed of a high amount of clay minerals. Smectite is the main mineralogical phase, which determines the swelling behaviour of clays and bentonites. In B25 bentonite and Friedland Clay, smectite is distributed in three different groups of smectite-bearing phases (Ca-smectite, diVS-ml, KS-ml), in Opalinus Clay only in two groups (diVS-ml, KS-ml).

Smectite is present in B25 bentonite as beidellite-rich Ca-smectite and furthermore as montmorillonite in illite-smectite mixed layer phases with K- and/or charge deficiency (diVS-ml) and in kaolinite-smectite mixed layer phases (KS-ml). Further minor phases are illite ($2M_1$, $1M$), kaolinite, quartz, and feldspar. 86% of mineral matter in initial B25 bentonite are clay mineral phases. Illite in fraction < 2 µm of original material occurs in two clusters: (i) reduced K in interlayer as well as octahedral layer is Al-rich (octahedral Al/Fe-ratio ~ 4.6) and (ii) high reduced K in interlayer and octahedral layer is Al-poor and Fe-rich (octahedral Al/Fe-ratio ~ 1.1).

Smectite is mainly found in the Friedland clay series (sum of clay mineral phases: 78%) in illite-smectite mixed layers (a minor phase) with K- and/or charge deficiency (diVS-ml) and in Ca-smectite as well as kaolinite-smectite mixed layer phases (both are trace phases). Beidellite is only a minor component of smectite in diVS-ml phases, whereas in Ca-smectite, it is the dominant smectite component. The main phase in Friedland clay is illite (1M), accompanied by illite ($2M_1$), kaolinite and quartz as minor phases. Illite in fraction < 2 µm is characterized by a reduced K in interlayer and its octahedral layer is Al- and Fe-rich. Friedland clay also contains traces of chlorite, feldspar, pyrite, calcite, and anatase. Calcite occurs as crystalline calcite and probably also as amorphous calcium carbonate.

Smectite is found in the Opalinus clay series (sum of clay mineral phases: 61%) in illite-smectite mixed layers with K- and/or charge deficiency (diVS-ml, a minor phase) and especially in kaolinite-smectite mixed layer phases (KS-ml, the main phase). Montmorillonite is the dominant smectite component. Illite ($2M_1$) and kaolinite (including KS-ml) are the main phases in Opalinus clay, accompanied by illite (1M), diVS-ml, quartz, and calcite as minor phases and traces of chlorite, feldspar, pyrite, siderite, dolomite, and anatase. Illite in fraction <2 µm of borehole BLT-A7 is characterized by high reduced K in interlayer and its octahedral layer is Al- and Fe-rich. Illite in fraction <2 µm of borehole BFS-B12 has a higher amount of K in interlayer (similar to Friedland clay) than in illite from borehole BLT-A7. Furthermore, borehole BFS-B12 shows three groups of illite in fraction < 2 µm differentiated mainly by specific octahedral Al/Fe-ratio.

Following the analytical principle of differential diagnostics for clay minerals, the results of XRD, as main analytical method, of the three bulk samples are consistent with IR, TA and TEM-EDX-results. The <2 µm fraction shows the highest frequency of smectite, dioctahedral vermiculite-smectite mixed layer (diVS-ml), illite-smectite mixed layer (IS-ml), and illite with a significant amount of interlayer K and a high content of Fe in the octahedral sheet, as well as significant substitution of Al for Si in the tetrahedral sheet. The same finding of high octahedral Fe is also observed in IR results. The TEM-EDX results are comparable with the oriented mount of XRD by classification into two and partially three clusters.

After the experimental runs, smectites remain the main phases, determining the swelling behaviour of clays. Each smectite-bearing group showed specific behaviour during the experiments. The role and behaviour of KS-ml remain largely unclear. The analytical evidence is mostly the result of modelling of X-ray diffractograms (oriented specimen) and indirect evaluation of thermogravimetry in comparison to powder X-ray diffractometry. Finally, in the experiments with increased thermal load, sample B25 showed slight "illitization," but Opalinus indicated contrasting behaviour of largely stability and unchanged conditions. Friedland clay is even stable in the development of %S in sum. In detail, %S of diVS-ml phases is increasing with rising thermal load in the experiments. It seems, this development is compensating the loss of Ca-smectite in treated Friedland clay in experiments higher than 60°C.

Additional overhead shaking experiments were applied to evaluate the specific dissolution potential of B25 and Opalinus clay according to Nguyen-Thanh et al. (2014). As Ca-Mg-interlayer type, the results suggested that Opalinus clay is characterized by slow-reacting smectites under limited reaction conditions, but under strong conditions (e.g. high temperature, high ionic strength of solution, 'fast' mass transport in sample body and only Na can act as protecting interlayer type, but Na is not really available there), it will turn to very fast reacting by losing most of the smectitic layer in smectite. The presence of pyrite especially acts as a strong influence on this behaviour. It is expected that the same behaviour would be found in Friedland clay. Otherwise, the specific dissolution potential of B25 bentonite showed as moderately reactive smectite, but under mentioned strong experimental conditions, this clay can react strongly and quickly, causing a complete loss of the smectitic layer in smectite phases.

2. Analytical Methods

2.1 X-ray diffraction (XRD)

Three clay materials of B25 bentonite, Opalinus and Friedland clays are analyzed both as random powders of the bulk materials (<40 µm) and oriented mounts of the clay fraction (< 2µm) by use of a Bruker Diffractometer D8 at Department of Material Sciences, Technical University Darmstadt. The equipment was operated at 30 mA and 40 kV, Cu-K$\alpha_{1,2}$ radiation, 0.5/25 soller collimator, automatic divergence slit, X'Celerator line focus detector. The data were recorded in the range of 4 to 70 °2Ɵ for randomly oriented powder samples and 4 to 40 °2Ɵ for oriented mounts.

2.1.1 Random oriented powders

The bulk samples were dried at 50 °C and ground in an agate mortar until the particles were as small as possible. The sample was brushed through a <0.4 µm sieve and carefully packed into the sample holder to avoid the preferred orientation of the particles. A glass slide was used to pack the sample firmly and create a smooth surface to minimize deformation during the rotation of the sample while measuring. A step size of 0.008° 2Ɵ, and 20 total added seconds for each measurement step were applied.

After identifying the main mineral components by comparison with the ICDD/PDF-4 Minerals database, the mineral phases were refined using the Rietveld program BGMN and the Profex user interface by Taut et al. (1998) and Doebelin and Kleeberg (2015). The B25, Opalinus, and Friedland clays contain a mixture of disordered phases (smectite, IS-ml). The smectite phase content is considered as 1w-smectite for Na-smectite and 2w-smectite for Ca-smectite. These results are then cross-checked with TEM-EDX results, XRF data, and DTA-TG to achieve the best fit for the quantification of mineral phases.

2.1.2 Oriented mounts

The clay suspension of the <2 µm fraction was prepared by Atterberg sedimentation. Oriented mounts were prepared by dispersing 45 mg of clay in 1.5 mL of deionized water and pipetting the dispersion onto glass slides. The mounts of oriented clays were scanned with a step size of 0.02° from 4° to 40° 2Ɵ. Clay minerals were identified according to the criteria of Brindley and Brown (1980), which are based on the reactions of clays to the following treatments:

- The swelling behaviour was tested by saturating the clay with ethylene glycol at 60 °C for at least 48 hours.
- Illite/smectite interstratification (IS-ml) was identified according to Moore and Reynolds (1989) and quantified using Sybilla© software.
- Heating the materials at 550 °C for 4 hours allowed for the identification and distinction of kaolinite and chlorite.

In addition, the XRD patterns of oriented specimens were modelled, in both air-dried and ethylene glycol-saturated states, with the Sybilla© software developed by Chevron™ (Aplin et al., 2006). This software is designed to calculate theoretical XRD patterns of the basal reflections of discrete clay minerals and interstratification structures. Sybilla©, based on the program designed by Drits and Sakharov (1976), allows direct comparison between experimental and calculated XRD profiles. Instrumental and experimental parameters of the goniometer were introduced but not further refined. The amount of interlayer species, octahedral iron, and the main value of coherent scattering domain sizes (T_{mean}) were considered as variable parameters during the fitting process.

2.2 X-ray Fluoresence (XRF)

Bulk samples were analysed for chemical composition using an X-ray fluorescence spectrometer S8 Tiger (Bruker). The samples were prepared as glass disks with a fully automated fusion technique. Loss on ignition (LOI) was determined at 1100 °C as an approximate measure of volatile H_2O. This method was applied only for the initial materials and these data were used to characterize the chemical composition of the bulk rocks and to cross-check the results of quantitative mineralogical composition identified by XRD of randomly oriented materials.

2.3 Fourier Transform Infrared (FTIR)

A Fourier Transform Infrared (FT-IR) spectroscopic study was conducted using the Varian 670-IR series FT-IR spectrometer. Powder samples (bulk samples) of approximately 1 to 2 mg were mixed homogeneously with 120 mg of KBr, which was pre-dried at 80 °C for at least 6 hours, and then pressed into a dye to form a pellet with a diameter of 13 mm. The spectra were recorded in the mid-infrared range, extending from 400 cm^{-1} to 4000 cm^{-1}, with multiple scans (e.g., 64 scans and 4 cm^{-1} resolution) at room temperature. Detailed investigations focused on the OH-stretching region between 3800 cm^{-1} and 3200 cm^{-1} and the OH-bending region between 1000 cm^{-1} and 750 cm^{-1}.

The FT-IR spectra were deconvoluted using Origin 2021 Peak Fitting software. A Gaussian distribution function was applied to smooth the spectra and to determine the exact values of peak position, full width at half maximum (FWHM), intensity, and area. The interpretation of the absorption spectra was primarily based on the works of Farmer (1974) and Farmer and Russell (1964).

2.4 Thermal analysis (TA)

Thermal analysis, including thermogravimetric (TG) investigation and differential thermal analysis (DTA), was performed using a NETZSCH STA 449 C at 3.5 kVA under an Ar atmosphere. The materials were milled to 40 µm and then dried at 35 °C for 1 hour. A 40 mg sample was heated to 1100 °C with a heating segment (S1) from around 35 °C up to 1100 °C, followed by an isothermal segment (S2) with a holding time of 20 minutes. Finally, the sample was rapidly cooled down to 1000 °C. Al_2O_3 was used as the reference material. The results were evaluated using NETZSCH Proteus Software.

2.5 Cation exchange capacity (CEC) and Brunauer–Emmett–Teller (BET) surface area and surface charge analysis

CEC measurements were conducted according to Gillman (1979). A 0.5 g sample of air-dried clay was mixed with 30 mL of 0.1 M aqueous $BaCl_2$ solution and shaken slowly on an end-over-end shaker (15 rpm) for 5 hours. The supernatant was removed by centrifugation and filtered with Whatman No. 41 filter paper. This procedure was repeated 5 times, and after each ion exchange, all liquid fractions were combined and analysed using atomic absorption spectroscopy (AAS) and ion chromatograph (IC) for Ca, Mg, K, Na, Al, Fe, and Mn. Finally, the concentrations of Ca, Mg, Na, and K were used for CEC calculation.

The surface charges of initial and reaction products were determined by polycation titration combined with streaming potential measurements using a particle charge detector (PCD-06) at the Department of Applied Geosciences, TU Darmstadt.

The Brunauer-Emmett-Teller specific surface area (SSA) was measured by N2 adsorption at 77 K in the relative pressure range of 0.05 to 0.3 (Quantachrome Autosorb-3B, USA) after degassing for 22 hours at 80 °C at the Department of Material Sciences, TU Darmstadt.

2.6 Scanning Electron Microscopy (SEM)

The scanning electron microscopy (SEM) analysis was conducted using an FEI Quanta 400 ESEM FEG instrument (FEI, Eindhoven, the Netherlands) equipped with an energy-dispersive X-ray detector (Oxford, Oxfordshire, UK). The analyses were performed manually, referred to as operator-controlled SEM. An acceleration voltage of 15 kV and a sample chamber pressure of around 1×10^{-5} mbar were used. The Oxford software Aztec was used for single EDX-point and EDX-mapping to control the measurements. Each measurement was conducted with a counting time of 5 to 10 seconds for X-ray microanalysis.

2.7 Transmission Electron Microscropy linked with energy dispersive X-ray spectroscopy (TEM-EDX)

The clay mineral phases in untreated and treated B25, Opalinus, and Friedland clays were characterized using transmission electron microscopy with energy-dispersive X-ray spectroscopy (TEM-EDX). The different clay mineral phases were identified and described based on their chemical composition variability, morphology, specific dissolution potential, and additional parameters. Parameters such as the distribution of smectite layers probability (%S) and the distribution of charges caused by exchangeable cations in the interlayer space were used as indicators for mineralogical alterations in subsequent treatment experiments with B25 and Opalinus clays.

The samples were suspended in deionized water and dispersed using ultrasonic treatment for approximately 20 minutes. The clay fraction (<2 µm) was separated by sedimentation and diluted with deionized water to obtain a clear suspension. This suspension was dropped onto carbon-coated Cu grids, air dried, and stored under controlled environmental conditions at 45% humidity.

TEM-EDX investigations were conducted on the <2 µm fraction using a FEI TECNAI G2 20 transmission electron microscope at the VNU University of Science, Vietnam National University, Hanoi. This equipment, operated at 200 kV with a LaB6 cathode, was equipped with an S-TWIN objective, a windowless EDAX energy-dispersive X-ray system, and a FEI Eagle 2k CCD TEM camera.

Approximately 200 individual clay particles per sample were characterized by TEM-EDX for crystal size, crystal habit, particle morphology, and element distribution. Crystal size, crystal habit, and particle morphology were described according to Henning & Störr (1986). Element distribution was quantified using calibrated k factors, following methods by Cliff & Lorimer (1975), Lorimer & Cliff (1976), and Mellini & Menichini (1985). These k values account for particle-specific behaviour against possible irradiation damage.

The elements O, Na, Mg, Al, Si, K, Ca, and Fe were quantified using the EDAX GENESIS–TEM Quant Materials procedure. This involved correcting acquired EDX spectra through background subtraction, Gaussian deconvolution, and applying k-factor corrections based on standards such as phyllosilicate (muscovite) and selected non-phyllosilicate standards. The average errors in element analysis, expressed as atomic proportions using the phyllosilicate standard, were approximately 10 (Na), 5 (Fe, Mg, K, Ti, Ca), and 1 (Si, Al).

Measurement parameters included a reduced time of 20 seconds per particle and a limited exposed area of 50 nm in diameter to avoid potential irradiation damage to particles. Particle stability during this measurement time was verified at the beginning of each measurement campaign.

Additional methodological details regarding TEM-EDX measurements and mathematical procedures for calculating mineral formulae can be found in Hoang-Minh et al. (2019). These procedures were further extended by applying the k-means clustering method to identify subgroups of observations within the dataset. Data were standardized (scaled) to ensure comparability, and Euclidean distances were employed as classical methods for distance measures. Optimal clusters were determined using the Elbow method and Gap statistics[1].

---

[1] *https://uc-r.github.io/kmeans_clustering*

3. Mineralogical Characterization of Initial Materials

3.1 Chemical composition (XRF)

The bulk chemical composition of the three initial powder materials (B25 bentonite, Opalinus, and Friedland clays), as analysed by XRF spectroscopy, is presented in Tab 3.1. The Opalinus clay contains a lower amount of SiO_2 and Fe_2O_3 but higher contents of TiO_2, MgO, CaO, Na_2O, K_2O, and P_2O_5 compared to B25 clay. Friedland clay shows less MgO but higher Fe_2O_3 and K_2O, with CaO and Fe_2O_3 being higher than in the other two clays. Otherwise, the other elements, such as Al_2O_3, are quite consistent among the three clays. The presence of calcite in Opalinus clay, as reported in XRD measurements, could explain the high amount of CaO, while the high sulphur content is due to the presence of pyrite in Opalinus and Friedland clays compared to B25 clay. The lower content of SiO_2 in Opalinus and Friedland clays is consistent with the mineralogical composition of clay minerals, where smectite is mostly absent, but micaceous minerals (illite, illite-ml) dominate in both materials.

***Tab 3.1** Chemical composition (XRF) of untreated materials of Opalinus and B25 clay*

Element (wt%)	SiO_2	TiO_2	Al_2O_3	Fe_2O_3	MnO	MgO	CaO	Na_2O	K_2O	P_2O_5	sum	LOI	total sum
B25 bentonite													
XRF	60.97	0.58	19.50	6.08	0.03	2.35	1.37	0.53	1.93	0.08	93.42	8.46	101.88
XRF[(a)]	61.50	0.50	21.10	6.40	0.10	4.00	3.80	0.40	2.00	0.10	100.00		
Opalinus clay													
XRF	45.95	0.84	19.60	5.86	0.05	2.57	9.00	0.64	2.87	0.19	87.57	14.43	102.00
XRF[(b)]	53.10	1.00	19.70	6.20	<0.1	2.30	3.00	0.60	2.60		91.00		
Friedland clay													
XRF[(c)]	56.7	0.94	18.09	7.31	0.035	2.01	0.54	0.96	3.01	0.11	88.21	9.12	99.32
XRF[(d)]	58.6	0.10	18.20	11.50	2.70	0.70	0.20	3.40	-	-	-	-	-
XRF	54.6	0.94	17.81	6.35	0.02	1.80	0.36	1.08	3.12	0.08	86.15	13.64	99.79
Element (ppm)	S	Cl	V	Cr	Ni	Cu	Zn	Rb	Sr	Zr			
XRF Opalinus	3172	380	179	489	94	56	190	1	279	130			
XRF B25 bentonite	132	0	0	474	79	77	129	1	50	274			

Note: (a) from Matschiavelli et al., 2019, (b) from Pearson et al., 2003, (c) from Hoang-Minh, 2006; (d) from Kasbohm, 2003

3.2 X-ray Diffraction (XRD)

3.2.1 B25-bentonite

The mineralogical composition of B25 bentonite was determined by BGMN-Rietveld refinement and is shown in Tab 3.2 and Fig 3.1A. The analysis revealed the presence of Illite 1*M* and 2M_1 as the second most abundant phases (15% and 17%) after Ca-smectite (32%). Other clay mineral phases include illite-smectite mixed layers (10%) and highly ordered kaolinite (14%). Non-clay mineral phases include quartz (10%) and traces of feldspar from orthoclase and albite (4%). The quantitative mineralogical composition analysis of the untreated B25 material showed results comparable to Ufer et al. (2008), although the amount of smectite (Ca-smectite + IS-ml) was lower than reported by Matschiavelli et al. (2019). However, our measurements indicated a higher content of illite (illite 1*M* and illite 2M_1), particularly illite 2M1, which is identified at 3.32, 3.20, 2.99, and 2.79 Å. The content of kaolinite is comparable to that in Matschiavelli et al. (2019) and lower than in Ufer et al. (2008). The amount of non-clay minerals (feldspar, quartz) is mostly consistent with both previous studies.

Tab 3.2. *Mineralogical composition of randomly oriented powder of B25, Opalinus and Friedland clays (original and compacted)*

B25 bentonite	***own results***	Ufer et al. 2008	Matschiavelli et al., 2019	***Opalinus clay***	***own results***	Gaucher et al., 2003	Bossart & Thury, 2008 *(min-best-max)*	Nagara, 2002
Ca-smectite	32%	43.2%	55%	Ca-smectite				
IS-ml	10%			IS-ml	3%	11 - 20%	5 - 11 - 20%	11%
Illite_1M	15%			Illite_1M	4%	17 - 40%	15 - 23 - 30%	23%
Illite_2M1	17%	16.6%	15%	Illite_2M1	18%			
Chlorite				Chlorite	12%	5 - 20%	3 - 10 - 18%	10%
Kaolinite	14%	21.9%	12%	Kaolinite	25%	15 - 32%	15 - 22 - 37%	22%
Σ clay	***86%***	***82%***	***82%***	***Σ clay***	***61%***		***28 - 66 - 93%***	***66%***
Quartz	10%	13.2%	10%	Quartz	13%	6 - 17%	10 - 14 - 32%	14%
Orthoclase	2%	1.7%		Orthoclase	1%	1 - 2%	0 - 1 - 6%	1%
Albite	2%	3.5%	3%	Albite	4%	1 - 2%	0 - 1 - 2%	1%
Pyrite				Pyrite	1%	1 - 2%	0 - 1 - 3%	1%
Calcite			1%	Calcite	17%	11 -28%	4 - 13 - 22%	13%
Siderite				Siderite	1%	1 - 4%	0 - 3 - 6%	3%
Dolomite			4%	Dolomite	2%	≤ 2%	≤ 1%	
Rutile			1%	Rutile				
Gypsum				Gypsum			≤ 0.5%	
Σ total	***100%***	***100%***	***100%***	***Σ total***	***100%***			***99%***

Friedland clay

Phases	Henning, 1971	Hoang, 2006	Karnland et al. (2006)	FIM (2009)	***own results (No19 initial)***	***Tonmehl Juli 2021 – Burgscholle***
Ca-smectite					5%	
Illite-smectite mixed layer structure	44%	40%	56%	33-42%	14%	12%
Illite 2M1	12%	14%	7%	25-30%	6%	33%
Illite 1M					34%	
Kaolinite (+ Chlorite)	11%	12%				
Kaolinite			11%	10-13%	16%	17%
Chlorite				3-4%	3%	5%
Σ clay	***67%***	***66%***	***74%***		***78%***	***67%***
Quartz	24%	27%	20%	16-20%	15%	16%
Feldspar	5%					
Plagioclase				0-2%	3%	2%
K-feldspar		2%	1%	0-1%	3%	1%
Anatase, Rutile		1%			1%	1%
Gypsum			1%			2%
Pyrite	1%	traces	1%		>1%	1%
Σ total	***97%***	***96%***	***97%***		***100%***	***99%***

In the same refinement, Ca-smectite and two kinds of illite and Ca-smectite are identified as following:

Smectite: $Al_{2.9}\,Ca_{1.46}\,Fe_{1.2}\,Mg_{0.4}\,Si_{7.5}\,O_{32.76}$

Illite 2*M*$_1$: $Al_{11.68}$ $Fe_{0.32}$ $K_{4.0}$ Si_{12} O_{48}

Illite 1*M*t: $Al_{5.98}$ $K_{1.4}$ $Si_{6.0}$ O_{24}

The oriented mount preparation for fraction <2µm indicated that B25 bentonite is dominated by 15Å-montmorilonite (divalent cation of Ca and/or Mg in the interlayer sheet) with specific peak at 15.4Å of the XRD-diffractogram from air-dried specimen (Fig. 1B). After ethylene-glycol saturation, the interlayer sheet was fully expanded to 17Å peak as well as the (001)/(002)-interference appeared at 8.59Å and (002)/(003) peak 5.63Å (Fig. 1B). It showed that smectite (montmorillonite, beidellite, etc.) is the dominant component in the clay fraction (<2µm) instead of IS-ml as expected. Moreover, the distance between (002) and (003) orders also confirmed the presence of this smectite phase.

Otherwise, the composition of clay minerals phases (<2 µm) of smectite, illite and kaolinite as well as mixed layer phases are modelled by Sybilla (Tab. 3.3, Fig. 3.2) and showed that there are two varieties of IS-ml: (1) IS R0 GLY (1) is pure montmorillonite and/or beidellite with 99% smectitic layer whereas distance of (002)/(003) at 5.42°2thetha, (2) IS R0 (2) contains 55% smectitic layer and 45% illitic layer where distance of (002)/(003) is 6.26°2thetha (Moore and Reynolds, 1997). In addition, the clay fraction contains 9% illite (d_{001}=9.99 Å, d_{002} = 4.97 Å and d_{003} = 3.31 Å) and 5% kaolinite at 7.17 Å, 3.57 Å together with 23% kaolinite-smectite mixed layer (KS-ml) with smectitic layer is 45% at 17.2 Å, 8.26 Å, 5.7 Å and 3.43 Å and distance of (001/002)/(002/005) = 15.24°2thetha.

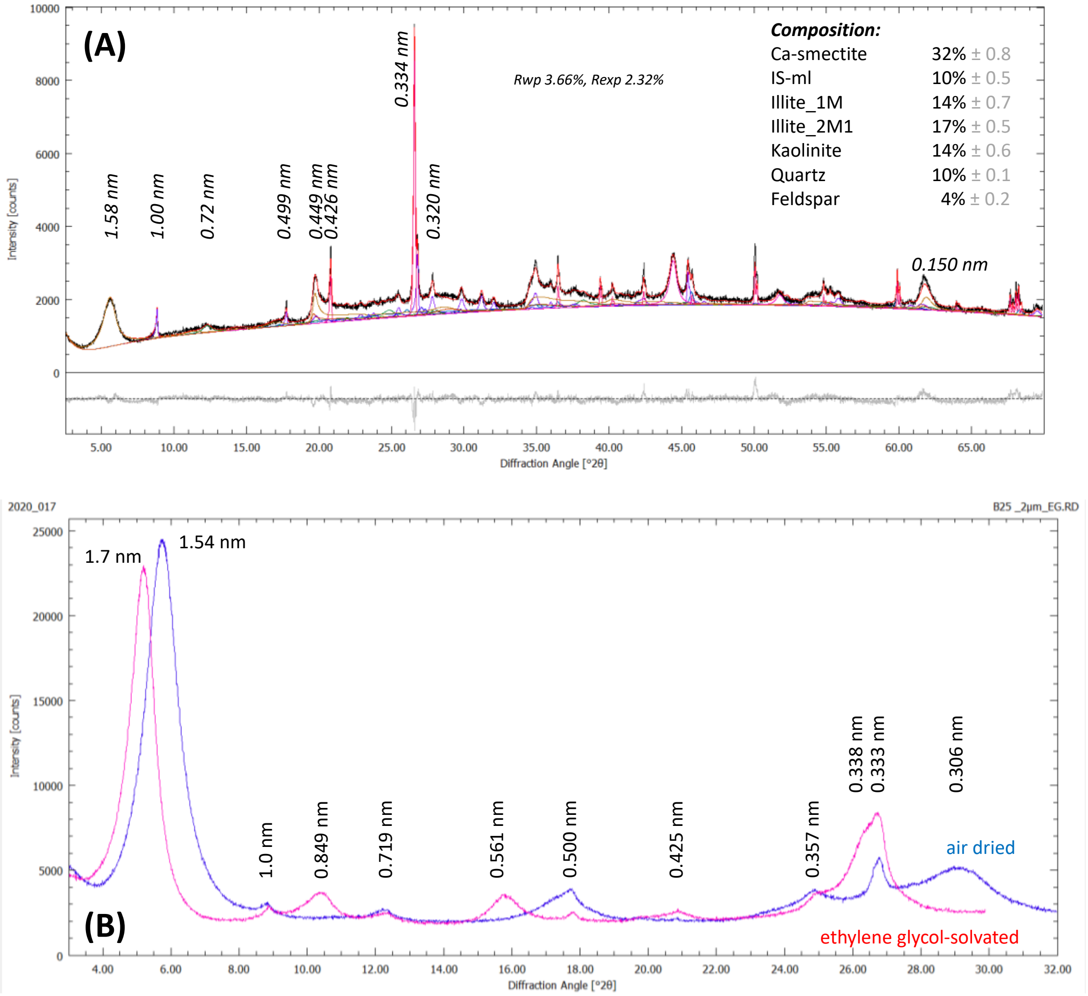

Fig 3.1 *(A) Diffractograms of randomly oriented powder (<40 µm) and oriented mount specimens (< 2 µm) (B) of B25 bentonite and interpretation of phases according to Profex-BGMN refinement (Rwp and Rexp are fitting parameters of refinement)*

Tab 3.3*Clay mineral matter of fraction < 2 µm by Syblla-modelling of XRD-oriented specimen of B25 bentonite, Opalinus, and Friedland clays*

Phases	content (%)	%S	T_{mean} (nm)	a(XII) phfu	Fe(VI) phfu
Oriented specimen of B25 bentonite, misfit = 11.28%					
IS R0 GLY(1)	47	99	4,4	0,06	0,24
IS R0 GLY(2)	16	55	14,4	0,21	0,03
Illite	9	-	13,1	0,3	0
Kaolinite	5	-	14,9	-	-
KS GL R0	n.d.	-	-	-	-
KS GL R1	23	45	11,2	0,15	0,38
Oriented specimen of Opalinus clay, misfit = 17.3%					
IS R0 GLY	10	11	24,4	0,59	0,00
ISS R0 GLY	8	29	12,5	0,50	0,17
Illite	12	18	0,56	0,00	-
Chlorite	7	18	-	-	-
Kaolinite	14	27	-	-	-
KS GL R0	14	16	23,7	0,05	0,00
KSS GL R0	36	44	18,5	0,11	0,00
Oriented specimen of Friedland clay (No19), misfit = 8.10%					
IS R0 GLY					
ISS R1 GLY	54	39	10.6	0.61	0.44
Illite	16	-	23.2	0.86	0.54
Chlorite	2	-	9.6	-	2.48
Kaolinite	10	-	17.3	-	-
KS GL R0	17	48	3.9	0.10	0.13

Note: Tmean – thickness of particles, %S-proportion of smectitic layer in mixed layer phases, a(XII) – interlayer charge, Fe(VI) – octahedral Fe, KS GLY R0 – kaolinite- one water layer smectite mixed layer, KSS GL R0 – kaolinite – one water layer smectite – two water layer smectite mixed layer

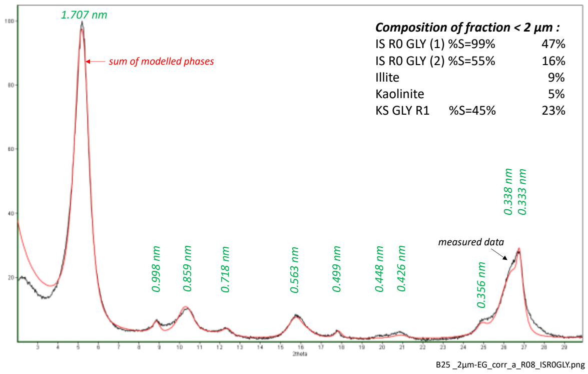

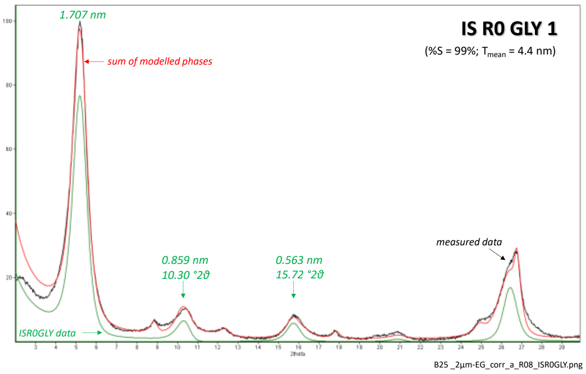

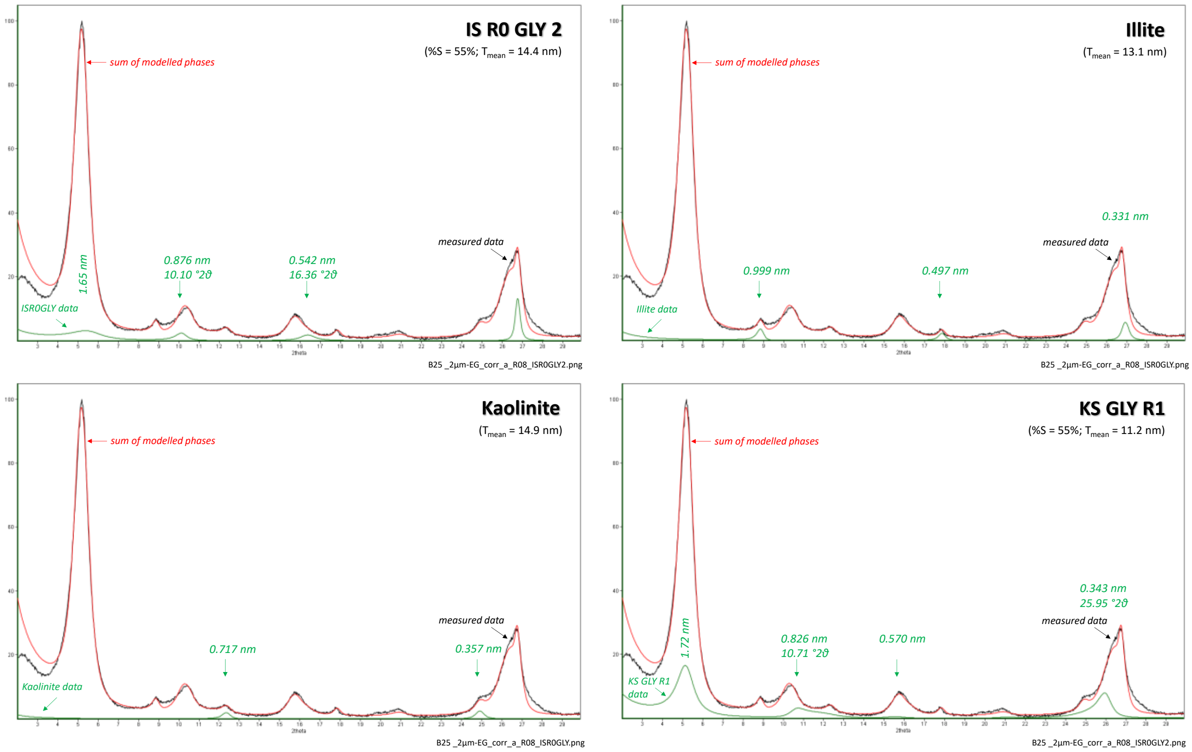

Fig 3.2. *Sybilla modelling of oriented mount specimen (XRD) of B25 bentonite*

3.2.2 Opalinus clay

The visual XRD patterns of randomly oriented material showed the presence of the following minerals: kaolinite, chlorite, illite, and illite-smectite mixed layers, with a total concentration of 62%. Quartz and calcite were found as the main non-clay minerals, along with traces of feldspar, pyrite, siderite, and dolomite. The quantitative amount of each phase was refined using BGMN Rietveld refinement, as shown in Fig 3.3A and Tab 3.2. This method also allowed for the modelling of the quantitative structural formulae of each phase:

IS-ml: $Al_{3.08}\ Fe_{0.28}K_{0.82}Mg_{0.8}Si_{7.84}O_{27.2}$

Illite 1*M*t: $Al_{5.98}K_{1.4}Si_6O_{24}$

Illite 2M_1: $Al_{11.68}Fe_{0.32}K_{2.97}Si_{12}O_{48}$

Due to a variable mineralogical composition of Opalinus (Bossart and Thury, 2008), the amount of total clay in our own sample is comparable with Nagara (2002) but the amount of non-clay minerals is changed from deposit to deposit /Tab 3.2/.

XRD-measurement with oriented samples, including air dried and ethylene glycol saturation, was used to characterize the expandable layers (Fig 3.3B). In the air-dried diffractogram, the IS-ml shows as broad/diffuse interference at ~ 11.6 Å peak and illite at 10 Å, 4.99 Å, kaolinite appeared at 7.17 Å, 3.57 Å and chlorite at 14.2 Å, 4.73 Å and 3.55 Å. Under ethylene glycol saturation, this clay indicated a strong limit of expandability due to a small amount of illite-smectite mixed layer. The small humps of 9.2 and 5.28 Å (Fig 3.3B) could suggest a presence of illite-smectite mixed layer with proportion of smectitic layer is ~25% (%S=25%).

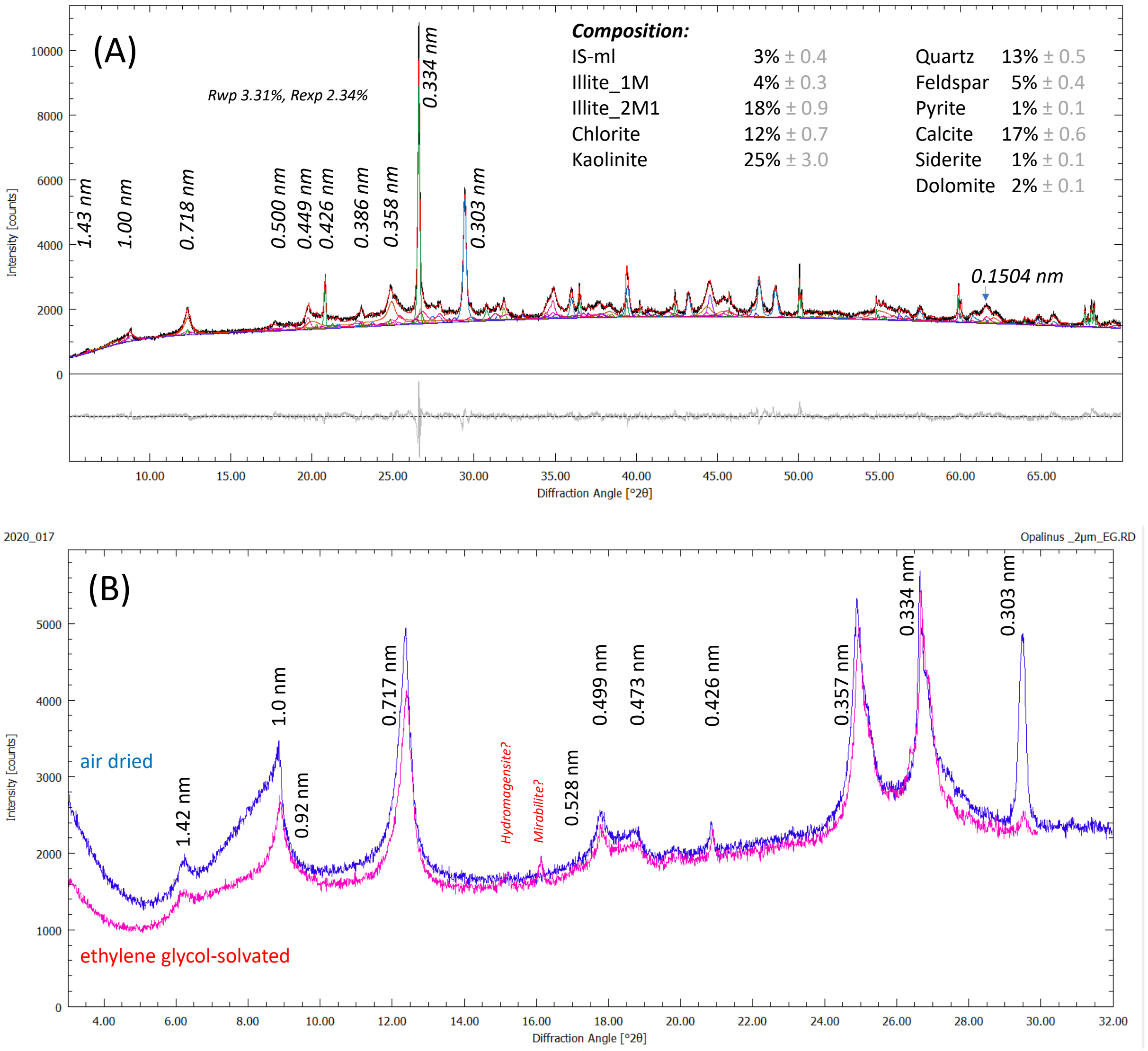

Fig 3.3. *(A) Diffractograms of randomly oriented powder (<40 µm) and oriented mount specimens (< 2 µm) (B) of Opalinus clay and interpretation of phases according to Profex-BGMN refinement and (Rwp and Rexp are fitting parameters of refinement)*

The Sybilla-modelling from oriented mount samples has indicated the presence of difference mixed layer phases including illite, chlorite and kaolinite (Tab 3.3, Fig 3.4).

- The IS R0 GLY (11%) appears at 9.81 Å and 5.04 Å with a distance of (002)/(003) is 8.58°2theta but the percentage of smectitic layer in IS-ml is only 11% and T_{mean} = 24.4 nm.
- The IS R0 GLY (29%) found as small hump at 10.7 Å which shows a low expandability for (001/002)-interferences because of high amount of 1w-smectite, the proportion of each layer as following: %I = 71%, %S-2w =9% and %S-1w =20% and T_{mean} = 12.5 nm.
- Illite (12%) is characterized by d(001) = 10 Å, d(002) = 5 Å and d(003) = 0.33 Å, the T_{mean} = 18 nm
- Chlorite (7%) showed at 14.3 Å, 7.11 Å, 4.74 Å, and 3.55 Å with T_{mean} = 11 nm
- Kaolinite (14%) is found at 7.16 Å and 3.58 Å with T_{mean} = 27 nm
- KS GLY R0 (14%) with 16% smectitic layer and 84% kaolinitic and Tmean = 23.7 appears at 7.48 Å and 3.52 Å where distance between (001/002) and (002/005) = 13.45°2thetha, this result is confirmed a percentage of 17% smectitic layer by Moore and Reynold (1997)

- KSS GLY R0 covers 36% of total clay mineral fraction in this sample with total smectitic layer is 44%, Tmean = 18.5 nm. This phase is characterized by a hump at 12.5 Å, 6.78 Å and 3.35 Å and the distance of (001/002) and (002)/(005) is 13.58 °2θ.

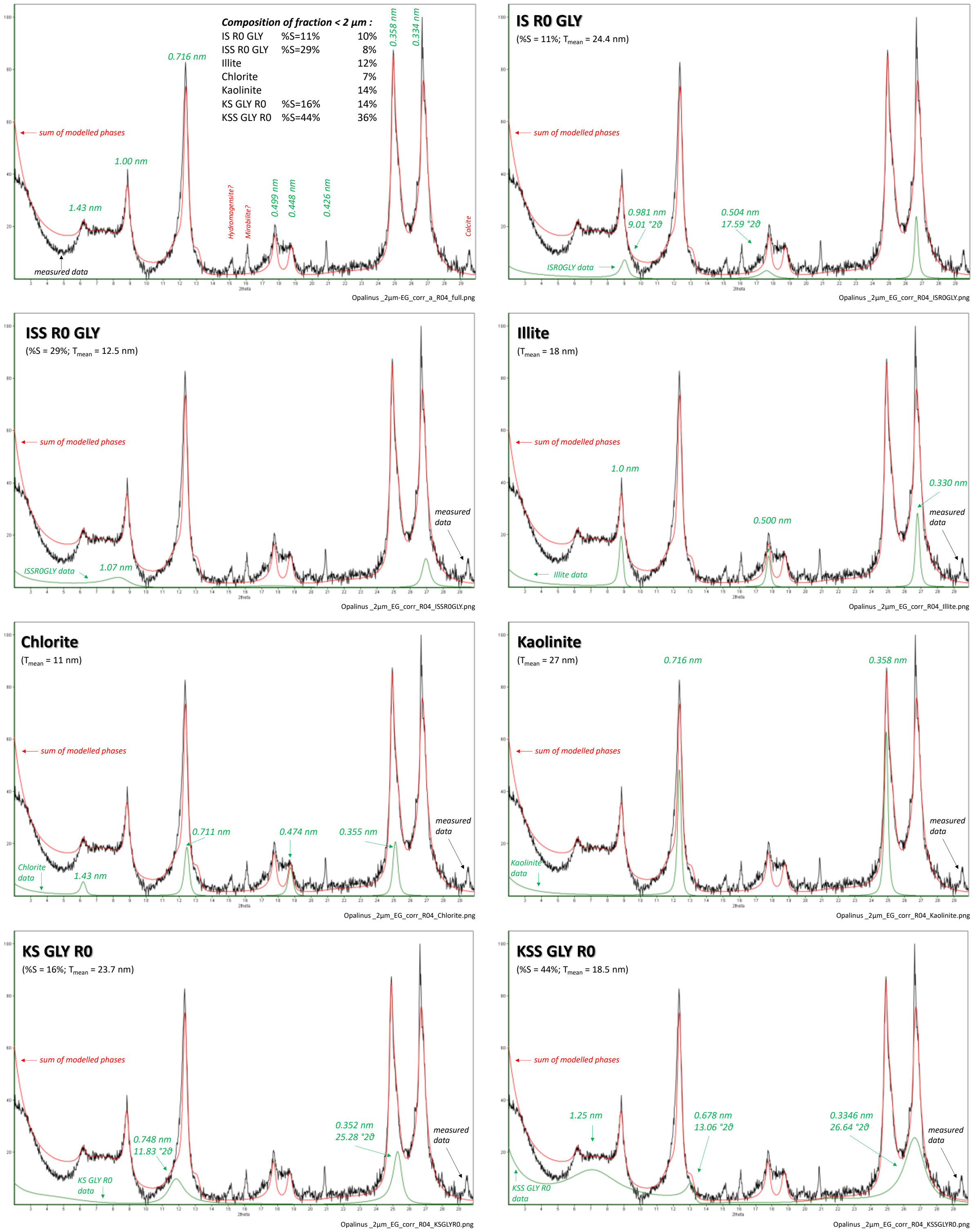

Fig 3.4 *Sybilla modelling of oriented mount specimen (XRD) of Opalinus clay*

3.2.3 Friedland clay

The visual XRD patterns of randomly oriented samples from two powder materials showed the presence of the following minerals: quartz, feldspar (albite, orthoclase) as non-clay minerals, and kaolinite, chlorite, illite, smectite, and illite-smectite mixed layer phases as clay minerals (Fig. 3.5), with traces of pyrite and anatase (<1 wt.%). The weight percent (wt.%) of each phase was calculated using BGMN-Rietveld refinement:

Powder material (untreated sample, used only for comparison of raw material):

- Illite-smectite mixed layer (IS-ml): 6 wt.%
- Illite (illite 1M and illite 2M1): 57 wt.%
- Chlorite: 2 wt.%
- Kaolinite: 20 wt.%
- Quartz: 13 wt.%
- Feldspars: 2 wt.%

Powder material (initial sample No19, parent material for experiments):

- Ca-smectite: 5 wt.%
- Illite-smectite mixed layer (IS-ml): 14 wt.%
- Illite (illite 1M and illite 2M1): 40 wt.%
- Chlorite: 3 wt.%
- Kaolinite: 16 wt.%
- Quartz: 15 wt.%
- Feldspars: 6 wt.%

XRD measurements with oriented samples, including air-dried and ethylene glycol saturated, were used to characterize the expandable layers. The smectite group of initial material (No19), which included the illite-smectite mixed layer (IS-ml), showed a peak at 12.5 Å under air-dried conditions, which increased to 17.9 Å with a new large reflection at 8.59 Å after ethylene glycol saturation. Illite was identified by a 9.98 Å peak. Chlorite and kaolinite were demonstrated at 7.16 and 7.07 Å, respectively, corresponding to the peaks of chlorite and kaolinite.

Proportions of illitic layers in IS-ml were calculated as described by Moore and Reynolds (1997). This calculation is based on the relationship between the positions of the (001/002) and (002/003) interferences taken from ethylene glycolated specimens. The Friedland clay (initial sample No19) was characterized by illite-smectite mixed layer phases with 39% of smectitic layers (Fig. 3.5).

Validating the Friedland Clay measurements with data from the literature is difficult. The open-cast mining company of the deposit "Siedlungsscholle" has closed and covered the well-known old areas of this deposit and opened a new exploitation field at the east margin. This material is located at the margin of the deposit and was in contact with glacial water during the Pleistocene. For this newly opened Eastfield, no new published data are available. A comparison of published mineralogical results from "Siedlungsscholle", the recent own measurement No19, and a former own measurement from the neighbouring deposit "Burgscholle" (Tab. 3.2) shows a remarkable coincidence of mineral matter between sample No19 (from "Siedlungsscholle" – new field at the east margin of this deposit) and the trade ware of the deposit "Burgscholle."

The clay fraction (<2 µm) was investigated in more detail using Sybilla modelling software, showing the presence of different mixed layer phases of high-charge illite/smectite mixed layer, low-charge beidellite, dioctahedral vermiculite/smectite mixed layer, kaolinite/smectite mixed layer, along with illite, chlorite, and kaolinite (Tab. 3.3).

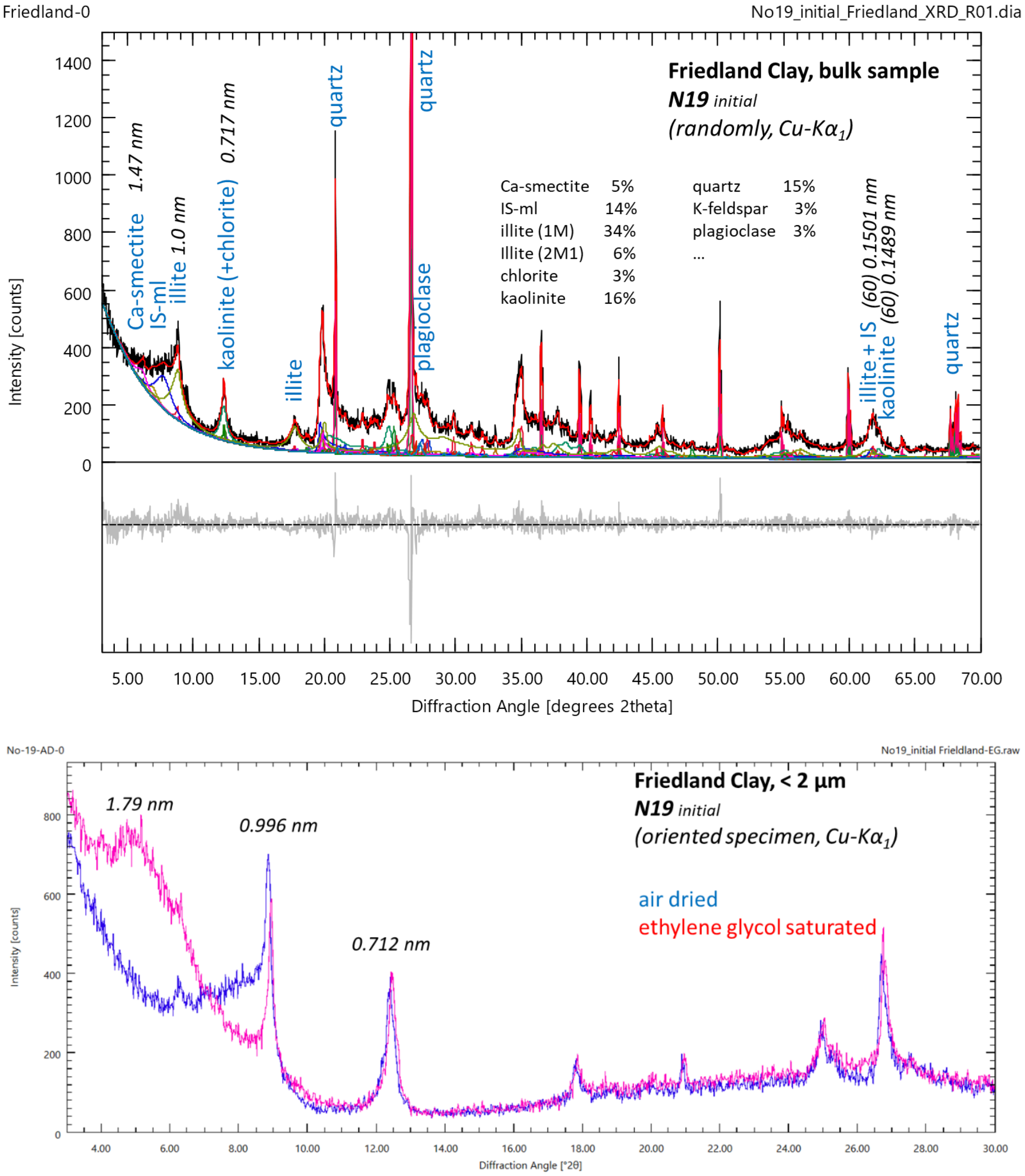

Fig 3.5. *(A) Diffractograms of randomly oriented powder (<40 µm) and oriented mount specimens (< 2 µm) (B) of Friedland clay and interpretation of phases according to Profex-BGMN refinement and (Rwp and Rexp are fitting parameters of refinement)*

- **ISS R0 GLY (54%):** At ~16 Å and 5.2 Å with a distance of (002)/(003) of 7.00°2θ, the percentage of smectitic layer (%S) in IS-ml is 39%.
- **Illite (16%):** Characterized by d(001) = 9.98 Å, d(002) = 5 Å, and d(003) = 0.33 Å.
- **Kaolinite (10%):** Found at 7.16 Å and 3.58 Å.
- **KS GLY R0 (17%):** With 48% smectitic layer and 52% kaolinitic at 8.74 Å and 3.40 Å, where the distance between (001/002) and (002/005) = 15.04°2θ.

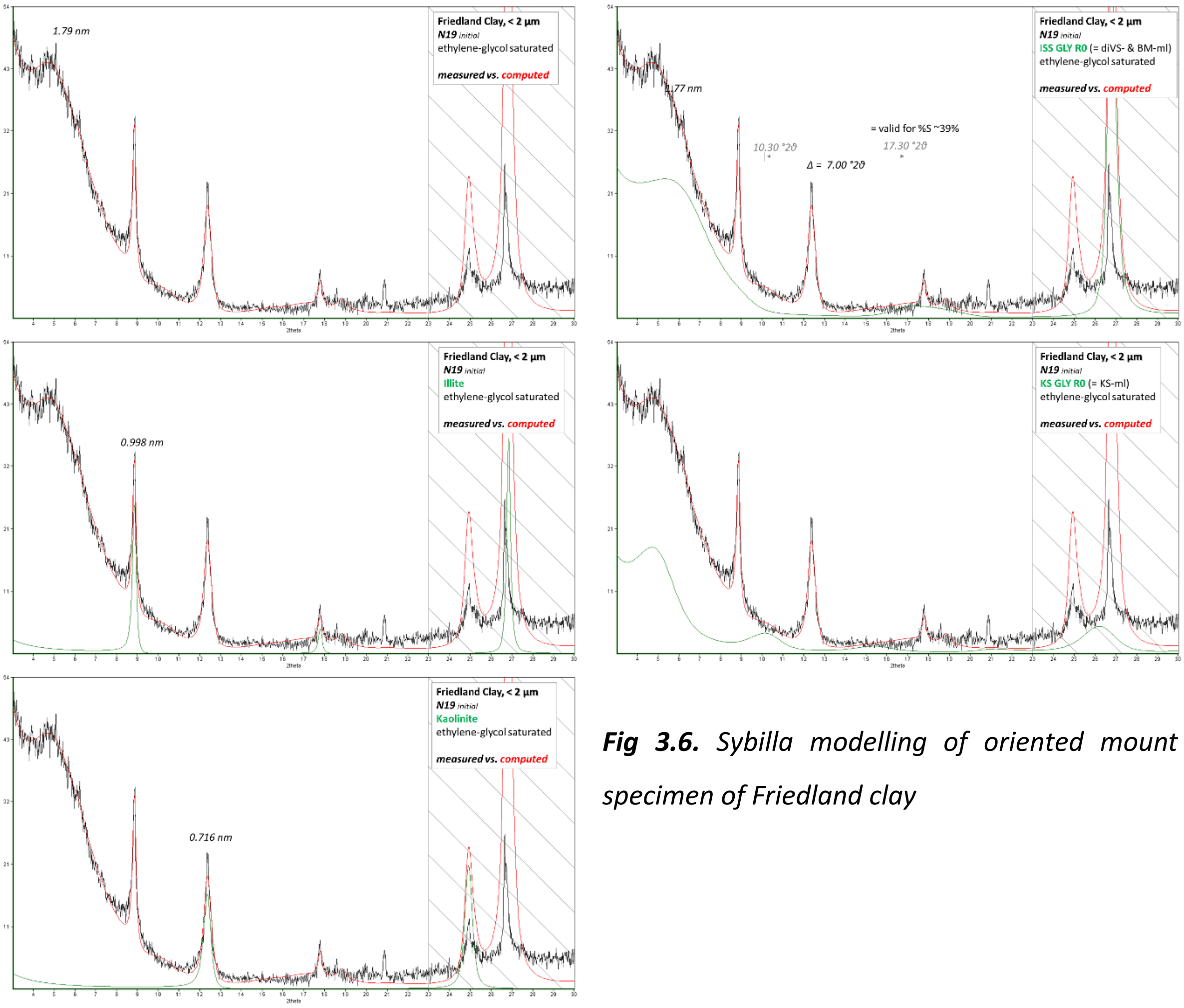

Fig 3.6. Sybilla modelling of oriented mount specimen of Friedland clay

3.3 Fourier Transform Infared (FTIR)

3.3.1 B25-bentonite

The FTIR spectroscopic analysis of B25 clay is shown in Fig. 3.7 left. It indicates that smectite is the dominant phase in the clay. The broad adsorption band at 3634 cm^{-1} (AlAlOH) is typical for Al-rich content of smectite (Madejova et al., 1996) and strongly associated with beidellites (Gate, 2005) but also Fe as presences of FeFeOH (3557 cm^{-1} and 3577 cm^{-1}) (Zviagina et al., 2004). The broad band at 3419 cm^{-1} represents the OH-stretching vibration of silanol (Si-OH) groups. These bands originated from the solid and H-O-H stretching oft he water molecules which were absorbend on the solid surface. Moreover, the band at 1635 cm^{-1} assigned to an overtone of the bending vibration of water, which is retained in the matrix.

In the OH-bending area, the broad bands at 1107 cm^{-1} and 1048 cm^{-1} represents the stretching vibrations of Si-O-Si group in tetrahedral sheets of smectite (Farmer and Russel, 1964, Emmerich et al., 1999). The spectral band at 910 cm^{-1} indicated the stretching vibration of AlOHAl and 873 cm^{-1}, 836 cm^{-1} corresponding to the AlOHFe and AlOHMg respectively. The coupled Al-O and Si-O out of plane vibration are assigned to the band at 621 cm^{-1}. The presence of muscovite is shown by different shared bands with smectite and kaolinite as well as quartz but the band at 750 cm^{-1} is typical ones for this phase as mentioned by Velde (1983) and kaolin at 693 cm^{-1} and 3700 cm^{-1}. It is note that, the two shoulders at 929 cm^{-1} in OH-bending region and 3646 cm^{-1} in OH-stretching region indicate the occurrences of beidellite type (Gates, 2005) and a bands at ~693 cm^{-1} shared with quartz is also assigned to Si-O in a ferruginous beidellite (Decarreau et al., 1992), in addition the occurrence of FeMgOH at 3557 and 3577 cm^{-1} suggested a high amount of Fe in smectite structures including beidellite. There were sharp bands at 780 cm^{-1} and 797 cm^{-1}, which confirms the occurrence of quartz. These results are in agreement with previous XRD-data.

3.3.2 Opalinus clay

FTIR scans of Opalinus clay (Fig. 3.7 right) shown strong distinct OH-stretching bands at 3620 cm^{-1}. A Si-O deformation band at 696 cm^{-1} indicated the presence of kaolin (Farmer and Russell, 1964). The tetraheral silica and quartz signals were assigned by Si-O stretching and Si-O vibration at 1111 cm^{-1} and 1038 cm^{-1}, respectively. The intensity of the Si-O vibration was proportional to the intensity of kaolinite bands. In the FTIR spectra, AlAlOH bending band assigned at 911 cm^{-1} which is typical for smectite and IS-ml (Farmer and Russell, 1964). The AlFe^{3+}OH band at 874 cm^{-1} shows a high intensity in comparision with 831 cm^{-1} of AlMgOH band. This is a sign of high content of Fe in octahedral sheet of dioctahedral minerals (e.g. smectite, illite, IS-ml) in Opalinus clay (Craciun, 1984; Gates, 2005). The FT-IR patterns of Opalinus clay show distinct Si-O stretching bands at double peaks of 778 and 798 cm^{-1}, indicating the presence of quartz. Moreover, the presence of calcite and pyrite was found at difference bands of 1428 cm^{-1} (calcite) and 1163 cm^{-1} and 1632 cm^{-1} (pyrite).

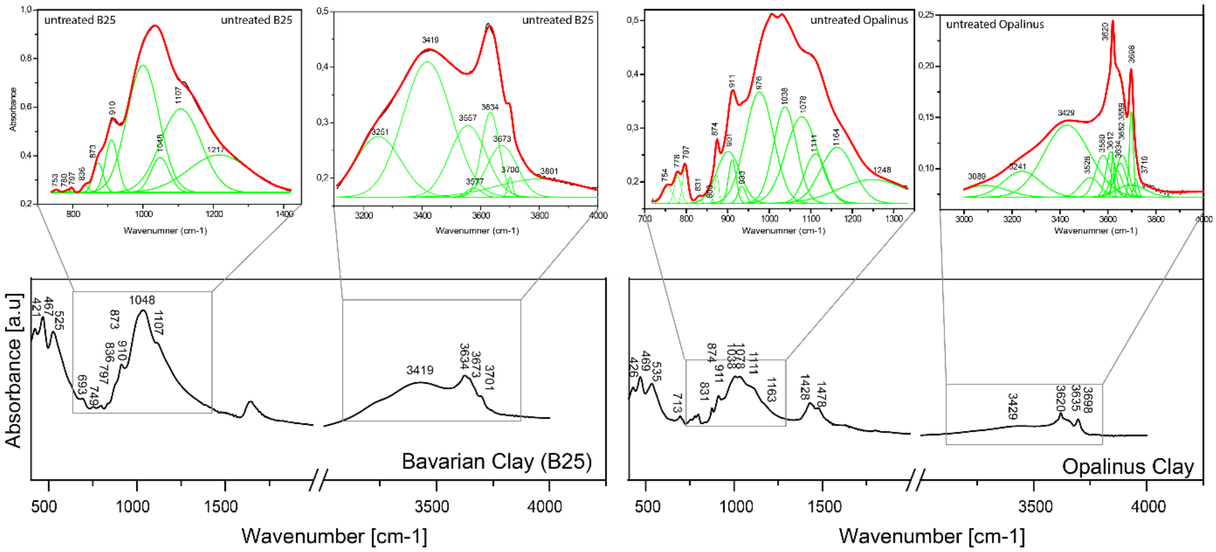

Fig 3.7 The FTIR-spectra of initial B25 bentonite and Opalinus clay

3.3.3 Friedland clay

FT-IR scans of Friedland clay (Fig. 3.8) showed strong distinct OH-stretching bands at 3623 cm^{-1}, ~ 3696 cm^{-1}. A Si-O-deformation band at 694 cm^{-1} indicated the presence of kaolinite and a possible absorption band of smectite was present at ~3600 cm^{-1} (Farmer and Russell, 1974). The tetrahedral silica and quartz signals were assigned by Si-O stretching and Si-O vibration at 1028 cm^{-1} and 987 cm^{-1}

respectively. The intensity of the Si-O vibration was proportional to the intensity of kaolinite bands. In FT-IR spectra, Al-OH-Al bending band assigned clearly at 909 cm^{-1} to a typical smectite and kaolinite (Farmer and Russell, 1974). The Al-OH-Fe^{3+} band at 882 cm^{-1} had low intensity reflecting the high Fe content of Friedland clay (Craciun, 1984; Russell and Fraser, 1994; Vantelon et al., 2001; Gates, 2005). Moreover, bending at 829cm^{-1} due to Al-OH-Mg and Al-O vibrations of illite rises to 753 cm^{-1}. An Al-O-Si band was also present (Farmer and Russell, 1974; Russell, 1987). In addition, the FT-IR patterns of Friedland clay show distinct Si-O stretching bands at double peaks of 779 cm^{-1} and 797 cm^{-1}, indicating the presence of quartz (Craciun, 1984).

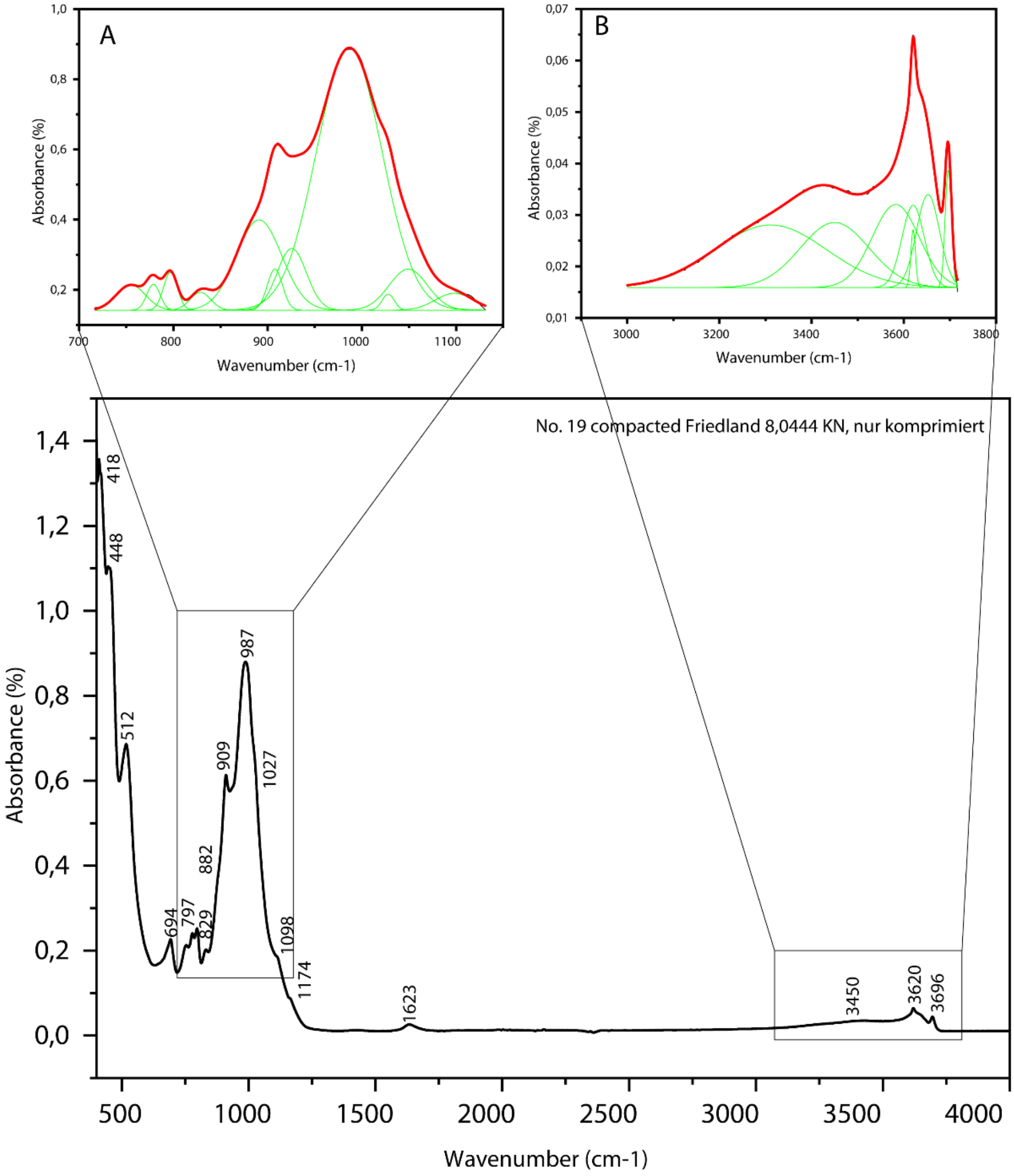

***Fig 3.8** Infrared spectrum of Friedland clay*

3.4 Thermal Analysis (DTA-TG)

Thermal gravimetry (TG) and differential thermal analysis (DTA) techniques were used to determine the elemental and mineralogical composition as well as to understand dehydration and dehydroxylation of the initial materials of B25 bentonite, Opalinus, and Friedland clays. The method additionally allowed to evaluate the temperature at which water is lost as well as the mass lost. The indication of the amount of strongly held water which is normally associated with swelling clays is provided. The small differences in the temperature at which water loss occurs also support the evidence on the presence of non-swelling and/or mixed layer minerals, as well as impurities in the rocks. Figures 3.9 and 3.10 depict the DTA/TG curve recorded the starting materials of three clays separately. In addition, the changes in the samples upon heating show both endothermic and exothermic peaks at different temperatures due to distinct mineralogical composition of the materials.

Tab 3.4 *The comparison of mass loss between DTA/TG and XRD for all phases and carbonate phases of B25 bentonite and Opalinus clay*

B25 bentonite		***Opalinus clay***	
300-1000°C *(as check for all phases)*		***300-1000°C*** *(as check for all phases)*	
meas.	5.17%	*meas.*	13.90%
XRD-calc.	5.15%	*XRD-calc.*	14.34%
700-1000°C *(as check especially for calcite)*		***700-1000°C*** *(as check especially for calcite+dolomite)*	
meas.	0.06%	*meas.*	6.45%
XRD-calc.	0%	*XRD-calc.*	6.96%

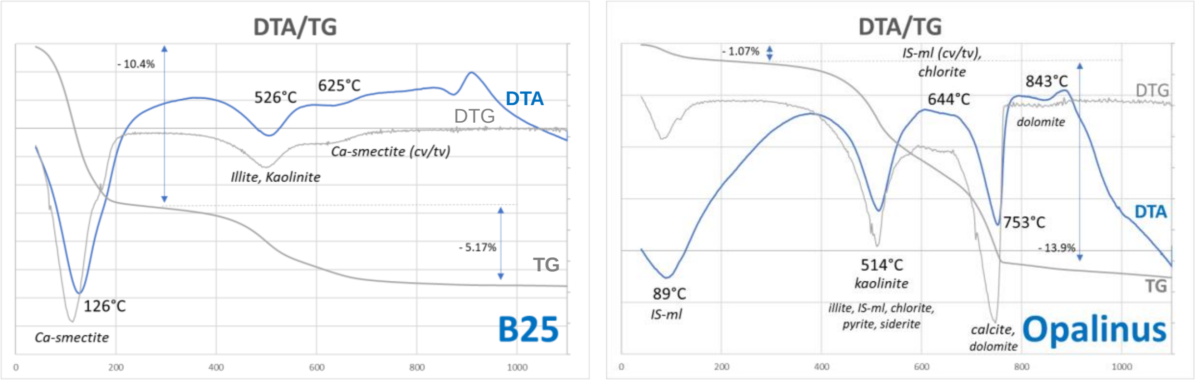

Fig 3.9 *DTA/TG curves of B25 bentonite and Opalinus clay*

3.4.1 B25-bentonite

The B25 bentonite shows a 3 steps of mass loss from room temperature up to 1000 °C. The first step is up to ~ 300 °C, shows the release of water molecules from the surface and interlayer sheet as well as water molecules coordinating exchangeable cations of smectite. High amount of smectite in B25 shows a dominant hydrated phase in bentonite, the mass loss of this step reached up to 10.4%. The second and third steps at the ranges of ~ 300 - ~ 550 °C and 550 – 700 °C, respectively, are related to dehydroxylation of clay minerals as smectite (400-800 °C), kaolinite (450-700 °C) and illite/muscovite (350-600 °C).

The changes in the sample upon heating is additionally interpreted by DTA curves. There are 4 endothermic peaks near 126 °C, 536 °C, 625 °C and nearby 900 °C. The first, most intense endothermic peak shows a shoulder at about 180 °C, which suggests a difference between removal of water molecules from the inner hydration shell of exchangeable cation and from less strongly bound water. Two endothermic peaks, near 526 °C and 625 °C on the DTA curves confirm that the changes observed on the TG curves in the 300 – 700 °C region are due two partly overlapping dehydroxylation processes. According to Brandley and Grim (1951) and Čičel et al. (1992), the endothermic peak near 900 °C is associated with the breakdown of the anhydrous montmorillonite to an „amorphous“ material from which new temperature phases crystallized near 920 °C.

The mass loss of the mineral phases from DTA/TG is cross checked with theoretical mass loss by XRD-results and show a good correlation at 300 – 1000 °C for all phases and 700 – 1000 °C for calcite (Tab 3.4)

3.4.2 Opalinus clay

The Opalinus clay is composed of low amount of smectite (IS-ml) but high amount of illite, chlorite and kaolinite in clay mineral group as shown in XRD-results (tab 3.2). It is responsible for a low mass loss (1.07%) from room temperature up to 1000 °C in the TG-curve of Opalinus clay. It means, aditionally to the dehydration of sample at 89°C, the escape of water molecules (beginning with 118°C – see DTG-signal) from the interlayer space and water molecules coordinating exchangeable cation is mostly absent in 2:1 fixed cation exchange phases (illite, chlorite) and 1:1 clay minerals (kaolinite) in the range up to 300 °C. The peaks in the range of 300 – 500 °C, and 550 – 700 °C are related to dehydroxylation of clay minerals including smectite (400 – 800 °C), kaolinite (450 – 700 °C), illite/muscovite (350 – 600 °C), chlorite (500 – 650 °C). Those steps are represented by 4 endothermic peaks near 89 °C, 514 °C, 644 °C and 843 °C in DTA curve. The first low intense endothermic peak at 118 °C is used to distinguish a removal of water molecules from the inner hydration shell of exchangeable cation in IS-ml from the less strongly bound water (Greene-Kelly, 1957). The two endothermic peaks near 514 and 644 °C on the DTA curves confirm that the changes observed on the TG curves in the region of 300 – 700 °C due to two partly overlapping dehydroxylation processes. Those endothermic peaks are contributed to kaolinite, illite, IS-ml, chlorite, pyrite, and siderite at 514 °C; chlorite, IS-ml (cv/tv) at 644 °C and carbonate of calcite, dolomite at 753 °C and finally 843 °C of dolomite.

The XRD-results of bulk sample have been validated by thermogravimetry (TG). The theoretical mass loss, calculated from XRD-results of bulk sample, was compared with the measured mass loss by TG. The XRD-results of raw Opalinus materials shows a theoretiocal mass loss of 14.34 % compared to the measured mass loss by TG with 13.9 % at 300 – 1000 °C. The content of carbonate phases (calcite + dolomite) is represented by a measured mass loss of 6.45% (by TG-measurement) in the range from 700 – 1000 °C). XRD calculation revealed 6.96% as theoretical mass loss caused by XRD-results for 14% calcite and 1% dolomite (tab 3.4).

3.4.3 Friedland clay

The DTA curve of smectite (Ca-smectite, illite-smectite mixed layer) in Friedland clay is shown in Fig. 3.10. The first endothermic effect observed in the range of 70 – 180 °C corresponds to dehydration of sample and the loss of interlayer water, the second and third correspond to the dehydroxylation what indicated by the mass loss of 1.85% (30 – 300 °C) observed in the TG curve. The TG analyses of other clay minerals phases as kaolinite (1:1 clay minerals), chlorite, illite (2:1 fixed cation exchange phases) show that the evolution of volatiles began at ~400 °C, peaked at ~500 °C and terminated at ~800 °C. These temperatures indicate the dehydroxylation of the clay minerals to the other phases (e.g., kaolinite to metakaolin and final destruction of the metakaolin structure at ~800 °C, illite changed to mullite or cristobalite, decomposition of smectite structure) at ~800 °C. Consequently, the mass loss at the range of 300 – 650 °C is 5.10% and 650 – 1000 °C is 1.16% and total mass loss of Friedland clay at 300 – 1000 °C reached 6.26%.

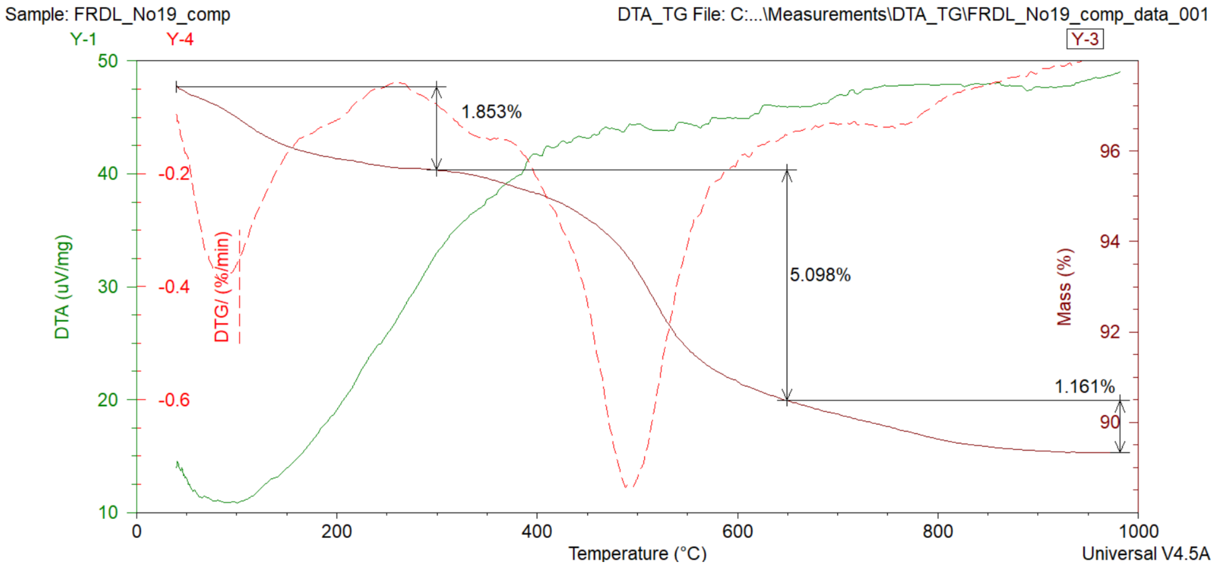

Fig 3.10 *DTA/TG curves of Friedland clay*

3.5 Scanning Electron Microscopy (SEM)

SEM observations were used to detect minerals that were unidentified by other methods (e.g., XRD, FTIR, DTA-TG, TEM-EDX) and to observe the effect of THMC experiments on the stability of clay and clay fabric at a microscopic scale with higher magnifications between 1000x and 3000x. The mineralogical composition was qualitatively identified using energy-dispersive X-ray spectroscopy (EDX) with an acceleration voltage of 15-20 kV. Additionally, the morphology and fabric of the clay were examined to interpret the changes between the compacted initial materials and the reaction products.

3.5.1 B25 bentonite

The photomicrographs in Fig. 3.11 show that the typical structures observed in the initial B25 bentonite are aggregated structures with very dense surfaces. These structures consist of aggregates 10 to 20 µm in diameter, as well as small clay platelets separated by an irregular porous network. Some grains of non-clay minerals are embedded between the clay aggregations or within the clay matrix. It is very common to observe some clay platelets acting as bridges, crossing inter-aggregate pores. The association of large and small aggregate clays shows a laminar structure. These aggregates are limited by large voids (>5 µm). Additionally, they show also an inner-aggregate porosity by voids with 1 – 2 µm as diameter. The presence of large grains such as muscovite, rutile, quartz, and Fe-oxides causes a large fracture system at the borders between the grains and the clay matrix/clay aggregates. Additionally, a laminar structure with thin smectite platelets in a face-to-face contact style is clearly observed, with interparticle pores (<2 µm) apparent. The micropore system develops along the 001-face of smectite platelets from face-to-face contact formations. Based on the morphology and EDX measurements, the dominance of smectite with impurities of non-clay minerals such as quartz, feldspar, Fe-oxides, and rutile is confirmed.

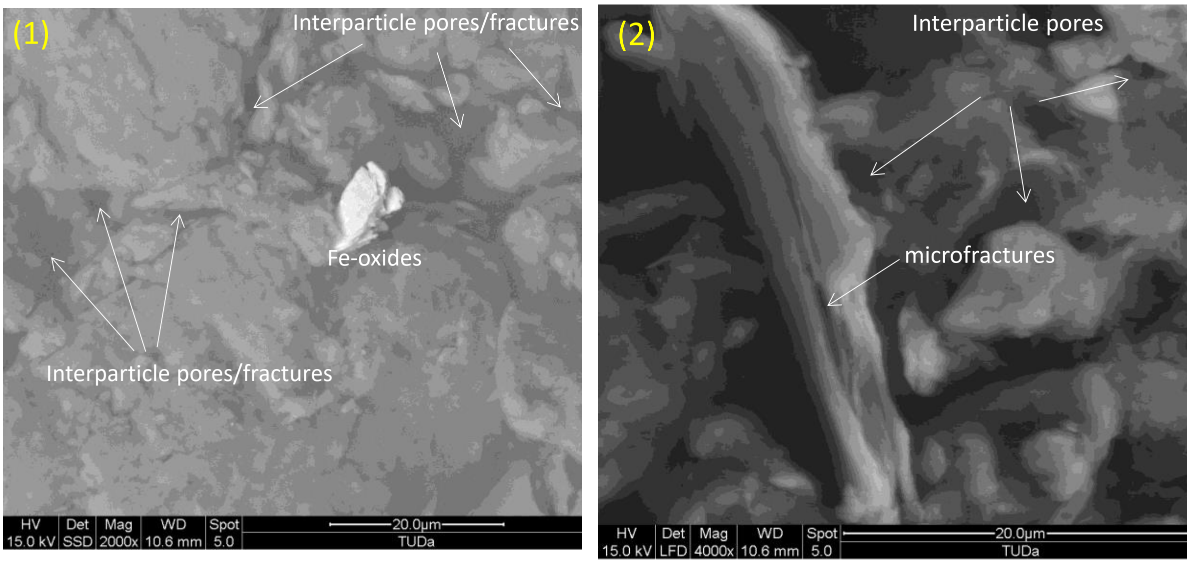

***Fig 3.11** SEM-images of initial compacted B25 bentonite.*

Note: (1) Compacted clay with a lot of linear and irregular shrinkage fractures, interparticles pores/fractures on the dense surface of clay pellet. (2) Loosely compacted clay with a large proportion of smectite causes an abundance of interparticle pores and cavities, likely due to volume reduction when dehydrated after the injection of OPA solution under saturated conditions. Additionally, large, thin, and platy mica particles with a system of linear microfractures between laminar sheets contribute to this phenomenon. The flocculation structure showed the edge-to-face and face-to-face contact style.

3.5.2 Opalinus clay

Electron micrographs of Opalinus clays (Fig. 3.12) show well-developed aggregate and small clay flake structures, with clay bridges acting as connectors in compacted Opalinus clay. The size of clay aggregates is variable (~25 µm), but the clay phases (smectite, illite/smectite) are very fine (1 – 2 µm) and widely distributed as a clay matrix with foliated textures. Non-clay mineral grains of various sizes appear as inclusions and/or embedded in the background of the fine-grained clay matrix, consequently forming abundant inter-particle and inter-aggregate pores. The inter-aggregate pores are angular in form, while inter-particle pores are mainly linear due to the laminar structure of the face-to-face contact style of smectite. The presence of fossils and pyrite, as well as other non-smectite phases, contributes to the widespread distribution of intracrystalline/intergranular macropores, but micropores from intracrystalline/intragranular structures are mostly observed on the crystal/granular surfaces of non-smectite particles. Additionally, linear shrinkage fracture systems are quite abundant in the samples.

In terms of mineralogical composition, SEM-EDX indicates the presence of all minerals detected by XRD. The clay matrix consists of fine-grained illite/smectite, carbonate fossils (shells, diatoms mainly composed of Ca), mica, calcite, quartz, and iron-hydro(oxides) associated with clusters of framboidal pyrite. No recrystallization of smectite to non-swelling clay or conversion processes is observed.

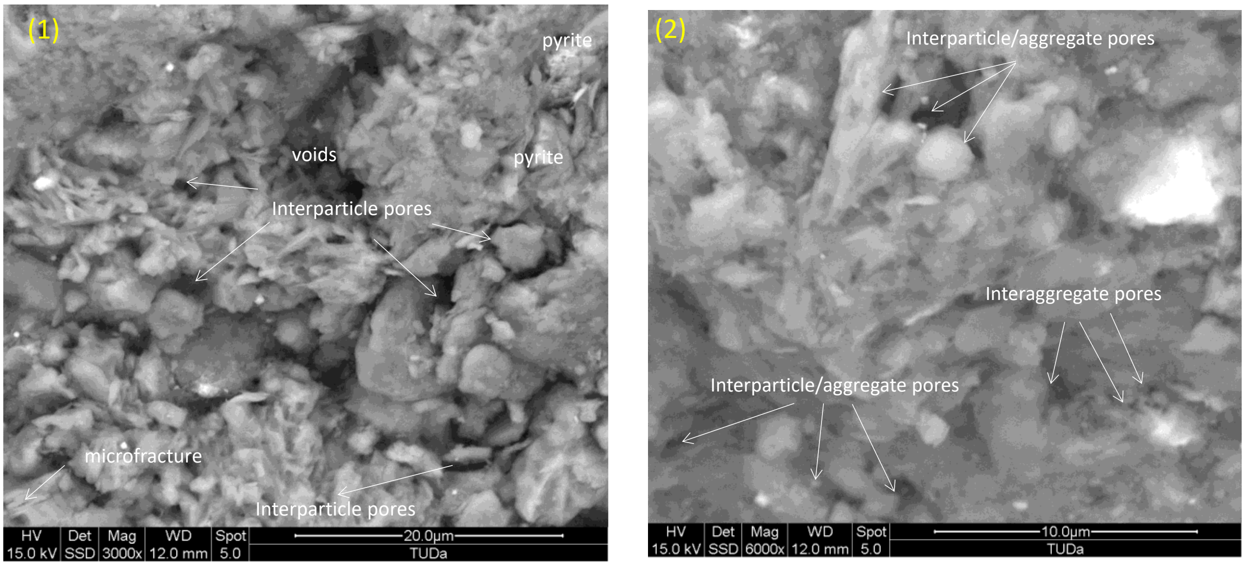

Fig 3.12 *SEM-images of compacted Opalinus*

Note: (1) Aggregation of platy illite-smectite mixed layer, interparticles and inter-aggregation pores and voids are observed with different angular form. The microfractures between sheet of illite-smectite flakes is observed due to the face-to-face and edge-to-face contact style. (2) the interparticle/aggregate pores on the loosely dense clay matrix.

3.5.3 Friedland clay

Under SEM-image observation, the initial Friedland clay (No19) is characterized by aggregated structures with a very dense clay matrix (Fig. 3.13). The small platy flakes of illite-smectite mixed-layer platelets form large aggregations (>25 µm). These are characterized by edge-to-face, face-to-face, and edge-to-edge contact styles, creating a system of pores, cavities, and fractures in different forms. The main component of the illite-smectite mixed layer in the rock shows characteristics of a disordered structure, resulting in lamellar slit and wedge-shaped pore systems.

The distribution of pores and minerals is commonly a combination of micropores between clay minerals and/or interparticle pores between clay minerals and non-clay phases. However, the most abundant are the interparticle pores of the illite-smectite mixed layer. The pore widths range from 2 nm to 10 µm. The shapes of the pores are mostly controlled by the crystal shapes of the lamellar illite-smectite mixed layer and the contact between them. The interaggregate pore fractures (shrinkage and contact surfaces between aggregate-aggregate and clay matrix-aggregate/impurities) are mostly linear and irregular in form, while voids and interparticle/granular/crystalline pores vary from linear to angular, spherical to irregularly polygonal. Intraparticle pores in Friedland clay are not clearly observed in clay minerals but are present in non-clay mineral phases (e.g., pyrite, Fe-oxides).

Fracture types are mainly developed in the illite/smectite mixed layer due to shrinkage and fractures between clay-clay aggregates and clay-impurities aggregates (such as clay and pyrite framboid, clay platelets, and interlayer microfractures). The length of fractures varies from 3 to 12 µm.

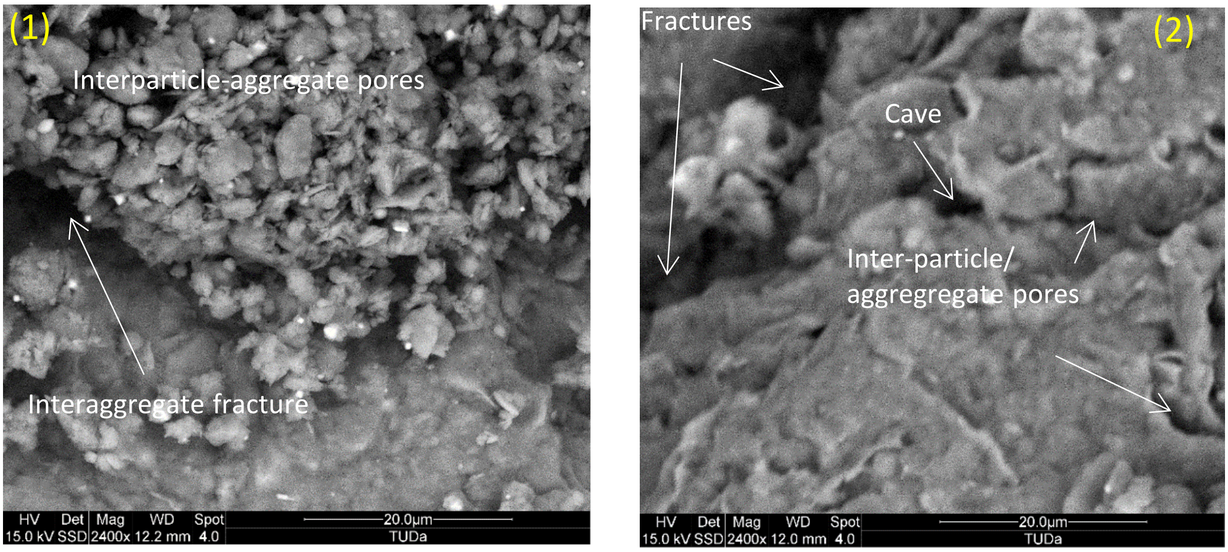

Fig 3.13 *SEM-images of initial Friedland clay*

Note: (1) large aggregate contains platy illite-smectite mixed layer particles. The large system of pores and voids appeared between aggregate of clays but micro interparticle pores are typical observed between illite-smectite platelets. The edge-to-face and face-to-face contact styles are found mainly in the contact between clay particles. (2) large angular fractures and caves (8 – 10 µm in diameter) formed between aggregate of clays but the small and linear fractures are found, too.

3.6 Cation exchange capacity (CEC), specific surface area (SSA) and surface charges

The cation exchange capacity (CEC) and specific surface area (SSA) and surface charge of the three starting materials are showed in (tab. 3.5). Swelling clays are characterized by a high interlayer cation population in the clay structure that releases in a high cation exchange capacity (CEC). The high amount of cation exchange sites is the consequence of the very high surface area of clay and high negative charge on these surfaces.

Barium chloride ($BaCl_2$) and calculation from TEM-EDX were used to determine CEC of two starting materials from Opalinus and B25 bentonite. The results show the smectite rich B25 bentonite is characterized by CEC of 45.15 meq/100 g ($BaCl_2$ method) and 48 meq/100 g (calculation from TEM-EDX) which compares to 56 meq/100 g from Matschiavelli et al (2019) . These different results are reasonable since Matschiavelli shows a higher content of Ca-smectite (55%) in comparison with our B25-material (content of 42% in total of Ca-smectite and IS-ml). Low cation exchange capacity of our bentonite material is also in agreement with low content of Mg as shown in XRF- and TEM-EDX-results (Tab. 1). Moreover, the substitution of Al for Si in tetrahedral sheet from TEM-EDX results and presence of ~750 cm^{-1} absorption band (Fig 3.7 left) are also a reason for this smaller CEC of our bentonite.

Otherwise, the CEC of Opalinus shows very high difference between $BaCl_2$-method (82.36 meq/100 g) and TEM-EDX calculation (52 meq/100 g) as well as Gaucher et al. (2004) as reference data. These authors presented that the CEC from Opalinus changed from 5 – 20.5 meq/100g. TEM-EDX could only support the CEC for clay fraction (< 2µm) which contain high amount of smectite in such fine fraction, it may also the reason for a higher CEC in compare with CEC of Gaucher et al. (2004). Carbonates (calcite, dolomite) can affect the CEC-measurements. Therefore, it is recommended the CEC of Opalinus clay needs to be repeated and cross-checked by additional methods (e.g. copper (II) triethylentetramine).

The CEC of Friedland clays were investigated largely by different authors as well as different methods, (e.g. BaCl2 solution, LiCl solution, ammonium acetate (NH4-Ac) and the copper triethylenetetramine (Cu-trien) methods) for the size fraction >62 µm of Carlson (2004). This author revealed the results in values of 37 cmol(+)/kg, 38 cmol(+)/kg, 35 cmol(+)/kg, and 42 cmol(+)/kg, respectively. It is apparently lower than our measurement. The smaller grain size (<40 µm) can be attributed to the higher CEC-value due to higher content of clay minerals, especially the presence of Ca-smectite can also be a reason for a higher CEC in compare with the other authors who collected materials in different deposits.

In general, the high swelling clay content but less CEC of B25 and Friedland clay can be explained by the dominance of divalent cations (e.g. Ca and Mg) in the interlayer sheet of smectite rather than monovalent (e.g. Na) exhibited a discernibly lower CEC. Otherwise, the use of $BaCl_2$ as exchangeable cations in the method of Hendershot and Duquitte (1986) has leaded to the overestimation of CEC in Opalinus clay because of dissolution of carbonate phases (e.g. calcite, dolomite and siderite).

The surface charge of all three starting materials showed a negative charge on the surface which are represented to clay minerals, especially smectite group. The Opalinus reached -8.3 µeq/l while B25 and Friedland showed the surface charge values from -13.7 to -19 µeq/l, respectively.

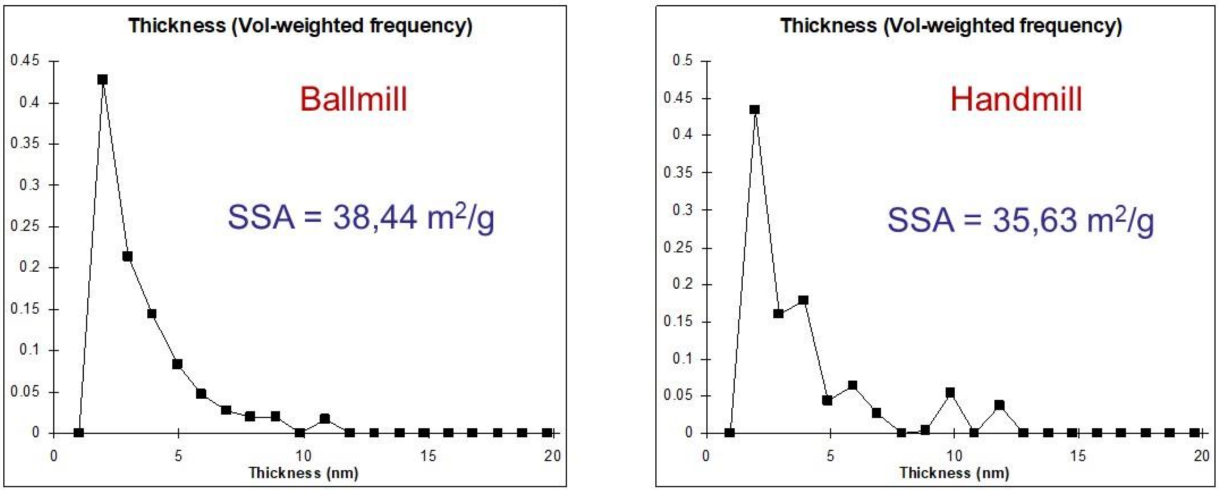

Fig 3.14 *Thickness distribution of grain size from bulk materials of ball mill and hand mill Opalinus clay*

Tab 3.5 *The CEC and BET-specific sureface area of initial B25 bentonite and Opalinus clay*

Sample	CEC (meq/100 g)	SSA (m^2/g)	Surface charge (µeq/l)
B25 Hand mill	45.15	90.39	-13.7
Opalinus Ball mill	88.23	38.44	-
Opalinus Hand mill	82.36	35.63	-8.3
Friedland clay	67.02	42.80	-19.0

The measurements indicated that the highest specific surface area is B25 bentonite that reached 90.39 m^2/g and the lowest ones is Opalinus clay (35.6 – 38.8 m^2/g), Friedland clay stays in the between with the SSA is 42.8 m^2/g. It is not clearly observed the big difference of SSA between hand milled (35.63 m^2/g) and ball milled (38.44 m^2/g) of Opalinus clay. It is compatible with the high amount of smectite and other of bulk materials as observed in XRD-measurement. Furthermore, in order to understand the possibility of mineralogical changes during the grinding of Opalinus claystone to powder, it could effect on the results of permeability experiments, a SSA of two Opalinus starting materials of ball mill and hand mill was analysed together with calculation of particles thickness from XRD. The results are shown in (Fig 3.14) that indicated a small difference between ball mill and hand mill in both SSA and thickness distribution of grain size. The hand mill materials is less homogenous than ball mill, but the concentration of particles at about 3 – 4 nm are the highest in both which caused a little bit smaller SSA in hand mill material.

3.7 Transmission Electron Microscopy coupled Energy-dispersive X-ray spectroscopy (TEM-EDX)

3.7.1 B25 - bentonite

The fraction < 2 µm of original B25 bentonite sample is mainly composed by dioctahedral vermiculite-smectite mixed layer phases (diVS-ml) and assumed beidellite-montmorillonite interstratifications (B:M ~50:50), abbreviated as BM-ml, and accompanied by montmorillonite and two types of illite. Furthermore, Si-surplus particles (Si, e.g. quartz) were identified in traces in this sample /fig. 3.15/.

	frequency-% *(n = 113 measured particles)*
BM-ml (Cluster1)	35%
diVS-ml (Cluster5)	56%
Montmorillonite (Cluster3)	2%
Illite (Cluster2)	3%
Illite (Cluster4)	2%
Si-surplus	3%

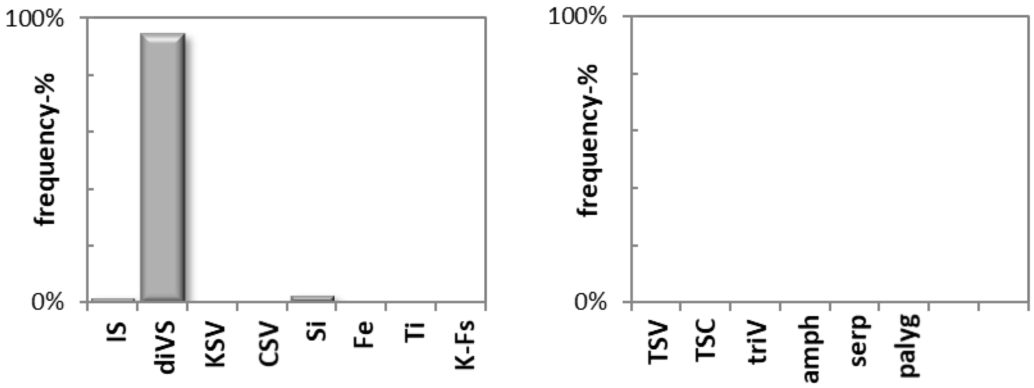

Fig. 3.15. *Distribution of mineral groups in fraction < 2 µm (in frequency-%)*

Note: ***IS*** *– illite-smectite-mixed layer series in sense of Środon et al. (1992), diVS – dioctahedral vermiculite-smectite illite-smectite-mixed layer series (= charge- and/or K-deficit),* ***KSV*** *– kaolinite-smectite-dioctahedral vermiculite-mixed layer series,* ***CSV*** *– chlorite-saponite-trioctahedral vermiculite-mixed layer series,* ***Si*** *– quartz or particles with Si-surplus,* ***Fe*** *– Fe-oxide or Fe-oxyhydroxide,* ***Ti*** *– Ti-bearing phases (e.g. rutile, anatase),* ***K-Fs*** *– K-feldspar*

Table 3.6. *Summarized chemical composition*

SiO_2	**TiO_2**	**Al_2O_3**	**Fe_2O_3**	**MnO**	**MgO**	**CaO**	**Na_2O**	**K_2O**	**P_2O_5**	**Σ**	
58.6%	0.0%	22.0%	5.9%		3.0%	1.0%	0.1%	1.1%	0.1%	0.92	measured particles
61.5%	0.5%	21.1%	6.4%	0.1%	4.0%	3.8%	0.4%	2.0%	0.1%	1.00	MAT19 (bulk sample)

All measured clay mineral phases summarized result following mineral formula computed from TEM-EDX-measurement of 110 individual particles:

$$Ca^{2+}_{0.10}\ Mg^{2+}_{0.08}\ Na^{+}_{0.01}\ K^{+}_{0.12}\quad Al^{3+}_{1.27}\ Fe^{3+}_{0.56}\ Mg^{2+}_{0.17}\ Ti^{4+}_{0.00}\ (OH)_2\quad Si^{4+}_{3.70}\ Al^{3+}_{0.30}\ O_{10}$$

SDOM *± 0.00 ± 0.00 ± 0.00 ± 0.01 ± 0.01 ± 0.01 ± 0.01 ± 0.00 ± 0.01 ± 0.01*

Legend: SDOM - standard deviation of the mean (= the standard deviation divided by the square root of the number of samples)

The interlayer charge is calculated as 0.48 per $(OH)_2\ O_{10}$ and the octahedral charge as 5.82 per $(OH)_2\ O_{10}$. The particles are characterized by a high octahedral Fe-amount.

The summarized chemical composition of all 110 computed particles is compared with chemical data from literature /tab. 3.6/. Such comparison is only limited valid because of different origin of samples and the differences in composition for fraction < 2 µm (the measured sample) and the bulk material (the applied literature data). The chemical composition averaged by measured particles show especially a lower amount of CaO, Na_2O and K_2O as the applied literature data, probably an indication for a higher concentration of feldspars in the bulk sample than in fraction < 2 µm.

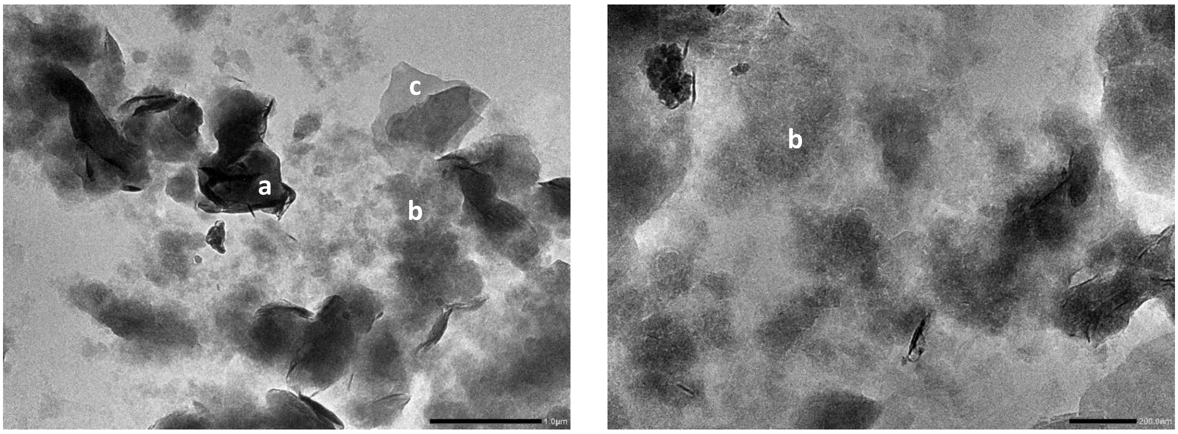

JEM-2100_MAG_X10k_B25-40um_I08.bmp

Magnification: 10k

(a) large (≤ 1 µm) xenomorph film-like platy crystals with folds;
(b) aggregates formed by small (≤ 200 nm) xenomorphous plates;
(c) large (≤ 1 µm) xenomorph plates, homogenous thickness

JEM-2100_MAG_X30k_B25-40um_I10.bmp

Magnification: 30k

(b) aggregates formed by small (≤ 200 nm) xenomorphous plates

Fig. 3.16. *Morphology of particles (TEM-micrographs)*

B25 bentonite is characterized by three morphological groups: (i) large (≤ 1 µm) xenomorph film-like platy crystals with folds, (ii) aggregates formed by small (≤ 200 nm) xenomorphous plates and (iii) large (≤ 1 µm) xenomorph plates with homogenous thickness (Fig. 3.16). Thin aggregates formed by small (≤ 200 nm) xenomorphous plates dominate the shapes of particles in the micrographs (Figs. 3.16, 3.17).

The distribution of %S-probability of all measured clay mineral phases (Fig. 3.18) also indicates the occurrence of three groups: (i) montmorillonite (in traces; %S-class = 100%), (ii) as main group a mixture of beidellite-montmorillonite interstratifications and diVS-ml (%S-max of this mixture at 70%) and (iii) illite with K- and charge deficit (%S-class = 0%).

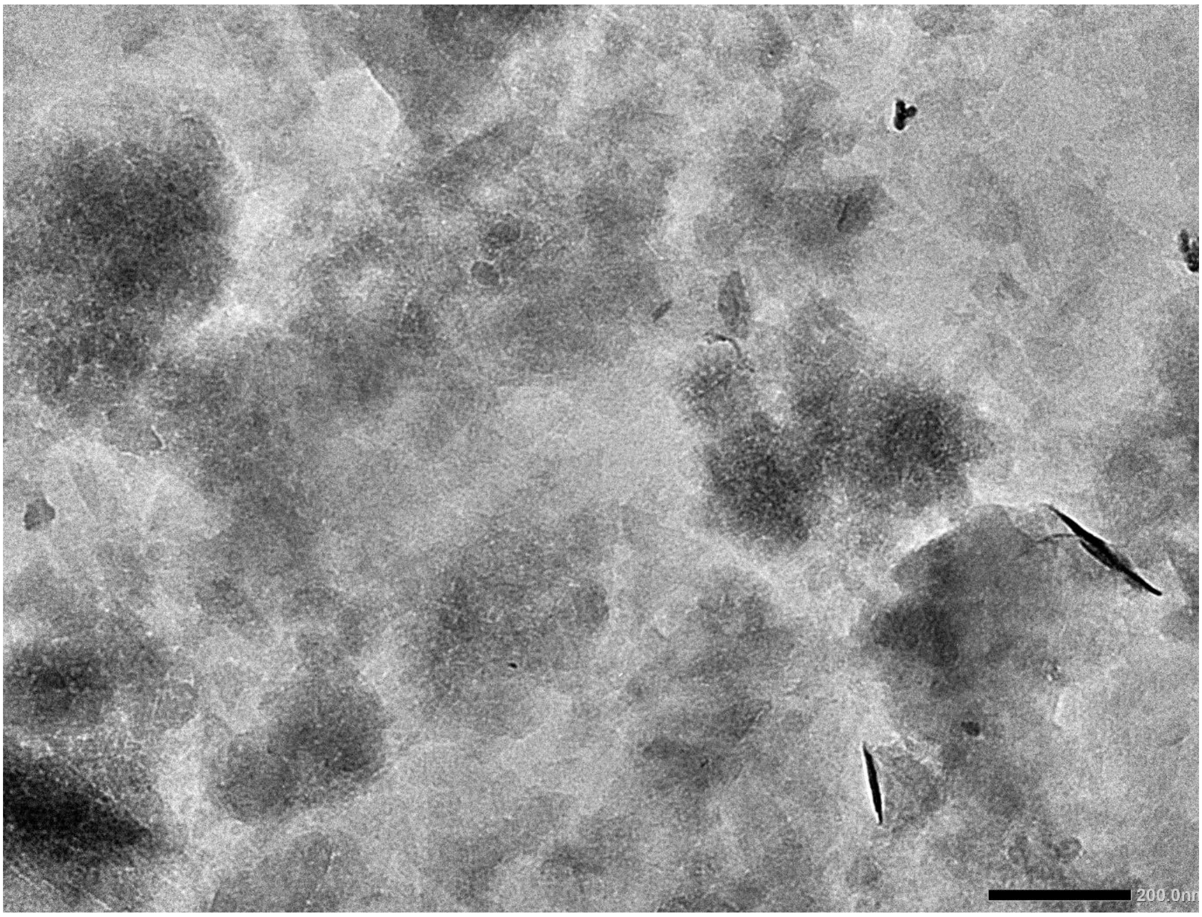

JEM-2100_MAG_X30k_B25-40um-I07.bmp

Magnification: 30k

aggregates formed by small (≤ 200 nm) xenomorphous plates

Fig. 3.17 *Morphology of particles (TEM-micrographs)*

The numerous measured particles by TEM-EDX allow a visualization of distribution of interlayer charges. Considering the TEM-EDX-determined cations Ca^{++}, Mg^{++} and Na^{+} and then computed their ratio as interlayer cations in the mineral formula, Ca^{++}, Mg^{++} and Na^{+} offer to characterize the degree of exchangeable charges in the interlayer space. This charge density of untreated B25 bentonite (< 2 µm) shows only a narrow interval at the maximal frequency-% of charge density at 0.35 per $(OH)_2\ O_{10}$ (fig.3.19). This narrow interval of interlayer charge density caused by exchangeable cations from 0.27 – 0.47 per $(OH)_2\ O_{10}$ represents mainly the BM- and diVS-ml phases. The few measured montmorillonite particles are part of this interval. Also, the measured illite particles (Cluster2) offer only a low number of exchangeable cations and indicating a lower degree of weathering.

Distribution of smectite layers probability (%S)

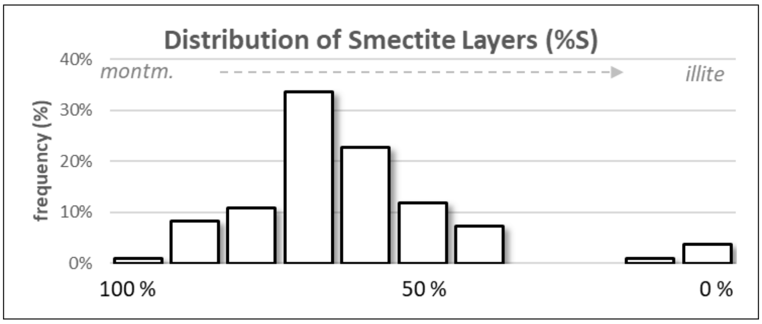

Description: *The distribution of %S-probability indicates the occurrence of three groups: (i) montmorillonite (in traces), (ii) mixture of beidellite-montmorillonite interstratifications (= assumption) with diVS-ml as well as (iii) illite with K-deficiency.*

Fig. 3.18a. *Distribution of smectite layers probability (%S)*

Differentiation by relation “Octahedral Mg vs. tetrahedral Si”?

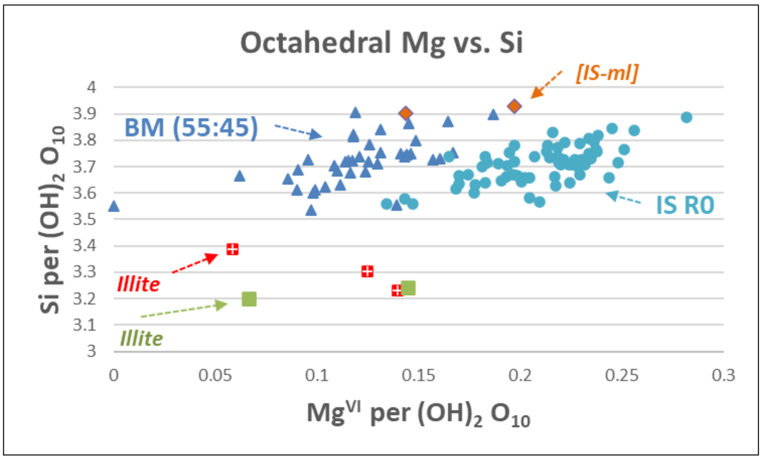

Description: *This diagram indicates the occurrence of two large groups of Mg in relation to tetrahedral Si as result of clustering. Probably, this distribution mirrors 2 phases (I) beidellite-montmorillonite interstratifications (labelled as BM 55:45) and (II) diVS-ml (labeled as IS R0 by Sybilla-processing of XRD-traces of EG-solvated fraction < 2 µm, %Sxrd=55%)*

Fig. 3.18b. *Distribution of octahedral Mg vs. tetrahedral Si [all per* $(OH)_2 O_{10}$*]*

Distribution of K in relation to tetrahedral Si

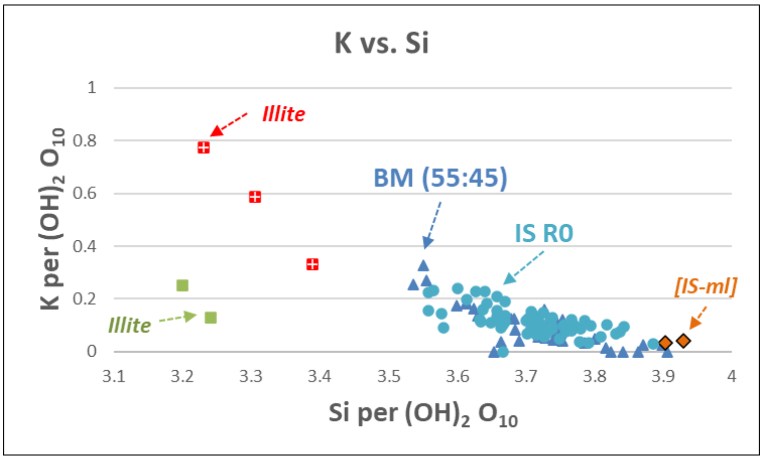

Description: *This diagram visualizes possible particles with a very low K (labelled groups as result of clustering)*

Fig. 3.18c. *Distribution of K in interlayer space vs. tetrahedral Si [all per* $(OH)_2 O_{10}$*]*

Distribution of charges (exchangeable from interlayer space)

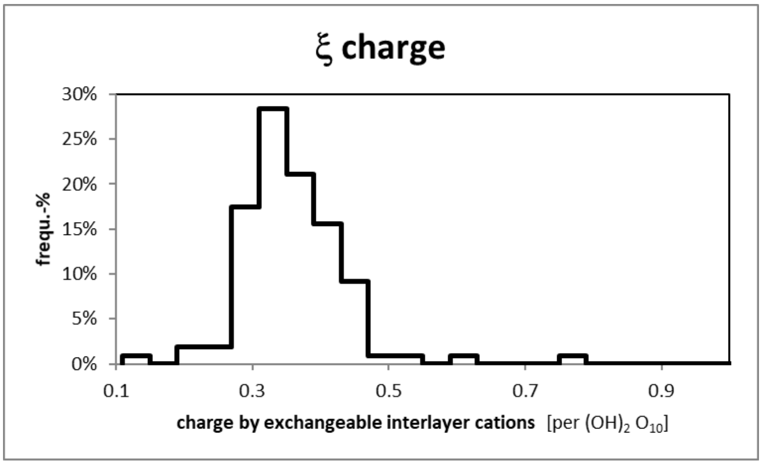

This diagram visualizes the distribution of exchangeable charges in the interlayer space (Ca, Mg, Na) determined and computed by TEM-EDX-data.

Description: *Maximal frequency-% of charge density at 0.35 per* $(OH)_2 O_{10}$*.*

Fig. 3.19. *Distribution of charges*

Result of Clustering & Comparison with XRD-data (Sybilla-processing)

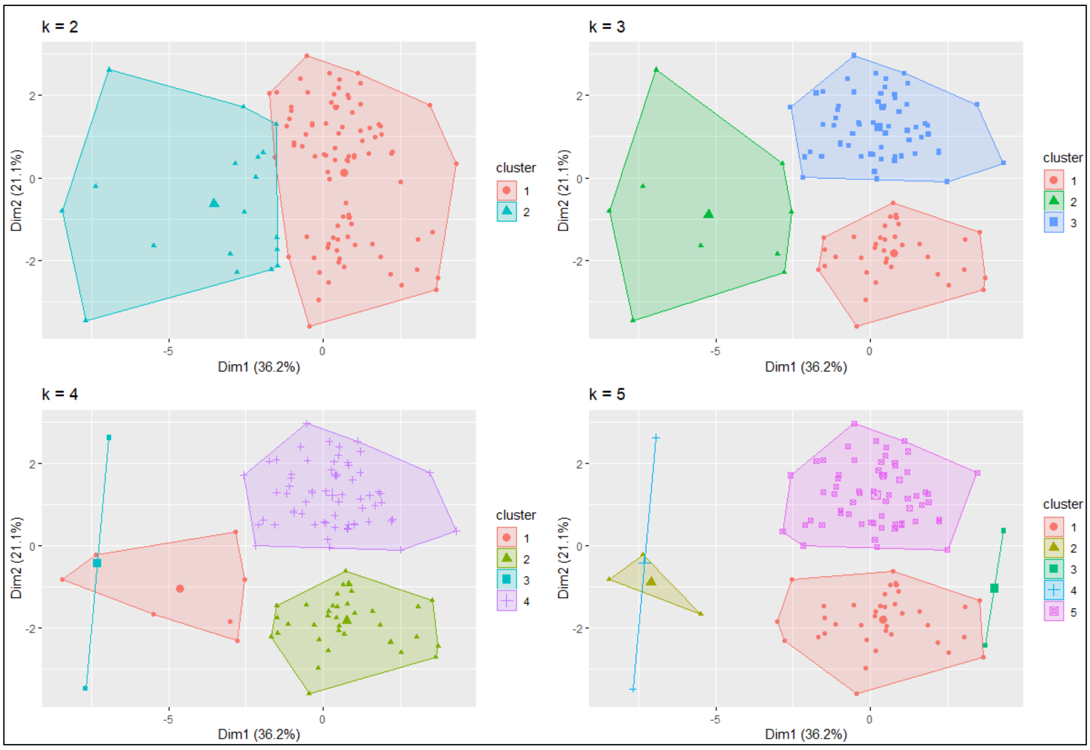

Fig. 3.20. *Clustering of all measured particles for clusters k = 2, k = 3, k = 4 and k = 5 (source for R-coding: https://uc-r.github.io/kmeans_clustering)*

The optimum of clusters was calculated with k = 5 (fig. 3.20). This number of clusters differentiates also clearly illite particles (Cluster2, Cluster4) from smectite-bearing phases (Cluster1, Cluster3, Cluster5) (fig. 21).

		Ca (XII)	Mg (XII)	Na (XII)	K (XII)	Cr3+ (VI)	Al (VI)	Fe3+ (VI)	Mg (VI)	Ti (VI)	Al (IV)	Si (IV)	XII	n_VI	%S
Cluster1	n = 40	0.04	0.11	0.00	0.09	0.00	1.32	0.56	0.12	0.00	0.28	3.72	0.4	2.0	58
Cluster2	n = 3	0.06	0.03	0.03	0.56	0.00	1.55	0.33	0.11	0.01	0.69	3.31	0.8	2.0	10
Cluster3	n = 2	0.11	0.09	0.00	0.04	0.00	1.31	0.46	0.17	0.00	0.08	3.92	0.4	1.9	92
Cluster4	n = 2	0.07	0.28	0.00	0.19	0.00	0.99	0.90	0.11	0.00	0.78	3.22	0.9	2.0	4
Cluster5	n = 63	0.13	0.05	0.01	0.12	0.00	1.22	0.56	0.21	0.00	0.29	3.71	0.5	2.0	56

Fig. 3.21. *Mineral formulae based on TEM-EDX-data summarized following the result of clustering for k=5*

Tab. 3.7 *Comparison of results from TEM-EDX- and XRD-measurements with clustering procedure*

	Sybilla-results	**TEM-EDX-results**	**Notes**
Cluster1	IS R0 (1) *(%S = 99%)*	BM-ml *(%S=100%, %B ~ 55%)*	*XRD: Montmorillonite and beidellite are only to distinguish by Green-Kelly-test (not available here).*
Cluster2	Illite	Illite	*K-deficit, Al(VI)-rich*
Cluster3	IS R0 (1) *(%S = 99%)*	IS-ml *(%S = 92%)*	*high charged Fe-rich Ca,Mg-montmorillonite*
Cluster4	Illite	Illite	*high K-deficit, nearby a Fe-illite*
Cluster5	IS R0 (2) *(%S = 55%)*	diVS-ml *(%S = 56%)*	*high K-deficit, Fe(VI)-rich*

The clustering of TEM-EDX-data offers a good agreement with the recent result of Sybilla-processing of XRD-traces from oriented specimen (tab. 3.7).

IS R0 (1): The X-ray diffraction pattern of the ethylene-glycol saturated oriented specimen shows a full expandability to 1.7 nm and a difference of 5.42°2θ between 2. and 3. order of smectite interferences. This distance is typically for montmorillonite (Moore & Reynolds, 1989). This result of XRD-processing let expect a maximum of particles for %S ~ 90-100% by TEM-EDX-measurements, but the maximum of particles measured by TEM-EDX is to find at %S=70% (fig. 3.18).

Montmorillonite and beidellite have the same behaviour concerning the expandability and they are only to distinguish by XRD using Li like by Greene-Kelly test (Green-Kelly 1952, 1953). So, combination of XRD- and TEM-results (full expandability by XRD and Si ~ 3.72 by TEM-EDX) led conclude the occurrence of 'beidellite-montmorillonite interstratifications', a beidellite-montmorillonite interstratification with about 55% beidellite and 45% montmorillonite layers (BM-ml 55:45).

The methodical combination of XRD-processing and TEM-EDX- data (incl. clustering) indicates further sub-groups of identified phases by Sybilla-procedure for illite-smectite mixed layer phases (IS R0 (1)): (i) BM-ml (Cluster1) and (ii) IS-ml (Cluster3) (tab. 3.7).

IS R0 (2): The Sybilla-procedure of XRD-traces (oriented mounts) has shown an occurrence of a second illite-smectite mixed layer phase with a smectite layers probability of %S = 55%. This situation is to find in Cluster5 (%S = 56%) representing a K- and charge deficient and Fe-rich dioctahedral vermiculite-smectite mixed layer phase (diV-ml) (tab. 3.7).

Illite: The Sybilla-procedure of XRD-traces (oriented mounts) draws the occurrence of illite. The clustering of TEM-EDX-data confirmed the Sybilla-results, but it indicates two sub-groups of illite: (i) illite (Cluster2) as K-deficient and Al(VI)-rich illite and (ii) illite (Cluster5) as very high K-deficient and Fe(VI)-rich illite (tab. 3.7).

The Sybilla-processing of XRD-traces (oriented mounts) also supports the existence of kaolinite and kaolinite-smectite mixed layer phases in fine fraction of B25 bentonite. Such phases were not to identify in TEM-EDX-database (a grain size effect?).

Specifics to the identified clay mineral groups

Montmorillonite as part of illite-smectite mixed-layer series *(IS-ml in sense of Środon et al., 1992)*

The term 'illite-smectite mixed layer series in sense of Środon et al. (1992)' describes illite-smectite interstratifications with a normal interlayer charge for illite layers of 0.89 (representing fixed K) and a normal interlayer charge for smectite layers of 0.40 per $(OH)_2\,O_{10}$. This series occurs in B25 bentonite (< 2 µm) in traces as end member of this series: montmorillonite. Only 2 of 110 measured particles belong so to this normal charged group IS-ml in sense of Środon et al. (1992).

Montmorillonite:

$$Ca_{0.11}\,Mg_{0.09}\,Na_{0.00}\,K_{0.04}\quad Al_{1.31}\,Fe^{3+}_{0.46}\,Mg_{0.17}\,Ti_{0.00}\,(OH)_2\quad Si_{3.92}\,Al_{0.08}\,O_{10}$$

Charge: XII = 0.44 VI = 5.64 IV = 15.92 **Σ = 22.00**
Probability of smectite layers (%S): 92%
Probability of illite layers (%I): 8%

Measured particles by TEM-EDX: 2
Result of clustering: Cluster3 (tab. 3.7)

The %S-probability of these particles (%S ~ 92%) indicates the occurrence of montmorillonite. Furthermore, the value for octahedral iron (0.46 per $(OH)_2\,O_{10}$) in the computed mineral formula characterizes this montmorillonite as Fe-rich.

The distribution of %S-probability, specified for normal charged IS-ml, indicates the occurrence only of one group of phases, here with %S mainly at 90% (fig. 3.22).

Distribution of smectite layers probability (%S) in IS-ml *(2 particles only)*

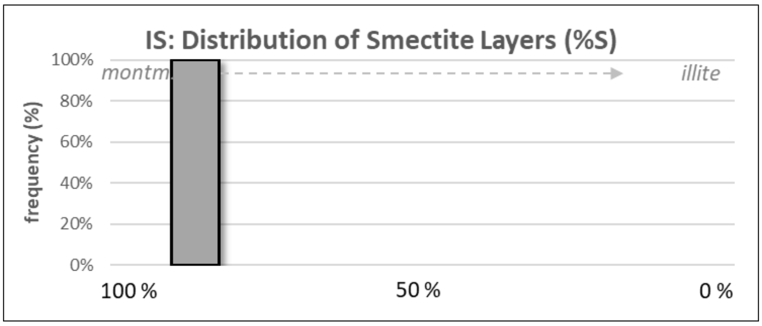

Description: *The distribution of %S-probability indicates also the occurrence of montmorillonite (confirmed as Cluster3).*

Fig. 3.22. *Distribution of smectite layers probability (%S) in IS-ml*

Beidellite-montmorillonite interstratifications (B:M ~50:50)

40 of 110 measured particles belong so to this assumed classification. The dioctahedral character of this group is proofed by X-ray diffraction. The position of the large (060)-interference of smectite is in the random oriented powder specimen at 1.497 Å.

The X-ray diffraction pattern of the ethylene-glycol saturated oriented specimen shows a full expandability to 1.7 nm and a difference of 5.42°2θ between 2. and 3. order of smectite interferences. This distance is typically for montmorillonite (Moore & Reynolds, 1989). This result of XRD-processing let expect a maximum of particles for %S ~ 90-100% by TEM-EDX-measurements, but the maximum of particles measured by TEM-EDX is to find at %S=70% (fig. 3.18).

Montmorillonite and beidellite have the same behaviour concerning the expandability and they are only to distinguish by XRD using Li by means of Greene-Kelly test (Green-Kelly 1952, 1953). So, combination of XRD- and TEM-results (full expandability by XRD and Si ~ 3.69 by TEM-EDX) led conclude the occurrence of 'beidellite-montmorillonite interstratifications', a beidellite-montmorillonite interstratification with about 55% beidellite and 45% montmorillonite layers (BM-ml55:45).

Beidellite-Montmorillonite interstratification (BM ~ 55%:45%) *(Cluster1):*

$$Ca_{0.04}\,Mg_{0.11}\,Na_{0.00}\,K_{0.09}\quad Al_{1.32}\,Fe^{3+}_{0.56}\,Mg_{0.12}\,Ti_{0.00}\,(OH)_2\quad Si_{3.72}\,Al_{0.28}\,O_{10}$$

Charge:	XII = 0.40	VI = 5.88	IV = 15.72	**Σ = 22.00**

Measured particles by TEM-EDX: 40
Result of clustering: Cluster1 (tab. 3.7)

Beidellitic structures are characterized by a low octahedral Mg-amount (because of high ratio of octahedral, 3-valent cations). A comparison of octahedral Mg vs. tetrahedral Si indicates the occurrence of two groups for octahedral Mg based on TEM-EDX-data (tab. 3.18b). The group with a lower Mg-ratio should represent the already mentioned BM-ml (55:45) phases (= IS GLY R0_1 with $\%S_{xrd}$ = 99%; see also Cluster1 in (tab. 3.7)) and the other group with a higher Mg-ratio is considered as diVS-ml (= IS GLY R0_2 with $\%S_{xrd}$ = 55%).

Using the results of clustering (see Cluster1 in (tab. 3.7)), the maximum of frequency-% is to find for particles in the Si(IV)-class 3.7 – 3.8 e phuc (fig. 3.32a), representing the mentioned relation 55% montmorillonite and 55% beidellite as ratio of interstratification. The mineral formulae, summarized in classes of tetrahedral Si, draw for the maximum an Fe-rich BM 55:45 phase with low K, but remarkable amount of Mg in the interlayer space (fig. 3.32b).

Distribution of BM-interstratifications (Cluster1)

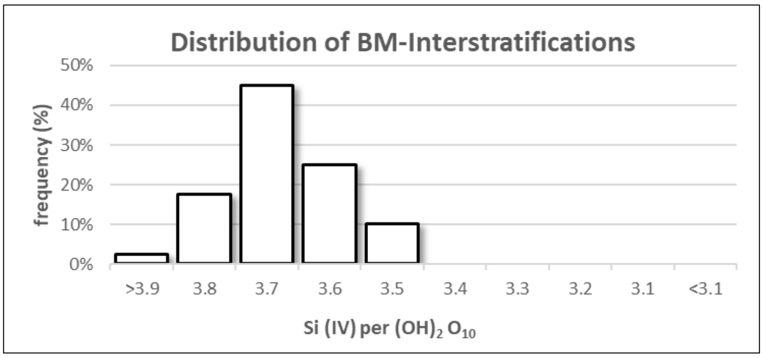

Description: *The distribution of BM-interstratifications (classified as Cluster1) draws a maximum of frequency (%) at tetrahedral Si-value between 3.7 – 3.8 e phuc*

Fig. 3.23a. *Distribution of assumed beidellite-montmorillonite interstratifications*

BM50:50		*particles (abs)*	**Ca (XII)**	**Mg (XII)**	**Na (XII)**	**K (XII)**	**Cr3+ (VI)**	**Al (VI)**	**Fe3+ (VI)**	**Mg (VI)**	**Ti (VI)**	**Al (IV)**	**Si (IV)**	**XII**	**n_VI**	**%S**
Si	>3.9	n = 1	0.00	0.11	0.00	0.00	0.00	1.32	0.56	0.12	0.00	0.09	3.91	0.2	2.0	90
Si	3.9-3.8	n = 7	0.04	0.11	0.00	0.02	0.00	1.34	0.51	0.14	0.00	0.16	3.84	0.3	2.0	79
Si	**3.8-3.7**	**n = 18**	**0.05**	**0.11**	**0.00**	**0.08**	**0.00**	**1.28**	**0.59**	**0.13**	**0.00**	**0.26**	**3.74**	**0.4**	**2.0**	**60**
Si	3.7-3.6	n = 10	0.04	0.12	0.00	0.11	0.00	1.36	0.54	0.10	0.00	0.35	3.65	0.4	2.0	48
Si	3.6-3.5	n = 4	0.05	0.08	0.00	0.26	0.00	1.40	0.51	0.08	0.00	0.44	3.56	0.5	2.0	35
Si	3.5-3.4	n = 0														
Si	3.4-3.3	n = 0														
Si	3.3-3.2	n = 0														
Si	3.2-3.1	n = 0														
Si	<3.1	n = 0														

Fig. 3.23b. *Computed averaged mineral formulae of phases in the different Si(IV)-classes*

Dioctahedral vermiculite-smectite mixed layer phase (diVS-ml)

The processing of XRD-traces (oriented mounts) by Sybilla-software has drawn the occurrence of two types of IS GLY R0-phases: (i) IS GLY R0 (1) with $\%S_{xrd}$ = 99% above discussed as BM-ml (50:50) and (ii) IS GLY R0 (2) with $S\%_{xrd}$ = 55% (see Cluster5 in (tab. 3.7).

Dioctahedral vermiculite-smectite mixed layer phase (diVS-ml):

$$Ca_{0.13}\ Mg_{0.05}\ Na_{0.01}\ K_{0.12}\quad Al_{1.22}\ Fe^{3+}_{0.56}\ Mg_{0.21}\ Ti_{0.00}\ (OH)_2\ \ Si_{3.71}\ Al_{0.29}\ O_{10}$$

Charge: XII = 0.50 VI = 5.79 IV = 15.71 **Σ = 22.00**
Probability of smectite layers (%S): 56%
Probability of illite layers (%I): 44%

Measured particles by TEM-EDX: 63
Result of clustering: Cluster5 (tab. 3.7)

The probability of smectite layers determined by TEM-EDX-data and Sybilla-processing of XRD-traces (oriented mounts) gives similar results: $\%S_{TEM}$ = 56% (fig. 3.24a) and $\%S_{XRD}$ = 55%.

The Rietveld refinement by Profex software (Döbelin & Kleeberg, 2015) draws for octahedral composition of this mixed layer phase in bulk sample: $Al^{3+}_{1.2}\ \ Fe^{3+}_{0.60}\ \ Mg^{2+}_{0.20}$ per ($(OH)_2\ O_{10}$) as best refinement result. This refinement of X-ray diffraction traces confirms additionally the Fe-rich occupation of octahedral layer as determined also by TEM-EDX (fig. 3.24b).

Distribution of smectite layers probability (%S) in diVS-ml (Cluster5)

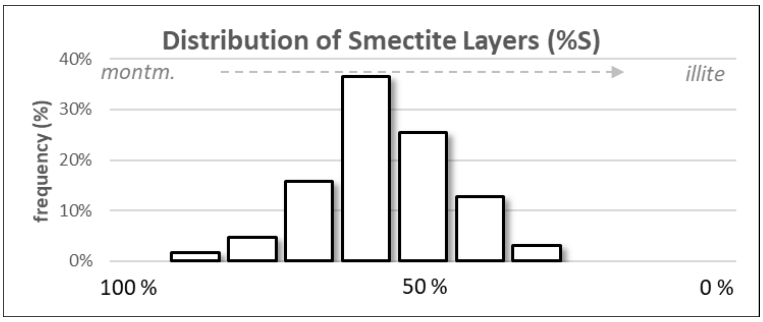

Description: *The distribution of diVS-ml (classified as Cluster5) draws a maximum of frequency (%) for smectite layer probability at 60%*

Fig. 3.24a. *Distribution of smectite layers probability in diVS-ml*

diVS-ml	*particles (abs)*	**Ca (XII)**	**Mg (XII)**	**Na (XII)**	**K (XII)**	**Cr3+ (VI)**	**Al (VI)**	**Fe3+ (VI)**	**Mg (VI)**	**Ti (VI)**	**Al (IV)**	**Si (IV)**	**XII**	**n_VI**	**%S**
%S >95%	n = 0														
%S 95-85%	n = 1	0.16	0.02	0.00	0.03	0.00	1.28	0.44	0.28	0.00	0.11	3.89	0.4	2.0	86
%S 85-75%	n = 3	0.10	0.05	0.02	0.08	0.00	1.33	0.43	0.24	0.00	0.16	3.84	0.4	2.0	77
%S 75-65%	n = 10	0.13	0.04	0.02	0.08	0.00	1.24	0.52	0.23	0.00	0.21	3.79	0.4	2.0	68
%S 65-55%	**n = 23**	**0.14**	**0.05**	**0.01**	**0.10**	**0.00**	**1.22**	**0.57**	**0.21**	**0.00**	**0.27**	**3.73**	**0.5**	**2.0**	**59**
%S 55-45%	n = 16	0.14	0.05	0.01	0.13	0.00	1.21	0.58	0.20	0.00	0.34	3.66	0.5	2.0	49
%S 45-35%	n = 8	0.13	0.06	0.02	0.17	0.00	1.19	0.62	0.18	0.00	0.40	3.60	0.6	2.0	41
%S 35-25%	n = 2	0.10	0.08	0.02	0.19	0.00	1.24	0.61	0.14	0.01	0.44	3.56	0.6	2.0	35
%S 25-15%	n = 0														
%S <15%	n = 0														

Fig. 3.24b. *Computed averaged mineral formulae of diVS-ml phases in the different smectite layers probability (%S)-classes*

Illite

The TEM-EDX-based distribution of %S-probability (Fig. 3.18a) indicates three possible groups: (i) the occurrence of montmorillonite with %S ~ 100%, (ii) BM-ml in mixture with diVS-ml (maximum at $Si_{tetrahedral}$ 3.74 per $(OH)_2$ O_{10} and (iii) illite with K- & charge-deficit. The clustering of TEM-EDX-data shows two illite clusters Cluster2 and Cluster4 (tab. 3.7).

Illite *(as end member of diVS-ml series; confirmed as Cluster2):*

$$Ca_{0.06}\ Mg_{0.03}\ Na_{0.03}\ K_{0.56}\quad Al_{1.55}\ Fe^{3+}_{0.33}\ Mg_{0.11}\ Ti_{0.01}\ (OH)_2\ \ Si_{3.31}\ Al_{0.69}\ O_{10}$$

Charge: XII = 0.78 VI = 5.91 IV = 15.31 **Σ = 22.00**
Probability of smectite layers (%S): 10%
Probability of illite layers (%I): 90%

Measured particles by TEM-EDX: 3

Illite *(as end member of diVS-ml series; confirmed as Cluster4):*

$$Ca_{0.07}\ Mg_{0.28}\ Na_{0.01}\ K_{0.19}\quad Al_{0.99}\ Fe^{3+}_{0.90}\ Mg_{0.11}\ Ti_{0.00}\ (OH)_2\ \ Si_{3.22}\ Al_{0.78}\ O_{10}$$

Charge: XII = 0.89 VI = 5.89 IV = 15.22 **Σ = 22.00**
Probability of smectite layers (%S): 4%
Probability of illite layers (%I): 96%

Measured particles by TEM-EDX: 2

Illite of Cluster2 is characterized by slight K-deficiency and Al-rich octahedral layer. Few smectite layers are not excluded because of Si(IV) = 3.31 e phuc.

Otherwise, illite particles of Cluster4 show a very high K-deficit and very Fe-rich octahedral layer.

The Rietveld refinement by Profex software (Döbelin & Kleeberg, 2015) indicates the occurrence of two polytypes for illite in B25 bentonite: $2M_1$- and 1M-polytype.

Kaolinite-montmorillonite mixed layer phases

The Excel-based procedure (Hoang-Minh et al., 2019) to identify possible clay mineral groups using the TEM-EDX-measurements also includes algorithms to classify kaolinite and kaolinite-montmorillonite mixed layer phases. These algorithms couldn't identify such phases basing on the measured TEM-EDX-data. Even also the clustering gives no indications for the occurrence of kaolinite-bearing phases.

Otherwise, the processing of XRD-traces (oriented mounts) by Sybilla-Software indicated the occurrence of kaolinite-montmorillonite mixed layer phases (KS GLY R1, $\%S_{xrd}$=45%). Such particles should be characterized by a low potassium (because of missing K in kaolinite structure). A visualization of TEM-EDX-measurements in a relation "K vs. Si" shows only two possible measurements (of 108 particles), which could represent phases with a very low potassium ratio in the structure (fig. 3.18c). The mean of particle thickness for KS GLY R1 was computed by Sybilla-software at 11 nm. Probably, this higher thickness is underrepresenting the kaolinite-bearing phases in the TEM-EDX-results in comparison to the finer particles of BM 50:50 in mixture with diVS-ml (T_{mean} ~ 4.4 nm).

Estimation of Specific Dissolution Potential *(in according to Nguyen-Thanh et al., 2014)*

Previous investigations have shown (summarized in Nguyen-Thanh et al., 2014), each bentonite or clay have a specific dissolution potential expressed as loss of smectite layer. The expected specific behaviour of smectite layers is classified using the mineral formula as result of TEM-EDX-measurements. The authors developed different experimental overhead rotation setups to determine the maximal possible loss of smectite layers under pre-defined conditions (fig. 3.25). These different experimental settings should represent different strength of acting forces in mineralogical alteration of original smectite (with water as low energy-level). The previous results with a large series of bentonites and clays allow to predict the expected rate of alteration of smectite layers distinguishing slow-reacting smectite layers (= sleepers), moderate-reacting smectite layers and fast-reacting smectite layers (= sprinters). The limits between these free classes are postulated only: sleepers are smectites with loss of smectite layers lower than Δ%S = 5% and are a sprinter with loss of smectite layers larger than Δ%S = 20%. Negative values for Δ%S mirroring a 'illitization'-like process and positive values represent a smectitization potential.

The modelled values for B25 bentonite (fig. 3.25) let expect mainly a moderate-reacting smectite with a change from the original $Si_{tetrahedral}$ 3.69 in direction to $Si_{tetrahedral}$ 3.60 per $(OH)_2$ O_{10} for the run products (Δ%S = -8%). Otherwise under strong conditions (e.g. higher temperature, high ionic strength, high saline solution), the modelling let assume for B25 bentonite a very fast and nearby complete loss of smectite layers (Δ%S = -96%).

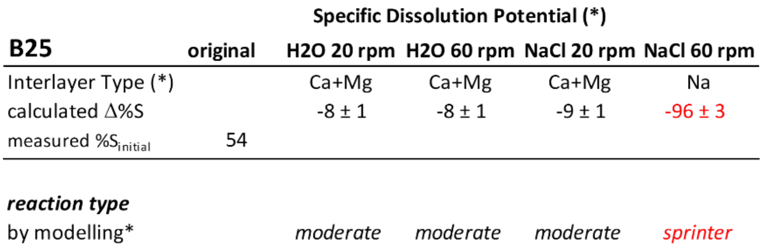

		Specific Dissolution Potential (*)			
B25	**original**	**H2O 20 rpm**	**H2O 60 rpm**	**NaCl 20 rpm**	**NaCl 60 rpm**
Interlayer Type (*)		Ca+Mg	Ca+Mg	Ca+Mg	Na
calculated Δ%S		-8 ± 1	-8 ± 1	-9 ± 1	-96 ± 3
measured $\%S_{initial}$	54				
reaction type					
by modelling*		*moderate*	*moderate*	*moderate*	*sprinter*

Description: *Overhead-rotation systems like H2O 20 rpm serve as indicator for rate of alteration of selected bentonite. Low grade reduction of smectitic layers (Δ%S) indicate a slow reaction of smectite phases (so-called sleeper).*
An opposite behaviour is called as sprinter.

Fig. 3.25. *Specific Dissolution Potential of B25 bentonite, < 2 µm (* in according to Nguyen-Thanh et al., 2014)*

The type of cations in the interlayer space (here type B with Ca + Mg) and the Fe-rich composition of octahedral layer are the driving forces for these estimations.

Following aspect could influence the expected behaviour for B25 bentonite: The alteration mechanisms and the rate of alteration of beidellite are unknown until now.

Finally, only further experiments with the selected bentonite can validate these estimations.

3.7.2 Opalinus clay

The fraction < 2 µm of Opalinus Clay original sample is mainly composed by two different types of dioctahedral vermiculite-smectite mixed layer phases (diVS-ml). Rarely, rutile and quartz were identified in traces in this sample (fig. 3.26).

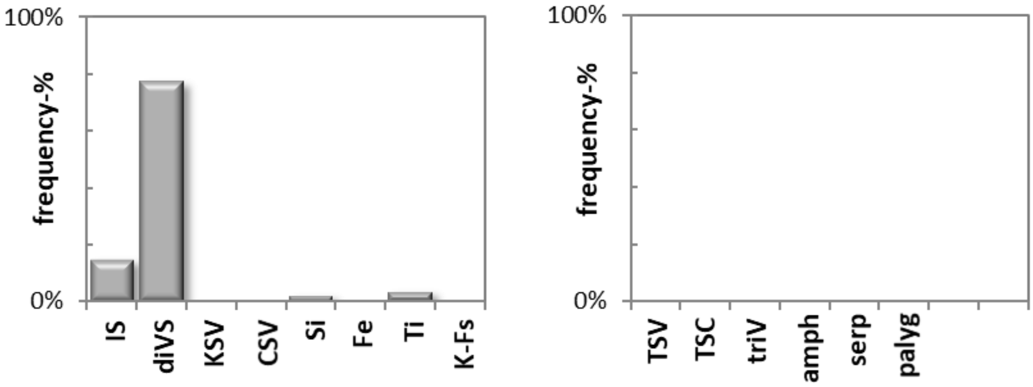

Fig. 3.26. *Distribution of mineral groups in fraction < 2 µm (in frequency-%)*

*Legend: **IS** – illite-smectite-mixed layer series in sense of Środon et al. (1992), diVS – dioctahedral vermiculite-smectite illite-smectite-mixed layer series (= charge- and/or K-deficit), **KSV** – kaolinite-smectite-dioctahedral vermiculite-mixed layer series, **CSV** – chlorite-saponite-trioctahedral vermiculite-mixed layer series, **Si** – quartz or particles with Si-surplus, **Fe** – Fe-oxide or Fe-oxyhydroxide, **Ti** – Ti-bearing phases (e.g. rutile, anatase), **K-Fs** – K-feldspar*

The measured and computed particles have shown a calculated CEC-value of 52 meq / 100 g located at surface and in the interlayer space.

	frequency-% *(n = 75 measured particles)*
diVS-ml	92%
Ti-phases	4%
Quartz	3%
Unknown phases	1%

All measured dioctahedral 2:1 clay mineral phases summarized result following mineral formula computed from TEM-EDX-measurement of 70 individual particles:

$$\boxed{Ca^{2+}_{0.09}\ Mg^{2+}_{0.06}\ Na^{+}_{0.01}\ K^{+}_{0.39}\quad Al^{3+}_{1.40}\ Fe^{3+}_{0.42}\ Mg^{2+}_{0.17}\ Ti^{4+}_{0.01}\ (OH)_2\quad Si^{4+}_{3.46}\ Al^{3+}_{0.54}\ O_{10}}$$

SDOM *± 0.01 ± 0.01 ± 0.0 ± 0.02 ± 0.02 ± 0.02 ± 0.01 ± 0.01 ± 0.02 ± 0.02*

Legend: SDOM - standard deviation of the mean (= the standard deviation divided by the square root of the number of samples)

The interlayer charge is calculated as 0.70 per $(OH)_2\ O_{10}$ and the octahedral charge as 5.83 per $(OH)_2\ O_{10}$. The particles are characterized by a high octahedral Fe-amount.

The summarized chemical composition of all 70 computed particles is listed (tab. 3.8).

Table 3.8. *Summarized chemical composition*

SiO_2	TiO_2	Al_2O_3	Fe_2O_3	MnO	MgO	CaO	Na_2O	K_2O	P_2O_5	Σ	
52.7%	0.1%	26.1%	4.3%		2.7%	1.3%	0.0%	3.4%	0.3%	0.91	measured particles
53.1%	1.0%	19.7%	6.2%	<0.1%	2.3%	3.0%	0.6%	2.6%		0.91	GAU03 (SHGN - bulk)

Opalinus Clay original sample is also characterized by two morphological groups: (i) large (≤ 1 µm) xenomorph platy crystals and (ii) aggregates, formed by small (≤ 200 nm) laths with idiomorph ends (fig. 3.27). Aggregates formed by small (≤ 200 nm) laths with idiomorph ends dominate the shapes of particles in the micrographs (fig. 3.27).

Distribution of smectite layers probability (%S)

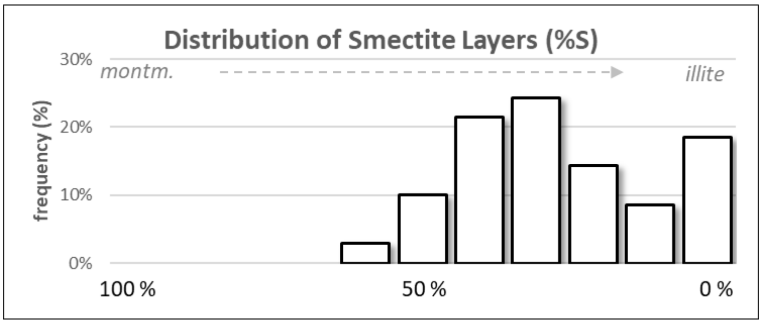

Description: *The distribution of %S-probability indicates two groups: (i) the occurrence of diVS-ml + IS-ml with %S mainly at 30-40% and (ii) illite with K- & charge-deficit.*

Fig. 3.28a. *Distribution of smectite layers probability (%S)*

Differentiation by relation "Octahedral Mg vs. tetrahedral Si"?

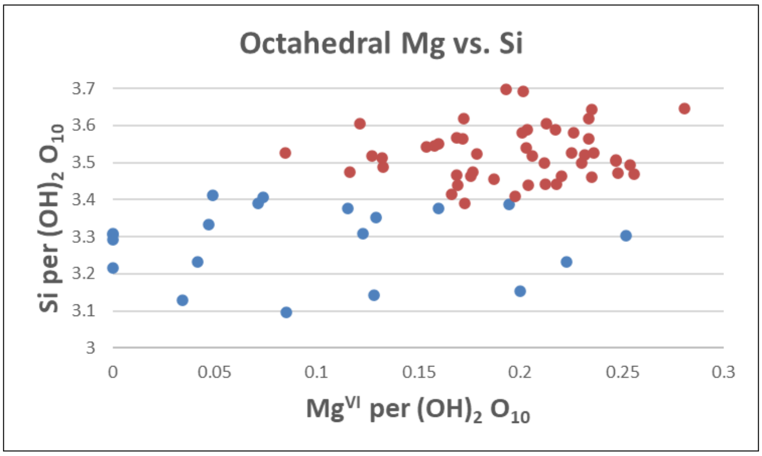

Description: *This diagram doesn't indicate any separation on low and high ratio of Mg in relation to tetrahedral Si (blue dots – Cluster1; red dots – Cluster2). Phases of Cluster2 are mostly characterized by Mg(VI) > 0.1 per* $(OH)_2$ O_{10}.

Fig. 3.28b. *Distribution of octahedral Mg vs. tetrahedral Si [all per* $(OH)_2$ O_{10}*]*

Distribution of K in relation to tetrahedral Si

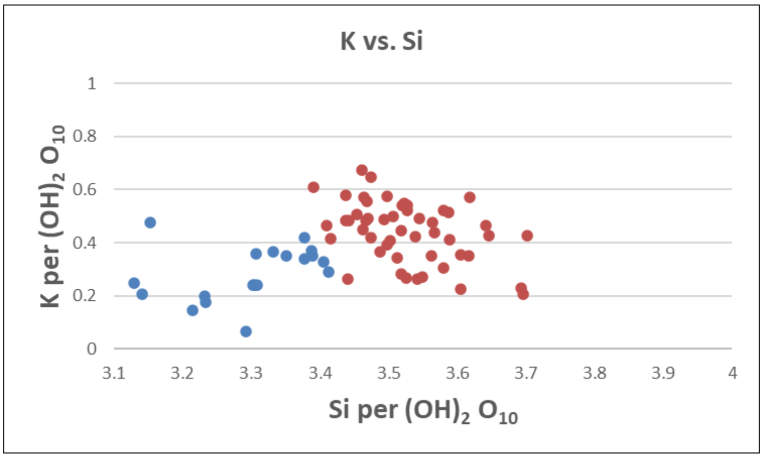

Description: *This diagram indicates a weak separation on low and high ratio of K in relation to tetrahedral Si (blue dots – Cluster1; red dots – Cluster2). Phases of Cluster1 are mostly characterized by K < 0.45 per* $(OH)_2$ O_{10}.

Fig. 3.28c. *Distribution of K in interlayer space vs. tetrahedral Si [all per* $(OH)_2$ O_{10}*]*

Distribution of charges (exchangeable from interlayer space)

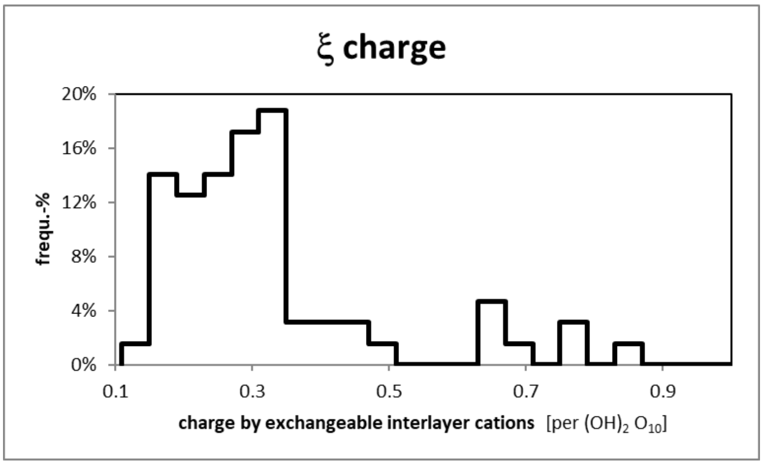

This diagram visualizes the distribution of exchangeable charges in the interlayer space (Ca, Mg, Na) determined and computed by TEM-EDX-data.

Description: *The charge density indicates a broad distribution of exchangeable interlayer cations lower than 0.35 per* $(OH)_2\ O_{10}$.

Fig. 3.29. *Distribution of charges*

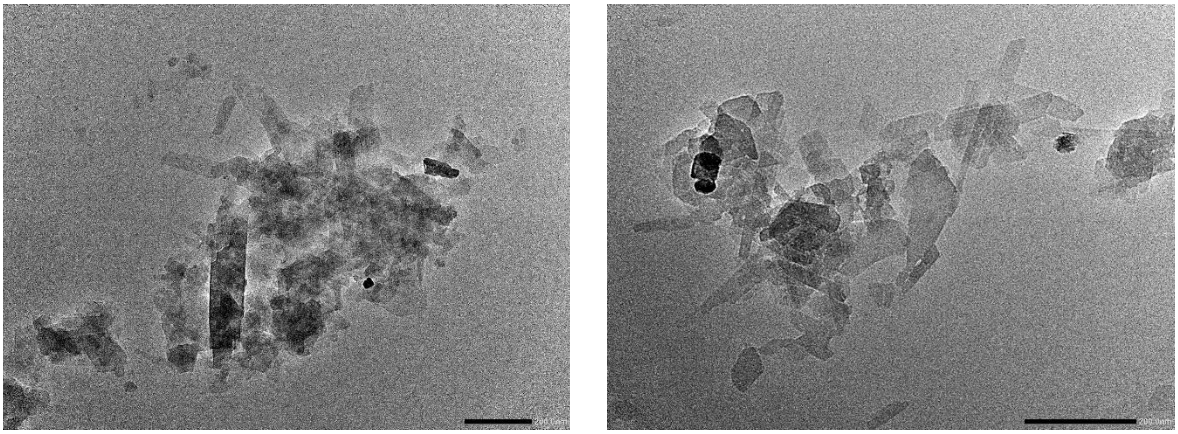

JEM-2100_MAG_X30k_Opalinus-40um-16.9_008.bmp *JEM-2100_MAG_X50k_Opalinus-40um-16.9_011.bmp*

Magnification: 30k Magnification: 50k

aggregates composed by slat-shaped crystals (length ~ 200 nm) with idiomorphic ends, commonly parallel or hexagonal intergrowths *(IS-ml and diVS-ml, not to distinguish by morphology of particles)*

Fig. 3.30a. *Morphology of particles (TEM-micrographs)*

The distribution of %S-probability of all measured clay mineral phases (fig. 3.28a) also indicates the occurrence of two groups: (i) diVS-ml with $\%S_{max}$=30-40% and (ii) illite with K-deficiency. A differentiation between

The numerous measured particles by TEM-EDX allow a visualization of distribution of interlayer charges. Considering the TEM-EDX-determined cations Ca^{++}, Mg^{++} and Na^{+} and then computed their ratio as interlayer cations in the mineral formula, Ca^{++}, Mg^{++} and Na^{+} offer to characterize the degree of exchangeable charges in the interlayer space. This charge density of Opalinus Clay original (< 2 µm) shows in this sample a maximal frequency-% of charge density at 0.35 per $(OH)_2\ O_{10}$ (fig. 3.29). This interval of interlayer charge density caused by exchangeable cations from 0.15 - 0.51 per $(OH)_2\ O_{10}$ represents mentioned two groups of diVS-ml.

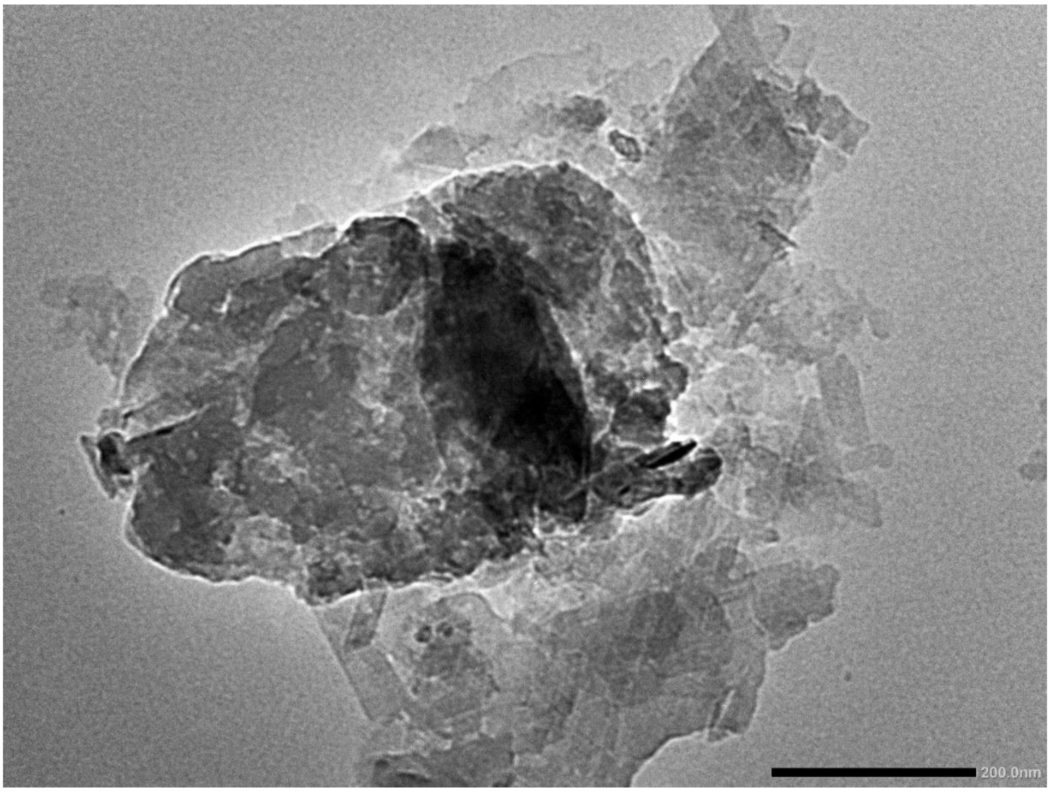

JEM-2100_MAG_X50k_Opalinus-40um-16.9_015.bmp
Magnification: 50k

former idiomorphic platy muscovite weathered into high charged dioctahedral vermiculite-smectite mixed layer phases with K-deficit (%S ~10%, %I ~ 90%)

Fig. 3.30b. *Morphology of particles (TEM-micrographs)*

Result of Clustering

The TEM-EDX-data offers a good agreement with the result of Sybilla-processing of XRD-traces from oriented specimen (tab. 3.9) considering traces of beidellite as further smectite component.

ISS R0: The X-ray diffraction pattern of the ethylene-glycol saturated oriented specimen shows a limited expandability to 1.46 nm. This result of XRD-pattern processing let expect a maximum of particles for %S ~ 50% by TEM-EDX-measurements, but the maximum of particles measured by TEM-EDX is to find at %S = 31%. Using a model for beidellite-montmorillonite-illite-mixed layer phases (BMI-ml) with 3.50, 4.00 and 3.20 as tetrahedral Si-value per $(OH)_2\ O_{10}$ the calculation of member ratios offers a solution for 10%-layer probability for %B and 40% for %S, if %I is given with 50% [see Cluster2 in (tab. 3.9)].

IS R0 (1): The Sybilla-procedure of XRD-traces (oriented mounts) has shown an occurrence of an illite-smectite mixed layer phase with a smectite layers probability of %S = 11%. This result of XRD-pattern processing is in good agreement with founded maximum of particles for %S ~ 9% by TEM-EDX-measurements (tab. 3.9).

The Sybilla-processing of XRD-traces (oriented mounts) also supports low amount of kaolinite and kaolinite-smectite mixed layer phases in fine fraction of sample.

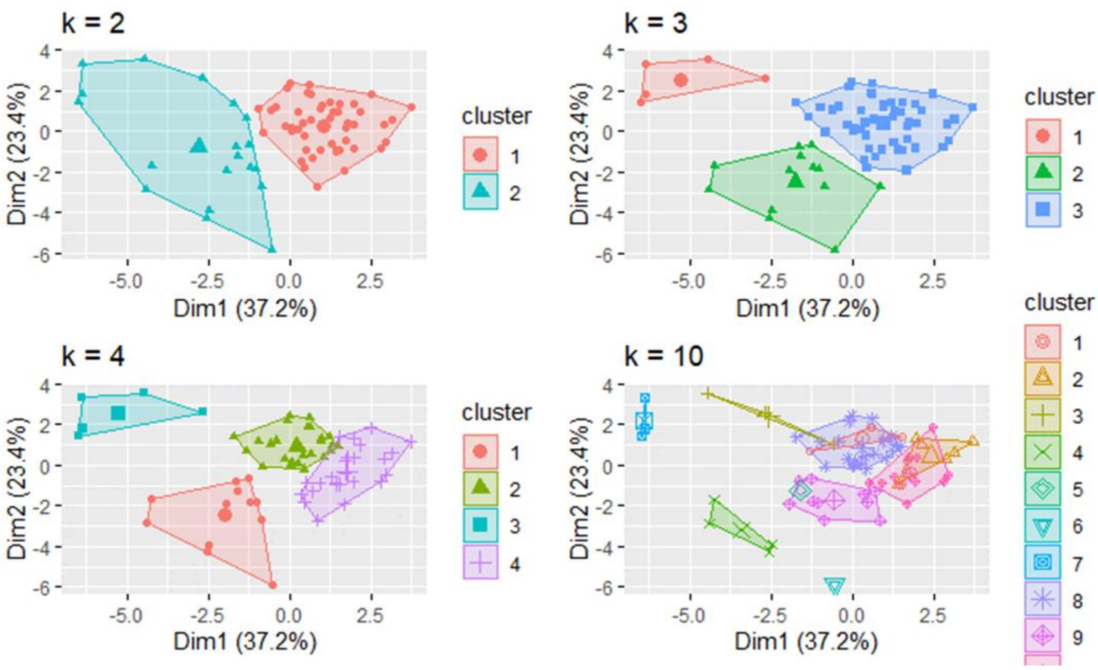

Fig. 3.31. *Clustering of all measured particles for clusters k = 2, k = 3, k = 4 and k = 10 (source for R-coding: https://uc-r.github.io/kmeans_clustering)*

The optimum of TEM-EDX-data-clusters, presented in fig. 3.31, was calculated with k = 2.

Tab. 3.9a *Comparison of results from TEM-EDX- and XRD-measurements*

	Sybilla-results	**TEM-EDX-results**	**Notes**
	Illite	diVS-ml (illite)	*very high K-deficit, low XII-charge deficit, Fe(VI)-rich, low Mg(VI)*
Cluster1	IS R0(1) *(%S = 11%)*	diVS-ml *(%S = 9%)*	*high K-deficit, low XII-charge deficit, Al(VI)- & Fe(VI)-rich*
Cluster2	ISS R0 *(%S = 48%)*	beid. diVS-ml *BMI 10:40:50*	*K-deficit, no XII-charge deficit, Fe(VI)-rich*

Tab. 3.9b. *Mineral formulae based on TEM-EDX-data summarized following the result of clustering for k=2*

		Ca (XII)	Mg (XII)	Na (XII)	K (XII)	Cr3+ (VI)	Al (VI)	Fe3+ (VI)	Mg (VI)	Ti (VI)	Al (IV)	Si (IV)	XII	n_VI	%S
Cluster1	n = 20	0.11	0.12	0.01	0.28	0.00	1.42	0.45	0.10	0.03	0.71	3.29	0.74	2.0	9
Cluster2	n = 50	0.08	0.04	0.00	0.44	0.00	1.39	0.41	0.20	0.00	0.47	3.53	0.68	2.0	31

Dioctahedral vermiculite-smectite mixed layer phase *(Cluster1)*

20 of 70 computed particles belong so to this assumed classification. The dioctahedral character of this group is proofed by X-ray diffraction. The position of the large (060)-interference of smectite is in the random oriented powder specimen at 1.497 Å.

Dioctahedral vermiculite-smectite mixed layer phase *(Cluster1)*

$$Ca_{0.11}\ Mg_{0.12}\ Na_{0.01}\ K_{0.28}\quad Al_{1.42}\ Fe^{3+}_{0.45}\ Mg_{0.10}\ Ti_{0.03}\ (OH)_2\ \ Si_{3.29}\ Al_{0.71}\ O_{10}$$

Charge: XII = 0.74 VI = 5.97 IV = 15.29 **Σ = 22.00**

Measured particles by TEM-EDX: 20

Probability of smectite layers (%S): 9%

Probability of illite layers (%I): 91%

Result of clustering: Cluster1 (tab 3.9)

A comparison of octahedral Mg vs. tetrahedral Si doesn't indicate any differentiation for octahedral Mg in comparison to Cluster2 based on TEM-EDX-data (fig. 2.28b). Particles of Cluster1 contain commonly Mg(VI) < 0.25 per $(OH)_2 O_{10}$ in octahedral layer. Also, a separation on low and high K in relation to Si is not to identify between Cluster1 and Cluster2 (fig. 28c). Phases of Cluster1 are mostly characterized by K < 0.45 per $(OH)_2 O_{10}$.

The mineral formulae, summarized in classes of %S, draws for the maximum an Al- & Fe-rich diVS-ml with a low Mg(VI) as well as low amount of K in the interlayer space (tab 3.10).

***Tab. 3.10.** Computed averaged mineral formulae of diVS-ml phases in the different smectite layers probability (%S)-classes*

diVS-ml	*particles (abs)*	**Ca (XII)**	**Mg (XII)**	**Na (XII)**	**K (XII)**	**Cr3+ (VI)**	**Al (VI)**	**Fe3+ (VI)**	**Mg (VI)**	**Ti (VI)**	**Al (IV)**	**Si (IV)**	**XII**	**n_VI**	**%S**
%S >95%	n = 0														
%S 95-85%	n = 0														
%S 85-75%	n = 0														
%S 75-65%	n = 0														
%S 65-55%	n = 0														
%S 55-45%	n = 0														
%S 45-35%	n = 0														
%S 35-25%	n = 0														
%S 25-15%	n = 6	0.09	0.09	0.01	0.35	0.00	1.49	0.40	0.11	0.00	0.61	3.39	0.72	2.0	17
%S <15%	**n = 14**	**0.13**	**0.13**	**0.01**	**0.25**	**0.00**	**1.39**	**0.48**	**0.09**	**0.04**	**0.76**	**3.24**	**0.76**	**2.0**	**6**

Dioctahedral vermiculite-smectite mixed layer phase *(beid. diVS-ml, Cluster2)*

$$Ca_{0.08}\ Mg_{0.04}\ Na_{0.00}\ K_{0.44}\quad Al_{1.39}\ Fe^{3+}_{0.41}\ Mg_{0.20}\ Ti_{0.00}\ (OH)_2\quad Si_{3.53}\ Al_{0.47}\ O_{10}$$

Charge: XII = 0.68 VI = 5.79 IV = 15.53 **Σ = 22.00**
Probability of smectite layers (%S): 50%
Probability of illite layers (%I): 50%
Measured particles by TEM-EDX: 50
Result of clustering: Cluster2 (tab. 3.9)

A comparison of octahedral Mg vs. tetrahedral Si doesn't indicate any differentiation for octahedral Mg in comparison to Cluster1 based on TEM-EDX-data (fig. 3.28b). Particles of Cluster2 contain commonly Mg(VI) > 0.1 per $(OH)_2 O_{10}$ in octahedral layer.

The mineral formulae, summarized in classes of %S, draws for the maximum an Al- & Fe-rich diVS-ml as well as reduced amount of K in the interlayer space (tab 3.11).

***Tab. 3.11.** Computed averaged mineral formulae of diVS-ml phases in the different smectite layers probability (%S)-classes*

beid. diVS-ml	*particles (abs)*	**Ca (XII)**	**Mg (XII)**	**Na (XII)**	**K (XII)**	**Cr3+ (VI)**	**Al (VI)**	**Fe3+ (VI)**	**Mg (VI)**	**Ti (VI)**	**Al (IV)**	**Si (IV)**	**XII**	**n_VI**	**%S**
%S >95%	n = 0														
%S 95-85%	n = 0														
%S 85-75%	n = 0														
%S 75-65%	n = 0														
%S 65-55%	n = 0														
%S 55-45%	n = 5	0.10	0.02	0.00	0.35	0.00	1.35	0.41	0.23	0.00	0.32	3.68	0.58	2.0	51
%S 45-35%	n = 11	0.07	0.04	0.01	0.41	0.00	1.39	0.40	0.20	0.00	0.41	3.59	0.64	2.0	39
%S 35-25%	**n = 20**	**0.08**	**0.04**	**0.01**	**0.44**	**0.00**	**1.44**	**0.37**	**0.19**	**0.00**	**0.49**	**3.51**	**0.68**	**2.0**	**30**
%S 25-15%	n = 14	0.08	0.05	0.00	0.50	0.00	1.32	0.47	0.20	0.00	0.56	3.44	0.76	2.0	22
%S <15%	n = 0														

Kaolinite-montmorillonite mixed layer phases

The Excel-based procedure (Hoang-Minh et al., 2019) to identify possible clay mineral groups using the TEM-EDX-measurements also includes algorithms to classify kaolinite and kaolinite-montmorillonite mixed layer phases. These algorithms couldn't compute no such phases basing on the measured TEM-EDX-data. Such particles have shown small hexagonal plates typically for kaolinite-bearing phases.

Estimation of Specific Dissolution Potential *(in according to Nguyen-Thanh et al., 2014)*

Previous investigations have shown (summarized in Nguyen-Thanh et al., 2014), each bentonite or clay have a specific dissolution potential expressed as loss of smectite layer. The expected specific behaviour of smectite layers is classified using the mineral formula as result of TEM-EDX-measurements. The authors developed different experimental overhead rotation setups to determine the maximal possible loss of smectite layers under pre-defined conditions. These different experimental settings should represent different strengths of acting forces in mineralogical alteration of original smectite (with water as low energy-level). The previous results with a large series of bentonites and clays allow to predict the expected rate of alteration of smectite layers distinguishing slow-reacting smectite layers (= sleepers), moderate-reacting smectite layers and fast-reacting smectite layers (= sprinters). The limits between these classes are postulated only: sleepers are smectites with loss of smectite layers lower than Δ%S = 5% and are a sprinter with loss of smectite layers larger than Δ%S = 20%. Negative values for Δ%S mirroring a 'illitization'-like process and positive values represent a smectitization potential.

The modelled values for Opalinus Clay (fig. 3.32) let expect mainly a slow-reacting smectite with a change from the original %S-value = 24% to 23% for the run products (Δ%S = -1%). Otherwise under strong conditions (e.g. higher temperature, high ionic strength, high saline solution), the modelling let assume for Opalinus Clay a very fast and nearby complete loss of smectite layers (Δ%S = -103%).

The type of cations in the interlayer space (here type B with Ca + Mg) and the Fe-rich composition of octahedral layer are the driving forces for these estimations.

Few aspects could influence the expected behaviour for Opalinus Clay:

1. The occurrence of pyrite let expect a higher degree of dissolution and so a higher loss of smectite layers than modelled.
2. Mixed layer phases offer a Si-buffer. Dissolved Si can again be precipitated in the alteration process as new-precipitated smectite layer. The key parameter is the grade of migration of dissolved Si far from the reaction site during the reaction. A fast transport of dissolved Si away from the reaction site is causing an 'illitization' and a slow transport away from the reaction site is offering partially a smectitization.

Finally, only further experiments with the selected clay can validate these estimations.

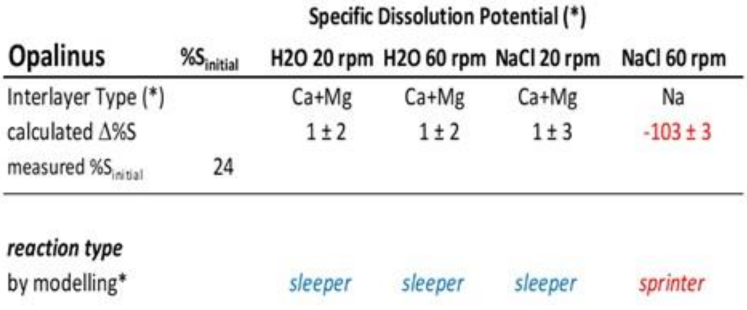

		Specific Dissolution Potential (*)			
Opalinus	$\%S_{initial}$	H2O 20 rpm	H2O 60 rpm	NaCl 20 rpm	NaCl 60 rpm
Interlayer Type (*)		Ca+Mg	Ca+Mg	Ca+Mg	Na
calculated Δ%S		1 ± 2	1 ± 2	1 ± 3	-103 ± 3
measured $\%S_{initial}$	24				
reaction type by modelling*		sleeper	sleeper	sleeper	sprinter

Description: *Overhead-rotation systems like H2O 20 rpm serve as indicator for rate of alteration of selected bentonite. Low grade reduction of smectitic layers (Δ%S) indicate a slow reaction of smectite phases (so-called sleeper). An opposite behaviour is called as sprinter*

Fig 3.32. *Specific Dissolution Potential of Opalinus Clay, < 2 µm (* in according to Nguyen-Thanh et al., 2014)*

3.7.3 Friedland clay

The fraction < 2 µm of Friedland Clay N10 sample is mainly composed by beidellite-montmorillonite-illite mixed layer phases (BMI-ml) and beidellitic dioctahedral vermiculite-smectite mixed layer phases (beid. diVS-ml). Furthermore, kaolinite and kaolinite-smectite-ml phases (with computed KSV =

60:25:15), chlorite-smectite-vermiculite mixed layer phases, Si-surplus particles (Si, e.g. quartz) and rutile were identified in traces in this sample (fig. 3.33).

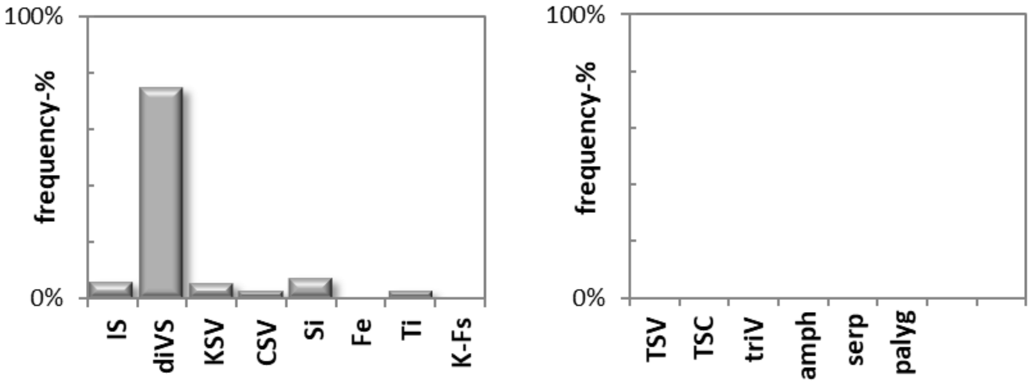

Fig. 3.33. *Distribution of mineral groups in fraction < 2 µm (in frequency-%)*

*Legend: **IS** – illite-smectite-mixed layer series in sense of Środon et al. (1992), diVS – dioctahedral vermiculite-smectite illite-smectite-mixed layer series (= charge- and/or K-deficit), **KSV** – kaolinite-smectite-dioctahedral vermiculite-mixed layer series, **CSV** – chlorite-saponite-trioctahedral vermiculite-mixed layer series, **Si** – quartz or particles with Si-surplus, **Fe** – Fe-oxide or Fe-oxyhydroxide, **Ti** – Ti-bearing phases (e.g. rutile, anatase), **K-Fs** – K-feldspar*

The measured and computed particles have shown a calculated CEC-value of 32 meq / 100 g located at surface and in the interlayer space.

	frequency-% *(n = 152 measured particles)*
BMI-ml	53%
beid. diVS-ml	28%
Kaolinite & KSV-ml	5%
CSV-ml	3%
Si-surplus	7%
Ti-phases	3%
Unknown	1%

All measured dioctahedral 2:1 clay mineral phases summarized result following mineral formula computed from TEM-EDX-measurement of 123 individual particles:

$$Ca^{2+}_{0.02}\ Mg^{2+}_{0.09}\ Na^{+}_{0.01}\ K^{+}_{0.35}\quad Al^{3+}_{1.36}\ Fe^{3+}_{0.52}\ Mg^{2+}_{0.10}\ Ti^{4+}_{0.02}\ (OH)_2\quad Si^{4+}_{3.49}\ Al^{3+}_{0.51}\ O_{10}$$

SDOM *± 0.00 ± 0.00 ± 0.00 ± 0.01 ± 0.02 ± 0.01 ± 0.01 ± 0.00 ± 0.01 ± 0.01*

Legend: SDOM - standard deviation of the mean (= the standard deviation divided by the square root of the number of samples)

Table 3.12. *Summarized chemical composition*

SiO_2	TiO_2	Al_2O_3	Fe_2O_3	MnO	MgO	CaO	Na_2O	K_2O	P_2O_5	Σ	
59.4%	0.3%	28.1%	5.9%		2.5%	0.3%	0.1%	3.3%	0.1%	1.00	measured particles of original Friedland Clay

The interlayer charge is calculated as 0.58 per $(OH)_2\ O_{10}$ and the octahedral charge as 5.93 per $(OH)_2\ O_{10}$. The particles are characterized by a high octahedral Fe-amount.

The summarized chemical composition of all 123 computed particles is listed (tab. 3.12).

Friedland Clay, Siedlungsscholle, East-field is characterized by two morphological groups: (i) large (≤ 1 µm) xenomorph platy crystals and (ii) aggregates, partially with folds, formed by small (≤ 100 nm) xenomorphous plates (fig. 3.34). Aggregates formed by small (≤ 100 nm) xenomorphous plates dominate the shapes of particles in the micrographs (fig. 3.34).

The distribution of %S-probability of all measured clay mineral phases (fig. 3.35a) also indicates the occurrence of two groups: (i) BMI- and beidellitic diVS-ml phases incl. illite with K-deficiency as well as (ii) montmorillonite (rare).

The numerous measured particles by TEM-EDX allow a visualization of distribution of interlayer charges. Considering the TEM-EDX-determined cations Ca^{++}, Mg^{++} and Na^{+} and then computed their ratio as interlayer cations in the mineral formula, Ca^{++}, Mg^{++} and Na^{+} offer to characterize the degree of exchangeable charges in the interlayer space. This charge density of Friedland Clay (< 2 µm) shows in this sample a broad interval with two maximal frequency-% of charge density at 0.15 and 0.23 per $(OH)_2$ O_{10} (fig. 3.37). This broad interval of interlayer charge density caused by exchangeable cations from 0.10 - 0.43 per $(OH)_2$ O_{10} represents mainly IS-ml (lowest peak at 0.15 per $(OH)_2$ O_{10}) and the diVS-ml phases with the other higher peak at 0.23 per $(OH)_2$ O_{10}.

The TEM-EDX-data offers a good agreement with the result of Sybilla-processing of XRD-traces from oriented specimen, but only under consideration of the option beidellite (tab. 3.13).

IS R0 (1): The X-ray diffraction pattern of the ethylene-glycol saturated oriented specimen shows a nearby full expandability to 1.67 nm and a difference of 5.68°2θ between 2. and 3. order of smectite interferences. This distance is typically for a probability of smectite layers (%S) of 80% (Moore & Reynolds, 1989). This result of XRD-processing let expect a maximum of particles for %S ~ 80% by TEM-EDX-measurements, but the maximum of particles measured by TEM-EDX is to find at %S=40% (fig. 3.35a). Using a model for beidellite-montmorillonite-illite-mixed layer phases (BMI-ml) with 3.50, 4.00 and 3.20 as tetrahedral Si-value per $(OH)_2$ O_{10} the calculation of member ratios offers a solution for 60%-layer probability for %B and 20% for %S, if %I is given with 20% (see Cluster2 in tab. 3.13).

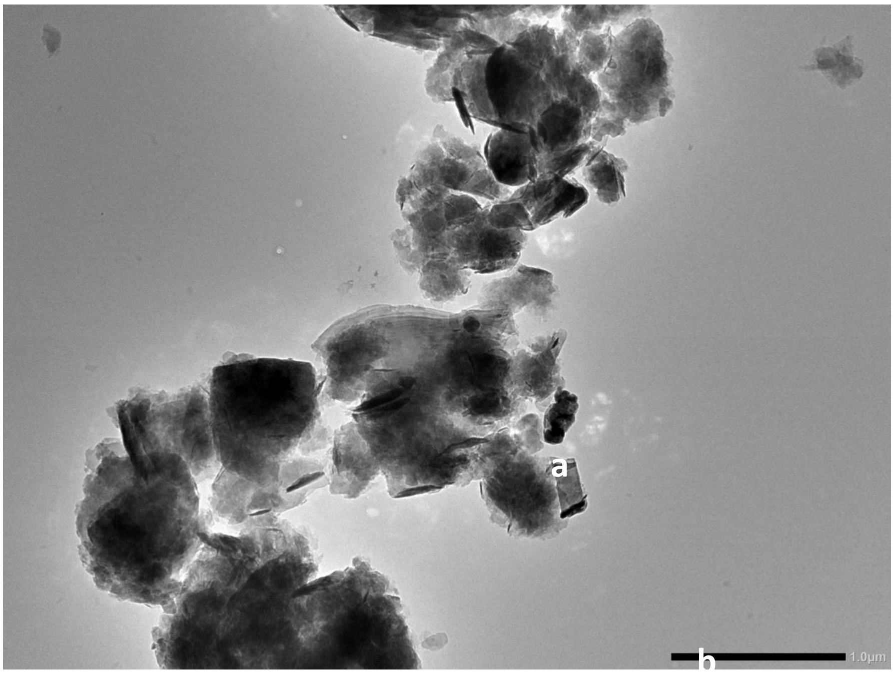

JEM-2100_MAG_X10k_007_AISZ-5ML.bmp

Magnification: 10k

(a) large (≤ 1 µm) xenomorph platy crystals;
(b) aggregates, partially with folds, formed by small (≤ 100 nm) xenomorph plates

***Fig. 3.34.** Morphology of particles (TEM-micrographs)*

Distribution of smectite layers probability (%S)

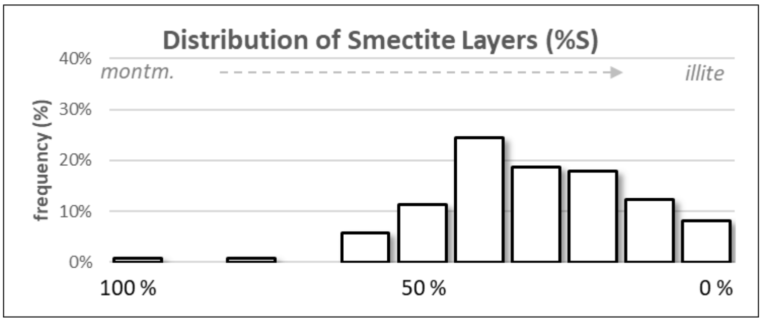

***Description:** The distribution of %S-probability indicates the occurrence of two groups: (i) BMI- and beidellitic diVS-ml phases incl. illite with K-deficiency as well as (ii) montmorillonite (rare).*

***Fig. 3.35a.** Distribution of smectite layers probability (%S)*

Differentiation by relation “Octahedral Mg vs. tetrahedral Si”?

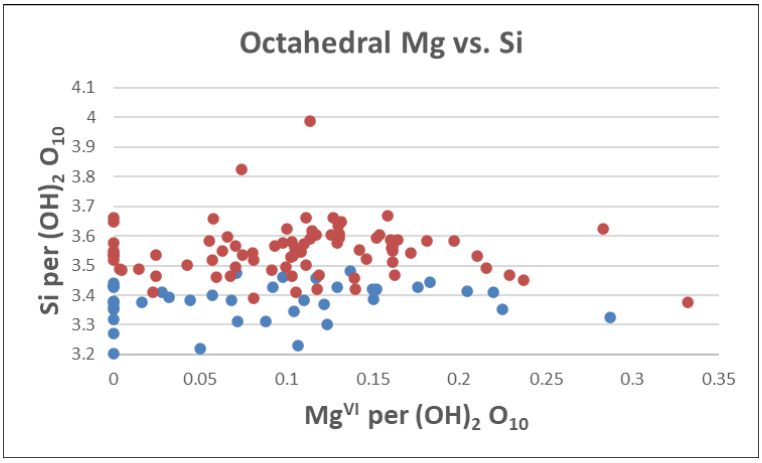

***Description:** This diagram doesn’t indicate any trend of Mg in relation to tetrahedral Si, also not between BMI-ml phases of cluster2 (red dots) and beidellitic diVS-ml phases of cluster1 (blue dots).*

***Fig. 3.35b.** Distribution of octahedral Mg vs. tetrahedral Si [all per $(OH)_2\ O_{10}$]*

Distribution of K in relation to tetrahedral Si

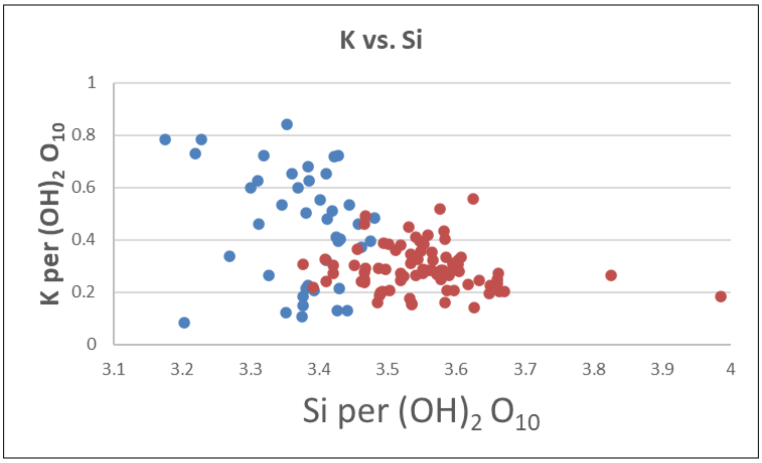

***Description:** This diagram visualizes a trend to higher K-values in beidellitic diVS-ml / cluster1 (blue dots) than in beidellite-montmorillonite-illite-ml phases / cluster2 (red dots).*

***Fig. 3.36.** Distribution of K in interlayer space vs. tetrahedral Si [all per $(OH)_2\ O_{10}$]*

Distribution of charges (exchangeable from interlayer space)

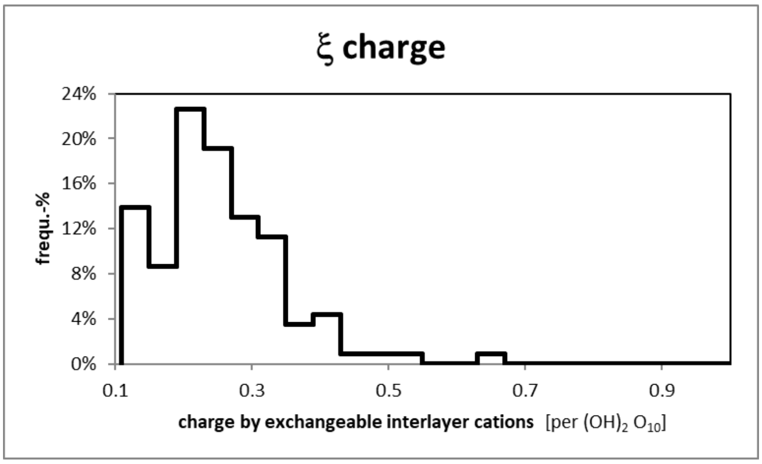

This diagram visualizes the distribution of exchangeable charges in the interlayer space (Ca, Mg, Na) determined and computed by TEM-EDX-data.

Description: *Bimodal distribution of charge density with (i) first maximal frequency-% at 0.15 per* $(OH)_2 O_{10}$ *(mica) as well as (ii) at 0.23 per* $(OH)_2 O_{10}$ *as second maximal frequency-%*

Fig. 3.37. *Distribution of charges*

Result of Clustering

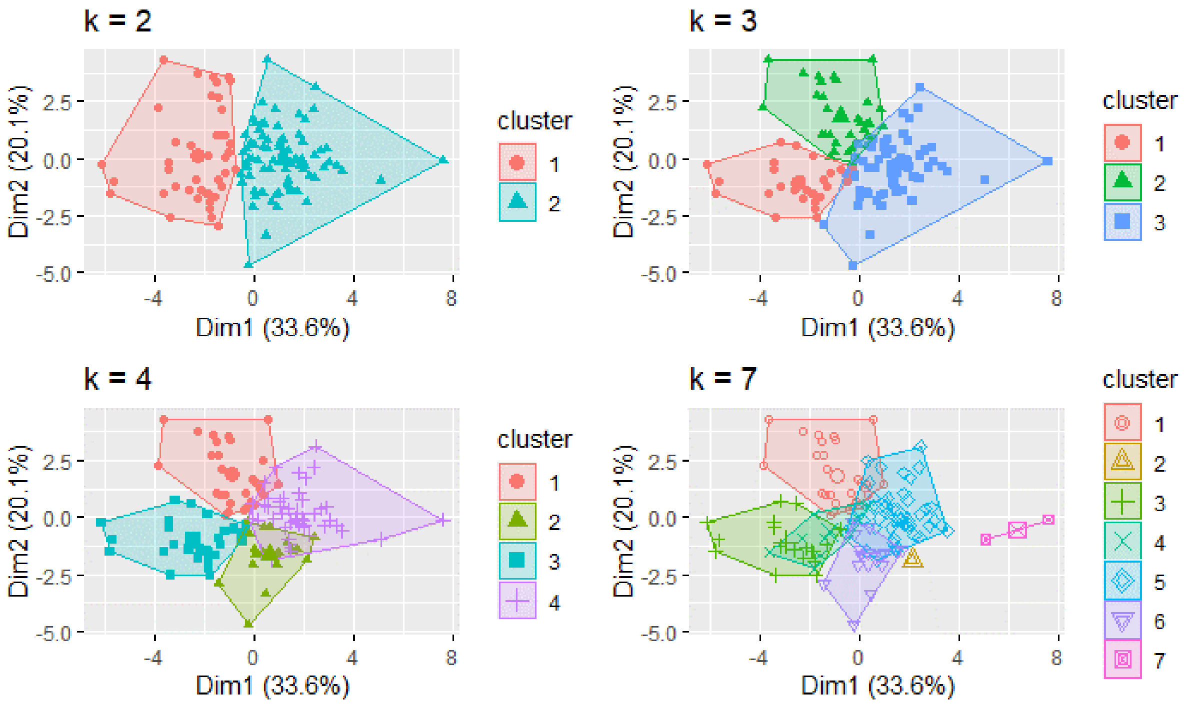

Fig. 3.38. *Clustering of all measured particles for clusters k = 2, k = 3, k = 4 and k = 7 (source for R-coding: https://uc-r.github.io/kmeans_clustering)*

The optimum of TEM-EDX-data-clusters (fig. 3.38) was calculated with k = 2 (here applied) and k=7.

Tab. 3.13a. *Mineral formulae based on TEM-EDX-data summarized following the result of clustering for k=2*

		Ca (XII)	Mg (XII)	Na (XII)	K (XII)	Cr3+ (VI)	Al (VI)	Fe3+ (VI)	Mg (VI)	Ti (VI)	Al (IV)	Si (IV)	XII	n_VI	%S
Cluster1	n = 42	0.01	0.08	0.01	0.45	0.00	1.50	0.40	0.08	0.03	0.63	3.37	0.65	2.0	15
Cluster2	n = 81	0.02	0.10	0.00	0.29	0.00	1.30	0.58	0.11	0.02	0.45	3.55	0.54	2.0	34

Tab. 3.13b. *Comparison of results from TEM-EDX- and XRD-measurements*

	Sybilla-results	**TEM-EDX-results**	**Notes**
	Illite	beid. diVS-ml (illite)	*high K-deficit, low XII-charge deficit, Al(VI)-rich, Fe(VI)-rich*
Cluster1	IS R0(2) *(%S = 25%)*	beid. diVS-ml, without illite *(BMI 05:15:75)*	*high K-deficit, charge deficit, Al(VI)-rich, Fe(VI)-rich*
Cluster2	IS R0(1) *(%S = 82%)*	BMI ~60:20:20	*XRD: Montmorillonite and beidellite is only to distinguish by Green-Kelly-test (not available here).*
	Kaolinite + KS GL R0		*in traces only*

IS R0 (2): The Sybilla-procedure of XRD-traces (oriented mounts) has shown an occurrence of a second illite-smectite mixed layer phase with a smectite layers probability of %S = 25%. This situation is to find also by TEM-EDX ($\%S_{TEM}$ = 15%). Using a model for beidellite-montmorillonite-illite-mixed layer phases (BMI-ml) with 3.50, 4.00 and 3.20 as tetrahedral Si-value per $(OH)_2\,O_{10}$ the calculation of member ratios offers a solution for 5%-layer probability for %B and 20% for %S, if %I is given with 75% (see Cluster2 in tab. 3.13a,b)]. That means, few parts of smectite layers are formed as beidellite in these phases. These phases represent remarkable K-amounts and slight charge deficit and Al- & Fe-rich, beidellitic dioctahedral vermiculite-smectite mixed layer phase (beid. diVS-ml) (tab. 3.13a,b).

The Sybilla-processing of XRD-traces (oriented mounts) also supports the existence of kaolinite and kaolinite-smectite mixed layer phases in fine fraction of sample. The mineral formula was to compute for only 3 particles of KSV-ml phases (average: %K 60%, %S 26%, %V 14%).

Specifics to the identified clay mineral groups

Beidellite-montmorillonite-illite-ml (BMI-ml 60:20:20) *(Cluster2)*

81 of 123 computed particles belong so to this assumed classification. The dioctahedral character of this group is proofed by X-ray diffraction. The position of the large (060)-interference of smectite is in the random oriented powder specimen at 1.497 Å.

Montmorillonite and beidellite have the same behaviour concerning the expandability and they are only to distinguish by XRD using Li by means of Greene-Kelly test (Greene-Kelly 1952, 1953). So, combination of XRD- and TEM-results (full expandability by XRD and Si ~ 3.55 by TEM-EDX) led conclude the occurrence of beidellite (fig. 3.39).

Beidellite-montmorillonite-illite-ml *(BMI 60:20:20)*

$$Ca_{0.02}\,Mg_{0.10}\,Na_{0.00}\,K_{0.29}\quad Al_{1.30}\,Fe^{3+}_{0.58}\,Mg_{0.11}\,Ti_{0.02}\,(OH)_2\quad Si_{3.55}\,Al_{0.45}\,O_{10}$$

Charge:	XII = 0.54	VI = 5.91	IV = 15.45	**Σ = 22.00**
Measured particles by TEM-EDX:	81			
Result of clustering:	Cluster2 (tab. 3.13)			

In this sample, beidellite is characterized by a low octahedral Mg-amount (because of high ratio of octahedral, 3-valent cations). A comparison of octahedral Mg vs. tetrahedral Si doesn't indicate any differentiation for octahedral Mg based on TEM-EDX-data [fig. 3.35b]. Particles of Cluster2 contain full interval of Mg(VI) from 0.0 to 0.3 per $(OH)_2\,O_{10}$ in octahedral layer. Particles of Cluster2 show also a trend to lower K in interlayer space than particles of Cluster1 (fig. 3.36),

Using the results of TEM-EDX data processing (see cluster2 in tab. 3.13), the maximum of frequency-% is to find for particles at 3.5-3.6e phuc (fig. 3.39). The mineral formulae, summarized in classes of %S, draws for the maximum an Fe-rich BMI-ml with low Mg(VI), but remarkable amount of K in the interlayer space (tab. 3.14).

Distribution of beidellite-montmorillonite-illite-ml phases (BMI-ml)

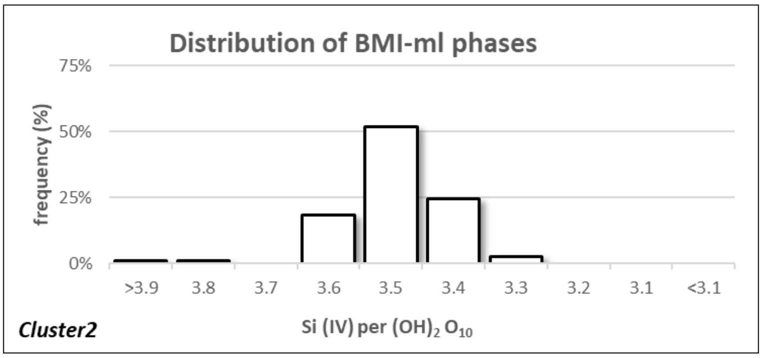

Description: *The distribution of BMI-ml phases (cluster2) draws a maximum of frequency (%) at tetrahedral Si-value between 3.5 – 3.6 e phuc.*

Fig. 3.39. *Distribution of smectite layer probability (%S) in diVS-ml*

Tab. 3.14. *Computed averaged mineral formulae of phases in the different Si(IV)-classes*

BMI 60:20:20?	*particles (abs)*	Ca (XII)	Mg (XII)	Na (XII)	K (XII)	Cr3+ (VI)	Al (VI)	Fe3+ (VI)	Mg (VI)	Ti (VI)	Al (IV)	Si (IV)	XII	n_VI	%S
Si >3.9	n = 1	0.03	0.06	0.00	0.18	0.00	1.32	0.48	0.11	0.00	0.01	3.99	0.37	1.9	106
Si 3.9-3.8	n = 1	0.02	0.10	0.00	0.27	0.00	1.32	0.52	0.07	0.00	0.17	3.83	0.52	1.9	75
Si 3.8-3.7	n = 0														
Si 3.7-3.6	n = 15	0.02	0.08	0.00	0.27	0.00	1.28	0.60	0.12	0.00	0.36	3.64	0.47	2.0	45
Si 3.6-3.5	**n = 42**	**0.02**	**0.08**	**0.01**	**0.31**	**0.00**	**1.32**	**0.57**	**0.10**	**0.02**	**0.45**	**3.55**	**0.52**	**2.0**	**34**
Si 3.5-3.4	n = 20	0.03	0.13	0.00	0.29	0.00	1.28	0.60	0.10	0.02	0.54	3.46	0.62	2.0	24
Si 3.4-3.3	n = 2	0.03	0.20	0.00	0.26	0.00	1.00	0.69	0.21	0.10	0.62	3.38	0.72	2.0	16
Si 3.3-3.2	n = 0														
Si 3.2-3.1	n = 0														
Si <3.1	n = 0														

Beidellitic dioctahedral vermiculite-smectite mixed layer phase (Cluster1)

(beid. diVS-ml, %S = 25%, without illite)

$$Ca_{0.02}\ Mg_{0.09}\ Na_{0.01}\ K_{0.40}\quad Al_{1.50}\ Fe^{3+}_{0.40}\ Mg_{0.08}\ Ti_{0.02}\ (OH)_2\quad Si_{3.42}\ Al_{0.58}\ O_{10}$$

Charge: XII = 0.62 VI = 5.96 IV = 15.42 **Σ = 22.00**
Probability of smectite layers (%S): 25%
Probability of illite layers (%I): 75%
Measured particles by TEM-EDX: 27

Illite as part of beid. diVS-ml series

$$Ca_{0.01}\ Mg_{0.07}\ Na_{0.01}\ K_{0.54}\quad Al_{1.49}\ Fe^{3+}_{0.39}\ Mg_{0.08}\ Ti_{0.05}\ (OH)_2\quad Si_{3.30}\ Al_{0.70}\ O_{10}$$

Charge: XII = 0.72 VI = 5.99 IV = 15.30 **Σ = 22.00**
Probability of smectite layers (%S): 9%
Probability of illite layers (%I): 91%
Measured particles by TEM-EDX: 15

Kaolinite-montmorillonite mixed layer phases

The Excel-based procedure (Hoang-Minh et al., 2019) to identify possible clay mineral groups using the TEM-EDX-measurements also includes algorithms to classify kaolinite and kaolinite-montmorillonite mixed layer phases. These algorithms could identify such phases basing on the measured TEM-EDX-data for only 3 particles. Such particles have shown small hexagonal plates typically for kaolinite-bearing phases.

References

Bossart, P.J., 2008, Mont terri rock laboratory project: programme 1996 to 2007 and results. Federal Office of Topography Swisstopo.

Bradley, W.F. and R.E. Grim, 1951, High temperature thermal effects of clay and related materials. American Mineralogist, 36(3-4): p. 182-201.

Breidung, K. P., 2002, Verwahrung von Kali- und Steinsalzbergwerken einschließlich langzeitsicherer Schachtabdichtungen. Kali und Salz, 2, p. 28–39.

Carlson, L., 2004. Bentonite Mineralogy. Part 1: Methods of investigation – a Literature review. Part 2: Mineralogical research of selected bentonites. Posiva Oy, Olkiluoto. p. 78.

Čičel, B., et al.,1992. Mineralogical composition and distribution of Si, Al, Fe, Mg and Cain the fine fractions of some Czech and Slovak bentonite. Geol. Carpathica, Ser. Clays, 43(1): p. 3-7.

Crâciun, C., 1984. Influence of the Fe3+ –for – Al3+ Octahedral Substitutions on the IR Spectra of Montmorillonite Minerals. Spectroscopy Letters, 17(10): p. 579-590.

Decarreau, A., O. Grauby, and S. Petit, 1992, The actual distribution of octahedral cations in 2:1 clay minerals: Results from clay synthesis. Applied Clay Science, 7(1): p. 147-167.

Döbelin, N., Kleeberg, R. (2015). Journal of Applied Crystallography 48, 1573-1580. DOI: 10.1107/S1600576715014685

Farmer, V.t. and J. Russell, 1964, The infra-red spectra of layer silicates. Spectrochimica acta, 20(7): p. 1149-1173.

Gates, W.P., 2005. Infrared Spectroscopy and the Chemistry of Dioctahedral Smectites, in The Application of Vibrational Spectroscopy to Clay Minerals and Layered Double Hydroxides, J.T. Kloprogge, Editor. 2005, Clay Minerals Society. p. 0.

Gaucher, E., A. Fernández, and H.N. Waber, 2003. Rock and Mineral Characterisation of the Opalinus Clay Formation. p. 281-303.

Greene-Kelly, R., 1955. Dehydration of the montmorillonite minerals. Mineralogical magazine and journal of the Mineralogical Society, 30(228): p. 604-615.

Hendershot, W.H. and M. Duquette, 1986. A Simple Barium Chloride Method for Determining Cation Exchange Capacity and Exchangeable Cations. Soil Science Society of America Journal, 50(3): p. 605-608.

Hoang-Minh, T., 2006. Characterization of clays and clay minerals in industrial application: substitution non-natural additives by clays in UV protection. Dissertation, Universtiy of Greifswald.

Karnland, O., S. Olsson, and U. Nilsson, 2006. Mineralogy and sealing properties of various bentonites and smectite-rich clay materials. Svensk Kärnbränslehantering AB (SKB). p. 70.

Kasbohm, J., 2003. Zur Langzeitstabilität von Na-Montmorillonit in hochsalinaren Lösungen. Habilitationsschrift, Universität Greifswald.

Laurich, B., Fourrière, A., Gräsle, W., 2019. LT-A Experiment: How fracture wetting leads to closure. Mont Terri Project, Technical Note 2020-29, October 2019.

Madejová, J., et al., 1996. Preparation and infrared spectroscopic characterization of reduced-charge montmorillonite with various Li contents. Clay Minerals, 31(2): p. 233-241.

Matschiavelli N, Kluge S, Podlech C, Standhaft D, Grathoff G, Ikeda-Ohno A, Warr LN, Chukharkina A, Arnold T, Cherkouk A. (2019). The Year-Long Development of Microorganisms in Uncompacted Bavarian Bentonite Slurries at 30 and 60 °C. Environ Sci Technol. 53(17),10514-10524. DOI: 10.1021/acs.est.9b02670.

Meleshyn A, Hinze M, Middelhoff M, Friedenberg L, Jantschik K, 2024, Thermische Integrität von Ton und Tonsteinen - Experiment und gekoppelte THMC-Simulationen (THMC-Sim): Gesellschaft für Anlagen- und Reaktorsicherheit, Braunschweig

Nagra, 2002, Project Opalinus Clay: Synthesis of the Geological Research Results – Feasibility of Disposing Spent Fuel Elements, Vitrified High-Level Radioactive as Well as Long-Lived Intermediate-Level Waste. National Cooperative for the Disposal of Radioactive Waste (Nagra): Wettingen, Switzerland.

Pearson, F., et al., 2003. Mont Terri Project - Geochemistry of Water in the Opalinus Clay Formation at the Mont Terri Rock Laboratory.

Sitz, P., Gruner, M., Rumphorst, K., 2003. Bentonitdichtelemente für langzeitsichere Schachtverschlüsse im Salinar. Kali und Salz 3, p. 6-13.

Taut, T., Kleeberg, R., Bergmann, J., 1998. The new Seifert Rietveld program BGMN and its application to quantitative phase analysis. Mater. Struct. 5, 57–64.

Ufer, K., et al., 2008. Quantitative phase analysis of bentonites by the rietveld method. Clays and Clay Minerals, 56(2): p. 272-282.

Vantelon, D., et al., 2001. Fe, Mg and Al distribution in the octahedral sheet of montmorillonites. An infrared study in the OH- bending region. Clay Minerals, 36(3): p. 369-379.

Velde, B., 1983. Infrared OH-stretch bands in potassic micas, talcs and saponites; influence of electronic configuration and site of charge compensation. American Mineralogist, 68(11-12): p. 1169-1173.

Zandanel, A., et al., 2002. Impacts of Crystalline Host Rock on Repository Barrier Materials at 250 °C: Hydrothermal Co-Alteration of Wyoming Bentonite and Steel in the Presence of Grimsel Granodiorite. Minerals, 12, DOI: 10.3390/min12121556.

Zviagina, B.B., et al., 2004. Interpretation of infrared spectra of dioctahedral smectites in the region of OH-stretching vibrations. Clays and Clay Minerals, 52(4): p. 399-410.

Part II. REACTION PRODUCTS

Introduction

It is expected a phase-analytical characterization of clay mineral phases in treated B25 bentonite, Opalinus Clay and Friedland Clay by X-ray diffraction (XRD) of bulk samples as powder specimen and for fraction < 2 µm as oriented specimen, by thermogravimetry of bulk sample (TG) and by transmission electron microscopy (TEM) for fraction < 2 µm. The treatment itself was carried out by GRS gGmbH in Braunschweig. The sample bodies were percolated by adapted Opalinus solution under different temperatures (35°C, 60°C, 100°C, 125°C, 150°C) and time intervals.

Specifically, for B25 bentonite: After the experiment, mostly three samples were investigated from each sample body – material from top position, from central part and from the bottom. The flow direction during the percolation was from the bottom to the top of the clay specimens.

Methodology, results, and graphs of measurements are summarized in separated supplements for all samples. These four supplements also contain the description of each applied method.

About selected mineralogical terms used in this report

Smectite (in senso of international classification)
→ ***Smectite*** (approached in this report)
  → montmorillonite
  → beidellite
  → beidellite-montmorillonite intergrowth (BM)
  …

→ ***Mixed-layer phases*** (approached in this report)
  → illite-smectite interstratification (IS-ml)*
    →beidellite-montmorillonite-illite interstratification (BMI-ml)
  → kaolinite-smectite-dioctahedral vermiculite interstratification (KSV-ml)
  …

* *term „IS-ml“: extended approach in senso of Środon et al., 1992*
  →normal charged:
    illite-smectite interstratification (IS-ml)
  →K- and/or charge deficit:
    dioctahedral vermiculite-smectite interstratification (diVS-ml)

The phase-analytical differential diagnostics of clay mineral matter, applied for this report, offer a more detailed view and discussion even to smectite-bearing intergrowths and interstratifications. The mineralogical terms applied in this report are presented and summarized here considering the framework of international classification for clay minerals.

Pure smectite minerals (e.g. montmorillonite, beidellite etc.) and smectite-bearing mixed-layer phases are summarized as members of term SMECTITE in senso of international classification of clay minerals. In result of investigation of B25 bentonite the connected occurrence of montmorillonite and beidellite was concluded. The distribution of these two smectite minerals in the measured particles is not clear: (i) vertically in *c*-axis as interstratification (= layer-by-layer) or (ii) horizontally in *ab*-axes more as intergrowth. In this report the term intergrowth is used so far only beidellite and montmorillonite which are members of measured particles.

Summary “Smectite behaviour”

Tab. I. *Overview about different smectite behaviour in all three sample-series*
(in direction of rising thermal load in experiments)

	B25 Bentonite	Friedland Clay	Opalinus Clay
Sum effect, mirrored by all dioctahedral particles (unclassified), measured by TEM			
tetrahedral Si	slight decreasing *(fig. 9)*	± constant *(at Si = 3.49 e phfu) (fig. 19)*	orig. vs treated: decreas. treatm.: ± constant *(at Si = 3.25 ± 0.05 e phfu)* *(fig. 26)*
Ca-smectite			
ratio in bulk sample	main phase *(tab. 1)*	minor phase, trace *(tab. 7)*	
smectite species	beidellite > montm. *((tab. 3))*	beidellite >> montm. *(tab. 9)*	
mass-% development	slight reduction *(from 35% to 25%) (fig. 2)*	± constant *(at 5% - 6%) (fig. 12)*	
%S-development	± constant *(at %S=70-100%) (tab. 3)*	± constant *(at %S=100%, available only ≤60°C) (tab. 9, fig. 14)*	
diVS-ml			
ratio in bulk sample	minor phase *(tab. 1)*	minor phase *(tab. 7)*	minor phase, trace *(tab. 13)*
smectite species	montm. >> beidellite *(tab. 4)*	montm. >> beidellite *(tab. 10)*	montm. >>> beidellite *(tab. 15)*
mass-% development	± stable *(variable 5% - 15%) (fig. 4)*	± stable *(variable 13%-16%) (fig. 12)*	%S=50%: destroyed %S=20%: no trend *(mass-% at 30% ±10%) (fig. 21)*
%S-development	reduction *(from 55% to 20%) (fig. 5)*	rising *(from 25% to 52%) (fig. 14)*	%S=50%: destroyed %S=20%: rising *(from 11% to 26%) (fig. 22)*
KS-ml			
ratio in bulk phase	minor phase *(tab. 1)*	minor phase *(tab. 7)*	minor phase *(tab. 13)*
smectite species	not to determine	not to determine	not to determine
mass-% development	rising *(< 2 µm: 25% → 45%) (fig. 7)*	± stable *(< 2 µm: variable at 10 %)* *(fig. 16)*	slight decreasing *(< 2 µm: 47% → 32%) (fig. 24)*
%S-development	rising *(< 2 µm: 45% → 70%) (fig. 8)*	± constant *(< 2 µm: ~50%) (fig. 17)*	± stable *(< 2 µm: at 40% ±8%) (fig. 25)*

Smectite is the main responsible mineralogical phase, which determines the swelling behaviour of clays and bentonites. In B25 bentonite and Friedland Clay, smectite is distributed in three different groups of smectite-bearing phases (Ca-smectite, diVS-ml, KS-ml), in Opalinus Clay only in two groups (diVS-ml, KS-ml). Each group has shown a specific behaviour during the experiments (tab. I).

The role played by the KS-ml phases shown is largely unclear. The analytical evidence is mostly only a result of the modelling of X-ray diffractograms (oriented specimen) and indirect evaluation of thermogravimetry in comparison to powder X-ray diffractometry.

In summary, in the experiments with increasing thermal load, sample B25 shows a slight 'illitization'. In contrast, the Friedland and Opalinus samples reveal largely stable, unchanged conditions.

1. Mineral matter in B25 bentonite

***Tab. 1.** Mineral matter of B25 bentonite (bulk sample)*

Sample	Ca-Smectite	diVS-ml	Illite (1M)	Illite (2M1)	Kaolinite + *KS-ml*	*Σ clay*	Quartz	K-feldspar	Plagioclase	Anhydrite	Cerussite	Analcime	Diaspore	Rutile + Anatase	Calcite	Natrolite	*Σ total*
B25 original	32%	10%	15%	17%	14%	*86%*	10%	2%	2%								*100%*
35°C, 93.6h, OPA																	
No4_T	37%	6%	10%	10%	7%	*70%*	12%	2%	12%	<1%		1%		1%	2%		*101%*
No4_C	34%	4%	18%	10%	7%	*73%*	13%	2%	9%	1%		<1%		<1%	2%		*97%*
No4_B	35%	5%	10%	10%	12%	*72%*	14%	3%	7%	1%		<1%		<1%	1%		*100%*
35°C, 285h, OPA.0.7 MPa																	
No23	28%	15%	8%	11%	15%	*77%*	14%	3%	4%	1%		<1%		<1%	1%		*100%*
60°C, 454h, OPA																	
No5_T	28%	3%	9%	10%	9%	*60%*	26%	3%	9%	1%				1%	2%		*100%*
No5_C	35%	3%	10%	10%	11%	*69%*	16%	2%	7%	2%		<1%	2%	1%	2%		*98%*
No5_B	28%	5%	22%	8%	6%	*68%*	16%	2%	8%	2%		<1%		1%	*1%		*100%*
100°C, 110h, OPA																	
No0_T	25%	11%	10%	10%	11%	*66%*	13%	4%	11%	2%	<1%	<1%		1%	*2%		*99%*
No0_C	26%	9%	14%	7%	13%	*69%*	9%	3%	12%	2%		<1%	2%	<1%	*2%	<1%	*100%*
No0_B	24%	12%	14%	7%	24%	*80%*	11%	2%	2%	1%	<1%	<1%		1%	<1%	2%	*100%*
100°C, 35d, OPA																	
No2_T	24%	12%	11%	10%	12%	*68%*	9%	3%	13%	2%		1%	<1%	1%	*2%	<1%	*100%*
No2_C	24%	15%	14%	9%	12%	*74%*	11%	2%	7%	1%		<1%	<1%	1%	*1%	<1%	*96%*
No2_B	30%	10%	9%	13%	14%	*74%*	10%	1%	8%	1%		<1%		<1%	1%	2%	*100%*
125°C, 98.6h, OPA																	
No15	31%	6%	20%	7%	12%	*76%*	11%	2%	5%	1%		1%	<1%	<1%	2%	2%	*100%*
150°C, 4d, OPA																	
No3_T	26%	14%	9%	9%	12%	*70%*	9%	3%	11%	1%		1%		<1%	*2%	<1%	*99%*
No3_C	21%	14%	13%	6%	12%	*65%*	8%	5%	12%	2%		<1%		1%	3%	<1%	*98%*
No3_B	20%	17%	7%	9%	13%	*66%*	10%	4%	14%	1%		1%		1%	2%	<1%	*99%*

***Legend:** Ca-Smectite – beidellite/montmorillonite-intergrowth; diVS-ml – IS-ml with K- and/or charge deficiency; * – including indications by TG for additional amount of amorphous calcium carbonate; standard deviation, absolute – see Supplement "XRD, powder"*

Smectite is mainly to find in B25 bentonite as beidellite-rich Ca-smectite and furthermore as montmorillonite in illite-smectite mixed layer phases with K- and/or charge deficiency (diVS-ml) and in kaolinite-smectite mixed layer phases. Further minor phases are illite, kaolinite, quartz, and feldspar. Compaction of bentonite material and the percolation and heating processes during the experiments cause traces of zeolites (analcime, natrolite), sulfates (anhydrite), carbonates (calcite – crystalline and probably also as amorphous calcite carbonate; cerussite), rutile, anatase as well as hydroxides (diaspore) (tab. 1). Generally, limit of detection of this applied Rietveld method is about 2 %. The here mentioned phases (tab. 1) with such low amount show in the samples their main peak not covered by possible sub-peaks of other verified phases.

A comparison of XRD-results with mass loss data from thermogravimetry measurements indicates the occurrence of an additional amorph phase, especially for samples from experiments at 60°C and 100°C. In these samples, the additional mass loss is mainly to find in temperature interval higher than 650°C in TG-measurement. This situation let assume amorph calcium carbonate (ACC) with 1-2% in marked samples (tab. 1).

Tab. 2. *B25 bentonite (original) composition – own measurement in comparison with literature*

B25 bentonite

	own results	Ufer et al., 2008	Kaufhold et al., 2012	Matschiavelli et al., 2019
Ca-smectite	32%	43.2%	61%	55%
diVS-ml	10%			
Illite_1M	15%			
Illite_2M1	17%	16.6%	17%	15%
Chlorite				
Kaolinite	14%	21.9%	4%	12%
Σ clay	***86%***	***82%***	***82%***	***82%***
Quartz	10%	13.2%	13%	10%
Orthoclase	2%	1.7%	5%	
Albite	2%	3.5%		3%
Pyrite				
Calcite				1%
Siderite				
Dolomite				4%
Rutile				1%
Gypsum				
Σ total	***100%***	***100%***	***100%***	***100%***

calculated DTA/TG-signal basing on XRD-results

mass loss 300-650°C	*XRD_calc*	*XRD_calc*	*XRD_calc*	*XRD_calc*	*mass loss (%)*
smectite (beidellite)	0.72%	0.98%	1.38%	1.24%	4.52
diVS-ml	0.43%				4.55
kaolinite	1.89%	3.04%	0.56%	1.67%	13.90
illite 1M	0.64%				4.41
mass loss 650-1000°C					
smectite (montm.)	0.76%	1.02%	1.45%	1.30%	4.74
illite 2M1	0.74%	0.73%	0.75%	0.66%	4.41
calcite				0.44%	44.00
dolomite				1.96%	48.99
					measured by TG
mass loss 300-650°C (%)	3.69%	4.02%	1.93%	2.91%	***3.72%***
mass loss 650-1000°C (%)	1.49%	1.76%	2.20%	4.36%	***1.47%***
mass loss 300-1000°C (%)	**5.18%**	**5.78%**	**4.13%**	**7.28%**	**5.19%**

Legend: *Ca-smectite – 50:50 beidellite-montmorillonite intergrowth; mass loss (%) – theoretical mass loss (in %) in thermogravimetry for 100% of certain phase used as basis unit to calculate the XRD_calc values for each by XRD detected phase*

Validation of B25 bentonite composition

The measured composition of original and uncompacted B25 bentonite is in a good agreement (tab. 2) with already published data from literature (Ufer et al, 2008; Kaufhold et al., 2012; Matschiavelli et al., 2019). Differences between here presented own measurements and literature references are to recognize in the amount of kaolinite, in listing of illite (1M) and summarizing of Ca-smectite and diVS-ml as total Ca-smectite in literature. Thermogravimetric investigations of B25 bentonite support the here reported results of kaolinite amount (tab. 2).

Generally, the here reported compositions of untreated and treated bentonite were verified by combination of following methods:

- TEM-EDX results, cross-checked by oriented specimen (XRD) after Sybilla-modelling of probability of smectite layers, also offer indications to the occurrence of beidellite
- XRD of powder samples (bulk) has been cross-checked by thermogravimetry using the mass loss to verify especially the XRD-results to kaolinite, indications to kaolinite-smectite mixed layer phases, and carbonates (see example: tab. 2).

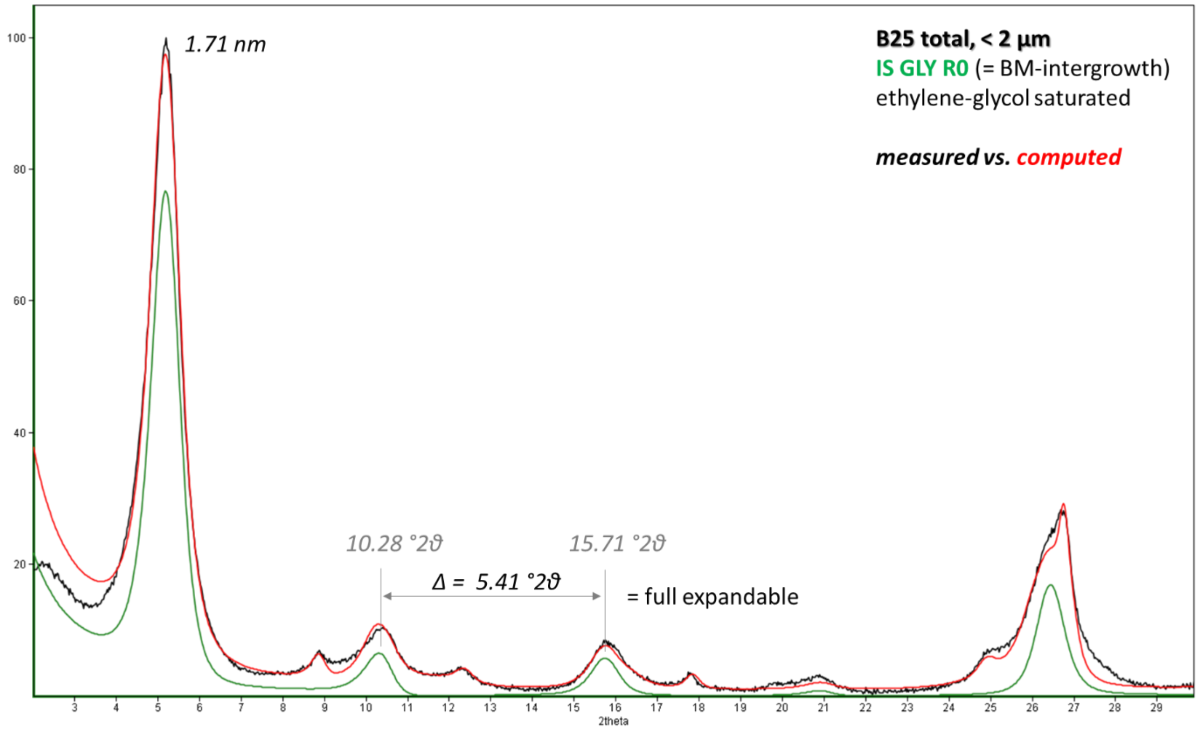

Fig. 1. *B25, original (< 2 µm) - X-ray diffraction pattern of the ethylene-glycol saturated oriented* ***specimen*** *(with computing of Ca-smectite by Sybilla-software – green line)*

Beidellite-rich Ca-Smectite

Identification by XRD: The X-ray diffraction pattern of the ethylene-glycol saturated oriented specimen shows a full expandability to 1.7 nm and a difference at 5.4° 2θ between 2. and 3. order of smectite interferences (fig. 1). This distance is typically for montmorillonite (Moore & Reynolds, 1989). An exception from this situation is drawn only by two samples (No 23 – 35°C, 0.7 MPa: %S = 80%; No 15 – 125°C: %S = 60%). Air dried oriented specimen show a (001)-interference at 1.41-1.56 nm and indicate a dominating Ca, Mg-occupation of interlayer space. Only sample No 15 (125°C) lets record this XRD-peak at 1.26 nm. This development could pronounce in this sample an interlayer occupation by mono-valent cations like Na or smectite with 1-water layer is under pressing the more typical 2-water layers.

Mineral formula by TEM-EDX and clustering: The full expandability of ethylene-glycol saturated oriented specimen let assume Si-values close to 4 per $(OH)_2$ O_{10} in computation of mineral formula basing on TEM-EDX-analyses but calculated were values between 3.47 - 3.78 e phuc. This situation is considered as intergrowth between beidellite (Si ~ 3.5), montmorillonite (Si ~ 4) and sometimes also in interstratification with illite (Si ~ 3.2).

Tab. 3. *Structural formulae for Ca-smectite B25 samples with estimation of beidellite-ratio*

		phase (low illite)	**mineral formula** *(clustering of TEM-EDX-results)*										**%S** *(XRD-oriented)*	**mass-%** *(XRD-oriented)*
			Ca	Mg	Na	K	Al	Fe^{3+}	Mg	Ti	Al	Si		
Original	B25_40µm	BMI 55:45:00	0.04	0.11	0.00	0.09	1.32	0.56	0.12	0.00	0.28	3.72	99%	47%
Orig., compacted	B25_repea	BMI 70:30:00	0.16	0.04	0.02	0.11	1.18	0.59	0.21	0.02	0.35	3.65		
OPA, 35°C	No4_T	BMI 100:00:00	0.08	0.12	0.01	0.14	1.00	0.92	0.08	0.01	0.50	3.50	100%	67%
	No4_C	BMI 100:00:00	0.15	0.06	0.05	0.21	0.95	0.88	0.15	0.01	0.53	3.47	100%	53%
	No4_B	BMI 80:20:00	0.17	0.01	0.00	0.07	1.02	0.83	0.22	0.00	0.41	3.59	100%	41%
OPA, 35°C, inj.	No23	BMI 35:45:20	0.11	0.08	0.00	0.09	1.24	0.59	0.17	0.01	0.31	3.69	82%	50%
OPA, 60°C	No5_T	BMI 65:35:00	0.05	0.12	0.00	0.09	1.28	0.60	0.11	0.01	0.33	3.67	100%	41%
	No5_C	BMI 65:35:00	0.07	0.11	0.00	0.05	1.12	0.77	0.10	0.01	0.33	3.67	100%	32%
		BMI 100:00:00	0.07	0.14	0.00	0.12	0.97	0.96	0.06	0.01	0.49	3.51		
	No5_B	BMI 85:15:00	0.08	0.00	0.22	0.33	0.96	0.74	0.30	0.01	0.42	3.58	100%	39%
OPA, 100°C	No0_T	BMI 55:45:00	0.08	0.09	0.00	0.06	1.27	0.58	0.14	0.01	0.28	3.72	99%	58%
	No0_C	BMI 50:45:05	0.12	0.08	0.00	0.07	1.24	0.57	0.18	0.01	0.29	3.71	94%	28%
	No0_B	BMI 70:30:00	0.18	0.04	0.01	0.10	1.18	0.60	0.22	0.01	0.34	3.66	100%	28%
OPA, 100°C	No2_T	BMI 70:30:00	0.09	0.10	0.00	0.11	1.24	0.61	0.15	0.00	0.34	3.66	100%	25%
		BMI 75:25:00	0.28	0.00	0.02	0.10	1.13	0.56	0.29	0.01	0.38	3.62		
	No2_C	BMI 65:35:00	0.10	0.07	0.01	0.12	1.23	0.59	0.17	0.01	0.33	3.67	100%	21%
	No2_B	BMI 45:55:00	0.15	0.05	0.00	0.03	1.26	0.52	0.22	0.00	0.22	3.78	100%	11%
		BMI 65:35:00	0.12	0.08	0.00	0.11	1.21	0.61	0.17	0.01	0.34	3.66		
		BMI 70:30:00	0.19	0.03	0.02	0.12	1.16	0.60	0.23	0.01	0.36	3.64		
		BMI 90:10:00	0.11	0.10	0.00	0.13	1.37	0.53	0.09	0.01	0.46	3.54		
		BMI 95:05:00	0.13	0.00	0.00	0.09	1.36	0.58	0.14	0.01	0.47	3.53		
OPA, 125°C	No15													
OPA, 150°C	No3_T	BMI 70:30:00	0.11	0.09	0.00	0.11	1.22	0.60	0.17	0.01	0.35	3.65	100%	26%
	No3_C	BMI 70:30:00	0.15	0.06	0.00	0.11	1.20	0.60	0.20	0.01	0.35	3.65	100%	38%
	No3_B	BMI 75:25:00	0.15	0.06	0.00	0.11	1.22	0.59	0.18	0.01	0.37	3.63	100%	40%

Legend: *BMI – beidellite-montmorillonite-illite; %S – probability of smectite layer; mass-% - result of Sybilla-modelling (oriented XRD) of fraction < 2 µm*

Beidellite-ratio in Ca-smectite is dominating in all samples. A BMI-ratio at 70:30:00 is commonly to observe. Samples No 23 (35°C) with a BMI-ratio of 35:40:20 and No 15 (125°C) without beidellite-dominated smectite (tab. 3) are again the only exceptions. The untreated Ca, Mg-smectite is characterized by high octahedral Fe^{3+} (0.56 per $(OH)_2$ O_{10}). This value is rising in all experimental samples, especially for reactions products of experiments at 35°C and 60°C (e.g. sample No4_T: 0.92 per $(OH)_2$ O_{10}). The calculated structural formulae (tab. 3) show variable tetrahedral Si-values (from 3.47 – 3.78 e phuc), but the full expandability is stable nearby in all samples.

Further indications for beidellite by FTIR: The FTIR spectroscopic analysis of B25 clay indicates that smectite is the dominant phase in this bentonite. The broad adsorption band at 3634 cm^{-1} (AlAlOH) is typical for Al-rich content of smectite (Madejova et al., 1996) and strongly associated with beidellites (Gate, 2005). Also, Fe is high present as FeFeOH (3557 cm^{-1} and 3577 cm^{-1}) (Zviagina et al., 2004). The two shoulders at 929 cm^{-1} in OH-bending region and 3646 cm^{-1} in OH-stretching region indicate the occurrence of beidellite (Gates, 2005). A band at ~693 cm^{-1} shared with quartz is also assigned to Si-O in a ferruginous beidellite (Decarreau et al., 1992).

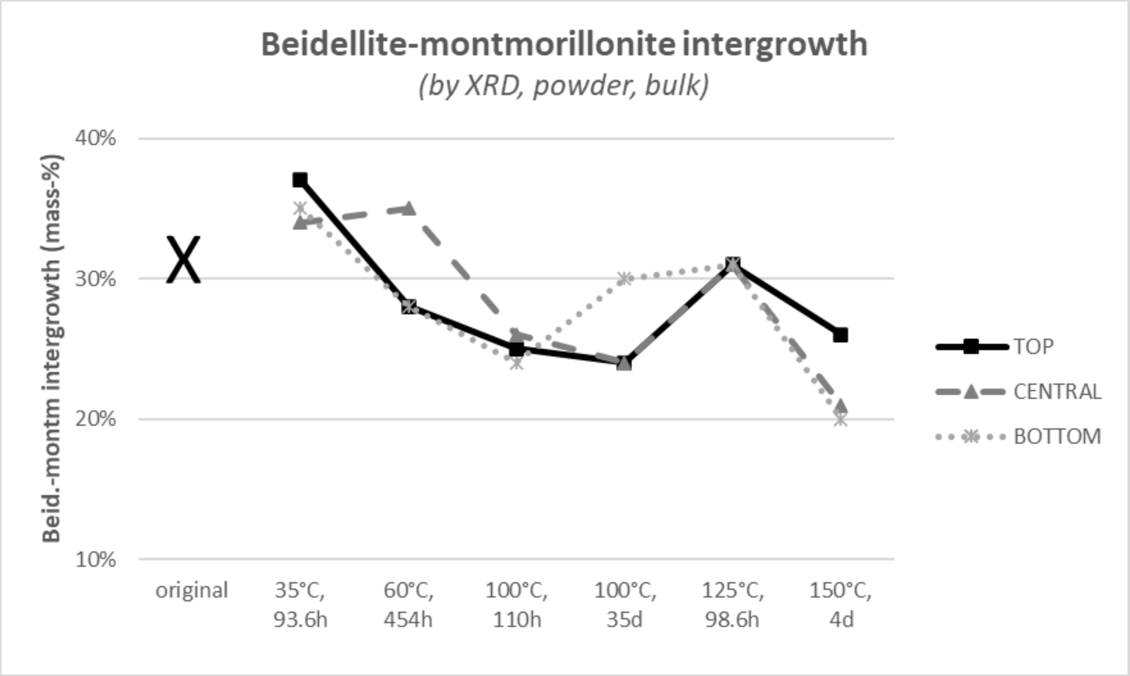

Fig. 2. *Mass distribution of Ca-smectite in bulk samples of B25 bentonite*
Note: *Sample No 15 (125°C) is only a single sample (without separation in top, central and bottom)*

Development of mass-distribution: Ca-smectite shows a trend to a slight mass reduction with increasing thermal load (fig. 2) from 35% in direction to 25%.

Special development in sample No15 (and partially also in sample No2_B): Sample No15 contains in the bulk material 31% Ca-smectite (proofed by XRD powder- & TG-measurements and Profex-processing). So, a remarkable amount of Ca-smectite with %S=100% should occur in fraction < 2 µm of sample No15. But XRD of oriented specimen for fraction < 2 µm of No15 shows only 10 % with %S = 60% (and further diVS-ml with 24% at %S=28%) (tab. 5). The data of oriented XRD are in good agreement with TEM & clustering. That means now, sample No15 has not in fraction < 2 µm the expected full expandable smectite, but 31% Ca-smectite in bulk powder sample. This situation between composition of bulk sample and material < 2 µm let assume that Ca-smectite is underwent a further process in this temperature level of experiments (125°C). In HTMC-experiments, smectite aggregates can filled by precipitated Si, which was dissolved before from smectite particles. In case of a low Si-dissolution rate, dissolved Si is transported away by flow of solution. In case of an increased Si-dissolution rate, the amount of dissolved Si is too high for the transport alone by flow of solution. The result of that is filling of smectite aggregates by precipitated Si-gel. Theses aggregates are “glued”. The grain size separation of bulk material into fraction < 2 µm by sedimentation (for XRD-measurement on oriented specimen) is not involving now the larger smectites aggregates solidified by before dissolved Si. So, such smectite aggregates occur only in a reduced amount or are missing (like in sample No15) than in fraction < 2 µm.

A similar development of reduced amount of full expandable smectite could be observed in sample No2_B (100°C). This sample is characterized by 30 % Ca-smectite in bulk material (tab. 1) and only 11% full expandable phases in fraction < 2 µm (tab. 5).

How is it possible to verify this assumed process? The bulk material is to separate in few fractions and each fraction is to measure by XRD (randomly oriented) related to distribution of Ca-smectite. An enrichment of Ca-smectite in fractions larger 2 µm should be to expect.

Identification by XRD: The X-ray diffraction pattern of the ethylene-glycol saturated oriented specimen draw a further group of swelling. The difference between 2. and 3. order of smectite interferences is variable representing smectite layer probabilities (%S) between 8 - 60% (%S_{mean} = 30-35%) (tab. 4). The smectite layer probability (%S) of uncompacted original B25 bentonite is to find at %S = 55% (fig. 3).

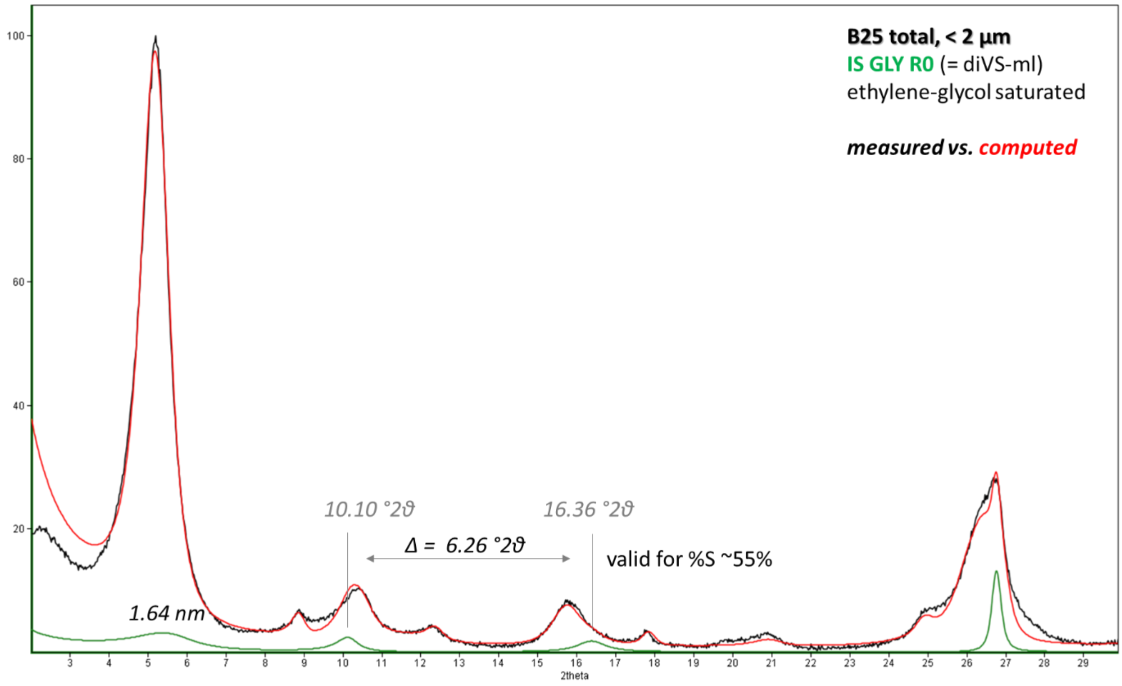

Fig. 3. *B25, original (< 2 µm) - X-ray diffraction pattern of the ethylene-glycol saturated oriented specimen (with computing of diVS-ml by Sybilla-software – green line)*

Tab. 4. *Structural formulae for diVS-ml phases in B25 samples with estimation of beidellite-ratio*

		phase (high illite)	mineral formula (clustering of TEM-EDX-results)										%S (XRD-oriented)	mass-% (XRD-oriented)
			Ca	Mg	Na	K	Al	Fe^{3+}	Mg	Ti	Al	Si		
Original	B25_40µm	BMI 00:55:45	0.13	0.05	0.01	0.12	1.22	0.56	0.21	0.00	0.29	3.71	55%	16%
Orig., compacted	B25_repeat	BMI 00:25:75	0.11	0.06	0.01	0.29	1.35	0.50	0.14	0.01	0.51	3.49		
OPA, 35°C	No4_T	BMI 00:30:70	0.03	0.01	0.05	0.62	1.10	0.66	0.22	0.02	0.54	3.46	30%	11%
	No4_C	BMI 10:30:60	0.13	0.05	0.26	0.35	0.77	0.77	0.44	0.01	0.54	3.46	38%	19%
	No4_B	BMI 10:30:60	0.15	0.09	0.00	0.16	0.95	0.92	0.12	0.01	0.55	3.45	38%	15%
OPA, 35°C	No23	BMI 00:40:60	0.32	0.00	0.00	0.14	1.03	0.56	0.40	0.01	0.41	3.59	45%	13%
		BMI 20:25:55	0.13	0.03	0.04	0.35	1.35	0.46	0.20	0.01	0.54	3.46		
OPA, 60°C	No5_T	BMI 05:35:60	0.05	0.13	0.00	0.29	1.24	0.63	0.11	0.02	0.56	3.44	33%	14%
	No5_C	BMI 20:20:60	0.05	0.10	0.00	0.34	1.18	0.72	0.08	0.02	0.58	3.42	39%	18%
	No5_B	BMI 40:15:45	0.13	0.00	0.22	0.38	0.84	0.85	0.30	0.01	0.57	3.43	55%	17%
OPA, 100°C	No0_T	BMI 00:35:65	0.09	0.11	0.00	0.16	1.18	0.67	0.14	0.02	0.43	3.57	30%	8%
	No0_C	BMI 00:30:70	0.10	0.10	0.00	0.17	1.30	0.57	0.12	0.01	0.46	3.54	30%	13%
	No0_B	BMI 00:25:75	0.22	0.04	0.02	0.19	1.12	0.63	0.24	0.01	0.51	3.49	25%	19%
OPA, 100°C	No2_T	BMI 00:25:75	0.12	0.05	0.01	0.34	1.39	0.45	0.17	0.00	0.52	3.48	20%	20%
	No2_C	BMI 00:25:75	0.08	0.10	0.01	0.26	1.27	0.59	0.13	0.02	0.53	3.47	23%	11%
	No2_B	BMI 00:30:70	0.18	0.02	0.01	0.27	1.23	0.53	0.21	0.03	0.49	3.51	8%	23%
OPA, 125°C	No15	BMI 05:55:40	0.15	0.05	0.03	0.11	1.19	0.60	0.21	0.01	0.35	3.65	60%	10%
		BMI 00:25:75	0.11	0.07	0.03	0.28	1.26	0.55	0.16	0.03	0.54	3.46	28%	24%
OPA, 150°C	No3_T	BMI 00:25:75	0.10	0.16	0.00	0.11	1.06	0.85	0.08	0.00	0.53	3.47	22%	11%
	No3_C	BMI 00:25:75	0.10	0.07	0.00	0.31	1.37	0.47	0.14	0.02	0.52	3.48	22%	10%
	No3_B	BMI 00:30:70	0.31	0.01	0.00	0.15	1.08	0.60	0.31	0.01	0.46	3.54	27%	9%

Legend: *BMI – beidellite-montmorillonite-illite; %S – probability of smectite layer*

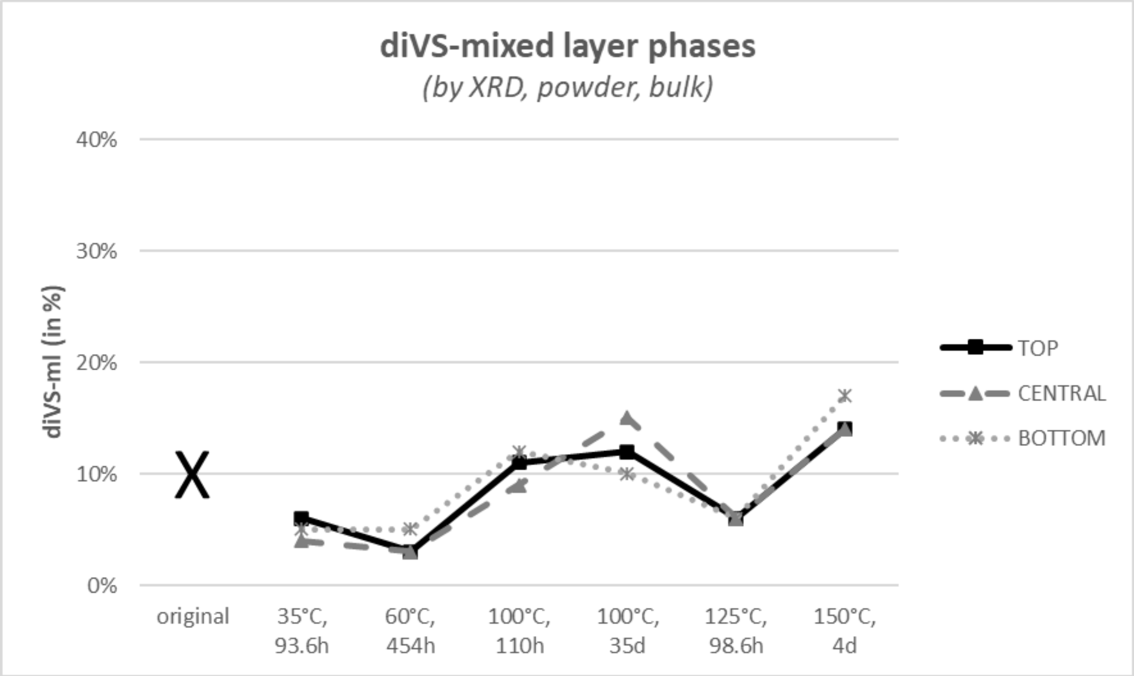

Fig. 4. *Mass distribution of diVS-ml in bulk samples of B25 bentonite*
Note: *Sample No 15 (125°C) is only a single sample (without separation in top, central and bottom)*

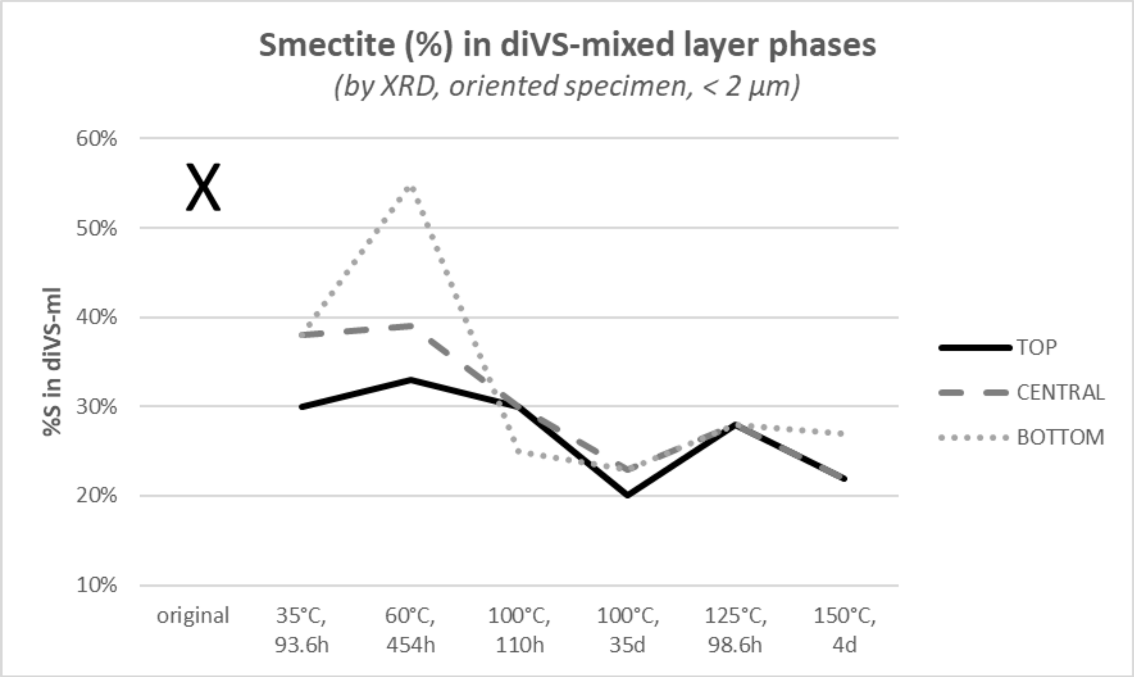

Fig. 5. *Smectite layer probability of diVS-ml in fraction < 2 µm of B25 bentonite*
Note: *Sample No 15 (125°C) is only a single sample (without separation in top, central and bottom)*

***Tab. 5.** Mineral matter of B25 bentonite (< 2 µm) – oriented specimen*

Sample	Beidellite-Montm. intergrowth	diVS-ml	Illite	Kaolinite	Kaolinite-Smectite-ml *(KS GL R1)*	Kaolinite-Smectite-ml *(KS GL R0)*	*Σ total*
B25 original	47% *(%S = 99%)*	16% *(%S = 55%)*	9%	5%	23% *(%S = 45%)*		*100%*
35°C, 93.6h, OPA							
No4_T	67% *(%S = 100%)*	11% *(%S = 30%)*	10%	5%		7% *(%S = 58%)*	*100%*
No4_C	53% *(%S = 100%)*	19% *(%S = 38%)*	6%	2%		21% *(%S = 65%)*	*101%*
No4_B	41% *(%S = 100%)*	15% *(%S = 38%)*	11%	6%		27% *(%S = 62%)*	*100%*
35°C, 285h, OPA, 0.7 MPa							
No23	50% *(%S = 82%)*	13% *(%S = 45%)*	10%	6%		22% *(%S = 57%)*	*101%*
60°C, 454h, OPA							
No5_T	41% *(%S = 100%)*	14% *(%S = 33%)*	8%	5%		31% *(%S = 61%)*	*99%*
No5_C	32% *(%S = 100%)*	18% *(%S = 39%)*	8%	6%		37% *(%S = 65%)*	*101%*
No5_B	39% *(%S = 100%)*	17% *(%S = 55%)*	13%	8%		23% *(%S = 65%)*	*100%*
100°C, 110h, OPA							
No0_T	58% *(%S = 99%)*	8% *(%S = 30%)*	20%	3%	12% *(%S = 45%)*		*101%*
No0_C	28% *(%S = 94%)*	13% *(%S = 30%)*	4%	7%	44% *(%S = 75%)*	4% *(%S = 48%)*	*100%*
No0_B	28% *(%S = 100%)*	19% *(%S = 25%)*	9%	8%	11% *(%S = 76%)*	25% *(%S = 58%)*	*100%*
100°C, 35d, OPA							
No2_T	25% *(%S = 100%)*	20% *(%S = 20%)*	2%	7%	37% *(%S = 79%)*	8% *(%S = 48%)*	*99%*
No2_C	21% *(%S = 100%)*	11% *(%S = 23%)*	3%	7%	47% *(%S = 78%)*	12% *(%S = 48%)*	*101%*
No2_B	11% *(%S = 100%)*	8% *(%S = 23%)*	11%	10%	51% *(%S = 75%)*	12% *(%S = 48%)*	*101%*
125°C, 98.6h, OPA							
No15	10% *(%S = 60%)*	24% *(%S = 28%)*	14%	18%	34% *(%S = 75%)*		*100%*
150°C, 4d, OPA							
No3_T	26% *(%S = 100%)*	11% *(%S = 22%)*	5%	6%	39% *(%S = 74%)*	13% *(%S = 48%)*	*100%*
No3_C	38% *(%S = 100%)*	10% *(%S = 22%)*	4%	6%	27% *(%S = 76%)*	16% *(%S = 48%)*	*101%*
No3_B	40% *(%S = 100%)*	9% *(%S = 27%)*	3%	5%	30% *(%S = 78%)*	13% *(%S = 48%)*	*100%*

***Legend:** diVS-ml – IS-ml with K- and/or charge deficiency; %S – probability of smectite layers*

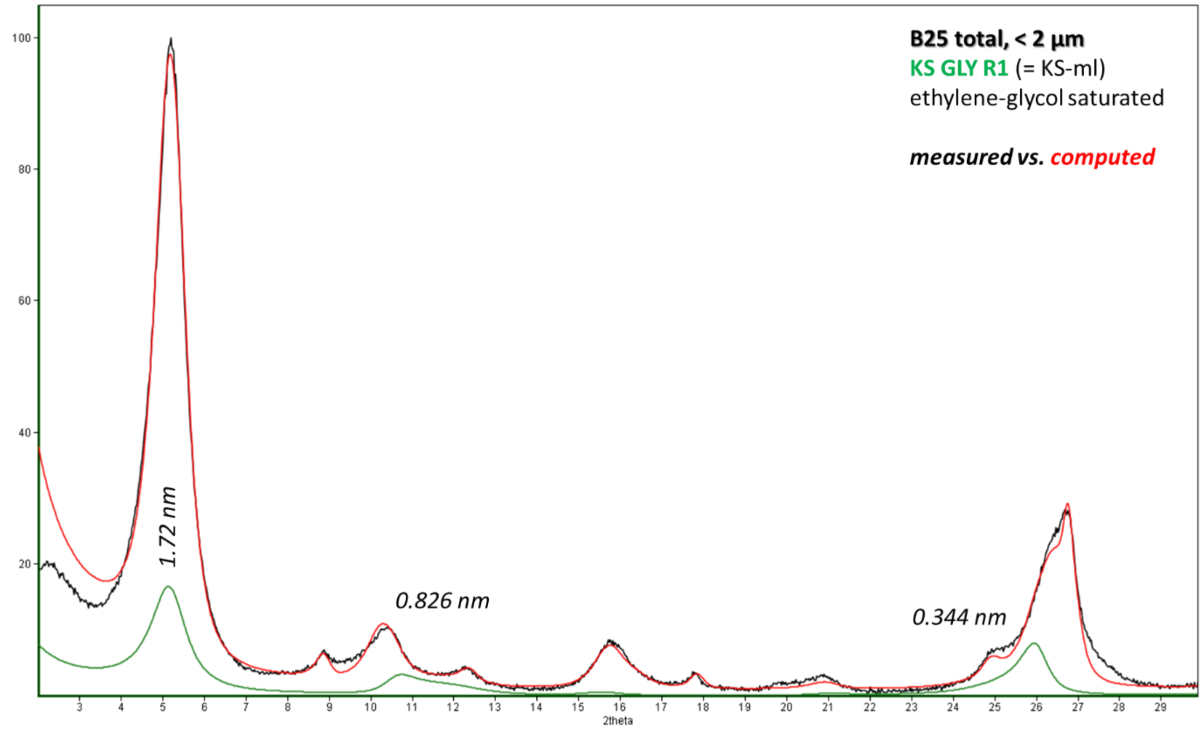

***Fig. 6.** B25, original (< 2 µm) - X-ray diffraction pattern of the ethylene-glycol saturated oriented specimen (with computing of KS-ml by Sybilla-software – green line)*

Mineral formula by TEM-EDX and clustering: The cross-checking between phases with limited expandability using ethylene-glycol saturated oriented specimen and TEM-EDX-data (incl. clustering) shows illite-smectite mixed layer phase with K- and charge deficiency. For these phases, montmorillonite is the dominating smectite component. Beidellite occurs in diVS-ml only in few samples in traces (only exception: sample No 5_B with BMI 40:15:45) (tab. 4). That means, reduced tetrahedral Si-values after experiments are linked with reduced swelling properties by a higher illite layer probability (%I).

Development of mass-distribution: diVS-ml phases show with increasing thermal load a slight variable mass distribution close to the original composition (fig. 4).

Development of expandability: diVS-ml phases in B25 bentonite draw with increasing thermal load a remarkable reduction of smectite layer probability from %S=55% (original B25) to close to 20% (150°C) (fig. 5).

Kaolinite-Smectite Mixed-Layer (KS-ml)

Identification by XRD: The occurrence of kaolinite-smectite mixed layer is mainly indicated by modelling of XRD-pattern of oriented specimen using Sybilla-software (developed by Chevron Inc.: Aplin et al., 2006) (tab. 5; fig. 6). Few particles, measured by TEM-EDX, indicated KS-ml phases, but it was not possible to calculate a valid structural formula.

Development of mass-distribution: KS-ml phases in fraction < 2 µm show as trend with increasing thermal load a rising ratio to the original composition (fig. 7).

Development of expandability: KS-ml phases in B25 bentonite (< 2 µm) draw with increasing thermal load a rising smectite layer probability from %S=45% (original B25) to close to 70% (150°C) (fig. 8).

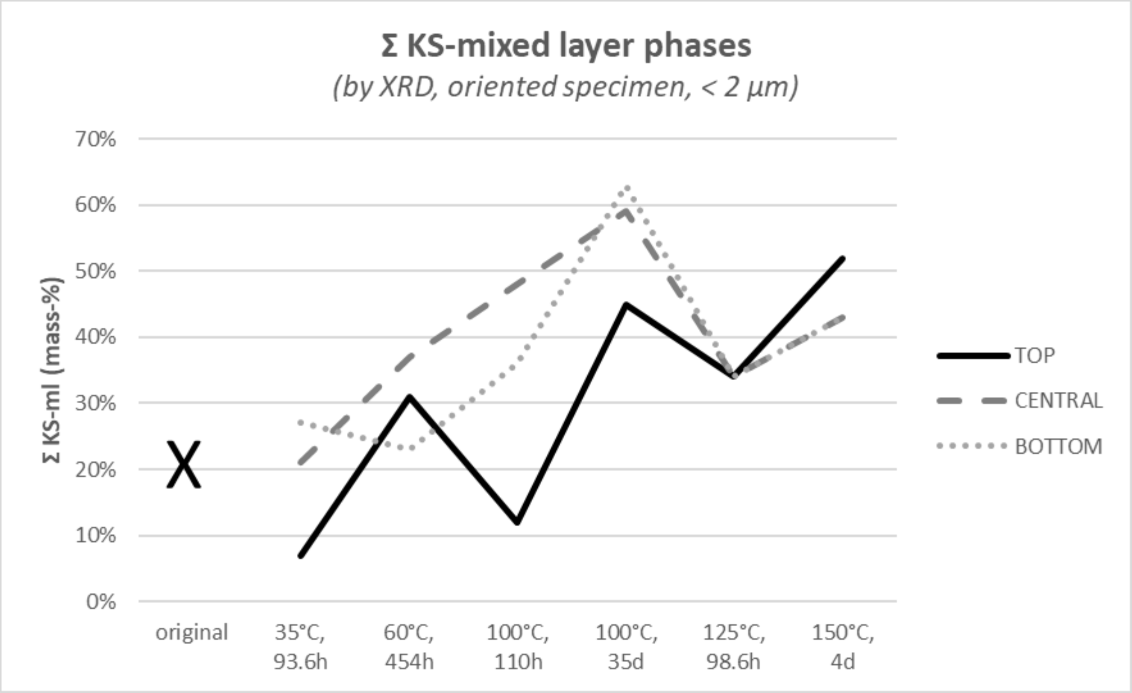

Fig. 7. *Mass distribution of KS-ml in samples of B25 bentonite (< 2 µm)*

Note: *Sample No 15 (125°C) is only a single sample (without separation in top, central and bottom)*

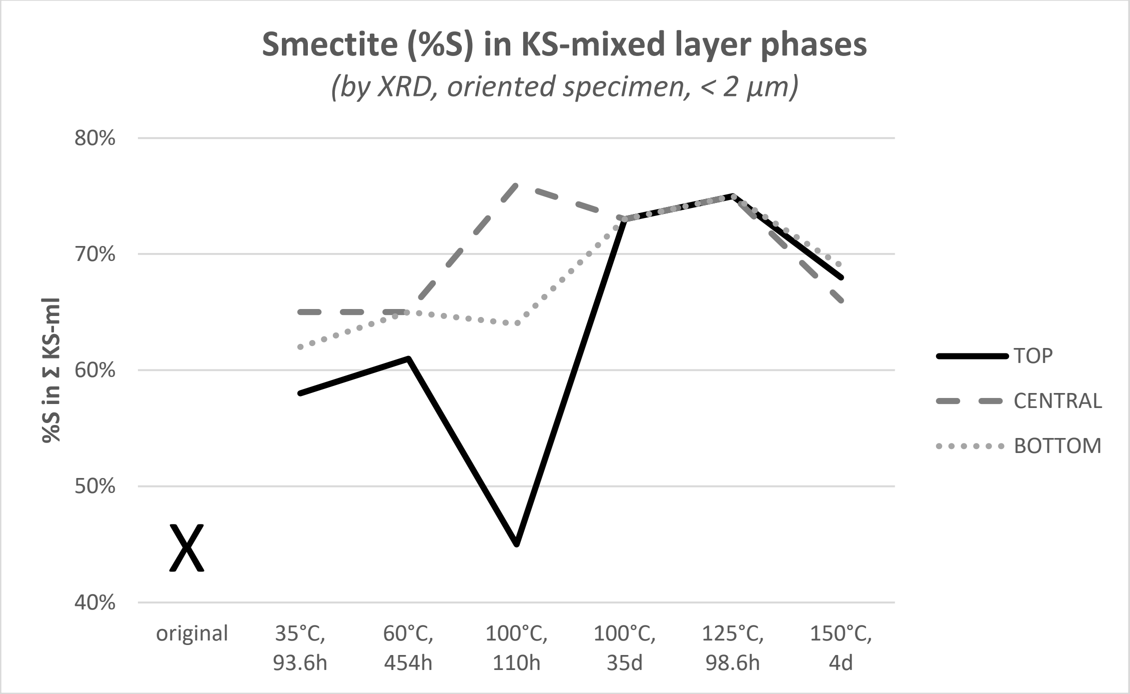

Fig. 8. *Smectite layer probability of KS-ml in fraction < 2 µm of B25 bentonite*

Note: *Sample No 15 (125°C) is only a single sample (without separation in top, central and bottom)*

Smectite-behaviour in experiments

Smectite is the main responsible mineralogical phase, which determines the swelling behaviour of bentonite. In B25 bentonite, smectite is distributed in three different groups of phases (Ca-smectite, diVS-ml, KS-ml). Each group has shown a specific behaviour during the experiments (tab. 6).

Tab. 6. *B25 – Overview about different smectite behaviour*

	role of phase in bulk sample	smectite species	mass-% development	%S-development	assumptions to expandab.
Ca-smectite	main phase *(tab. 1)*	beidellite > montm. *(tab. 3)*	slight reduction *(from 35% to 25%)* *(fig. 2)*	± constant *(at %S=70-100%)* *(tab. 3)*	slight impact for reduction
diVS-ml	minor phase *(tab. 1)*	montm. >> beidellite *(tab. 4)*	± stable *(variable 5% - 15%)* *(fig. 4)*	reduction *(from 55% to 20%)* *(fig. 5)*	slight impact for reduction
KS-ml	minor phase *(tab. 1)*	not to determine	rising *(< 2 µm: 25% → 45%)* *(fig. 7)*	rising *(< 2 µm: 45% → 70%)* *(fig. 8)*	increasing

(in direction of rising thermal load in experiments)

The summarizing impact of Ca-smectite together with diVS-ml on expandability is mirrored by TEM-EDX-measurements (fig. 9). The original material shows the highest tetrahedral Si-value per $(OH)_2$ O_{10} with Si = 3.72. The first Si-downfall at 35°C is caused by the beidellitization of Ca-smectite (tab. 3) (see BMI at 100:00:00). The expandability should be not limited at 35°C.

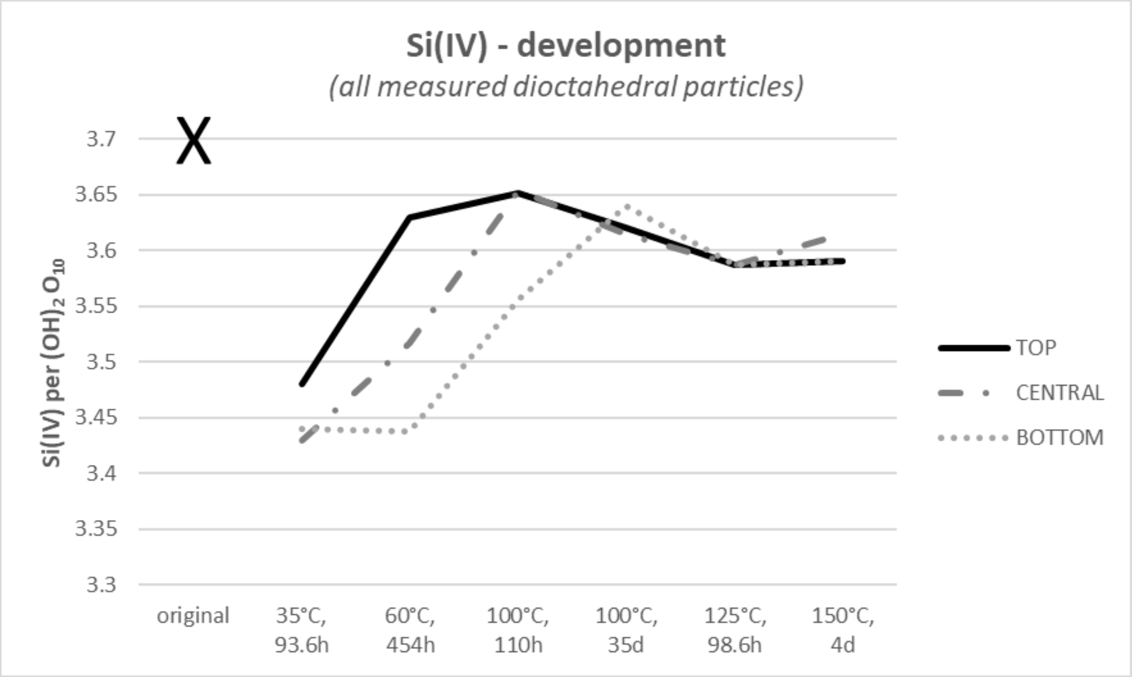

Fig. 9. *Behaviour of tetrahedral Si per $(OH)_2$ O_{10} in fraction < 2 µm of B25 bentonite*

Note: *Sample No 15 (125°C) is only a single sample (without separation in top, central and bottom); KS-ml not included here*

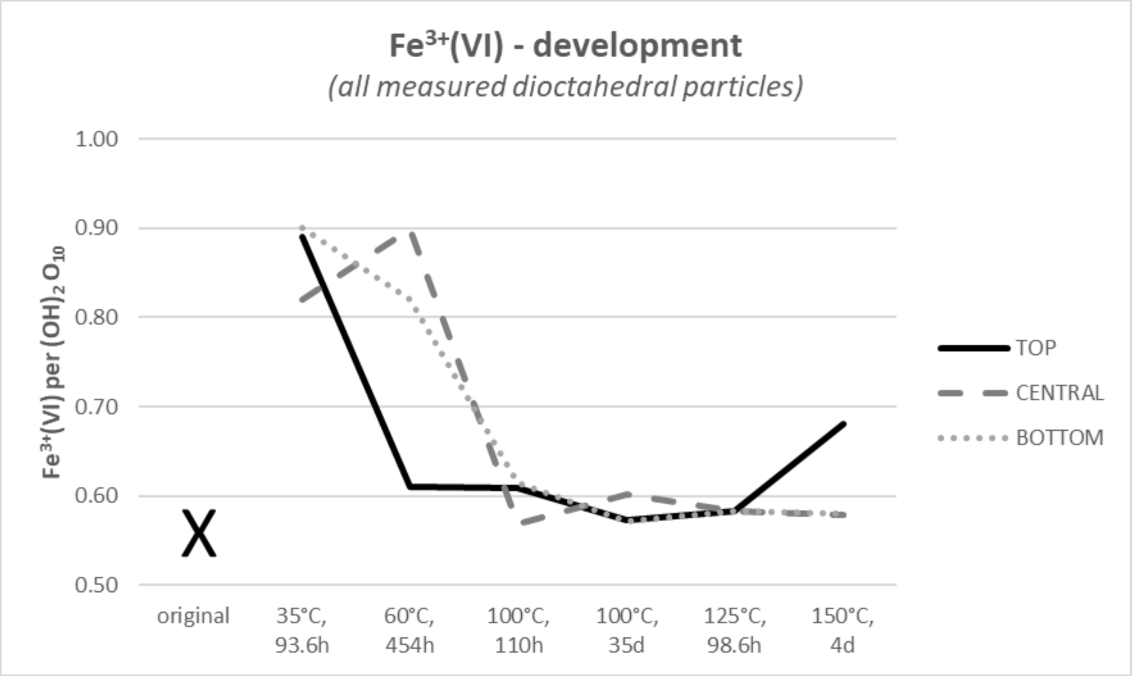

Fig. 10. *Development of octahedral Fe^{3+} per $(OH)_2$ O_{10} in fraction < 2 µm of B25 bentonite*

Note: *Sample No 15 (125°C) is only a single sample (without separation in top, central and bottom); KS-ml not included here*

This beidellitization of Ca-smectite at 35°C is linked with a very high octahedral Fe^{3+}-amount (> 0.8 per $(OH)_2$ O_{10}) (fig. 10) and a reduced octahedral Al (~ 1.0 per $(OH)_2$ O_{10}) (tab. 3). The degree of this beidellitization is lower at temperatures higher than 35°C with a BMI in average ~70:30:00 (tab. 3), but the “illitization” of diVS-ml started now (fig. 5). A reduction of expandability could be expected.

The additional contribution of KS-ml on expandability of the total sample is not really to evaluate. The rising mass of KS-ml (< 2 µm) by higher thermal load during the experiments (tab. 6; fig. 7) and the even rising smectite layer probability (tab. 6; fig. 8) let assume a certain degree of compensation of expected lost expandability by Ca-smectite and diVS-ml.

TEM-EDX: Illite-behaviour in experiments

Only few particles of illite could be measured in fraction < 2 µm by TEM-EDX. Because of these low numbers of measured illite particles, the following messages are not full valid by statistics.

The available TEM-EDX-measurements indicate the occurrence of two illite groups: (i) Al(VI)-rich with a low to moderate K-deficit and (ii) Fe(VI)-rich ($\geq$ 0.9 per $(OH)_2\,O_{10}$) with a high K-deficit (tab. Illite_B25). Both groups are not to distinguish in all samples by clustering because of often low numbers of illite particles. The octahedral Fe seems to substitute Al in a certain degree in both groups in experiments ≤ 60°C. The opposite development in octahedral Al/Fe-ratio (again Fe-reduction) is to observe in experiments > 60°C. This observed variable result concerning illite could represented by alteration of composition, but also by degradation of larger illite particles than feeding the fraction < 2 µm.

	Ca (XII)	Mg (XII)	Na (XII)	K (XII)	Cr3+ (VI)	Al (VI)	Fe3+ (VI)	Mg (VI)	Ti (VI)	Al (IV)	Si (IV)	XII	n_VI	%S	K-deficit	charge-deficit
B25 original																
Cluster2 *(n=3)*	0.06	0.03	0.03	0.56	0.00	1.55	0.33	0.11	0.01	0.69	3.31	0.79	2.0	10	43%	7%
Cluster4 *(n=2)*	0.07	0.28	0.00	0.19	0.00	0.99	0.90	0.11	0.00	0.78	3.22	0.88	2.0	4	80%	-2%
B25 treated																
No4_T *35°C, 93.6h*																
Cluster2 *(n=6)*	0.01	0.03	0.08	0.71	0.00	1.28	0.60	0.10	0.01	0.78	3.22	0.87	2.0	4	24%	0%
No4_C *35°C, 93.6h*																
Cluster4 *(n=6)*	0.09	0.06	0.12	0.51	0.00	1.18	0.56	0.25	0.02	0.70	3.30	0.93	2.0	9	48%	-10%
No4_B *35°C, 93.6h*																
Cluster1 *(n=6)*	0.10	0.02	0.03	0.61	0.00	1.24	0.60	0.13	0.03	0.75	3.25	0.87	2.0	4	34%	0%
Cluster3 *(n=7)*	0.15	0.16	0.00	0.18	0.00	0.59	1.28	0.06	0.06	0.80	3.20	0.80	2.0	4	81%	7%
No5_T *60°C, 454h*																
Cluster1 *(n=3)*	0.03	0.25	0.00	0.35	0.00	0.88	0.95	0.10	0.07	0.87	3.13	0.90	2.0	0	61%	-2%
No5_C *60°C, 454h*																
Cluster3 *(n=8)*	0.08	0.23	0.00	0.18	0.00	0.57	1.29	0.10	0.04	0.75	3.25	0.81	2.0	6	81%	5%
Cluster5 *(n=6)*	0.03	0.05	0.00	0.59	0.00	1.13	0.72	0.13	0.03	0.68	3.32	0.77	2.0	11	41%	8%
No5_B *60°C, 454h*																
Cluster1 *(n=27)*	0.13	0.01	0.19	0.44	0.00	0.93	0.81	0.25	0.01	0.68	3.32	0.91	2.0	11	56%	-9%
No0_T *100°C, 110h*																
Cluster2 *(n=3)*	0.07	0.17	0.02	0.25	0.00	1.15	0.72	0.11	0.02	0.67	3.33	0.76	2.0	12	75%	9%
No0_C *100°C, 110h*																
Note: no illite detected																
No0_B *100°C, 110h*																
Cluster1 *(n=3)*	0.17	0.07	0.02	0.30	0.00	1.51	0.38	0.11	0.00	0.69	3.31	0.80	2.0	10	69%	5%
Cluster4 *(n=2)*	0.14	0.22	0.03	0.15	0.00	0.79	1.00	0.21	0.01	0.70	3.30	0.90	2.0	9	84%	-6%
No2_T *100°C, 35d*																
Cluster1 *(n=4)*	0.04	0.11	0.01	0.44	0.00	1.36	0.53	0.10	0.02	0.66	3.34	0.75	2.0	13	57%	10%
No2_C *100°C, 35d*																
Cluster1 *(n=4)*	0.07	0.24	0.02	0.28	0.00	0.92	0.82	0.24	0.02	0.69	3.31	0.91	2.0	10	72%	-9%
No2_B *100°C, 35d*																
Note: no illite detected																
No15 *125°C, 98.6h*																
Cluster2 *(n=9)*	0.07	0.08	0.02	0.49	0.00	1.35	0.51	0.13	0.01	0.70	3.30	0.81	2.0	9	50%	4%
No3_T *150°C, 4d*																
Cluster1 *(n=4)*	0.08	0.12	0.00	0.31	0.00	1.13	0.81	0.06	0.00	0.67	3.33	0.73	2.0	12	69%	13%
No3_C *150°C, 4d*																
Cluster2 *(n=4)*	0.07	0.10	0.09	0.43	0.00	1.39	0.49	0.11	0.01	0.75	3.25	0.85	2.0	6	55%	2%
No3_B *150°C, 4d*																
Cluster2 *(n=1)*	0.08	0.13	0.00	0.27	0.00	1.74	0.25	0.00	0.01	0.73	3.27	0.69	2.0	7	72%	19%

Tab. Illite_B25. *B25 bentonite: Illite in fraction < 2 µm (by TEM-EDX)*

Legend: *(n=3) – number of illite particles measured by TEM-EDX; XII – interlayer charge; n_VI – number of atoms in octahedral layer per $(OH)_2\ O_{10}$; %S – probability of smectite layers in senso of Środon et al. (1992); K-deficit, charge-deficit – in senso of Środon et al. (1992) (normal K in illite = 0.89 per $(OH)_2\ O_{10}$)*

"Top – Central – Bottom" - Development of Reactions

The flow direction of adapted Opalinus solution during the experiments was arranged from bottom to top. Differences are only to observe in short term experiments for ≤ 100°C (figs. 9, 10). The Si-behaviour (fig. 9) mirrors probably a beidellitization of Ca-smectite (alteration into pure beidellite) (tab. 3) with a highest impact at the bottom area. This process is accompanied by enrichment of octahedral Fe (tab. 10), especially to see in experiment at 60°C.

2. Mineral matter in Friedland Clay

***Tab. 7**. Mineral matter of Friedland Clay-series (bulk sample)*

Sample	Ca-Smectite	IS-ml	Illite (1M)	Illite (2M1)	Chlorite	Kaolinite + *KS-ml*	*Σ clay*	Quartz	K-feldspar	Plagioclase	Pyrite	Calcite	Anatase	*Σ total*
orig., compact. **No19**	5% *(±0.9)*	14% *(±0.3)*	34% *(±0.9)*	6% *(±0.3)*	3% *(±0.3)*	16% *(±0.6)*	78%	15% *(±0.6)*	3% *(±0.2)*	3% *(±0.2)*	<1% *(±0.1)*		1% *(±0.1)*	*100%*
35°C, 46.3h, OPA **No10**	6% *(±0.3)*	13% *(±1.6)*	26% *(±0.7)*	7% *(±0.3)*	6% *(±0.6)*	11% *(±0.5)*	69%	22% *(±0.8)*	5% *(±0.3)*	3% *(±0.2)*	<1% *(±0.1)*	*<1% *(±0.1)*	1% *(±0.1)*	*100%*
60°C, 45.9h, OPA **No11**	5% *(±0.5)*	13% *(±0.4)*	28% *(±0.9)*	8% *(±0.3)*	5% *(±0.6)*	15% *(±0.6)*	73%	17% *(±0.8)*	5% *(±0.3)*	3% *(±0.2)*	<1% *(±0.1)*	*	1% *(±0.1)*	*100%*
100°C, 40h, OPA **No16**	6% *(±0.8)*	16% *(±0.6)*	26% *(±0.6)*	8% *(±0.2)*	5% *(±0.4)*	15% *(±0.5)*	75%	16% *(±0.5)*	4% *(±0.3)*	3% *(±0.2)*	<1% *(±0.1)*	*<1% *(±0.2)*	1% *(±0.1)*	*100%*
125°C, 40h, OPA **No20**	3% *(±0.6)*	16% *(±1.0)*	33% *(±1.0)*	7% *(±0.4)*	8% *(±0.8)*	12% *(±0.8)*	78%	15% *(±0.9)*	3% *(±0.2)*	3% *(±0.3)*	<1% *(±0.1)*		1% *(±0.1)*	*100%*
150°C, 68.3 h, OPA **No21**	8% *(±1.6)*	13% *(±0.5)*	30% *(±1.2)*	7% *(±0.4)*	3% *(±0.6)*	16% *(±0.8)*	76%	16% *(±0.5)*	3% *(±0.2)*	4% *(±0.3)*	<1% *(±0.1)*		1% *(±0.1)*	*100%*
without transport cell														
100°C, OPA **No12**	7% *(±0.4)*	7% *(±0.5)*	29% *(±0.9)*	8% *(±0.4)*	4% *(±0.6)*	18% *(±0.7)*	73%	19% *(±0.5)*	4% *(±0.3)*	3% *(±0.3)*	<1% *(±0.1)*	<1% *(±0.1)*	1% *(±0.1)*	*100%*

***Legend:** * - including indications by TG for additional amount of amorphous calcium carbonate; (±0.1) – standard deviation, absolute*

Smectite is mainly to find in Friedland Clay-series in illite-smectite mixed layers (a minor phase) with K- and/or charge deficiency (diVS-ml) and in Ca-smectite as well as kaolinite-smectite mixed layer phases (both are trace phases). Smectite in diVS-ml phases shows only a slight ratio of beidellite. Moreover, in Ca-smectite, beidellite is the dominating smectite component.

The main phase in Friedland Clay is illite accompanied by kaolinite and quartz as further minor phases. In traces, the Friedland Clay also contains chlorite, feldspar, pyrite, calcite and anatase. Calcite occurs as crystalline calcite and probably also as amorphous calcite carbonate. Compaction of clay material and the percolation and heating processes during the experiments don't cause any mineralogical neoformations (tab. 7).

Validation of Friedland Clay composition by literature

The validation of own Friedland Clay measurements with data from literature is difficult. The open cast mining company of deposit "Siedlungsscholle" has closed and covered the well-known old areas of this deposit and opened here a new exploitation field at the east margin. This material is located at the margin of deposit and was in contact with glacial water in Pleistocene. For this new opened Eastfield, no new published data were not to find. A comparison of published mineralogical results ("Siedlungsscholle"), the recent own measurement No19, and a former own measurement from neighboured deposit "Burgscholle" (tab. 8) shows a remarkable coincidence of mineral matter

Tab. 8. *Friedland Clay (initial) composition – own measurement of this project (No19) in comparison with literature and former own other measurements*

	|----	Deposit: Siedlungsscholle			----|	|- Burgscholle -|
Phase	***Henning (1971)***	**Hoang (2006)**	**Karnland et al. (2006)**	**FIM (2009)**	**own sample (No19)**	***Tonmehl, Juli 2021***
Ca-smectite					5%	
Illite-smectite mixed layer structure	44%	40%	56%	33-42%	14%	12%
Illite 2M1	12%	14%	7%	25-30%	6%	33%
Illite 1M					34%	9%
Kaolinite (+ Chlorite)	11%	12%				
Kaolinite			11%	10-13%	16%	17%
Chlorite				3-4%	3%	5%
Quartz	24%	27%	20%	16-20%	15%	16%
Feldspar	5%					
Plagioclase				0-2%	3%	2%
K-Feldspar		2%	1%	0-1%	3%	1%
Anatase, Rutile		1%			1%	1%
Gypsum			1%			2%
Pyrite	1%	traces	1%		<1%	1%

between sample No19 (belongs to "Siedlungsscholle" – new field at the east margin of this deposit) and the trade ware of deposit "Burgscholle".

Glacitectonics in Pleistocene divided the occurrence of Friedland clay in few separate blocks (Schollen). The block "Siedlungsscholle" is the source of Friedland clay used in this project. Another block, "Burgscholle", is located only few kilometres to east from "Siedlungsscholle". The material from deposit "Burgscholle" is characterized by a higher degree of interaction with former glacial water.

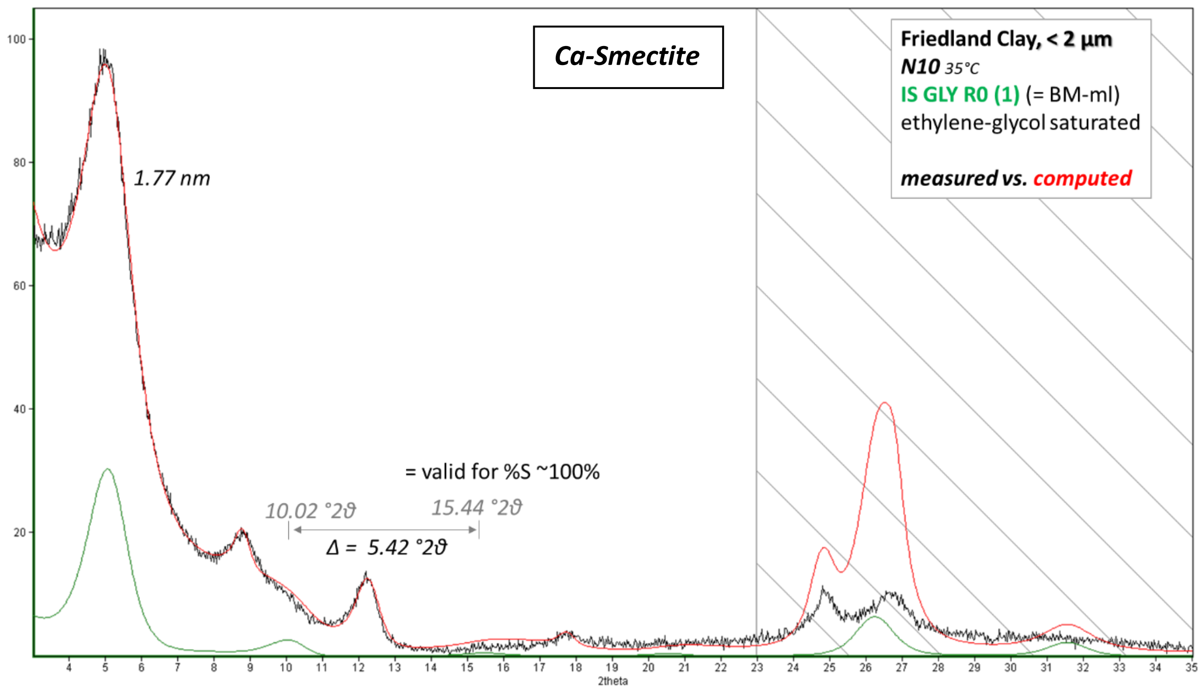

Fig. 11. *Friedland Clay No10, 35°C, 46.3 h (< 2 µm) - X-ray diffraction pattern of the ethylene-glycol saturated oriented specimen (with computing of Ca-smectite by Sybilla-software – green line)*

Beidellite-rich Ca-Smectite

Identification by XRD: The X-ray diffraction pattern of the ethylene-glycol saturated oriented specimen of samples “Friedland initial”, “No10” (35°C) and “No11” (60°C) show an expandability closed to 1.7 nm or higher and a difference at 5.42-5.68°2θ between 2. and 3. order of smectite interferences (fig. 11). This distance is typically for full expandable smectite like montmorillonite (Moore & Reynolds, 1997) or beidellite.

The XRD-pattern of bulk samples show for all samples the occurrence of Ca-smectite ((tab. 7)). Otherwise, only for the above mentioned three samples were found phases with a full expandability in the clay fraction (< 2 µm).

Mineral formula by TEM-EDX and clustering: The full expandability of ethylene-glycol saturated oriented specimen let assume Si-values close to 4 per $(OH)_2 O_{10}$ in computation of mineral formula by TEM-EDX-analyses, but values have been calculated between 3.53 - 3.56 e phuc. This situation is considered as intergrowth between beidellite (Si ~ 3.5), montmorillonite (Si ~ 4) and sometimes also in interstratification with illite (Si ~ 3.2).

Beidellite-ratio in Ca-smectite is dominating in all three mentioned samples. The BMI-ratios for these three samples indicate the occurrence of pure beidellite (but “Friedland initial” with 20% illite layer probability). The calculated structural formulae (tab. 9) show variable tetrahedral Si-values (from 3.53 - 3.56 e phuc), but the full expandability is stable nearby in all mentioned three samples (tab. 9).

Tab. 9. *Structural formulae for Ca-smectite in Frieland Clay-series with estimation of beidellite-ratio*

		phase (low illite)	**mineral formula** *(clustering of TEM-EDX-results)*										**%S** *(XRD-oriented)*	**mass-%** *(XRD-oriented)*
			Ca	Mg	Na	K	Al	Fe^{3+}	Mg	Ti	Al	Si		
Original	Friedland	BMI 60:20:20	0.02	0.10	0.00	0.29	1.30	0.58	0.11	0.02	0.45	3.55	82%	11%
orig., compr.	No19													
OPA, 35°C	No10	BMI 95:05:00	0.04	0.03	0.14	0.35	1.21	0.58	0.19	0.02	0.47	3.53	100%	11%
OPA, 60°C	No11	BMI 80:15:05	0.09	0.02	0.03	0.32	1.20	0.61	0.19	0.02	0.44	3.56	94%	17%
OPA, 100°C	No16													
OPA, 125°C	No20													
OPA, 150°C	No21													

Legend: *BMI – beidellite-montmorillonite-illite; %S – probability of smectite layer*

Further indications by FTIR: The Al-OH-Fe^{3+} band at 882 cm^{-1} had a low intensity reflecting the high Fe content of Friedland clay (Craciun, 1984; Russell & Fraser, 1994; Vantelon et al., 2001; Gates, 2005).

Development of mass-distribution: Ca-smectite shows a nearby constant mass distribution in all experimental stages (fig. 12) surrounding a level at 5-6%.

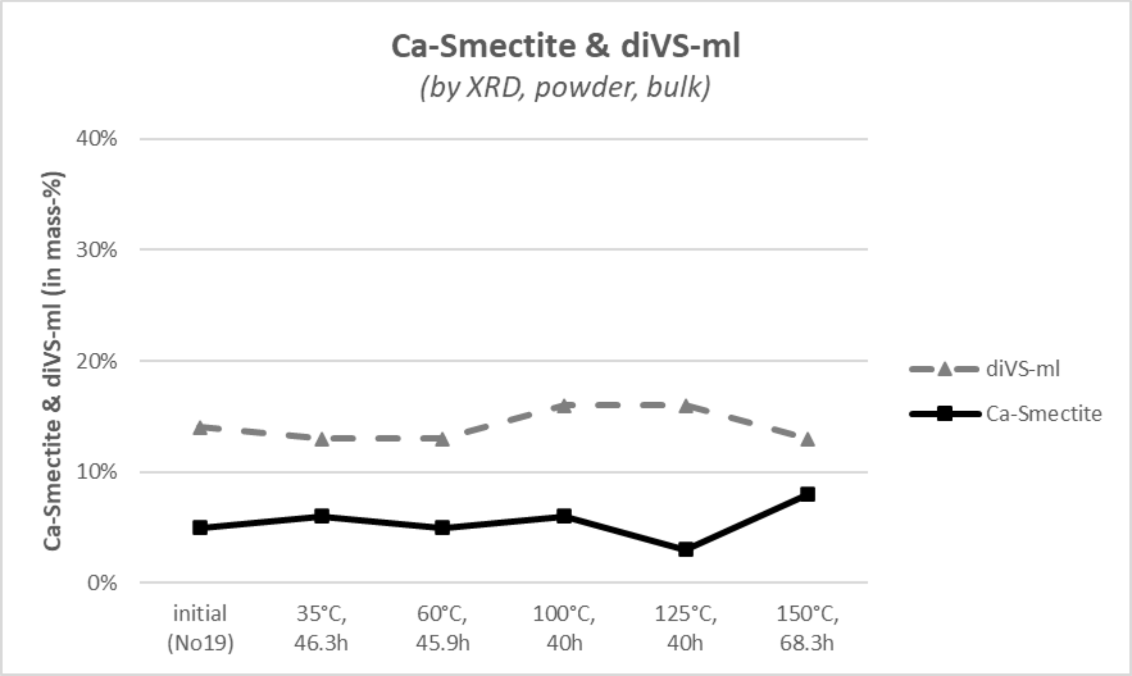

Fig. 12. *Mass distribution of Ca-smectite (black line) and diVS-ml (dashed line) in bulk samples of Friedland Clay-series*

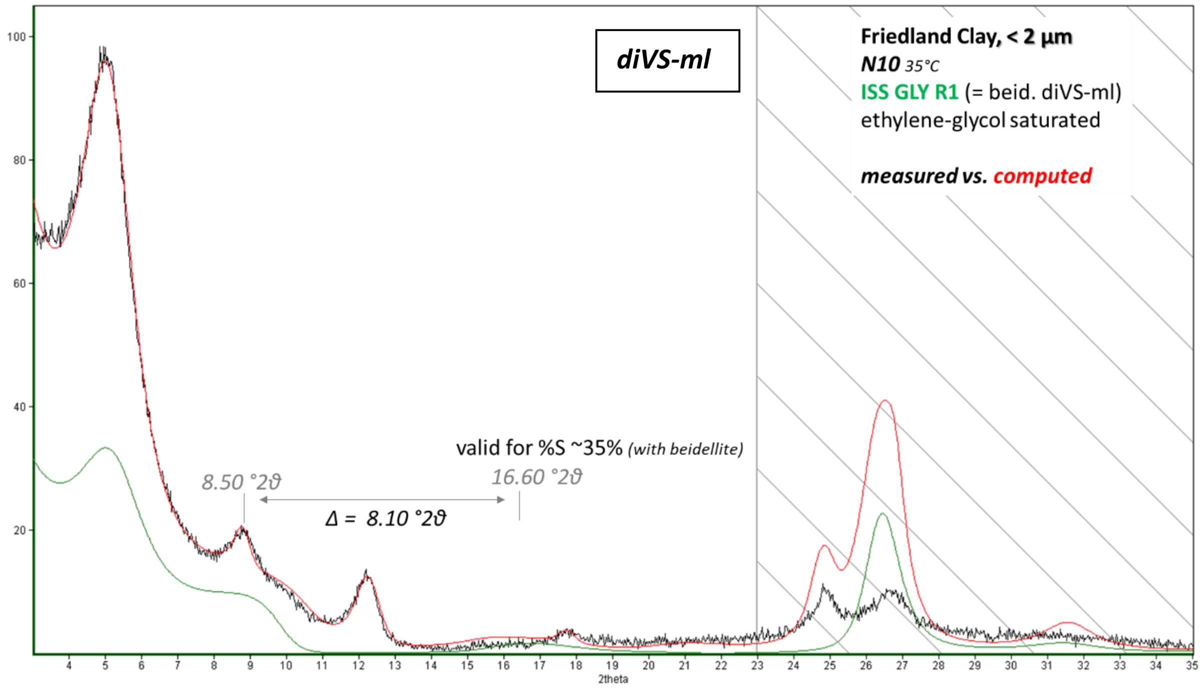

Fig. 13. *Friedland Clay N10, 35°C (< 2 µm) - X-ray diffraction pattern of the ethylene-glycol saturated oriented specimen (with computing of diVS-ml by Sybilla-software – green line)*

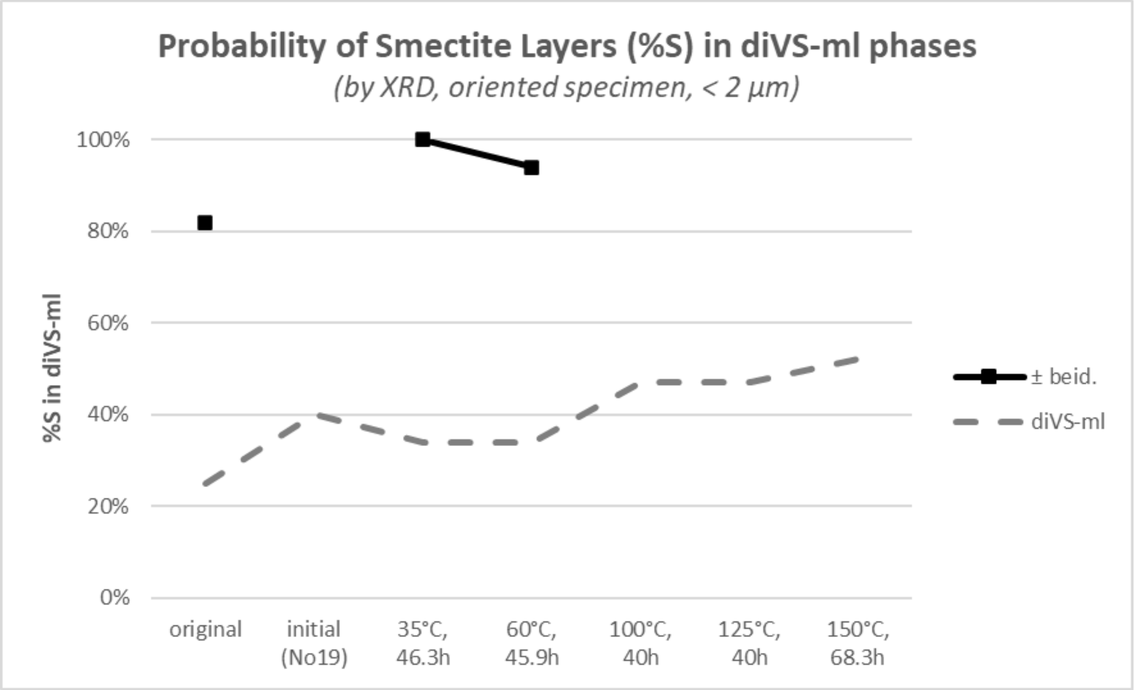

Fig. 14. *Smectite layer probability of beidellite (solid line) and diVS-ml (dashed line) in fraction < 2 µm of Friedland Clay-series*

Dioctahedral Vermiculite-Smectite Mixed-Layer (diVS-ml)

Identification by XRD: The X-ray diffraction pattern of the ethylene-glycol saturated oriented draws a further group of swelling clay mineral phases. The difference between 2. and 3. order of smectite interferences is variable representing smectite layer probabilities (%S) between 10 - 52% (see example: fig. 13). These diVS-ml phases are distributed in two groups: (i) %S at 40% (from %S = 34% to %S = 52%) and (ii) %S at 20% (from %S = 10% to %S = 30%) (tab. 10). The smectite layer probability (%S) of uncompacted original Friedland Clay is to find at %S = 25%.

Mineral formula by TEM-EDX and clustering: The cross-checking between phases with limited expandability of ethylene-glycol saturated oriented specimen and TEM-EDX-data (incl. clustering) shows illite-smectite mixed layer phase with K- and charge deficiency. These phases are mainly dominated by montmorillonite as smectite component. Beidellite occurs in diVS-ml only in traces (tab. 10). That means, increased tetrahedral Si-values after experiments are linked with rising swelling properties by a decreased illite layer probability (%I).

Development of mass-distribution: diVS-ml phases show with a slight variable mass distribution (13%-16%) close to the original composition (fig. 12, tab. 7).

Development of expandability: diVS-ml phases in fraction < 2 µm of Friedland Clay-series draw a slight increasing smectite layer probability with increasing thermal load in experiments from %S = 25% (Friedland initial) to 52% (150°C) (fig. 14).

Tab. 10. *Structural formulae for diVS-ml phases in Friedland Clay samples with estimation of beidellite-ratio*

		phase (high illite)	**mineral formula** *(clustering of TEM-EDX-results)*										**%S** *(XRD-oriented)*	**mass-%** *(XRD-oriented)*
			Ca	Mg	Na	K	Al	Fe^{3+}	Mg	Ti	Al	Si		
Original	Friedland	BMI 05:20:75	0.01	0.08	0.01	0.45	1.50	0.40	0.08	0.03	0.63	3.37	25%	2%
initial	No19	BMI 00:40:60	0.03	0.01	0.27	0.35	1.16	0.60	0.21	0.01	0.49	3.51	40%	54%
		BMI 30:10:60	0.02	0.03	0.20	0.48	1.42	0.42	0.14	0.01	0.63	3.37	40%	
OPA, 35°C	No10	BMI 15:20:65	0.04	0.09	0.13	0.31	1.43	0.46	0.10	0.01	0.59	3.41	34%	40%
OPA, 60°C	No11	BMI 00:35:65	0.10	0.05	0.03	0.31	1.24	0.58	0.15	0.03	0.52	3.48	34%	49%
OPA, 100°C	No16	BMI 15:20:65	0.01	0.04	0.12	0.49	1.40	0.45	0.14	0.01	0.59	3.41	36%	11%
		BMI 10:40:50	0.03	0.03	0.13	0.37	1.20	0.62	0.16	0.01	0.47	3.53	47%	57%
OPA, 125°C	No20	BMI 15:30:55	0.05	0.01	0.23	0.38	1.15	0.60	0.24	0.01	0.51	3.49	47%	67%
		BMI 00:10:90	0.05	0.07	0.16	0.34	1.54	0.37	0.08	0.01	0.68	3.32	10%	6%
OPA, 150°C	No21	BMI 05:45:50	0.03	0.02	0.12	0.35	1.20	0.61	0.18	0.01	0.42	3.58	52%	51%
		BMI 10:20:70	0.02	0.07	0.09	0.41	1.46	0.43	0.09	0.02	0.62	3.38	30%	7%

Legend: *BMI – beidellite-montmorillonite-illite; %S – probability of smectite layer*

Tab. 11. *Mineral matter of Friedland Clay-series (< 2 µm) – oriented specimen*

Sample	**Ca-Smectite (BMI-ml)** *(IS GLY R0_V1)*	**beid. diVS-ml** *(IS GLY R0_V2 or ISS GLY R1)*	**Illite**	**Chlorite**	**Kao-linite**	**Kaolinite-Smectite-ml** *(KS GL R0)*		*Σ total*
FRIEDLAND* original	11% *(%S = 82%)*	2% *(%S = 25%)*	13%	15%	48%	11% *(%S = 23%)*		*100%*
initial **No19**		54% *(%S = 39%)*	16%	2%	10%	17% *(%S = 48%)*		*99%*
35°C, 46.3h **No10**	11% *(%S = 100%)*	40% *(%S = 34%)*	11%		12%	27% *(%S = 51%)*		*101%*
60°C, 45.9h **No11**	17% *(%S = 94%)*	49% *(%S = 34%)*	7%		13%	14% *(%S = 48%)*		*100%*
100°C, 40h **No16**		11% *(%S = 36%)* 57% *(%S = 47%)*	16%		13%	4% *(%S = 50%)*		*101%*
125°C, 40h **No20**		6% *(%S = 10%)* 67% *(%S = 47%)*	11%		10%	6% *(%S = 48%)*		*100%*
150°C, 68.3h **No21**		7% *(%S = 30%)* 51% *(%S = 52%)*	24%	4%	9%	6% *(%S = 50%)*		*101%*
without transport cell *100°C* **No12**	35% *(%S = 79%)*	27% *(%S = 34%)*	11%		11%	16% *(%S = 40%)*		*100%*

Kaolinite-Smectite Mixed-Layer (KS-ml)

Identification by XRD: The occurrence of kaolinite-smectite mixed layer is mainly indicated by modelling of XRD-pattern of oriented specimen using Sybilla-software (developed by Chevron Inc.: Aplin et al., 2006) (tab. 11; fig. 15). Few particles, measured by TEM-EDX, indicated the occurrence of KS-ml phases, but it was not possible to calculate a valid structural formula.

Development of mass-distribution: KS-ml phases in fraction < 2 µm show a variable development without any significant trend with increasing thermal load (fig. 16).

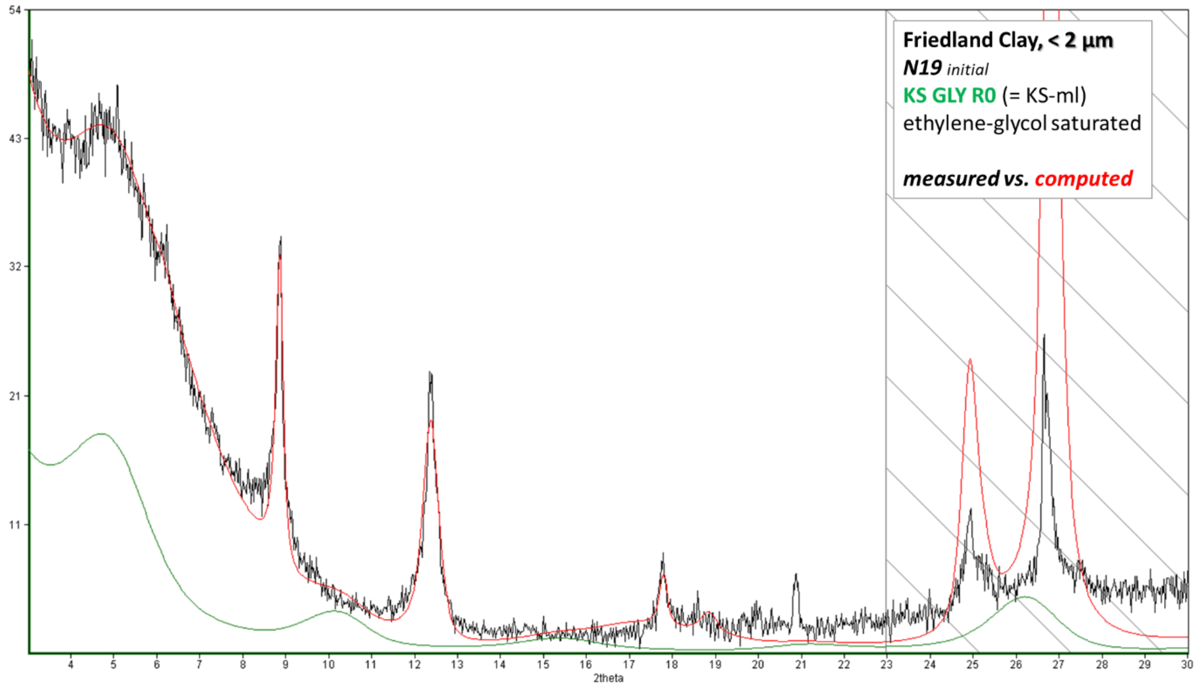

Fig. 15. *Friedland Clay No19, initial (< 2 µm) - X-ray diffraction pattern of the ethylene-glycol saturated oriented specimen (with computing of KS-ml by Sybilla-software – green line)*

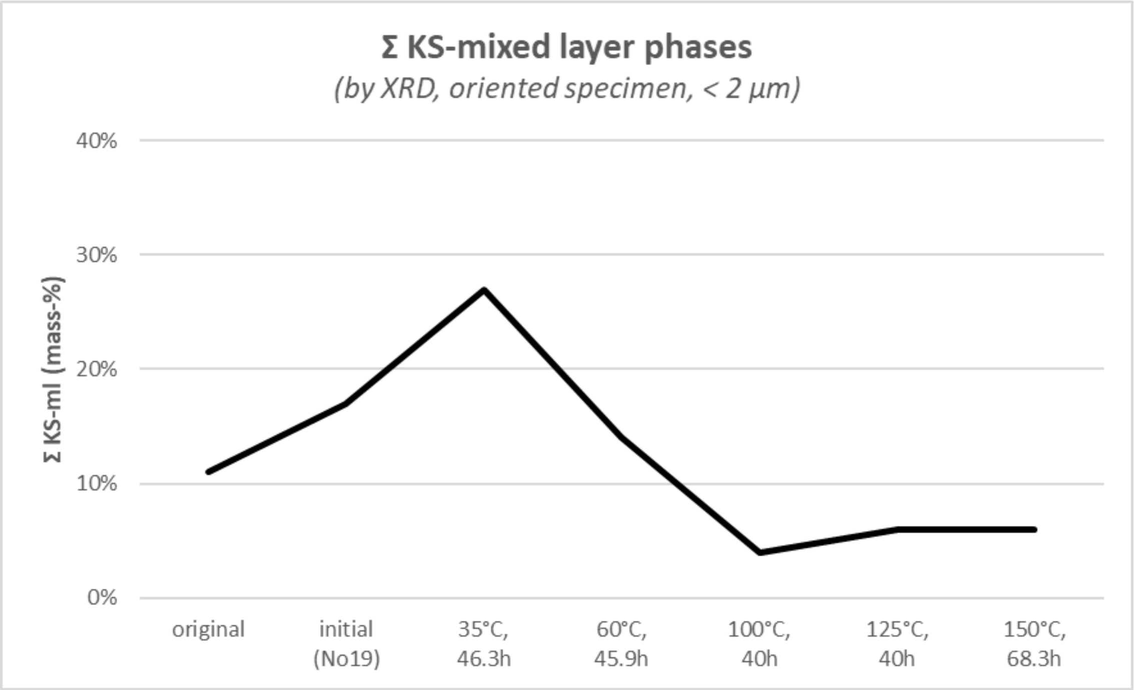

Fig. 16. *Mass distribution of KS-ml in samples of Friedland Clay-series (< 2 µm)*

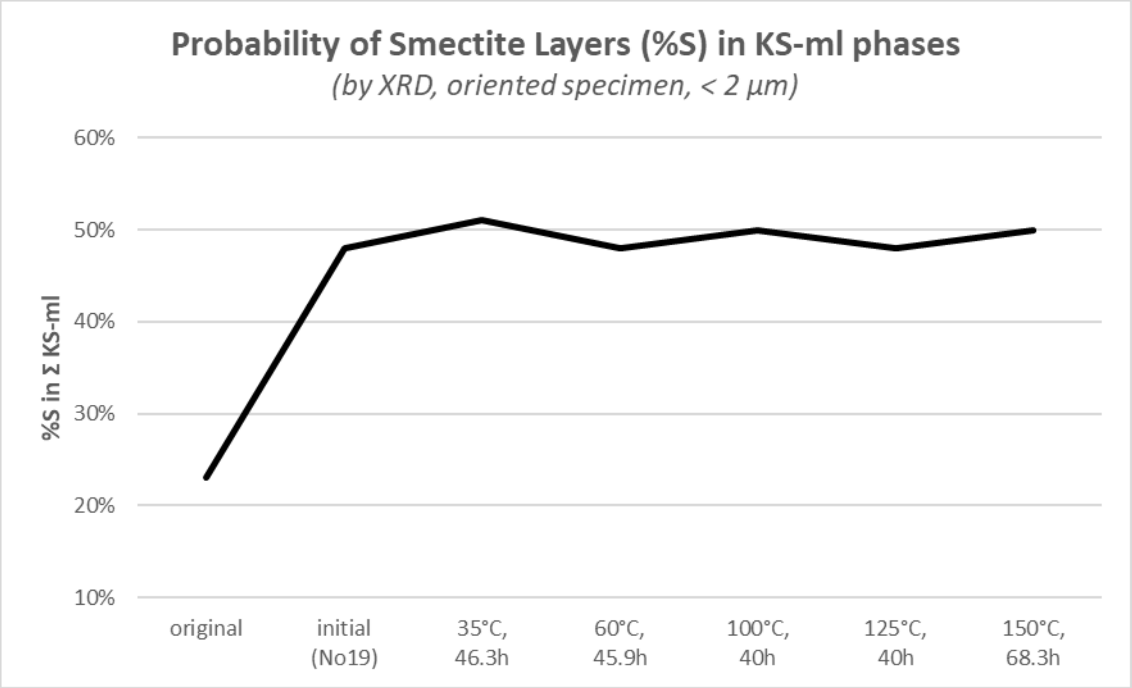

Fig. 17. *Smectite layer probability of KS-ml in fraction < 2 µm of Friedland Clay-series*

Development of expandability: KS-ml phases in Friedland Clay-series (< 2 µm) draw a higher smectite layer probability than %S=23% from original Friedland Clay staying to close to 50% (fig. 17). With increasing thermal load, the smectite layer probability is running nearby constant at %S= ~50%.

Smectite-behaviour in experiments

Smectite is the main responsible mineralogical phase, which determines the swelling behaviour of clays. In Friedland Clay, smectite is distributed in three different groups of phases (Ca-smectite, diVS-ml, KS-ml). Each group has shown a specific behaviour during the experiments (tab. 12).

Tab. 12. *Friedland Clay – Overview about different smectite behaviour (in direction of rising thermal load in experiments)*

	role of phase in bulk sample	smectite species	mass-% development	%S-development	assumptions to expandab.
Ca-smectite	minor phase, trace *(tab. 7)*	beidellite >> montm. *(tab. 9)*	± constant *(at 5% - 6%)* *(fig. 12)*	± constant *(at %S=100%, only ≤60°C)* *(tab. 9) (fig. 14)*	slight impact for increasing in low temperat. level
diVS-ml	minor phase *(tab. 7)*	montm. >> beidellite *(tab. 10)*	± stable *(variable 13%-16%)* *(fig. 12)*	rising *(from 25% to 52%)* *(fig. 14)*	impact for rising
KS-ml	minor phase *(tab. 7)*	not to determine	± stable *(< 2 µm: variable at 10 %) (fig. 16)*	constant *(< 2 µm: ~50%)* *(fig. 17)*	constant contribution for expandability

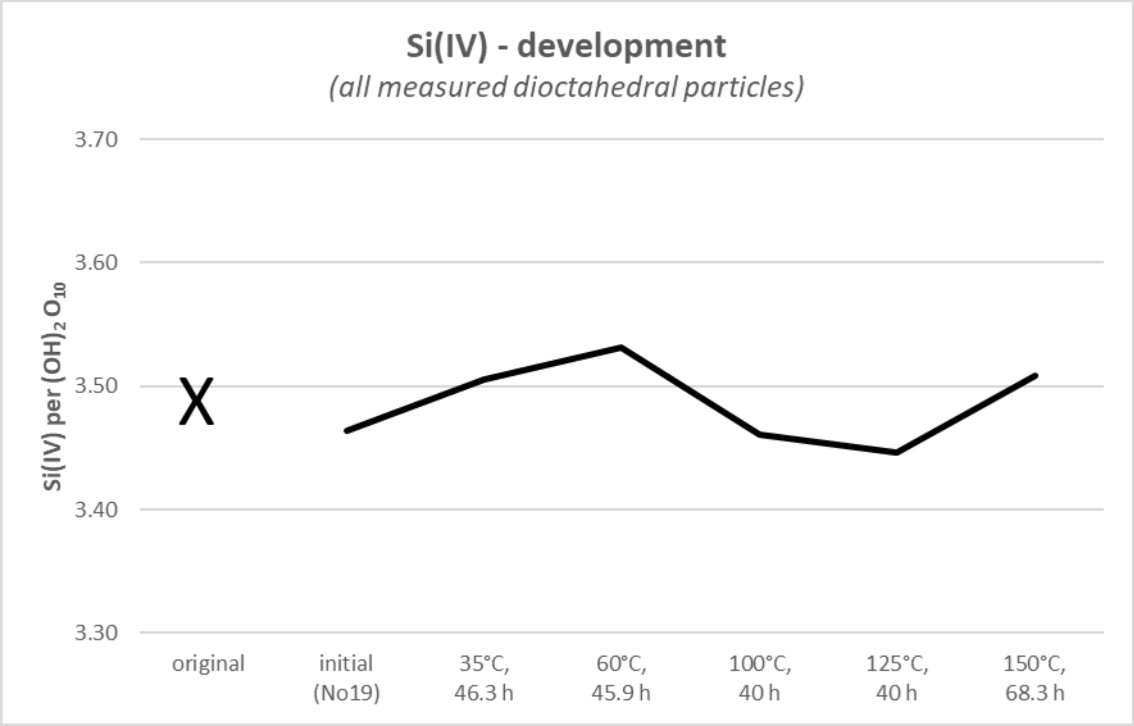

Fig. 18. *Behaviour of tetrahedral Si per $(OH)_2$ O_{10} in fraction < 2 µm of Friedland Clay*
Note: *KS-ml not included here*

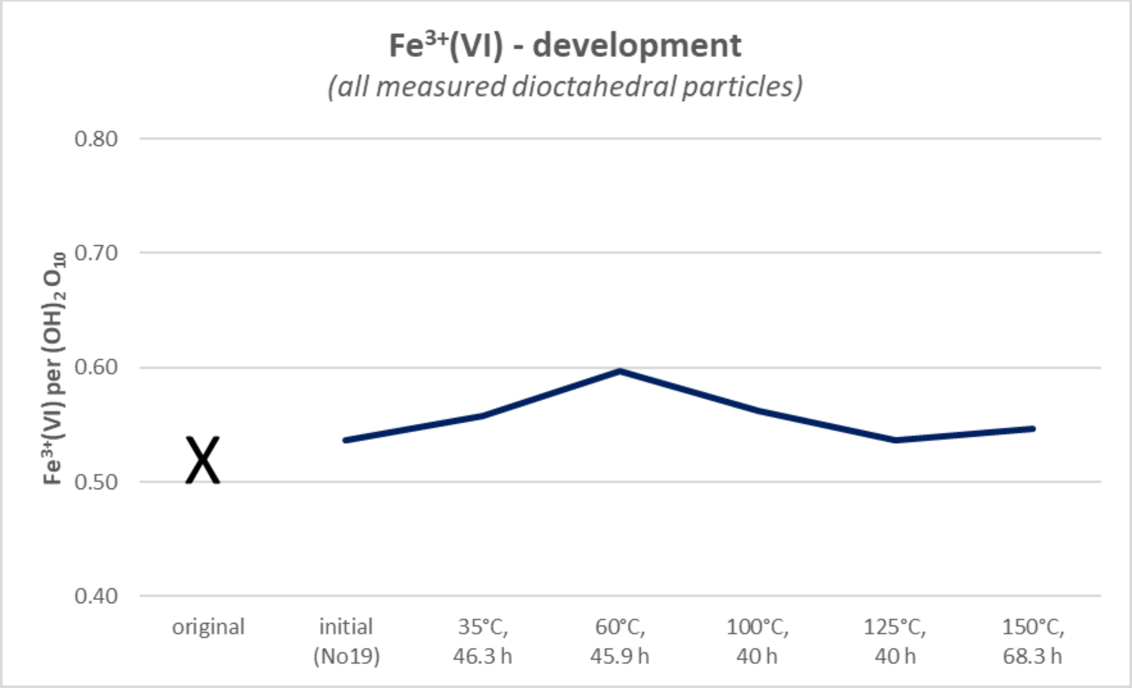

Fig. 19. *Development of octahedral Fe^{3+} per $(OH)_2$ O_{10} in fraction < 2 µm of Friedland Clay*
Note: *KS-ml not included here*

The summarizing impact of Ca-smectite including with diVS-ml on expandability is mirrored by TEM-EDX-measurements (fig. 18)/. The original material shows an average value for development of tetrahedral Si-value per $(OH)_2$ O_{10} with Si = 3.49. The tetrahedral Si-values of all measured particles from all experiments are constant with a slight variability from Si 3.45 – 3.53. A trend related to increasing thermal load by experiments is not to recognize.

The octahedral layer of all Ca-smectite and diVS-ml phases don't show real changes in all experiments (fig. 19).

The additional contribution of KS-ml on expandability of the total sample is not real to evaluate. The variable mass distribution of KS-ml (< 2 µm) by higher thermal load during the experiments (tab. 12; fig. 16) and the even constant smectite layer probability (tab. 12; fig. 17) let assume a more stabilizing contribution for expandability of sample.

TEM-EDX: Illite-behaviour in experiments

Ca. 20% of all measured particles in each sample were identified as illite. A very limited number of illite particles (N10 – 35°C) or a lack of illite particles (N11 – 60°C) was only detected in these two samples.

The available TEM-EDX-measurements indicate the occurrence of only one illite group: Al(VI)-rich, with a high to moderate K-deficit and Fe(VI) at 0.4 per $(OH)_2 O_{10}$ (tab. Illite_Friedland). The composition of this illite group is stable in all experiments – exception: experiment at 125° (sample N20). Illite in sample N20 shows an octahedral Al-enrichment substituting Fe(VI).

The reduced number or the lack of illite in samples N10 and N11 could be caused by a slight smectitization of illite particles (fig. 18). The Al-development of illite in sample N20 (125°C) let assume a degradation of larger illite particles, which than feed the fine fraction < 2 µm.

	Ca (XII)	Mg (XII)	Na (XII)	K (XII)	Cr3+ (VI)	Al (VI)	Fe3+ (VI)	Mg (VI)	Ti (VI)	Al (IV)	Si (IV)	XII	n_VI	%S	K-deficit	charge-deficit
Friedland original																
Cluster1 *(n=15)*	0.01	0.07	0.01	0.54	0.00	1.49	0.39	0.08	0.05	0.70	3.30	0.72	2.0	9	45%	15%
No19 *initial*																
Cluster2 *(n=15)*	0.03	0.03	0.25	0.47	0.00	1.42	0.42	0.13	0.02	0.71	3.29	0.83	2.0	9	52%	2%
Opalinus treated																
N10 *35°C, 48.3h*																
Cluster1 *(n=4)*	0.02	0.07	0.14	0.45	0.00	1.49	0.41	0.09	0.00	0.67	3.33	0.76	2.0	12	56%	8%
N11 *60°C, 45.9h*	Note: No illite measured by TEM-EDX.															
N16 *100°C, 40h*																
Cluster1 *(n=20)*	0.01	0.03	0.10	0.65	0.00	1.46	0.40	0.12	0.02	0.75	3.25	0.84	2.0	6	31%	2%
No20 *125°C, 40h*																
Cluster1 *(n=21)*	0.05	0.08	0.17	0.34	0.00	1.61	0.33	0.07	0.01	0.74	3.26	0.77	2.0	7	65%	11%
No21 *150°C, 68.3h*																
Cluster2 *(n=16)*	0.02	0.07	0.09	0.49	0.00	1.48	0.40	0.09	0.04	0.72	3.28	0.75	2.0	8	49%	12%

Tab. Illite_Friedland. *Friedland Clay: Illite in fraction < 2 µm (by TEM-EDX)*

Legend: *(n=4) – number of illite particles measured by TEM-EDX; XII – interlayer charge; n_VI – number of atoms in octahedral layer per $(OH)_2 O_{10}$; %S – probability of smectite layers in senso of Środon et al. (1992); K-deficit, charge-deficit – in senso of Środon et al. (1992) (normal K in illite = 0.89 per $(OH)_2 O_{10}$)*

3. Mineral matter in Opalinus Clay

***Tab. 13.** Mineral matter of Opalinus Clay-series (bulk sample)*

Sample	Ca-Smectite	diVS-ml	Illite (1M)	Illite (2M1)	Chlorite	Kaolinite + KS-ml	*Σ clay*	Quartz	K-feldspar	Plagioclase	Pyrite	Calcite	Siderite	Dolomite	Anatase	*Σ total*
Opalin. Clay original, BLT-A7		3% *(±0.4)*	4% *(±0.3)*	18% *(±0.9)*	12% *(±0.7)*	25% *(±3.0)*	*61%*	13% *(±0.5)*	1% *(±0.2)*	4% *(±0.2)*	1% *(±0.1)*	17% *(±0.6)*	1% *(±0.1)*	2% *(±0.1)*		*100%*
. Opalin. Clay original, BFS-B12 **No6**		9% *(±0.5)*	2% *(±0.2)*	13% *(±0.6)*	4% *(±0.3)*	50% *(±1.6)*	78%	9% *(±0.3)*	1% *(±0.2)*	2% *(±0.2)*	<1% *(±0.1)*	8% *(±0.3)*	<1% *(±0.1)*	<1% *(±0.1)*	<1% *(±0.1)*	*100%*
35°C, 144h, OPA **No22** BFS-B12		12% *(±0.7)*	2% *(±0.5)*	22% *(±0.8)*	7% *(±0.4)*	25% *(±1.2)*	67%	14% *(±0.5)*	2% *(±0.3)*	3% *(±0.3)*	1% *(±0.1)*	10% *(±0.1)*	1% *(±0.1)*	1% *(±0.1)*	1% *(±0.1)*	*100%*
60°C, 45.4h, OPA **No9** BFS-B12		12% *(±0.7)*	1% *(±0.3)*	19% *(±0.9)*	3% *(±0.3)*	35% *(±2.2)*	69%	13% *(±0.7)*	1% *(±0.2)*	2% *(±0.2)*	1% *(±0.1)*	*10% *(±0.3)*	<1% *(±0.1)*	1% *(±0.1)*		*99%*
60°C, 95.3h, OPA **No7** BFS-B12		9% *(±0.5)*	1% *(±0.4)*	3% *(±0.3)*	<1% *(±0.1)*	13% *(±0.8)*	28%	6% *(±0.4)*	1% *(±0.2)*	1% *(±0.2)*	<1% *(±0.1)*	***60%** *(±0.6)*	<1% *(±0.1)*	1% *(±0.1)*		*98%*
100°C, 69.3h, OPA **No8** BFS-B12		12% *(±1.0)*	3% *(±0.5)*	11% *(±0.4)*	8% *(±0.7)*	27% *(±1.2)*	61%	14% *(±0.6)*	3% *(±0.3)*	4% *(±0.3)*	2% *(±0.1)*	*14% *(±0.3)*	2% *(±0.1)*	1% *(±0.1)*		*100%*
125°C, 48.5h, OPA **No14** BFS-B12		16% *(±0.7)*	5% *(±0.5)*	10% *(±0.4)*	7% *(±0.9)*	25% *(±1.2)*	63%	14% *(±0.6)*	3% *(±0.3)*	4% *(±0.3)*	1% *(±0.1)*	*11% *(±0.3)*	2% *(±0.1)*	<1% *(±0.1)*		*99%*
150°C, 48.6 h, OPA **No13** BFS-B12		8% *(±0.9)*	<1% *(±0.1)*	16% *(±1.1)*	4% *(±0.4)*	53% *(±3.2)*	81%	8% *(±0.5)*	1% *(±0.2)*	1% *(±0.1)*	1% *(±0.1)*	*7% *(±0.4)*	<1% *(±0.1)*	<1% *(±0.1)*		*99%*
without transport cell																
35°C, OPA **No9a** BFS-B12		10% *(±0.3)*	2% *(±0.2)*	25% *(±0.6)*	4% *(±0.5)*	29% *(±0.8)*	70%	15% *(±0.4)*	1% *(±0.2)*	3% *(±0.2)*	1% *(±0.1)*	*9% *(±0.2)*	<1% *(±0.1)*	1% *(±0.1)*		*99%*
125°C, OPA **No9b** BFS-B12		10% *(±0.4)*	3% *(±0.3)*	20% *(±0.6)*	1% *(±0.2)*	32% *(±0.9)*	65%	14% *(±0.3)*	2% *(±0.2)*	2% *(±0.2)*	1% *(±0.1)*	*11% *(±0.2)*	<1% *(±0.1)*	1% *(±0.1)*		*96%*

***Legend:** * - including indications by TG for additional amount of amorphous calcium carbonate; (±0.1) – standard deviation, absolute; BLT-A7, BFS-B12 - boreholes*

***Note:** sample No7 ("white" clay) is composed mainly by calcite = indication for sometimes inhomogeneous distribution of calcite in sample body; all other samples belong to the so-called "grey" clay*

Smectite is to find in Opalinus Clay-series in illite-smectite mixed layers (a minor phase) with K- and/or charge deficiency (diVS-ml) and especially in kaolinite-smectite mixed layer phases (a main phase). Montmorillonite is the dominating smectite component.

Illite and kaolinite (incl. KS-ml) are the main phases in Opalinus Clay, accompanied by diVS-ml, quartz, and calcite as minor phases and in traces by chlorite, feldspar, pyrite, siderite, dolomite and anatase. Calcite occurs as crystalline calcite (see values in tab. 13) and additionally also as amorphous calcite carbonate. The percolation and heating processes during the experiments don't cause any mineralogical neoformations (tab. 13).

Validation of Opalinus Clay composition

The measured composition of original Opalinus Clay from the borehole BLT-A7 is in a good agreement (tab. 14) with already published data from literature (Gaucher et al., 2003; Bossart & Thury, 2008; Nagara, 2002). Differences between here presented own measurements and literature references are to recognize in the amount of diVS-ml (lower for own measurement). Thermogravimetric investigations of Opalinus Clay support the here reported results of diVS-ml, kaolinite, and carbonate amount (tab. 14). The differences in mass loss values of original sample BFL-B12 between measured by thermogravimetry and calculated from XRD-results indicate the occurrence of amorph calcium carbonate (ACC) (tab. 14).

Tab. 14. *Opalinus Clay (original) composition – own measurement in comparison with literature*

	Opalinus				
	own results				
	BLT-A7	BFL-B12	Pearson et al., 2003	Bossart & Thury, 2008 *(min-best-max)*	NAGRA, 2002
Ca-smectite					
IS-ml	3%	9%	11 - 20%	5 - 11 - 20%	11%
Illite_1M	4%	2%	17 - 40%	15 - 23 - 30%	23%
Illite_2M1	18%	13%			
Chlorite	12%	4%	5 - 20%	3 - 10 - 18%	10%
Kaolinite	25%	50%	15 - 32%	15 - 22 - 37%	22%
Σ clay	***61%***	***78%***		***28 - 66 - 93%***	***66%***
Quartz	13%	9%	6 - 17%	10 - 14 - 32%	14%
Orthoclase	1%	1%	1 - 2%	0 - 1 - 6%	1%
Albite	4%	2%	1 - 2%	0 - 1 - 2%	1%
Pyrite	1%	<1%	1 - 2%	0 - 1 - 3%	1%
Calcite	17%	8%	11 -28%	4 - 13 - 22%	13%
Siderite	1%	<1%	1 - 4%	0 - 3 - 6%	3%
Dolomite	2%	<1%	≤ 2%	≤ 1%	
Rutile		<1%			
Gypsum				≤ 0.5%	
Σ total	***100%***	***100%***			***99%***

DTG/TG, mass loss (as proof)			
300-1000°C *(as check for all phases)*			
meas. by TG	13.90%	13.73%	
calc. by XRD	13.89%	11.60%	
650-1000°C *(as check especially for calcite+dolomite)*			
meas. by TG	7.75%	7.23%	*This difference between TG and XRD let assume the additional occurrence of 6% ACC in BFL-B12.*
calc. by XRD	7.89%	4.35%	

Generally, the here reported compositions of untreated and treated bentonite were verified by combination of following methods:

- TEM-EDX results, cross-checked by oriented specimen (XRD) after Sybilla-modelling of probability of smectite layers, also offer indications to the occurrence of beidellite
- XRD of powder samples (bulk) has been cross-checked by thermogravimetry using the mass loss to verify especially the XRD-results to kaolinite, indications to kaolinite-smectite mixed layer phases, and carbonates (see example: tab. 2, tab. 14).

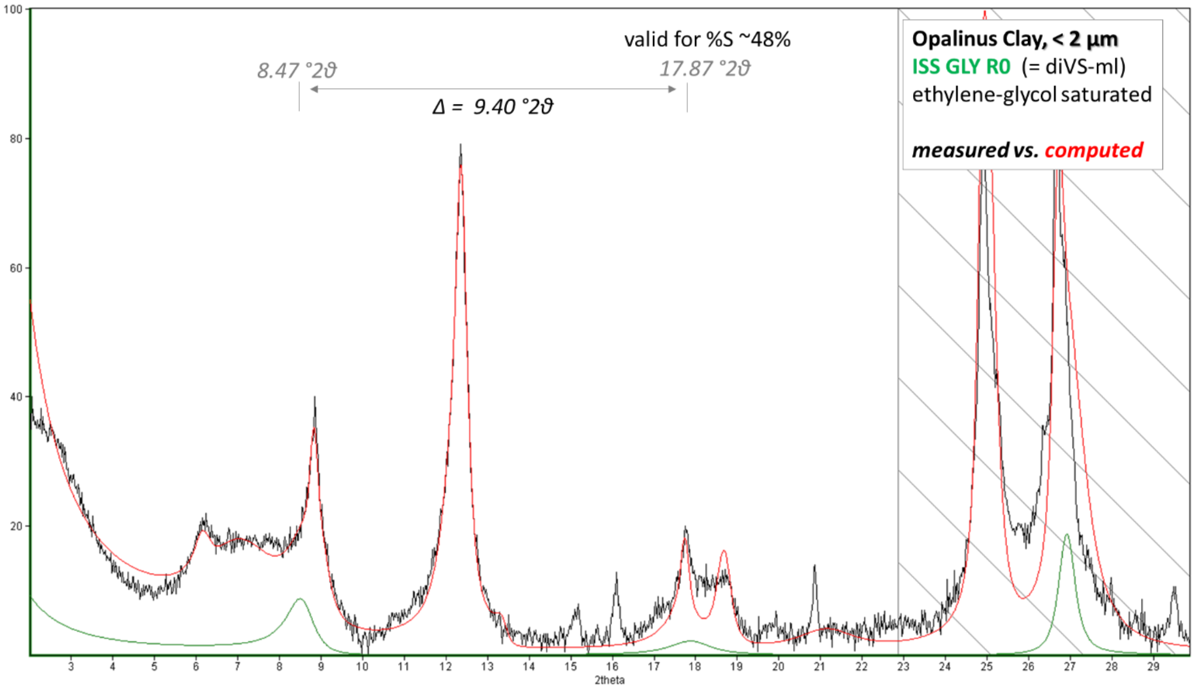

Fig. 20. *Opalinus Clay, original (< 2 µm) - X-ray diffraction pattern of the ethylene-glycol saturated oriented specimen (with computing of diVS-ml group I by Sybilla-software – green line)*

Tab. 15. *Structural formulae for diVS-ml phases (group I) in Opalinus Clay samples with estimation of beidellite-ratio*

		phase (low smectite)	**mineral formula** *(clustering of TEM-EDX-results)*										**%S** *(XRD-oriented)*	**mass-%** *(XRD-oriented)*
			Ca	Mg	Na	K	Al	Fe^{3+}	Mg	Ti	Al	Si		
Original	OPAL_40µm	BMI 10:40:50	0.08	0.04	0.00	0.44	1.39	0.41	0.20	0.00	0.47	3.53	48%	11%
		BMI 00:09:91	0.11	0.12	0.01	0.28	1.42	0.45	0.10	0.03	0.71	3.29	11%	18%
OPA, 35°C	No22	BMI 00:15:85	0.10	0.03	0.03	0.56	1.42	0.39	0.18	0.01	0.67	3.33	16%	44%
OPA, 60°C	No9	BMI 00:20:80	0.10	0.00	0.04	0.56	1.34	0.42	0.24	0.00	0.58	3.42	23%	21%
OPA, 100°C	No8	BMI 00:20:80	0.06	0.04	0.00	0.55	1.40	0.40	0.19	0.00	0.56	3.44	26%	22%
OPA, 125°C	No14	BMI 00:20:80	0.08	0.00	0.05	0.59	1.27	0.46	0.28	0.00	0.55	3.45	24%	31%
OPA, 150°C	N013	BMI 00:15:85	0.05	0.00	0.09	0.68	1.36	0.42	0.22	0.00	0.65	3.35	16%	42%

Legend: *BMI – beidellite-montmorillonite-illite; %S – probability of smectite layer*

Dioctahedral Vermiculite-Smectite Mixed-Layer (diVS-ml)

Identification by XRD: The X-ray diffraction pattern of the ethylene-glycol saturated oriented specimen draw for diVS-ml phases two groups of swelling. First group is characterized with a smectite layer probability (%S) at 15-20%. Exception: Opalinus clay, original contain two diVS-ml phases (tab. 15): (i) with %S = 50% (fig. 20) and (ii) with %S = 11%, both basing on the differences between 2. and 3. order of smectite interferences.

Second group of diVS-ml contains only traces of smectite (%S ≤ 5%) (tab. 16), even basing on the difference between 2. and 3. order of smectite interferences, close to pure illite.

Tab. 16. *Structural formulae for diVS-ml phases (group II) in Opalinus Clay samples with estimation of beidellite-ratio*

		phase (~ illite)	**mineral formula** *(clustering of TEM-EDX-results)*										**%S** *(XRD-oriented)*	**mass-%** *(XRD-oriented)*
			Ca	Mg	Na	K	Al	Fe^{3+}	Mg	Ti	Al	Si		
Original	OPAL_40µm													
OPA, 35°C	No22	BMI 00:05:95	0.10	0.14	0.03	0.33	1.58	0.37	0.05	0.01	0.80	3.20	0%	14%
		BMI 00:05:95	*0.10*	*0.10*	*0.02*	*0.51*	*1.26*	*0.55*	*0.16*	*0.03*	*0.82*	*3.18*		
OPA, 60°C	No9	BMI 00:05:95	0.15	0.07	0.04	0.43	1.41	0.43	0.14	0.02	0.81	3.19	0%	14%
OPA, 100°C	No8	BMI 00:05:95	0.12	0.13	0.04	0.32	1.56	0.38	0.07	0.00	0.82	3.18	0%	29%
OPA, 125°C	No14	*BMI 00:05:95*	*0.08*	*0.15*	*0.00*	*0.44*	*1.28*	*0.57*	*0.13*	*0.02*	*0.79*	*3.21*	0%	26%
		BMI 00:05:95	0.12	0.13	0.04	0.32	1.56	0.38	0.07	0.00	0.82	3.18		
OPA, 150°C	N013	*BMI 00:05:95*	*0.10*	*0.03*	*0.14*	*0.57*	*1.33*	*0.45*	*0.21*	*0.01*	*0.77*	*3.23*	0%	14%
		BMI 00:00:100	*0.06*	*0.16*	*0.06*	*0.45*	*1.21*	*0.64*	*0.11*	*0.05*	*0.92*	*3.08*		
		BMI 00:00:100	0.20	0.05	0.13	0.34	1.67	0.24	0.09	0.00	0.88	3.12		

Legend: *BMI – beidellite-montmorillonite-illite; %S – probability of smectite layer*

Mineral formula by TEM-EDX and clustering: The cross-checking between phases with limited expandability using ethylene-glycol saturated oriented specimen and TEM-EDX-data (incl. clustering) shows illite-smectite mixed layer phase with K- and charge deficiency. For these phases, montmorillonite is the only smectite component. Beidellite is to assume in traces (BMI 10:40:50) only in one sample, in diVS-ml of group I of untreated Opalinus Clay, original (tab. 15).

Further indications by FTIR: The $AlFe^{3+}OH$ band at 874 cm^{-1} shows a high intensity in comparison with 831 cm^{-1} of AlMgOH band. This is a sign of high content of Fe in octahedral sheet of dioctahedral minerals (e.g. smectite, illite, IS-ml) in Opalinus clay (Craciun, 1984; Gates, 2005).

Development of mass-distribution: diVS-ml phases (group I) show with increasing thermal load a broader variable mass distribution (absolute ± 10%) at the original composition of 29% (fig. 21).

Development of expandability: diVS-ml phases (group I) draw with increasing thermal load at the beginning a rising smectite layer probability from %S=11% (original Opalinus Clay) to close to 26% (100°C) and higher 100°C again a downfall to 16% (16%) (fig. 22). Otherwise, the high smectite diVS-ml phases of sample Opalinus original are immediately removed by the experiments.

Kaolinite-Smectite Mixed-Layer (KS-ml)

Identification by XRD: The occurrence of kaolinite-smectite mixed layer is mainly indicated by modelling of XRD-pattern of oriented specimen using Sybilla-software (developed by Chevron Inc.: Aplin et al., 2006) (tab. 17; fig. 23). Few particles, measured by TEM-EDX, indicated KS-ml phases, but it was not possible to calculate a valid structural formula.

Development of mass-distribution: KS-ml phases in fraction < 2 µm show as trend with increasing thermal load a slight decreasing ratio to the original composition (fig. 24). A cross-check between XRD powder analysis of bulk sample and thermogravimetry (bulk sample) indicates for sample "Opalinus, original" 20 % kaolinite and 5% KS-ml phases.

Development of expandability: KS-ml phases in Opalinus Clay (< 2 µm) draw with increasing thermal load a ± constant smectite layer probability at %S=40% (fig. 25).

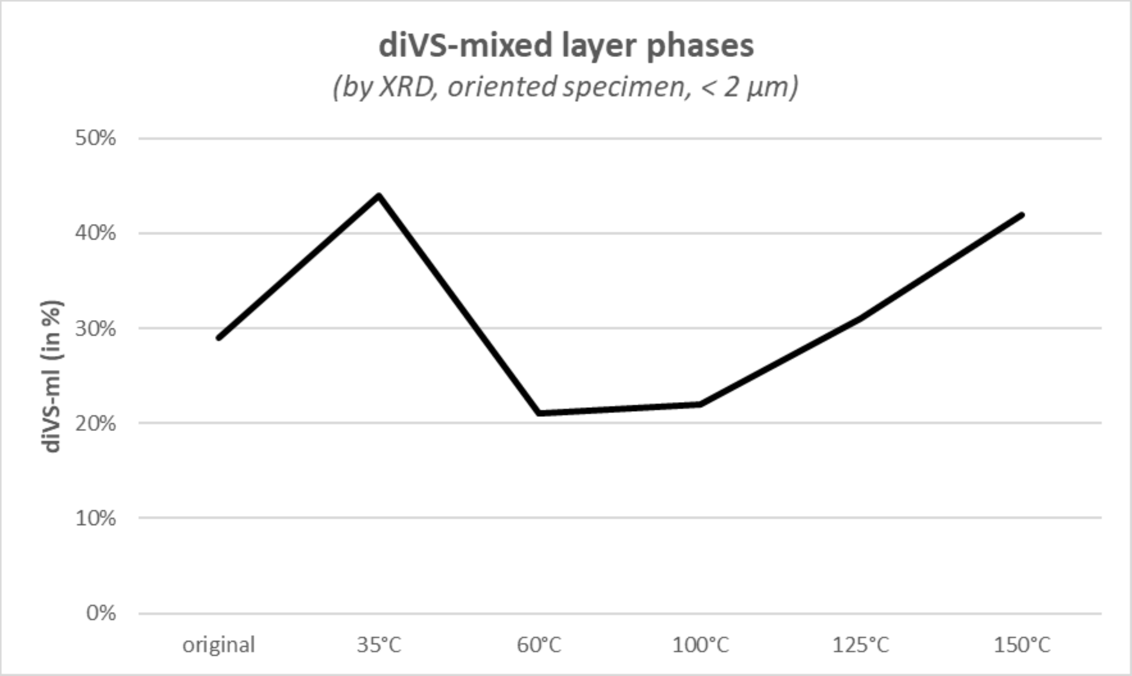

Fig. 21. *Mass distribution of diVS-ml (group I) in bulk samples of Opalinus Clay*

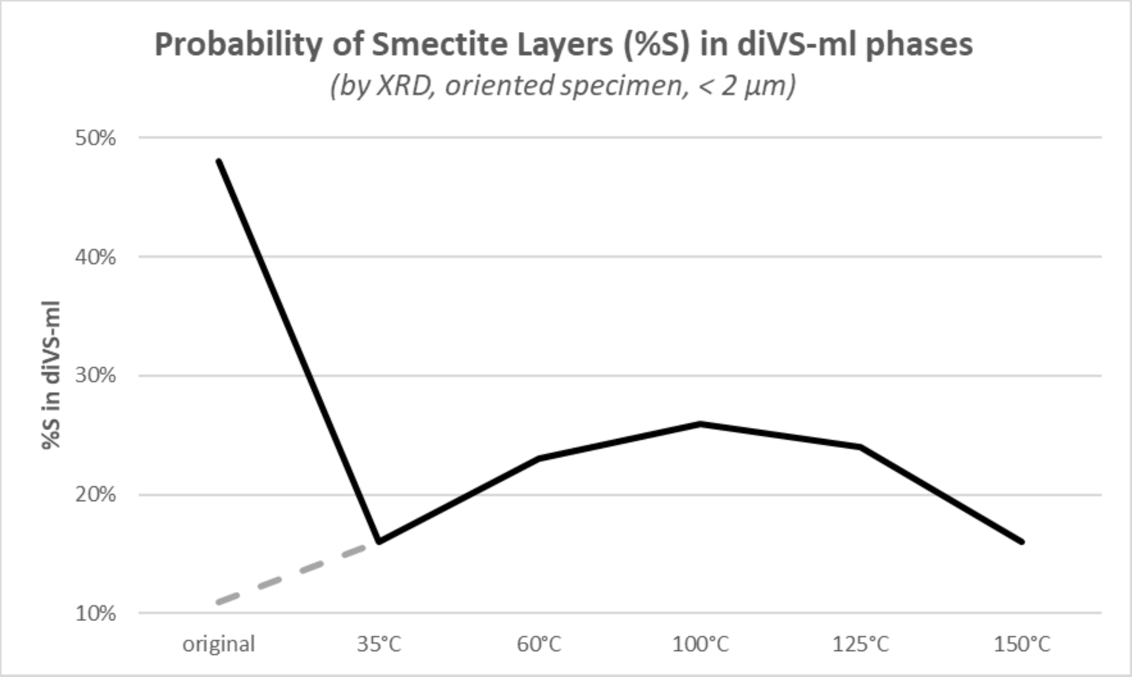

Fig. 22. *Smectite layer probability of diVS-ml (group I) in fraction < 2 µm of Opalinus Clay*

Tab. 17. *Mineral matter of Opalinus Clay (< 2 µm) – oriented specimen*

Sample	**diVS-ml** *(IS GLY R0)*	**diVS-ml** *(ISS GLY R0)*	**Illite**	**Chlorite**	**Kao-linite**	**Kaolinite-Smectite-ml** *(KS GL R0)*	**Kaolinite-Smectite-ml** *(KSS GL R0)*	*Σ total*
OPALINUS original	18% *(%S = 11%)*	11% *(%S = 48%)*	8%	8%	8%	20% *(%S = 14%)*	27% *(%S = 61%)*	*100%*
35°C, 144h **No22**	44% *(%S = 16%)*		14%	4%	7%		32% *(%S = 37%)*	*100%*
60°C, 45.4h **No9**	21% *(%S = 23%)*		14%	5%	16%	10% *(%S = 14%)*	34% *(%S = 53%)*	*100%*
60°C, 95.3h **No7**	32% *(%S = 20%)*		12%	5%	12%	13% *(%S = 9%)*	26% *(%S = 55%)*	*100%*
100°C, 69.3h **No8**	22% *(%S = 26%)*		29%	5%	12%	6% *(%S = 14%)*	27% *(%S = 53%)*	*101%*
125°C, 48.5h **No14**	31% *(%S = 24%)*		26%	5%	8%	12% *(%S = 26%)*	19% *(%S = 35%)*	*101%*
150°C, 48.6h **No13**	42% *(%S = 16%)*		14%	4%	8%	2% *(%S = 28%)*	30% *(%S = 45%)*	*102%*
Without transport cell *35°C* **No9a**	25% *(%S = 20%)*		14%	4%	15%	10% *(%S = 9%)*	31% *(%S = 55%)*	*99%*
125°C **No9b**	13% *(%S = 29%)*		30%	4%	13%	7% *(%S = 14%)*	35% *(%S = 56%)*	*102%*

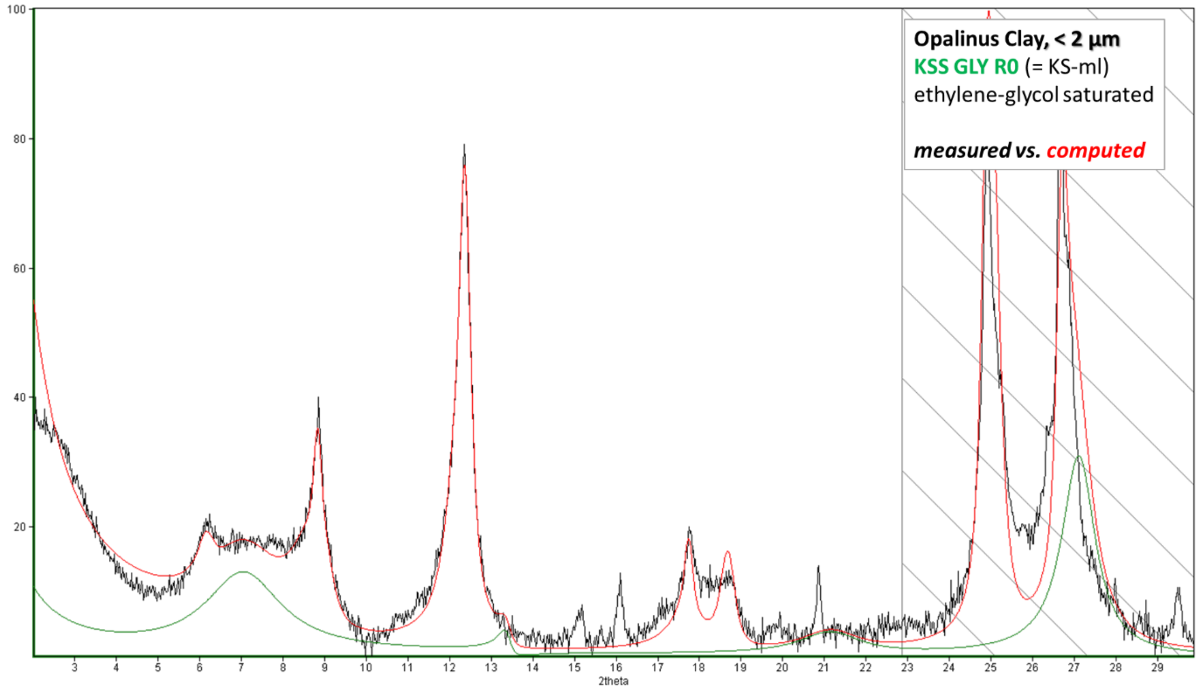

Fig. 23. *Opalinus Clay, original (< 2 µm) - X-ray diffraction pattern of the ethylene-glycol saturated oriented specimen (with computing of KS-ml by Sybilla-software – green line)*

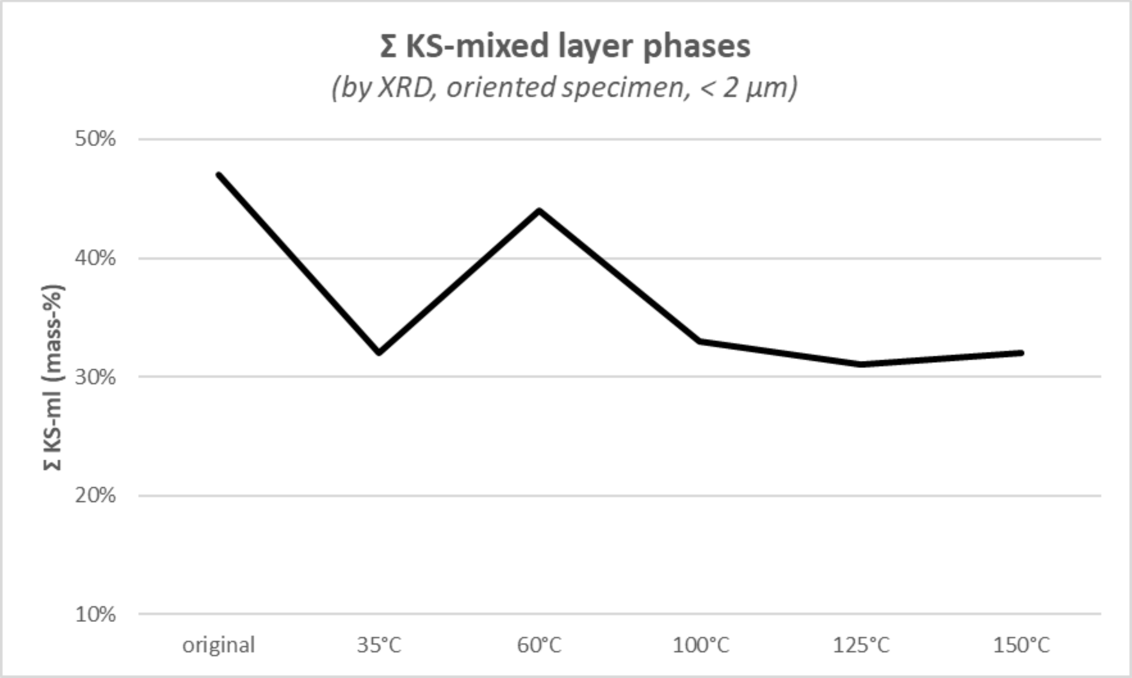

Fig. 24. *Mass distribution of KS-ml in samples of Opalinus Clay (< 2 µm)*

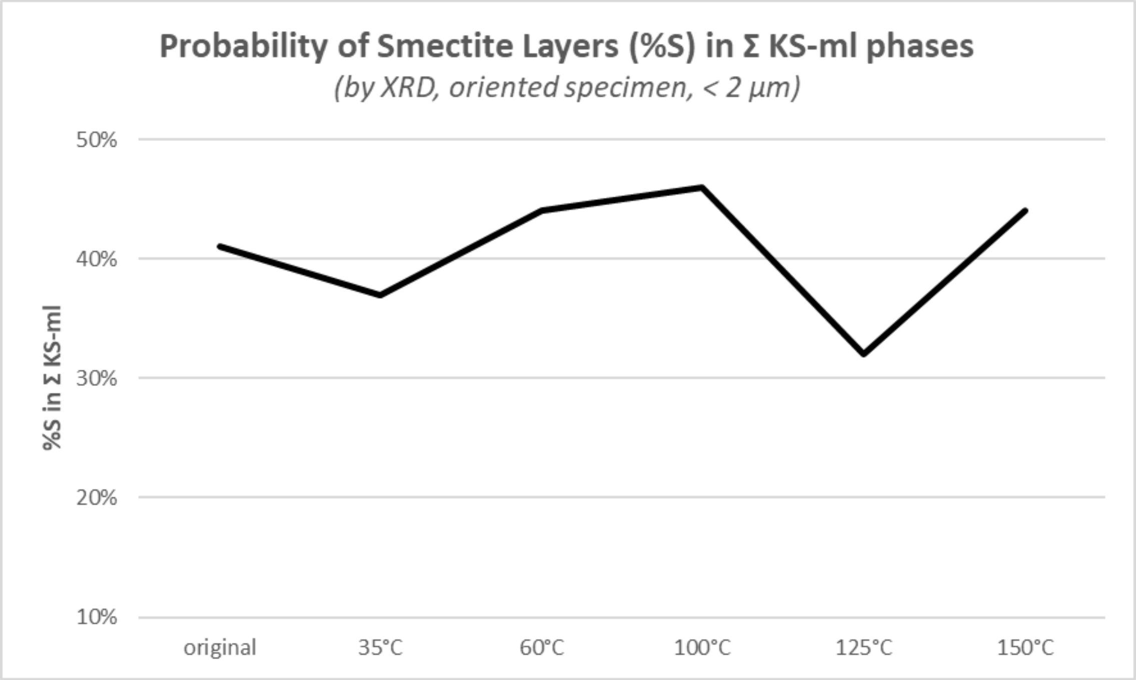

Fig. 25. *Smectite layer probability of KS-ml in fraction < 2 µm of Opalinus Clay-series*

Smectite-behaviour in experiments

Smectite is the main responsible mineralogical phase, which determines the swelling behaviour of clays and bentonites. In Opalinus Clay, smectite is distributed in only two different groups of phases (diVS-ml, KS-ml). Each group has shown a specific behaviour during the experiments (tab. 18).

Tab. 18. *Opalinus Clay – Overview about different smectite behaviour (in direction of rising thermal load in experiments)*

	role of phase in bulk sample	smectite species	mass-% development	%S-development	assumptions to expandab.
diVS-ml *(%S ~ 50%)*	minor phase *(tab. 13)*	montm. >> beidellite *(tab. 15)*	destroyed by each experim. *(fig. 21)*	destroyed by each experim. *(fig. 22)*	reduction
diVS-ml *(%S ~ 20%)*	minor phase *(tab. 13)*	montm. *(tab. 15)*	no trend *(variable at 30% ±10%) (fig. 21)*	≤100°C: rising *(from 11% to 26%)* *(fig. 22)*	slight rising impact
KS-ml	minor phase *(tab. 13)*	not to determine	slight decreas. *(< 2 µm: 47% → 32%)* *(fig. 24)*	± stable *(< 2 µm: at 40% ±8%)* *(fig. 25)*	slight decreasing

The summarizing impact of diVS-ml phases on expandability is mirrored by TEM-EDX-measurements (fig. 26). The original material shows the highest tetrahedral Si-value per $(OH)_2\ O_{10}$ with Si = 3.46. The first Si-downfall to 35°C is caused by the loss of diVS-ml with %S~50% from untreated sample "Opalinus, original" (tab. 17). Following the %S-development of diVS-ml with %S ~ 20%, a rising smectite ratio is to observe also by Si-development until 100°C.

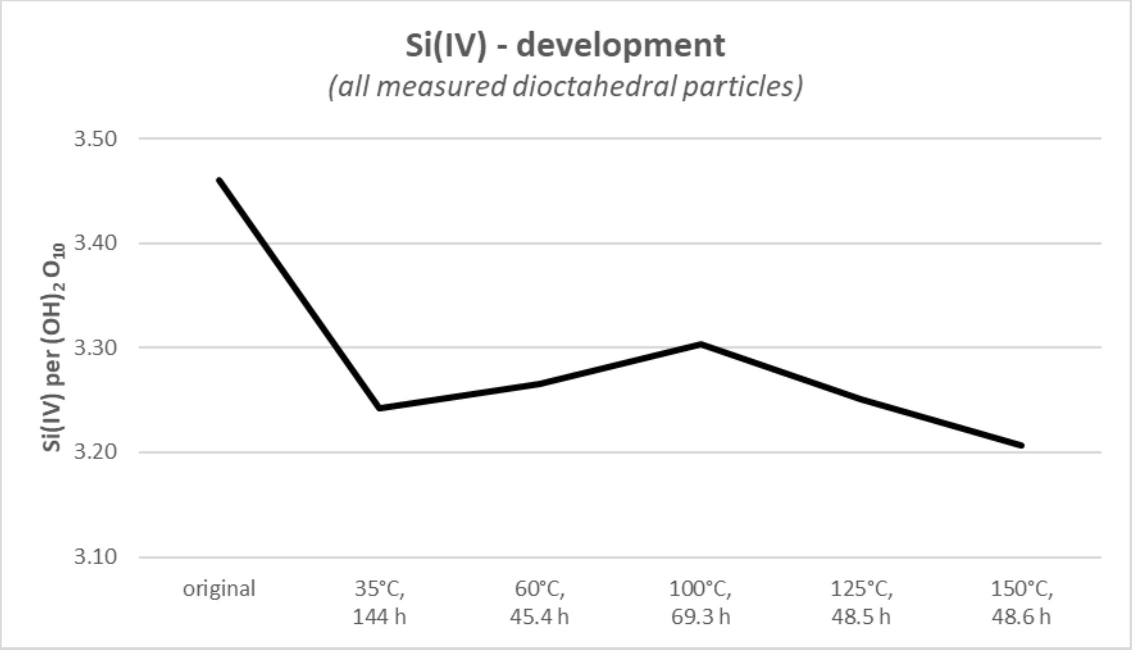

Fig. 26. *Behaviour of tetrahedral Si per $(OH)_2\ O_{10}$ in fraction < 2 µm of Opalinus Clay*
Note: *KS-ml not included here*

TEM-EDX: Illite-behaviour in experiments

All samples are dominated in fraction < 2 µm by illite and offer that's why a sufficient number of illite particles for TEM-EDX-measurements.

The available TEM-EDX-measurements indicate the occurrence of three illite groups: (i) Al(VI)-rich (> 1.5 per $(OH)_2\ O_{10}$), Fe(VI) ≤ 0.4 per $(OH)_2\ O_{10}$ and low Mg(VI) (< 0.1 per $(OH)_2\ O_{10}$), with a high K-deficit; (ii) Al(VI)-rich (< 1.5 per $(OH)_2\ O_{10}$), Fe(VI) ≤ 0.4 per $(OH)_2\ O_{10}$ and moderate Mg(VI) (~ 0.2 per $(OH)_2\ O_{10}$), with only a moderate K-deficit; (iii) Al(VI)-reduced (< 1.3 per $(OH)_2\ O_{10}$), Fe(VI)-rich > 0.5 per $(OH)_2\ O_{10}$ and moderate Mg(VI) (~ 0.2 per $(OH)_2\ O_{10}$), with a moderate K-deficit. These three illite groups are well to recognize in experiments at 35°C (sample No22), at 125°C (sample No14) and at 150°C (sample No13) (fig. Illite_Opalinus). Cluster1 of sample No22 represents illite group (i), Cluster2 mirrors illite group (ii) and Cluster3 shows the illite group (iii). Cluster2 of sample No14 represents illite group (i), Cluster3 mirrors illite group (ii) and Cluster1 shows the illite group (iii). Cluster2 and Cluster4 of sample No13 represent illite group (i), Cluster3 mirrors alteration in illite group (ii) and Cluster1 shows the illite group (iii). Experiments at 60°C (sample No9) and at 100°C (sample No8) show a reduced differentiation of illite particles. Cluster1 of sample No9 seems to mix illite groups (ii) and (iii). In sample No8, illite group (ii) was not identified here.

Following the above introduced division of clusters in this system of illite groups, illite group (i) is nearby unchanged in composition in all experiments. Only a slight substitution of Al by Fe in octahedral layer is to observe with increasing thermal load in experiments. Illite group (ii) is few times not to differentiate after treatment of clay (60°C, 100°C) and shows in experiment at 150°C (No13) a slight substitution of Fe by Al, now with a higher K-deficit. Illite group (iii) shows the same development (enrichment of octahedral Fe by Al-substitution) with increasing thermal load as illite group (i) but linked with slight continuous changes in composition. All these mentioned low-changed compositions in illite groups (i) + (iii) and the more variable behaviour of illite group (ii) could be caused by alteration processes and/or by changes in the thickness of particles. Thinner particles offer a higher surface in interaction with solutions than thicker particles and aggregates. So, thinner particles resist in solutions better, if they contain a higher octahedral Al-ratio and less Fe and Mg (less sheet stress by effect of Fe, Mg-cation diameter).

Tab. 18 Illite_Opalinus. *Opalinus Clay: Illite in fraction < 2 µm (by TEM-EDX)*

	Ca (XII)	Mg (XII)	Na (XII)	K (XII)	Cr3+ (VI)	Al (VI)	Fe3+ (VI)	Mg (VI)	Ti (VI)	Al (IV)	Si (IV)	XII	n_VI	%S	K-deficit	charge-deficit
Opalinus original																
BLT-A7																
Cluster1 *(n=14)*	0.13	0.13	0.01	0.25	0.00	1.39	0.48	0.09	0.04	0.76	3.24	0.76	2.0	6	74%	12%
Opalinus treated																
BFS-B12																
No22 *35°C, 144h*																
Cluster1 *(n=22)*	0.10	0.14	0.03	0.33	0.00	1.58	0.37	0.05	0.01	0.80	3.20	0.83	2.0	3	64%	5%
Cluster2 *(n=30)*	0.10	0.03	0.03	0.56	0.00	1.43	0.39	0.17	0.01	0.68	3.32	0.84	2.0	11	44%	-1%
Cluster3 *(n=34)*	0.10	0.10	0.02	0.51	0.00	1.26	0.55	0.16	0.03	0.82	3.18	0.95	2.0	2	44%	-8%
No9 *60°C, 45.4h*																
Cluster1 *(n=64)*	0.15	0.07	0.04	0.43	0.00	1.41	0.43	0.14	0.02	0.81	3.19	0.93	2.0	3	53%	-6%
Cluster2 *(n=20)*	0.10	0.01	0.03	0.62	0.00	1.37	0.39	0.23	0.01	0.68	3.32	0.88	2.0	11	38%	-5%
No8 *100°C, 69.3h*																
Cluster1 *(n=38)*	0.08	0.15	0.00	0.44	0.00	1.28	0.57	0.13	0.02	0.79	3.21	0.90	2.0	4	52%	-3%
Cluster2 *(n=52)*	0.06	0.08	0.00	0.54	0.00	1.52	0.35	0.12	0.01	0.69	3.31	0.81	2.0	10	45%	4%
No14 *125°C, 48.5h*																
Cluster1 *(n=33)*	0.11	0.10	0.06	0.47	0.00	1.18	0.59	0.19	0.04	0.82	3.18	0.96	2.0	2	48%	-9%
Cluster2 *(n=38)*	0.12	0.13	0.04	0.32	0.00	1.56	0.38	0.07	0.00	0.82	3.18	0.87	2.0	2	65%	1%
Cluster3 *(n=50)*	0.12	0.02	0.06	0.57	0.00	1.36	0.40	0.23	0.01	0.70	3.30	0.91	2.0	9	42%	-8%
No13 *150°C, 48.6h*																
Cluster1 *(n=10)*	0.06	0.16	0.06	0.45	0.00	1.21	0.64	0.11	0.05	0.92	3.08	0.97	2.0	-2	48%	-8%
Cluster2 *(n=9)*	0.05	0.00	0.09	0.68	0.00	1.39	0.40	0.21	0.00	0.68	3.32	0.88	2.0	11	32%	-5%
Cluster3 *(n=15)*	0.20	0.05	0.13	0.34	0.00	1.67	0.24	0.09	0.00	0.88	3.12	0.97	2.0	0	61%	-9%
Cluster4 *(n=38)*	0.10	0.03	0.14	0.57	0.00	1.33	0.45	0.21	0.01	0.77	3.23	0.98	2.0	5	39%	-13%

Legend: *(n=22) – number of illite particles measured by TEM-EDX; XII – interlayer charge; n_VI – number of atoms in octahedral layer per (OH)$_2$ O$_{10}$; %S – probability of smectite layers in senso of Środon et al. (1992); K-deficit, charge-deficit – in senso of Środon et al. (1992) (normal K in illite = 0.89 per (OH)$_2$ O$_{10}$)*

References

Aplin, A.C., Matenaar, I.F., McCarty, D.K., van der Pluijm, B.A. (2006). Clays Clay Miner 54, 500-514. DOI: 10.1346/CCMN.2006.0540411

Bergmann, J., Friedel, P., Kleeberg, R., 1998. BGMN — a new fundamental parameter based Rietveld program for laboratory X-ray sources, its use in quantitative analysis and structure investigations. CPD Newsl. 20, 5–8.

Bossart, P., Tury, M. (Ed.) (2008. Mont Terri Rock Laboratory. Project, Programme 1996 to 2007 and Results, Federal Office of Topography

Cliff, G. & Lorimer, G. W. (1975). J. Microsc. 103, 203–207.

Döbelin, N., Kleeberg, R. (2015). Journal of Applied Crystallography 48, 1573-1580. DOI: 10.1107/S1600576715014685

Henning, K.-H. (1971): Mineralogische Untersuchung des eozänen Tones der Lagerstätte Friedland (Bezirk Neubrandenburg).- In: Ber.dtsch.Ges.geol.Wiss., B.- 16 (5), 5-39.

Henning, K.-H. & Störr, M. (1986). Electron Micrographs (TEM, SEM) of Clays and Clay Minerals, p. 325. Akademie-Verlag Berlin.

Hoang-Minh, T., Kasbohm, J., Nguyen-Thanh, L., Nga, P. T., Lai, L. T., Duong, N. T., Thanh, N. D., Thuyet, N. T. M., Anh, D. D., Pusch, R., Knutsson, S. & Ferreiro Mahlmann, R. (2019). J. Appl. Cryst. 52, 133-147. DOI: 10.1107/S1600576718018162

Karnland, O., Olsson, S., and Nilsson, U. (2006) Mineralogy and sealing properties of various bentonites and smectite-rich clay materials. In: Technical Report of SKB TR-06-30, SKB, Stockholm, Sweden, 112 pp.

Kaufhold, S., Hein, M., Dohrmann, R., and Ufer, K. (2012). Quantification of the mineralogical composition of clays using FTIR spectroscopy. Vibrational Spectroscopy 59, 29 – 39. DOI: 10.1016/j.vibspec.2011.12.012

Kleeberg, R., Ufer, K., and Bergmann, J. (2010) Rietveld analysis with BGMN Rietveld method physical basics profile modelling quantification. In: BGMN workshop Freiberg 2010. Technische Universität Bergakademie Freiberg. Freiberg, Germany, 87 pp.

Lee, B.D., Sears, S.K., Graham, R.C., Amrhein, C., Vali, H., 2003. Secondary mineral genesis from chlorite and serpentine in an ultramafic soil toposequence. Soil Sci. Soc. Am. J. 67, 1309–1317. http://dx.doi.org/10.2136/sssaj2003.1309.

Lorimer, G. W. & Cliff, G. (1976). Electron Microscopy in Mineralogy, edited by H. R. Wenk, pp. 506–519. Berlin: Springer Verlag.

Matschiavelli N, Kluge S, Podlech C, Standhaft D, Grathoff G, Ikeda-Ohno A, Warr LN, Chukharkina A, Arnold T, Cherkouk A. (2019). The Year-Long Development of Microorganisms in Uncompacted Bavarian Bentonite Slurries at 30 and 60 °C. Environ Sci Technol. 53(17),10514-10524. DOI: 10.1021/acs.est.9b02670.

Mellini, M. & Menichini, R. (1985). R. Soc. Ital. Miner. Petrol. 40, 261–266.

Moore, D.M., Reynolds, R.C., 1997. X-ray Diffraction and the Identification and Analysis of Clay Minerals, 2nd ed. Oxford University Press.

NAGRA (2002). Project Opalinus Clay - Safety Report – Demonstration of disposal feasibility for spent fuel, vitrified high-level waste and long-lived intermediate-level waste (Entsorgungsnachweis). TECHNICAL REPORT 02-05. ISSN 1015-2636

Nguyen-Thanh, L., Herbert, H.-J., Kasbohm, J., Hoang-Minh, T. & Mählmann, R. F. (2014). Clays Clay Miner. 62, 425–446.

Pearson, F.J., Arcos, D., Bath, A., Boisson, J.-Y., Fernández, A. M., Gäbler, H.-E., Gaucher, E., Gautschi, A., Griffault, L., Hernán, P., and Waber, H. N. (2003. Mont Terri Project – Geochemistry of Water in the Opalinus Clay Formation at the Mont Terri Rock Laboratory. No. 5, Berichte des BWG, Serie Geologie – Rapports de l'OFEG, Série Géologie – Rapporti dell'UFAEG, Serie Geologia – Reports of the FOWG, Geology Series.

Środoń, J., Elsass, F., McHardy, W. J. & Morgan, D. J. (1992). Clay Miner. 27, 137–158.

Ufer, K., Roth, G., Kleeberg, R., Stanjek, H., Dohrmann, R., Bergmann, J., 2004. Description of X-ray powder pattern of turbostratically disordered layer structures with a Rietveld compatible approach. Z. Krist. 219, 519–527. doi.org/10.1524/zkri.219.9.519.44039.

Ufer, K., Stanjek, H., Roth, G., Dohrmann, R., Kleeberg, R., Kaufhold, S. (2008) Quantitative phase analysis of bentonites by the Rietveld method. Clays and Clay Minerals, 56, 272-282. dx.doi.org/10.1346/CCMN.2008.0560210.

Part III. SUPPLEMENTS

S1. Overhead shaking experiments of B25-bentonite and Opalinus clay

Content

Sample - B25 (< 2 µm), original material

Preparation for TEM

- raw material: <40 µm powder of original B25-sample
- suspension on particles < 2 µm on carbon-filmed Cu-grid
- air-dried and humidity-controlled storing

Mineral Matter

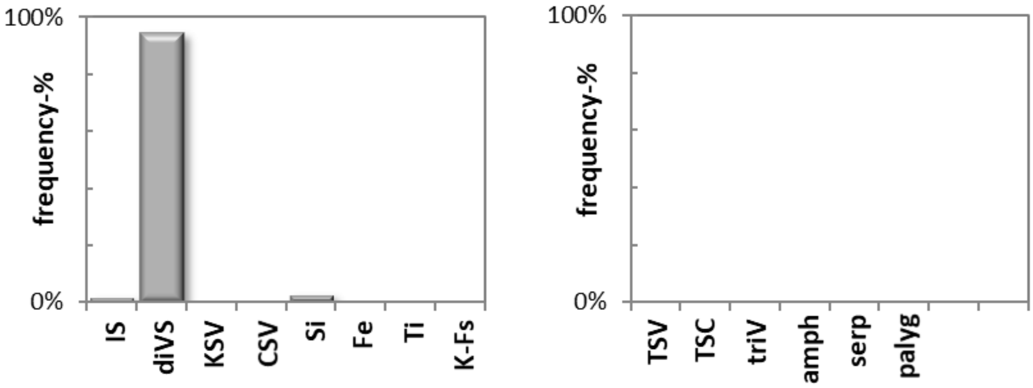

Fig. 49. Distribution of mineral groups in fraction < 2 µm (in frequency-%)
Legend: ***IS*** *– illite-smectite-mixed layer series in sense of Środon et al. (1992), diVS – dioctahedral vermiculite-smectite illite-smectite-mixed layer series (= charge- and/or K-deficit),* ***KSV*** *– kaolinite-smectite-dioctahedral vermiculite-mixed layer series,* ***CSV*** *– chlorite-saponite-trioctahedral vermiculite-mixed layer series,* ***Si*** *– quartz or particles with Si-surplus,* ***Fe*** *– Fe-oxide or Fe-oxyhydroxide,* ***Ti*** *– Ti-bearing phases (e.g. rutile, anatase),* ***K-Fs*** *– K-feldspar*

Clay Mineral Composition

Illite-smectite mixed-layer series (summarized: IS + diVS):

$$Ca_{0.10}\,Mg_{0.08}\,Na_{0.01}\,K_{0.12}\quad Al_{1.27}\,Fe^{3+}_{0.56}\,Mg_{0.17}\,Ti_{0.00}\,(OH)_2\quad Si_{3.70}\,Al_{0.30}\,O_{10}$$

Charge: XII = 0.48 VI = 5.82 IV = 15.70 **Σ = 22.00**
Probability of smectite layers (%S): 54%
Probability of illite layers (%I): 46%
Specific Dissolution Potential (ΔS%)
for H2O, 20 + 60 rpm -8 (= slow reacting)
for NaCl, 20 rpm -9 (= slow reacting)
for NaCl, 60 rpm -96 (= fast reacting, 'illitization')
CEC_{calc}: 48 meq / 100 g (literature: 56 meq / 100 g [MAT19])

Measured particles: 110

Table 11. *Summarized chemical composition*

SiO_2	TiO_2	Al_2O_3	Fe_2O_3	MnO	MgO	CaO	Na_2O	K_2O	P_2O_5	Σ	
58.6%	0.0%	22.0%	5.9%		3.0%	1.0%	0.1%	1.1%	0.1%	0.92	measured particles
61.5%	0.5%	21.1%	6.4%	0.1%	4.0%	3.8%	0.4%	2.0%	0.1%	1.00	MAT19 (bulk sample)

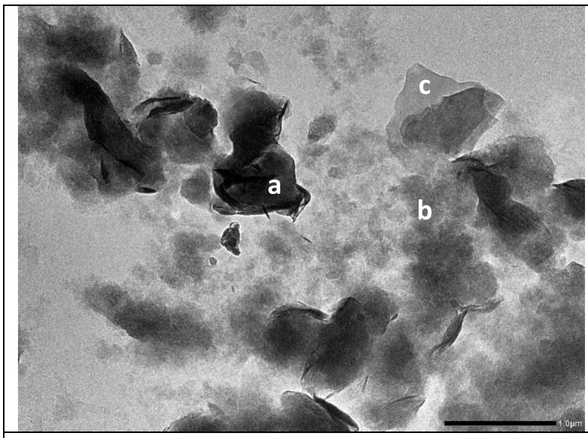	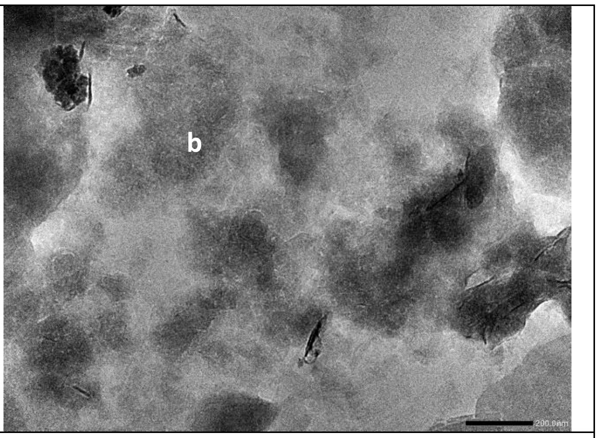
JEM-2100_MAG_X10k_B25-40um_I08.bmp Magnification: 10k (d) large (≤ 1 µm) xenomorph film-like platy crystals with folds; (e) aggregates formed by small (≤ 200 nm) xenomorphous plates; (f) large (≤ 1 µm) xenomorph plates, homogenous thickness	*JEM-2100_MAG_X30k_B25-40um_I10.bmp* Magnification: 30k (b) aggregates formed by small (≤ 200 nm) xenomorphous plates

Fig. 50. *Morphology of particles (TEM-micrographs)*

Distribution of smectite layers probability (%S)

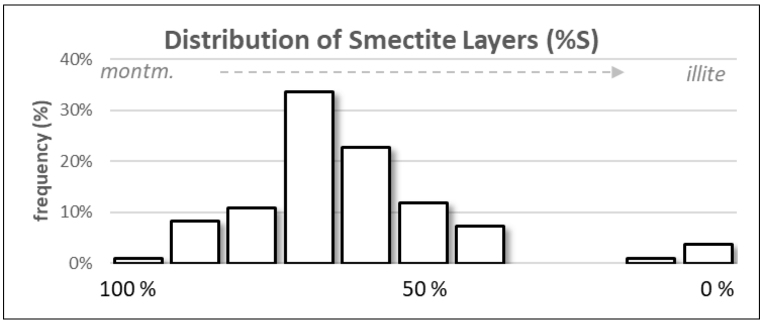

Description: *The distribution of %S-probability indicates the occurrence of three groups: (i) montmorillonite (in traces), (ii) mixture of beidellite-montmorillonite interstratifications (= assumption) with diVS-ml as well as (iii) illite with K-deficiency.*

Fig. 51. *Distribution of smectite layers probability (%S)*

Distribution of charges (exchangeable from interlayer space)

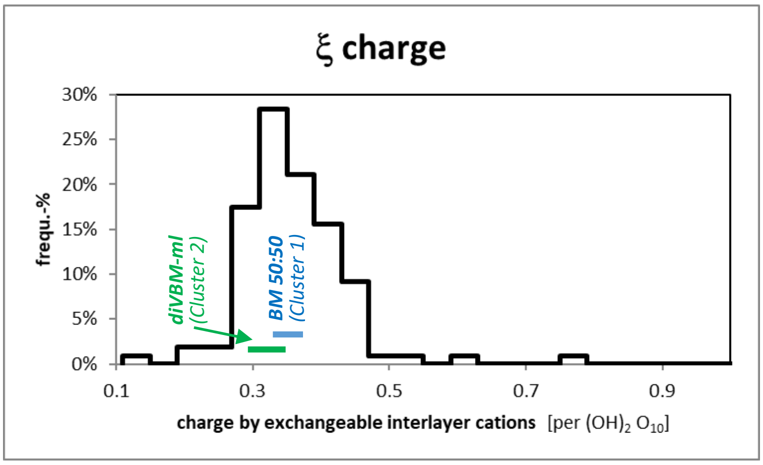

This diagram visualizes the distribution of exchangeable charges in the interlayer space (Ca, Mg, Na) determined and computed by TEM-EDX-data.

Description: *Maximal frequency-% of charge density at 0.35 per* $(OH)_2 O_{10}$.

Fig. 52. *Distribution of charges*

Beidellite-montmorillonite interstratification (BM ~ 50%:50%) *(Cluster1):*

$$Ca_{0.10}\ Mg_{0.07}\ Na_{0.01}\ K_{0.09}\quad Al_{1.26}\ Fe^{3+}_{0.56}\ Mg_{0.18}\ Ti_{0.00}\ (OH)_2\quad Si_{3.74}\ Al_{0.26}\ O_{10}$$

Charge: XII = 0.44 VI = 5.82 IV = 15.74 **Σ = 22.00**

Probability of montmorillonite layers (%M): 52%
Probability of beidellite layers (%B): 48%

Measured particles: 92

Distribution of BM-interstratifications (Cluster1)

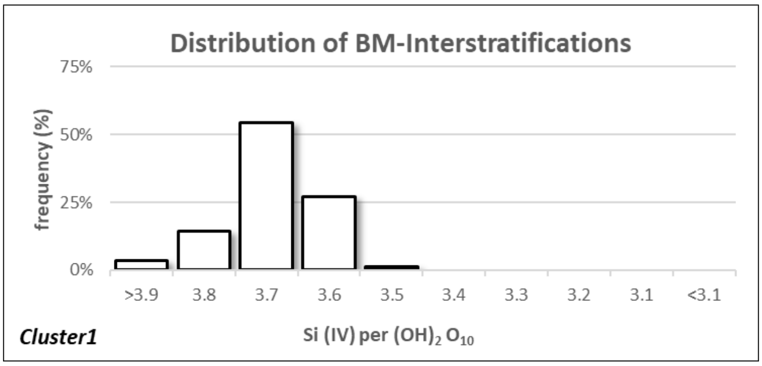

Description: *The distribution of BM-interstratifications (classified as Cluster1) draws a maximum of frequency (%) for tetrahedral Si-value at 3.7 e phuc*

Fig. 53a. *Distribution of assumed beidellite-montmorillonite interstratifications*

Cluster 1 BM 50:50		*particles (abs)*	Ca (XII)	Mg (XII)	Na (XII)	K (XII)	Cr3+ (VI)	Al (VI)	Fe3+ (VI)	Mg (VI)	Ti (VI)	Al (IV)	Si (IV)	XII	n_VI	%S
Si	>3.9	n = 3	0.07	0.10	0.00	0.02	0.00	1.31	0.49	0.15	0.00	0.09	3.91	0.4	2.0	92
Si	3.9-3.8	n = 13	0.07	0.08	0.01	0.04	0.00	1.32	0.49	0.19	0.00	0.16	3.84	0.3	2.0	76
Si	**3.8-3.7**	**n = 50**	**0.11**	**0.07**	**0.01**	**0.09**	**0.00**	**1.24**	**0.57**	**0.19**	**0.00**	**0.26**	**3.74**	**0.4**	**2.0**	**53**
Si	3.7-3.6	n = 25	0.11	0.08	0.01	0.12	0.00	1.26	0.57	0.17	0.00	0.34	3.66	0.5	2.0	35
Si	3.6-3.5	n = 1	0.16	0.11	0.00	0.09	0.00	1.03	0.77	0.20	0.00	0.42	3.58	0.6	2.0	18
Si	3.5-3.4	n = 0														
Si	3.4-3.3	n = 0														
Si	3.3-3.2	n = 0														
Si	3.2-3.1	n = 0														
Si	<3.1	n = 0														

Fig. 53b. *Computed averaged mineral formulae of phases in the different Si(IV)-classes*

Dioctahedral vermiculite-beidellite/montmorillonite mixed layer phases (diVBM-ml):
(charge- and/or K-deficit; confirmed as Cluster2):

$$Ca_{0.08}\ Mg_{0.09}\ Na_{0.01}\ K_{0.27}\quad Al_{1.31}\ Fe^{3+}_{0.56}\ Mg_{0.12}\ Ti_{0.01}\ (OH)_2\quad Si_{3.50}\ Al_{0.50}\ O_{10}$$

Charge: XII = 0.61 VI = 5.89 IV = 15.50 **Σ = 22.00**
Probability of montmorillonite layers (%M): ~30%
Probability of beidellite layers (%B): ~20%
Probability of dioct. vermiculite layers (%V): ~50%

Measured particles: 18

Estimation of %M, %B, %I: $0.30 * 4\ Si_{montm} + 0.20 * 3.5\ Si_{beid} + 0.50 * 3.2\ Si_{verm} = \mathbf{3.50\ Si_{total}}$ **(phfu)**
%I by XRD: 45% for IS R0 GLY (2)

Distribution of smectite layers probability (%S) in diVS-ml (Cluster2)

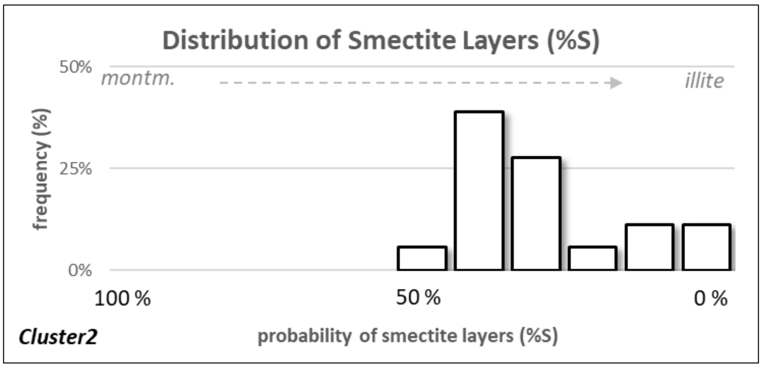

Description: *The distribution of %S-probability of diVS-ml (classified as Cluster2) indicates the occurrence of two groups: (i) diVS-ml with a maximum of frequency (%) for smectite layer probability at 40% as well as (ii) illite with K-deficiency.*

Fig. 54a. *Distribution of smectite layers probability in diVS-ml*

Cluster 2 IS R0 diVS	*particles (abs)*	Ca (XII)	Mg (XII)	Na (XII)	K (XII)	Cr3+ (VI)	Al (VI)	Fe3+ (VI)	Mg (VI)	Ti (VI)	Al (IV)	Si (IV)	XII	n_VI	%S
%S >95%	n = 0														
%S 95-85%	n = 0														
%S 85-75%	n = 0														
%S 75-65%	n = 0														
%S 65-55%	n = 0														
%S 55-45%	n = 1	0.13	0.04	0.00	0.18	0.00	1.21	0.56	0.20	0.03	0.36	3.64	0.5	2.0	46
%S 45-35%	**n = 7**	**0.08**	**0.09**	**0.01**	**0.19**	**0.00**	**1.30**	**0.57**	**0.13**	**0.01**	**0.40**	**3.60**	**0.5**	**2.0**	**40**
%S 35-25%	**n = 5**	**0.08**	**0.07**	**0.01**	**0.25**	**0.00**	**1.34**	**0.55**	**0.10**	**0.01**	**0.45**	**3.55**	**0.5**	**2.0**	**34**
%S 25-15%	n = 1	0.06	0.08	0.04	0.33	0.00	1.50	0.42	0.06	0.02	0.61	3.39	0.7	2.0	17
%S 15- 5%	n = 2	0.10	0.13	0.02	0.36	0.00	1.08	0.78	0.13	0.01	0.73	3.27	0.9	2.0	8
%S <5%	n = 2	0.03	0.15	0.00	0.51	0.00	1.49	0.41	0.10	0.00	0.78	3.22	0.9	2.0	4

Fig. 54b. *Computed averaged mineral formulae of diVS-ml phases in the different smectite layers probability (%S)-classes*

[ATTENTION: value for %S by TEM is too low in comparison to %S by XRD = 55% - is that an indication for interstratification with beidellite?]

Distribution of diVBM-interstratifications (Cluster2)

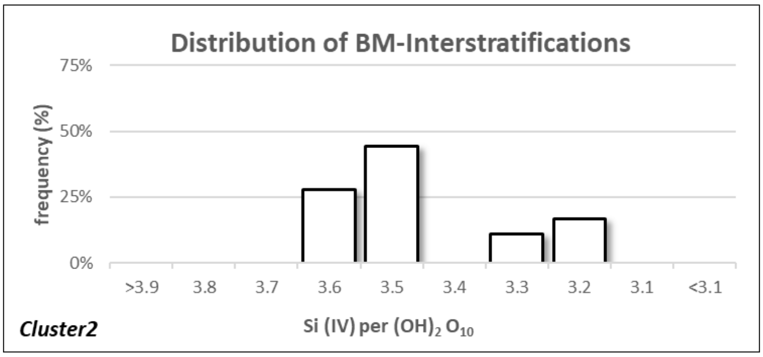

Description: *The distribution of diVBM-interstratifications (classified as Cluster2) draws a maximum of frequency (%) for tetrahedral Si-value at 3.5 e phuc*

Fig. 55a. *Distribution of assumed dioctahedral vermiculite-beidellite-montmorillonite interstratifications*

Cluster 2 diVBM 50:20:30	*particles (abs)*	Ca (XII)	Mg (XII)	Na (XII)	K (XII)	Cr3+ (VI)	Al (VI)	Fe3+ (VI)	Mg (VI)	Ti (VI)	Al (IV)	Si (IV)	XII	n_VI	%V, %B,%M
Si >3.9	n = 0														
Si 3.9-3.8	n = 0														
Si 3.8-3.7	n = 0														
Si 3.7-3.6	n = 5	0.07	0.08	0.01	0.19	0.00	1.30	0.56	0.13	0.01	0.38	3.62	0.5	2.0	35:20:45
Si 3.6-3.5	**n = 8**	**0.09**	**0.07**	**0.00**	**0.22**	**0.00**	**1.31**	**0.56**	**0.12**	**0.01**	**0.44**	**3.56**	**0.5**	**2.0**	**45:15:40**
Si 3.5-3.4	n = 0														
Si 3.4-3.3	n = 2	0.06	0.05	0.04	0.46	0.00	1.50	0.39	0.09	0.02	0.65	3.35	0.7	2.0	75:10:15
Si 3.3-3.2	n = 3	0.07	0.19	0.00	0.38	0.00	1.21	0.68	0.12	0.00	0.78	3.22	0.9	2.0	95: 5: 0
Si 3.2-3.1	n = 0														
Si <3.1	n = 0														

Fig. 55b. *Computed averaged mineral formulae of phases in the different Si(IV)-classes*

Mineral Matter – Specification

Result of Clustering & Comparison with XRD-data (Sybilla-processing)

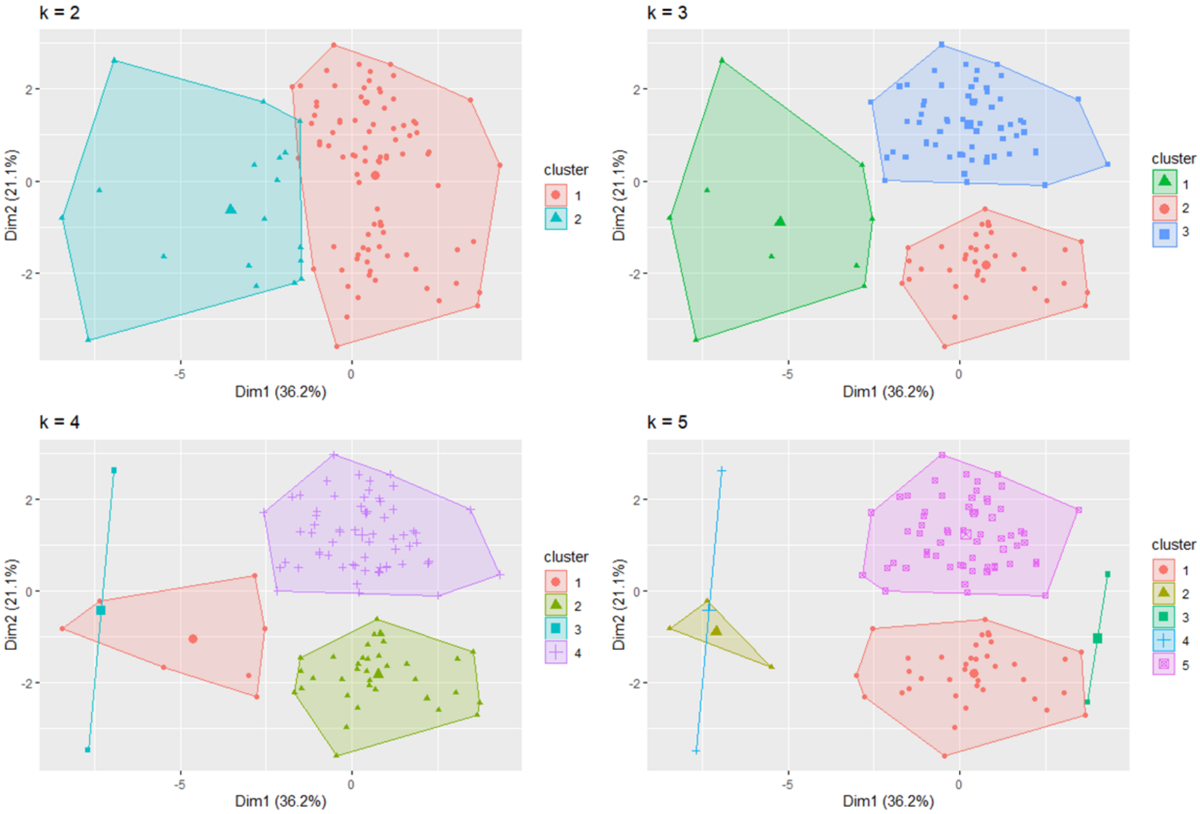

Fig. 56. *Clustering of all measured particles for clusters k = 2, k = 3, k = 4 and k = 5 (source for R-coding: https://uc-r.github.io/kmeans_clustering)*

		Ca (XII)	Mg (XII)	Na (XII)	K (XII)	Cr3+ (VI)	Al (VI)	Fe3+ (VI)	Mg (VI)	Ti (VI)	Al (IV)	Si (IV)	XII	n_VI	%S
Cluster1	n = 92	0.10	0.07	0.01	0.09	0.00	1.26	0.56	0.18	0.00	0.26	3.74	0.45	2.0	52
Cluster2	n = 18	0.08	0.09	0.01	0.27	0.00	1.31	0.56	0.12	0.01	0.50	3.50	0.61	2.0	28

Fig. 57. *Mineral formulae based on TEM-EDX-data summarized following the result of clustering for k=2*

	Sybilla-modelling of XRD-results	**TEM-EDX-results**	**Notes**
Cluster1	IS R0 *(%S = 99%)**	BM 50:50 *(%B=48%, %S = 52%)*	*K in traces only, Fe(VI)-rich*
Cluster2	IS R0 *(%S = 55%)*	diVBM-ml *(%I=50%, %BM=50%)*	*high K-deficit, Fe(VI)-rich, low Mg(VI)*

Tab. 12. *Comparison of results from TEM-EDX- and XRD-measurements with clustering procedure*
(- beidellite is to verify by XRD only by Li-test)*

Sample - B25 (< 2 µm), treated H_2O 20 rpm

Preparation for TEM

- raw material: <40 µm powder of B25-sample after treatment by H_2O 20 rpm
- suspension on particles < 2 µm on carbon-filmed Cu-grid
- air-dried and humidity-controlled storing

Mineral Matter

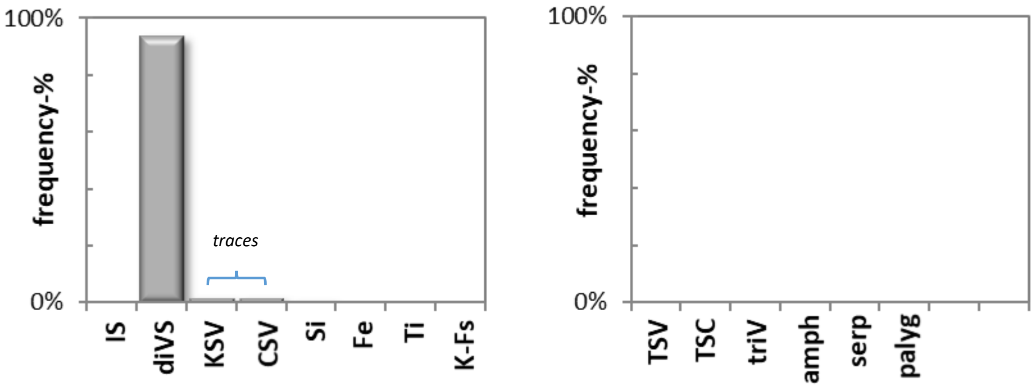

Fig. 58. *Distribution of mineral groups in fraction < 2 µm (in frequency-%)*
Legend: ***IS*** *– illite-smectite-mixed layer series in sense of Środon et al. (1992), diVS – dioctahedral vermiculite-smectite illite-smectite-mixed layer series (= charge- and/or K-deficit),* ***KSV*** *– kaolinite-smectite-dioctahedral vermiculite-mixed layer series,* ***CSV*** *– chlorite-saponite-trioctahedral vermiculite-mixed layer series,* ***Si*** *– quartz or particles with Si-surplus,* ***Fe*** *– Fe-oxide or Fe-oxyhydroxide,* ***Ti*** *– Ti-bearing phases (e.g. rutile, anatase),* ***K-Fs*** *– K-feldspar*

Clay Mineral Composition

Dioctahedral vermiculite-smectite mixed-layer series *(charge- and/or K-deficit):*

$$Ca_{0.09}\ Mg_{0.08}\ Na_{0.01}\ K_{0.13}\quad Al_{1.25}\ Fe^{3+}_{0.59}\ Mg_{0.15}\ Ti_{0.01}\ (OH)_2\quad Si_{3.64}\ Al_{0.36}\ O_{10}$$

Charge: XII = 0.50 VI = 5.86 IV = 15.64 **Σ = 22.00**

Probability of smectite layers (%S):	46%
Probability of illite layers (%I):	54%
CEC_{calc}:	49 meq / 100 g
Measured particles:	92

Table 13. *Summarized chemical composition*

SiO_2	TiO_2	Al_2O_3	Fe_2O_3	MnO	MgO	CaO	Na_2O	K_2O	P_2O_5	Σ	
59.5%	0.1%	23.2%	6.5%		3.0%	1.0%	0.1%	1.2%	0.0%	0.94	measured particles
58.6%	0.0%	22.0%	5.9%		3.0%	1.0%	0.1%	1.1%	0.1%	0.92	original B25 (< 2µm)

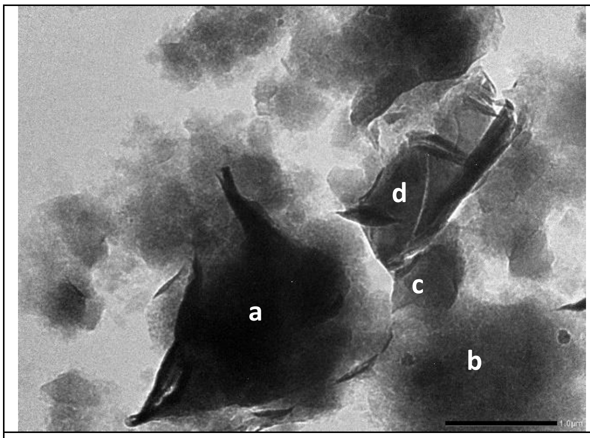 	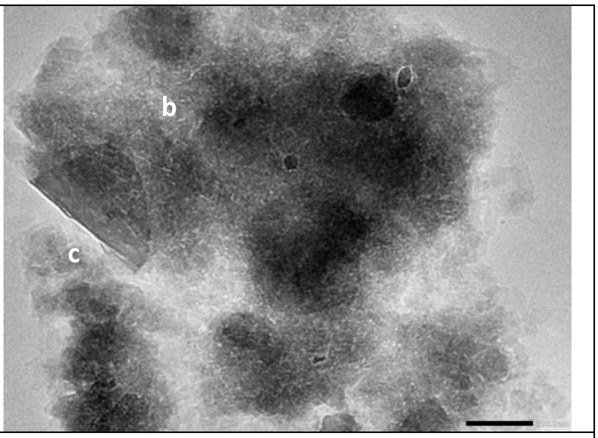
JEM-2100_MAG_X10k_B25-H2O-20r_006.bmp Magnification: 10k (a) large (~ 1 µm) xenomorph film-like platy crystals with folds *(diVS-ml mainly with %S-range 40-60%)*; (b) aggregates formed by small (≤ 200 nm) xenomorphous platy crystals *(diVS-ml mainly with %S-range 60-70%)*; (c) large (≤ 1 µm) xenomorph plates, homogenous thickness (*dioctahedral vermiculite*) (d) large (≤ 1 µm) xenomorph plates with indications for partial dissolution processes *(assumed: CSV-ml with %C=30%, %S=30%; %V=40%)*	*JEM-2100_MAG_X30k_B25-H2O-20r_003.bmp* Magnification: 30k (c) aggregates formed by small (≤ 200 nm) xenomorphous platy crystals *(diVS-ml mainly with %S-range 45-60%)* (d) large (≤ 1 µm) xenomorph plates, homogenous thickness *(diVS-ml mainly with %S-range < 40%)*

Fig. 59. *Morphology of particles (TEM-micrographs)*

Distribution: Smectite layers probability (%S)

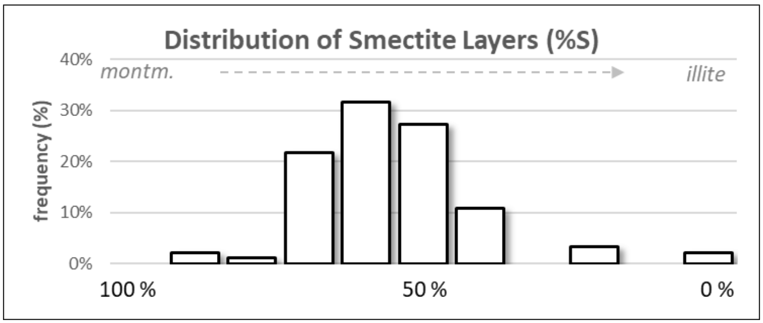

Description: *The distribution of %S-probability indicates the occurrence of three groups: (i) montmorillonite (in traces), (ii) diVS-ml with %S-range of 50-60% (= main group) and (iii) illite with K- and charge deficit.*

Fig. 60. *Distribution of smectite layers probability (%S)*

Distribution: Charge density of exchangeable cations

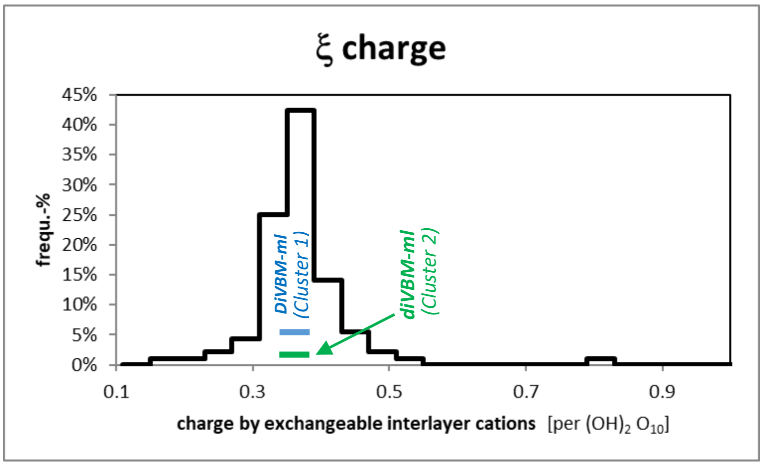

This diagram visualizes the distribution of exchangeable charges in the interlayer space (Ca, Mg, Na) determined and computed by TEM-EDX-data.

Description: *Narrow charge density distribution of exchangeable interlayer cations at 0.37 per* $(OH)_2\ O_{10}$.

Fig. 61. *Distribution of charges*

Dioctahedral vermiculite-beidellite/montmorillonite-ml (diVBM ~10%:50%:40%) *(Cluster1):*

$$\mathrm{Ca_{0.10}\ Mg_{0.08}\ Na_{0.01}\ K_{0.11}\quad Al_{1.22}\ Fe^{3+}_{0.61}\ Mg_{0.17}\ Ti_{0.01}\ (OH)_2\ \ Si_{3.68}\ Al_{0.32}\ O_{10}}$$

Charge: XII = 0.48 VI = 5.84 IV = 15.68 **Σ = 22.00**

Probability of montmorillonite layers (%M): 40%
Probability of beidellite layers (%B): 54%
Probability of illite layers (%I): 6%

Measured particles: 71

Estimation of %M, %B, %I: 0.40 * 4 $\mathrm{Si_{montm}}$ + 0.54 * 3.5 $\mathrm{Si_{beid}}$ + 0.06 * 3.2 $\mathrm{Si_{verm}}$ = **3.68 $\mathrm{Si_{total}}$ (phfu)**
%I by XRD: 5% for IS R0 GLY (1)

Distribution of BM-interstratifications (Cluster1)

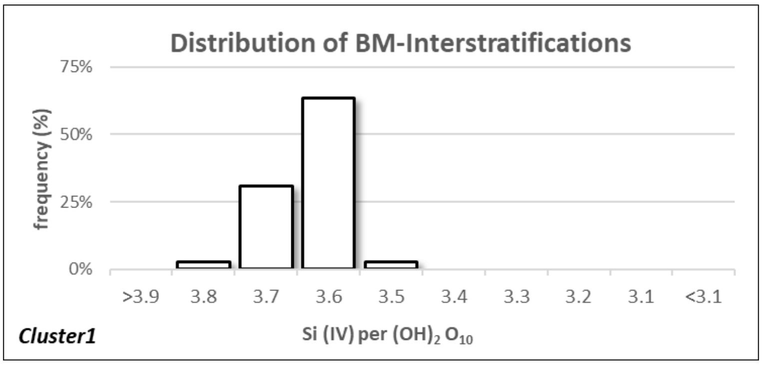

Description: *The distribution of BM-interstratifications (classified as Cluster1) draws a maximum of frequency (%) at tetrahedral Si-value between 3.6 – 3.7 e phuc*

Fig. 62a. *Distribution of assumed beidellite-montmorillonite interstratifications*

Cluster 1 diVBM 5:55:40	*particles (abs)*	**Ca (XII)**	**Mg (XII)**	**Na (XII)**	**K (XII)**	**Cr3+ (VI)**	**Al (VI)**	**Fe3+ (VI)**	**Mg (VI)**	**Ti (VI)**	**Al (IV)**	**Si (IV)**	**XII**	**n_VI**	**%V, %B,%M**
Si >3.9	n = 0														
Si 3.9-3.8	n = 2	0.10	0.08	0.00	0.01	0.00	1.30	0.46	0.23	0.01	0.14	3.86	0.4	2.0	0:30:70
Si 3.8-3.7	n = 22	0.11	0.06	0.01	0.09	0.00	1.25	0.57	0.18	0.00	0.27	3.73	0.4	2.0	5:50:45
Si 3.7-3.6	**n = 45**	**0.10**	**0.08**	**0.01**	**0.13**	**0.00**	**1.21**	**0.63**	**0.16**	**0.01**	**0.35**	**3.65**	**0.5**	**2.0**	**5:60:35**
Si 3.6-3.5	n = 2	0.09	0.10	0.01	0.14	0.00	1.13	0.71	0.14	0.02	0.41	3.59	0.5	2.0	15:60:25
Si 3.5-3.4	n = 0														
Si 3.4-3.3	n = 0														
Si 3.3-3.2	n = 0														
Si 3.2-3.1	n = 0														
Si <3.1	n = 0														

Fig. 62b. *Computed averaged mineral formulae of phases in the different Si(IV)-classes*

Dioctahedral vermiculite-beidellite/montmorillonite mixed layer phases (diVBM-ml):
(charge- and/or K-deficit; confirmed as Cluster2):

$$\mathrm{Ca_{0.08}\ Mg_{0.11}\ Na_{0.03}\ K_{0.19}\quad Al_{1.37}\ Fe^{3+}_{0.53}\ Mg_{0.10}\ Ti_{0.00}\ (OH)_2\ \ Si_{3.52}\ Al_{0.48}\ O_{10}}$$

Charge: XII = 0.57 VI = 5.91 IV = 15.52 **Σ = 22.00**
Probability of montmorillonite layers (%M): 30%
Probability of beidellite layers (%B): 25%
Probability of illite layers (%I): 45%

Measured particles: 30

Estimation of %M, %B, %I: 0.30 * 4 $\mathrm{Si_{montm}}$ + 0.25 * 3.5 $\mathrm{Si_{beid}}$ + 0.45 * 3.2 $\mathrm{Si_{verm}}$ = **3.52 $\mathrm{Si_{total}}$ (phfu)**
%I by XRD: 43% for IS R0 GLY (2)

Distribution of smectite layers probability (%S) in diVS-ml (Cluster2)

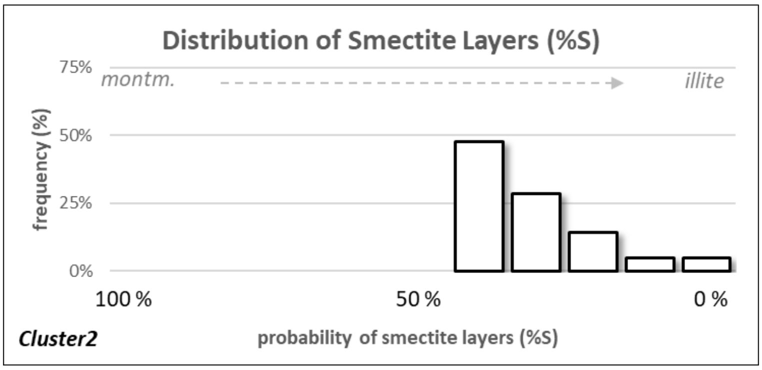

Description: *The distribution of diVS-ml (classified as Cluster2) draws a maximum of frequency (%) for smectite layer probability at 40% shows also traces of illite*

Fig. 63a. *Distribution of smectite layers probability in diVS-ml*

Cluster 2 IS+Illite diVS	*particles (abs)*	Ca (XII)	Mg (XII)	Na (XII)	K (XII)	Cr3+ (VI)	Al (VI)	Fe3+ (VI)	Mg (VI)	Ti (VI)	Al (IV)	Si (IV)	XII	n_VI	%S
%S >95%	n = 0														
%S 95-85%	n = 0														
%S 85-75%	n = 0														
%S 75-65%	n = 0														
%S 65-55%	n = 0														
%S 55-45%	n = 0														
%S 45-35%	**n = 10**	**0.08**	**0.10**	**0.01**	**0.15**	**0.00**	**1.34**	**0.55**	**0.11**	**0.00**	**0.41**	**3.59**	**0.5**	**2.0**	**39**
%S 35-25%	n = 6	0.08	0.08	0.01	0.23	0.00	1.40	0.51	0.09	0.00	0.46	3.54	0.6	2.0	32
%S 25-15%	n = 3	0.05	0.13	0.02	0.24	0.00	1.47	0.44	0.07	0.02	0.57	3.43	0.6	2.0	21
%S 15- 5%	n = 1	0.03	0.07	0.31	0.19	0.00	1.73	0.25	0.02	0.00	0.70	3.30	0.7	2.0	9
%S <5%	n = 1	0.11	0.30	0.00	0.14	0.00	0.76	1.10	0.14	0.00	0.83	3.17	1.0	2.0	2

Fig. 63b. *Computed averaged mineral formulae of diVS-ml phases in the different smectite layers probability (%S)-classes*

[ATTENTION: value for %S by TEM is too low in comparison to %S by XRD = 57% - is that an indication for interstratification with beidellite?]

Distribution of diVBM-interstratifications (Cluster2)

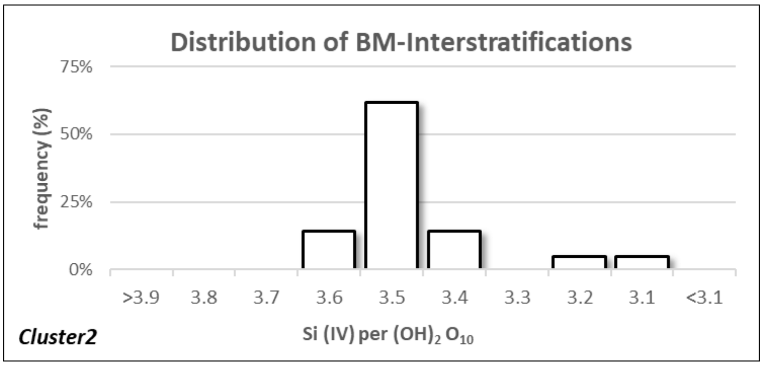

Description: *The distribution of diVBM-interstratifications (classified as Cluster2) draws a maximum of frequency (%) for tetrahedral Si-value at 3.5 e phuc*

Fig. 64a. *Distribution of assumed dioctahedral vermiculite-beidellite-montmorillonite interstratifications*

Cluster 2 diVBM 45:25:30	*particles (abs)*	Ca (XII)	Mg (XII)	Na (XII)	K (XII)	Cr3+ (VI)	Al (VI)	Fe3+ (VI)	Mg (VI)	Ti (VI)	Al (IV)	Si (IV)	XII	n_VI	%V, %B,%M
Si >3.9	n = 0														
Si 3.9-3.8	n = 0														
Si 3.8-3.7	n = 0														
Si 3.7-3.6	n = 3	0.08	0.08	0.03	0.17	0.00	1.39	0.49	0.12	0.00	0.39	3.61	0.5	2.0	35:20:45
Si 3.6-3.5	**n = 13**	**0.08**	**0.09**	**0.01**	**0.18**	**0.00**	**1.36**	**0.54**	**0.10**	**0.00**	**0.44**	**3.56**	**0.5**	**2.0**	**40:25:35**
Si 3.5-3.4	n = 3	0.05	0.13	0.02	0.24	0.00	1.47	0.44	0.07	0.02	0.57	3.43	0.6	2.0	55:25:20
Si 3.4-3.3	n = 0														
Si 3.3-3.2	n = 1	0.03	0.07	0.31	0.19	0.00	1.73	0.25	0.02	0.00	0.70	3.30	0.7	2.0	85: 5:10
Si 3.2-3.1	n = 1	0.11	0.30	0.00	0.14	0.00	0.76	1.10	0.14	0.00	0.83	3.17	1.0	2.0	100: 0: 0
Si <3.1	n = 0														

Fig. 64b. *Computed averaged mineral formulae of phases in the different Si(IV)-classes*

Chlorite-saponite-trioctahedral vermiculite mixed-layer series (CSV-ml):

$Ca_{0.07}\ Mg_{0.09}\ Na_{0.00}\ K_{0.07}\quad Al_{0.86}\ Fe^{2+}_{2.11}\ Mg_{0.82}\ Ti_{0.00}\ (OH)_{3.8}\ \ Si_{2.99}\ Al_{1.01}\ O_{10}$

Charge: XII = 0.38 VI = 8.43 (n^{VI}= 3.80) IV = 14.99 **Σ = 23.80**

Probability of chlorite layers (%C): 30% *min – max: 30%*

Probability of saponite layers (%S): 30% *min – max: 25 … 40%*

Probability of trioct. vermiculite layers (%V): 40% *min – max: 30 … 45%*

Measured particles: 2

Mineral Matter – Specification

Result of Clustering & Comparison with XRD-data (Sybilla-processing)

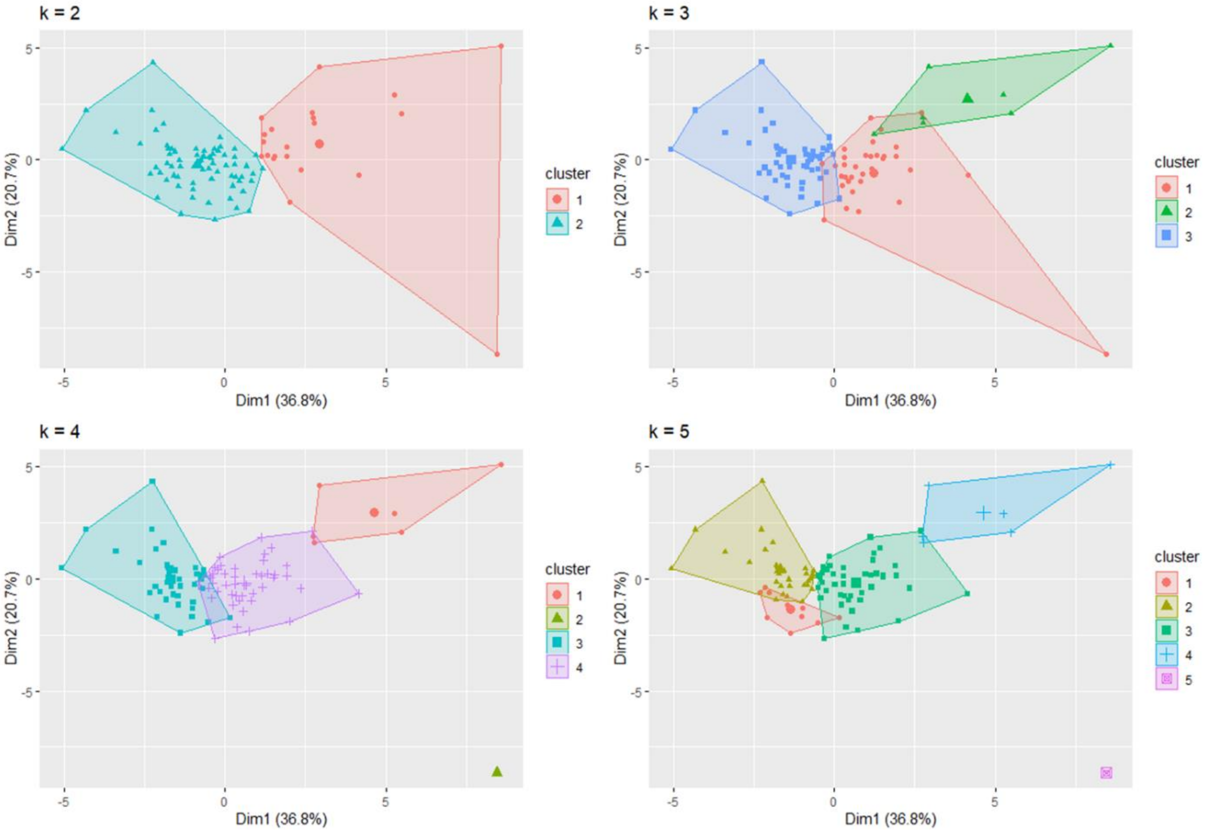

Fig. 65. *Clustering of all measured particles for clusters k = 2, k = 3, k = 4 and k = 5 (source for R-coding: https://uc-r.github.io/kmeans_clustering)*

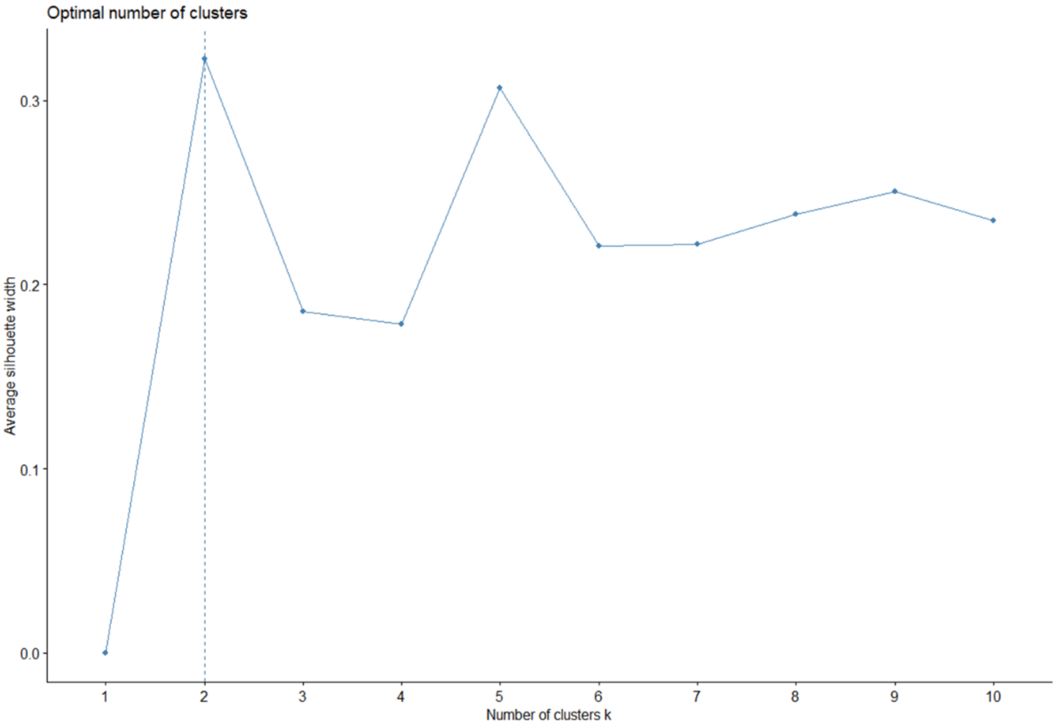

Fig. 66. *Optimal number of clusters determined by silhouette method for k = 2 (source for R-coding: https://uc-r.github.io/kmeans_clustering)*

		Ca (XII)	Mg (XII)	Na (XII)	K (XII)	Cr3+ (VI)	Al (VI)	Fe3+ (VI)	Mg (VI)	Ti (VI)	Al (IV)	Si (IV)	XII	n_VI	%S
Cluster1	n = 71	0.10	0.08	0.01	0.11	0.00	1.22	0.61	0.17	0.01	0.32	3.68	0.48	2.0	95
Cluster2	n = 21	0.08	0.11	0.03	0.19	0.00	1.37	0.53	0.10	0.00	0.48	3.52	0.57	2.0	55

Fig. 67. *Mineral formulae based on TEM-EDX-data summarized following the result of clustering for k=2*

	Sybilla-modelling of XRD-results	**TEM-EDX-results**	**Notes**
Cluster1	IS R0 *(%S = 95%)**	B-IS 50:10:40 *(%B=49%, %I=9% %M = 41%)*	*low K, Fe(VI)-rich*
Cluster2	IS R0 *(%S = 57%)*	diVBM-ml *(%I=45%, %BM=55%)*	*high K-deficit, Fe(VI)-rich, low Mg(VI)*

Tab. 14. *Comparison of results from TEM-EDX- and XRD-measurements with clustering procedure*
(- beidellite is to verify by XRD only by Li-test)*

Sample - B25 (< 2 µm), treated H_2O 60 rpm

Preparation for TEM

- raw material: <40 µm powder of B25-sample after treatment by H_2O 60 rpm
- suspension on particles < 2 µm on carbon-filmed Cu-grid
- air-dried and humidity-controlled storing

Mineral Matter

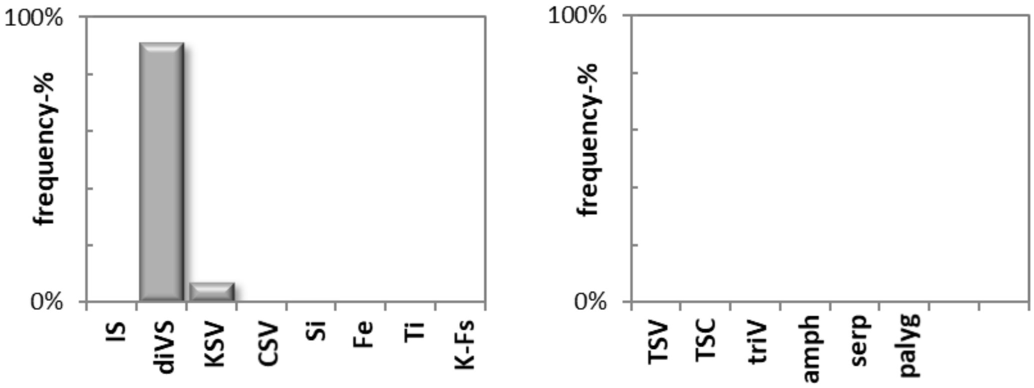

Fig. 68. *Distribution of mineral groups in fraction < 2 µm (in frequency-%)*
Legend: ***IS*** *– illite-smectite-mixed layer series in sense of Środon et al. (1992), diVS – dioctahedral vermiculite-smectite illite-smectite-mixed layer series (= charge- and/or K-deficit),* ***KSV*** *– kaolinite-smectite-dioctahedral vermiculite-mixed layer series,* ***CSV*** *– chlorite-saponite-trioctahedral vermiculite-mixed layer series,* ***Si*** *– quartz or particles with Si-surplus,* ***Fe*** *– Fe-oxide or Fe-oxyhydroxide,* ***Ti*** *– Ti-bearing phases (e.g. rutile, anatase),* ***K-Fs*** *– K-feldspar*

Clay Mineral Composition

Dioctahedral vermiculite-smectite mixed-layer series *(charge- and/or K-deficit):*

$$Ca_{0.19}\, Mg_{0.02}\, Na_{0.09}\, K_{0.15}\quad Al_{1.17}\, Fe^{3+}_{0.56}\, Mg_{0.26}\, Ti_{0.01}\, (OH)_2\quad Si_{3.60}\, Al_{0.40}\, O_{10}$$

Charge: XII = 0.67 VI = 5.73 IV = 15.60 **Σ = 22.00**
Probability of smectite layers (%S): 40%
Probability of illite layers (%I): 60%
CEC_{calc}: 79 meq / 100 g

Measured particles: 126

Table 15. *Summarized chemical composition*

SiO_2	**TiO_2**	**Al_2O_3**	**Fe_2O_3**	**MnO**	**MgO**	**CaO**	**Na_2O**	**K_2O**	**P_2O_5**	**Σ**	
54.2%	0.1%	20.9%	5.6%		3.3%	2.8%	0.8%	1.2%	0.0%	0.89	measured particles
58.6%	0.0%	22.0%	5.9%		3.0%	1.0%	0.1%	1.1%	0.1%	0.92	original B25 (< 2µm)

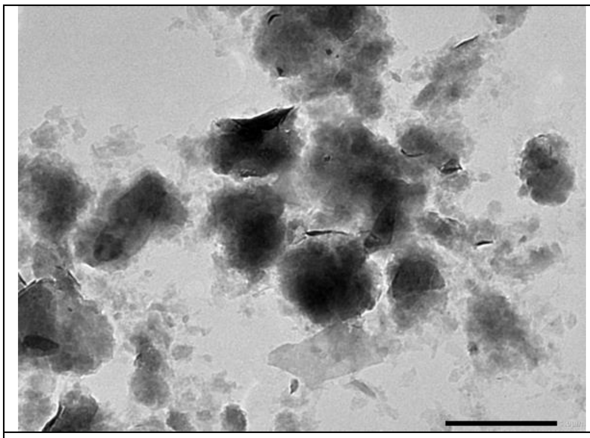	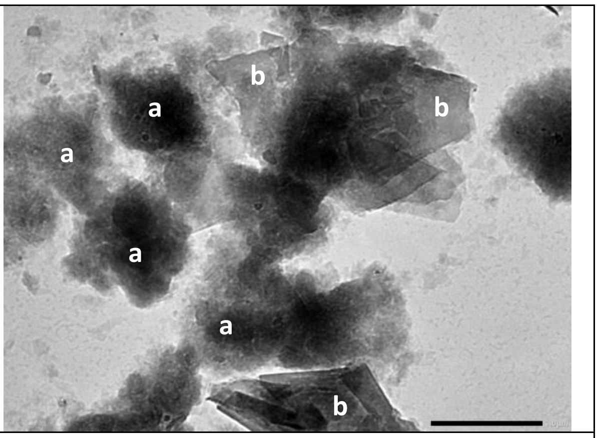
JEM-2100_MAG_X10k_B25-H2O-60r_009.bmp Magnification: 10k large (≤ 1 µm) xenomorphic film-like platy crystals with folds *(diVS-ml mainly with %S-range 25-40%)*	*JEM-2100_MAG_X10k_B25-H2O-60r_012.bmp* Magnification: 10k (a) aggregates formed by small (≤ 100 nm) xenomorphic platy crystals *(diVS-ml mainly with %S-range 40-60%);* *(b)* large (> 1 µm) xenomorph plates, homogenous thickness *(probably KSV-ml with beidellite as smectite compound)*

Fig. 69. *Morphology of particles (TEM-micrographs)*

Distribution: Smectite layers probability (%S)

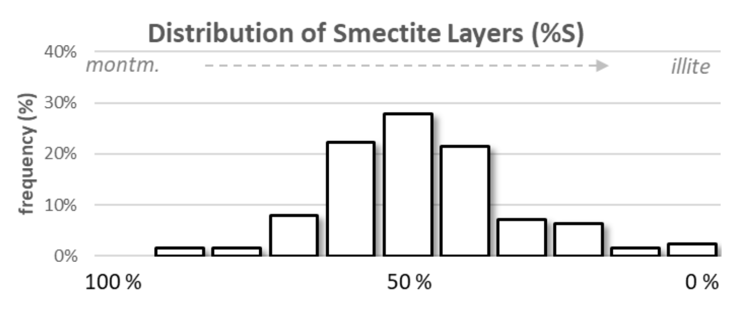

Description: *The distribution of %S-probability in diVS-ml indicates the occurrence of two groups: (i) diVS-ml with %S-range of 40-60% (= main group) and (ii) illite with K- and charge deficit (in traces).*

Fig. 70. *Distribution of smectite layers probability (%S)*

Distribution: Charge density of exchangeable cations

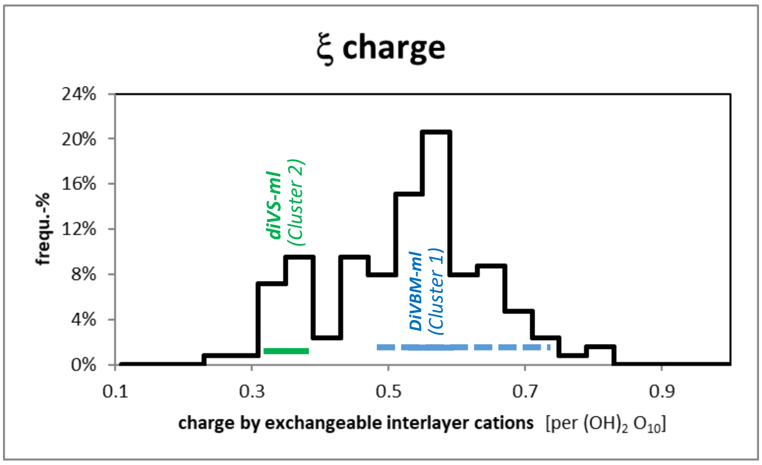

This diagram visualizes the distribution of exchangeable charges in the interlayer space (Ca, Mg, Na) determined and computed by TEM-EDX-data.

Description: *Broad charge density distribution of exchangeable interlayer cations with a maximum at 0.59 per $(OH)_2 O_{10}$.*

Fig. 71. *Distribution of charges*

Dioctahedral vermiculite-beidellite/montmorillonite-ml (diVBM ~20%:50%:30%) *(Cluster1):*

$Ca_{0.22}\ Mg_{0.00}\ Na_{0.11}\ K_{0.15}\quad Al_{1.13}\ Fe^{3+}_{0.56}\ Mg_{0.30}\ Ti_{0.00}\ (OH)_2\ \ Si_{3.59}\ Al_{0.41}\ O_{10}$

Charge: XII = 0.72 VI = 5.69 IV = 15.59 **Σ = 22.00**

Probability of montmorillonite layers (%M): 30%
Probability of beidellite layers (%B): 50%
Probability of illite layers (%I): 20%

Measured particles: 102

Estimation of %M, %B, %I: 0.50 * 4 Si_{montm} + 0.30 * 3.5 Si_{beid} + 0.20 * 3.2 Si_{verm} = **3.59 Si_{total} (phfu)**
%I by XRD: 78% for IS R0 GLY (1)

Distribution of diVBM-interstratifications (Cluster1)

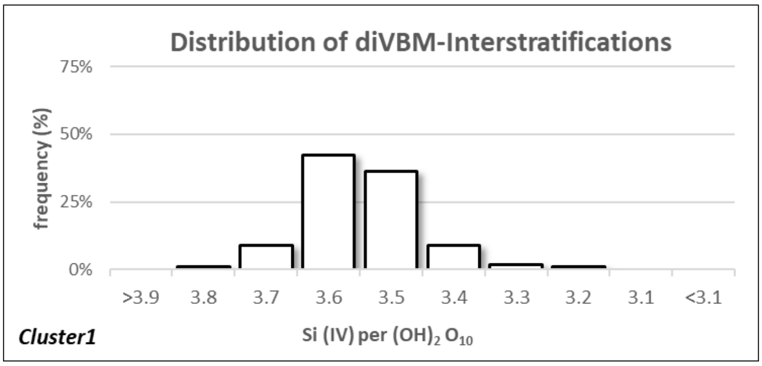

Description: *The distribution of diVBM-interstratifications (classified as Cluster1) draws a maximum of frequency (%) at tetrahedral Si-value between 3.5 – 3.6 e phuc*

Fig. 72a. *Distribution of assumed beidellite-montmorillonite interstratifications*

Cluster 1 diVBM 20:50:30		*particles (abs)*	**Ca (XII)**	**Mg (XII)**	**Na (XII)**	**K (XII)**	**Cr3+ (VI)**	**Al (VI)**	**Fe3+ (VI)**	**Mg (VI)**	**Ti (VI)**	**Al (IV)**	**Si (IV)**	**XII**	**n_VI**	**%V, %B,%M**
Si	>3.9	n = 0														
Si	3.9-3.8	n = 1	0.26	0.00	0.00	0.00	0.00	1.07	0.55	0.38	0.00	0.16	3.84	0.5	2.0	0:35:65
Si	3.8-3.7	n = 9	0.19	0.00	0.11	0.11	0.00	1.15	0.54	0.31	0.00	0.28	3.72	0.6	2.0	5:50:45
Si	**3.7-3.6**	**n = 43**	**0.22**	**0.00**	**0.12**	**0.13**	**0.00**	**1.12**	**0.56**	**0.31**	**0.00**	**0.36**	**3.64**	**0.7**	**2.0**	**15:50:35**
Si	**3.6-3.5**	**n = 37**	**0.23**	**0.01**	**0.10**	**0.17**	**0.00**	**1.11**	**0.59**	**0.29**	**0.01**	**0.44**	**3.56**	**0.7**	**2.0**	**25:50:25**
Si	3.5-3.4	n = 9	0.22	0.01	0.12	0.23	0.00	1.19	0.53	0.25	0.02	0.56	3.44	0.8	2.0	35:55:10
Si	3.4-3.3	n = 2	0.26	0.02	0.20	0.15	0.00	1.38	0.40	0.20	0.00	0.66	3.34	0.9	2.0	60:35: 5
Si	3.3-3.2	n = 1	0.31	0.03	0.13	0.12	0.00	1.29	0.51	0.20	0.00	0.74	3.26	0.9	2.0	80:20: 0
Si	3.2-3.1	n = 0														
Si	<3.1	n = 0														

Fig. 72b. *Computed averaged mineral formulae of phases in the different Si(IV)-classes*

Dioctahedral vermiculite-smectite mixed layer phases (diVS-ml):
(charge- and/or K-deficit; confirmed as Cluster2):

$Ca_{0.08}\ Mg_{0.10}\ Na_{0.01}\ K_{0.12}\quad Al_{1.34}\ Fe^{3+}_{0.53}\ Mg_{0.12}\ Ti_{0.01}\ (OH)_2\ \ Si_{3.63}\ Al_{0.37}\ O_{10}$

Charge: XII = 0.49 VI = 5.88 IV = 15.63 **Σ = 22.00**
Probability of smectite layers (%S): 45%
Probability of illite layers (%I): 55%

Measured particles: 24

%I by XRD: 56% for IS R0 GLY (2)

Distribution of smectite layers probability (%S) in diVS-ml (Cluster2)

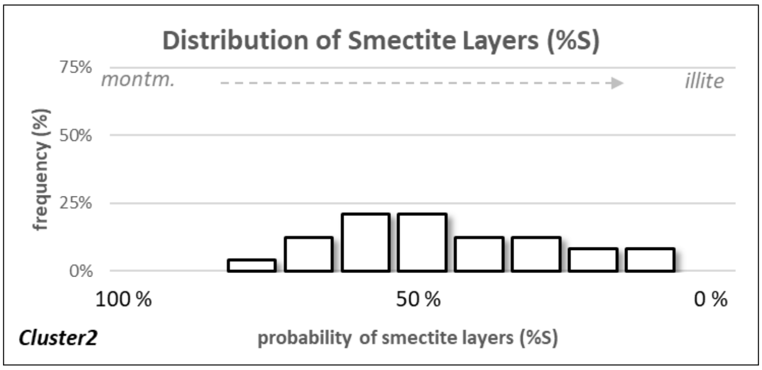

Description: *The distribution of diVS-ml (classified as Cluster2) draws a maximum of frequency (%) for smectite layer probability at 50-60% and shows also traces of illite*

Fig. 73a. *Distribution of smectite layers probability in diVS-ml*

Cluster 2 IS R0 diVS	*particles (abs)*	**Ca (XII)**	**Mg (XII)**	**Na (XII)**	**K (XII)**	**Cr3+ (VI)**	**Al (VI)**	**Fe3+ (VI)**	**Mg (VI)**	**Ti (VI)**	**Al (IV)**	**Si (IV)**	**XII**	**n_VI**	**%S**
%S >95%	n = 0														
%S 95-85%	n = 0														
%S 85-75%	n = 1	0.15	0.04	0.00	0.00	0.00	1.28	0.47	0.24	0.00	0.14	3.86	0.4	2.0	82
%S 75-65%	n = 3	0.08	0.09	0.00	0.04	0.00	1.29	0.53	0.17	0.00	0.20	3.80	0.4	2.0	71
%S 65-55%	**n = 5**	**0.07**	**0.10**	**0.00**	**0.06**	**0.00**	**1.30**	**0.56**	**0.14**	**0.01**	**0.28**	**3.72**	**0.4**	**2.0**	**58**
%S 55-45%	**n = 5**	**0.07**	**0.10**	**0.00**	**0.10**	**0.00**	**1.21**	**0.63**	**0.15**	**0.02**	**0.32**	**3.68**	**0.5**	**2.0**	**51**
%S 45-35%	n = 3	0.07	0.10	0.00	0.16	0.00	1.30	0.58	0.12	0.00	0.39	3.61	0.5	2.0	42
%S 35-25%	n = 3	0.06	0.10	0.02	0.21	0.00	1.37	0.54	0.09	0.01	0.47	3.53	0.5	2.0	32
%S 25-15%	n = 2	0.10	0.11	0.03	0.19	0.00	1.57	0.37	0.06	0.00	0.57	3.43	0.6	2.0	20
%S 15- 5%	n = 2	0.10	0.11	0.00	0.29	0.00	1.65	0.31	0.04	0.00	0.67	3.33	0.7	2.0	12
%S <5%	n = 0														

Fig. 73b. *Computed averaged mineral formulae of diVS-ml phases in the different smectite layers probability (%S)-classes*

Mineral Matter – Specification

Result of Clustering & Comparison with XRD-data (Sybilla-processing)

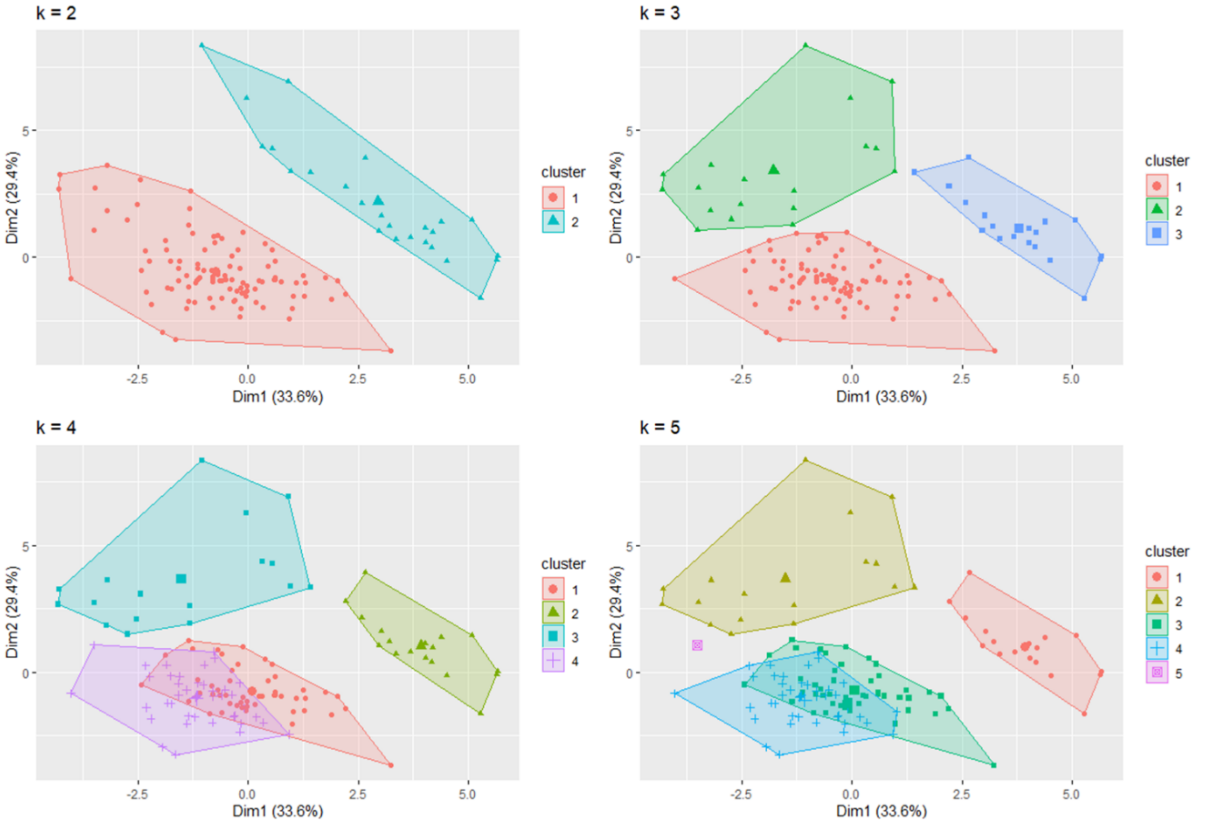

Fig. 74. *Clustering of all measured particles for clusters k = 2, k = 3, k = 4 and k = 5 (source for R-coding: https://uc-r.github.io/kmeans_clustering)*

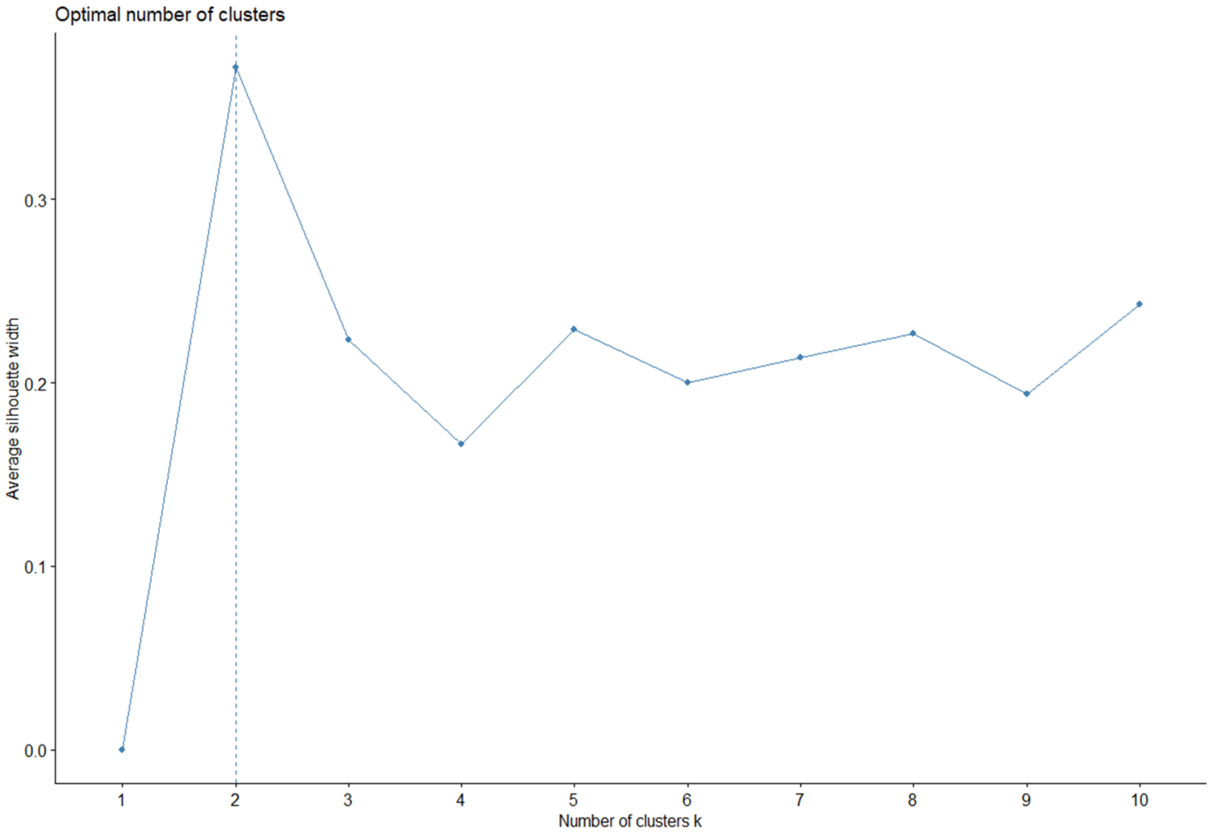

Fig. 75. *Optimal number of clusters determined by silhouette method for k = 2 (source for R-coding: https://uc-r.github.io/kmeans_clustering)*

		Ca (XII)	Mg (XII)	Na (XII)	K (XII)	Cr3+ (VI)	Al (VI)	Fe3+ (VI)	Mg (VI)	Ti (VI)	Al (IV)	Si (IV)	XII	n_VI	%S
Cluster1	n = 102	0.22	0.00	0.11	0.15	0.00	1.13	0.56	0.30	0.00	0.41	3.59	0.7	2.0	80
Cluster2	n = 24	0.08	0.10	0.01	0.12	0.00	1.34	0.53	0.12	0.01	0.37	3.63	0.5	2.0	45

Fig. 76. *Mineral formulae based on TEM-EDX-data summarized following the result of clustering for k=2*

	Sybilla-modelling of XRD-results	**TEM-EDX-results**	**Notes**
Cluster1	IS R0 *(%S = 78%)**	diVBM-ml *(%B=50%,* *%I=20% %M = 30%)*	*low K, Fe(VI)-rich*
Cluster2	IS R0 *(%S = 44%)*	diVS-ml *(%S=45%)*	*high K-deficit, Fe(VI)-rich, low Mg(VI)*

Tab. 16. *Comparison of results from TEM-EDX- and XRD-measurements with clustering procedure*
(- beidellite is to verify by XRD only by Li-test)*

Sample - B25 (< 2 µm), treated NaCl 20 rpm

Preparation for TEM

- raw material: <40 µm powder of B25-sample after treatment by NaCl 20 rpm
- suspension on particles < 2 µm on carbon-filmed Cu-grid
- air-dried and humidity-controlled storing

Mineral Matter

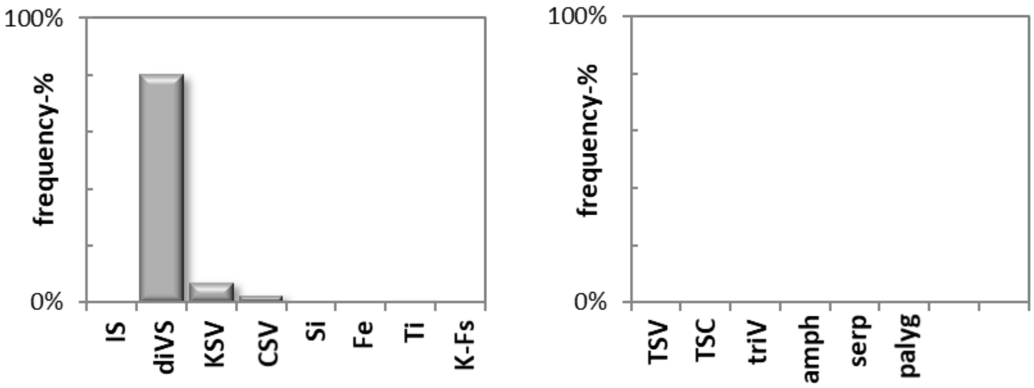

Fig. 77. *Distribution of mineral groups in fraction < 2 µm (in frequency-%)*
Legend: ***IS*** *– illite-smectite-mixed layer series in sense of Środon et al. (1992), diVS – dioctahedral vermiculite-smectite illite-smectite-mixed layer series (= charge- and/or K-deficit),* ***KSV*** *– kaolinite-smectite-dioctahedral vermiculite-mixed layer series,* ***CSV*** *– chlorite-saponite-trioctahedral vermiculite-mixed layer series,* ***Si*** *– quartz or particles with Si-surplus,* ***Fe*** *– Fe-oxide or Fe-oxyhydroxide,* ***Ti*** *– Ti-bearing phases (e.g. rutile, anatase),* ***K-Fs*** *– K-feldspar*

Clay Mineral Composition

Dioctahedral vermiculite-smectite mixed-layer series *(charge- and/or K-deficit):*

$$Ca_{0.09}\ Mg_{0.09}\ Na_{0.00}\ K_{0.16}\quad Al_{1.29}\ Fe^{3+}_{0.57}\ Mg_{0.13}\ Ti_{0.01}\ (OH)_2\quad Si_{3.60}\ Al_{0.40}\ O_{10}$$

Charge: XII = 0.52 VI = 5.88 IV = 15.60 **Σ = 22.00**
Probability of smectite layers (%S): 40%
Probability of illite layers (%I): 60%
CEC$_{calc}$: 47 meq / 100 g

Measured particles: 88

Table 17. *Summarized chemical composition*

SiO_2	TiO_2	Al_2O_3	Fe_2O_3	MnO	MgO	CaO	Na_2O	K_2O	P_2O_5	Σ	
56.6%	0.1%	23.6%	6.0%		2.7%	0.9%	0.0%	1.4%	0.3%	0.92	measured particles
58.6%	0.0%	22.0%	5.9%		3.0%	1.0%	0.1%	1.1%	0.1%	0.92	original B25 (< 2µm)

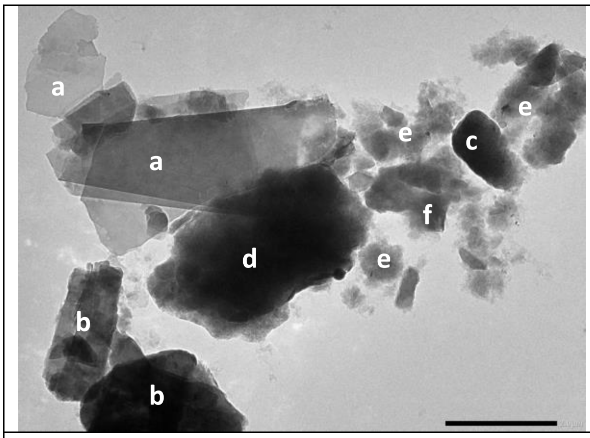	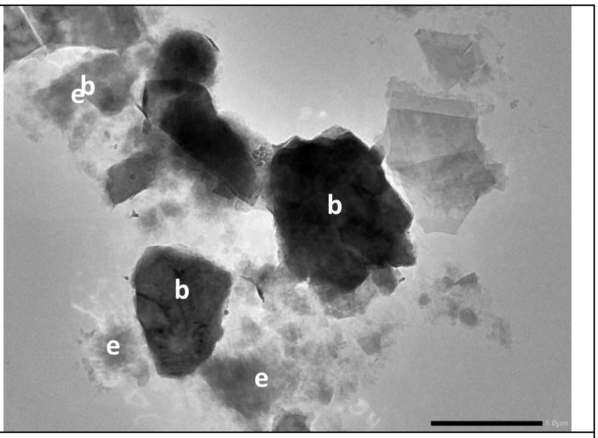
JEM-2100_MAG_X5000_B25-NaCl-20r_001.bmp	*JEM-2100_MAG_X10k_B25-NaCl-20r_005.bmp*
Magnification: 5k (a) large (> 1 µm) xenomorph plates, homogenous thickness *(probably KSV-ml)*; (b) large (> 1 µm) and thick xenomorphic platy crystals *(illite with K- and charge deficit)*; (c) large (> 1 µm) and thick xenomorphic platy crystals *(beidellite)*; (d) large (> 1 µm), inhomogeneous thick platy crystals *(diVS-ml mainly with %S-range at 30%)*; (e) aggregates composed by small (≤ 200 nm) xenomorphic platy crystals *(diVS-ml mainly with %S-range 40-60%)*; (f) large (≤ 1 µm) xenomorphic film-like platy crystals with folds *(diVS-ml mainly with %S-range at 80%)*	Magnification: 10k (b) large (> 1 µm) and thick xenomorphic platy crystals *(illite with K- and charge deficit)*; (e) aggregates formed by small (≤ 200 nm) xenomorphic platy crystals *(diVS-ml mainly with %S-range 40-70%)*

Fig. 78. *Morphology of particles (TEM-micrographs)*

Distribution: Smectite layers probability (%S)

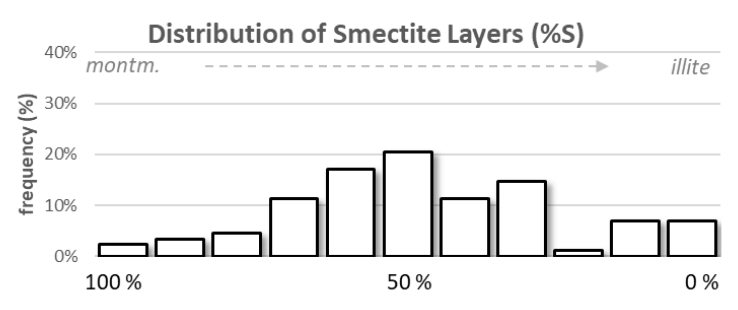

Description: *The distribution of %S-probability in diVS-ml indicates the occurrence of three groups: (i) low charged montmorillonite (in traces), (ii) diVS-ml with %S-range of 30-70% (= main group) and (iii) illite with K- and charge deficit.*

Fig. 79. *Distribution of smectite layers probability (%S)*

Distribution: Charge density of exchangeable cations

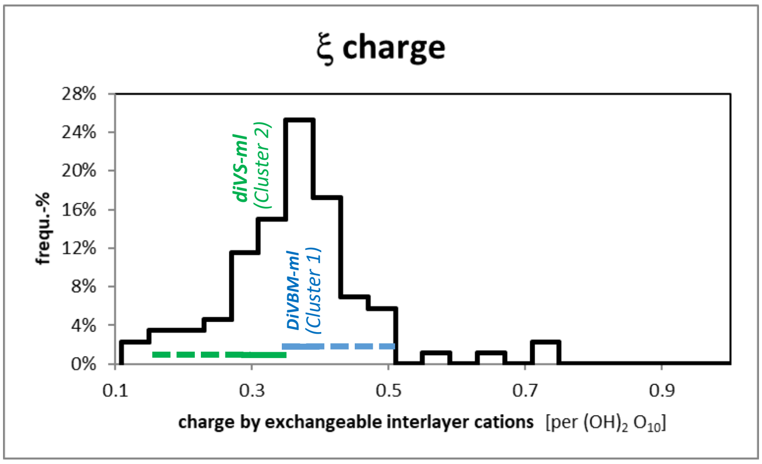

This diagram visualizes the distribution of exchangeable charges in the interlayer space (Ca, Mg, Na) determined and computed by TEM-EDX-data.

Description: *Asymmetric broadening of charge density distribution of exchangeable interlayer cations with a maximum at 0.39 per $(OH)_2\ O_{10}$.*

Fig. 80. *Distribution of charges*

Dioctahedral vermiculite-beidellite/montmorillonite-ml (diVBM ~15%:45%:40%) *(Cluster1):*

$$Ca_{0.10}\ Mg_{0.10}\ Na_{0.00}\ K_{0.09}\quad Al_{1.21}\ Fe^{3+}_{0.63}\ Mg_{0.16}\ Ti_{0.00}\ (OH)_2\ \ Si_{3.67}\ Al_{0.33}\ O_{10}$$

Charge: XII = 0.48 VI = 5.85 IV = 15.67 **Σ = 22.00**

Probability of montmorillonite layers (%M): 42%
Probability of beidellite layers (%B): 43%
Probability of illite layers (%I): 15%

Measured particles: 59

Estimation of %M, %B, %I: 0.42 * 4 Si_{montm} + 0.43 * 3.5 Si_{beid} + 0.15 * 3.2 Si_{verm} = **3.67 Si_{total} (phfu)**
%I by XRD: 16% for IS R0 GLY (1)

Distribution of BM-interstratifications (Cluster1)

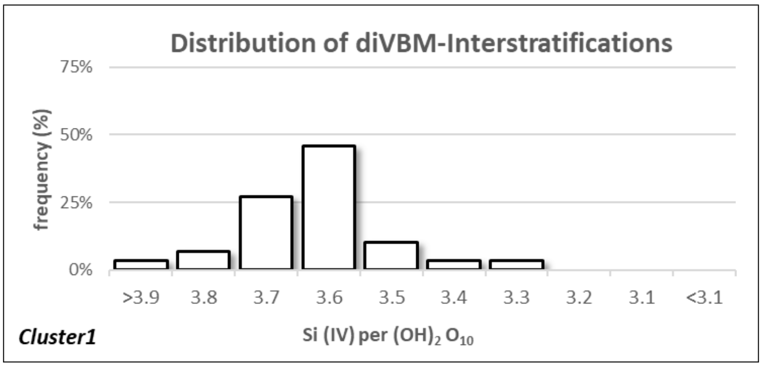

***Description:** The distribution of BM-interstratifications (classified as Cluster1) draws a maximum of frequency (%) at tetrahedral Si-value between 3.6 – 3.7 e phuc*

***Fig. 81a.** Distribution of assumed beidellite-montmorillonite interstratifications*

Cluster 1 diVBM 15:45:40		*particles (abs)*	**Ca (XII)**	**Mg (XII)**	**Na (XII)**	**K (XII)**	**Cr3+ (VI)**	**Al (VI)**	**Fe3+ (VI)**	**Mg (VI)**	**Ti (VI)**	**Al (IV)**	**Si (IV)**	**XII**	**n_VI**	**%V, %B,%M**
Si	>3.9	n = 2	0.09	0.08	0.00	0.00	0.00	1.38	0.37	0.25	0.00	0.10	3.90	0.3	2.0	0:20:80
Si	3.9-3.8	n = 4	0.08	0.08	0.00	0.00	0.00	1.34	0.47	0.19	0.00	0.16	3.84	0.3	2.0	0:35:65
Si	3.8-3.7	n = 16	0.09	0.09	0.00	0.06	0.00	1.25	0.59	0.16	0.00	0.25	3.75	0.4	2.0	5:40:55
Si	**3.7-3.6**	**n = 27**	**0.09**	**0.10**	**0.00**	**0.11**	**0.00**	**1.20**	**0.67**	**0.14**	**0.00**	**0.35**	**3.65**	**0.5**	**2.0**	**10:55:35**
Si	3.6-3.5	n = 6	0.14	0.11	0.00	0.10	0.00	1.14	0.70	0.16	0.01	0.45	3.55	0.6	2.0	25:50:25
Si	3.5-3.4	n = 2	0.12	0.10	0.00	0.29	0.00	1.18	0.60	0.23	0.00	0.51	3.49	0.7	2.0	30:55:15
Si	3.4-3.3	n = 2	0.11	0.24	0.00	0.07	0.00	0.98	0.87	0.15	0.00	0.63	3.37	0.8	2.0	60:30:10
Si	3.3-3.2	n = 0														
Si	3.2-3.1	n = 0														
Si	<3.1	n = 0														

***Fig. 81b.** Computed averaged mineral formulae of phases in the different Si(IV)-classes*

Dioctahedral vermiculite-beidellite/montmorillonite mixed layer phases (diVBM-ml):
(charge- and/or K-deficit; confirmed as Cluster2):

$$Ca_{0.06}\ Mg_{0.08}\ Na_{0.01}\ K_{0.30}\quad Al_{1.45}\ Fe^{3+}_{0.46}\ Mg_{0.07}\ Ti_{0.02}\ (OH)_2\ \ Si_{3.45}\ Al_{0.55}\ O_{10}$$

Charge: XII = 0.60 VI = 5.95 IV = 15.45 **Σ = 22.00**
Probability of montmorillonite layers (%M): 20%
Probability of beidellite layers (%B): 30%
Probability of illite layers (%I): 50%

Measured particles: 29

Estimation of %M, %B, %I: 0.20 * 4 Si_{montm} + 0.30 * 3.5 Si_{beid} + 0.50 * 3.2 Si_{verm} = **3.45 Si_{total} (phfu)**
%I by XRD: 50% for IS R0 GLY (2)

Distribution of smectite layers probability (%S) as diVS-ml (Cluster2)

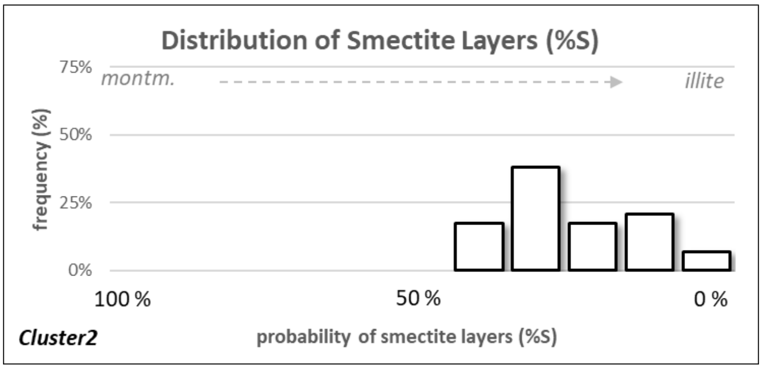

Description: *The distribution of diVS-ml (classified as Cluster2) draws a maximum of frequency (%) for smectite layer probability at 30% shows also traces of illite*

Fig. 82a. *Distribution of smectite layers probability in diVS-ml*

Cluster 2 IS R0 diVS	*particles (abs)*	Ca (XII)	Mg (XII)	Na (XII)	K (XII)	Cr3+ (VI)	Al (VI)	Fe3+ (VI)	Mg (VI)	Ti (VI)	Al (IV)	Si (IV)	XII	n_VI	%S
%S >95%	n = 0														
%S 95-85%	n = 0														
%S 85-75%	n = 0														
%S 75-65%	n = 0														
%S 65-55%	n = 0														
%S 55-45%	n = 0														
%S 45-35%	n = 5	0.06	0.06	0.00	0.25	0.00	1.41	0.48	0.10	0.01	0.41	3.59	0.5	2.0	39
%S 35-25%	**n = 11**	**0.08**	**0.09**	**0.02**	**0.18**	**0.00**	**1.36**	**0.54**	**0.08**	**0.02**	**0.48**	**3.52**	**0.5**	**2.0**	**30**
%S 25-15%	n = 5	0.08	0.08	0.02	0.30	0.00	1.46	0.46	0.08	0.01	0.57	3.43	0.6	2.0	20
%S 15- 5%	n = 6	0.03	0.08	0.00	0.44	0.00	1.60	0.36	0.04	0.02	0.70	3.30	0.7	2.0	10
%S <5%	n = 2	0.04	0.05	0.03	0.65	0.00	1.67	0.25	0.07	0.01	0.80	3.20	0.8	2.0	3

Fig. 82b. *Computed averaged mineral formulae of diVS-ml phases in the different smectite layers probability (%S)-classes [ATTENTION: value for %S by TEM is too low in comparison to %S by XRD = 50% - is that an indication for interstratification with beidellite?]*

Distribution of diVBM-interstratifications (Cluster2)

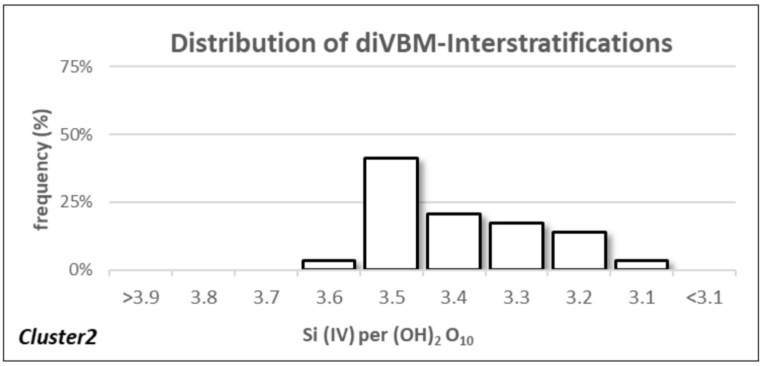

Description: *The distribution of diVBM-interstratifications (classified as Cluster2) draws a maximum of frequency (%) for tetrahedral Si-value at 3.5 e phuc*

Fig. 83a. *Distribution of assumed dioctahedral vermiculite-beidellite-montmorillonite interstratifications*

Cluster 2 diVBM 50:30:20	*particles (abs)*	Ca (XII)	Mg (XII)	Na (XII)	K (XII)	Cr3+ (VI)	Al (VI)	Fe3+ (VI)	Mg (VI)	Ti (VI)	Al (IV)	Si (IV)	XII	n_VI	%V, %B,%M
Si >3.9	n = 0														
Si 3.9-3.8	n = 0														
Si 3.8-3.7	n = 0														
Si 3.7-3.6	n = 1	0.08	0.00	0.00	0.20	0.00	1.33	0.63	0.00	0.04	0.40	3.60	0.4	2.0	35:25:40
Si 3.6-3.5	**n = 12**	**0.08**	**0.08**	**0.00**	**0.22**	**0.00**	**1.35**	**0.53**	**0.10**	**0.02**	**0.45**	**3.55**	**0.5**	**2.0**	**40:25:35**
Si 3.5-3.4	n = 6	0.08	0.12	0.03	0.15	0.00	1.44	0.51	0.05	0.00	0.53	3.47	0.6	2.0	50:30:20
Si 3.4-3.3	n = 5	0.06	0.09	0.02	0.37	0.00	1.54	0.37	0.08	0.01	0.64	3.36	0.7	2.0	60:35: 5
Si 3.3-3.2	n = 4	0.03	0.04	0.01	0.60	0.00	1.64	0.30	0.04	0.03	0.74	3.26	0.7	2.0	80:20: 0
Si 3.2-3.1	n = 1	0.03	0.07	0.00	0.60	0.00	1.83	0.18	0.00	0.00	0.81	3.19	0.8	2.0	100: 0: 0
Si <3.1	n = 0														

Fig. 83b. *Computed averaged mineral formulae of phases in the different Si(IV)-classes*

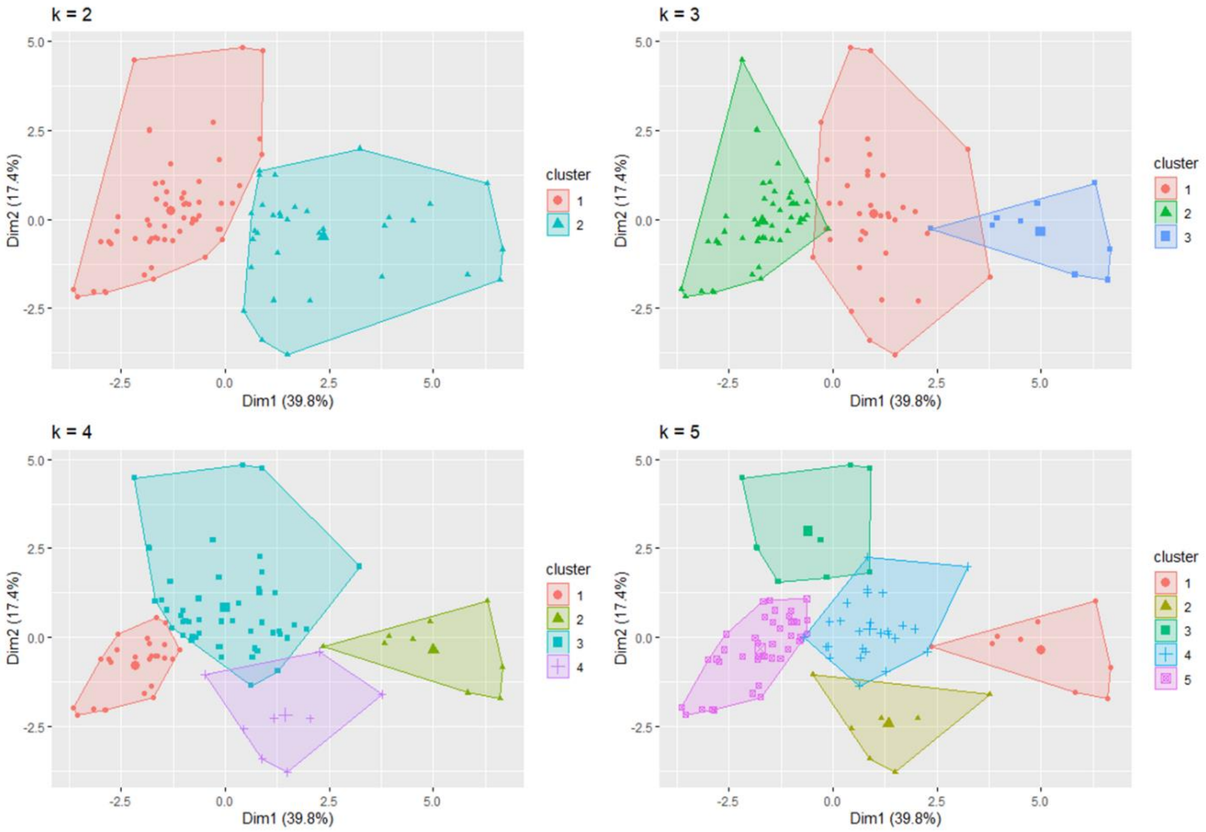

Fig. 84. Clustering of all measured particles for clusters k = 2, k = 3, k = 4 and k = 5 (source for R-coding: https://uc-r.github.io/kmeans_clustering)

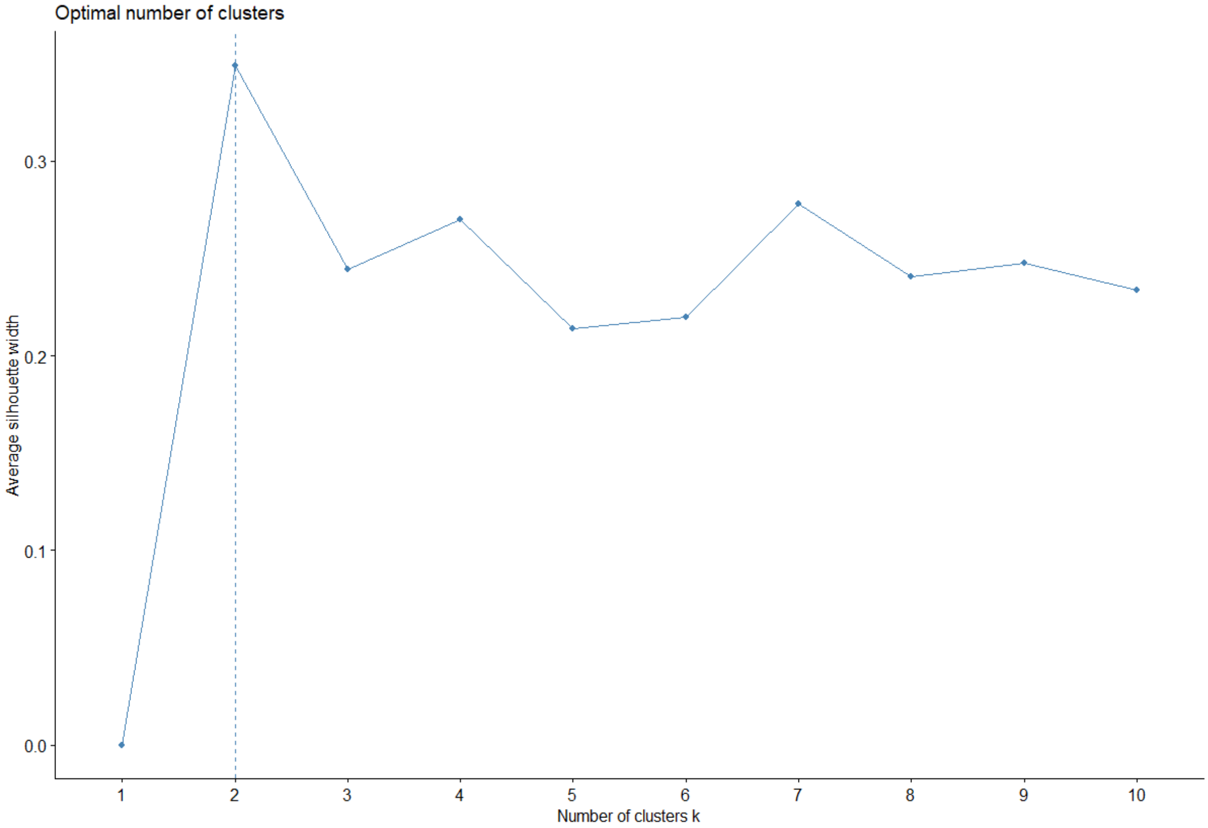

Fig. 85. Optimal number of clusters determined by silhouette method for k = 2 (source for R-coding: https://uc-r.github.io/kmeans_clustering)

		Ca (XII)	Mg (XII)	Na (XII)	K (XII)	Cr3+ (VI)	Al (VI)	Fe3+ (VI)	Mg (VI)	Ti (VI)	Al (IV)	Si (IV)	XII	n_VI	%S
Cluster1	n = 59	0.10	0.10	0.00	0.09	0.00	1.21	0.63	0.16	0.00	0.33	3.67	0.5	2.0	85
Cluster2	n = 29	0.06	0.08	0.01	0.30	0.00	1.45	0.46	0.07	0.02	0.55	3.45	0.6	2.0	50

Fig. 86. *Mineral formulae based on TEM-EDX-data summarized following the result of clustering for k=2*

	Sybilla-modelling of XRD-results	**TEM-EDX-results**	**Notes**
Cluster1	IS R0 *(%S = 83%)**	diVBM 15:45:40 *(%B=43%,* *%I=15% %M = 42%)*	*low K, Fe(VI)-rich*
Cluster2	ISS R0 + IS R0(2) *(%S = 47%)*	diVBM-ml *(%I=50%, %BM=50%)*	*K-deficit, Fe(VI)-rich, low Mg(VI)*

Tab. 18. *Comparison of results from TEM-EDX- and XRD-measurements with clustering procedure*
(- beidellite is to verify by XRD only by Li-test)*

Sample - B25 (< 2 µm), treated NaCl 60 rpm

Preparation for TEM

- raw material: <40 µm powder of B25-sample after treatment by NaCl 60 rpm
- suspension on particles < 2 µm on carbon-filmed Cu-grid
- air-dried and humidity-controlled storing

Mineral Matter

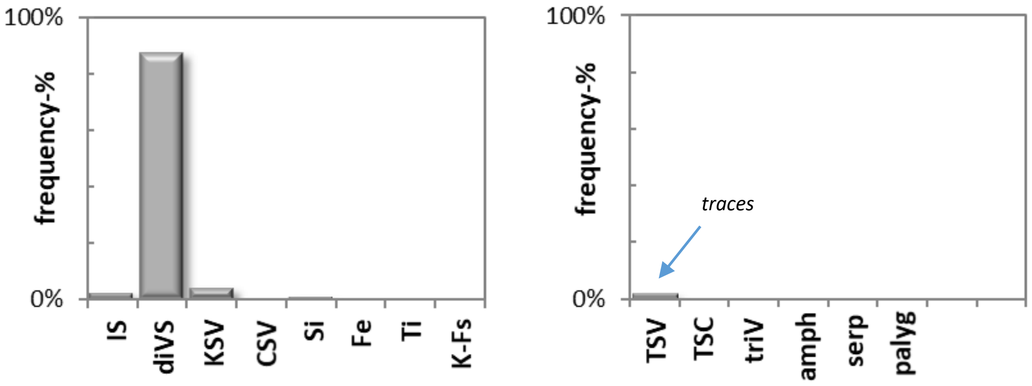

Fig. 87. *Distribution of mineral groups in fraction < 2 µm (in frequency-%)*
Legend: ***IS*** *– illite-smectite-mixed layer series in sense of Środon et al. (1992), diVS – dioctahedral vermiculite-smectite illite-smectite-mixed layer series (= charge- and/or K-deficit),* ***KSV*** *– kaolinite-smectite-dioctahedral vermiculite-mixed layer series,* ***CSV*** *– chlorite-saponite-trioctahedral vermiculite-mixed layer series,* ***Si*** *– quartz or particles with Si-surplus,* ***Fe*** *– Fe-oxide or Fe-oxyhydroxide,* ***Ti*** *– Ti-bearing phases (e.g. rutile, anatase),* ***K-Fs*** *– K-feldspar*

Clay Mineral Composition

Illite-smectite mixed-layer series (summarized: IS + diVS):

$$Ca_{0.12}\ Mg_{0.08}\ Na_{0.00}\ K_{0.16}\quad Al_{1.26}\ Fe^{3+}_{0.58}\ Mg_{0.15}\ Ti_{0.00}\ (OH)_2\quad Si_{3.59}\ Al_{0.41}\ O_{10}$$

Charge: XII = 0.56 VI = 5.85 IV = 15.59 **Σ = 22.00**
Probability of smectite layers (%S): 39%
Probability of illite layers (%I): 61%
CEC_{calc}: 52 meq / 100 g

Measured particles: 116

Table 19. *Summarized chemical composition*

SiO_2	TiO_2	Al_2O_3	Fe_2O_3	MnO	MgO	CaO	Na_2O	K_2O	P_2O_5	Σ	
61.7%	0.1%	25.4%	6.7%		3.1%	1.4%	0.0%	1.5%	0.0%	1.00	measured particles
58.6%	0.0%	22.0%	5.9%		3.0%	1.0%	0.1%	1.1%	0.1%	0.92	original B25 (< 2µm)

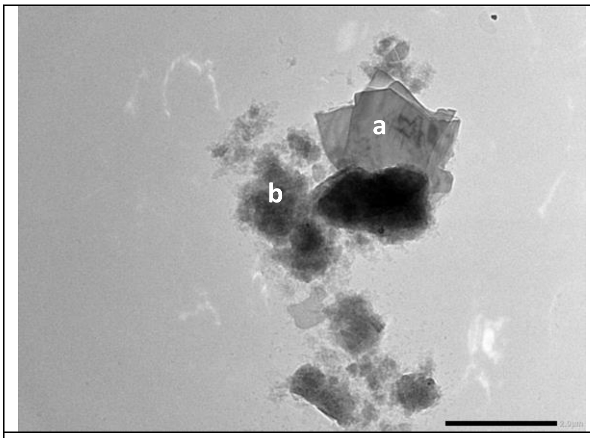

JEM-2100_MAG_X5000_B25-NaCl-60r_006.bmp

Magnification: 5k

(a) large (> 2 µm) xenomorphic plates with slight Moirè-properties *(illite, normal charged and K-amount)*; (b) aggregates composed by small (≤ 200 nm) xenomorphic platy crystals *(diVS-ml mainly with %S-range 30-40%)*

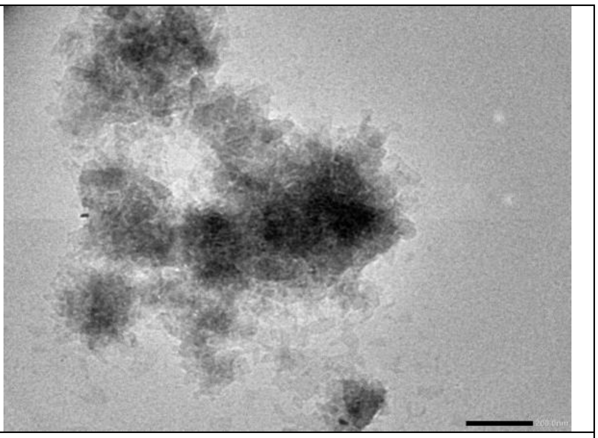

JEM-2100_MAG_X30k_B25-NaCl-60r_011.bmp

Magnification: 30k

aggregates composed by small (≤ 200 nm) xenomorphic platy crystals *(diVS-ml mainly with %S-range 40-60%)*

Fig. 88. *Morphology of particles (TEM-micrographs)*

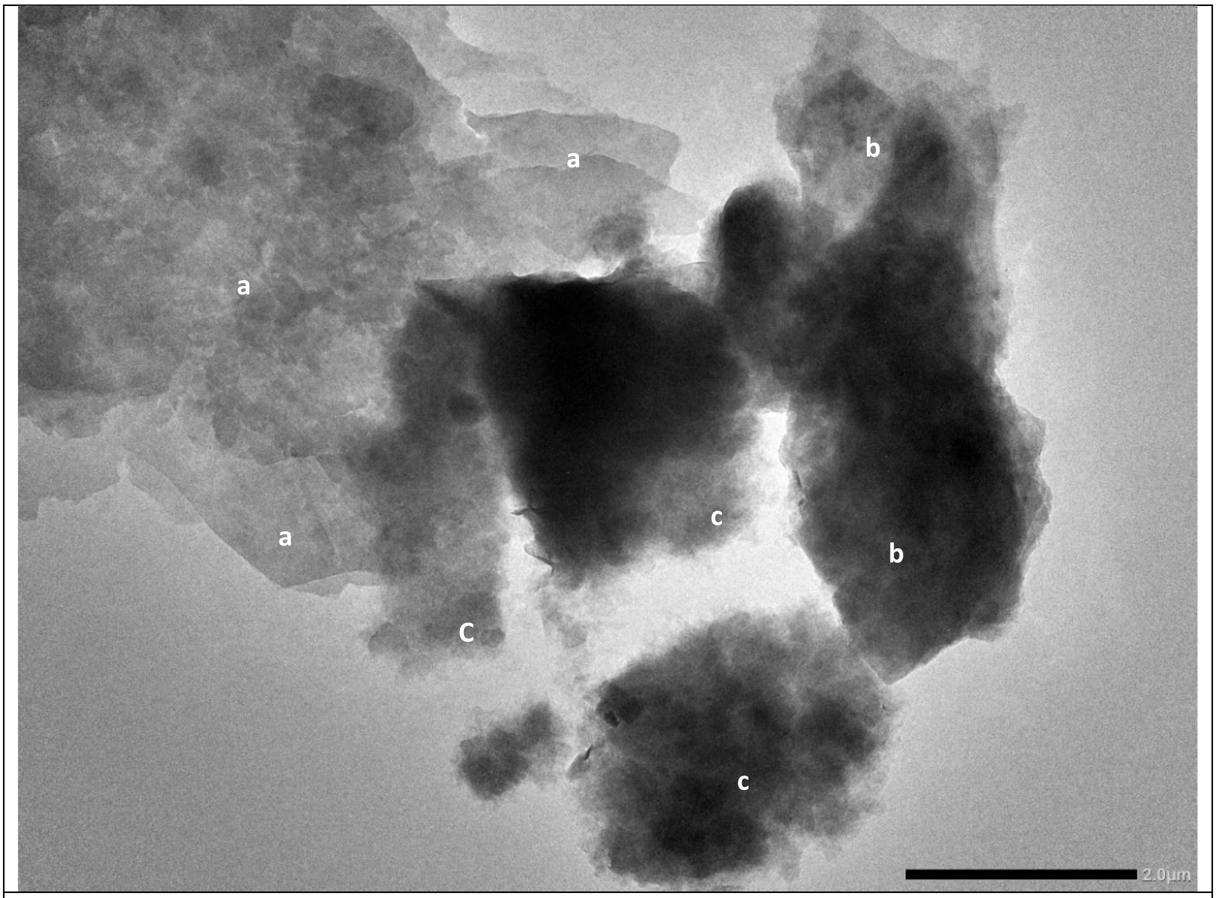

JEM-2100_MAG_X5000_B25-NaCl-60r_009.bmp

Magnification: 5k

overview: (a) aggregates composed by large (< 2 µm) and small xenomorphic thin platy crystals *(probably KSV-ml)*; (b) large (> 2 µm) xenomorphic and thick platy crystals (probably TSV-ml); (c) aggregates composed by small (< 200 nm) xenomorphic platy crystals (diVS-ml with %S-range of 30-50%)

Fig. 89. *Morphology of particles (TEM-micrographs)*

Distribution: Smectite layers probability (%S)

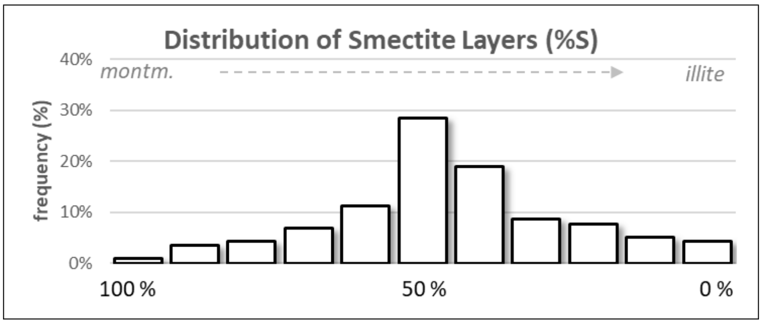

__Description:__ The distribution of %S-probability indicates the occurrence of three groups: (i) montmorillonite (in traces), (ii) diVS-ml with %S-range of 30-70% (= main group) and (iii) illite.

Fig. 90. *Distribution of smectite layers probability (%S)*

Distribution: Charge density of exchangeable cations

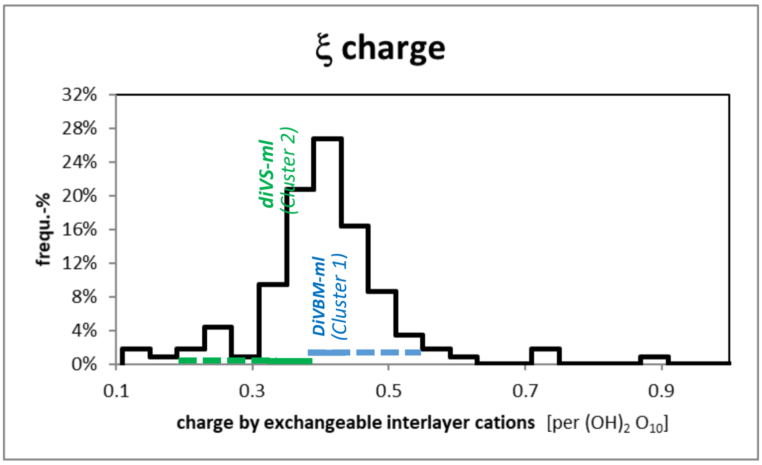

This diagram visualizes the distribution of exchangeable charges in the interlayer space (Ca, Mg, Na) determined and computed by TEM-EDX-data.

__Description:__ Narrowed charge density distribution of exchangeable interlayer cations with a maximum at 0.39 per $(OH)_2\ O_{10}$.

Fig. 91. *Distribution of charges*

Illite-smectite mixed-layer series *(IS-ml in sense of Środon et al., 1992):*

$$Ca_{0.05}\ Mg_{0.04}\ Na_{0.03}\ K_{0.45}\quad Al_{1.39}\ Fe^{3+}_{0.43}\ Mg_{0.15}\ Ti_{0.00}\ (OH)_2\quad Si_{3.59}\ Al_{0.41}\ O_{10}$$

Charge: XII = 0.66 VI = 5.75 IV = 15.59 **Σ = 22.00**
Probability of smectite layers (%S): 39%
Probability of illite layers (%I): 61%

Measured particles: 3

Distribution of smectite layers probability (%S) in IS-ml *(3 particles only)*

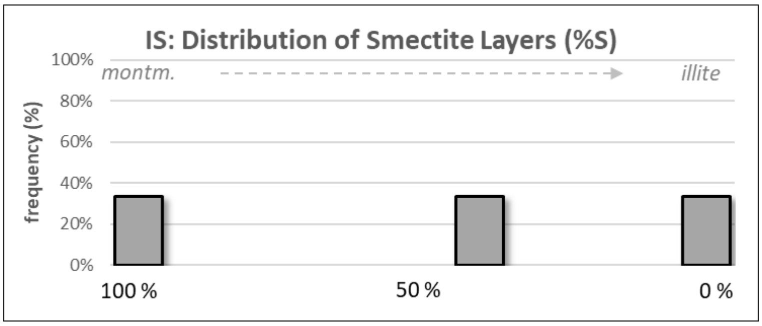

Fig. 57. *Distribution of smectite layers probability (%S)*

***Dioctahedral vermiculite-smectite mixed-layer series** (charge- and/or K-deficit):*

$$\mathrm{Ca_{0.12}\ Mg_{0.08}\ Na_{0.00}\ K_{0.15}\quad Al_{1.26}\ Fe^{3+}_{0.58}\ Mg_{0.15}\ Ti_{0.01}\ (OH)_2\ \ Si_{3.59}\ Al_{0.41}\ O_{10}}$$

Charge: XII = 0.56 VI = 5.85 IV = 15.59 **Σ = 22.00**

Probability of smectite layers (%S):	39%
Probability of illite layers (%I):	61%

Measured particles:	113

Distribution of smectite layers probability (%S) in diVS-ml

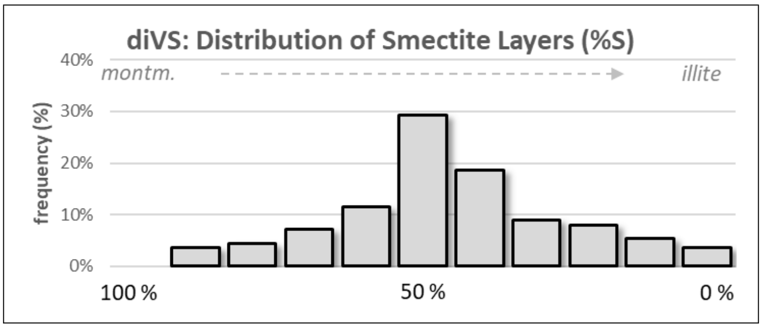

***Description:** The distribution of %S-probability in diVS-ml indicates the occurrence of two groups: (i) diVS-ml with %S-range at 40-50% (= main group) and (ii) illite with K- and charge deficit.*

***Fig. 58.** Distribution of smectite layers probability (%S)*

Talc-saponite-trioctahedral vermiculite mixed-layer series (TSV-ml):

$$\mathrm{Ca_{0.09}\ Mg_{0.00}\ Na_{0.00}\ K_{0.50}\quad Al_{0.48}\ Fe^{2+}_{1.84}\ Mg_{0.58}\ Ti_{0.00}\ (OH)_2\ \ Si_{3.06}\ Al_{0.94}\ O_{10}}$$

Charge: XII = 0.67 VI = 6.28 IV = 15.06 **Σ = 22.00**

Probability of talc layers (%T):	10%	*min – max: 2 … 15%*
Probability of saponite layers (%S):	30%	*min – max: 20 … 35%*
Probability of trioctahedral vermiculite layers (%V):	60%	*min – max: 60 … 65%*

Indications for Alteration Processes

Task of this chapter is the identification of possible indications for alteration processes caused by the overhead-rotation experiments.

Clay Mineral Matter

OPALINUS	**original**	**H2O 20 rpm**	**H2O 60 rpm**	**NaCl 20 rpm**	**NaCl 60 rpm**	**notes**
IS-ml	16%	11%	8%	3%	8%	decreasing ratio until NaCl 20 rpm
diVS-ml	84%	89%	91%	91%	76%	increasing ratio until NaCl 20 rpm
CSV-ml	n.d.	n.d.	1%	n.d.	2%	occurrence after strong treatment
TSV-ml	n.d.	n.d.	n.d.	6%	8%	
KSV-ml	n.d.	n.d.	n.d.	n.d.	7%	

Table 11. *Opalinus: Development of frequency-% for different mixed layer phases*
Legend: ***IS*** *– illite-smectite-mixed layer series in sense of Środon et al. (1992), diVS – dioctahedral vermiculite-smectite illite-smectite-mixed layer series (= charge- and/or K-deficit),* ***KSV*** *– kaolinite-smectite-dioctahedral vermiculite-mixed layer series,* ***CSV*** *– chlorite-saponite-trioctahedral vermiculite-mixed layer series;*
100 frequency-% = IS-ml + diVS-ml + CSV-ml + TSV-ml + KSV-ml; n.d. – not detected

The TEM-results show a decreasing ratio of IS-ml phases and increasing ratio diVS-ml phases in the total clay mineral matter. Other mixed layer phases (CSV, TSV, KSV) occur only in samples representing a higher treatment degree of original Opalinus clay.

B25	**original**	**H2O 20 rpm**	**H2O 60 rpm**	**NaCl 20 rpm**	**NaCl 60 rpm**	**notes**
IS-ml	2%	0%	0%	0%	2%	no valid occurrence, in traces only
diVS-ml	98%	96%	93%	89%	92%	decreasing ratio until NaCl 60 rpm
CSV-ml	n.d.	2%	n.d.	3%	n.d.	occurrence after treatment
TSV-ml	n.d.	n.d.	n.d.	n.d.	2%	
KSV-ml	n.d.	2%	7%	8%	4%	

Table 12. *B25: Development of frequency-% for different mixed layer phases*

IS-ml phases are missing nearby completely in all samples. So, the occurrence of other mixed layer phases (CSV, TSV, KSV) reduces after experimental treatments the ratio of diVS-ml phases in comparison to the original B25-sample.

Conclusions: IS-ml phases with K- & charge deficit (= diVS-ml) form the main constituent of clay mineral matter in all samples. The ratio reduction of IS-ml phases (in sense of Środon et al., 1992) is caused by overhead-rotation. Degradation of particles and alteration into diVS-ml phases are the main processes for these IS-ml phases.
The occurrence of other mixed layer phases (e.g. CSV, KSV and TSV) are considered as result of disaggregation of larger particles caused by overhead-rotation experiments.

Characterization of IS- + diVS-ml

Overview about development of selected parameter of computed mineral formulae [per $(OH)_2 O_{10}$)] in overhead-rotation experiments:

Opalinus IS+diVS

	original	H2O 20 rpm	H2O 60 rpm	NaCl 20 rpm	NaCl 60 rpm	notes
Ca	0.09 ± 0.01	0.08 ± 0.00	0.10 ± 0.01	0.11 ± 0.01	0.06 ± 0.00	
Mg	0.06 ± 0.01	0.08 ± 0.01	0.07 ± 0.01	0.08 ± 0.01	0.09 ± 0.01	
Na	0.01 ± 0.00	0.00 ± 0.00	0.01 ± 0.00	0.00 ± 0.00	0.00 ± 0.00	
K	0.39 ± 0.02	0.43 ± 0.01	0.44 ± 0.01	0.43 ± 0.01	0.45 ± 0.02	slight increasing by treatment
Al(VI)	1.40 ± 0.02	1.40 ± 0.02	1.39 ± 0.02	1.42 ± 0.02	1.42 ± 0.02	
Fe3+	0.42 ± 0.02	0.44 ± 0.01	0.43 ± 0.01	0.42 ± 0.01	0.43 ± 0.02	
Mg	0.17 ± 0.01	0.16 ± 0.01	0.18 ± 0.01	0.15 ± 0.01	0.14 ± 0.01	
Si	3.46 ± 0.02	3.39 ± 0.01	3.39 ± 0.01	3.33 ± 0.01	3.35 ± 0.01	slight decreasing by treatment
chargeXII	0.70 ± 0.01	0.76 ± 0.01	0.78 ± 0.01	0.81 ± 0.01	0.76 ± 0.01	increasing (role of NaCl 60r ?)
chargeVI-deficit	-0.17 ± 0.10	-0.15 ± 0.10	-0.17 ± 0.11	-0.15 ± 0.08	-0.12 ± 0.10	special role of NaCl 60r ?
chargeIV-deficit	-0.54 ± 0.14	-0.61 ± 0.13	-0.61 ± 0.11	-0.67 ± 0.11	-0.65 ± 0.14	increasing
%S	24 ± 2	17 ± 1	17 ± 1	12 ± 1	14 ± 1	decreasing by treatment
CECcalc	52 ± 5	43 ± 5	67 ± 5	52 ± 5	40 ± 5	
CECXII	40 ± 5	41 ± 5	44 ± 5	49 ± 5	39 ± 5	

Table 13. *Opalinus: Development of selected components and parameters in mineral formula of IS- & diVS-phases*

Legend: %S - probability of smectite layers in mixed layer phases; CECcalc – cation exchange capacity (in meq / 100 g) calculated as sum of all exchangeable cations detected by TEM-EDX-measurements; CECXII – cation cation exchange capacity (in meq / 100 g) calculated as sum of all exchangeable cations in interlayer space detected by TEM-EDX-measurements and computed for mineral formula

Opalinus series: Tetrahedral Si is reduced by experiments and the probability of smectite layers in the mixed layer phases (%S) and the tetrahedral charge deficit (chargeIV-deficit) mirror this development of Si (= pseudo-illitization). The increasing tetrahedral charge deficit is compensated mainly by rising interlayer charge (chargeXII) represented by rising K-amount. The octahedral charge deficit is nearby constant (incl. octahedral Fe^{3+}). The overhead-rotation experiment in NaCl at 60 rpm draws for few parameters a specific development (e.g. Ca, $charge_{XII}$, $charge_{VI\text{-}deficit}$, CEC_{XII}).

B25 series: Like the behavior of Opalinus series - tetrahedral Si is reduced by experiments and the probability of smectite layers in the mixed layer phases (%S) and the tetrahedral charge deficit (chargeIV-deficit) mirror this development of Si (= pseudo-illitization). The increasing tetrahedral charge deficit is compensated mainly by rising interlayer charge (chargeXII) represented mainly by

B25 IS+diVS

	original	H2O 20 rpm	H2O 60 rpm	NaCl 20 rpm	NaCl 60 rpm	notes
Ca	0.10 ± 0.00	0.09 ± 0.00	0.19 ± 0.01	0.09 ± 0.00	0.12 ± 0.00	no real change (H2O 60r ?)
Mg	0.08 ± 0.00	0.08 ± 0.00	0.02 ± 0.00	0.09 ± 0.01	0.08 ± 0.00	no real change (H2O 60r ?)
Na	0.01 ± 0.00	0.01 ± 0.00	0.09 ± 0.01	0.00 ± 0.00	0.00 ± 0.00	no real change (H2O 60r ?)
K	0.12 ± 0.01	0.13 ± 0.01	0.15 ± 0.01	0.16 ± 0.02	0.16 ± 0.01	slight increasing by treatment
Al(VI)	1.27 ± 0.01	1.25 ± 0.01	1.17 ± 0.01	1.29 ± 0.02	1.26 ± 0.01	special role of H2O 60r ?
Fe3+	0.56 ± 0.01	0.59 ± 0.01	0.56 ± 0.01	0.57 ± 0.02	0.58 ± 0.01	no real change
Mg	0.17 ± 0.01	0.15 ± 0.01	0.26 ± 0.01	0.13 ± 0.01	0.15 ± 0.01	slight decreasing (H2O 60r?)
Si	3.70 ± 0.01	3.64 ± 0.01	3.60 ± 0.01	3.60 ± 0.02	3.59 ± 0.01	decreasing by treatment
chargeXII	0.48 ± 0.01	0.50 ± 0.01	0.67 ± 0.01	0.52 ± 0.01	0.56 ± 0.01	increasing (H2O 60r?)
chargeVI-deficit	-0.17 ± 0.06	-0.15 ± 0.06	-0.27 ± 0.09	-0.12 ± 0.08	-0.15 ± 0.06	slight decreasing?? (H2O 60 r ?)
chargeIV-deficit	-0.30 ± 0.12	-0.36 ± 0.10	-0.40 ± 0.11	-0.40 ± 0.16	-0.41 ± 0.14	increasing
%S	54 ± 2	46 ± 1	40 ± 1	40 ± 2	39 ± 2	decreasing by treatment
CECcalc	48 ± 5	49 ± 5	105 ± 5	47 ± 5	52 ± 5	special role by H2O 60r?
CECXII	47 ± 5	49 ± 5	79 ± 5	47 ± 5	52 ± 5	special role by H2O 60r?

Table 14. *B25: Development of selected components and parameters in mineral formula of IS- & diVS-phases*

rising K-amount. The octahedral charge deficit is nearby constant (incl. octahedral Fe^{3+}). The overhead-rotation experiment in H$_2$O at 60 rpm draws for few parameters (e.g. Ca, charge$_{\text{XII}}$, charge$_{\text{VI-deficit}}$, CEC$_{\text{XII}}$) a specific development.

Here, the series of IS- and diVS-ml is classified in four groups by charge-deficit: (i) IS-ml (IS), (ii) high charge diVS-ml (hc diVS), (iii) medium charge diVS-ml (mc diVS) and (iv) low charge diVS-ml (lc diVS). IS-ml are considered in sense of Środon et al. (1992) with an interlayer charge of 0.89 for illite layers and 0.40 for smectite layers, hc diVS have a normal charge (0.92 for illite layers; 0.40 for smectite layers) and additionally a certain K-deficit, mc diVS show a reduced charge (0.72 for illite layers; 0.30 for smectite layers) and lc diVS are characterized by 0.62 as interlayer charge of illite layers and 0.20 as interlayer charge of smectite layers. These charges are only postulated as limits for the four groups in experience of former TEM-EDX-measurements.

Opalinus IS- & diVS-ml

	original	H2O 20 rpm	H2O 60 rpm	NaCl 20 rpm	NaCl 60 rpm	notes
frequency-%						
IS	13%	11%	8%	3%	9%	decreasing ratio by treatment
hc diVS	50%	54%	70%	70%	53%	main group, increasing by treatmer
mc diVS	30%	33%	19%	25%	32%	decreasing (role of NaCl 60r?)
lc diVS	7%	2%	3%	1%	6%	decreasing ratio by treatment
Al(VI)						
IS	1.33	1.43	1.43	1.56	1.36	increasing data from high
hc diVS	1.30	1.31	1.32	1.36	1.34	charge to low charge diVS-ml;
mc diVS	1.54	1.50	1.53	1.56	1.50	± increasing data with rising
lc diVS	1.61	1.68	1.78	2.00	1.83	degree of treatment
Fe3+(VI)						
IS	0.43	0.35	0.34	0.23	0.39	decreasing data from high
hc diVS	0.50	0.49	0.47	0.47	0.49	charge to low charge diVS-ml;
mc diVS	0.34	0.40	0.38	0.35	0.39	± decreasing data with rising
lc diVS	0.22	0.35	0.25	0.00	0.18	degree of treatment
Mg(VI)						
IS	0.22	0.21	0.23	0.23	0.25	decreasing data from IS-ml to
hc diVS	0.20	0.19	0.20	0.17	0.17	low charge diVS-ml;
mc diVS	0.12	0.09	0.09	0.09	0.11	± constant data with rising
lc diVS	0.06	0.00	0.00	0.00	0.00	degree of treatment
XII-charge						
IS	0.70	0.77	0.75	0.77	0.72	decreasing data from high
hc diVS	0.76	0.79	0.81	0.84	0.82	charge to low charge diVS-ml;
mc diVS	0.65	0.71	0.71	0.75	0.72	± increasing data with rising
lc diVS	0.54	0.64	0.53	0.30	0.45	degree of treatment (!! lc diVS)
Si(IV)						decreasing data from IS-ml to
IS	3.58	3.47	3.49	3.43	3.52	low charge diVS-ml;
hc diVS	3.45	3.40	3.39	3.33	3.34	± decreasing data with rising
mc diVS	3.47	3.36	3.37	3.32	3.35	degree of treatment
lc diVS	3.27	3.26	3.28	3.18	3.31	(exception: lc diVS-ml)

Table 15. *Opalinus: Development of selected components and parameters in mineral formula of different charge groups of IS- & diVS-phases*

Legend: ***Al(VI)*** *– atoms of Al^{3+} in octahedral sheet;* ***Si(IV)*** *– atoms of Si^{4+} in tetrahedral sheet;* ***XII-charge*** *– interlayer charge per (OH)$_2$ O$_{10}$*

Opalinus-series: High charge diVS-ml phases (K-reduced, normal charge) dominate the IS- & diVS-ml series in Opalinus clay in original material, but also in the run products of experiments. The development of diVS-ml composition shows for all selected parameter nearby the same process even in original and treated material *from high to low charge species*:

Tetrahedral layer: Increasing charge deficit caused by decreasing Si-amount (= “illitization”)
Octahedral layer: Increasing ratio of cations with a low ion radius (more Al^{3+}, less Fe^{3+} and Mg^{2+})
Interlayer space: Lowering of interlayer charge

The development of larger and high charge particles into fine and low charge particles in the original material is assumed as natural alteration by disaggregation at smectite layers of stacks accompanied by K-leaching. The compensation of rising tetrahedral charge deficit is arranged by reduction of octahedral charge (Mg - Al substitution). Partially, a small charge surplus was calculated in octahedral layer by means of an occupation slightly higher than 2 atoms [until 2.05 per $(OH)_2\ O_{10}$].

The composition of particles also mirrors a higher *intensity of treatment by overhead-rotation*:

Tetrahedral layer: Increasing charge deficit caused by decreasing Si-amount (= “illitization”)
Octahedral layer: Increasing ratio of cations with a low ion radius without change of charge (more Al^{3+}, less Fe^{3+}, but nearby constant Mg^{2+})
Interlayer space: Increasing interlayer charge compensating the rising charge^{IV}-deficit

The strong treatment in NaCl-solution at 60 rpm is commonly not following the mentioned trend indicated by the other overhead-rotation experiments.

B25-series: Medium charge diVS-ml phases (with slight charge- & K-deficits) dominate the IS- & diVS-ml series in B25 in original material, but also in the run products of experiments (exception: hc diVS-ml are the main group in run products of experiment in H_2O at 60 rpm!). The development of diVS-ml composition shows for all selected parameter nearby the same process even in original and treated material *from high to low charge species*:

Tetrahedral layer: Decreasing charge deficit caused by increasing Si-amount (= smectitization)
Octahedral layer: Increasing ratio of cations with a low ion radius with lowering of layer charge deficit (more Al^{3+}, less Fe^{3+}, even less Mg^{2+})
Interlayer space: Decreasing interlayer charge mirroring the lowering of charge-deficit in tetrahedral and octahedral layers

The composition of particles also mirrors a higher *intensity of treatment by overhead-rotation*:

Tetrahedral layer: Increasing charge deficit caused by decreasing Si-amount (= “illitization”)
Octahedral layer: No real trends are to recognize caused by experiments
Interlayer space: Increasing interlayer charge with experiments

The development of larger and high charge particles into fine and low charge particles in the original material is assumed as natural alteration by disaggregation at smectite layers of stacks accompanied by K-leaching. The increased charge deficit in tetrahedral layer caused by experiments is mainly compensated by increased interlayer charge.

For all parameter, the sample NaCl 60 rpm, representing the most intensive treatment, seems to play a special role. Probably a further mechanism is influencing the alteration process.

B25 IS- & diVS-ml

	original	H2O 20 rpm	H2O 60 rpm	NaCl 20 rpm	NaCl 60 rpm	notes
frequency-%						
IS	2%	0%	0%	0%	3%	
hc diVS	17%	10%	81%	8%	12%	special role of H2O 60r ?
mc diVS	71%	83%	17%	78%	83%	the main group, mostly
lc diVS	10%	8%	2%	14%	3%	
Al(VI)						
IS	1.31				1.39	
hc diVS	1.18	1.12	1.13	1.22	1.20	increasing data from high charge to low charge diVS-ml
mc diVS	1.27	1.25	1.33	1.29	1.27	
lc diVS	1.35	1.48	1.39	1.37	1.32	
Fe3+(VI)						
IS	0.46				0.43	
hc diVS	0.61	0.64	0.56	0.58	0.58	decreasing data from hc to lc diVS-ml only for original sample and experiments in
mc diVS	0.55	0.60	0.53	0.57	0.59	
lc diVS	0.54	0.47	0.50	0.58	0.55	
Mg(VI)						
IS	0.17				0.15	
hc diVS	0.21	0.24	0.30	0.20	0.21	decreasing data from high charge to low charge diVS-ml
mc diVS	0.17	0.15	0.13	0.14	0.15	
lc diVS	0.10	0.04	0.10	0.04	0.07	
XII-charge						
IS	0.44				0.66	decreasing data from high charge to low charge diVS-ml; ± increasing data with rising degree of treatment
hc diVS	0.59	0.62	0.72	0.80	0.62	
mc diVS	0.47	0.49	0.50	0.50	0.55	
lc diVS	0.34	0.45	0.40	0.46	0.50	
Si(IV)						
IS	3.92				3.59	increasing data from high charge to low charge diVS-ml; ± decreasing data with rising degree of treatment
hc diVS	3.62	3.62	3.59	3.39	3.59	
mc diVS	3.70	3.65	3.62	3.63	3.59	
lc diVS	3.76	3.60	3.70	3.53	3.51	

Table 16. *B25: Development of selected components and parameters in mineral formula of different charge groups of IS- & diVS-phases*
Legend: ***Al(VI)*** *– atoms of Al^{3+} in octahedral sheet;* ***Si(IV)*** *– atoms of Si^{4+} in tetrahedral sheet;* ***XII-charge*** *– interlayer charge per $(OH)_2\ O_{10}$*

Charge distribution of exchangeable cations in interlayer space

The TEM-EDX-measurements and their approach for the computation of diVS-ml mineral formulae visualize the distribution of exchangeable charges in the interlayer space (Ca, Mg, Na). This distribution indicates a different behavior of exchangeable cations controlled mainly by the development of interlayer charge.

Opalinus: The diVS-ml phases in the original Opalinus clay-material show a limited interval of distribution without a specified maximum charge from 0.15 … 0.35 by exchangeable cations per $(OH)_2\ O_{10}$. The treatment experiments are broadening this interval and shift this field to higher charges. The experiment NaCl 60 rpm shows a special role of this treatment process by a low peak maximum of charge at 0.29.

B25: The diVS-ml phases in the original B25 sample show a limited interval of distribution from 0.27 … 0.47 by exchangeable cations per $(OH)_2 O_{10}$ with a peak maximum of charge at 0.35. The treatment experiments cause only a slight broadening of this interval combined with a shift to higher charges. The strong broadening of charge distribution in sample H_2O 60 rpm visualized the special role of this treatment process for B25-series.

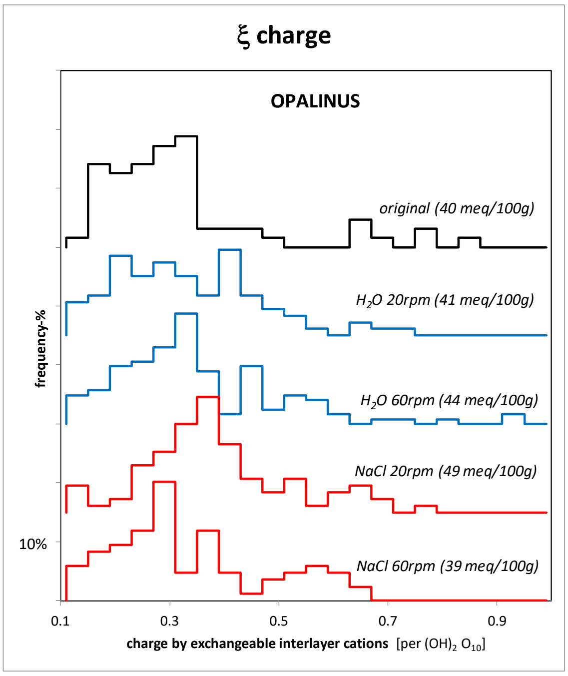

interval = 0.15 … 0.35; width = 0.2; ?max ~ 0.27 (?) = no real peak maximum

interval = 0.11 … 0.55; width = 0.44; ?max ~ 0.31 (?) = no real peak maximum
= broadening of charge density

interval = 0.11 … 0.59; width = 0.48; max at ~ 0.35
= broadening of charge density & increased charge by exchangeable cations

interval = 0.15 … 0.70; width = 0.48; max at ~ 0.39
= broadening of charge density & increased charge by exchangeable cations

interval = 0.11 … 0.67; width = 0.56; max at ~ 0.29
= less broadening of charge density & lower increased charge by exchangeable cations

Table 17. *Opalinus: Development of interlayer charges by exchangeable cations (Ca, Mg)*
Legend: *This diagram visualizes the distribution of exchangeable charges in the interlayer space (Ca, Mg, Na) determined and computed by TEM-EDX-data; 40 meq/100 g – average of charge of exchangeable cations in interlayer space*

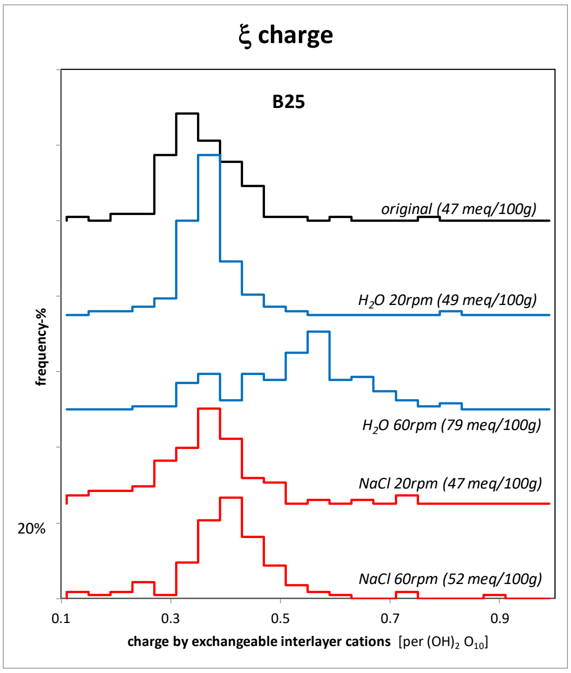

interval = 0.27 … 0.47; width = 0.2; max at 0.35

interval = 0.31 … 0.43; width = 0.12; max at 0.39
= narrowing of charge density & slight increased charge by exchangeable cations

interval = 0.31 … 0.75; width = 0.44; max at ~ 0.59
= broadening of charge density & increased charge by exchangeable cations

interval = 0.27 … 0.51; width = 0.24; max at ~ 0.43
= slight broadening of charge density & slight increased charge by exchangeable cations

interval = 0.31 … 0.55; width = 0.24; max at ~ 0.39
= slight shifting of charge density intervall & slight increased charge by exchangeable cations

Table 18. *B25: Development of interlayer charges by exchangeable cations (Ca, Mg)*
Legend: *This diagram visualizes the distribution of exchangeable charges in the interlayer space (Ca, Mg, Na) determined and computed by TEM-EDX-data; 40 meq/100 g – average of charge of exchangeable cations in interlayer space*

Rate of Alteration – Comparison between Model and Measurement

Nguyen-Thanh et al. (2014) described a model to estimate the rate of alteration for bentonites. The bentonites were classed as 'slow-reacting bentonite', 'moderate-reacting bentonite', or 'fast-reacting bentonite' corresponding to a relatively low (ΔP specific dissolution potential: < -5%), moderate (-5% < ΔP < -20%), or high specific dissolution potential (ΔP > -20%), respectively.

The larger the amount of octahedral Fe and Mg compared to octahedral Al, the greater the specific dissolution potential. They found that the interlayer composition has a discernible impact on the rate of alteration. In experiments with rotation speeds of 60 rpm and a 1 M NaCl solution, Na^+ was found to be the stabilizing cation in the interlayers of all the smectites. The Na-stabilizing mechanism was identified in only some of the smectites (type A) in experiments with 20 rpm (1 M NaCl solution). A second stabilization mechanism (by interlayer cations; Ca and Mg) was identified for other smectites (type B). Each bentonite has a specific rate of alteration. 'Slow-reacting bentonite' and clay with smectite-illite interstratifications are recommended as potential clay barriers in HLW repositories.

Opalinus: The estimation of specific dissolution potential for Opalinus clay using the mineral formula in according to Nguyen-Thanh et al. (2014) let expect a slow-reacting clay for the experiments in water (20 rpm, 60 rpm) and in NaCl-solution with 20 rpm. The measurement of run products in those three experiments have shown a more moderate-reacting clay. The probability of smectite layers of original Opalinus clay was reduced by experiments from 24% $\%S_{initial}$ to 12 … 17% $\%S_{experiment}$. X-ray diffraction reported the occurrence of pyrite in Opalinus clay. Pyrite could promote additional dissolution processes in the experiments, which are not considered in the modeling by Nguyen-Thanh et al. (2014).

The missing Na-cations in the interlayer space are responsible for the characterization of Opalinus clay as sprinter (fast-reacting clay) with an estimated complete loss of all smectite layers for experiments in NaCl-solution at 60 rpm. Otherwise, the measurements of these run products show a certain amount of smectite layers (14% $\%S_{experiment}$). Following this characterization by the model, the most of fine particles should be dissolved and recrystallized during the experiments. Indications for this assumption are the commonly announced special role of NaCl 60 rpm-experiments and the change in morphology of particles recorded by TEM in comparison to the other three experiments. Particles of untreated Opalinus clay were characterized as aggregates composed by slat-shaped crystals (length ~ 200 nm) with idiomorphic ends and underwent commonly parallel or hexagonal intergrowths. Run products of NaCl 60 rpm-experiments show nearby only aggregates composed by small xenomorphic platy crystals.

		Specific Dissolution Potential (*)			
Opalinus	**$\%S_{initial}$**	**H2O 20 rpm**	**H2O 60 rpm**	**NaCl 20 rpm**	**NaCl 60 rpm**
Interlayer Type (*)		Ca+Mg	Ca+Mg	Ca+Mg	Na
calculated $\Delta\%S$		1 ± 2	1 ± 2	1 ± 3	-103 ± 3
measured $\%S_{initial}$	24				
expected $\%S_{experiment}$		24 ± 2	24 ± 2	24 ± 3	0
measured $\%S_{experiment}$		17 ± 1	17 ± 1	12 ± 1	14 ± 1
reaction type					
by modelling*		*sleeper*	*sleeper*	*sleeper*	*sprinter*
by experiment		***moderate***	***moderate***	***moderate***	***sprinter***

***Legend** : (*) - in according to Nguyen-Thanh et al., 2014*

***Table 19.** Opalinus: Development of Specific Dissolution Potential*

B25: The estimation of specific dissolution potential for B25-series using the mineral formula in according to Nguyen-Thanh et al. (2014) let expect a moderate-reacting clay for the experiments in water (20 rpm, 60 rpm) and in NaCl-solution with 20 rpm (Δ%S: -8 … -9%). The investigations of run products from those three experiments confirm this material as moderate-reacting clay. The probability of smectite layers of original B25 clay was reduced by experiments from 54% $\%S_{initial}$ to 40 … 46% $\%S_{experiment}$.

The missing Na-cations in the interlayer space are responsible for the characterization of B25 clay even as sprinter (fast-reacting clay) with an estimated complete loss of all smectite layers for experiments in NaCl-solution at 60 rpm. Otherwise, the measurements of these run products show a certain amount of smectite layers (39% $\%S_{experiment}$). Following this characterization by the model, the most of fine particles should be dissolved and recrystallized during the experiments. Indications for this assumption are the commonly announced special role of NaCl 60 rpm-experiments and the change in morphology of particles recorded by TEM in comparison to the other three experiments. The particles of untreated B25 clay, characterized as large (≤ 1 µm) xenomorph film-like platy crystals with folds, are not to find in run products of NaCl 60 rpm-experiments. Aggregates composed by small (< 200 nm) xenomorphic platy crystals control the morphology of particles in this treated material.

		Specific Dissolution Potential (*)			
B25	**original**	**H2O 20 rpm**	**H2O 60 rpm**	**NaCl 20 rpm**	**NaCl 60 rpm**
Interlayer Type (*)		Ca+Mg	Ca+Mg	Ca+Mg	Na
calculated Δ%S		-8 ± 1	-8 ± 1	-9 ± 1	-96 ± 3
measured $\%S_{initial}$	54				
expected $\%S_{experiment}$		46 ± 1	46 ± 1	45 ± 1	0
measured $\%S_{experiment}$		46 ± 1	40 ± 1	40 ± 2	39 ± 2
reaction type					
by modelling*		*moderate*	*moderate*	*moderate*	*sprinter*
by experiment		***moderate***	***moderate***	***moderate***	***sprinter***

***Legend** : (*) - in according to Nguyen-Thanh et al., 2014*

***Table 20.** B25: Development of Specific Dissolution Potential*

Conclusions: The Opalinus- and B25-sample series show a nearby similar behavior in result of over-head-rotation experiments. Low charge species of diVS-ml phases survive treatment procedure only in cases of lowered stress parameters (e.g. in octahedra: preferred cations with a smaller ion radius like Al^{3+} and Fe^{3+} in comparison to Mg^{2+}).

The loss of tetrahedral Si increases the tetrahedral charge deficit (= "illitization") with higher intensity of treatment. This tetrahedral charge deficit is compensated mainly by an increasing interlayer charge represented by a higher K-amount.

The assumption for the mechanism behind of this observation is: The treatment is mainly breaking larger particles/stacks preferred at smectite layers. Furthermore, lower charged diVS-ml phases undergo easier dissolution processes. Only particles with less stress parameter in the mineral pattern survive the treatment.

References

Aplin, A.C., Matenaar, I.F., McCarty, D.K., van der Pluijm, B.A. (2006). Clays Clay Miner ***54****, 500-514. DOI: 10.1346/CCMN.2006.0540411*

Cliff, G. & Lorimer, G. W. (1975). J. Microsc. ***103****, 203–207.*

Crâciun, C. (1984). Spectrosc. Lett. ***17****, 579–590.*

Döbelin, N., Kleeberg, R. (2015). Journal of Applied Crystallography ***48****, 1573-1580. DOI: 10.1107/S1600576715014685*

Farmer, V. C. (1974). Editor. The Infrared Spectra of Minerals, Monograph 4. London: Mineralogical Society.

Farmer, V. C. & Russell, J. D. (1964). Spectrochim. Acta, ***20*** *, 1149-1173.*

Gaucher, E.C., Fernández, A. M. & Waber, H.N. (2003): Annex 9: Rock and Mineral Characterisation of the Opalinus Clay Formation. in: Pearson, F. J., Arcos, D., Bath, A., Boisson, J.-Y., Fernández, A. M., Gäbler, H.-E., Gaucher, E., Gautschi, A., Griffault, L., Hernán, P. & Waber, H. N. (2003): Mont Terri Project – Geochemistry of Water in the Opalinus Clay Formation at the Mont Terri Rock Laboratory. Berichte des BWG, Serie Geologie – Rapports de l’OFEG, Série Géologie – Rapporti dell’UFAEG, Serie Geologia – Reports of the FOWG, Geology Series, ***5****, 281-303.*

Goodman, B. A., Russell, J. D., Fraser, A. R. & Woodhams, F. W. D. (1976). Clays Clay Miner. ***24****, 52-59.*

Henning, K.-H. & Störr, M. (1986). Electron Micrographs (TEM, SEM) of Clays and Clay Minerals, p. 325. Akademie-Verlag Berlin.

Hoang-Minh, T., Kasbohm, J., Nguyen-Thanh, L., Nga, P. T., Lai, L. T., Duong, N. T., Thanh, N. D., Thuyet, N. T. M., Anh, D. D., Pusch, R., Knutsson, S. & Ferreiro Mahlmann, R. (2019). J. Appl. Cryst. ***52****, 133-147. doi: https://doi.org/10.1107/S1600576718018162*

Lorimer, G. W. & Cliff, G. (1976). Electron Microscopy in Mineralogy, edited by H. R. Wenk, pp. 506–519. Berlin: Springer Verlag.

Madejová, J. & Komadel, P (2001). Clays Clay Miner. ***49*** *, 410-432.*

Madejová, J., Komadel, P. & Čičel, B. (1994). Clay Miner. ***29****, 319-326.*

Matschiavelli, N., Kluge, S., Podlech, C., Standhaft, D., Grathoff, G., Ikeda-Ohno, A., Warr, L.N., Chukharkina, A., Arnold, T. & Cherkouk, A. (2019). Environmental Science & Technology. ***53*** *(17), 10514-10524, DOI: 10.1021/acs.est.9b02670*

Mellini, M. & Menichini, R. (1985). R. Soc. Ital. Miner. Petrol. ***40****, 261–266.*

Moore, D.M., Reynolds, R.C. (1989). X-ray Diffraction and the Identification and Analysis of Clay Minerals, Oxford University Press, New York, 332 + xvi pp.

Nguyen-Thanh, L., Herbert, H.-J., Kasbohm, J., Hoang-Minh, T. & Mählmann, R. F. (2014). Clays Clay Miner. ***62****, 425–446.*

Środoń, J., Elsass, F., McHardy, W. J. & Morgan, D. J. (1992). Clay Miner. ***27****, 137–158.*

Content

Sample - Opalinus (< 2 µm), original material

Preparation for TEM

- raw material: <40 µm powder of original Opalinus-sample
- suspension on particles < 2 µm on carbon-filmed Cu-grid
- air-dried and humidity-controlled storing

Mineral Matter

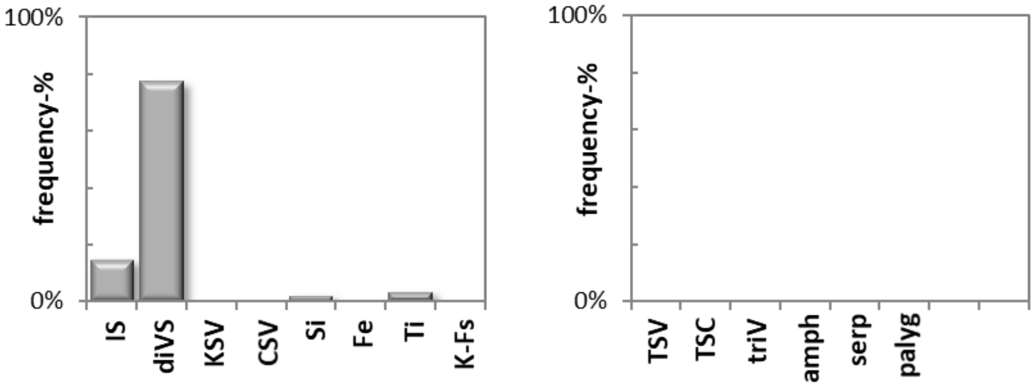

Fig. 1. *Distribution of mineral groups in fraction < 2 µm (in frequency-%)*
Legend: ***IS*** *– illite-smectite-mixed layer series in sense of Środon et al. (1992), diVS – dioctahedral vermiculite-smectite illite-smectite-mixed layer series (= charge- and/or K-deficit),* ***KSV*** *– kaolinite-smectite-dioctahedral vermiculite-mixed layer series,* ***CSV*** *– chlorite-saponite-trioctahedral vermiculite-mixed layer series,* ***Si*** *– quartz or particles with Si-surplus,* ***Fe*** *– Fe-oxide or Fe-oxyhydroxide,* ***Ti*** *– Ti-bearing phases (e.g. rutile, anatase),* ***K-Fs*** *– K-feldspar*

Clay Mineral Composition

Illite-smectite mixed-layer series (summarized: IS + diVS):

$$\mathrm{Ca_{0.09}\,Mg_{0.06}\,Na_{0.01}\,K_{0.39}\quad Al_{1.40}\,Fe^{3+}_{0.42}\,Mg_{0.17}\,Ti_{0.01}\,(OH)_2\quad Si_{3.46}\,Al_{0.54}\,O_{10}}$$

Charge: XII = 0.7 VI = 5.83 IV = 15.46 **Σ = 21.99**

Probability of smectite layers (%S): 24%
Probability of illite layers (%I): 76%
Specific Dissolution Potential (ΔS%)
for H2O, 20 + 60 rpm 1 (= slow reacting, interlayer group: Ca+Mg (= type B))
for NaCl, 20 rpm 1 (= slow reacting, interlayer group: Ca+Mg (= type B))
for NaCl, 60 rpm -103 (= fast reacting, ‘illitization’, interlayer group: Na (= type A))
CEC$_{calc}$: 52 meq / 100 g

Measured particles: 70

Table 1. *Summarized chemical composition*

SiO_2	TiO_2	Al_2O_3	Fe_2O_3	MnO	MgO	CaO	Na_2O	K_2O	P_2O_5	Σ	
52.7%	0.1%	26.1%	4.3%		2.7%	1.3%	0.0%	3.4%	0.3%	0.91	measured particles
53.1%	1.0%	19.7%	6.2%	<0.1%	2.3%	3.0%	0.6%	2.6%		0.91	GAU03 (SHGN - bulk)

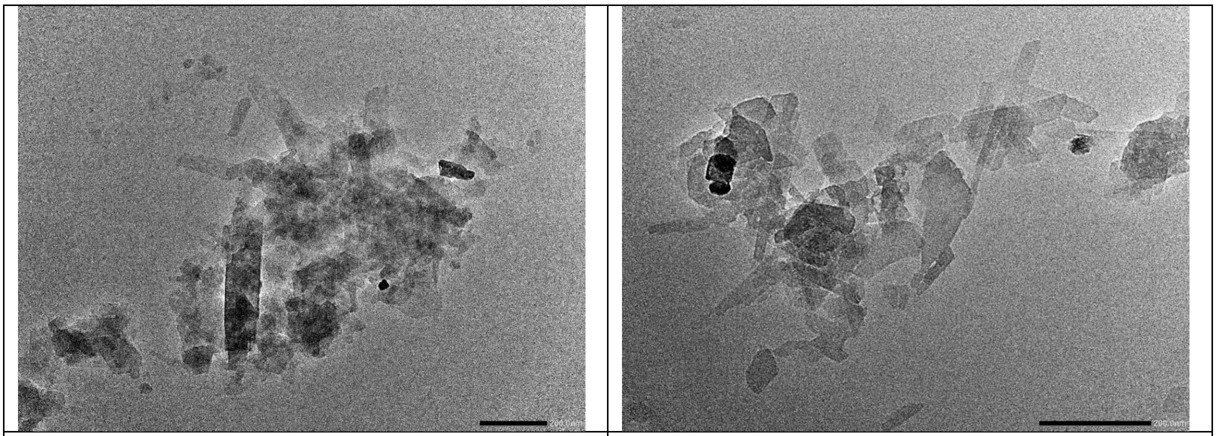

JEM-2100_MAG_X30k_Opalinus-40um-16.9_008.bmp Magnification: 30k	*JEM-2100_MAG_X50k_Opalinus-40um-16.9_011.bmp* Magnification: 50k

aggregates composed by slat-shaped crystals (length ~ 200 nm) with idiomorphic ends, commonly parallel or hexagonal intergrowths *(IS-ml and diVS-ml, not to distinguish by morphology of particles)*

Fig. 2. *Morphology of particles (TEM-micrographs)*

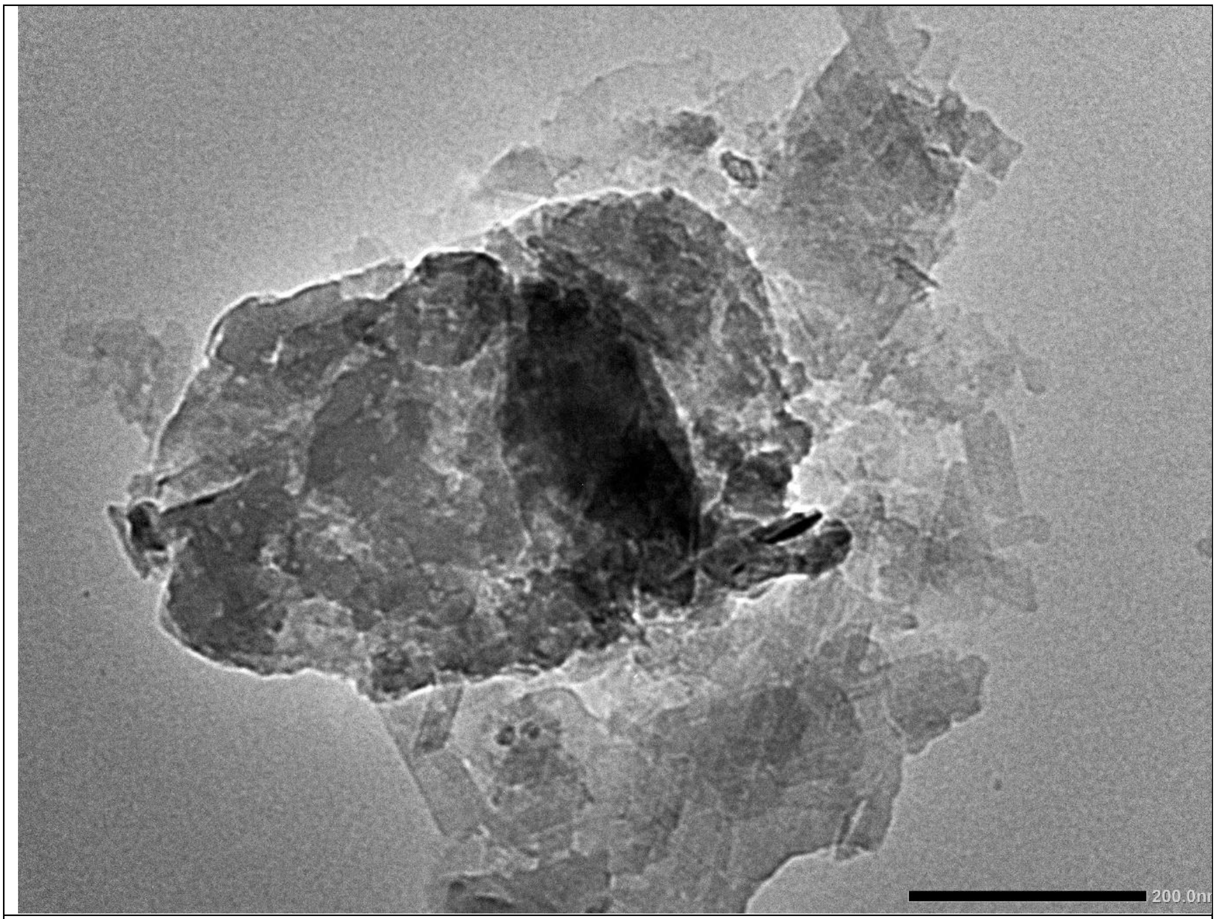

JEM-2100_MAG_X50k_Opalinus-40um-16.9_015.bmp
Magnification: 50k

former idiomorphic platy muscovite weathered into high charged dioctahedral vermiculite-smectite mixed layer phases with K-deficit (%S ~10%, %I ~ 90%)

Fig. 3. *Morphology of particles (TEM-micrographs)*

Distribution of smectite layers probability (%S)

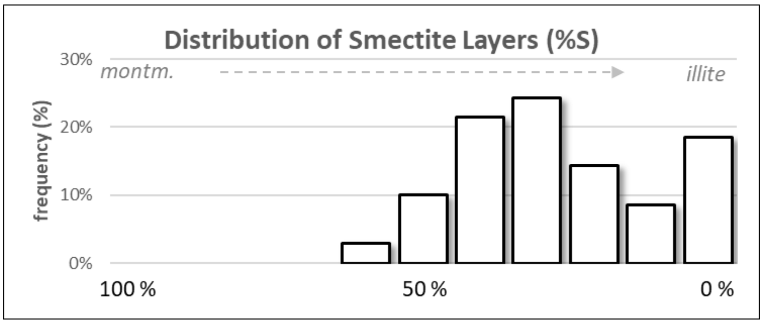

Description: *The distribution of %S-probability indicates two groups: (i) the occurrence of diVS-ml + IS-ml with %S mainly at 30-40% and (ii) illite with K- & charge-deficit.*

Fig. 4a. *Distribution of smectite layers probability (%S)*

Differentiation by relation “Octahedral Mg vs. tetrahedral Si”?

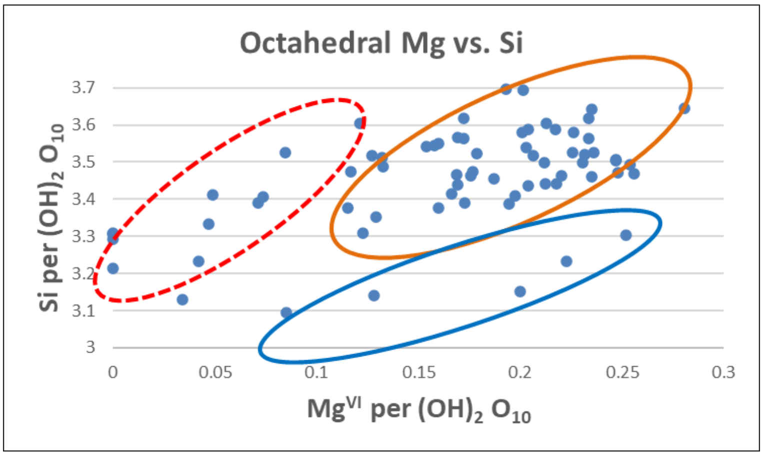

Description: *This diagram indicates the occurrence of three Mg-groups in relation to tetrahedral Si. Probably, this distribution of TEM-EDX-data mirrors three phases modelled already by Sybilla-processed oriented XRD-traces:*

(I) brown: ISS GLY R0 with %S ~29%, (II) red: IS GLY R0 with %S ~11% and (III) blue: illite

Fig. 4b. *Distribution of octahedral Mg vs. tetrahedral Si [all per$(OH)_2 O_{10}$]*

Distribution of K in relation to tetrahedral Si

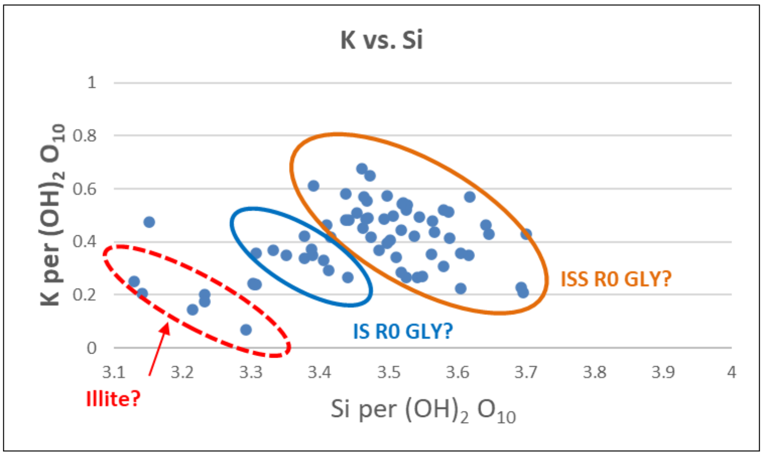

Description: *This diagram indicates the occurrence of three groups in relation of K to tetrahedral Si. Probably, this distribution of TEM-EDX-data mirrors three phases modelled already by Sybilla-processed oriented XRD-traces:*

(I) brown: ISS GLY R0 with $\%S_{XRD}$ ~29%, (II) blue: IS GLY R0 with $\%S_{XRD}$ ~11% and (III) red: Illite

Fig. 4c. *Distribution of K vs. tetrahedral Si [all per$(OH)_2 O_{10}$]*

Distribution of charges (exchangeable from interlayer space)

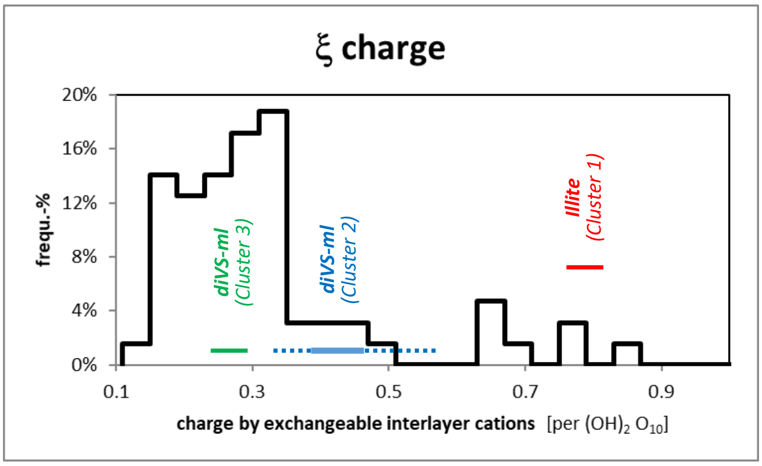

This diagram visualizes the distribution of exchangeable charges in the interlayer space (Ca, Mg, Na) determined and computed by TEM-EDX-data.

Description: *The charge density indicates a broad distribution of exchangeable interlayer cations lower than 0.35 per $(OH)_2\ O_{10}$.*

Fig. 5. *Distribution of charges (incl. averaged charges of cluster 1-3 of fig. 9)*

Dioctahedral vermiculite-smectite mixed-layer series
(charge- and/or K-deficit; confirmed as Cluster3):

$Ca_{0.08}\ Mg_{0.04}\ Na_{0.01}\ K_{0.44}\quad Al_{1.38}\ Fe^{3+}_{0.42}\ Mg_{0.20}\ Ti_{0.00}\ (OH)_2\quad Si_{3.52}\ Al_{0.48}\ O_{10}$

Charge:	XII = 0.69	VI = 5.79	IV = 15.52	**Σ = 22.00**
Probability of smectite layers (%S):	31%			
Probability of illite layers (%I):	69%			
Measured particles:	50			

Distribution of smectite layers probability (%S) in Cluster3

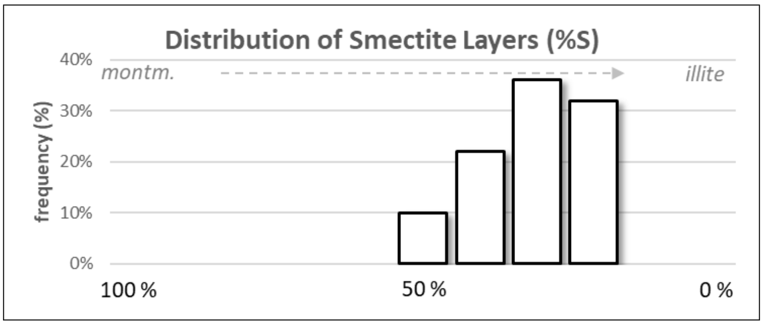

Description: *The distribution of %S-probability indicates the occurrence mainly of diVS-ml with %S mainly at 30%.*

Fig. 6a. *Distribution of smectite layers probability (%S) in IS-ml*

diVS-ml	*particles (abs)*	**Ca (XII)**	**Mg (XII)**	**Na (XII)**	**K (XII)**	**Cr3+ (VI)**	**Al (VI)**	**Fe3+ (VI)**	**Mg (VI)**	**Ti (VI)**	**Al (IV)**	**Si (IV)**	**XII**	**n_VI**	**%S**
%S >95%	n = 0														
%S 95-85%	n = 0														
%S 85-75%	n = 0														
%S 75-65%	n = 0														
%S 65-55%	n = 0														
%S 55-45%	n = 5	0.10	0.02	0.00	0.35	0.00	1.35	0.41	0.23	0.00	0.32	3.68	0.6	2.0	51
%S 45-35%	n = 11	0.07	0.04	0.01	0.41	0.00	1.39	0.40	0.20	0.00	0.41	3.59	0.6	2.0	39
%S 35-25%	**n = 18**	**0.08**	**0.04**	**0.01**	**0.45**	**0.00**	**1.42**	**0.38**	**0.19**	**0.00**	**0.49**	**3.51**	**0.7**	**2.0**	**30**
%S 25-15%	n = 16	0.09	0.05	0.00	0.48	0.00	1.32	0.47	0.20	0.00	0.56	3.44	0.8	2.0	21
%S 15- 5%	n = 0														
%S <5%	n = 0														

Fig. 6b. *Computed averaged mineral formulae for diVS-ml phases of Cluster3 in the different %S-classes*

Dioctahedral vermiculite-smectite mixed-layer series

(charge- and/or K-deficit; confirmed as Cluster2):

$$Ca_{0.07}\ Mg_{0.11}\ Na_{0.00}\ K_{0.28}\quad Al_{1.64}\ Fe^{3+}_{0.29}\ Mg_{0.06}\ Ti_{0.01}\ (OH)_2\ \ Si_{3.35}\ Al_{0.65}\ O_{10}$$

Charge: XII = 0.66 VI = 5.98 IV = 15.35 **Σ = 21.99**

Probability of smectite layers (%S): 14%

Probability of illite layers (%I): 86%

Measured particles: 14

Distribution of smectite layers probability (%S) in Cluster2

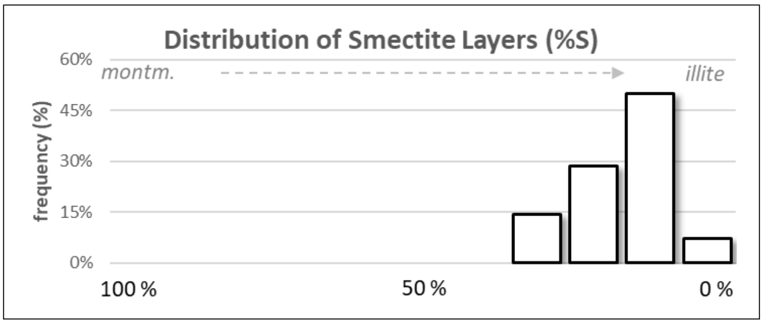

Description: *The distribution of %S-probability indicates the occurrence of diVS-ml with %S mainly at 10%.*

Fig. 7a. *Distribution of smectite layers probability (%S) in diVS-ml*

diVS-ml	*particles (abs)*	**Ca (XII)**	**Mg (XII)**	**Na (XII)**	**K (XII)**	**Cr3+ (VI)**	**Al (VI)**	**Fe3+ (VI)**	**Mg (VI)**	**Ti (VI)**	**Al (IV)**	**Si (IV)**	**XII**	**n_VI**	**%S**
%S >95%	n = 0														
%S 95-85%	n = 0														
%S 85-75%	n = 0														
%S 75-65%	n = 0														
%S 65-55%	n = 0														
%S 55-45%	n = 0														
%S 45-35%	n = 0														
%S 35-25%	n = 2	0.07	0.08	0.00	0.32	0.00	1.68	0.21	0.11	0.00	0.49	3.51	0.6	2.0	29
%S 25-15%	n = 4	0.06	0.11	0.00	0.35	0.00	1.57	0.35	0.08	0.00	0.60	3.40	0.7	2.0	17
%S 15- 5%	**n = 7**	**0.08**	**0.11**	**0.00**	**0.26**	**0.00**	**1.66**	**0.27**	**0.05**	**0.02**	**0.70**	**3.30**	**0.6**	**2.0**	**10**
%S <5%	n = 1	0.07	0.24	0.00	0.15	0.00	1.65	0.36	0.00	0.00	0.78	3.22	0.8	2.0	4

Fig. 7b. *Computed averaged mineral formulae diVS-ml phases of Cluster2 in the different %S-classes*

Illite *(as end member of diVS-ml series; confirmed as Cluster1):*

$$Ca_{0.22}\,Mg_{0.15}\,Na_{0.02}\,K_{0.21}\quad Al_{1.04}\,Fe^{3+}_{0.82}\,Mg_{0.14}\,Ti_{0.00}\,(OH)_2\quad Si_{3.18}\,Al_{0.82}\,O_{10}$$

Charge: XII = 0.95 VI = 5.87 IV = 15.18 **Σ = 22.00**

Probability of smectite layers (%S): 2%

Probability of illite layers (%I): 98%

Measured particles: 5

Illite	*particles (abs)*	**Ca (XII)**	**Mg (XII)**	**Na (XII)**	**K (XII)**	**Cr3+ (VI)**	**Al (VI)**	**Fe3+ (VI)**	**Mg (VI)**	**Ti (VI)**	**Al (IV)**	**Si (IV)**	**XII**	**n_VI**	**%S**
%S >95%	n = 0														
%S 95-85%	n = 0														
%S 85-75%	n = 0														
%S 75-65%	n = 0														
%S 65-55%	n = 0														
%S 55-45%	n = 0														
%S 45-35%	n = 0														
%S 35-25%	n = 0														
%S 25-15%	n = 0														
%S 15- 5%	n = 2	0.33	0.05	0.00	0.22	0.00	1.12	0.64	0.24	0.00	0.73	3.27	1.0	2.0	7
%S <5%	n = 3	0.14	0.22	0.03	0.20	0.00	0.98	0.93	0.08	0.00	0.88	3.12	1.0	2.0	0

Fig. 8. *Computed averaged mineral formulae f illite (Cluster1) in the different %S-classes*

Mineral Matter – Specification

Result of Clustering & Comparison with XRD-data (Sybilla-processing)

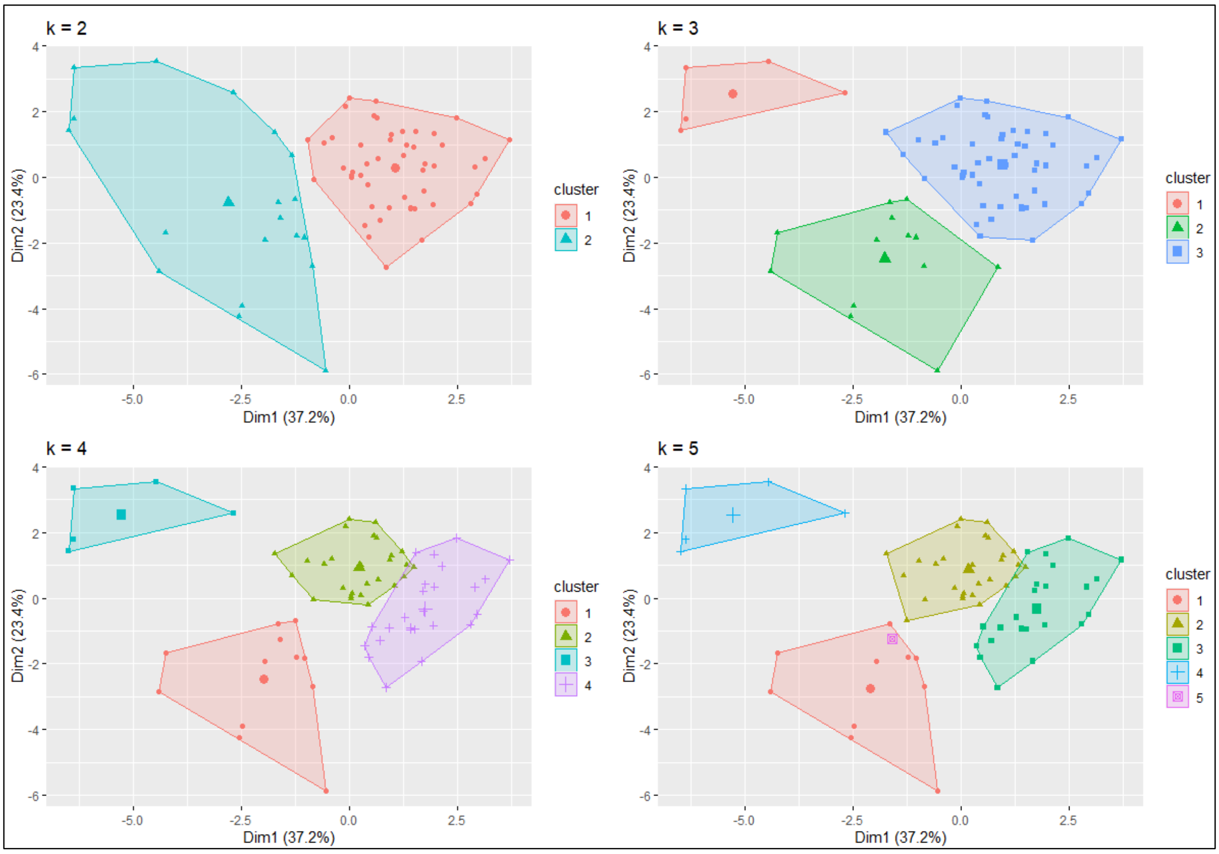

Fig. 9. *Clustering of all measured particles for clusters k = 2, k = 3, k = 4 and k = 5 (source for R-coding: https://uc-r.github.io/kmeans_clustering)*

The optimum of clusters was calculated with k = 3. This number of clusters differentiates also clearly illite particles (Cluster1) from smectite-bearing phases (Cluster2, Cluster3).

		Ca (XII)	Mg (XII)	Na (XII)	K (XII)	Cr3+ (VI)	Al (VI)	Fe3+ (VI)	Mg (VI)	Ti (VI)	Al (IV)	Si (IV)	XII	n_VI	%S
Cluster1	n = 5	0.22	0.15	0.02	0.21	0.00	1.04	0.82	0.14	0.00	0.82	3.18	1.0	2.0	2
Cluster2	n = 14	0.07	0.11	0.00	0.28	0.00	1.64	0.29	0.06	0.01	0.65	3.35	0.7	2.0	14
Cluster3	n = 50	0.08	0.04	0.01	0.44	0.00	1.38	0.42	0.20	0.00	0.48	3.52	0.7	2.0	31

Fig. 10. *Mineral formulae based on TEM-EDX-data summarized following the result of clustering for k=3*

	Sybilla-results	**TEM-EDX-results**	**Notes**
Cluster1	Illite	Illite	*high K-deficit, Fe(VI)-rich*
Cluster2	IS R0 *(%S = 11%)*	diVS-ml *(%S = 14%)*	*high K-deficit, Al(VI)-rich, low Mg(VI)*
Cluster3	ISS R0 *(%S = 29%)*	diVS-ml *(%S = 31%)*	*K-deficit, Fe(VI)- & Mg(VI)-rich*

Tab. 2. *Comparison of results from TEM-EDX- and XRD-measurements with clustering procedure*

Sample - Opalinus (< 2 µm), treated H_2O - 20 rpm

Preparation for TEM

- raw material: <40 µm powder of Opalinus-sample, treated by H_2O at 20 rpm for 30 days
- suspension on particles < 2 µm on carbon-filmed Cu-grid
- air-dried and humidity-controlled storing

Mineral Matter

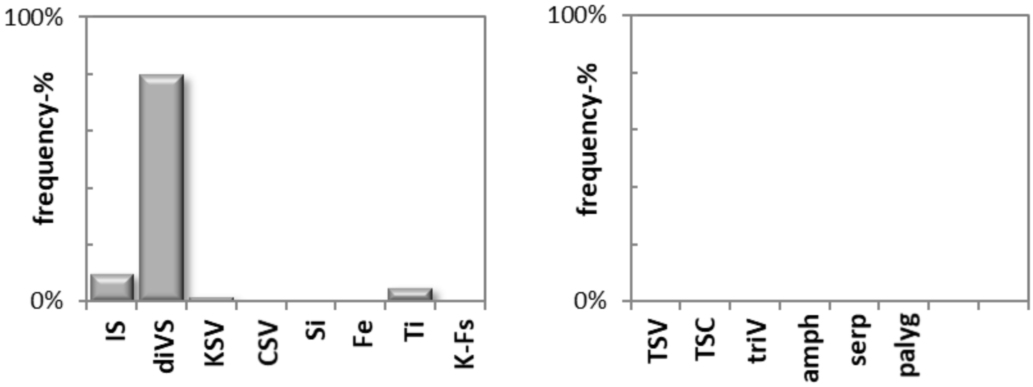

Fig. 11. *Distribution of mineral groups in fraction < 2 µm (in frequency-%)*
Legend: ***IS*** *– illite-smectite-mixed layer series in sense of Środon et al. (1992), diVS – dioctahedral vermiculite-smectite illite-smectite-mixed layer series (= charge- and/or K-deficit),* ***KSV*** *– kaolinite-smectite-dioctahedral vermiculite-mixed layer series,* ***CSV*** *– chlorite-saponite-trioctahedral vermiculite-mixed layer series,* ***Si*** *– quartz or particles with Si-surplus,* ***Fe*** *– Fe-oxide or Fe-oxyhydroxide,* ***Ti*** *– Ti-bearing phases (e.g. rutile, anatase),* ***K-Fs*** *– K-feldspar*

Clay Mineral Composition

Illite-smectite mixed-layer series (summarized: IS + diVS):

$$Ca_{0.08}\,Mg_{0.08}\,Na_{0.00}\,K_{0.43}\quad Al_{1.40}\,Fe^{3+}_{0.44}\,Mg_{0.16}\,Ti_{0.01}\,(OH)_2\quad Si_{3.39}\,Al_{0.61}\,O_{10}$$

Charge: XII = 0.76 VI = 5.85 IV = 15.39 **Σ = 22.00**
Probability of smectite layers (%S): 17%
Probability of illite layers (%I): 83%
CEC_{calc}: 43 meq / 100 g

Measured particles: 91

Table 3. *Summarized chemical composition*

SiO_2	TiO_2	Al_2O_3	Fe_2O_3	MnO	MgO	CaO	Na_2O	K_2O	P_2O_5	Σ	
51.3%	0.1%	26.8%	4.5%		2.8%	0.8%	0.0%	3.7%	0.0%	0.90	measured particles
52.7%	0.1%	26.1%	4.3%		2.7%	1.3%	0.0%	3.4%	0.3%	0.91	Opalinus, original

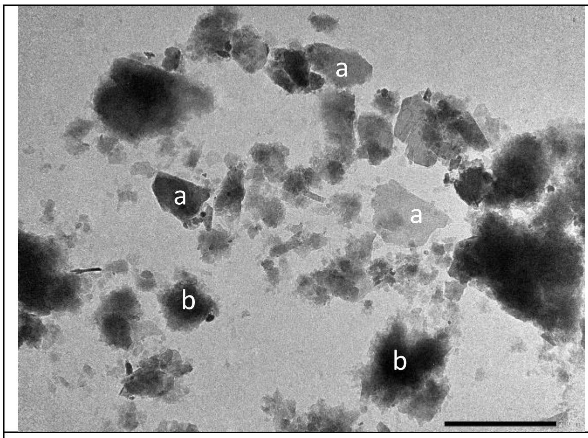	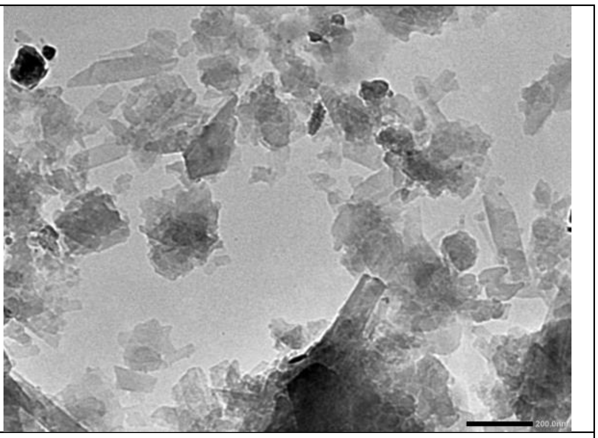
JEM-2100_MAG_X5000_Opalinus-20r-H2O_003.bmp Magnification: 5k	*JEM-2100_MAG_X30k_Opalinus-20r-H2O_008.bmp* Magnification: 30k
(a) Mixture of xenomorphic plates (length + 1 µm) *[= diVS-ml and IS-ml with %S < 10%]* and (b) aggregates composed by slat-shaped crystals *[= diVS-ml with %S-range 10-20%]*	aggregates composed by slat-shaped crystals (length ~ 200 nm) with hypidiomorphic ends, commonly hexagonal intergrowths *(mainly diVS-ml with %S-range 20-30%)*

Fig. 12. *Morphology of particles (TEM-micrographs)*

Distribution of smectite layers probability (%S)

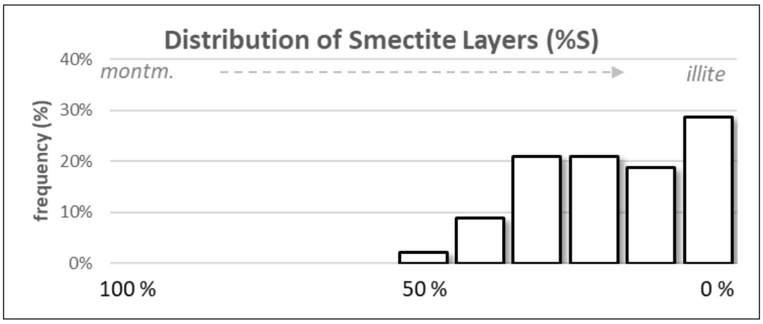

Description: *The distribution of %S-probability indicates two groups: (i) the occurrence of diVS-ml + IS-ml with %S mainly at 20-30% and (ii) illite with K- & charge-deficit.*

Fig. 13. *Distribution of smectite layers probability (%S)*

Distribution of charges (exchangeable from interlayer space)

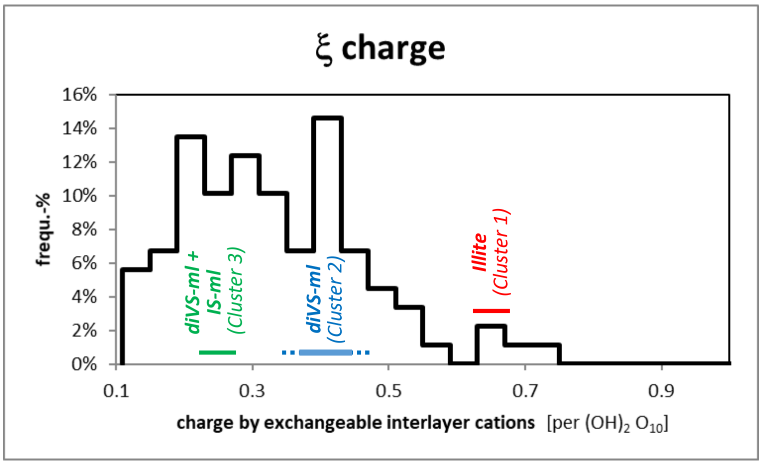

This diagram visualizes the distribution of exchangeable charges in the interlayer space (Ca, Mg, Na) determined and computed by TEM-EDX-data.

Description: *The charge density indicates an overly broad distribution of exchangeable interlayer cations lower than 0.55 per* $(OH)_2 O_{10}$.

Fig. 14. *Distribution of charges*

Dioctahedral vermiculite-smectite mixed-layer series** (mixed with IS-ml)**:
*(diVS-ml with charge- and/or K-deficit; group confirmed as Cluster3)**:***

$$Ca_{0.08}\ Mg_{0.04}\ Na_{0.00}\ K_{0.50}\quad Al_{1.37}\ Fe^{3+}_{0.43}\ Mg_{0.20}\ Ti_{0.00}\ (OH)_2\quad Si_{3.46}\ Al_{0.54}\ O_{10}$$

Charge: XII = 0.75 VI = 5.79 IV = 15.46 **Σ = 22.00**
Probability of smectite layers (%S): 24%
Probability of illite layers (%I): 76%

Measured particles: 55

Distribution of smectite layers probability (%S) in Cluster3

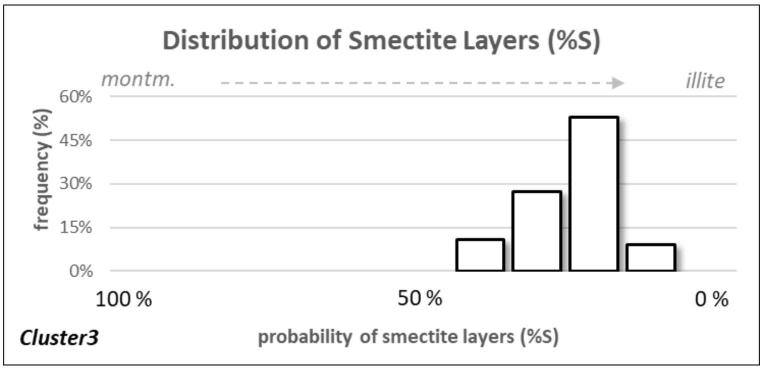

***Description:** The distribution of %S-probability indicates the occurrence of mixed layer phases with a %S mainly at 20%.*

***Fig. 15a.** Distribution of smectite layers probability (%S) in diVS-ml & IS-ml*

Cluster 3 ISS R0 + IS R0(2)	*particles (abs)*	Ca (XII)	Mg (XII)	Na (XII)	K (XII)	Cr3+ (VI)	Al (VI)	Fe3+ (VI)	Mg (VI)	Ti (VI)	Al (IV)	Si (IV)	XII	n_VI	%S
%S >95%	n = 0														
%S 95-85%	n = 0														
%S 85-75%	n = 0														
%S 75-65%	n = 0														
%S 65-55%	n = 0														
%S 55-45%	n = 0														
%S 45-35%	n = 6	0.07	0.03	0.00	0.47	0.00	1.35	0.43	0.20	0.00	0.41	3.59	0.7	2.0	38
%S 35-25%	n = 15	0.08	0.03	0.00	0.49	0.00	1.36	0.41	0.23	0.00	0.49	3.51	0.7	2.0	29
%S 25-15%	**n = 29**	**0.08**	**0.05**	**0.00**	**0.48**	**0.00**	**1.37**	**0.43**	**0.19**	**0.00**	**0.57**	**3.43**	**0.8**	**2.0**	**21**
%S <15%	n = 5	0.08	0.03	0.00	0.62	0.00	1.37	0.43	0.19	0.01	0.68	3.32	0.9	2.0	11

***Fig. 15b.** Computed averaged mineral formulae diVS- & IS-ml phases of Cluster3 in the different %S-classes*

Dioctahedral vermiculite-smectite mixed-layer series:
*(charge- and/or K-deficit; confirmed as Cluster2)**:***

$$Ca_{0.07}\ Mg_{0.13}\ Na_{0.00}\ K_{0.34}\quad Al_{1.51}\ Fe^{3+}_{0.39}\ Mg_{0.08}\ Ti_{0.02}\ (OH)_2\quad Si_{3.31}\ Al_{0.69}\ O_{10}$$

Charge: XII = 0.74 VI = 5.95 IV = 15.31 **Σ = 22.00**
Probability of smectite layers (%S): 10%
Probability of illite layers (%I): 90%

Measured particles: 29

Distribution of smectite layers probability (%S) in Cluster2 (diVS-ml)

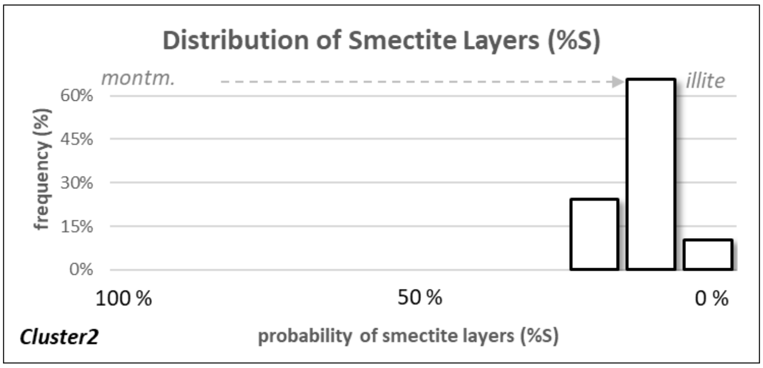

***Description:** The distribution of %S-probability indicates the occurrence of diVS-ml with %S mainly at 10%.*

***Fig. 16a.** Distribution of smectite layers probability (%S) in diVS-ml (Cluster2)*

Cluster 2 IS R0 (1)	*particles (abs)*	**Ca (XII)**	**Mg (XII)**	**Na (XII)**	**K (XII)**	**Cr3+ (VI)**	**Al (VI)**	**Fe3+ (VI)**	**Mg (VI)**	**Ti (VI)**	**Al (IV)**	**Si (IV)**	**XII**	**n_VI**	**%S**
%S >95%	n = 0														
%S 95-85%	n = 0														
%S 85-75%	n = 0														
%S 75-65%	n = 0														
%S 65-55%	n = 0														
%S 55-45%	n = 0														
%S 45-35%	n = 0														
%S 35-25%	n = 0														
%S 25-15%	n = 7	0.06	0.10	0.01	0.36	0.00	1.55	0.35	0.09	0.01	0.60	3.40	0.7	2.0	17
%S 15- 5%	**n = 19**	**0.08**	**0.13**	**0.00**	**0.34**	**0.00**	**1.49**	**0.41**	**0.09**	**0.01**	**0.69**	**3.31**	**0.8**	**2.0**	**10**
%S <5%	n = 3	0.06	0.18	0.00	0.27	0.00	1.55	0.41	0.00	0.07	0.88	3.12	0.7	2.0	0

***Fig. 16b.** Computed averaged mineral formulae diVS-ml phases of Cluster2 in the different %S-classes*

***Illite** (as end member of diVS-ml series; confirmed as Cluster1):*

$$Ca_{0.07}\ Mg_{0.24}\ Na_{0.00}\ K_{0.33}\quad Al_{1.14}\ Fe^{3+}_{0.75}\ Mg_{0.10}\ Ti_{0.01}\ (OH)_2\quad Si_{3.14}\ Al_{0.86}\ O_{10}$$

Charge: XII = 0.96 VI = 5.90 IV = 15.14 **Σ = 22.00**
Probability of smectite layers (%S): 0%
Probability of illite layers (%I): 100%

Measured particles: 7

Distribution of smectite layers probability (%S) in Cluster1

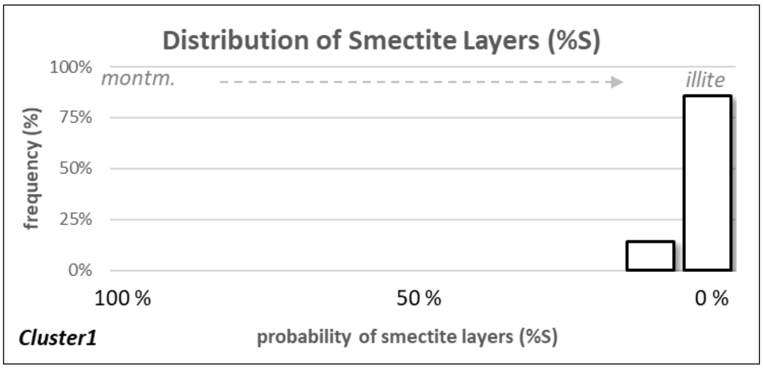

***Description:** The distribution of %S-probability indicates the occurrence of illite (%S mainly at 0%).*

***Fig. 17a.** Distribution of smectite layers probability (%S) in illite (Cluster1)*

Cluster 1 Illite	particles (abs)	Ca (XII)	Mg (XII)	Na (XII)	K (XII)	Cr3+ (VI)	Al (VI)	Fe3+ (VI)	Mg (VI)	Ti (VI)	Al (IV)	Si (IV)	XII	n_VI	%S
%S >95%	n = 0														
%S 95-85%	n = 0														
%S 85-75%	n = 0														
%S 75-65%	n = 0														
%S 65-55%	n = 0														
%S 55-45%	n = 0														
%S 45-35%	n = 0														
%S 35-25%	n = 0														
%S 25-15%	n = 0														
%S 15- 5%	n = 1	0.13	0.12	0.00	0.32	0.00	1.14	0.79	0.07	0.00	0.73	3.27	0.8	2.0	7
%S <5%	**n = 6**	**0.06**	**0.26**	**0.00**	**0.33**	**0.00**	**1.14**	**0.74**	**0.10**	**0.01**	**0.88**	**3.12**	**1.0**	**2.0**	**0**

Fig. 17b. *Computed averaged mineral formulae f illite (Cluster1) in the different %S-classes*

Mineral Matter – Specification

Result of Clustering & Comparison with XRD-data (Sybilla-processing)

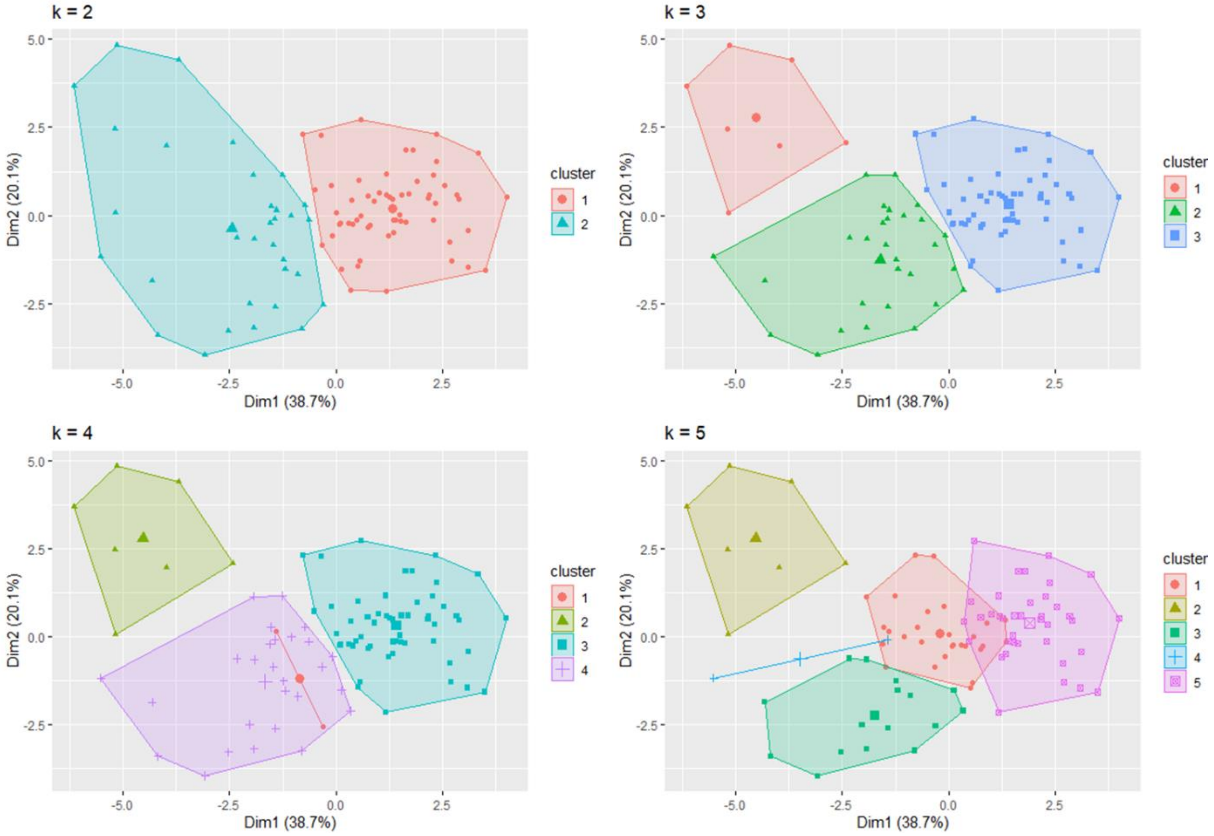

Fig. 18. *Clustering of all measured particles for clusters k = 2, k = 3, k = 4 and k = 5 (source for R-coding: https://uc-r.github.io/kmeans_clustering)*

The optimum of clusters was calculated with k = 3. This number of clusters differentiates also clearly illite particles (Cluster1) from smectite-bearing phases (Cluster2, Cluster3).

k=3		Ca (XII)	Mg (XII)	Na (XII)	K (XII)	Cr3+ (VI)	Al (VI)	Fe3+ (VI)	Mg (VI)	Ti (VI)	Al (IV)	Si (IV)	XII	n_VI	%S
Cluster1	n = 7	0.07	0.24	0.00	0.33	0.00	1.14	0.75	0.10	0.01	0.86	3.14	0.94	2.0	0
Cluster2	n = 29	0.07	0.13	0.00	0.34	0.00	1.51	0.39	0.08	0.02	0.69	3.31	0.74	2.0	10
Cluster3	n = 55	0.08	0.04	0.00	0.50	0.00	1.37	0.43	0.20	0.00	0.54	3.46	0.75	2.0	24

Fig. 19. *Mineral formulae based on TEM-EDX-data summarized following the result of clustering for k=3*

	Sybilla-modelling of XRD-results	TEM-EDX-results	Notes

Cluster1	Illite	Illite	*high K-deficit, Fe(VI)-rich*
Cluster2	IS R0 *(%S = 9%)*	diVS-ml *(%S = 10%)*	*high K-deficit, Al(VI)-rich, low Mg(VI)*
Cluster3	ISS R0 *(%S = 28%)* + IS R0 *(%S = 32%)*	diVS-ml + IS-ml *(%S = 24%)*	*K-deficit, Fe(VI)- & Mg(VI)-rich*

Tab. 4. *Comparison of results from TEM-EDX- and XRD-measurements with clustering procedure*

Sample - Opalinus (< 2 µm), treated H_2O - 60 rpm

Preparation for TEM

- raw material: < 40 µm powder of Opalinus-sample, treated by H_2O at 60 rpm for 30 days
- suspension on particles < 2 µm on carbon-filmed Cu-grid
- air-dried and humidity-controlled storing

Mineral Matter

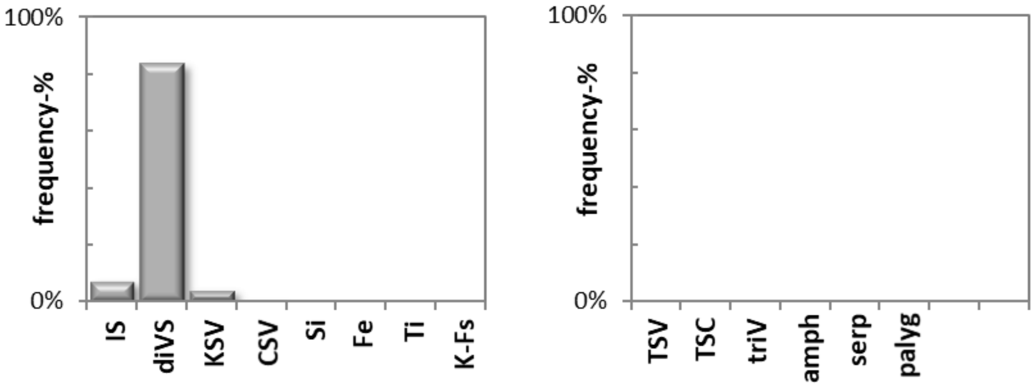

Fig. 20. *Distribution of mineral groups in fraction < 2 µm (in frequency-%)*
Legend: ***IS*** *– illite-smectite-mixed layer series in sense of Środon et al. (1992), diVS – dioctahedral vermiculite-smectite illite-smectite-mixed layer series (= charge- and/or K-deficit),* ***KSV*** *– kaolinite-smectite-dioctahedral vermiculite-mixed layer series,* ***CSV*** *– chlorite-saponite-trioctahedral vermiculite-mixed layer series,* ***Si*** *– quartz or particles with Si-surplus,* ***Fe*** *– Fe-oxide or Fe-oxyhydroxide,* ***Ti*** *– Ti-bearing phases (e.g. rutile, anatase),* ***K-Fs*** *– K-feldspar*

Clay Mineral Composition

Illite-smectite mixed-layer series (summarized: IS + diVS):

$$Ca_{0.10}\,Mg_{0.07}\,Na_{0.01}\,K_{0.44}\quad Al_{1.39}\,Fe^{3+}_{0.43}\,Mg_{0.18}\,Ti_{0.00}\,(OH)_2\quad Si_{3.39}\,Al_{0.61}\,O_{10}$$

Charge: XII = 0.78 VI = 5.83 IV = 15.39 **Σ = 22.00**
Probability of smectite layers (%S): 17%
Probability of illite layers (%I): 83%
CEC_{calc}: 67 meq / 100 g

Measured particles: 127

Table 5. *Summarized chemical composition*

SiO_2	TiO_2	Al_2O_3	Fe_2O_3	MnO	MgO	CaO	Na_2O	K_2O	P_2O_5	Σ	
51.1%	0.0%	26.6%	4.4%		2.9%	1.8%	0.1%	3.7%	0.0%	0.90	measured particles
52.7%	0.1%	26.1%	4.3%		2.7%	1.3%	0.0%	3.4%	0.3%	0.91	Opalinus, original

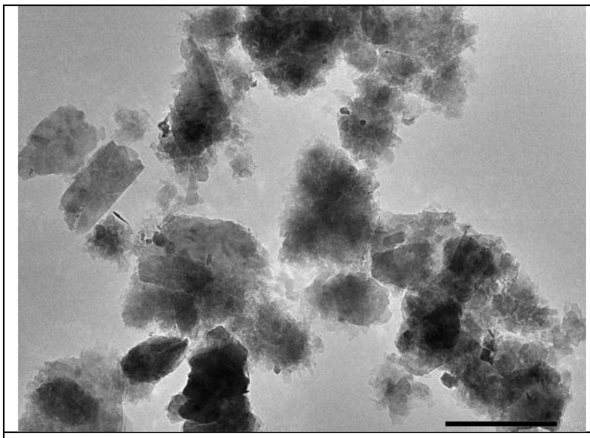	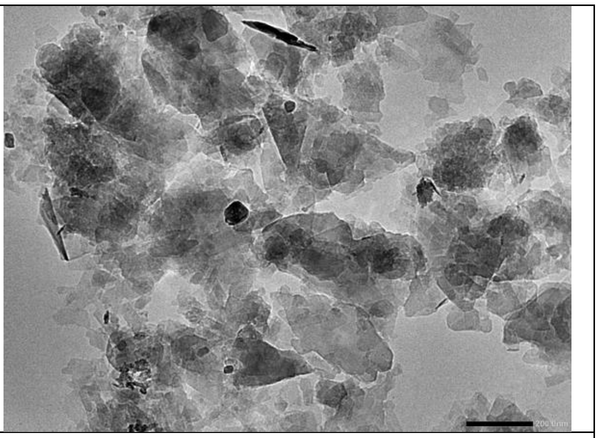
JEM-2100_MAG_X10k_Opalinus-60r-H2O_I12.bmp Magnification: 10k	*JEM-2100_MAG_X30k_Opalinus-60r-H2O_I04.bmp* Magnification: 30k
Mixture of xenomorphic plates (length + 1 µm) *[= diVS-ml and IS-ml with %S < 10%?]* and aggregates composed by slat-shaped crystals *[= diVS-ml with %S-range 10-20%]*	aggregates composed mainly by slat-shaped crystals (length ~ 200 nm) with hypidiomorphic ends, commonly hexagonal intergrowths *(mainly diVS-ml with %S-range 20-30%)*

Fig. 21. *Morphology of particles (TEM-micrographs)*

Distribution of smectite layers probability (%S)

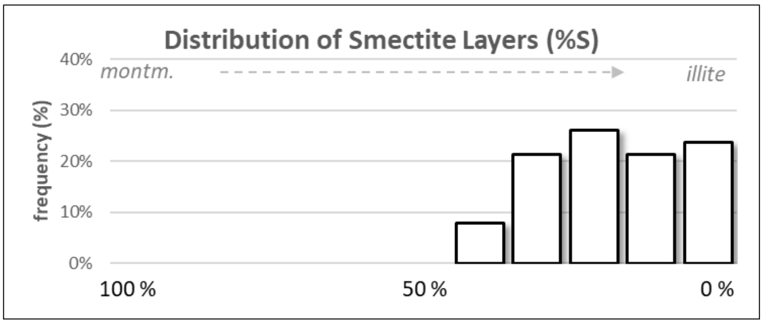

Description: *The distribution of %S-probability indicates two groups: (i) the occurrence of diVS-ml + IS-ml with %S mainly at 20% and (ii) illite with K- & charge-deficit.*

Fig. 22. *Distribution of smectite layers probability (%S)*

Distribution of charges (exchangeable from interlayer space)

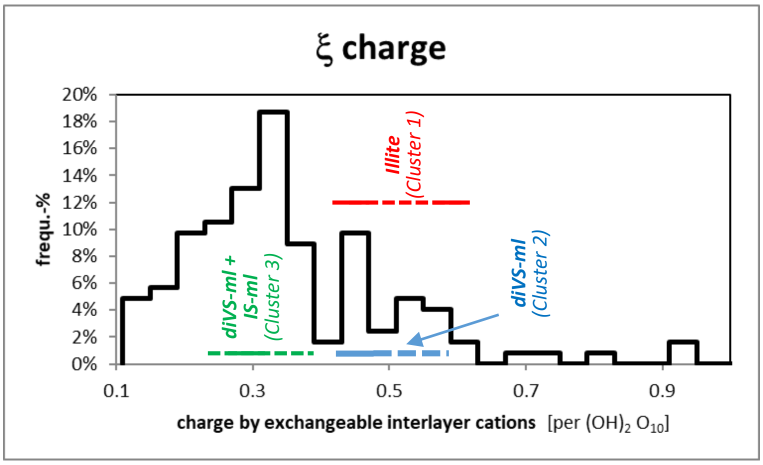

This diagram visualizes the distribution of exchangeable charges in the interlayer space (Ca, Mg, Na) determined and computed by TEM-EDX-data.

Description: *The charge density indicates a broad distribution of exchangeable interlayer cations with a maximum at 0.33 per* $(OH)_2$ O_{10}.

Fig. 23. *Distribution of charges*

Dioctahedral vermiculite-smectite mixed-layer series *(mixed with IS-ml)****:***
*(diVS-ml with charge- and/or K-deficit; group confirmed as Cluster3)****:***

$$Ca_{0.09}\ Mg_{0.05}\ Na_{0.00}\ K_{0.48}\quad Al_{1.39}\ Fe^{3+}_{0.41}\ Mg_{0.21}\ Ti_{0.00}\ (OH)_2\quad Si_{3.45}\ Al_{0.55}\ O_{10}$$

Charge: XII = 0.76 VI = 5.79 IV = 15.45 **Σ = 22.00**
Probability of smectite layers (%S): 24%
Probability of illite layers (%I): 76%

Measured particles: 55

Distribution of smectite layers probability (%S) in diVS-ml

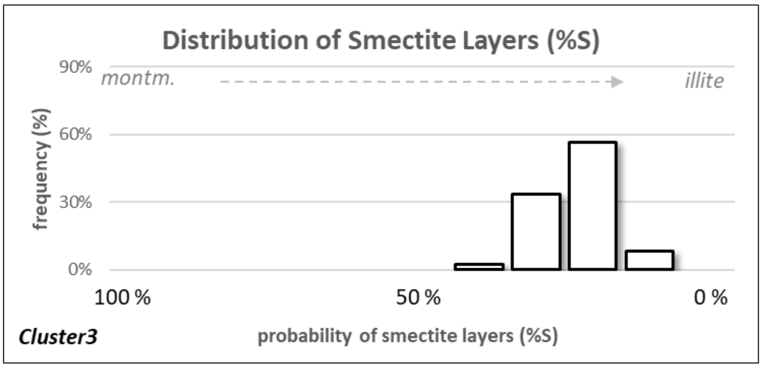

Description: *The distribution of %S-probability indicates the occurrence of mixed layer phases with a %S mainly at 20%.*

Fig. 24a. *Distribution of smectite layers probability (%S) in diVS-ml & IS-ml*

Cluster 3 ISS+IS R0(2)	*particles (abs)*	Ca (XII)	Mg (XII)	Na (XII)	K (XII)	Cr3+ (VI)	Al (VI)	Fe3+ (VI)	Mg (VI)	Ti (VI)	Al (IV)	Si (IV)	XII	n_VI	%S
%S >95%	n = 0														
%S 95-85%	n = 0														
%S 85-75%	n = 0														
%S 75-65%	n = 0														
%S 65-55%	n = 0														
%S 55-45%	n = 0														
%S 45-35%	n = 2	0.17	0.02	0.00	0.30	0.00	1.38	0.37	0.25	0.00	0.43	3.57	0.7	2.0	36
%S 35-25%	n = 29	0.09	0.03	0.01	0.50	0.00	1.36	0.39	0.24	0.00	0.49	3.51	0.7	2.0	30
%S 25-15%	**n = 49**	**0.09**	**0.06**	**0.00**	**0.47**	**0.00**	**1.38**	**0.43**	**0.19**	**0.00**	**0.58**	**3.42**	**0.8**	**2.0**	**20**
%S 15- 5%	n = 7	0.10	0.05	0.00	0.50	0.00	1.54	0.31	0.15	0.00	0.65	3.35	0.8	2.0	13
%S <5%	n = 0														

Fig. 24b. *Computed averaged mineral formulae diVS- & IS-ml phases of Cluster3 in the different %S-classes*

Dioctahedral vermiculite-smectite mixed-layer series:
*(charge- and/or K-deficit; confirmed as Cluster2)****:***

$$Ca_{0.14}\ Mg_{0.09}\ Na_{0.03}\ K_{0.43}\quad Al_{1.17}\ Fe^{3+}_{0.63}\ Mg_{0.20}\ Ti_{0.00}\ (OH)_2\quad Si_{3.29}\ Al_{0.71}\ O_{10}$$

Charge: XII = 0.90 VI = 5.81 IV = 15.29 **Σ = 22.00**
Probability of smectite layers (%S): 8%
Probability of illite layers (%I): 92%

Measured particles: 19

Distribution of smectite layers probability (%S) in Cluster2 (diVS-ml)

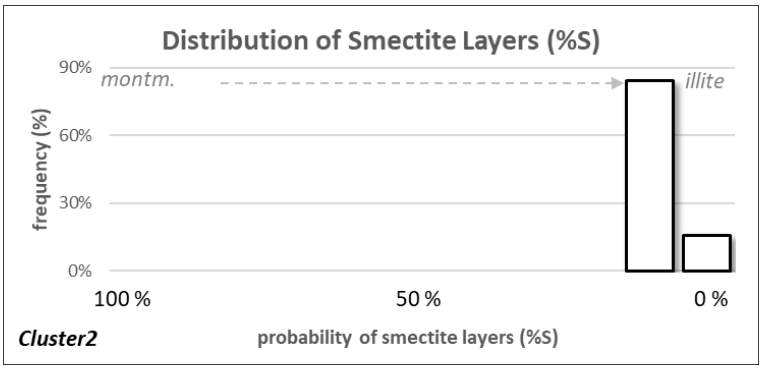

Description: *The distribution of %S-probability indicates the occurrence of diVS-ml with %S mainly at 10%.*

Fig. 25a. *Distribution of smectite layers probability (%S) in diVS-ml (Cluster2)*

Cluster 2 IS R0 (1)	*particles (abs)*	Ca (XII)	Mg (XII)	Na (XII)	K (XII)	Cr3+ (VI)	Al (VI)	Fe3+ (VI)	Mg (VI)	Ti (VI)	Al (IV)	Si (IV)	XII	n_VI	%S
%S >95%	n = 0														
%S 95-85%	n = 0														
%S 85-75%	n = 0														
%S 75-65%	n = 0														
%S 65-55%	n = 0														
%S 55-45%	n = 0														
%S 45-35%	n = 0														
%S 35-25%	n = 0														
%S 25-15%	n = 0														
%S 15- 5%	**n = 16**	**0.14**	**0.08**	**0.02**	**0.45**	**0.00**	**1.16**	**0.63**	**0.21**	**0.00**	**0.69**	**3.31**	**0.9**	**2.0**	**10**
%S <5%	n = 3	0.12	0.17	0.05	0.34	0.00	1.22	0.65	0.13	0.00	0.84	3.16	1.0	2.0	1

Fig. 25b. *Computed averaged mineral formulae diVS-ml phases of Cluster2 in the different %S-classes*

Illite *(as end member of diVS-ml series; confirmed as Cluster1):*

$$Ca_{0.09}\ Mg_{0.15}\ Na_{0.01}\ K_{0.26}\quad Al_{1.63}\ Fe^{3+}_{0.34}\ Mg_{0.04}\ Ti_{0.01}\ (OH)_2\quad Si_{3.23}\ Al_{0.77}\ O_{10}$$

Charge: XII = 0.74 VI = 6.03 IV = 15.23 **Σ = 22.00**
Probability of smectite layers (%S): 5%
Probability of illite layers (%I): 95%

Measured particles: 18

Distribution of smectite layers probability (%S) in Cluster1

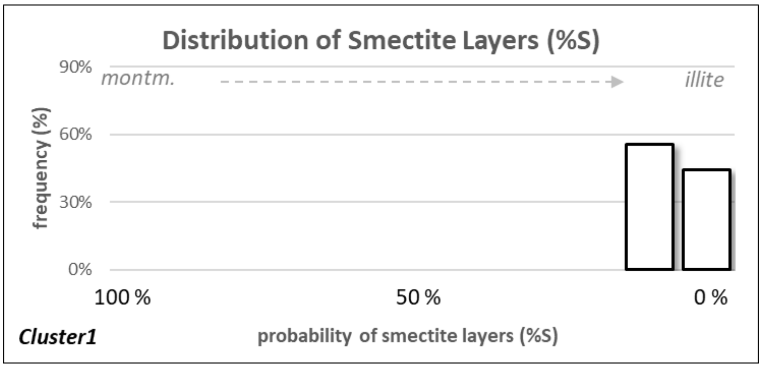

Description: *The distribution of %S-probability indicates the occurrence of illite (%S mainly at 0%).*

Fig. 26a. *Distribution of smectite layers probability (%S) in illite (Cluster1)*

Cluster 1 Illite	*particles (abs)*	**Ca** (XII)	**Mg** (XII)	**Na** (XII)	**K** (XII)	**Cr3+** (VI)	**Al** (VI)	**Fe3+** (VI)	**Mg** (VI)	**Ti** (VI)	**Al** (IV)	**Si** (IV)	**XII**	**n_VI**	**%S**
%S >95%	n = 0														
%S 95-85%	n = 0														
%S 85-75%	n = 0														
%S 75-65%	n = 0														
%S 65-55%	n = 0														
%S 55-45%	n = 0														
%S 45-35%	n = 0														
%S 35-25%	n = 0														
%S 25-15%	n = 0														
%S 15- 5%	**n = 10**	**0.05**	**0.14**	**0.00**	**0.30**	**0.00**	**1.63**	**0.33**	**0.04**	**0.01**	**0.70**	**3.30**	**0.7**	**2.0**	**10**
%S <5%	n = 8	0.14	0.17	0.02	0.20	0.00	1.63	0.34	0.03	0.02	0.86	3.14	0.8	2.0	1

Fig. 26b. *Computed averaged mineral formulae f illite (Cluster1) in the different %S-classes*

Mineral Matter – Specification

Result of Clustering & Comparison with XRD-data (Sybilla-processing)

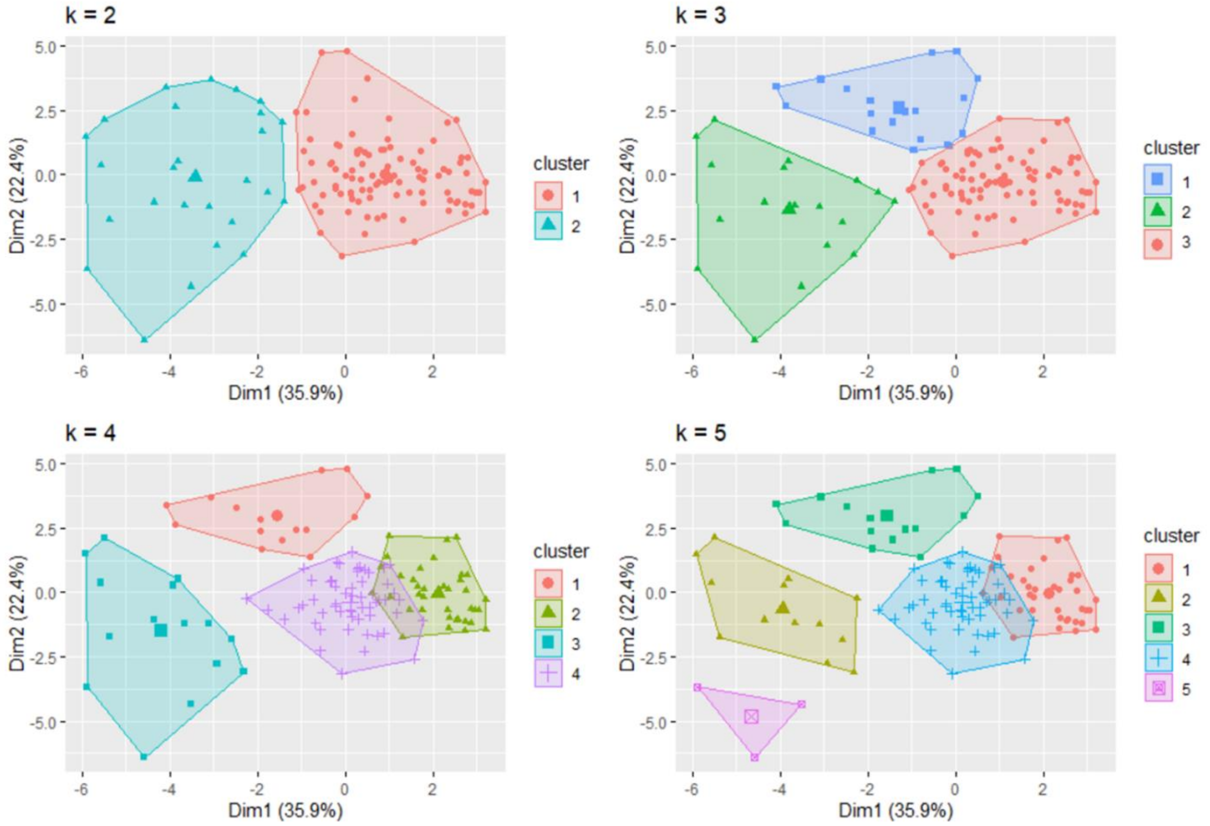

Fig. 27. *Clustering of all measured particles for clusters k = 2, k = 3, k = 4 and k = 5 (source for R-coding: https://uc-r.github.io/kmeans_clustering)*

The optimum of clusters was calculated with k = 3. This number of clusters differentiates also clearly illite particles (Cluster1) from smectite-bearing phases (Cluster2, Cluster3).

k=3		**Ca** (XII)	**Mg** (XII)	**Na** (XII)	**K** (XII)	**Cr3+** (VI)	**Al** (VI)	**Fe3+** (VI)	**Mg** (VI)	**Ti** (VI)	**Al** (IV)	**Si** (IV)	**XII**	**n_VI**	**%S**
Cluster1	n = 18	0.09	0.15	0.01	0.26	0.00	1.63	0.34	0.04	0.01	0.77	3.23	0.7	2.0	5
Cluster2	n = 19	0.14	0.09	0.03	0.43	0.00	1.17	0.63	0.20	0.00	0.71	3.29	0.9	2.0	8
Cluster3	n = 87	0.09	0.05	0.00	0.48	0.00	1.39	0.41	0.21	0.00	0.55	3.45	0.8	2.0	23

Fig. 28. *Mineral formulae based on TEM-EDX-data summarized following the result of clustering for k=3*

Sample - Opalinus (< 2 µm), treated NaCl - 20 rpm

Preparation for TEM

- raw material: < 40 µm powder of Opalinus-sample, treated by 1 m NaCl-solution at 20 rpm for 30 d
- suspension on particles < 2 µm on carbon-filmed Cu-grid
- air-dried and humidity-controlled storing

Mineral Matter

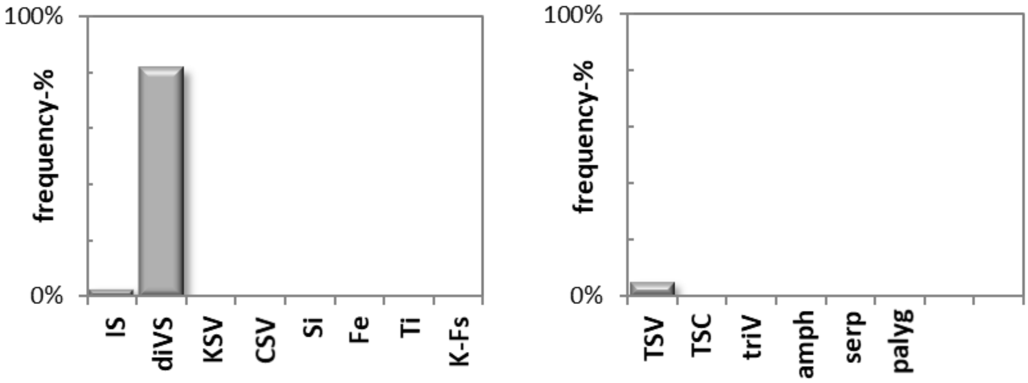

Fig. 29. *Distribution of mineral groups in fraction < 2 µm (in frequency-%)*
Legend: ***IS*** *– illite-smectite-mixed layer series in sense of Środon et al. (1992), diVS – dioctahedral vermiculite-smectite illite-smectite-mixed layer series (= charge- and/or K-deficit),* ***KSV*** *– kaolinite-smectite-dioctahedral vermiculite-mixed layer series,* ***CSV*** *– chlorite-saponite-trioctahedral vermiculite-mixed layer series,* ***Si*** *– quartz or particles with Si-surplus,* ***Fe*** *– Fe-oxide or Fe-oxyhydroxide,* ***Ti*** *– Ti-bearing phases (e.g. rutile, anatase),* ***K-Fs*** *– K-feldspar, TSV – talc-saponite-trioctahedral vermiculite-mixed layer series*

Clay Mineral Composition

Illite-smectite mixed-layer series (summarized: IS + diVS):

$$Ca_{0.11}\ Mg_{0.08}\ Na_{0.00}\ K_{0.43}\quad Al_{1.42}\ Fe^{3+}_{0.42}\ Mg_{0.15}\ Ti_{0.00}\ (OH)_2\ \ Si_{3.33}\ Al_{0.67}\ O_{10}$$

Charge: XII = 0.81 VI = 5.86 IV = 15.33 **Σ = 22.00**
Probability of smectite layers (%S): 12%
Probability of illite layers (%I): 88%
CEC_{calc}: 52 meq / 100 g

Measured particles: 87

Table 7. *Summarized chemical composition*

SiO_2	TiO_2	Al_2O_3	Fe_2O_3	MnO	MgO	CaO	Na_2O	K_2O	P_2O_5	Σ	
50.0%	0.0%	27.8%	4.3%		2.7%	1.2%	0.0%	3.6%	0.0%	0.90	measured particles
52.7%	0.1%	26.1%	4.3%		2.7%	1.3%	0.0%	3.4%	0.3%	0.91	Opalinus, original

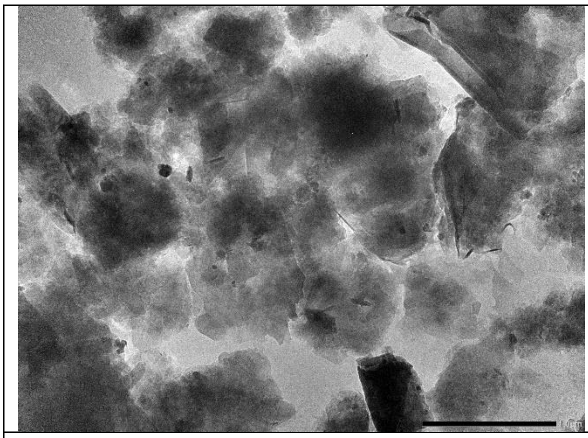	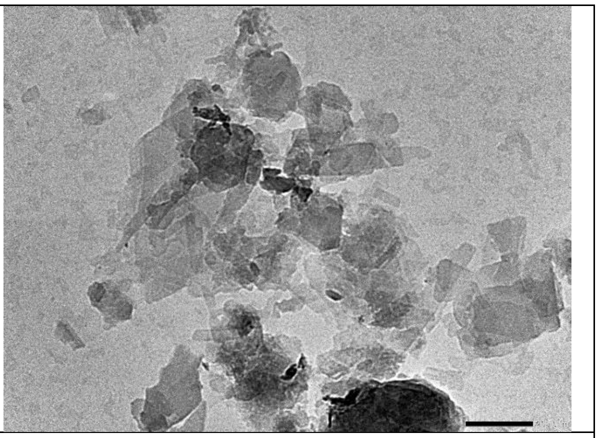
JEM-2100_MAG_X12k_Opalinus-NaCl-20r_013.bmp Magnification: 12k	*JEM-2100_MAG_X30k_Opalinus-NaCl-20r_002.bmp* Magnification: 30k
Xenomorphic platy crystals (length ~ 1 µm) with folds at margins *[IS-ml with %S ~20%]* and smaller xenomorphic platy crystals (length << 1 µm) *[= diVS-ml with %S < 10%]*	Xenomorphic plates and slat-shaped crystals (length ~ 200 nm) with hypidiomorphic ends *(diVS-ml mainly with %S < 15%)*

Fig. 30. *Morphology of particles (TEM-micrographs)*

Distribution of smectite layers probability (%S)

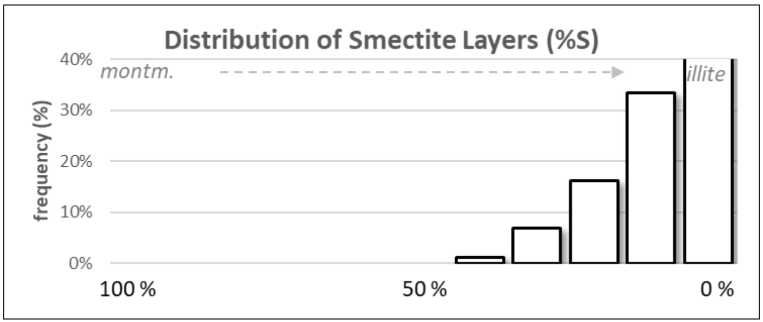

Description: *The distribution of %S-probability indicates two groups: (i) the occurrence of diVS-ml + IS-ml with %S mainly at 10% and (ii) illite with K- & charge-deficit.*

Fig. 31. *Distribution of smectite layers probability (%S)*

Distribution of charges (exchangeable from interlayer space)

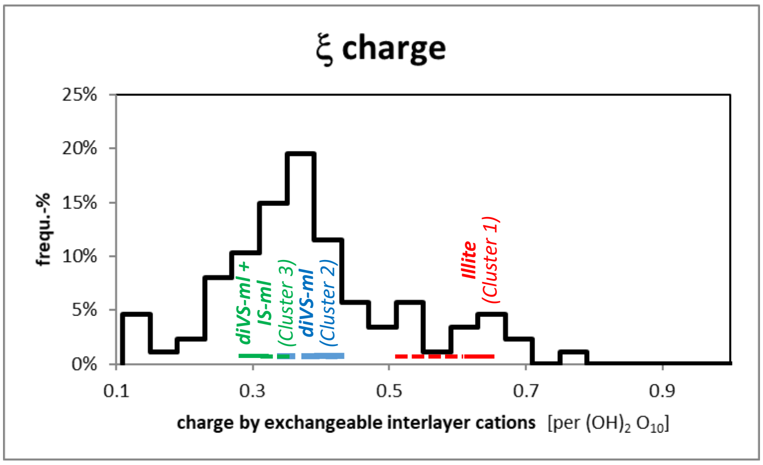

This diagram visualizes the distribution of exchangeable charges in the interlayer space (Ca, Mg, Na) determined and computed by TEM-EDX-data.

Description: *The charge density indicates a broad distribution of exchangeable interlayer cations at 0.37 (by illite with K-deficit?) and at 0.65 (diVS-ml) per $(OH)_2$ O_{10}.*

Fig. 32. *Distribution of charges*

***Dioctahedral vermiculite-smectite mixed-layer series** (mixed with IS-ml):*
(diVS-ml with charge- and/or K-deficit; group confirmed as Cluster3):

$$Ca_{0.11}\ Mg_{0.04}\ Na_{0.00}\ K_{0.49}\quad Al_{1.37}\ Fe^{3+}_{0.43}\ Mg_{0.20}\ Ti_{0.00}\ (OH)_2\quad Si_{3.40}\ Al_{0.60}\ O_{10}$$

Charge: XII = 0.80 VI = 5.80 IV = 15.40 **Σ = 22.00**
Probability of smectite layers (%S): 18%
Probability of illite layers (%I): 82%

Measured particles: 47

Distribution of smectite layers probability (%S) in diVS-ml

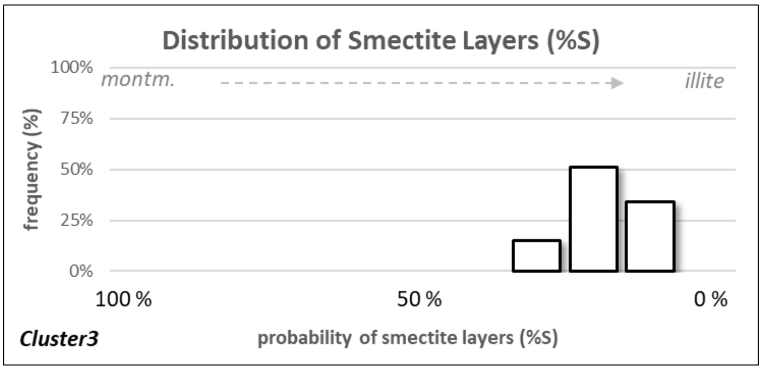

***Description:** The distribution of %S-probability indicates the occurrence of mixed layer phases with a %S mainly at 20%.*

***Fig. 33a.** Distribution of smectite layers probability (%S) in diVS-ml & IS-ml*

Cluster 3 ISS+IS R0(2)	particles (abs)	Ca (XII)	Mg (XII)	Na (XII)	K (XII)	Cr3+ (VI)	Al (VI)	Fe3+ (VI)	Mg (VI)	Ti (VI)	Al (IV)	Si (IV)	XII	n_VI	%S
%S >95%	n = 0														
%S 95-85%	n = 0														
%S 85-75%	n = 0														
%S 75-65%	n = 0														
%S 65-55%	n = 0														
%S 55-45%	n = 0														
%S 45-35%	n = 0														
%S 35-25%	n = 7	0.14	0.03	0.00	0.44	0.00	1.32	0.43	0.25	0.00	0.50	3.50	0.8	2.0	28
%S 25-15%	**n = 24**	**0.11**	**0.04**	**0.00**	**0.50**	**0.00**	**1.40**	**0.39**	**0.20**	**0.00**	**0.59**	**3.41**	**0.8**	**2.0**	**19**
%S 15- 5%	n = 16	0.11	0.06	0.00	0.50	0.00	1.33	0.48	0.18	0.00	0.66	3.34	0.8	2.0	13
%S <5%	n = 0														

***Fig. 33b.** Computed averaged mineral formulae diVS- & IS-ml phases of Cluster3 in the different %S-classes*

Dioctahedral vermiculite-smectite mixed-layer series:
(charge- and/or K-deficit; confirmed as Cluster2):

$$Ca_{0.12}\ Mg_{0.08}\ Na_{0.00}\ K_{0.37}\quad Al_{1.56}\ Fe^{3+}_{0.35}\ Mg_{0.09}\ Ti_{0.00}\ (OH)_2\quad Si_{3.29}\ Al_{0.71}\ O_{10}$$

Charge: XII = 0.78 VI = 5.93 IV = 15.29 **Σ = 22.00**
Probability of smectite layers (%S): 9%
Probability of illite layers (%I): 91%

Measured particles: 29

Distribution of smectite layers probability (%S) in Cluster2 (diVS-ml)

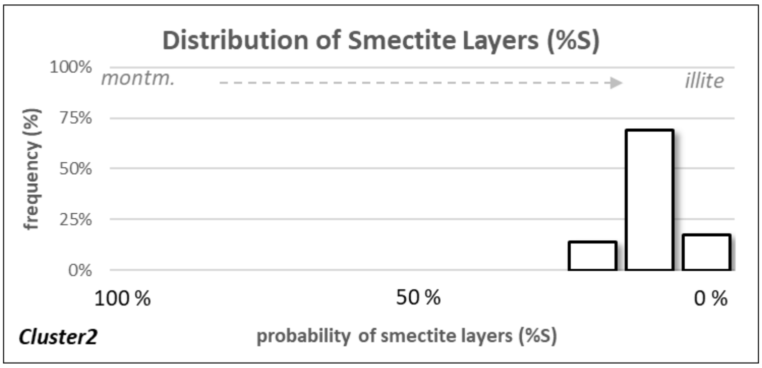

Description: *The distribution of %S-probability indicates the occurrence of diVS-ml with %S mainly at 10%.*

Fig. 34a. *Distribution of smectite layers probability (%S) in diVS-ml (Cluster2)*

Cluster 2 IS R0 (1)	*particles (abs)*	Ca (XII)	Mg (XII)	Na (XII)	K (XII)	Cr3+ (VI)	Al (VI)	Fe3+ (VI)	Mg (VI)	Ti (VI)	Al (IV)	Si (IV)	XII	n_VI	%S
%S >95%	n = 0														
%S 95-85%	n = 0														
%S 85-75%	n = 0														
%S 75-65%	n = 0														
%S 65-55%	n = 0														
%S 55-45%	n = 0														
%S 45-35%	n = 0														
%S 35-25%	n = 0														
%S 25-15%	n = 4	0.09	0.07	0.02	0.38	0.00	1.63	0.27	0.10	0.00	0.62	3.38	0.7	2.0	16
%S 15- 5%	**n = 20**	**0.13**	**0.08**	**0.00**	**0.38**	**0.00**	**1.53**	**0.37**	**0.10**	**0.00**	**0.70**	**3.30**	**0.8**	**2.0**	**9**
%S <5%	n = 5	0.12	0.10	0.00	0.31	0.00	1.63	0.32	0.05	0.00	0.81	3.19	0.7	2.0	3

Fig. 34b. *Computed averaged mineral formulae diVS-ml phases of Cluster2 in the different %S-classes*

Illite *(as end member of diVS-ml series; confirmed as Cluster1):*

$$\mathrm{Ca_{0.09}\,Mg_{0.21}\,Na_{0.00}\,K_{0.32}\quad Al_{1.30}\,Fe^{3+}_{0.60}\,Mg_{0.10}\,Ti_{0.01}\,(OH)_2\quad Si_{3.15}\,Al_{0.85}\,O_{10}}$$

Charge: XII = 0.92 VI = 5.93 IV = 15.15 **Σ = 22.00**

Probability of smectite layers (%S): 1%

Probability of illite layers (%I): 99%

Measured particles: 11

Distribution of smectite layers probability (%S) in Cluster1

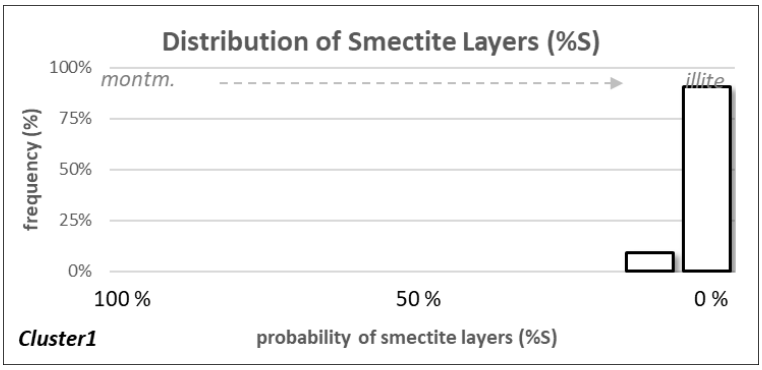

Description: *The distribution of %S-probability indicates the occurrence of illite (%S mainly at 0%).*

Fig. 35a. *Distribution of smectite layers probability (%S) in illite (Cluster1)*

Cluster 1 Illite	particles (abs)	Ca (XII)	Mg (XII)	Na (XII)	K (XII)	Cr3+ (VI)	Al (VI)	Fe3+ (VI)	Mg (VI)	Ti (VI)	Al (IV)	Si (IV)	XII	n_VI	%S
%S >95%	n = 0														
%S 95-85%	n = 0														
%S 85-75%	n = 0														
%S 75-65%	n = 0														
%S 65-55%	n = 0														
%S 55-45%	n = 0														
%S 45-35%	n = 0														
%S 35-25%	n = 0														
%S 25-15%	n = 0														
%S 15- 5%	n = 1	0.16	0.11	0.00	0.40	0.00	1.25	0.56	0.19	0.00	0.74	3.26	0.9	2.0	6
%S <5%	**n = 10**	**0.09**	**0.22**	**0.00**	**0.31**	**0.00**	**1.30**	**0.60**	**0.09**	**0.01**	**0.87**	**3.13**	**0.9**	**2.0**	**0**

Fig. 35b. *Computed averaged mineral formulae f illite (Cluster1) in the different %S-classes*

Talc-saponite-trioctahedral vermiculite mixed-layer series (TSV-ml):

$$Ca_{0.13}\ Mg_{0.01}\ Na_{0.00}\ K_{0.32}\quad Al_{0.77}\ Fe^{2+}_{1.50}\ Mg_{0.48}\ Ti_{0.05}\ (OH)_2\ \ Si_{2.92}\ Al_{1.08}\ O_{10}$$

Charge: XII = 0.60 VI = 6.47 IV = 14.92 **Σ = 22.00**

Probability of talc layers (%T): 4% *min – max: 5 … 10%*

Probability of saponite layers (%S): 61% *min – max: 14 … 97%*

Probability of trioct. vermiculite layers (%V): 35% *min – max: 1 … 86%*

Measured particles: 5

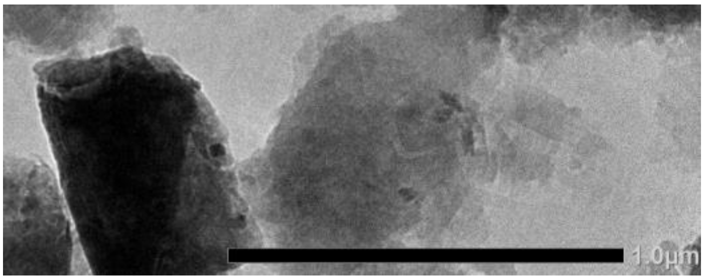

Zoom from
JEM-2100_MAG_X12k_Opalinus-NaCl-20r_013.bmp

Left: xenomorphic plate computed as TSV-ml with %T:%S:%V = 10:75:15

Fig. 36. *Morphology of particles (TEM-micrographs)*

Mineral Matter – Specification

Result of Clustering & Comparison with XRD-data (Sybilla-processing)

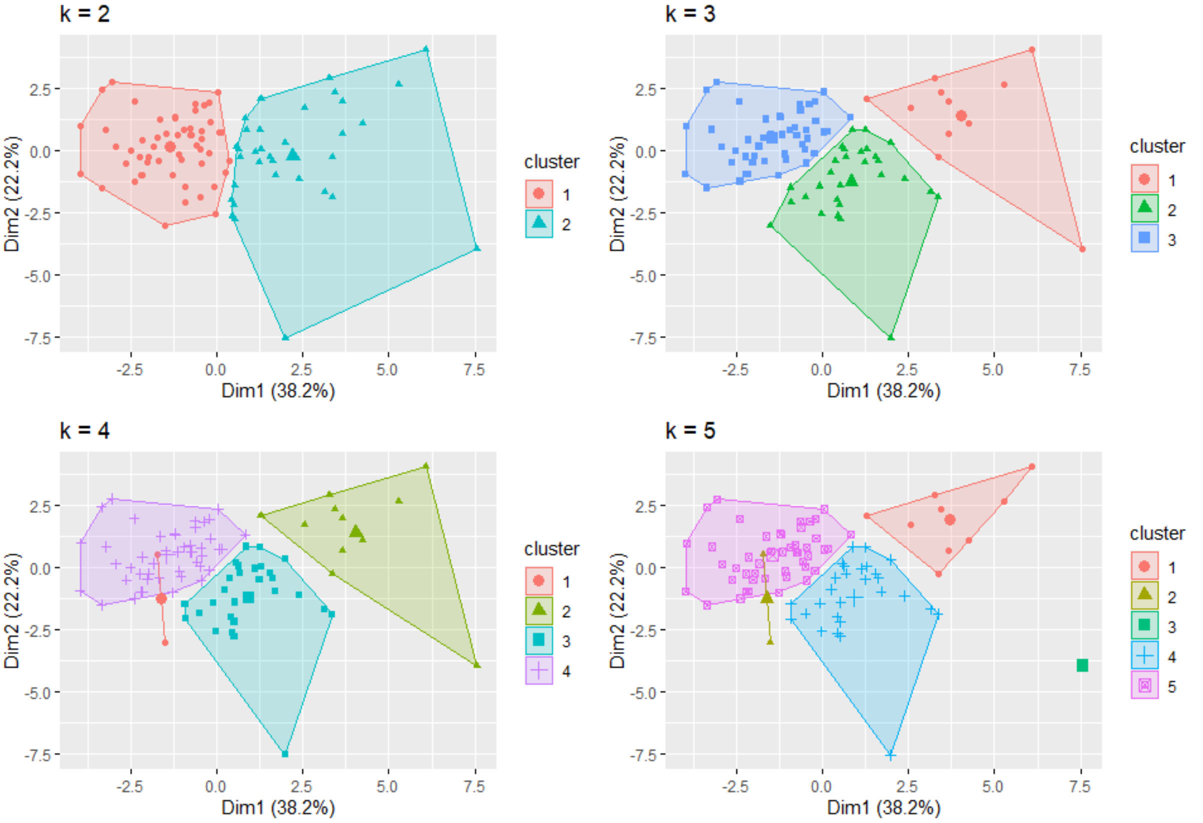

Fig. 37. *Clustering of all measured particles for clusters k = 2, k = 3, k = 4 and k = 5 (source for R-coding: https://uc-r.github.io/kmeans_clustering)*

The optimum of clusters was calculated with k = 3. This number of clusters differentiates also clearly illite particles (Cluster1) from smectite-bearing phases (Cluster2, Cluster3).

		Ca (XII)	Mg (XII)	Na (XII)	K (XII)	Cr3+ (VI)	Al (VI)	Fe3+ (VI)	Mg (VI)	Ti (VI)	Al (IV)	Si (IV)	XII	n_VI	%S
Cluster1	n = 11	0.09	0.21	0.00	0.32	0.00	1.30	0.60	0.10	0.01	0.85	3.15	0.93	2.0	1
Cluster2	n = 29	0.12	0.08	0.00	0.37	0.00	1.56	0.35	0.09	0.00	0.71	3.29	0.78	2.0	9
Cluster3	n = 47	0.11	0.04	0.00	0.49	0.00	1.37	0.43	0.20	0.00	0.60	3.40	0.80	2.0	18

Fig. 38. *Mineral formulae based on TEM-EDX-data summarized following the result of clustering for k=3*

	Sybilla-modelling of XRD-results	**TEM-EDX-results**	**Notes**
Cluster1	Illite	Illite	*high K-deficit, Fe(VI)-rich, low Mg(VI)*
Cluster2	IS R0 *(%S = 9%)*	diVS-ml *(%S = 9%)*	*high K-deficit, Al(VI)-rich, low Mg(VI)*
Cluster3		diVS-ml + IS-ml *(%S = 18%)*	*K-deficit, Fe(VI)- & Mg(VI)-rich*

Tab. 8. *Comparison of results from TEM-EDX- and XRD-measurements with clustering procedure*

Sample – Opalinus (< 2 µm), treated NaCl – 60 rpm

Preparation for TEM

- raw material: < 40 µm powder of Opalinus-sample, treated by 1 m NaCl-solution at 60 rpm for 30 d
- suspension on particles < 2 µm on carbon-filmed Cu-grid
- air-dried and humidity-controlled storing

Mineral Matter

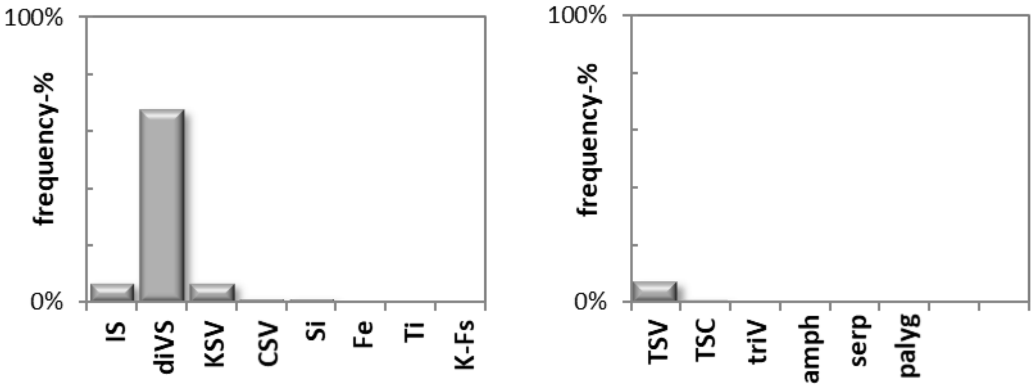

Fig. 39. *Distribution of mineral groups in fraction < 2 µm (in frequency-%)*
Legend: ***IS*** *– illite-smectite-mixed layer series in sense of Środon et al. (1992), diVS – dioctahedral vermiculite-smectite illite-smectite-mixed layer series (= charge- and/or K-deficit),* ***KSV*** *– kaolinite-smectite-dioctahedral vermiculite-mixed layer series,* ***CSV*** *– chlorite-saponite-trioctahedral vermiculite-mixed layer series,* ***Si*** *– quartz or particles with Si-surplus,* ***Fe*** *– Fe-oxide or Fe-oxyhydroxide,* ***Ti*** *– Ti-bearing phases (e.g. rutile, anatase),* ***K-Fs*** *– K-feldspar,* ***TSV*** *– talc-saponite-trioctahedral vermiculite-mixed layer series*

Clay Mineral Composition

Illite-smectite mixed-layer series (summarized: IS + diVS):

$$Ca_{0.06}\ Mg_{0.09}\ Na_{0.00}\ K_{0.45}\quad Al_{1.42}\ Fe^{3+}_{0.43}\ Mg_{0.14}\ Ti_{0.01}\ (OH)_2\quad Si_{3.35}\ Al_{0.65}\ O_{10}$$

Charge: XII = 0.77 VI = 5.88 IV = 15.35 **Σ = 22.00**
Probability of smectite layers (%S): 14%
Probability of illite layers (%I): 86%
CEC_{calc}: 40 meq / 100 g

Measured particles: 95

Table 9. *Summarized chemical composition*

SiO_2	TiO_2	Al_2O_3	Fe_2O_3	MnO	MgO	CaO	Na_2O	K_2O	P_2O_5	Σ	
51.8%	0.1%	28.2%	4.5%		2.8%	0.7%	0.0%	3.9%	0.1%	0.92	measured particles
52.7%	0.1%	26.1%	4.3%		2.7%	1.3%	0.0%	3.4%	0.3%	0.91	Opalinus, original

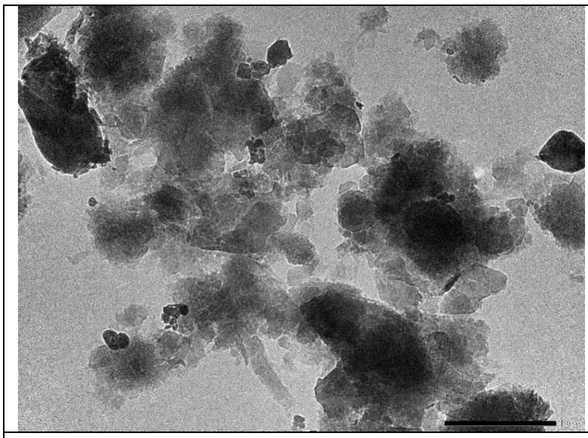	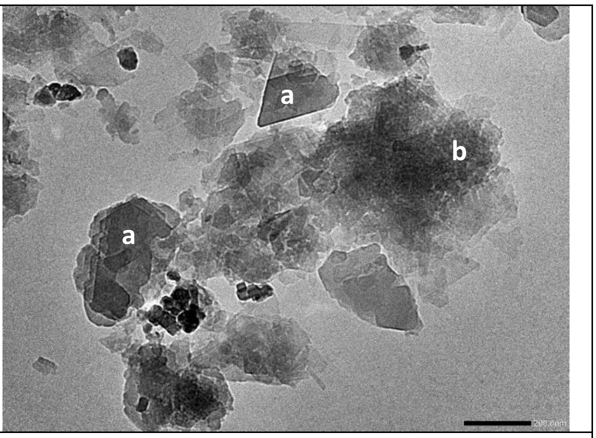
JEM-2100_MAG_X10k_Opalinus-NaCl-60r_05.bmp Magnification: 10k	*JEM-2100_MAG_X30k_Opalinus-NaCl-60r_I10.bmp* Magnification: 30k
Aggregates composed by mainly xenomorphic platy crystals (length << 1 µm) *[IS-ml and diVS-ml are not to distinguish by morphology]*	a) Idiomorphic plates *(a - kaolinite)* partially with dis-solution marks and b) slat-shaped crystals (length ~ 200 nm) with hypidiomorphic ends mainly as aggregates in hexagonal intergrowths *(diVS-ml mainly with %S-range 15-25%)*

Fig. 40. *Morphology of particles (TEM-micrographs)*

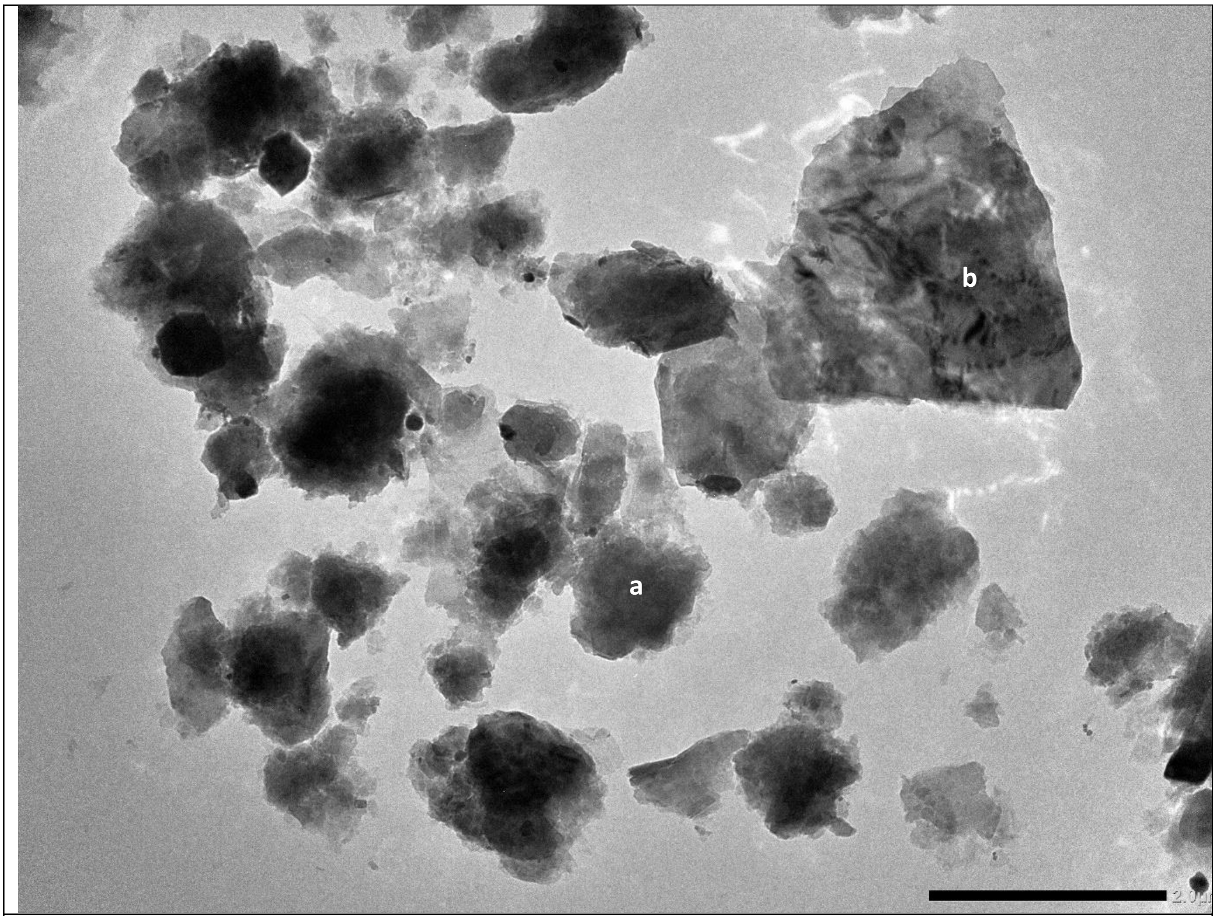

JEM-2100_MAG_X5000_Opalinus-NaCl-60r_I12.bmp

Magnification: 5k
overview: a) mainly aggregates composed by small xenomorphic platy crystals *(diVS-ml and IS-ml)* and b) a large plate (> 2 µm) with Moiré-effects in right top corner (*illite*)

Fig. 41. *Morphology of particles (TEM-micrographs)*

Distribution of smectite layers probability (%S)

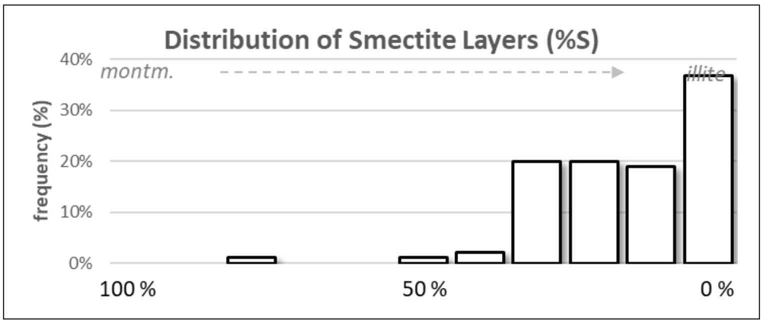

Description: *The distribution of %S-probability indicates two groups: (i) the occurrence of diVS-ml + IS-ml with %S mainly at 20-30% and (ii) illite.*

Fig. 42. *Distribution of smectite layers probability (%S)*

Distribution of charges (exchangeable from interlayer space)

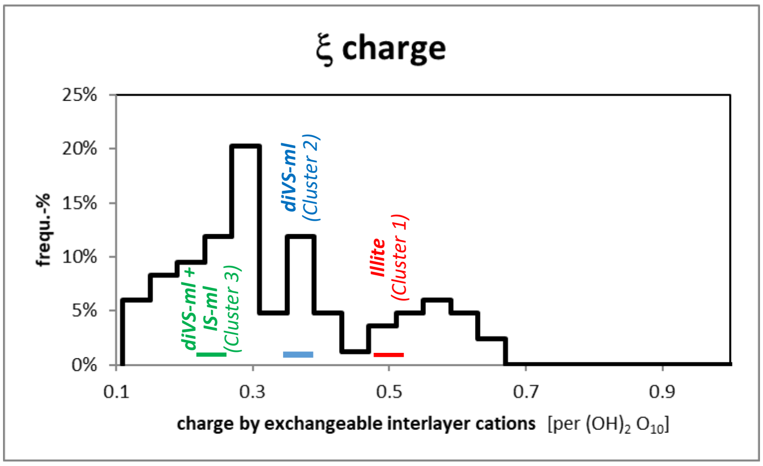

This diagram visualizes the distribution of exchangeable charges in the interlayer space (Ca, Mg, Na) determined and computed by TEM-EDX-data.

Description: *The charge density indicates a bimodal distribution of exchangeable interlayer cations at 0.30 (diVS-ml) and at 0.55 (by illite with K-deficit?) per* $(OH)_2\ O_{10}$.

Fig. 43. *Distribution of charges*

Dioctahedral vermiculite-smectite mixed-layer series *(mixed with IS-ml):*
(diVS-ml with charge- and/or K-deficit; group confirmed as Cluster3):

$$Ca_{0.06}\ Mg_{0.05}\ Na_{0.00}\ K_{0.52}\quad Al_{1.34}\ Fe^{3+}_{0.44}\ Mg_{0.21}\ Ti_{0.01}\ (OH)_2\quad Si_{3.44}\ Al_{0.56}\ O_{10}$$

Charge: XII = 0.75 VI = 5.81 IV = 15.44 **Σ = 22.00**
Probability of smectite layers (%S): 22%
Probability of illite layers (%I): 78%

Measured particles: 54

Distribution of smectite layers probability (%S) in diVS-ml

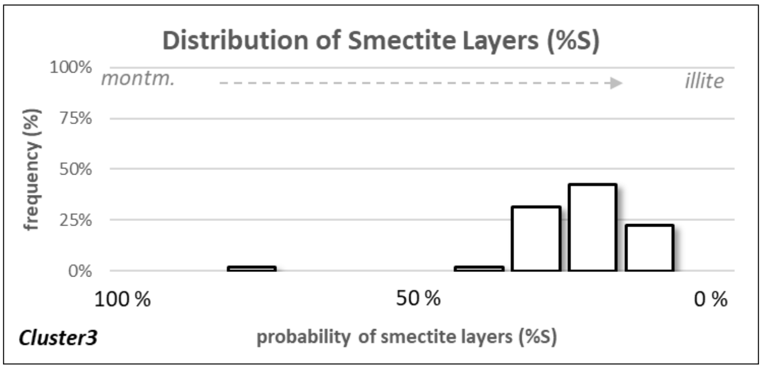

Description: *The distribution of %S-probability indicates the occurrence of mixed layer phases with a %S mainly at 20%.*

Fig. 44a. *Distribution of smectite layers probability (%S) in diVS-ml & IS-ml*

Cluster 3 ISS+IS R0(2)	*particles (abs)*	**Ca (XII)**	**Mg (XII)**	**Na (XII)**	**K (XII)**	**Cr3+ (VI)**	**Al (VI)**	**Fe3+ (VI)**	**Mg (VI)**	**Ti (VI)**	**Al (IV)**	**Si (IV)**	**XII**	**n_VI**	**%S**
%S >95%	n = 0														
%S 95-85%	n = 0														
%S 85-75%	n = 1	0.07	0.06	0.00	0.23	0.00	1.41	0.41	0.09	0.00	0.13	3.87	0.5	1.9	84
%S 75-65%	n = 0														
%S 65-55%	n = 0														
%S 55-45%	n = 0														
%S 45-35%	n = 1	0.00	0.07	0.00	0.46	0.00	1.42	0.39	0.19	0.00	0.41	3.59	0.6	2.0	40
%S 35-25%	n = 17	0.05	0.05	0.00	0.51	0.00	1.35	0.42	0.23	0.00	0.50	3.50	0.7	2.0	28
%S 25-15%	**n = 23**	**0.06**	**0.05**	**0.00**	**0.54**	**0.00**	**1.31**	**0.47**	**0.21**	**0.01**	**0.58**	**3.42**	**0.8**	**2.0**	**20**
%S 15- 5%	n = 12	0.09	0.07	0.00	0.52	0.00	1.38	0.43	0.19	0.00	0.67	3.33	0.8	2.0	12
%S <5%	n = 0														

Fig. 44b. *Computed averaged mineral formulae diVS- & IS-ml phases of Cluster3 in the different %S-classes*

Dioctahedral vermiculite-smectite mixed-layer series:

(charge- and/or K-deficit; confirmed as Cluster2):

$$Ca_{0.05}\ Mg_{0.11}\ Na_{0.00}\ K_{0.34}\quad Al_{1.67}\ Fe^{3+}_{0.28}\ Mg_{0.06}\ Ti_{0.00}\ (OH)_2\quad Si_{3.31}\ Al_{0.69}\ O_{10}$$

Charge: XII = 0.70 VI = 5.99 IV = 15.31 **Σ = 22.00**

Probability of smectite layers (%S): 11%

Probability of illite layers (%I): 89%

Measured particles: 24

Distribution of smectite layers probability (%S) in Cluster2 (diVS-ml)

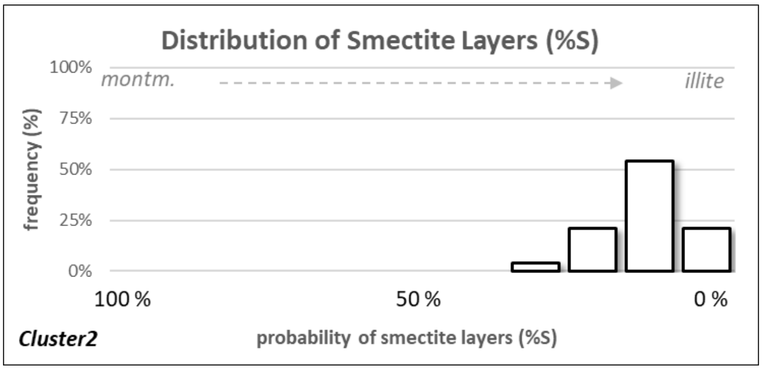

Description: *The distribution of %S-probability indicates the occurrence of diVS-ml with %S mainly at 10%.*

Fig. 45a. *Distribution of smectite layers probability (%S) in diVS-ml (Cluster2)*

Cluster 2 IS R0 (1)	*particles (abs)*	**Ca (XII)**	**Mg (XII)**	**Na (XII)**	**K (XII)**	**Cr3+ (VI)**	**Al (VI)**	**Fe3+ (VI)**	**Mg (VI)**	**Ti (VI)**	**Al (IV)**	**Si (IV)**	**XII**	**n_VI**	**%S**
%S >95%	n = 0														
%S 95-85%	n = 0														
%S 85-75%	n = 0														
%S 75-65%	n = 0														
%S 65-55%	n = 0														
%S 55-45%	n = 0														
%S 45-35%	n = 0														
%S 35-25%	n = 1	0.00	0.17	0.00	0.15	0.00	1.70	0.31	0.00	0.00	0.51	3.49	0.5	2.0	27
%S 25-15%	n = 5	0.08	0.09	0.00	0.32	0.00	1.62	0.29	0.10	0.00	0.58	3.42	0.7	2.0	20
%S 15- 5%	**n = 13**	**0.05**	**0.12**	**0.01**	**0.39**	**0.00**	**1.64**	**0.31**	**0.05**	**0.00**	**0.70**	**3.30**	**0.7**	**2.0**	**10**
%S <5%	n = 5	0.04	0.11	0.00	0.26	0.00	1.78	0.20	0.03	0.00	0.80	3.20	0.6	2.0	3

Fig. 45b. *Computed averaged mineral formulae diVS-ml phases of Cluster2 in the different %S-classes*

Illite *(as end member of diVS-ml series; confirmed as Cluster1):*

$$Ca_{0.06}\ Mg_{0.19}\ Na_{0.00}\ K_{0.37}\quad Al_{1.33}\ Fe^{3+}_{0.60}\ Mg_{0.06}\ Ti_{0.01}\ (OH)_2\quad Si_{3.14}\ Al_{0.86}\ O_{10}$$

Charge: XII = 0.88 VI = 5.98 IV = 15.14 **Σ = 22.00**

Probability of smectite layers (%S): 1%

Probability of illite layers (%I): 99%

Measured particles: 17

Distribution of smectite layers probability (%S) in Cluster1

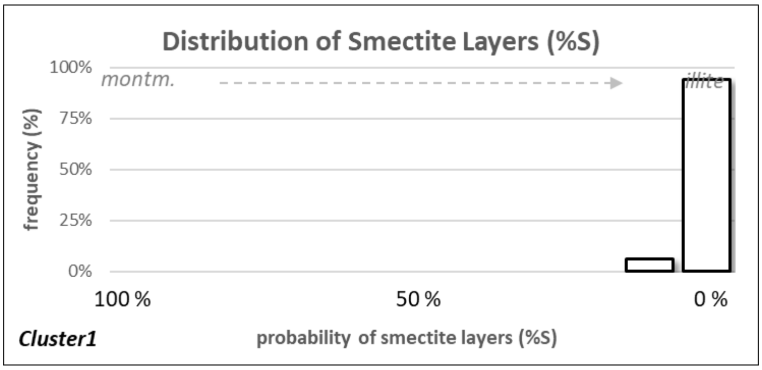

***Description:** The distribution of %S-probability indicates the occurrence of illite (%S mainly at 0%).*

***Fig. 46a.** Distribution of smectite layers probability (%S) in illite (Cluster1)*

Cluster 1 Illite	*particles (abs)*	Ca (XII)	Mg (XII)	Na (XII)	K (XII)	Cr3+ (VI)	Al (VI)	Fe3+ (VI)	Mg (VI)	Ti (VI)	Al (IV)	Si (IV)	XII	n_VI	%S
%S >95%	n = 0														
%S 95-85%	n = 0														
%S 85-75%	n = 0														
%S 75-65%	n = 0														
%S 65-55%	n = 0														
%S 55-45%	n = 0														
%S 45-35%	n = 0														
%S 35-25%	n = 0														
%S 25-15%	n = 0														
%S 15- 5%	n = 1	0.09	0.20	0.00	0.31	0.00	1.43	0.41	0.16	0.00	0.74	3.26	0.9	2.0	7
%S <5%	**n = 16**	**0.06**	**0.19**	**0.00**	**0.38**	**0.00**	**1.32**	**0.62**	**0.06**	**0.02**	**0.86**	**3.14**	**0.9**	**2.0**	**0**

***Fig. 46b.** Computed averaged mineral formulae f illite (Cluster1) in the different %S-classes*

Talc-saponite-trioctahedral vermiculite mixed-layer series (TSV-ml):

$$Ca_{0.07}\ Mg_{0.05}\ Na_{0.00}\ K_{0.27}\quad Al_{0.86}\ Fe^{2+}_{1.42}\ Mg_{0.56}\ Ti_{0.01}\ (OH)_2\quad Si_{2.93}\ Al_{1.07}\ O_{10}$$

Charge: XII = 0.51 VI = 6.57 IV = 14.93 **Σ = 22.00**

Probability of talc layers (%T): 5% *min – max: 0 … 15%*

Probability of saponite layers (%S): 61% *min – max: 2 … 96%*

Probability of tricot. vermiculite layers (%V): 34% *min – max: 1 … 96%*

Measured particles: 9

Mineral Matter – Specification

Result of Clustering & Comparison with XRD-data (Sybilla-processing)

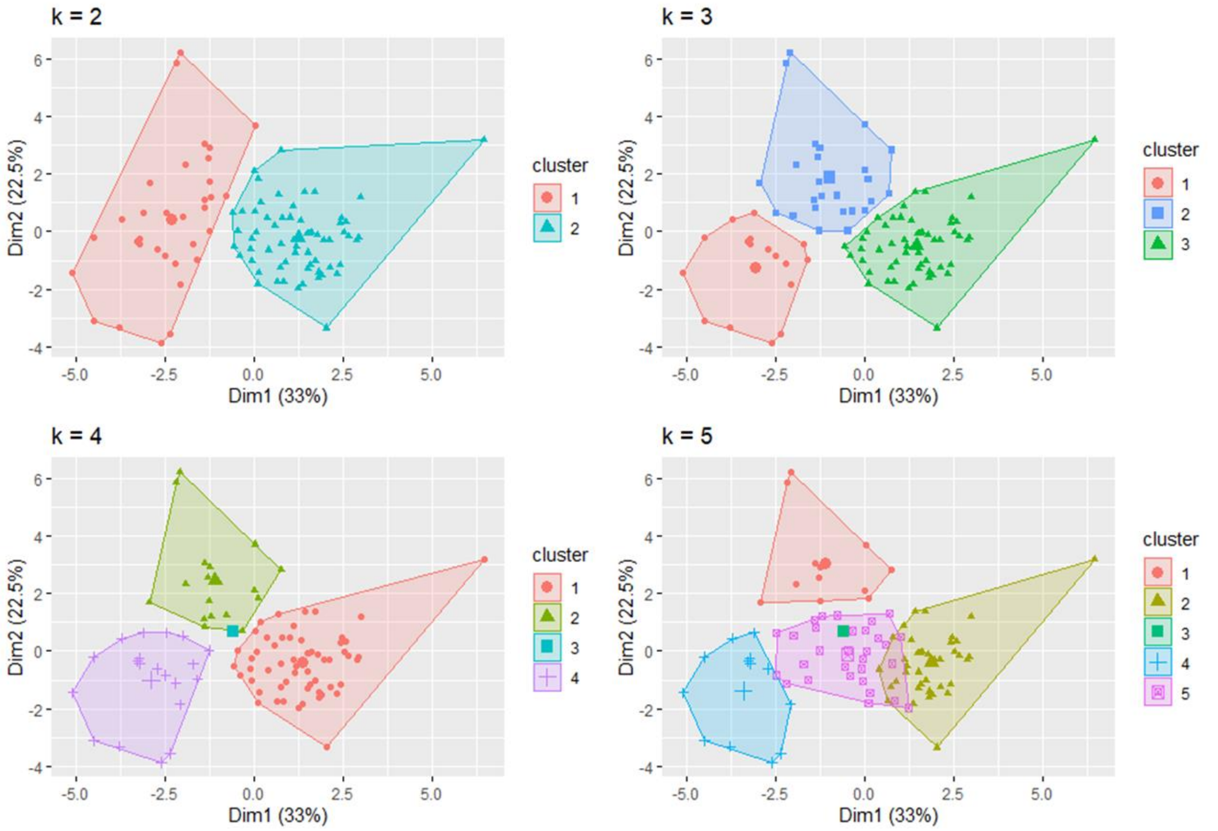

Fig. 47. *Clustering of all measured particles for clusters k = 2, k = 3, k = 4 and k = 5 (source for R-coding: https://uc-r.github.io/kmeans_clustering)*

The optimum of clusters was calculated with k = 3. This number of clusters differentiates also clearly illite particles (Cluster1) from smectite-bearing phases (Cluster2, Cluster3).

		Ca (XII)	Mg (XII)	Na (XII)	K (XII)	Cr3+ (VI)	Al (VI)	Fe3+ (VI)	Mg (VI)	Ti (VI)	Al (IV)	Si (IV)	XII	n_VI	%S
Cluster1	n = 17	0.06	0.19	0.00	0.37	0.00	1.33	0.60	0.06	0.01	0.86	3.14	0.88	2.0	1
Cluster2	n = 24	0.05	0.11	0.00	0.34	0.00	1.67	0.28	0.06	0.00	0.69	3.31	0.68	2.0	11
Cluster3	n = 54	0.06	0.05	0.00	0.52	0.00	1.34	0.44	0.21	0.01	0.56	3.44	0.75	2.0	22

Fig. 48. *Mineral formulae based on TEM-EDX-data summarized following the result of clustering for k=3*

	Sybilla-modelling of XRD-results	**TEM-EDX-results**	**Notes**
Cluster1	Illite	Illite	*high K-deficit, Fe(VI)-rich, low Mg(VI)*
Cluster2	IS R0 *(%S = 9%)*	diVS-ml *(%S = 9%)*	*high K-deficit, Al(VI)-rich, low Mg(VI)*
Cluster3	ISS R0 *(%S = 28%)* + IS R0 *(%S = 29%)*	diVS-ml + IS-ml *(%S = 22%)*	*K-deficit, Fe(VI)- & Mg(VI)-rich*

Tab. 10. *Comparison of results from TEM-EDX- and XRD-measurements with clustering procedure*

References

Aplin, A.C., Matenaar, I.F., McCarty, D.K., van der Pluijm, B.A. (2006). Clays Clay Miner ***54****, 500-514. DOI: 10.1346/CCMN.2006.0540411*

Cliff, G. & Lorimer, G. W. (1975). J. Microsc. ***103****, 203–207.*

Crâciun, C. (1984). Spectrosc. Lett. ***17****, 579–590.*

Döbelin, N., Kleeberg, R. (2015). Journal of Applied Crystallography ***48****, 1573-1580. DOI: 10.1107/S1600576715014685*

Farmer, V. C. (1974). Editor. The Infrared Spectra of Minerals, Monograph 4. London: Mineralogical Society.

Farmer, V. C. & Russell, J. D. (1964). Spectrochim. Acta, ***20*** *, 1149-1173.*

Gaucher, E.C., Fernández, A. M. & Waber, H.N. (2003): Annex 9: Rock and Mineral Characterisation of the Opalinus Clay Formation. in: Pearson, F. J., Arcos, D., Bath, A., Boisson, J.-Y., Fernández, A. M., Gäbler, H.-E., Gaucher, E., Gautschi, A., Griffault, L., Hernán, P. & Waber, H. N. (2003): Mont Terri Project – Geochemistry of Water in the Opalinus Clay Formation at the Mont Terri Rock Laboratory. Berichte des BWG, Serie Geologie – Rapports de l'OFEG, Série Géologie – Rapporti dell'UFAEG, Serie Geologia – Reports of the FOWG, Geology Series, ***5****, 281-303.*

Goodman, B. A., Russell, J. D., Fraser, A. R. & Woodhams, F. W. D. (1976). Clays Clay Miner. ***24****, 52-59.*

Henning, K.-H. & Störr, M. (1986). Electron Micrographs (TEM, SEM) of Clays and Clay Minerals, p. 325. Akademie-Verlag Berlin.

Hoang-Minh, T., Kasbohm, J., Nguyen-Thanh, L., Nga, P. T., Lai, L. T., Duong, N. T., Thanh, N. D., Thuyet, N. T. M., Anh, D. D., Pusch, R., Knutsson, S. & Ferreiro Mahlmann, R. (2019). J. Appl. Cryst. ***52****, 133-147. doi: https://doi.org/10.1107/S1600576718018162*

Lorimer, G. W. & Cliff, G. (1976). Electron Microscopy in Mineralogy, edited by H. R. Wenk, pp. 506–519. Berlin: Springer Verlag.

Madejová, J. & Komadel, P (2001). Clays Clay Miner. ***49*** *, 410-432.*

Madejová, J., Komadel, P. & Čičel, B. (1994). Clay Miner. ***29****, 319-326.*

Matschiavelli, N., Kluge, S., Podlech, C., Standhaft, D., Grathoff, G., Ikeda-Ohno, A., Warr, L.N., Chukharkina, A., Arnold, T. & Cherkouk, A. (2019). Environmental Science & Technology. ***53*** *(17), 10514-10524, DOI: 10.1021/acs.est.9b02670*

Mellini, M. & Menichini, R. (1985). R. Soc. Ital. Miner. Petrol. ***40****, 261–266.*

Moore, D.M., Reynolds, R.C. (1989). X-ray Diffraction and the Identification and Analysis of Clay Minerals, Oxford University Press, New York, 332 + xvi pp.

Nguyen-Thanh, L., Herbert, H.-J., Kasbohm, J., Hoang-Minh, T. & Mählmann, R. F. (2014). Clays Clay Miner. ***62****, 425–446.*

Środoń, J., Elsass, F., McHardy, W. J. & Morgan, D. J. (1992). Clay Miner. ***27****, 137–158.*

S2. X-ray Diffraction (XRD)

SUPPLEMENT – XRD: Powder, bulk

Content

Methodology – X-ray diffraction of powder samples

It is expected a characterization of clay mineral phases in treated B25 bentonite by X-ray diffraction (XRD) of bulk samples as powder specimen. The treatment itself was carried out by GRS gGmbH in Braunschweig. The sample bodies were percolated by adapted Opalinus solution under different temperatures (35°C, 60°C, 100°C, 125°C, 150°C) and time intervals.

After the experiment, three samples were investigated from each sample body – material from top position, from central part and from the bottom. The flow direction of percolation was oriented from the top to the bottom of sample body.

Powder XRD is a non-destructive analytical technique used to identify the crystalline composition of solid materials through diffraction of X-rays by the lattice planes of atoms within materials. Incident X-ray are hit on the samples and reflected from the parallel planes of atoms of minerals. They are realized by distinguishing orientation through Miller indices. The diffraction patterns indicated bulk properties of structure. The Bragg law equation was applied to observe the relationship between the wavelength of the incident beam (λ), the angle of incident beam entry and parallel planes of atoms causing the diffraction (θ), as well as the distance between these planes (d). The delivered XRD-pattern represents scans of randomly oriented powders of bulk samples to determine their general mineral composition. XRD-diffractograms of powder materials from studied rocks were recorded over the range 4 – 70 °2θ, using Panalytical X'Pert Pro Diffractometer (Cu- $K\alpha_{1,2}$ radiation; 40 kV; 30 mA; 0.5/25 soller collimator, automatic divergence slit, step size 0.008 °2Θ; time per step 50 s; X'Celerator Scientific line focus detector; 240 mm goniometer PW3050/60 radius) at Institute of Geosciences, Goethe University in Frankfurt am Main. The processing of XRD powder patterns included Rietveld refinement for semi-quantitative determination of essential mineral components by using the software PROFEX (Döbelin and Kleeberg, 2015) as a graphical interface, which has embedded the BGMN software package (Bergmann et al., 1998; Kleeberg et al., 2010; Ufer et al., 2004, 2008). The d(060)-value was used to determine the main contribution of individual clay components in the samples (Lee et al., 2003; Moore and Reynolds, 1997). Results of thermogravimetry (TG) are used for an additional cross-checking with XRD results.

References:

Bergmann, J., Friedel, P., Kleeberg, R., 1998. BGMN — a new fundamental parameter based Rietveld program for laboratory X-ray sources, its use in quantitative analysis and structure investigations. CPD Newsl. 20, 5–8.

Döbelin, N., Kleeberg, R. (2015). Journal of Applied Crystallography 48, 1573-1580. DOI: 10.1107/S1600576715014685

Kleeberg, R., Ufer, K., and Bergmann, J. (2010) Rietveld analysis with BGMN Rietveld method physical basics profile modelling quantification. In: BGMN workshop Freiberg 2010. Technische Universität Bergakademie Freiberg. Freiberg, Germany, 87 pp.

Lee, B.D., Sears, S.K., Graham, R.C., Amrhein, C., Vali, H., 2003. Secondary mineral genesis from chlorite and serpentine in an ultramafic soil toposequence. Soil Sci. Soc. Am. J. 67, 1309–1317. http://dx.doi.org/10.2136/sssaj2003.1309.

Moore, D.M., Reynolds, R.C., 1997. X-ray Diffraction and the Identification and Analysis of Clay Minerals, 2nd ed. Oxford University Press.

Ufer, K., Roth, G., Kleeberg, R., Stanjek, H., Dohrmann, R., Bergmann, J., 2004. Description of X-ray powder pattern of turbostratically disordered layer structures with a Rietveld compatible approach. Z. Krist. 219, 519–527. doi.org/10.1524/zkri.219.9.519.44039.

Ufer, K., Stanjek, H., Roth, G., Dohrmann, R., Kleeberg, R., Kaufhold, S. (2008) Quantitative phase analysis of bentonites by the Rietveld method. Clays and Clay Minerals, 56, 272-282. dx.doi.org/10.1346/CCMN.2008.0560210.

Data Sheet – Mineral matter in bulk powder of B25-series

Sample	Ca-Smectite	IS-ml	Illite (1M)	Illite (2M1)	Kaolinite + *KS-ml*	*Σ clay*	Quartz	K-feldspar	Plagioclase	Anhydrite	Cerussite	Analcime	Diaspore	Rutile + Anatase	Calcite	Natrolite	*Σ total*
B25 original	32% *(±0.8)*	10% *(±0.5)*	15% *(±0.7)*	17% *(±0.5)*	14% *(±0.6)*	*86%*	10% *(±0.1)*	2% *(±0.1)*	2% *(±0.1)*								*100%*
35°C, 93.6h, OPA																	
No4_T	37% *(±0.8)*	6% *(±0.8)*	10% *(±0.7)*	10% *(±0.4)*	7% *(±0.3)*	70%	12% *(±0.8)*	2% *(±0.2)*	12% *(±0.2)*	<1% *(±0.1)*		1% *(±0.1)*		1% *(±0.1)*	2% *(±0.2)*		*101%*
No4_C	34% *(±1.2)*	4% *(±0.5)*	18% *(±0.9)*	10% *(±0.5)*	7% *(±0.6)*	73%	13% *(±0.6)*	2% *(±0.2)*	9% *(±0.8)*	1% *(±0.1)*		<1% *(±0.1)*		<1% *(±0.1)*	2% *(±0.3)*		*97%*
No4_B	35% *(±1.4)*	5% *(±1.1)*	10% *(±0.8)*	10% *(±0.4)*	12% *(±0.8)*	72%	14% *(±0.6)*	3% *(±0.2)*	7% *(±0.6)*	1% *(±0.2)*		<1% *(±0.1)*		<1% *(±0.1)*	1% *(±0.4)*		*100%*
35°C, 285h, OPA.0.7 MPa																	
No23	28% *(±1.7)*	15% *(±1.9)*	8% *(±0.8)*	11% *(±0.4)*	15% *(±1.4)*	77%	14% *(±0.4)*	3% *(±0.2)*	4% *(±0.7)*	1% *(±0.2)*		<1% *(±0.1)*		<1% *(±0.1)*	1% *(±0.3)*		*100%*
60°C, 454h, OPA																	
No5_T	28% *(±1.4)*	3% *(±0.6)*	9% *(±0.8)*	10% *(±0.5)*	9% *(±1.1)*	60%	26% *(±0.7)*	3% *(±0.2)*	9% *(±0.9)*	1% *(±0.1)*				1% *(±0.1)*	2% *(±0.3)*		*100%*
No5_C	35% *(±0.8)*	3% *(±0.4)*	10% *(±0.8)*	10% *(±0.4)*	11% *(±0.8)*	69%	16% *(±0.7)*	2% *(±0.2)*	7% *(±0.7)*	2% *(±0.2)*		<1% *(±0.1)*	2% *(±0.1)*	1% *(±0.1)*	2% *(±0.3)*		*98%*
No5_B	28% *(±1.0)*	5% *(±0.5)*	22% *(±1.0)*	8% *(±0.5)*	6% *(±1.0)*	68%	16% *(±0.6)*	2% *(±0.1)*	8% *(±0.7)*	2% *(±0.2)*		<1% *(±0.1)*		1% *(±0.1)*	*1% *(±0.3)*		*100%*
100°C, 110h, OPA																	
No0_T	25% *(±1.6)*	11% *(±1.4)*	10% *(±0.6)*	10% *(±0.3)*	11% *(±0.7)*	66%	13% *(±0.6)*	4% *(±0.2)*	11% *(±0.6)*	2% *(±0.1)*	<1%	<1% *(±0.1)*		1% *(±0.1)*	*2% *(±0.2)*		*99%*
No0_C	26% *(±0.9)*	9% *(±0.7)*	14% *(±0.7)*	7% *(±0.5)*	13% *(±1.0)*	69%	9% *(±0.4)*	3% *(±0.2)*	12% *(±0.7)*	2% *(±0.2)*		<1% *(±0.1)*	2% *(±0.2)*	<1% *(±0.1)*	*2% *(±0.3)*	<1% *(±0.1)*	*100%*
No0_B	24% *(±1.9)*	12% *(±1.4)*	14% *(±1.3)*	7% *(±0.7)*	24% *(±1.8)*	80%	11% *(±1.0)*	2% *(±0.3)*	2% *(±0.2)*	1% *(±0.2)*	<1%	<1% *(±0.1)*		1% *(±0.1)*	<1% *(±0.4)*	2% *(±0.3)*	*100%*
100°C, 35d, OPA																	
No2_T	24% *(±1.2)*	12% *(±1.0)*	11% *(±0.6)*	10% *(±0.3)*	12% *(±0.7)*	68%	9% *(±0.3)*	3% *(±0.3)*	13% *(±0.7)*	2% *(±0.1)*		1% *(±0.1)*	<1% *(±0.1)*	1% *(±0.1)*	*2% *(±0.2)*	<1% *(±0.1)*	*100%*
No2_C	24% *(±1.1)*	15% *(±0.7)*	14% *(±0.6)*	9% *(±0.3)*	12% *(±0.8)*	74%	11% *(±0.2)*	2% *(±0.2)*	7% *(±0.5)*	1% *(±0.1)*		<1% *(±0.1)*	<1% *(±0.1)*	1% *(±0.1)*	*1% *(±0.2)*	<1% *(±0.1)*	*96%*
No2_B	30% *(±0.9)*	10% *(±0.6)*	9% *(±0.6)*	13% *(±0.3)*	14% *(±0.8)*	74%	10% *(±0.3)*	1% *(±0.1)*	8% *(±0.6)*	1% *(±0.1)*		<1% *(±0.1)*		<1% *(±0.1)*	1% *(±0.2)*	2% *(±0.2)*	*100%*
125°C, 98.6h, OPA																	
No15	31% *(±1.3)*	6% *(±0.6)*	20% *(±0.9)*	7% *(±0.5)*	12% *(±1.1)*	76%	11% *(±0.7)*	2% *(±0.2)*	5% *(±0.2)*	1% *(±0.1)*		1% *(±0.1)*	<1% *(±0.1)*	<1% *(±0.1)*	2% *(±0.3)*	2% *(±0.2)*	*100%*
150°C, 4d, OPA																	
No3_T	26% *(±1.4)*	14% *(±1.1)*	9% *(±0.6)*	9% *(±0.4)*	12% *(±1.0)*	70%	9% *(±0.3)*	3% *(±0.2)*	11% *(±0.7)*	1% *(±0.1)*		1% *(±0.1)*		<1% *(±0.1)*	*2% *(±0.2)*	<1% *(±0.1)*	*99%*
No3_C	21% *(±1.1)*	14% *(±0.9)*	13% *(±0.8)*	6% *(±0.5)*	12% *(±0.9)*	65%	8% *(±0.2)*	5% *(±0.2)*	12% *(±0.7)*	2% *(±0.2)*		<1% *(±0.1)*		1% *(±0.1)*	3% *(±0.3)*	<1% *(±0.2)*	*98%*
No3_B	20% *(±1.2)*	17% *(±1.0)*	7% *(±0.6)*	9% *(±0.3)*	13% *(±0.5)*	66%	10% *(±0.2)*	4% *(±0.2)*	14% *(±0.5)*	1% *(±0.1)*		1% *(±0.1)*		1% *(±0.1)*	2% *(±0.2)*	<1% *(±0.1)*	*99%*

***Legend:** * - including indications by TG for additional amount of amorphous calcium carbonate; (±0.1) – standard deviation, absolute*

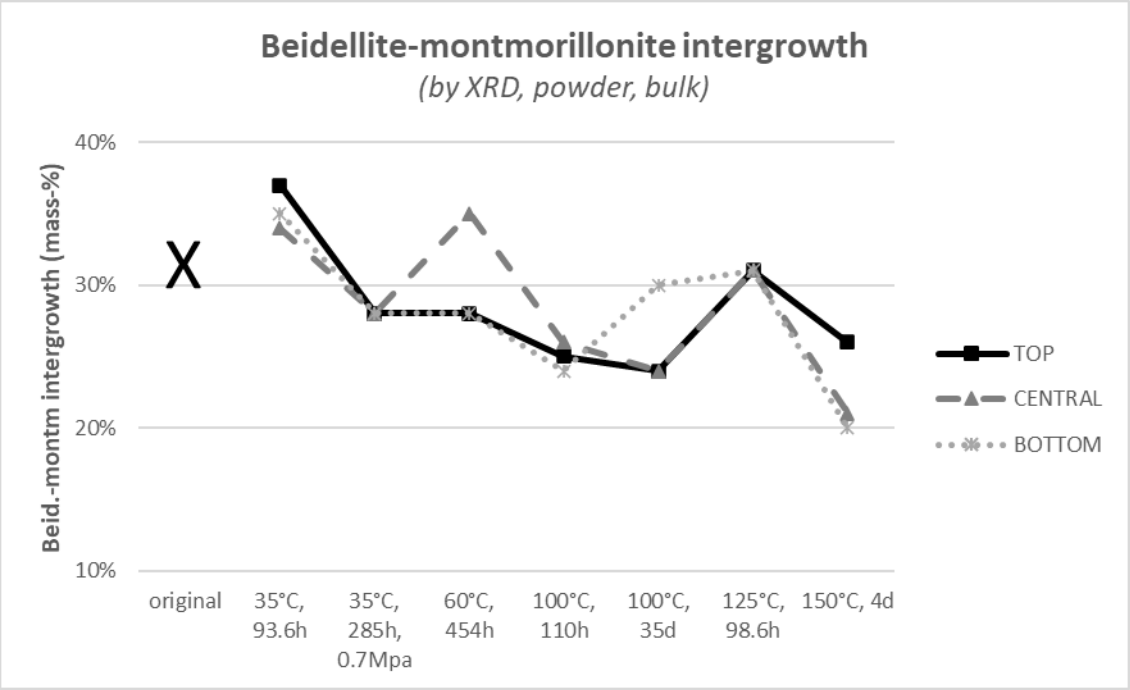
Beidellite-montmorillonite intergrowth
(by XRD, powder, bulk)
Beid.-montm intergrowth (mass-%)
40%
30%
20%
10%
X
original
35°C, 93.6h
35°C, 285h, 0.7Mpa
60°C, 454h
100°C, 110h
100°C, 35d
125°C, 98.6h
150°C, 4d
TOP
CENTRAL
BOTTOM

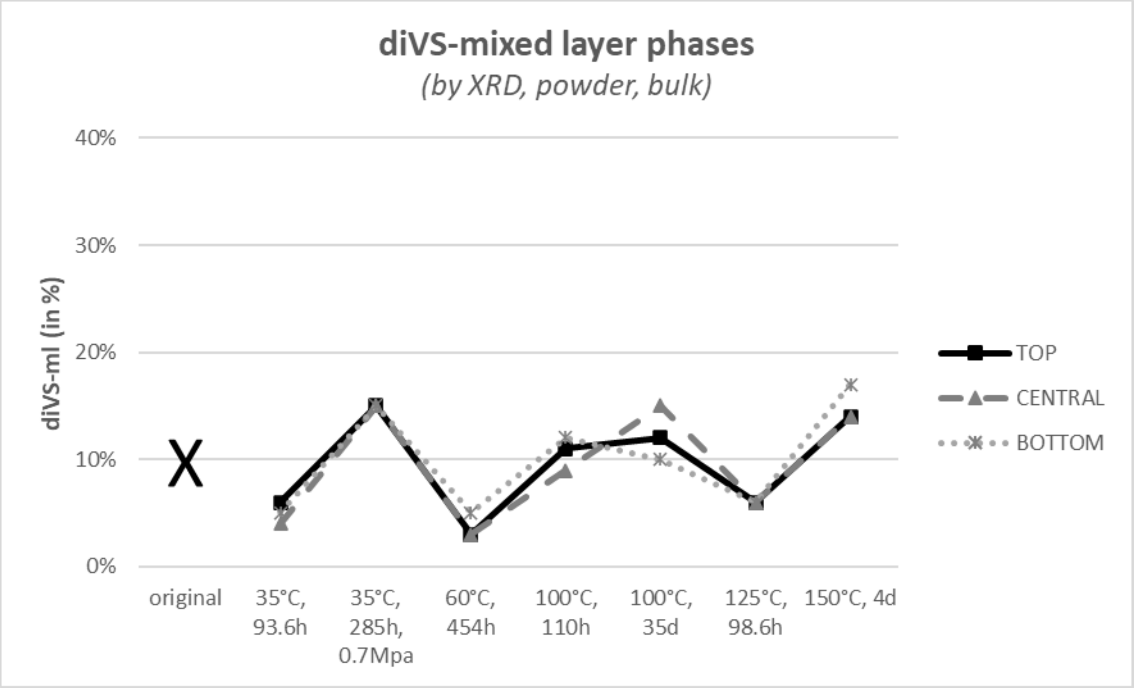
diVS-mixed layer phases
(by XRD, powder, bulk)
diVS-ml (in %)
40%
30%
20%
10%
0%
X
original
35°C, 93.6h
35°C, 285h, 0.7Mpa
60°C, 454h
100°C, 110h
100°C, 35d
125°C, 98.6h
150°C, 4d
TOP
CENTRAL
BOTTOM

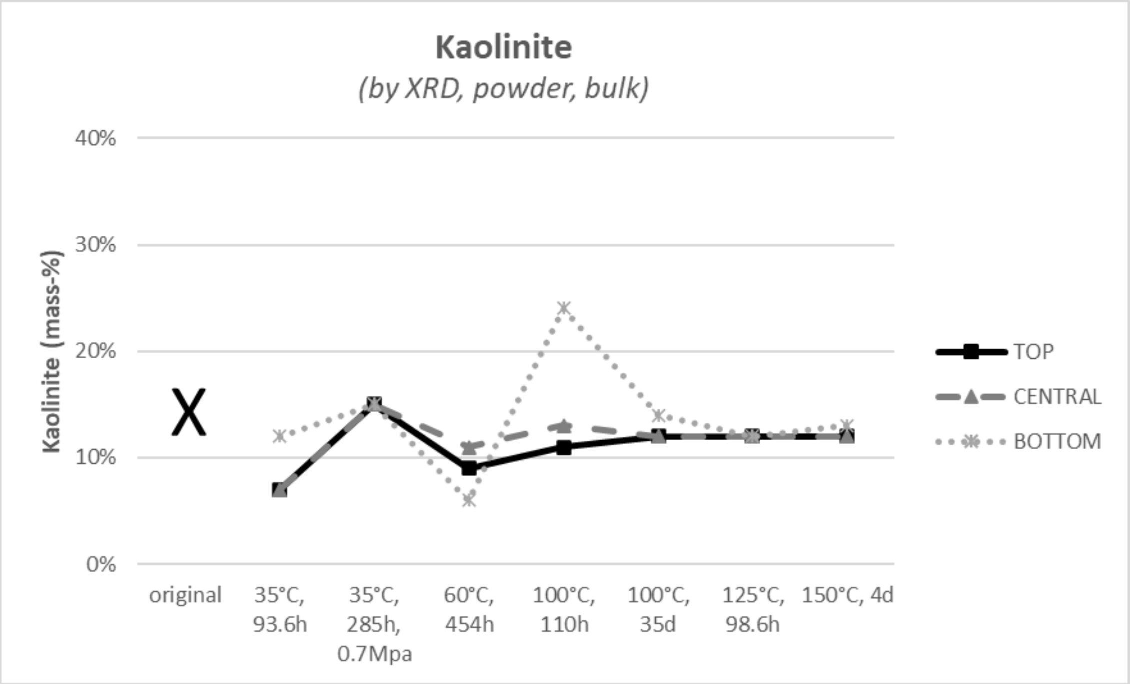
Kaolinite
(by XRD, powder, bulk)
Kaolinite (mass-%)
40%
30%
20%
10%
0%
X
original
35°C, 93.6h
35°C, 285h, 0.7Mpa
60°C, 454h
100°C, 110h
100°C, 35d
125°C, 98.6h
150°C, 4d
TOP
CENTRAL
BOTTOM

Data Sheet – Mineral matter in bulk powder of Friedland Clay-series

Sample	**Ca-Smectite**	**IS-ml**	**Illite (1M)**	**Illite (2M1)**	**Chlorite**	**Kaolinite +** *KS-ml*	*Σ clay*	**Quartz**	**K-feldspar**	**Plagioclase**	**Pyrite**	**Calcite**	**Anatase**	*Σ total*
orig., compact. **No19**	5% *(±0.9)*	14% *(±0.3)*	34% *(±0.9)*	6% *(±0.3)*	3% *(±0.3)*	16% *(±0.6)*	78%	15% *(±0.6)*	3% *(±0.2)*	3% *(±0.2)*	<1% *(±0.1)*	*	1% *(±0.1)*	*100%*
35°C, 46.3h, OPA **No10**	6% *(±0.3)*	13% *(±1.6)*	26% *(±0.7)*	7% *(±0.3)*	6% *(±0.6)*	11% *(±0.5)*	69%	22% *(±0.8)*	5% *(±0.3)*	3% *(±0.2)*	<1% *(±0.1)*	*<1% *(±0.1)*	1% *(±0.1)*	*100%*
60°C, 45.9h, OPA **No11**	5% *(±0.5)*	13% *(±0.4)*	28% *(±0.9)*	8% *(±0.3)*	5% *(±0.6)*	15% *(±0.6)*	73%	17% *(±0.8)*	5% *(±0.3)*	3% *(±0.2)*	<1% *(±0.1)*	*	1% *(±0.1)*	*100%*
100°C, 40h, OPA **No16**	6% *(±0.8)*	16% *(±0.6)*	26% *(±0.6)*	8% *(±0.2)*	5% *(±0.4)*	15% *(±0.5)*	75%	16% *(±0.5)*	4% *(±0.3)*	3% *(±0.2)*	<1% *(±0.1)*	*<1% *(±0.2)*	1% *(±0.1)*	*100%*
125°C, 40h, OPA **No20**	3% *(±0.6)*	16% *(±1.0)*	33% *(±1.0)*	7% *(±0.4)*	8% *(±0.8)*	12% *(±0.8)*	78%	15% *(±0.9)*	3% *(±0.2)*	3% *(±0.3)*	<1% *(±0.1)*	*	1% *(±0.1)*	*100%*
150°C, 68.3 h, OPA **No21**	8% *(±1.6)*	13% *(±0.5)*	30% *(±1.2)*	7% *(±0.4)*	3% *(±0.6)*	16% *(±0.8)*	76%	16% *(±0.5)*	3% *(±0.2)*	4% *(±0.3)*	<1% *(±0.1)*	*	1% *(±0.1)*	*100%*
without transport cell														
100°C, OPA **No12**	7% *(±0.4)*	7% *(±0.5)*	29% *(±0.9)*	8% *(±0.4)*	4% *(±0.6)*	18% *(±0.7)*	73%	19% *(±0.5)*	4% *(±0.3)*	3% *(±0.3)*	<1% *(±0.1)*	*1% *(±0.1)*	1% *(±0.1)*	*100%*

Legend: ** - including indications by TG for additional amount of amorphous calcium carbonate; (±0.1) – standard deviation, absolute*

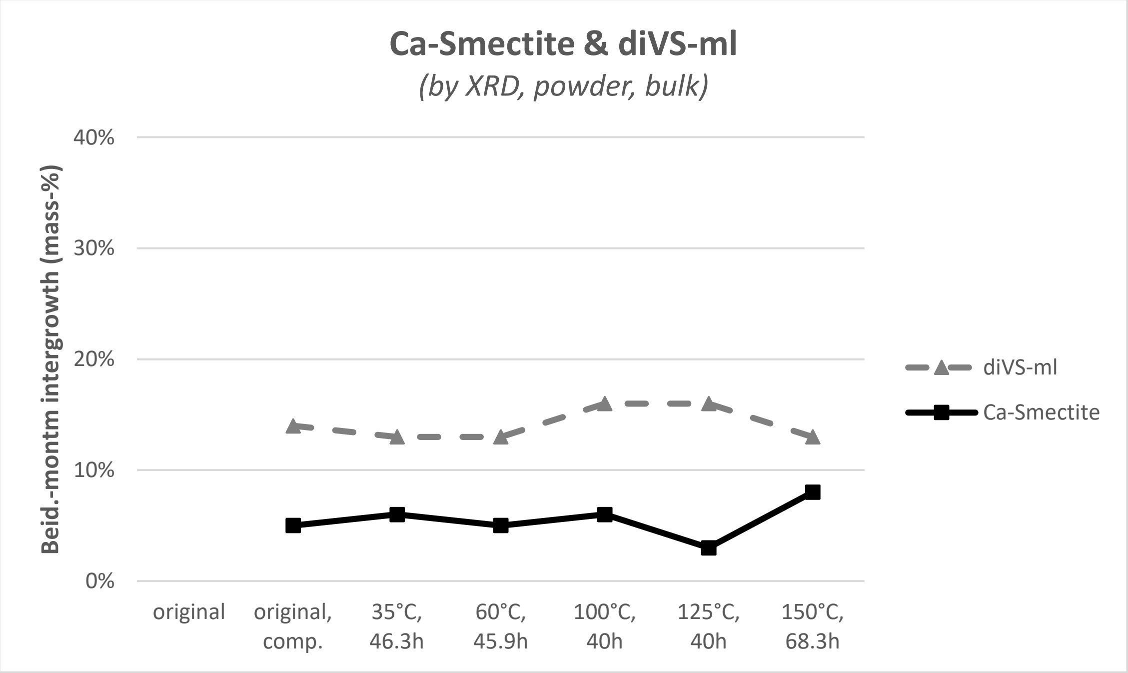

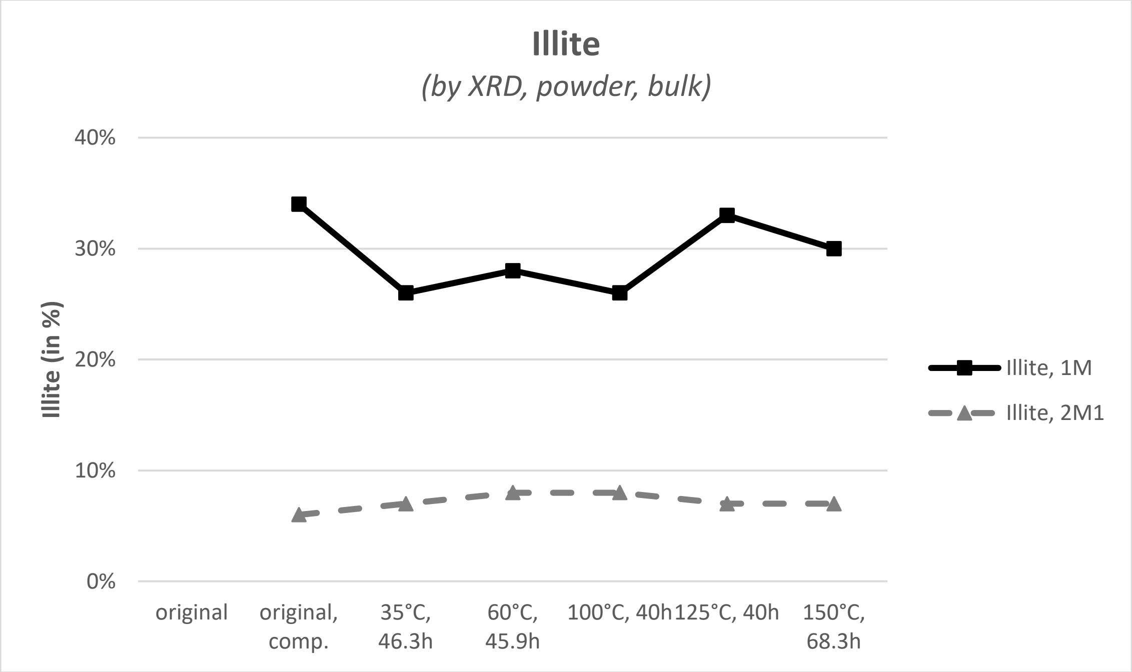
Illite
(by XRD, powder, bulk)
Illite (in %)
40%
30%
20%
10%
0%
original
original, comp.
35°C, 46.3h
60°C, 45.9h
100°C, 40h
125°C, 40h
150°C, 68.3h
Illite, 1M
Illite, 2M1

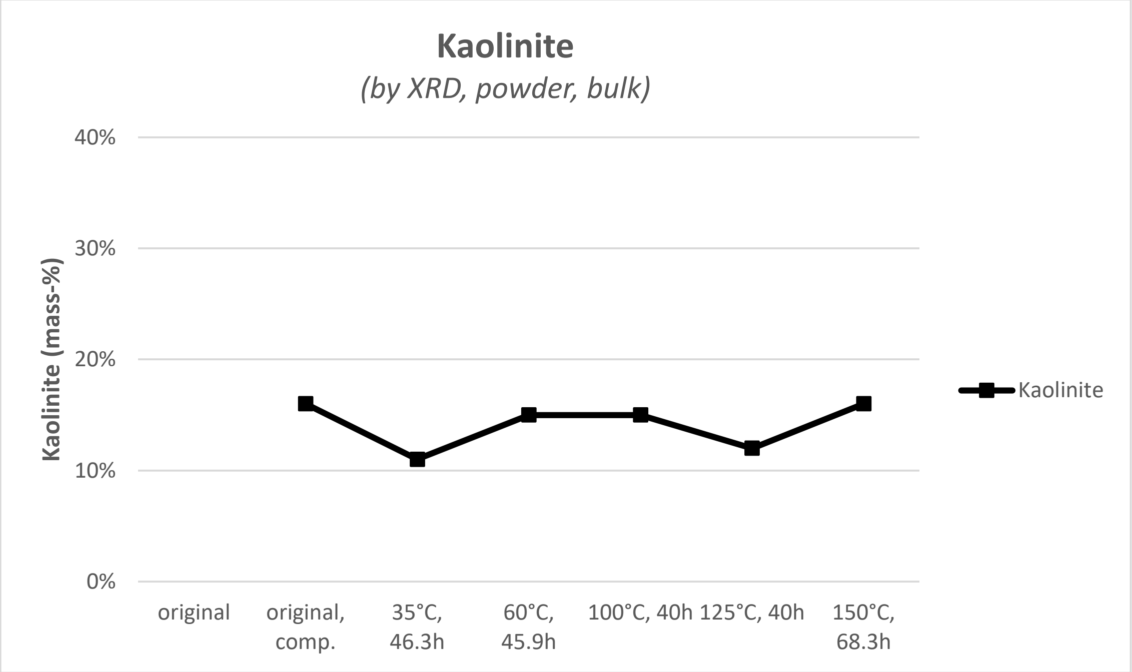
Kaolinite
(by XRD, powder, bulk)
Kaolinite (mass-%)
40%
30%
20%
10%
0%
original
original, comp.
35°C, 46.3h
60°C, 45.9h
100°C, 40h
125°C, 40h
150°C, 68.3h
Kaolinite

Data Sheet – Mineral matter in bulk powder of Opalinus Clay-series

Sample	Ca-Smectite	diVS-ml	Illite (1M)	Illite (2M1)	Chlorite	Kaolinite + KS-ml	*Σ clay*	Quartz	K-feldspar	Plagioclase	Pyrite	Calcite	Siderite	Dolomite	Anatase	*Σ total*
Opalin. Clay original		3% *(±0.4)*	4% *(±0.3)*	18% *(±0.9)*	12% *(±0.7)*	25% *(±3.0)*	*61%*	13% *(±0.5)*	1% *(±0.2)*	4% *(±0.2)*	1% *(±0.1)*	17% *(±0.6)*	1% *(±0.1)*	2% *(±0.1)*		*100%*
orig., compact. **No6**		9% *(±0.5)*	2% *(±0.2)*	13% *(±0.6)*	4% *(±0.3)*	50% *(±1.6)*	78%	9% *(±0.3)*	1% *(±0.2)*	2% *(±0.2)*	<1% *(±0.1)*	8% *(±0.3)*	<1% *(±0.1)*	<1% *(±0.1)*	<1% *(±0.1)*	*100%*
35°C, 144h, OPA **No22**		12% *(±0.7)*	2% *(±0.5)*	22% *(±0.8)*	7% *(±0.4)*	25% *(±1.2)*	67%	14% *(±0.5)*	2% *(±0.3)*	3% *(±0.3)*	1% *(±0.1)*	*10% *(±0.1)*	1% *(±0.1)*	1% *(±0.1)*	1% *(±0.1)*	*100%*
60°C, 45.4h, OPA **No9**		12% *(±0.7)*	1% *(±0.3)*	19% *(±0.9)*	3% *(±0.3)*	35% *(±2.2)*	69%	13% *(±0.7)*	1% *(±0.2)*	2% *(±0.2)*	1% *(±0.1)*	*10% *(±0.3)*	<1% *(±0.1)*	1% *(±0.1)*		*99%*
60°C, 95.3h, OPA **No7**		9% *(±0.5)*	1% *(±0.4)*	3% *(±0.3)*	<1% *(±0.1)*	13% *(±0.8)*	28%	6% *(±0.4)*	1% *(±0.2)*	1% *(±0.2)*	<1% *(±0.1)*	*60% *(±0.6)*	<1% *(±0.1)*	1% *(±0.1)*		*98%*
100°C, 69.3h, OPA **No8**		12% *(±1.0)*	3% *(±0.5)*	11% *(±0.4)*	8% *(±0.7)*	27% *(±1.2)*	61%	14% *(±0.6)*	3% *(±0.3)*	4% *(±0.3)*	2% *(±0.1)*	*14% *(±0.3)*	2% *(±0.1)*	1% *(±0.1)*		*100%*
125°C, 48.5h, OPA **No14**		16% *(±0.7)*	5% *(±0.5)*	10% *(±0.4)*	7% *(±0.9)*	25% *(±1.2)*	63%	14% *(±0.6)*	3% *(±0.3)*	4% *(±0.3)*	1% *(±0.1)*	*11% *(±0.3)*	2% *(±0.1)*	<1% *(±0.1)*		*99%*
150°C, 48.6 h, OPA **No13**		8% *(±0.9)*	<1% *(±0.1)*	16% *(±1.1)*	4% *(±0.4)*	53% *(±3.2)*	81%	8% *(±0.5)*	1% *(±0.2)*	1% *(±0.1)*	1% *(±0.1)*	*7% *(±0.4)*	<1% *(±0.1)*	<1% *(±0.1)*		*99%*
without transport cell																
35°C, OPA **No9a**		10% *(±0.3)*	2% *(±0.2)*	25% *(±0.6)*	4% *(±0.5)*	29% *(±0.8)*	70%	15% *(±0.4)*	1% *(±0.2)*	3% *(±0.2)*	1% *(±0.1)*	*9% *(±0.2)*	<1% *(±0.1)*	1% *(±0.1)*		*99%*
125°C, OPA **No9b**		10% *(±0.4)*	3% *(±0.3)*	20% *(±0.6)*	1% *(±0.2)*	32% *(±0.9)*	65%	14% *(±0.3)*	2% *(±0.2)*	2% *(±0.2)*	1% *(±0.1)*	*11% *(±0.2)*	<1% *(±0.1)*	1% *(±0.1)*		*96%*

Legend: ** - including indications by TG for additional amount of amorphous calcium carbonate; (±0.1) – standard deviation, absolute*

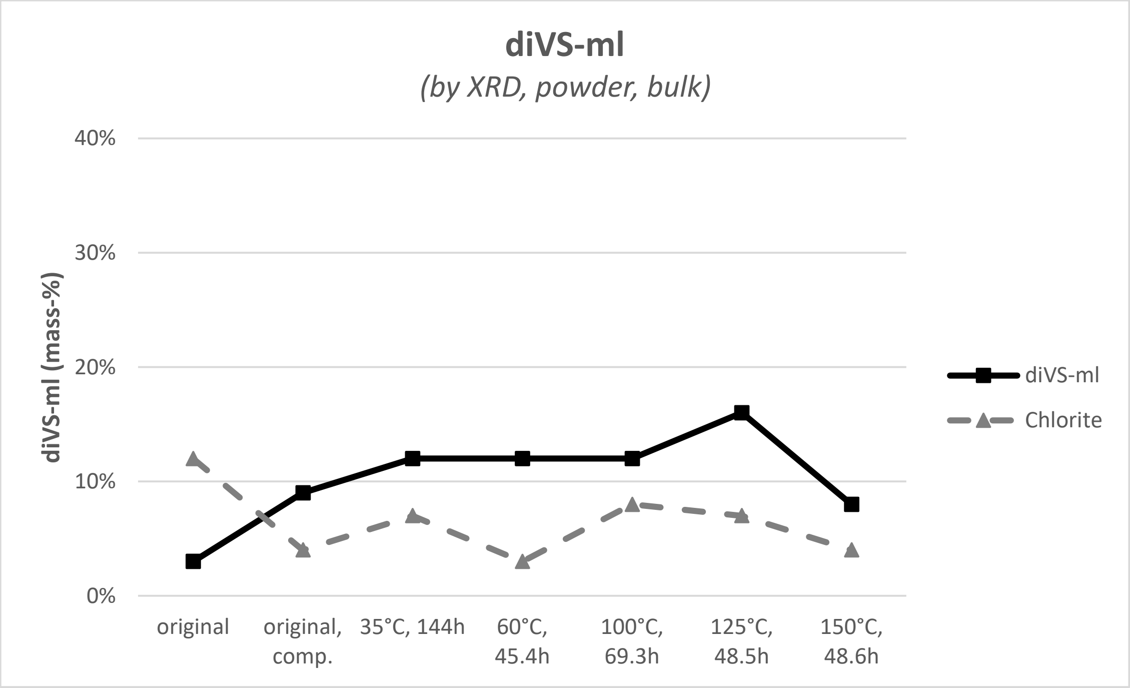

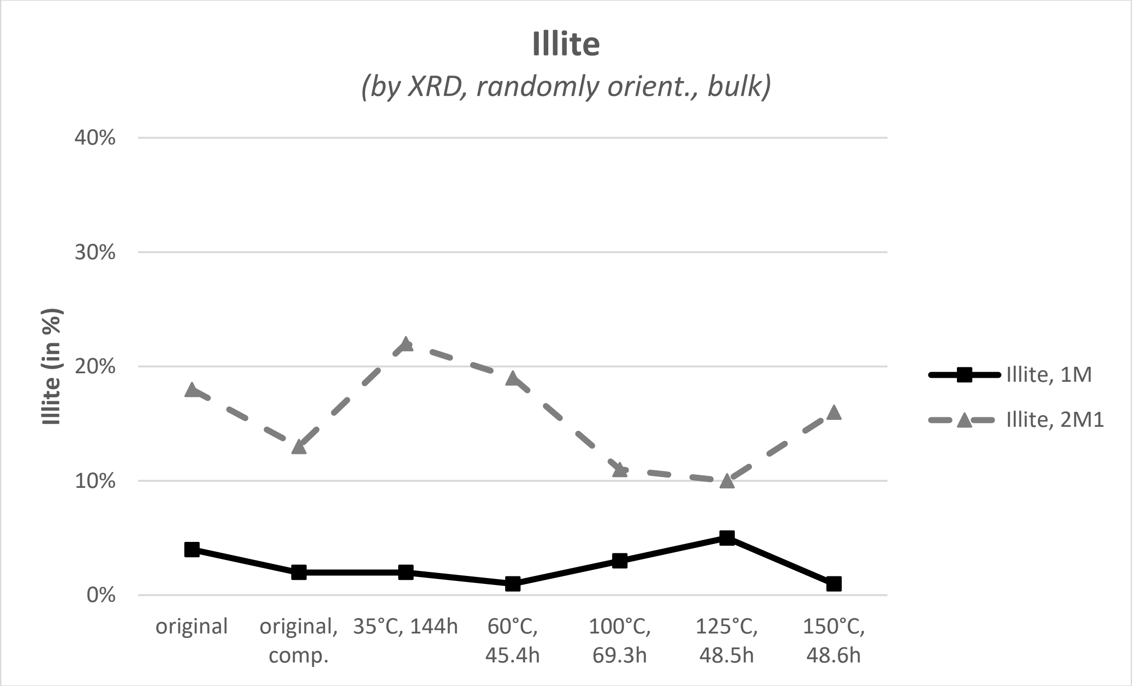
Illite
(by XRD, randomly orient., bulk)
Illite (in %)
40%
30%
20%
10%
0%
original
original, comp.
35°C, 144h
60°C, 45.4h
100°C, 69.3h
125°C, 48.5h
150°C, 48.6h
Illite, 1M
Illite, 2M1

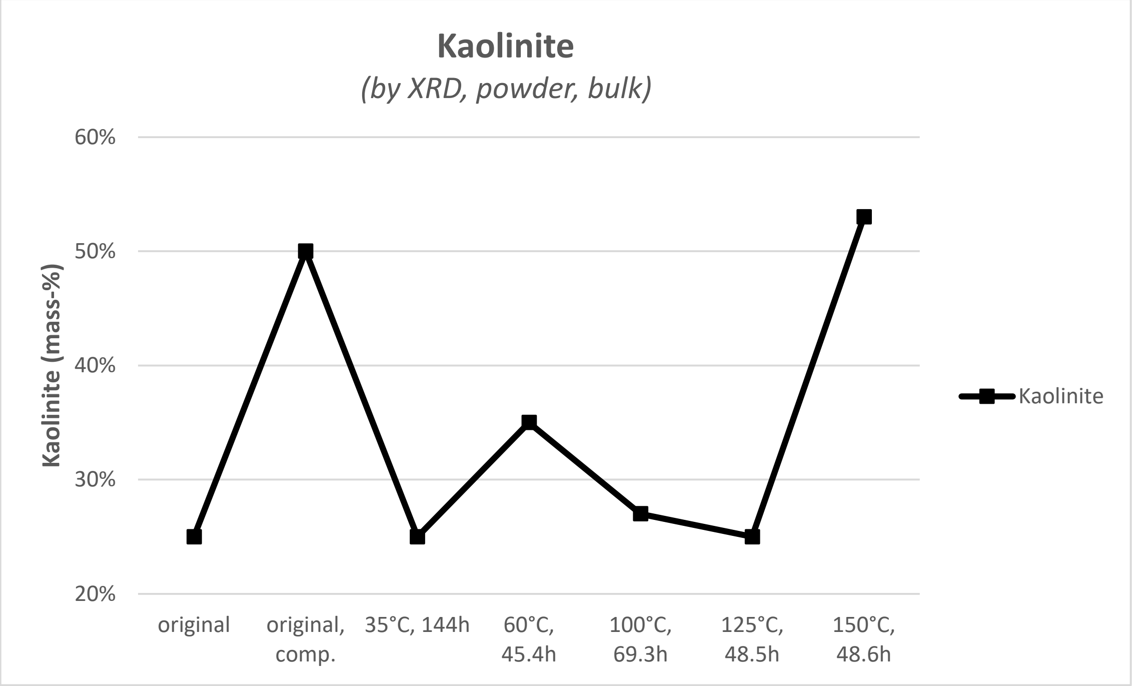
Kaolinite
(by XRD, powder, bulk)
Kaolinite (mass-%)
60%
50%
40%
30%
20%
original
original, comp.
35°C, 144h
60°C, 45.4h
100°C, 69.3h
125°C, 48.5h
150°C, 48.6h
Kaolinite

Data Sheet – B25 total (bulk), original material *(uncompacted)*

Sample Information

2020_017				
File Name	B25 - Total_R22.dia			
Instrument configuration	PW1830_TU Darmstadt_adopted.geq			
Wavelength	CU (1.5406 Å)			
Directory	C:/Users/kasbo/Documents/Data_Laptop/Profex_data/BGE_Project/random			
Date of Refinement	Freitag Mai 14, 2021			
Operator	kasbo			
Statistics	R_{wp} = 3.66	R_{exp} = 2.32	χ^2 = 2.4888	GoF = 1.5776

Diffraction Pattern

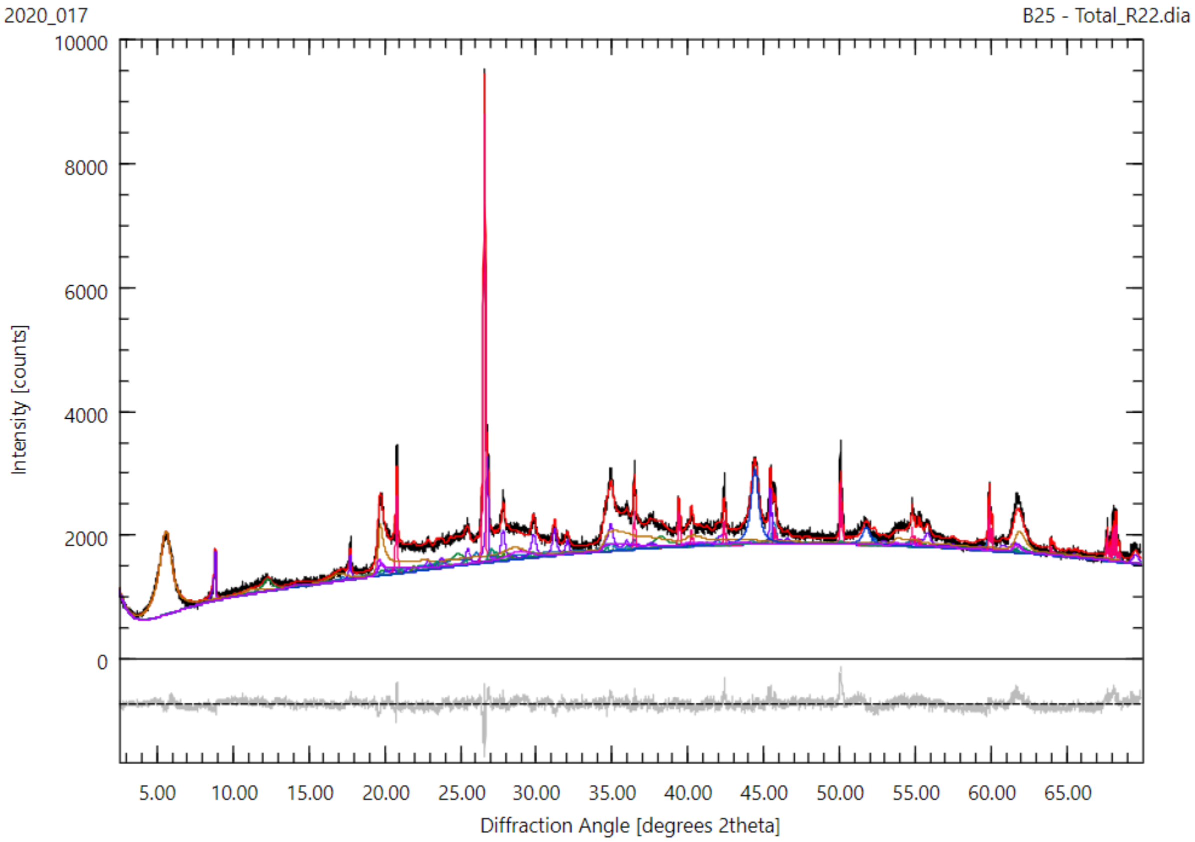

Data Sheet – B25 No4_T (bulk), treated material *(OPA, 35°C, 93.6 hours)*

Profex

Sample Information

No4-T-0				
File Name	No4-T_R01.dia			
Instrument configuration	D8_Advance_Sol-X_Darmstadt.geq			
Wavelength	CU (1.5406 Å)			
Directory	C:/Users/kasbo/Documents/Data_Laptop/Profex_data/BGE_Project/random			
Date of Refinement	Montag November 13, 2023			
Operator	kasbo			
Statistics	R_{wp} = 15.22	R_{exp} = 11.51	χ^2 = 1.7486	GoF = 1.3223

Diffraction Pattern

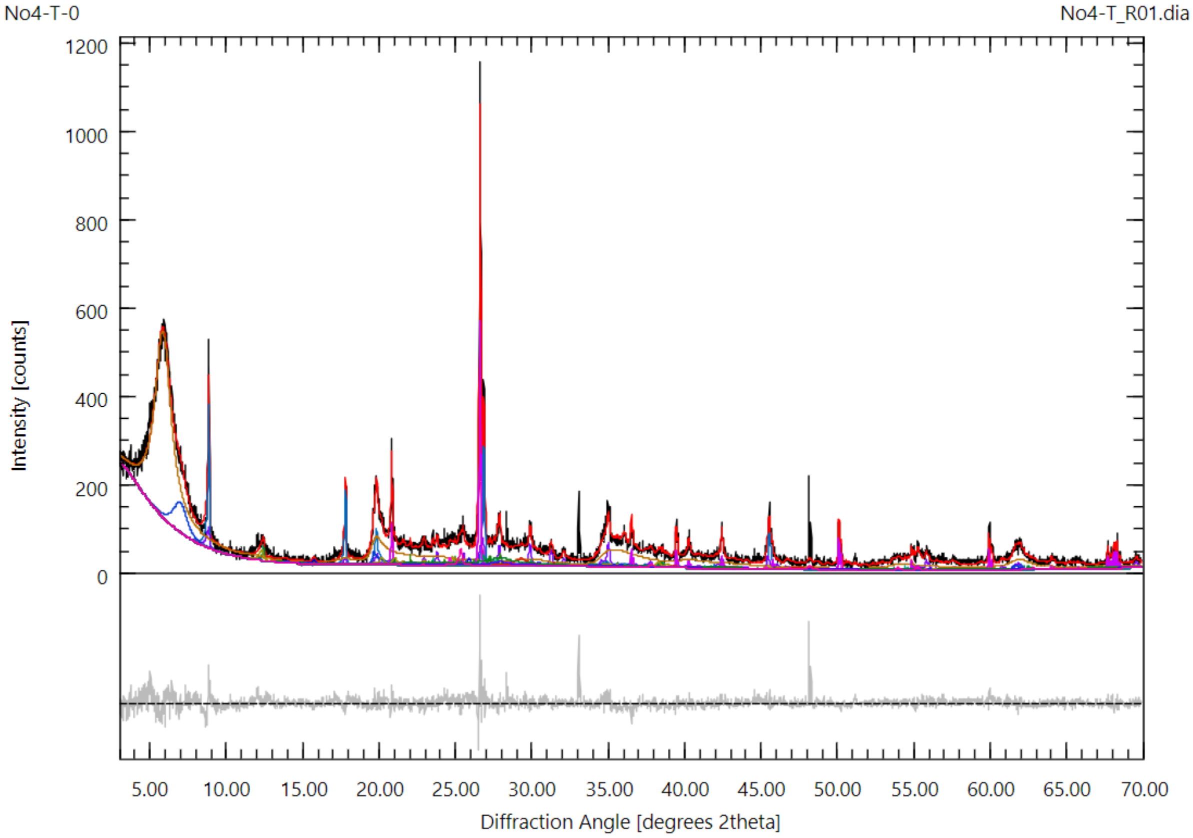

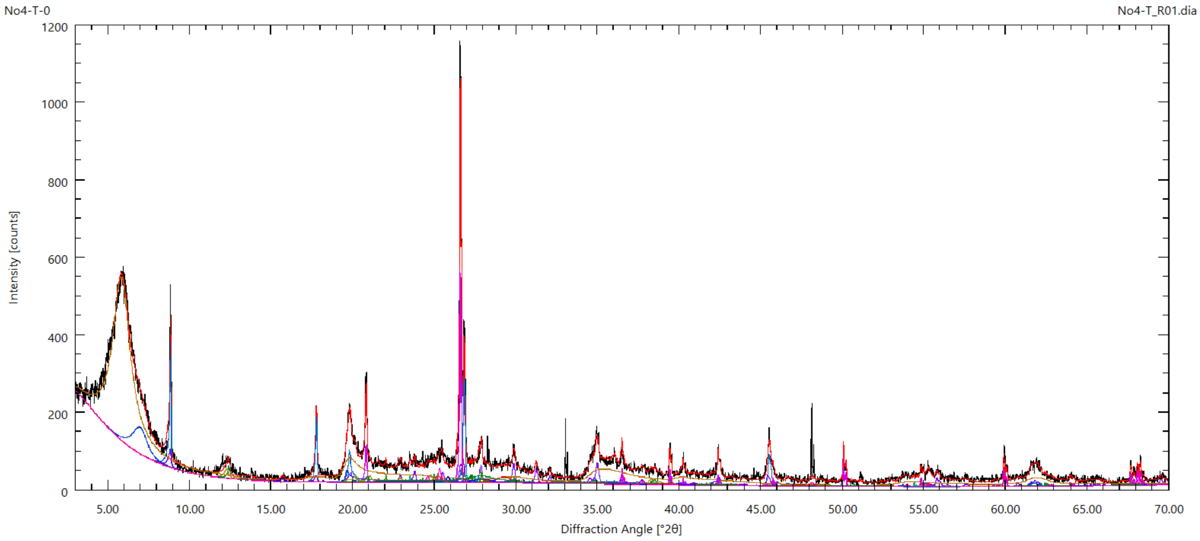
No4-T-0
No4-T_R01.dia
Intensity [counts]
1200
1000
800
600
400
200
0
5.00
10.00
15.00
20.00
25.00
30.00
35.00
40.00
45.00
50.00
55.00
60.00
65.00
70.00
Diffraction Angle [°2θ]

Data Sheet – B25 No4_C (bulk), treated material *(OPA, 35°C, 93.6 hours)*

Sample Information

No4-C-0				
File Name	No4-C_R01.dia			
Instrument configuration	D8_Advance_Sol-X_Darmstadt.geq			
Wavelength	CU (1.5406 Å)			
Directory	C:/Users/kasbo/Documents/Data_Laptop/Profex_data/BGE_Project/random			
Date of Refinement	Samstag Oktober 28, 2023			
Operator	kasbo			
Statistics	R_{wp} = 14.25	R_{exp} = 12.10	χ^2 = 1.3869	GoF = 1.1777

Diffraction Pattern

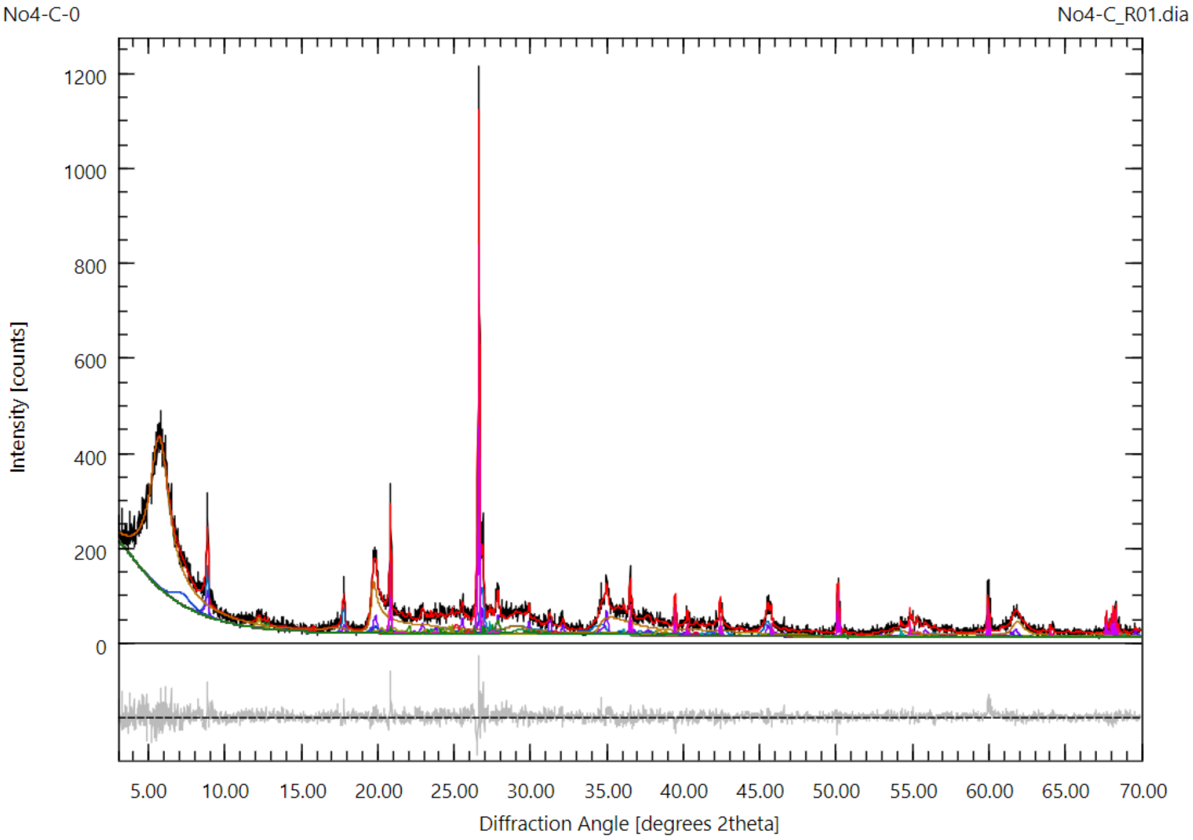

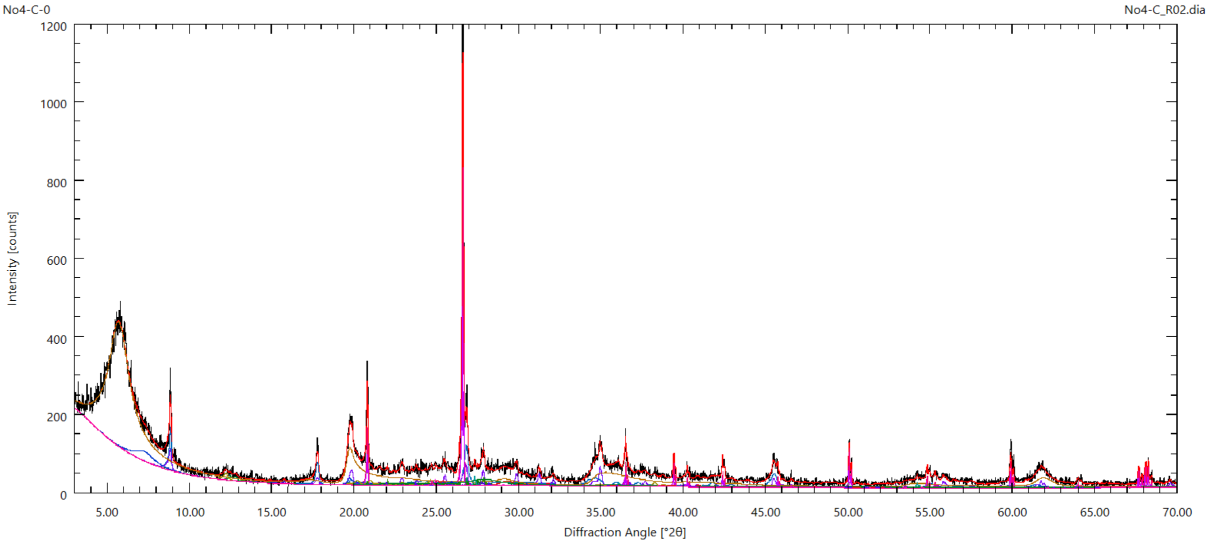
No4-C-0
No4-C_R02.dia
Intensity [counts]
0
200
400
600
800
1000
1200
5.00
10.00
15.00
20.00
25.00
30.00
35.00
40.00
45.00
50.00
55.00
60.00
65.00
70.00
Diffraction Angle [°2θ]

Data Sheet – B25 No4_B (bulk), treated material *(OPA, 35°C, 93.6 hours)*

Profex

Sample Information

No4-B-0				
File Name	No4-B_R01.dia			
Instrument configuration	D8_Advance_Sol-X_Darmstadt.geq			
Wavelength	CU (1.5406 Å)			
Directory	C:/Users/kasbo/Documents/Data_Laptop/Profex_data/BGE_Project/random			
Date of Refinement	Montag November 13, 2023			
Operator	kasbo			
Statistics	R_{wp} = 15.16	R_{exp} = 11.91	χ^2 = 1.6202	GoF = 1.2729

Diffraction Pattern

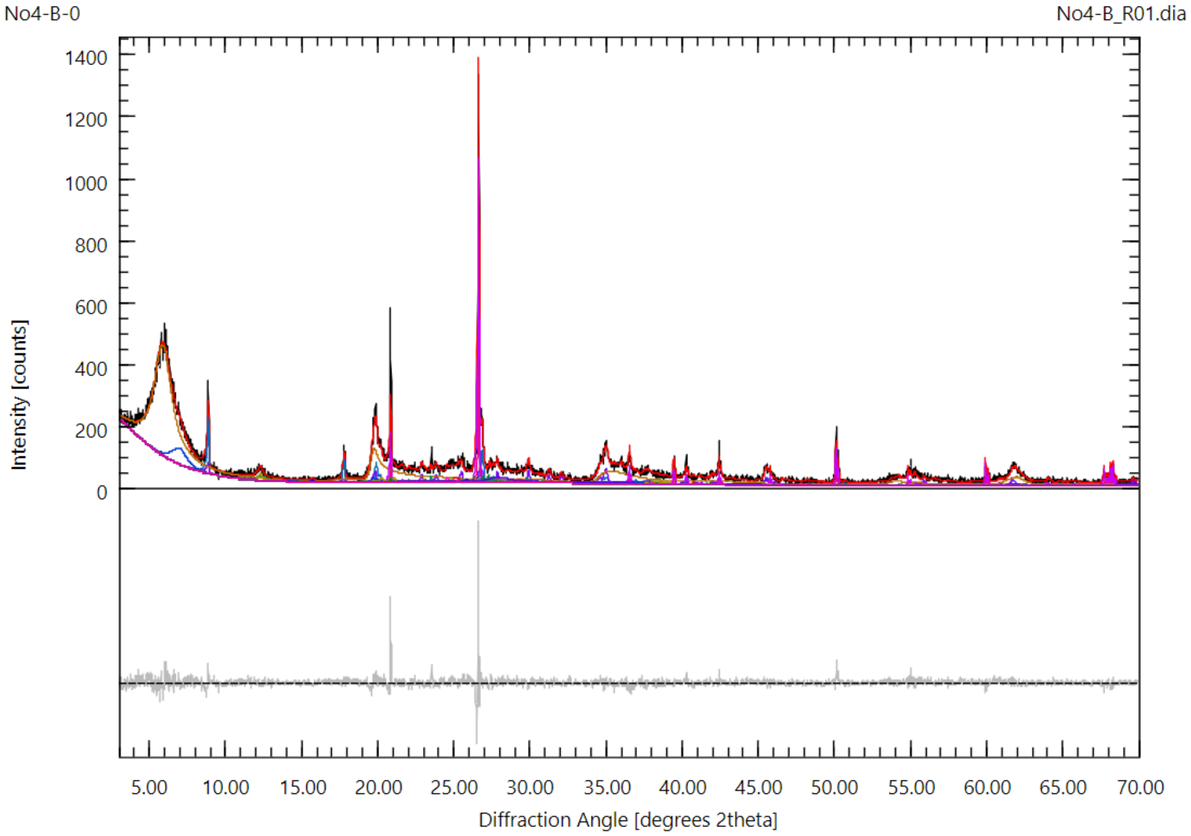

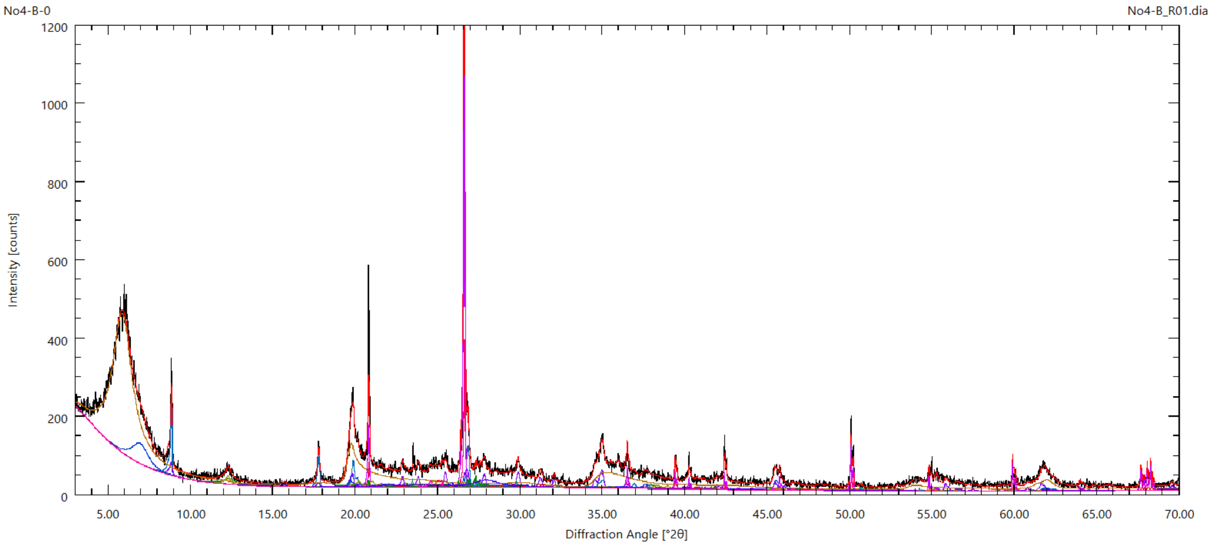
No4-B-0
No4-B_R01.dia
Intensity [counts]
0
200
400
600
800
1000
1200
5.00
10.00
15.00
20.00
25.00
30.00
35.00
40.00
45.00
50.00
55.00
60.00
65.00
70.00
Diffraction Angle [°2θ]

Data Sheet – B25 No23 (bulk), treated material *(OPA, 35°C, 285 h, 0.7 MPa)*

Sample Information

No23-0				
File Name	No-23-002-5s_R01.dia			
Instrument configuration	D8_Advance_Sol-X_Darmstadt.geq			
Wavelength	CU (1.5406 Å)			
Directory	C:/Users/kasbo/Documents/Data_Laptop/Profex_data/BGE_Project/random			
Date of Refinement	Sonntag November 26, 2023			
Operator	kasbo			
Statistics	R_{wp} = 16.34	R_{exp} = 12.60	χ^2 = 1.6818	GoF = 1.2968

Diffraction Pattern

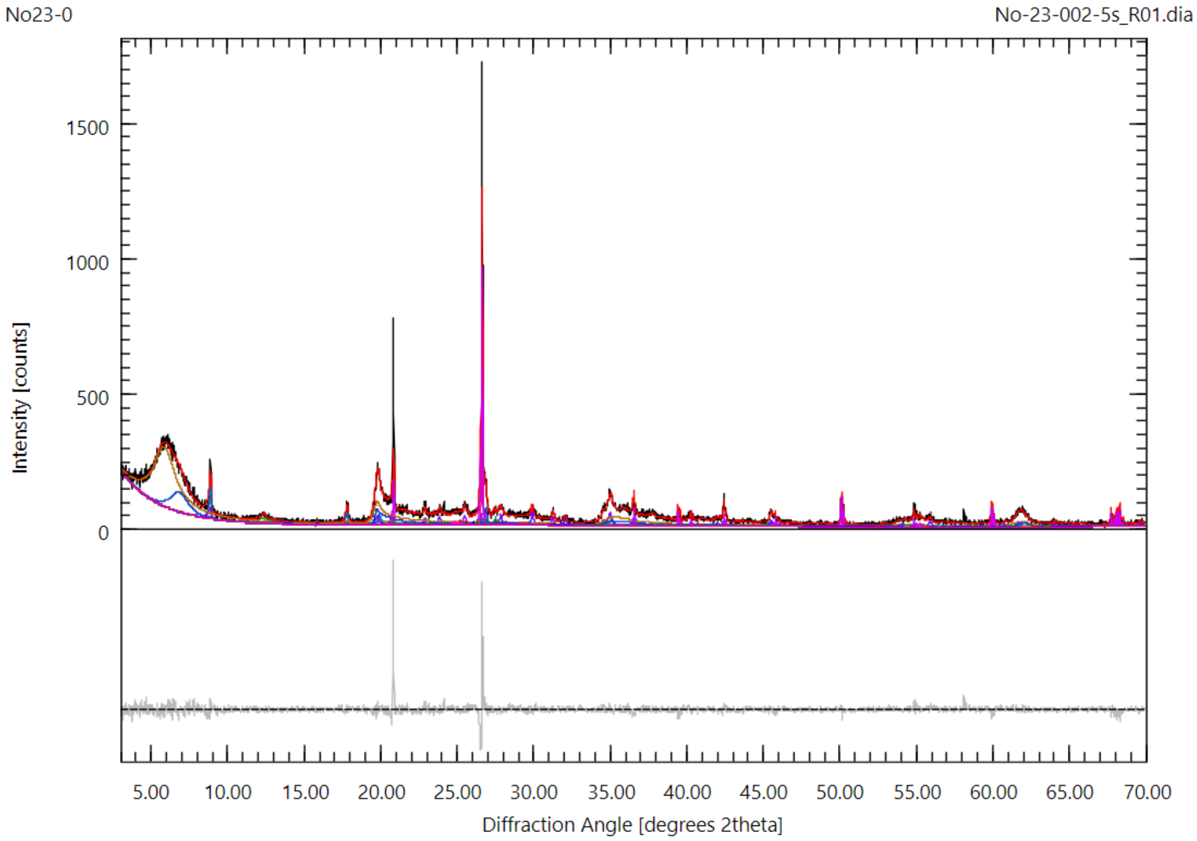

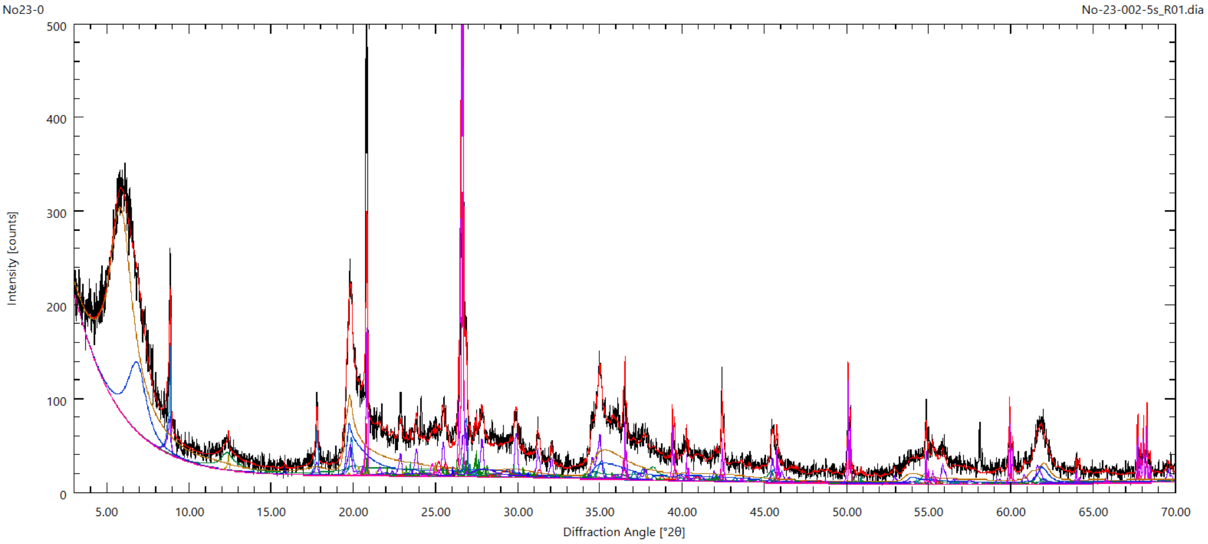
No23-0
No-23-002-5s_R01.dia
Intensity [counts]
500
400
300
200
100
0
5.00
10.00
15.00
20.00
25.00
30.00
35.00
40.00
45.00
50.00
55.00
60.00
65.00
70.00
Diffraction Angle [°2θ]

Data Sheet – B25 No5_T (bulk), treated material *(OPA, 60°C, 454 hours)*

Sample Information

No5_T				
File Name	No5-T_R03.dia			
Instrument configuration	D8_Advance_Sol-X_Darmstadt.geq			
Wavelength	CU (1.5406 Å)			
Directory	C:/Users/kasbo/Documents/Data_Laptop/Profex_data/BGE_Project/random			
Date of Refinement	Mittwoch November 01, 2023			
Operator	kasbo			
Statistics	R_{wp} = 20.12	R_{exp} = 11.78	χ^2 = 2.9172	GoF = 1.7080

Diffraction Pattern

No5_T

No5-T_R03.dia

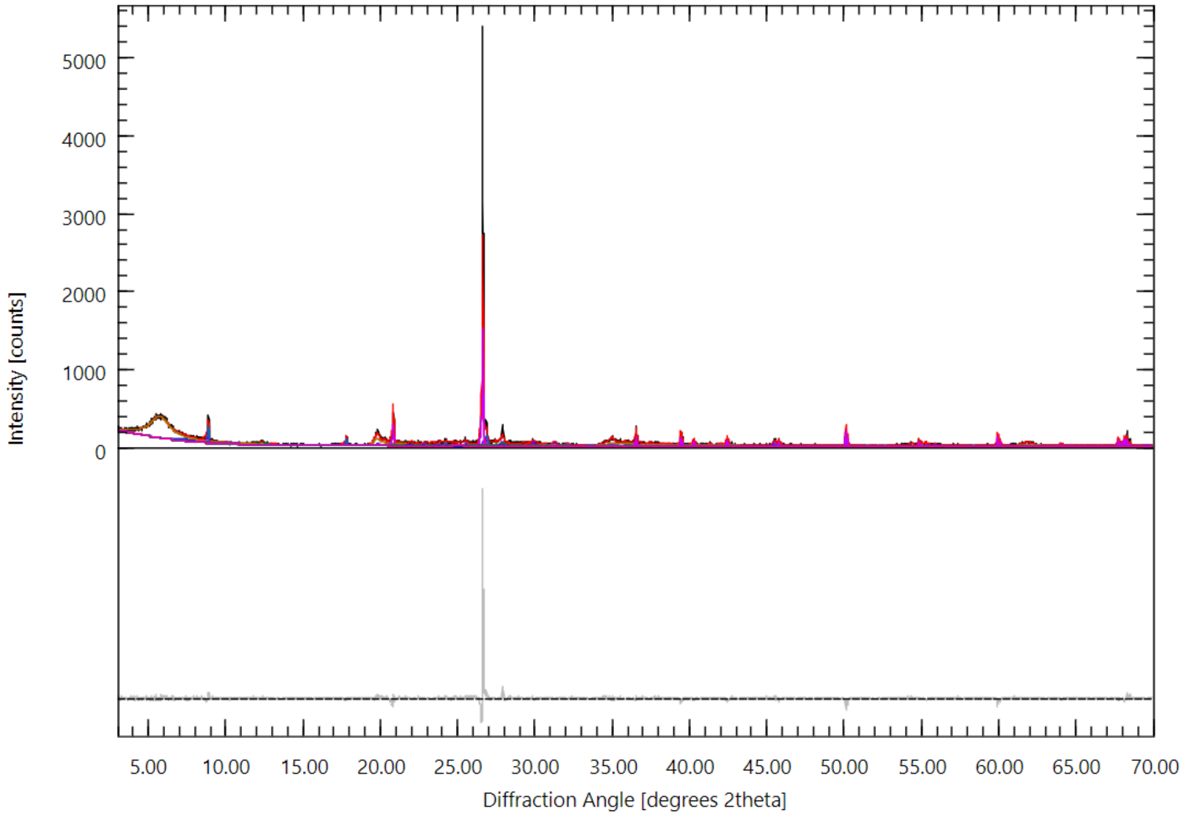

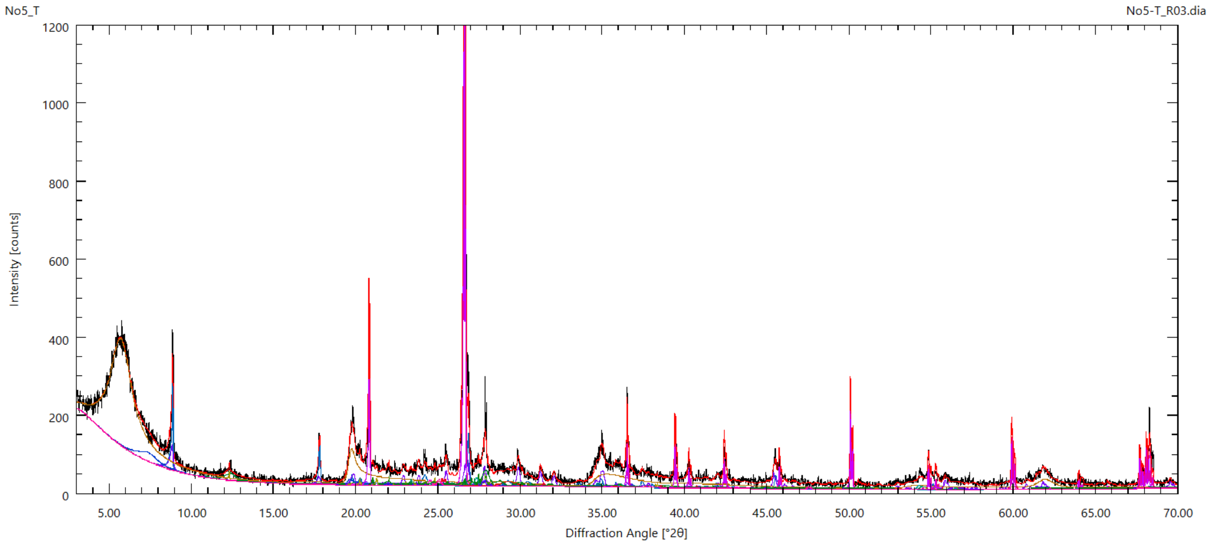
No5_T
No5-T_R03.dia
Intensity [counts]
1200
1000
800
600
400
200
0
5.00
10.00
15.00
20.00
25.00
30.00
35.00
40.00
45.00
50.00
55.00
60.00
65.00
70.00
Diffraction Angle [°2θ]

Data Sheet – B25 No5_C (bulk), treated material *(OPA, 60°C, 454 hours)*

Sample Information

No5-C-0				
File Name	No5-C_R02.dia			
Instrument configuration	D8_Advance_Sol-X_Darmstadt.geq			
Wavelength	CU (1.5406 Å)			
Directory	C:/Users/kasbo/Documents/Data_Laptop/Profex_data/BGE_Project/random			
Date of Refinement	Dienstag Oktober 31, 2023			
Operator	kasbo			
Statistics	R_{wp} = 17.76	R_{exp} = 11.15	χ^2 = 2.5371	GoF = 1.5928

Diffraction Pattern

No5-C-0

No5-C_R02.dia

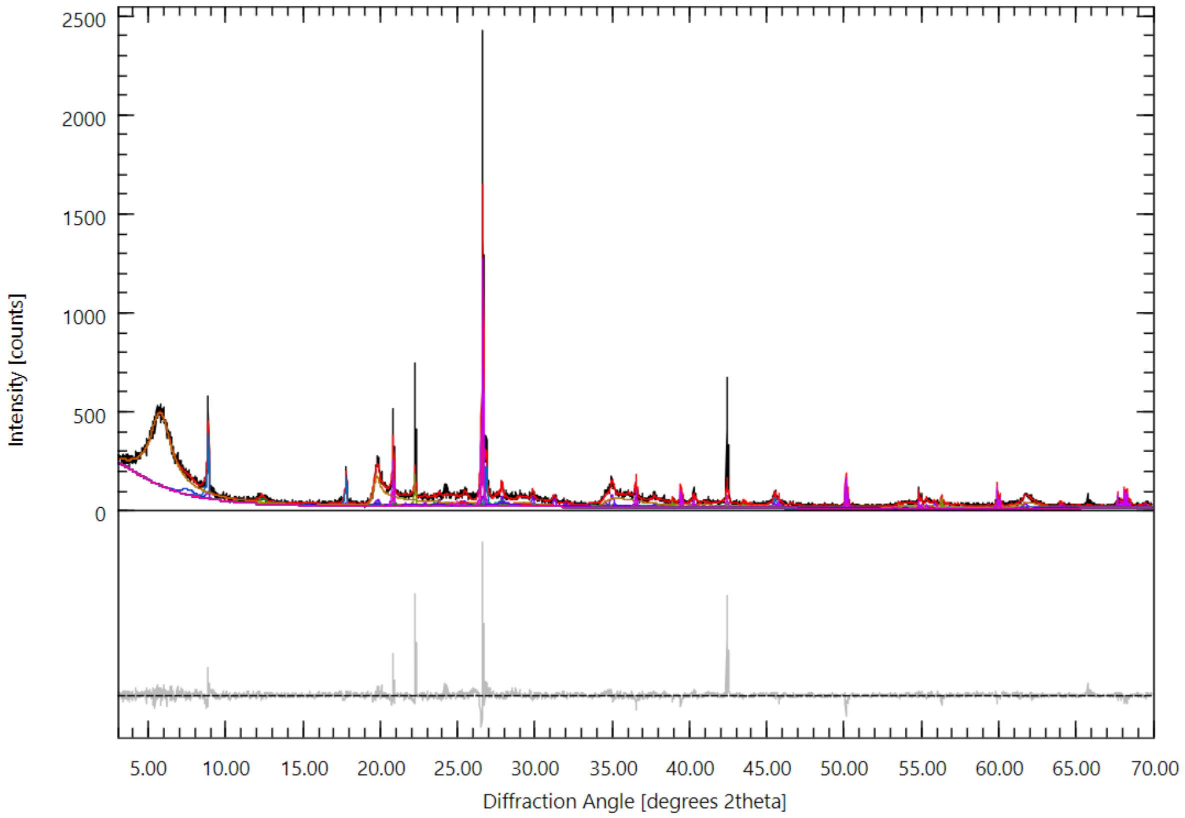

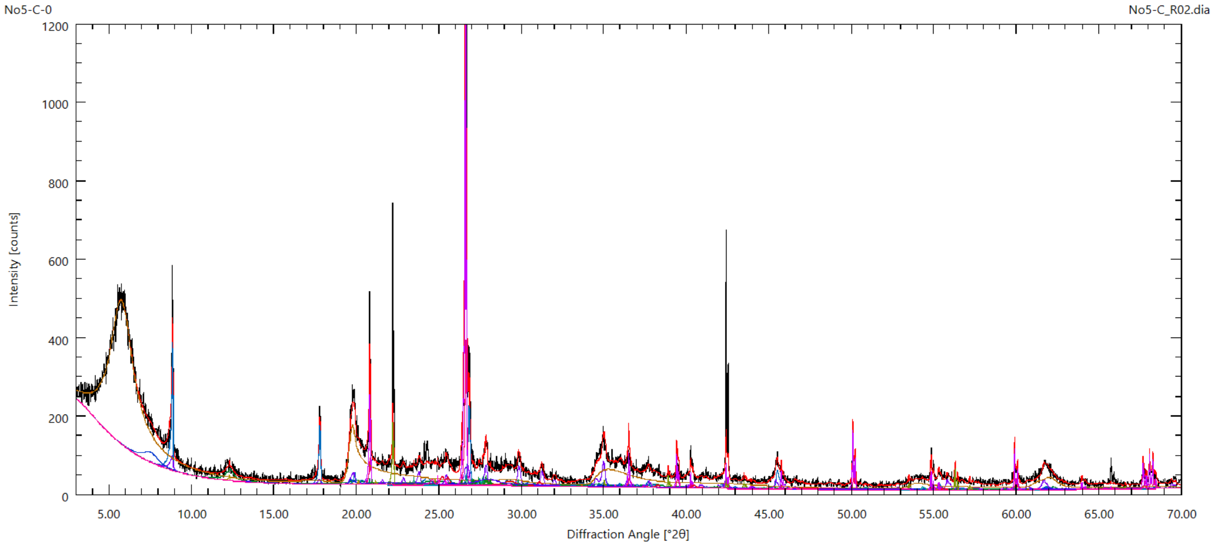
No5-C-0
No5-C_R02.dia
Intensity [counts]
0
200
400
600
800
1000
1200
5.00
10.00
15.00
20.00
25.00
30.00
35.00
40.00
45.00
50.00
55.00
60.00
65.00
70.00
Diffraction Angle [°2θ]

Data Sheet – B25 No5_B (bulk), treated material *(OPA, 60°C, 454 hours)*

Profex

Sample Information

No5-B-0				
File Name	No5-B_R02.dia			
Instrument configuration	D8_Advance_Sol-X_Darmstadt.geq			
Wavelength	CU (1.5406 Å)			
Directory	C:/Users/kasbo/Documents/Data_Laptop/Profex_data/BGE_Project/random			
Date of Refinement	Mittwoch November 01, 2023			
Operator	kasbo			
Statistics	R_{wp} = 16.33	R_{exp} = 11.67	χ^2 = 1.9581	GoF = 1.3993

Diffraction Pattern

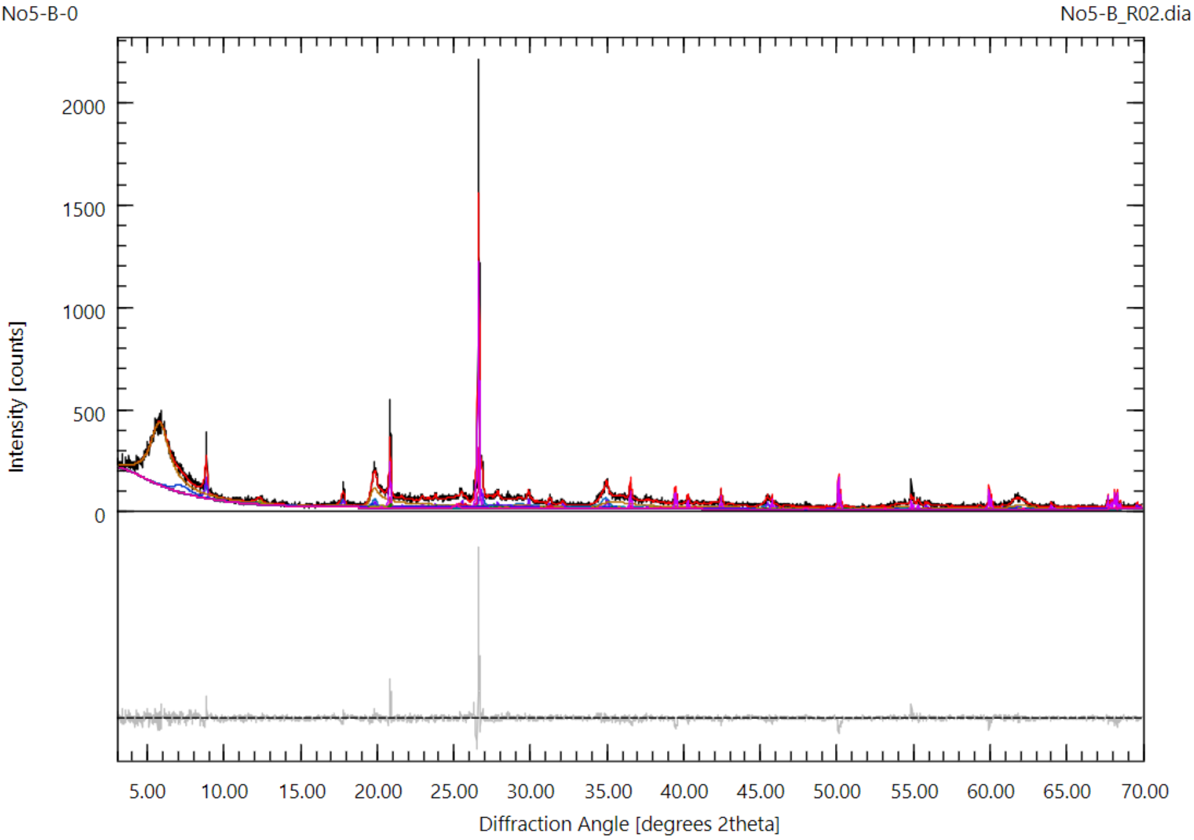

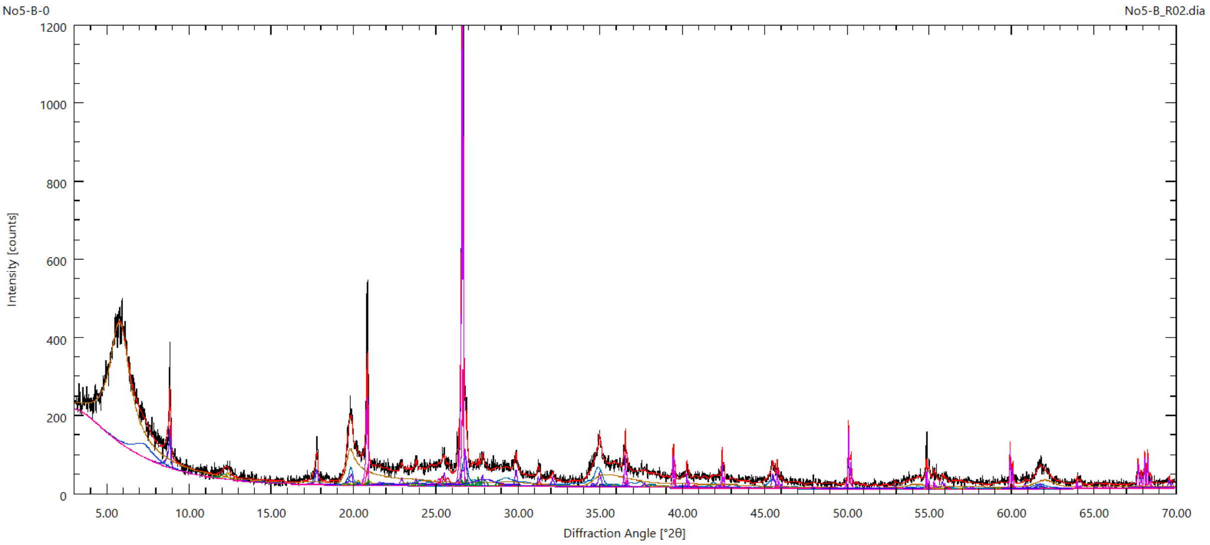
No5-B-0
No5-B_R02.dia
Intensity [counts]
0
200
400
600
800
1000
1200
5.00
10.00
15.00
20.00
25.00
30.00
35.00
40.00
45.00
50.00
55.00
60.00
65.00
70.00
Diffraction Angle [°2θ]

Data Sheet – B25 No0_T (bulk), treated material *(OPA, 100°C, 110 hours)*

Profex

Sample Information

No0-T-0				
File Name	No0-Top_T08.dia			
Instrument configuration	D8_Advance_Sol-X_Darmstadt.geq			
Wavelength	CU (1.5406 Å)			
Directory	C:/Users/kasbo/Documents/Data_Laptop/Profex_data/BGE_Project/random			
Date of Refinement	Sonntag November 05, 2023			
Operator	kasbo			
Statistics	R_{wp} = 14.24	R_{exp} = 8.21	χ^2 = 3.0084	GoF = 1.7345

Diffraction Pattern

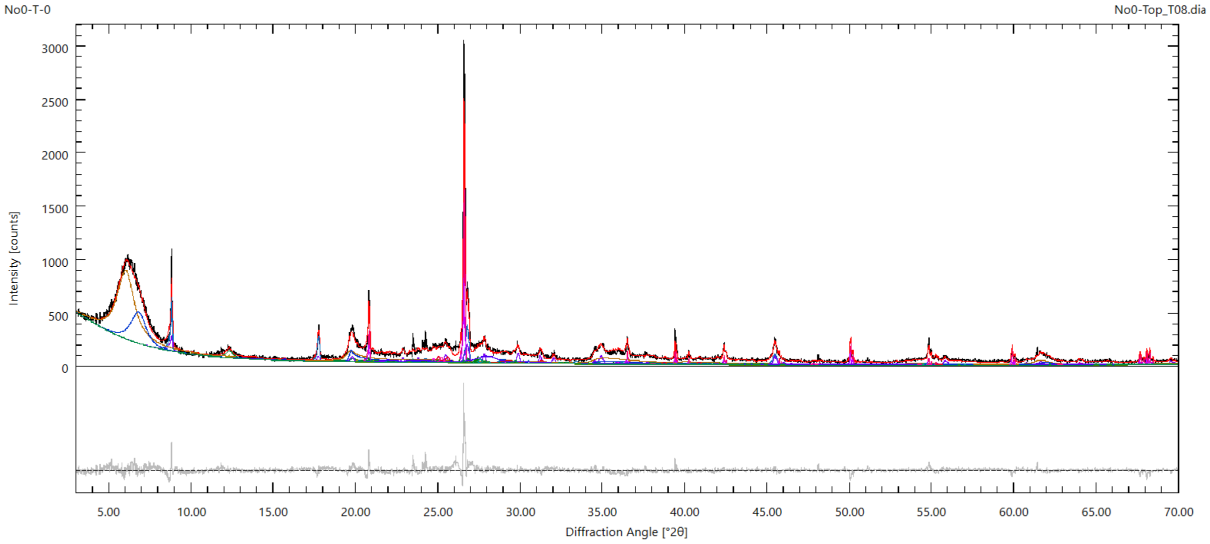

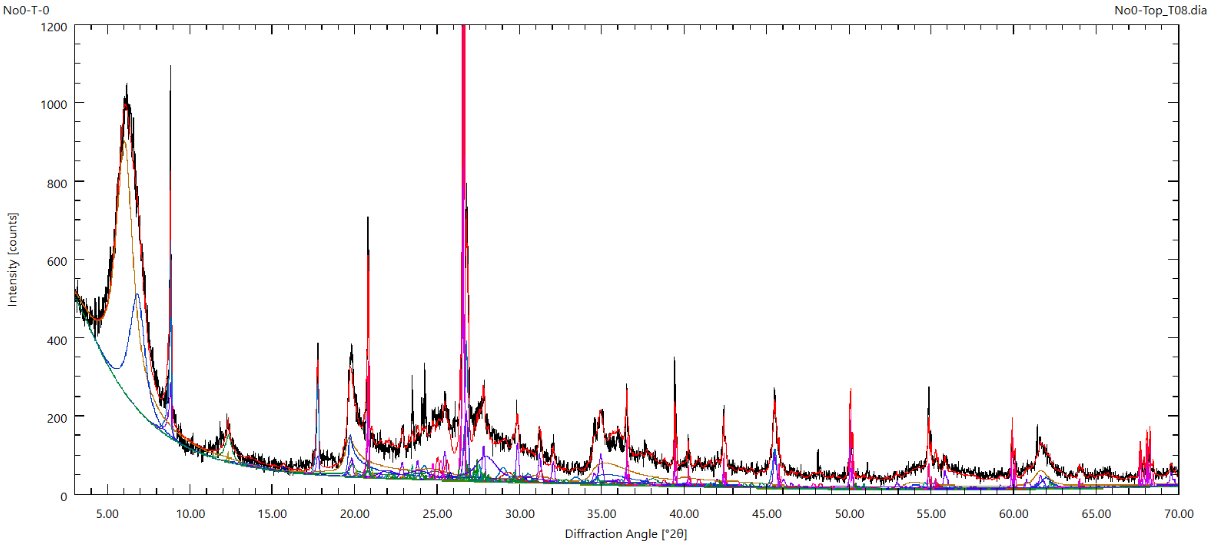
No0-T-0
No0-Top_T08.dia
Intensity [counts]
1200
1000
800
600
400
200
0
5.00
10.00
15.00
20.00
25.00
30.00
35.00
40.00
45.00
50.00
55.00
60.00
65.00
70.00
Diffraction Angle [°2θ]

Data Sheet – B25 No0_C (bulk), treated material *(OPA, 100°C, 110 hours)*

Profex

Sample Information

No0-C-0				
File Name	No0-C_enter_T07.dia			
Instrument configuration	D8_Advance_Sol-X_Darmstadt.geq			
Wavelength	CU (1.5406 Å)			
Directory	C:/Users/kasbo/Documents/Data_Laptop/Profex_data/BGE_Project/random			
Date of Refinement	Montag November 06, 2023			
Operator	kasbo			
Statistics	R_{wp} = 15.33	R_{exp} = 9.08	χ^2 = 2.8504	GoF = 1.6883

Diffraction Pattern

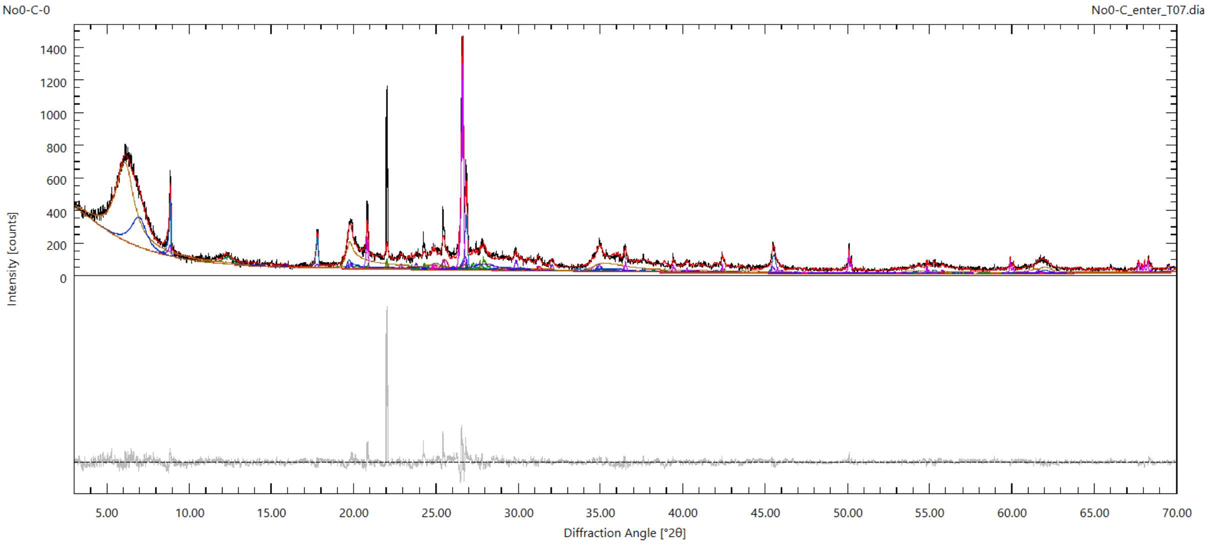

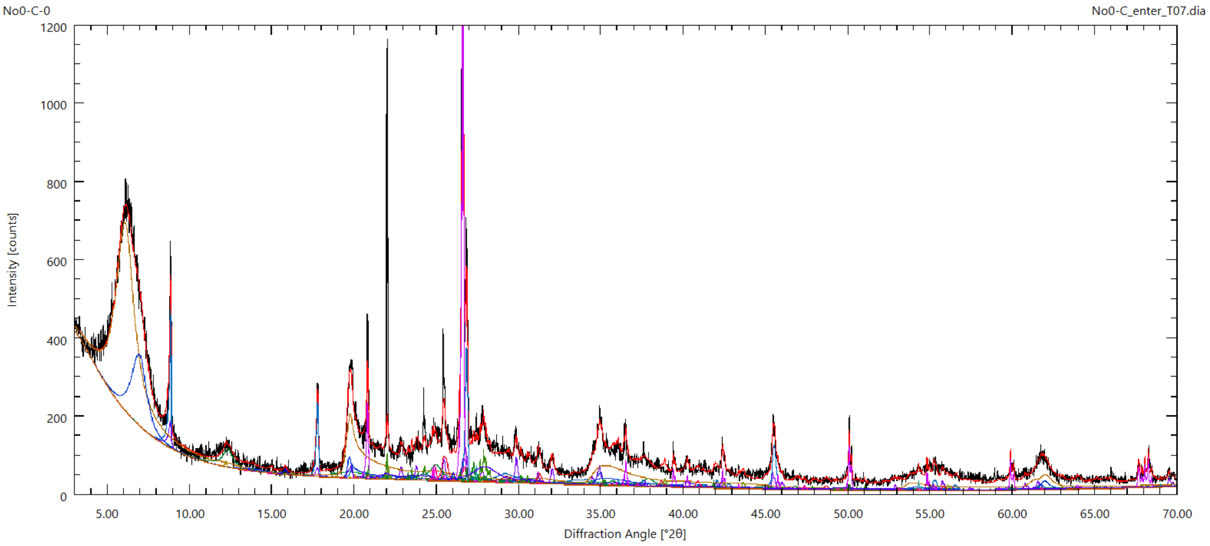
No0-C-0
No0-C_enter_T07.dia
Intensity [counts]
0
200
400
600
800
1000
1200
5.00
10.00
15.00
20.00
25.00
30.00
35.00
40.00
45.00
50.00
55.00
60.00
65.00
70.00
Diffraction Angle [°2θ]

Data Sheet – B25 No0_B (bulk), treated material *(OPA, 100°C, 110 hours)*

Profex

Sample Information

No0-B -0				
File Name	No0-B_ottom_T06.dia			
Instrument configuration	D8_Advance_Sol-X_Darmstadt.geq			
Wavelength	CU (1.5406 Å)			
Directory	C:/Users/kasbo/Documents/Data_Laptop/Profex_data/BGE_Project/random			
Date of Refinement	Sonntag November 05, 2023			
Operator	kasbo			
Statistics	R_{wp} = 13.60	R_{exp} = 11.84	χ^2 = 1.3194	GoF = 1.1486

Diffraction Pattern

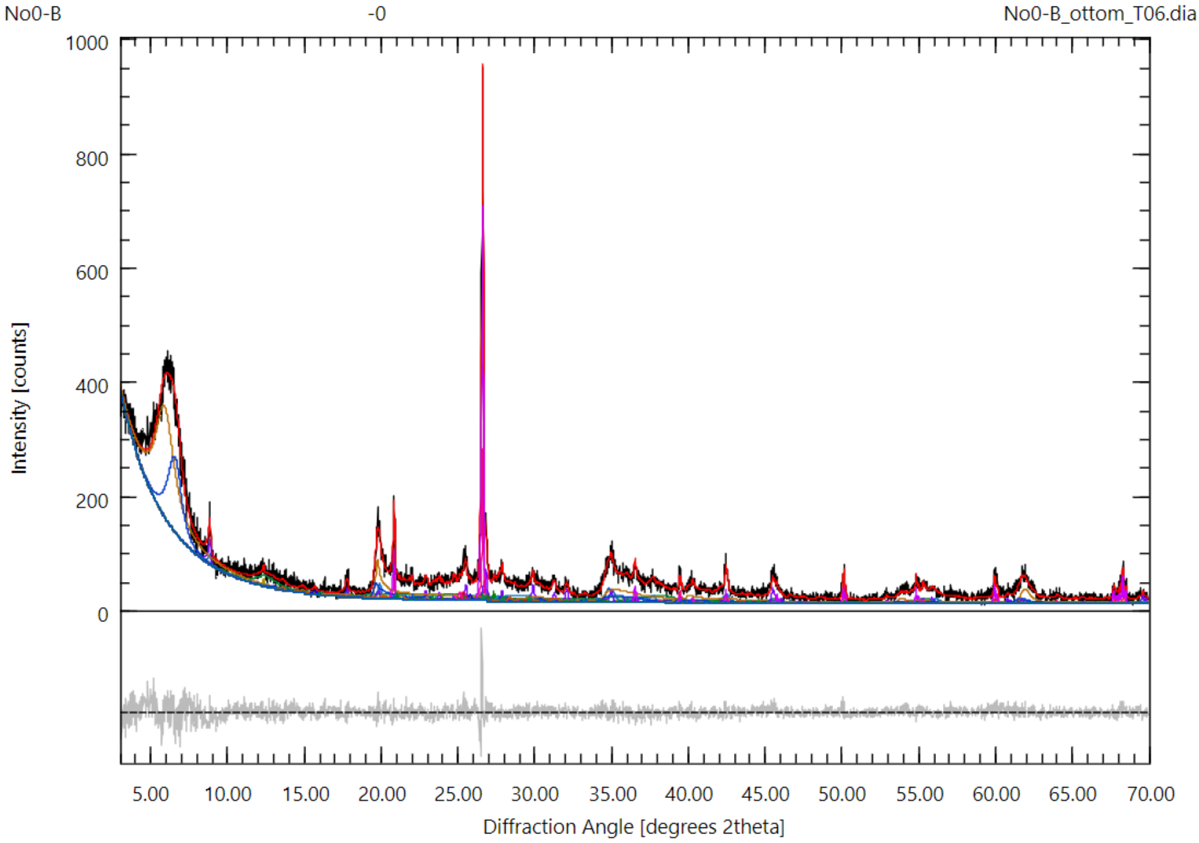

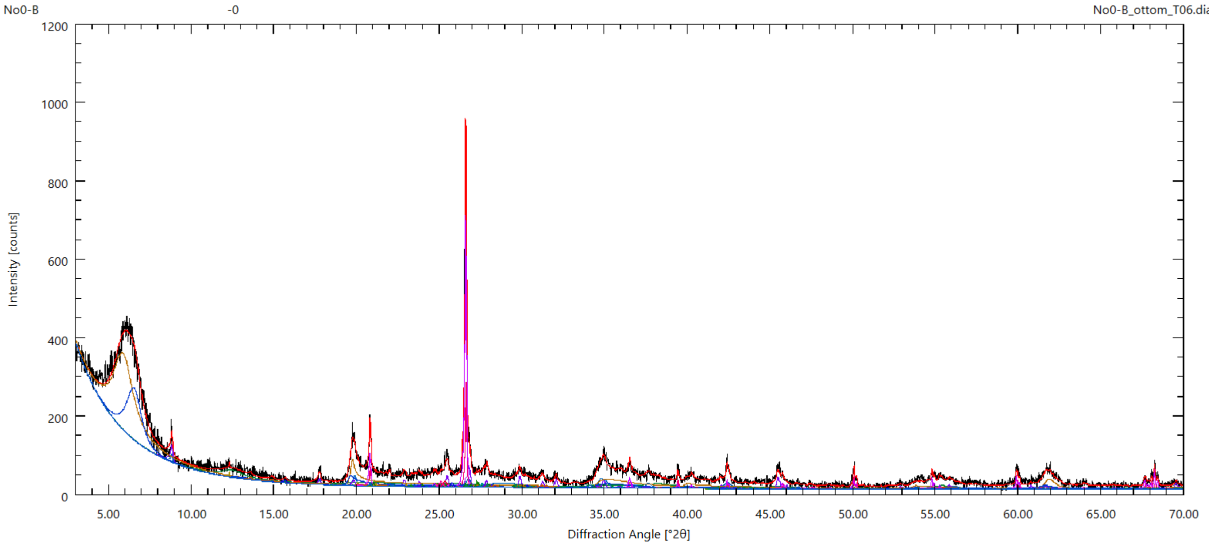
No0-B
-0
No0-B_ottom_T06.dia
Intensity [counts]
1200
1000
800
600
400
200
0
5.00
10.00
15.00
20.00
25.00
30.00
35.00
40.00
45.00
50.00
55.00
60.00
65.00
70.00
Diffraction Angle [°2θ]

Data Sheet – B25 No2_T (bulk), treated material *(OPA, 100°C, 35 days)*

Profex

Sample Information

No2-T-0				
File Name	No2-T_op_T08.dia			
Instrument configuration	D8_Advance_Sol-X_Darmstadt.geq			
Wavelength	CU (1.5406 Å)			
Directory	C:/Users/kasbo/Documents/Data_Laptop/Profex_data/BGE_Project/random			
Date of Refinement	Montag November 06, 2023			
Operator	kasbo			
Statistics	R_{wp} = 13.10	R_{exp} = 8.26	χ^2 = 2.5153	GoF = 1.5860

Diffraction Pattern

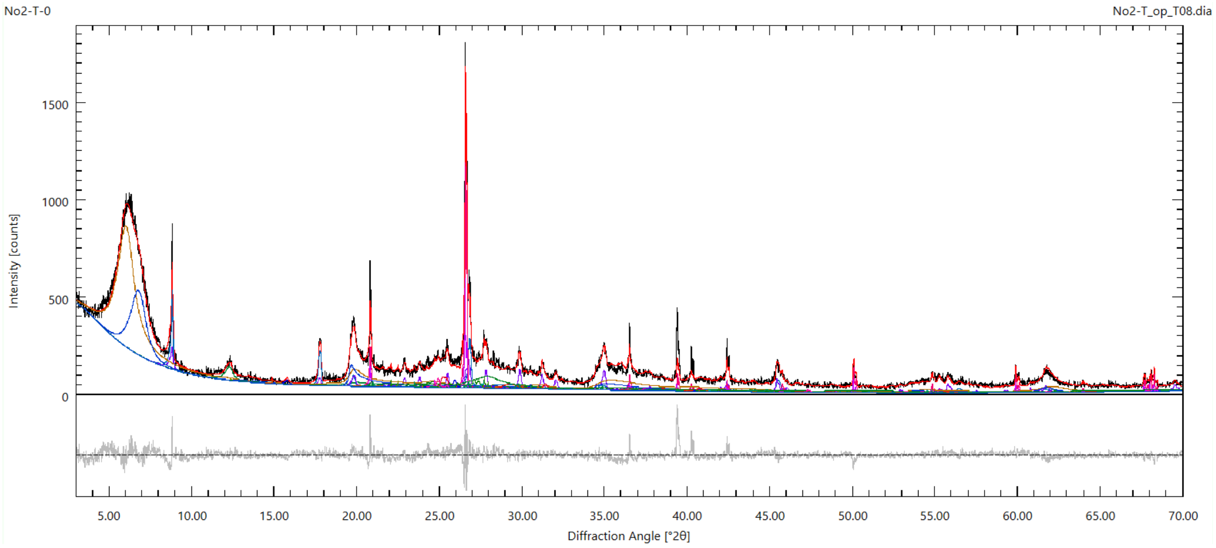

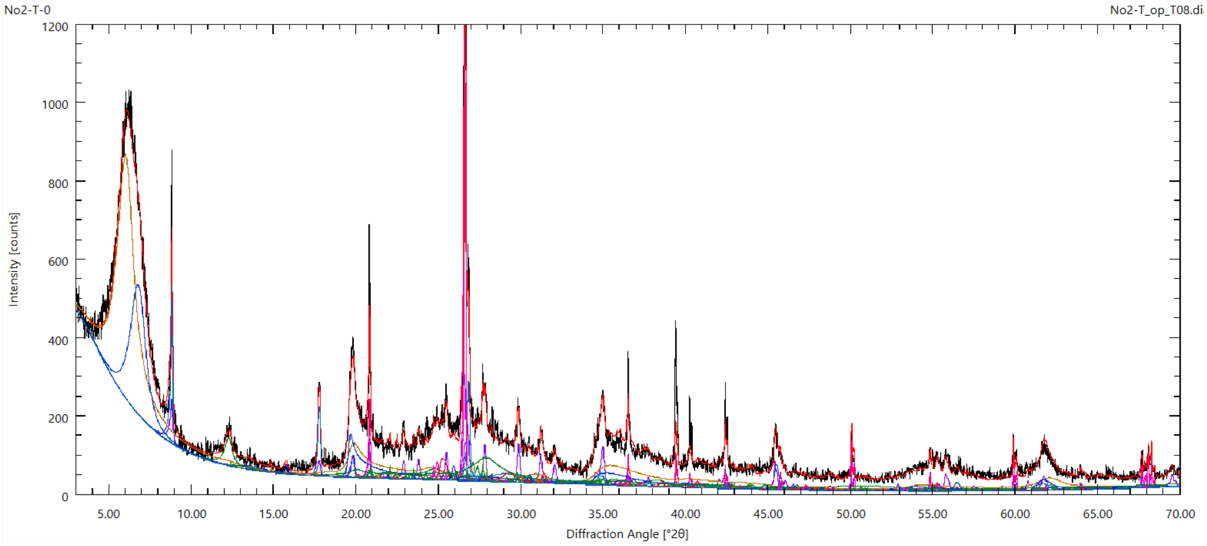
No2-T-0
No2-T_op_T08.di
Intensity [counts]
0
200
400
600
800
1000
1200
5.00
10.00
15.00
20.00
25.00
30.00
35.00
40.00
45.00
50.00
55.00
60.00
65.00
70.00
Diffraction Angle [°2θ]

Data Sheet – B25 No2_C (bulk), treated material *(OPA, 100°C, 35 days)*

Profex

Sample Information

No2-C-0				
File Name	No2-C_RP_R01.dia			
Instrument configuration	D8_Advance_Sol-X_Darmstadt.geq			
Wavelength	CU (1.5406 Å)			
Directory	C:/Users/kasbo/Documents/Data_Laptop/Profex_data/BGE_Project/random			
Date of Refinement	Dienstag Januar 30, 2024			
Operator	kasbo			
Statistics	R_{wp} = 12.46	R_{exp} = 7.95	χ^2 = 2.4564	GoF = 1.5673

Diffraction Pattern

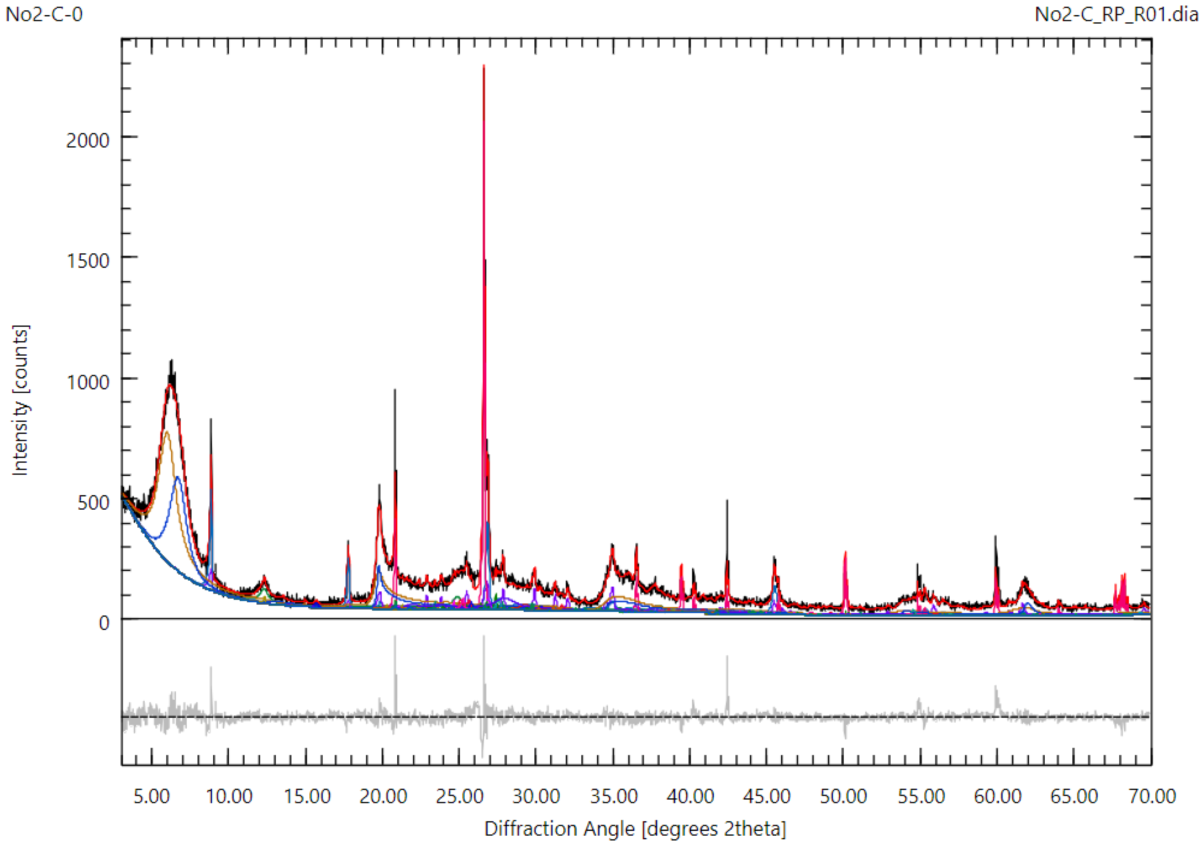

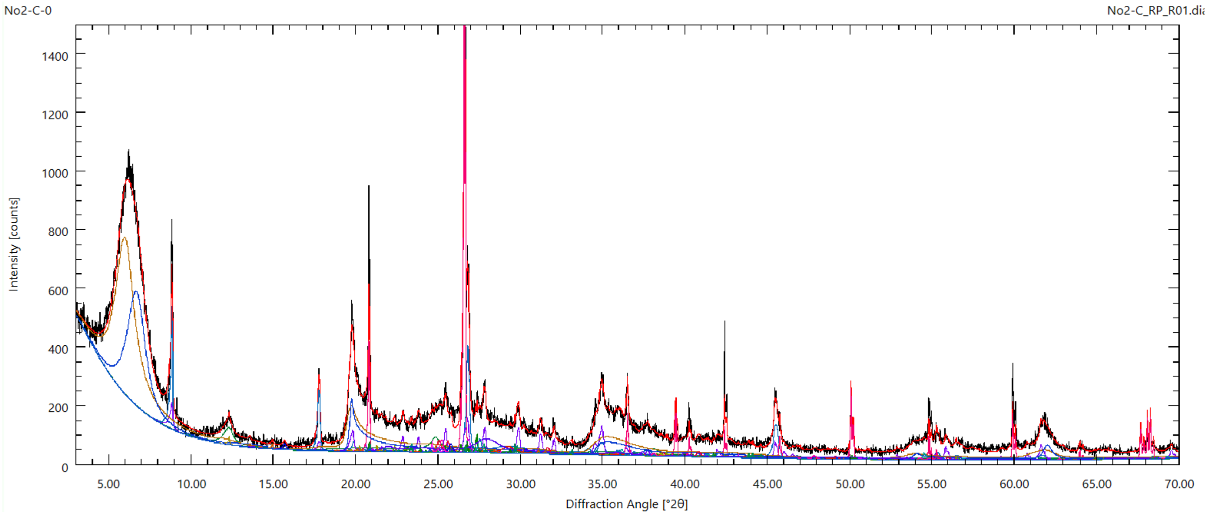
No2-C-0
No2-C_RP_R01.dia
Intensity [counts]
1400
1200
1000
800
600
400
200
0
5.00
10.00
15.00
20.00
25.00
30.00
35.00
40.00
45.00
50.00
55.00
60.00
65.00
70.00
Diffraction Angle [°2θ]

Data Sheet – B25 No2_B (bulk), treated material *(OPA, 100°C, 35 days)*

Sample Information

No2-B-0				
File Name	No2-B_ottom_T05.dia			
Instrument configuration	D8_Advance_Sol-X_Darmstadt.geq			
Wavelength	CU (1.5406 Å)			
Directory	C:/Users/kasbo/Documents/Data_Laptop/Profex_data/BGE_Project/random			
Date of Refinement	Montag November 06, 2023			
Operator	kasbo			
Statistics	R_{wp} = 12.88	R_{exp} = 8.91	χ^2 = 2.0897	GoF = 1.4456

Diffraction Pattern

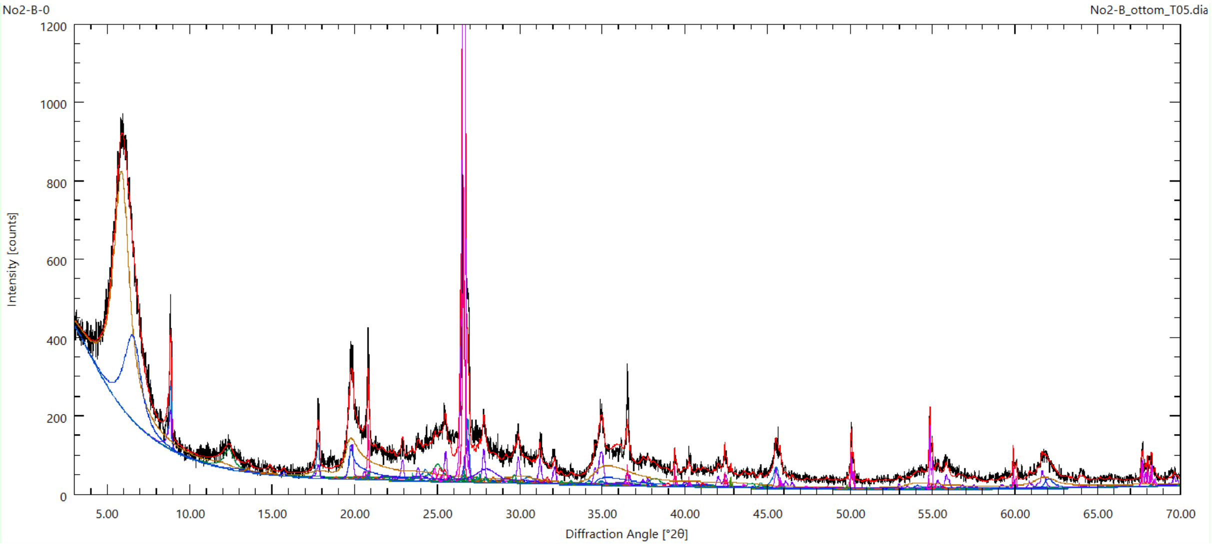

Data Sheet – B25 No15 (bulk), treated material *(OPA, 125°C, 98.6 h)*

Sample Information

No15-0				
File Name	No15_B25+125°C-VersuchD_R05.dia			
Instrument configuration	D8_Advance_Sol-X_Darmstadt.geq			
Wavelength	CU (1.5406 Å)			
Directory	C:/Users/kasbo/Documents/Data_Laptop/Profex_data/BGE_Project/random			
Date of Refinement	Mittwoch November 01, 2023			
Operator	kasbo			
Statistics	R_{wp} = 15.14	R_{exp} = 11.71	χ^2 = 1.6716	GoF = 1.2929

Diffraction Pattern

No15-0 No15_B25+125°C-VersuchD_R05.dia

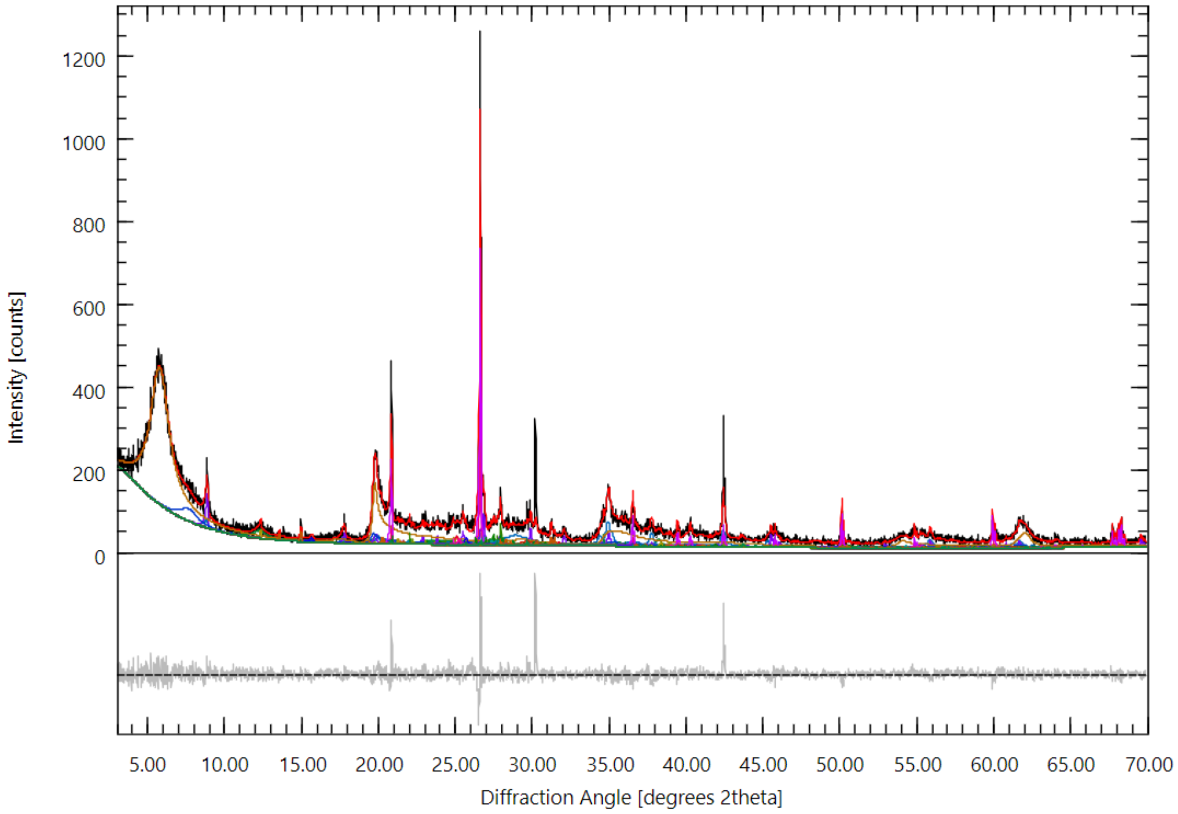

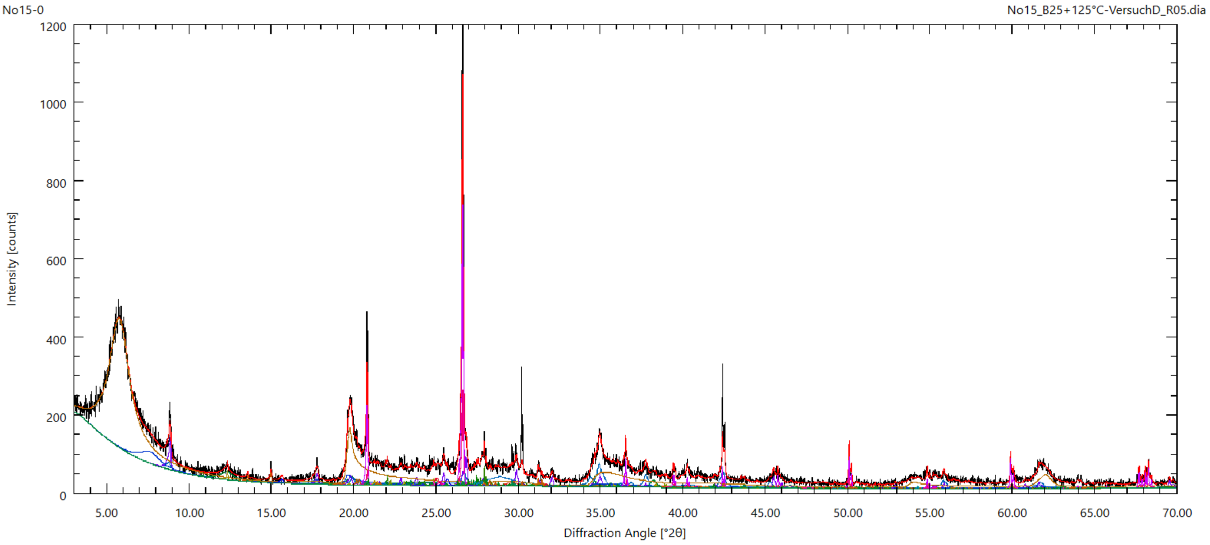
No15-0
No15_B25+125°C-VersuchD_R05.dia
Intensity [counts]
1200
1000
800
600
400
200
0
5.00
10.00
15.00
20.00
25.00
30.00
35.00
40.00
45.00
50.00
55.00
60.00
65.00
70.00
Diffraction Angle [°2θ]

Data Sheet – B25 No3_T (bulk), treated material *(OPA, 150°C, 96 h)*

Profex

Sample Information

No3-T-0				
File Name	No3-T_RD_R01.dia			
Instrument configuration	D8_Advance_Sol-X_Darmstadt.geq			
Wavelength	CU (1.5406 Å)			
Directory	C:/Users/kasbo/Documents/Data_Laptop/Profex_data/BGE_Project/random			
Date of Refinement	Montag Januar 29, 2024			
Operator	kasbo			
Statistics	R_{wp} = 13.39	R_{exp} = 8.20	χ^2 = 2.6665	GoF = 1.6329

Diffraction Pattern

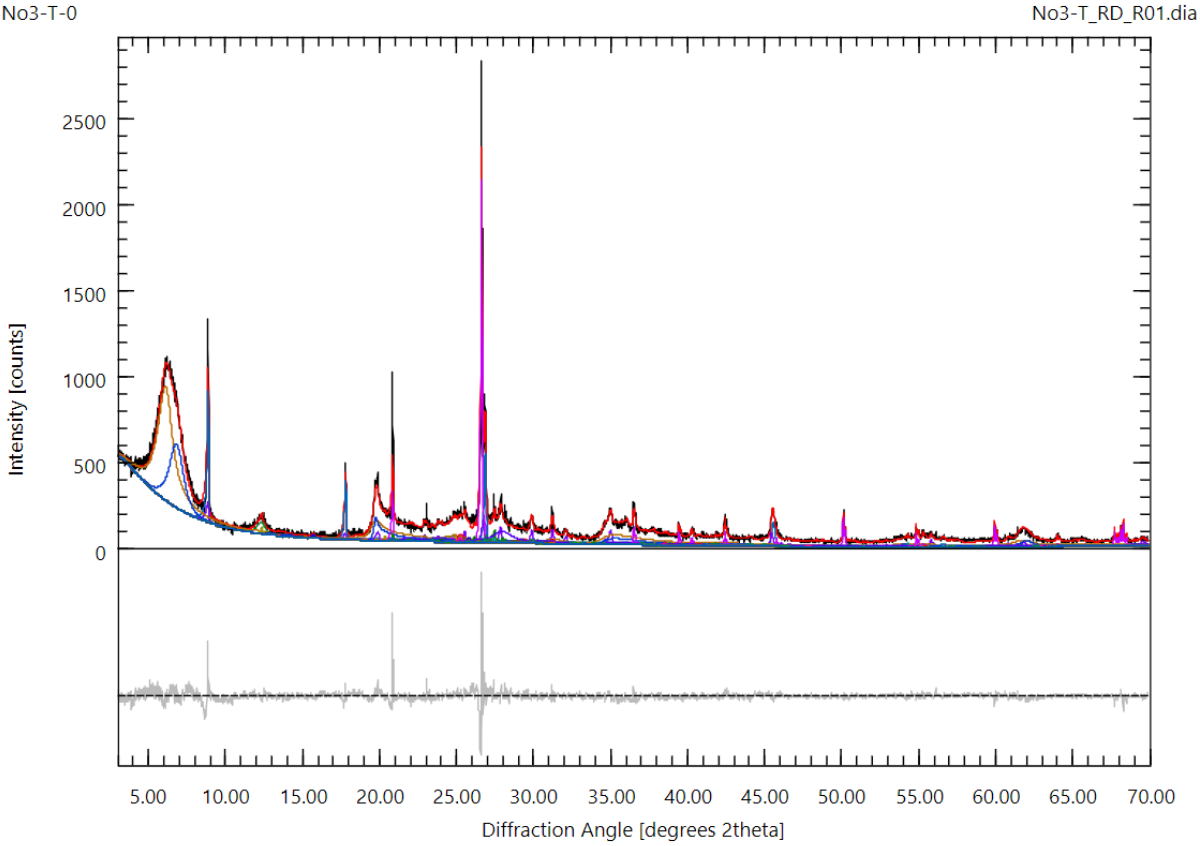

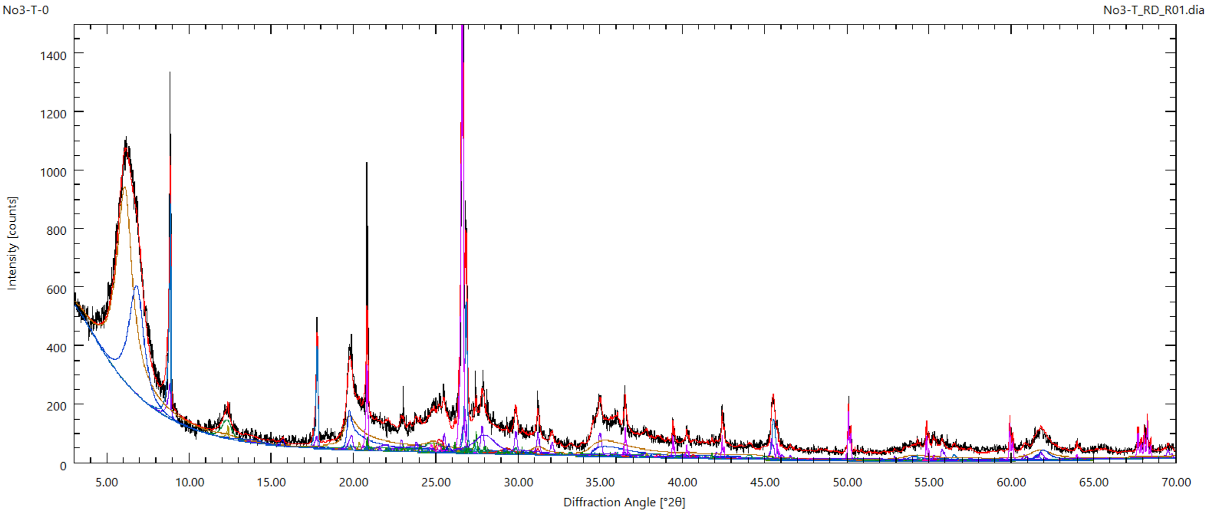
No3-T-0
No3-T_RD_R01.dia
Intensity [counts]
0
200
400
600
800
1000
1200
1400
5.00
10.00
15.00
20.00
25.00
30.00
35.00
40.00
45.00
50.00
55.00
60.00
65.00
70.00
Diffraction Angle [°2θ]

Data Sheet – B25 No3_C (bulk), treated material *(OPA, 150°C, 96 h)*

Profex

Sample Information

No3-C-0				
File Name	No3-C_RD_R02.dia			
Instrument configuration	D8_Advance_Sol-X_Darmstadt.geq			
Wavelength	CU (1.5406 Å)			
Directory	C:/Users/kasbo/Documents/Data_Laptop/Profex_data/BGE_Project/random			
Date of Refinement	Montag Januar 29, 2024			
Operator	kasbo			
Statistics	R_{wp} = 19.18	R_{exp} = 7.64	χ^2 = 6.3025	GoF = 2.5105

Diffraction Pattern

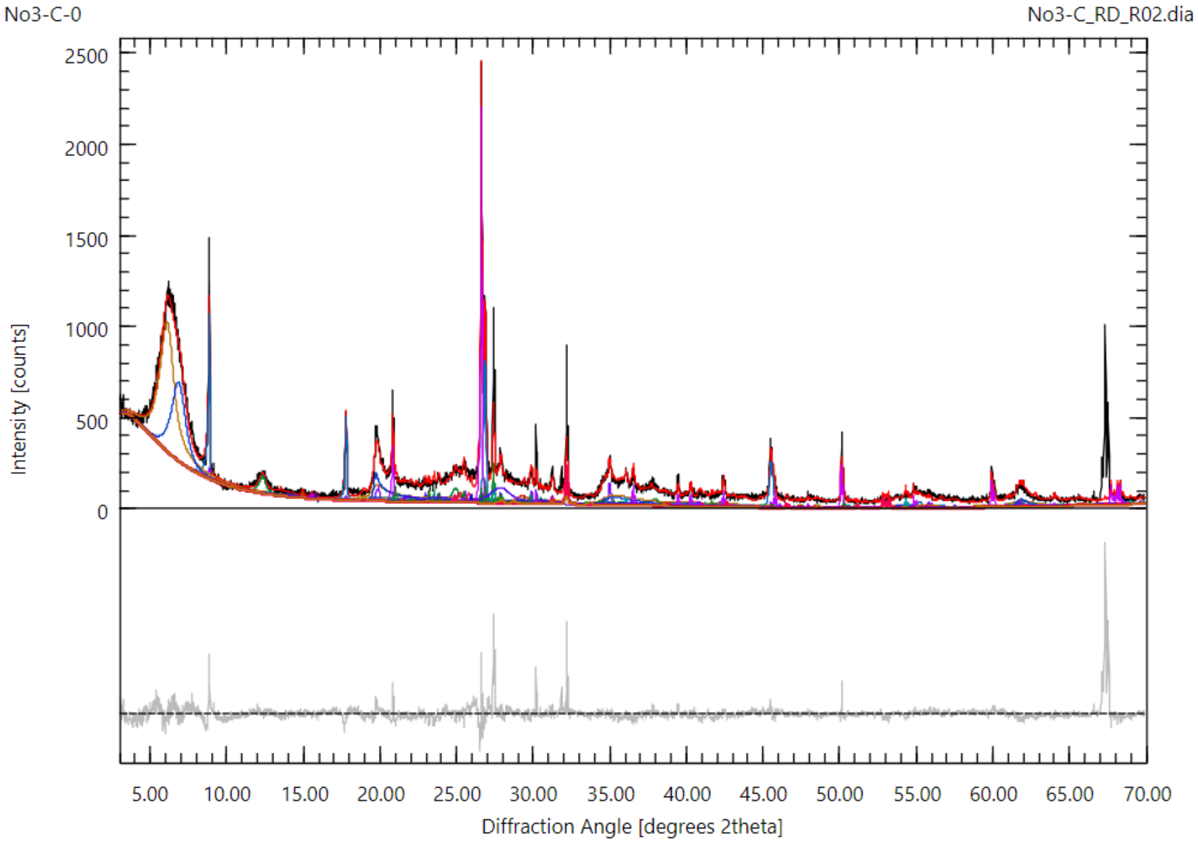

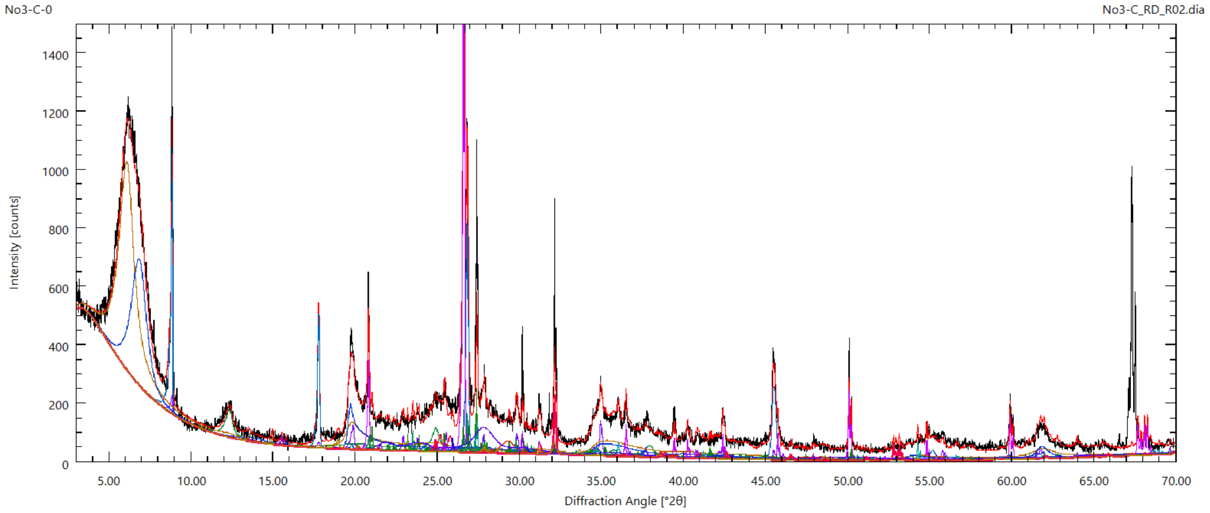
No3-C-0
No3-C_RD_R02.dia
Intensity [counts]
0
200
400
600
800
1000
1200
1400
5.00
10.00
15.00
20.00
25.00
30.00
35.00
40.00
45.00
50.00
55.00
60.00
65.00
70.00
Diffraction Angle [°2θ]

Data Sheet – B25 No3_B (bulk), treated material *(OPA, 150°C, 96 h)*

Sample Information

No3-B-0				
File Name	No3-B_RD_R01.dia			
Instrument configuration	D8_Advance_Sol-X_Darmstadt.geq			
Wavelength	CU (1.5406 Å)			
Directory	C:/Users/kasbo/Documents/Data_Laptop/Profex_data/BGE_Project/random			
Date of Refinement	Montag Januar 29, 2024			
Operator	kasbo			
Statistics	R_{wp} = 12.89	R_{exp} = 7.81	χ^2 = 2.7240	GoF = 1.6504

Diffraction Pattern

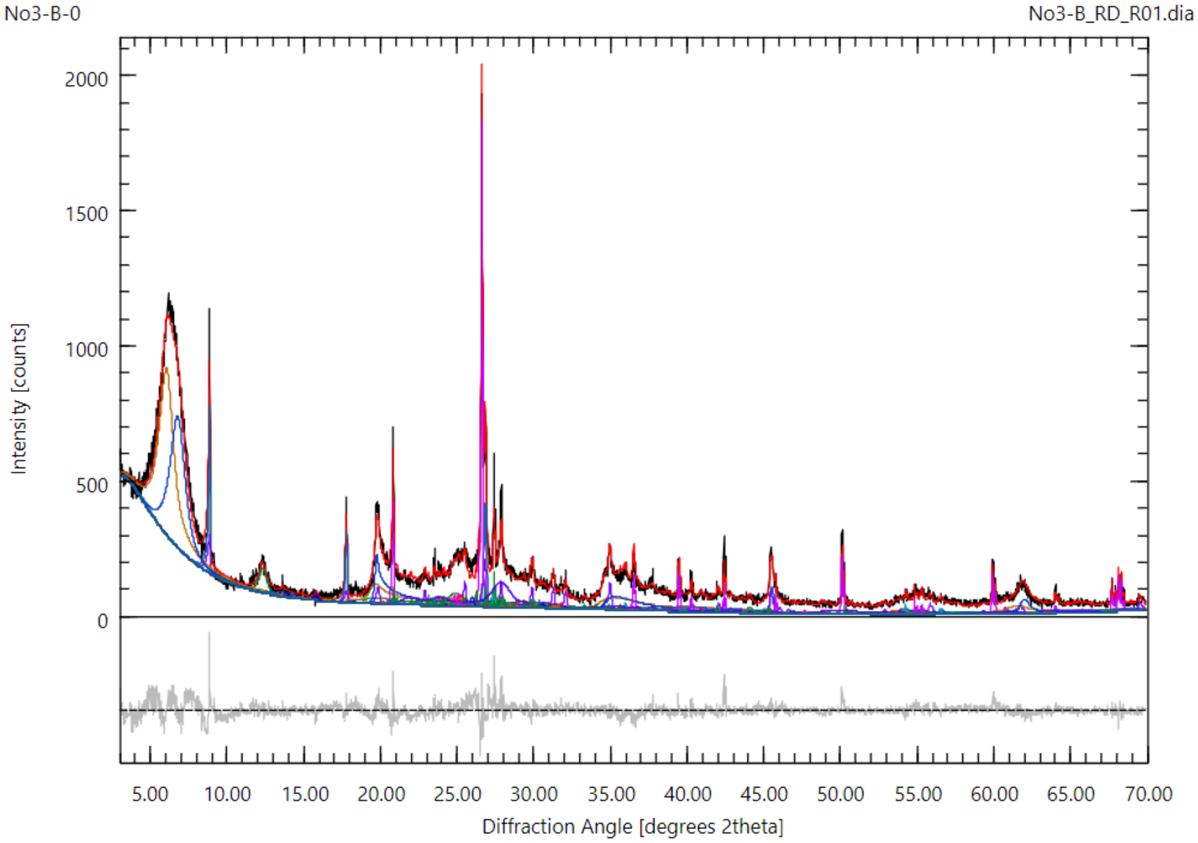

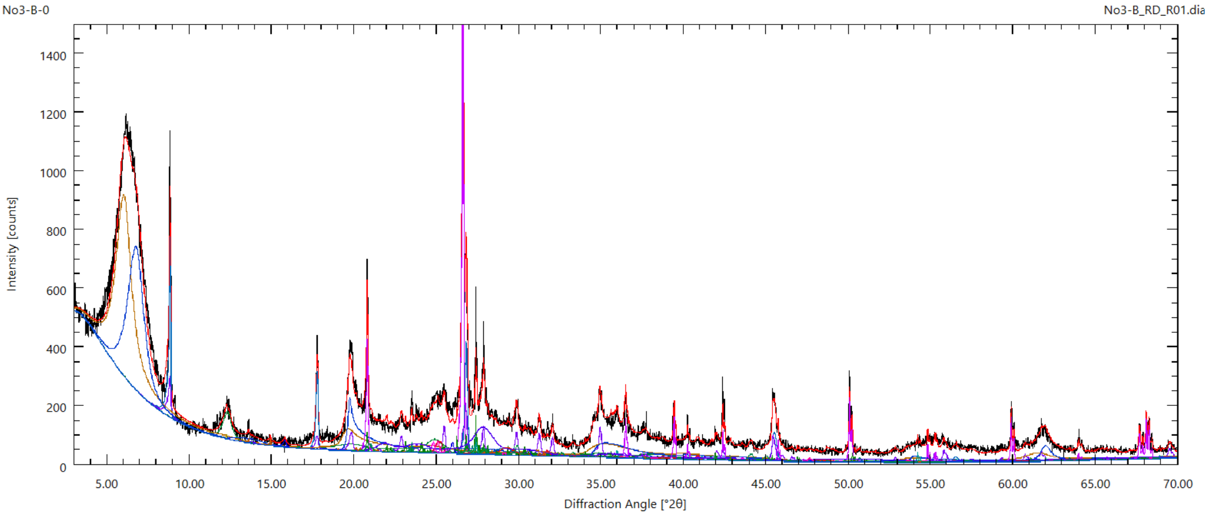
No3-B-0
No3-B_RD_R01.dia
Intensity [counts]
0
200
400
600
800
1000
1200
1400
5.00
10.00
15.00
20.00
25.00
30.00
35.00
40.00
45.00
50.00
55.00
60.00
65.00
70.00
Diffraction Angle [°2θ]

Data Sheet – Friedland Clay (bulk), original material *(uncompacted)*

Data Sheet – Friedland Clay No19 (bulk), original material *(compacted)*

Sample Information

Friedland-0				
File Name	No19_initial_Friedland_XRD_R01.dia			
Instrument configuration	D8_Advance_Sol-X_Darmstadt.geq			
Wavelength	CU (1.5406 Å)			
Directory	C:/Users/kasbo/Documents/Data_Laptop/Profex_data/BGE_Project/random			
Date of Refinement	Donnerstag Februar 01, 2024			
Operator	kasbo			
Statistics	R_{wp} = 12.19	R_{exp} = 8.30	χ^2 = 2.1570	GoF = 1.4687

Diffraction Pattern

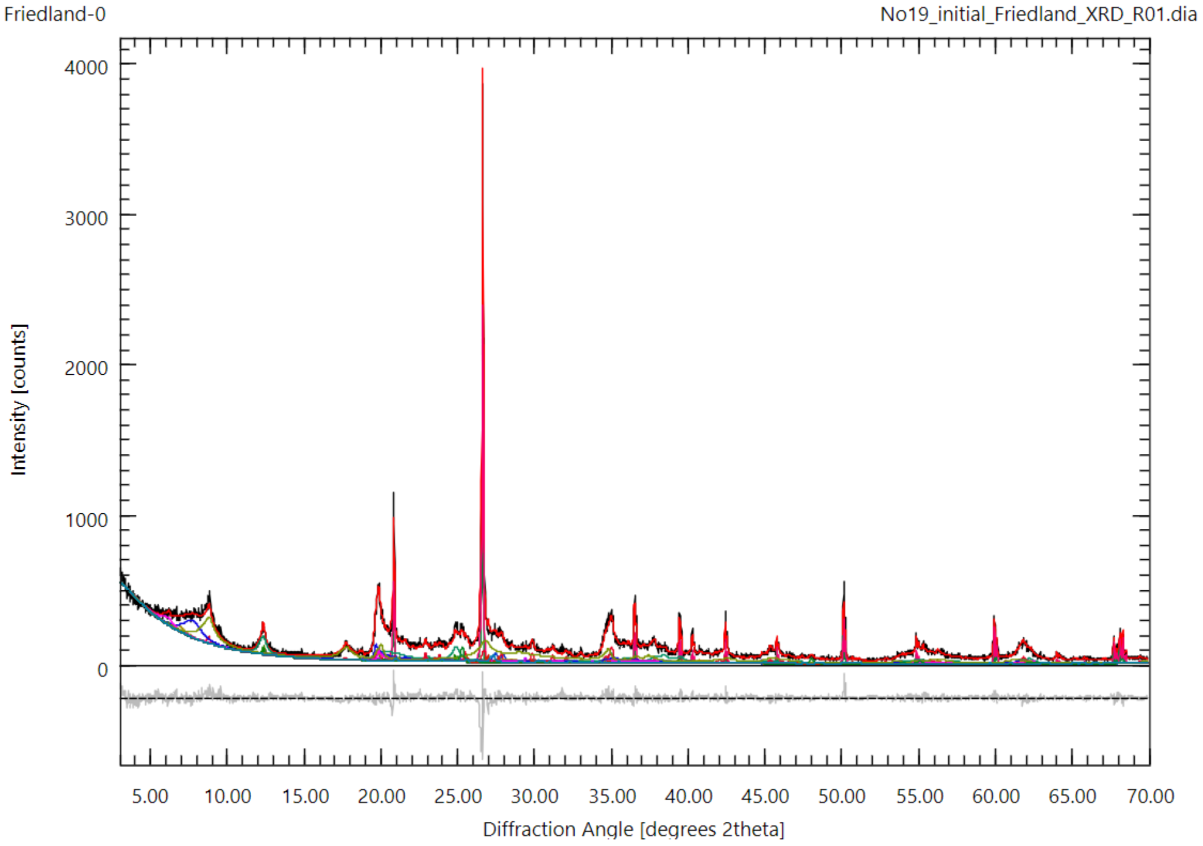

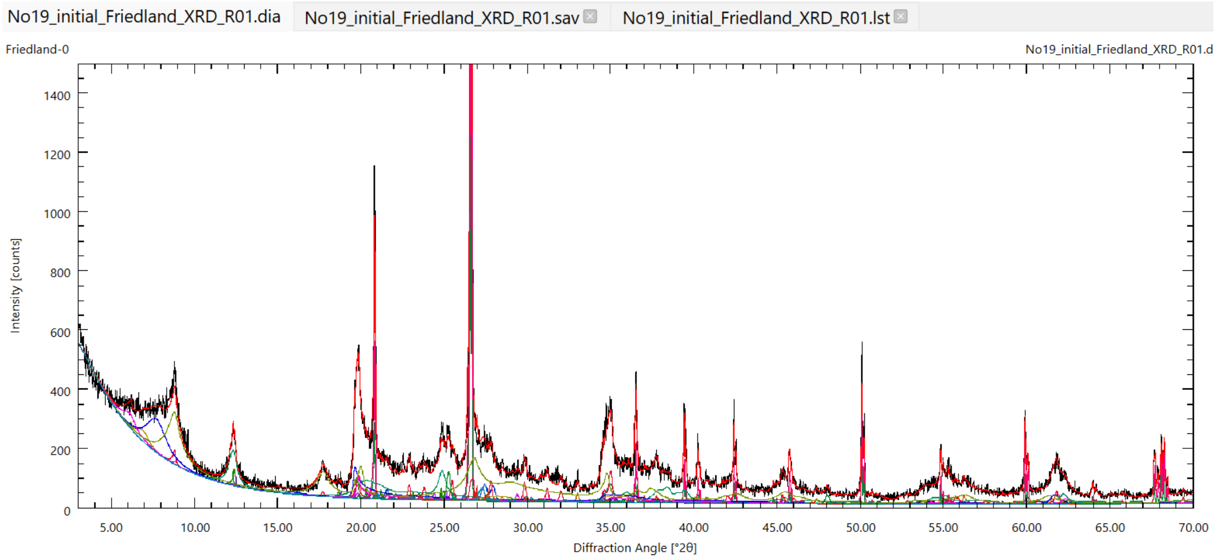
No19_initial_Friedland_XRD_R01.dia
No19_initial_Friedland_XRD_R01.sav
No19_initial_Friedland_XRD_R01.lst
Friedland-0
No19_initial_Friedland_XRD_R01.d
Intensity [counts]
1400
1200
1000
800
600
400
200
0
5.00
10.00
15.00
20.00
25.00
30.00
35.00
40.00
45.00
50.00
55.00
60.00
65.00
70.00
Diffraction Angle [°2θ]

Data Sheet – Friedland No10 (bulk), treated material *(OPA, 35°C, 46.3 h)*

Profex

Sample Information

No10-FRT-35C-0				
File Name	No10-FRT-35C_R03.dia			
Instrument configuration	D8_Advance_Sol-X_Darmstadt.geq			
Wavelength	CU (1.5406 Å)			
Directory	C:/Users/kasbo/Documents/Data_Laptop/Profex_data/BGE_Project/random			
Date of Refinement	Sonntag Oktober 29, 2023			
Operator	kasbo			
Statistics	R_{wp} = 11.53	R_{exp} = 7.80	χ^2 = 2.1851	GoF = 1.4782

Diffraction Pattern

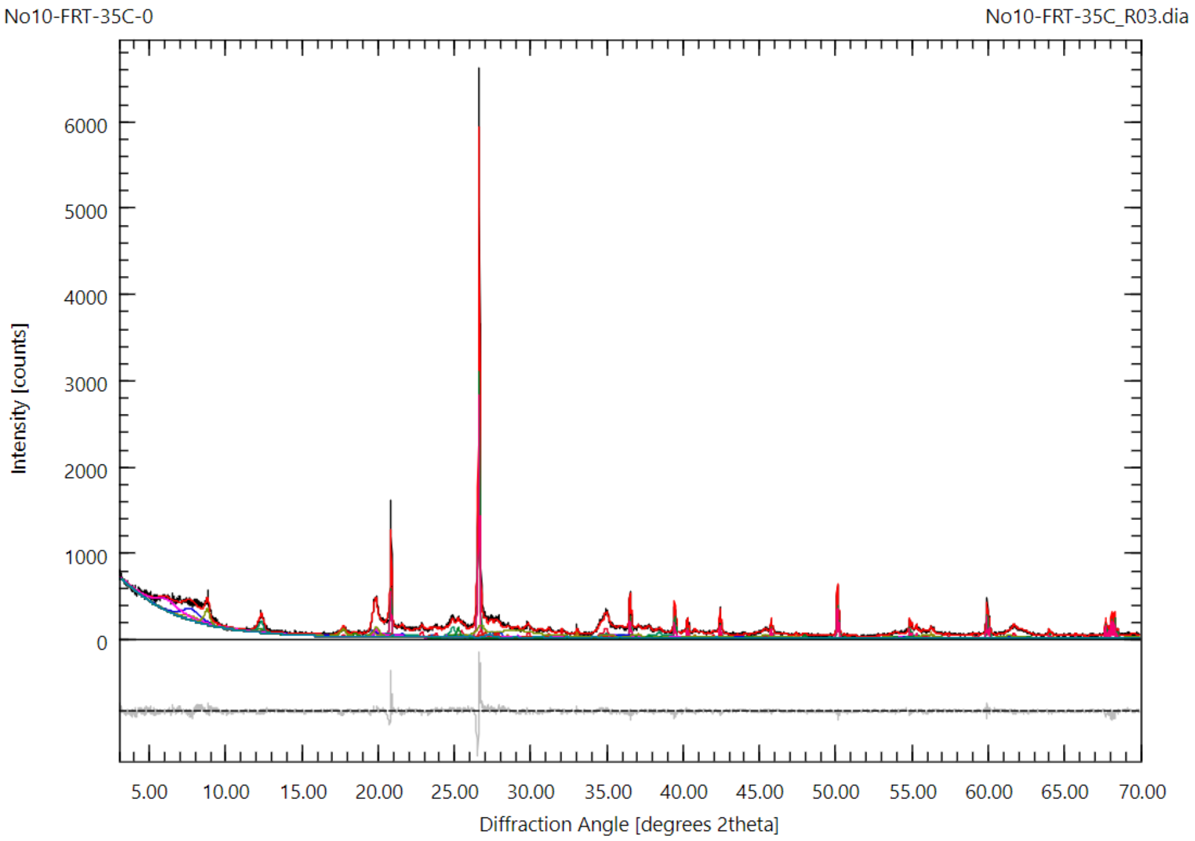

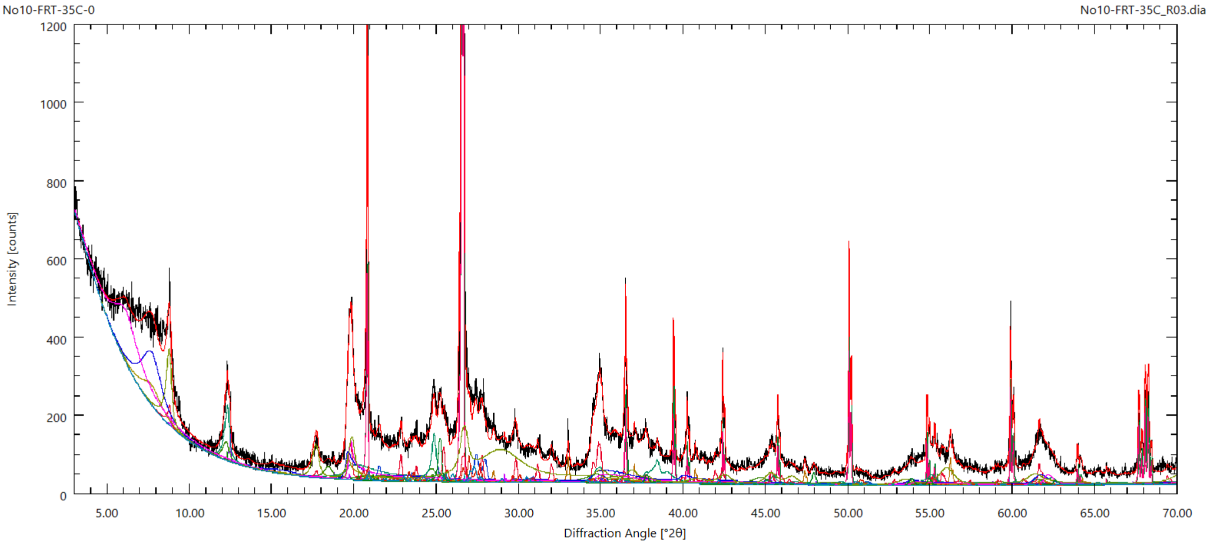
No10-FRT-35C-0
No10-FRT-35C_R03.dia
Intensity [counts]
0
200
400
600
800
1000
1200
5.00
10.00
15.00
20.00
25.00
30.00
35.00
40.00
45.00
50.00
55.00
60.00
65.00
70.00
Diffraction Angle [°2θ]

Data Sheet – Friedland No11 (bulk), treated material *(OPA, 60°C, 45.9 h)*

Profex

Sample Information

No11-0				
File Name	No11_FRDL_60grd_R01.dia			
Instrument configuration	D8_Advance_Sol-X_Darmstadt.geq			
Wavelength	CU (1.5406 Å)			
Directory	C:/Users/kasbo/Documents/Data_Laptop/Profex_data/BGE_Project/random			
Date of Refinement	Sonntag Oktober 29, 2023			
Operator	kasbo			
Statistics	R_{wp} = 10.74	R_{exp} = 7.77	χ^2 = 1.9106	GoF = 1.3822

Diffraction Pattern

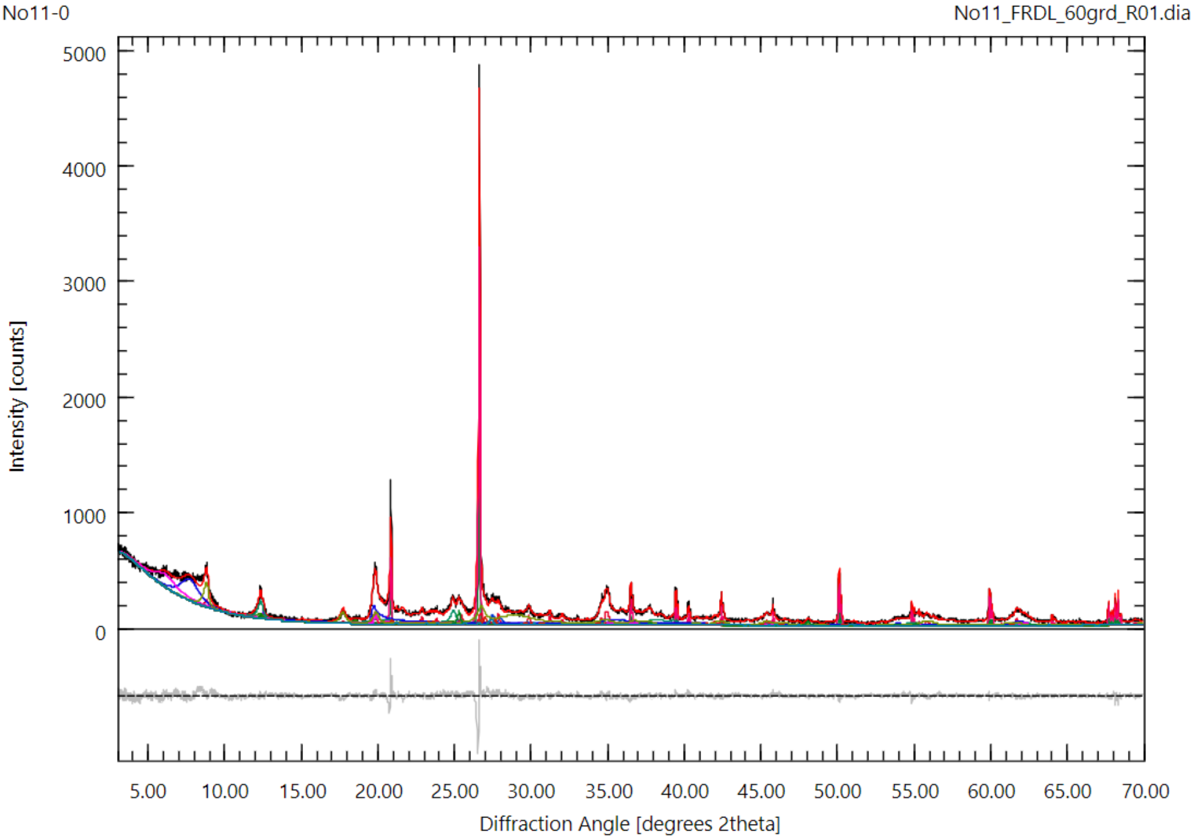

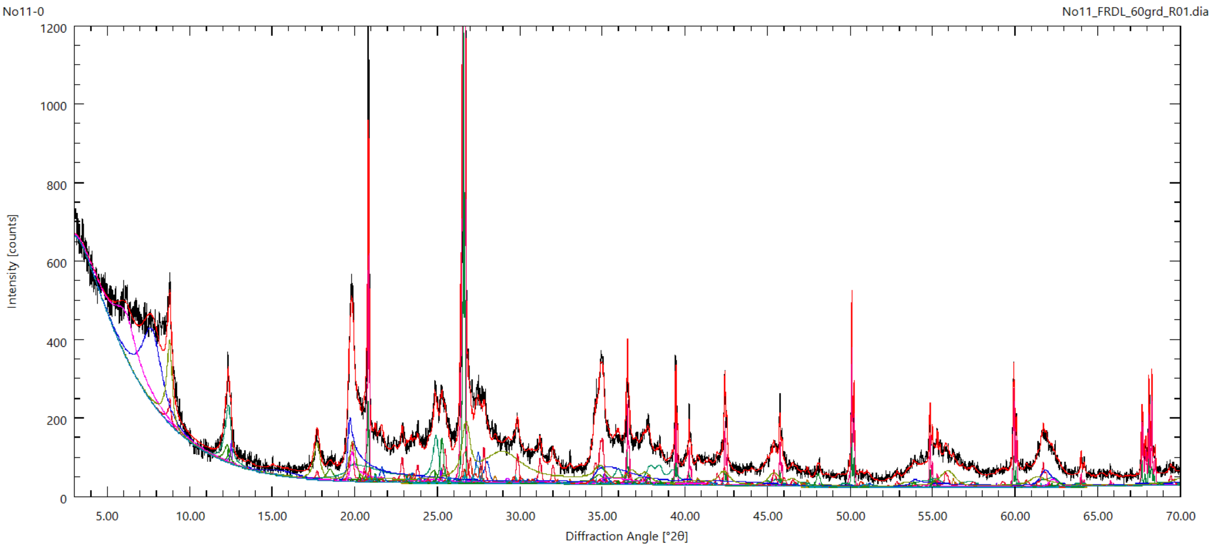
No11-0
No11_FRDL_60grd_R01.dia
Intensity [counts]
1200
1000
800
600
400
200
0
5.00
10.00
15.00
20.00
25.00
30.00
35.00
40.00
45.00
50.00
55.00
60.00
65.00
70.00
Diffraction Angle [°2θ]

Data Sheet – Friedland No16 (bulk), treated material *(OPA, 100°C, 40 h)*

Profex

Sample Information

No16-0				
File Name	No16_FRDL_100grd_R01.dia			
Instrument configuration	D8_Advance_Sol-X_Darmstadt.geq			
Wavelength	CU (1.5406 Å)			
Directory	C:/Users/kasbo/Documents/Data_Laptop/Profex_data/BGE_Project/random			
Date of Refinement	Montag Oktober 30, 2023			
Operator	kasbo			
Statistics	R_{wp} = 9.94	R_{exp} = 6.95	χ^2 = 2.0455	GoF = 1.4302

Diffraction Pattern

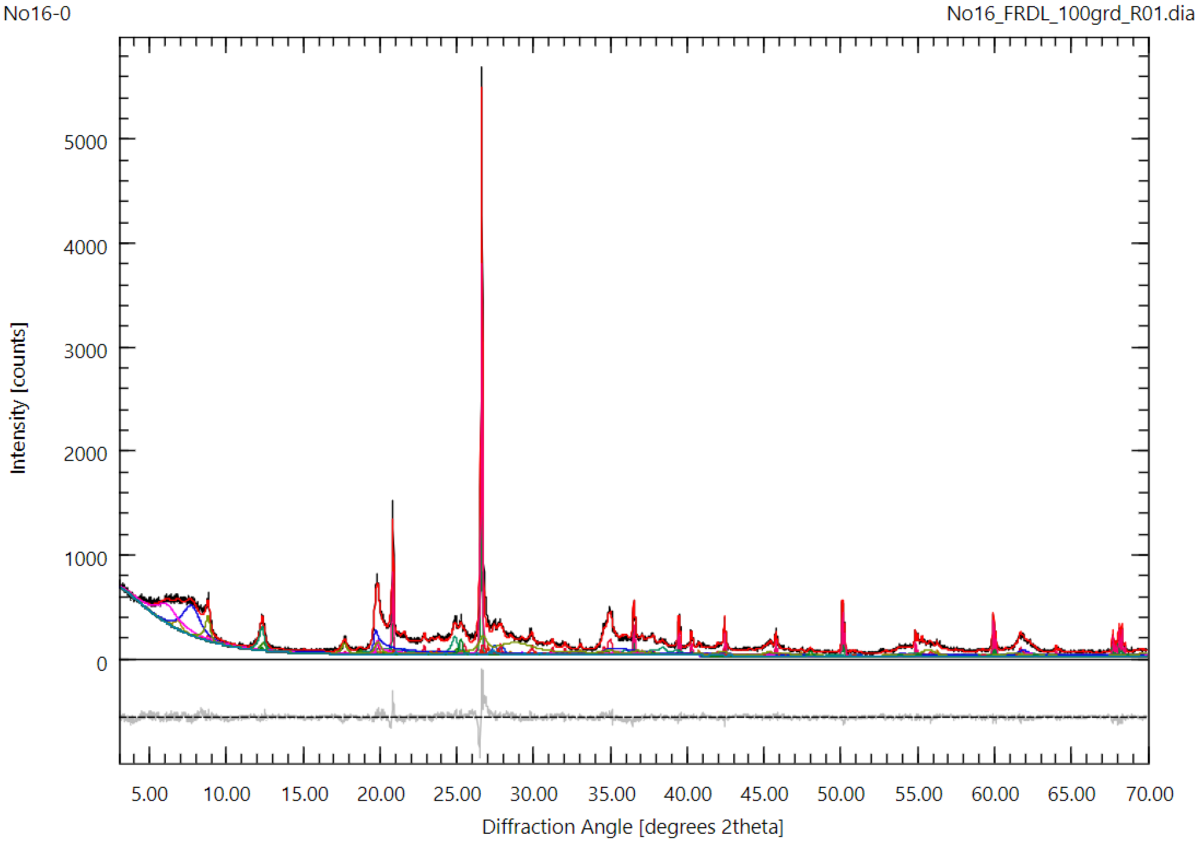

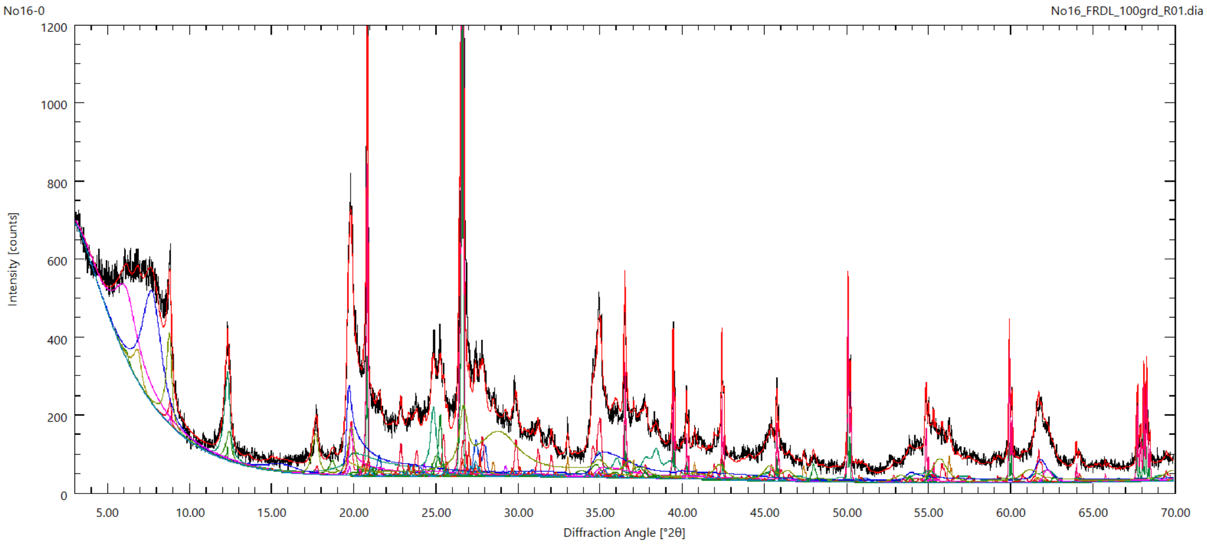
No16-0
No16_FRDL_100grd_R01.dia
Intensity [counts]
1200
1000
800
600
400
200
0
5.00
10.00
15.00
20.00
25.00
30.00
35.00
40.00
45.00
50.00
55.00
60.00
65.00
70.00
Diffraction Angle [°2θ]

Data Sheet – Friedland No20 (bulk), treated material *(OPA, 125°C)*

Profex

Sample Information

No-20-0				
File Name	No-20_FRDL125_R01.dia			
Instrument configuration	D8_Advance_Sol-X_Darmstadt.geq			
Wavelength	CU (1.5406 Å)			
Directory	C:/Users/kasbo/Documents/Data_Laptop/Profex_data/BGE_Project/random			
Date of Refinement	Dienstag Dezember 19, 2023			
Operator	kasbo			
Statistics	R_{wp} = 15.02	R_{exp} = 12.84	χ^2 = 1.3684	GoF = 1.1698

Diffraction Pattern

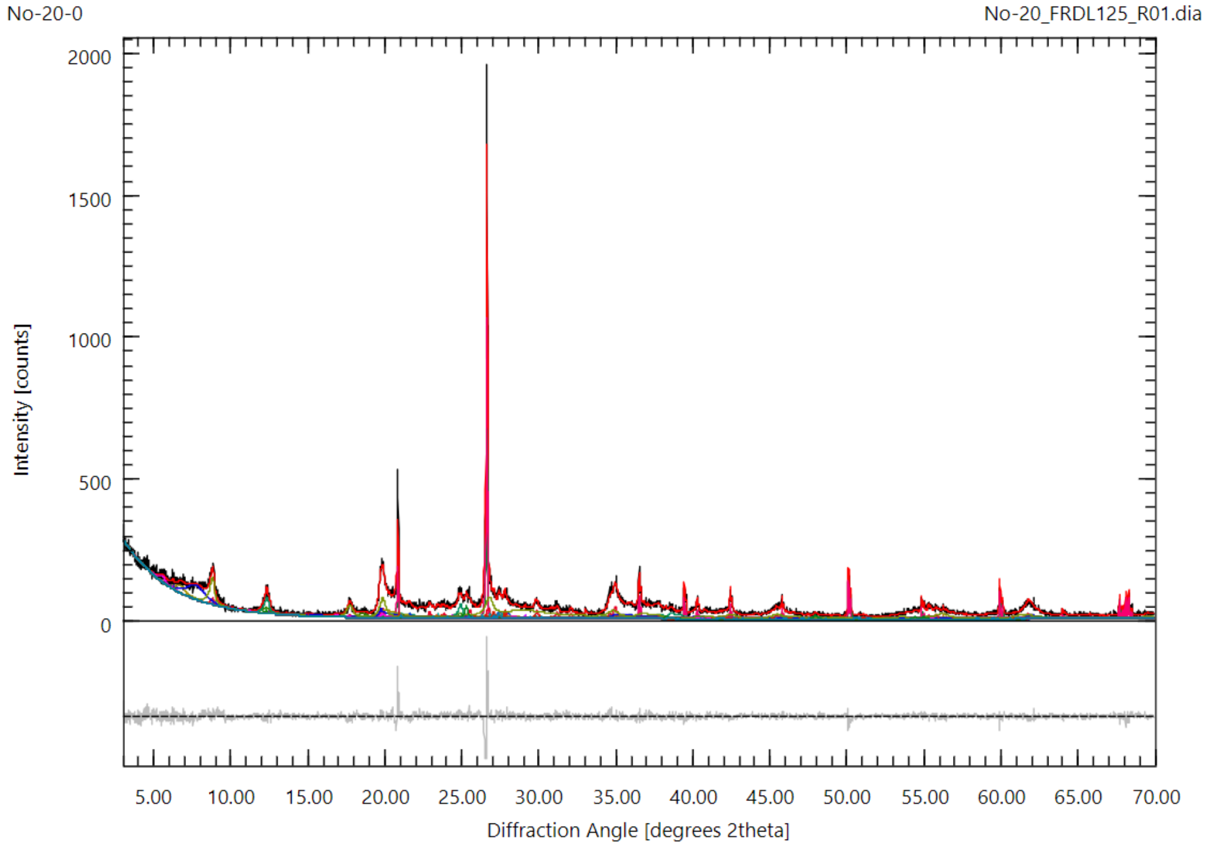

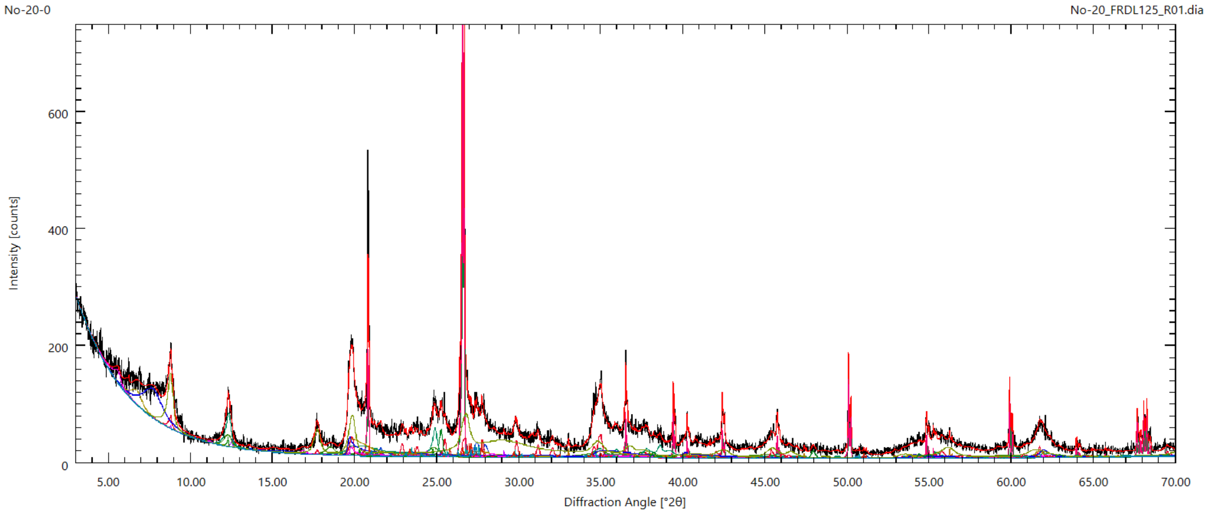
No-20-0
No-20_FRDL125_R01.dia
Intensity [counts]
0
200
400
600
5.00
10.00
15.00
20.00
25.00
30.00
35.00
40.00
45.00
50.00
55.00
60.00
65.00
70.00
Diffraction Angle [°2θ]

Data Sheet – Friedland No21 (bulk), treated material *(OPA, 150°C)*

Profex

Sample Information

No-21-0				
File Name	No-21_FRDL150_R01.dia			
Instrument configuration	D8_Advance_Sol-X_Darmstadt.geq			
Wavelength	CU (1.5406 Å)			
Directory	C:/Users/kasbo/Documents/Data_Laptop/Profex_data/BGE_Project/random			
Date of Refinement	Dienstag Dezember 19, 2023			
Operator	kasbo			
Statistics	R_{wp} = 14.37	R_{exp} = 12.94	χ^2 = 1.2332	GoF = 1.1105

Diffraction Pattern

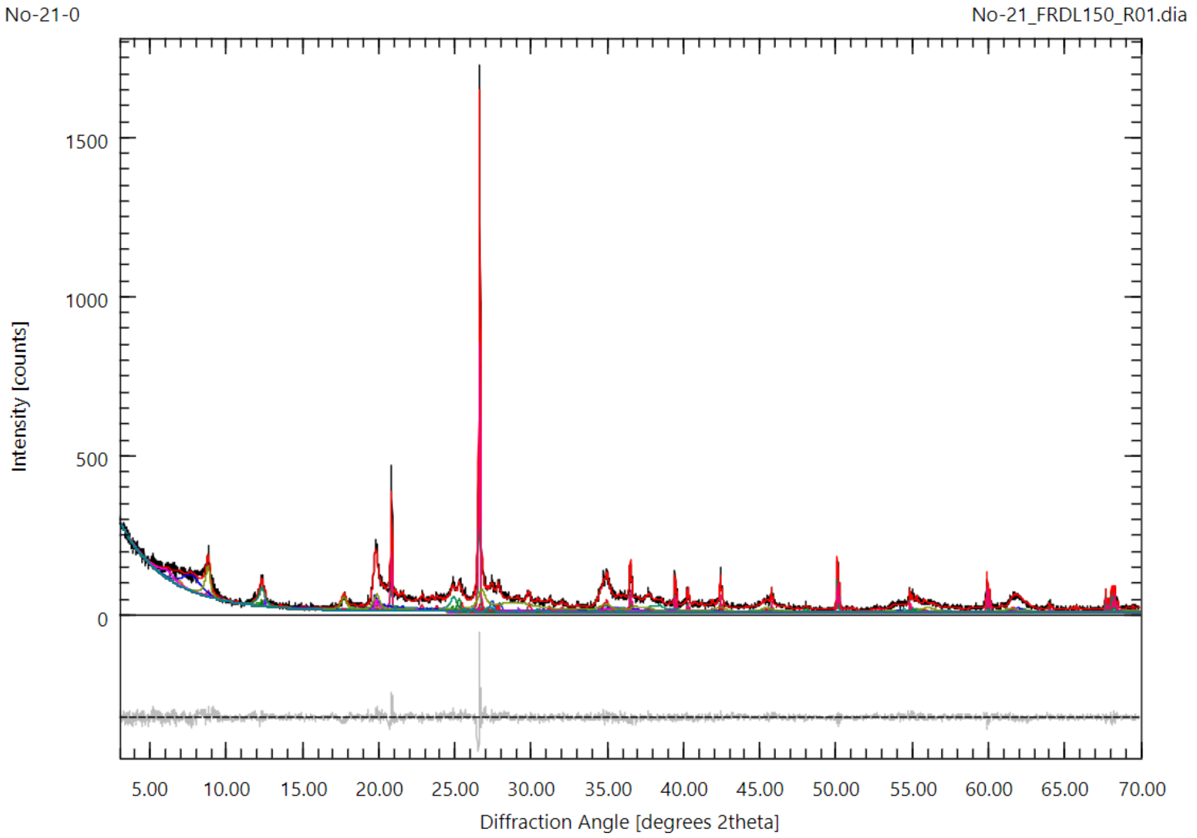

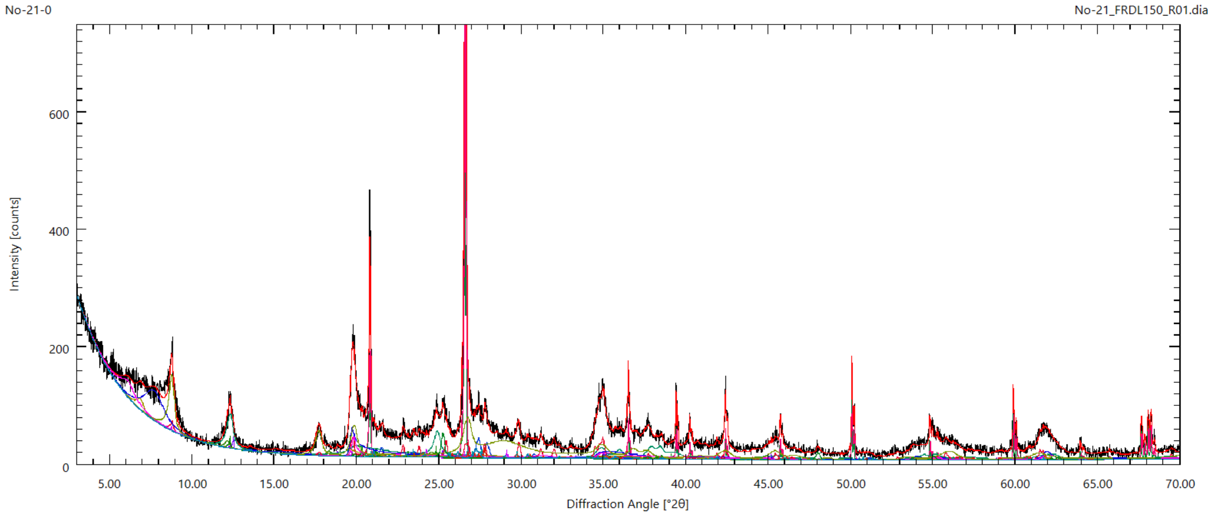
No-21-0
No-21_FRDL150_R01.dia
Intensity [counts]
0
200
400
600
5.00
10.00
15.00
20.00
25.00
30.00
35.00
40.00
45.00
50.00
55.00
60.00
65.00
70.00
Diffraction Angle [°2θ]

Data Sheet – Friedland No12 (bulk), treated material *(OPA, 100°C)*

[without transport cell]

Sample Information

No12-0				
File Name	No12_R03.dia			
Instrument configuration	D8_Advance_Sol-X_Darmstadt.geq			
Wavelength	CU (1.5406 Å)			
Directory	C:/Users/kasbo/Documents/Data_Laptop/Profex_data/BGE_Project/random			
Date of Refinement	Dienstag November 14, 2023			
Operator	kasbo			
Statistics	R_{wp} = 15.06	R_{exp} = 12.93	χ^2 = 1.3566	GoF = 1.1647

Diffraction Pattern

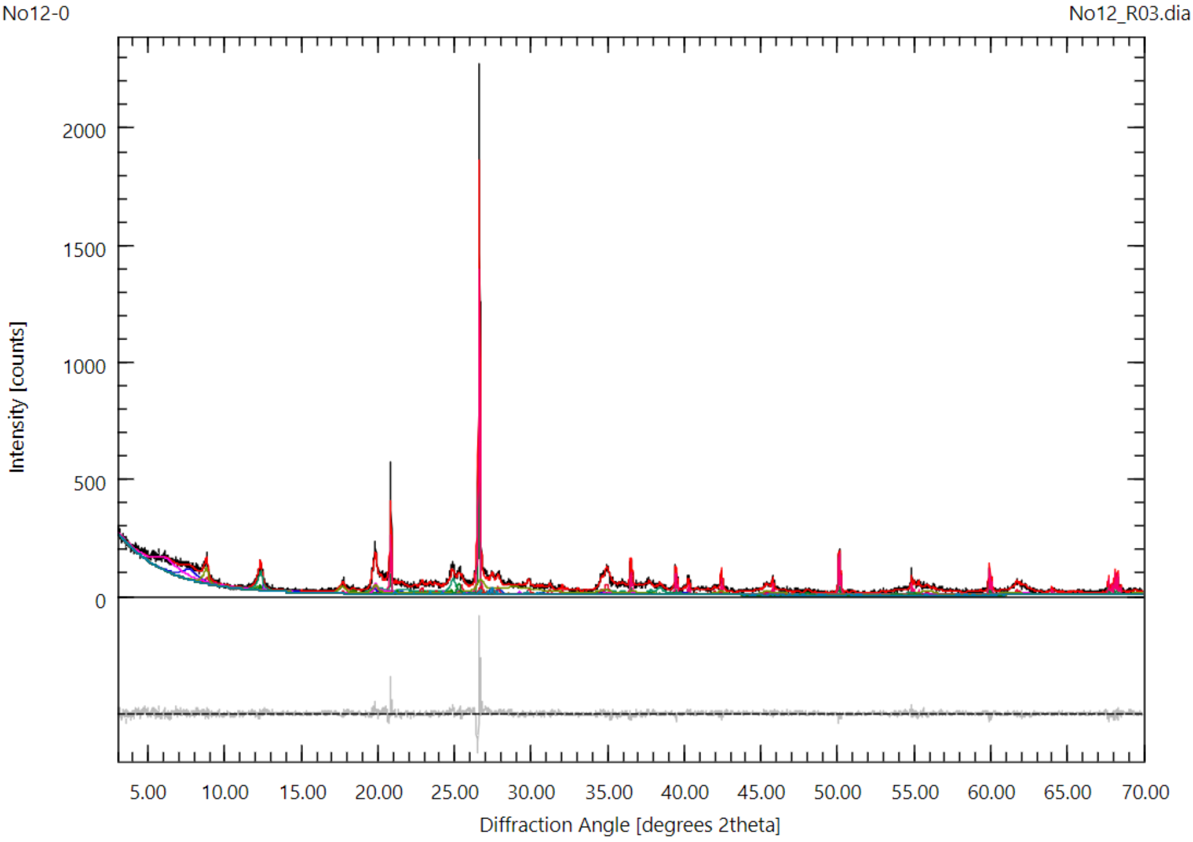

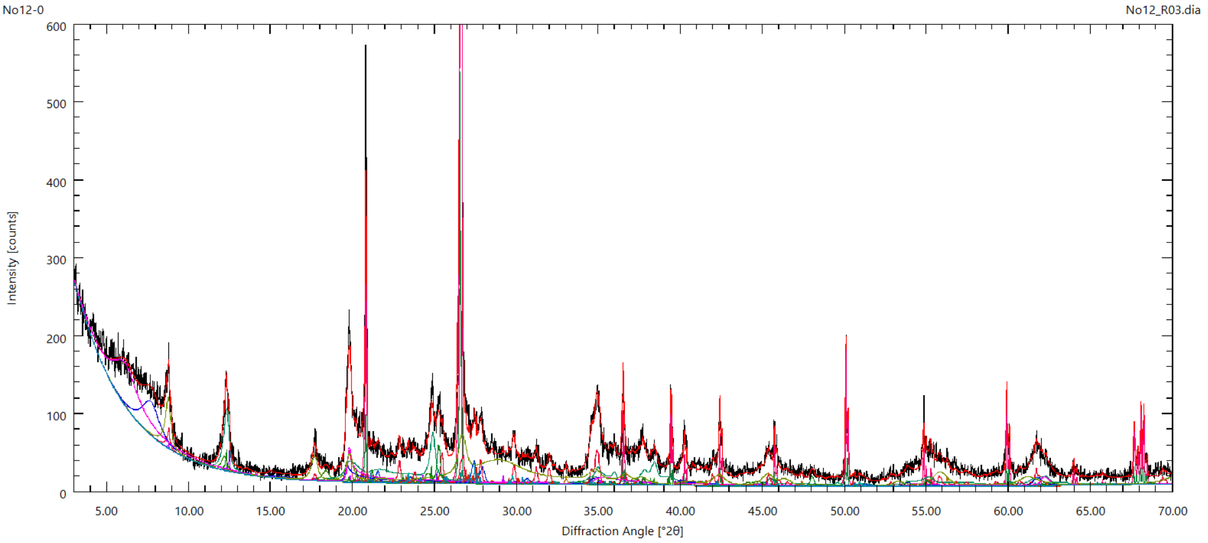
No12-0
No12_R03.dia
Intensity [counts]
0
100
200
300
400
500
600
5.00
10.00
15.00
20.00
25.00
30.00
35.00
40.00
45.00
50.00
55.00
60.00
65.00
70.00
Diffraction Angle [°2θ]

Data Sheet – Opalinus Clay (bulk), original material *(uncompacted)*

Sample Information

2020_017				
File Name	Opalinus total_R13.dia			
Instrument configuration	PW1830_TU Darmstadt_adopted.geq			
Wavelength	CU (1.5406 Å)			
Directory	C:/Users/kasbo/Documents/Data_Laptop/Profex_data/BGE_Project/random			
Date of Refinement	Dienstag Juli 06, 2021			
Operator	kasbo			
Statistics	R_{wp} = 3.31	R_{exp} = 2.34	χ^2 = 2.0009	GoF = 1.4145

Diffraction Pattern

2020_017

Opalinus total_R13.dia

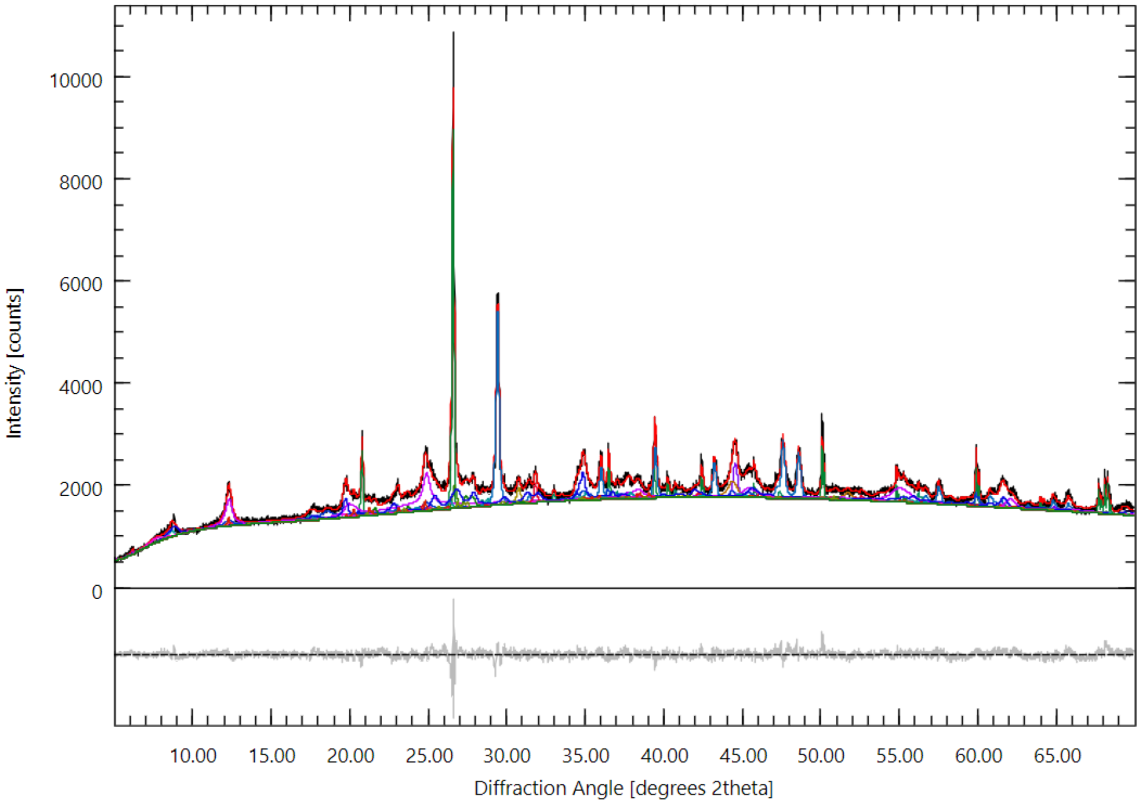

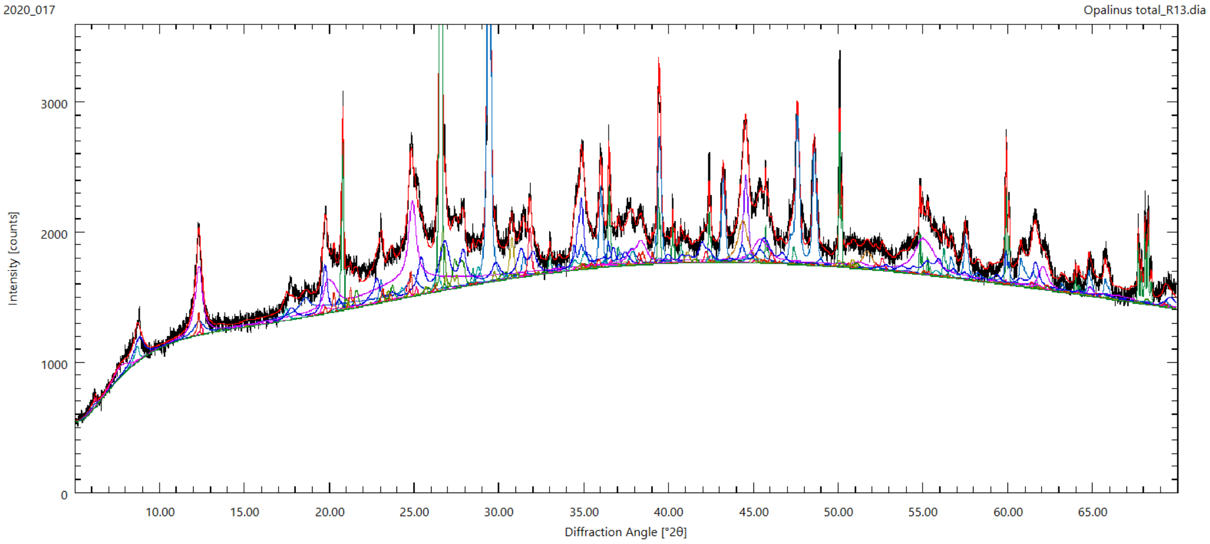
2020_017
Opalinus total_R13.dia
Intensity [counts]
0
1000
2000
3000
10.00
15.00
20.00
25.00
30.00
35.00
40.00
45.00
50.00
55.00
60.00
65.00
Diffraction Angle [°2θ]

Data Sheet – Opalinus Clay No6 (bulk), original material

Profex

Sample Information

Opalinus-0				
File Name	No6_XRD_initial Opalinus_R02.dia			
Instrument configuration	D8_Advance_Sol-X_Darmstadt.geq			
Wavelength	CU (1.5406 Å)			
Directory	C:/Users/kasbo/Documents/Data_Laptop/Profex_data/BGE_Project/random			
Date of Refinement	Dienstag Januar 30, 2024			
Operator	kasbo			
Statistics	R_{wp} = 12.31	R_{exp} = 8.65	χ^2 = 2.0253	GoF = 1.4231

Diffraction Pattern

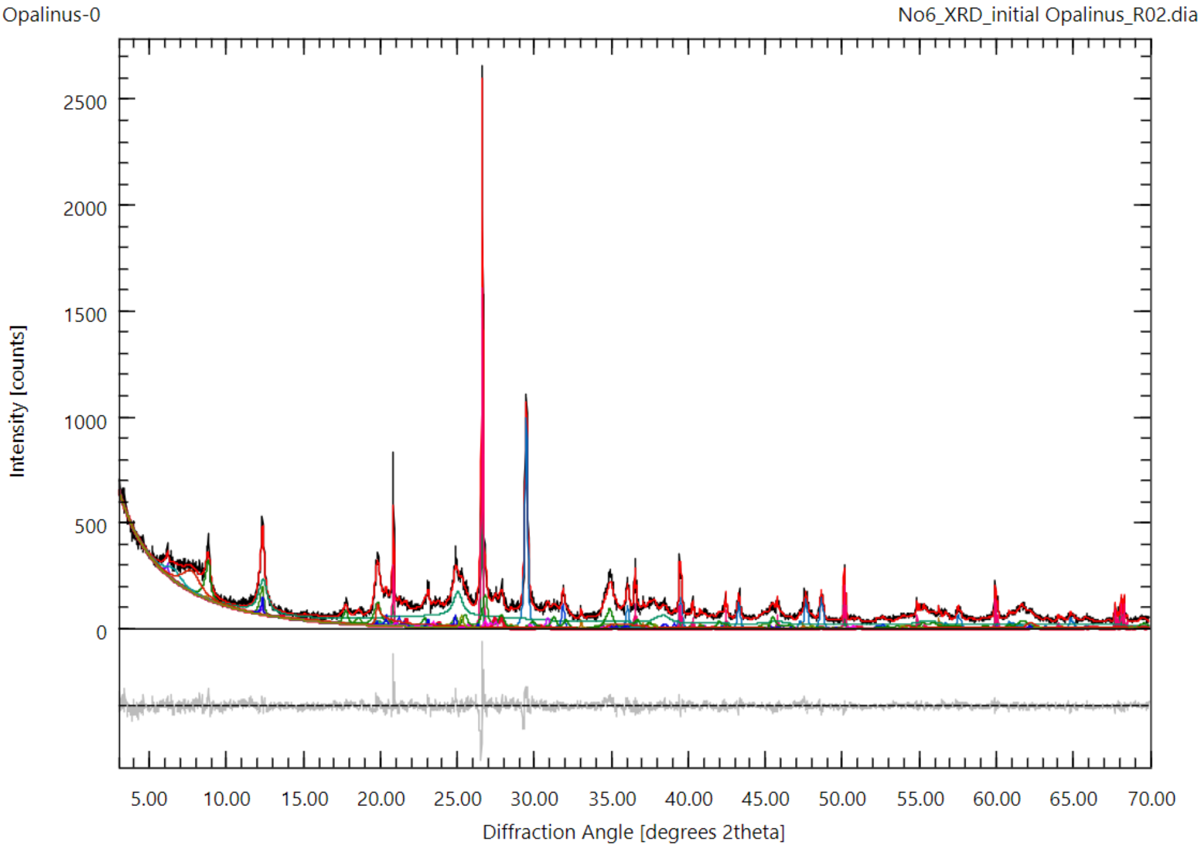

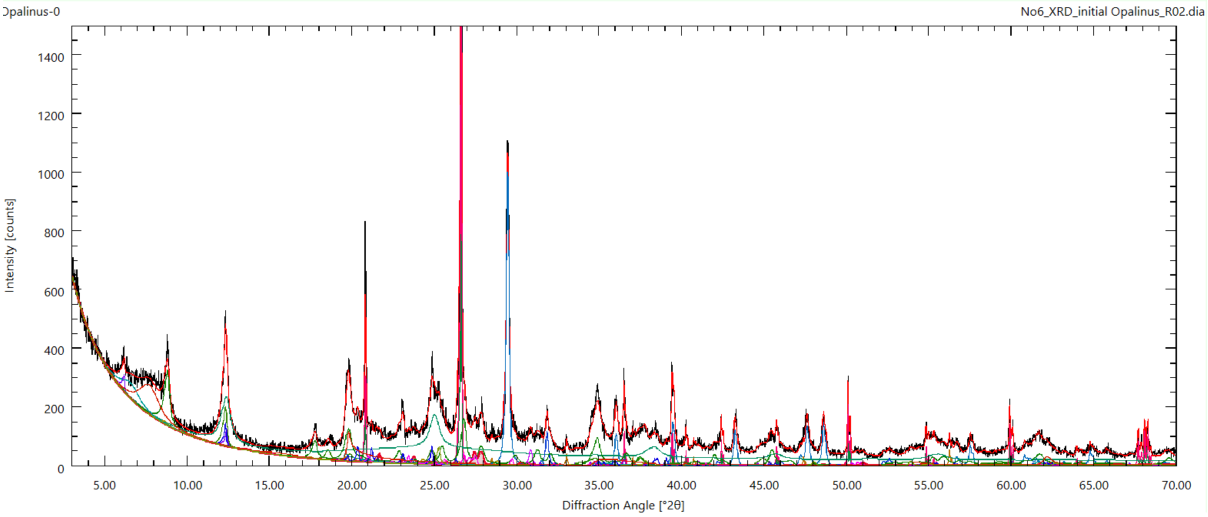
Opalinus-0
No6_XRD_initial Opalinus_R02.dia
Intensity [counts]
1400
1200
1000
800
600
400
200
0
5.00
10.00
15.00
20.00
25.00
30.00
35.00
40.00
45.00
50.00
55.00
60.00
65.00
70.00
Diffraction Angle [°2θ]

Data Sheet – Opalinus No22 (bulk), treated material *(OPA, 35°C, 144 h)*

Profex

Sample Information

No-22-0				
File Name	No-22_OPA35_R02.dia			
Instrument configuration	D8_Advance_Sol-X_Darmstadt.geq			
Wavelength	CU (1.5406 Å)			
Directory	C:/Users/kasbo/Documents/Data_Laptop/Profex_data/BGE_Project/random			
Date of Refinement	Dienstag Dezember 19, 2023			
Operator	kasbo			
Statistics	R_{wp} = 15.70	R_{exp} = 13.24	χ^2 = 1.4061	GoF = 1.1858

Diffraction Pattern

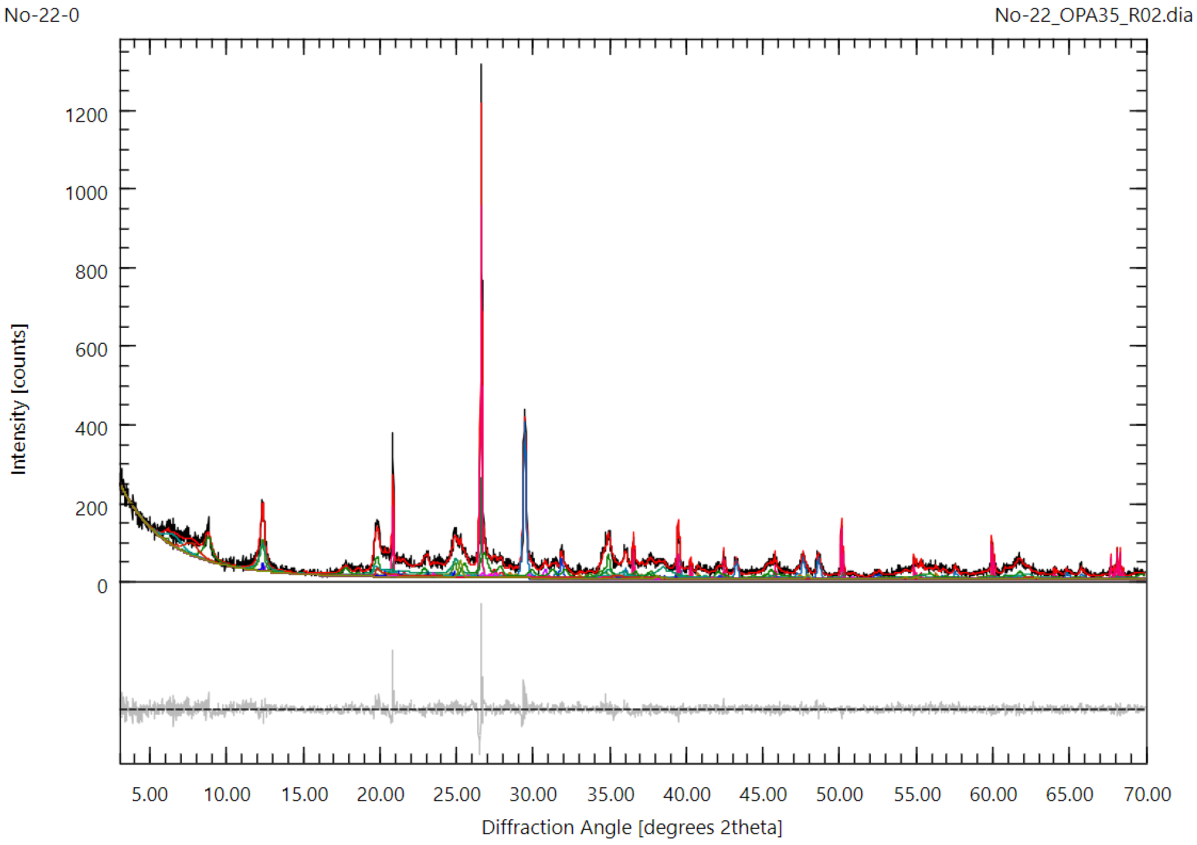

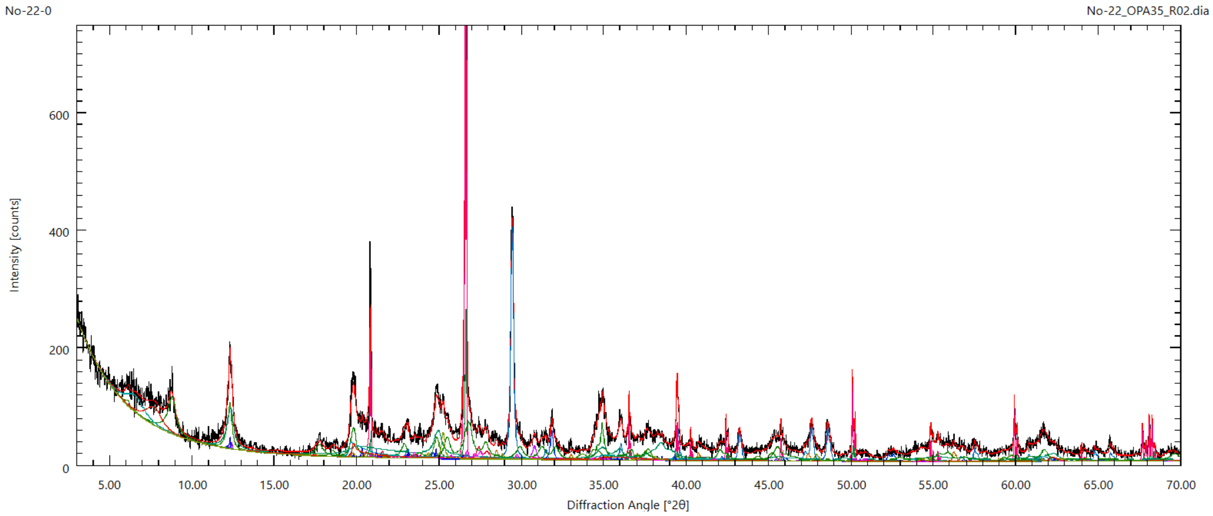
No-22-0
No-22_OPA35_R02.dia
Intensity [counts]
0
200
400
600
5.00
10.00
15.00
20.00
25.00
30.00
35.00
40.00
45.00
50.00
55.00
60.00
65.00
70.00
Diffraction Angle [°2θ]

Data Sheet – Opalinus No9 (bulk), treated material *(OPA, 60°C, 45.4 h)*

Profex

Sample Information

No9-OP4-0				
File Name	No9-OP4_R01.dia			
Instrument configuration	D8_Advance_Sol-X_Darmstadt.geq			
Wavelength	CU (1.5406 Å)			
Directory	C:/Users/kasbo/Documents/Data_Laptop/Profex_data/BGE_Project/random			
Date of Refinement	Samstag Oktober 28, 2023			
Operator	kasbo			
Statistics	R_{wp} = 11.13	R_{exp} = 8.32	χ^2 = 1.7895	GoF = 1.3377

Diffraction Pattern

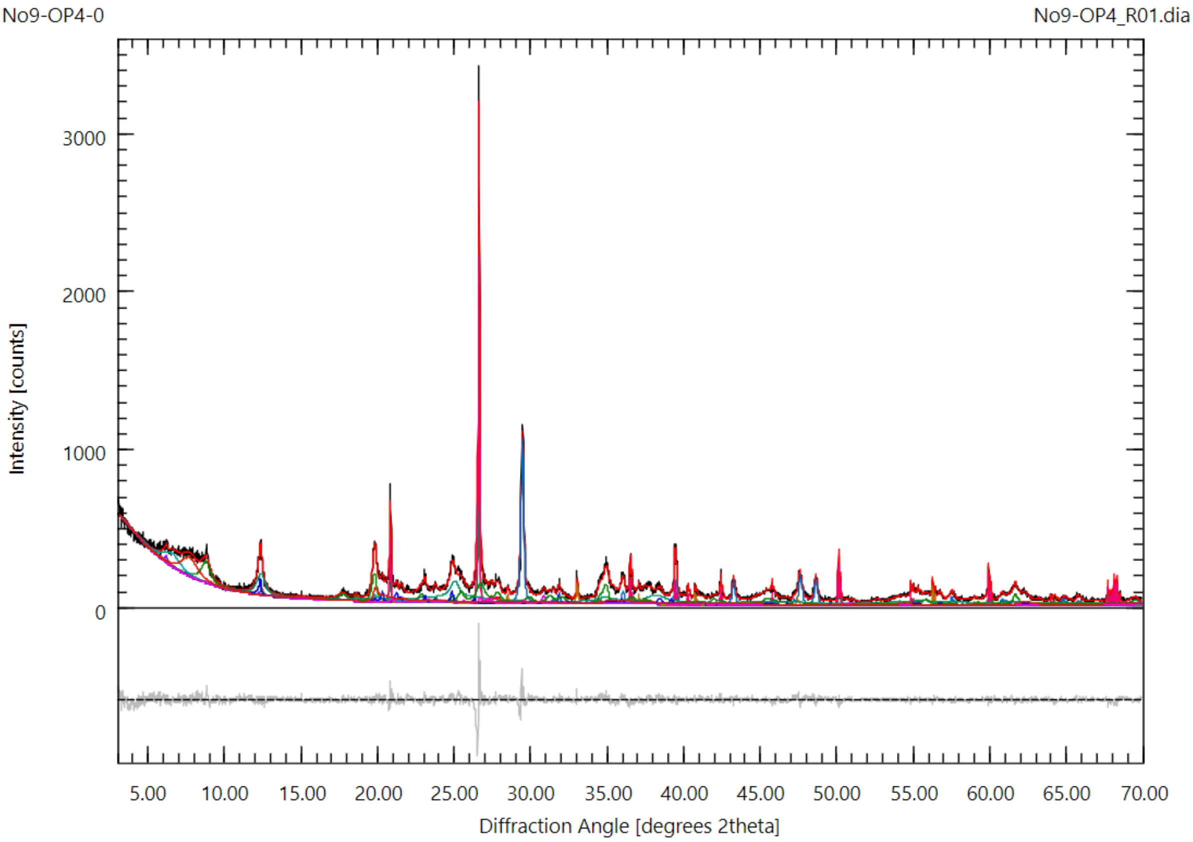

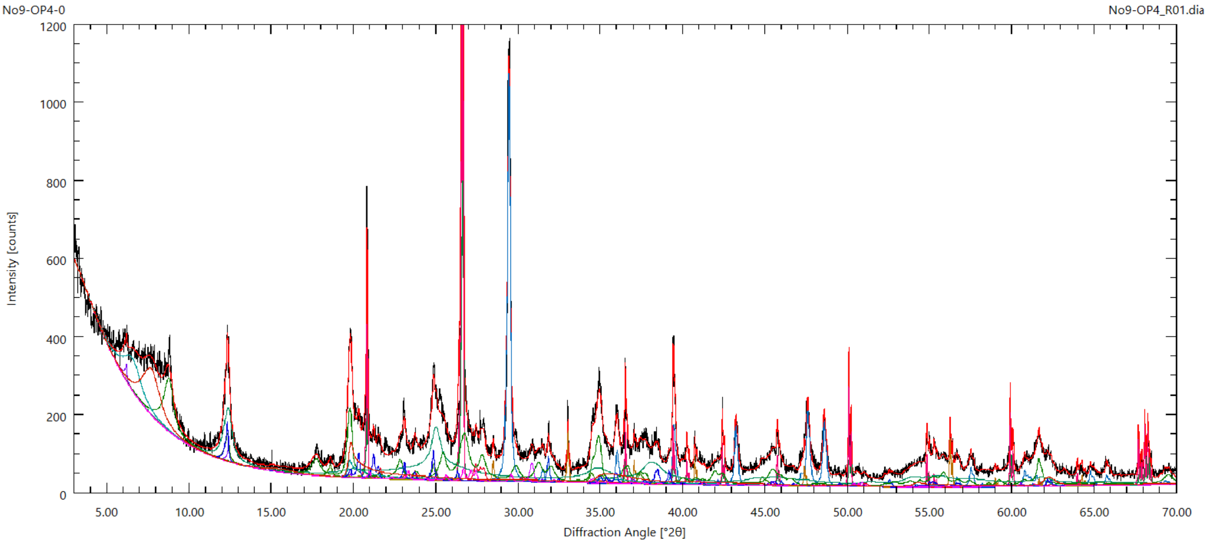
No9-OP4-0
No9-OP4_R01.dia
Intensity [counts]
0
200
400
600
800
1000
1200
5.00
10.00
15.00
20.00
25.00
30.00
35.00
40.00
45.00
50.00
55.00
60.00
65.00
70.00
Diffraction Angle [°2θ]

Data Sheet – Opalinus No7 (bulk), treated material *(OPA, 60°C, 95.3 h)*

Sample Information

No7-OP2-0				
File Name	No7-OP2_R03.dia			
Instrument configuration	D8_Advance_Sol-X_Darmstadt.geq			
Wavelength	CU (1.5406 Å)			
Directory	C:/Users/kasbo/Documents/Data_Laptop/Profex_data/BGE_Project/random			
Date of Refinement	Samstag Oktober 28, 2023			
Operator	kasbo			
Statistics	R_{wp} = 15.10	R_{exp} = 9.51	χ^2 = 2.5211	GoF = 1.5878

Diffraction Pattern

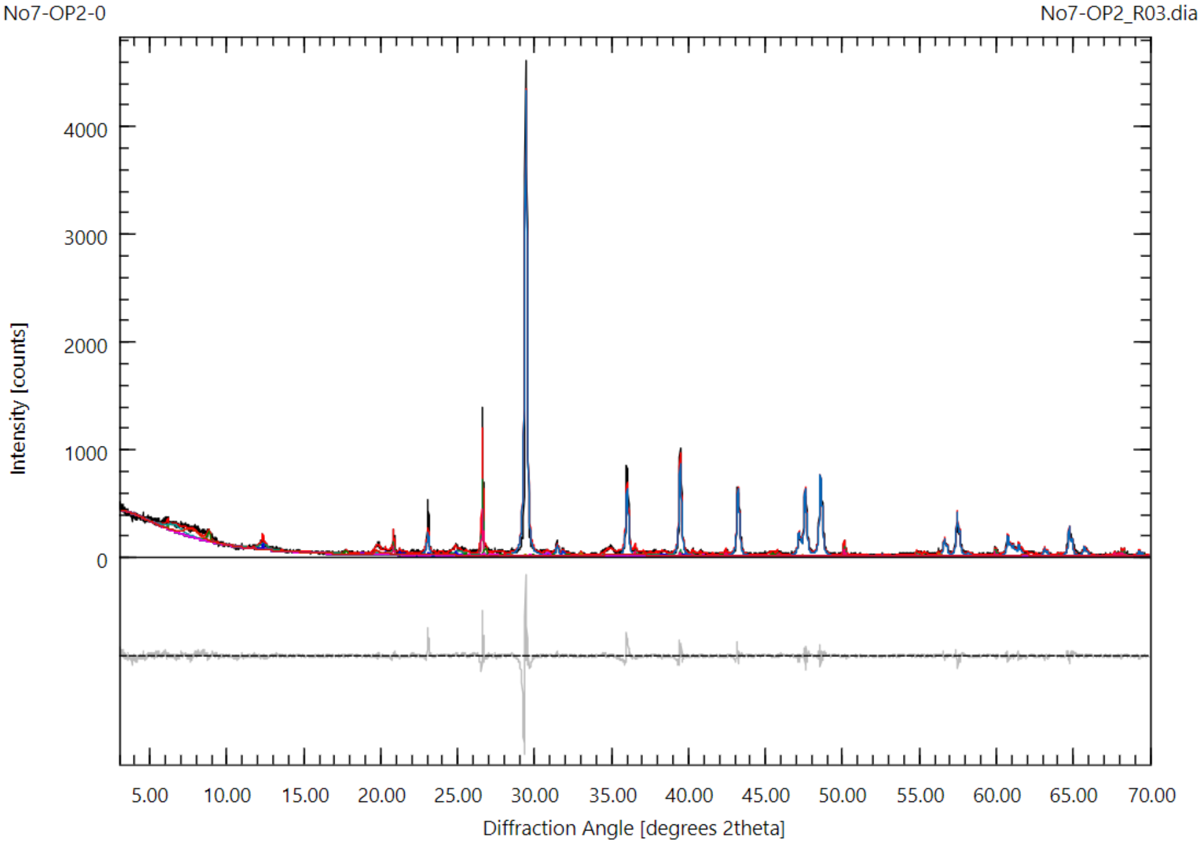

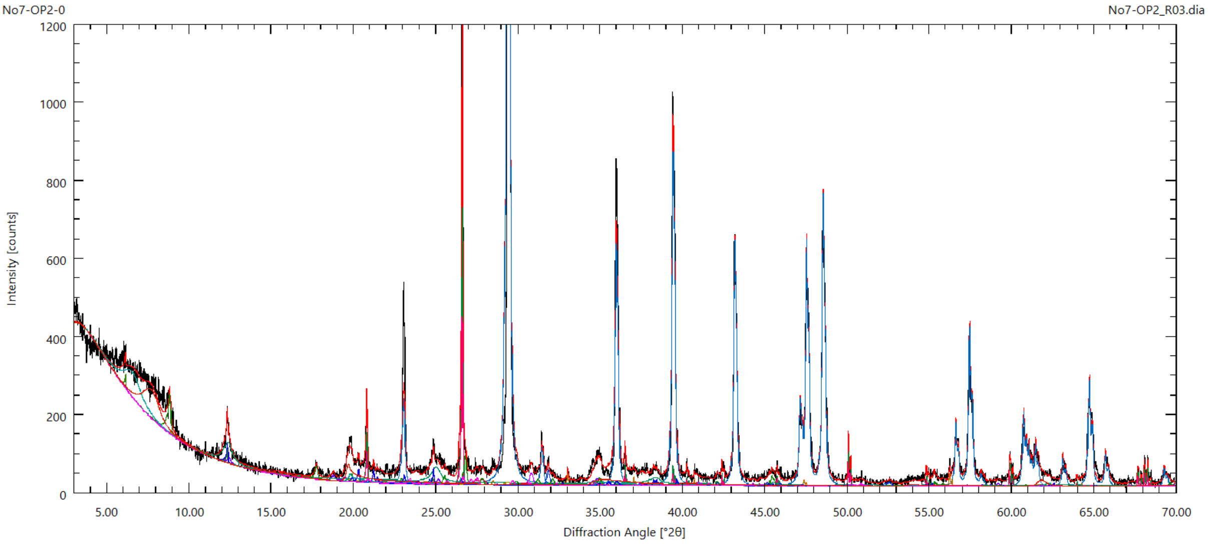
No7-OP2-0
No7-OP2_R03.dia
Intensity [counts]
1200
1000
800
600
400
200
0
5.00
10.00
15.00
20.00
25.00
30.00
35.00
40.00
45.00
50.00
55.00
60.00
65.00
70.00
Diffraction Angle [°2θ]

Data Sheet – Opalinus No8 (bulk), treated material *(OPA, 100°C, 69.3 h)*

Profex

Sample Information

No8-OP3-0				
File Name	No8-OP3_R01.dia			
Instrument configuration	D8_Advance_Sol-X_Darmstadt.geq			
Wavelength	CU (1.5406 Å)			
Directory	C:/Users/kasbo/Documents/Data_Laptop/Profex_data/BGE_Project/random			
Date of Refinement	Montag November 13, 2023			
Operator	kasbo			
Statistics	R_{wp} = 17.60	R_{exp} = 13.63	χ^2 = 1.6674	GoF = 1.2913

Diffraction Pattern

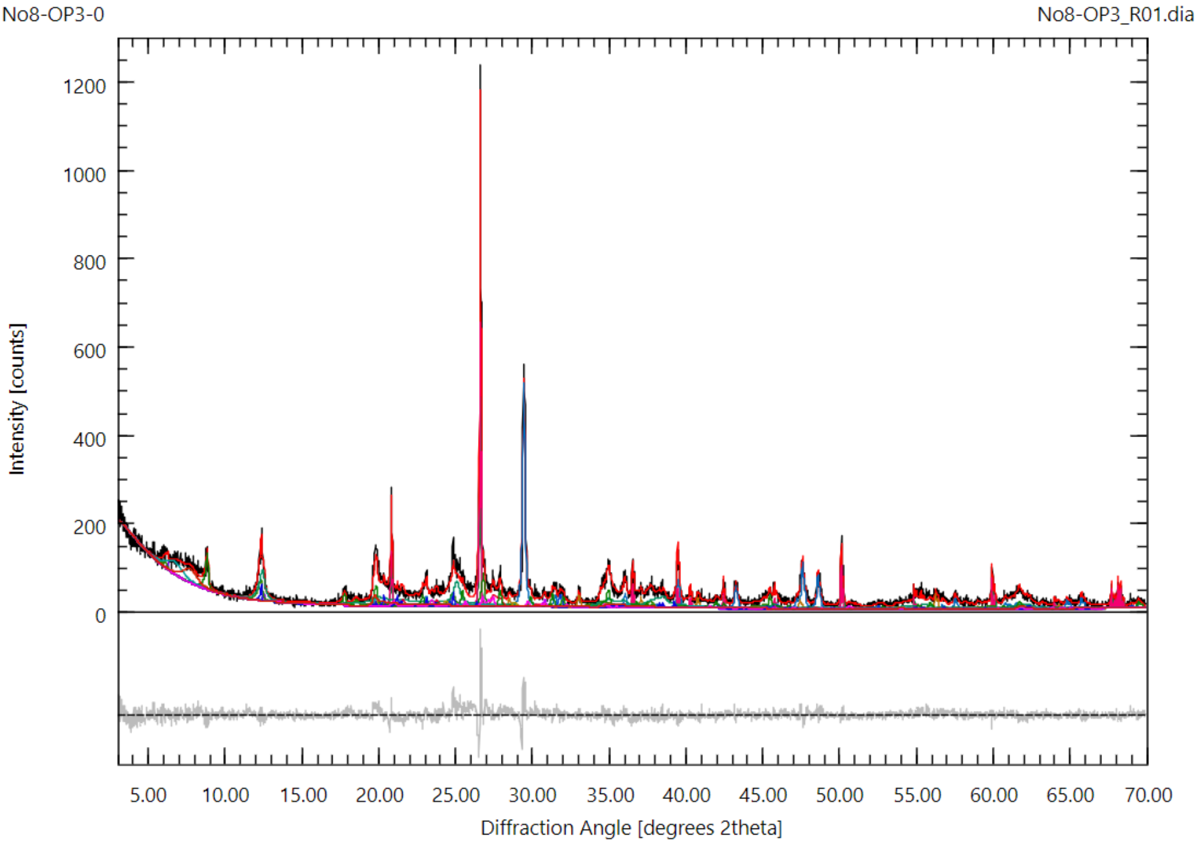

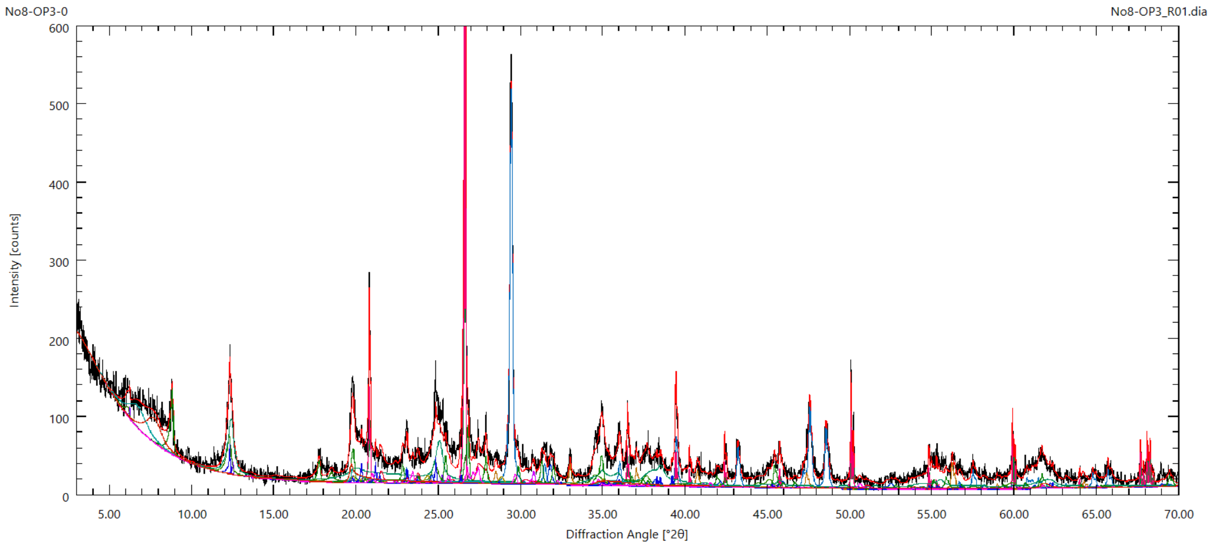
No8-OP3-0
No8-OP3_R01.dia
Intensity [counts]
0
100
200
300
400
500
600
5.00
10.00
15.00
20.00
25.00
30.00
35.00
40.00
45.00
50.00
55.00
60.00
65.00
70.00
Diffraction Angle [°2θ]

Data Sheet – Opalinus No14 (bulk), treated material *(OPA, 125°C, 48.5 h)*

Sample Information

No14-0				
File Name	No14_OPA versuch C_R01.dia			
Instrument configuration	D8_Advance_Sol-X_Darmstadt.geq			
Wavelength	CU (1.5406 Å)			
Directory	C:/Users/kasbo/Documents/Data_Laptop/Profex_data/BGE_Project/random			
Date of Refinement	Samstag Oktober 28, 2023			
Operator	kasbo			
Statistics	R_{wp} = 16.62	R_{exp} = 12.86	χ^2 = 1.6702	GoF = 1.2924

Diffraction Pattern

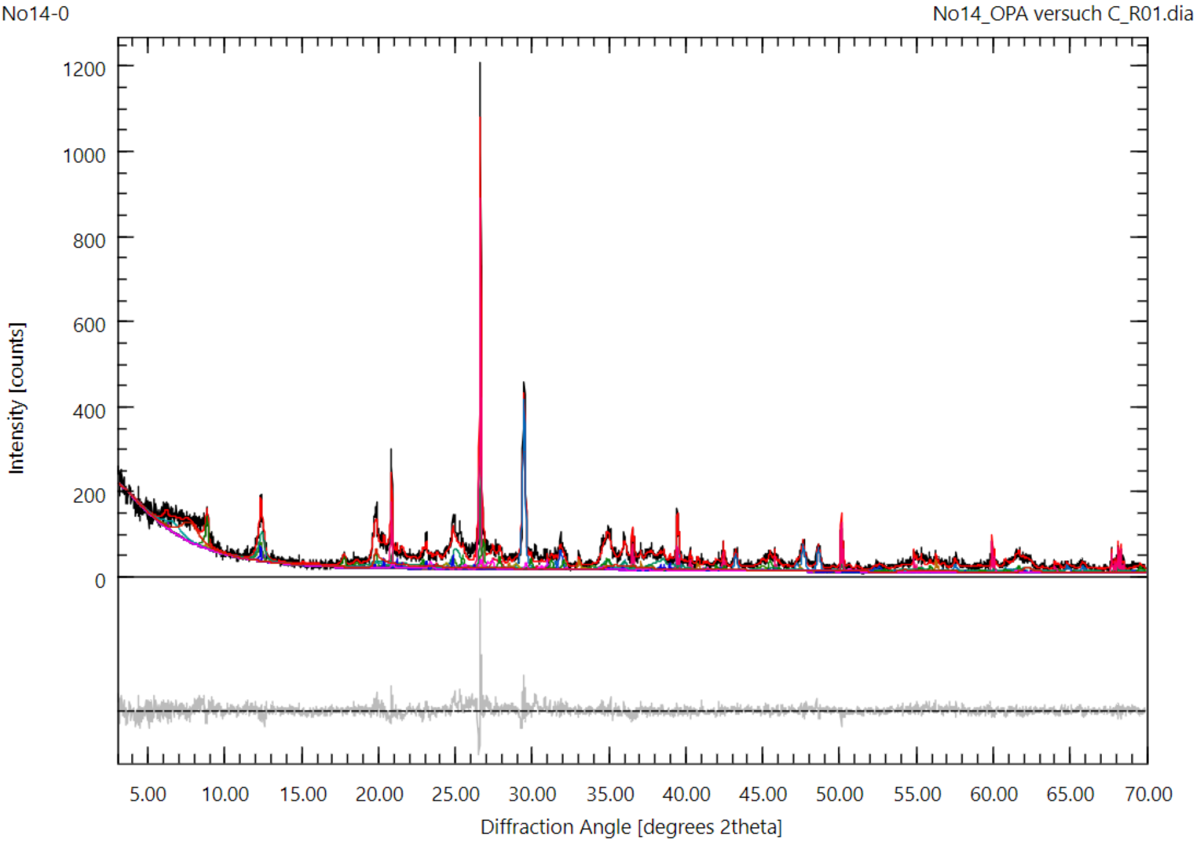

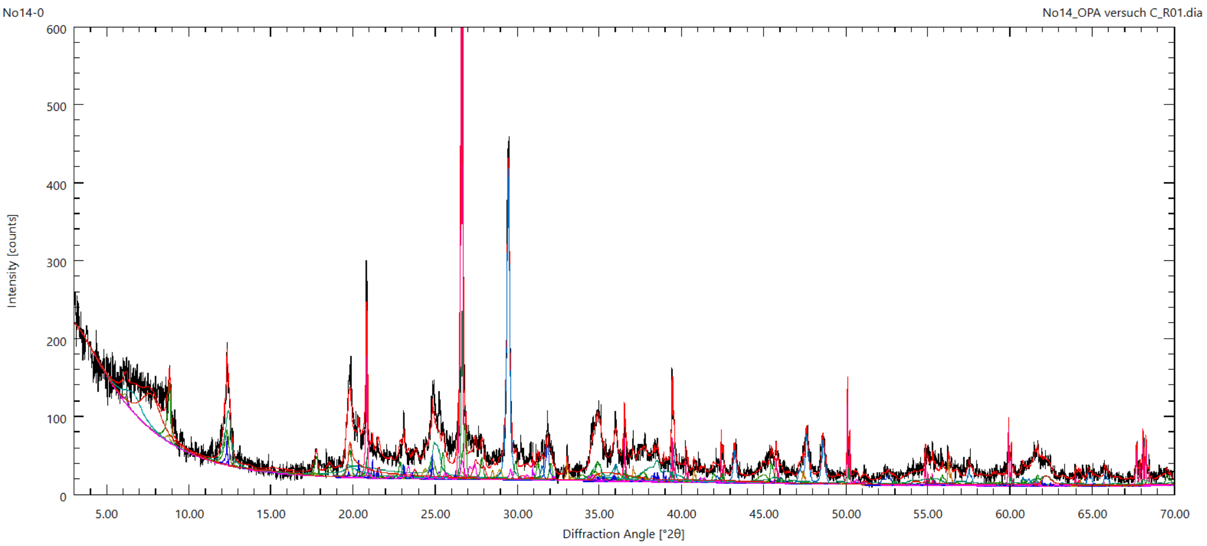
No14-0
No14_OPA versuch C_R01.dia
Intensity [counts]
600
500
400
300
200
100
0
5.00
10.00
15.00
20.00
25.00
30.00
35.00
40.00
45.00
50.00
55.00
60.00
65.00
70.00
Diffraction Angle [°2θ]

Data Sheet – Opalinus No13 (bulk), treated material *(OPA, 150°C, 48.6 h)*

Profex

Sample Information

No13-0				
File Name	No13_R01.dia			
Instrument configuration	D8_Advance_Sol-X_Darmstadt.geq			
Wavelength	CU (1.5406 Å)			
Directory	C:/Users/kasbo/Documents/Data_Laptop/Profex_data/BGE_Project/random			
Date of Refinement	Montag November 13, 2023			
Operator	kasbo			
Statistics	R_{wp} = 15.86	R_{exp} = 12.58	χ^2 = 1.5894	GoF = 1.2607

Diffraction Pattern

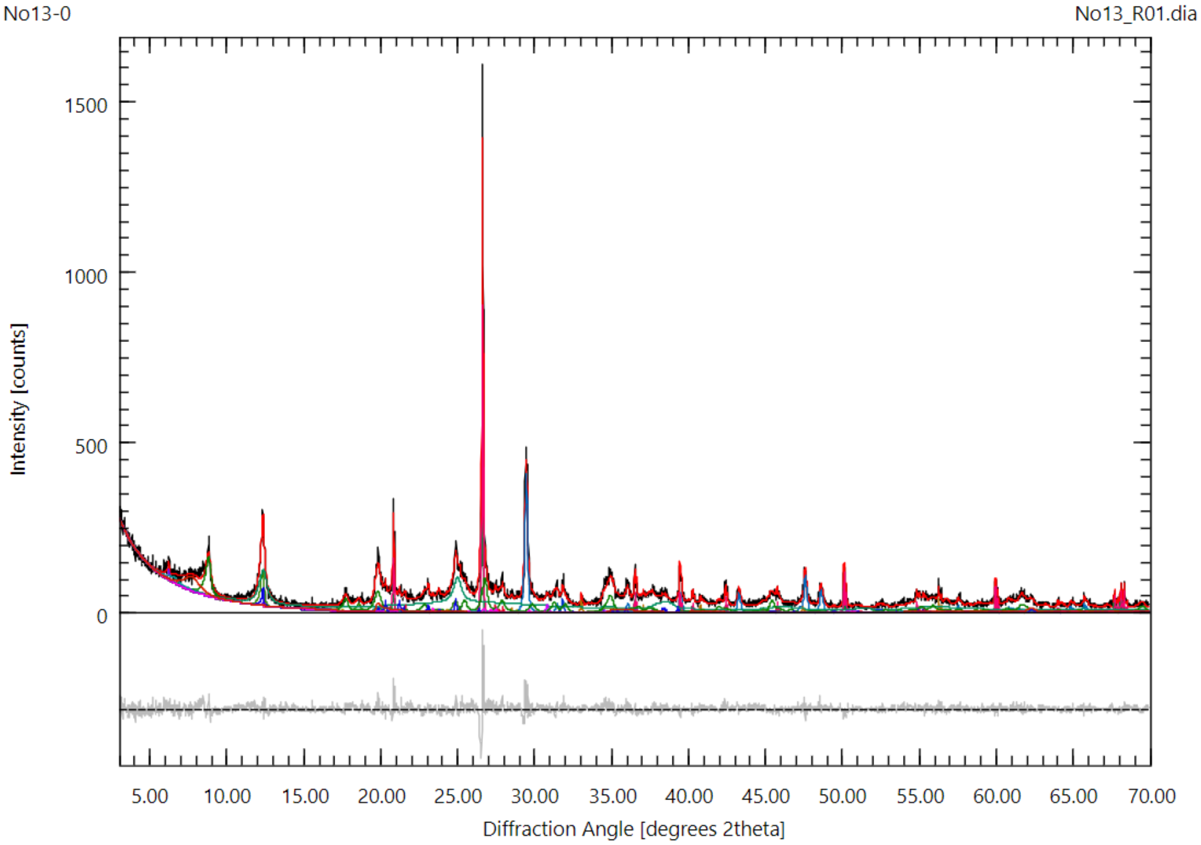

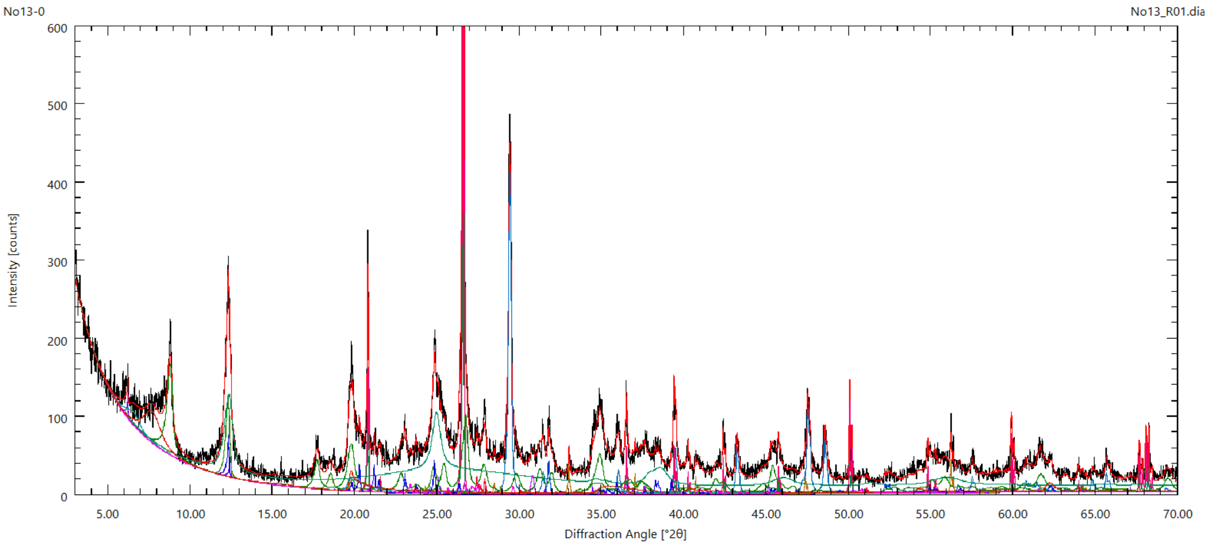
No13-0
No13_R01.dia
Intensity [counts]
0
100
200
300
400
500
600
5.00
10.00
15.00
20.00
25.00
30.00
35.00
40.00
45.00
50.00
55.00
60.00
65.00
70.00
Diffraction Angle [°2θ]

Data Sheet – Opalinus No9a (bulk), treated material *(OPA, 35°C)*

[without transport cell]

Profex

Sample Information

No9a-OP5-0				
File Name	No9a-OP5_R01.dia			
Instrument configuration	D8_Advance_Sol-X_Darmstadt.geq			
Wavelength	CU (1.5406 Å)			
Directory	C:/Users/kasbo/Documents/Data_Laptop/Profex_data/BGE_Project/random			
Date of Refinement	Samstag Oktober 28, 2023			
Operator	kasbo			
Statistics	R_{wp} = 12.13	R_{exp} = 8.39	χ^2 = 2.0902	GoF = 1.4458

Diffraction Pattern

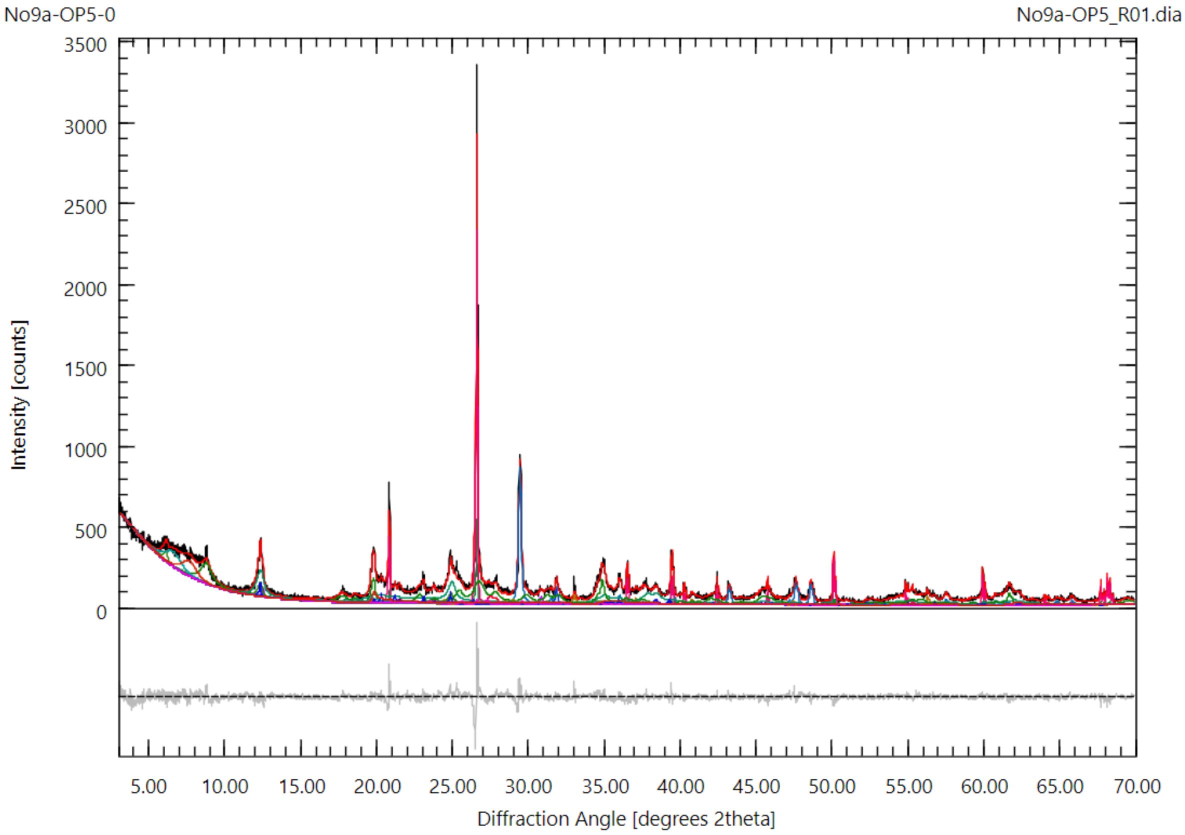

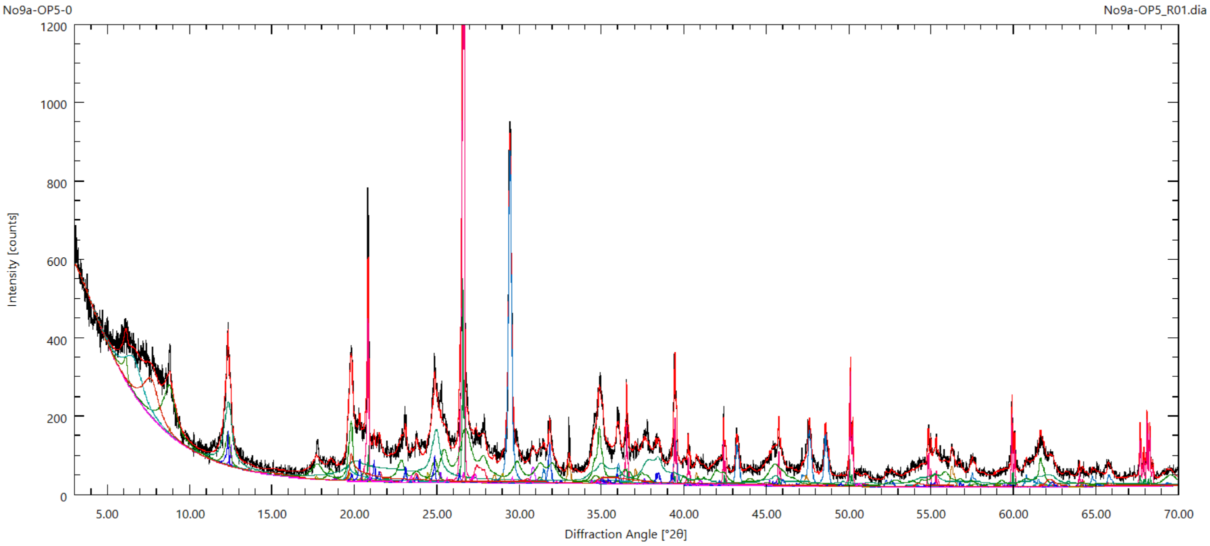
No9a-OP5-0
No9a-OP5_R01.dia
Intensity [counts]
1200
1000
800
600
400
200
0
5.00
10.00
15.00
20.00
25.00
30.00
35.00
40.00
45.00
50.00
55.00
60.00
65.00
70.00
Diffraction Angle [°2θ]

Data Sheet – Opalinus No9b (bulk), treated material *(OPA, 125°C)*

[without transport cell]

Profex

Sample Information

File Name	No9b-OP06_R01.dia			
Instrument configuration				
Wavelength	(1.5406 Å)			
Directory	C:/Users/kasbo/Documents/Data_Laptop/Profex_data/BGE_Project/random			
Date of Refinement				
Operator	kasbo			
Statistics	R_{wp} = 0.00	R_{exp} = 0.00	χ^2 = 0.0000	GoF = 0.0000

Diffraction Pattern

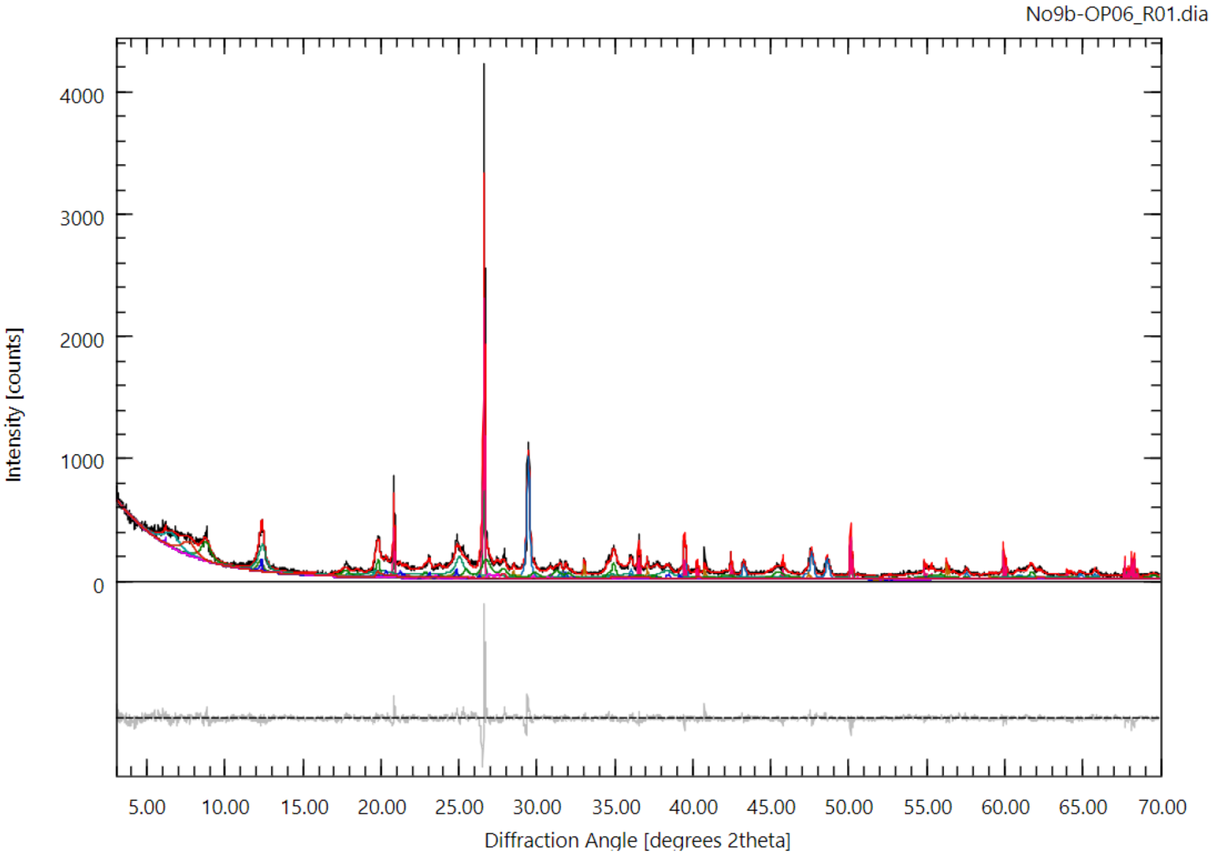

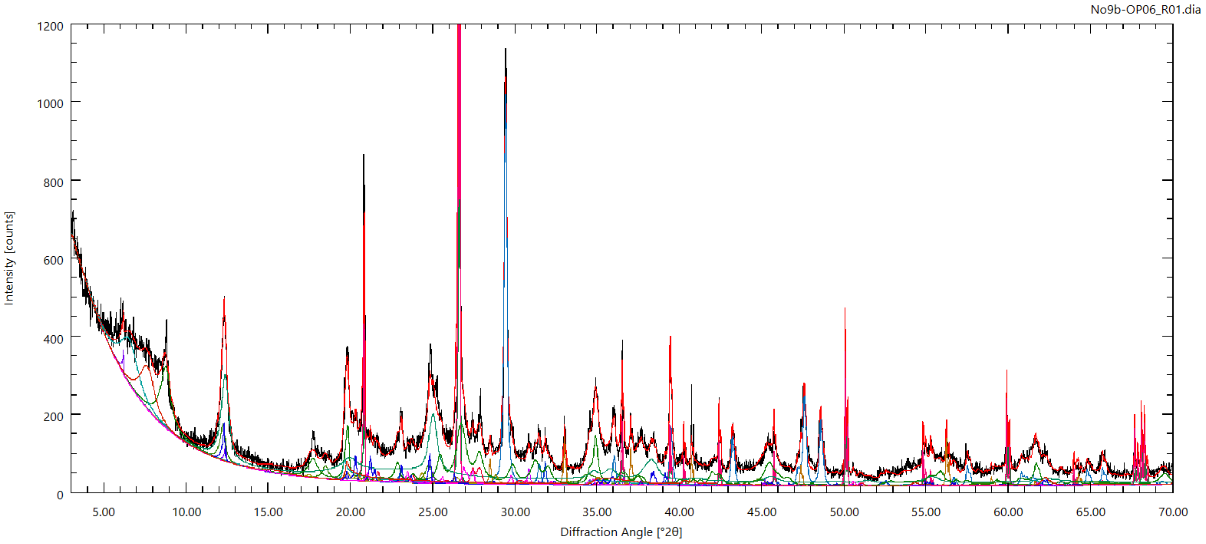
No9b-OP06_R01.dia
Intensity [counts]
0
200
400
600
800
1000
1200
5.00
10.00
15.00
20.00
25.00
30.00
35.00
40.00
45.00
50.00
55.00
60.00
65.00
70.00
Diffraction Angle [°2θ]

SUPPLEMENT – XRD: Oriented, < 2 µm

Content

Methodology – X-ray diffraction of oriented specimen

It is expected a characterization of clay mineral phases in treated B25 bentonite by X-ray diffraction (XRD) of oriented specimen (fraction < 2 µm). The treatment itself was carried out by GRS gGmbH in Braunschweig. The sample bodies were percolated by adapted Opalinus solution under different temperatures (35°C, 60°C, 100°C, 125°C, 150°C) and time intervals.

After the experiment, three samples were investigated from each sample body – material from top position, from central part and from the bottom. The flow direction of percolation was oriented from the top to the bottom of sample body.

Furthermore, percolated samples of Opalinus Clay and Friedland Clay (Siedlungsscholle, Ost-Feld) were also analyzed.

The XRD analyses on oriented samples of <2 µm material (separated by sedimentation) were performed in air-dried and ethylene glycol-solvated specimens for identification of expandable clay minerals. The specimens were analyzed by using a SIEMENS Theta/2Theta D5000 goniometer equipped with a Cu tube ($K\alpha_{1,2}$-radiation) and a secondary monochromator (fixed divergence slide: 0.2 mm; collimator: 0.2; receiving slit size: 0.1 mm; step size: 0.02 °2θ; scan step time: 1 s; measured interval: 3.0 - 35.0 °2θ at the clay laboratory, Technical University Darmstadt.

Obtained XRD patterns were modelled with the Sybilla software developed by Chevron Inc. (Aplin et al., 2006), which is a program to compare the measured X-ray diffractogram with a modelled pattern of the basal reflections to better determine discrete clay minerals and interstratifications. The quantities of interlayer ion species and octahedral Fe as well as the mean value of coherent scattering domain sizes (T mean) were considered as variables in the fitting process. This modelling of oriented XRD patterns was also applied to validate the TEM-EDX measurements concerning possible precipitations of Fe, Al or amorphous silica on particles.

References:

Aplin, A.C., Matenaar, I.F., McCarty, D.K., van der Pluijm, B.A. (2006). Clays Clay Miner 54, 500-514. DOI: 10.1346/CCMN.2006.0540411

OVERVIEW – Mineral matter in fraction < 2 µm of treated B25-series

Sample	**Beidellite-Montm. intergrowth**	**diVS-ml**	**Illite**	**Kaolinite**	**Kaolinite-Smectite-ml** *(KS GL R1)*	**Kaolinite-Smectite-ml** *(KS GL R0)*	*Σ total*
B25 original	47% *(%S = 99%)*	16% *(%S = 55%)*	9%	5%	23% *(%S = 45%)*		*100%*
35°C, 93.6h, OPA							
No4_T	67% *(%S = 100%)*	11% *(%S = 30%)*	10%	5%		7% *(%S = 58%)*	*100%*
No4_C	53% *(%S = 100%)*	19% *(%S = 38%)*	6%	2%		21% *(%S = 65%)*	*101%*
No4_B	41% *(%S = 100%)*	15% *(%S = 38%)*	11%	6%		27% *(%S = 62%)*	*100%*
35°C, 285h, OPA, 0.7 MPa							
No23	50% *(%S = 82%)*	13% *(%S = 45%)*	10%	6%		22% *(%S = 57%)*	*101%*
60°C, 454h, OPA							
No5_T	41% *(%S = 100%)*	14% *(%S = 33%)*	8%	5%		31% *(%S = 61%)*	*99%*
No5_C	32% *(%S = 100%)*	18% *(%S = 39%)*	8%	6%		37% *(%S = 65%)*	*101%*
No5_B	39% *(%S = 100%)*	17% *(%S = 55%)*	13%	8%		23% *(%S = 65%)*	*100%*
100°C, 110h, OPA							
No0_T	58% *(%S = 99%)*	8% *(%S = 30%)*	20%	3%	12% *(%S = 45%)*		*101%*
No0_C	28% *(%S = 94%)*	13% *(%S = 30%)*	4%	7%	44% *(%S = 75%)*	4% *(%S = 48%)*	*100%*
No0_B	28% *(%S = 100%)*	19% *(%S = 25%)*	9%	8%	11% *(%S = 76%)*	25% *(%S = 58%)*	*100%*
100°C, 35d, OPA							
No2_T	25% *(%S = 100%)*	20% *(%S = 20%)*	2%	7%	37% *(%S = 79%)*	8% *(%S = 48%)*	*99%*
No2_C	21% *(%S = 100%)*	11% *(%S = 23%)*	3%	7%	47% *(%S = 78%)*	12% *(%S = 48%)*	*101%*
No2_B	11% *(%S = 100%)*	8% *(%S = 23%)*	11%	10%	51% *(%S = 75%)*	12% *(%S = 48%)*	*101%*
125°C, 98.6h, OPA							
No15	10% *(%S = 60%)*	24% *(%S = 28%)*	14%	18%	34% *(%S = 75%)*		*100%*
150°C, 4d, OPA							
No3_T	26% *(%S = 100%)*	11% *(%S = 22%)*	5%	6%	39% *(%S = 74%)*	13% *(%S = 48%)*	*100%*
No3_C	38% *(%S = 100%)*	10% *(%S = 22%)*	4%	6%	27% *(%S = 76%)*	16% *(%S = 48%)*	*101%*
No3_B	40% *(%S = 100%)*	9% *(%S = 27%)*	3%	5%	30% *(%S = 78%)*	13% *(%S = 48%)*	*100%*

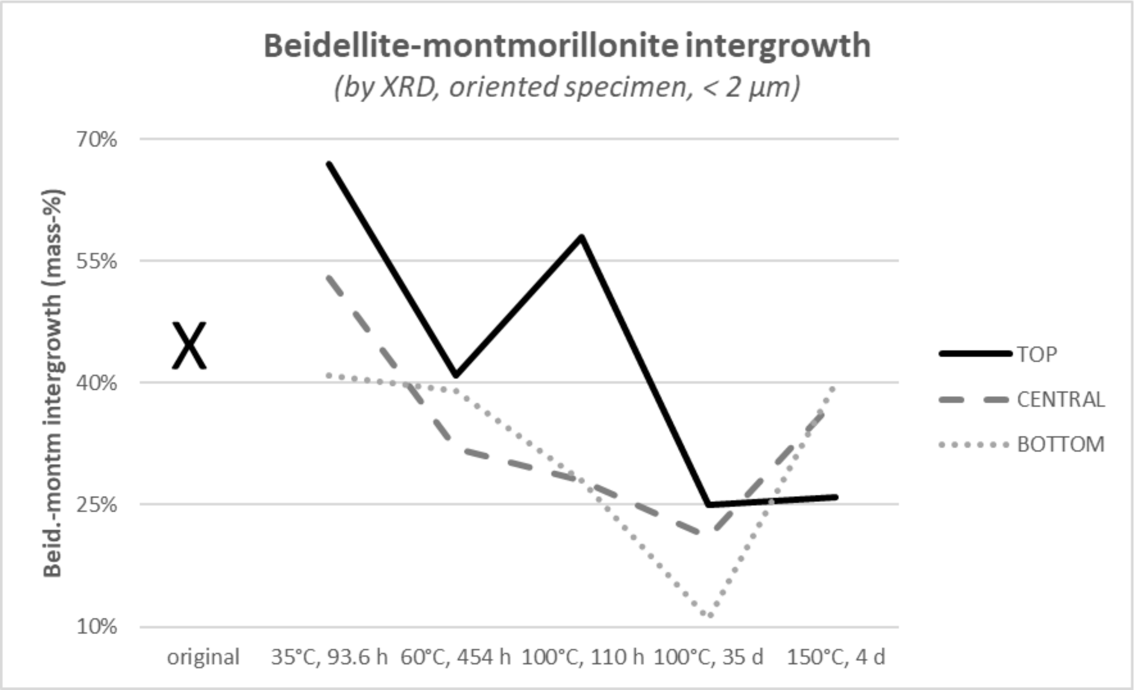

Trend: Rising treatment level deals to a reduced portion of Ca-smectite phases (assumed: an intergrowth between beidellite and montmorillonite in a different ratio - see TEM-EDX measurements), full expandability is drawn in all experiments for this intergrowth.

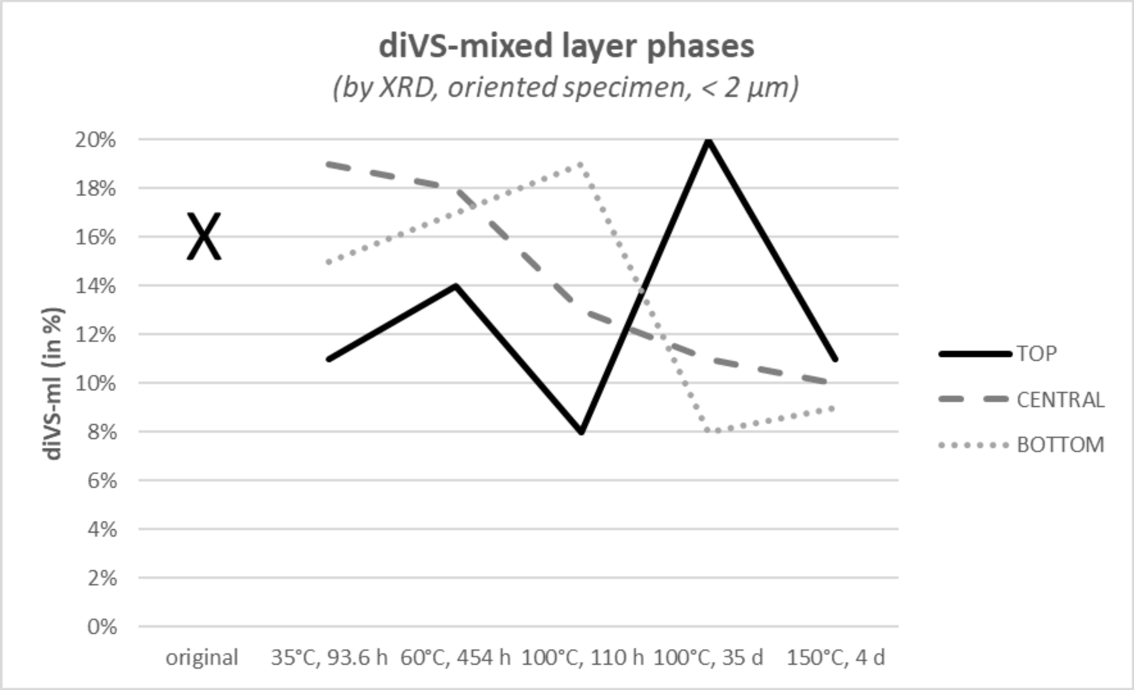

Trend: A certain trend is not to recognize for mass distribution of dioctahedral vermiculite - smectite mixed layer phases (diVS-ml).

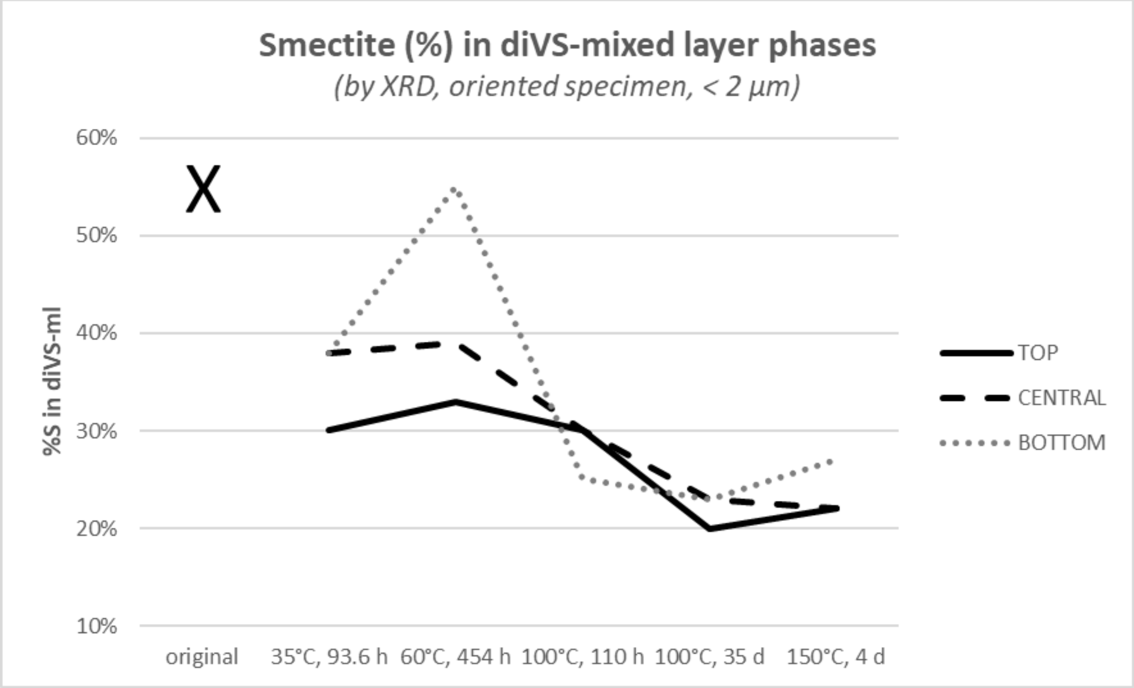

Trend: The probability of smectite layers (%S) in diVS-ml and the expandability of diVS-ml are decreasing with rising treatment level as well as lower than the original material.

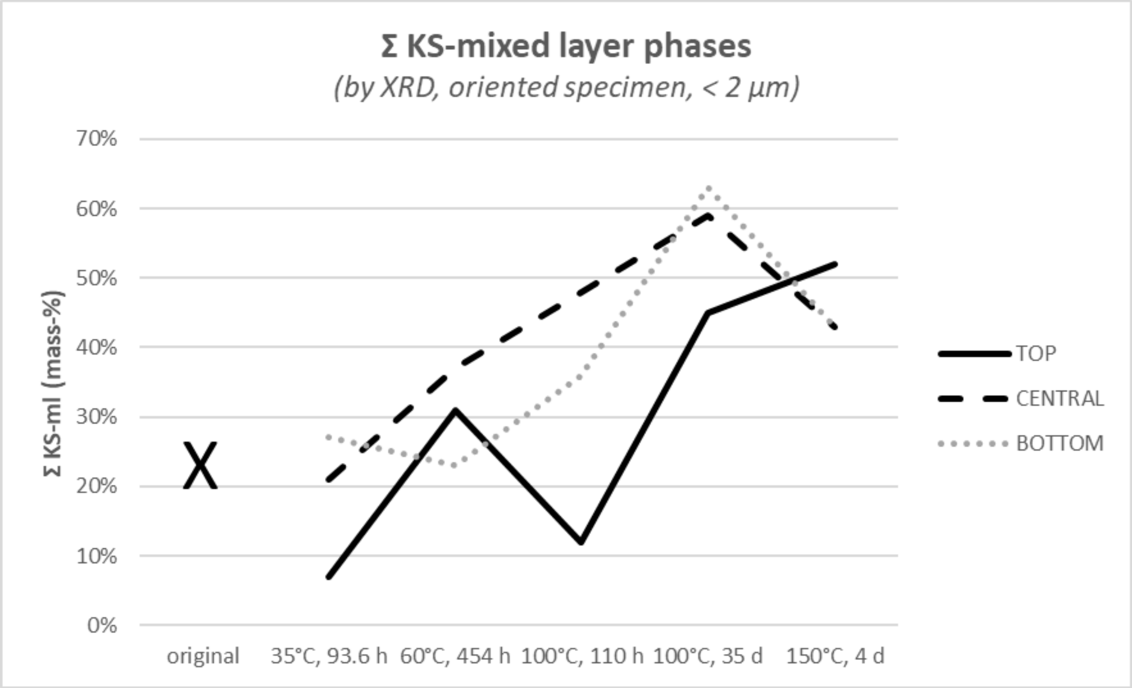

Trend: The mass distribution of kaolinite-smectite mixed layer phases (KS-ml) is rising with increased treatment level and higher than in the original, untreated B25 bentonite.

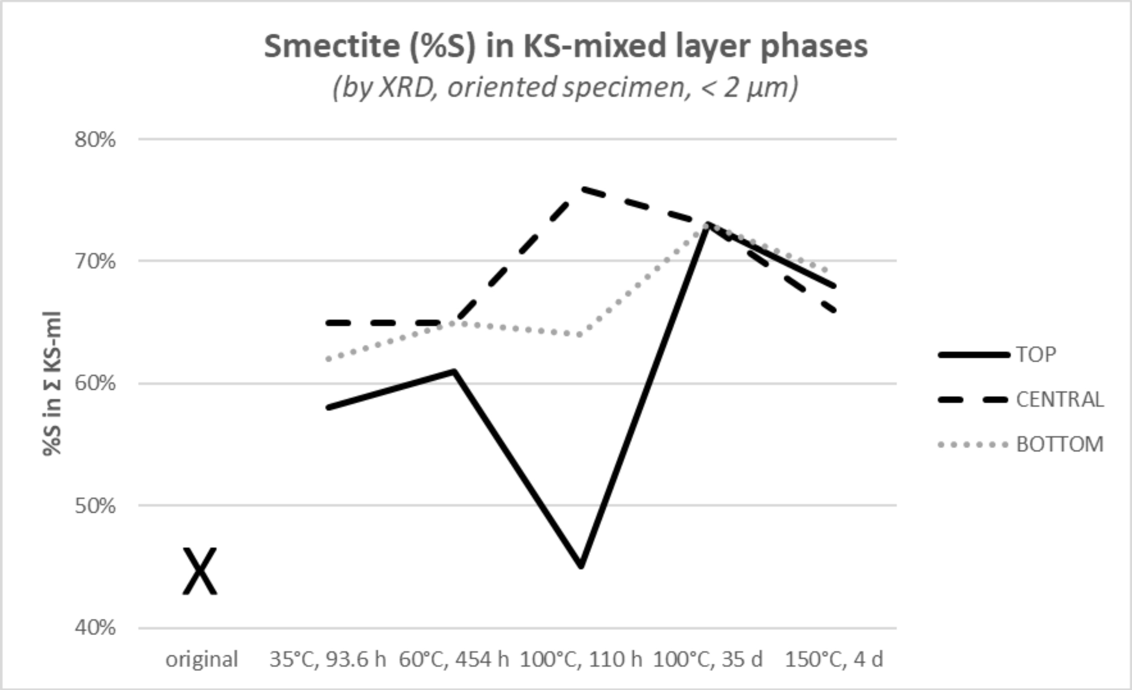

Trend: The probability of smectite layers (%S) in KS-ml and the expandability of KS-ml are rising with increased treatment level as well as higher than the original material.

OVERVIEW – Mineral matter in fraction < 2 µm of treated OPALINUS

Sample	**diVS-ml** *(IS GLY R0)*	**diVS-ml** *(ISS GLY R0)*	**Illite**	**Chlorite**	**Kao-linite**	**Kaolinite-Smectite-ml** *(KS GL R0)*	**Kaolinite-Smectite-ml** *(KSS GL R0)*	*Σ total*
OPALINUS original	18% *(%S = 11%)*	11% *(%S = 48%)*	8%	8%	8%	20% *(%S = 14%)*	27% *(%S = 61%)*	*100%*
35°C, 144h **No22**	44% *(%S = 16%)*		14%	4%	7%		32% *(%S = 37%)*	*100%*
60°C, 45.4h **No9**	21% *(%S = 23%)*		14%	5%	16%	10% *(%S = 14%)*	34% *(%S = 53%)*	*100%*
60°C, 95.3h **No7**	32% *(%S = 20%)*		12%	5%	12%	13% *(%S = 9%)*	26% *(%S = 55%)*	*100%*
100°C, 69.3h **No8**	22% *(%S = 26%)*		29%	5%	12%	6% *(%S = 14%)*	27% *(%S = 53%)*	*101%*
125°C, 48.5h **No14**	31% *(%S = 24%)*		26%	5%	8%	12% *(%S = 26%)*	19% *(%S = 35%)*	*101%*
150°C, 48.6h **No13**	42% *(%S = 16%)*		14%	4%	8%	2% *(%S = 28%)*	30% *(%S = 45%)*	*102%*
Without transport cell *35°C* **No9a**	25% *(%S = 20%)*		14%	4%	15%	10% *(%S = 9%)*	31% *(%S = 55%)*	*99%*
125°C **No9b**	13% *(%S = 29%)*		30%	4%	13%	7% *(%S = 14%)*	35% *(%S = 56%)*	*102%*

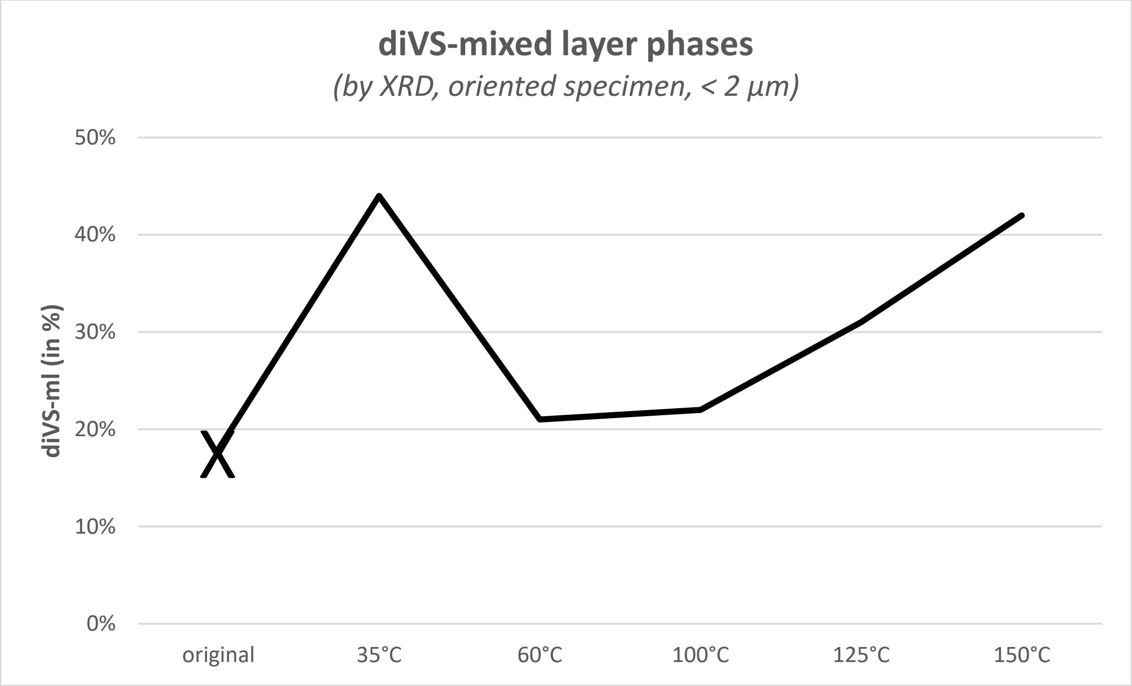

Trend: Increasing ratio of mass distribution by experiments in comparison to original clay.

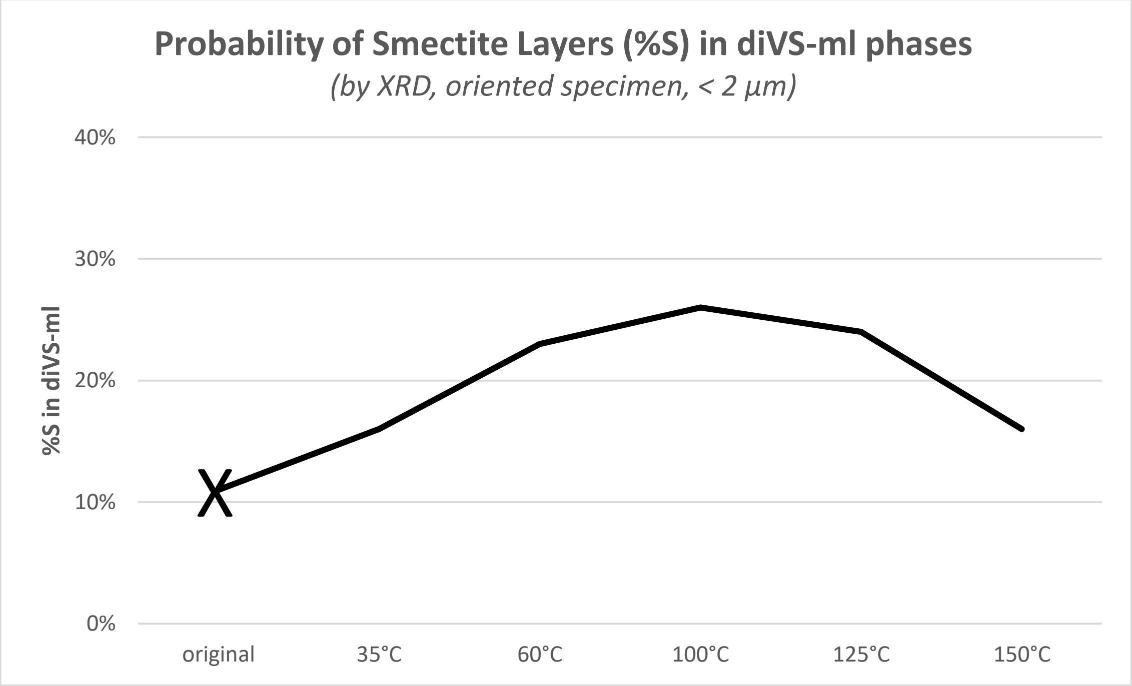

Trend: Moderate smectitization caused by experiments in comparison to original clay.

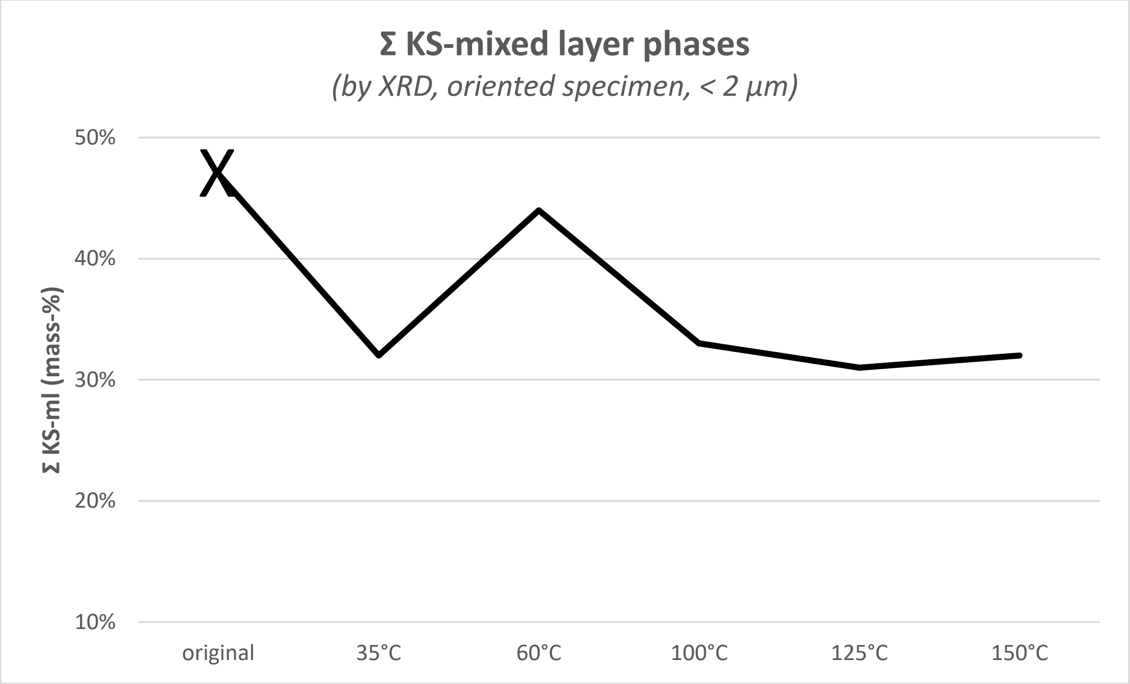

Trend: Slight decreasing of mass distribution by experiments in comparison to original clay.

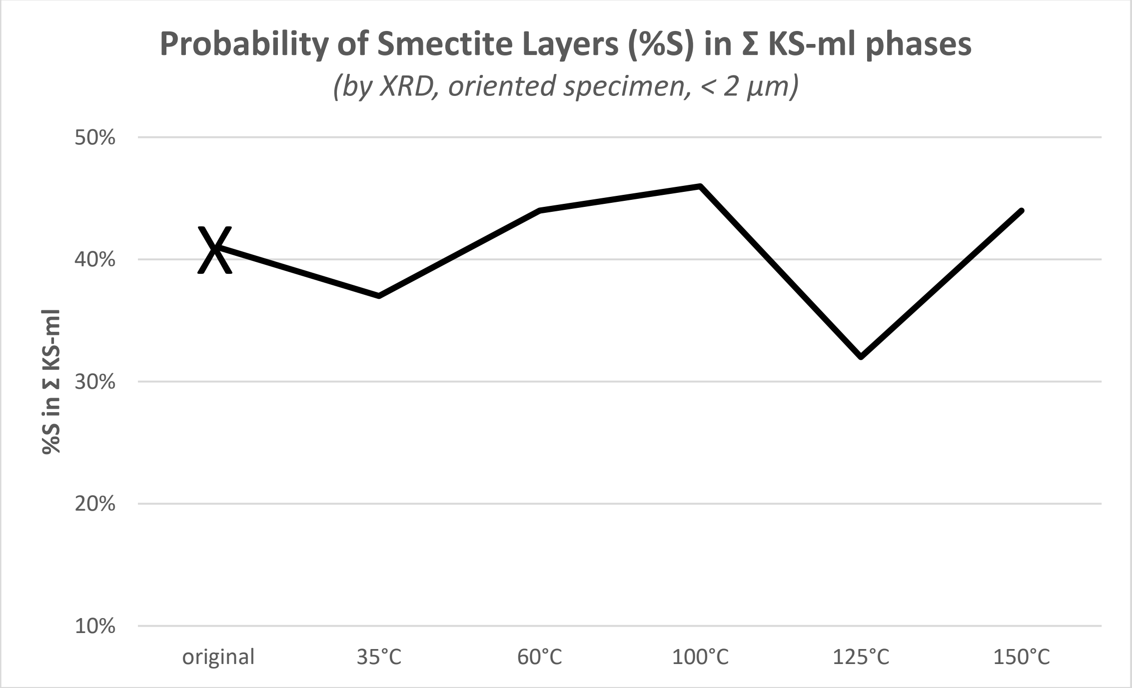

Trend: No significant trend caused by experiments in comparison to original clay.

OVERVIEW – Mineral matter in fraction < 2 µm of treated FRIEDLAND

Sample	**BMI-ml** *(IS GLY R0_V1)*	**beid. diVS-ml** *(IS GLY R0_V2 or ISS GLY R1)*	**Illite**	**Chlorite**	**Kao-linite**	**Kaolinite-Smectite-ml** *(KS GL R0)*		*Σ total*
FRIEDLAND* original	11% *(%S = 82%)*	2% *(%S = 25%)*	13%	15%	48%	11% *(%S = 23%)*		*100%*
orig., compacted **No19**		54% *(%S = 39%)*	16%	2%	10%	17% *(%S = 48%)*		*99%*
35°C, 46.3h **No10**	11% *(%S = 100%)*	40% *(%S = 34%)*	11%		12%	27% *(%S = 51%)*		*101%*
60°C, 45.9h **No11**	17% *(%S = 94%)*	49% *(%S = 34%)*	7%		13%	14% *(%S = 48%)*		*100%*
100°C, 40h **No16**		11% *(%S = 36%)* 57% *(%S = 47%)*	16%		13%	4% *(%S = 50%)*		*101%*
125°C, 40h **No20**		6% *(%S = 10%)* 67% *(%S = 47%)*	11%		10%	6% *(%S = 48%)*		*100%*
150°C, 68.3h **No21**		7% *(%S = 30%)* 51% *(%S = 52%)*	24%	4%	9%	6% *(%S = 50%)*		*101%*
without transport cell *100°C* **No12**	35% *(%S = 79%)*	27% *(%S = 34%)*	11%		11%	16% *(%S = 40%)*		*100%*

*** Friedland (MV),** Siedlungsscholle, Ost-Feld (= neues Abbaufeld)

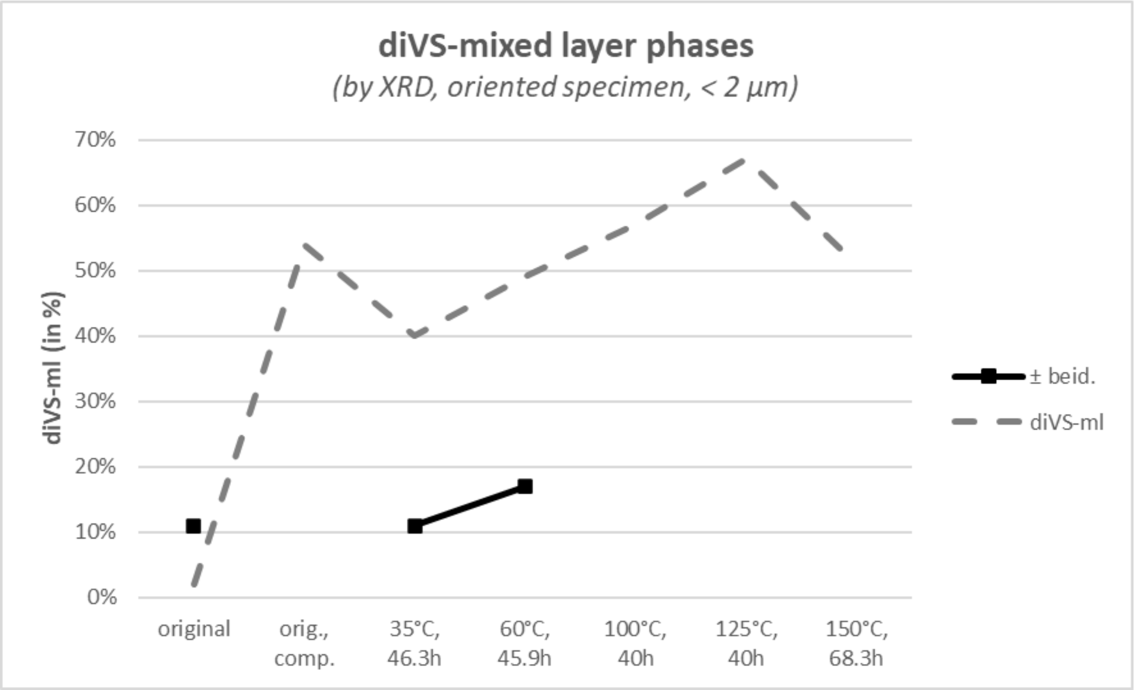

Trend: Beidellite (solid line) disappears with increasing thermal pressure. Increasing mass-% for illite-rich diVS-ml phase (dashed line).

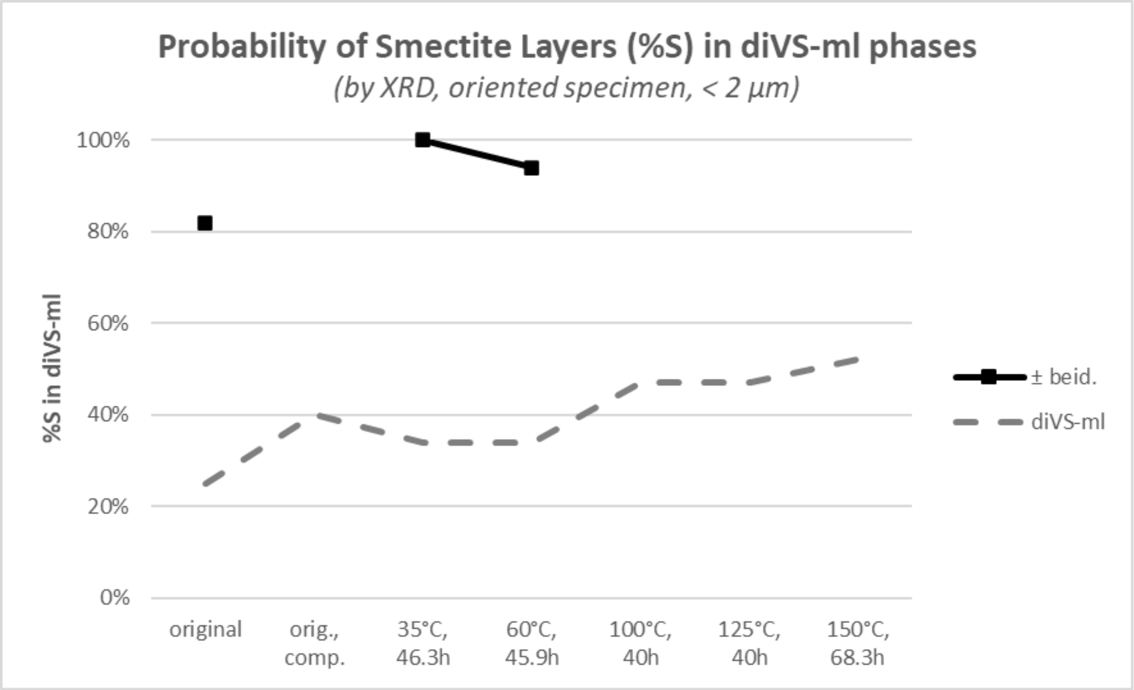

Trend: Slight increasing %S for illite-rich diVS-ml phase (dashed line) with increasing thermal pressure.

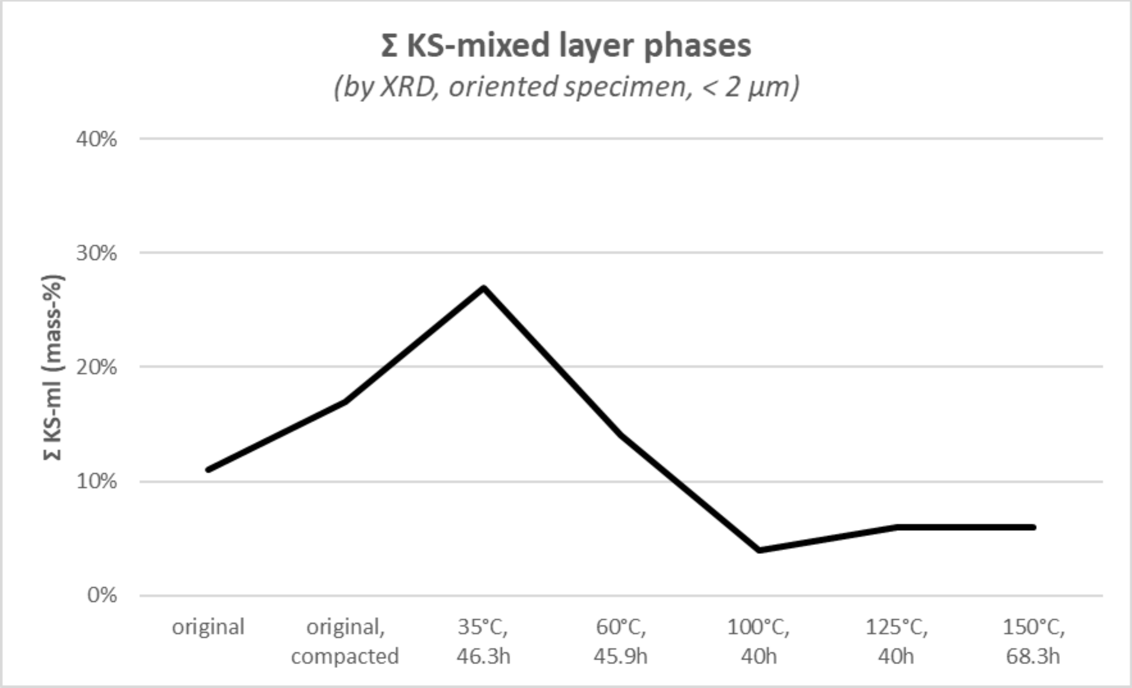

Trend: No significant trend.

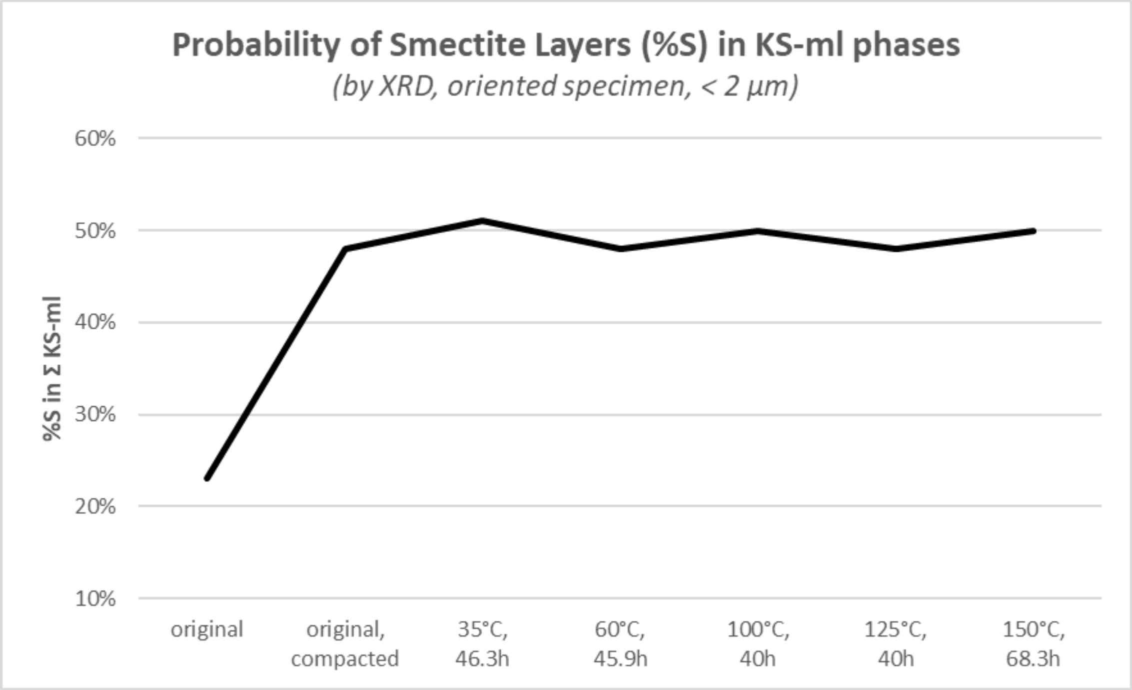

Trend: Trend to increased, but constant %S.

Data Sheet – B25 total (< 2 µm), original material *(uncompacted)*

Diffraction pattern of oriented specimen & modelling by Sybilla

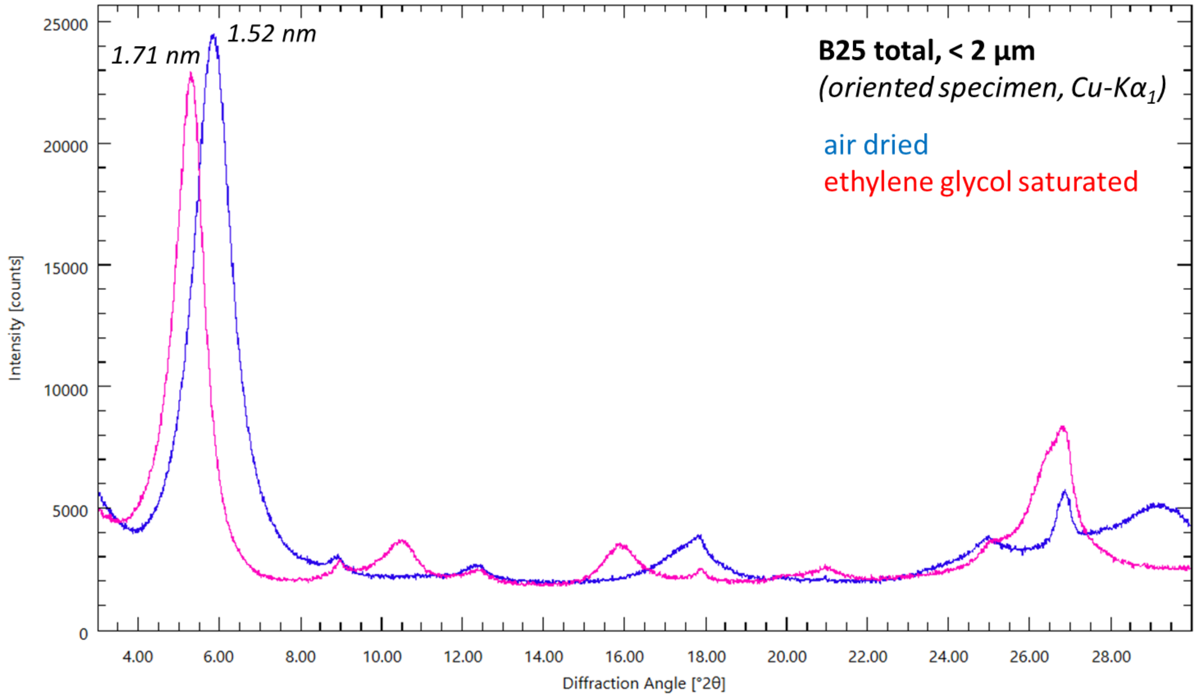

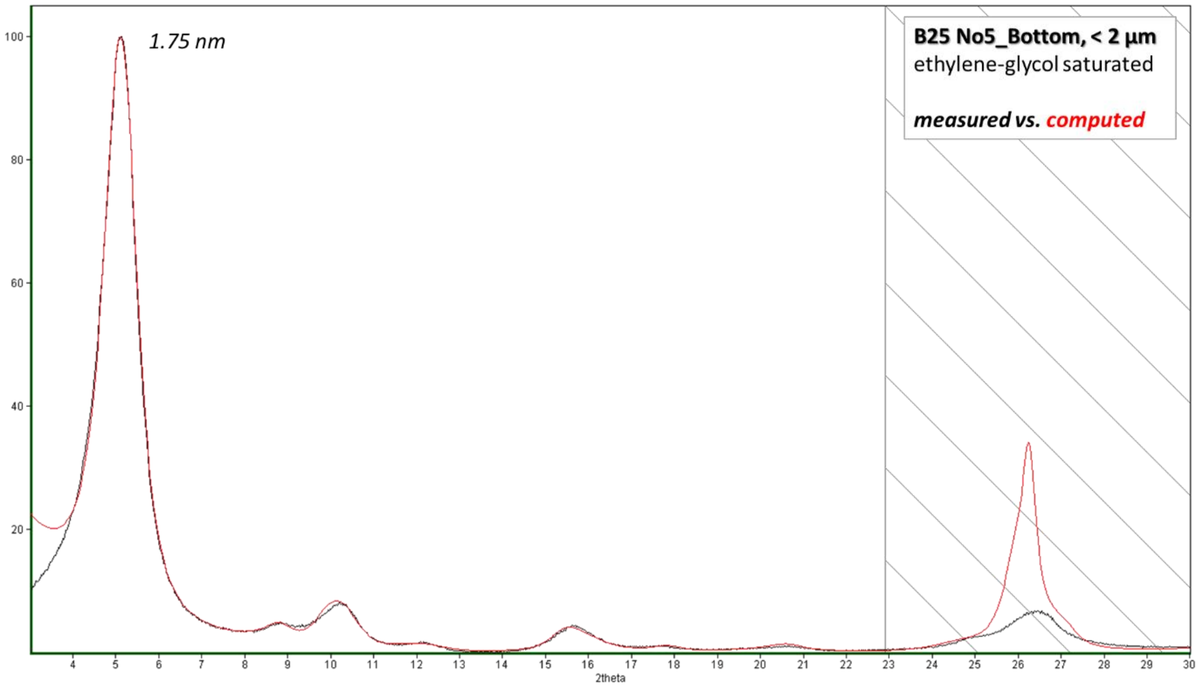

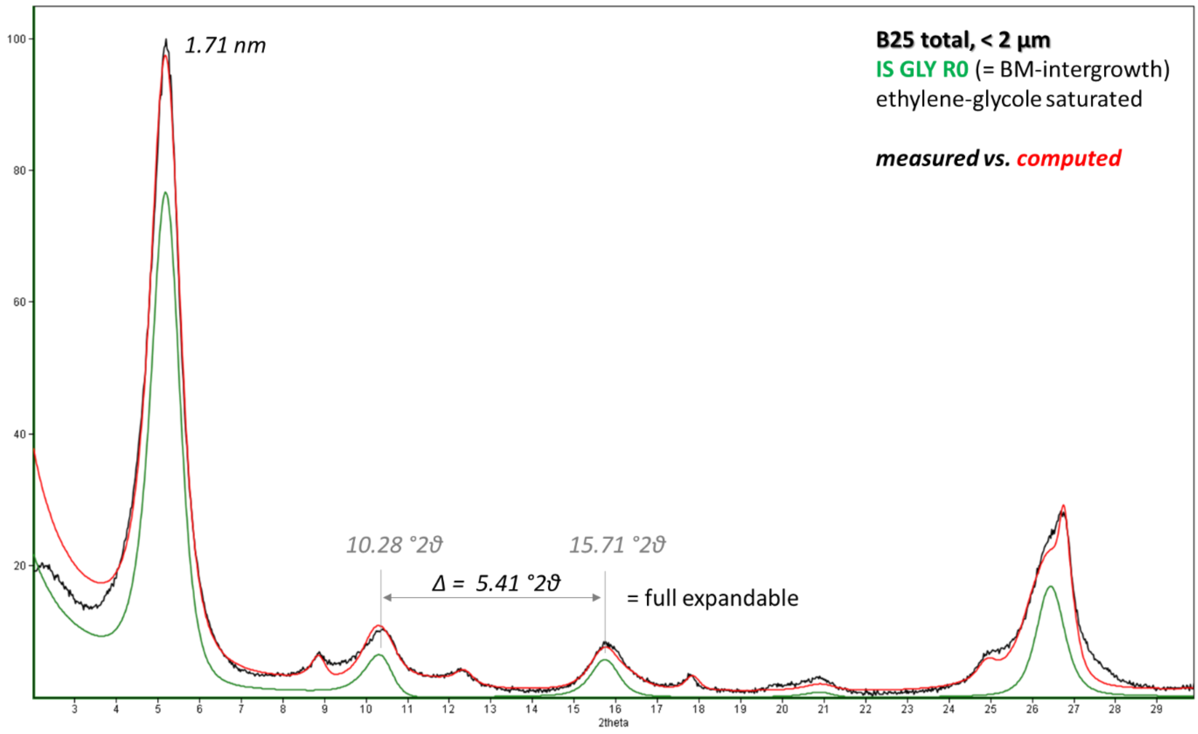
B25 total, < 2 µm
IS GLY R0 (= BM-intergrowth)
ethylene-glycole saturated
measured vs. computed
1.71 nm
10.28 °2ϑ
15.71 °2ϑ
Δ = 5.41 °2ϑ
= full expandable
100
80
60
40
20
3 4 5 6 7 8 9 10 11 12 13 14 15 16 17 18 19 20 21 22 23 24 25 26 27 28 29
2theta

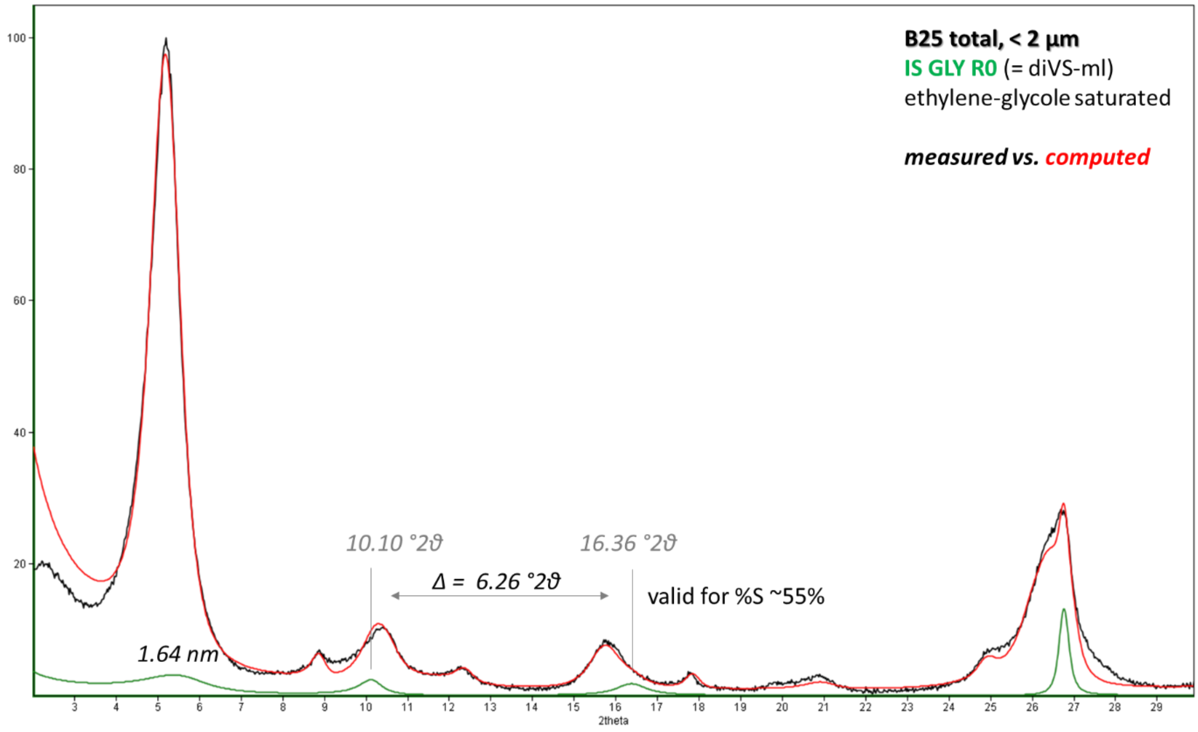
B25 total, < 2 µm
IS GLY R0 (= diVS-ml)
ethylene-glycole saturated
measured vs. computed
1.64 nm
10.10 °2ϑ
16.36 °2ϑ
Δ = 6.26 °2ϑ
valid for %S ~55%
100
80
60
40
20
3 4 5 6 7 8 9 10 11 12 13 14 15 16 17 18 19 20 21 22 23 24 25 26 27 28 29
2theta

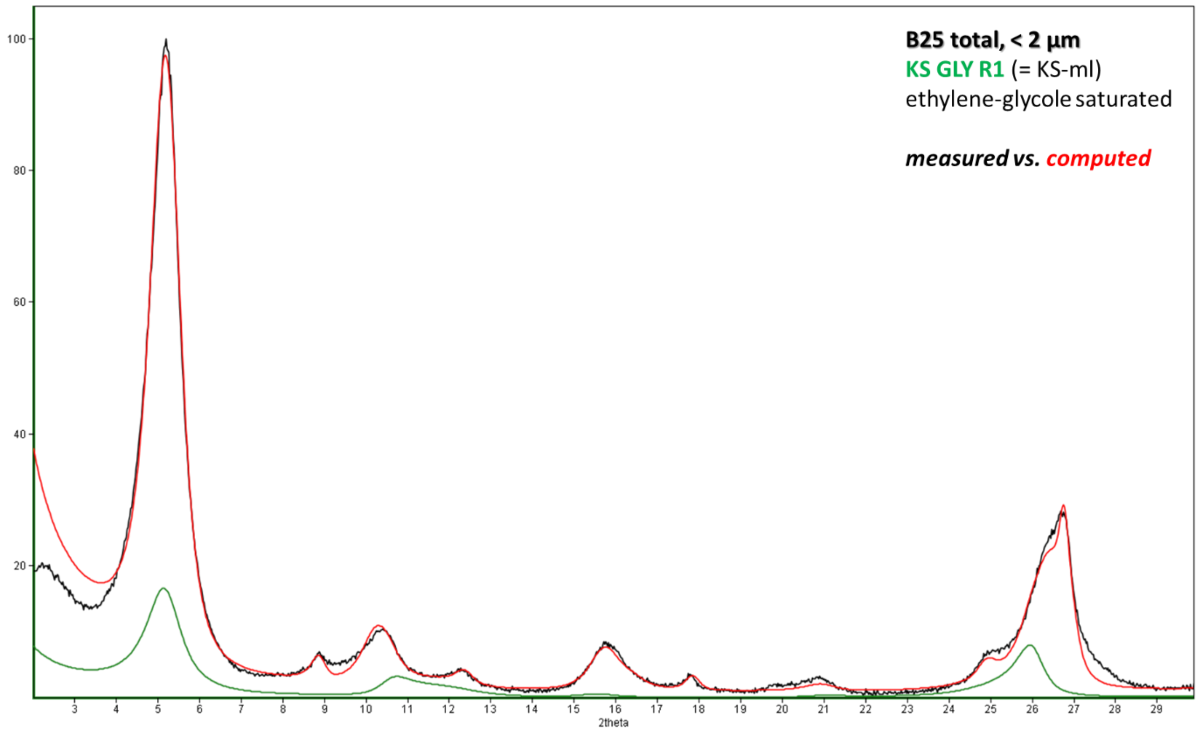
B25 total, < 2 µm
KS GLY R1 (= KS-ml)
ethylene-glycole saturated
measured vs. computed
100
80
60
40
20
3
4
5
6
7
8
9
10
11
12
13
14
15
16
17
18
19
20
21
22
23
24
25
26
27
28
29
2theta

Data Sheet – B25 No4_T (< 2 µm), treated material *(OPA, 35°C, 93.6 hours)*

Diffraction pattern of oriented specimen & modelling by Sybilla

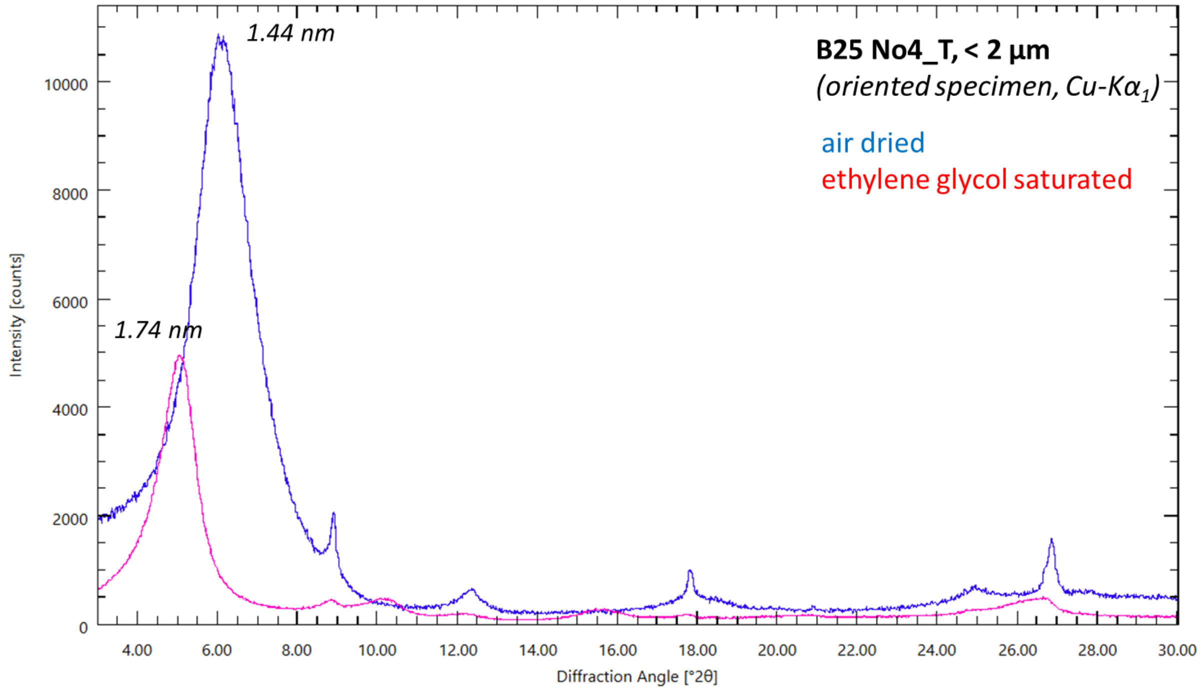

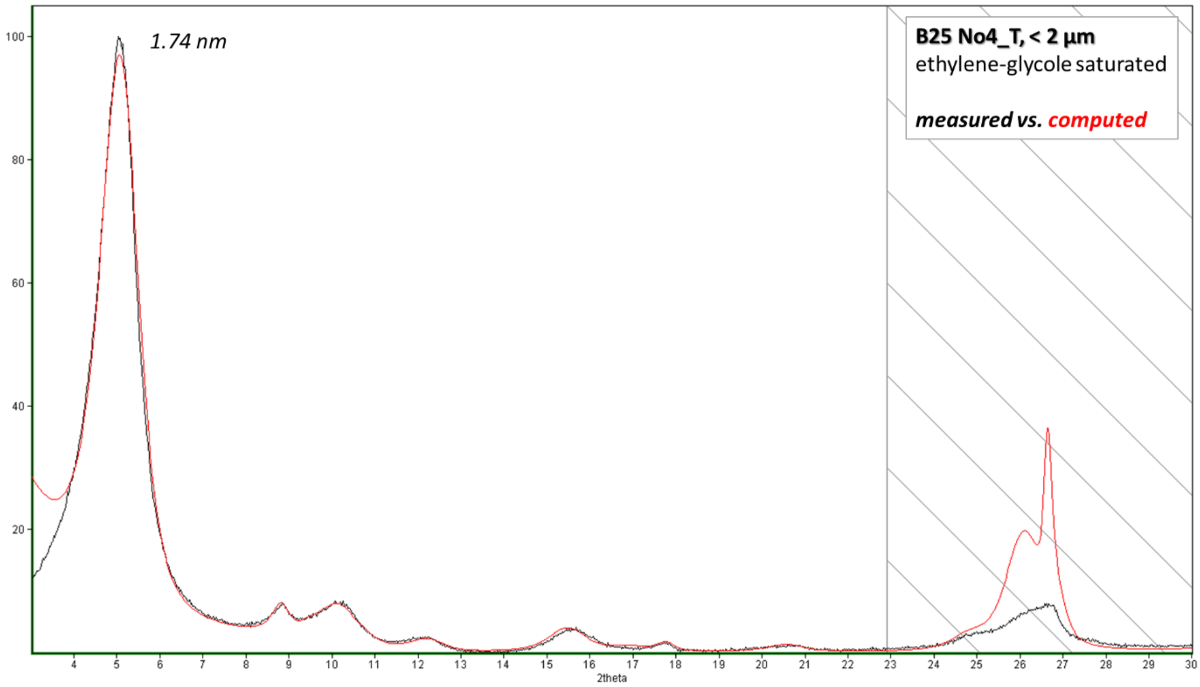

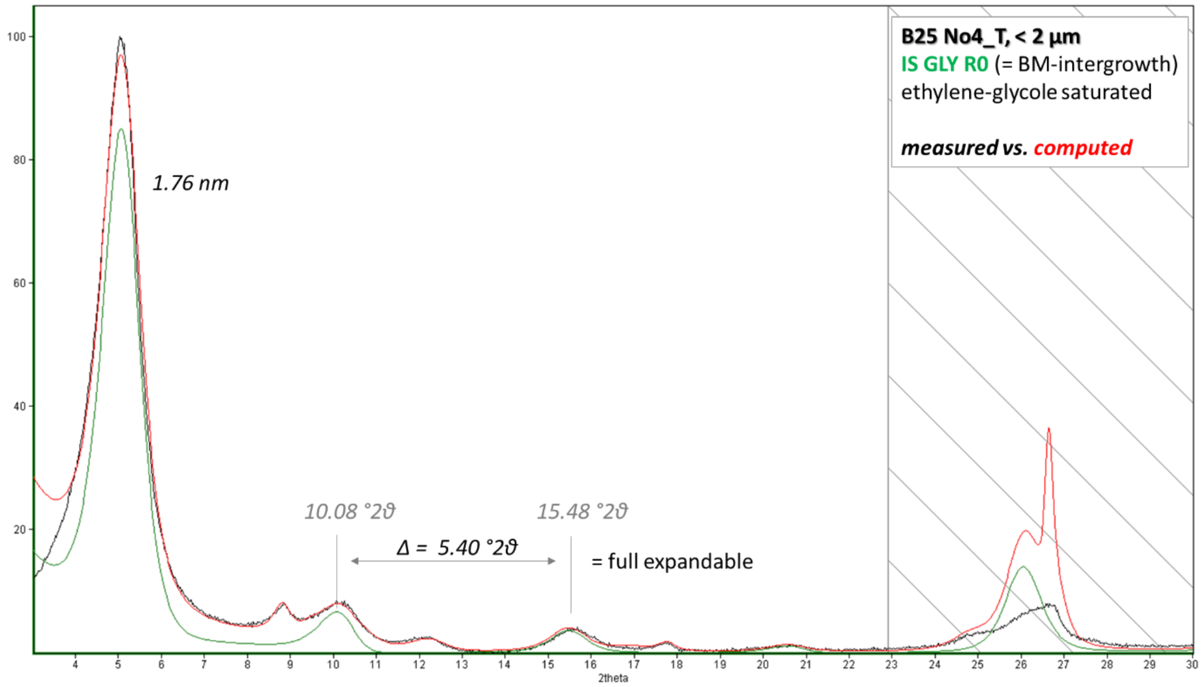
B25 No4_T, < 2 µm
IS GLY R0 (= BM-intergrowth)
ethylene-glycole saturated
measured vs. computed
1.76 nm
10.08 °2ϑ
15.48 °2ϑ
Δ = 5.40 °2ϑ
= full expandable
100
80
60
40
20
4
5
6
7
8
9
10
11
12
13
14
15
16
17
18
19
20
21
22
23
24
25
26
27
28
29
30
2theta

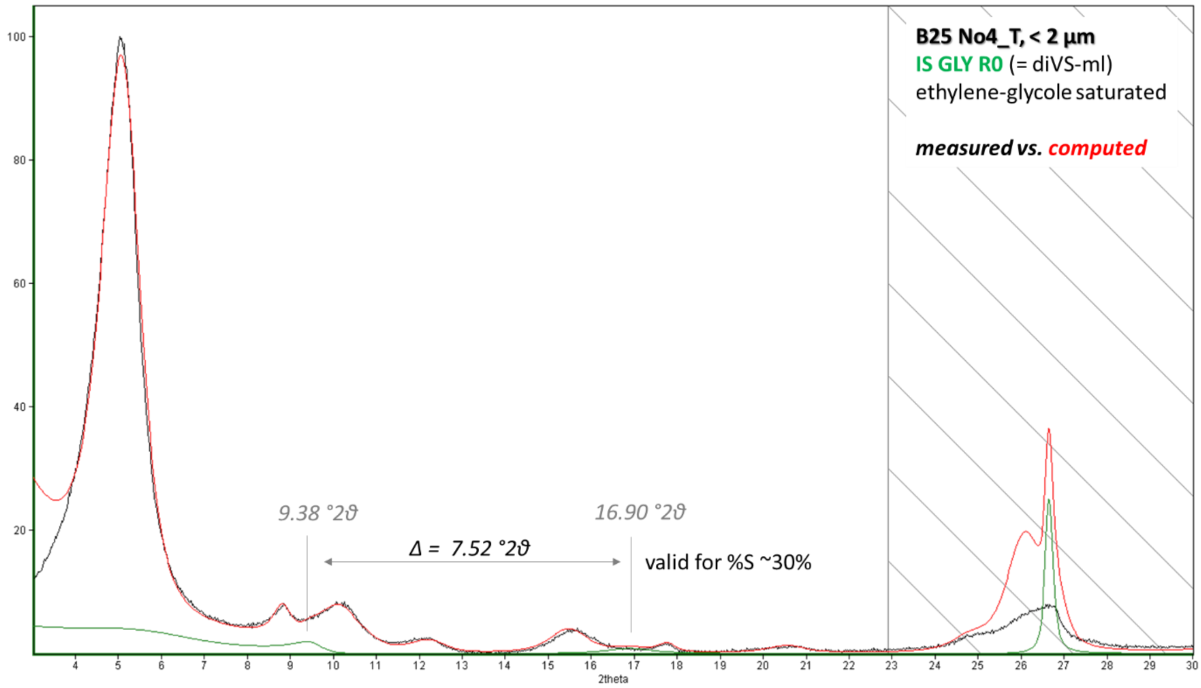
B25 No4_T, < 2 µm
IS GLY R0 (= diVS-ml)
ethylene-glycole saturated
measured vs. computed
9.38 °2ϑ
16.90 °2ϑ
Δ = 7.52 °2ϑ
valid for %S ~30%
100
80
60
40
20
4
5
6
7
8
9
10
11
12
13
14
15
16
17
18
19
20
21
22
23
24
25
26
27
28
29
30
2theta

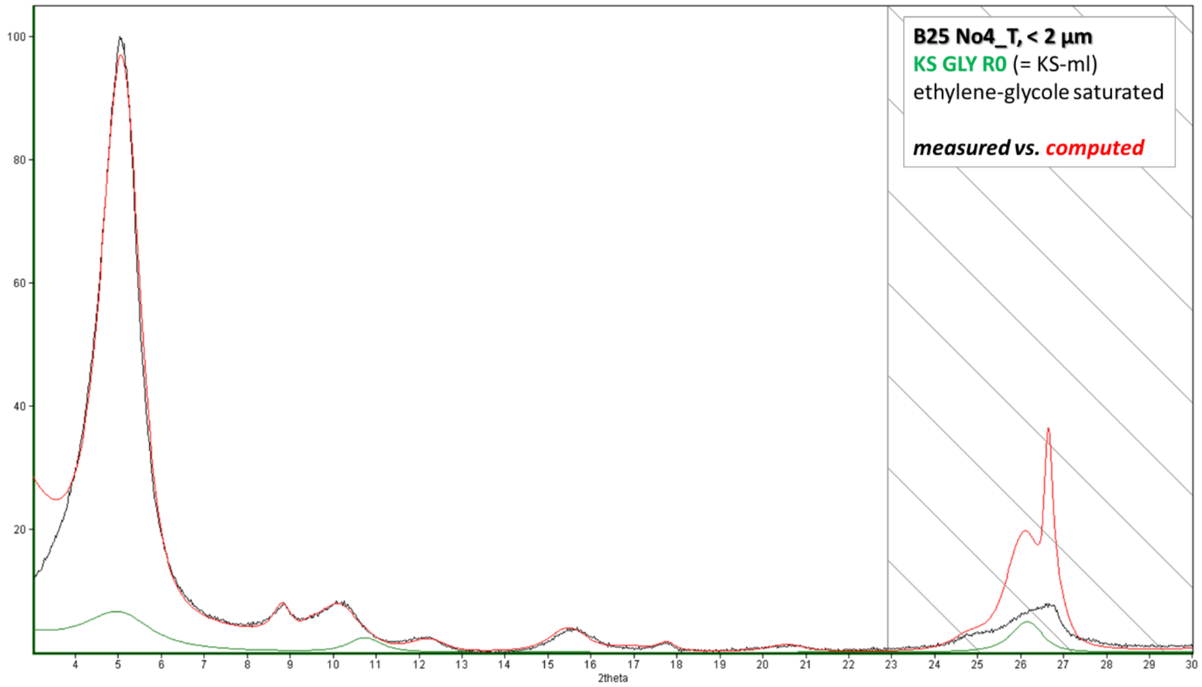
B25 No4_T, < 2 µm
KS GLY R0 (= KS-ml)
ethylene-glycole saturated
measured* vs. *computed
100
80
60
40
20
4
5
6
7
8
9
10
11
12
13
14
15
16
17
18
19
20
21
22
23
24
25
26
27
28
29
30
2theta

Data Sheet – B25 No4_M (< 2 µm), treated material *(OPA, 35°C, 93.6 hours)*

Diffraction pattern of oriented specimen & modelling by Sybilla

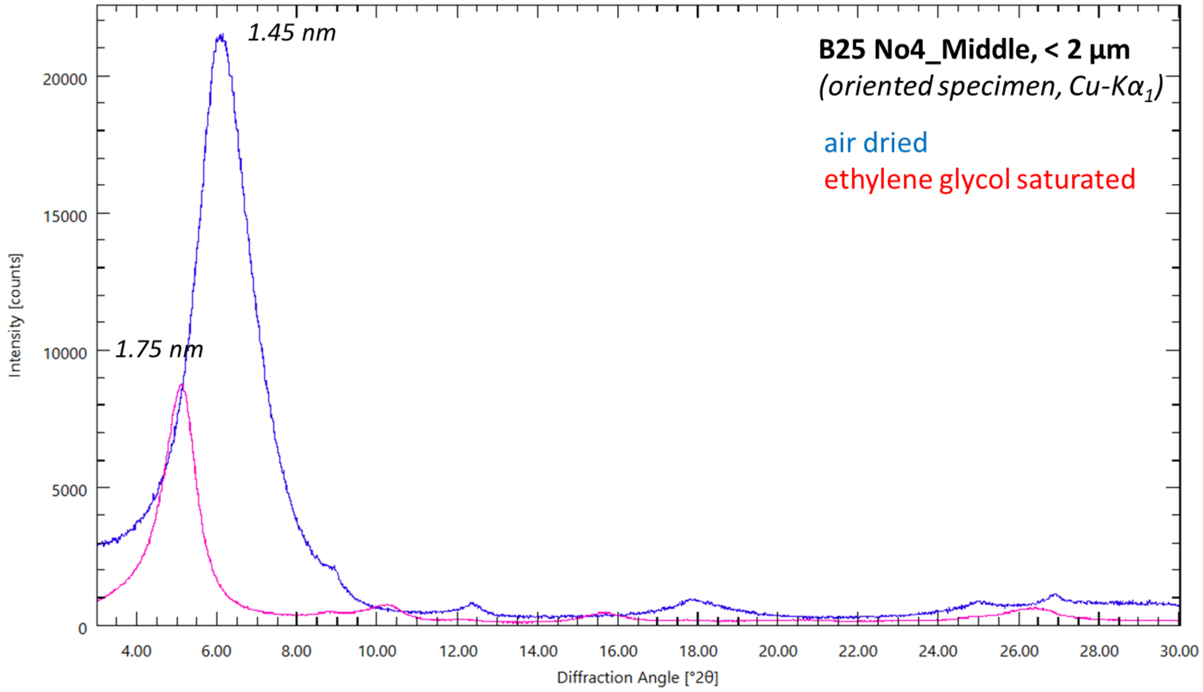

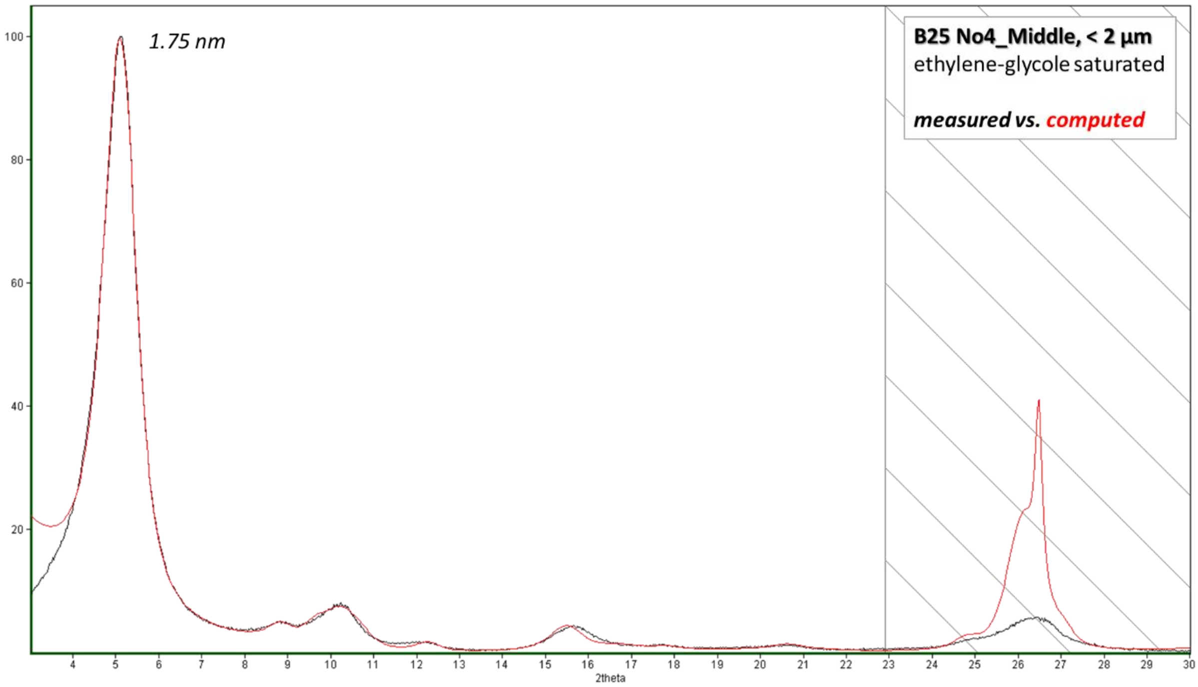

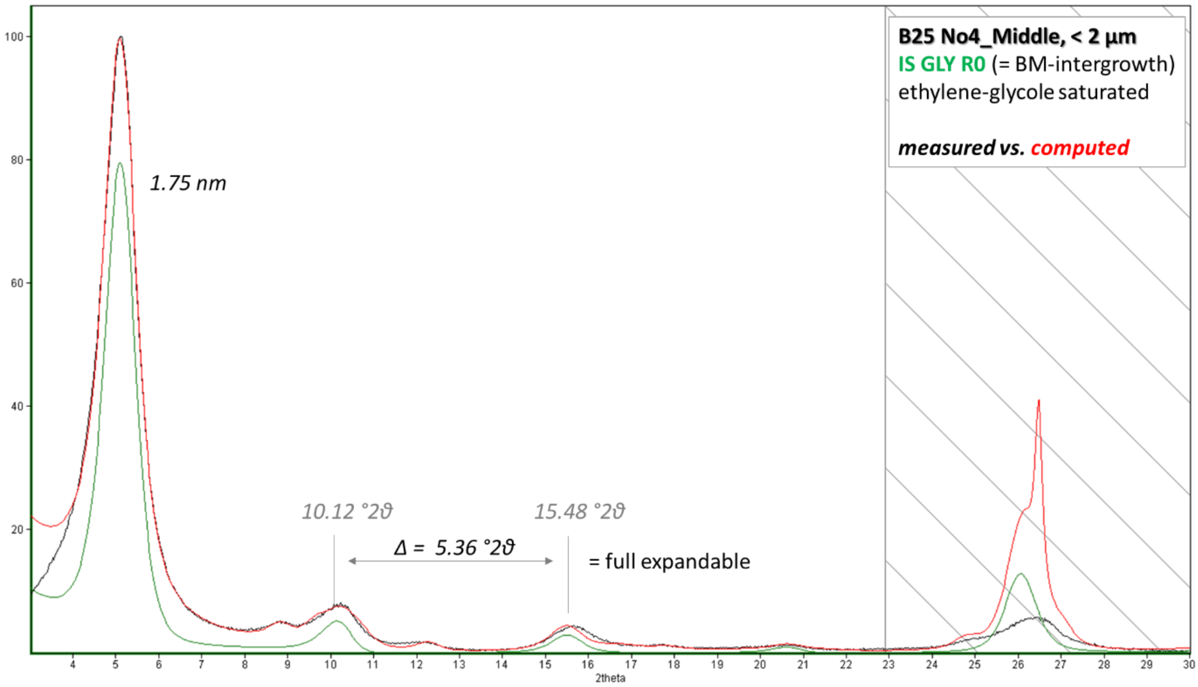
B25 No4_Middle, < 2 µm
IS GLY R0 (= BM-intergrowth)
ethylene-glycole saturated
measured vs. computed
1.75 nm
10.12 °2ϑ
15.48 °2ϑ
Δ = 5.36 °2ϑ
= full expandable
100
80
60
40
20
4
5
6
7
8
9
10
11
12
13
14
15
16
17
18
19
20
21
22
23
24
25
26
27
28
29
30
2theta

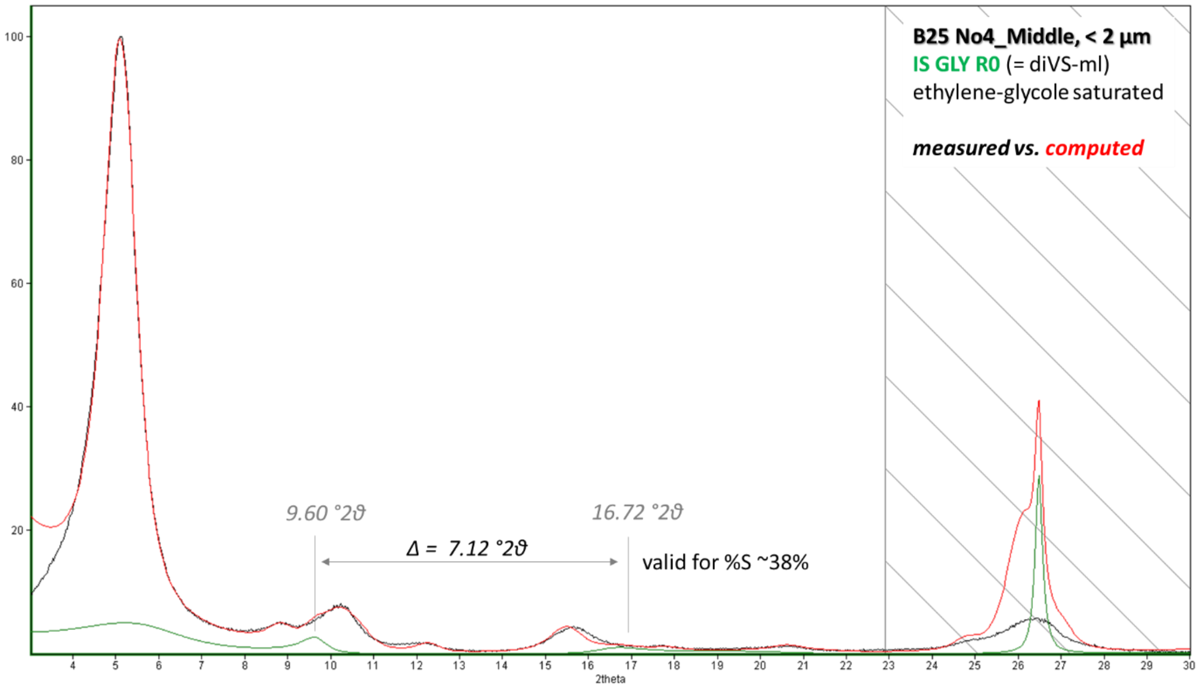
B25 No4_Middle, < 2 µm
IS GLY R0 (= diVS-ml)
ethylene-glycole saturated
measured vs. computed
9.60 °2ϑ
16.72 °2ϑ
Δ = 7.12 °2ϑ
valid for %S ~38%
100
80
60
40
20
4
5
6
7
8
9
10
11
12
13
14
15
16
17
18
19
20
21
22
23
24
25
26
27
28
29
30
2theta

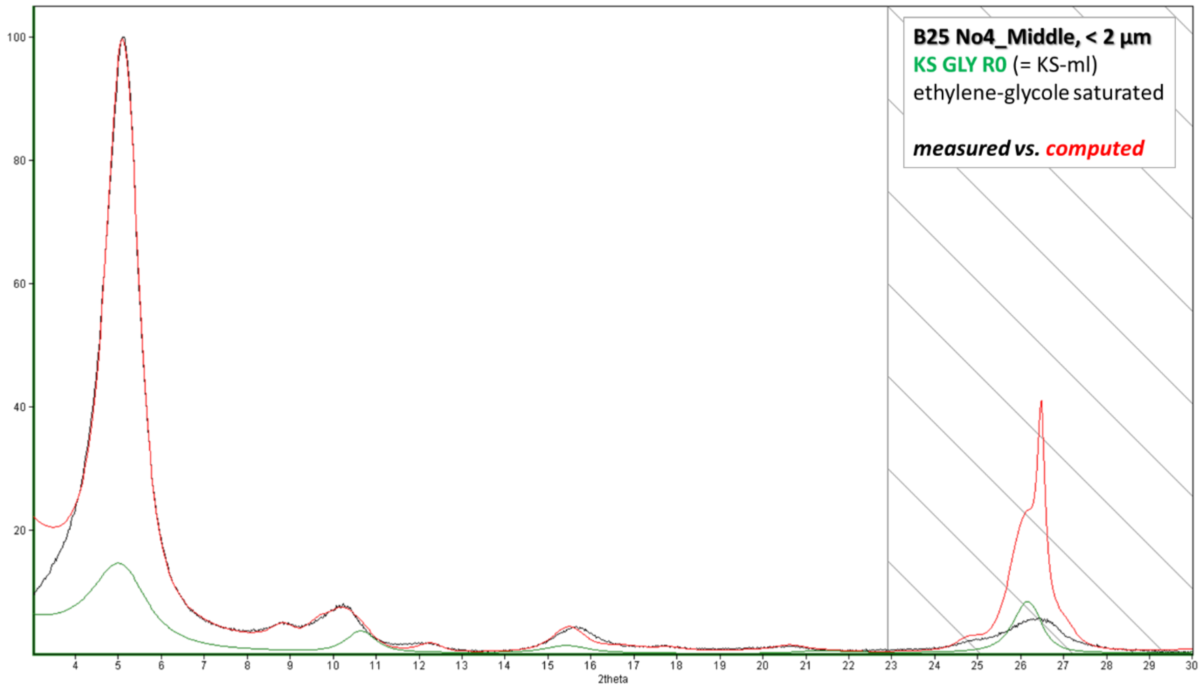
B25 No4_Middle, < 2 µm
KS GLY R0 (= KS-ml)
ethylene-glycole saturated
measured vs. computed
100
80
60
40
20
4
5
6
7
8
9
10
11
12
13
14
15
16
17
18
19
20
21
22
23
24
25
26
27
28
29
30
2theta

Data Sheet – B25 No4_B (< 2 µm), treated material *(OPA, 35°C, 93.6 hours)*

Diffraction pattern of oriented specimen & modelling by Sybilla

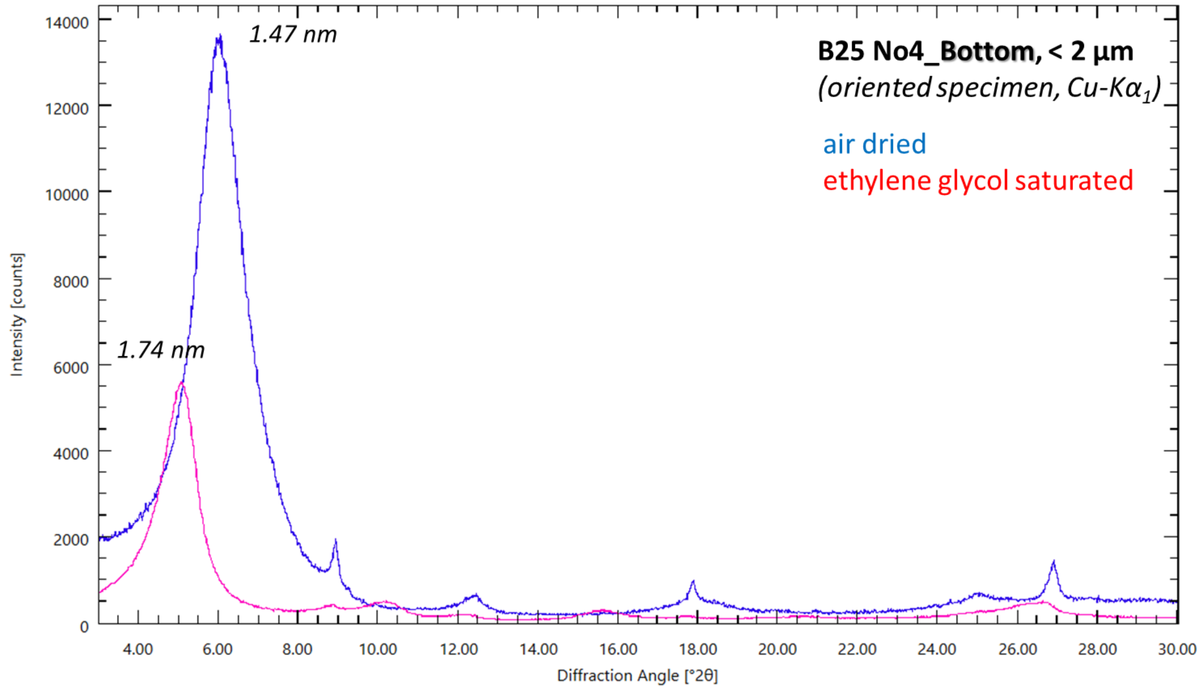

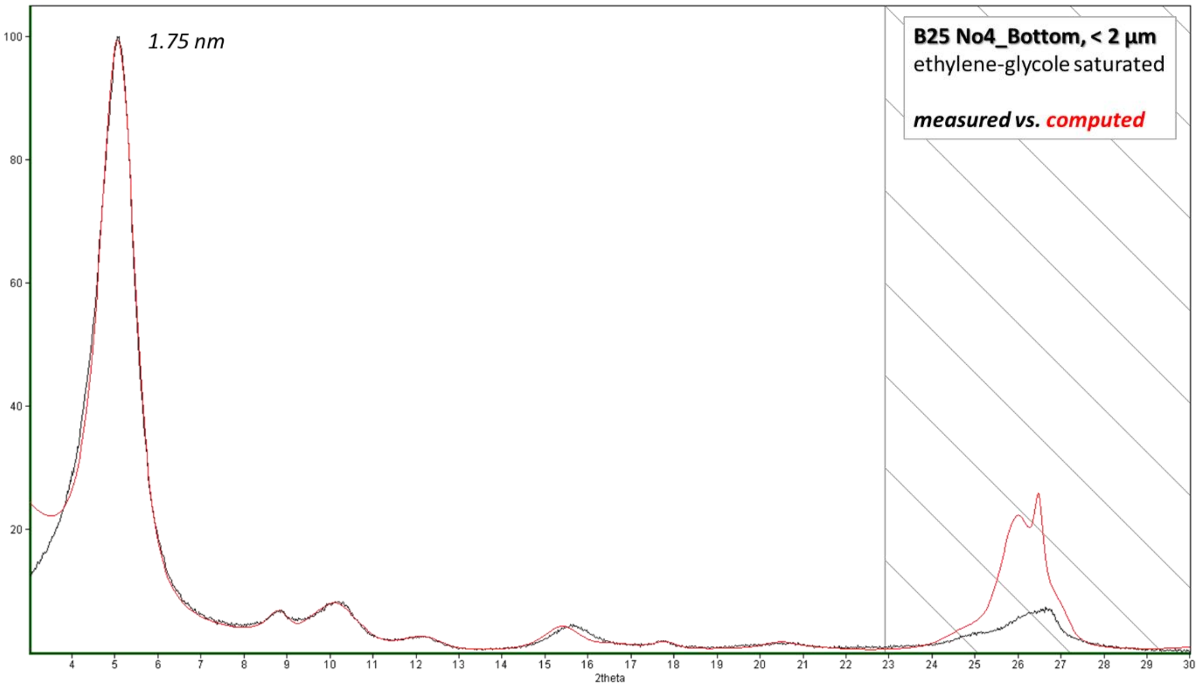

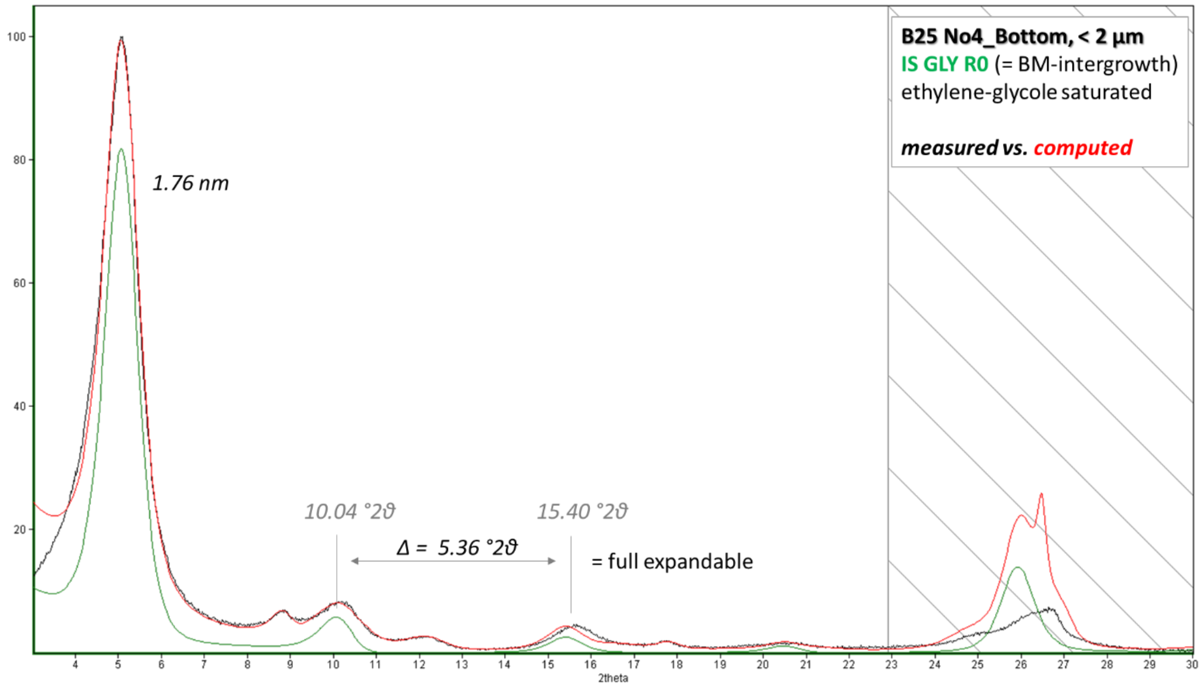
B25 No4_Bottom, < 2 µm
IS GLY R0 (= BM-intergrowth)
ethylene-glycole saturated
measured vs. computed
1.76 nm
10.04 °2ϑ
15.40 °2ϑ
Δ = 5.36 °2ϑ
= full expandable
100
80
60
40
20
4
5
6
7
8
9
10
11
12
13
14
15
16
17
18
19
20
21
22
23
24
25
26
27
28
29
30
2theta

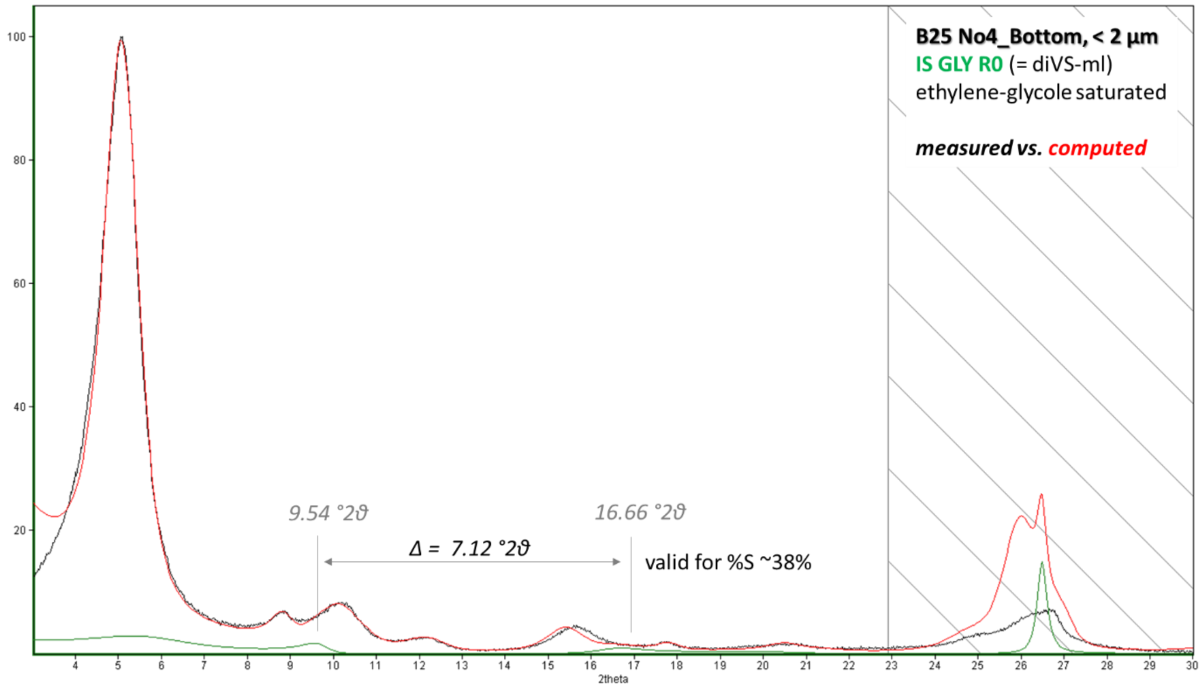
B25 No4_Bottom, < 2 µm
IS GLY R0 (= diVS-ml)
ethylene-glycole saturated
measured vs. computed
9.54 °2ϑ
16.66 °2ϑ
Δ = 7.12 °2ϑ
valid for %S ~38%
100
80
60
40
20
4
5
6
7
8
9
10
11
12
13
14
15
16
17
18
19
20
21
22
23
24
25
26
27
28
29
30
2theta

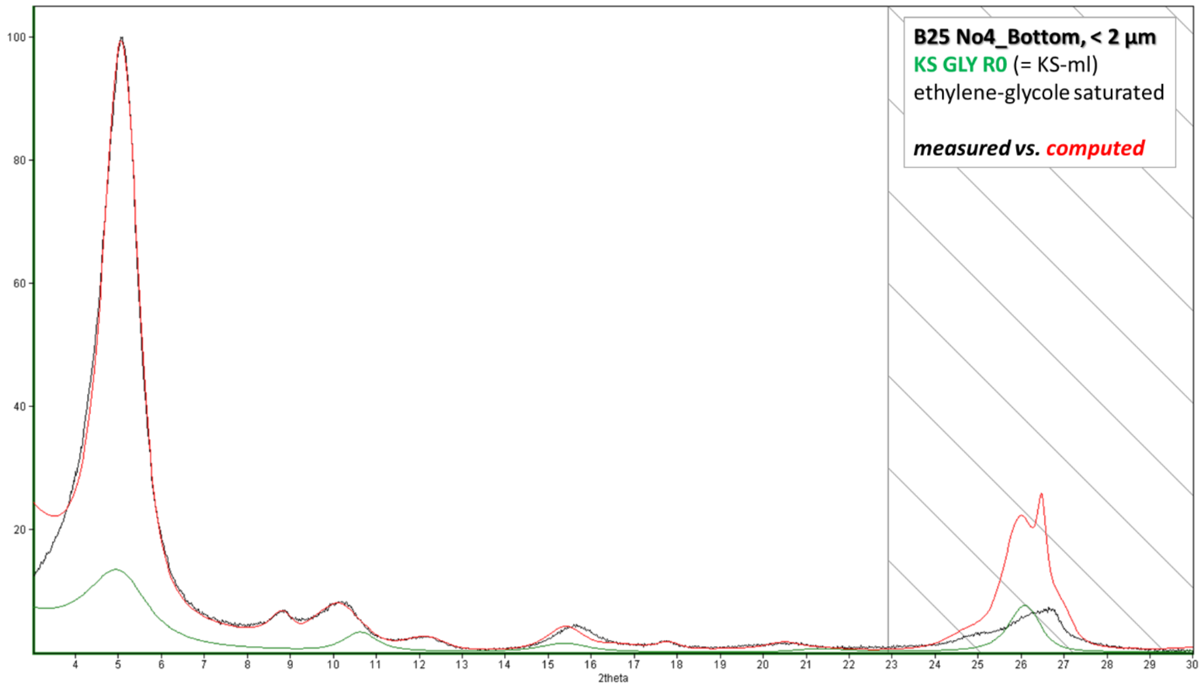
B25 No4_Bottom, < 2 µm
KS GLY R0 (= KS-ml)
ethylene-glycole saturated
measured* vs. *computed
100
80
60
40
20
4
5
6
7
8
9
10
11
12
13
14
15
16
17
18
19
20
21
22
23
24
25
26
27
28
29
30
2theta

Data Sheet – B25 No23 (< 2 µm), treated material *(OPA, 35°C, 285 h, 0.7 MPa)*

Diffraction pattern of oriented specimen & modelling by Sybilla

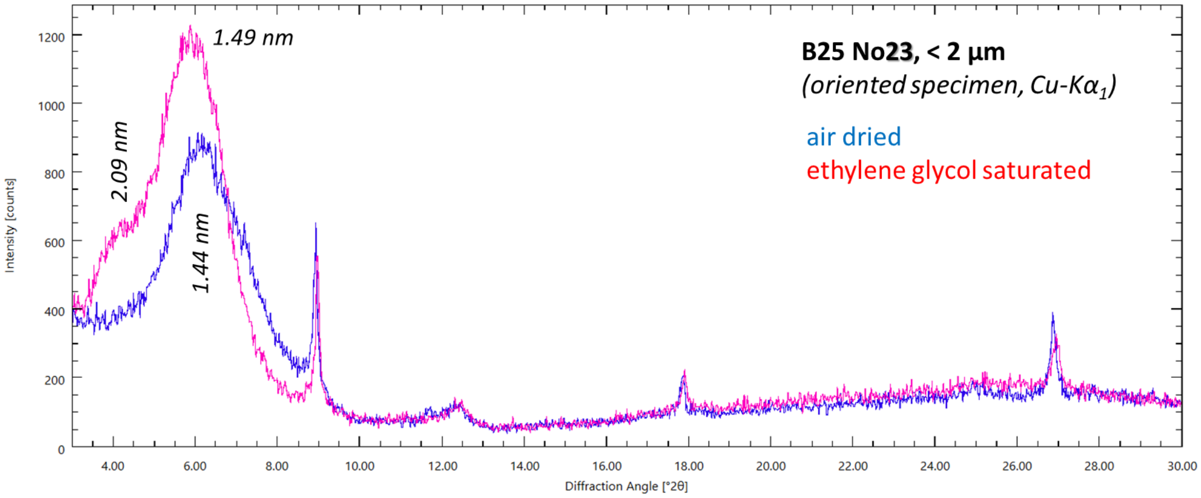

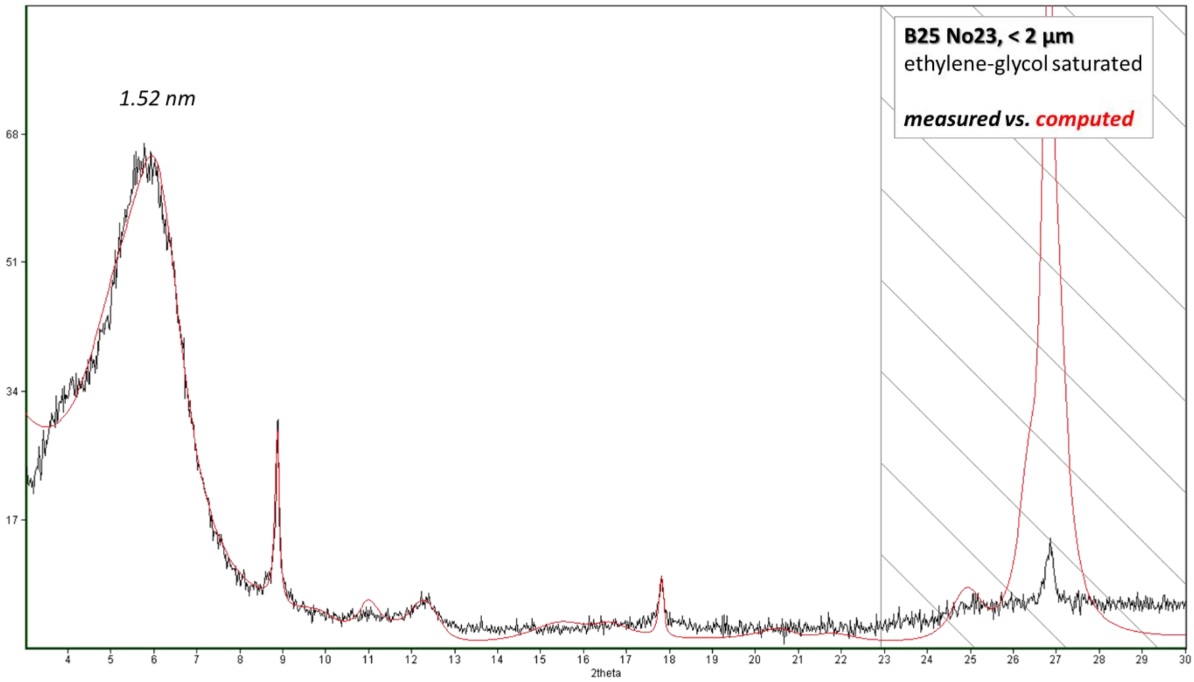

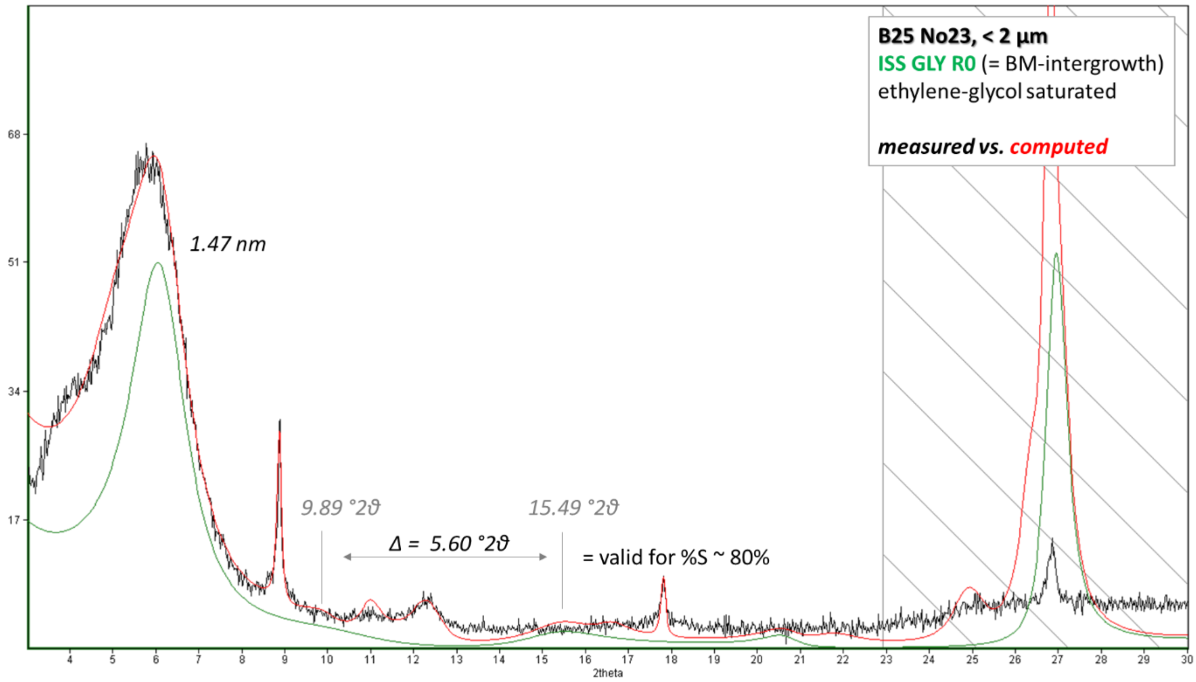
B25 No23, < 2 µm
ISS GLY R0 (= BM-intergrowth)
ethylene-glycol saturated
measured vs. computed
1.47 nm
9.89 °2ϑ
15.49 °2ϑ
Δ = 5.60 °2ϑ
= valid for %S ~ 80%
68
51
34
17
4
5
6
7
8
9
10
11
12
13
14
15
16
17
18
19
20
21
22
23
24
25
26
27
28
29
30
2theta

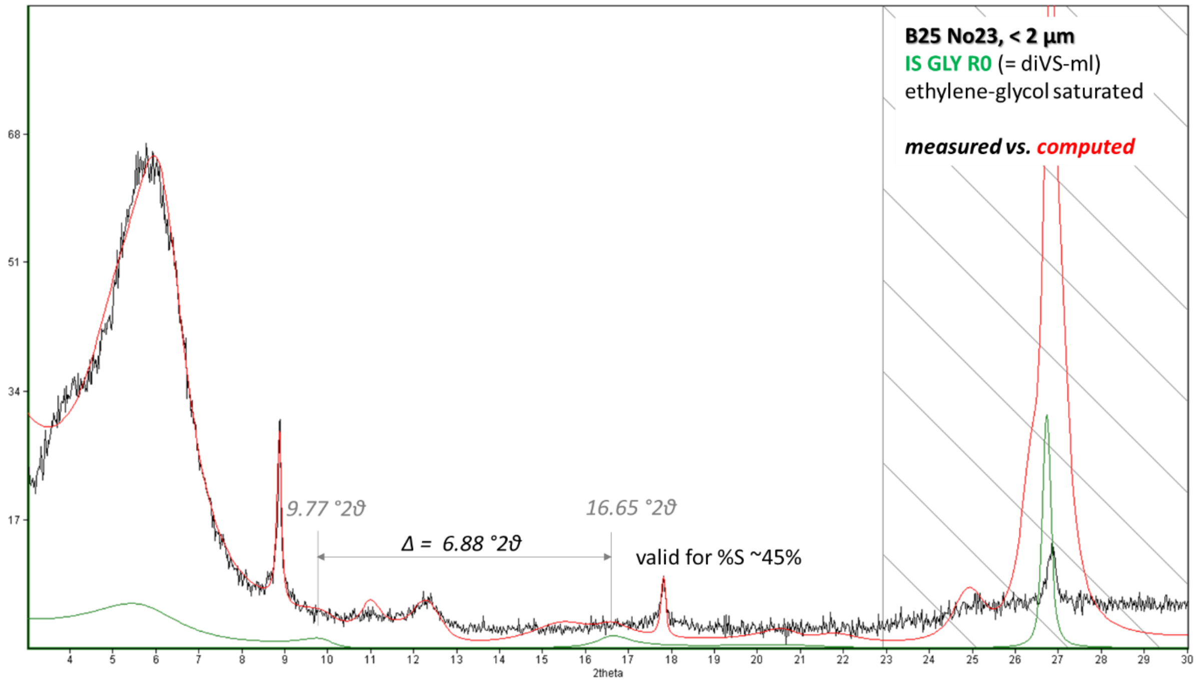
B25 No23, < 2 µm
IS GLY R0 (= diVS-ml)
ethylene-glycol saturated
measured vs. computed
9.77 °2ϑ
16.65 °2ϑ
Δ = 6.88 °2ϑ
valid for %S ~45%
68
51
34
17
4
5
6
7
8
9
10
11
12
13
14
15
16
17
18
19
20
21
22
23
24
25
26
27
28
29
30
2theta

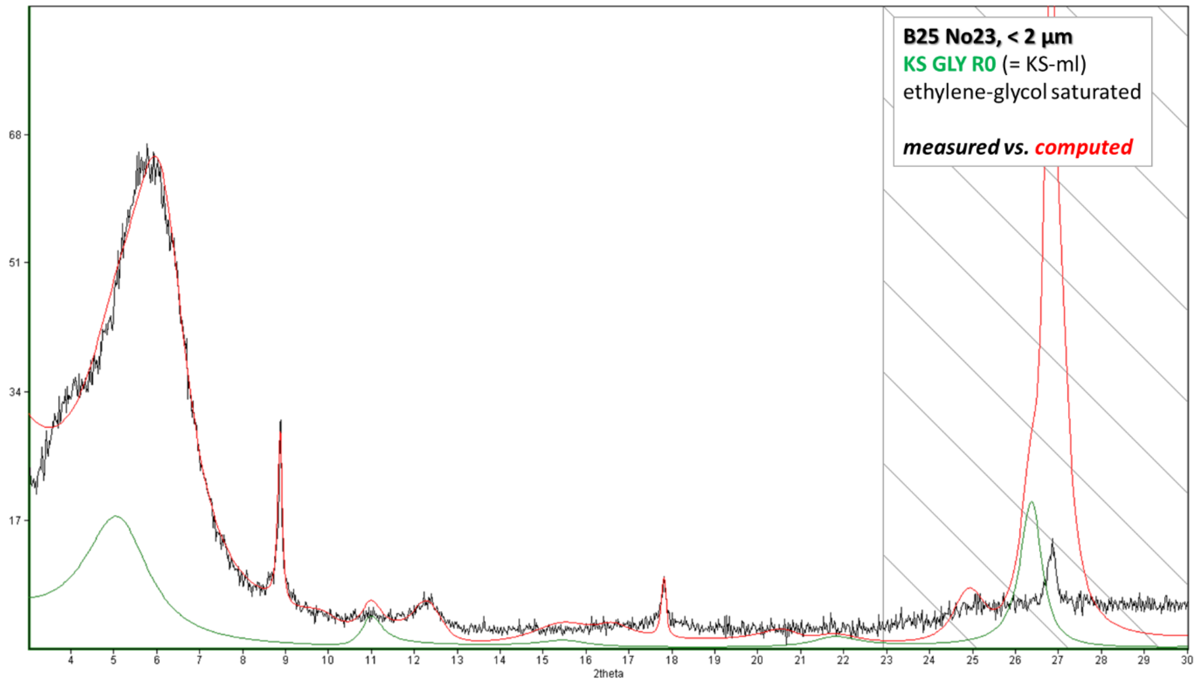
B25 No23, < 2 µm
KS GLY R0 (= KS-ml)
ethylene-glycol saturated
measured vs. computed
68
51
34
17
4
5
6
7
8
9
10
11
12
13
14
15
16
17
18
19
20
21
22
23
24
25
26
27
28
29
30
2theta

S

Data Sheet – B25 No5_T (< 2 µm), treated material *(OPA, 60°C, 454 hours)*

Diffraction pattern of oriented specimen & modelling by Sybilla

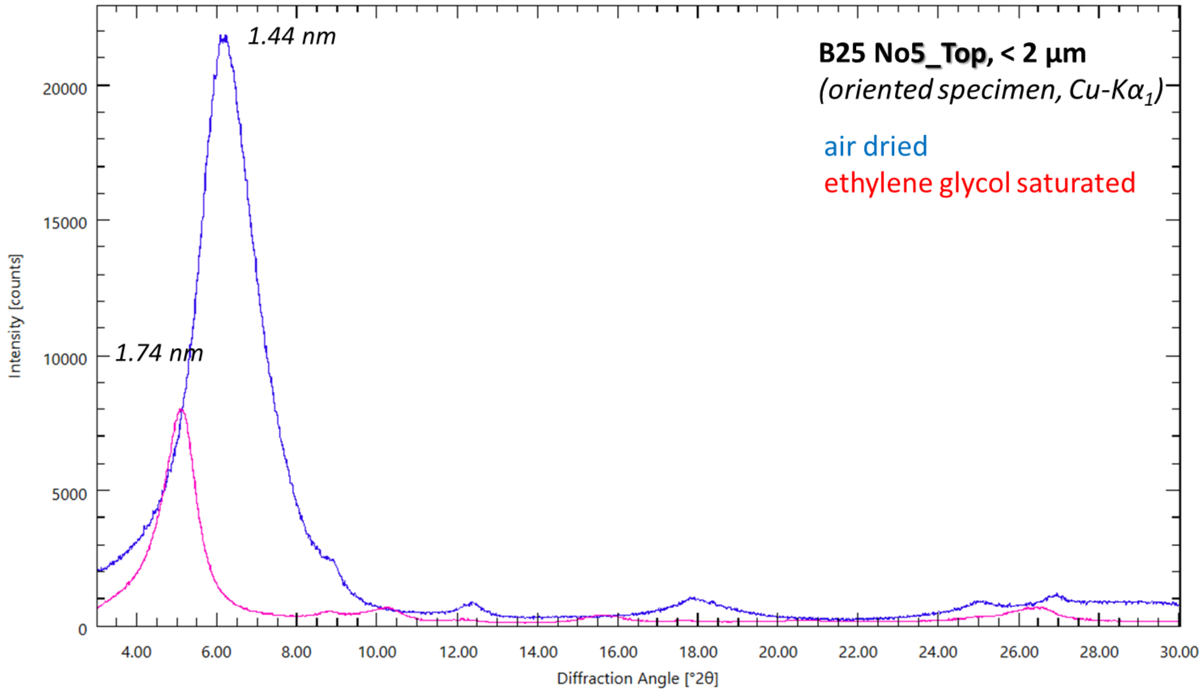

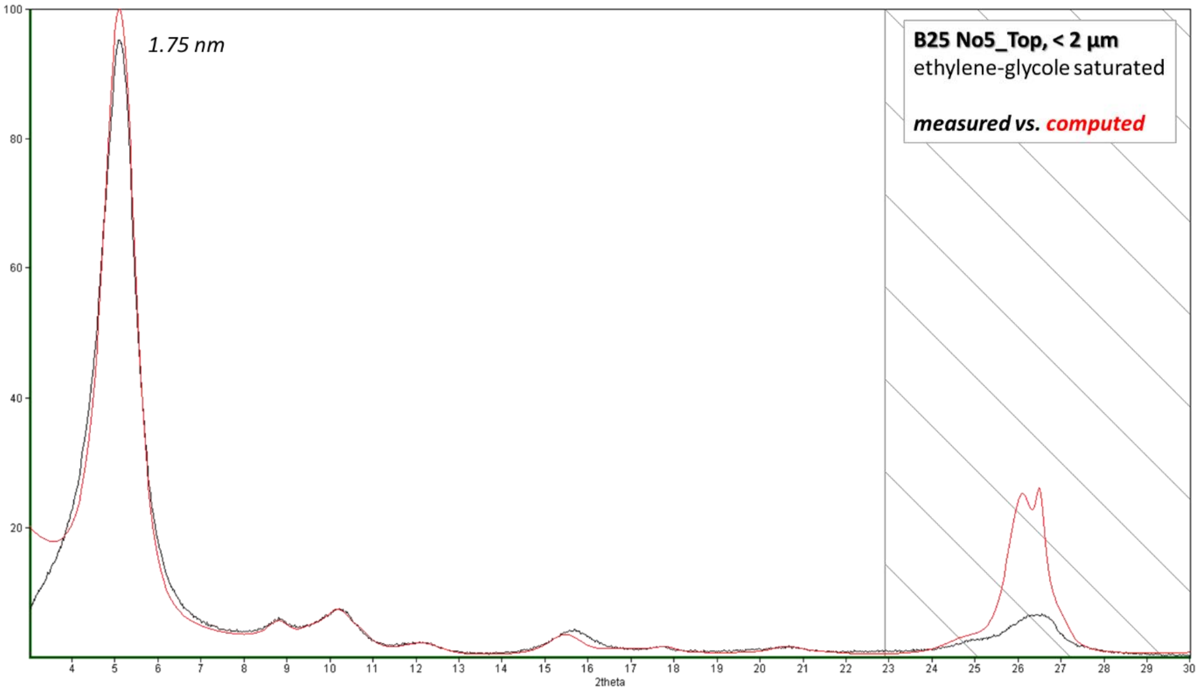

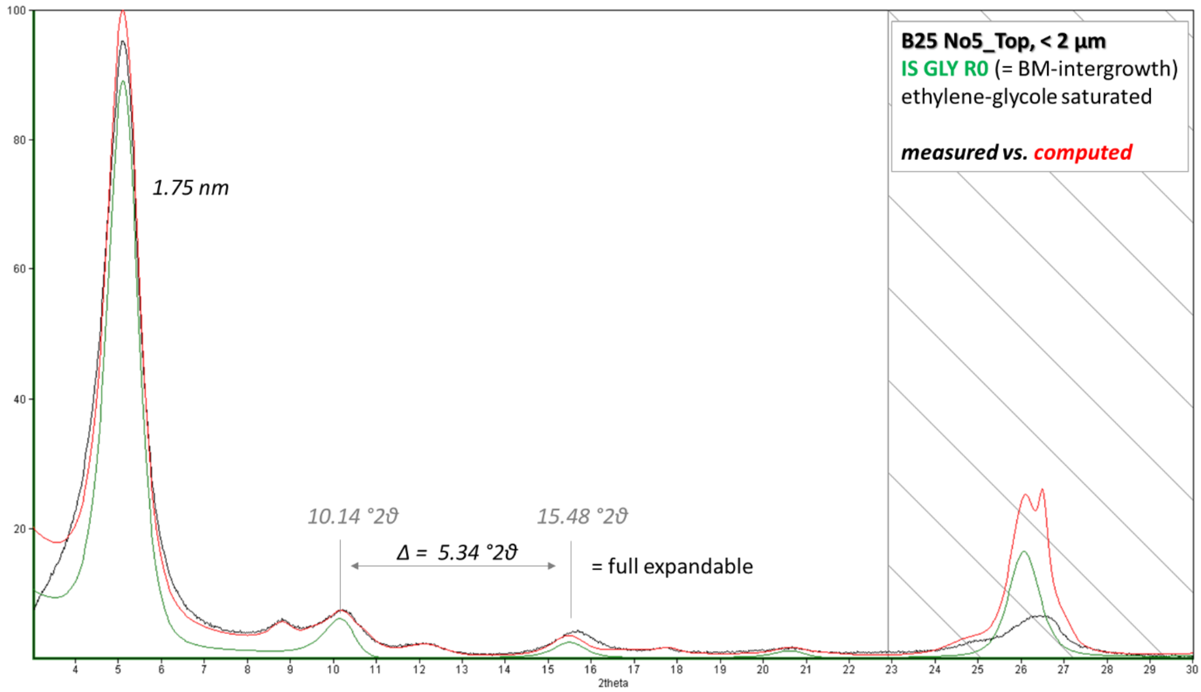
B25 No5_Top, < 2 µm
IS GLY R0 (= BM-intergrowth)
ethylene-glycole saturated
measured vs. computed
1.75 nm
10.14 °2ϑ
15.48 °2ϑ
Δ = 5.34 °2ϑ
= full expandable
100
80
60
40
20
4
5
6
7
8
9
10
11
12
13
14
15
16
17
18
19
20
21
22
23
24
25
26
27
28
29
30
2theta

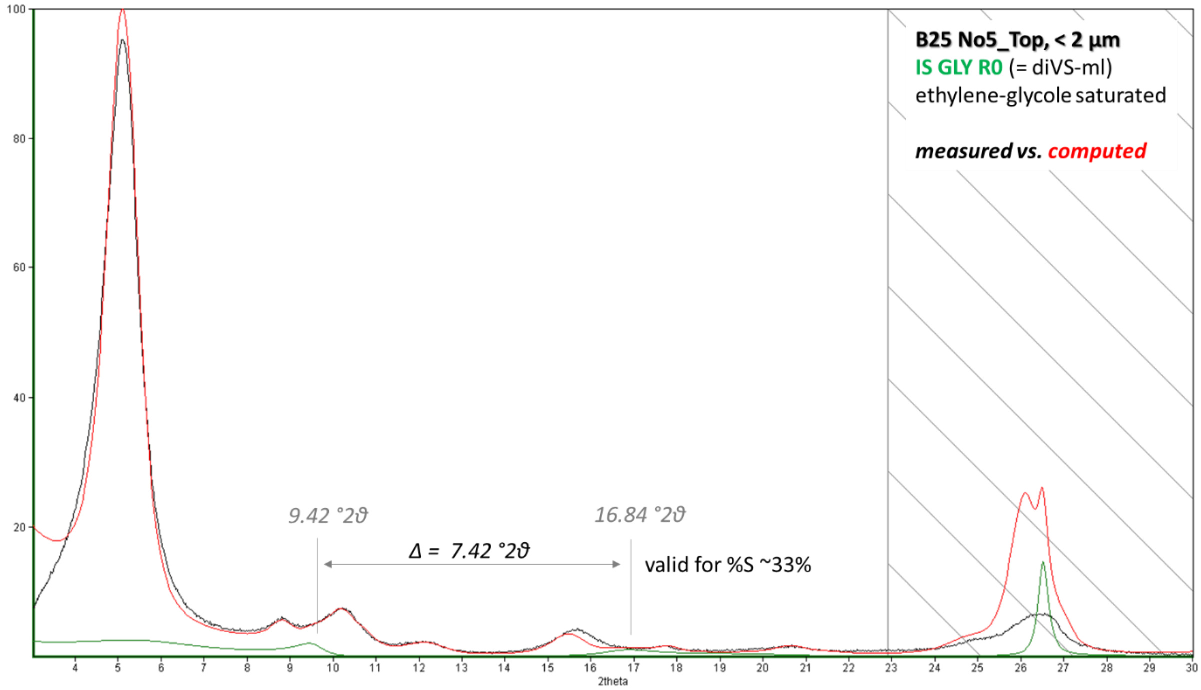
B25 No5_Top, < 2 µm
IS GLY R0 (= diVS-ml)
ethylene-glycole saturated
measured vs. computed
9.42 °2ϑ
16.84 °2ϑ
Δ = 7.42 °2ϑ
valid for %S ~33%
100
80
60
40
20
4
5
6
7
8
9
10
11
12
13
14
15
16
17
18
19
20
21
22
23
24
25
26
27
28
29
30
2theta

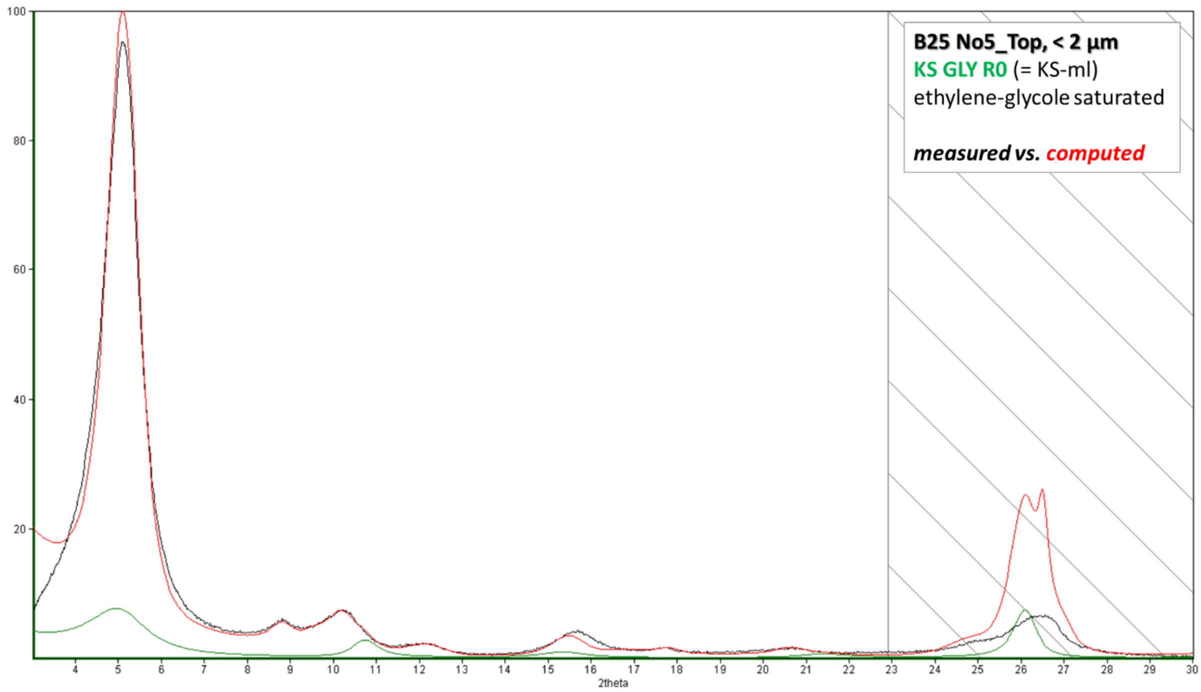
B25 No5_Top, < 2 µm
KS GLY R0 (= KS-ml)
ethylene-glycole saturated
measured vs. computed
100
80
60
40
20
4
5
6
7
8
9
10
11
12
13
14
15
16
17
18
19
20
21
22
23
24
25
26
27
28
29
30
2theta

Data Sheet – B25 No5_M (< 2 µm), treated material *(OPA, 60°C, 454 hours)*

Diffraction pattern of oriented specimen & modelling by Sybilla

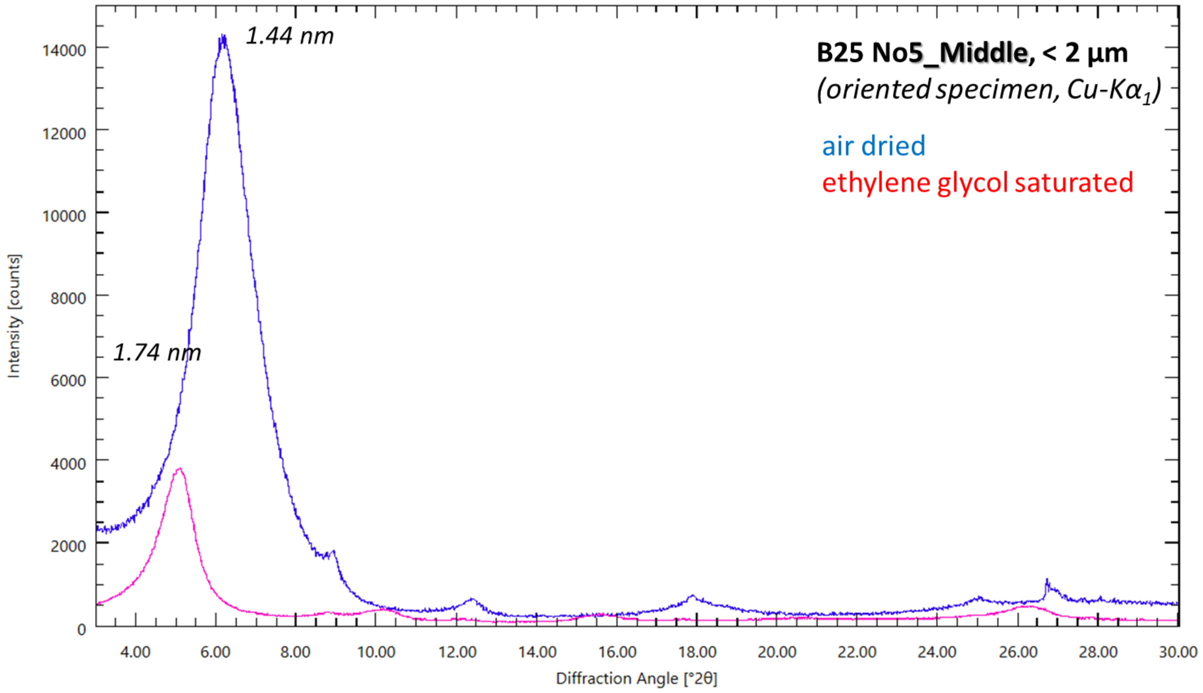

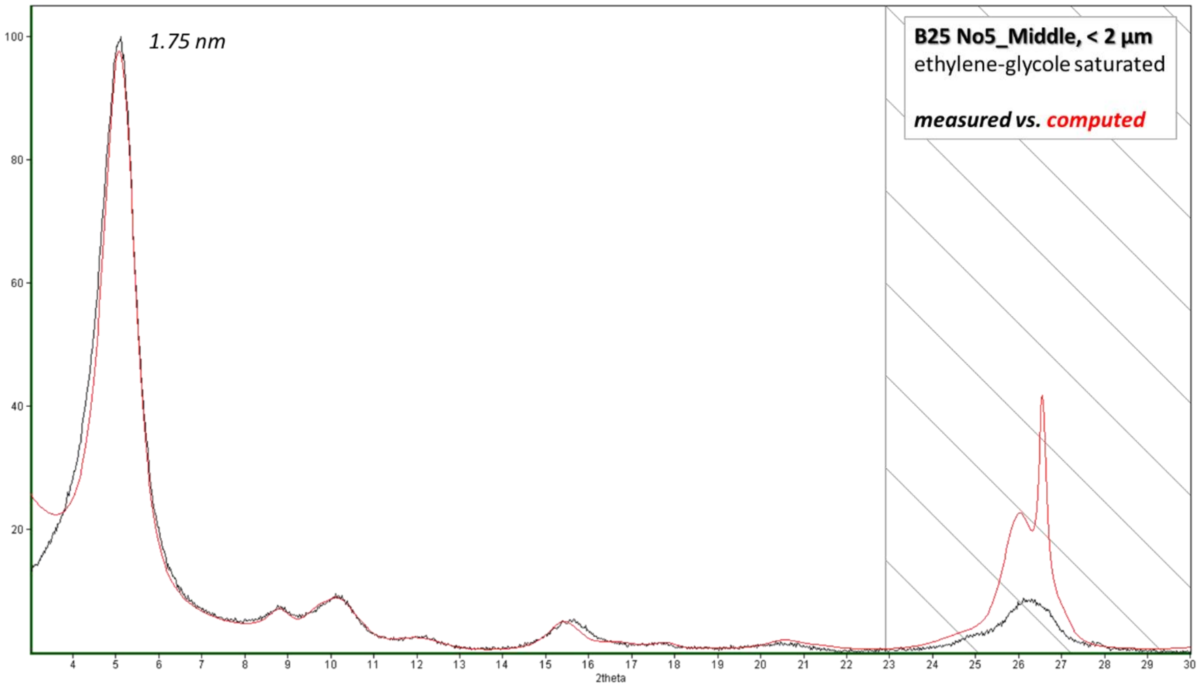

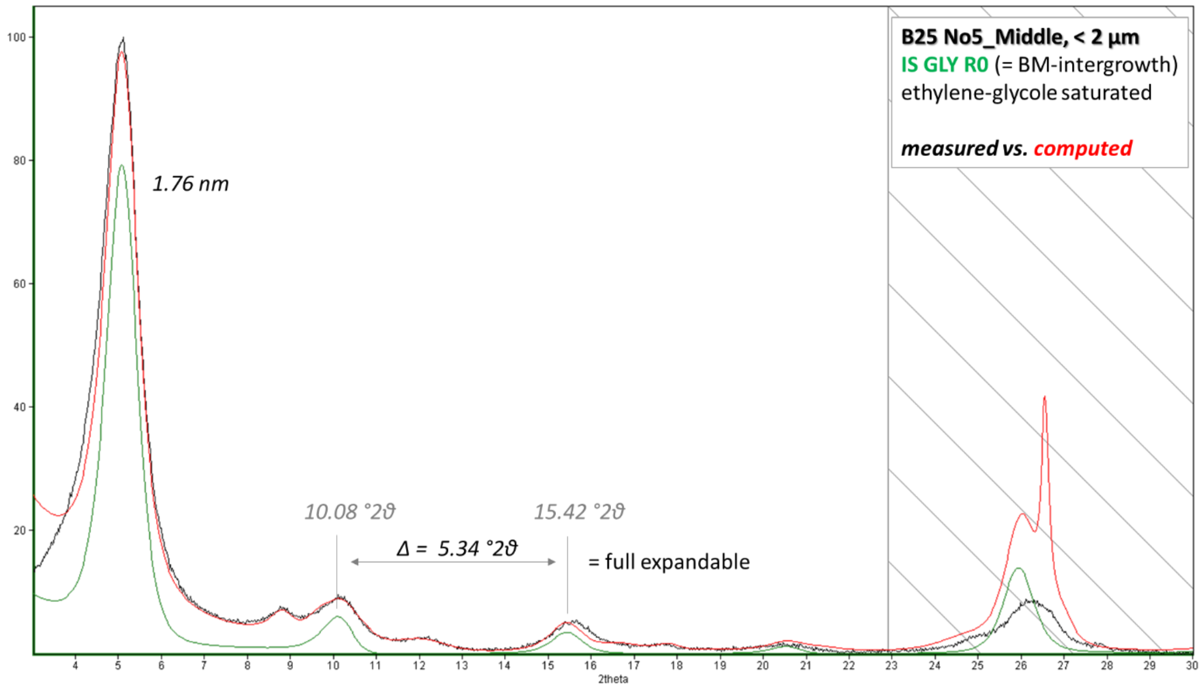
B25 No5_Middle, < 2 µm
IS GLY R0 (= BM-intergrowth)
ethylene-glycole saturated
measured vs. computed
1.76 nm
10.08 °2ϑ
15.42 °2ϑ
Δ = 5.34 °2ϑ
= full expandable
100
80
60
40
20
4
5
6
7
8
9
10
11
12
13
14
15
16
17
18
19
20
21
22
23
24
25
26
27
28
29
30
2theta

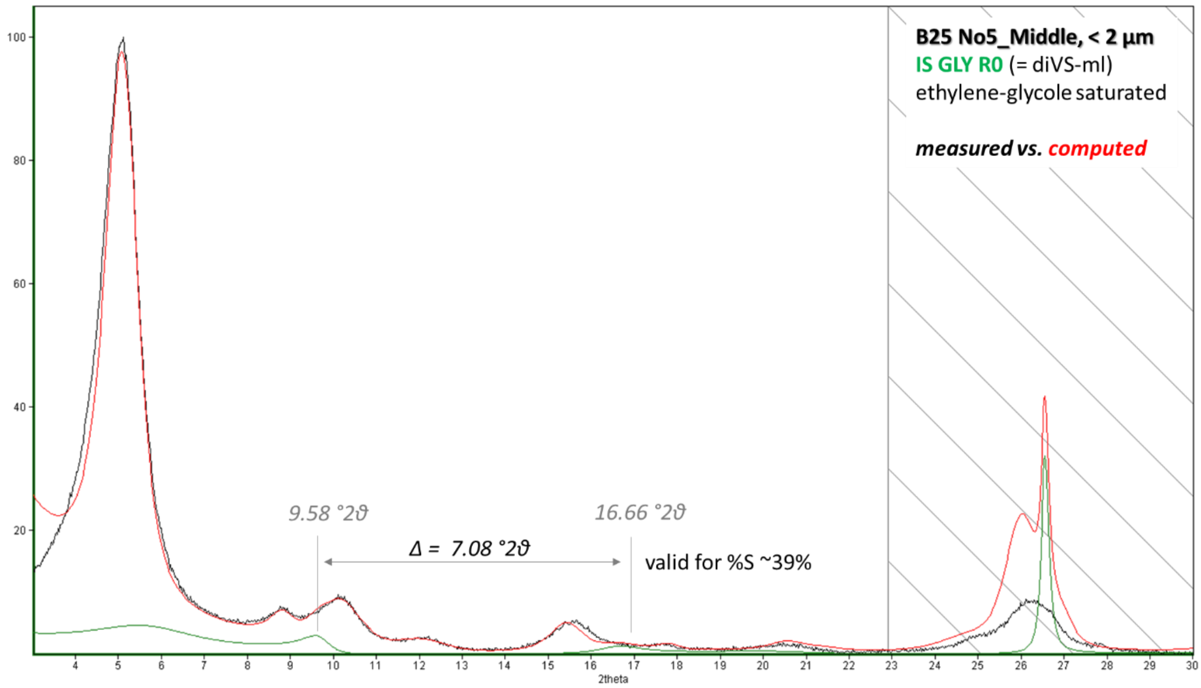
B25 No5_Middle, < 2 µm
IS GLY R0 (= diVS-ml)
ethylene-glycole saturated
measured vs. computed
9.58 °2ϑ
16.66 °2ϑ
Δ = 7.08 °2ϑ
valid for %S ~39%
100
80
60
40
20
4
5
6
7
8
9
10
11
12
13
14
15
16
17
18
19
20
21
22
23
24
25
26
27
28
29
30
2theta

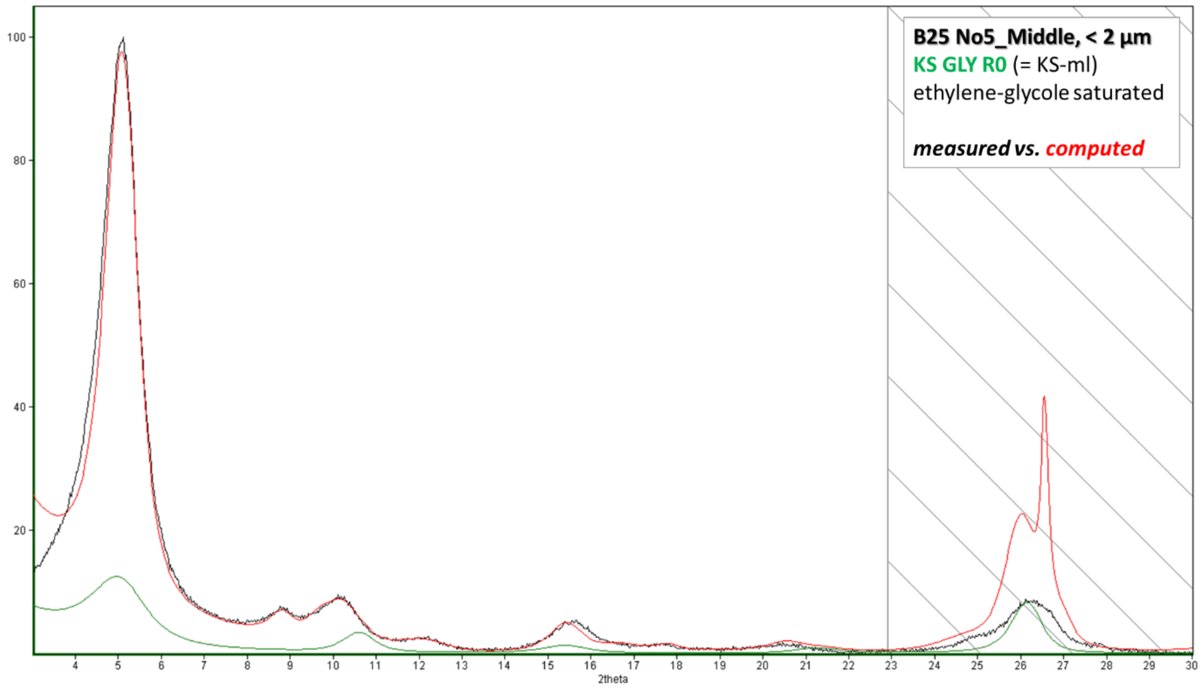
B25 No5_Middle, < 2 µm
KS GLY R0 (= KS-ml)
ethylene-glycole saturated
measured vs. computed
100
80
60
40
20
4
5
6
7
8
9
10
11
12
13
14
15
16
17
18
19
20
21
22
23
24
25
26
27
28
29
30
2theta

Data Sheet – B25 No5_B (< 2 µm), treated material *(OPA, 60°C, 454 hours)*

Diffraction pattern of oriented specimen & modelling by Sybilla

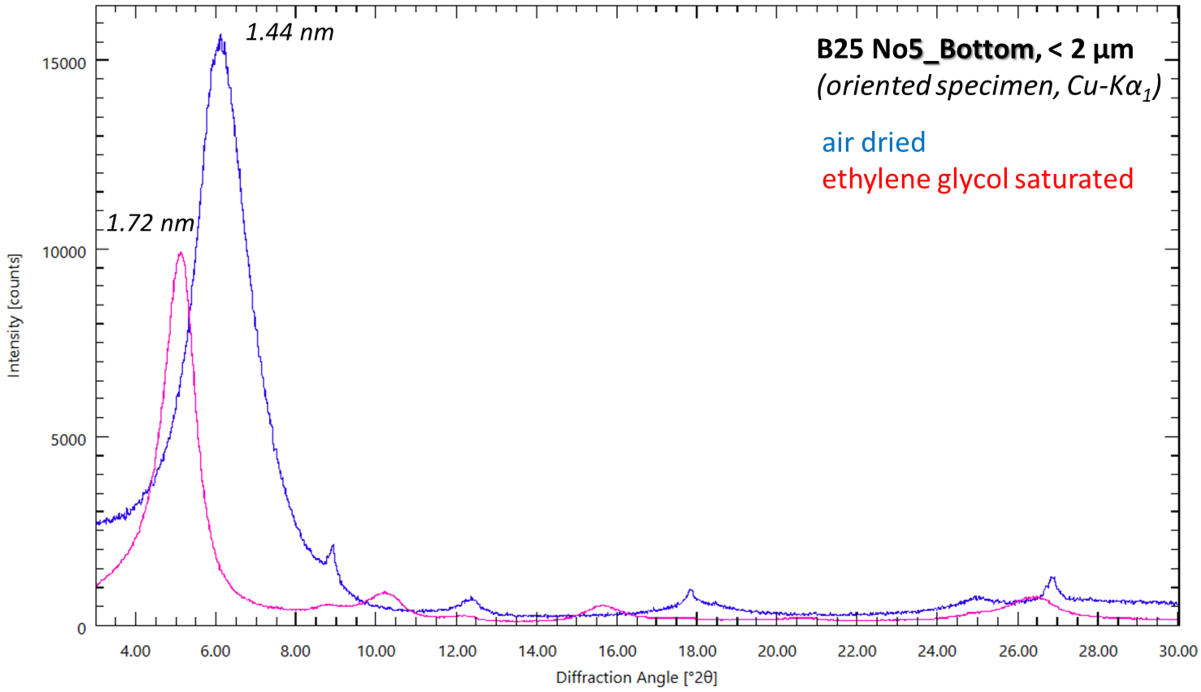

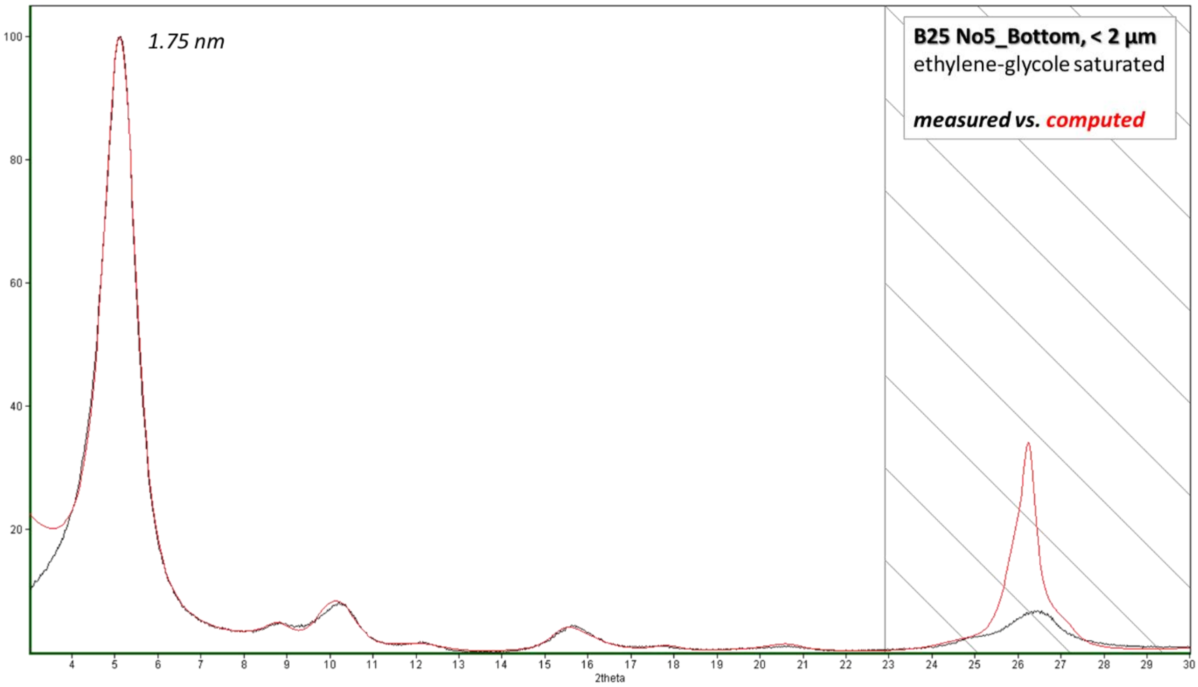

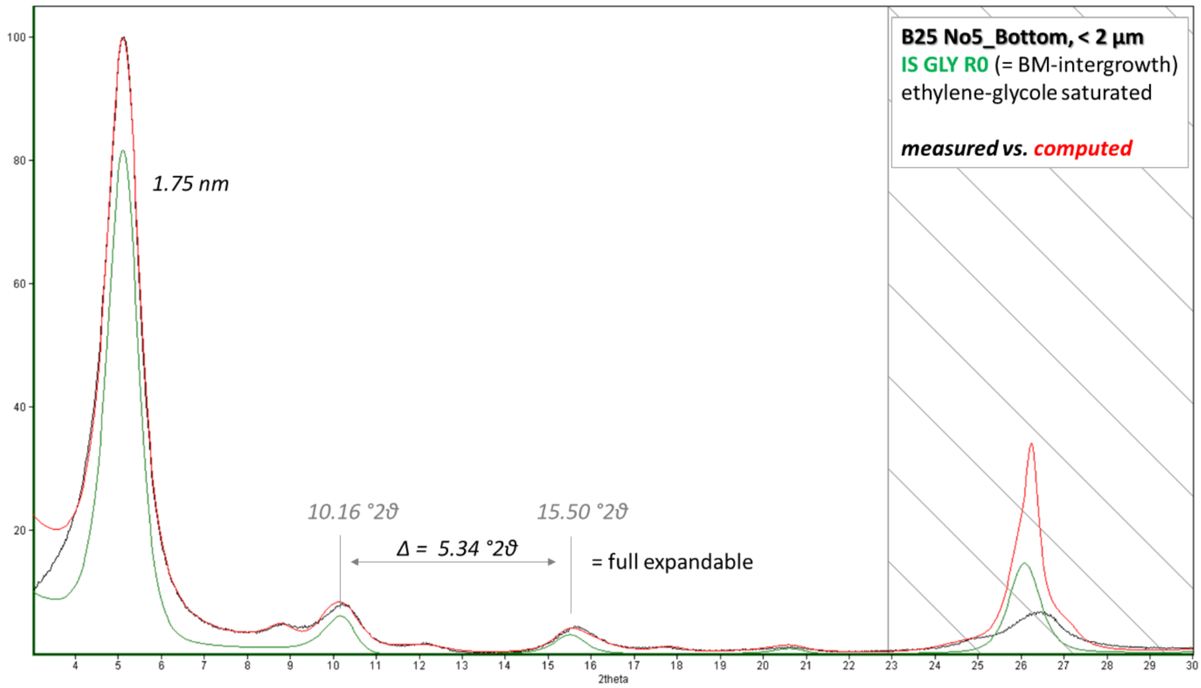
B25 No5_Bottom, < 2 µm
IS GLY R0 (= BM-intergrowth)
ethylene-glycole saturated
measured* vs. *computed
1.75 nm
10.16 °2ϑ
15.50 °2ϑ
Δ = 5.34 °2ϑ
= full expandable
100
80
60
40
20
4
5
6
7
8
9
10
11
12
13
14
15
16
17
18
19
20
21
22
23
24
25
26
27
28
29
30
2theta

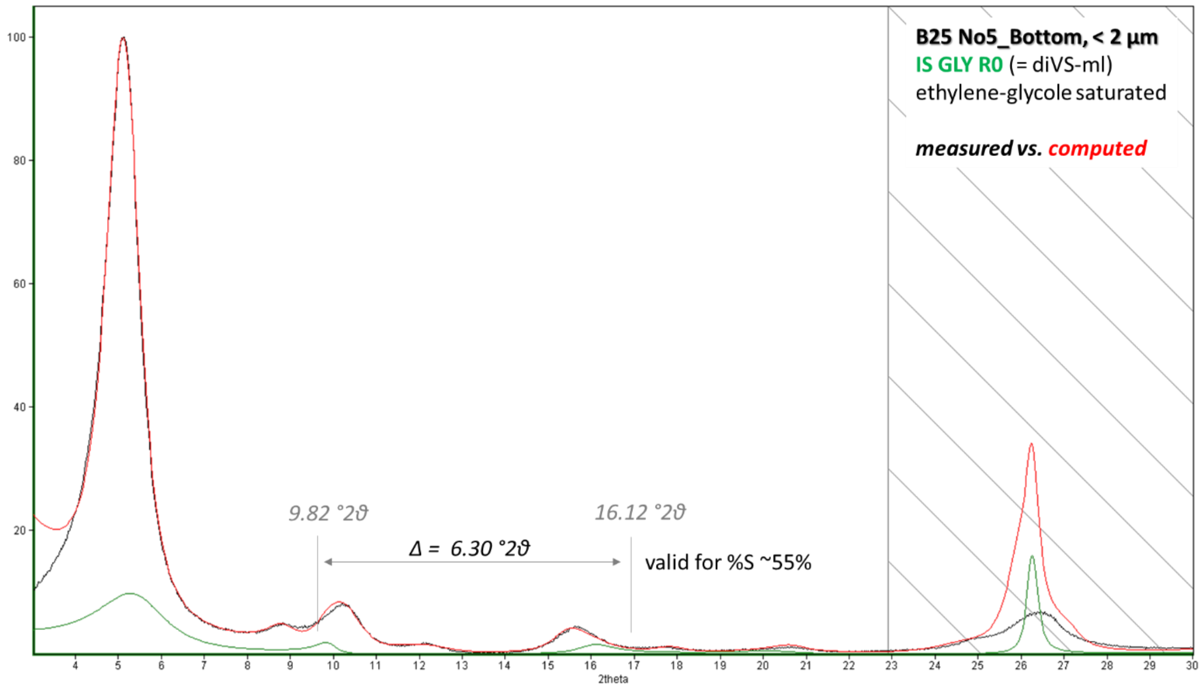
B25 No5_Bottom, < 2 µm
IS GLY R0 (= diVS-ml)
ethylene-glycole saturated
measured* vs. *computed
9.82 °2ϑ
16.12 °2ϑ
Δ = 6.30 °2ϑ
valid for %S ~55%
100
80
60
40
20
4
5
6
7
8
9
10
11
12
13
14
15
16
17
18
19
20
21
22
23
24
25
26
27
28
29
30
2theta

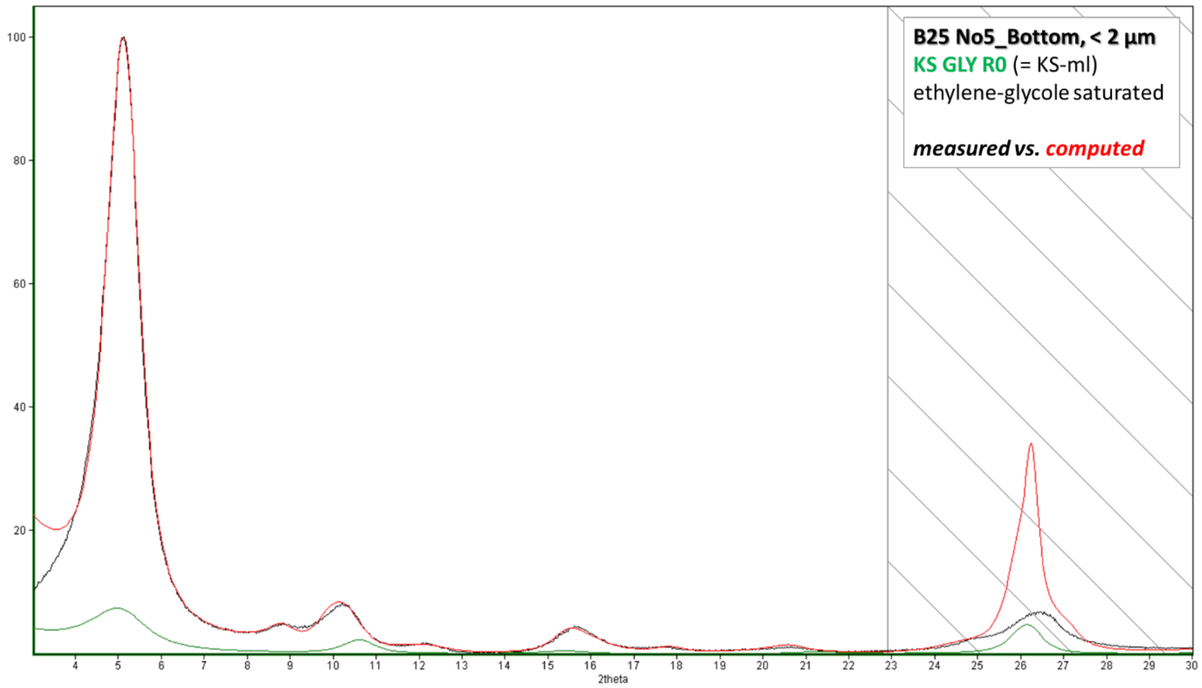
B25 No5_Bottom, < 2 µm
KS GLY R0 (= KS-ml)
ethylene-glycole saturated
measured vs. computed
100
80
60
40
20
4
5
6
7
8
9
10
11
12
13
14
15
16
17
18
19
20
21
22
23
24
25
26
27
28
29
30
2theta

Data Sheet – B25 No0_T (< 2 µm), treated material *(OPA, 100°C, 110 hours)*

Diffraction pattern of oriented specimen & modelling by Sybilla

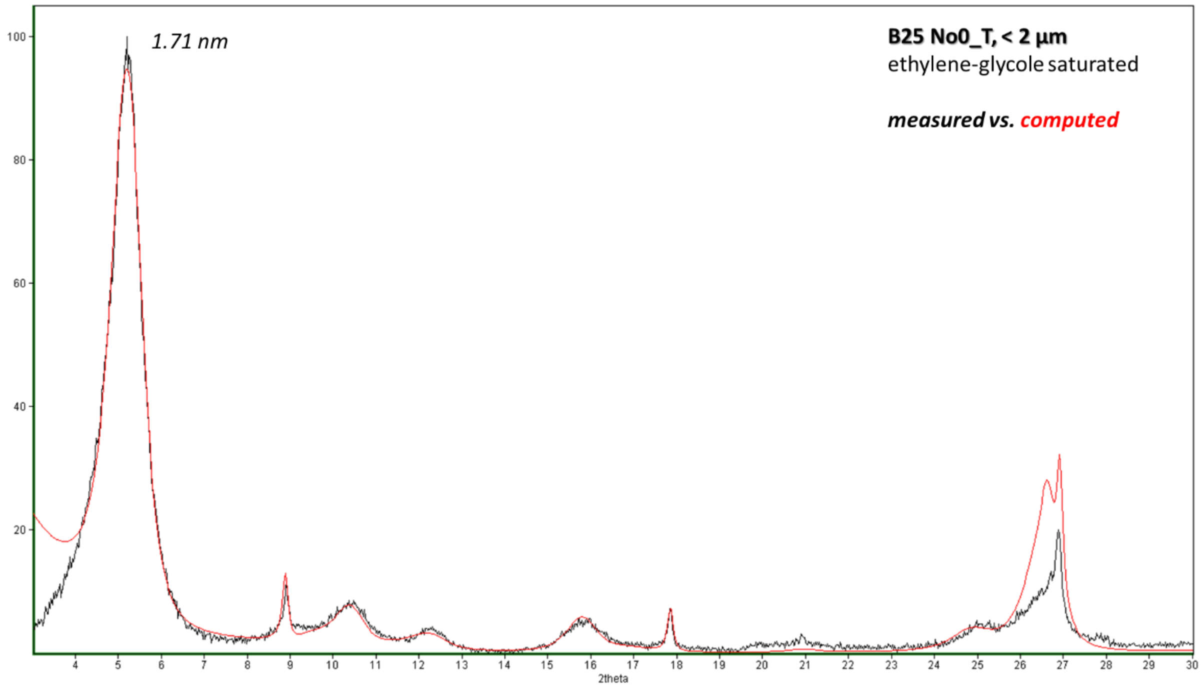

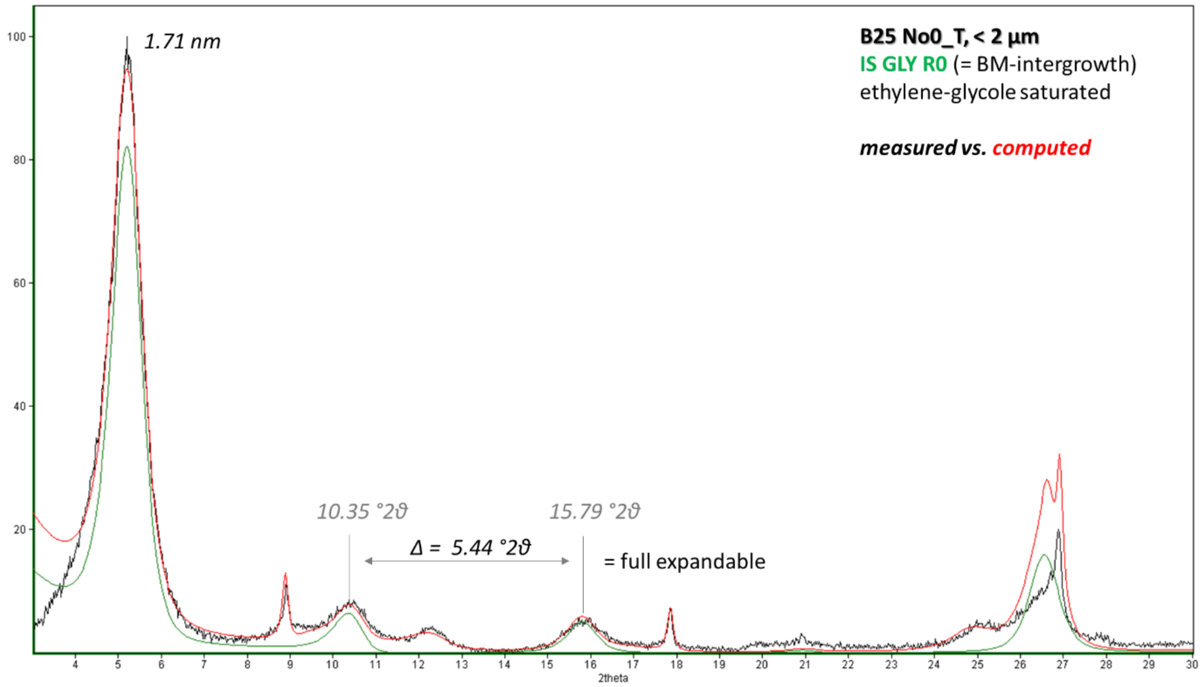

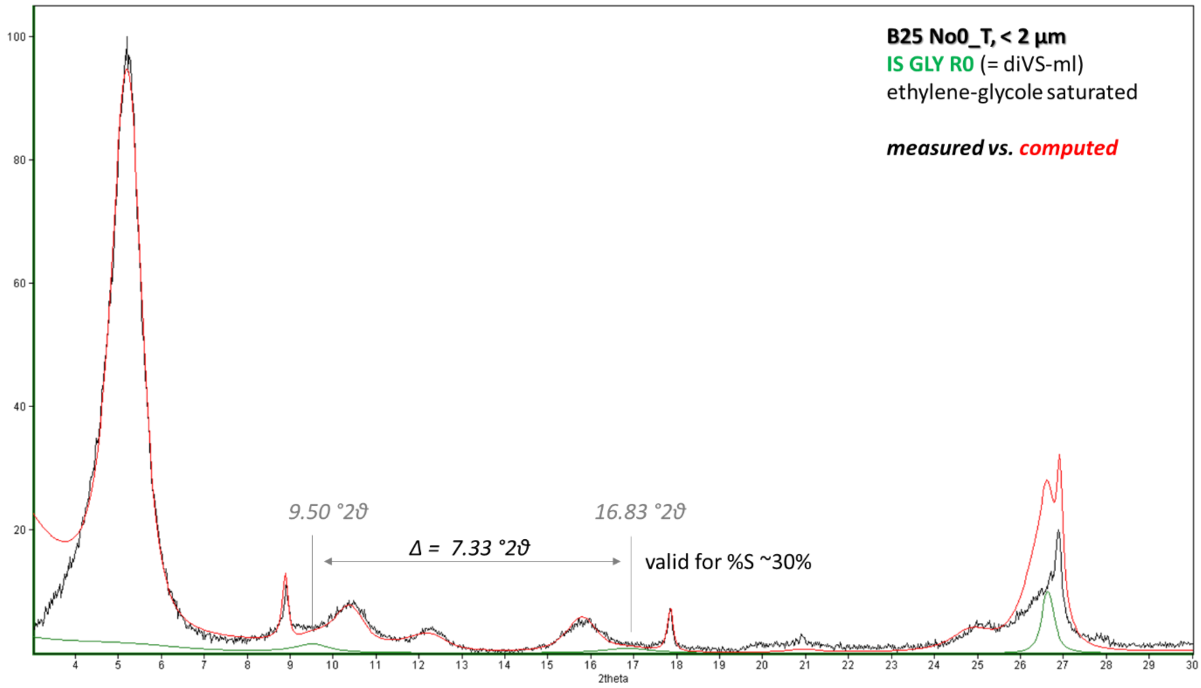
B25 No0_T, < 2 µm
IS GLY R0 (= diVS-ml)
ethylene-glycole saturated
measured vs. computed
9.50 °2ϑ
16.83 °2ϑ
Δ = 7.33 °2ϑ
valid for %S ~30%
100
80
60
40
20
4
5
6
7
8
9
10
11
12
13
14
15
16
17
18
19
20
21
22
23
24
25
26
27
28
29
30
2theta

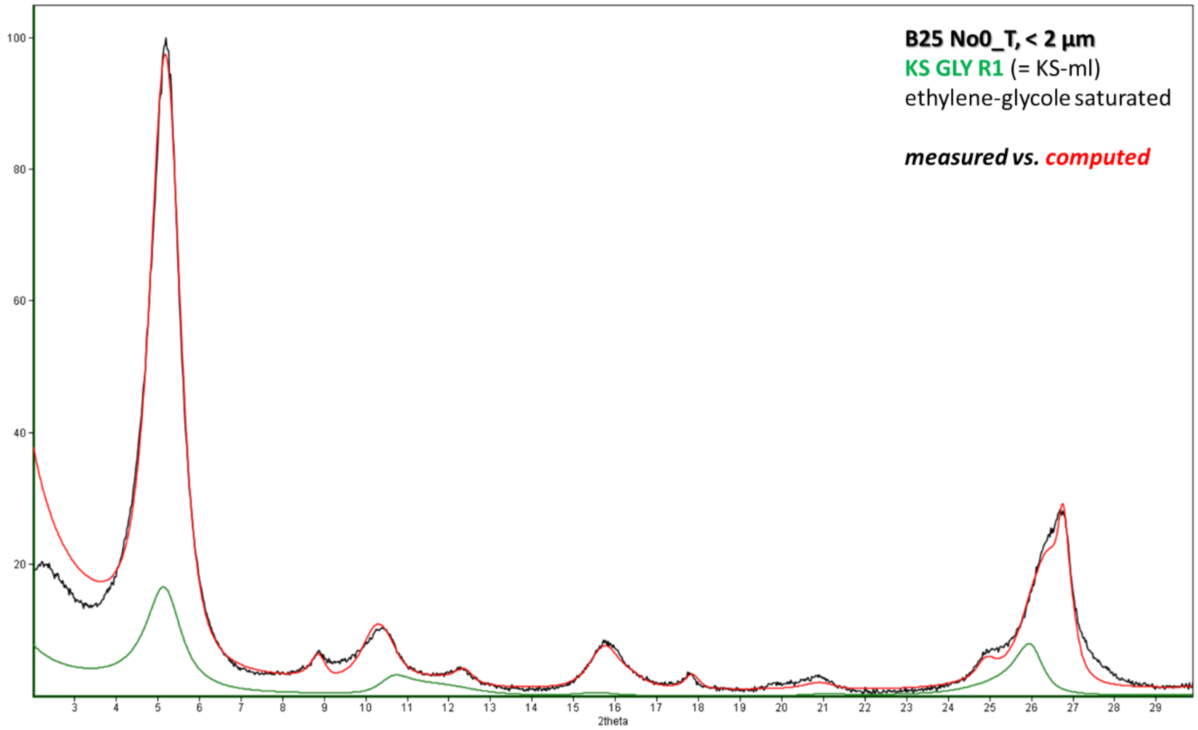
B25 No0_T, < 2 µm
KS GLY R1 (= KS-ml)
ethylene-glycole saturated
measured vs. computed
100
80
60
40
20
3
4
5
6
7
8
9
10
11
12
13
14
15
16
17
18
19
20
21
22
23
24
25
26
27
28
29
2theta

Data Sheet – B25 No0_C (< 2 µm), treated material *(OPA, 100°C, 110 hours)*

Diffraction pattern of oriented specimen & modelling by Sybilla

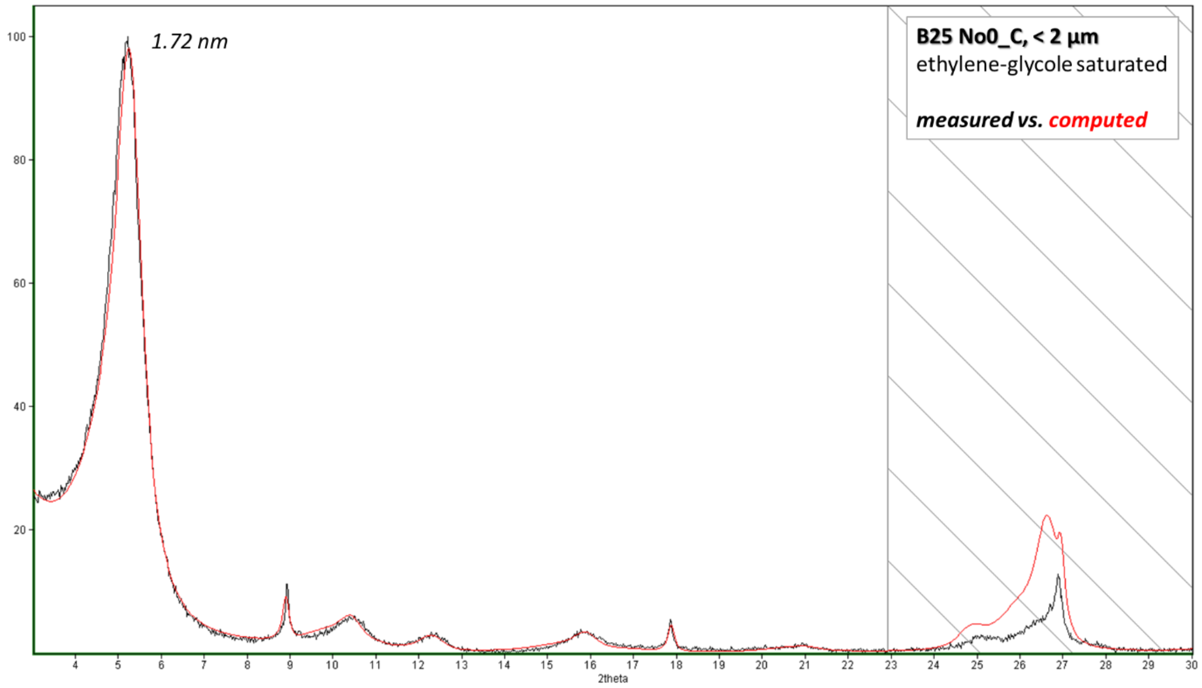

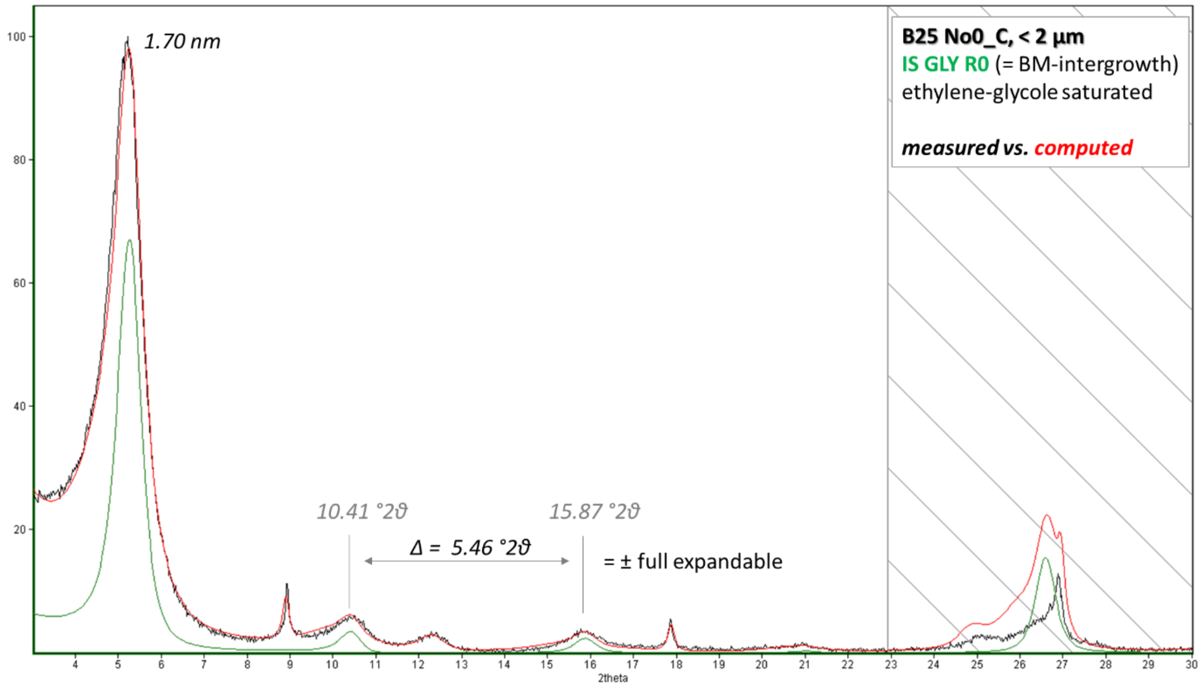

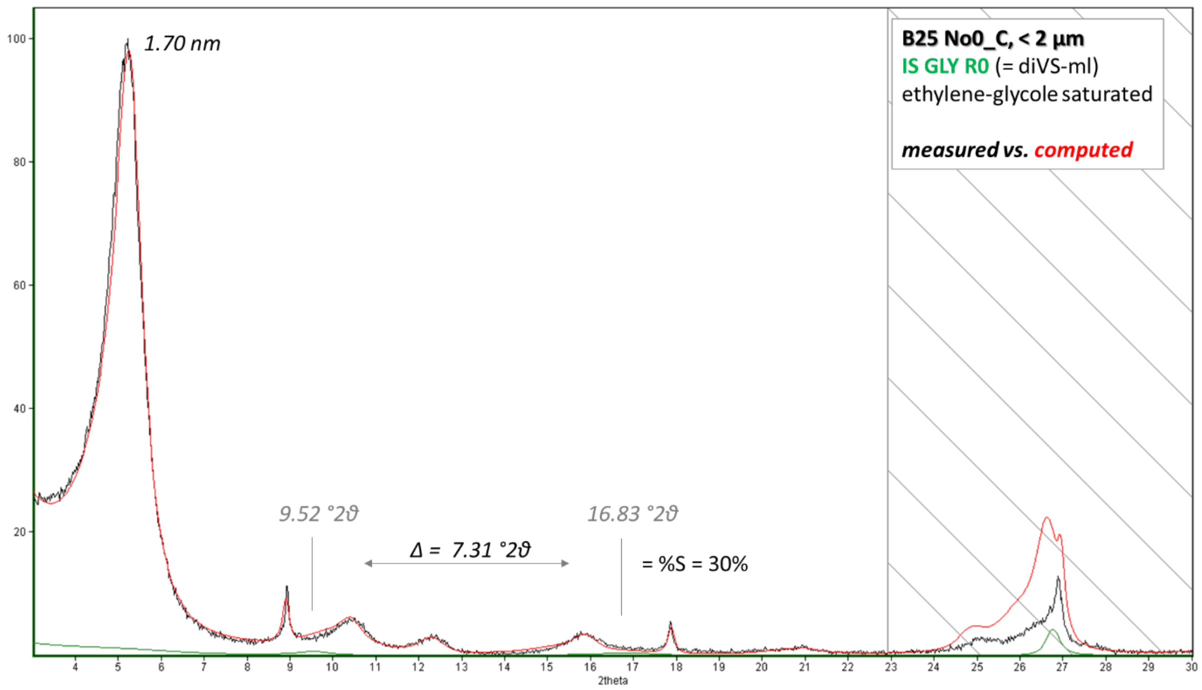
B25 No0_C, < 2 µm
IS GLY R0 (= diVS-ml)
ethylene-glycole saturated
measured vs. computed
1.70 nm
9.52 °2ϑ
16.83 °2ϑ
Δ = 7.31 °2ϑ
= %S = 30%
100
80
60
40
20
4
5
6
7
8
9
10
11
12
13
14
15
16
17
18
19
20
21
22
23
24
25
26
27
28
29
30
2theta

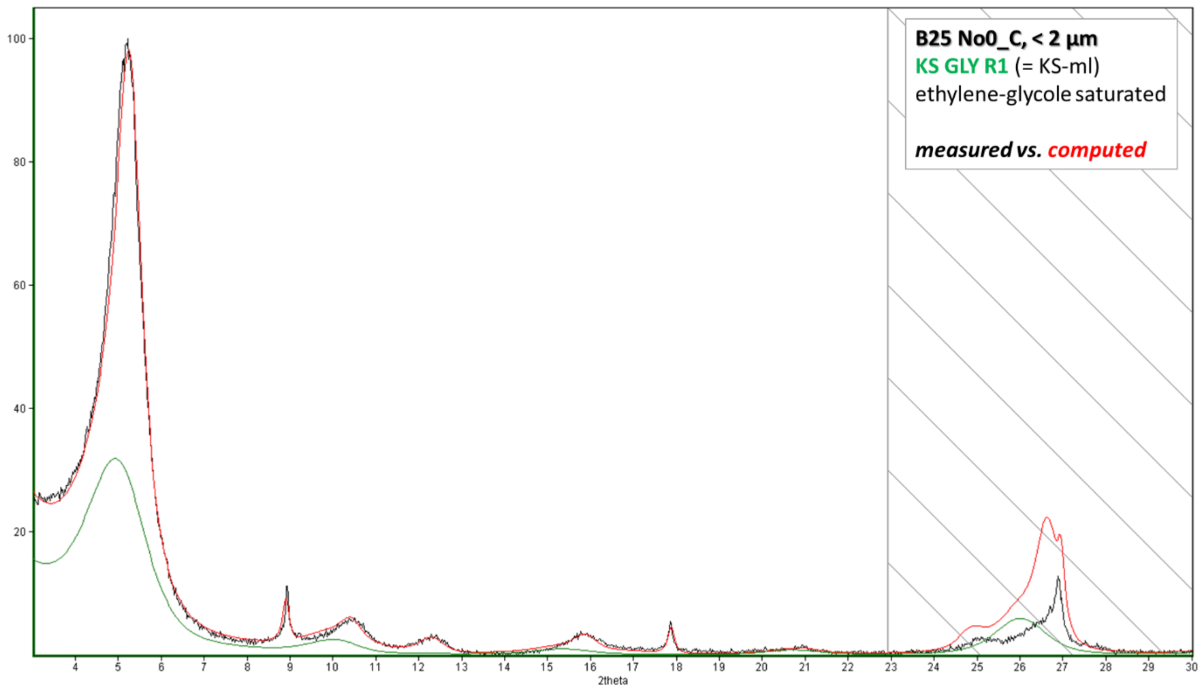
B25 No0_C, < 2 µm
KS GLY R1 (= KS-ml)
ethylene-glycole saturated
measured vs. computed
100
80
60
40
20
4
5
6
7
8
9
10
11
12
13
14
15
16
17
18
19
20
21
22
23
24
25
26
27
28
29
30
2theta

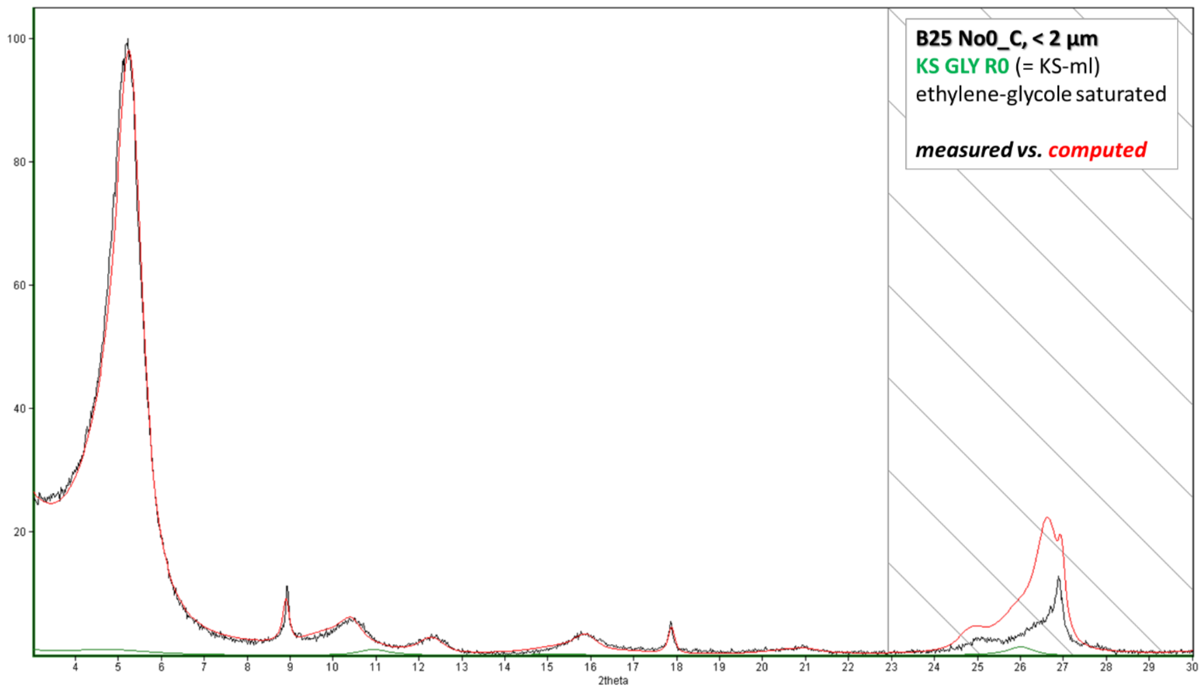
B25 No0_C, < 2 µm
KS GLY R0 (= KS-ml)
ethylene-glycole saturated
measured* vs. *computed
100
80
60
40
20
4
5
6
7
8
9
10
11
12
13
14
15
16
17
18
19
20
21
22
23
24
25
26
27
28
29
30
2theta

Data Sheet – B25 No0_B (< 2 µm), treated material *(OPA, 100°C, 110 hours)*

Diffraction pattern of oriented specimen & modelling by Sybilla

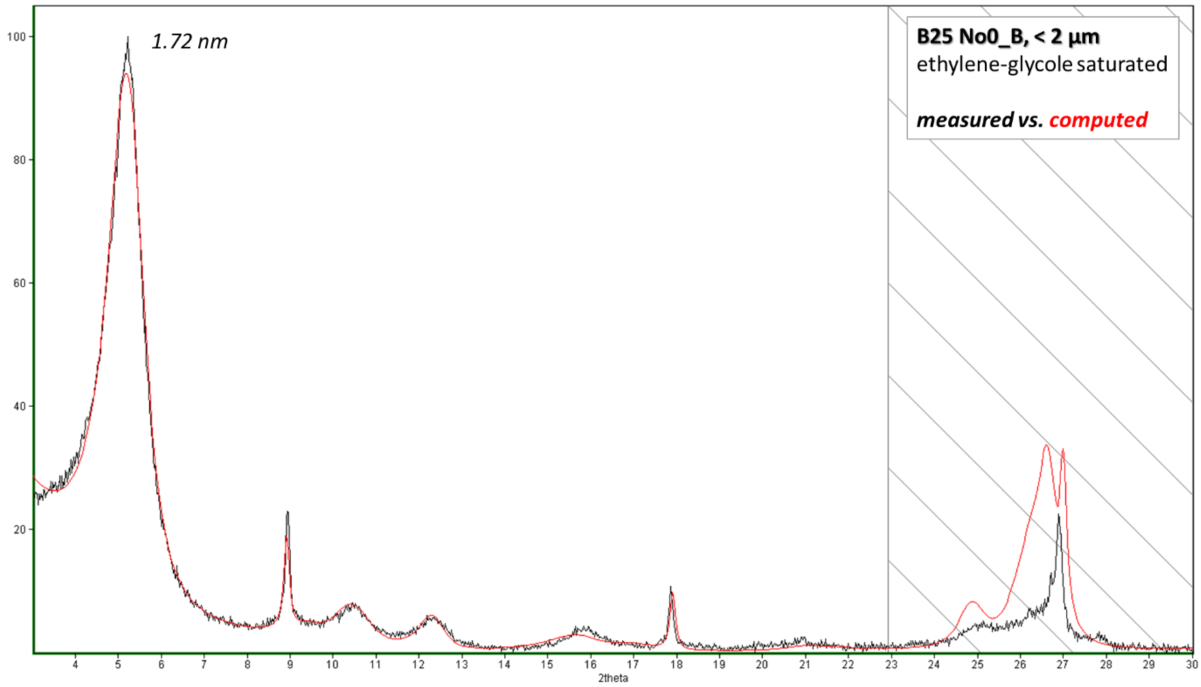

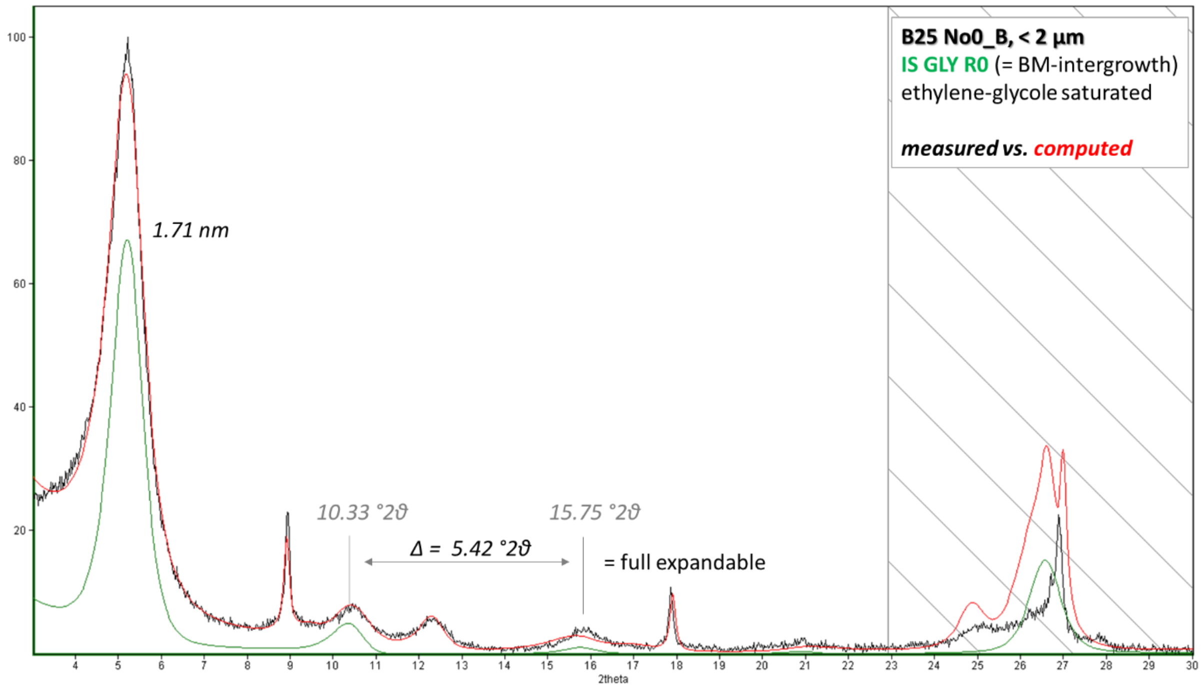
B25 No0_B, < 2 µm
IS GLY R0 (= BM-intergrowth)
ethylene-glycole saturated
measured vs. computed
1.71 nm
10.33 °2ϑ
15.75 °2ϑ
Δ = 5.42 °2ϑ
= full expandable
100
80
60
40
20
4
5
6
7
8
9
10
11
12
13
14
15
16
17
18
19
20
21
22
23
24
25
26
27
28
29
30
2theta

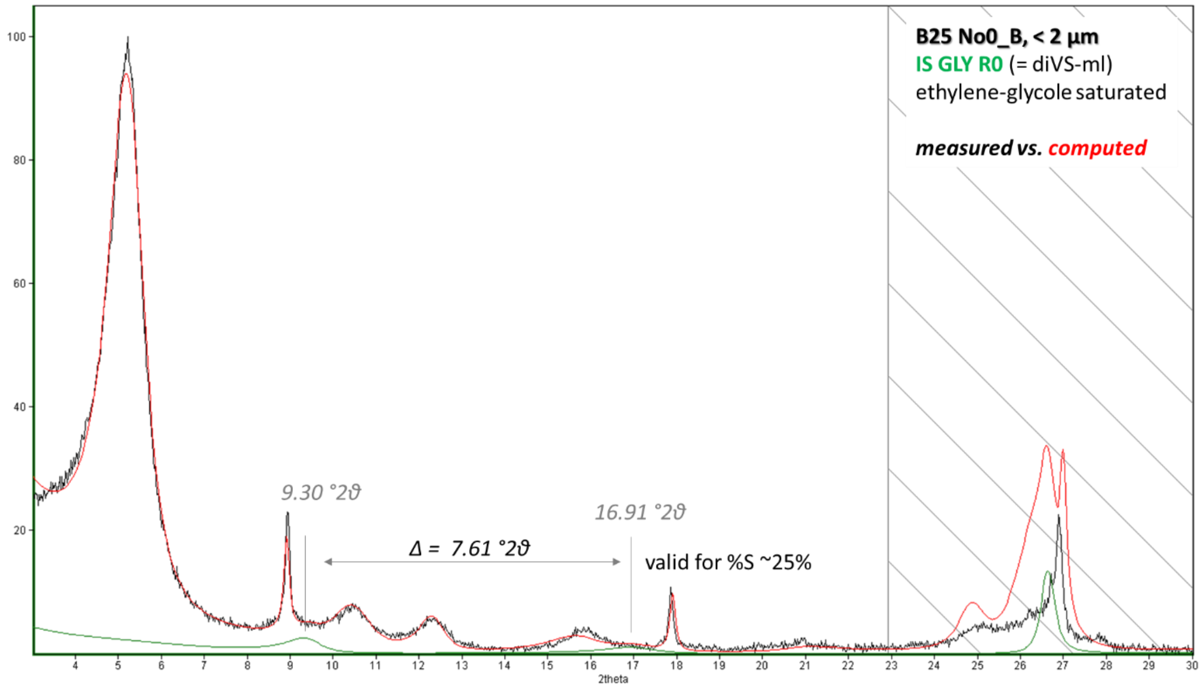
B25 No0_B, < 2 µm
IS GLY R0 (= diVS-ml)
ethylene-glycole saturated
measured vs. computed
9.30 °2ϑ
16.91 °2ϑ
Δ = 7.61 °2ϑ
valid for %S ~25%
100
80
60
40
20
4
5
6
7
8
9
10
11
12
13
14
15
16
17
18
19
20
21
22
23
24
25
26
27
28
29
30
2theta

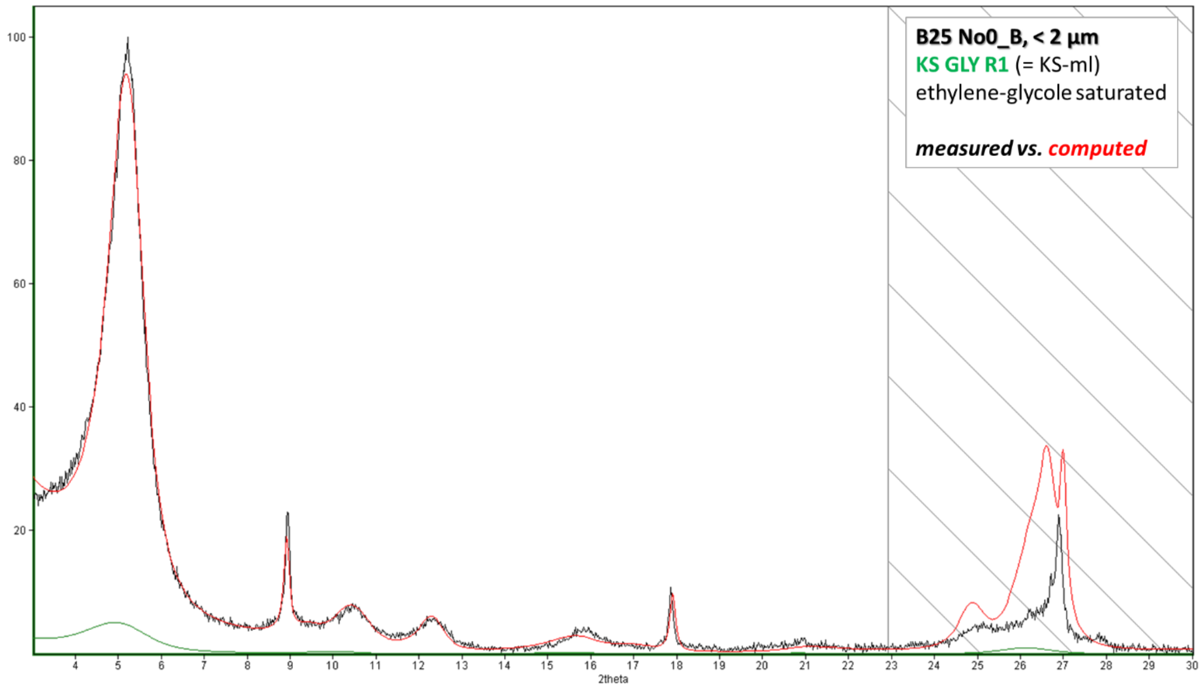
B25 No0_B, < 2 µm
KS GLY R1 (= KS-ml)
ethylene-glycole saturated
measured vs. computed
100
80
60
40
20
4
5
6
7
8
9
10
11
12
13
14
15
16
17
18
19
20
21
22
23
24
25
26
27
28
29
30
2theta

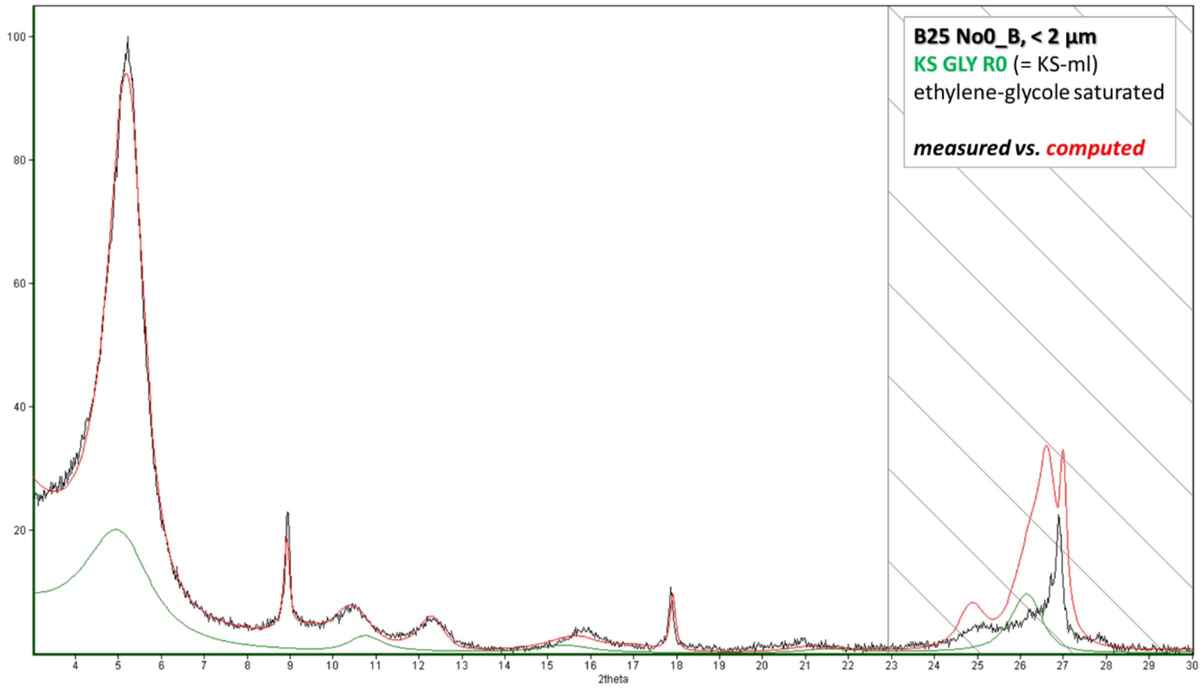
B25 No0_B, < 2 µm
KS GLY R0 (= KS-ml)
ethylene-glycole saturated
measured vs. computed
100
80
60
40
20
4
5
6
7
8
9
10
11
12
13
14
15
16
17
18
19
20
21
22
23
24
25
26
27
28
29
30
2theta

Data Sheet – B25 No2_T (< 2 µm), treated material *(OPA, 100°C, 35 days)*

Diffraction pattern of oriented specimen & modelling by Sybilla

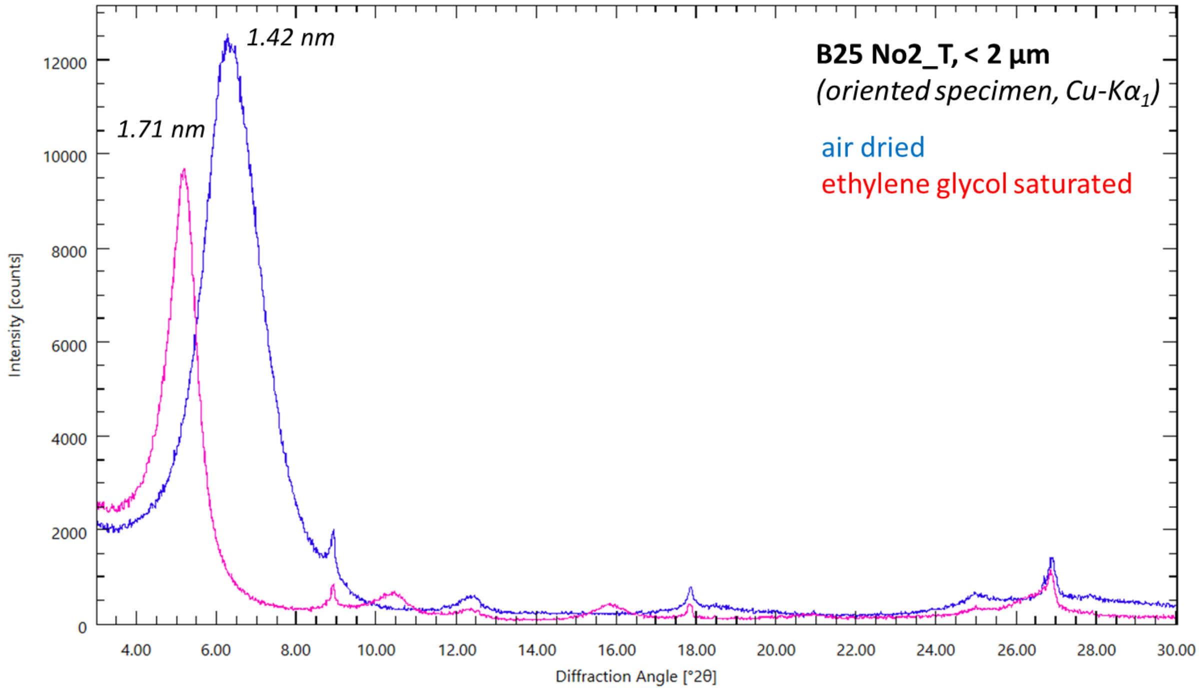

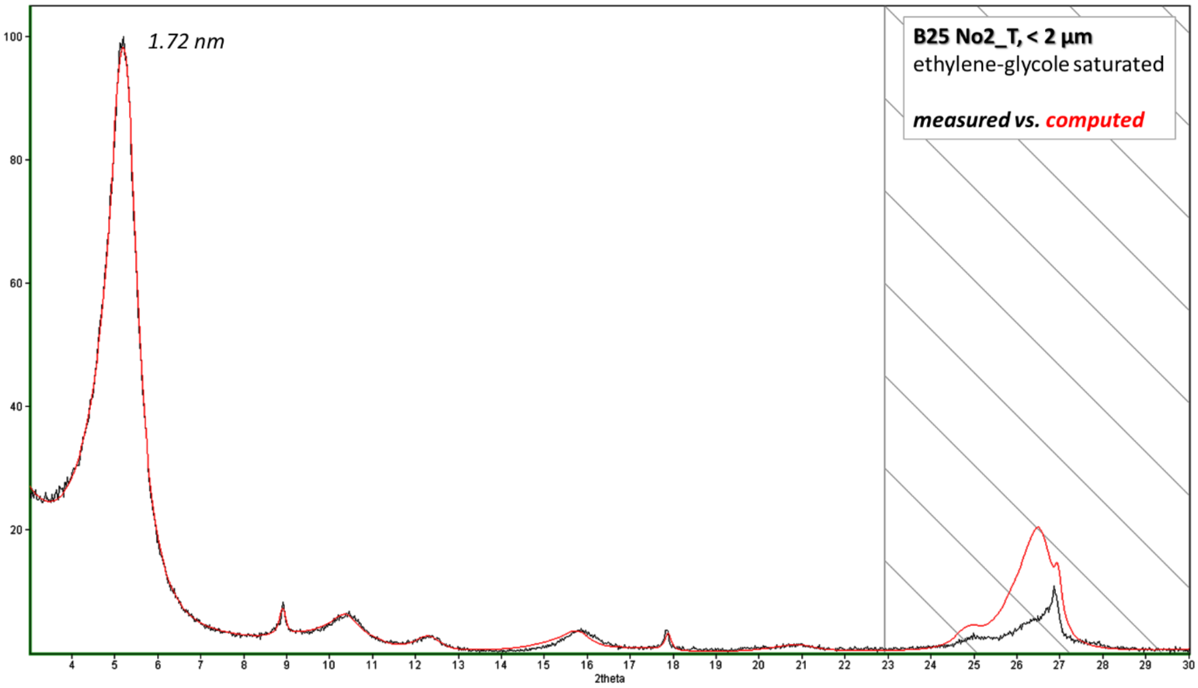

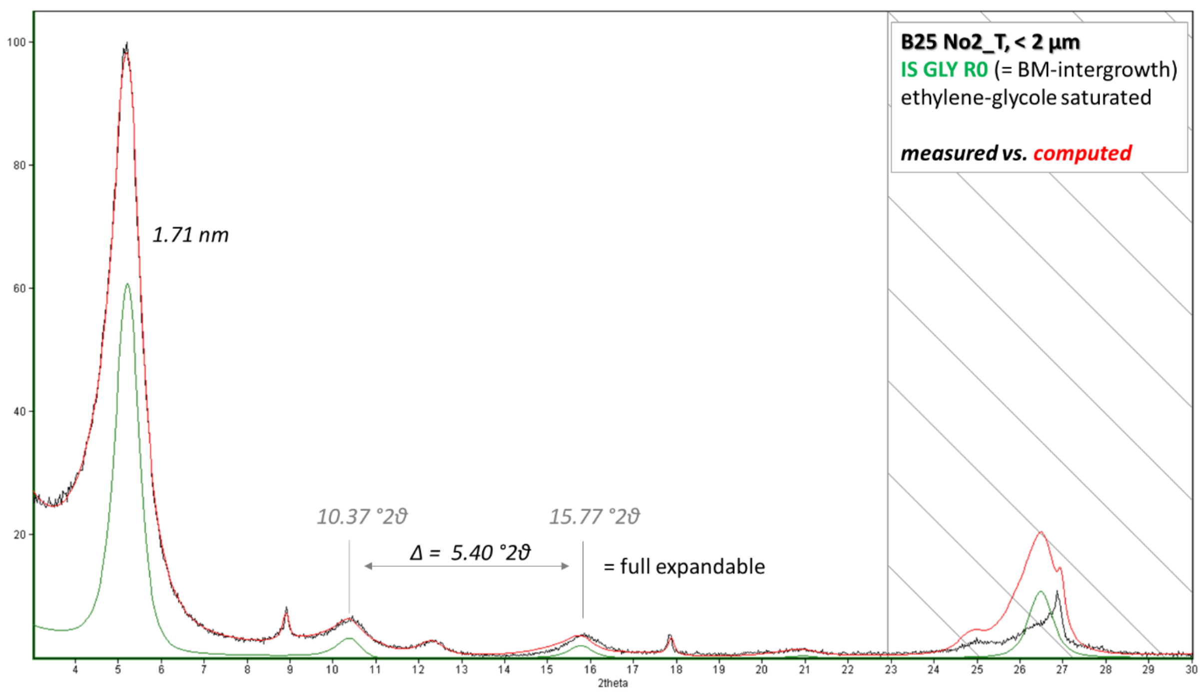
B25 No2_T, < 2 µm
IS GLY R0 (= BM-intergrowth)
ethylene-glycole saturated
measured vs. computed
1.71 nm
10.37 °2ϑ
15.77 °2ϑ
Δ = 5.40 °2ϑ
= full expandable
100
80
60
40
20
4 5 6 7 8 9 10 11 12 13 14 15 16 17 18 19 20 21 22 23 24 25 26 27 28 29 30
2theta

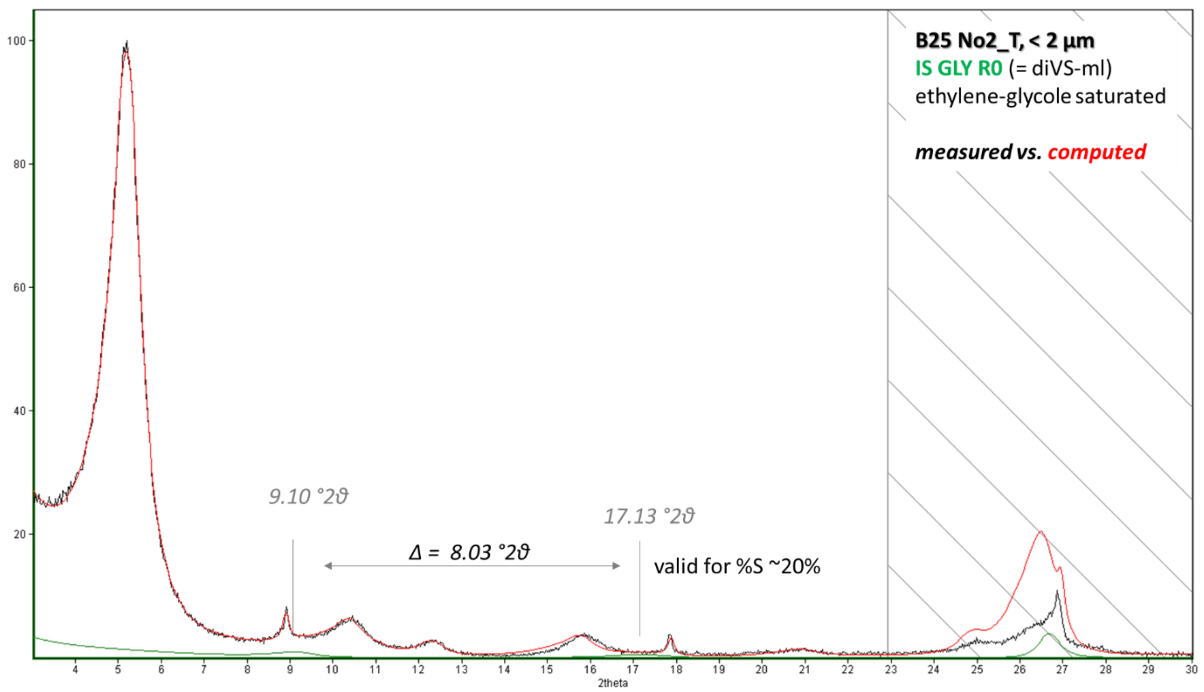
B25 No2_T, < 2 µm
IS GLY R0 (= diVS-ml)
ethylene-glycole saturated
measured vs. computed
9.10 °2ϑ
17.13 °2ϑ
Δ = 8.03 °2ϑ
valid for %S ~20%
100
80
60
40
20
4 5 6 7 8 9 10 11 12 13 14 15 16 17 18 19 20 21 22 23 24 25 26 27 28 29 30
2theta

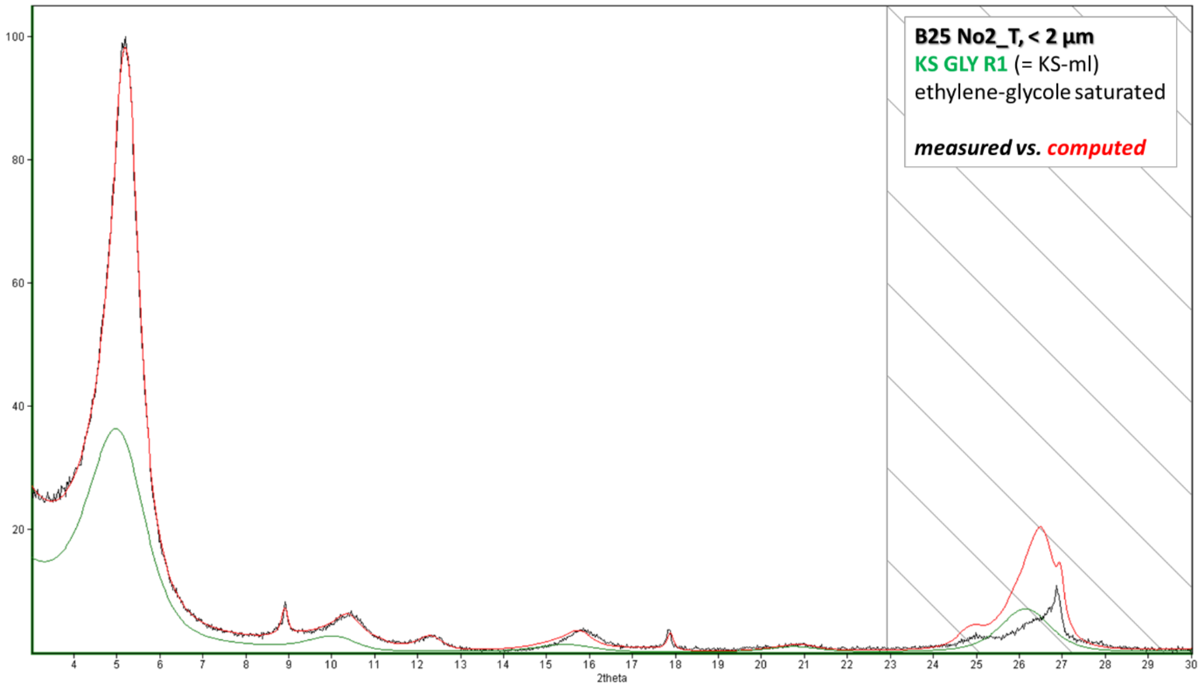
B25 No2_T, < 2 µm
KS GLY R1 (= KS-ml)
ethylene-glycole saturated
measured vs. computed
100
80
60
40
20
4
5
6
7
8
9
10
11
12
13
14
15
16
17
18
19
20
21
22
23
24
25
26
27
28
29
30
2theta

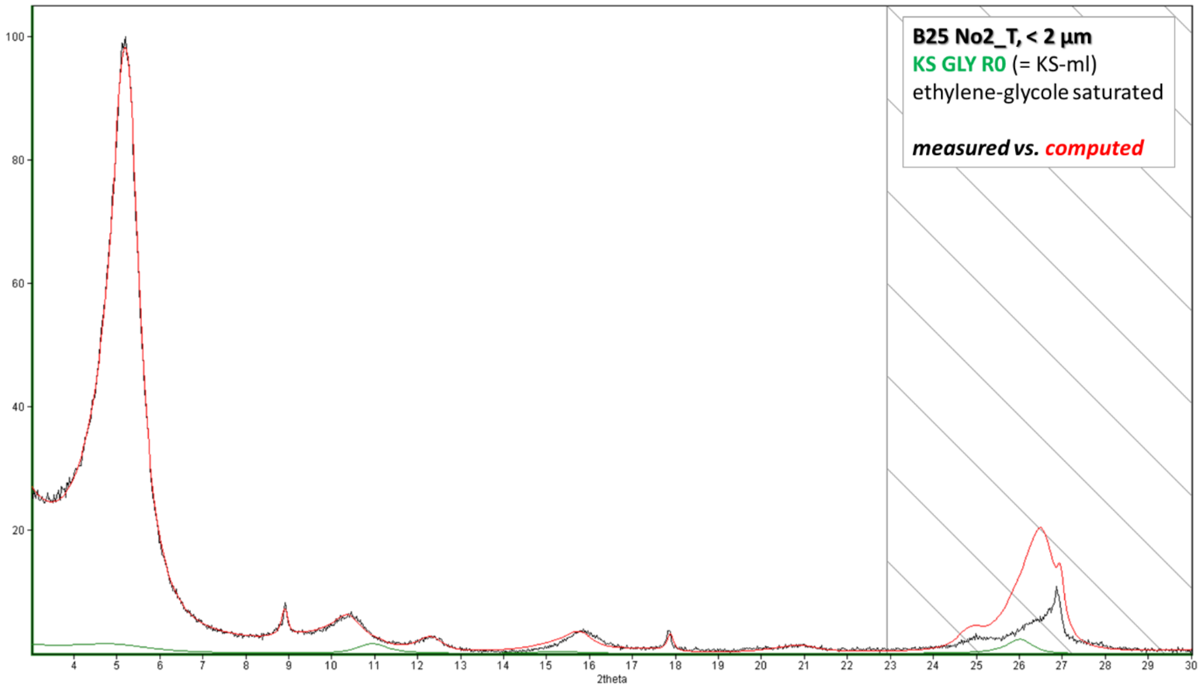
B25 No2_T, < 2 µm
KS GLY R0 (= KS-ml)
ethylene-glycole saturated
measured vs. computed
100
80
60
40
20
4
5
6
7
8
9
10
11
12
13
14
15
16
17
18
19
20
21
22
23
24
25
26
27
28
29
30
2theta

Data Sheet – B25 No2_C (< 2 µm), treated material *(OPA, 100°C, 35 days)*

Diffraction pattern of oriented specimen & modelling by Sybilla

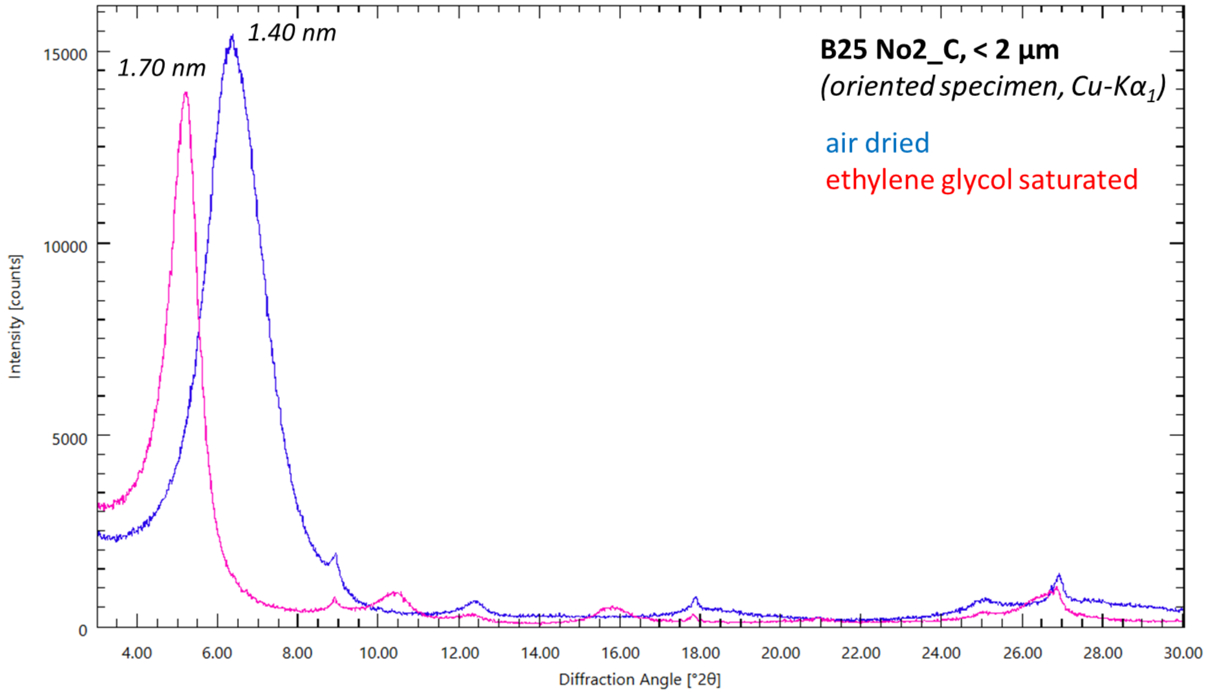

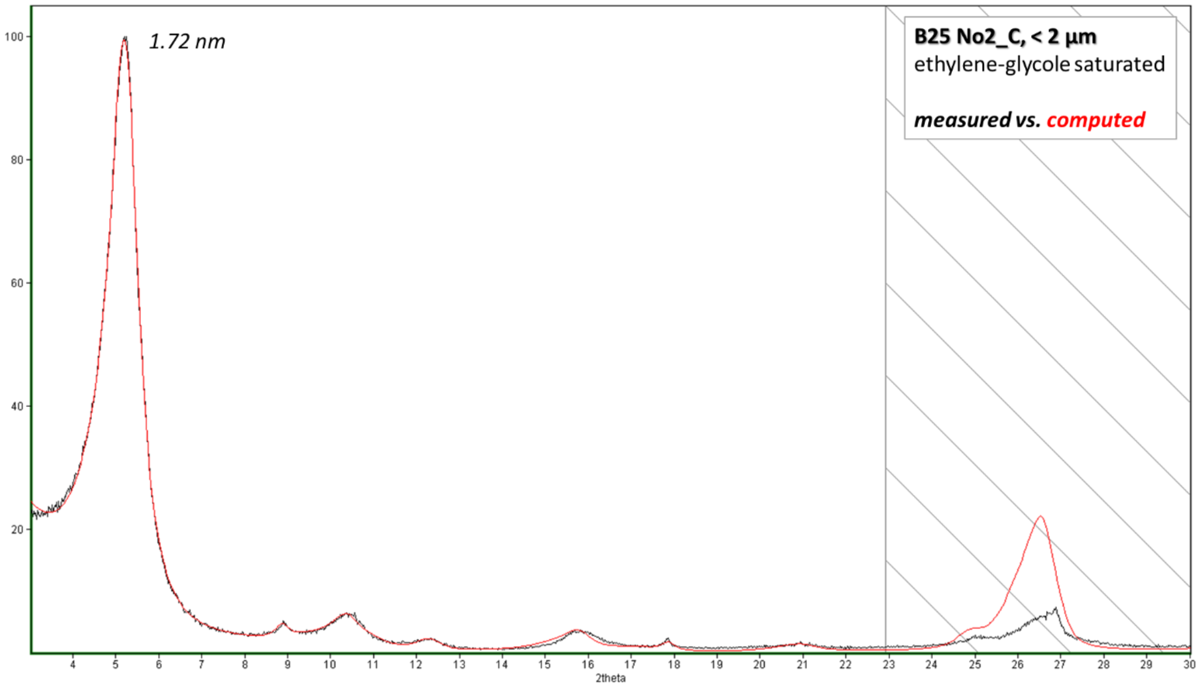

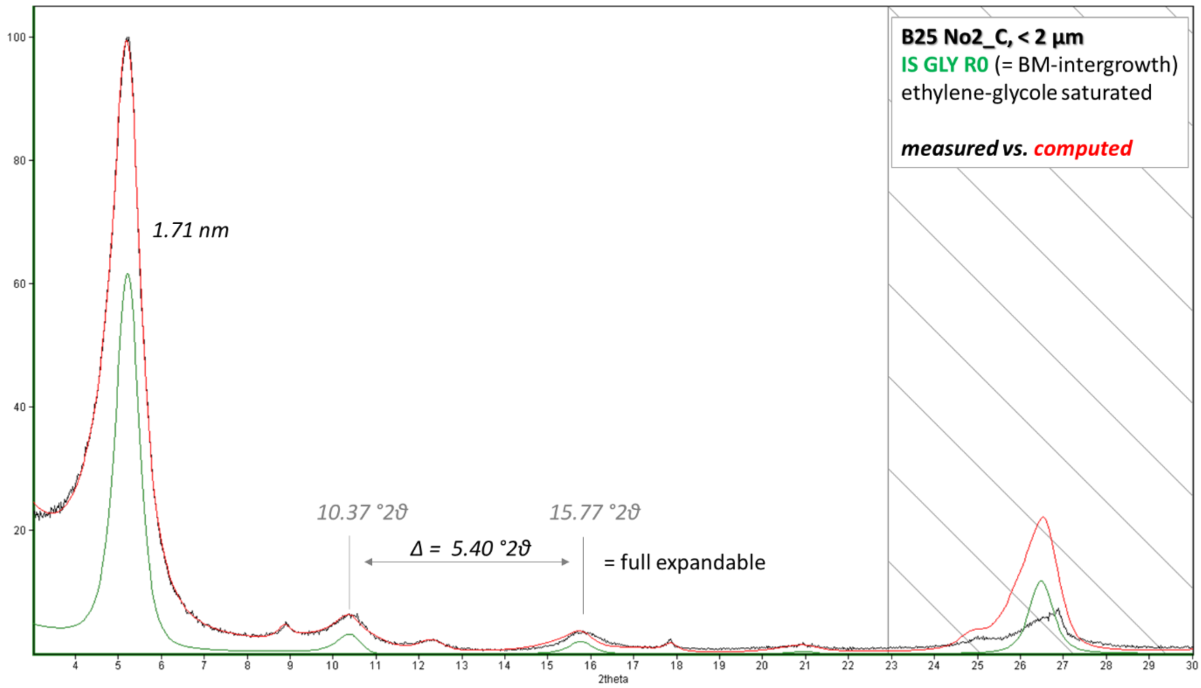
B25 No2_C, < 2 µm
IS GLY R0 (= BM-intergrowth)
ethylene-glycole saturated
measured* vs. *computed
1.71 nm
10.37 °2ϑ
15.77 °2ϑ
Δ = 5.40 °2ϑ
= full expandable
100
80
60
40
20
4
5
6
7
8
9
10
11
12
13
14
15
16
17
18
19
20
21
22
23
24
25
26
27
28
29
30
2theta

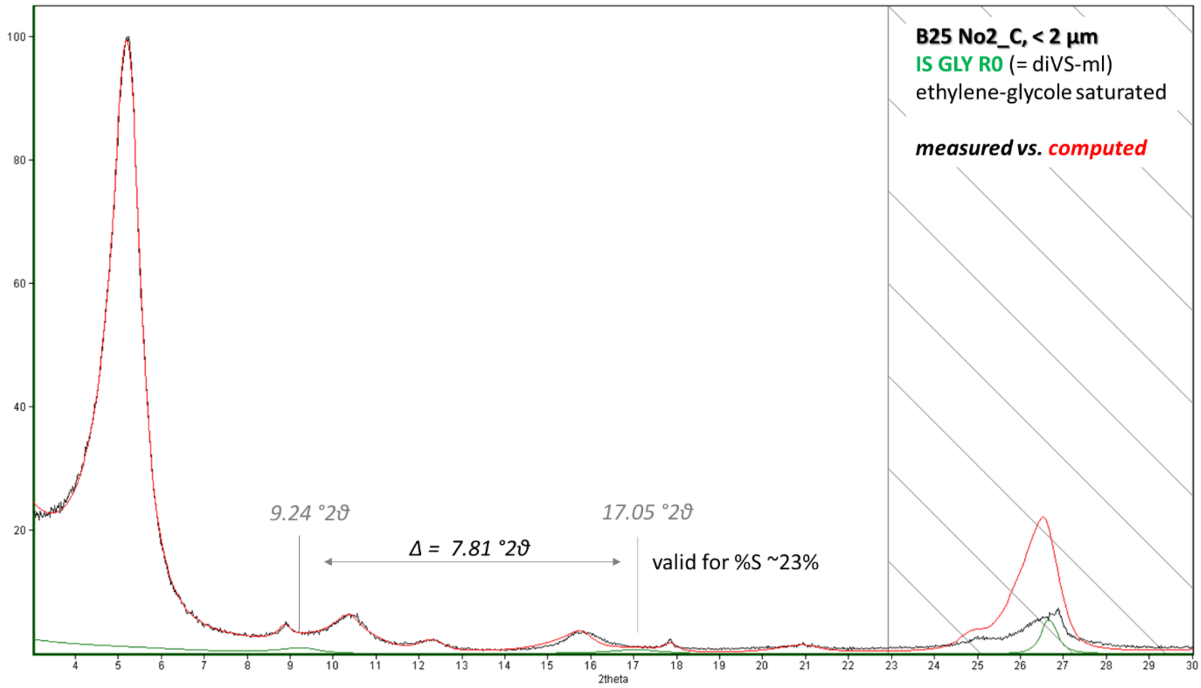
B25 No2_C, < 2 µm
IS GLY R0 (= diVS-ml)
ethylene-glycole saturated
measured* vs. *computed
9.24 °2ϑ
17.05 °2ϑ
Δ = 7.81 °2ϑ
valid for %S ~23%
100
80
60
40
20
4
5
6
7
8
9
10
11
12
13
14
15
16
17
18
19
20
21
22
23
24
25
26
27
28
29
30
2theta

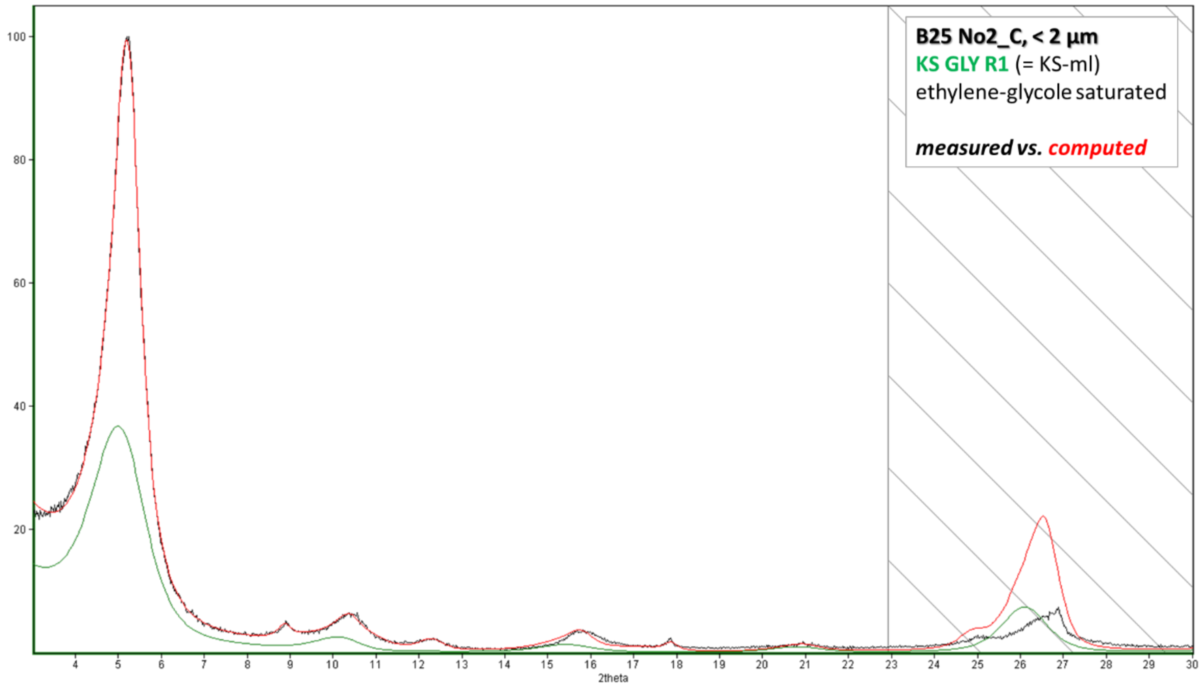
B25 No2_C, < 2 µm
KS GLY R1 (= KS-ml)
ethylene-glycole saturated
measured vs. computed
100
80
60
40
20
4
5
6
7
8
9
10
11
12
13
14
15
16
17
18
19
20
21
22
23
24
25
26
27
28
29
30
2theta

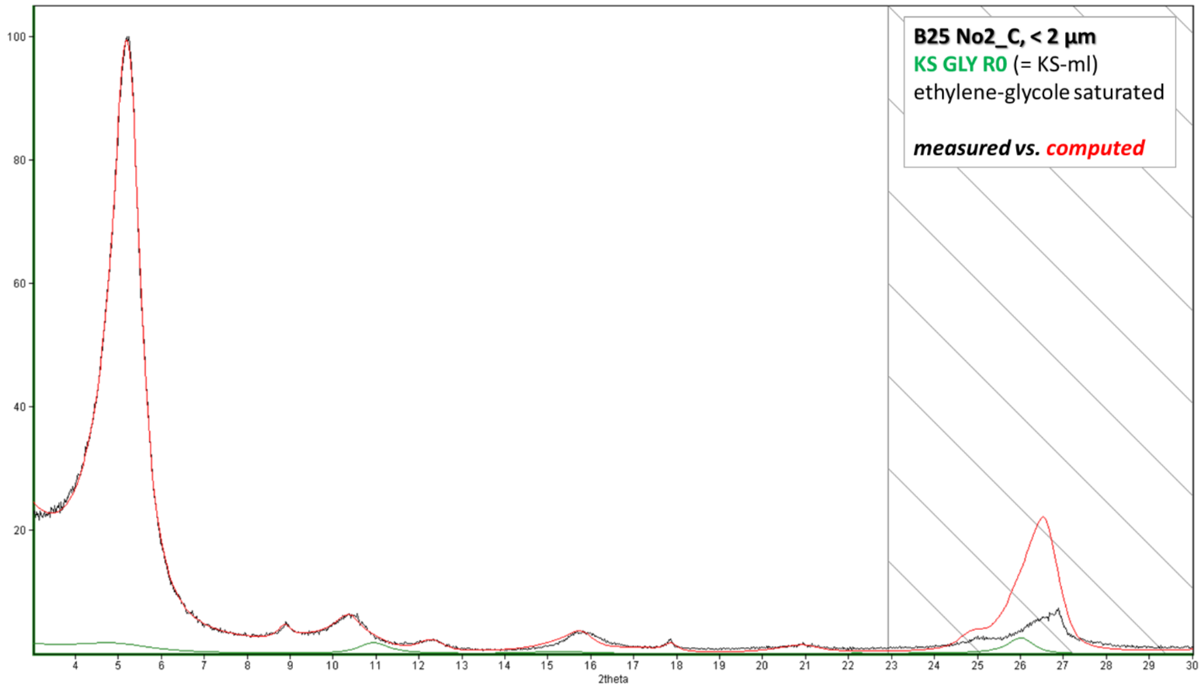
B25 No2_C, < 2 µm
KS GLY R0 (= KS-ml)
ethylene-glycole saturated
measured vs. computed
100
80
60
40
20
4
5
6
7
8
9
10
11
12
13
14
15
16
17
18
19
20
21
22
23
24
25
26
27
28
29
30
2theta

Data Sheet – B25 No2_B (< 2 µm), treated material *(OPA, 100°C, 35 days)*

Diffraction pattern of oriented specimen & modelling by Sybilla

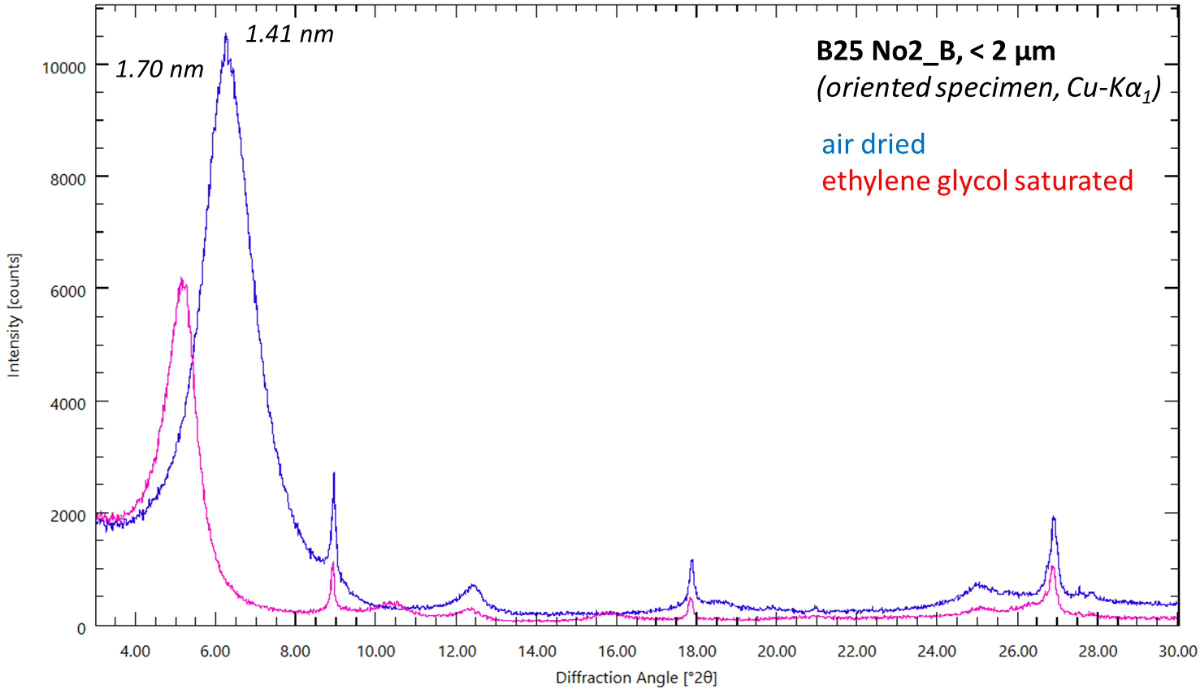

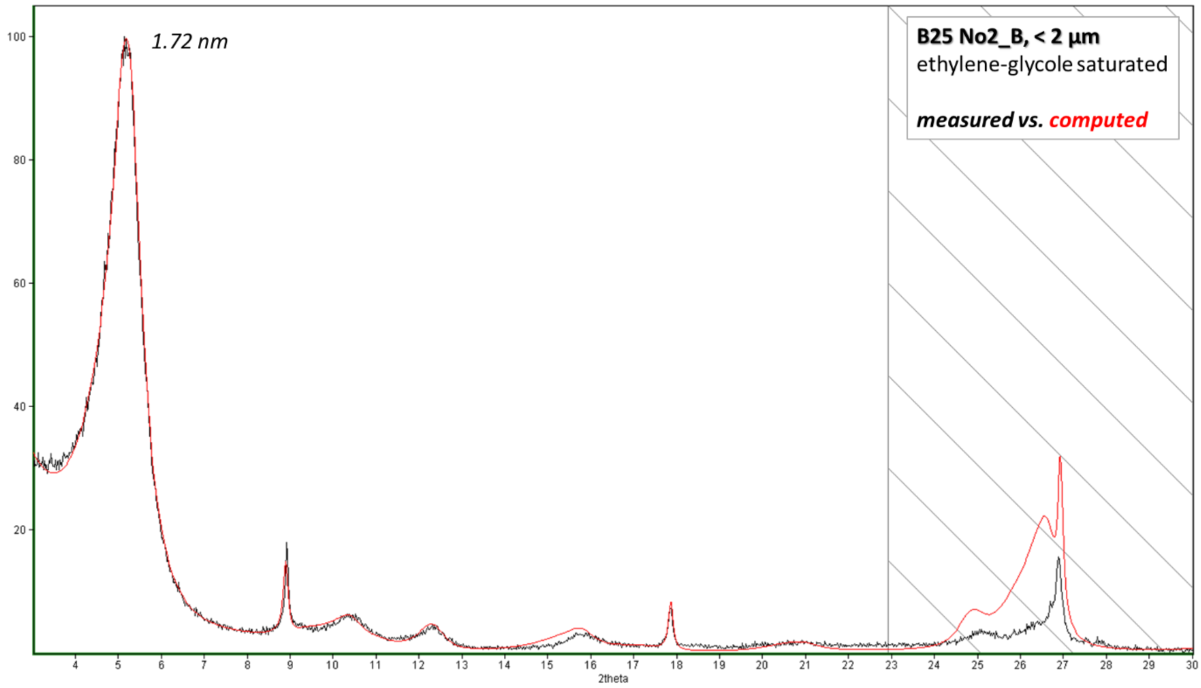

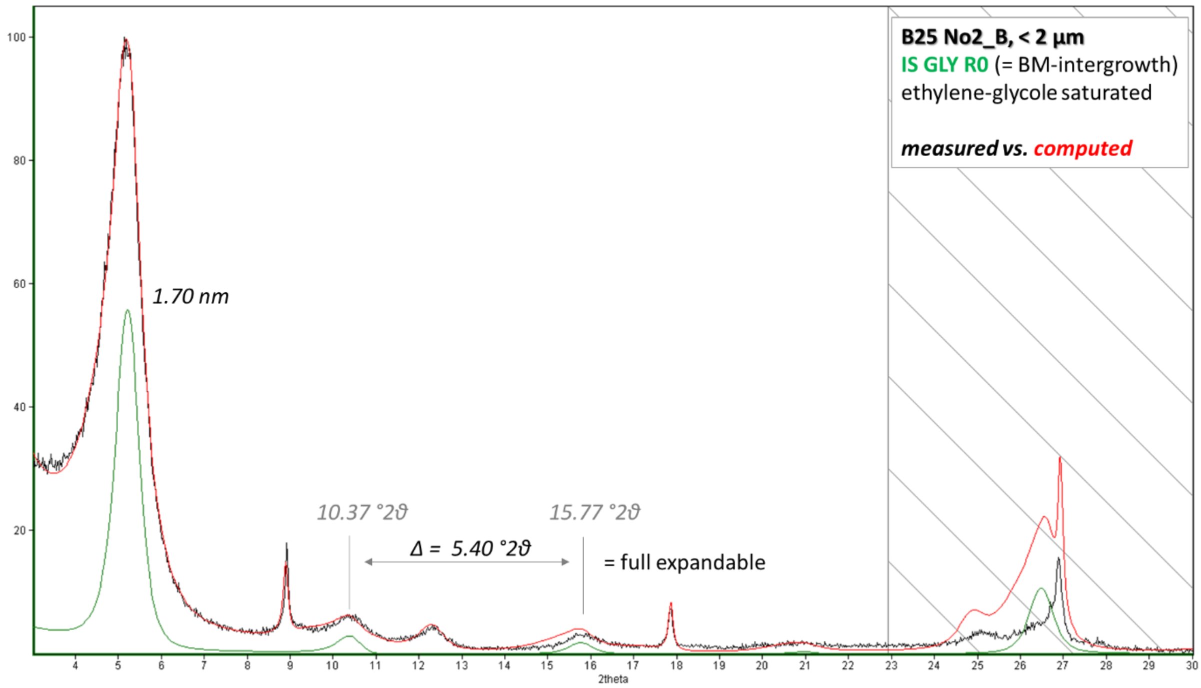
B25 No2_B, < 2 µm
IS GLY R0 (= BM-intergrowth)
ethylene-glycole saturated
measured vs. computed
1.70 nm
10.37 °2ϑ
15.77 °2ϑ
Δ = 5.40 °2ϑ
= full expandable
100
80
60
40
20
4
5
6
7
8
9
10
11
12
13
14
15
16
17
18
19
20
21
22
23
24
25
26
27
28
29
30
2theta

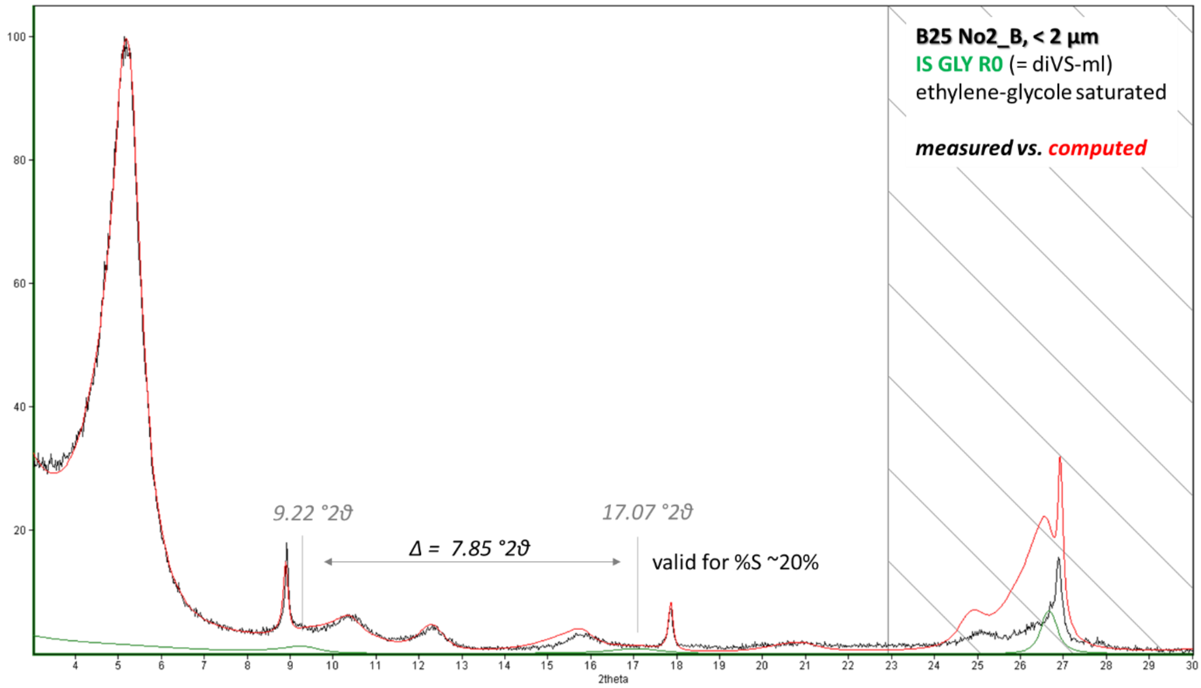
B25 No2_B, < 2 µm
IS GLY R0 (= diVS-ml)
ethylene-glycole saturated
measured vs. computed
9.22 °2ϑ
17.07 °2ϑ
Δ = 7.85 °2ϑ
valid for %S ~20%
100
80
60
40
20
4
5
6
7
8
9
10
11
12
13
14
15
16
17
18
19
20
21
22
23
24
25
26
27
28
29
30
2theta

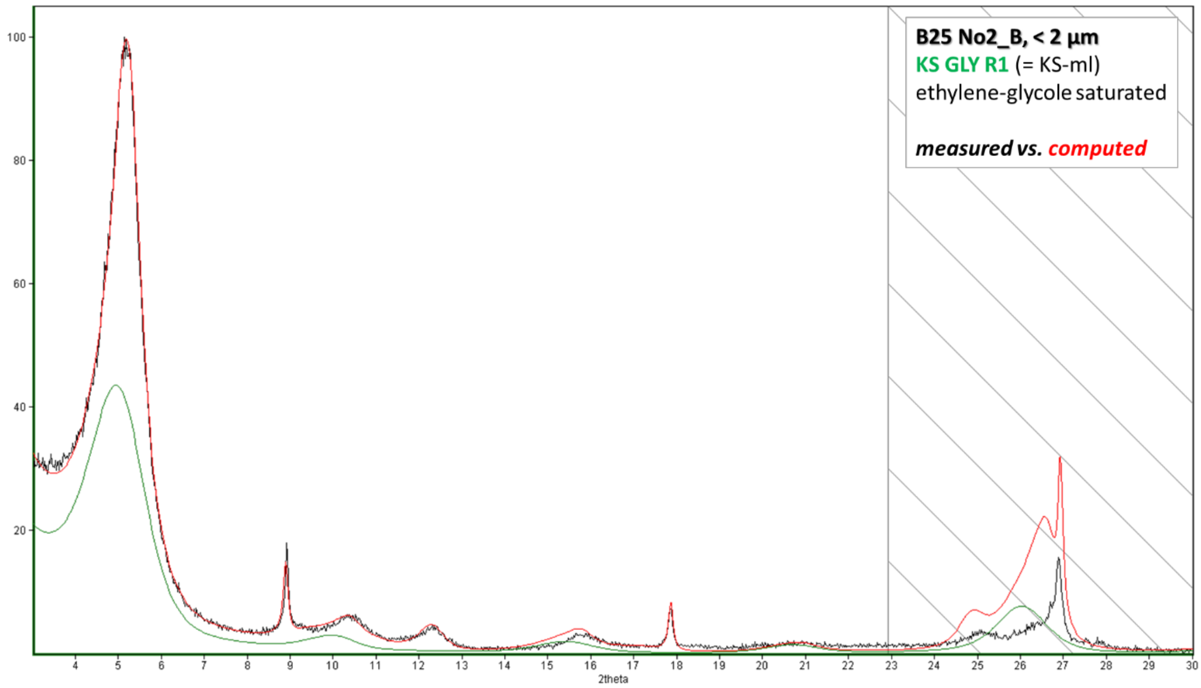
B25 No2_B, < 2 µm
KS GLY R1 (= KS-ml)
ethylene-glycole saturated
measured vs. computed
100
80
60
40
20
4
5
6
7
8
9
10
11
12
13
14
15
16
17
18
19
20
21
22
23
24
25
26
27
28
29
30
2theta

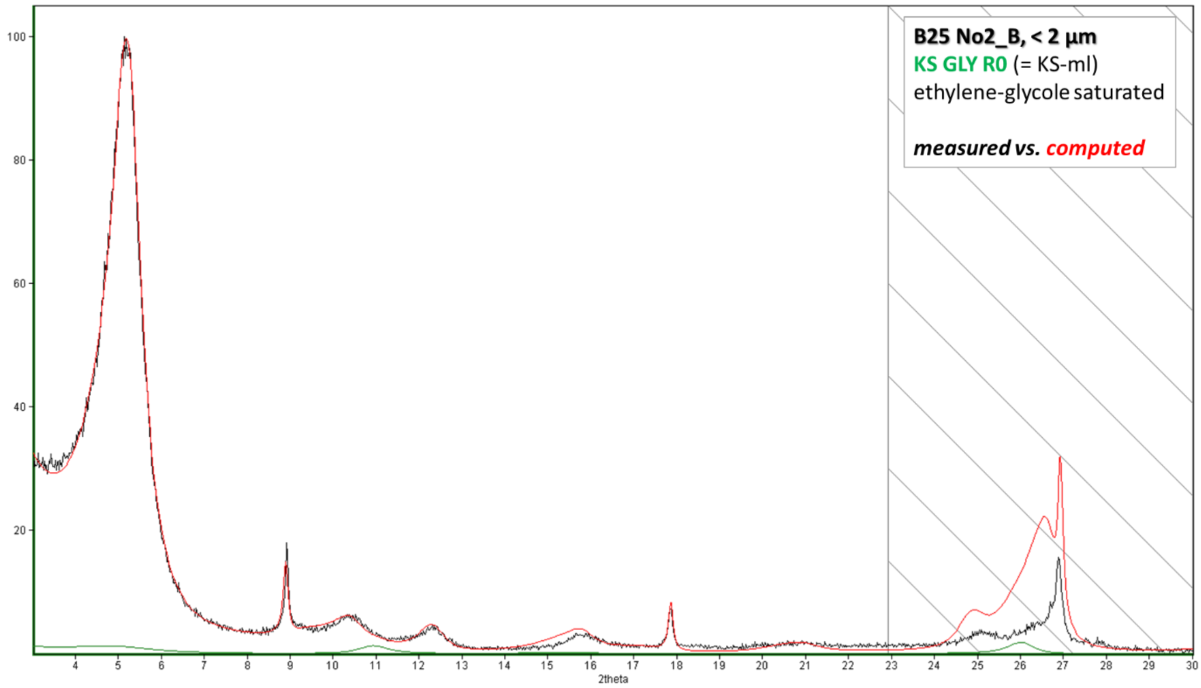
B25 No2_B, < 2 µm
KS GLY R0 (= KS-ml)
ethylene-glycole saturated
measured vs. computed
100
80
60
40
20
4
5
6
7
8
9
10
11
12
13
14
15
16
17
18
19
20
21
22
23
24
25
26
27
28
29
30
2theta

Data Sheet – B25 No15 (< 2 µm), treated material *(OPA, 125°C, 98.5 hours)*

Diffraction pattern of oriented specimen & modelling by Sybilla

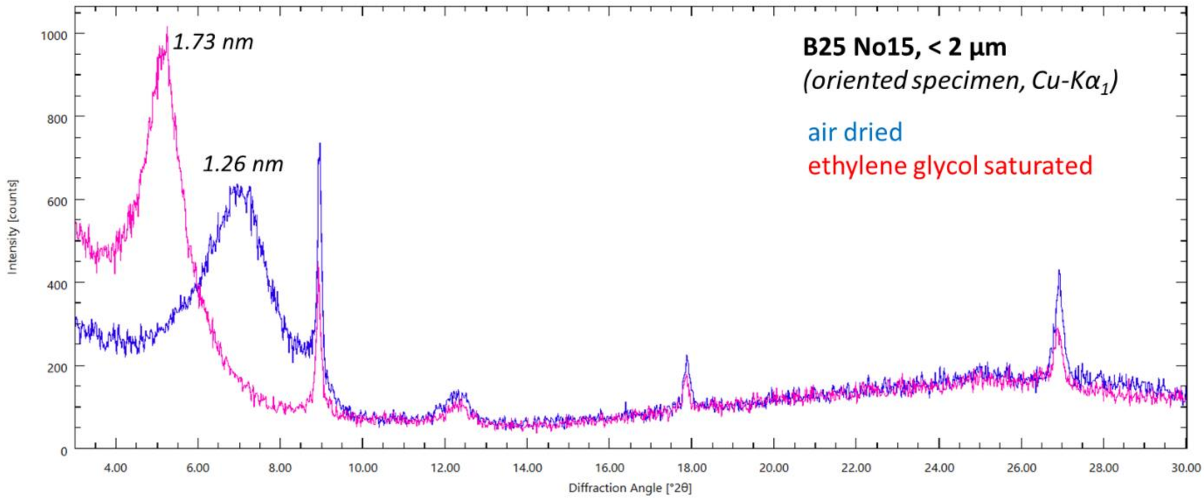

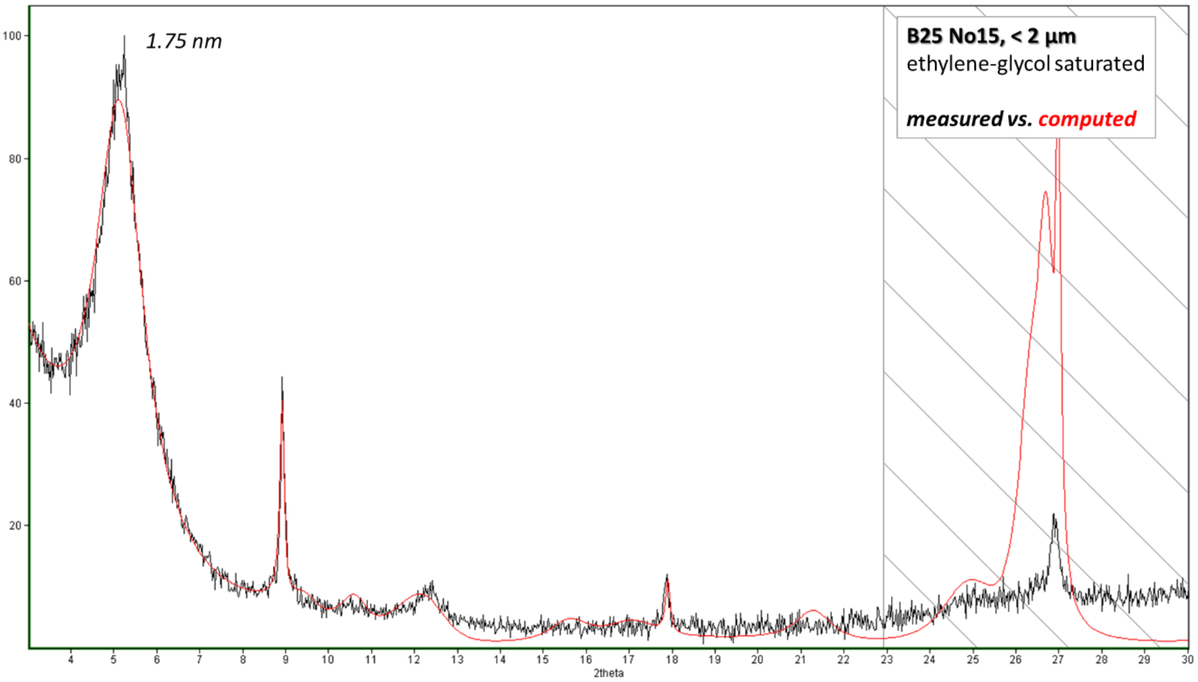

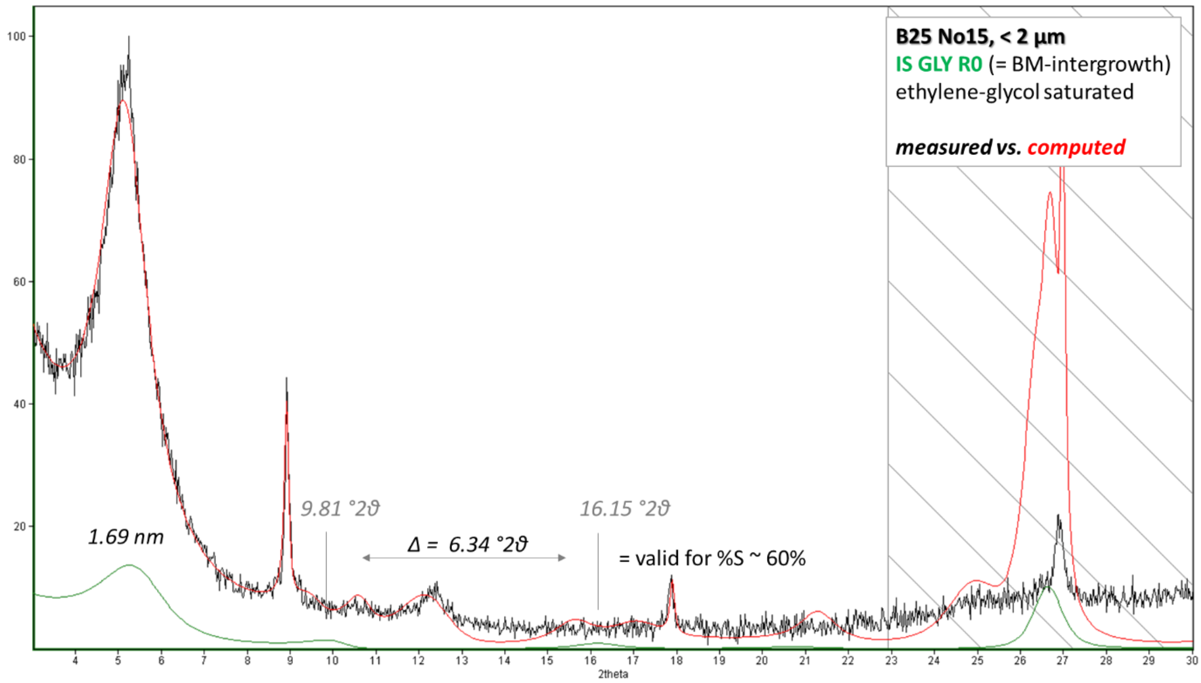
B25 No15, < 2 µm
IS GLY R0 (= BM-intergrowth)
ethylene-glycol saturated
measured* vs. *computed
1.69 nm
9.81 °2ϑ
Δ = 6.34 °2ϑ
16.15 °2ϑ
= valid for %S ~ 60%
100
80
60
40
20
4 5 6 7 8 9 10 11 12 13 14 15 16 17 18 19 20 21 22 23 24 25 26 27 28 29 30
2theta

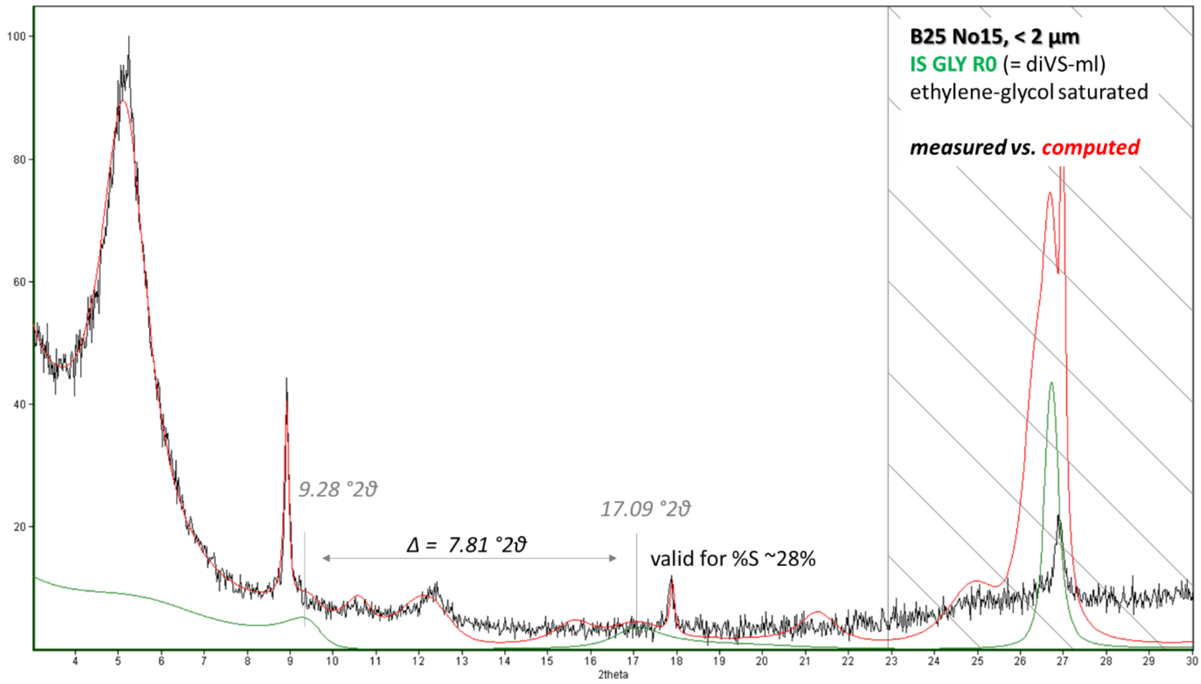
B25 No15, < 2 µm
IS GLY R0 (= diVS-ml)
ethylene-glycol saturated
measured* vs. *computed
9.28 °2ϑ
Δ = 7.81 °2ϑ
17.09 °2ϑ
valid for %S ~28%
100
80
60
40
20
4 5 6 7 8 9 10 11 12 13 14 15 16 17 18 19 20 21 22 23 24 25 26 27 28 29 30
2theta

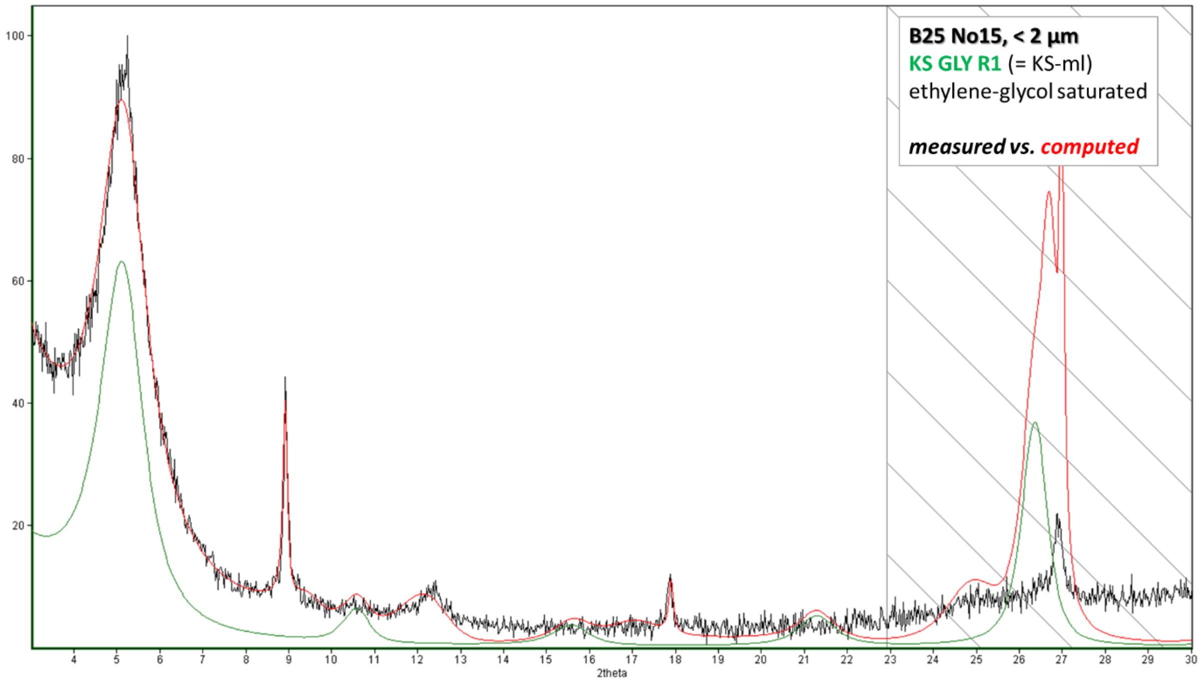
B25 No15, < 2 µm
KS GLY R1 (= KS-ml)
ethylene-glycol saturated
measured* vs. *computed
100
80
60
40
20
4
5
6
7
8
9
10
11
12
13
14
15
16
17
18
19
20
21
22
23
24
25
26
27
28
29
30
2theta

Data Sheet – B25 No3_T (< 2 µm), treated material *(OPA, 150°C, 4 days)*

Diffraction pattern of oriented specimen & modelling by Sybilla

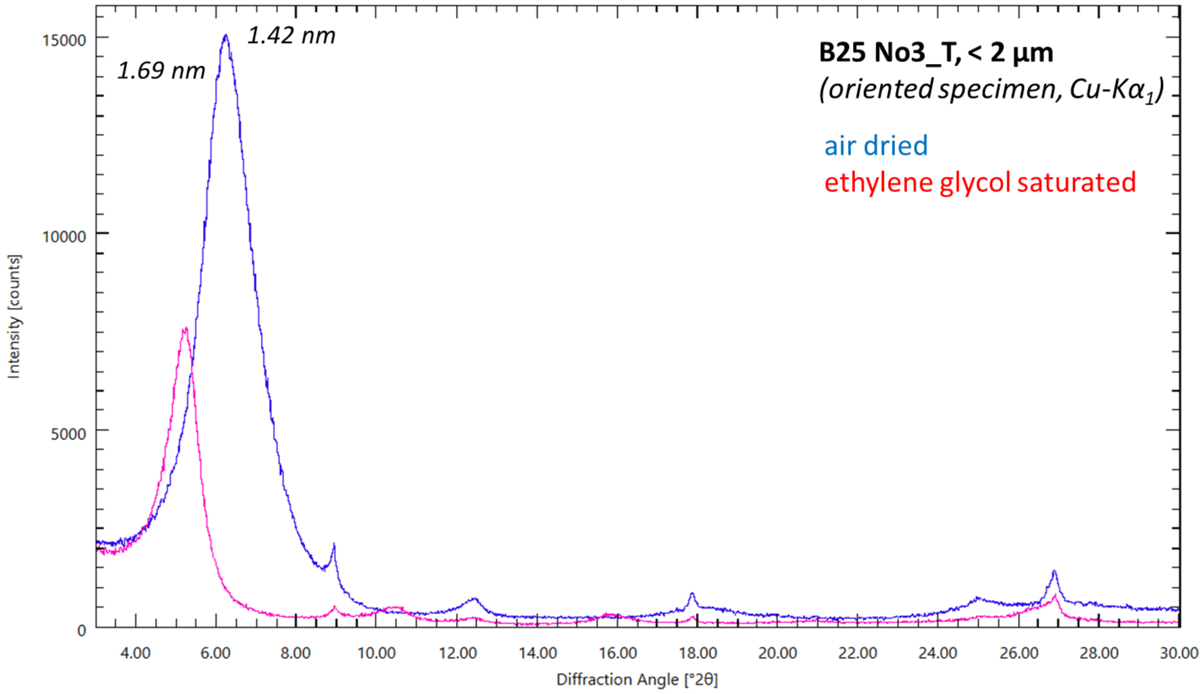

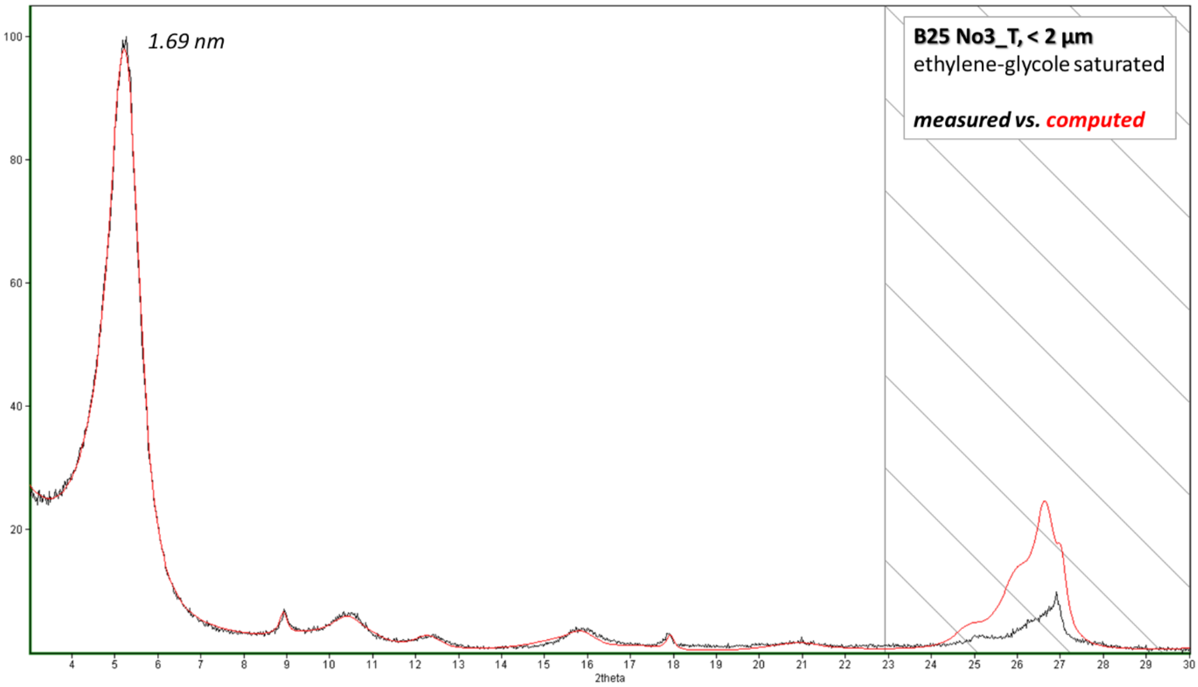

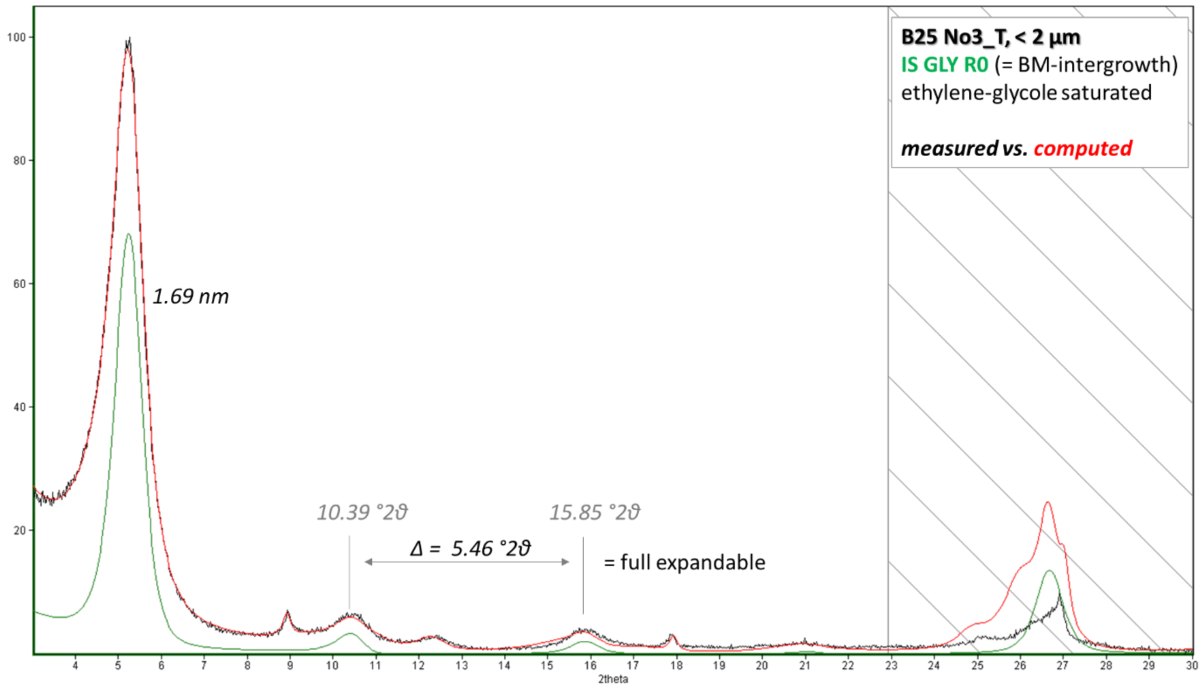
B25 No3_T, < 2 µm
IS GLY R0 (= BM-intergrowth)
ethylene-glycole saturated
measured* vs. *computed
1.69 nm
10.39 °2ϑ
15.85 °2ϑ
Δ = 5.46 °2ϑ
= full expandable
100
80
60
40
20
4
5
6
7
8
9
10
11
12
13
14
15
16
17
18
19
20
21
22
23
24
25
26
27
28
29
30
2theta

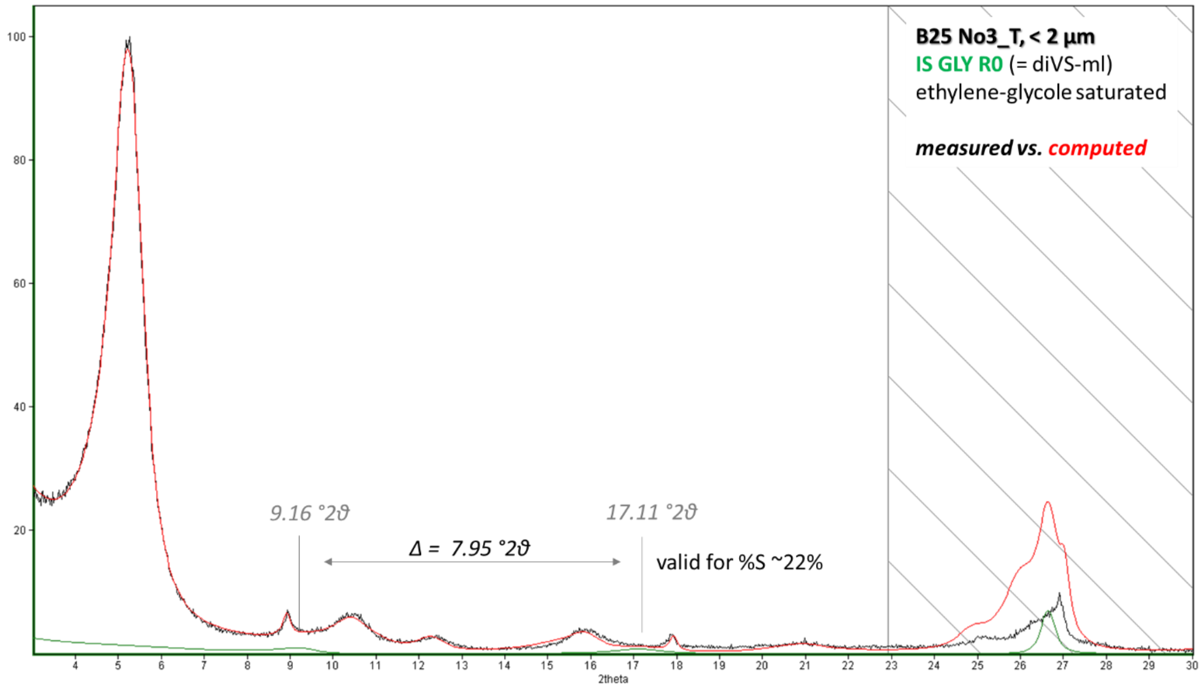
B25 No3_T, < 2 µm
IS GLY R0 (= diVS-ml)
ethylene-glycole saturated
measured* vs. *computed
9.16 °2ϑ
17.11 °2ϑ
Δ = 7.95 °2ϑ
valid for %S ~22%
100
80
60
40
20
4
5
6
7
8
9
10
11
12
13
14
15
16
17
18
19
20
21
22
23
24
25
26
27
28
29
30
2theta

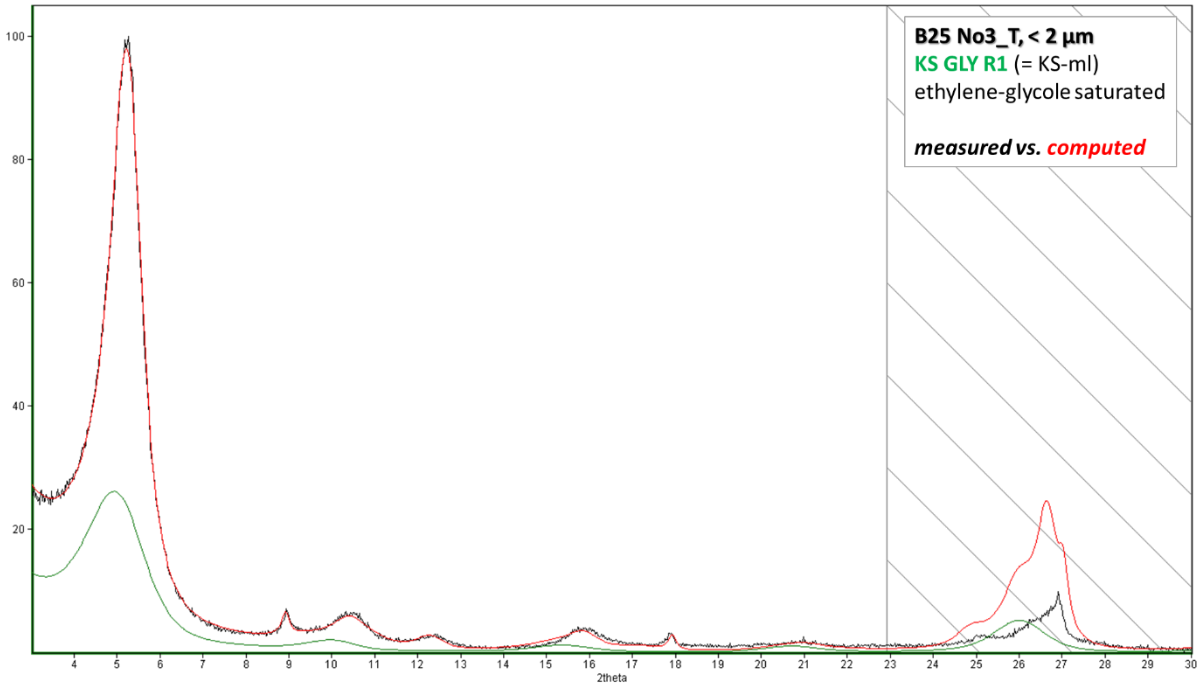
B25 No3_T, < 2 µm
KS GLY R1 (= KS-ml)
ethylene-glycole saturated
measured vs. *computed*
100
80
60
40
20
4
5
6
7
8
9
10
11
12
13
14
15
16
17
18
19
20
21
22
23
24
25
26
27
28
29
30
2theta

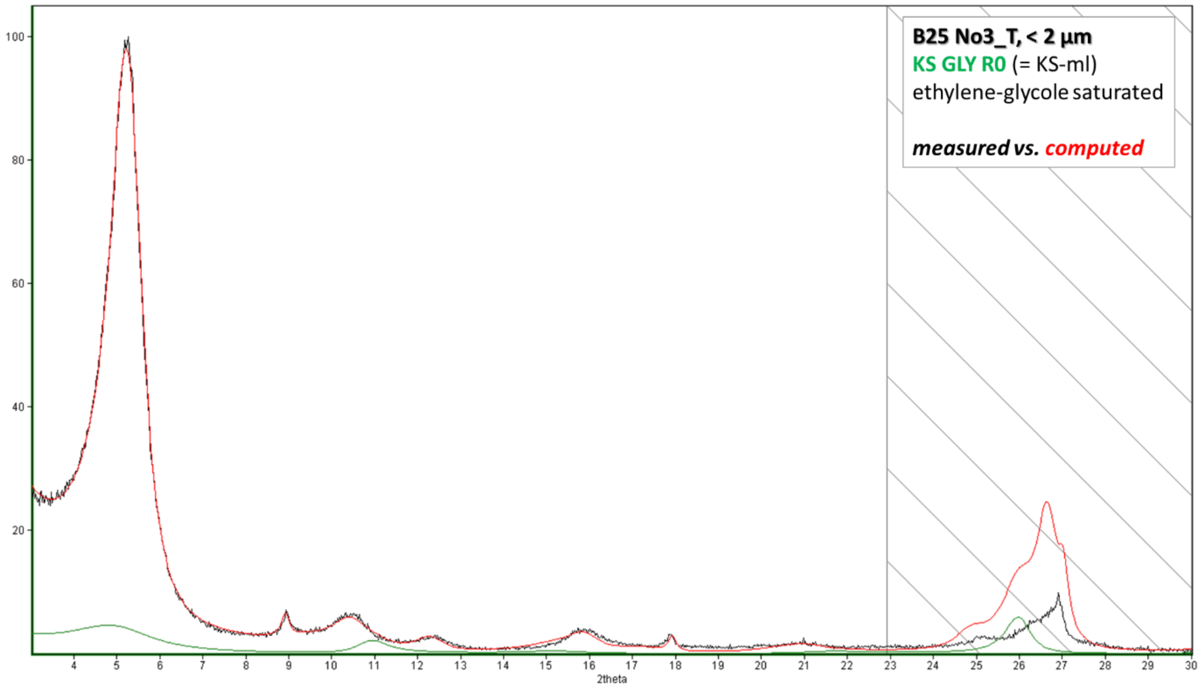
B25 No3_T, < 2 µm
KS GLY R0 (= KS-ml)
ethylene-glycole saturated
measured vs. *computed*
100
80
60
40
20
4
5
6
7
8
9
10
11
12
13
14
15
16
17
18
19
20
21
22
23
24
25
26
27
28
29
30
2theta

Data Sheet – B25 No3_C (< 2 µm), treated material *(OPA, 150°C, 4 days)*

Diffraction pattern of oriented specimen & modelling by Sybilla

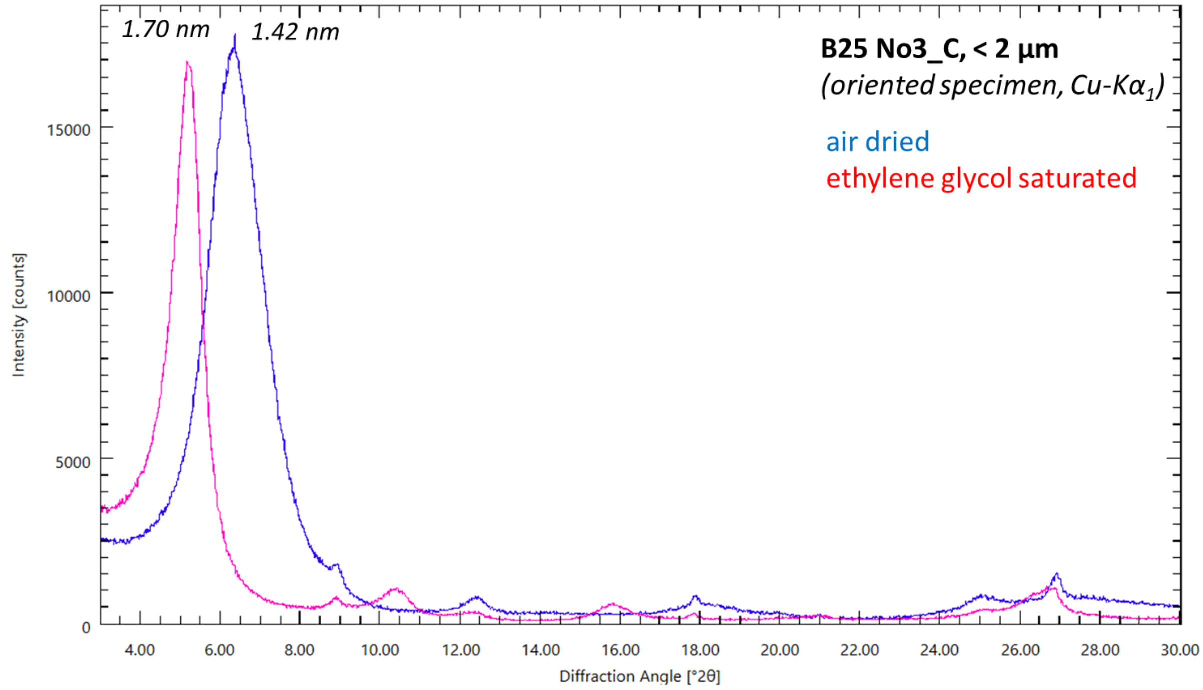

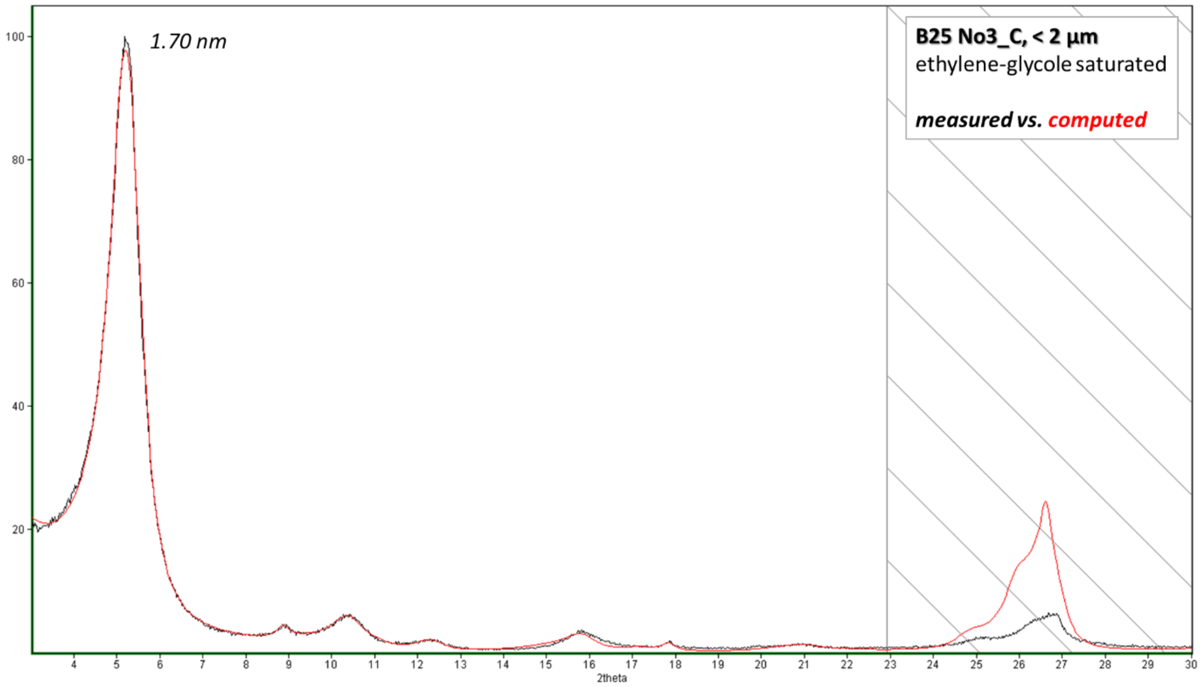

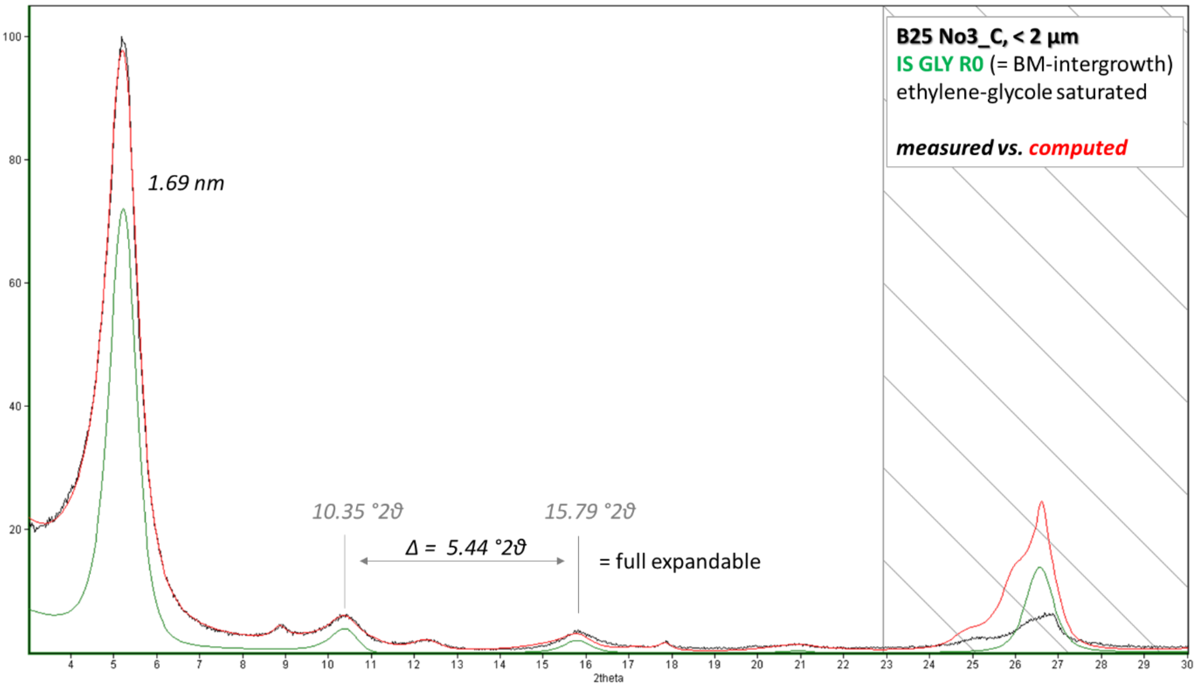
B25 No3_C, < 2 µm
IS GLY R0 (= BM-intergrowth)
ethylene-glycole saturated
measured vs. computed
1.69 nm
10.35 °2ϑ
15.79 °2ϑ
Δ = 5.44 °2ϑ
= full expandable
100
80
60
40
20
4
5
6
7
8
9
10
11
12
13
14
15
16
17
18
19
20
21
22
23
24
25
26
27
28
29
30
2theta

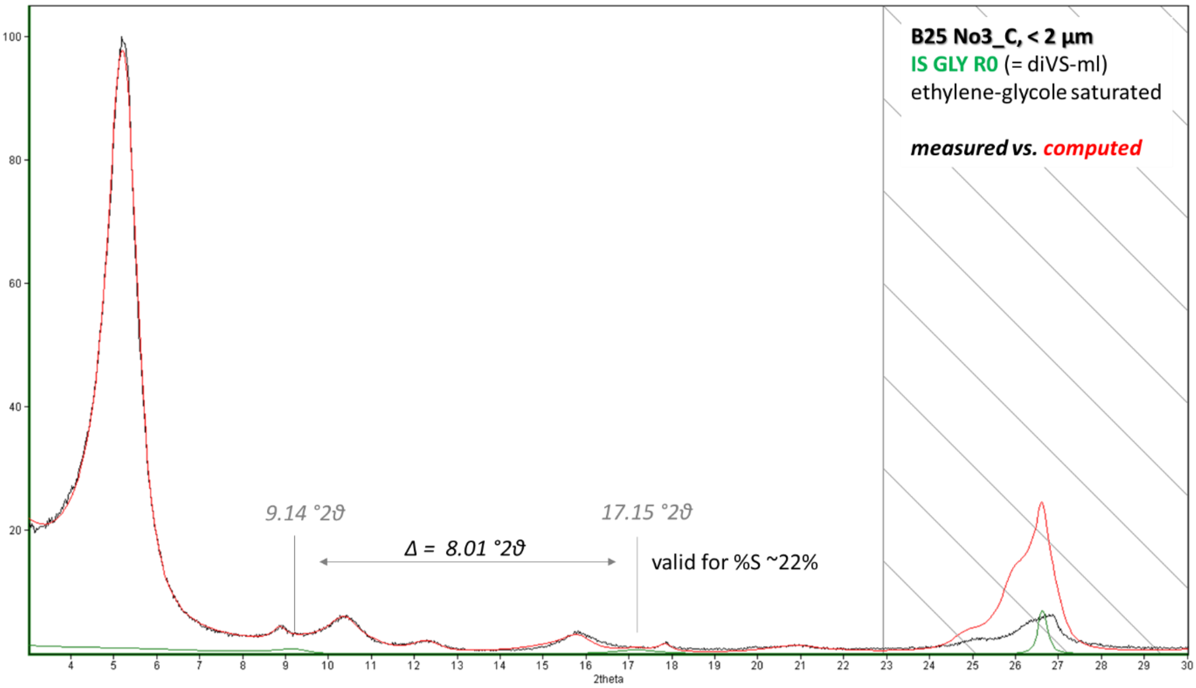
B25 No3_C, < 2 µm
IS GLY R0 (= diVS-ml)
ethylene-glycole saturated
measured vs. computed
9.14 °2ϑ
17.15 °2ϑ
Δ = 8.01 °2ϑ
valid for %S ~22%
100
80
60
40
20
4
5
6
7
8
9
10
11
12
13
14
15
16
17
18
19
20
21
22
23
24
25
26
27
28
29
30
2theta

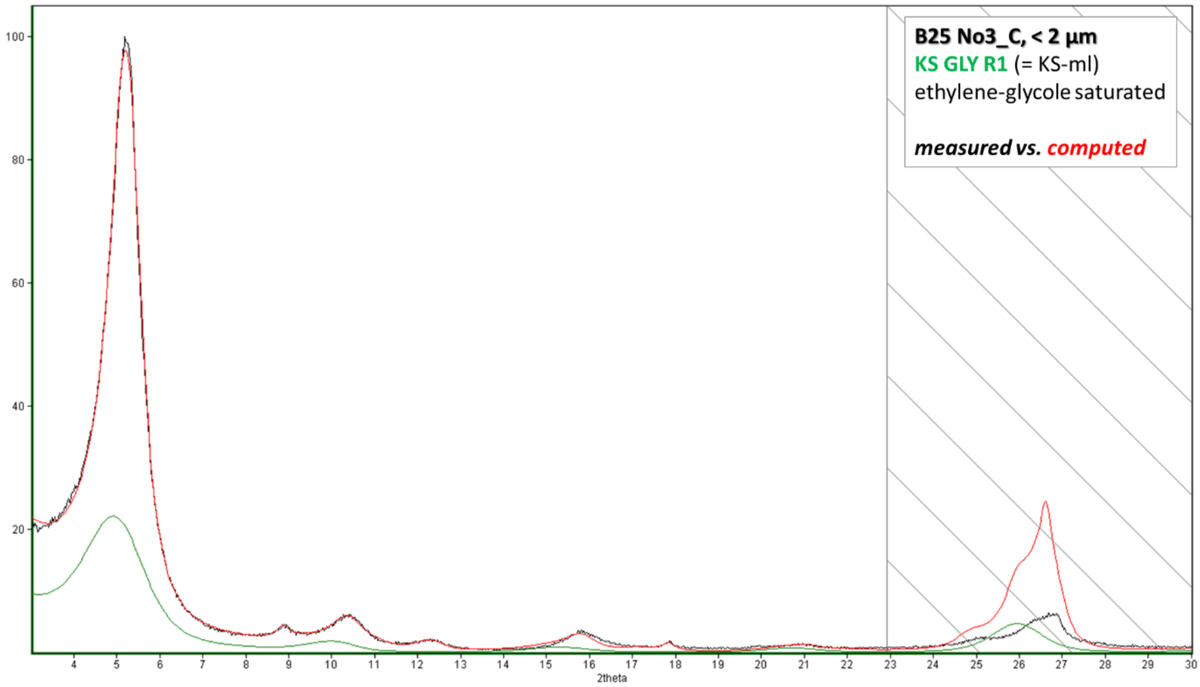
B25 No3_C, < 2 µm
KS GLY R1 (= KS-ml)
ethylene-glycole saturated
measured* vs. *computed
100
80
60
40
20
4
5
6
7
8
9
10
11
12
13
14
15
16
17
18
19
20
21
22
23
24
25
26
27
28
29
30
2theta

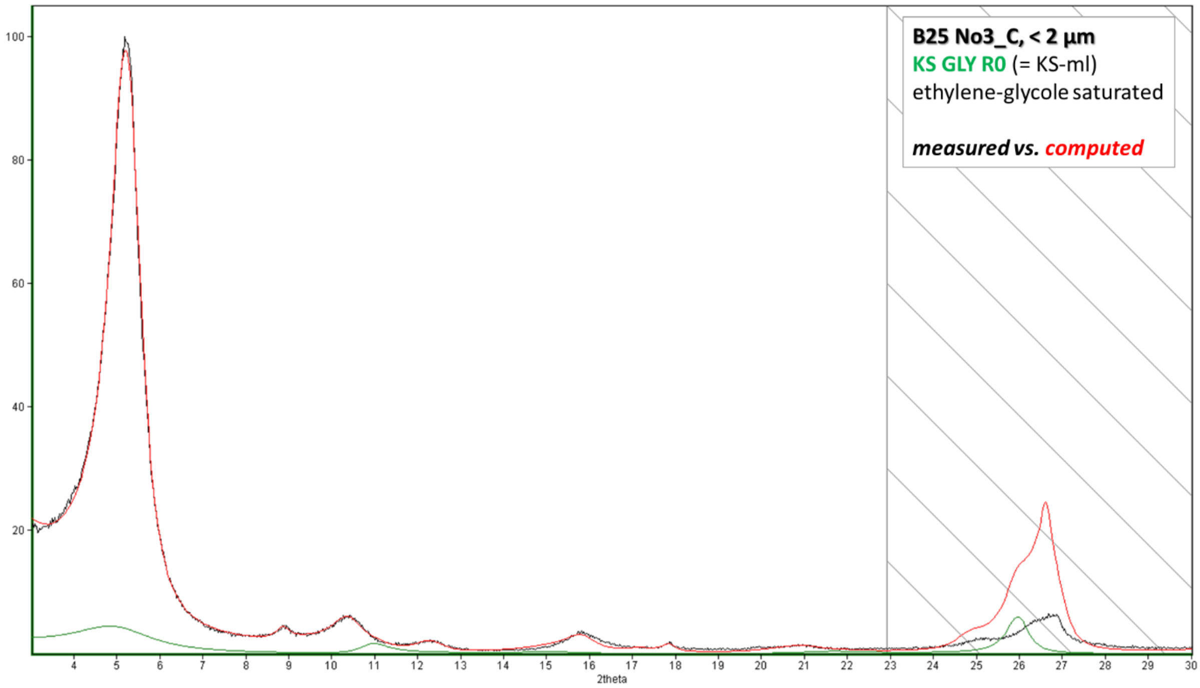
B25 No3_C, < 2 µm
KS GLY R0 (= KS-ml)
ethylene-glycole saturated
measured* vs. *computed
100
80
60
40
20
4
5
6
7
8
9
10
11
12
13
14
15
16
17
18
19
20
21
22
23
24
25
26
27
28
29
30
2theta

Data Sheet – B25 No3_B (< 2 µm), treated material *(OPA, 150°C, 4 days)*

Diffraction pattern of oriented specimen & modelling by Sybilla

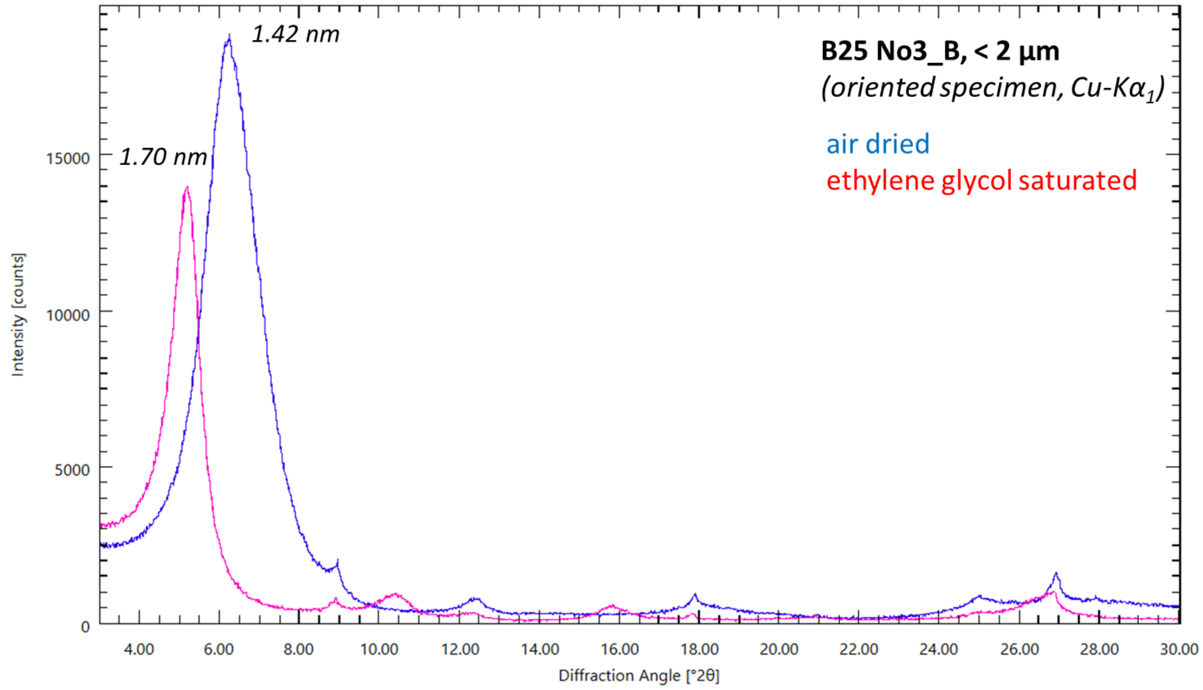

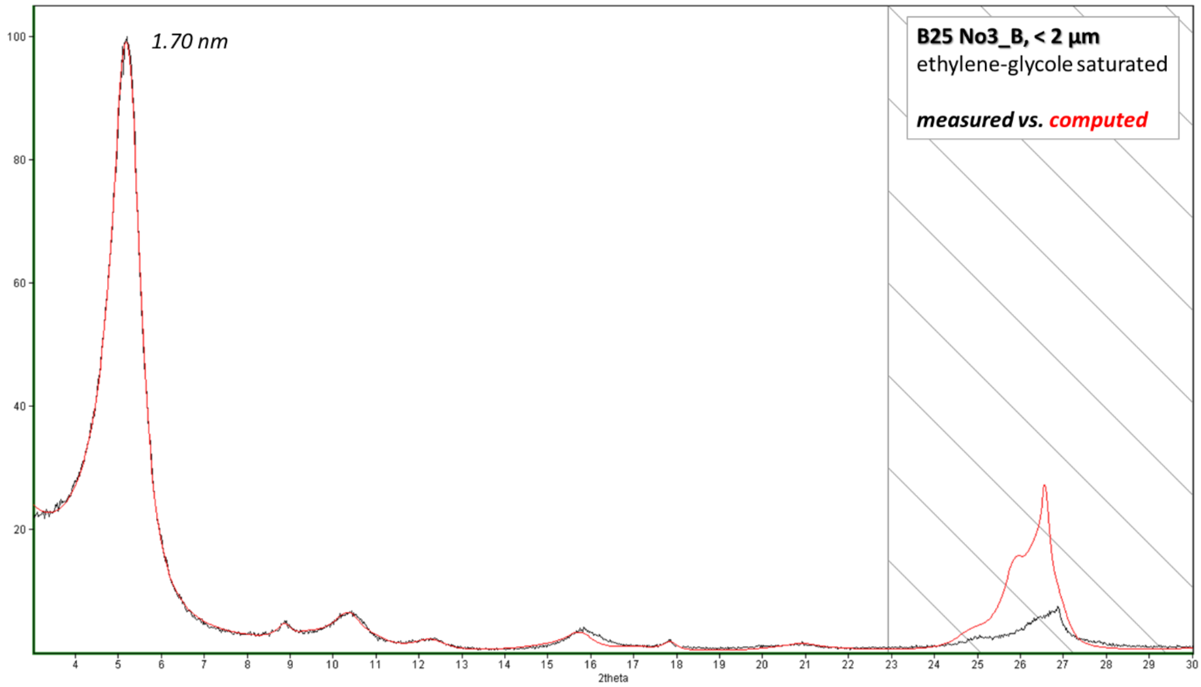

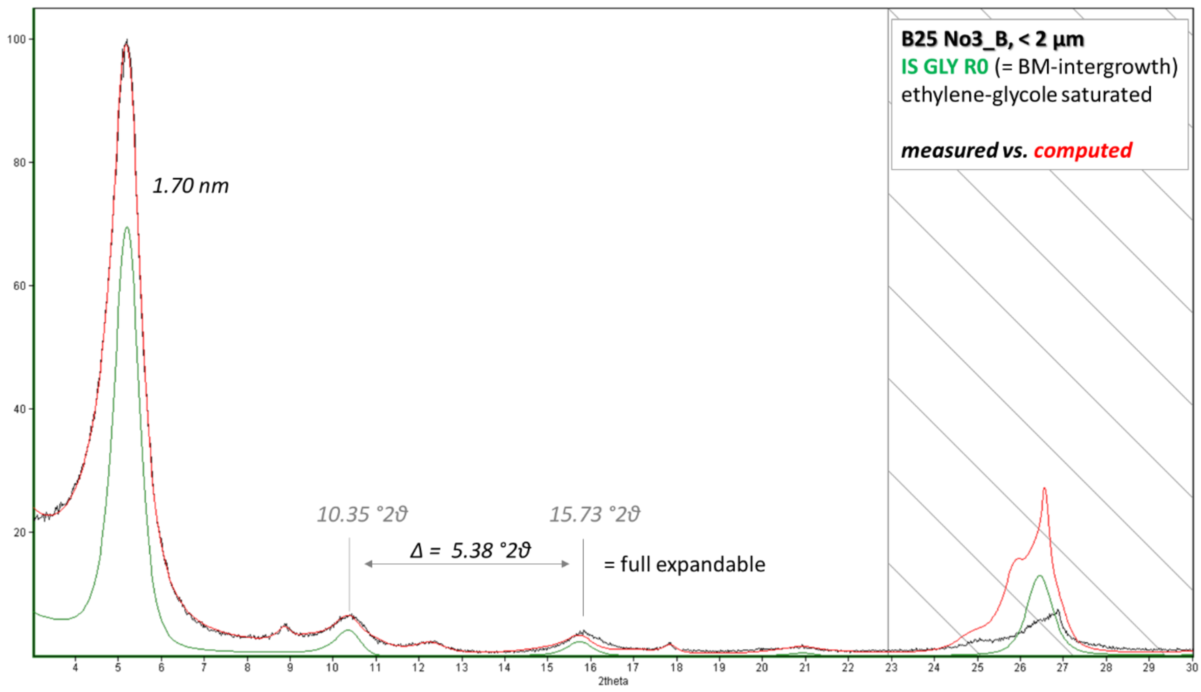
B25 No3_B, < 2 µm
IS GLY R0 (= BM-intergrowth)
ethylene-glycole saturated
measured* *vs.* *computed
1.70 nm
10.35 °2ϑ
15.73 °2ϑ
Δ = 5.38 °2ϑ
= full expandable
100
80
60
40
20
4
5
6
7
8
9
10
11
12
13
14
15
16
17
18
19
20
21
22
23
24
25
26
27
28
29
30
2theta

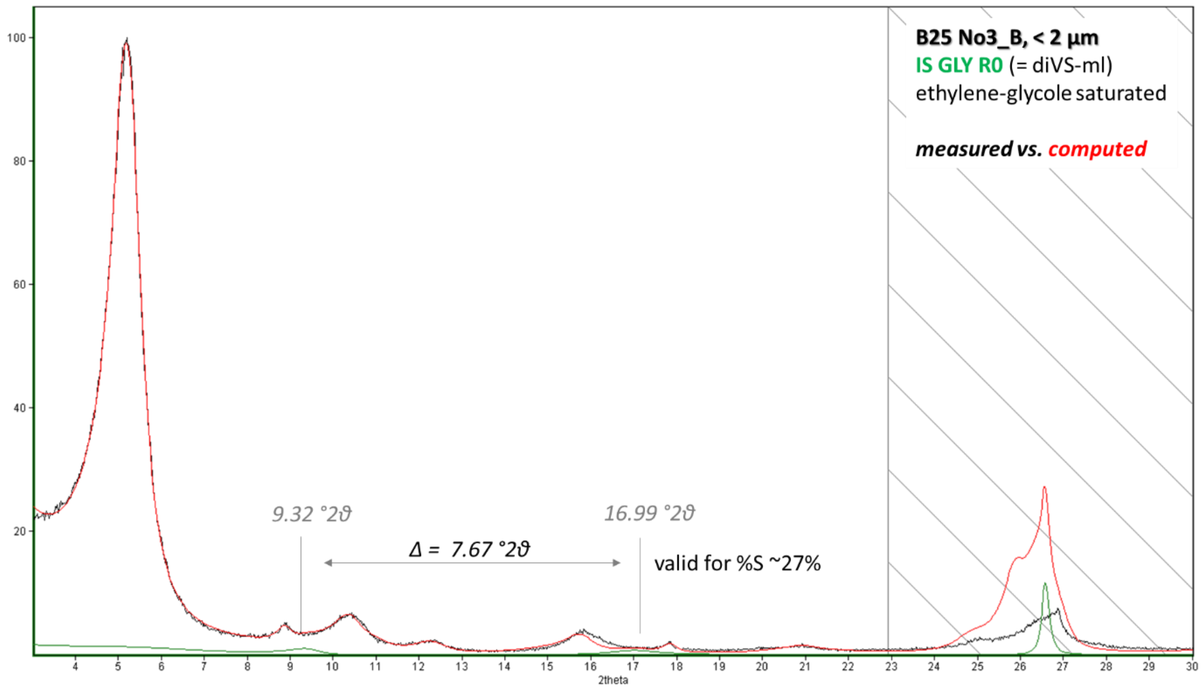
B25 No3_B, < 2 µm
IS GLY R0 (= diVS-ml)
ethylene-glycole saturated
measured* *vs.* *computed
9.32 °2ϑ
16.99 °2ϑ
Δ = 7.67 °2ϑ
valid for %S ~27%
100
80
60
40
20
4
5
6
7
8
9
10
11
12
13
14
15
16
17
18
19
20
21
22
23
24
25
26
27
28
29
30
2theta

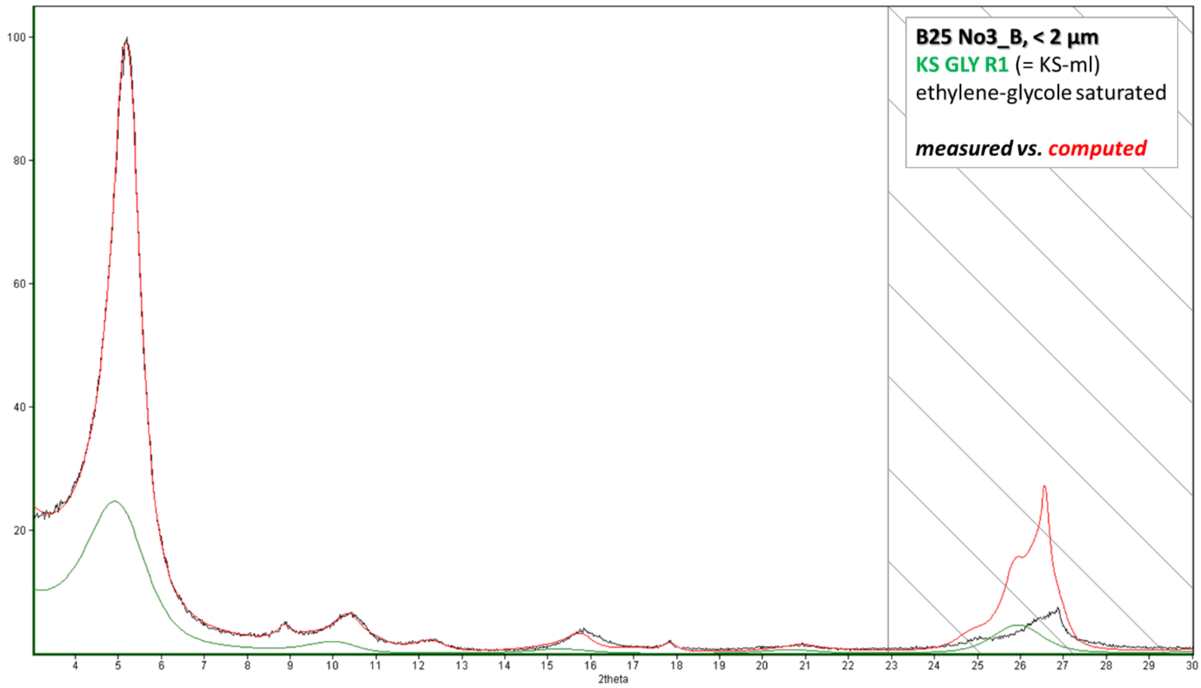
B25 No3_B, < 2 µm
KS GLY R1 (= KS-ml)
ethylene-glycole saturated
measured vs. computed
100
80
60
40
20
4
5
6
7
8
9
10
11
12
13
14
15
16
17
18
19
20
21
22
23
24
25
26
27
28
29
30
2theta

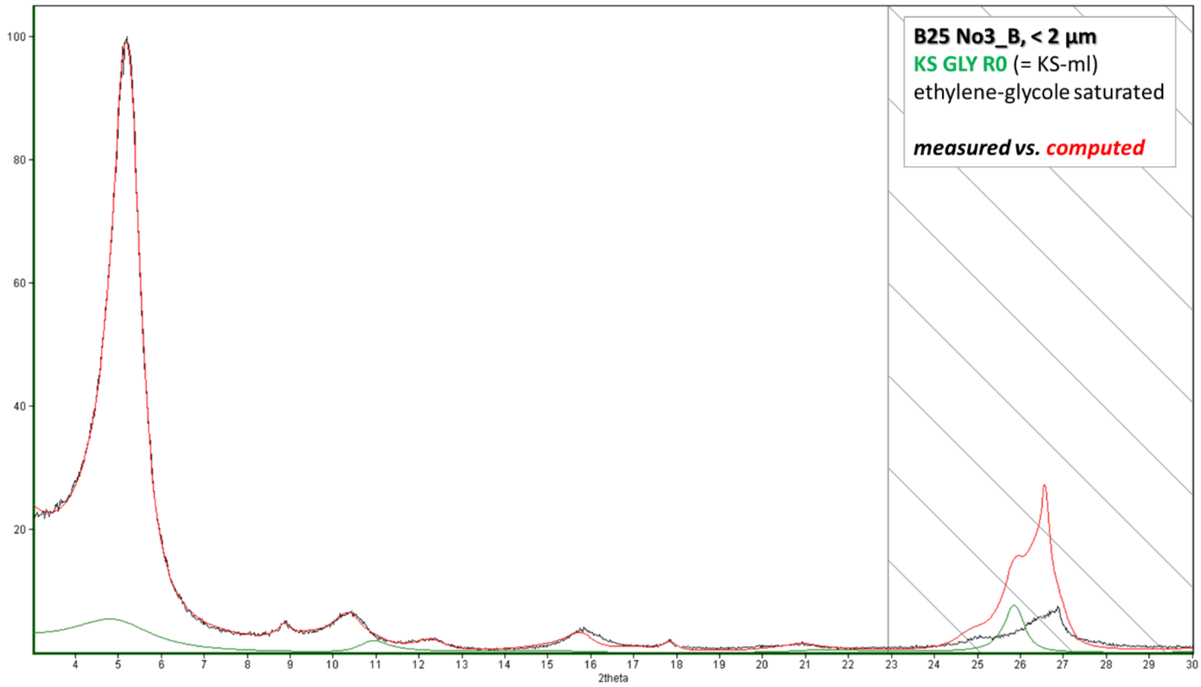
B25 No3_B, < 2 µm
KS GLY R0 (= KS-ml)
ethylene-glycole saturated
measured vs. computed
100
80
60
40
20
4
5
6
7
8
9
10
11
12
13
14
15
16
17
18
19
20
21
22
23
24
25
26
27
28
29
30
2theta

Data Sheet – OPALINUS (< 2 µm), all experiments

Diffraction pattern of oriented specimen & modelling by Sybilla

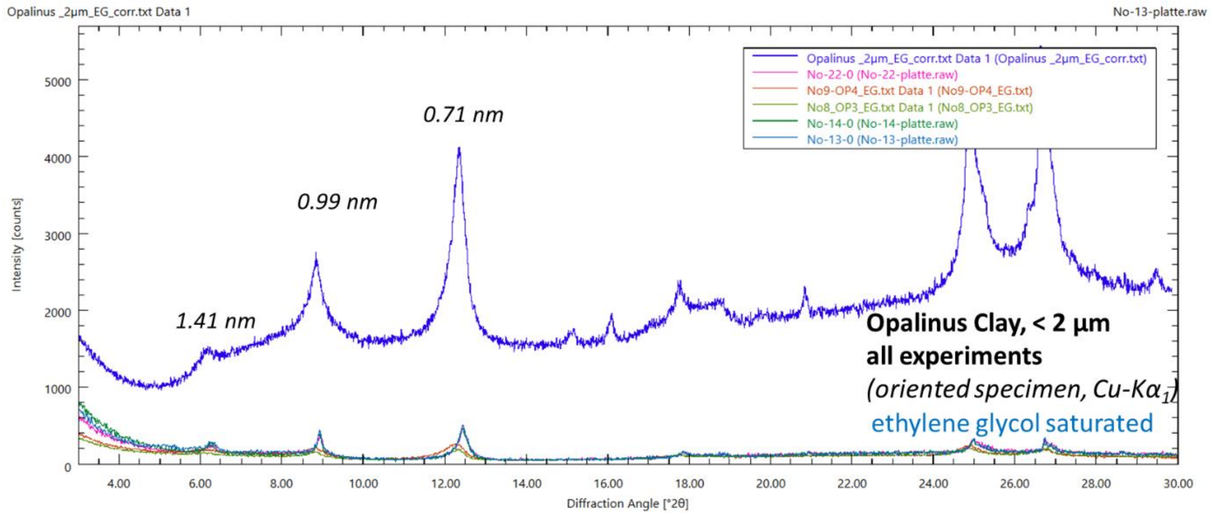

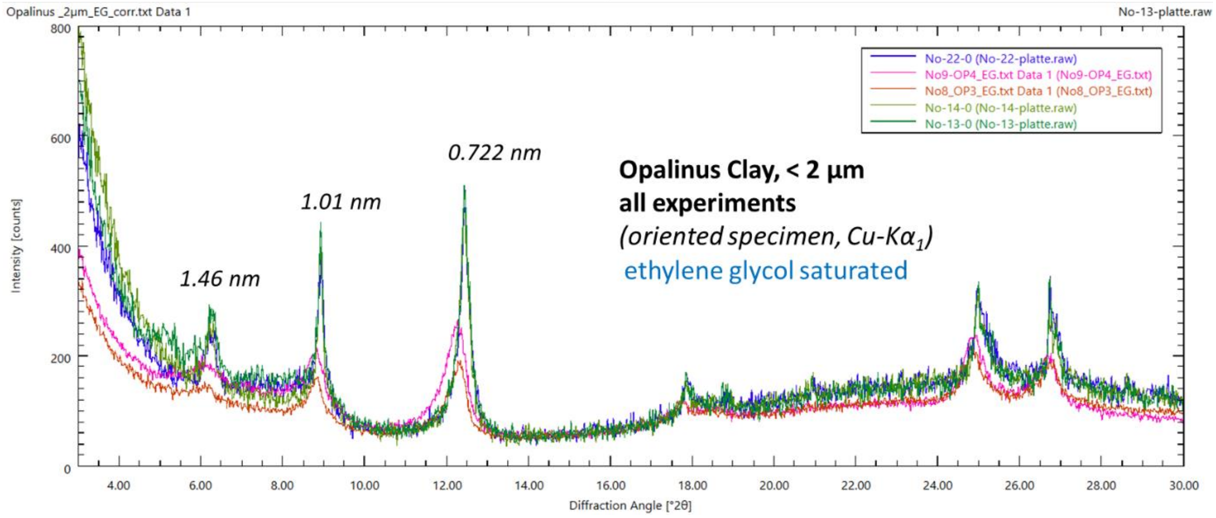

Data Sheet – OPALINUS (< 2 µm), untreated material

Diffraction pattern of oriented specimen & modelling by Sybilla

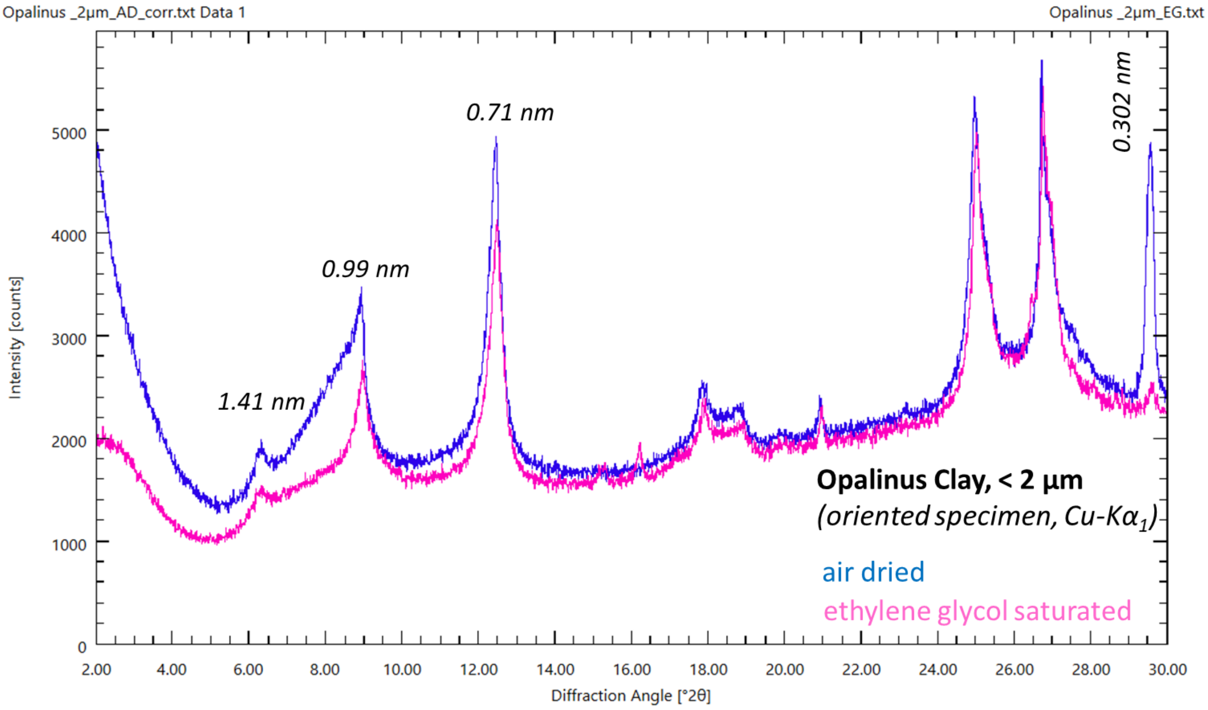

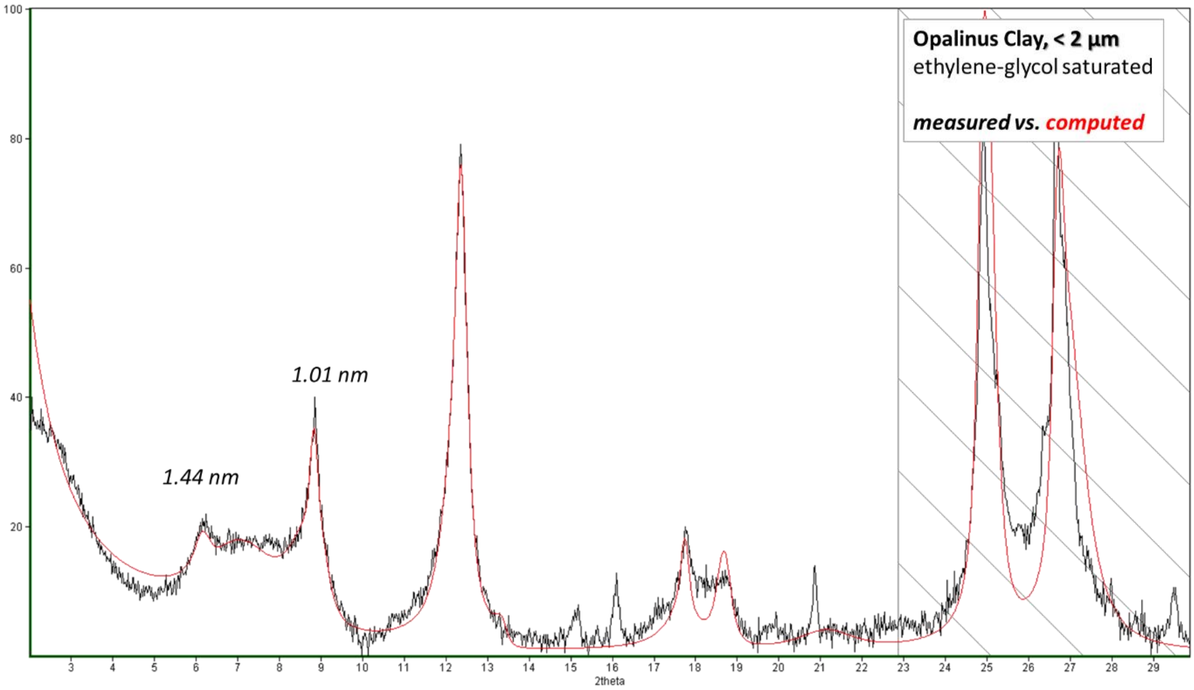

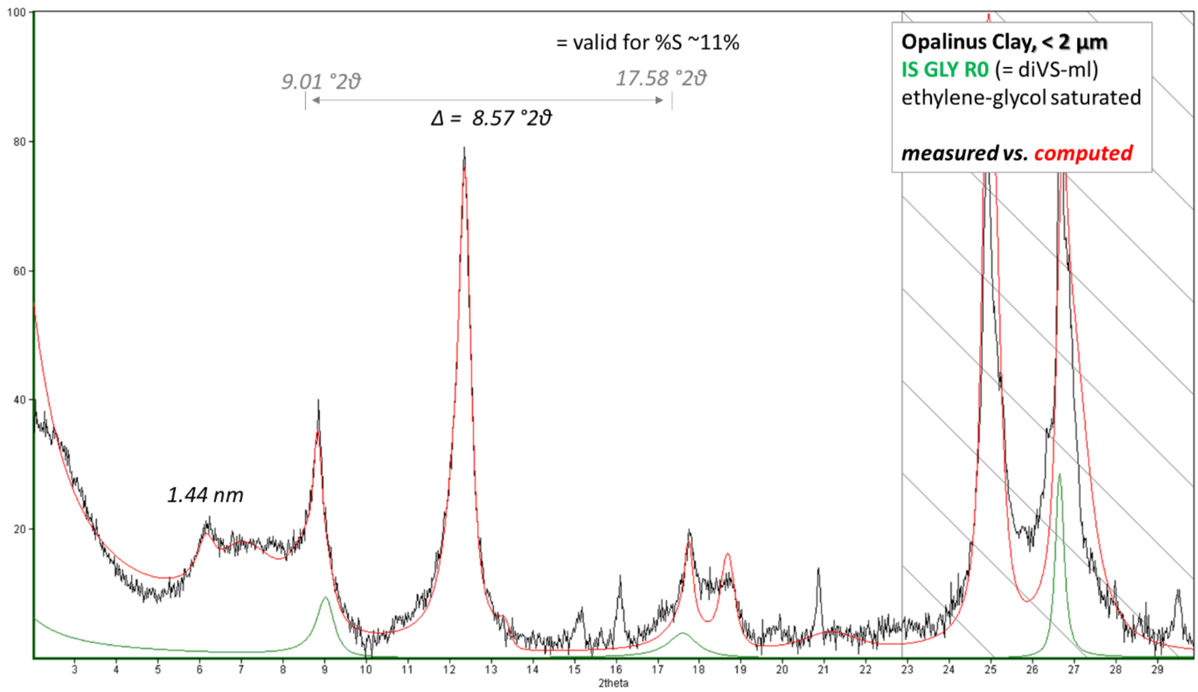
= valid for %S ~11%
9.01 °2ϑ
17.58 °2ϑ
Δ = 8.57 °2ϑ
1.44 nm
Opalinus Clay, < 2 µm
IS GLY R0 (= diVS-ml)
ethylene-glycol saturated
measured vs. computed
100
80
60
40
20
3
4
5
6
7
8
9
10
11
12
13
14
15
16
17
18
19
20
21
22
23
24
25
26
27
28
29
2theta

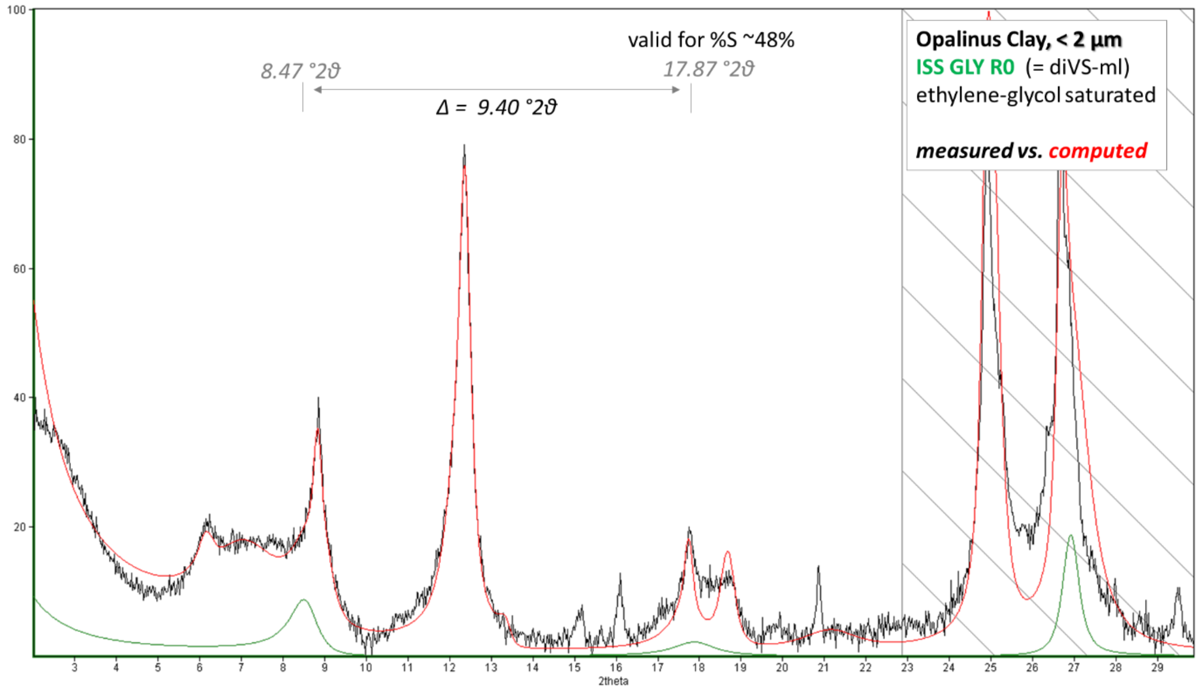
valid for %S ~48%
8.47 °2ϑ
17.87 °2ϑ
Δ = 9.40 °2ϑ
Opalinus Clay, < 2 µm
ISS GLY R0 (= diVS-ml)
ethylene-glycol saturated
measured vs. computed
100
80
60
40
20
3
4
5
6
7
8
9
10
11
12
13
14
15
16
17
18
19
20
21
22
23
24
25
26
27
28
29
2theta

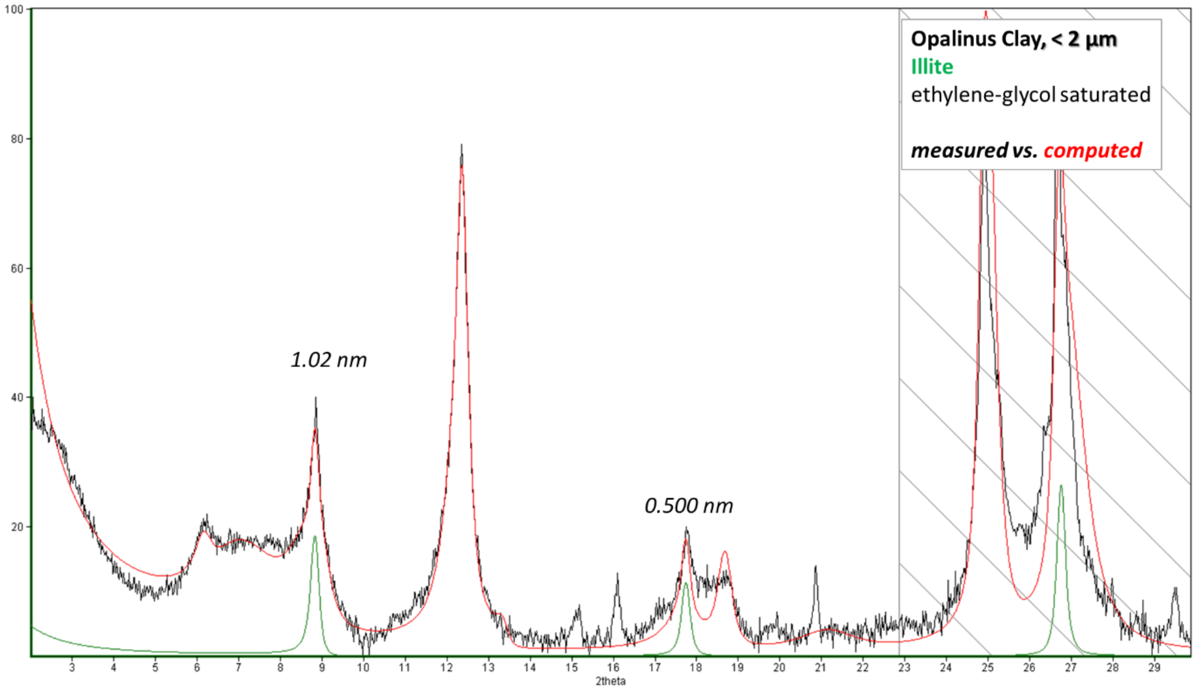
Opalinus Clay, < 2 µm
Illite
ethylene-glycol saturated
measured vs. computed
1.02 nm
0.500 nm
100
80
60
40
20
3
4
5
6
7
8
9
10
11
12
13
14
15
16
17
18
19
20
21
22
23
24
25
26
27
28
29
2theta

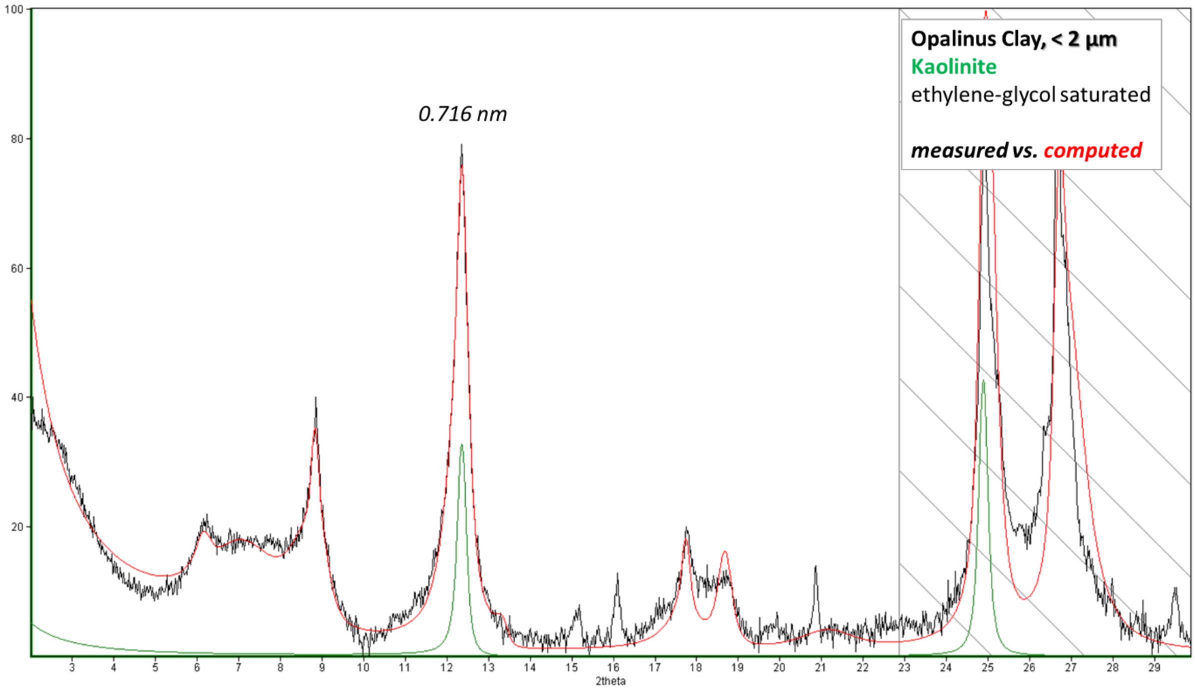
Opalinus Clay, < 2 µm
Kaolinite
ethylene-glycol saturated
measured vs. computed
0.716 nm
100
80
60
40
20
3
4
5
6
7
8
9
10
11
12
13
14
15
16
17
18
19
20
21
22
23
24
25
26
27
28
29
2theta

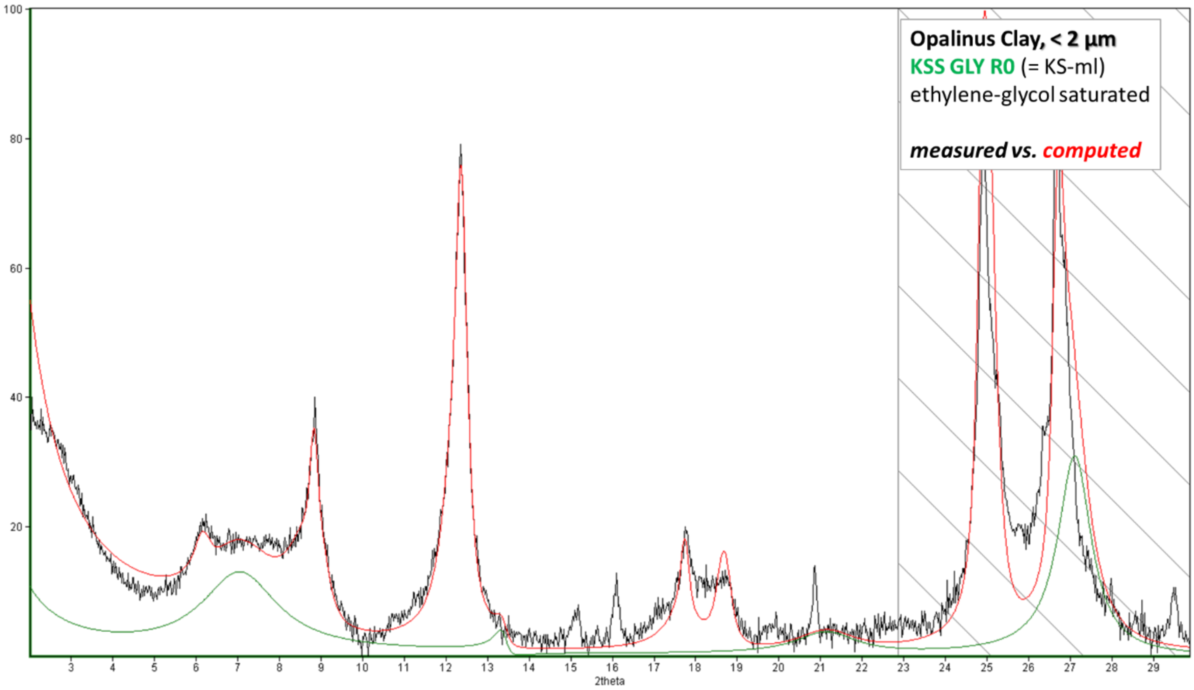
Opalinus Clay, < 2 µm
KSS GLY R0 (= KS-ml)
ethylene-glycol saturated
measured vs. computed
100
80
60
40
20
3
4
5
6
7
8
9
10
11
12
13
14
15
16
17
18
19
20
21
22
23
24
25
26
27
28
29
2theta

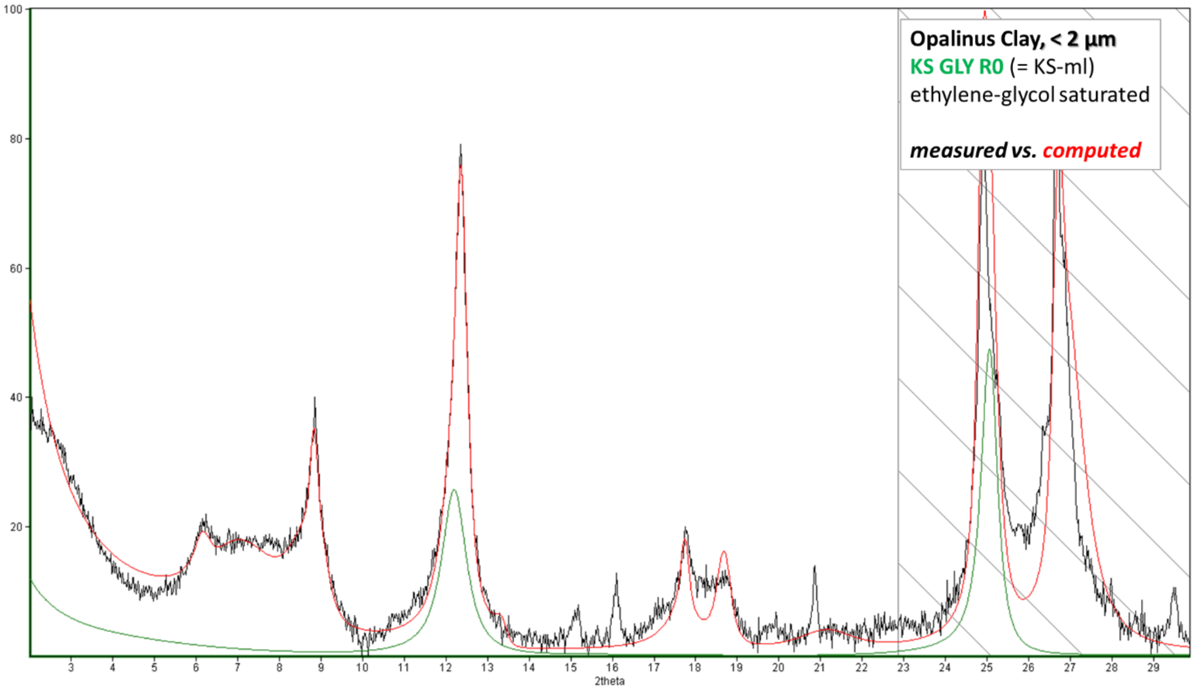
Opalinus Clay, < 2 µm
KS GLY R0 (= KS-ml)
ethylene-glycol saturated
measured vs. computed
100
80
60
40
20
3
4
5
6
7
8
9
10
11
12
13
14
15
16
17
18
19
20
21
22
23
24
25
26
27
28
29
2theta

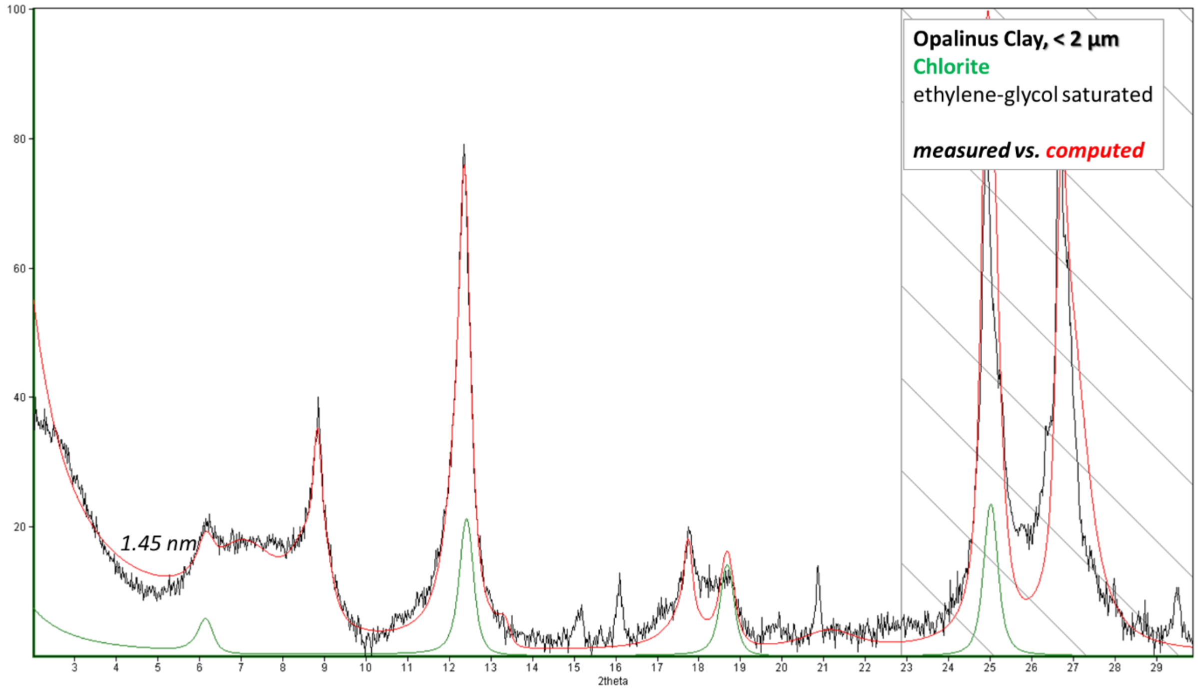
Opalinus Clay, < 2 µm
Chlorite
ethylene-glycol saturated
measured vs. computed
1.45 nm
100
80
60
40
20
3
4
5
6
7
8
9
10
11
12
13
14
15
16
17
18
19
20
21
22
23
24
25
26
27
28
29
2theta

Data Sheet – OPALINUS No22 (< 2 µm), treated material *(35°C, 144 hours)*

Diffraction pattern of oriented specimen & modelling by Sybilla

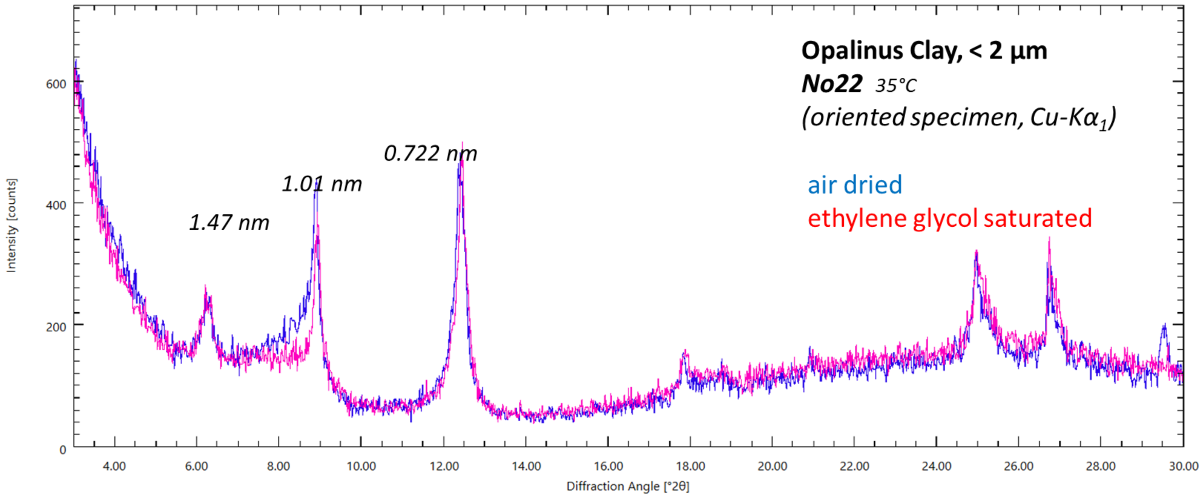

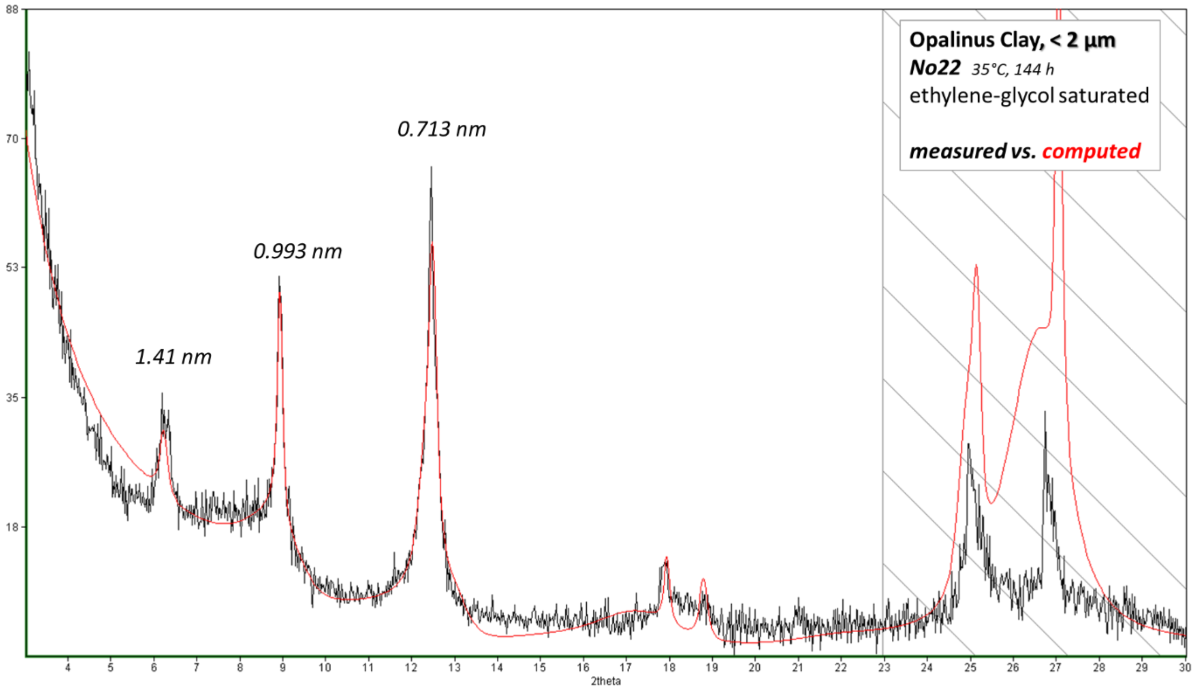

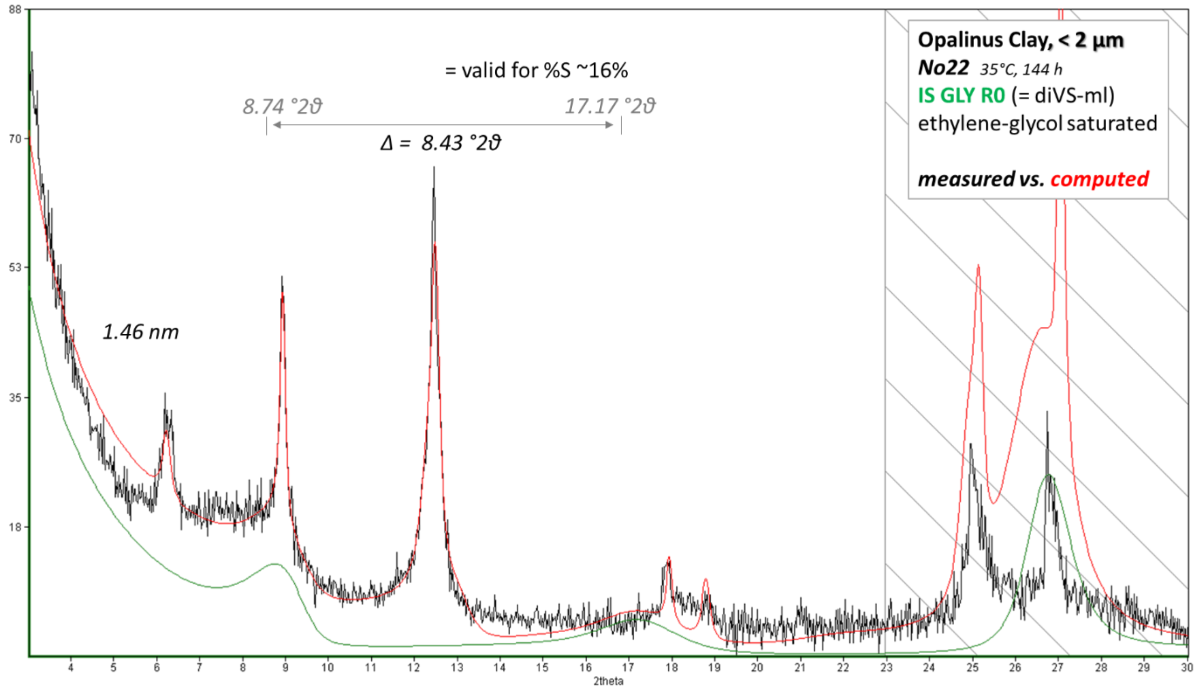
Opalinus Clay, < 2 µm
No22 35°C, 144 h
IS GLY R0 (= diVS-ml)
ethylene-glycol saturated
measured vs. computed
= valid for %S ~16%
8.74 °2ϑ
17.17 °2ϑ
Δ = 8.43 °2ϑ
1.46 nm
88
70
53
35
18
4
5
6
7
8
9
10
11
12
13
14
15
16
17
18
19
20
21
22
23
24
25
26
27
28
29
30
2theta

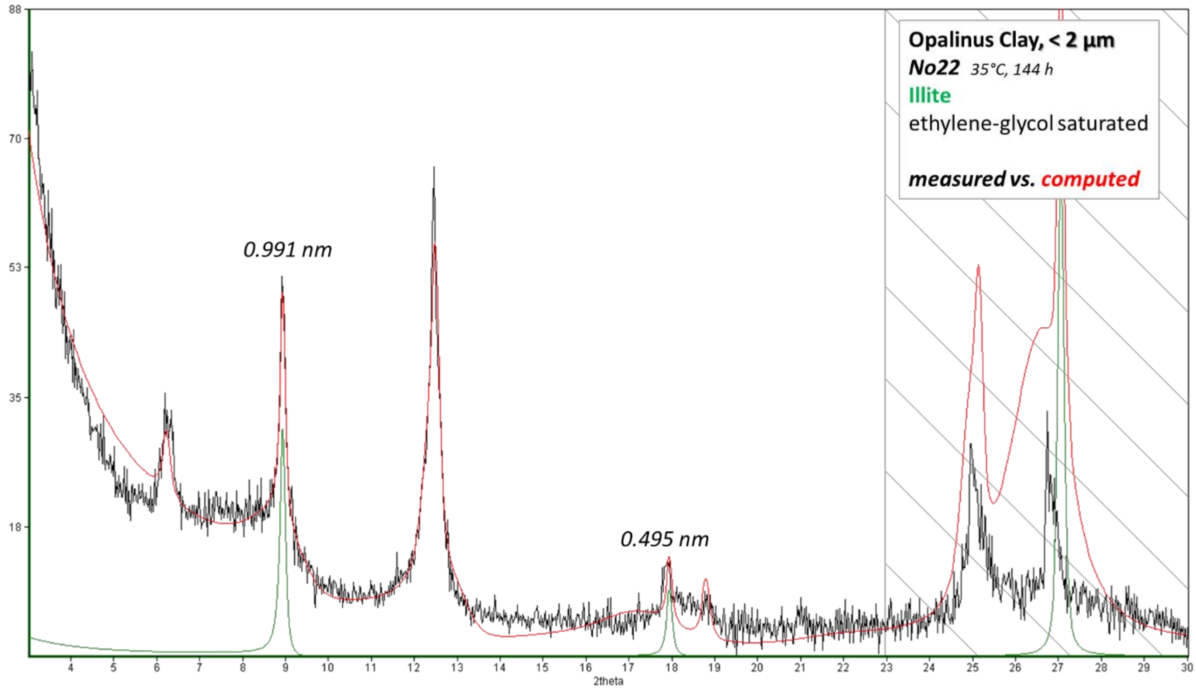
Opalinus Clay, < 2 µm
No22 35°C, 144 h
Illite
ethylene-glycol saturated
measured vs. computed
0.991 nm
0.495 nm
88
70
53
35
18
4
5
6
7
8
9
10
11
12
13
14
15
16
17
18
19
20
21
22
23
24
25
26
27
28
29
30
2theta

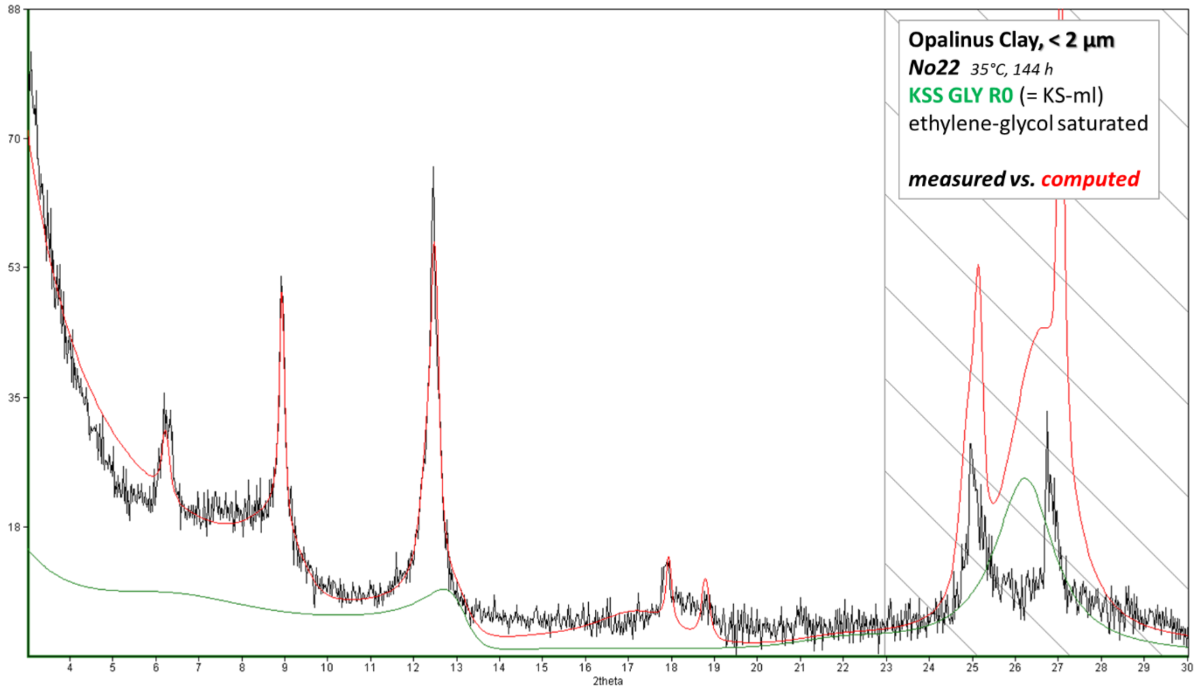
Opalinus Clay, < 2 µm
No22 *35°C, 144 h*
KSS GLY R0 (= KS-ml)
ethylene-glycol saturated
measured* vs. *computed
88
70
53
35
18
4
5
6
7
8
9
10
11
12
13
14
15
16
17
18
19
20
21
22
23
24
25
26
27
28
29
30
2theta

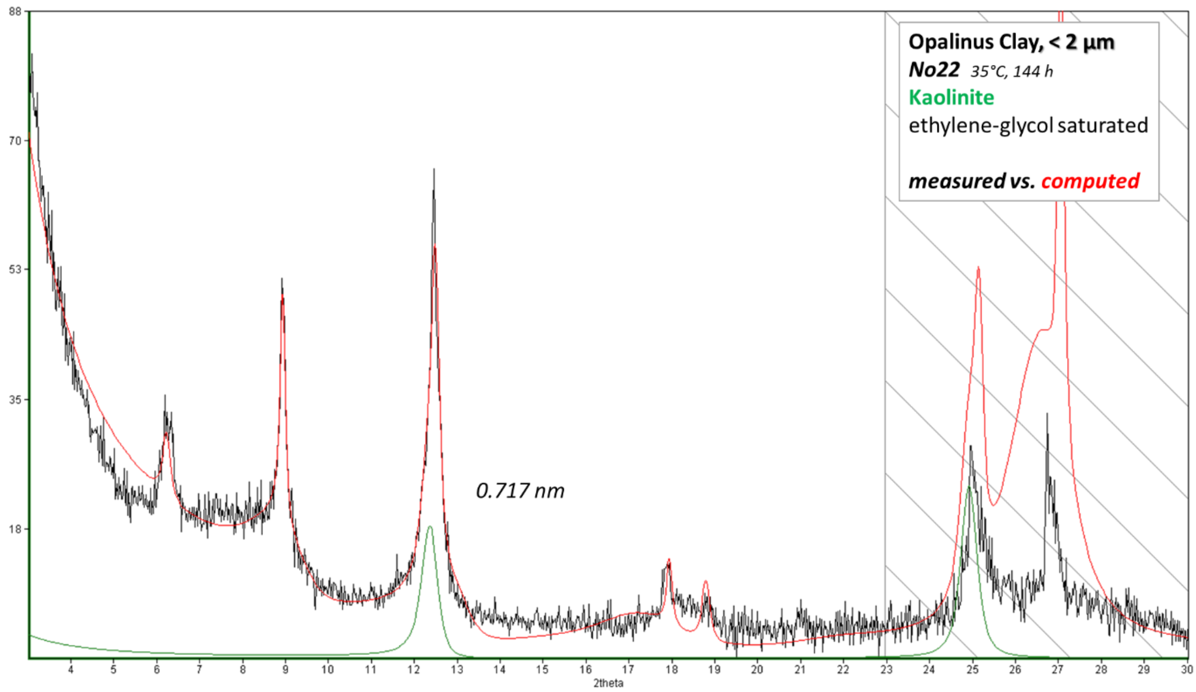
Opalinus Clay, < 2 µm
No22 *35°C, 144 h*
Kaolinite
ethylene-glycol saturated
measured* vs. *computed
0.717 nm
88
70
53
35
18
4 5 6 7 8 9 10 11 12 13 14 15 16 17 18 19 20 21 22 23 24 25 26 27 28 29 30
2theta

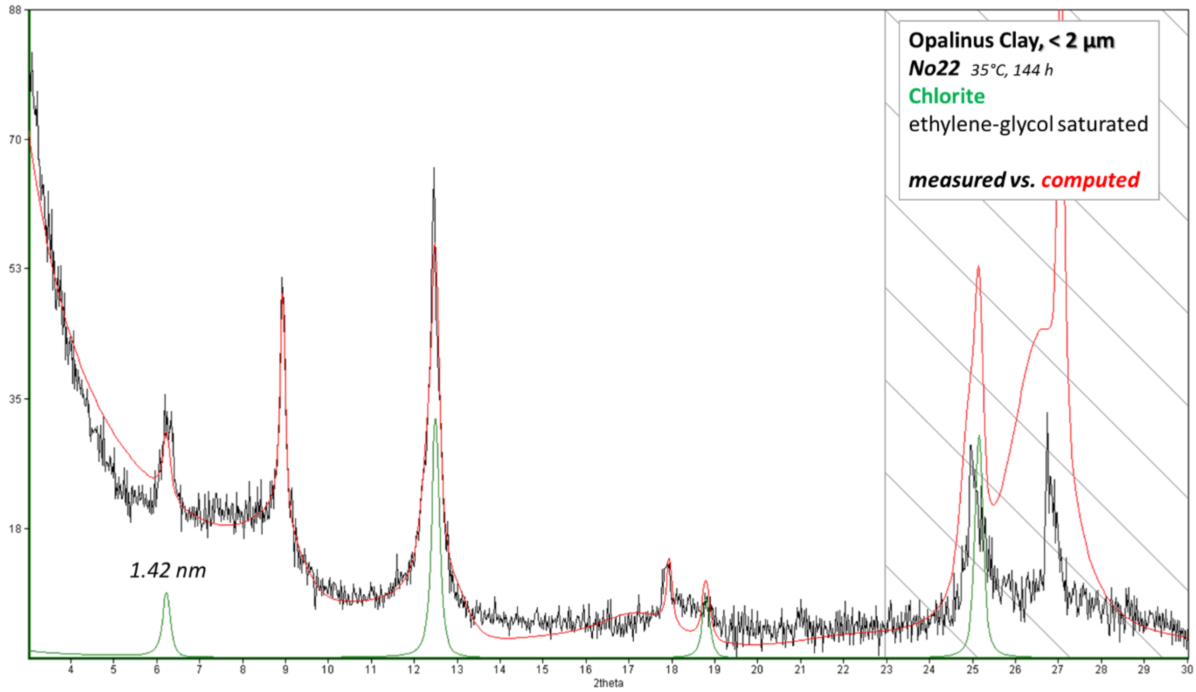
Opalinus Clay, < 2 µm
No22 *35°C, 144 h*
Chlorite
ethylene-glycol saturated
measured* vs. *computed
1.42 nm
88
70
53
35
18
4 5 6 7 8 9 10 11 12 13 14 15 16 17 18 19 20 21 22 23 24 25 26 27 28 29 30
2theta

Data Sheet – OPALINUS No9a (< 2 µm), treated material *(35°C)*

Diffraction pattern of oriented specimen & modelling by Sybilla

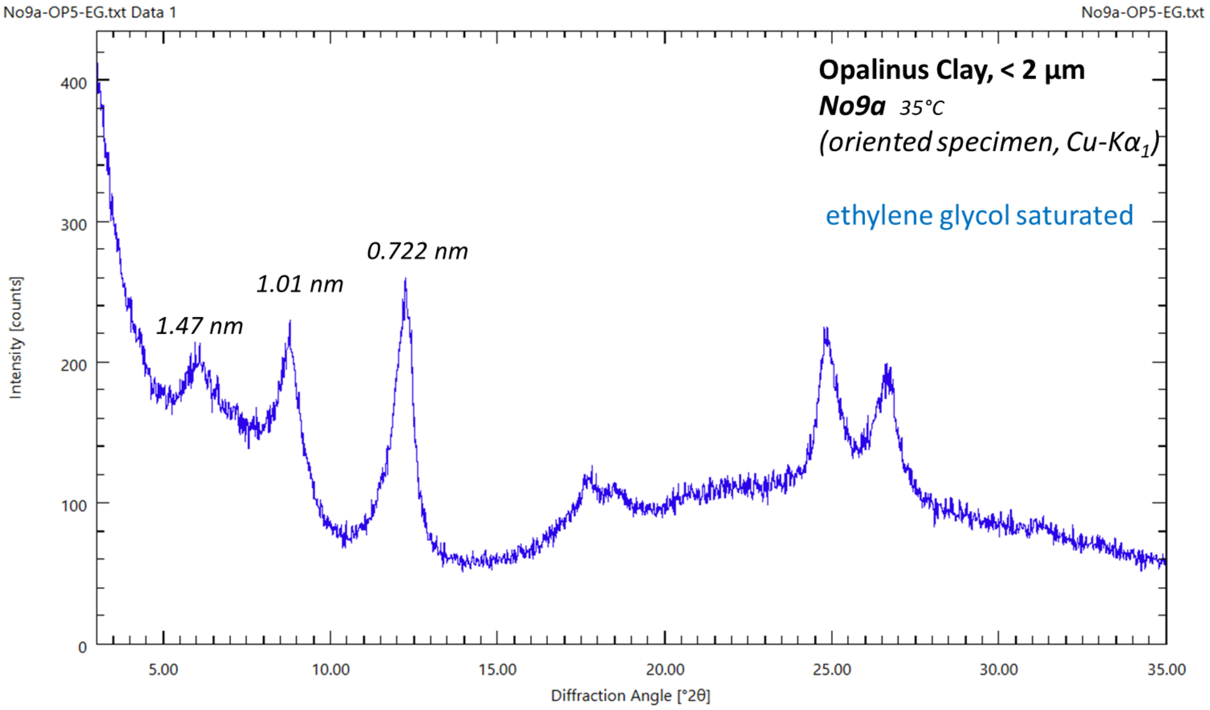

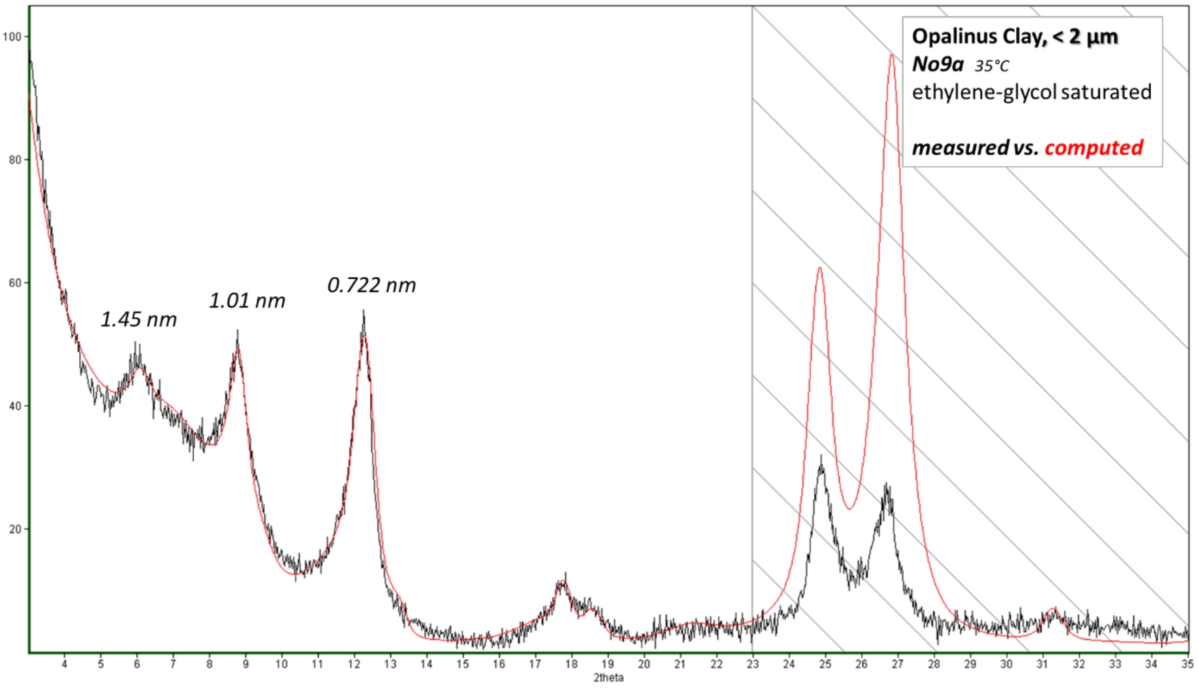

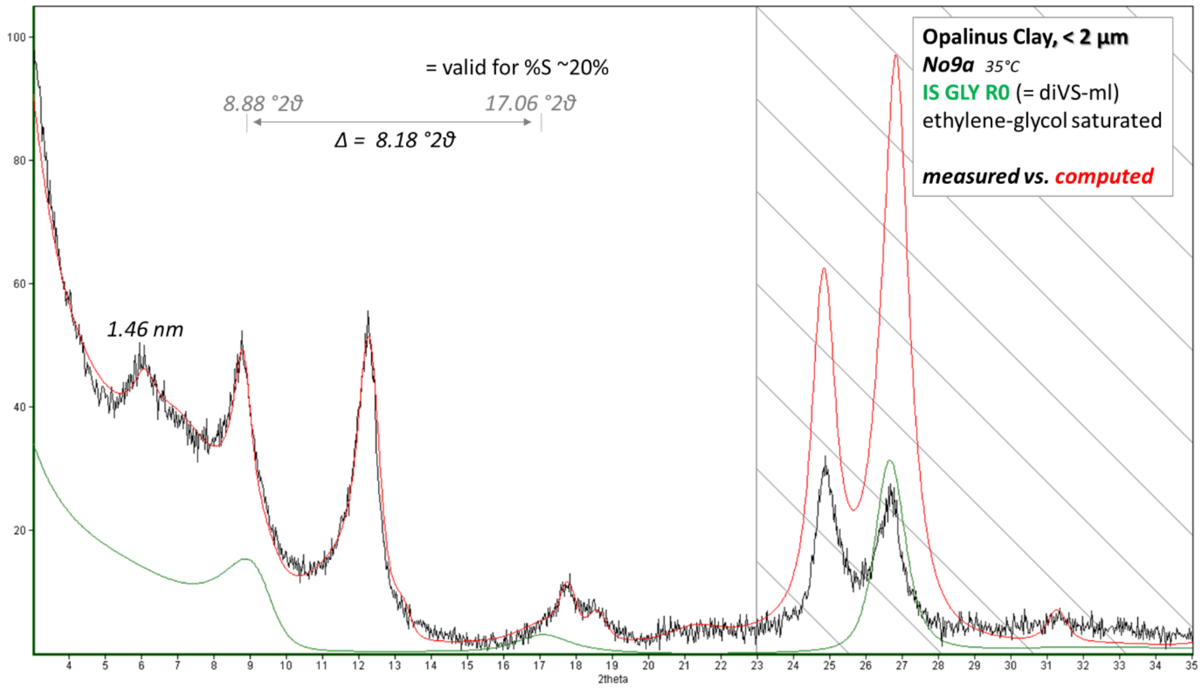
Opalinus Clay, < 2 µm
No9a 35°C
IS GLY R0 (= diVS-ml)
ethylene-glycol saturated
measured vs. computed
= valid for %S ~20%
8.88 °2ϑ
17.06 °2ϑ
Δ = 8.18 °2ϑ
1.46 nm
100
80
60
40
20
4 5 6 7 8 9 10 11 12 13 14 15 16 17 18 19 20 21 22 23 24 25 26 27 28 29 30 31 32 33 34 35
2theta

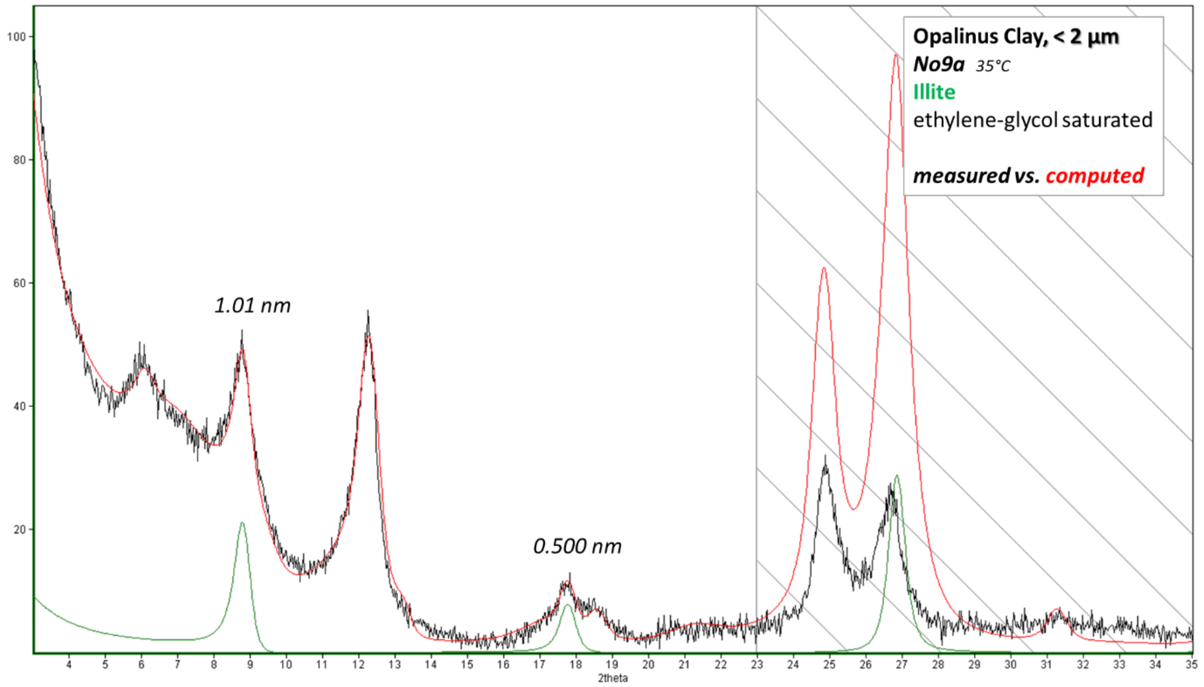
Opalinus Clay, < 2 µm
No9a 35°C
Illite
ethylene-glycol saturated
measured vs. computed
1.01 nm
0.500 nm
100
80
60
40
20
4 5 6 7 8 9 10 11 12 13 14 15 16 17 18 19 20 21 22 23 24 25 26 27 28 29 30 31 32 33 34 35
2theta

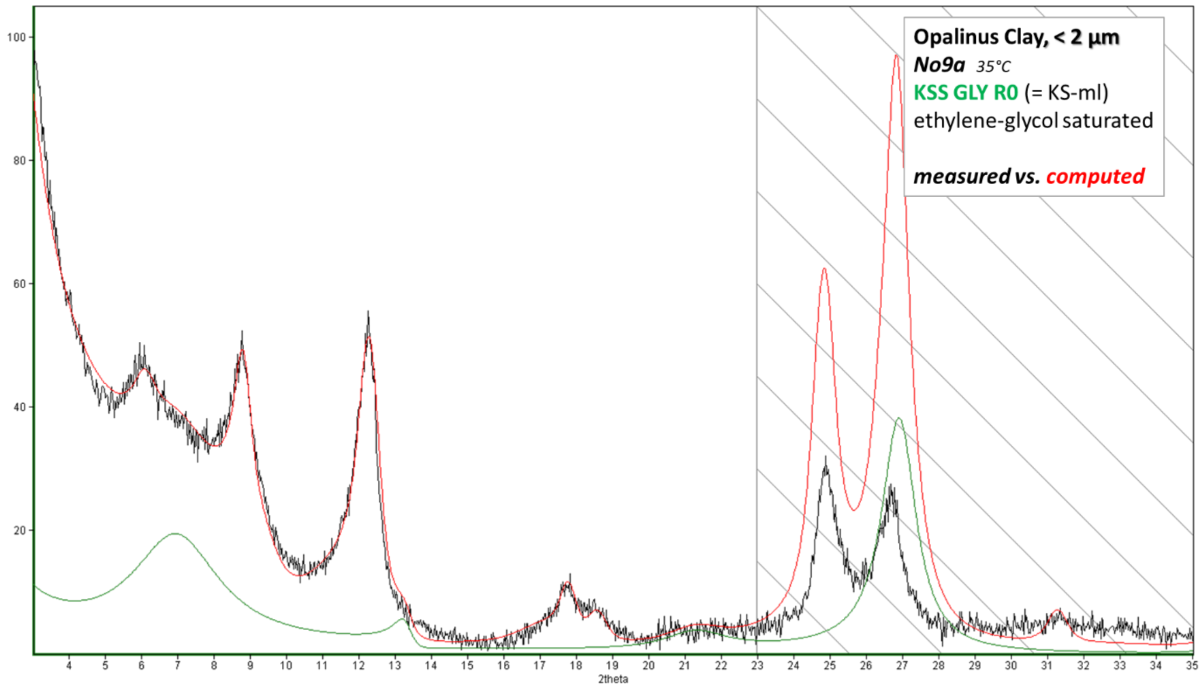
Opalinus Clay, < 2 µm
No9a 35°C
KSS GLY R0 (= KS-ml)
ethylene-glycol saturated
measured vs. computed
100
80
60
40
20
4 5 6 7 8 9 10 11 12 13 14 15 16 17 18 19 20 21 22 23 24 25 26 27 28 29 30 31 32 33 34 35
2theta

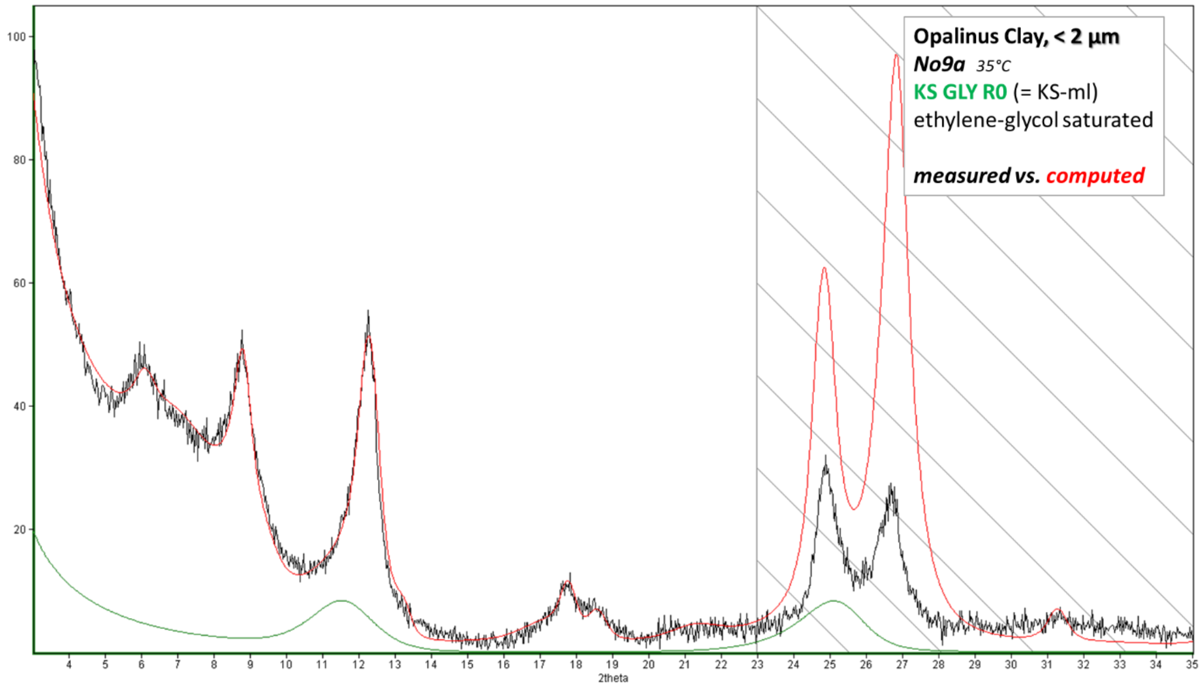
Opalinus Clay, < 2 µm
No9a 35°C
KS GLY R0 (= KS-ml)
ethylene-glycol saturated
measured vs. computed
100
80
60
40
20
4 5 6 7 8 9 10 11 12 13 14 15 16 17 18 19 20 21 22 23 24 25 26 27 28 29 30 31 32 33 34 35
2theta

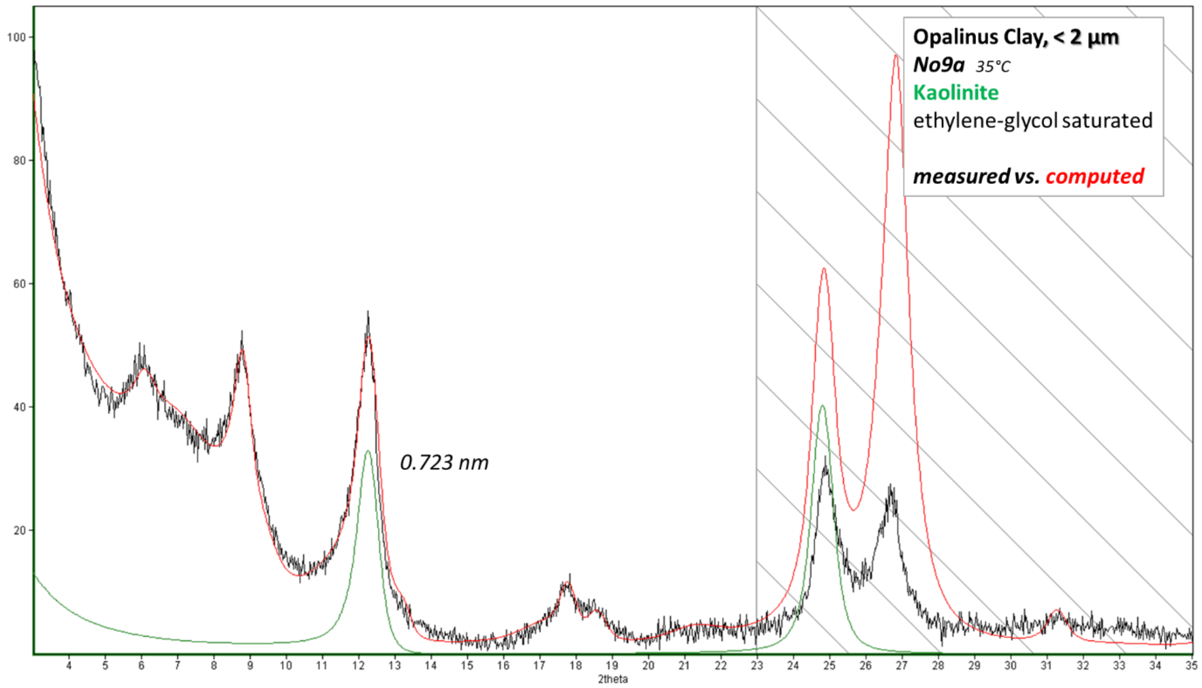
Opalinus Clay, < 2 µm
No9a 35°C
Kaolinite
ethylene-glycol saturated
measured vs. computed
0.723 nm
100
80
60
40
20
4 5 6 7 8 9 10 11 12 13 14 15 16 17 18 19 20 21 22 23 24 25 26 27 28 29 30 31 32 33 34 35
2theta

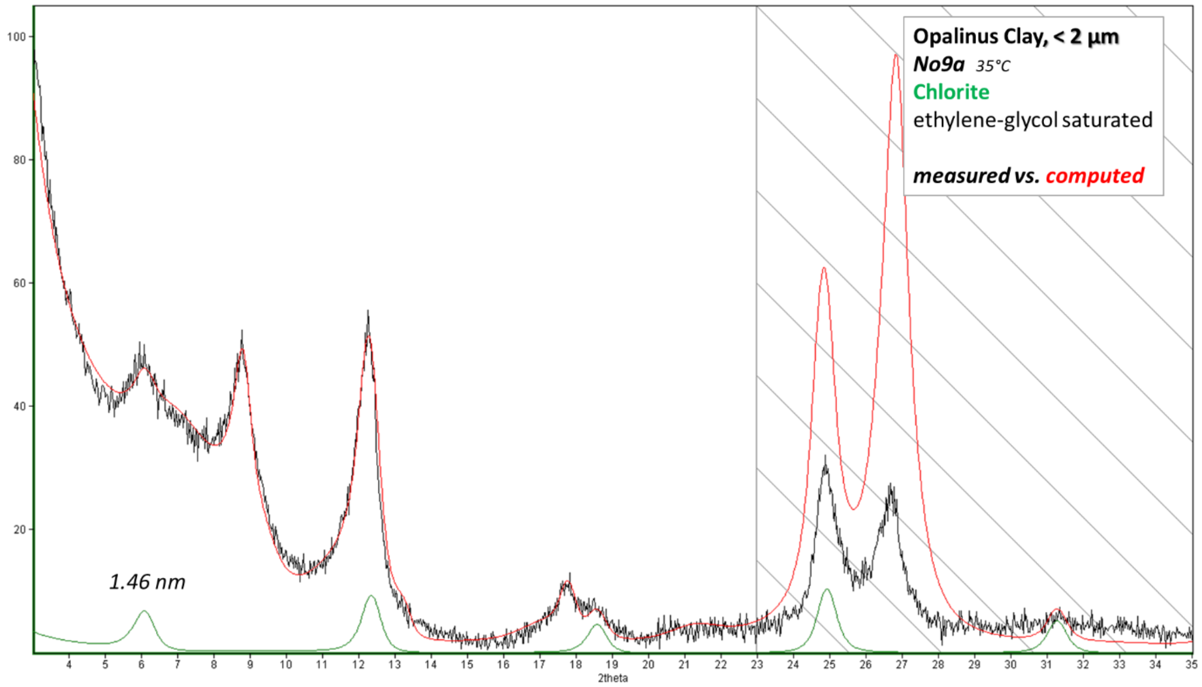
Opalinus Clay, < 2 µm
No9a 35°C
Chlorite
ethylene-glycol saturated
measured vs. computed
1.46 nm
100
80
60
40
20
4 5 6 7 8 9 10 11 12 13 14 15 16 17 18 19 20 21 22 23 24 25 26 27 28 29 30 31 32 33 34 35
2theta

Data Sheet – OPALINUS No7 (< 2 µm), treated material *(60°C)*

Diffraction pattern of oriented specimen & modelling by Sybilla

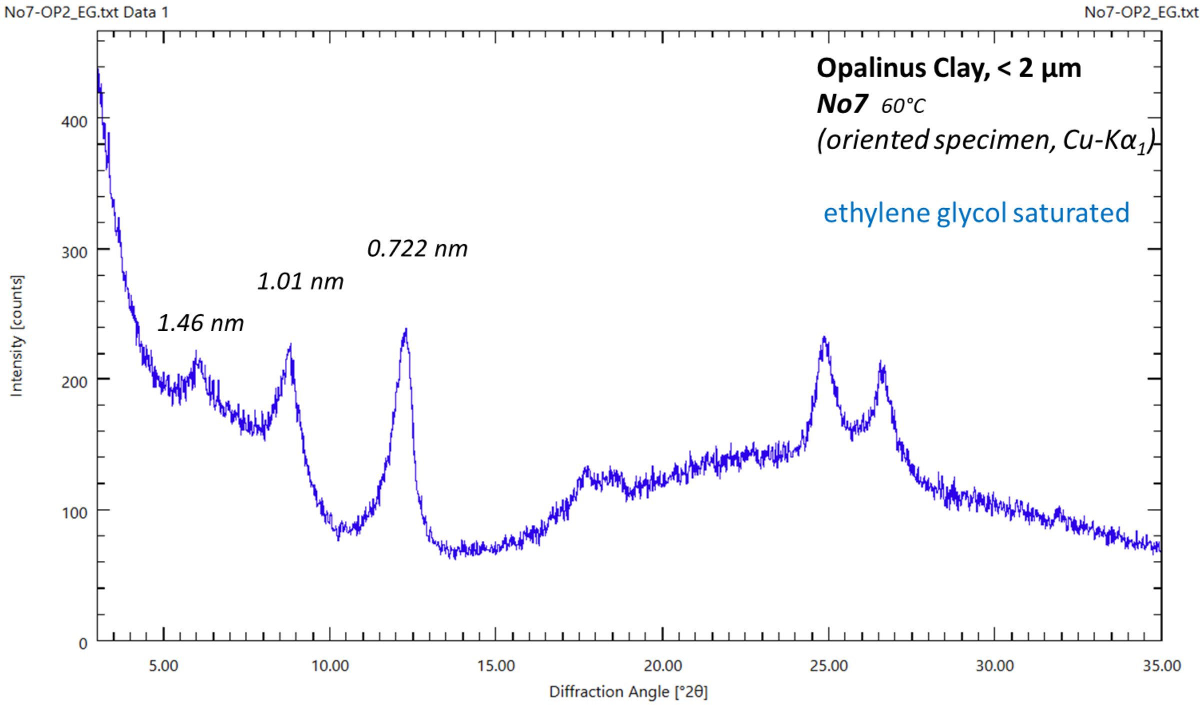

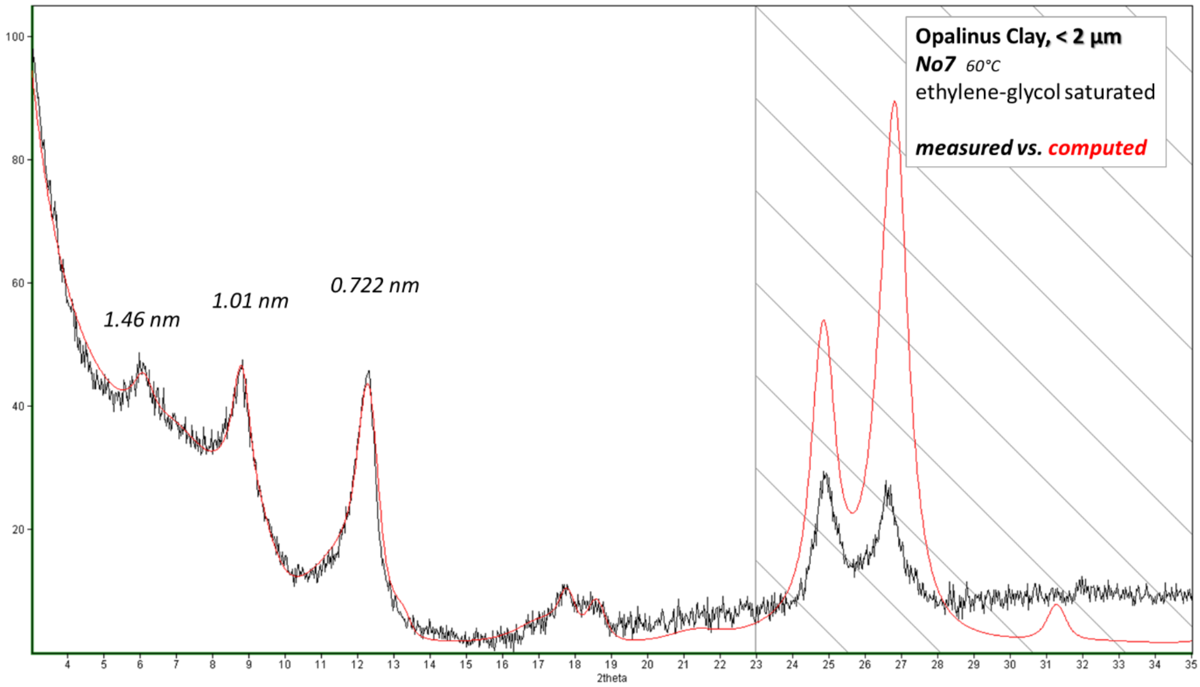

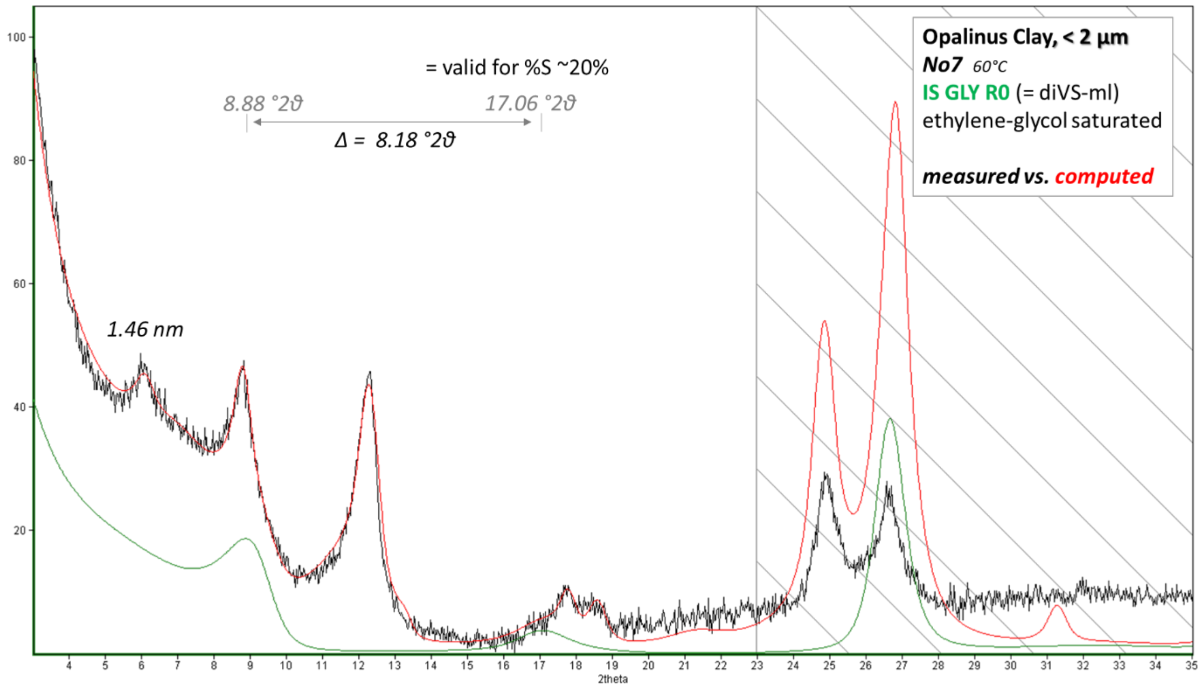
Opalinus Clay, < 2 µm
No7 60°C
IS GLY R0 (= diVS-ml)
ethylene-glycol saturated
measured vs. computed
= valid for %S ~20%
8.88 °2ϑ
17.06 °2ϑ
Δ = 8.18 °2ϑ
1.46 nm
100
80
60
40
20
4 5 6 7 8 9 10 11 12 13 14 15 16 17 18 19 20 21 22 23 24 25 26 27 28 29 30 31 32 33 34 35
2theta

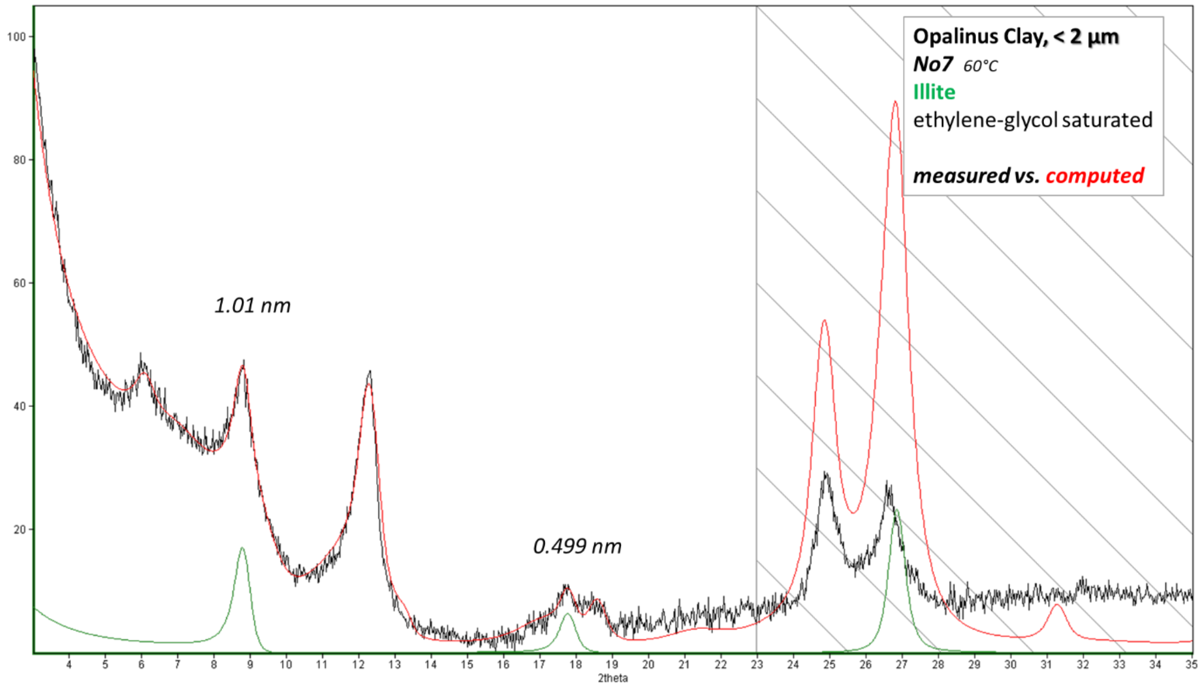
Opalinus Clay, < 2 µm
No7 60°C
Illite
ethylene-glycol saturated
measured vs. computed
1.01 nm
0.499 nm
100
80
60
40
20
4 5 6 7 8 9 10 11 12 13 14 15 16 17 18 19 20 21 22 23 24 25 26 27 28 29 30 31 32 33 34 35
2theta

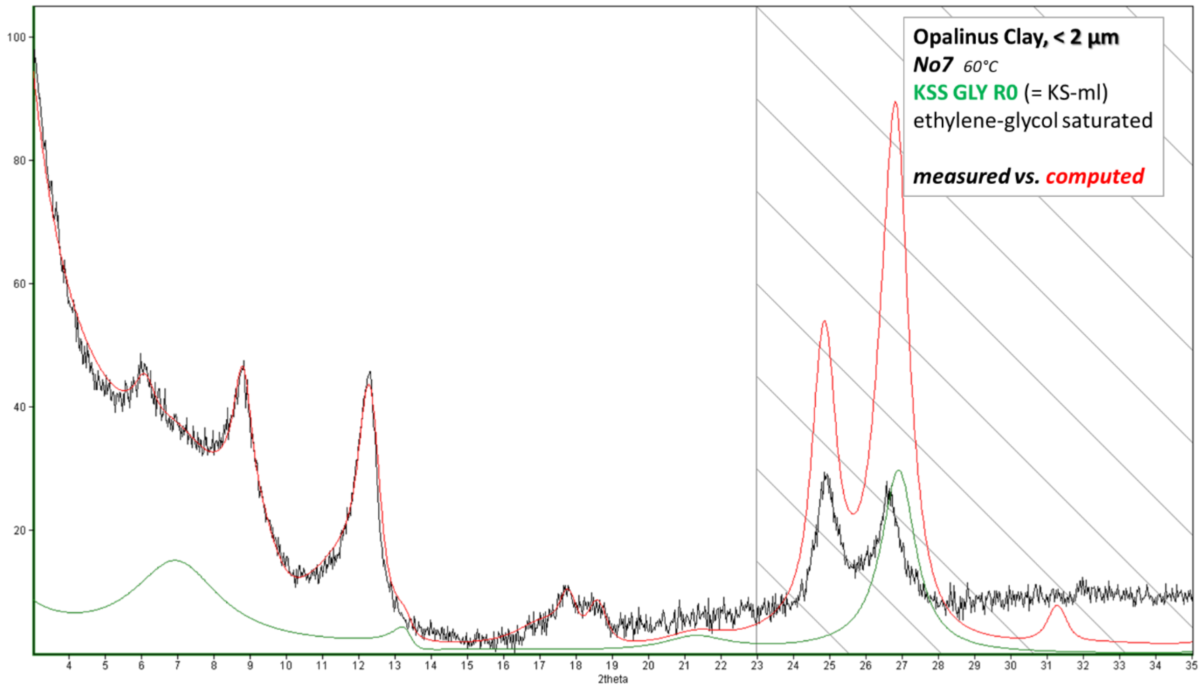
Opalinus Clay, < 2 µm
No7 60°C
KSS GLY R0 (= KS-ml)
ethylene-glycol saturated
measured vs. computed
100
80
60
40
20
4 5 6 7 8 9 10 11 12 13 14 15 16 17 18 19 20 21 22 23 24 25 26 27 28 29 30 31 32 33 34 35
2theta

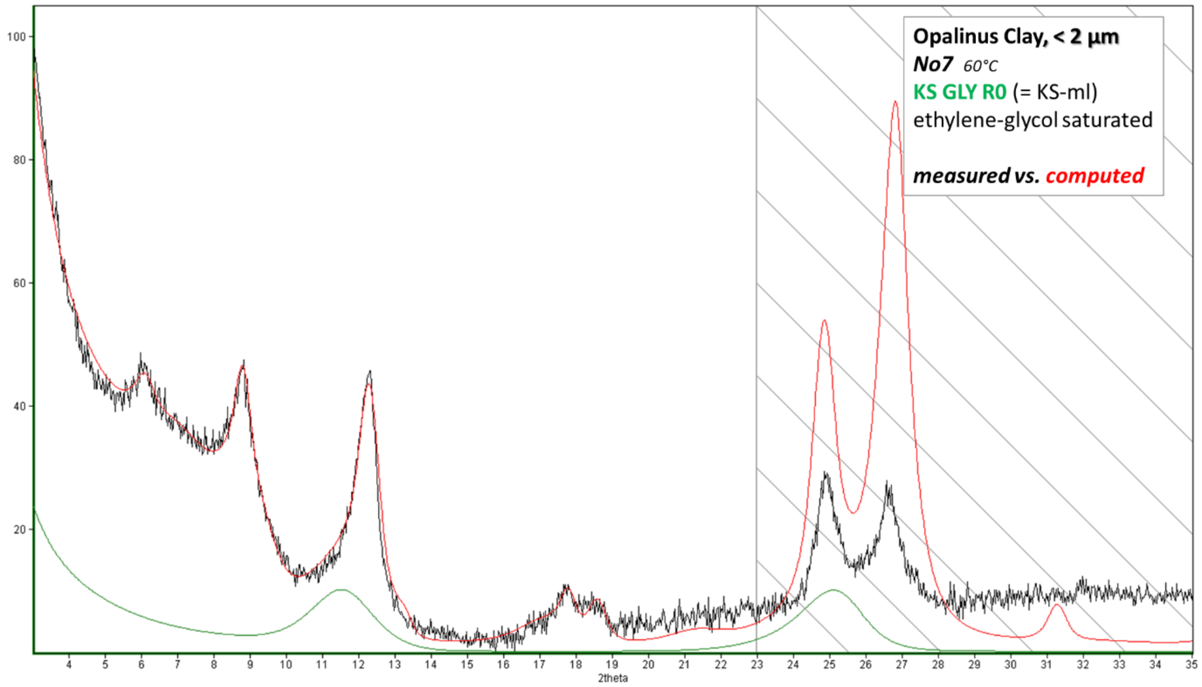
Opalinus Clay, < 2 µm
No7 60°C
KS GLY R0 (= KS-ml)
ethylene-glycol saturated
measured vs. computed
100
80
60
40
20
4 5 6 7 8 9 10 11 12 13 14 15 16 17 18 19 20 21 22 23 24 25 26 27 28 29 30 31 32 33 34 35
2theta

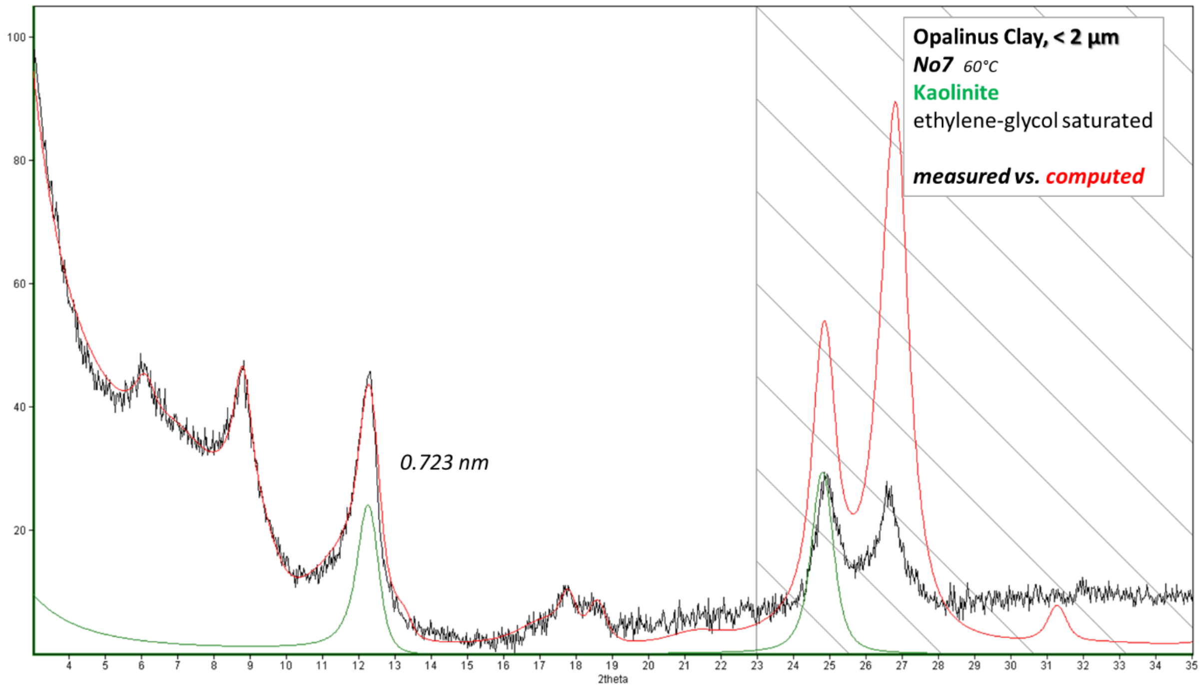
Opalinus Clay, < 2 µm
No7 *60°C*
Kaolinite
ethylene-glycol saturated
measured* *vs.* *computed
0.723 nm
100
80
60
40
20
4
5
6
7
8
9
10
11
12
13
14
15
16
17
18
19
20
21
22
23
24
25
26
27
28
29
30
31
32
33
34
35
2theta

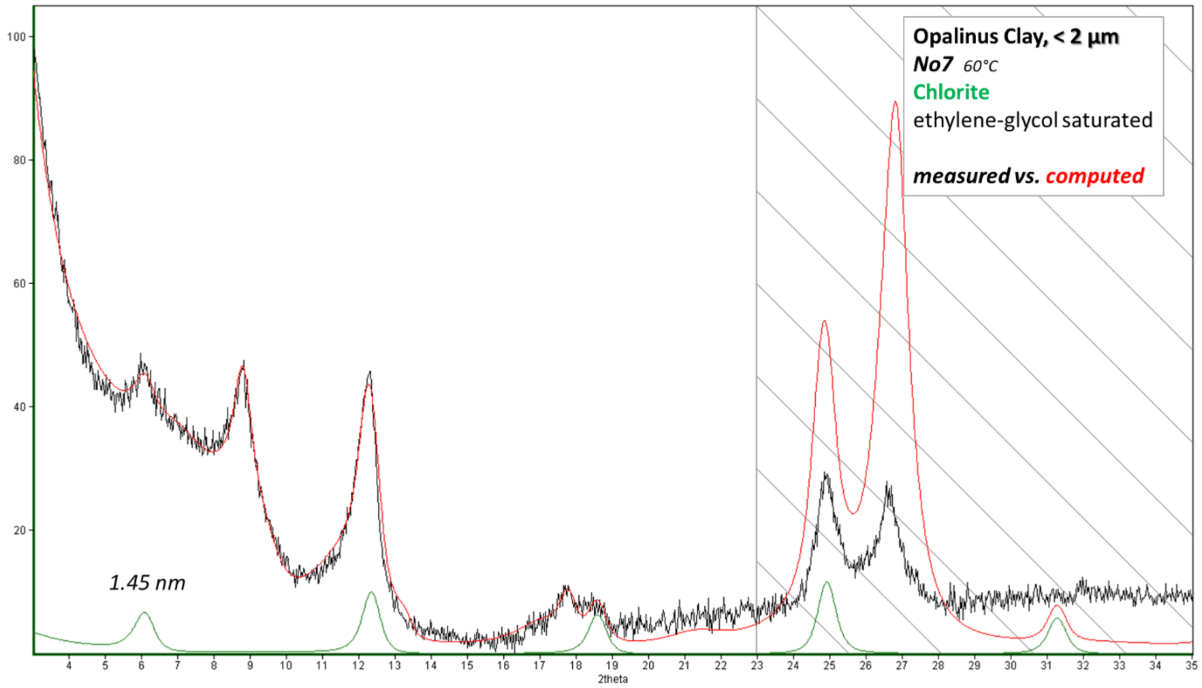
Opalinus Clay, < 2 µm
No7 *60°C*
Chlorite
ethylene-glycol saturated
measured* *vs.* *computed
1.45 nm
100
80
60
40
20
4
5
6
7
8
9
10
11
12
13
14
15
16
17
18
19
20
21
22
23
24
25
26
27
28
29
30
31
32
33
34
35
2theta

Data Sheet – OPALINUS No9 (< 2 µm), treated material *(60°C)*

Diffraction pattern of oriented specimen & modelling by Sybilla

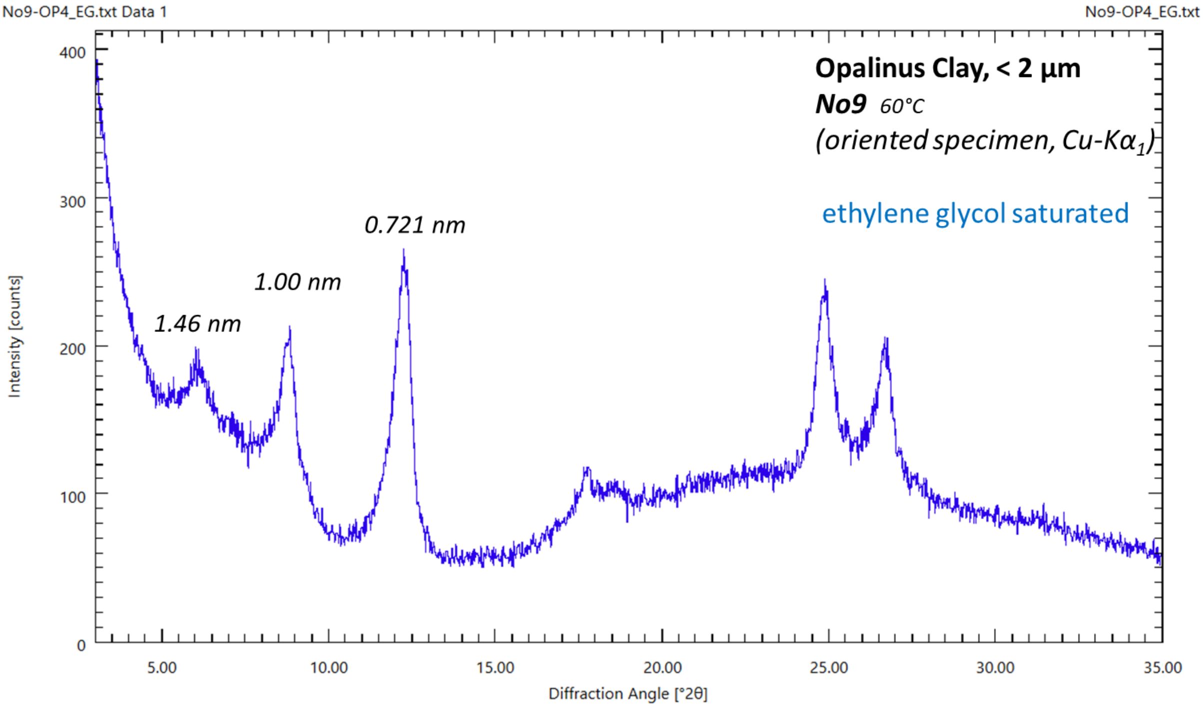

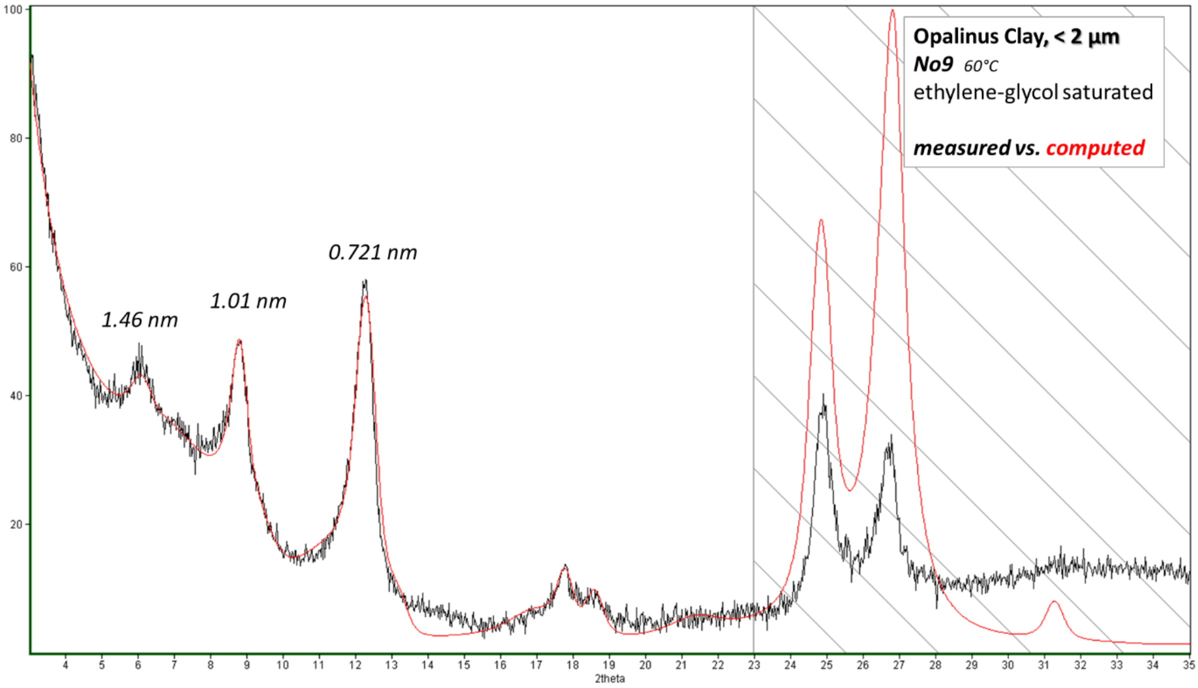

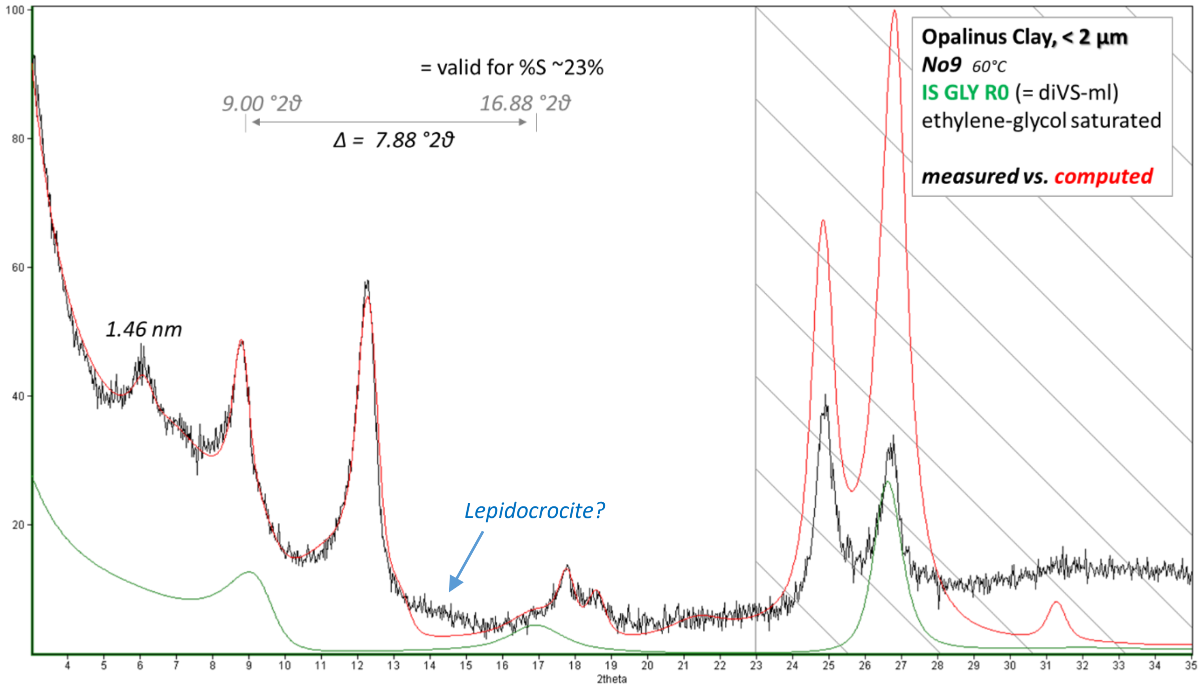
Opalinus Clay, < 2 µm
No9 60°C
IS GLY R0 (= diVS-ml)
ethylene-glycol saturated
measured vs. computed
= valid for %S ~23%
9.00 °2ϑ
16.88 °2ϑ
Δ = 7.88 °2ϑ
1.46 nm
Lepidocrocite?
2theta
100
80
60
40
20
4
5
6
7
8
9
10
11
12
13
14
15
16
17
18
19
20
21
22
23
24
25
26
27
28
29
30
31
32
33
34
35

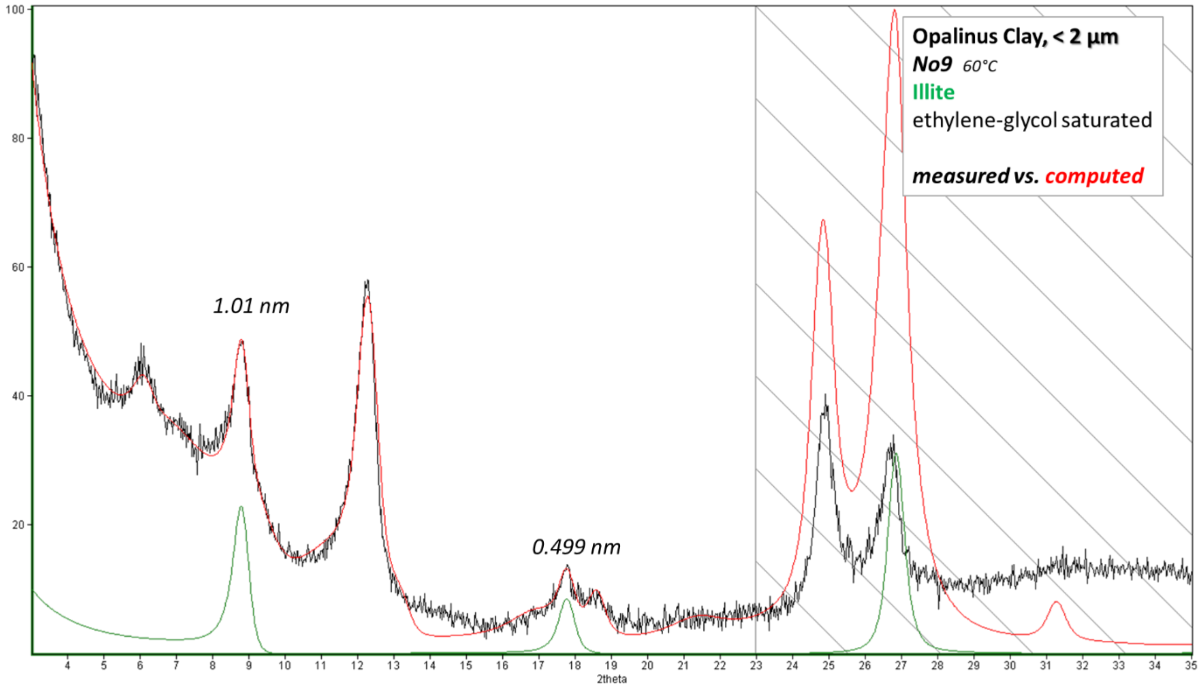
Opalinus Clay, < 2 µm
No9 60°C
Illite
ethylene-glycol saturated
measured vs. computed
1.01 nm
0.499 nm
2theta
100
80
60
40
20
4
5
6
7
8
9
10
11
12
13
14
15
16
17
18
19
20
21
22
23
24
25
26
27
28
29
30
31
32
33
34
35

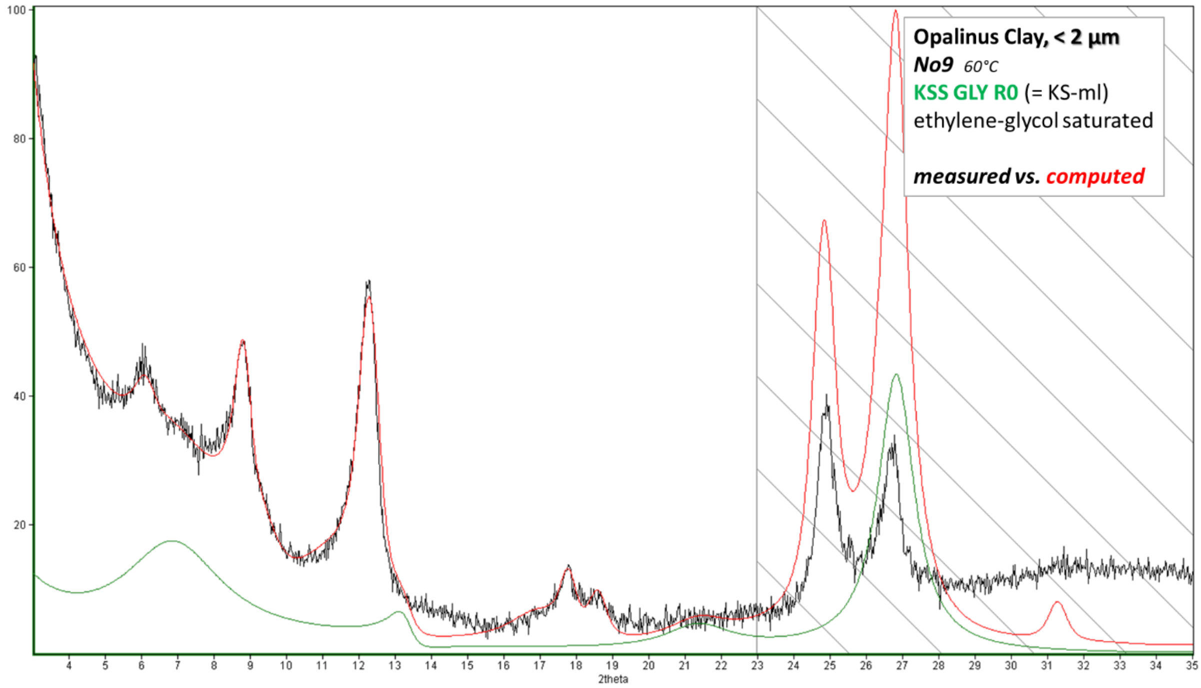
Opalinus Clay, < 2 µm
No9 60°C
KSS GLY R0 (= KS-ml)
ethylene-glycol saturated
measured vs. computed
100
80
60
40
20
4
5
6
7
8
9
10
11
12
13
14
15
16
17
18
19
20
21
22
23
24
25
26
27
28
29
30
31
32
33
34
35
2theta

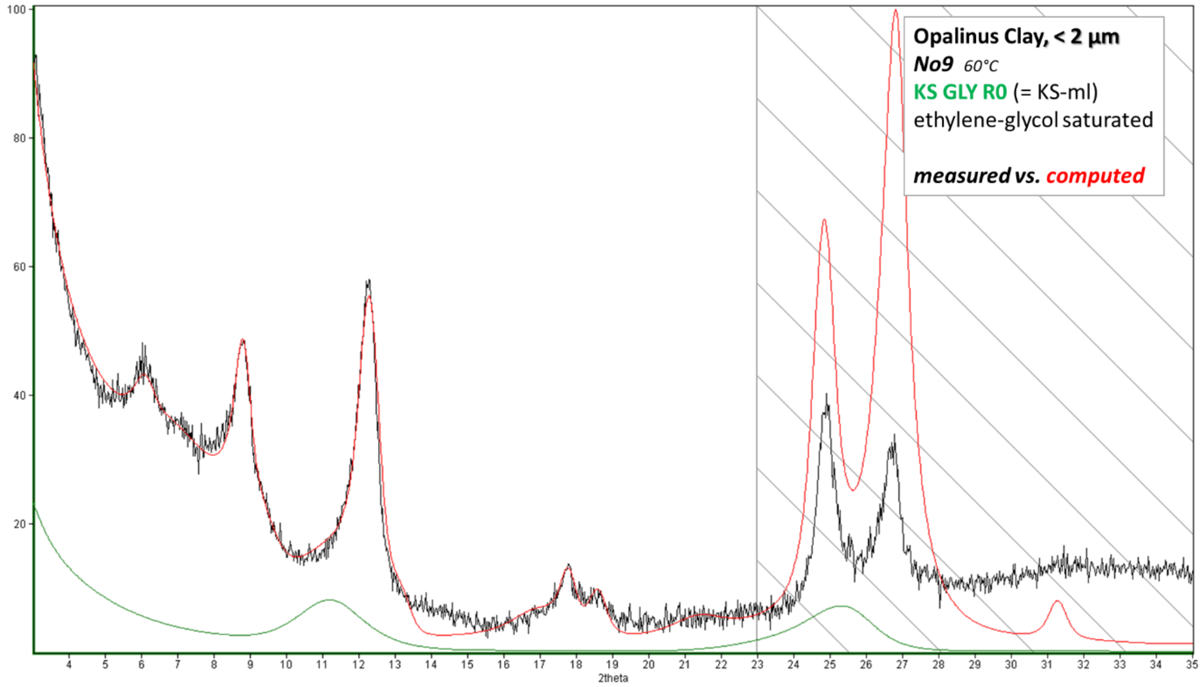
Opalinus Clay, < 2 µm
No9 60°C
KS GLY R0 (= KS-ml)
ethylene-glycol saturated
measured vs. computed
100
80
60
40
20
4
5
6
7
8
9
10
11
12
13
14
15
16
17
18
19
20
21
22
23
24
25
26
27
28
29
30
31
32
33
34
35
2theta

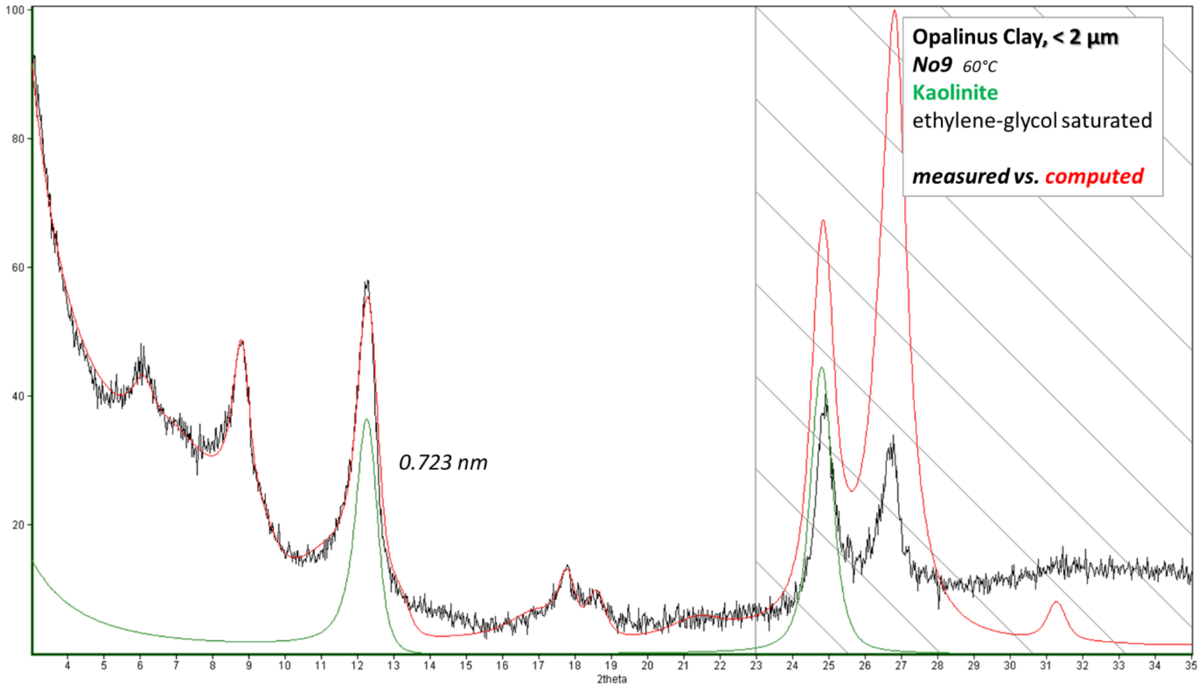
Opalinus Clay, < 2 µm
No9 60°C
Kaolinite
ethylene-glycol saturated
measured vs. computed
0.723 nm
100
80
60
40
20
4
5
6
7
8
9
10
11
12
13
14
15
16
17
18
19
20
21
22
23
24
25
26
27
28
29
30
31
32
33
34
35
2theta

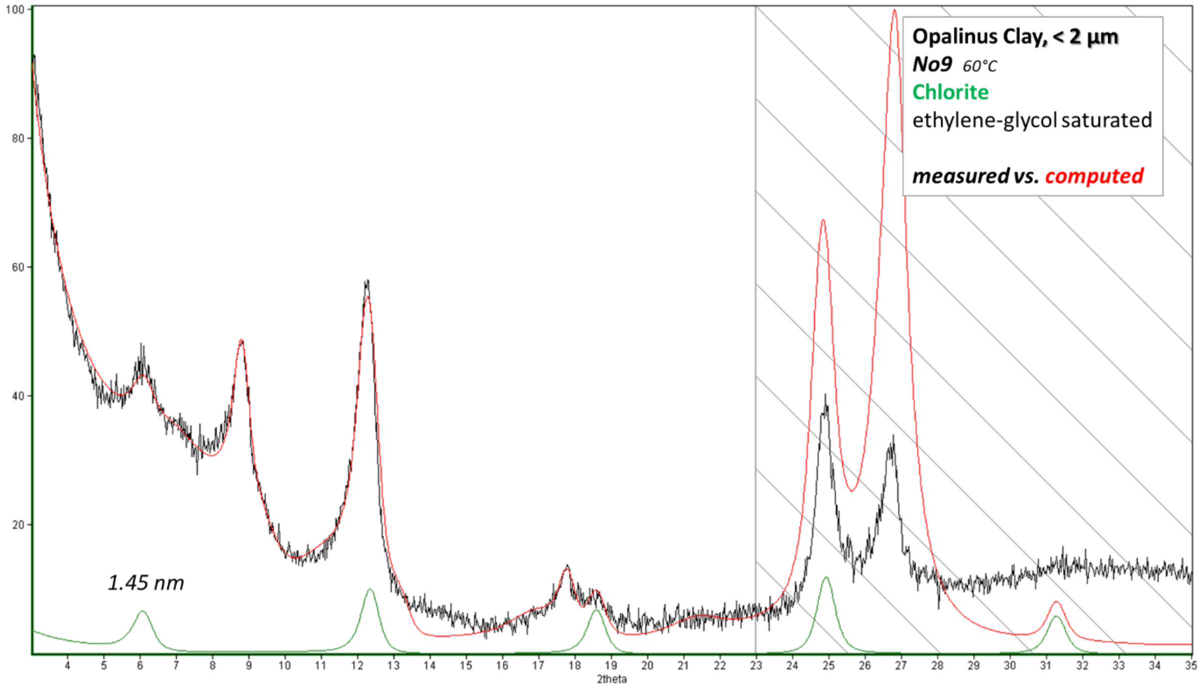
Opalinus Clay, < 2 µm
No9 60°C
Chlorite
ethylene-glycol saturated
measured vs. computed
1.45 nm
100
80
60
40
20
4
5
6
7
8
9
10
11
12
13
14
15
16
17
18
19
20
21
22
23
24
25
26
27
28
29
30
31
32
33
34
35
2theta

Data Sheet – OPALINUS No8 (< 2 µm), treated material *(100°C)*

Diffraction pattern of oriented specimen & modelling by Sybilla

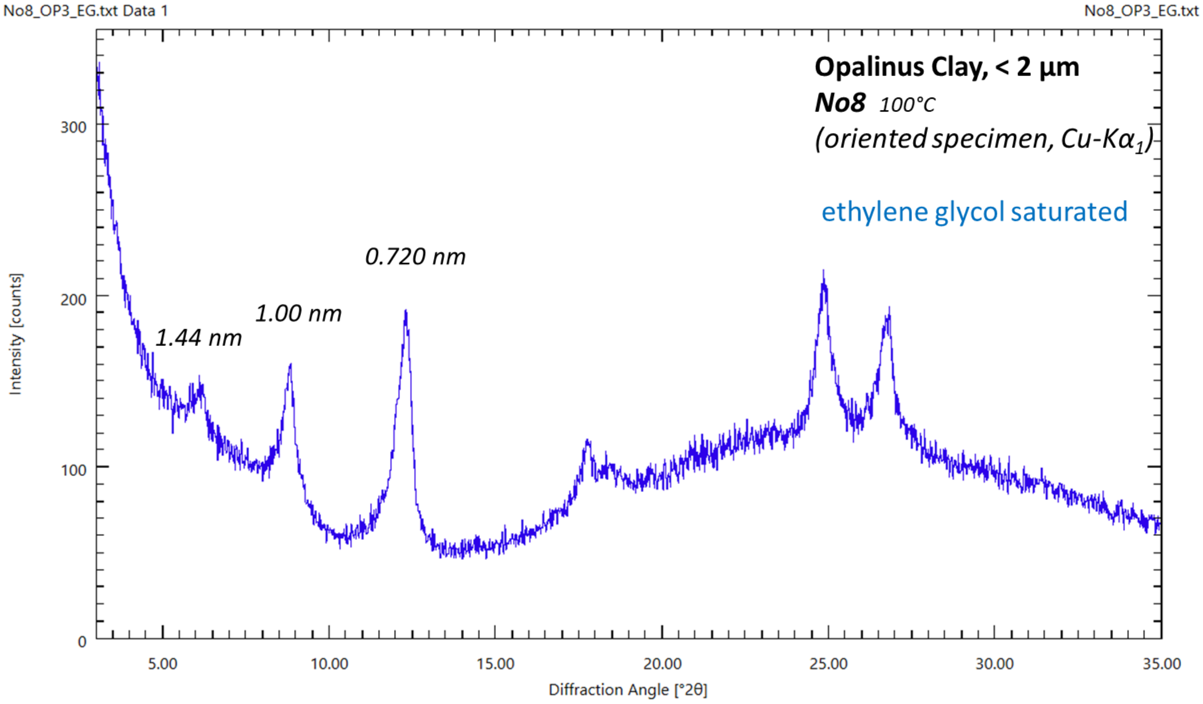

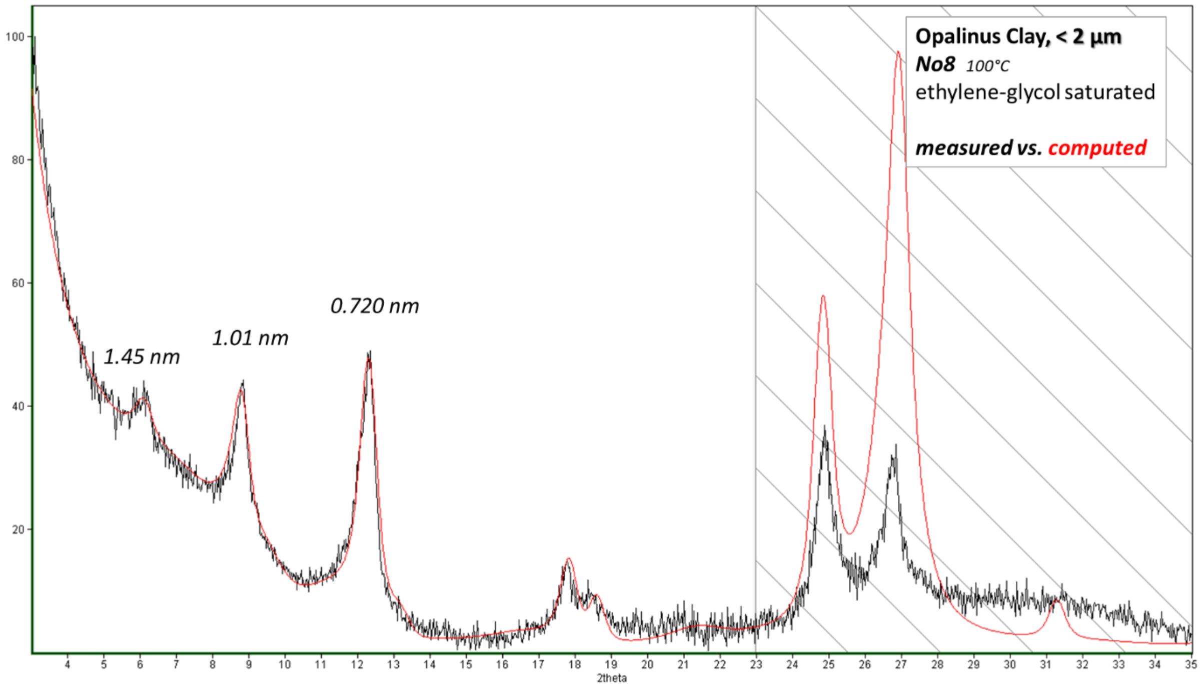

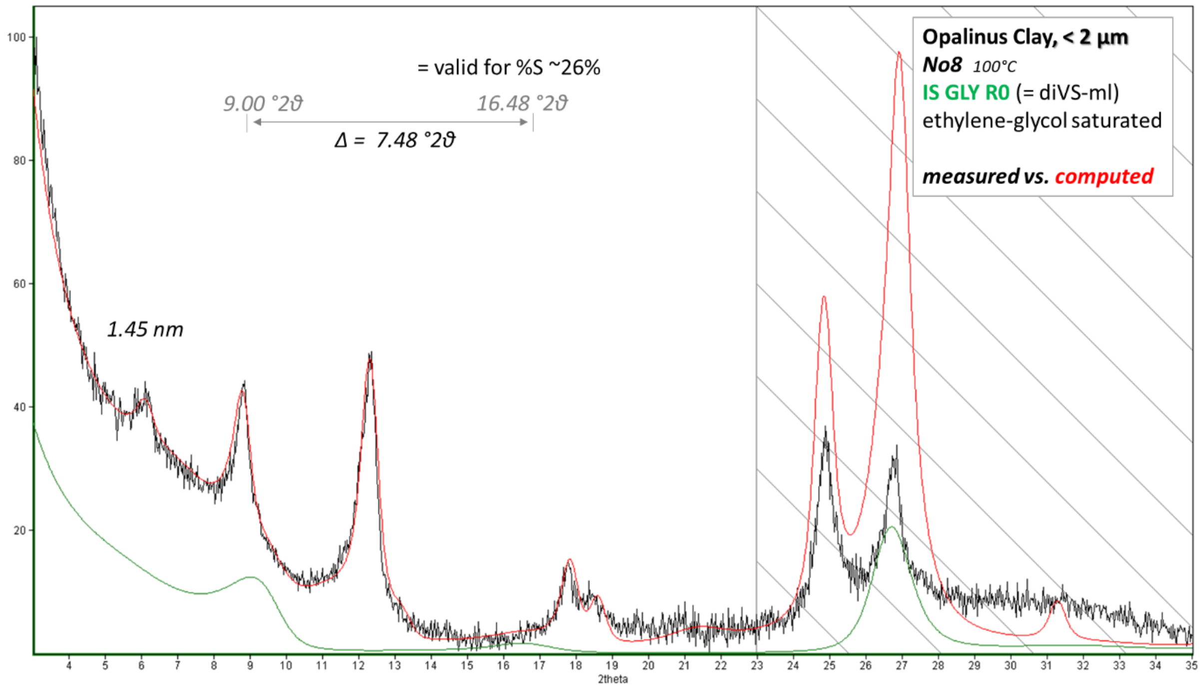
Opalinus Clay, < 2 µm
No8 100°C
IS GLY R0 (= diVS-ml)
ethylene-glycol saturated
measured vs. computed
= valid for %S ~26%
9.00 °2ϑ
16.48 °2ϑ
Δ = 7.48 °2ϑ
1.45 nm
100
80
60
40
20
4
5
6
7
8
9
10
11
12
13
14
15
16
17
18
19
20
21
22
23
24
25
26
27
28
29
30
31
32
33
34
35
2theta

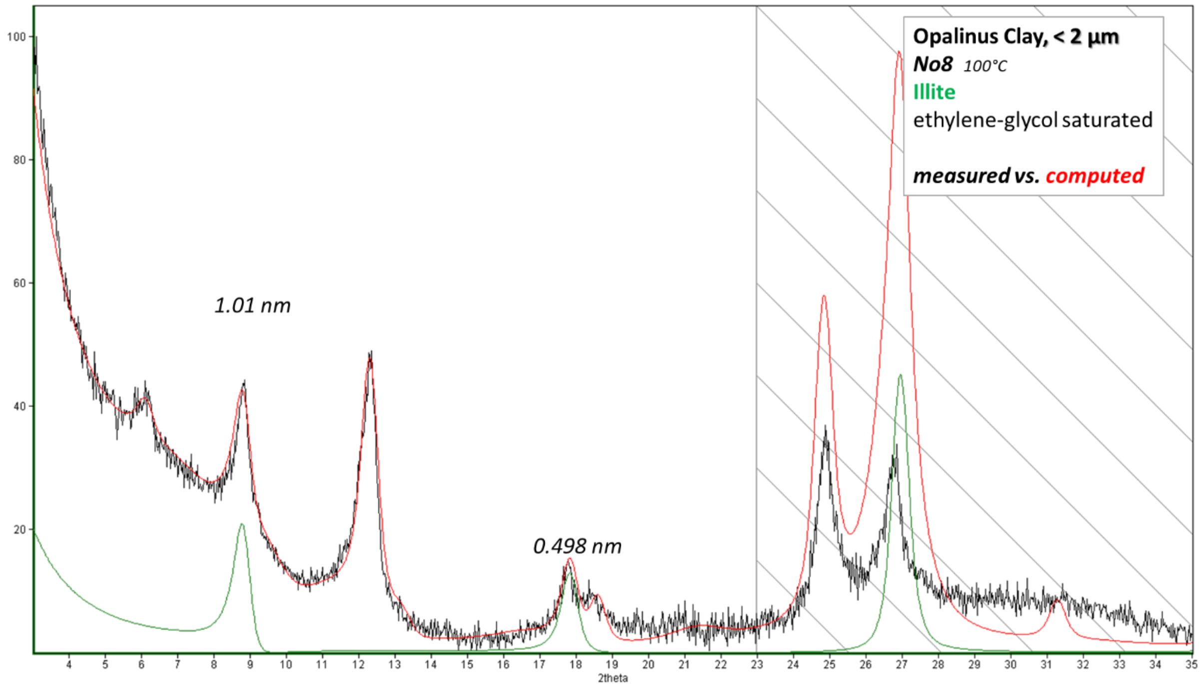
Opalinus Clay, < 2 µm
No8 100°C
Illite
ethylene-glycol saturated
measured vs. computed
1.01 nm
0.498 nm
100
80
60
40
20
4
5
6
7
8
9
10
11
12
13
14
15
16
17
18
19
20
21
22
23
24
25
26
27
28
29
30
31
32
33
34
35
2theta

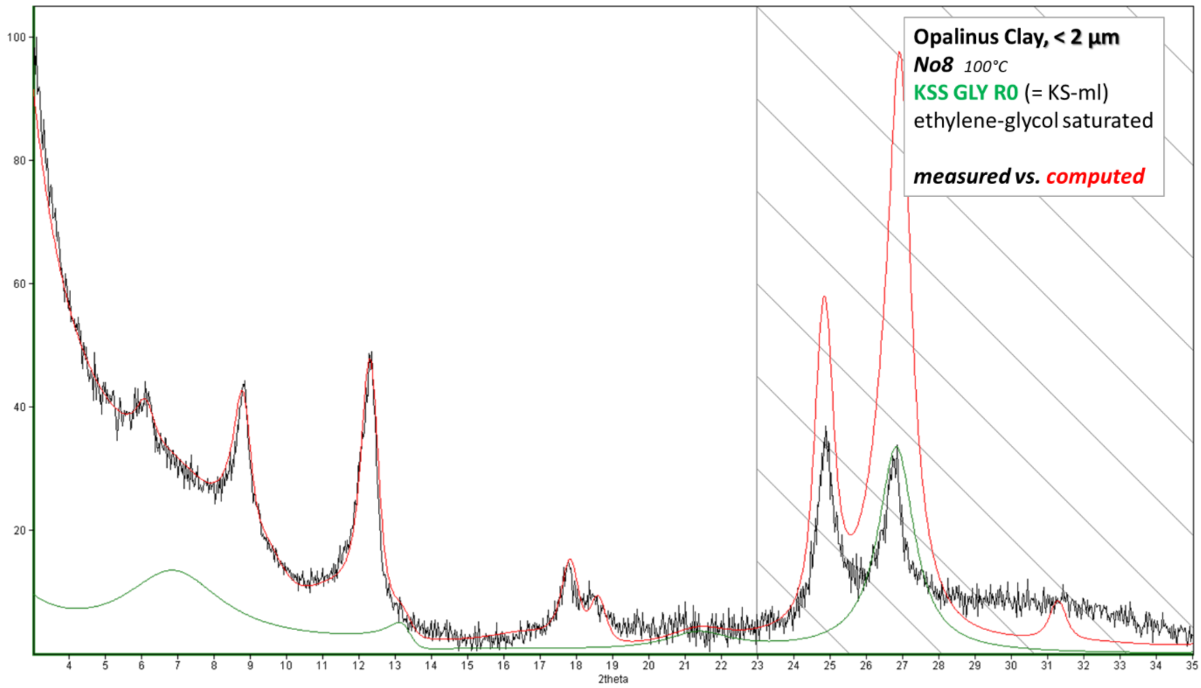
Opalinus Clay, < 2 µm
No8 100°C
KSS GLY R0 (= KS-ml)
ethylene-glycol saturated
measured vs. computed
100
80
60
40
20
4
5
6
7
8
9
10
11
12
13
14
15
16
17
18
19
20
21
22
23
24
25
26
27
28
29
30
31
32
33
34
35
2theta

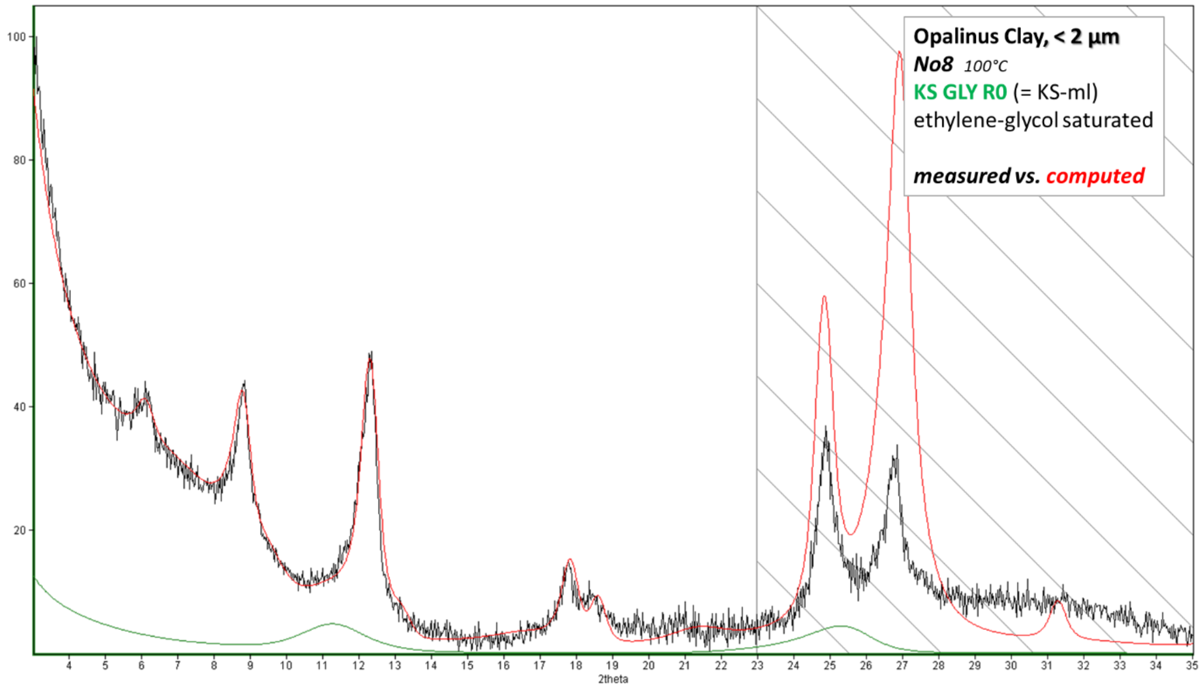
Opalinus Clay, < 2 µm
No8 100°C
KS GLY R0 (= KS-ml)
ethylene-glycol saturated
measured vs. computed
100
80
60
40
20
4
5
6
7
8
9
10
11
12
13
14
15
16
17
18
19
20
21
22
23
24
25
26
27
28
29
30
31
32
33
34
35
2theta

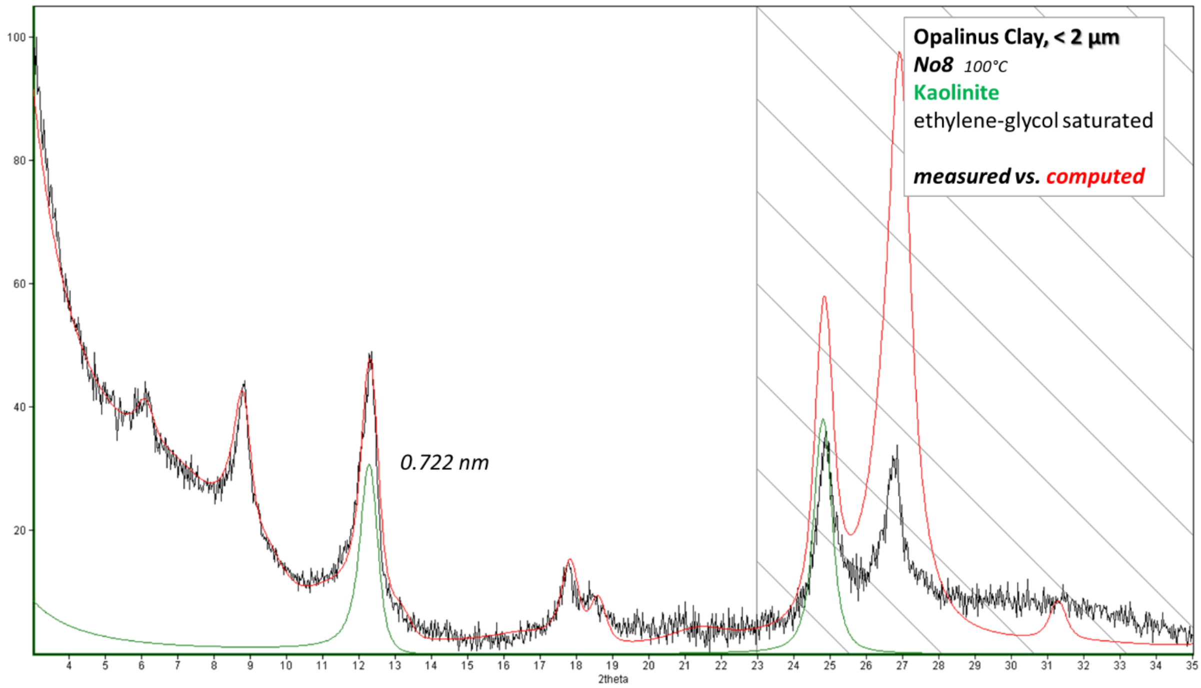
Opalinus Clay, < 2 µm
No8 100°C
Kaolinite
ethylene-glycol saturated
measured vs. computed
0.722 nm
100
80
60
40
20
4 5 6 7 8 9 10 11 12 13 14 15 16 17 18 19 20 21 22 23 24 25 26 27 28 29 30 31 32 33 34 35
2theta

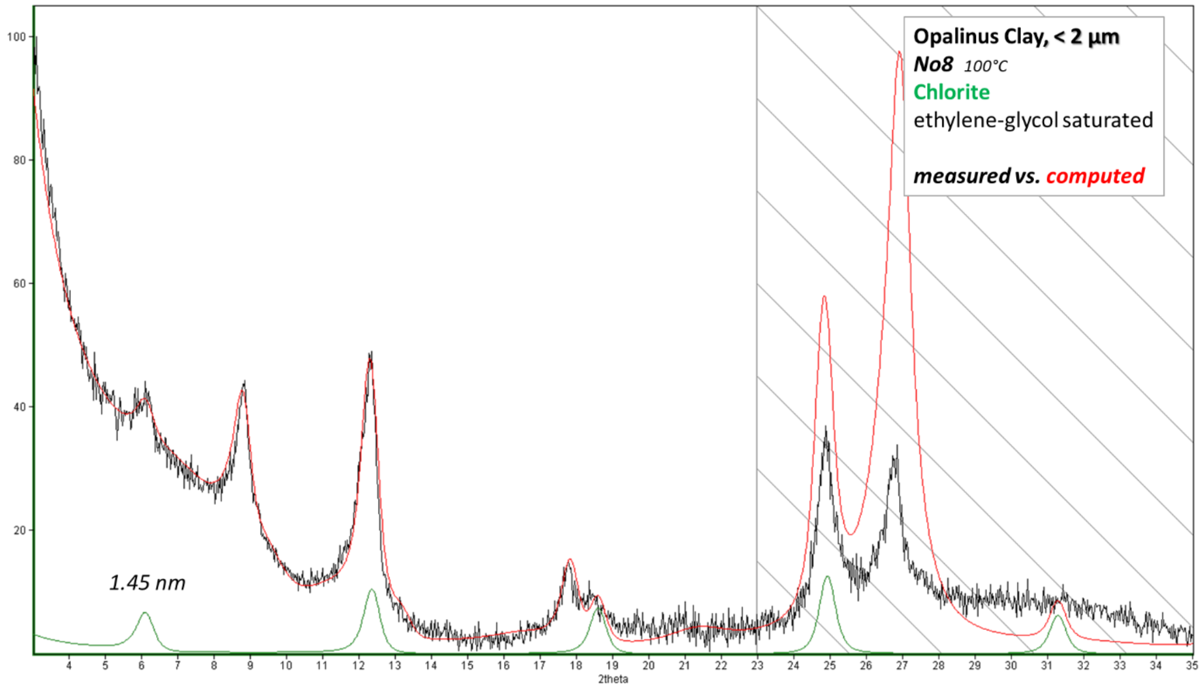
Opalinus Clay, < 2 µm
No8 100°C
Chlorite
ethylene-glycol saturated
measured vs. computed
1.45 nm
100
80
60
40
20
4 5 6 7 8 9 10 11 12 13 14 15 16 17 18 19 20 21 22 23 24 25 26 27 28 29 30 31 32 33 34 35
2theta

Data Sheet – OPALINUS No14 (< 2 µm), treated material *(125°C, 48.5 h)*

Diffraction pattern of oriented specimen & modelling by Sybilla

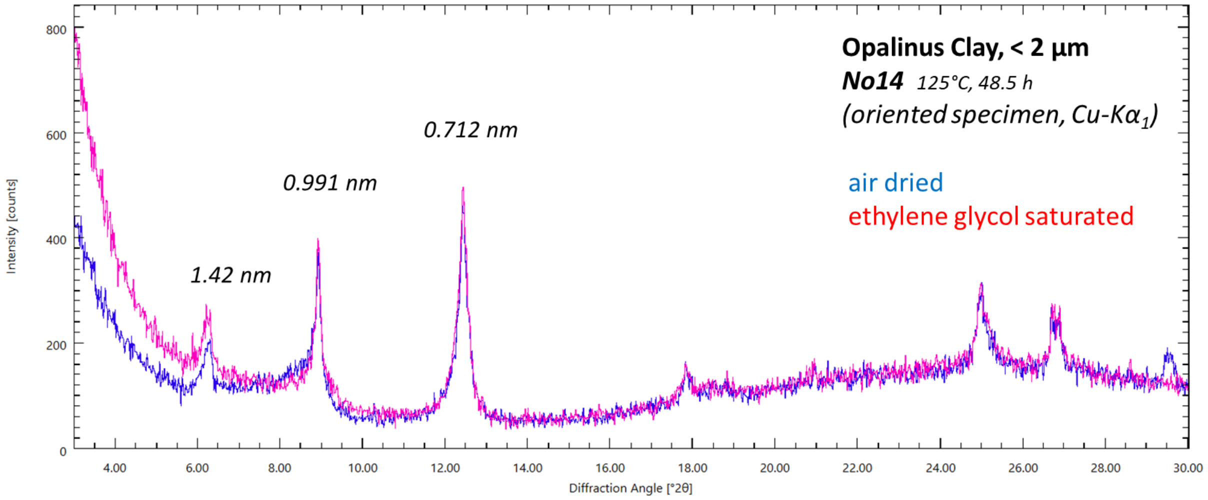

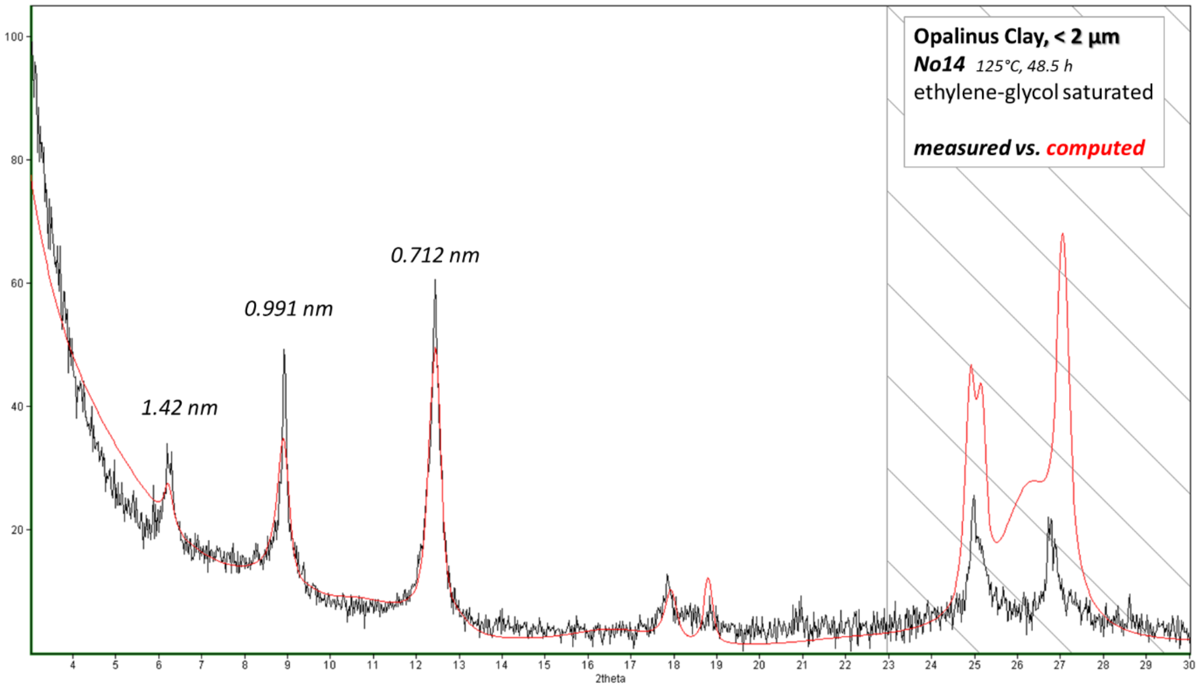

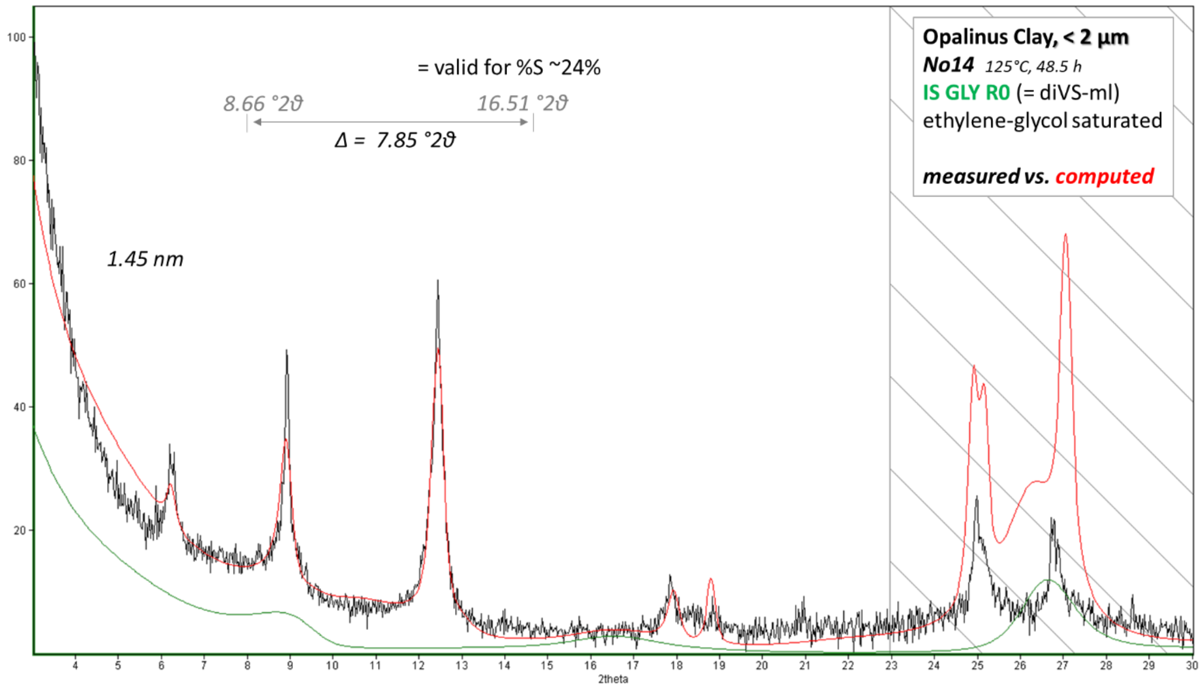
Opalinus Clay, < 2 µm
No14 125°C, 48.5 h
IS GLY R0 (= diVS-ml)
ethylene-glycol saturated
measured vs. computed
= valid for %S ~24%
8.66 °2ϑ
16.51 °2ϑ
Δ = 7.85 °2ϑ
1.45 nm
100
80
60
40
20
4
5
6
7
8
9
10
11
12
13
14
15
16
17
18
19
20
21
22
23
24
25
26
27
28
29
30
2theta

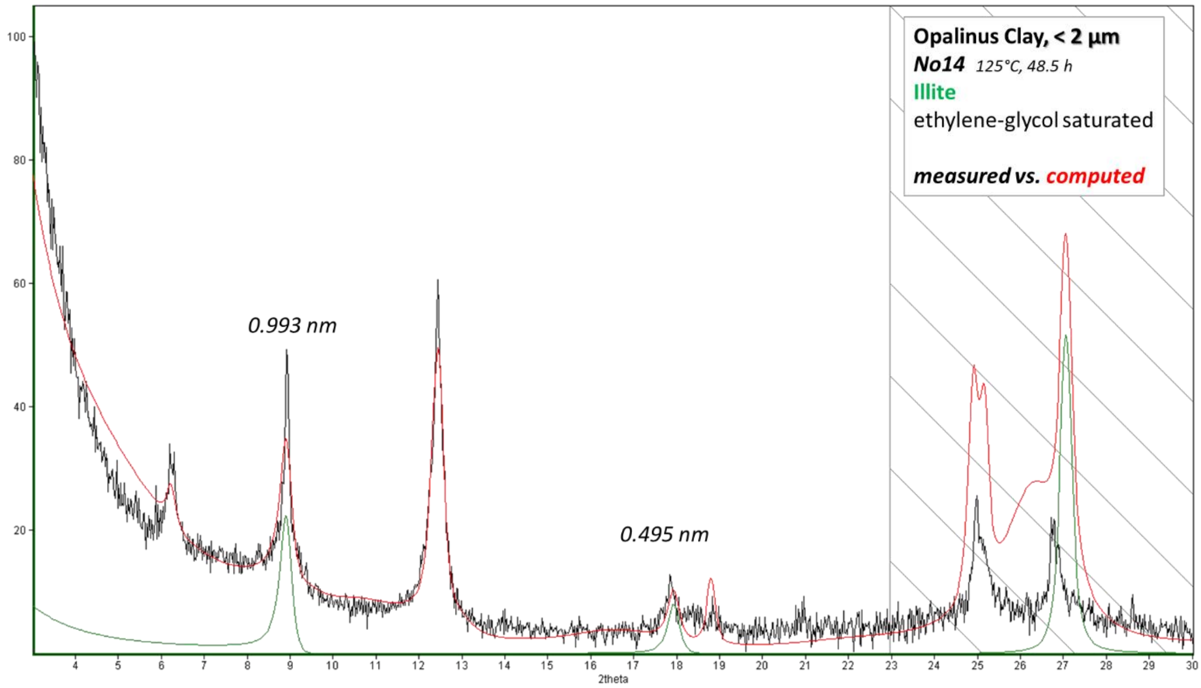
Opalinus Clay, < 2 µm
No14 125°C, 48.5 h
Illite
ethylene-glycol saturated
measured vs. computed
0.993 nm
0.495 nm
100
80
60
40
20
4
5
6
7
8
9
10
11
12
13
14
15
16
17
18
19
20
21
22
23
24
25
26
27
28
29
30
2theta

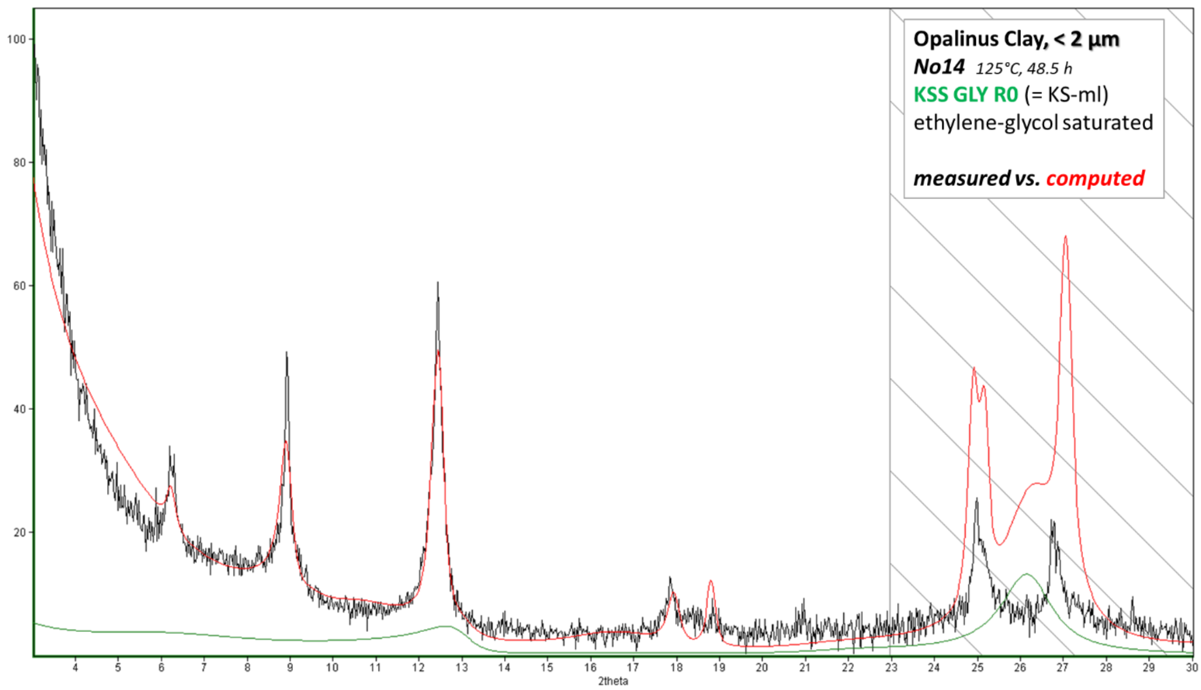
Opalinus Clay, < 2 µm
No14 125°C, 48.5 h
KSS GLY R0 (= KS-ml)
ethylene-glycol saturated
measured vs. computed
100
80
60
40
20
4
5
6
7
8
9
10
11
12
13
14
15
16
17
18
19
20
21
22
23
24
25
26
27
28
29
30
2theta

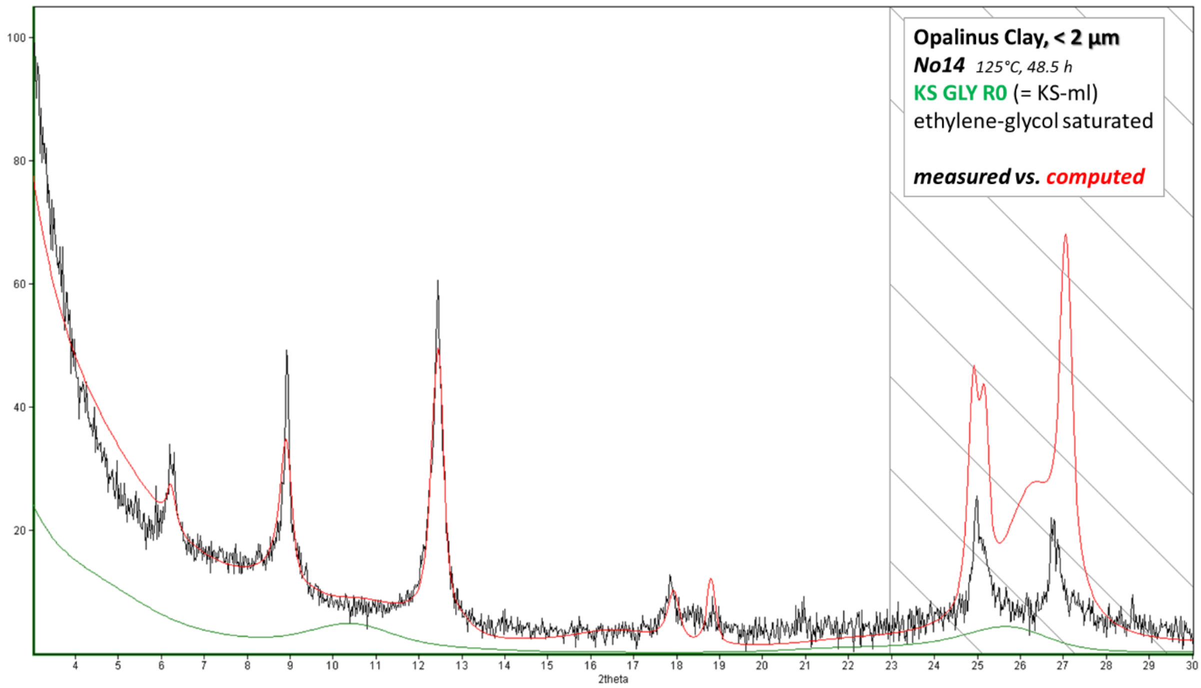
Opalinus Clay, < 2 µm
No14 125°C, 48.5 h
KS GLY R0 (= KS-ml)
ethylene-glycol saturated
measured vs. computed
100
80
60
40
20
4
5
6
7
8
9
10
11
12
13
14
15
16
17
18
19
20
21
22
23
24
25
26
27
28
29
30
2theta

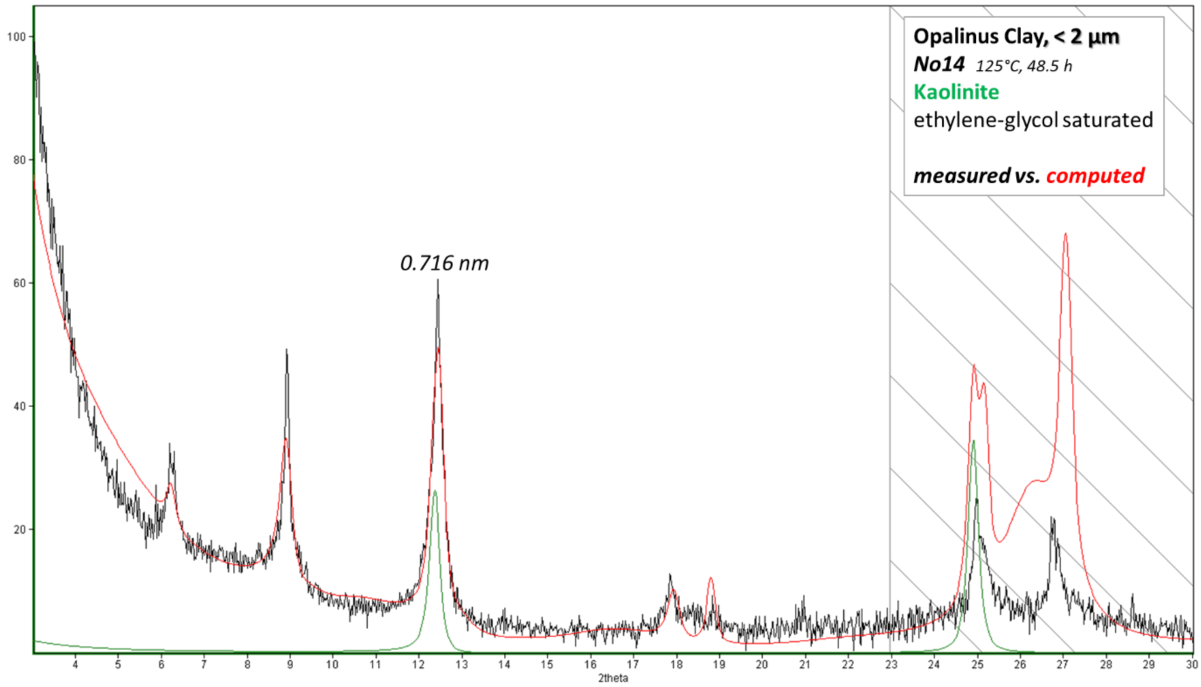
Opalinus Clay, < 2 µm
No14 *125°C, 48.5 h*
Kaolinite
ethylene-glycol saturated
measured* vs. *computed
0.716 nm
100
80
60
40
20
4
5
6
7
8
9
10
11
12
13
14
15
16
17
18
19
20
21
22
23
24
25
26
27
28
29
30
2theta

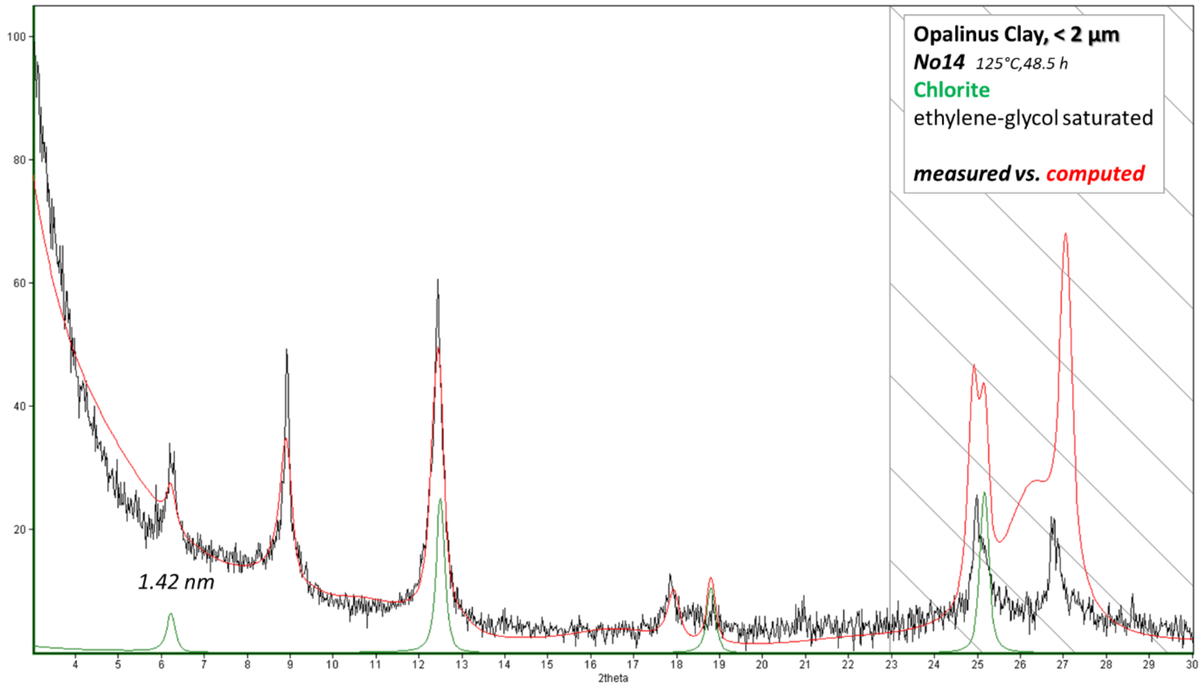
Opalinus Clay, < 2 µm
No14 *125°C,48.5 h*
Chlorite
ethylene-glycol saturated
measured* vs. *computed
1.42 nm
100
80
60
40
20
4
5
6
7
8
9
10
11
12
13
14
15
16
17
18
19
20
21
22
23
24
25
26
27
28
29
30
2theta

Data Sheet – OPALINUS No13 (< 2 µm), treated material *(150°C, 48.6 h)*

Diffraction pattern of oriented specimen & modelling by Sybilla

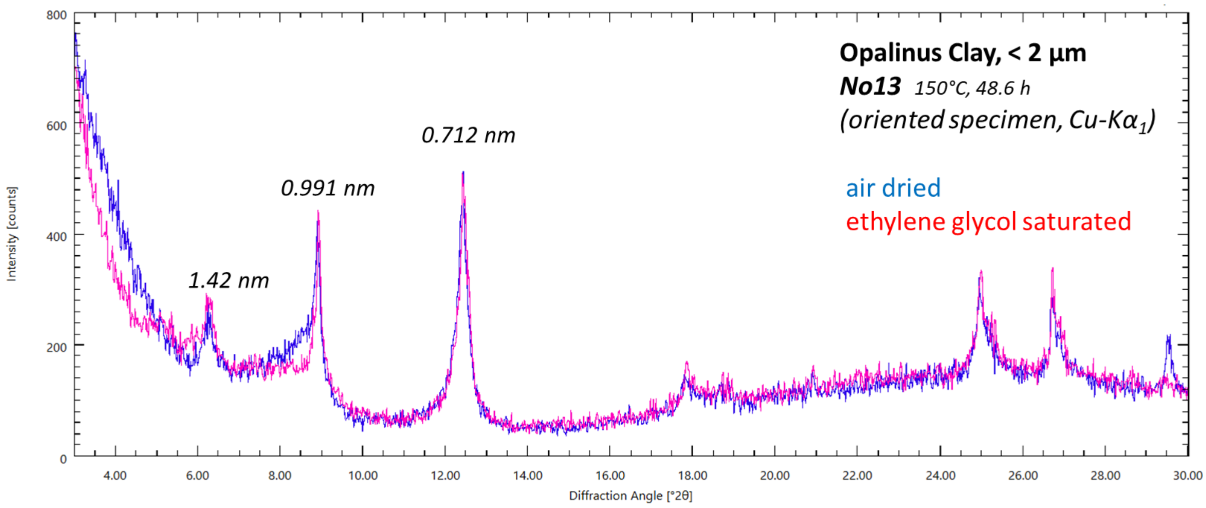

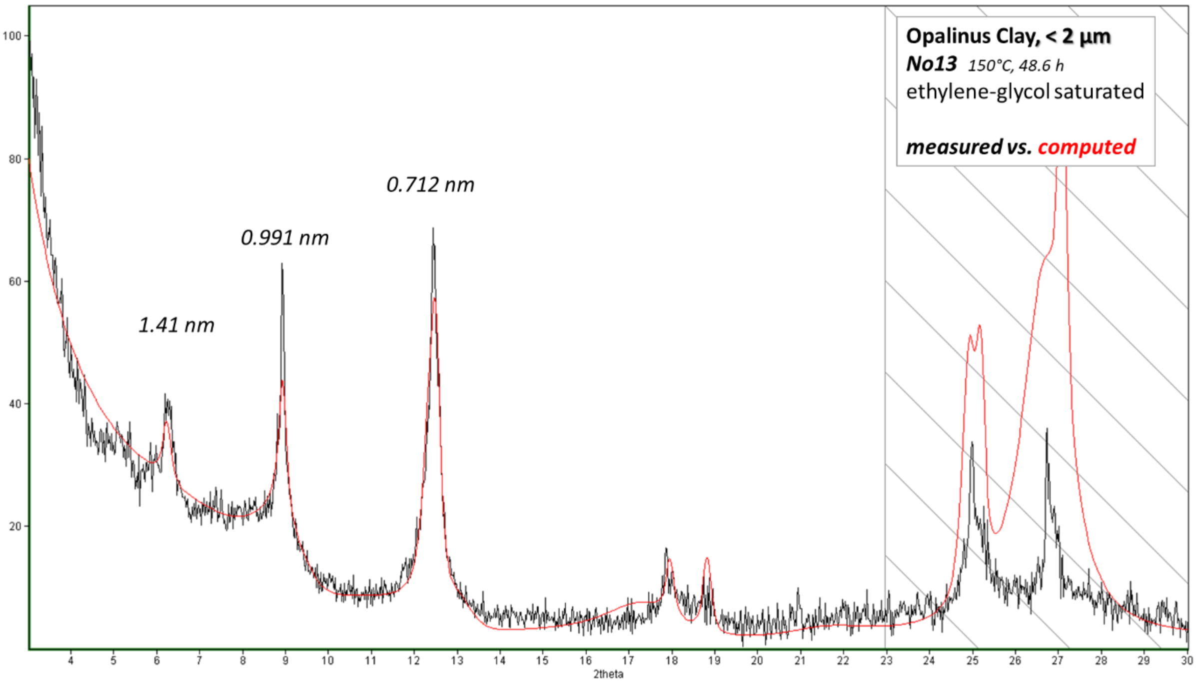

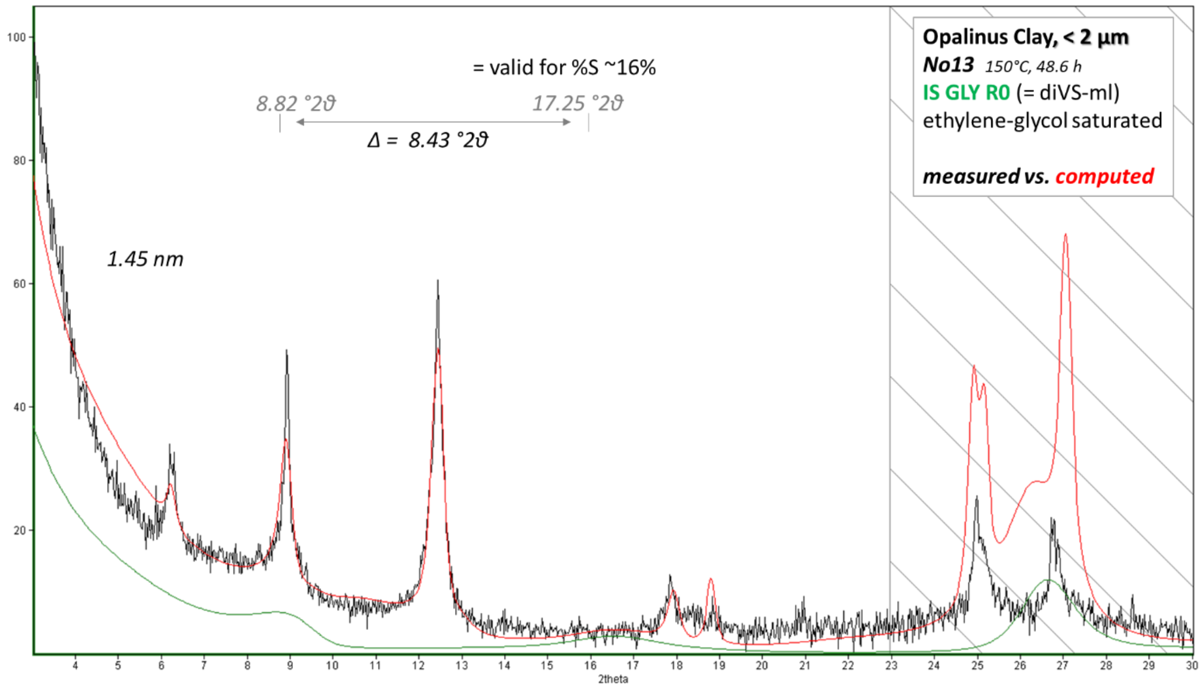
Opalinus Clay, < 2 µm
No13 150°C, 48.6 h
IS GLY R0 (= diVS-ml)
ethylene-glycol saturated
measured vs. computed
= valid for %S ~16%
8.82 °2ϑ
17.25 °2ϑ
Δ = 8.43 °2ϑ
1.45 nm
100
80
60
40
20
4
5
6
7
8
9
10
11
12
13
14
15
16
17
18
19
20
21
22
23
24
25
26
27
28
29
30
2theta

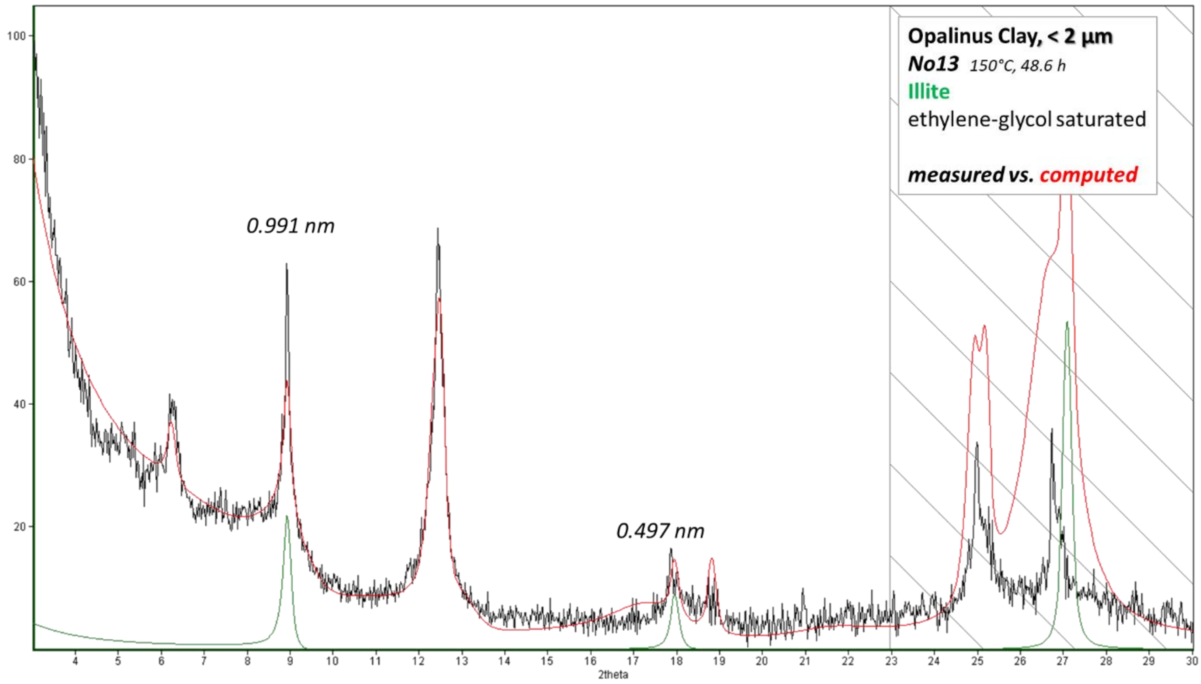
Opalinus Clay, < 2 µm
No13 150°C, 48.6 h
Illite
ethylene-glycol saturated
measured vs. computed
0.991 nm
0.497 nm
100
80
60
40
20
4
5
6
7
8
9
10
11
12
13
14
15
16
17
18
19
20
21
22
23
24
25
26
27
28
29
30
2theta

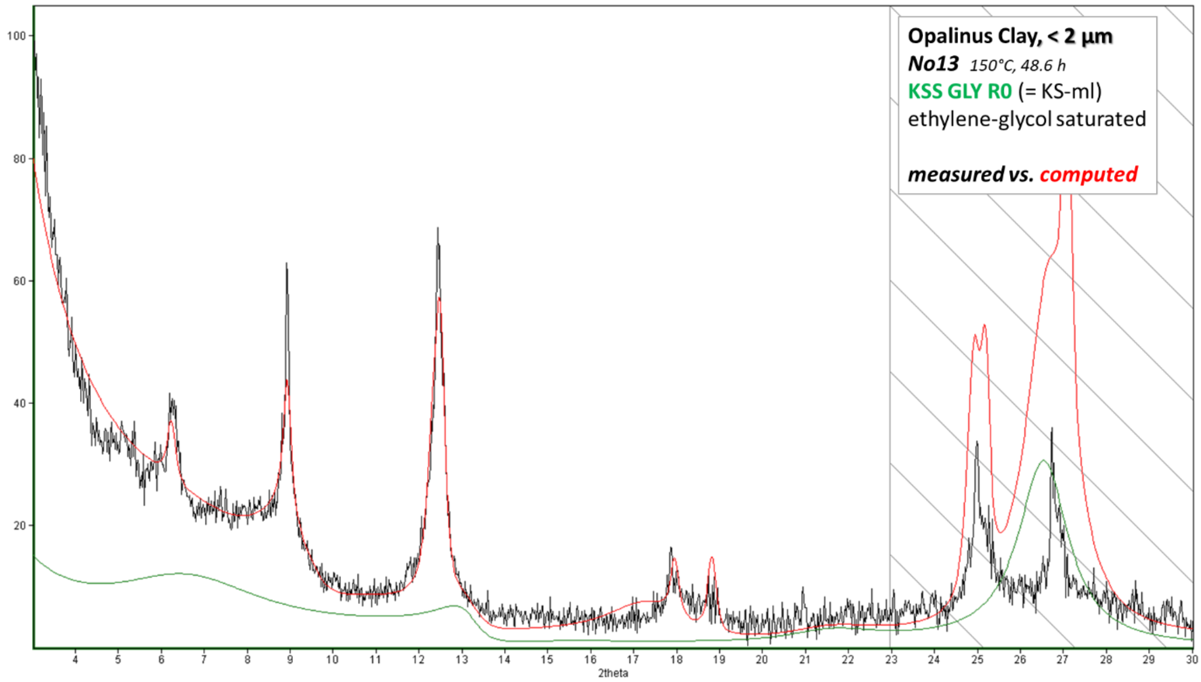
Opalinus Clay, < 2 µm
No13 *150°C, 48.6 h*
KSS GLY R0 (= KS-ml)
ethylene-glycol saturated
measured* vs. *computed
100
80
60
40
20
4
5
6
7
8
9
10
11
12
13
14
15
16
17
18
19
20
21
22
23
24
25
26
27
28
29
30
2theta

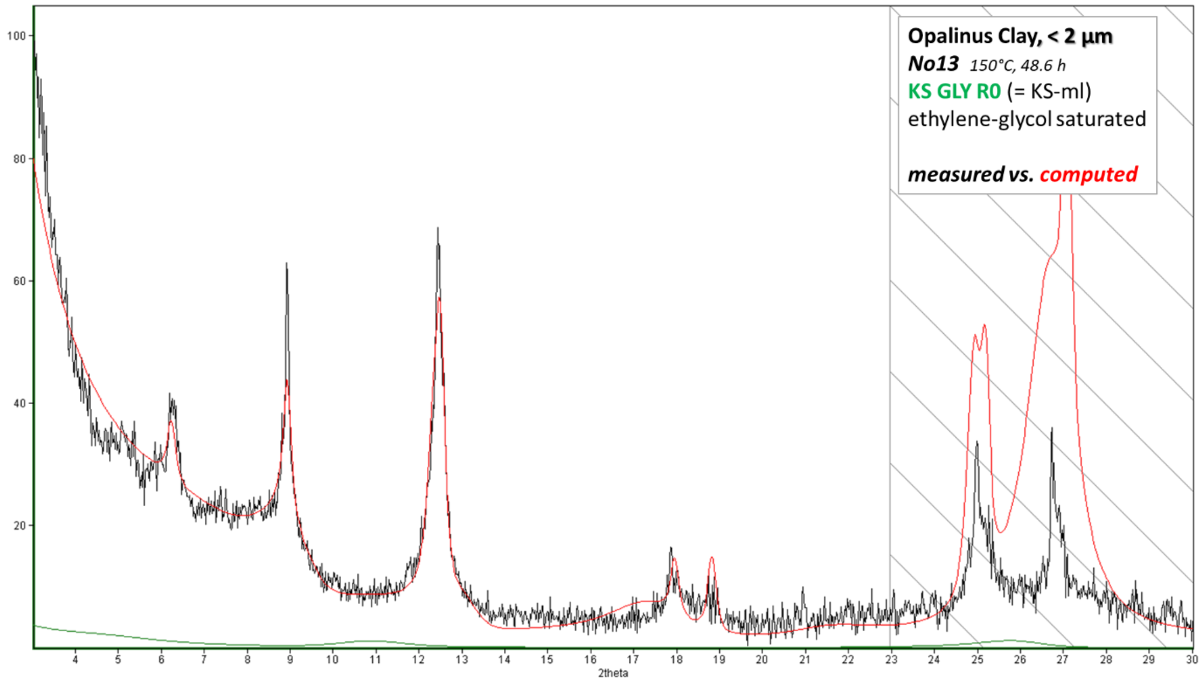
Opalinus Clay, < 2 µm
No13 *150°C, 48.6 h*
KS GLY R0 (= KS-ml)
ethylene-glycol saturated
measured* vs. *computed
100
80
60
40
20
4
5
6
7
8
9
10
11
12
13
14
15
16
17
18
19
20
21
22
23
24
25
26
27
28
29
30
2theta

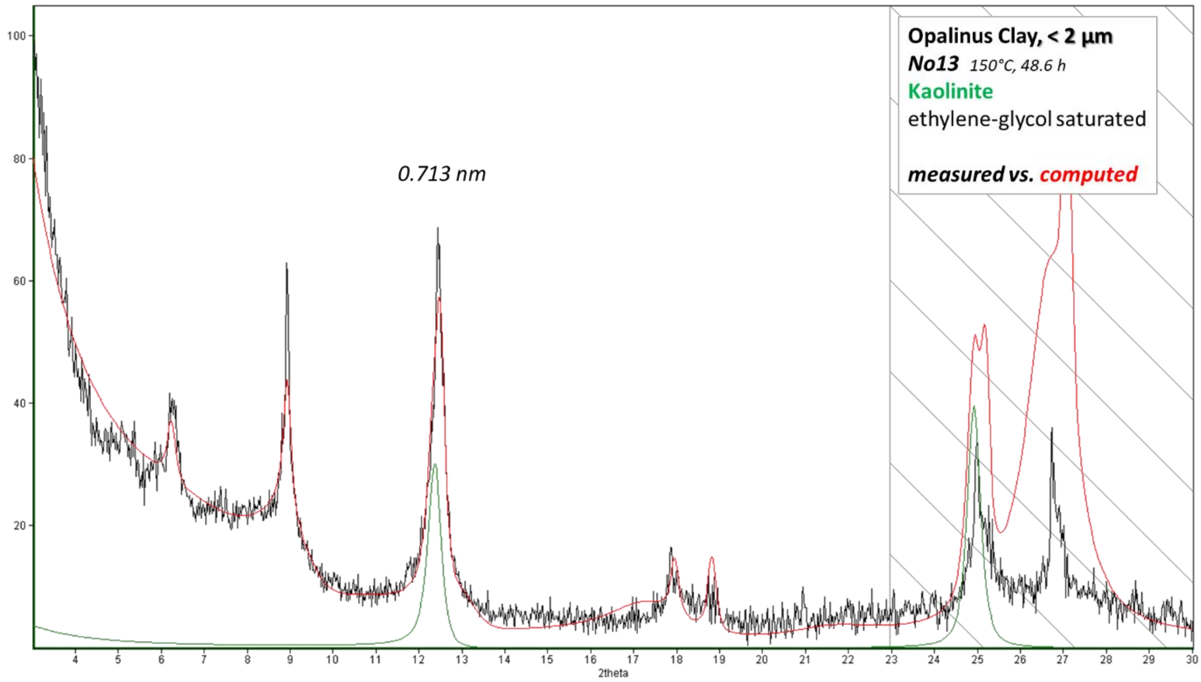
Opalinus Clay, < 2 µm
No13 150°C, 48.6 h
Kaolinite
ethylene-glycol saturated
measured vs. computed
0.713 nm
100
80
60
40
20
4
5
6
7
8
9
10
11
12
13
14
15
16
17
18
19
20
21
22
23
24
25
26
27
28
29
30
2theta

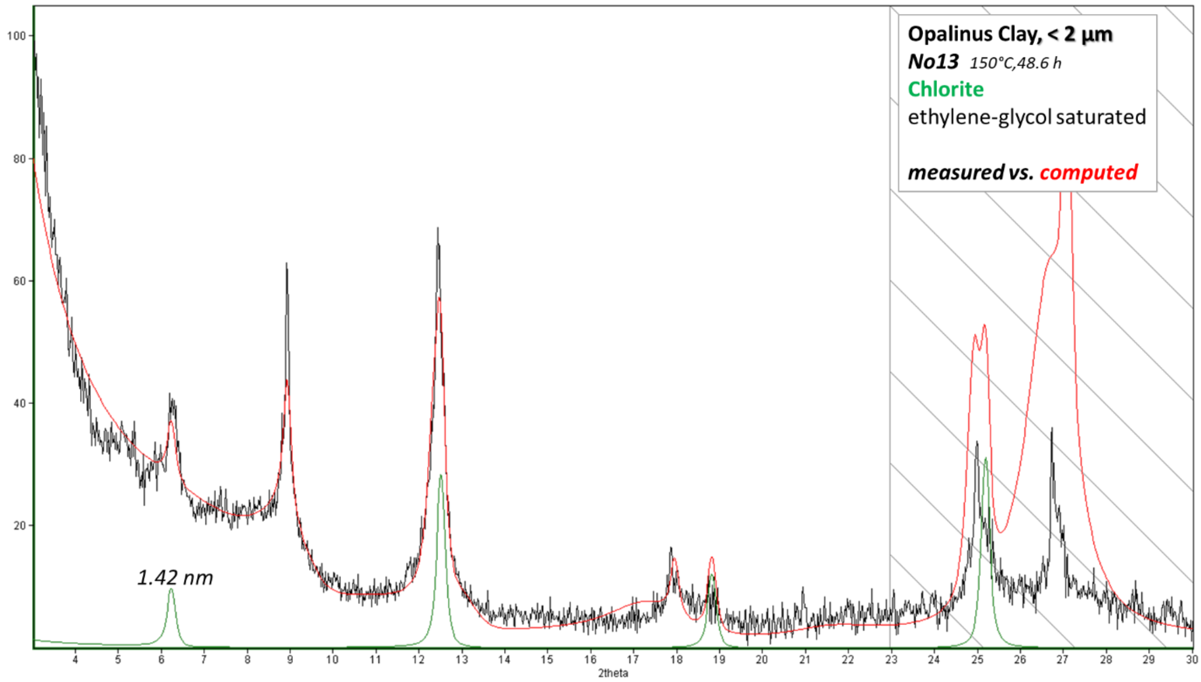
Opalinus Clay, < 2 µm
No13 150°C,48.6 h
Chlorite
ethylene-glycol saturated
measured vs. computed
1.42 nm
100
80
60
40
20
4
5
6
7
8
9
10
11
12
13
14
15
16
17
18
19
20
21
22
23
24
25
26
27
28
29
30
2theta

Data Sheet – OPALINUS No9b (< 2 µm), treated material *(125°C)*

Diffraction pattern of oriented specimen & modelling by Sybilla

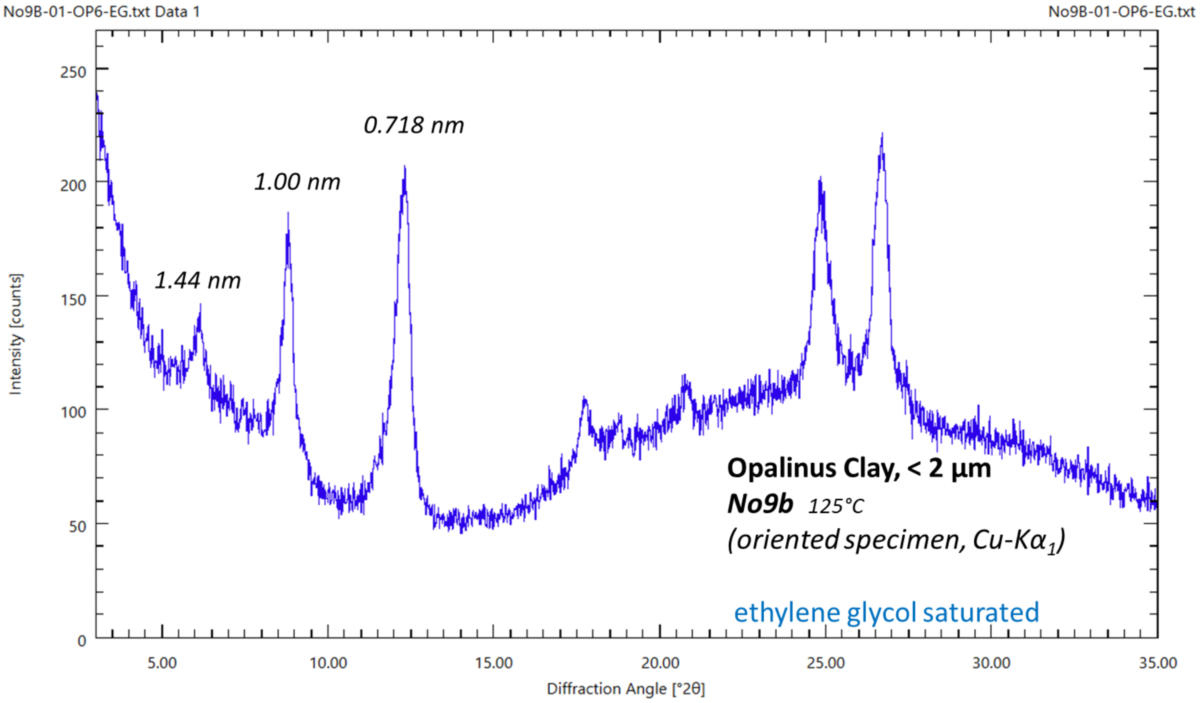

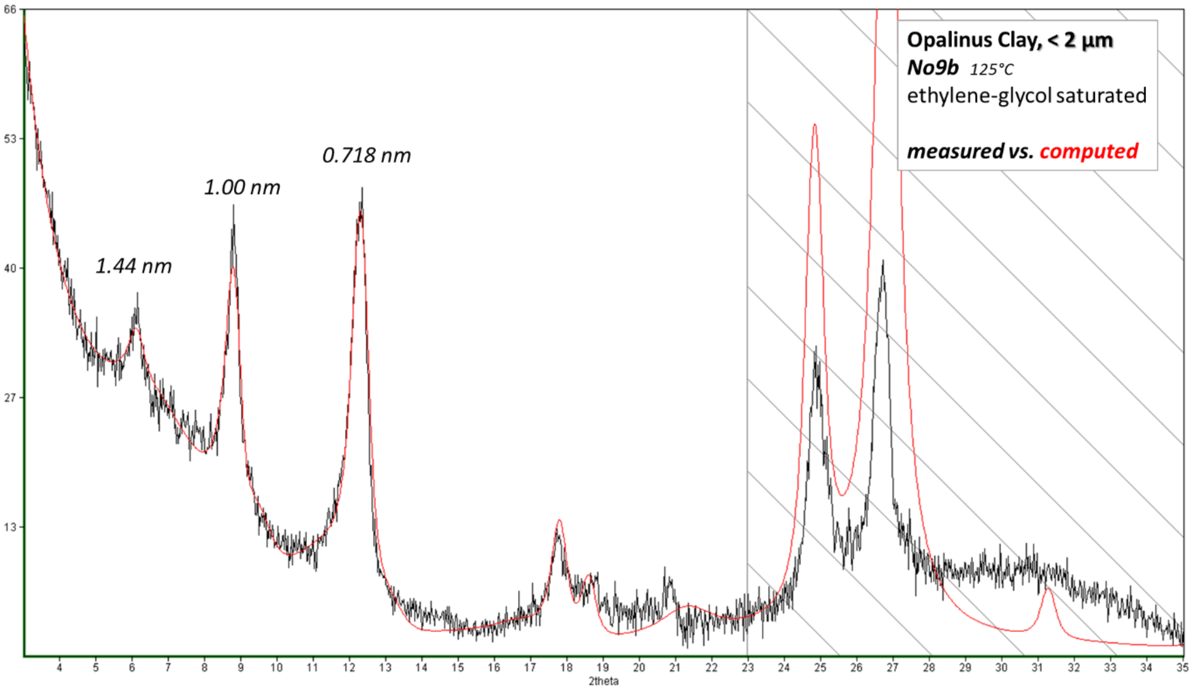

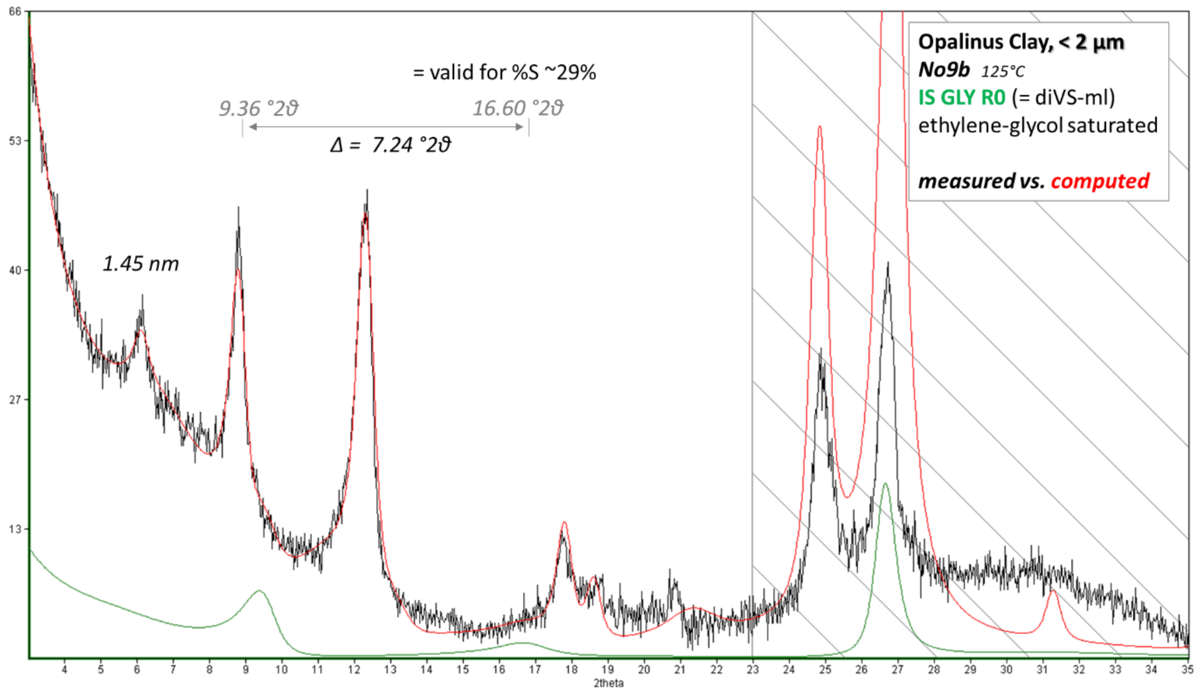
66
53
40
27
13
= valid for %S ~29%
9.36 °2ϑ
16.60 °2ϑ
Δ = 7.24 °2ϑ
1.45 nm
Opalinus Clay, < 2 µm
No9b 125°C
IS GLY R0 (= diVS-ml)
ethylene-glycol saturated
measured vs. computed
4 5 6 7 8 9 10 11 12 13 14 15 16 17 18 19 20 21 22 23 24 25 26 27 28 29 30 31 32 33 34 35
2theta

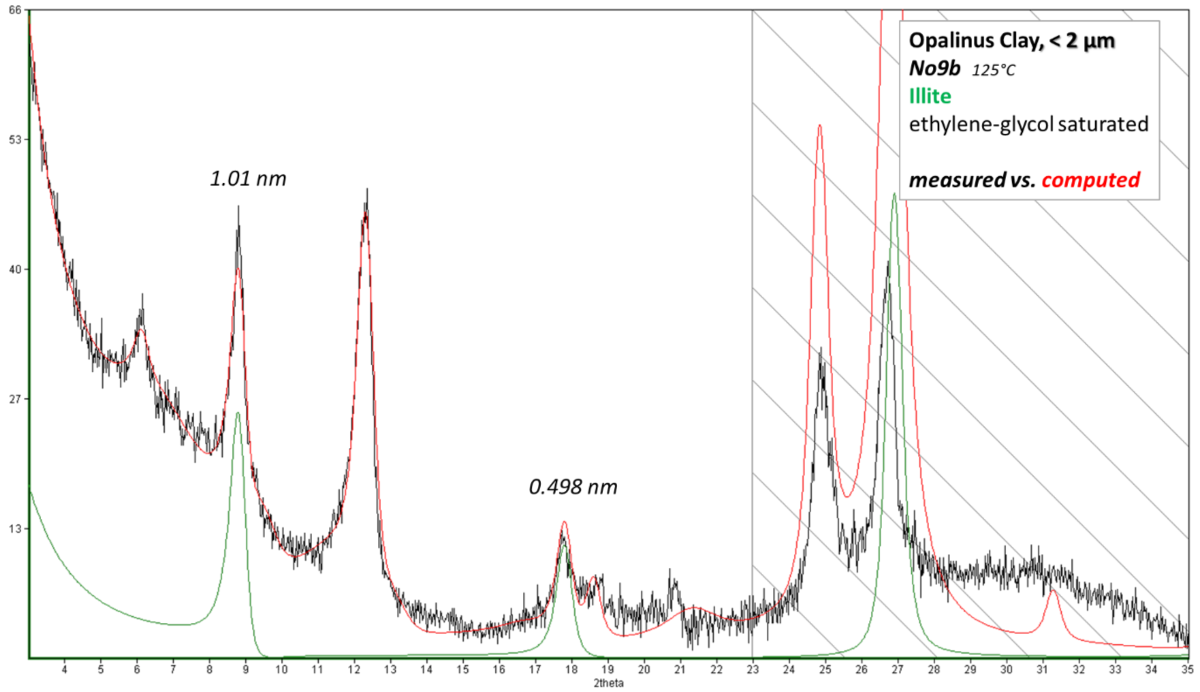
66
53
40
27
13
1.01 nm
0.498 nm
Opalinus Clay, < 2 µm
No9b 125°C
Illite
ethylene-glycol saturated
measured vs. computed
4 5 6 7 8 9 10 11 12 13 14 15 16 17 18 19 20 21 22 23 24 25 26 27 28 29 30 31 32 33 34 35
2theta

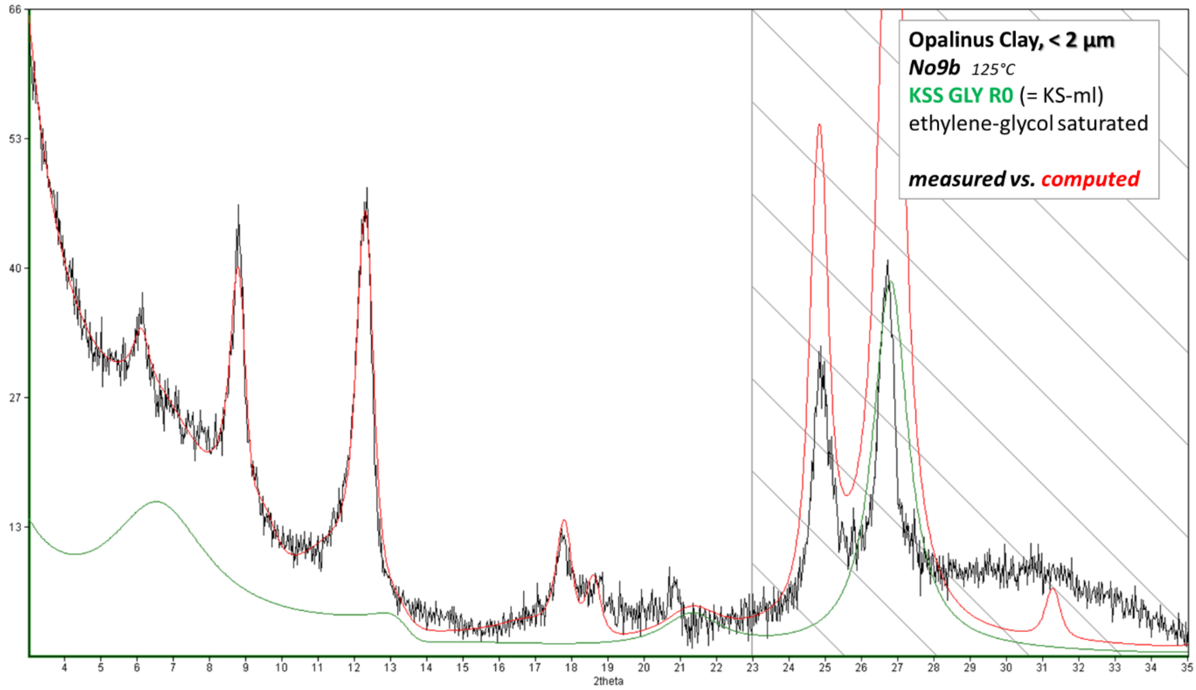
Opalinus Clay, < 2 µm
No9b 125°C
KSS GLY R0 (= KS-ml)
ethylene-glycol saturated
measured vs. computed
66
53
40
27
13
4
5
6
7
8
9
10
11
12
13
14
15
16
17
18
19
20
21
22
23
24
25
26
27
28
29
30
31
32
33
34
35
2theta

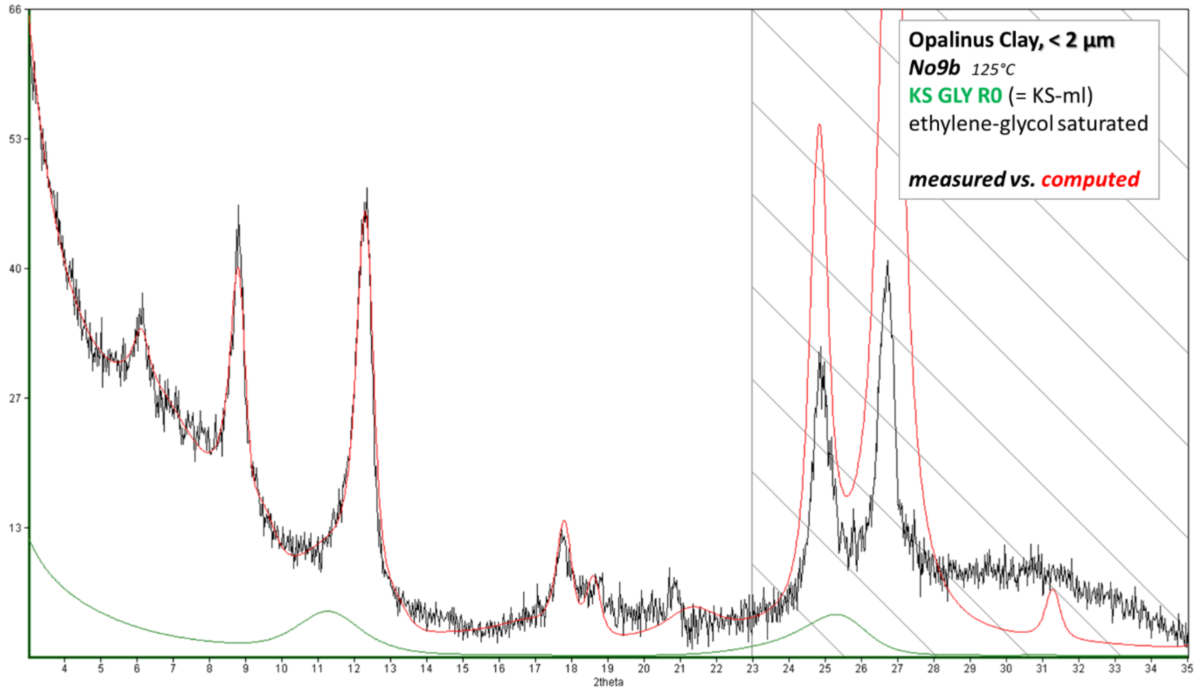
Opalinus Clay, < 2 µm
No9b 125°C
KS GLY R0 (= KS-ml)
ethylene-glycol saturated
measured vs. computed
66
53
40
27
13
4
5
6
7
8
9
10
11
12
13
14
15
16
17
18
19
20
21
22
23
24
25
26
27
28
29
30
31
32
33
34
35
2theta

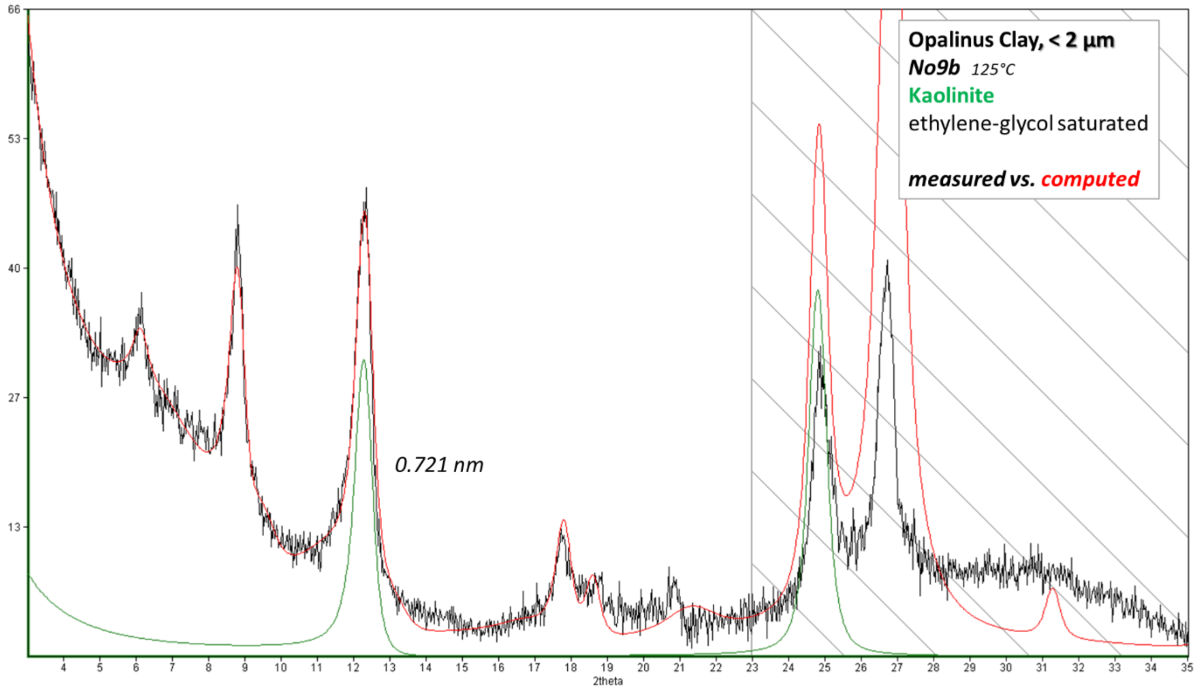
Opalinus Clay, < 2 µm
No9b *125°C*
Kaolinite
ethylene-glycol saturated
measured* vs. *computed
0.721 nm
66
53
40
27
13
4
5
6
7
8
9
10
11
12
13
14
15
16
17
18
19
20
21
22
23
24
25
26
27
28
29
30
31
32
33
34
35
2theta

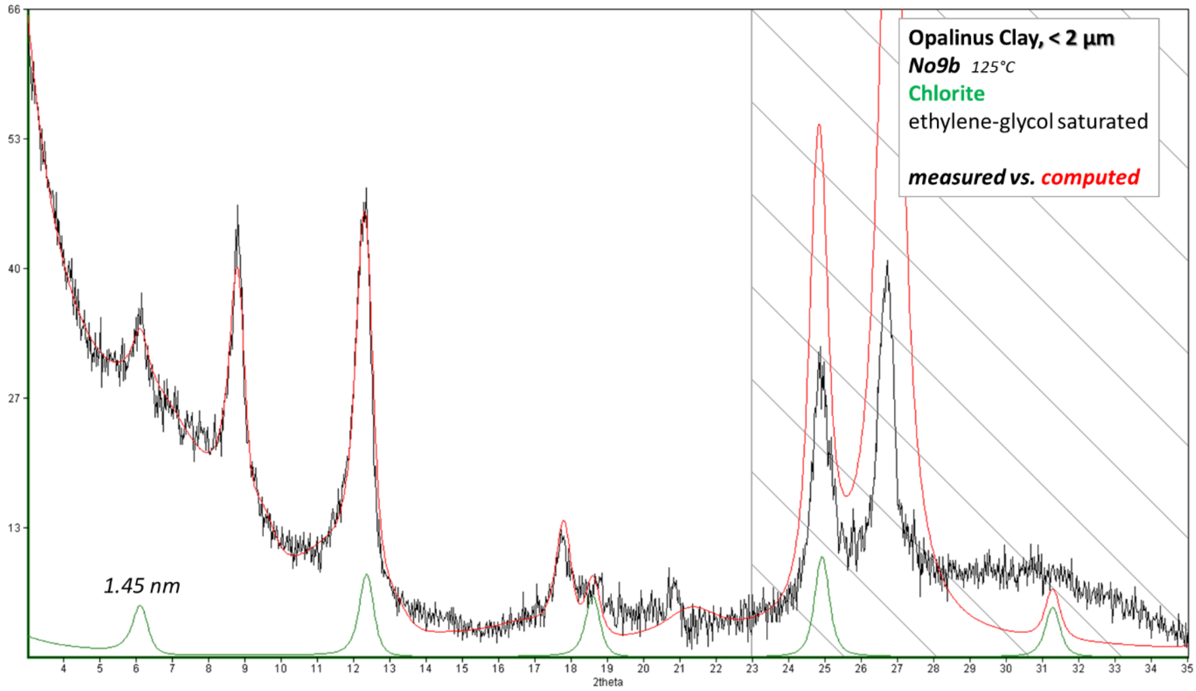
Opalinus Clay, < 2 µm
No9b *125°C*
Chlorite
ethylene-glycol saturated
measured* vs. *computed
1.45 nm
66
53
40
27
13
4
5
6
7
8
9
10
11
12
13
14
15
16
17
18
19
20
21
22
23
24
25
26
27
28
29
30
31
32
33
34
35
2theta

Data Sheet – FRIEDLAND (< 2 µm), all experiments

Diffraction pattern of oriented specimen & modelling by Sybilla

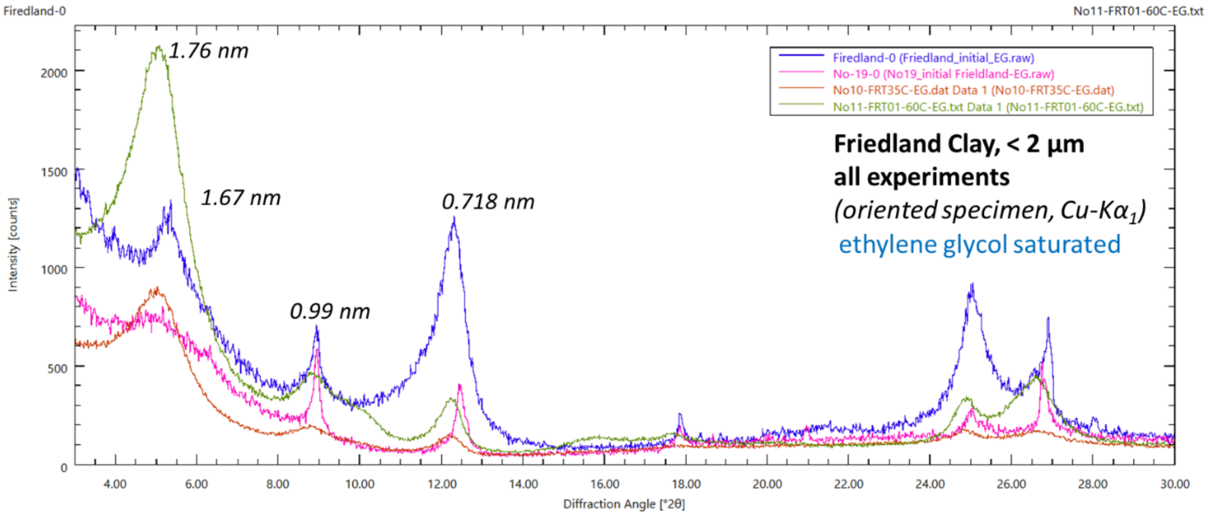

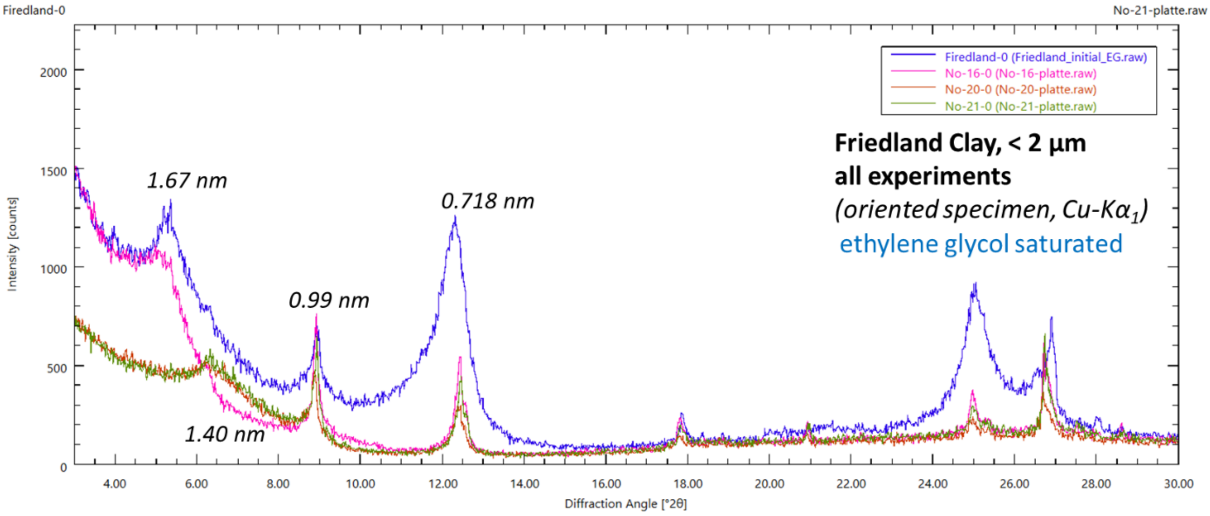

Data Sheet – FRIEDLAND (< 2 µm), untreated material

Diffraction pattern of oriented specimen & modelling by Sybilla

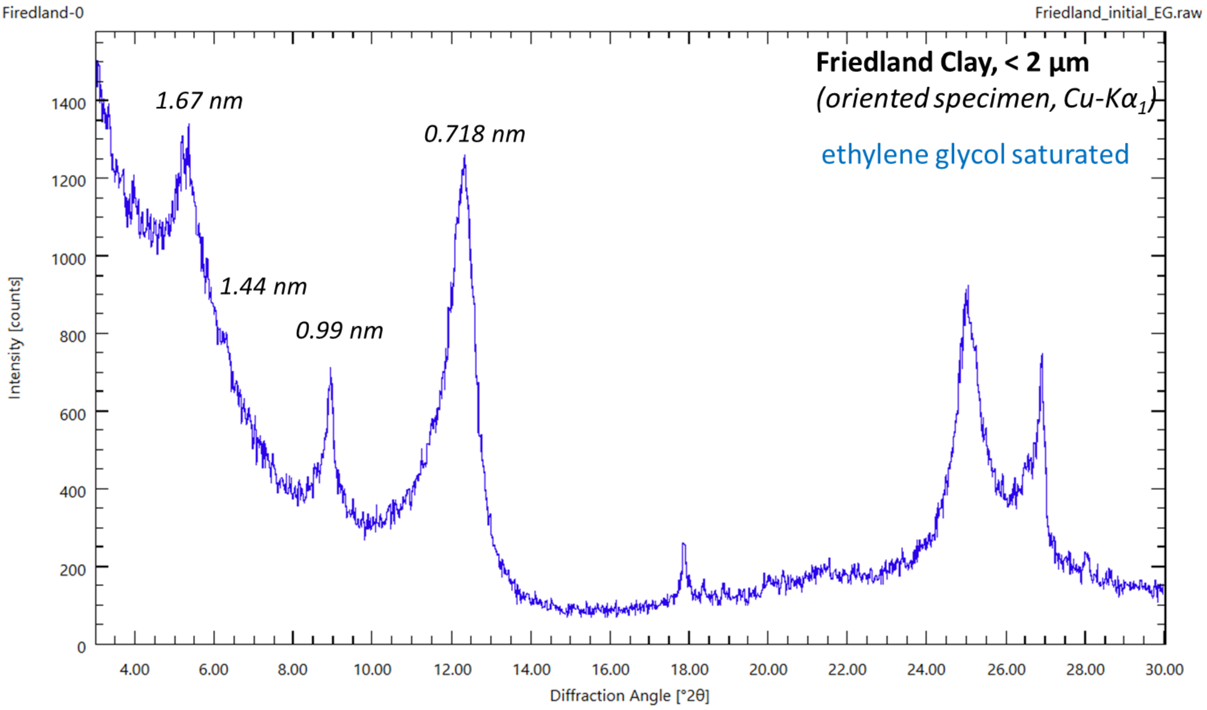

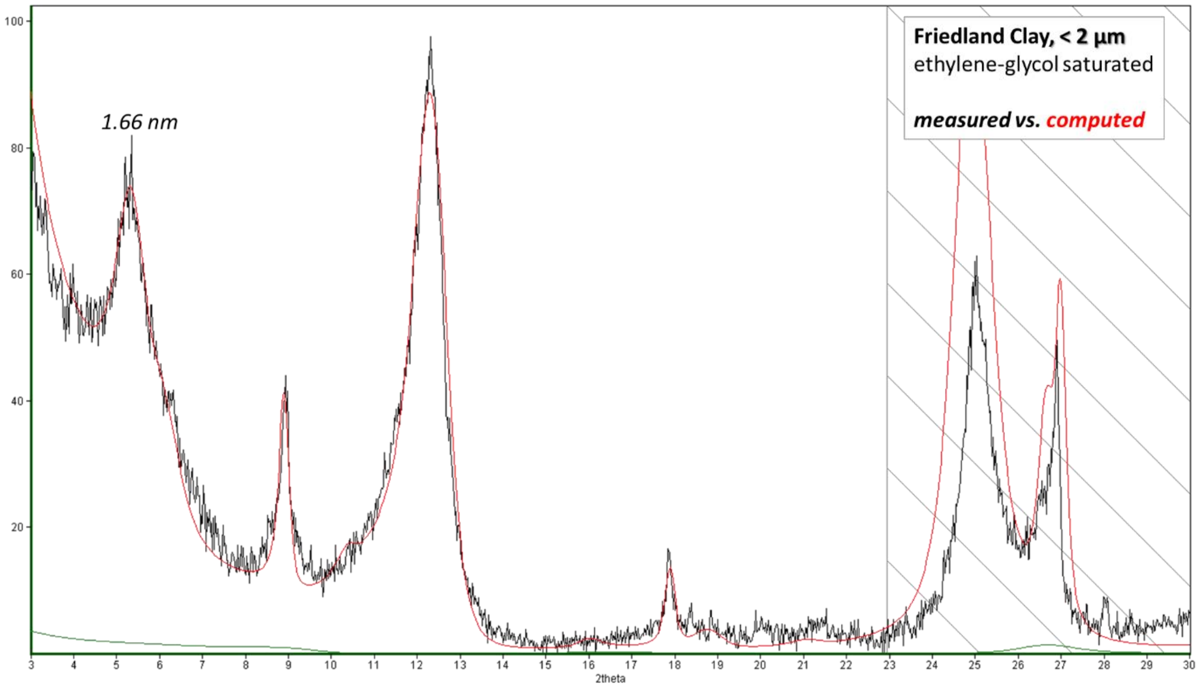

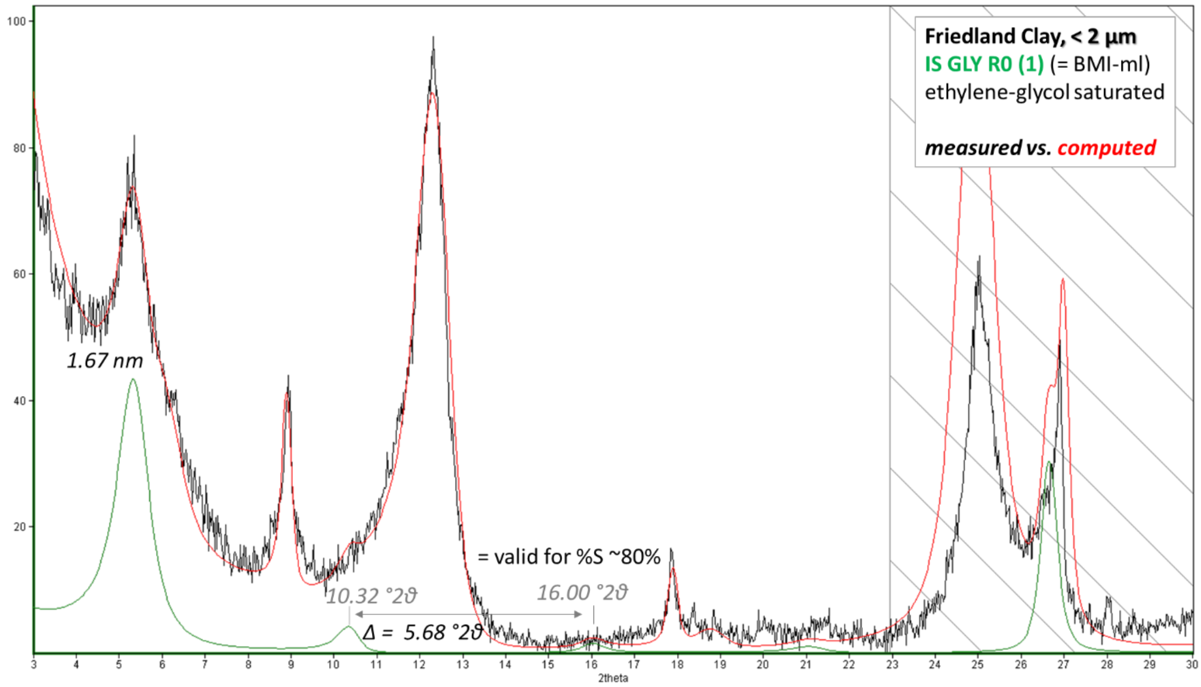

Friedland Clay, < 2 µm
IS GLY R0 (1) (= BMI-ml)
ethylene-glycol saturated
measured vs. computed
1.67 nm
= valid for %S ~80%
10.32 °2ϑ
16.00 °2ϑ
Δ = 5.68 °2ϑ
100
80
60
40
20
3
4
5
6
7
8
9
10
11
12
13
14
15
16
17
18
19
20
21
22
23
24
25
26
27
28
29
30
2theta

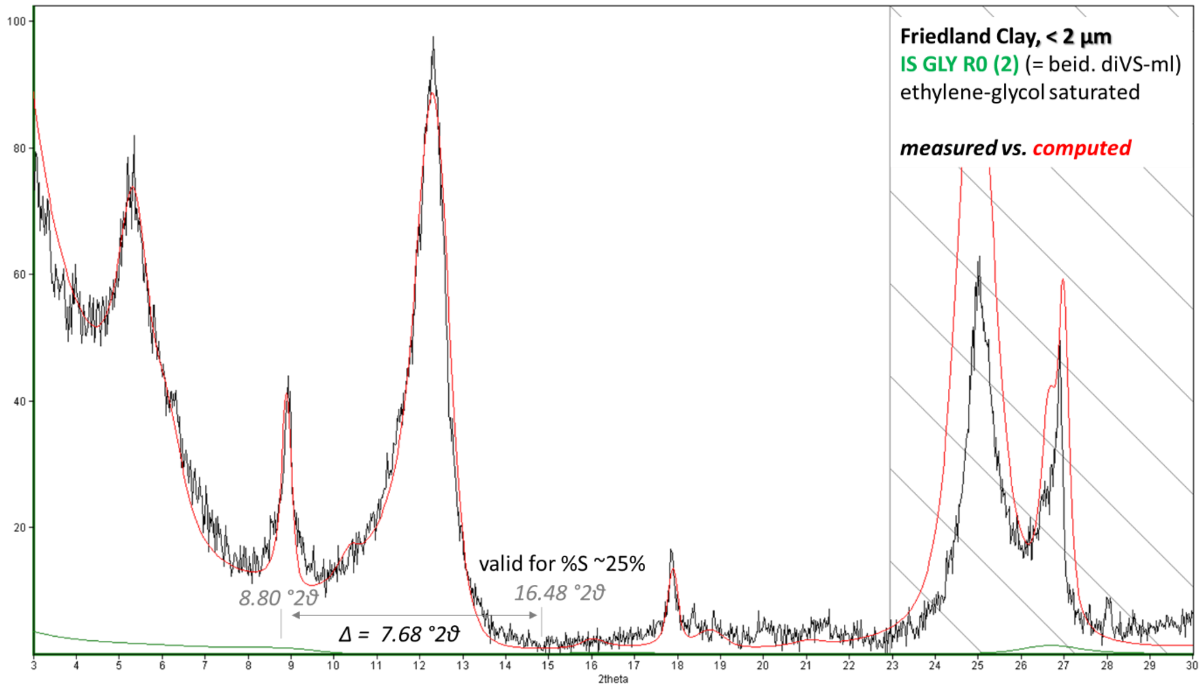

Friedland Clay, < 2 µm
IS GLY R0 (2) (= beid. diVS-ml)
ethylene-glycol saturated
measured vs. computed
valid for %S ~25%
8.80 °2ϑ
16.48 °2ϑ
Δ = 7.68 °2ϑ
100
80
60
40
20
3
4
5
6
7
8
9
10
11
12
13
14
15
16
17
18
19
20
21
22
23
24
25
26
27
28
29
30
2theta

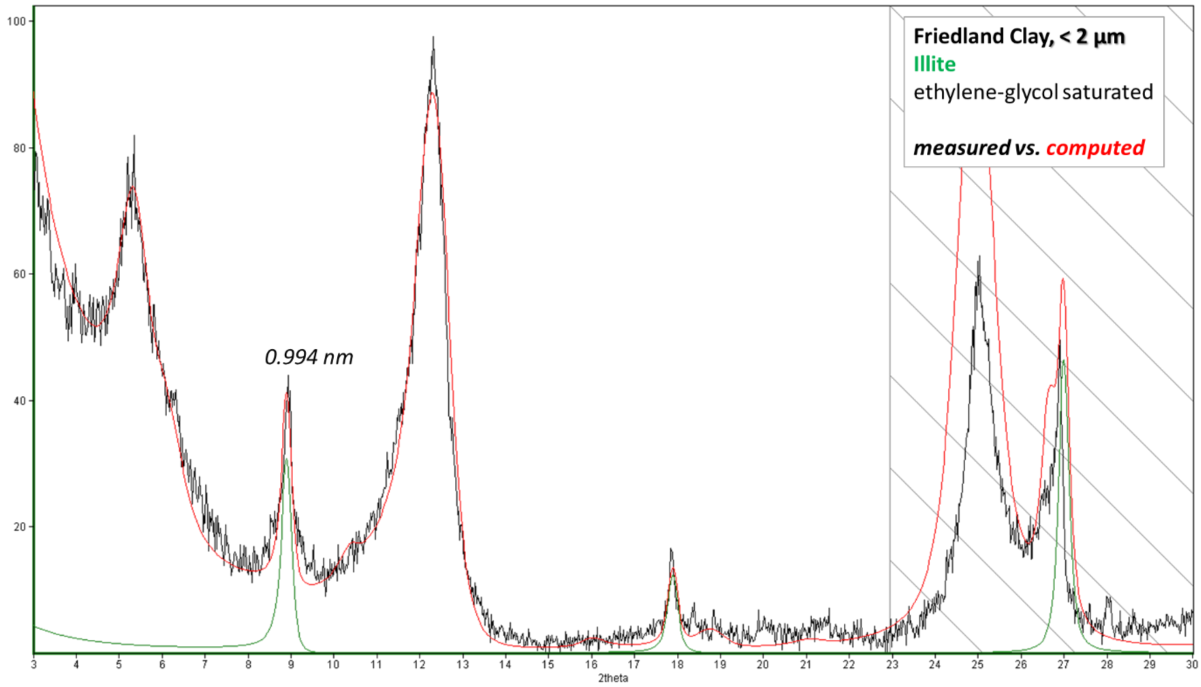
Friedland Clay, < 2 µm
Illite
ethylene-glycol saturated
measured vs. computed
0.994 nm
100
80
60
40
20
3 4 5 6 7 8 9 10 11 12 13 14 15 16 17 18 19 20 21 22 23 24 25 26 27 28 29 30
2theta

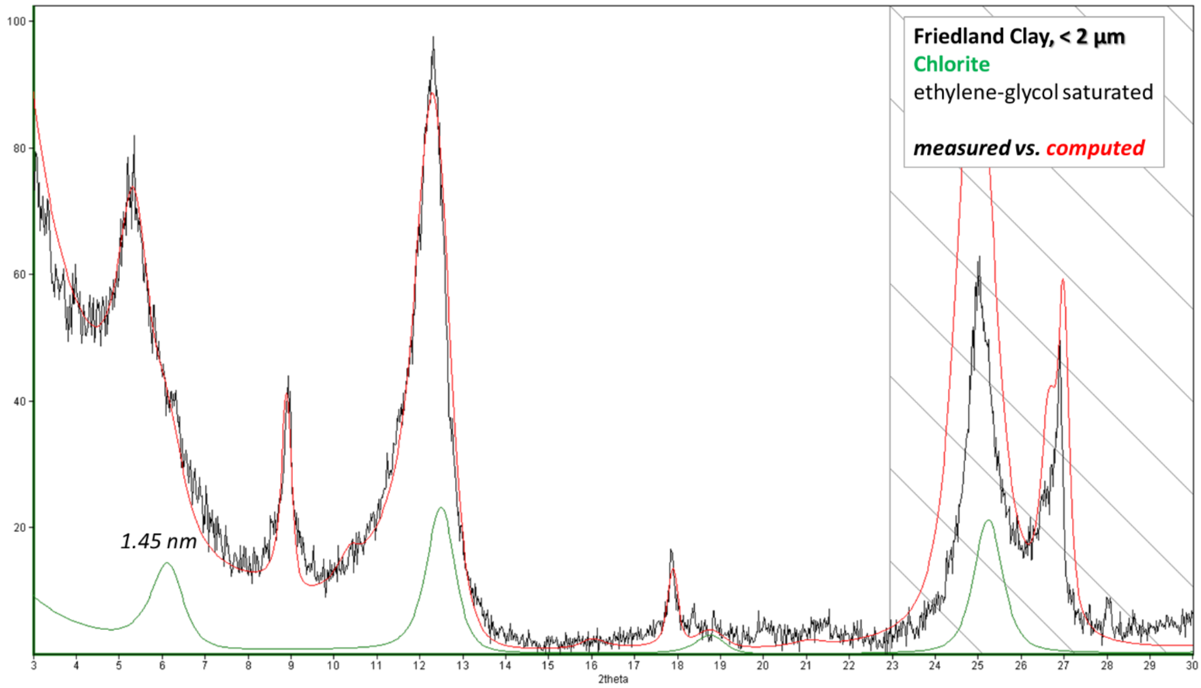
Friedland Clay, < 2 µm
Chlorite
ethylene-glycol saturated
measured vs. computed
1.45 nm
100
80
60
40
20
3 4 5 6 7 8 9 10 11 12 13 14 15 16 17 18 19 20 21 22 23 24 25 26 27 28 29 30
2theta

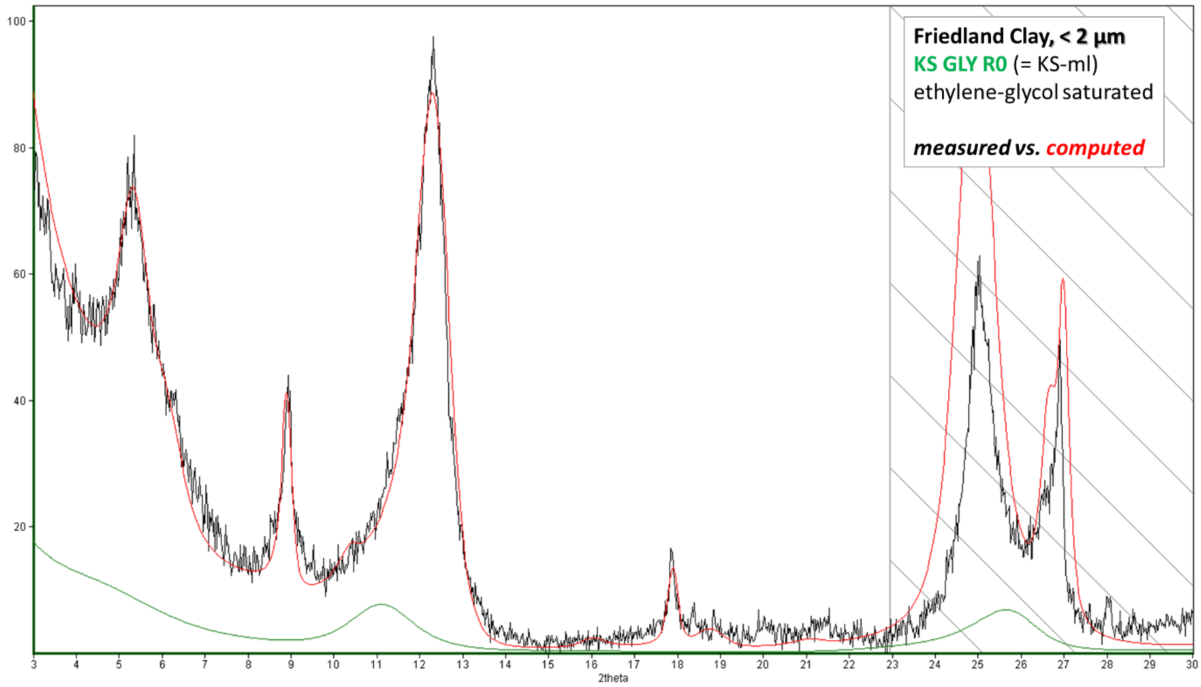
Friedland Clay, < 2 µm
KS GLY R0 (= KS-ml)
ethylene-glycol saturated
measured* vs. *computed
100
80
60
40
20
3
4
5
6
7
8
9
10
11
12
13
14
15
16
17
18
19
20
21
22
23
24
25
26
27
28
29
30
2theta

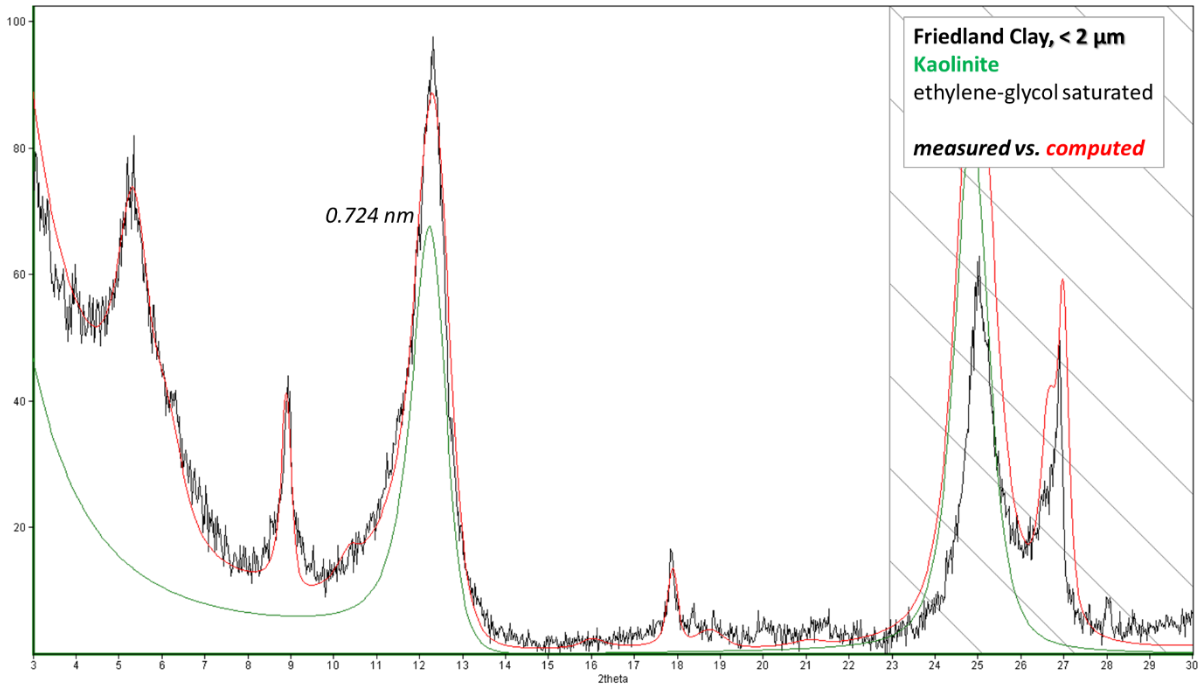
Friedland Clay, < 2 µm
Kaolinite
ethylene-glycol saturated
measured* vs. *computed
0.724 nm
100
80
60
40
20
3
4
5
6
7
8
9
10
11
12
13
14
15
16
17
18
19
20
21
22
23
24
25
26
27
28
29
30
2theta

Data Sheet – FRIEDLAND No19 (< 2 µm), compacted material *(untreated)*

Diffraction pattern of oriented specimen & modelling by Sybilla

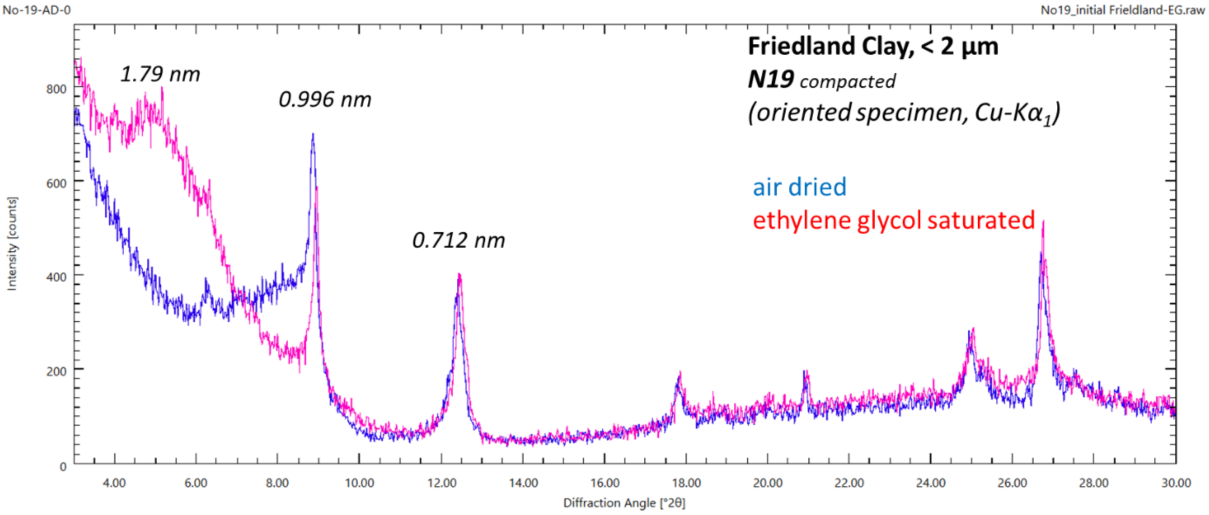

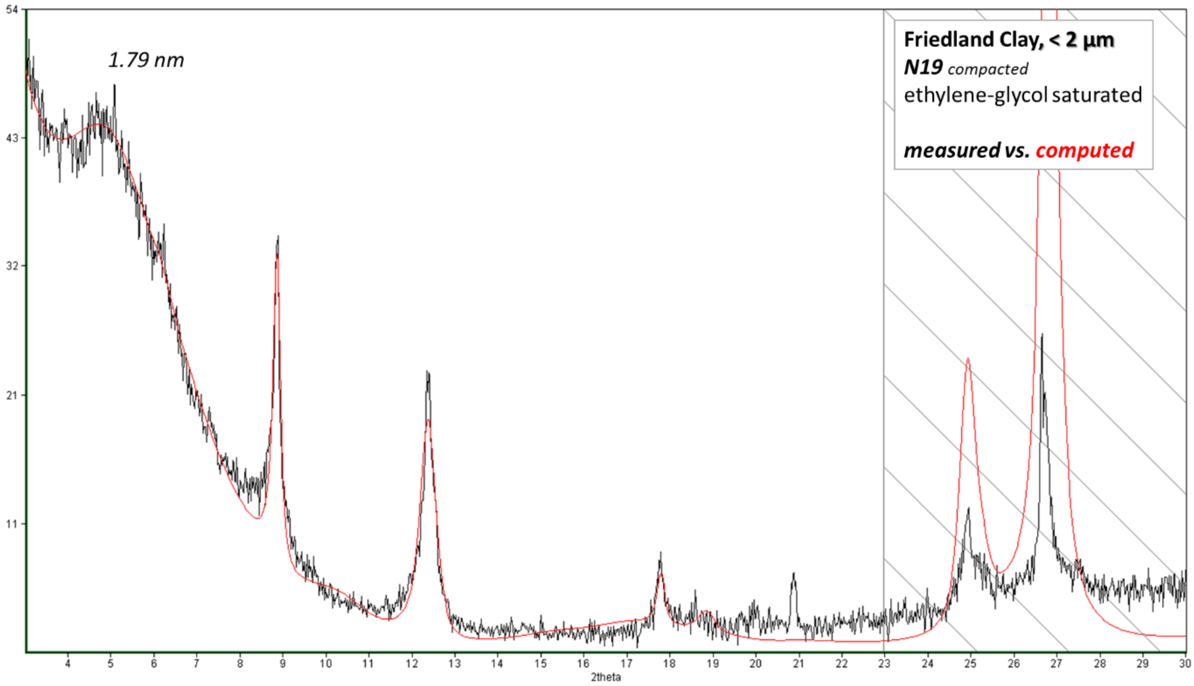

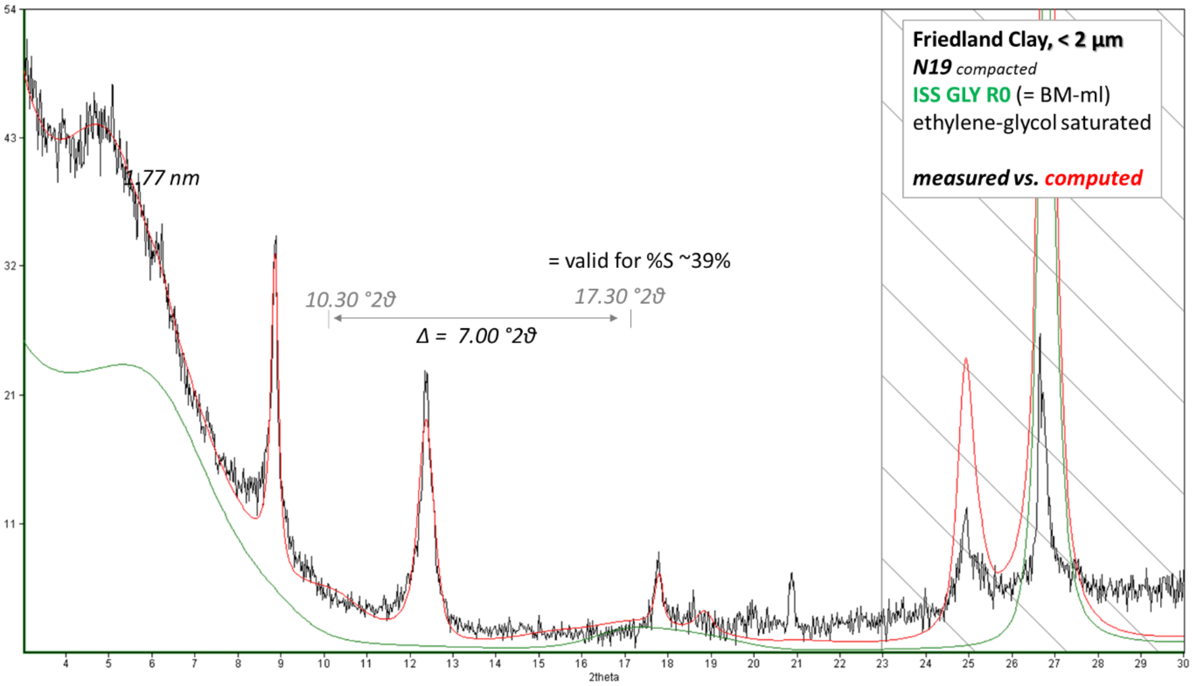
Friedland Clay, < 2 µm
N19 *compacted*
ISS GLY R0 (= BM-ml)
ethylene-glycol saturated
measured vs. computed
1.77 nm
= valid for %S ~39%
10.30 °2ϑ
17.30 °2ϑ
Δ = 7.00 °2ϑ
54
43
32
21
11
4
5
6
7
8
9
10
11
12
13
14
15
16
17
18
19
20
21
22
23
24
25
26
27
28
29
30
2theta

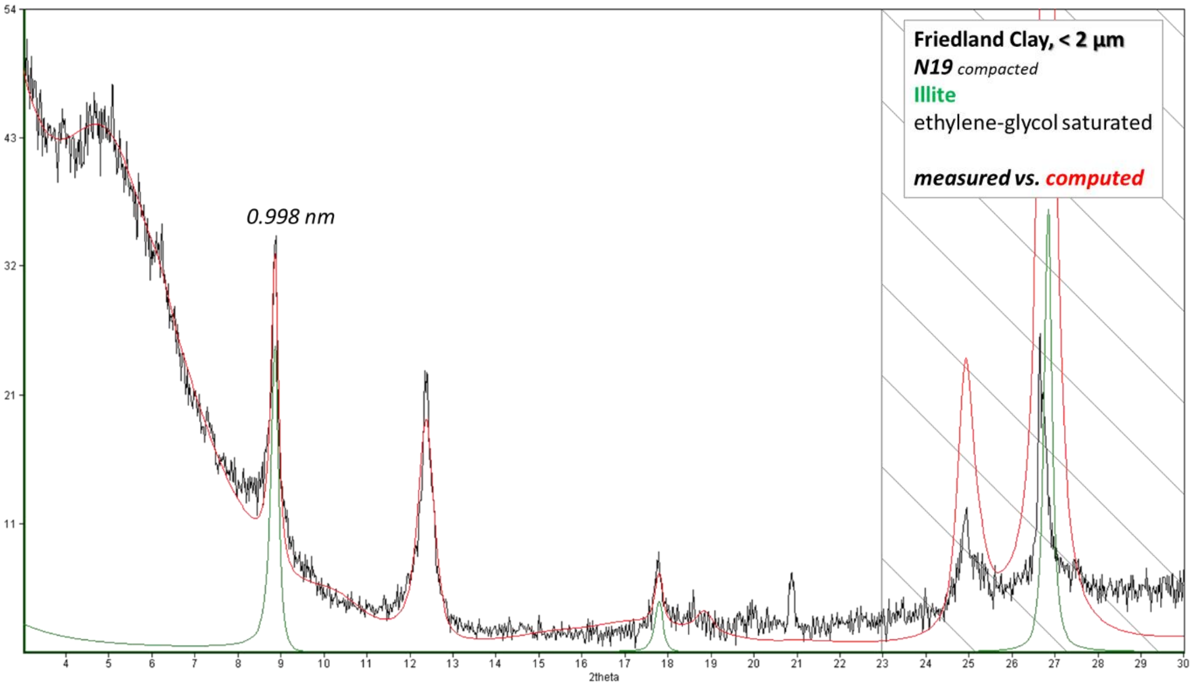
Friedland Clay, < 2 µm
N19 *compacted*
Illite
ethylene-glycol saturated
measured vs. computed
0.998 nm
54
43
32
21
11
4
5
6
7
8
9
10
11
12
13
14
15
16
17
18
19
20
21
22
23
24
25
26
27
28
29
30
2theta

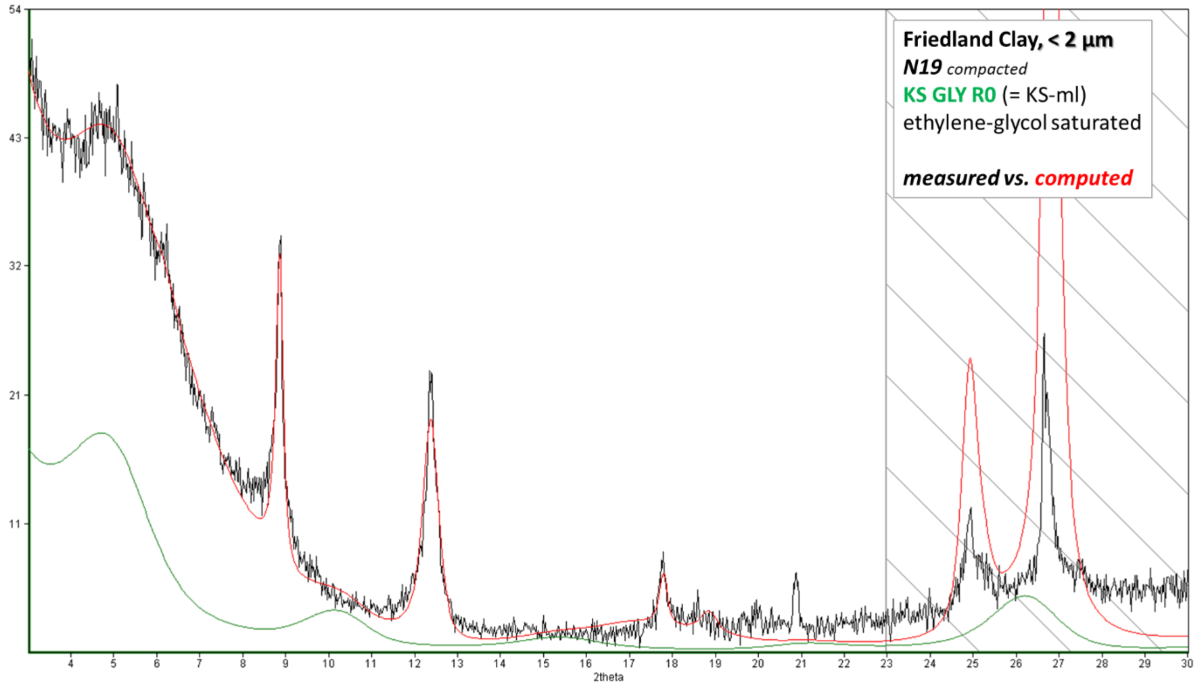
Friedland Clay, < 2 µm
N19 compacted
KS GLY R0 (= KS-ml)
ethylene-glycol saturated
measured vs. computed
54
43
32
21
11
4 5 6 7 8 9 10 11 12 13 14 15 16 17 18 19 20 21 22 23 24 25 26 27 28 29 30
2theta

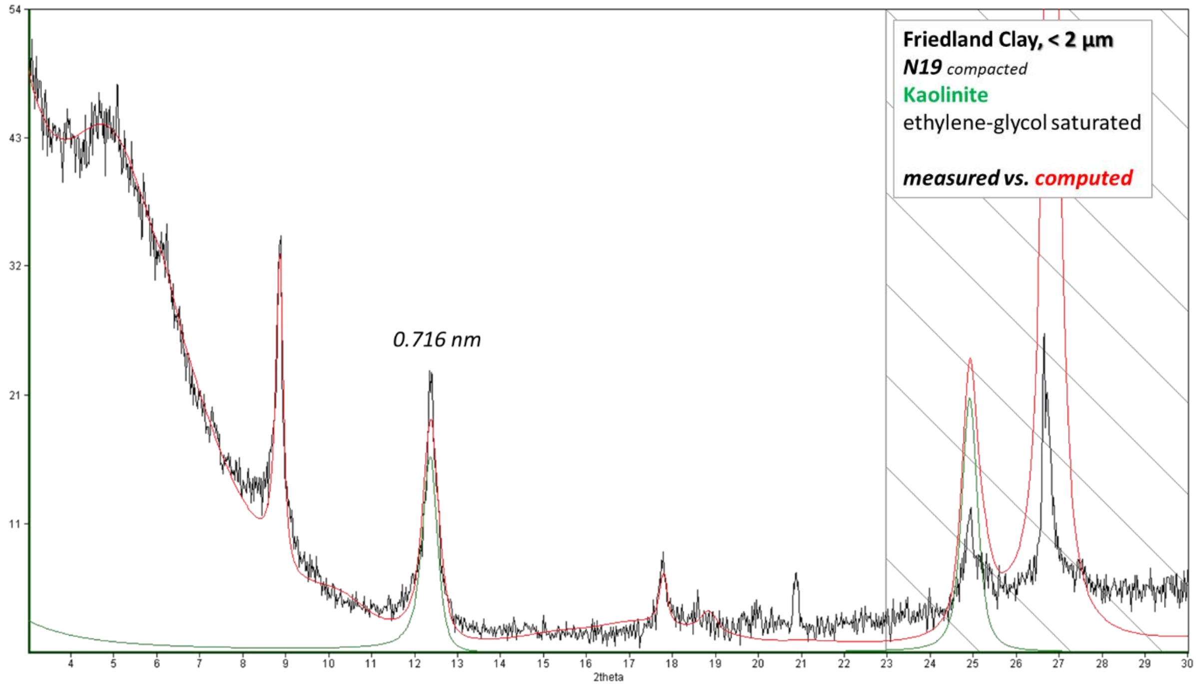
Friedland Clay, < 2 µm
N19 compacted
Kaolinite
ethylene-glycol saturated
measured vs. computed
0.716 nm
54
43
32
21
11
4 5 6 7 8 9 10 11 12 13 14 15 16 17 18 19 20 21 22 23 24 25 26 27 28 29 30
2theta

Data Sheet – FRIEDLAND No10 (< 2 µm), treated material *(35°C)*

Diffraction pattern of oriented specimen & modelling by Sybilla

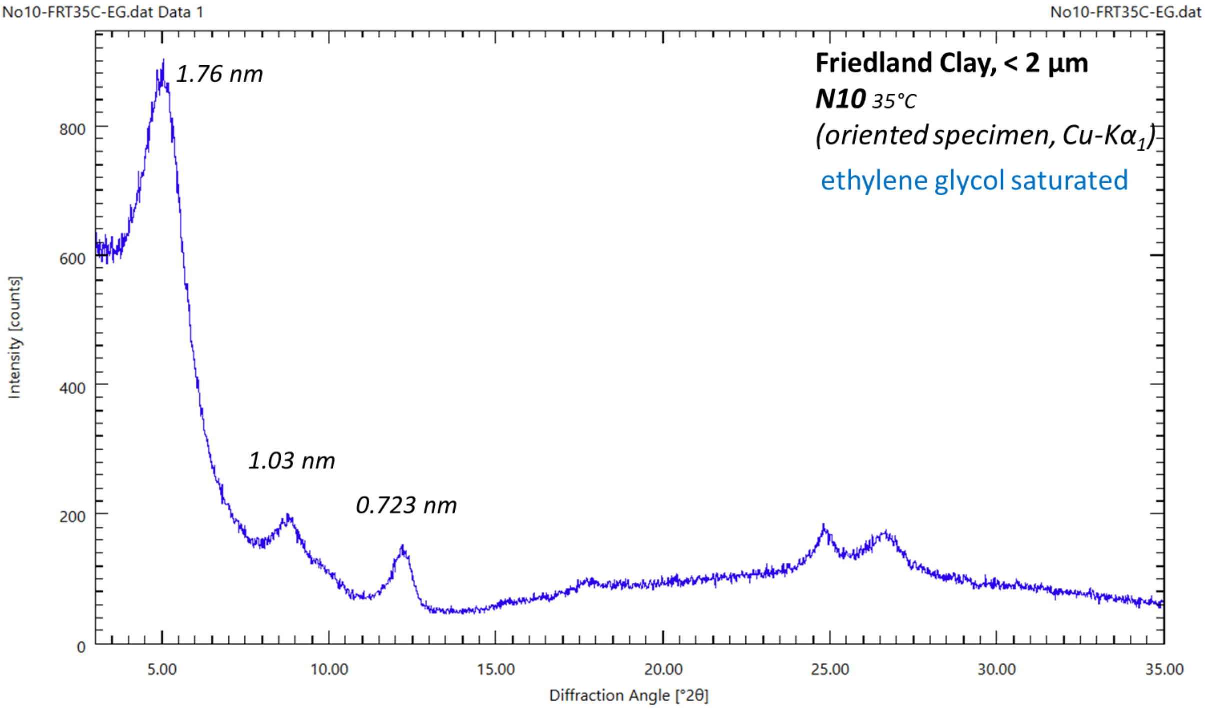

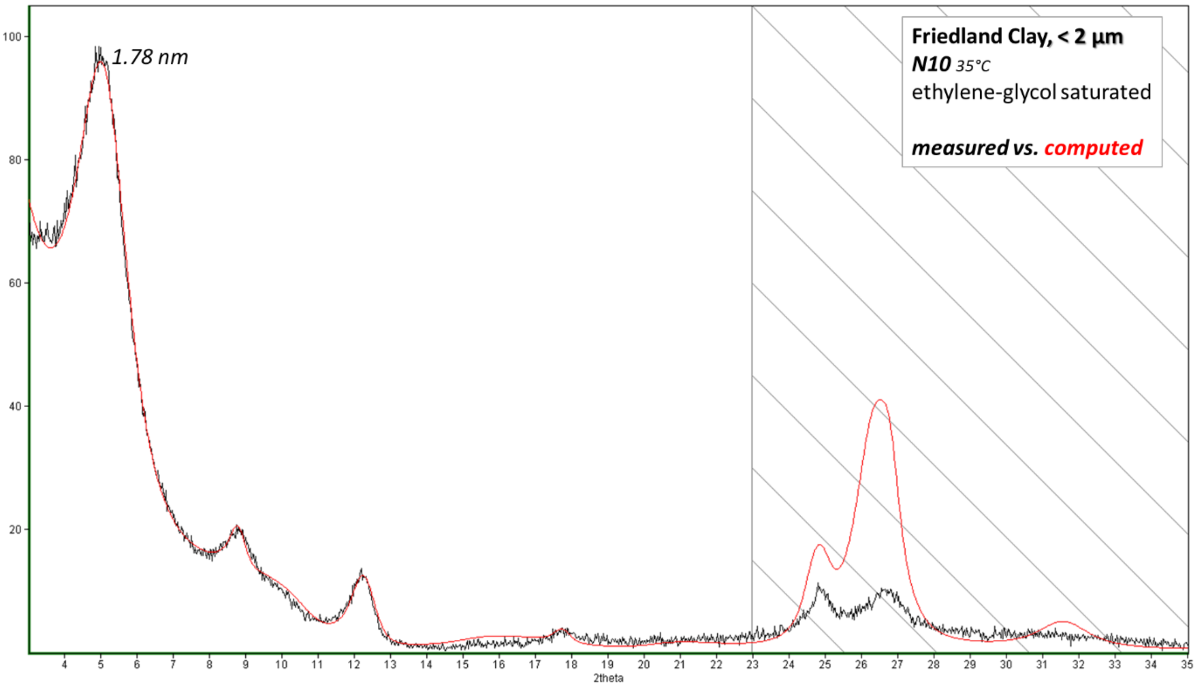

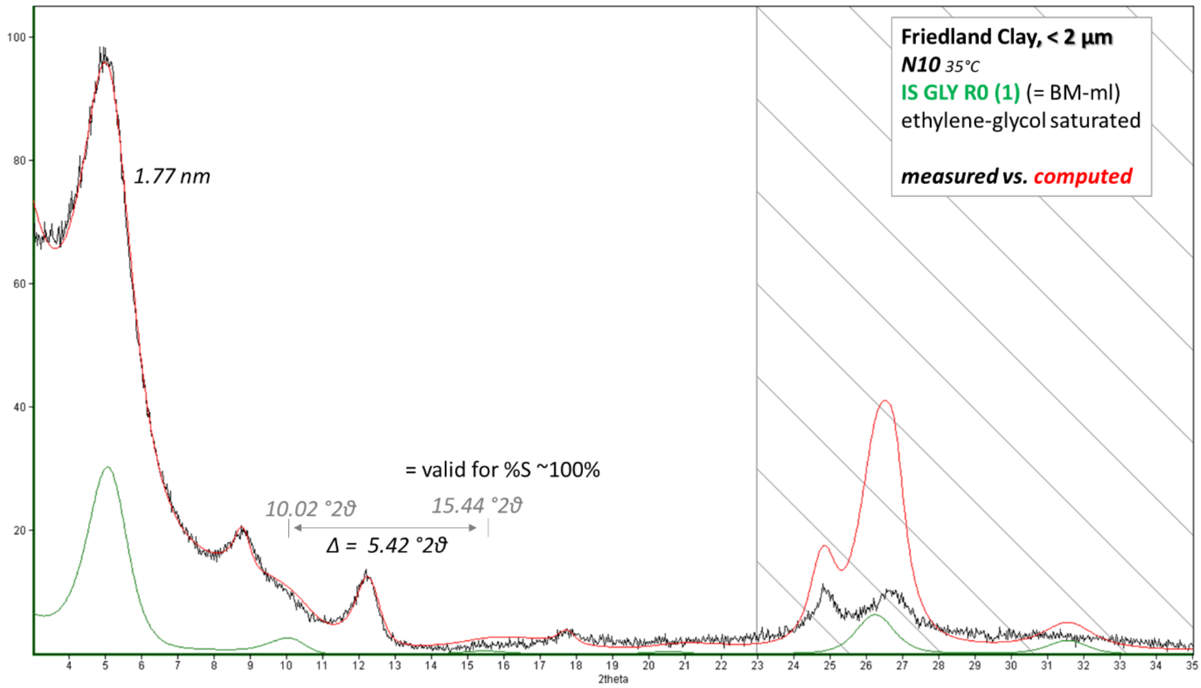
Friedland Clay, < 2 µm
N10 35°C
IS GLY R0 (1) (= BM-ml)
ethylene-glycol saturated
measured vs. computed
1.77 nm
= valid for %S ~100%
10.02 °2ϑ
15.44 °2ϑ
Δ = 5.42 °2ϑ
100
80
60
40
20
4 5 6 7 8 9 10 11 12 13 14 15 16 17 18 19 20 21 22 23 24 25 26 27 28 29 30 31 32 33 34 35
2theta

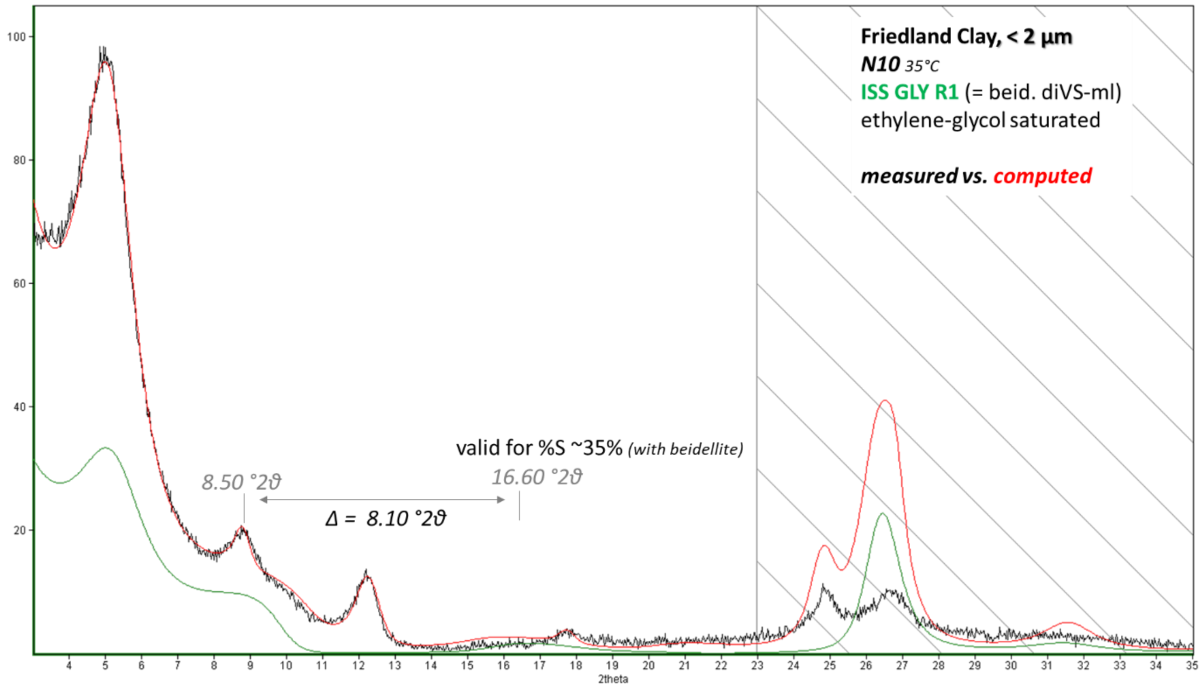
Friedland Clay, < 2 µm
N10 35°C
ISS GLY R1 (= beid. diVS-ml)
ethylene-glycol saturated
measured vs. computed
valid for %S ~35% (with beidellite)
8.50 °2ϑ
16.60 °2ϑ
Δ = 8.10 °2ϑ
100
80
60
40
20
4 5 6 7 8 9 10 11 12 13 14 15 16 17 18 19 20 21 22 23 24 25 26 27 28 29 30 31 32 33 34 35
2theta

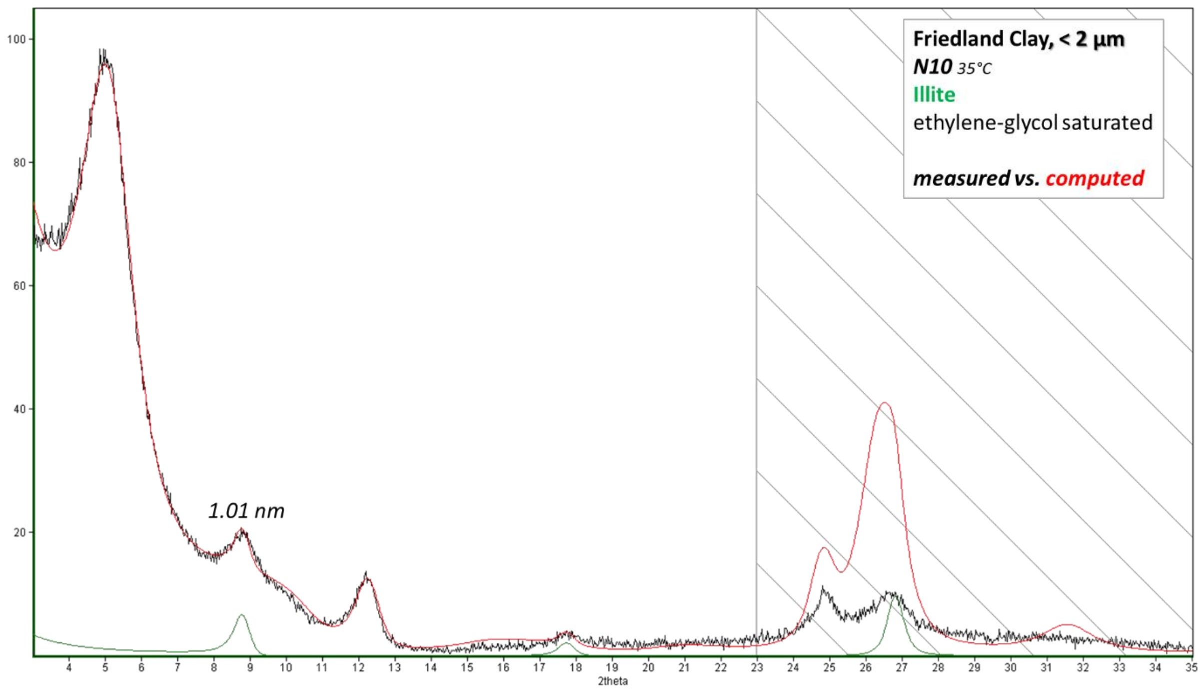
Friedland Clay, < 2 µm
N10 35°C
Illite
ethylene-glycol saturated
measured vs. computed
1.01 nm
100
80
60
40
20
4 5 6 7 8 9 10 11 12 13 14 15 16 17 18 19 20 21 22 23 24 25 26 27 28 29 30 31 32 33 34 35
2theta

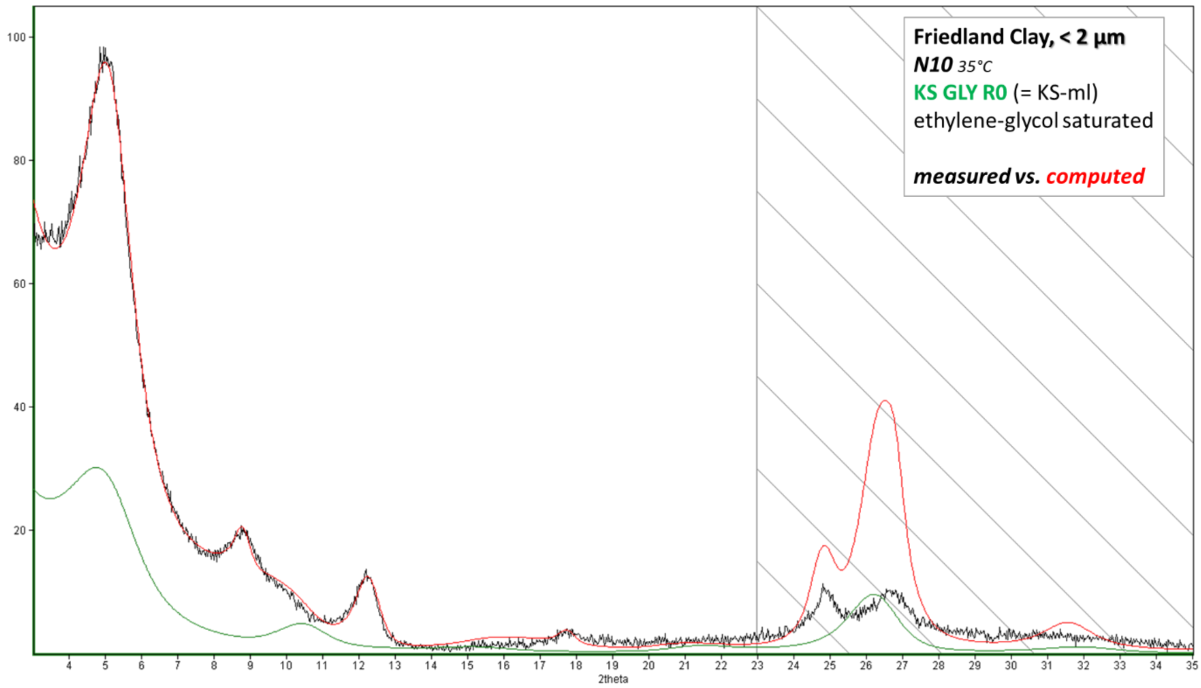
Friedland Clay, < 2 µm
N10 35°C
KS GLY R0 (= KS-ml)
ethylene-glycol saturated
measured vs. computed
100
80
60
40
20
4
5
6
7
8
9
10
11
12
13
14
15
16
17
18
19
20
21
22
23
24
25
26
27
28
29
30
31
32
33
34
35
2theta

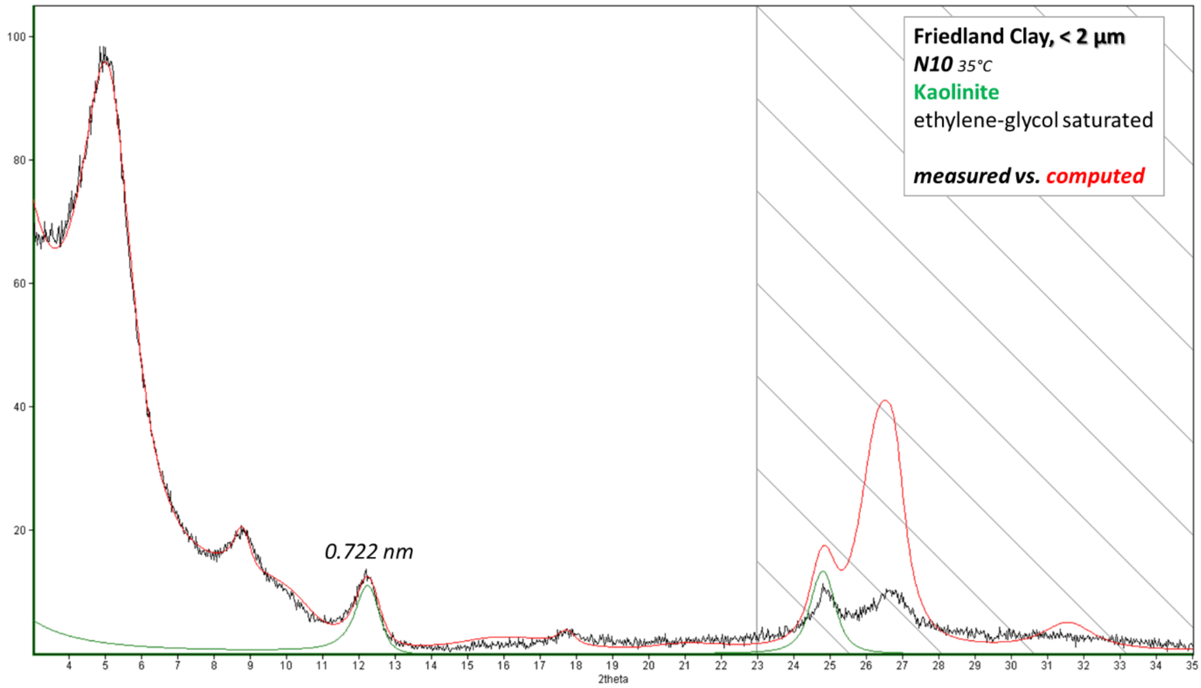
Friedland Clay, < 2 µm
N10 35°C
Kaolinite
ethylene-glycol saturated
measured vs. computed
0.722 nm
100
80
60
40
20
4
5
6
7
8
9
10
11
12
13
14
15
16
17
18
19
20
21
22
23
24
25
26
27
28
29
30
31
32
33
34
35
2theta

Data Sheet – FRIEDLAND No11 (< 2 µm), treated material *(60°C)*

Diffraction pattern of oriented specimen & modelling by Sybilla

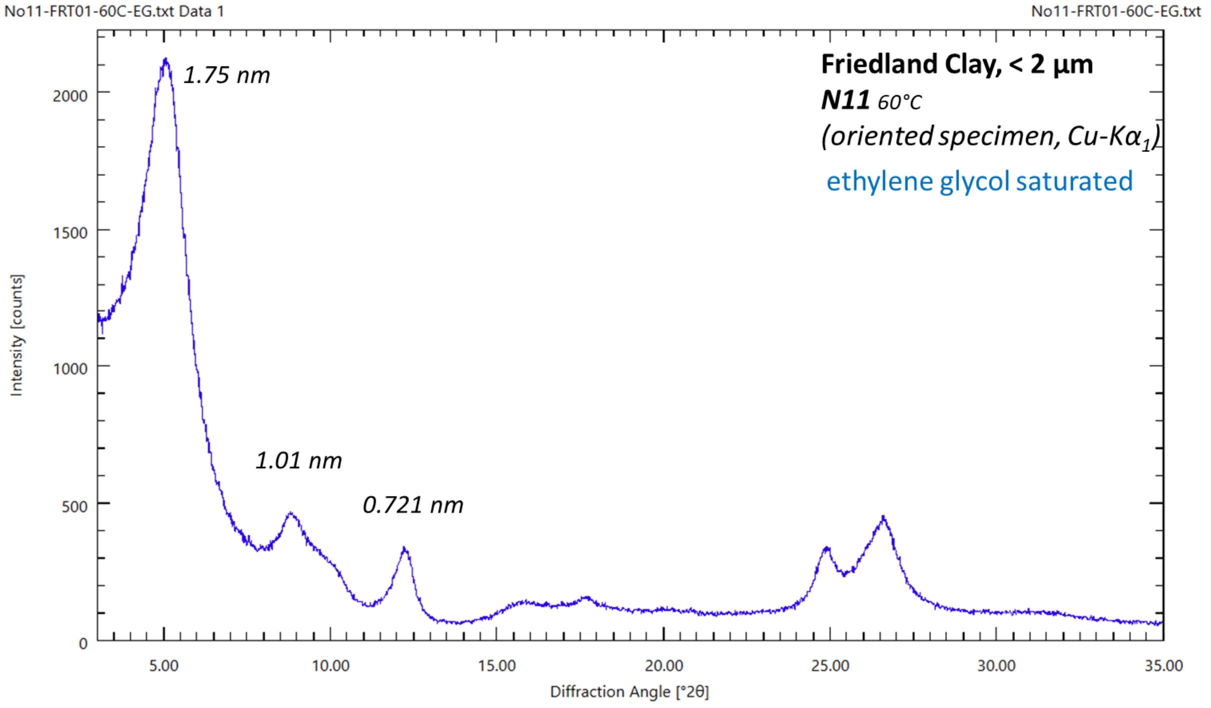

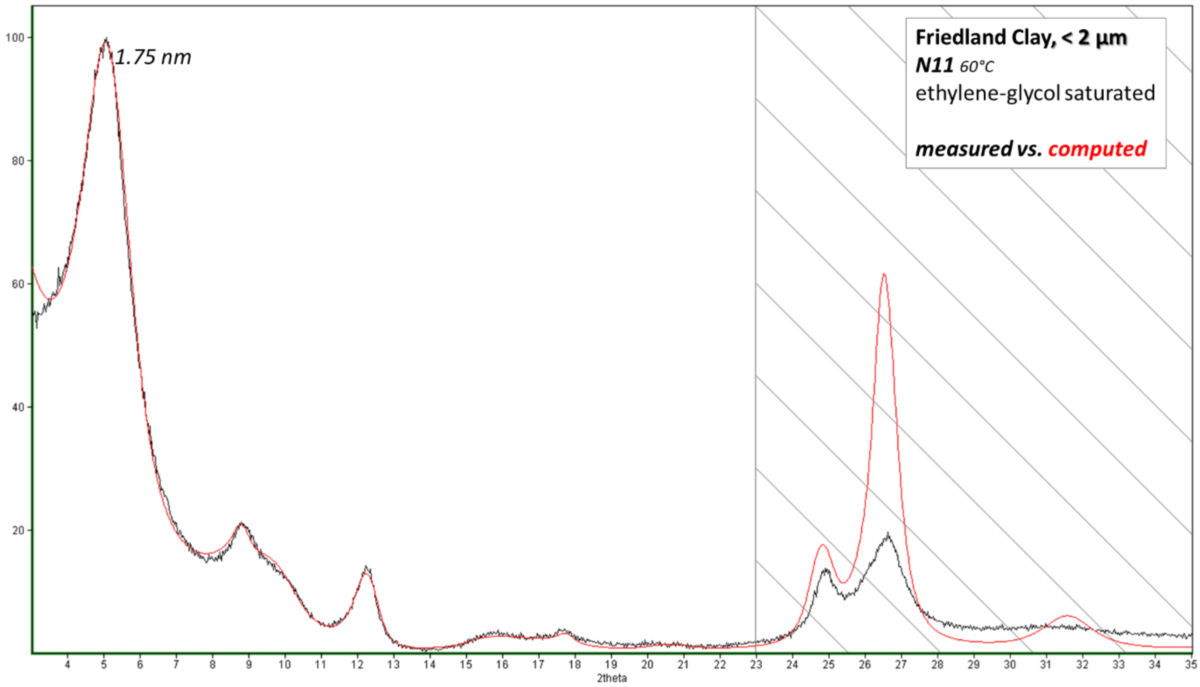

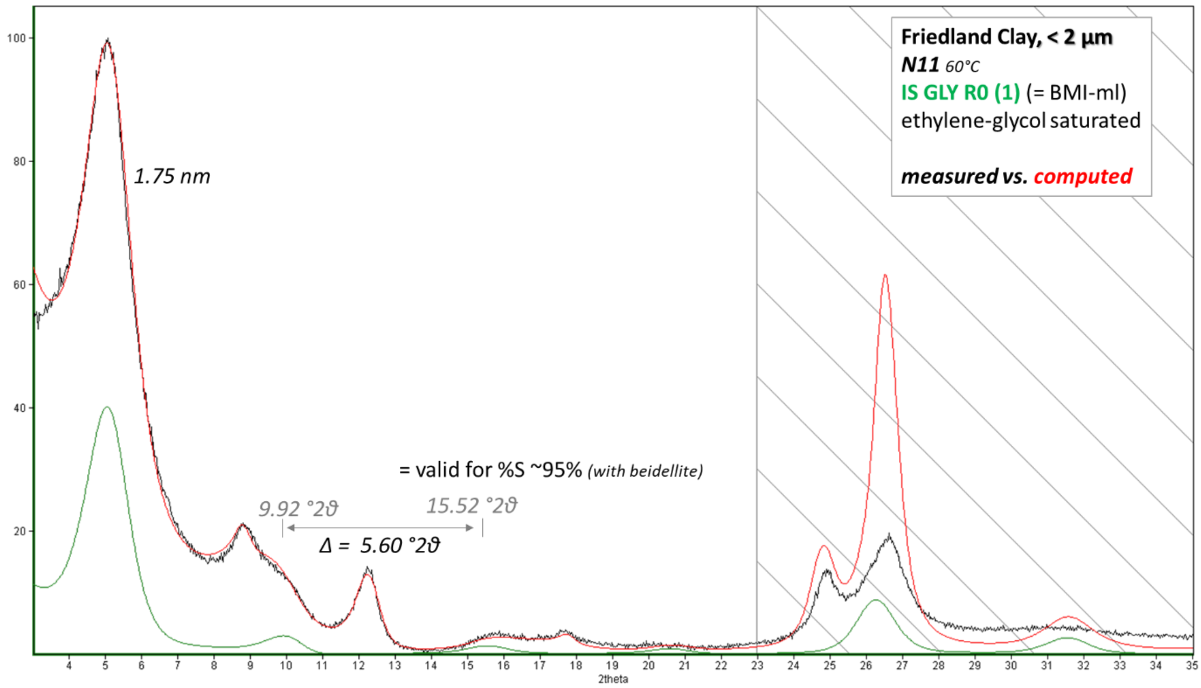
Friedland Clay, < 2 µm
N11 60°C
IS GLY R0 (1) (= BMI-ml)
ethylene-glycol saturated
measured vs. computed
1.75 nm
= valid for %S ~95% (with beidellite)
9.92 °2ϑ
15.52 °2ϑ
Δ = 5.60 °2ϑ
100
80
60
40
20
4
5
6
7
8
9
10
11
12
13
14
15
16
17
18
19
20
21
22
23
24
25
26
27
28
29
30
31
32
33
34
35
2theta

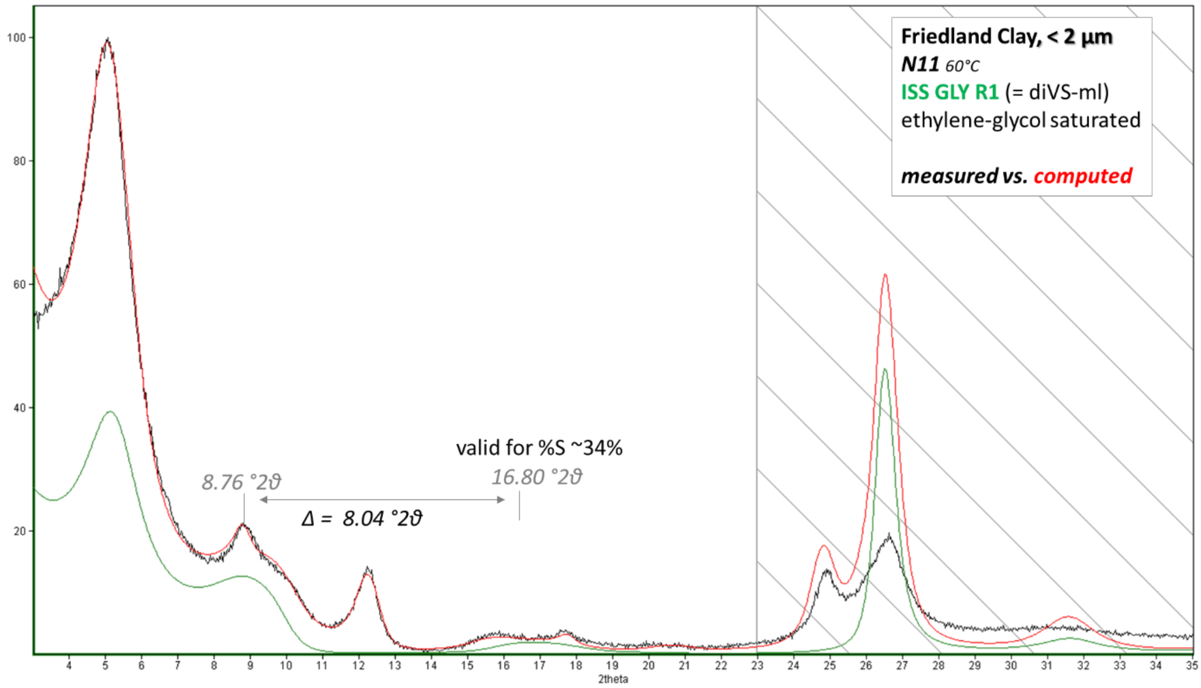
Friedland Clay, < 2 µm
N11 60°C
ISS GLY R1 (= diVS-ml)
ethylene-glycol saturated
measured vs. computed
valid for %S ~34%
8.76 °2ϑ
16.80 °2ϑ
Δ = 8.04 °2ϑ
100
80
60
40
20
4
5
6
7
8
9
10
11
12
13
14
15
16
17
18
19
20
21
22
23
24
25
26
27
28
29
30
31
32
33
34
35
2theta

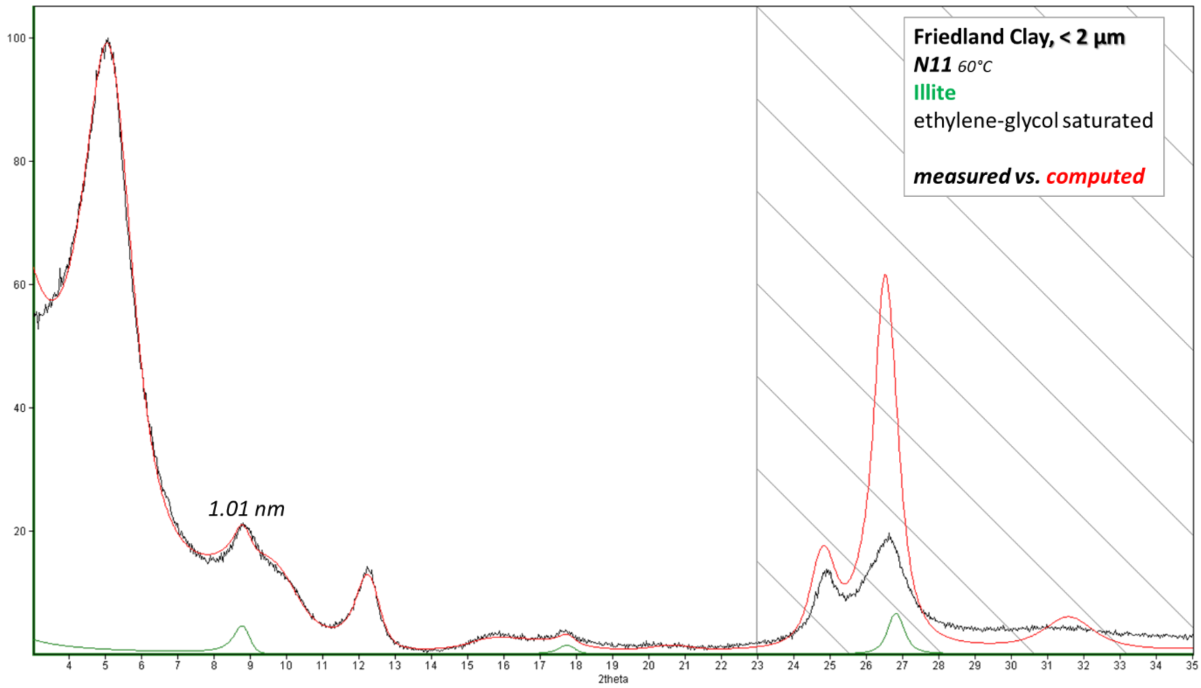
Friedland Clay, < 2 µm
N11 *60°C*
Illite
ethylene-glycol saturated
measured* vs. *computed
1.01 nm
100
80
60
40
20
4
5
6
7
8
9
10
11
12
13
14
15
16
17
18
19
20
21
22
23
24
25
26
27
28
29
30
31
32
33
34
35
2theta

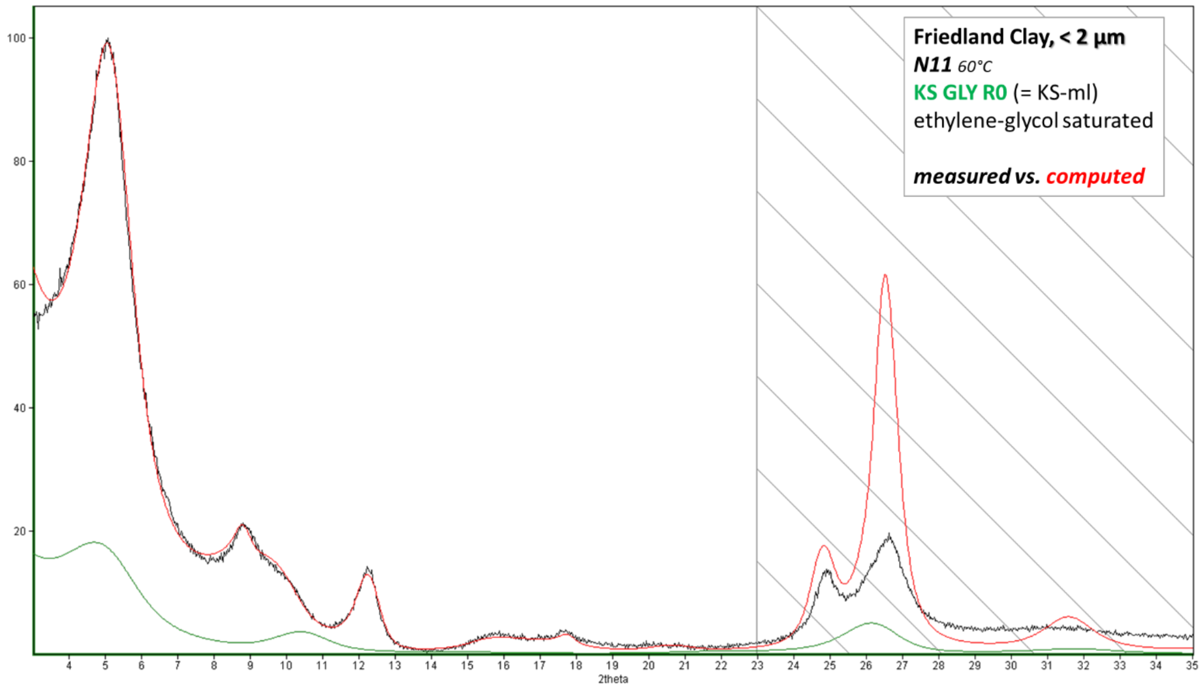
Friedland Clay, < 2 µm
N11 *60°C*
KS GLY R0 (= KS-ml)
ethylene-glycol saturated
measured* vs. *computed
100
80
60
40
20
4
5
6
7
8
9
10
11
12
13
14
15
16
17
18
19
20
21
22
23
24
25
26
27
28
29
30
31
32
33
34
35
2theta

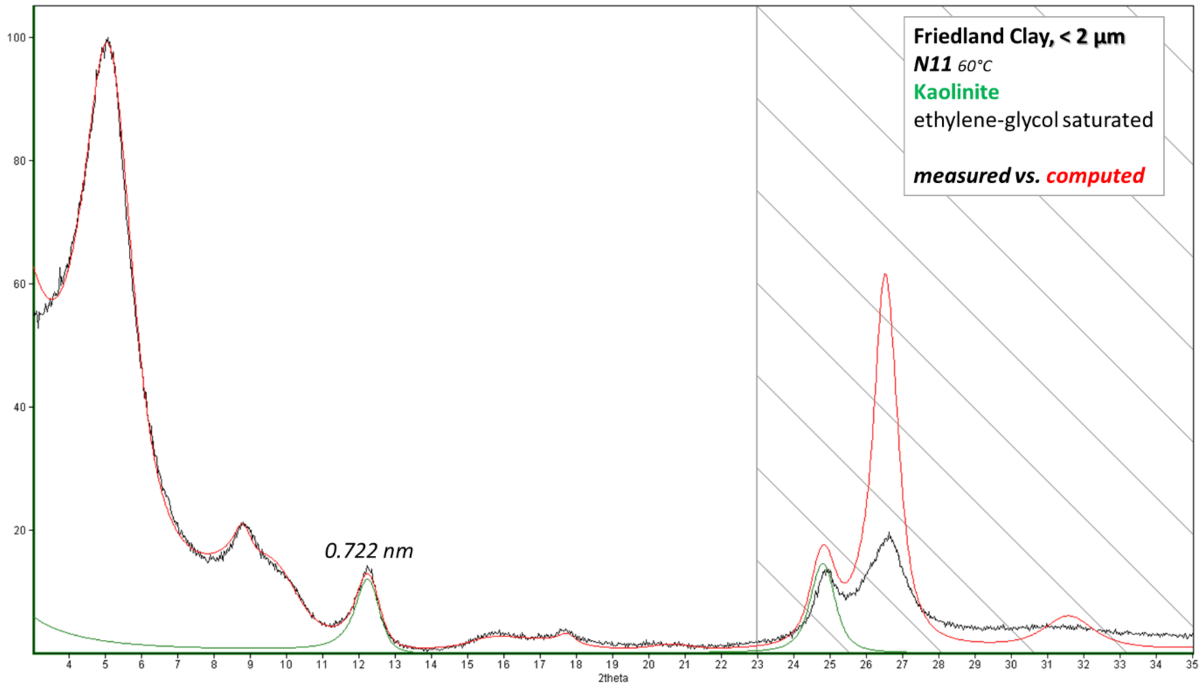
Friedland Clay, < 2 µm
N11 *60°C*
Kaolinite
ethylene-glycol saturated
measured* vs. *computed
0.722 nm
100
80
60
40
20
4
5
6
7
8
9
10
11
12
13
14
15
16
17
18
19
20
21
22
23
24
25
26
27
28
29
30
31
32
33
34
35
2theta

Data Sheet – FRIEDLAND No16 (< 2 µm), treated material *(100°C)*

Diffraction pattern of oriented specimen & modelling by Sybilla

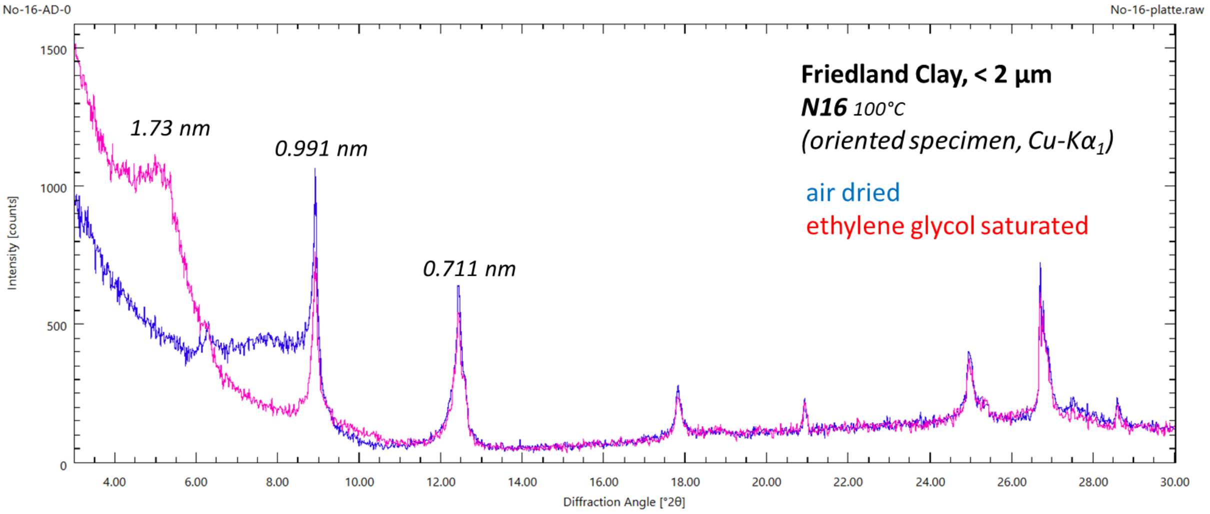

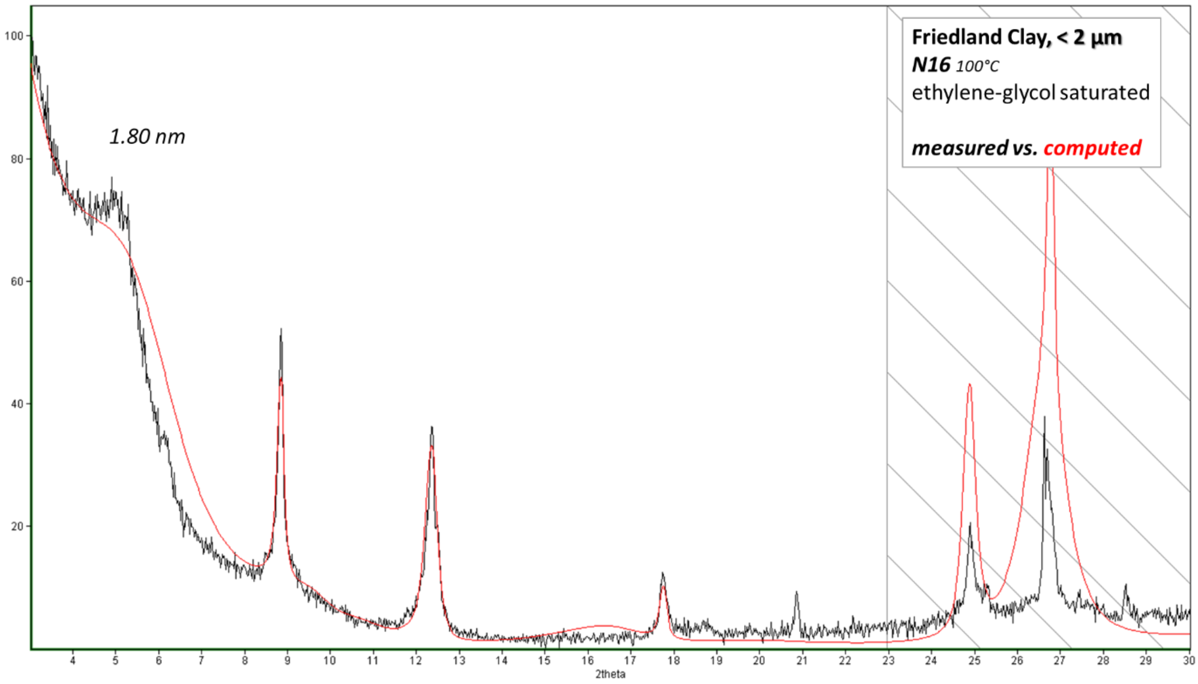

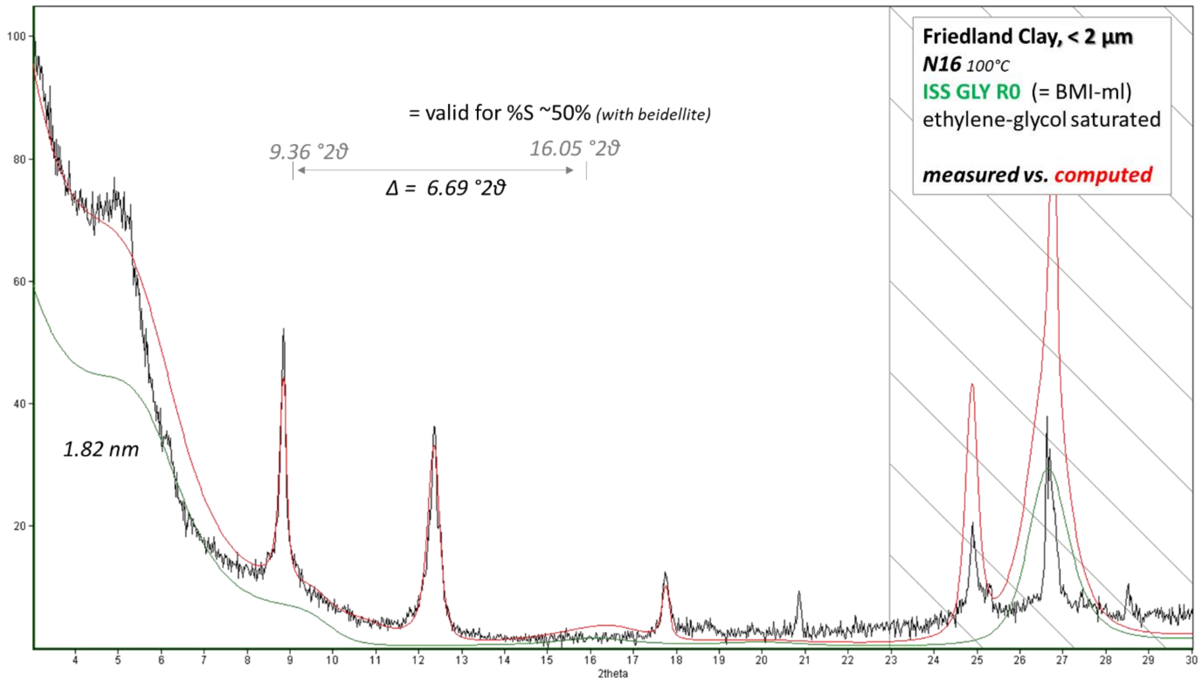
Friedland Clay, < 2 µm
N16 100°C
ISS GLY R0 (= BMI-ml)
ethylene-glycol saturated
measured vs. computed
= valid for %S ~50% (with beidellite)
9.36 °2ϑ
16.05 °2ϑ
Δ = 6.69 °2ϑ
1.82 nm
100
80
60
40
20
4
5
6
7
8
9
10
11
12
13
14
15
16
17
18
19
20
21
22
23
24
25
26
27
28
29
30
2theta

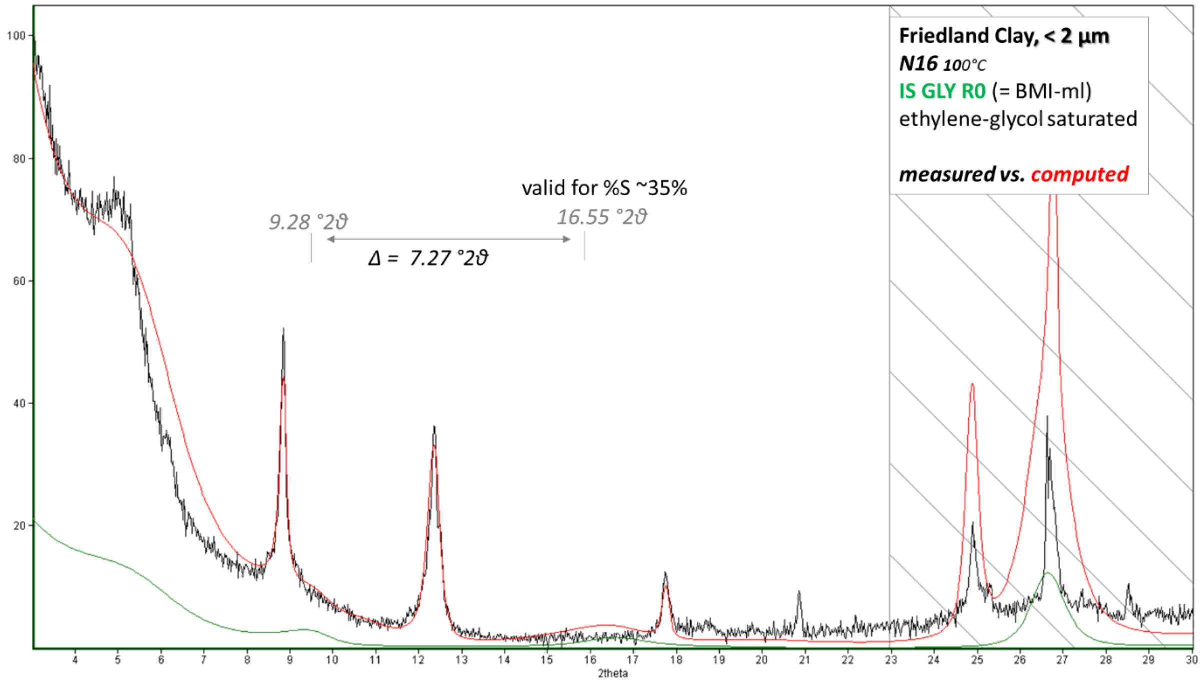
Friedland Clay, < 2 µm
N16 100°C
IS GLY R0 (= BMI-ml)
ethylene-glycol saturated
measured vs. computed
valid for %S ~35%
9.28 °2ϑ
16.55 °2ϑ
Δ = 7.27 °2ϑ
100
80
60
40
20
4
5
6
7
8
9
10
11
12
13
14
15
16
17
18
19
20
21
22
23
24
25
26
27
28
29
30
2theta

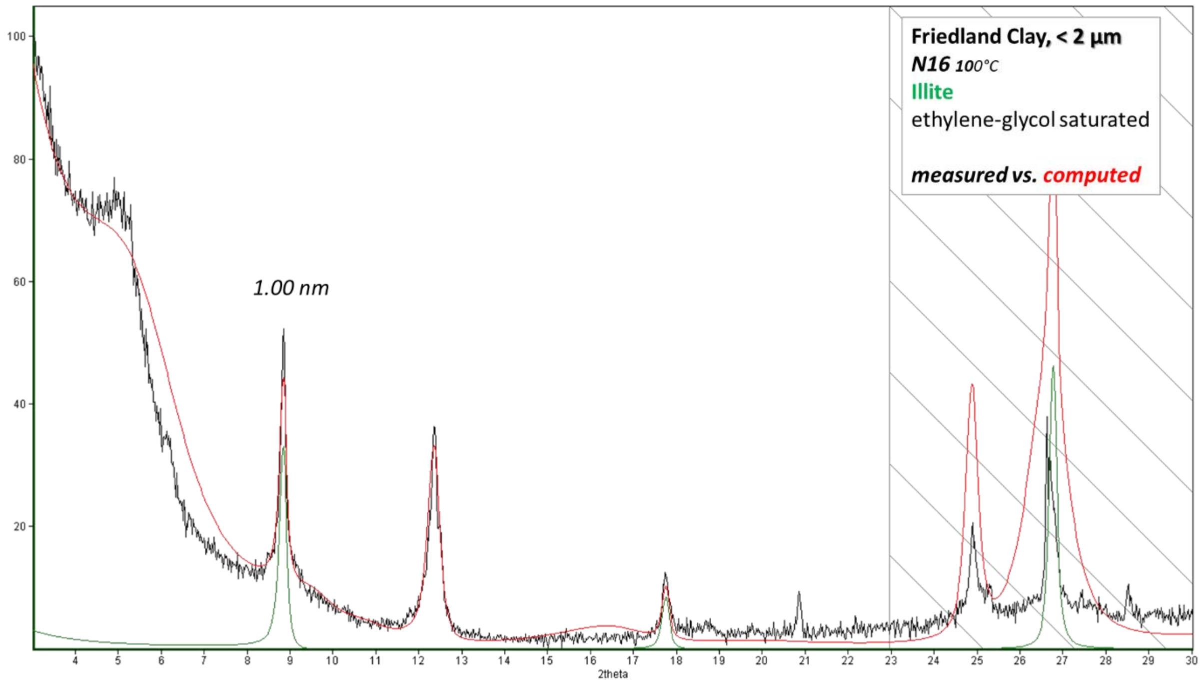
Friedland Clay, < 2 µm
N16 *100°C*
Illite
ethylene-glycol saturated
measured* vs. *computed
1.00 nm
100
80
60
40
20
4
5
6
7
8
9
10
11
12
13
14
15
16
17
18
19
20
21
22
23
24
25
26
27
28
29
30
2theta

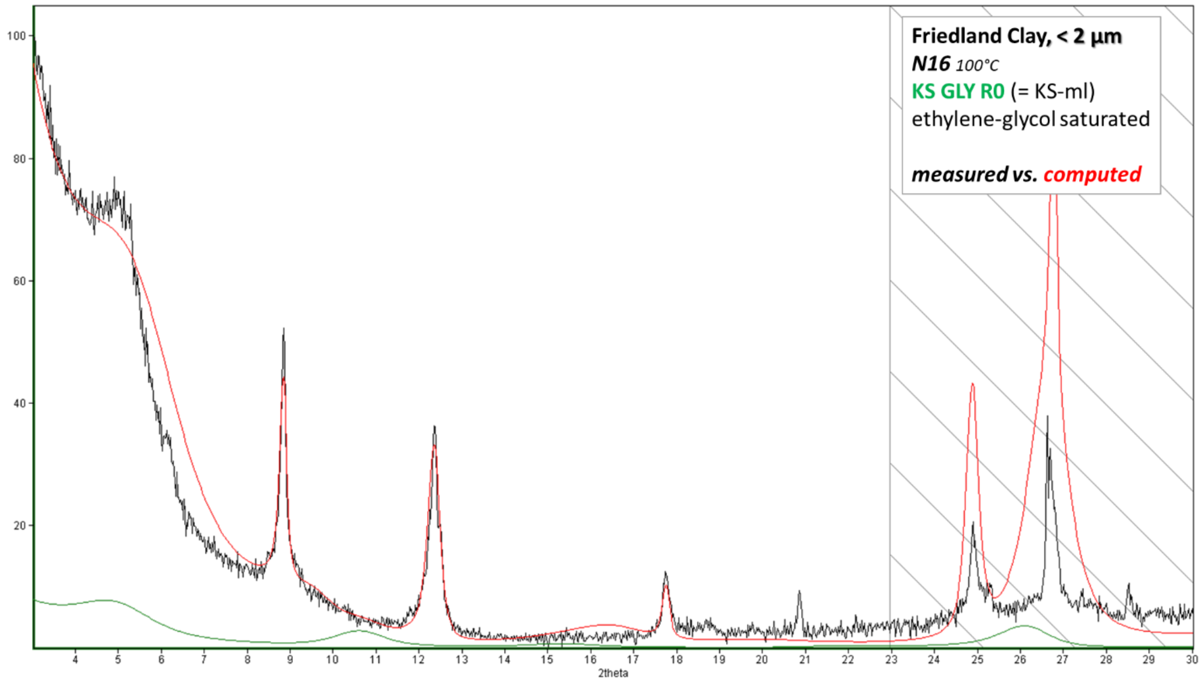
Friedland Clay, < 2 µm
N16 *100°C*
KS GLY R0 (= KS-ml)
ethylene-glycol saturated
measured **vs.** ***computed***
100
80
60
40
20
4
5
6
7
8
9
10
11
12
13
14
15
16
17
18
19
20
21
22
23
24
25
26
27
28
29
30
2theta

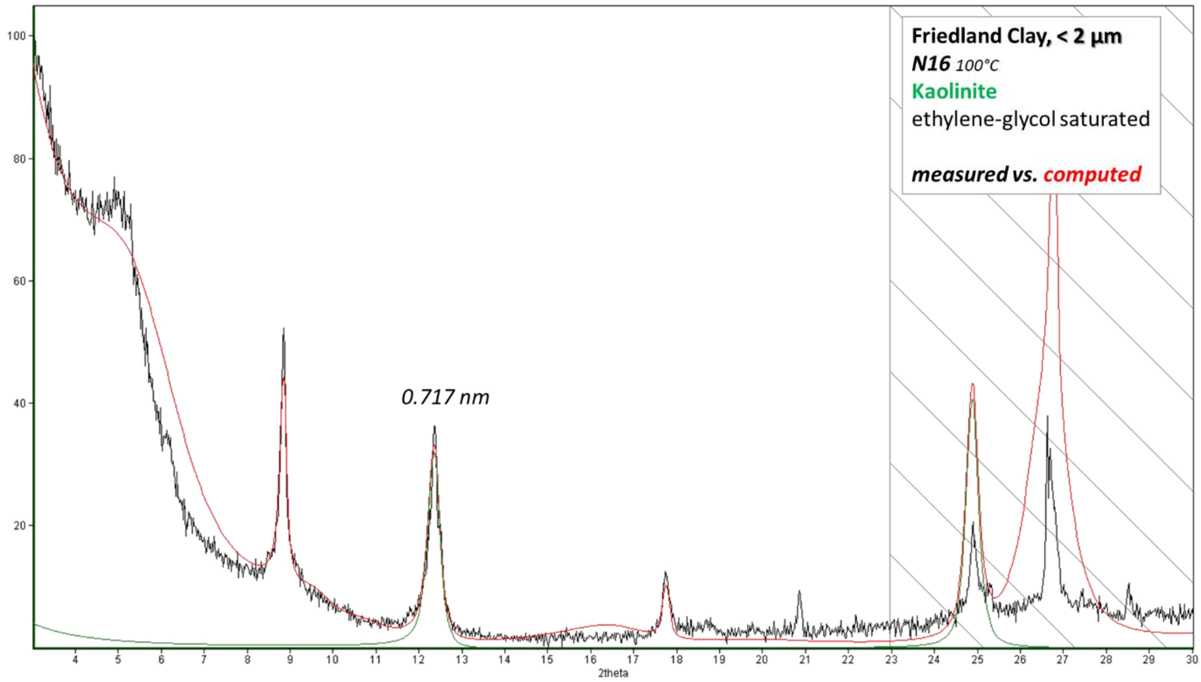
Friedland Clay, < 2 µm
N16 *100°C*
Kaolinite
ethylene-glycol saturated
measured **vs.** ***computed***
0.717 nm
100
80
60
40
20
4
5
6
7
8
9
10
11
12
13
14
15
16
17
18
19
20
21
22
23
24
25
26
27
28
29
30
2theta

Data Sheet – FRIEDLAND No20 (< 2 µm), treated material *(125°C)*

Diffraction pattern of oriented specimen & modelling by Sybilla

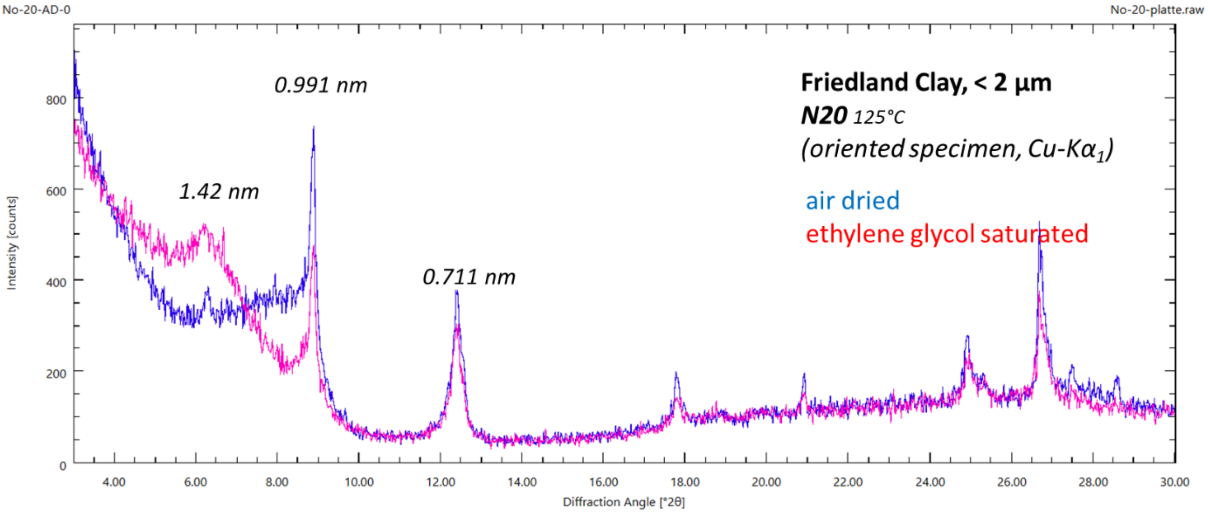

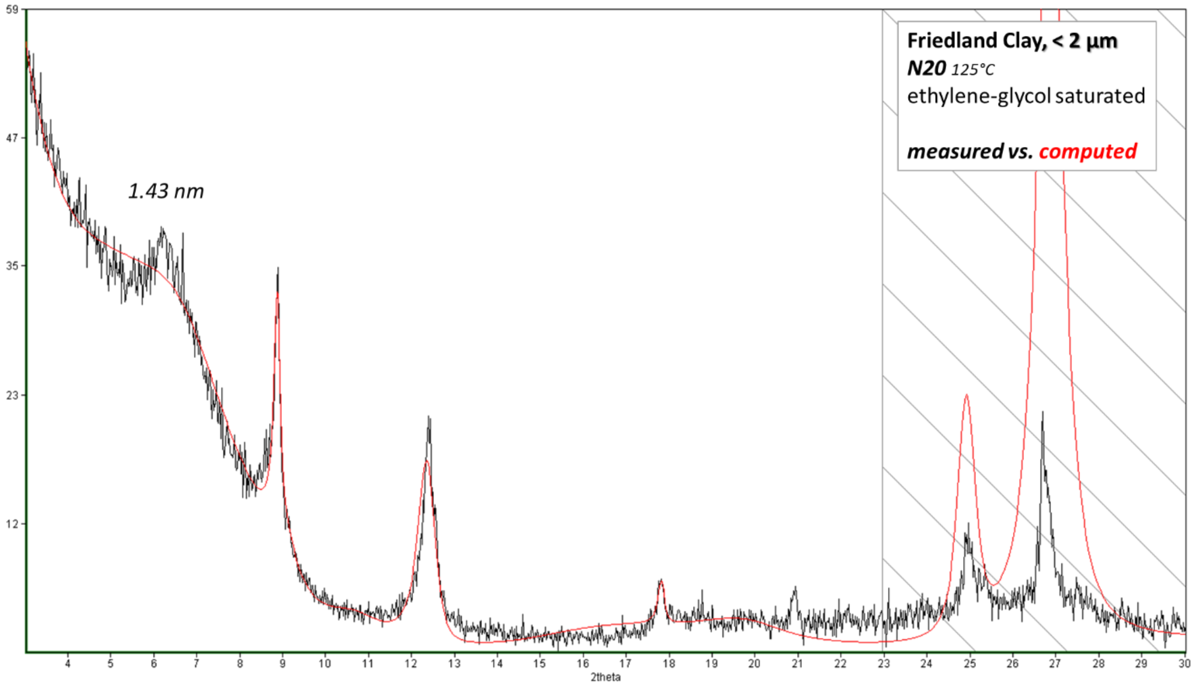

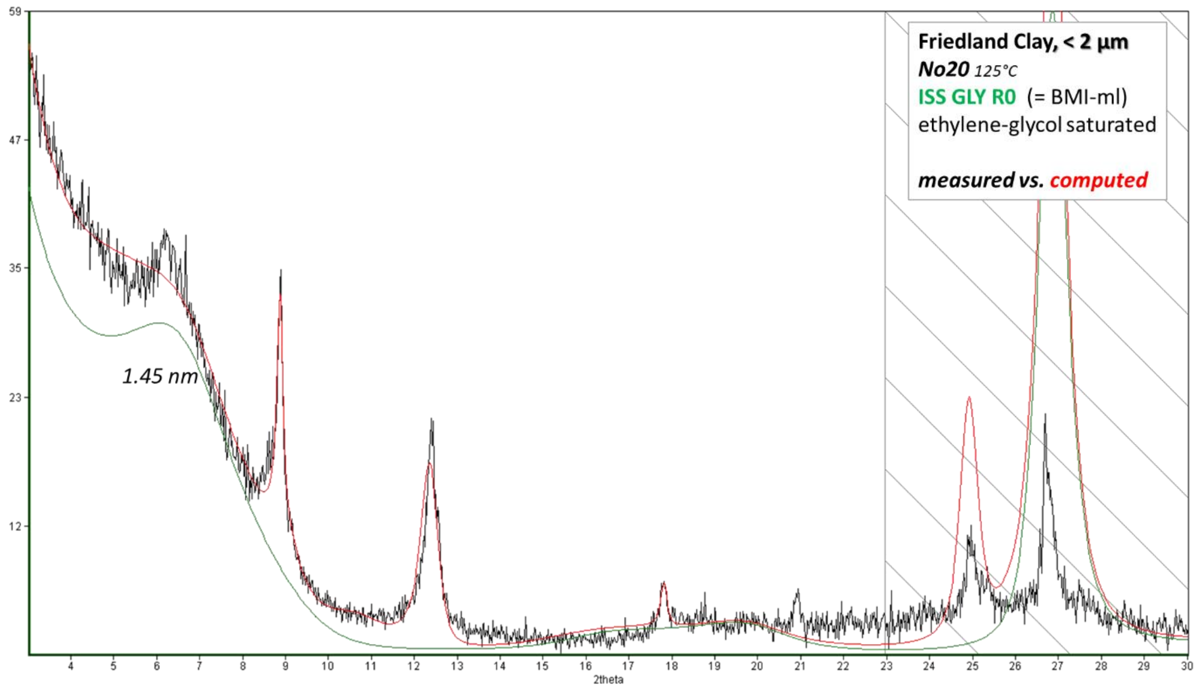
Friedland Clay, < 2 µm
No20 125°C
ISS GLY R0 (= BMI-ml)
ethylene-glycol saturated
measured vs. computed
1.45 nm
59
47
35
23
12
4 5 6 7 8 9 10 11 12 13 14 15 16 17 18 19 20 21 22 23 24 25 26 27 28 29 30
2theta

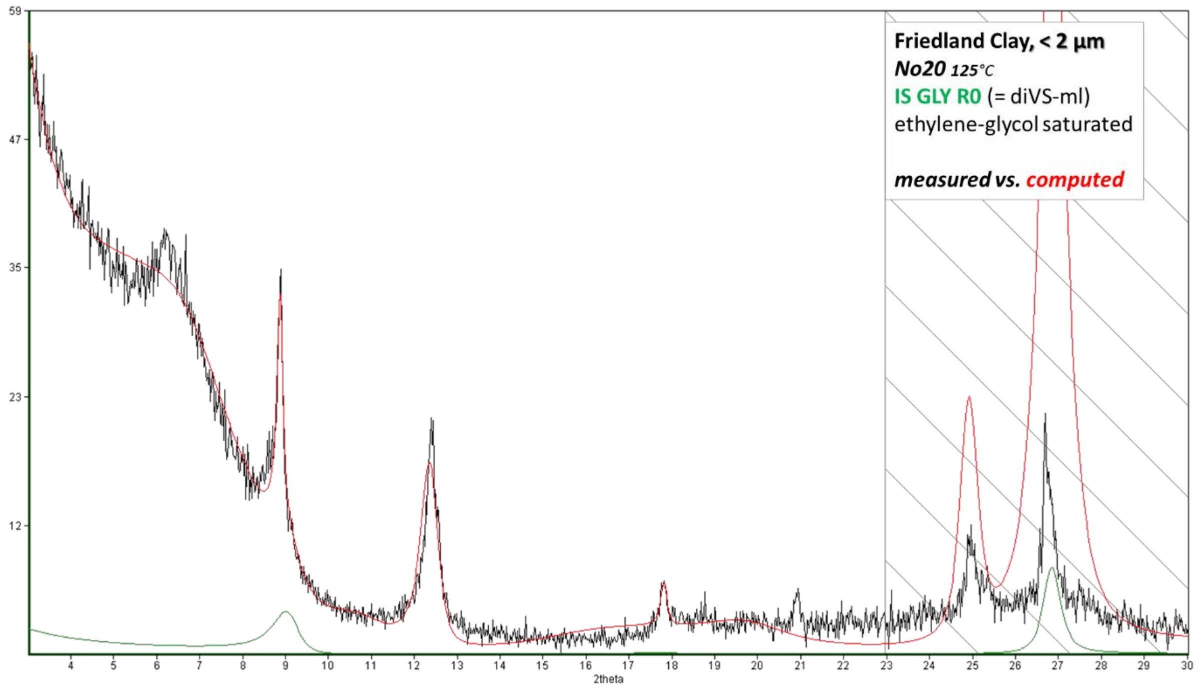
Friedland Clay, < 2 µm
No20 125°C
IS GLY R0 (= diVS-ml)
ethylene-glycol saturated
measured vs. computed
59
47
35
23
12
4 5 6 7 8 9 10 11 12 13 14 15 16 17 18 19 20 21 22 23 24 25 26 27 28 29 30
2theta

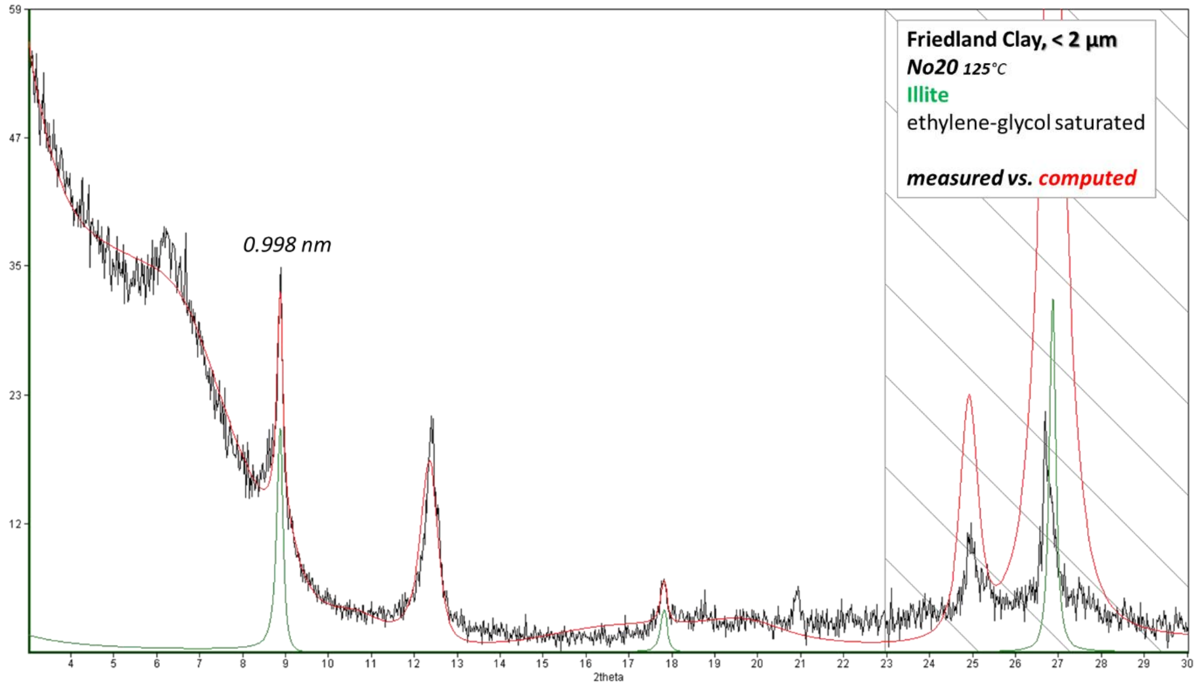
Friedland Clay, < 2 µm
No20 125°C
Illite
ethylene-glycol saturated
measured vs. computed
0.998 nm
59
47
35
23
12
4
5
6
7
8
9
10
11
12
13
14
15
16
17
18
19
20
21
22
23
24
25
26
27
28
29
30
2theta

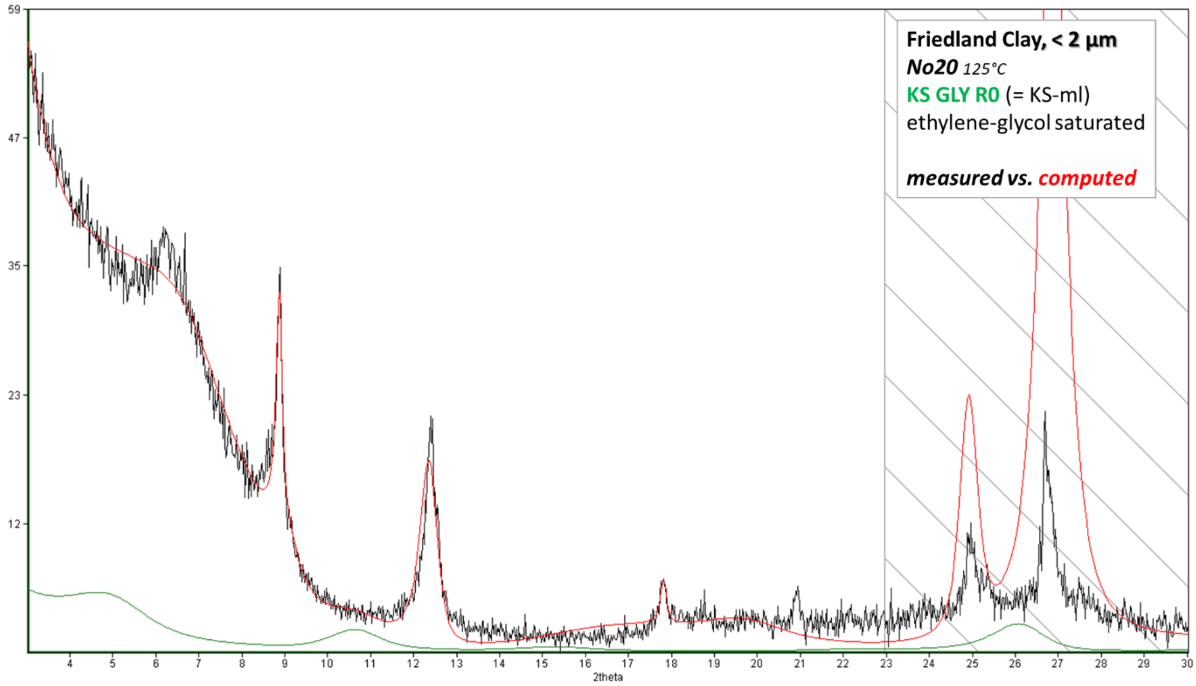
Friedland Clay, < 2 µm
No20 *125°C*
KS GLY R0 (= KS-ml)
ethylene-glycol saturated
measured* vs. *computed
59
47
35
23
12
4
5
6
7
8
9
10
11
12
13
14
15
16
17
18
19
20
21
22
23
24
25
26
27
28
29
30
2theta

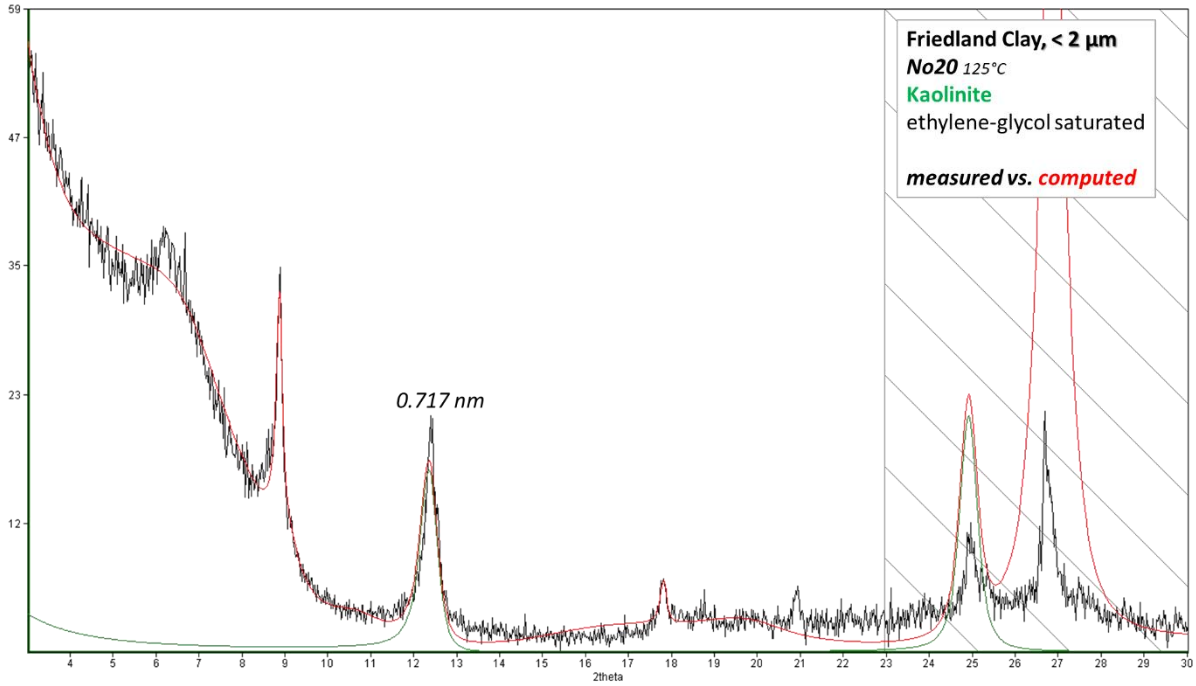
Friedland Clay, < 2 µm
No20 *125°C*
Kaolinite
ethylene-glycol saturated
measured* vs. *computed
0.717 nm
59
47
35
23
12
4
5
6
7
8
9
10
11
12
13
14
15
16
17
18
19
20
21
22
23
24
25
26
27
28
29
30
2theta

Data Sheet – FRIEDLAND No21 (< 2 µm), treated material *(150°C)*

Diffraction pattern of oriented specimen & modelling by Sybilla

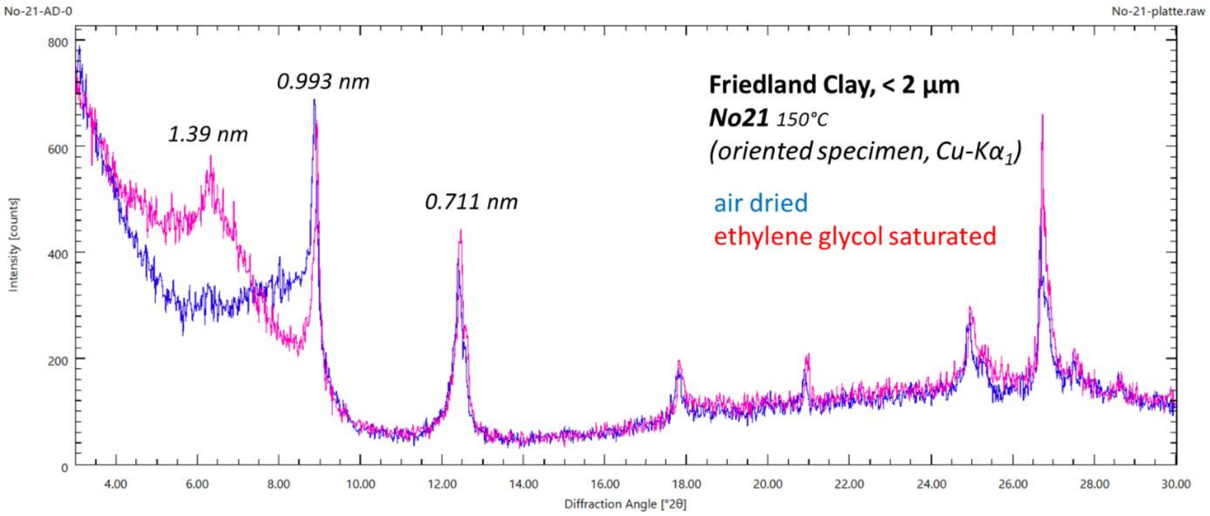

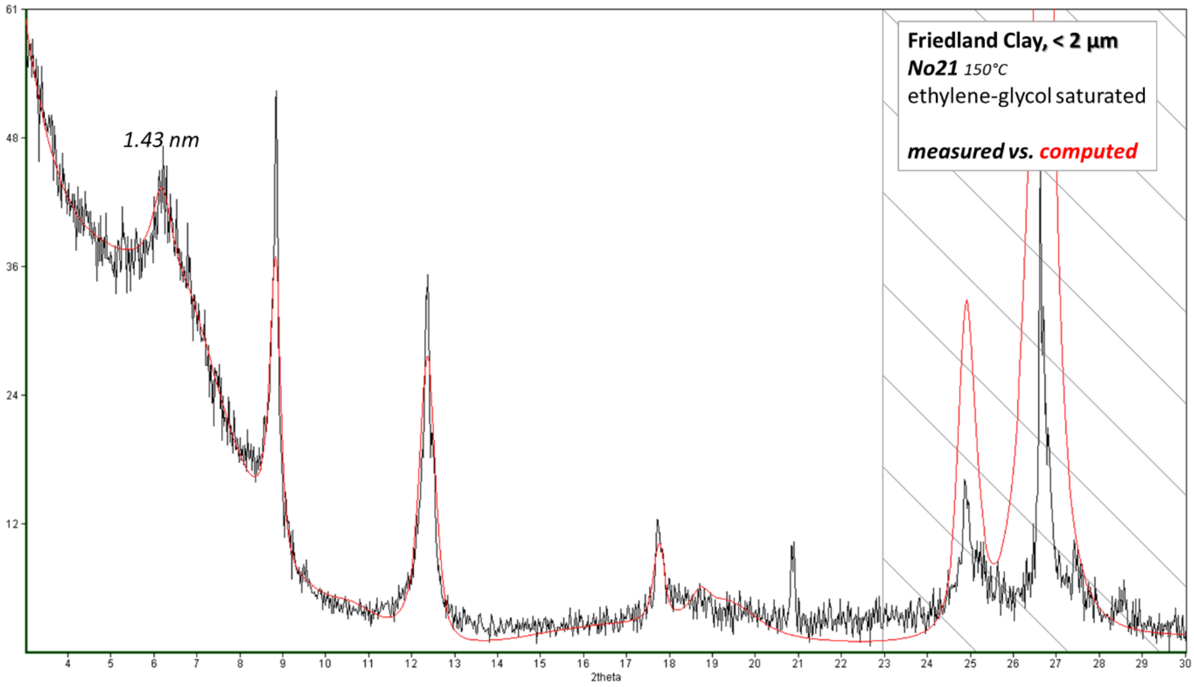

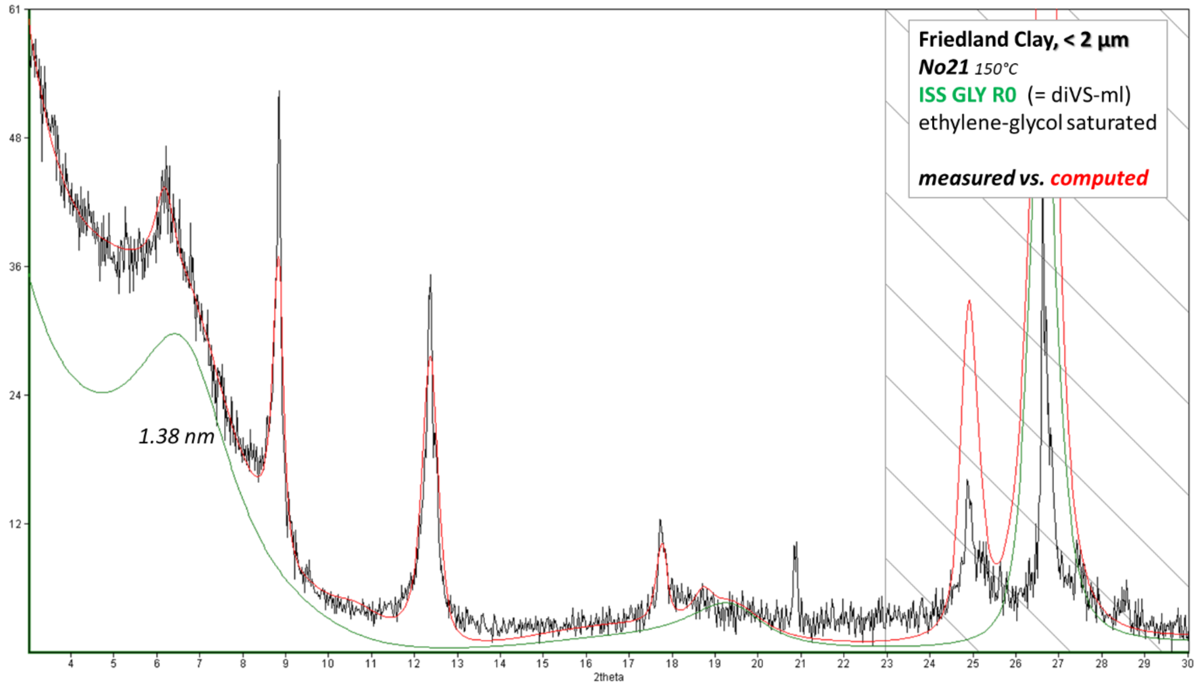
Friedland Clay, < 2 µm
No21 150°C
ISS GLY R0 (= diVS-ml)
ethylene-glycol saturated
measured vs. computed
1.38 nm
61
48
36
24
12
4 5 6 7 8 9 10 11 12 13 14 15 16 17 18 19 20 21 22 23 24 25 26 27 28 29 30
2theta

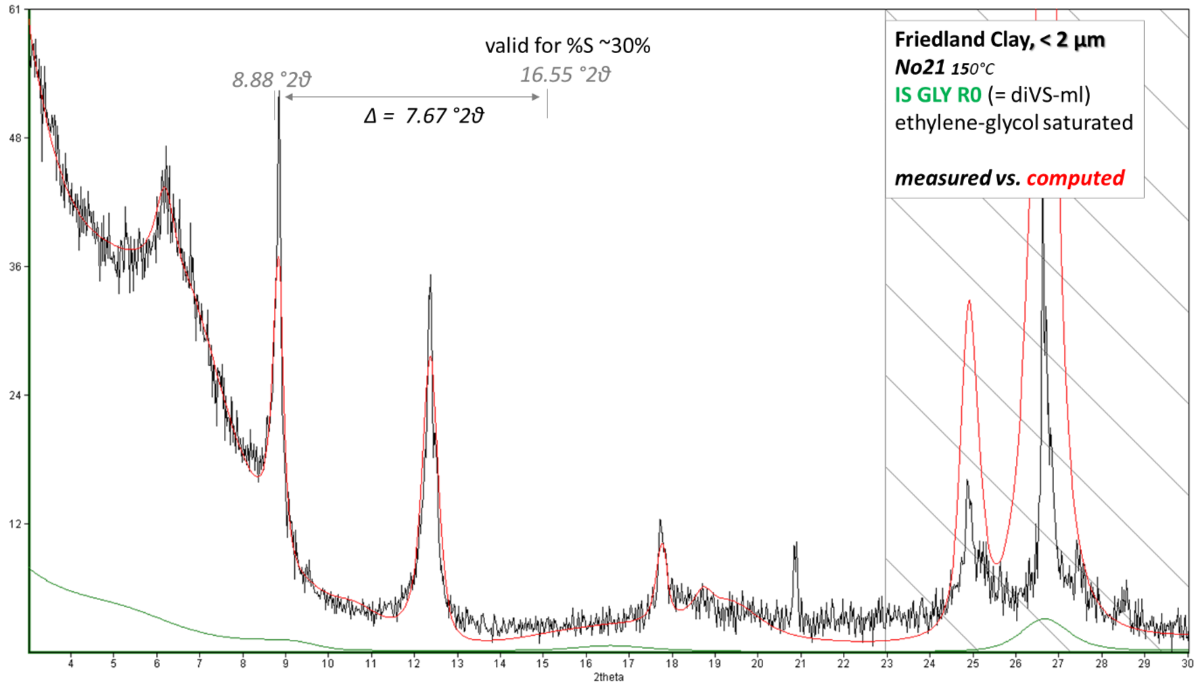
Friedland Clay, < 2 µm
No21 150°C
IS GLY R0 (= diVS-ml)
ethylene-glycol saturated
measured vs. computed
valid for %S ~30%
8.88 °2ϑ
16.55 °2ϑ
Δ = 7.67 °2ϑ
61
48
36
24
12
4 5 6 7 8 9 10 11 12 13 14 15 16 17 18 19 20 21 22 23 24 25 26 27 28 29 30
2theta

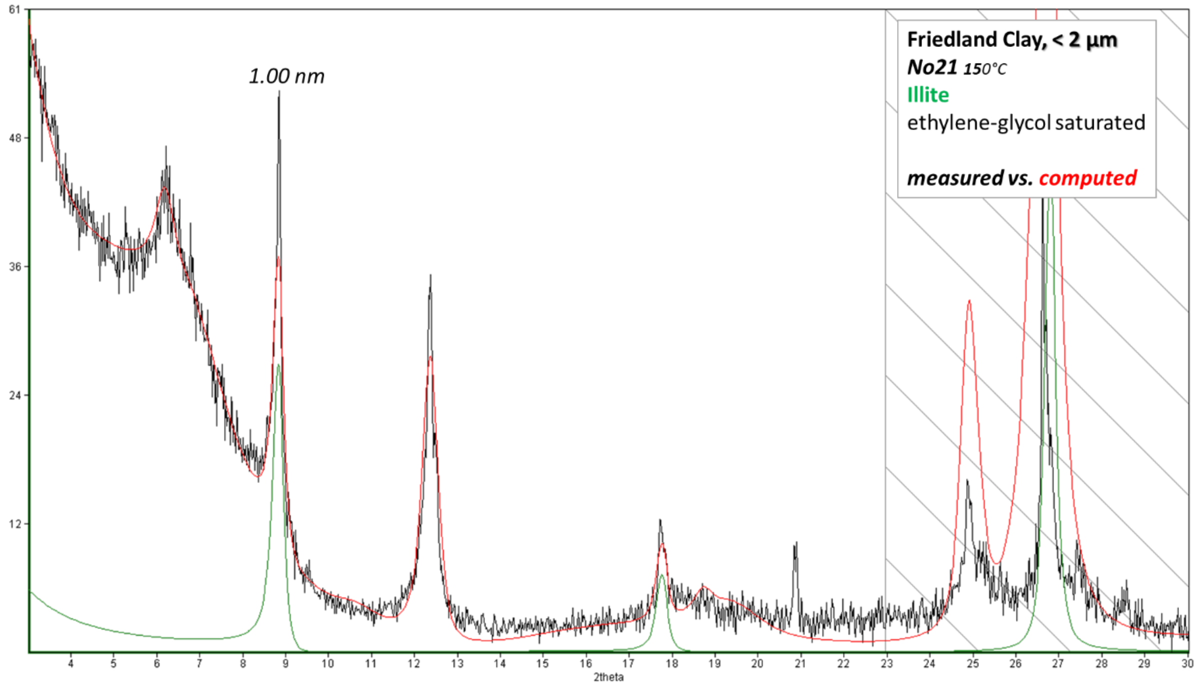
Friedland Clay, < 2 µm
No21 150°C
Illite
ethylene-glycol saturated
measured vs. computed
1.00 nm
61
48
36
24
12
4
5
6
7
8
9
10
11
12
13
14
15
16
17
18
19
20
21
22
23
24
25
26
27
28
29
30
2theta

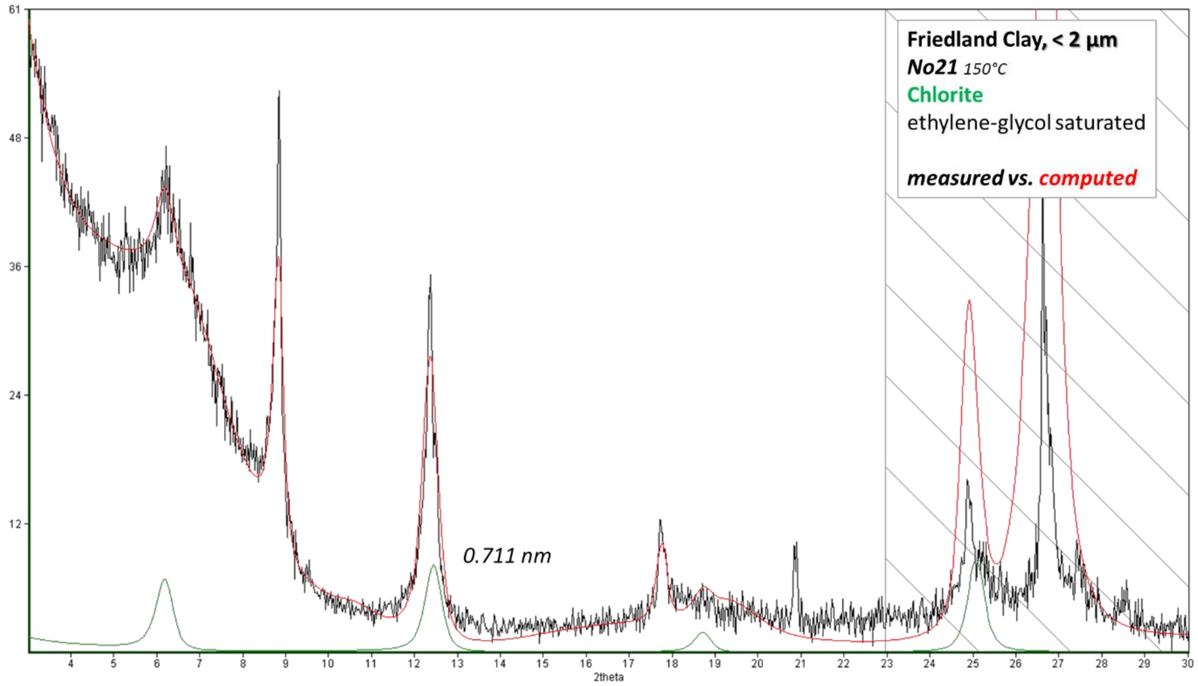
Friedland Clay, < 2 µm
No21 150°C
Chlorite
ethylene-glycol saturated
measured vs. computed
0.711 nm
61
48
36
24
12
4
5
6
7
8
9
10
11
12
13
14
15
16
17
18
19
20
21
22
23
24
25
26
27
28
29
30
2theta

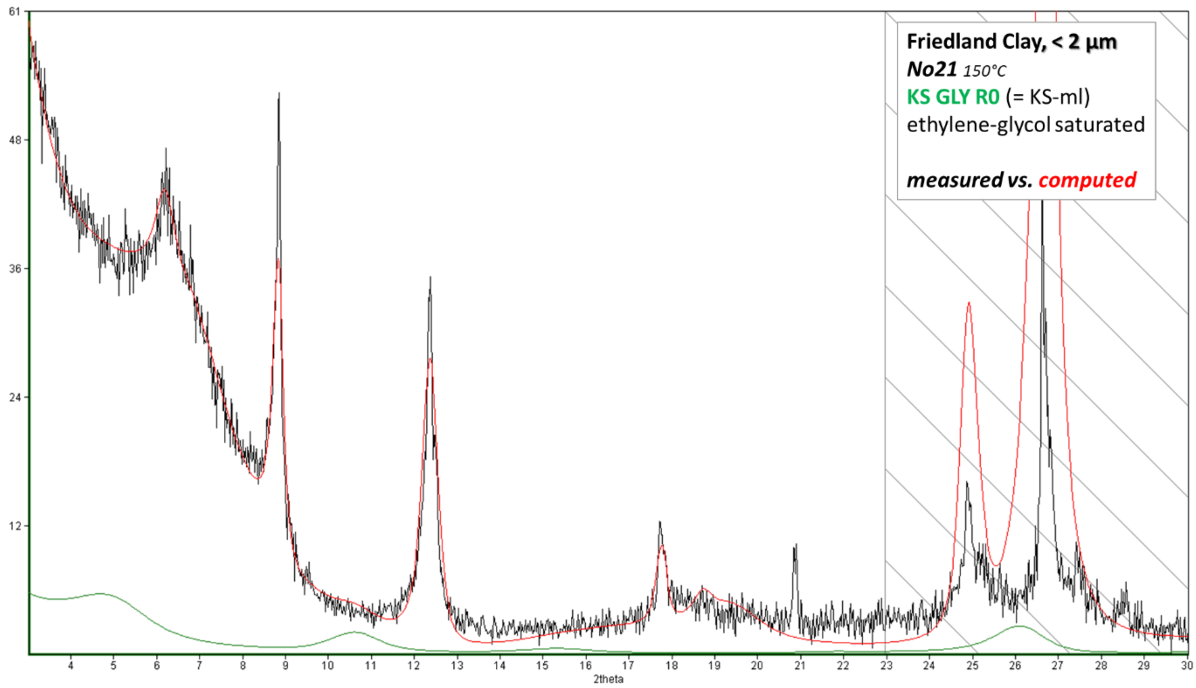
Friedland Clay, < 2 µm
No21 150°C
KS GLY R0 (= KS-ml)
ethylene-glycol saturated
measured vs. computed
61
48
36
24
12
4
5
6
7
8
9
10
11
12
13
14
15
16
17
18
19
20
21
22
23
24
25
26
27
28
29
30
2theta

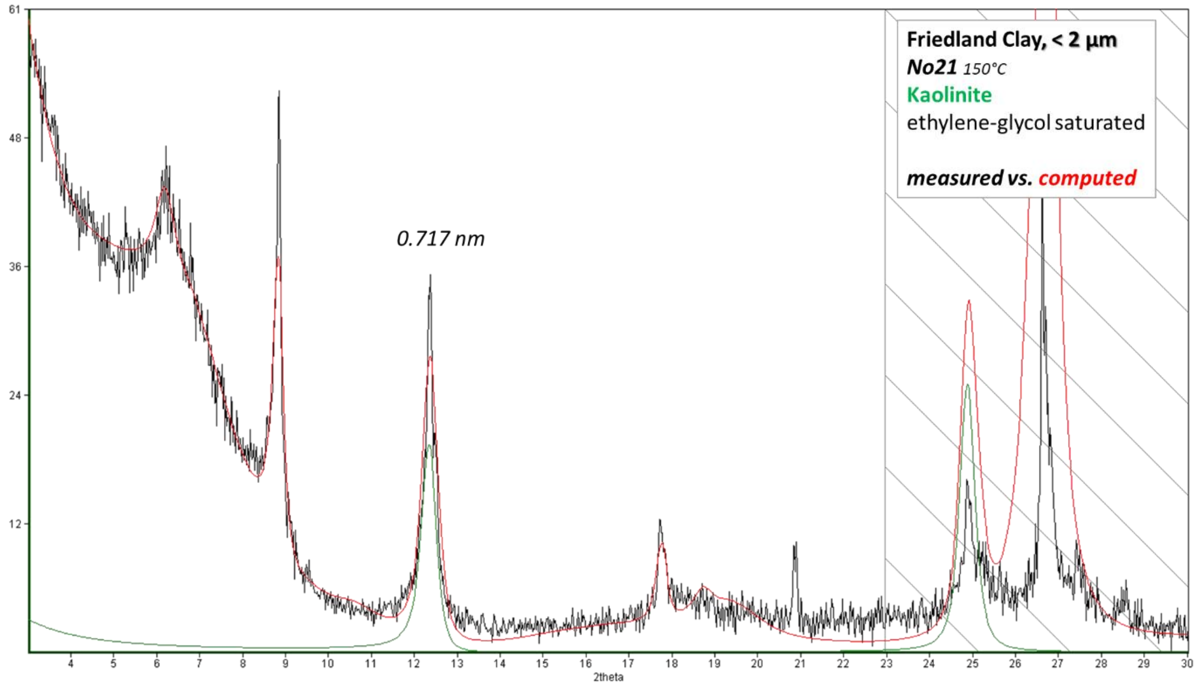
Friedland Clay, < 2 µm
No21 150°C
Kaolinite
ethylene-glycol saturated
measured vs. computed
0.717 nm
61
48
36
24
12
4
5
6
7
8
9
10
11
12
13
14
15
16
17
18
19
20
21
22
23
24
25
26
27
28
29
30
2theta

Data Sheet – FRIEDLAND No12 (< 2 µm), treated material *(100°C)*

Diffraction pattern of oriented specimen & modelling by Sybilla

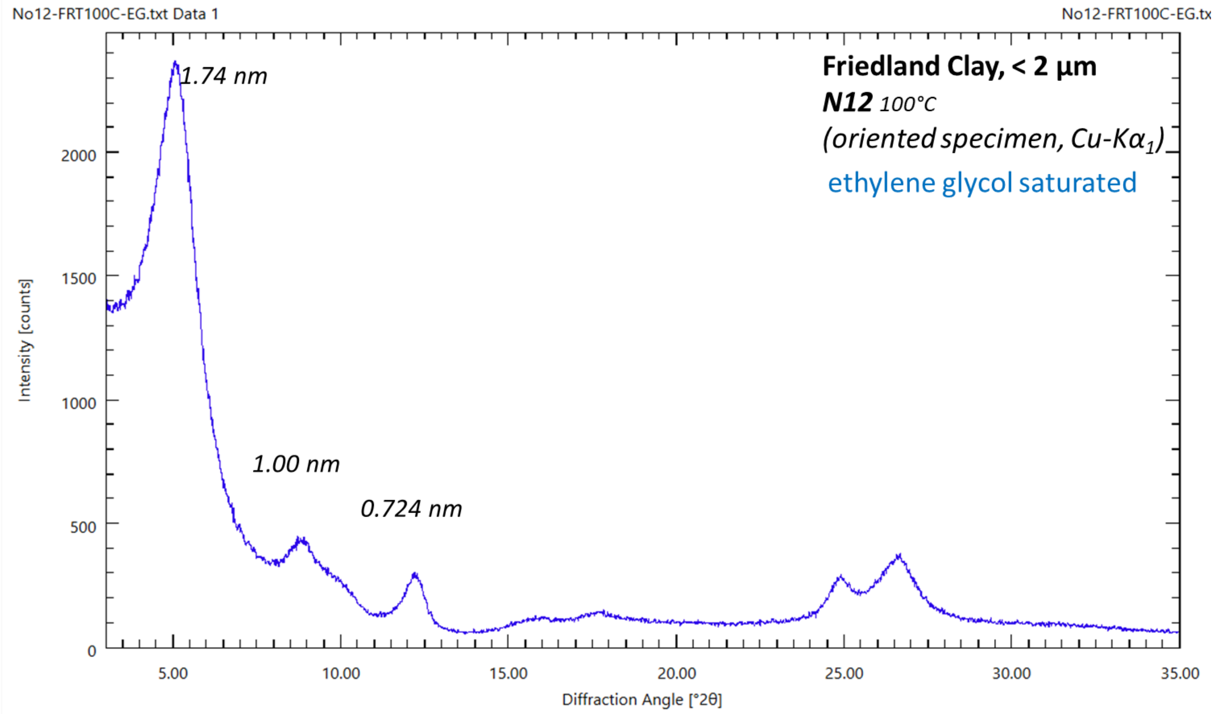

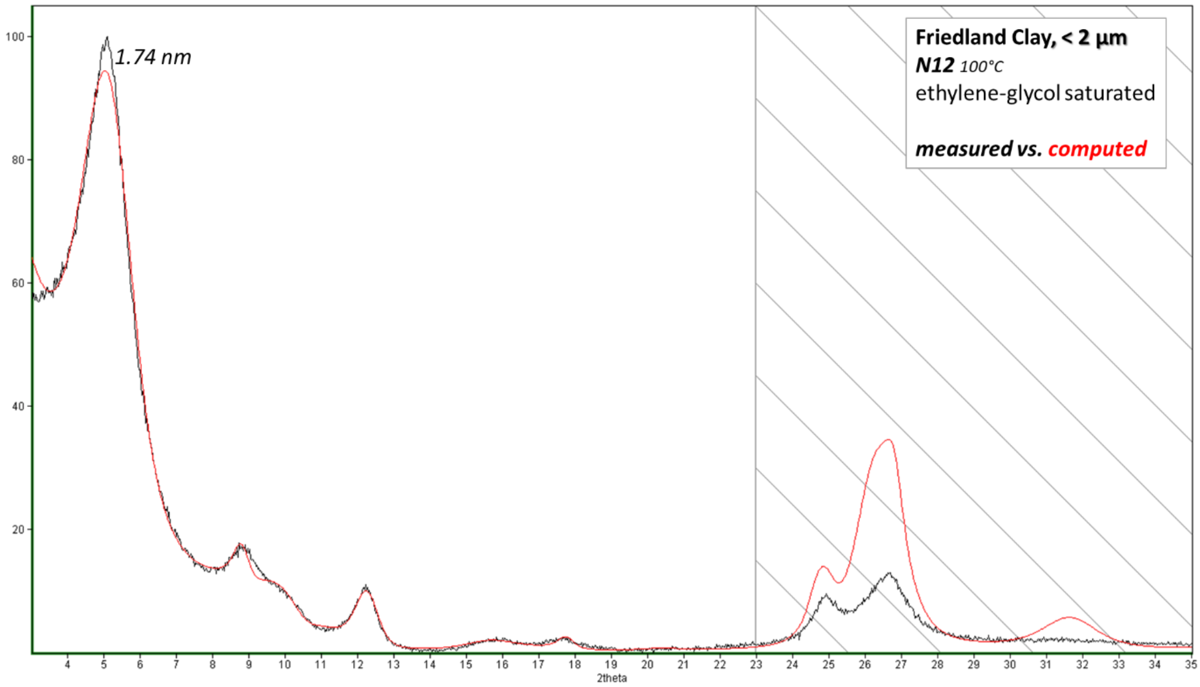

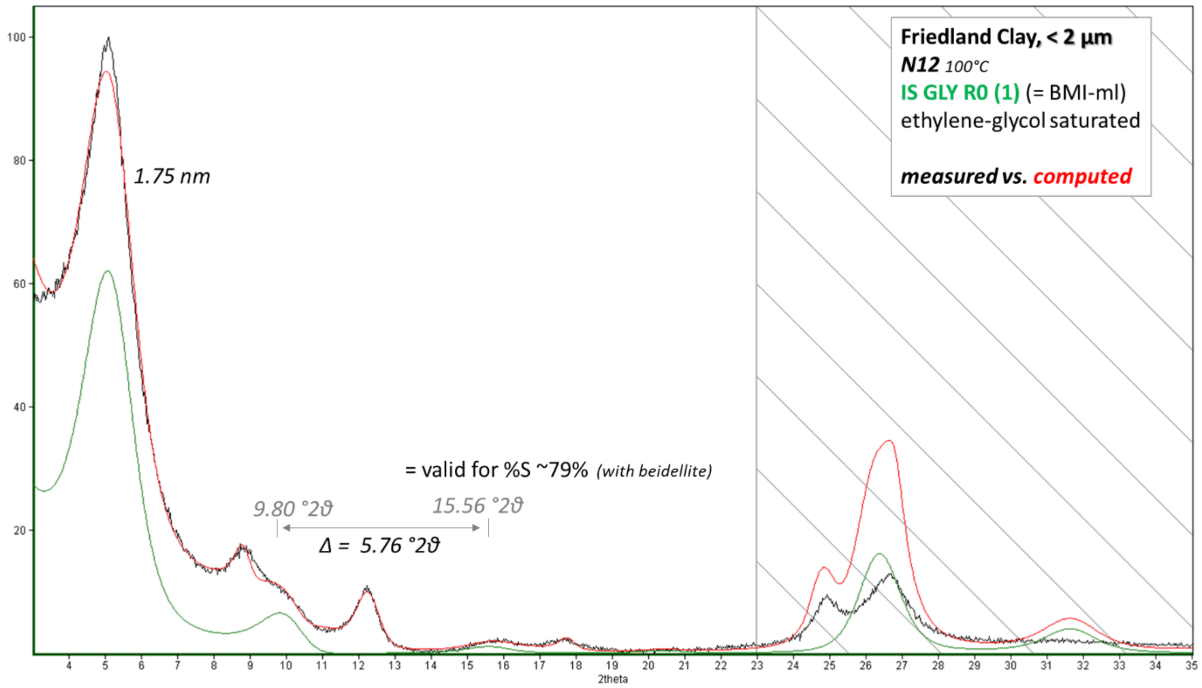
Friedland Clay, < 2 µm
N12 100°C
IS GLY R0 (1) (= BMI-ml)
ethylene-glycol saturated
measured vs. computed
1.75 nm
= valid for %S ~79% (with beidellite)
9.80 °2ϑ
15.56 °2ϑ
Δ = 5.76 °2ϑ
100
80
60
40
20
4
5
6
7
8
9
10
11
12
13
14
15
16
17
18
19
20
21
22
23
24
25
26
27
28
29
30
31
32
33
34
35
2theta

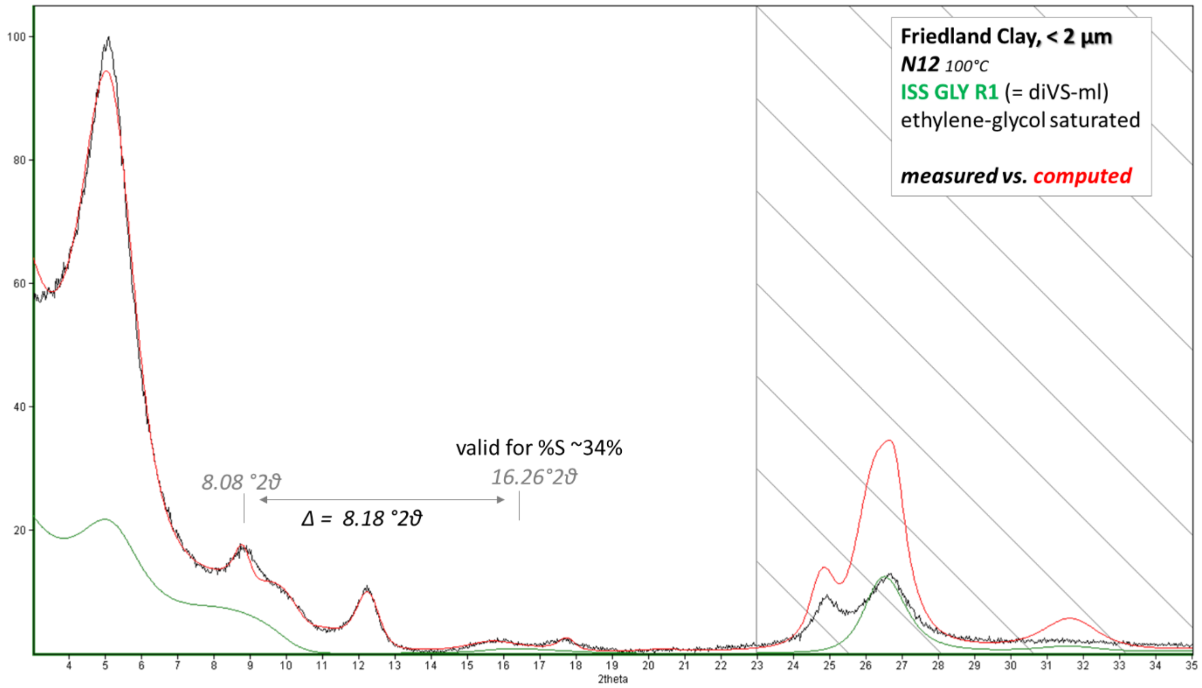
Friedland Clay, < 2 µm
N12 100°C
ISS GLY R1 (= diVS-ml)
ethylene-glycol saturated
measured vs. computed
valid for %S ~34%
8.08 °2ϑ
16.26°2ϑ
Δ = 8.18 °2ϑ
100
80
60
40
20
4
5
6
7
8
9
10
11
12
13
14
15
16
17
18
19
20
21
22
23
24
25
26
27
28
29
30
31
32
33
34
35
2theta

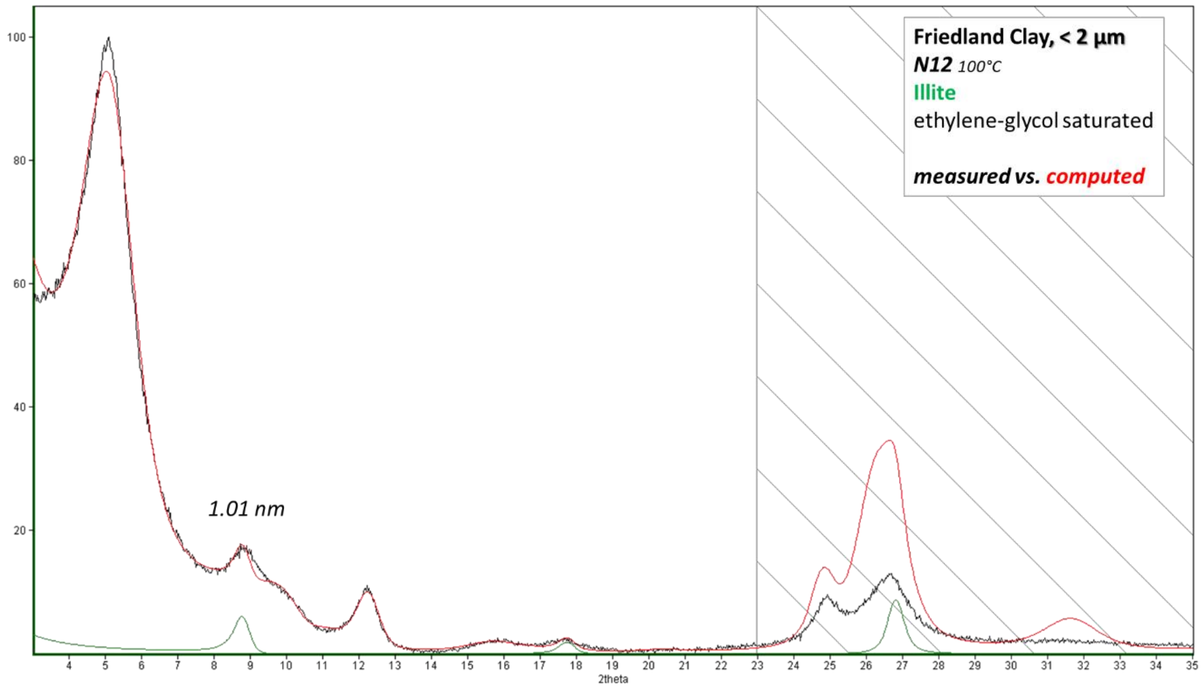
Friedland Clay, < 2 µm
N12 100°C
Illite
ethylene-glycol saturated
measured vs. computed
1.01 nm
100
80
60
40
20
4
5
6
7
8
9
10
11
12
13
14
15
16
17
18
19
20
21
22
23
24
25
26
27
28
29
30
31
32
33
34
35
2theta

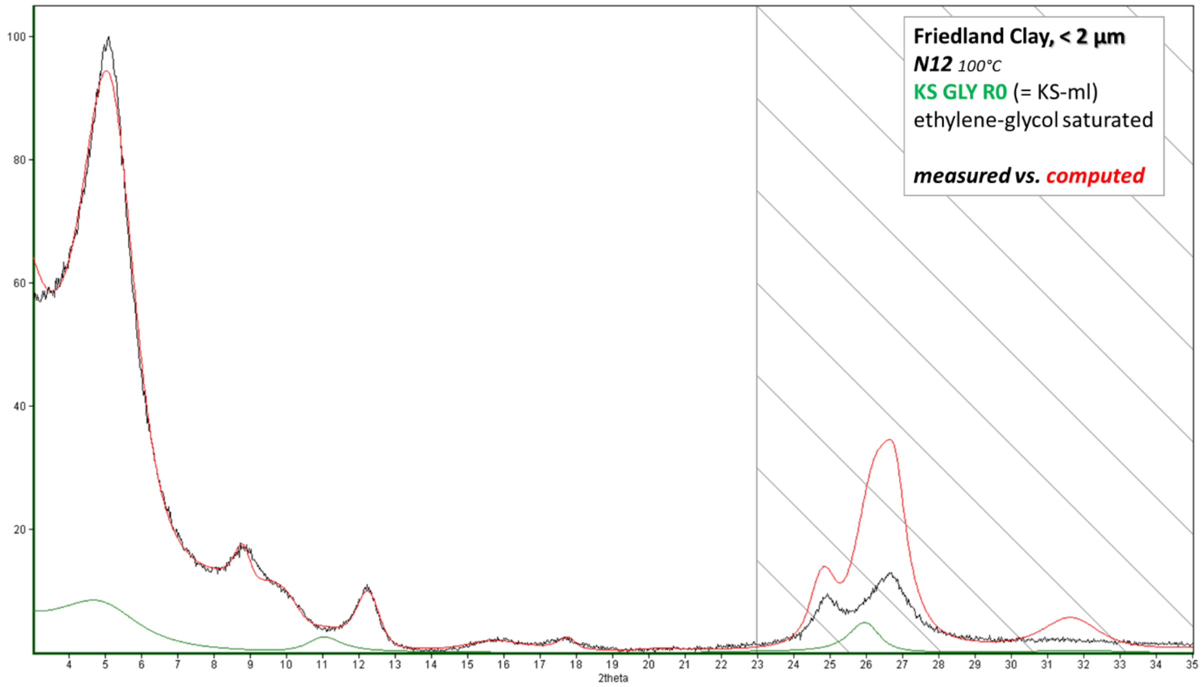
Friedland Clay, < 2 µm
N12 *100°C*
KS GLY R0 (= KS-ml)
ethylene-glycol saturated
measured* vs. *computed
100
80
60
40
20
4
5
6
7
8
9
10
11
12
13
14
15
16
17
18
19
20
21
22
23
24
25
26
27
28
29
30
31
32
33
34
35
2theta

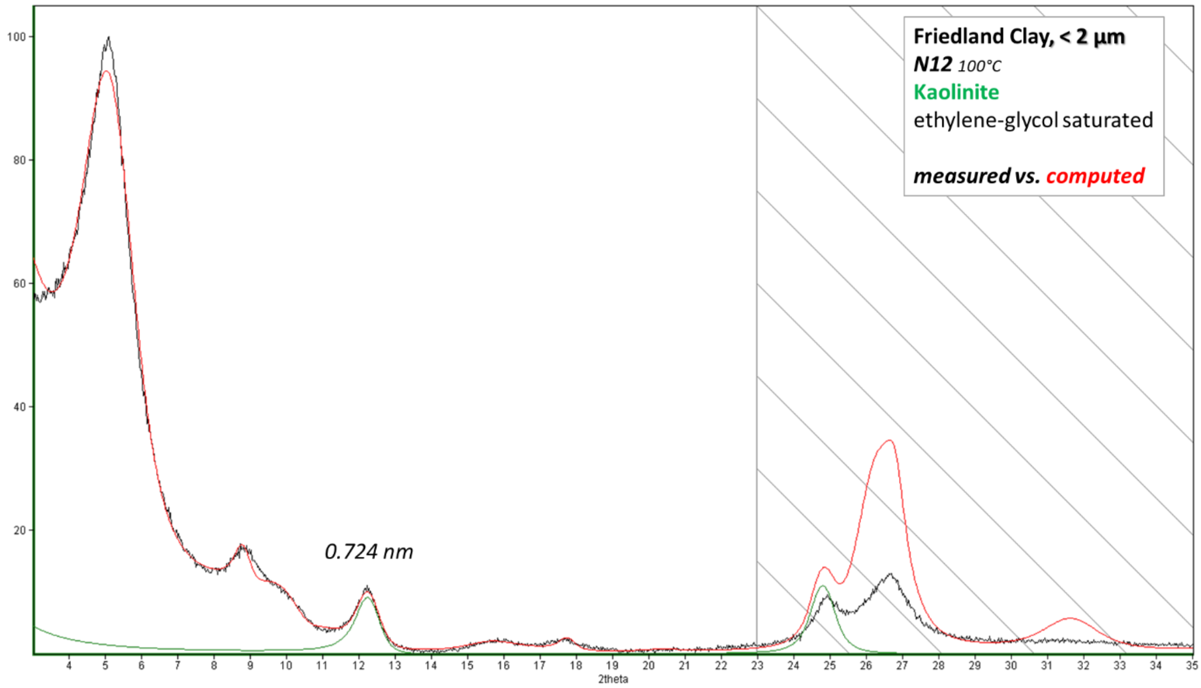
Friedland Clay, < 2 µm
N12 *100°C*
Kaolinite
ethylene-glycol saturated
measured* vs. *computed
0.724 nm
100
80
60
40
20
4
5
6
7
8
9
10
11
12
13
14
15
16
17
18
19
20
21
22
23
24
25
26
27
28
29
30
31
32
33
34
35
2theta

S3. Fourier Transform Infared Spectroscopy (FTIR)

SUPPLEMENT – FTIR: bulks

Content

Methodology – Fourier Transform Infrared (FTIR) of powder samples

Fourier Transform Infrared (FITR) spectroscopic study was implemented by the Varian 670-IR series FT-IR spectrometer. The powder samples (bulk samples) of approximately 1 to 2 mg were mixed homogenously in 120 mg of KBr, which was pre-dried at 80 °C for at least 6 hours, then placed into a dye under pressure to form a pellet of 13 mm in diameter. The spectra are recorded in the mid-infrared range, which extends from 400 cm^{-1} to 4000 cm^{-1} with multiple scan (*e.g.*, 64 scans and 4 cm^{-1} resolution), at room temperature. The OH-stretching region between 3800 cm^{-1} and 3200 cm^{-1} and the OH-bending region between 1000 cm^{-1} and 750 cm^{-1} were investigated in detail. The FT-IR spectra were deconvoluted by Origin 2021 Peak Fitting. A Gaussian distribution function was applied to smooth the spectra and to provide the exact value of peak position, FWHM, intensity, and area. The interpretation of the absorption spectra followed mainly those given by Farmer (1974) and Farmer and Russel (1964).

References:

Gates, W.P., 2005. Infrared Spectroscopy and the Chemistry of Dioctahedral Smectites, in The Application of Vibrational Spectroscopy to Clay Minerals and Layered Double Hydroxides, J.T. Kloprogge, Editor. 2005, Clay Minerals Society. p. 0.

Goodman, B.A., Russell, J.D., Fraser, A.R. and Woodhams, F.W.D. 1976. A Mössbauer and I.R. spectroscopic study of the structure of nontronite. Clays and Clay Minerals 24, 53-59

Inoue, A. 1989. Infared spectra of interstratified illite/smectite from hydrothermall altered tuffs (Shinzan, Japan) and diagenetic bentonites (Kinnekulle, Sweden). Clay Science, 7, 263-275

Farmer, V.C. 1974. The layer silicates. Chapter 15 in: The IR Spectra of Minerals (V.C. Farmer, editor). Mineralogical Society, London. 539p

Farmer, V.C. and Russell, J.D. 1964. The infra-red spectra of layer silicates. Spectrochim. Acta 20, 1149-1173

Russell, J.D., and Fraser, A.R. 1994. Infrared methods. Chapter 1 In Clay Mineralogy: Spectroscopic and Chemical Determinative Methods. (M.J. Wilson, ed.) Mineralgoical Society, London.

Reaction Products

B25 - bentonite

The reaction products materials of B25 bentonite at 35 °C, 60 °C, 100 °C and 150 °C in cylinder form were divided into 3 parts of top cylinder (No0_T), center cylinder (No0-C), and bottom cylinder (No0_B) according to the changes in colour (macroscopy observation) and textures (microscopy under SEM-observation). They are characterized by FITR spectrocopic studies in the mid-infrared range from 400 – 4000 cm^{-1}. The monoclinic and triclinic layer structure of smectite and kaolinite reveals four well resolved (-OH) bands in FTIR spectra. There are some minor changes that found between untreated and treated mtaerials.

In OH-stretching regions, the bands at 3701 cm^{-1} of initial materials shifted to 3695 – 3698 cm^{-1} are assigned to the stretching vibration of surface hydroxyl groups of kaolinite. The vibrations of inner hydroxyl groups of Al-Al-OH in smectite at 3634 cm^{-1} in smectite of untreated B25 which associated with beidellites as mentioned by Gate, 2005 have shifted to lower wavenumber of 3621 – 3629 cm^{-1} in reaction products is related to change of beidellites to montmorillonite with high content of octahedral Mg^{2+}-content (Gate, 2005).

It is noted that, in the 520 cm^{-1} to 1100 cm^{-1} region of octahedral cations-OH bending and lattice deformation, not all the band are assigned for any one smectite but some are discernable in the spectra of most dioctahedral smectite. The strongest bands near 1000 – 1040 cm^{-1} belong to Si^{4+}-O stretching. According to Inoue (1989), the position of this band can use to identifed the subsitution of Al, Fe for Si in tetrahedral sheet. It means that, the isomorphic substitution in tetrahedral sheet of initial materials and all the reaction products at higher than 100 °C were apparently occurs except B25 bentonite at 35 °C 0.7 Ma but the tetrahedral sheet of other reaction products at lower temperatures of 35 °C and 60 °C seem to be occupied mainly by Si^{4+}. The presence of shoulders at nearly 930 cm^{-1} proved the high content of Fe in tetrahedral sheet of B25 bentonite as mentioned by Goodman et al. (1976)

The observations and assignments of the other bands follow:

- AlAlOH-bands are almost unchanged between initial materials (912 cm^{-1}) to reaction products (907 – 915 cm^{-1}) which belong to smectites. Anyway, it is depend on the condition of THMC experiment the exact wavenumber of this band can be related to tretrahedral Al^{3+} and octahedral Mg^{2+} and Fe^{3+} content, higher wavenumber bands are associated with higher content of octahedral Al^{3+} but lower wavenumbers being assigned to octahedral Mg^{2+} and Fe^{3+} (Gates, 2005). It indicated that after the experiment runs, the subsitution of Fe and Mg was occured in the octahedral sheet of B25-bentonite but this conclusion is quite strictly due to low variation of wavenumber between initial material and reaction products.
- FeAlOH vibration appeared at 875 cm^{-1} for initial materials and 860 – 879 cm^{-1} for reaction products and they are all represented for Fe-bearing smectite in compare with montmorillonite at 870 cm-1 (Gates, 2005)
- MgAlOH bands are characterized at about 830 cm^{-1}, this band shifted to lower wavenumbers after experiment which show high amount of Fe in octahedral sheet until the Mg value reach below ~0.5 Mg per unit cell and the presence of shoulders at ~866 cm^{-1} showed exist of beidellite in all range of experiments (Gates, 2005).

The presence of quartz in the B25 bentonite has limited the intepretation of chemical structure of smectite, especially octahedral occupacies at 750 – 500 cm^{-1} area due to several overlapping bands with quarzt whose intensities are highl correlated tot he chemistr of the octahedral sheet (Gates, 2005). In general the B25 bentonite composed of mainly two types of smectite, Al-smectite (illite/smectite mixed layer) and beidellite, they are both contain remarkable amount of Fe in the octahedral sheet and tetrahedral sheet. The transformation of them after experiment runs have not apparently detected due to small changes of wavenumbers of bands between initial materials and reactions products.

Tab. 1. *Band assignments (cm^{-1}) for IR spectral features in starting materials and reaction products in THMC-experiments of Bavarian (B25) clays*

untreated B25	B25+OPA+100 °C+110h (No0)			B25+OPA+100 °C+35d (No2)			B25+OPA+150 °C+4d (No3)			Assignment	Phases
	bottom	middle	top	bottom	middle	top	bottom	middle	top		
421	420	419	408	420	413	410	412	409	409	Si-O bend	
467	457	458	443	452	449	448	450	442	451	Si-O-Si bending	Quartz/Illite/smectite (beidelite)
525	515	514	514	513	512	513	512	512	513	Si-O-Al deformation	Kaolin/Illite/smectite (Beidelite, Montm, IS-ml)
693	690	691	690	691	691	691	690	690	691	Si-O, Al-O$_{ap}$ and Si-O	Quartz, ferruginous beidellite,
753	751	752	748	750	747	752	752	740	749	Al-O-Si stretch	Kaolin, illite, illite/smectite mixed layer
779	780	777	778	778	777	780	780	778	777	Si-O	Quartz
797	797	797	792	797	797	796	796	794	790	Si-O bend	Quartz/Kaolin
833	829	829	828	829	829	828	828	829	829	FeAlOH	Smectite (Montm, IS-ml)/Illite
875	865	860	879	878	865	879	863	865	874	MgAlOH	Smectite (Montm, IS-ml)/Illite
912	909	909	908	908	907	908	904	908	909	AlAlOH	Smectite (Montm, IS-ml)/Illite
1034	1034	1032	1022	1022	1027	1030	1031	979	1034	Si-O stretching	Smectite (Montm., beidelite, IS-ml)/Illite/Kaolin
3626	3627	3623	3621	3628	3625	3625	3629	3625	3627	v4 Stretch inner OH	Kaolin/Illite/Smectite
3698	3696	3695	3697	3697	3698	3697	3697	3695	3696	N1 Stretch inner surface OH	Kaolin

Tab. 1 *(continued)*

untreated B25	B25+OPA+35°C+93.6h (No4)			B25+OPA+60°C+454h (No5)					Assignment	Phases
	bottom	middle	top	bottom	middle	top	No15_B25 VSD 125 °C	No23_B25 290h 0.7Ma 35°C		
421	420	420	417	419	421	419	417	415	Si-O bend	
467	456	460	456	457	450	457	453	447	Si-O-Si bending	Quartz/Illite/smectite (beidelite)
525	516	519	512	517	512	517	512	509	Si-O-Al deformation	Kaolin/Illite/smectite (Beidelite, Montm, IS-ml)
693	691	692	691	689	690	690	684	692	Si-O, Al-O$_{ap}$ and Si-O	Quartz, ferruginous beidellite,
753	751	751	748	752	749	751	743	745	Al-O-Si stretch	Kaolin, illite, illite/smectite mixed layer
779	779	779	780	779	778	779	779	780	Si-O	Quartz
797	797	793	795	795	796	791	796	797	Si-O bend	Quartz/Kaolin
833	829	829	829	830	829	829	832	828	FeAlOH	Smectite (Montm, IS-ml)/Illite
875	876	875	865	867	876	877	878	877	MgAlOH	Smectite (Montm, IS-ml)/Illite
912	909	909	908	910	908	915	910	908	AlAlOH	Smectite (Montm, IS-ml)/Illite
1034	1036	1040	1035	1036	1037	1035	1033	1032	Si-O stretching	Smectite (Montm., beidelite, IS-ml)/Illite/Kaolin
3626	3624	3624	3632	3627	3625	3625	3629	3626	v4 Stretch inner OH	Kaolin/Illite/Smectite
3698	3696	3698	3698	3697	3697	3696	3696	3696	N1 Stretch inner surface OH	Kaolin

Note: * shoulder

Opalinus clay

The band assignments (cm-1) for IR spectral features of starting materials and reaction products in THMC-experiments of Opalinus clay are presented in /tab. 2/ and data sheet in supplements. The mineralogical composition of Opalinus clay shows no difference between untreated and treated materials although the position of bands (wavenumer) have slightly shifted to lower or higher frequencies – depend on the which reflect a change in structure of clay minerals.

OH stretching region of octaedral cation at 3500 – 3700 cm^{-1}: quantitative differences can not be observed in the OH-stretching band spectra of smectite that are associated with the identities oft he OH-shareing octahedral cation pairs in OPA clay. The postion of the main absortion band is near 3620 cm^{-1} (AlAlOH) have shown an almost unchanged wavenumber except the material at 60 °C of VSB which shows 3635 cm-1. The occurences of illite/muscovite in OPA clay can be a reason for this undetecable change of this band because the micaeous minerals could be decomposed into an overlapping bands whose intensities were correlated to the chemistry of octahedral cation pairs (Gates, 2005).

A strong band near 1024 – 1038 cm^{-1}, associated with Si4+-O stretching, is present in the spectra of all initial and reation products. The exact position of this band is dependent on the structural chemistry, for example the lowest wavenumber at 1015 cm-1 is typical for illite (Si = 3.0 formula unit) but 1037 cm^{-1} is fully montmorillonite (Si = 4.0 formula unit) (Inoue, 1989), it means that the OPA clay seems to change from higher smectitic layer smectite (montmorillonite type) to illitic type (illite/smectite mixed layer) after the experiment runs.

In the OH-bending regions, the octahedral cations of Al, Fe, and Mg are assigned by AlAlOH, FeAlOH, and MgAlOH at ~ 910 cm^{-1}; ~ 830 cm^{-1}, and ~ 874 cm^{-1}. The AlAlOH and FeAlOH band showed a slightly shift toward lower wavenumber which is opposite to MgAlOH band. This change indicated probably the occurence of substitution between Al and Fe, Mg in octahedral sheet but not clearly. The absence of band at 812 – 816 cm^{-1} showed a poorly Fe in chemical structure of OPA clay in both initial and reaction products. A shoulder at ~ 750 cm^{-1} in initial material has appeared to real band at compacted and reaction products which showed the overlapping of kaolinite and intertratified illite/smectite phases (Russell and Fraser, 1994) in OPA clay.

In general, it is hard to see the real change in structure of OPA after THMC-experiment runs but a small changed could be concluded, especially the of Al or/and Fe for Si in tetrahedral sheet. The impurities as calcite, pyrite are remained in the reaction products but they are not deeply investigate in this method.

Tab. 2. *Band assignments (cm^{-1}) for IR spectral features in starting materials and reaction products in THMC-experiments of Opalinus clay.*

untreated OPA	No6_ Opalinus compacted	No9a-OP5+ 35 °C	No. 22 - OPA + 35 °C - VSE	No. 7 - OP2+ 60 °C - VSB	No09_ Opalinus VSE 60°C	No8-OP3+ 100 °C	No09b-01_OP06+ 125 °C	No14_Opalinus VSC 125°C	No13_Opalinus VSB 150°C	Assignment	Phases
426	422	423	419	426	419	422	423	421	421	Si-O bend	
469	459	455	462	466	456	462	458	453	457	Si-O-Si bending	Quartz/Illite/smectite (beidelite)
535	522	522	525	529	522	525	522	521	517	Si-O-Al deformation	Kaolin/Illite/smectite (Beidelite, Montm, IS-ml)
696	689	693	969	696	689	695	689	694	694	Si-O	Quartz
751*	749	749	751	749	749	750	749	752	743	Al-O-Si stretch	Kaolin, illite
778	779	778	780	778	779	778	780	779	780	Si-O	Quartz
798	799	798	798	799	796	797	798	799	798	Si-O bend	Quartz/Kaolin

831	827	828	828	830	833	828	828	828	829	FeAlOH	Smectite (Montm, IS-ml)/Illite
874	874	874	873	873	875	874	874	876	873	MgAlOH	Smectite (Montm, IS-ml)/Illite
911	908	909	983	910	908	908	908	909	910	AlAlOH	Smectite (Montm, IS-ml)/Illite
988	988	986	983	1005	989	983	1001	1000	992	Si-O stretching	Smectite (Montm., beidelite, IS-ml)/Illite/Kaolin
1038	1031	1027	1024	1026	1029	1028	1025	1028	1028		
1163	1162	1166	1115	1169	1166	1166	1114	1115	1112	-	Pyrite
1428	1432	1429	1442	1416	1439	1436	1432	1433	1433	-	carbonate
1632	1625	1630	1635	1635	1635	1635	1639	1637	1641	-	Pyrite
				1796							carbonate
3620	3620	3619	3620	3635	3619	3619	3619	3619	3620	v4 Stretch inner OH	Kaolin/Illite/Smectite
3698	3695	3695	3697	3695	3695	3694	3695	3695	3695	N1 Stretch inner surface OH	Kaolin

Note: * shoulder

Friedland clay

The mineralogical composition of Friedland clay under FTIR-investigation of FTIR is compatible with previous XRD-measurement. The AlAlOH of smectite in stretching region (3623 cm^{-1}) is shifted to lower wavenumber (3618-3620 cm^{-1}) after experiment runs which indicated an influence of cation pair mass and decreased valence (Gates, 2005). According to Madejova et al. (1994), the presence of FeMgOH at ~3580 cm^{-1} is assigned for FeMgOH of Fe-smectite, this band moved to lower wavenumber for the reaction products of low temperature runs but higher for high temperature runs. It indicated the substitution of Mg for Fe in octahedral sheet of reaction products.

The OH-bending region is composed of bands from AlAlOH, FeAlOH, and MgAlOH which are characterized the spectra of octahedral cations from dioctahedral smectites. The AlAlOH band is almost unchanged after experiment runs which have moeratedly resolved band of 909 – 911 cm^{-1} of Al dominace in octahedral sheet with participant of Fe and Mg. The FeAlOH band appeared at higher wavenumbers 882 cm-1 and shifted to 880 – 885 cm^{-1} of montmorillonite (Gates, 2005). Otherwises, the low frequencies of FeAlOH at 829 – 834 cm^{-1} is in range of Fe-bearing smectites. In addition, the Si-O of tetrahedral seet showed a large shift between initial and reaction materials. At 100 °C experiment, the lowest wavenumber is found but the others are showed the higher wavenumber in compare with starting materials, it mean that the Si is still acted as main cation in tetrahedral sheet but Si-surplus at 35 °C and 125 °C experiment as view point of Inoue (1989).

In general, the analysis oft he infared spectra of Friedland clay confirms a change in tetrahedral sheet of smectite but octahedral sheet showed a less effect from THMC-experiments. The main Al octahedral cation remains largely occupation but high amount of Fe is also expected in octahedral sheet. Unfortunately, it is impossible from the present data to interprete the sign of large transformation of FRT clay as well as presence of interstratifications phases.

Tab. 3. *Band assignments (cm^{-1}) for IR spectral features in starting materials and reaction products in THMC-experiments of Opalinus clay.*

untreated Friedland clay (No19)	2_No10_Friedland VSC 35 °C	3_No11_Friedland VSC 60°C	4_No12_Friedland 100°C	5_No20_Friedland VSC 125 °C	6_No16_Friedland VSD 125 °C	7_No21_Friedland VSC 150 °C	Assignment	Phases
418	419	422	426	422	417	422	Si-O bend	
448	446	449	466	449	445	459	Si-O-Si bending	Quartz/Illite/smectite (beidelite)
512	516	516	529	516	515	519	Si-O-Al deformation	Kaolin/Illite/smectite (Beidelite, Montm, IS-ml)
694	693	693	696	693	690	693	Si-O	Quartz
754*	753	755	759	755	752	753	Al-O-Si stretch	Kaolin
779	779	779	779	779	779	779	Si-O	Quartz
797	797	797	798	797	797	798	Si-O bend	Quartz/Kaolin

829	834	830	830	830	829	829	FeAlOH	Smectite (Montm, IS-ml)/Illite
882	880	880	882	885	880	880	MgAlOH	Smectite (Montm, IS-ml)/Illite
909	909	909	911	911	908	909	AlAlOH	Smectite (Montm, IS-ml)/Illite
987	988	985	980	991	981	993		
1028	1074	1032	1023	1028	1044	1030	Si-O stretching	Smectite (Montm., beidelite, IS-ml)/Illite/Kaolin
1163	1169	1166	1107	1108	1168	1166	-	Pyrite
1632	1632	1639	1632	1632	1635	1627	-	HOH
3587	3577	3576	-	3589	3572	3587	FeMgOH	Fe-smectite
3623	3620	3619	3618	3620	3620	3620	v4 Stretch inner OH	Kaolin/Illite/Smectite
3696	3696	3695	3696	3696	3694	3696	N1 Stretch inner surface OH	Kaolin

Note: * shoulder

Data Sheet – B25 bentonite, treated materials *(OPA, 35 °C, 93.6h)*

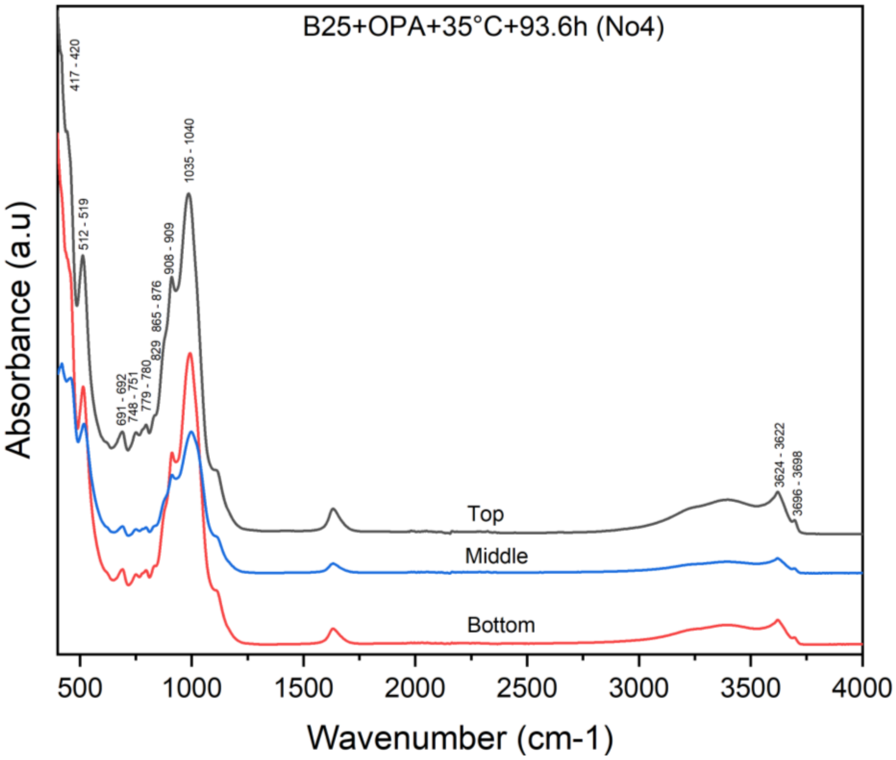

Fig. 1. FTIR-spectra of B25+OPA+35 °C+93.6 h in the top, center and bottom of clay cylinder

Tab. 4. Decomposition of FTIR-spectra of B25+OPA+35 °C+93.6 h in the top, center and bottom of clay cylinder by Gaussian of Origin 2021

Top				Middle				Bottom			
Area Fit	Center Max	Max Height	FWHM	Area Fit	Center Max	Max Height	FWHM	Area Fit	Center Max	Max Height	FWHM
9,48206	748,50377	0,10208	87,26233	2,18795	738,69969	0,02088	98,41916	9,48206	748,50377	0,10208	87,26233
0,19539	780,61635	0,01484	12,37198	0,34334	750,57577	0,01302	24,76861	0,19539	780,61635	0,01484	12,37198
0,61591	795,92435	0,03371	17,16519	1,3448	793,50253	0,02956	42,73957	0,61591	795,92435	0,03371	17,16519
1,05785	859,0814	0,05123	19,39928	0,47861	830,52833	0,02028	22,1667	1,05785	859,0814	0,05123	19,39928
2,18544	874,25983	0,09897	20,74352	3,06964	868,65325	0,04823	59,79104	2,18544	874,25983	0,09897	20,74352
14,90171	907,55025	0,29642	47,22804	0,46391	911,81063	0,02226	19,57563	14,90171	907,55025	0,29642	47,22804
68,9626	987,15947	0,72455	89,41603	29,31083	998,8206	0,28911	95,24315	68,9626	987,15947	0,72455	89,41603
1,64617	1035,27267	0,04994	30,96916	0,9917	1040,50565	0,02844	32,75361	1,64617	1035,27267	0,04994	30,96916
23,73441	874,25201	0,16354	136,33852	0,26299	868,65325	0,01105	22,35988	23,73441	874,25201	0,16354	136,33852
0,85135	831,6684	0,03313	24,14027	8,08884	911,81063	0,11525	65,93617	0,85135	831,6684	0,03313	24,14027
0,17614	829,31993	0,01329	12,45249	0,06902	828,67003	0,00514	12,61149	0,17614	829,31993	0,01329	12,45249
0,7667	865,0129	0,03715	19,38958	0,01063	836,70646	0,00146	6,86103	0,7667	865,0129	0,03715	19,38958
3,20756	880,23948	0,11196	26,91316	0,12591	860,9024	0,00741	15,96388	3,20756	880,23948	0,11196	26,91316
5,58014	908,25447	0,1909	27,46059	0,88136	874,89131	0,03733	22,1812	5,58014	908,25447	0,1909	27,46059
0,68216	931,09793	0,03609	17,75844	0,48321	889,85954	0,02349	19,32318	0,68216	931,09793	0,03609	17,75844
				1,90183	909,06713	0,07143	25,01317				
38,2759	2666,62217	0,03623	992,45387	0,50868	930,50042	0,02216	21,56121	38,2759	2666,62217	0,03623	992,45387
13,1613	3224,56836	0,04995	247,52103					13,1613	3224,56836	0,04995	247,52103
23,79007	3433,87343	0,08693	257,09044	19,12874	3146,99218	0,02498	719,29762	23,79007	3433,87343	0,08693	257,09044
4,26634	3574,72634	0,03907	102,59697	0,6086	3206,97658	0,00433	132,09085	4,26634	3574,72634	0,03907	102,59697
5,94866	3632,19763	0,07806	71,59303	10,00385	3433,92345	0,0282	333,20812	5,94866	3632,19763	0,07806	71,59303
1,17477	3698,22475	0,03221	34,26192	3,41143	3624,42845	0,02342	136,82705	1,17477	3698,22475	0,03221	34,26192
				0,46939	3624,42875	0,0106	41,58286				
				0,13916	3698,96053	0,0069	18,95915				

Data Sheet – B25 bentonite, treated materials *(35 °C, 0.7Ma, 290h-VSD)*

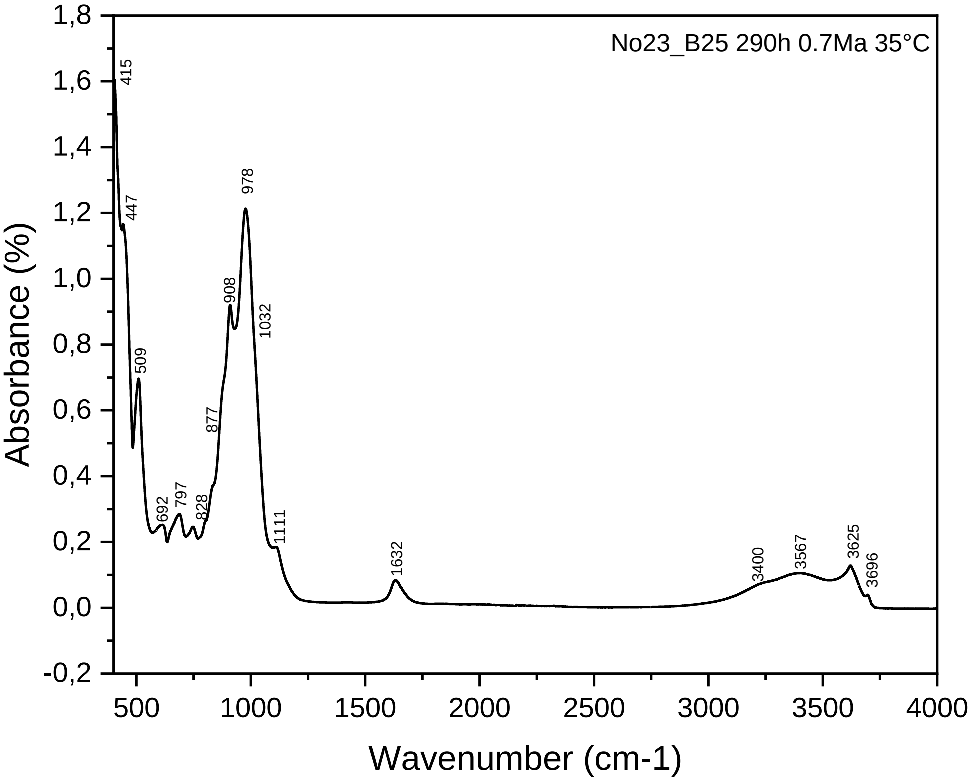

Fig. 2. FTIR-spectrum of bulk material of B25+35 °C+290h_VSD

Tab. 5. Decomposition of FTIR-spectra of B25+35 °C+290h_VSD by Gaussian of Origin 2021

Area Fit	Center Max	Max Height	FWHM
1,34172	748,67673	0,04559	27,64799
0,43557	780,56088	0,01999	20,46996
0,47799	797,65151	0,03026	14,84105
10,55632	838,33902	0,18462	53,71613
7,10655	870,91241	0,23549	28,35038
31,68778	906,44795	0,61489	48,41303
82,56992	977,95743	1,02248	75,86377
6,88687	1032,25612	0,16064	40,27574
2,13076	713,49977	0,03076	65,06852
41,67375	748,59033	0,82964	47,1889
0,43651	827,77527	0,02564	15,99361
6,97849	877,39713	0,20643	31,75878
9,5107	907,5655	0,32664	27,35319
1,94032	930,39222	0,07911	23,04119
2,01808	3141,38437	0,01209	156,84344
1,24179	3220,69651	0,01204	96,88652
32,46519	3400,15279	0,0919	331,86889
1,69941	3567,24894	0,023	69,42308
5,30726	3625,59165	0,0796	62,63272
0,21544	3695,79829	0,01422	14,23035

Data Sheet – B25 bentonite, treated materials *(OPA, 60 °C, 454h)*

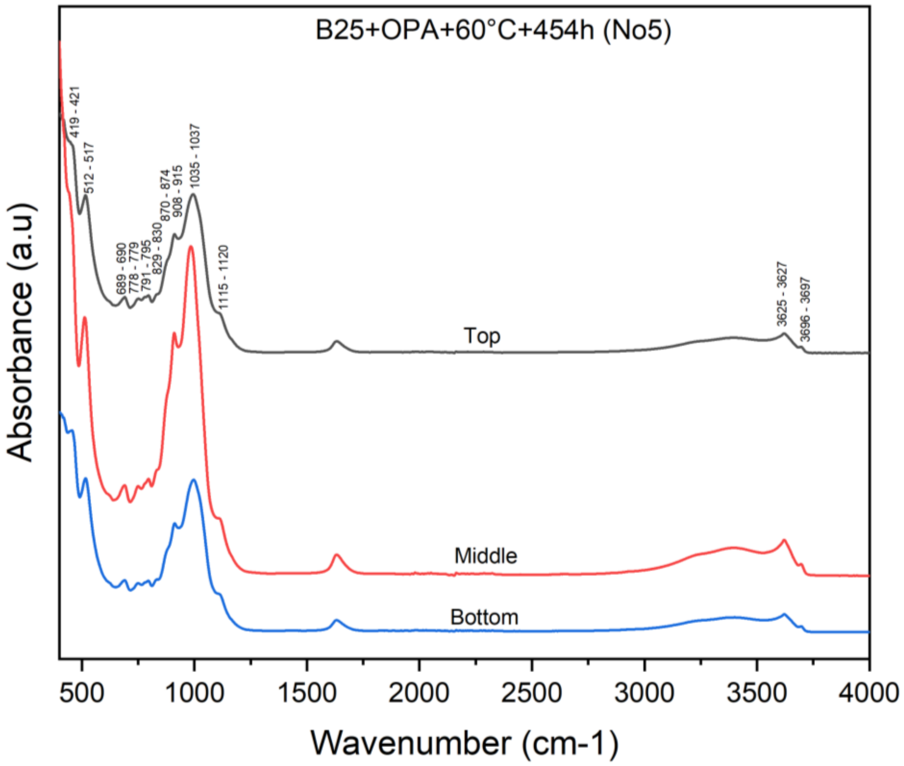

Fig. 3. FTIR-spectra of B25+OPA+100 °C+35d in the top, center and bottom of clay cylinder

Tab. 6. Decomposition of FTIR-spectra of B25+OPA+100 °C+35d in the top, center and bottom of clay cylinder by Gaussian of Origin 2021

Top				Middle				Bottom			
Area Fit	Center Max	Max Height	FWHM	Area Fit	Center Max	Max Height	FWHM	Area Fit	Center Max	Max Height	FWHM
0,94308	751,01222	0,02547	34,78376	4,60288	748,65826	0,05629	76,81703	1,19697	752,27899	0,025	44,98062
10,6139	751,01339	0,0186	536,12727	0,44098	796,39535	0,02366	17,51036	0,22775	779,23418	0,01392	15,37292
1,33457	790,90335	0,03506	35,76447	1,09437	835,54472	0,03865	26,59944	0,57364	795,92635	0,02715	19,84901
0,47722	829,92019	0,02231	20,09253	25,97272	870,33358	0,12288	198,56245	0,57712	829,55147	0,01992	27,21231
0,61327	862,3214	0,01609	35,80764	4,31558	870,33411	0,14233	28,48478	1,41536	873,57535	0,04369	30,43126
0,41492	873,81413	0,01745	22,33854	17,6062	907,84043	0,34929	47,35231	1,80925	873,57535	0,017	99,99458
17,5148	915,33667	0,18486	89,0105	68,36052	986,26246	0,75578	84,97258	1,67181	909,65751	0,05412	29,02198
10,60682	990,68229	0,147	67,78299	1,94695	1036,64286	0,05936	30,81388	13,58773	927,73154	0,13992	91,22623
10,75838	990,72538	0,14806	68,26378					20,65286	994,73746	0,28134	68,96305
7,49396	1034,74266	0,13663	51,52626	0,18596	829,16646	0,01348	12,95614	5,8862	1036,78241	0,11446	48,30944
0,6098	909,50984	0,02868	19,97786	0,56404	861,83238	0,03294	16,0852				
				2,98952	876,41036	0,12719	22,08124	0,11328	829,6285	0,0076	14,00076
0,09772	829,13678	0,00693	13,25293	0,88887	890,4699	0,04972	16,7942	0,45033	867,04562	0,01975	21,4216
0,06891	862,0128	0,00514	12,59447	6,34229	908,13017	0,22588	26,37723	1,45853	882,1774	0,04888	28,02958
1,62185	876,75648	0,05371	28,36557	1,00236	930,10862	0,0513	18,35539	2,52068	909,80157	0,08765	27,01831
2,85466	908,92359	0,08669	30,93596					0,40226	931,68326	0,02008	18,82032
0,19781	933,74782	0,01181	15,73628	1,88504	3077,84346	0,0099	178,78908				
				5,95169	3217,04223	0,03229	173,16126	8,78452	3286,93117	0,02746	300,4735
4,86822	3121,52489	0,01072	426,60338	18,2841	3404,8001	0,06988	245,80237	0,75907	3379,37913	0,00671	106,25373
4,17355	3237,42955	0,0199	197,04464	3,44699	3564,27839	0,02567	126,15736	3,38574	3475,62386	0,01968	161,58745
6,60693	3397,87518	0,03293	188,46257	4,84505	3625,35635	0,05126	88,79179	3,01345	3603,73069	0,02392	118,34929
6,16944	3565,27542	0,02815	205,91598	0,68261	3625,35635	0,01889	33,94956	0,93535	3627,40689	0,01791	49,07356
0,18751	3565,28104	0,00417	42,23221	0,20336	3697,12994	0,01314	14,54078	0,05717	3696,52517	0,00482	11,14006
2,03637	3625,00418	0,03042	62,87946								
0,12626	3696,49928	0,00753	15,74598								

Data Sheet – B25 bentonite, treated materials *(OPA, 100 °C, 35d)*

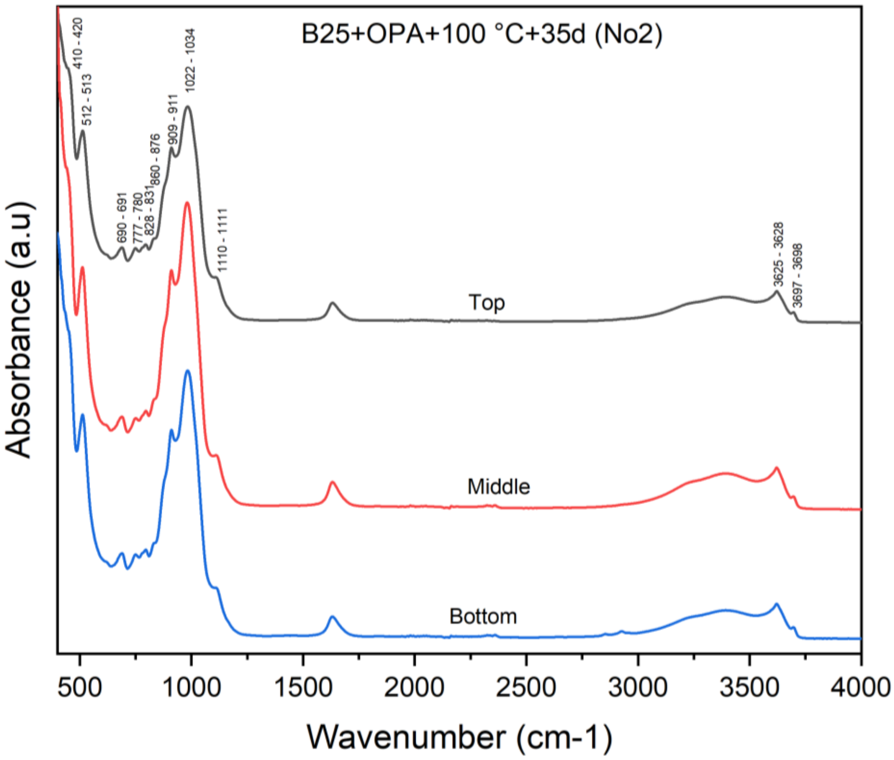

Fig. 4. FTIR-spectra of B25+OPA+100 °C+35d in the top, center and bottom of clay cylinder

Tab. 7. Decomposition of FTIR-spectra of B25+OPA+100 °C+35d in the top, center and bottom of clay cylinder by Gaussian of Origin 2021

Top				Center				Bottom			
Area Fit	Center Max	Max Height	FWHM	Area Fit	Center Max	Max Height	FWHM	Area Fit	Center Max	Max Height	FWHM
48,73495	752,8565	0,29618	154,5792	0,76851	746,59166	0,02909	24,81567	4,00319	749,57114	0,0674	55,80084
0,27559	779,96883	0,01838	14,08274	2,7311	796,14614	0,04789	53,57104	0,19293	777,7848	0,00922	19,65247
1,09611	795,89251	0,05084	20,25606	8,13503	796,14614	0,03761	203,19617	2,69482	797,27491	0,07261	34,86542
5,27453	827,77409	0,12769	38,80422	0,73277	829,14373	0,0402	17,12486	2,60241	831,43109	0,08961	27,2812
16,29919	874,36877	0,30078	50,90772	2,92492	859,61749	0,07271	37,79036	2,08603	859,99967	0,06111	32,06779
8,1423	911,26515	0,20587	37,15451	5,83927	909,33593	0,08549	64,16708	7,81829	876,05983	0,18546	39,60284
102,55866	983,93688	0,73606	130,89537	29,57119	909,33593	0,37612	73,86039	14,69641	910,23225	0,31521	43,80017
0,14038	1029,88012	0,00911	14,48081	48,24652	982,47595	0,6999	64,75842	60,84938	982,52492	0,63723	89,707
				9,00936	1026,8028	0,19923	42,48187	1,85115	1022,3619	0,04969	34,99675
0,19088	827,78092	0,01297	13,82378								
3,52514	878,75083	0,10134	32,67929	0,27683	829,05057	0,01706	15,24863	0,18179	828,55813	0,01395	12,24538
0,18621	894,22716	0,01412	12,38642	1,15214	865,13647	0,05572	19,42411	3,94815	878,21578	0,11608	31,9521
3,10865	908,3951	0,13059	22,3632	2,05249	878,21426	0,08988	21,45354	4,60102	908,39835	0,16729	25,83746
0,83731	927,44911	0,03928	20,02798	7,49751	906,83672	0,1875	37,56424	0,58291	929,66462	0,03243	16,88784
42,71935	2786,83011	0,0404	993,25214	12,29587	3159,77847	0,02421	477,06783	15,08789	3231,1338	0,03555	398,71503
7,61045	3117,17777	0,02263	315,91656	11,10567	3240,00746	0,04909	212,53928	3,2984	3231,14884	0,02062	150,3046
10,70087	3247,79439	0,05007	200,7846	20,20128	3421,97145	0,08966	211,67361	9,6492	3385,00038	0,05161	175,64831
14,02648	3398,12397	0,07254	181,65275	4,31669	3550,73296	0,03618	112,07531	6,44326	3505,37579	0,03833	157,92837
22,6709	3587,49261	0,08808	241,80892	8,29086	3625,17146	0,08329	93,51026	7,39754	3611,90808	0,0564	123,21941
2,2962	3624,6332	0,03921	55,02041	0,70201	3625,17162	0,02103	31,35276	0,14066	3621,14302	0,00909	14,54453
0,2378	3697,89022	0,01323	16,88575	0,40834	3698,49478	0,02027	18,9221	1,66544	3628,47402	0,02955	52,94563
								0,26432	3697,39757	0,01512	16,42145

Data Sheet – B25 bentonite, treated materials *(OPA, 100 °C, 110h)*

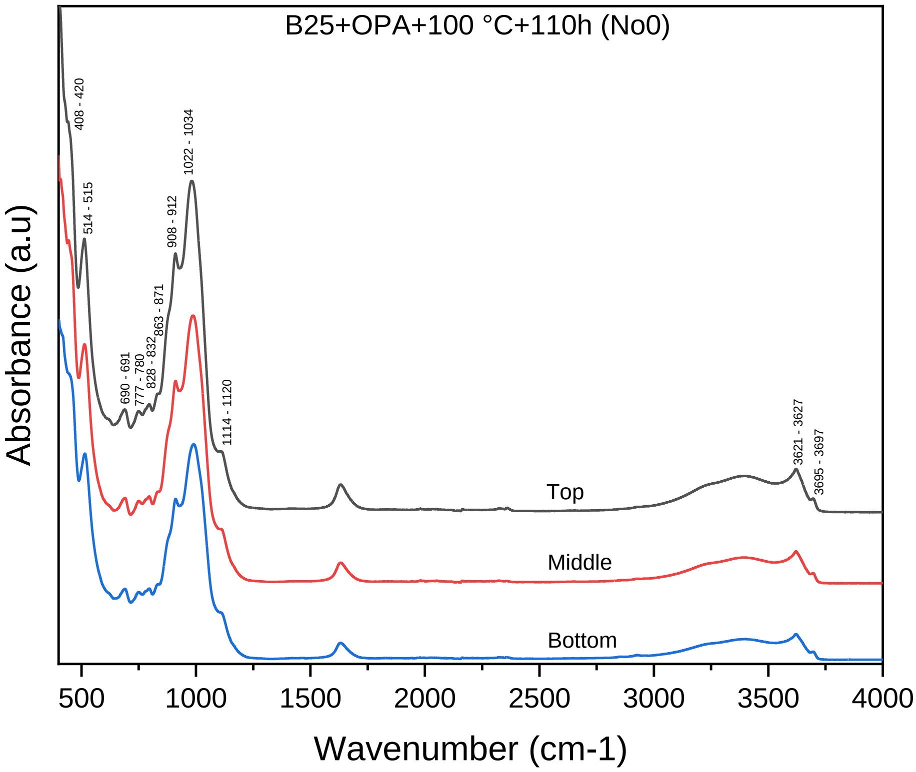

Fig. 5. FTIR-spectra of B25+OPA+100 °C+110h in the top, center and bottom of clay cylinder

Tab. 8. Decomposition of FTIR-spectra of B25+OPA+100 °C+110h in the top, center and bottom of clay cylinder by Gaussian of Origin 2021

Top				Center				Bottom			
Area Fit	Center Max	Max Height	FWHM	Area Fit	Center Max	Max Height	FWHM	Area Fit	Center Max	Max Height	FWHM
1,65	748,52	0,04	39,41	4,98	752,02	0,07	69,03	0,12	829,30	0,01	12,58
1,67	792,90	0,05	33,79	0,06	777,47	0,01	9,42	0,41	865,10	0,02	18,36
0,80	828,53	0,04	19,48	2,11	798,00	0,06	33,15	1,86	880,06	0,07	26,13
48,30	828,53	0,11	417,18	2,05	830,18	0,08	25,32	3,43	908,65	0,12	27,93
0,73	870,56	0,04	18,80	3,73	863,46	0,10	34,41	0,39	931,54	0,02	17,34
35,31	912,14	0,37	89,11	25,42	911,52	0,36	66,14				
1,16	912,14	0,05	19,94	3,98	958,32	0,10	39,37	5,69	750,66	0,07	80,39
31,83	980,27	0,52	57,19	33,58	988,77	0,50	62,52	1,70	796,51	0,05	33,72
17,75	1022,12	0,31	54,08	9,92	1032,42	0,19	48,06	2,54	831,85	0,07	32,14
1,53	939,02	0,01	104,87					5,05	869,29	0,13	37,66
				0,18	828,97	0,01	14,60	11,93	908,17	0,21	52,91
0,23	828,78	0,02	13,58	0,30	860,38	0,02	14,88	0,42	908,33	0,03	15,17
0,39	864,54	0,02	16,71	1,29	872,12	0,06	19,91	45,76	988,32	0,45	95,07
3,74	879,32	0,12	29,03	2,04	887,50	0,08	24,59	1,92	1034,66	0,05	36,50
5,49	908,42	0,19	27,13	3,72	908,96	0,15	24,03				
0,60	930,91	0,03	16,58	0,85	929,44	0,04	19,64	9,78	3279,05	0,03	279,53
								1,05	3375,65	0,01	108,52
14,26	3026,68	0,01	1710,45	2,65	3149,77	0,01	217,55	4,65	3470,13	0,03	162,48
3,20	3027,41	0,01	283,58	0,81	3217,55	0,01	106,54	3,90	3600,87	0,03	120,01
17,33	3264,02	0,06	252,56	19,08	3400,07	0,06	318,10	1,23	3627,09	0,02	48,82
10,25	3414,28	0,06	159,49	0,58	3541,39	0,01	63,65	0,07	3696,27	0,01	11,13
3,96	3503,85	0,04	102,19	0,36	3568,60	0,01	38,19				
1,44	3543,42	0,02	54,46	3,85	3623,14	0,05	66,60				
0,51	3569,51	0,01	34,76	0,14	3695,34	0,01	14,01				
8,85	3621,33	0,10	81,07								
0,63	3697,11	0,02	25,72								

Data Sheet – B25 bentonite, treated materials *(OPA, 125 °C, VSD)*

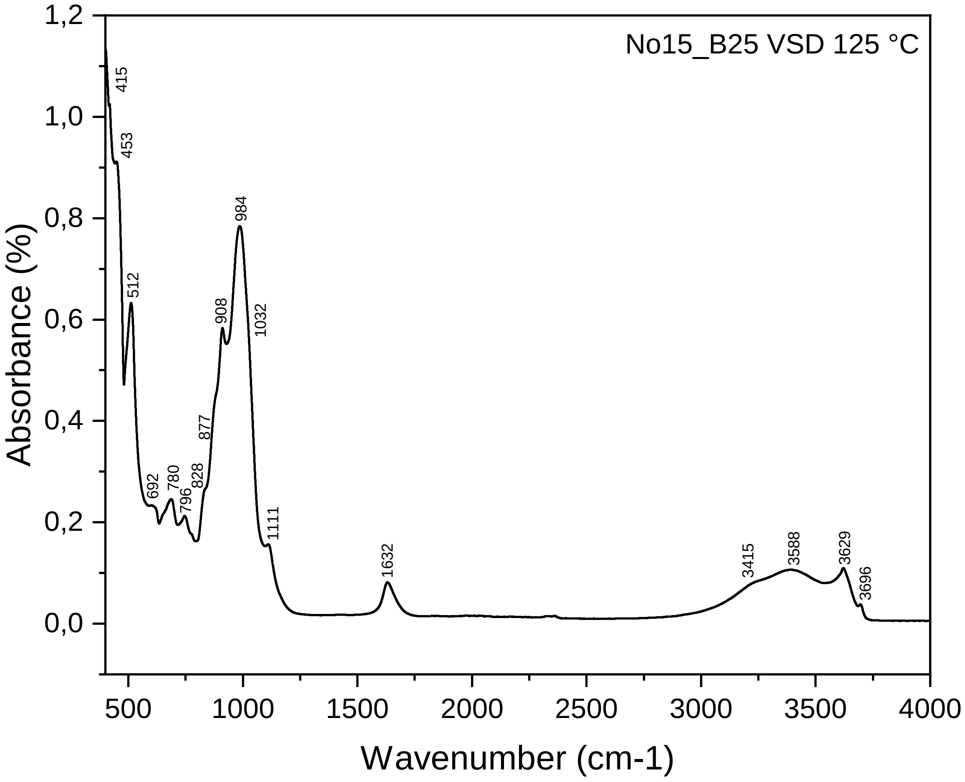

Fig. 6. FTIR-spectrum of bulk material of B25+125 °C_VSD

Tab. 9. Decomposition of FTIR-spectra of B25+125 °C_VSD by Gaussian of Origin 2021

Area Fit	Center Max	Max Height	FWHM
3,63926	831,58578	0,10153	33,67259
7,25274	870,3172	0,1766	38,581
0,90835	908,26954	0,04974	17,15666
54,27863	985,37513	0,63483	80,32296
5,00808	1032,87415	0,11527	40,81417
19,39372	910,61253	0,32181	56,61455
0,20607	820,93005	0,01292	14,98936
1,35717	831,96324	0,05288	24,11205
7,20521	878,06092	0,15266	44,3389
4,10126	910,06866	0,1543	24,96992
0,7783	930,52737	0,0403	18,14344
13,49922	3215,66278	0,03168	400,26159
4,0504	3219,85698	0,02303	165,2228
20,48826	3415,57521	0,07854	245,07556
5,4014	3588,15196	0,03962	128,06057
3,41315	3629,21575	0,0513	62,50778
0,37608	3696,30138	0,01756	20,12082

Data Sheet – B25 bentonite, treated materials *(OPA, 150°C, 4d)*

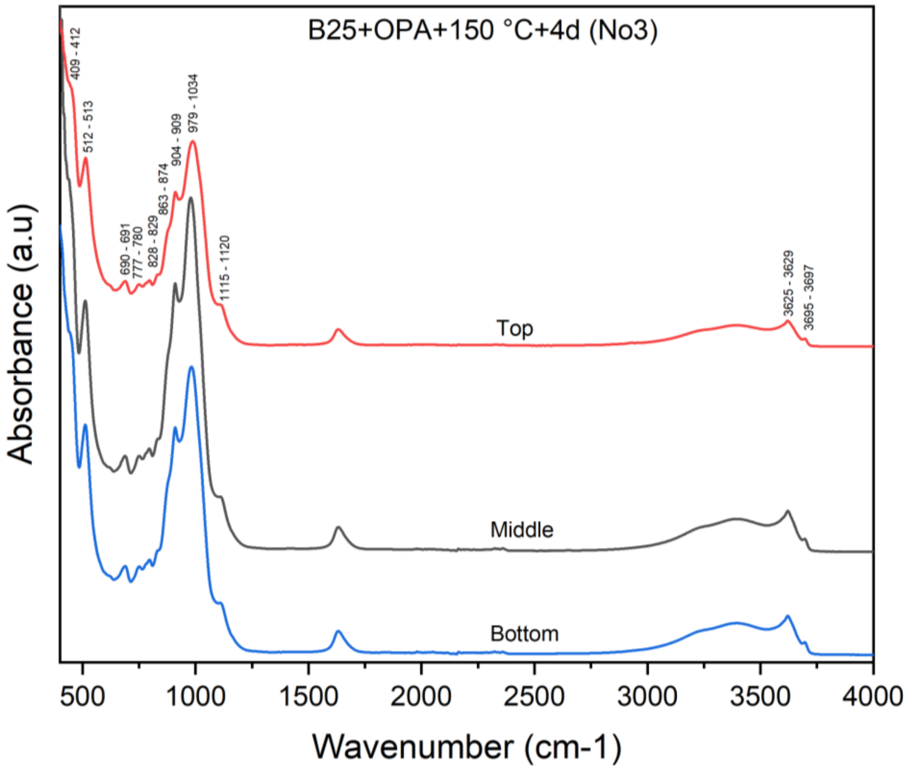

Fig. 7. FTIR-spectra of B25+OPA+150 °C+4d in the top, center and bottom of clay cylinder

Tab. 10. Decomposition of FTIR-spectra of B25+OPA+150 °C+4d in the top, center and bottom of clay cylinder by Gaussian of Origin 2021

Top				**Bottom**				**Center**			
Area Fit	Center Max	Max Height	FWHM	Area Fit	Center Max	Max Height	FWHM	Area Fit	Center Max	Max Height	FWHM
0,66329	749,40096	0,0217	28,7115	4,94119	752,76729	0,07823	59,33964	13,5863	739,95387	0,13091	97,50179
19,82115	790,53381	0,0623	298,86958	0,54651	780,01655	0,03155	16,27495	1,51543	794,66888	0,05617	25,34708
0,94728	790,56838	0,02816	31,60502	1,34312	796,14333	0,06292	20,05394	9,48771	794,66888	0,08991	99,13841
0,67323	830,99838	0,02691	23,49887	5,99582	833,27484	0,12308	45,76417	5,60736	832,33049	0,14681	35,88223
15,73842	908,7682	0,15228	97,09201	3,4519	868,31904	0,12392	26,16972	15,79188	873,01891	0,37931	39,11174
5,40014	908,7682	0,13415	37,81674	28,9869	906,19133	0,45016	60,49214	18,14879	908,17274	0,45323	37,61779
45,3885	990,17197	0,49808	85,60846	59,48906	983,0897	0,72218	77,38527	103,2434	979,4186	0,99403	97,57288
2,77926	1034,91786	0,06789	38,45767	3,60536	1031,06621	0,10202	33,19962				
2,0567	872,03698	0,07198	26,8423								
				0,92879	827,98136	0,03081	28,31912	0,2988	828,53663	0,01981	14,17071
0,17297	829,11514	0,01154	14,08059	0,11154	853,09796	0,00935	11,2088	1,17925	865,33307	0,05537	20,00802
0,31095	861,38773	0,01999	14,6153	0,88106	863,29347	0,05011	16,51658	4,77276	881,12534	0,16246	27,59883
1,53237	874,30121	0,07145	20,14877	1,44391	875,50529	0,07167	18,9253	7,73829	908,09361	0,27585	26,35353
1,19825	889,21994	0,05458	20,62361	9,39156	904,08315	0,18929	46,6111	0,98783	930,11736	0,05427	17,09824
3,58784	908,99375	0,13725	24,55703	0,62689	908,54994	0,04094	14,38335				
0,64505	929,78124	0,03327	18,2117	0,36229	962,40158	0,01924	17,68939				
9,69454	3248,80842	0,03608	252,39086	12,75968	3223,79134	0,04126	290,51382	4,34109	3190,35314	0,02201	185,27245
10,42773	3433,06937	0,04651	210,63618	1,52902	3223,79296	0,01226	117,20594	30,6632	3405,80527	0,08686	331,63636
4,73497	3596,04984	0,03515	126,54713	15,33194	3397,657	0,06925	207,98002	1,55806	3567,79651	0,02232	65,57699
1,78982	3627,05924	0,03257	51,62707	6,03182	3530,64129	0,03422	165,57245	5,15006	3625,44495	0,07895	61,28189
0,09	3696,70958	0,00746	11,3355	6,45435	3612,98448	0,05425	111,77247	0,18871	3695,78109	0,01259	14,08608
				0,14013	3621,12901	0,00953	13,80721				
				1,88929	3628,59544	0,03454	51,38663				
				0,24701	3697,03103	0,01502	15,45211				

Data Sheet – Opalinus, untreated compacted materials

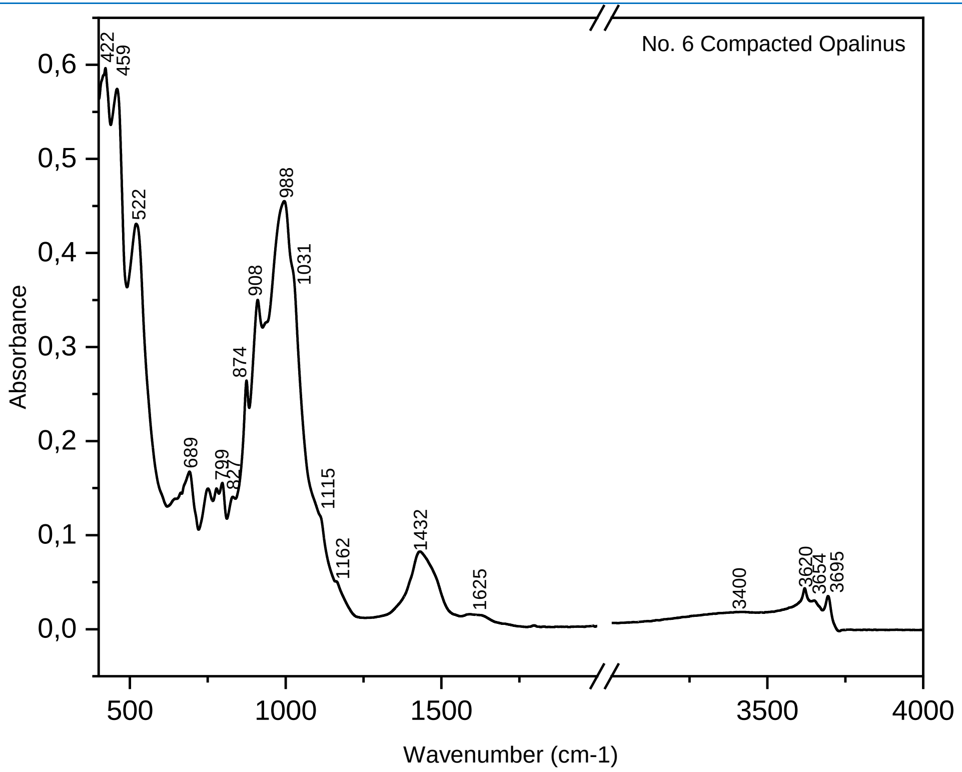

Fig. 8. FTIR-spectrum of initial material of compacted Opalinus clay

Tab. 11. Decomposition of FTIR-spectra of initial material of OPA by Gaussian of Origin 2021

Area Fit	Center Max	Max Height	FWHM
1,07	750,25	0,04	24,71
0,90	779,49	0,04	22,35
0,57	797,78	0,04	13,59
0,66	829,15	0,03	23,16
2,75	868,67	0,07	35,31
0,88	873,99	0,06	12,84
1,99	894,02	0,09	20,86
2,15	908,60	0,11	18,76
3,21	924,46	0,09	32,44
22,60	988,19	0,21	102,07
9,77	993,88	0,11	83,84
4,91	993,88	0,03	167,67
0,60	1031,91	0,03	19,19
0,20051	827,51226	0,01258	14,97079
0,55488	866,27728	0,02864	18,20052
0,63242	874,06194	0,05386	11,03072
7,62971	2861,0268	0,01154	621,25587
13,67435	3440,62177	0,02422	530,50171
1,26285	3599,07286	0,01067	111,18362
0,48149	3620,44902	0,01094	41,35363
0,14171	3620,4493	0,0114	11,67502
0,46529	3655,02339	0,01383	31,60026
0,13162	3678,15072	0,00592	20,89782
0,50444	3695,4844	0,02705	17,51668

Data Sheet – Opalinus, treated materials *(OPA, 150°C, 4d)*

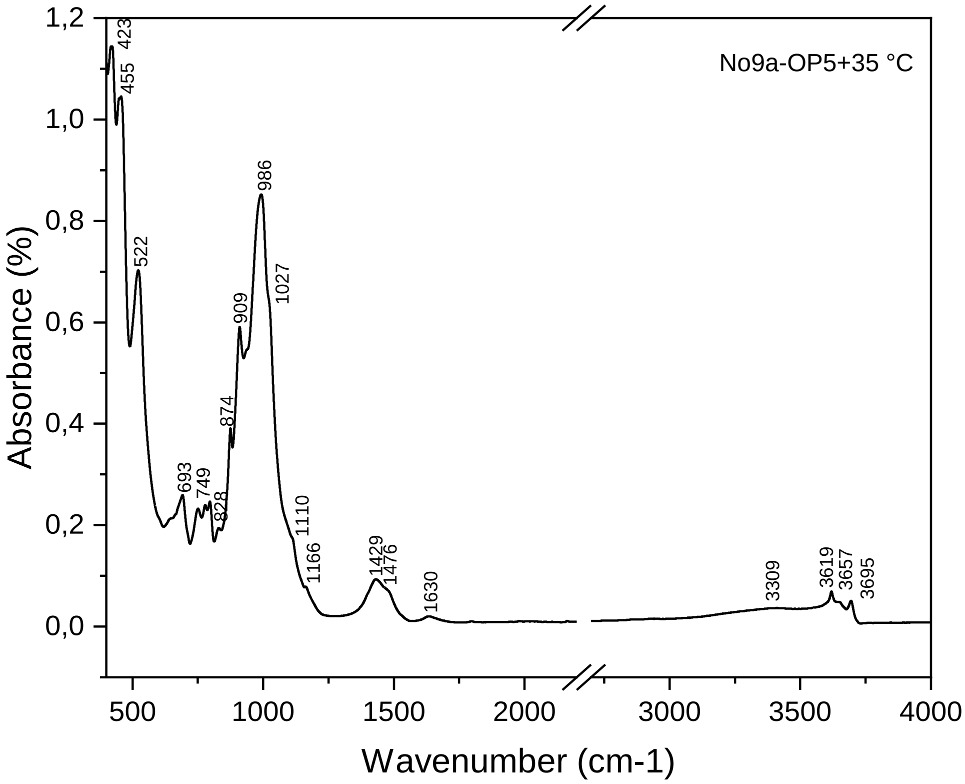

Fig. 9. FTIR-spectrum of OPA + 35 °C

Tab. 12. Decomposition of FTIR-spectrum of OPA + 35 ° by Gaussian of Origin 2021

Area Fit	Center Max	Max Height	FWHM	Area Fit	Center Max	Max Height	FWHM
1,79	750,16	0,07	25,62	0,19	828,47	0,01	13,16
1,71	779,70	0,07	22,99	0,82	866,50	0,04	18,23
0,85	797,44	0,06	12,30	0,99	874,32	0,09	10,90
4,11	873,74	0,05	72,80				
2,71	873,74	0,14	18,37	4,84	3309,20	0,01	315,35
12,02	908,59	0,33	33,78	3,26	3458,13	0,01	215,74
1,94	935,52	0,09	19,74	2,06	3587,59	0,02	116,82
56,12	985,66	0,66	79,82	0,22	3619,12	0,02	11,84
1,20	999,65	0,06	19,34	1,09	3657,33	0,02	51,95
1,69	1026,94	0,09	17,93	0,57	3695,11	0,03	17,17
3,33	1044,05	0,08	37,08	0,79	3619,12	0,01	51,06
1,50	1081,25	0,04	38,66				

Data Sheet – Opalinus, treated materials *(OPA, 35°C, VSE)*

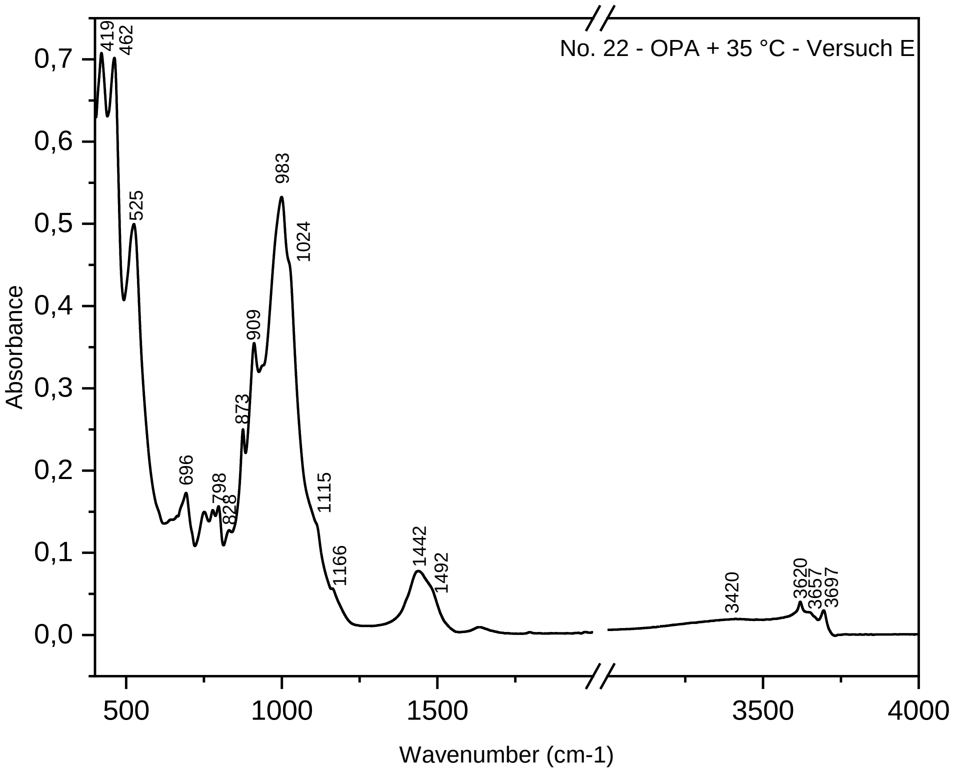

Fig. 10. FTIR-spectrum of OPA + 35 °C – VSE

Tab. 13. Decomposition of FTIR-spectrum of OPA + 35 °C – VSE by Gaussian of Origin 2021

Area Fit	Center Max	Max Height	FWHM	Area Fit	Center Max	Max Height	FWHM
1,76	751,36	0,05	33,90	0,15	828,04	0,01	13,83
0,85	780,08	0,04	18,57	0,61	868,23	0,03	18,96
0,79	797,60	0,05	14,62	0,59	874,96	0,05	10,65
0,24	827,18	0,01	15,69				
0,77	873,47	0,06	12,49	5,75	3420,68	0,01	402,98
1,31	908,61	0,07	18,77	0,64	3582,48	0,01	95,93
20,38	927,76	0,19	100,04	0,13	3619,54	0,01	11,28
8,21	982,89	0,19	40,08	0,59	3619,54	0,01	48,35
1,56	1000,64	0,07	19,71	0,19	3690,41	0,01	15,92
8,96	1023,93	0,20	43,06	0,15	3697,77	0,01	11,92
16,83	1023,99	0,13	123,34	0,51	3656,73	0,01	41,71

Data Sheet – Opalinus, treated materials *(OPA, 60°C, VSB)*

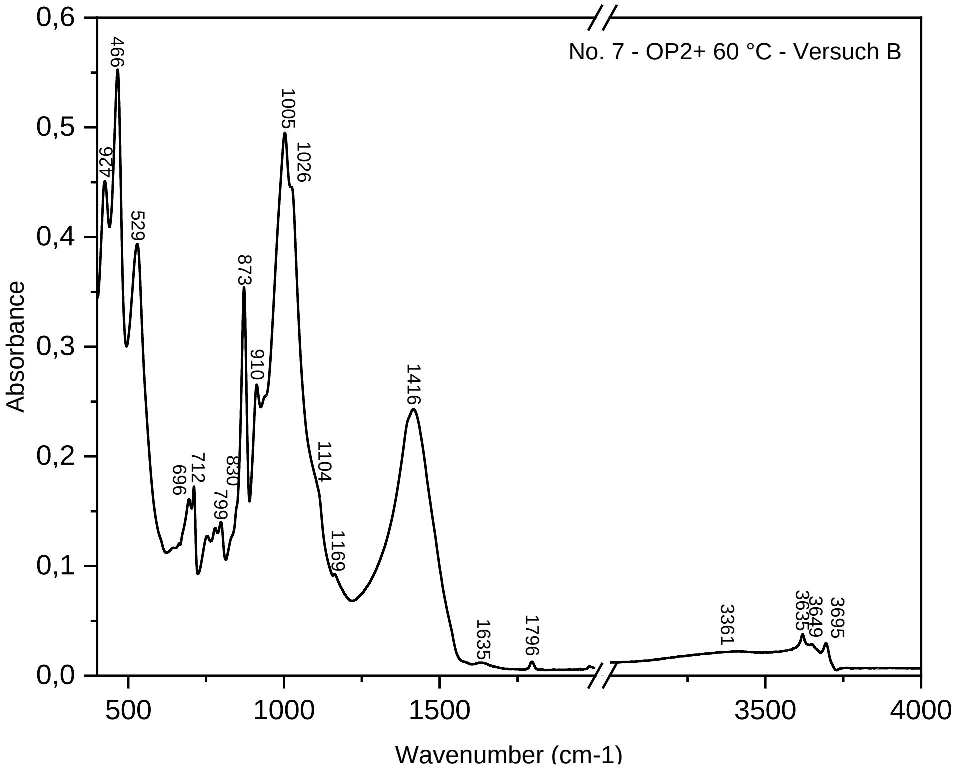

Fig. 11. FTIR-spectrum of OPA + 60 °C – Versuch B

Tab. 14. Decomposition of FTIR-spectrum of OPA + 60 °C – VSB by Gaussian of Origin 2021

Area Fit	Center Max	Max Height	FWHM	Area Fit	Center Max	Max Height	FWHM
12,11846	751,44865	0,06181	184,18279	0,07925	830,77339	0,00648	11,49257
0,58851	751,44865	0,0251	22,02916	0,22026	847,24473	0,01685	12,27859
1,47188	784,38405	0,03854	35,87343	1,62467	864,58656	0,09457	16,13995
0,24693	799,42252	0,02212	10,48689	2,00282	873,0972	0,15673	12,00471
6,16132	860,23429	0,09446	61,27862	0,26326	880,68758	0,03352	7,37768
3,86472	871,96481	0,20197	17,97597	0,1303	900,30241	0,01465	8,356
7,79846	918,09478	0,21585	33,941	0,93415	909,74302	0,06287	13,95948
0,55666	1000,82272	0,03193	16,37982	0,84575	920,92426	0,04151	19,13921
49,1635	1005,15238	0,42661	108,26214	0,29601	936,16455	0,02075	13,39954
361,54986	1103,89648	0,03783	8978,0377				
5,35933	1103,89676	0,09057	55,59008	4,7574	3411,13636	0,01077	415,14586
4,31837	1168,70707	0,04882	83,09891	0,72007	3603,79699	0,0065	104,06464
0,46336	1031,31172	0,03016	14,43433	0,15374	3619,03897	0,0101	14,29538
				0,00305	3634,54591	4,98E-04	5,7588
				0,0268	3649,27832	0,00185	13,62379
				0,54744	3649,27832	0,00744	69,15407
				0,19962	3694,67314	0,01252	14,97375

Data Sheet – Opalinus, treated materials *(OPA, 60°C, VSE)*

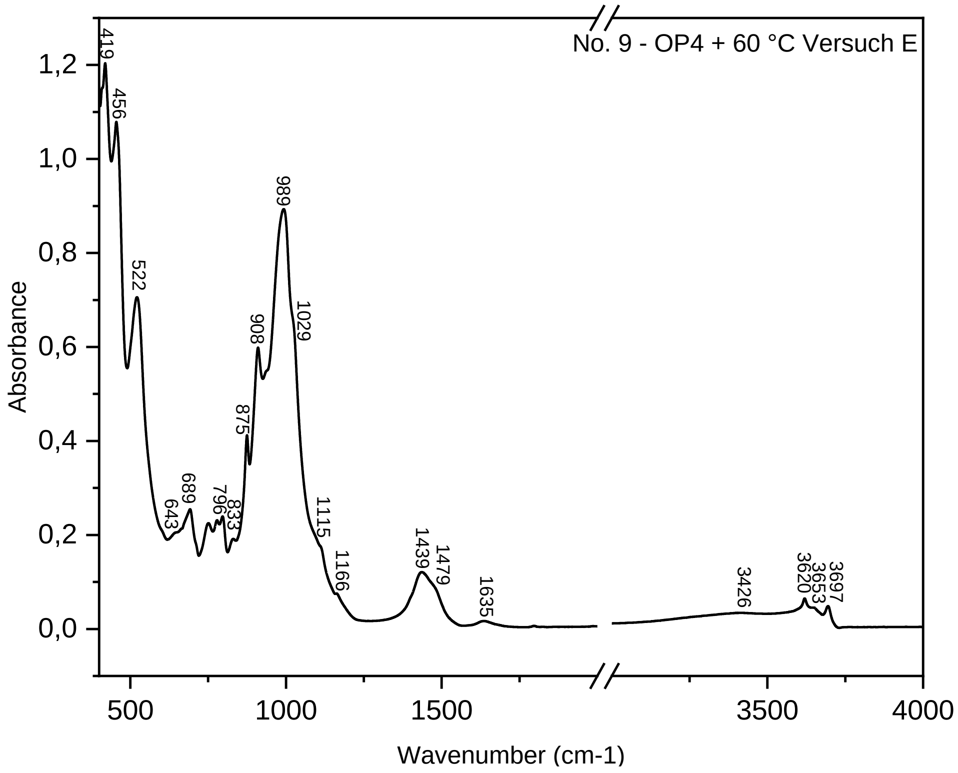

Fig. 12. FTIR-spectrum of OPA + 60 °C – VSE

Tab. 15. Decomposition of FTIR-spectrum of OPA + 60 °C – VSE by Gaussian of Origin 2021

Area Fit	Center Max	Max Height	FWHM	Area Fit	Center Max	Max Height	FWHM
1,33	750,32	0,06	21,78	0,03	833,43	0,00	7,23
1,58	779,58	0,06	24,09	0,52	862,45	0,03	17,53
0,76	797,57	0,06	12,00	1,06	875,05	0,10	9,91
0,43	831,64	0,02	17,99	0,13	827,24	0,01	11,55
4,84	874,13	0,14	32,84	0,66	869,83	0,05	12,88
0,91	874,13	0,09	9,80	0,02	883,62	0,00	5,35
10,46	908,43	0,33	29,75				
1,90	934,38	0,09	19,97	4,84	3309,20	0,01	315,35
4,20	989,04	0,10	38,81	3,26	3458,13	0,01	215,74
63,09	989,04	0,63	94,64	2,06	3587,59	0,02	116,82
0,82	1029,04	0,06	13,62	0,22	3619,12	0,02	11,84
				1,09	3657,33	0,02	51,95
				0,57	3695,11	0,03	17,17
				0,79	3619,12	0,01	51,06

Data Sheet – Opalinus, treated materials *(OPA, 100°C, VSD)*

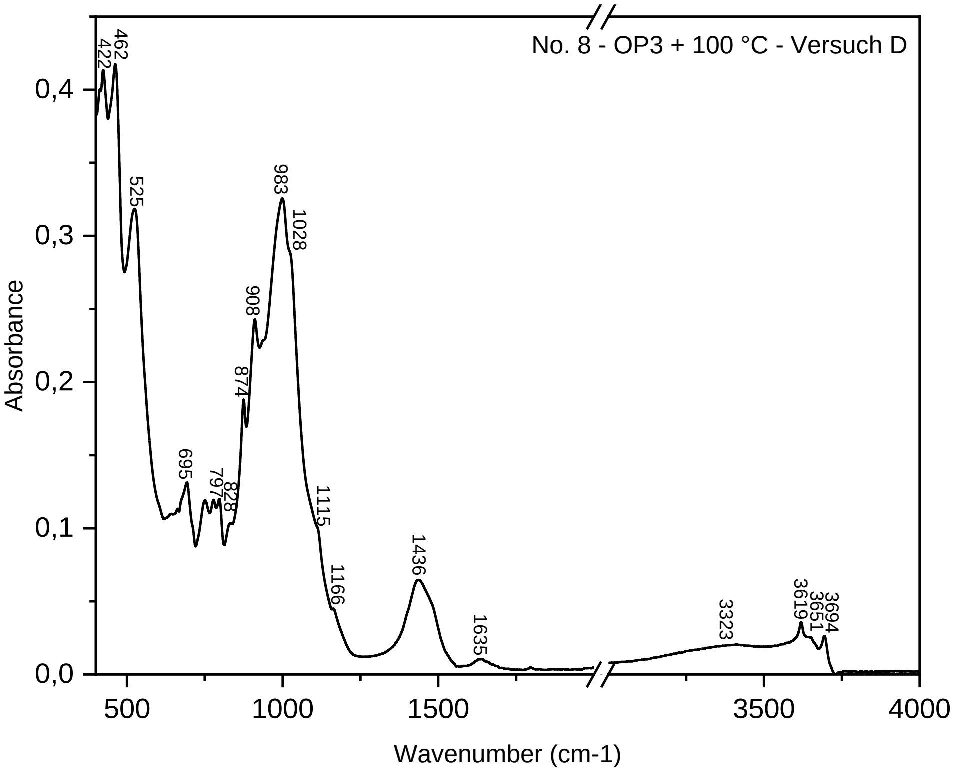

Fig. 13. FTIR-spectrum of OPA + 100 °C – Versuch D

Tab. 16. Decomposition of FTIR-spectrum of OPA + 100 °C – Versuch D by Gaussian of Origin 2021

Area Fit	Center Max	Max Height	FWHM	Area Fit	Center Max	Max Height	FWHM
1,16	750,80	0,03	31,93	0,13	828,08	0,01	15,04
0,65	780,13	0,03	20,21	0,36	867,07	0,02	17,56
0,42	797,54	0,03	13,13	0,11	874,64	0,01	10,06
0,10	827,83	0,01	12,42	0,30	874,64	0,02	11,74
0,58	872,65	0,04	14,07				
0,70	907,83	0,03	18,92	5,94	3410,36	0,01	424,11
15,62	930,76	0,14	107,33	0,65	3592,61	0,01	97,22
5,91	982,96	0,12	44,66	0,20	3614,83	0,01	36,27
1,52	1003,51	0,05	26,46	0,10	3619,00	0,01	10,79
0,50	1028,11	0,03	18,38	0,53	3650,88	0,01	55,31
8,52	1029,98	0,15	54,47	0,02	3650,88	0,00	11,88
1,54	1085,61	0,03	53,25	0,23	3694,22	0,01	15,91

Data Sheet – Opalinus, treated materials *(OPA, 125°C, VSE)*

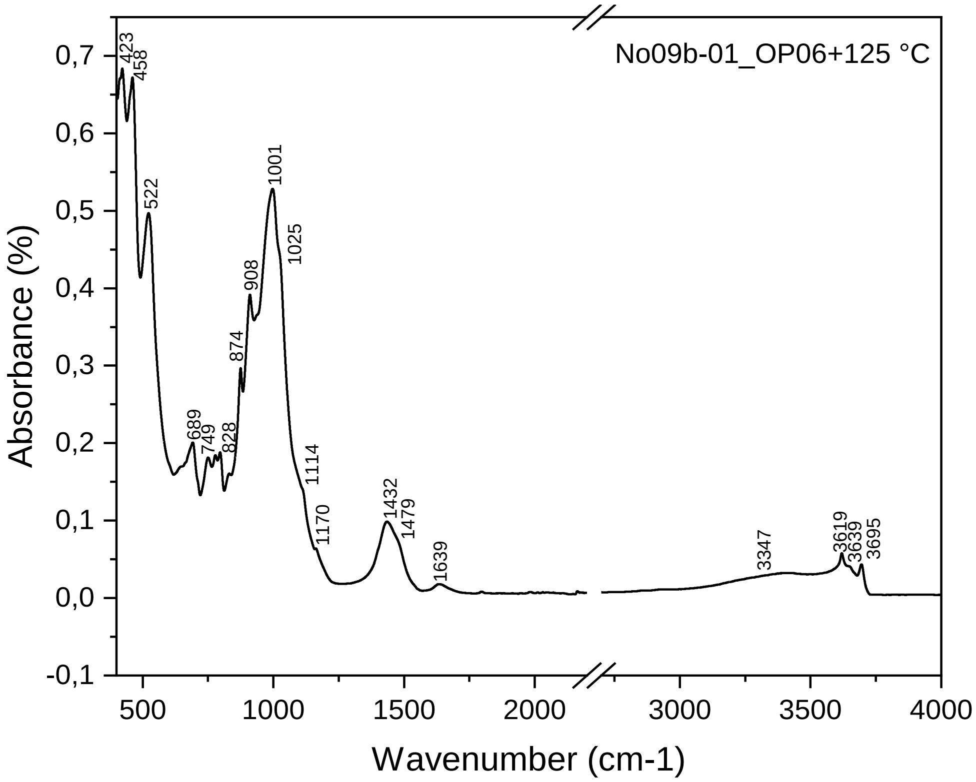

Fig. 14. FTIR-spectrum of OPA + 125 °C – VSE

Tab. 17. Decomposition of FTIR-spectrum of OPA + 125 °C – VSE by Gaussian of Origin 2021

Area Fit	Center Max	Max Height	FWHM	Area Fit	Center Max	Max Height	FWHM
1,22	749,81	0,05	25,24	0,23	828,22	0,01	17,75
1,18	779,51	0,05	23,94	0,82	868,04	0,04	21,06
0,55	797,72	0,04	12,46	0,58	874,19	0,05	10,80
0,15	827,94	0,01	11,95	0,04	897,31	0,00	9,41
0,97	872,73	0,07	13,98				
1,22	907,67	0,06	19,15	5,73	3319,62	0,02	330,89
22,68	928,32	0,21	99,26	1,97	3447,53	0,01	182,18
9,33	982,27	0,20	44,38	1,77	3571,18	0,01	123,24
1,69	1000,81	0,07	21,12	0,19	3619,38	0,01	12,31
4,83	1025,11	0,13	34,83	2,37	3639,26	0,03	87,81
12,38	1025,15	0,14	82,38	0,44	3695,21	0,02	16,88

Data Sheet – Opalinus, treated materials *(OPA, 125°C, VSC)*

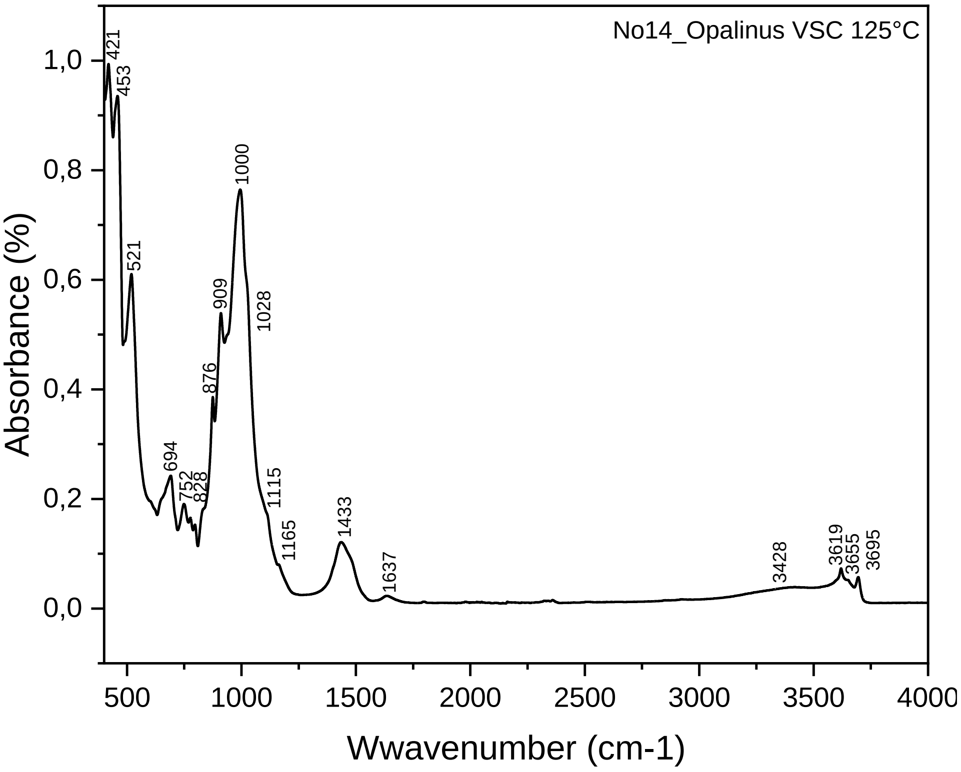

Fig. 15. FTIR-spectrum of OPA + 125 °C – VSC

Tab. 18. Decomposition of FTIR-spectrum of OPA + 125 °C – VSC by Gaussian of Origin 2021

Area Fit	Center Max	Max Height	FWHM	Area Fit	Center Max	Max Height	FWHM
3,77	828,99	0,10	36,22	0,93	828,68	0,04	22,76
0,66	873,70	0,06	9,79	0,75	873,64	0,07	10,28
11,84	875,85	0,24	45,76	5,52	908,53	0,20	26,43
9,75	909,22	0,32	28,62	0,86	933,58	0,05	17,05
3,31	933,49	0,13	24,20	0,90	971,23	0,03	25,21
63,19	986,04	0,67	89,12	3,40	873,64	0,09	36,37
1,18	999,72	0,05	20,20				
1,28	1028,23	0,07	18,43	10,82	3428,06	0,02	425,91
5,49	1044,95	0,10	50,88	2,00	3611,55	0,02	94,82
7,92	1098,16	0,11	64,92	0,32	3619,04	0,02	15,60
				0,72	3654,53	0,01	53,89
				0,51	3694,90	0,03	16,15

Data Sheet – Opalinus, treated materials *(OPA, 150 °C, VSB)*

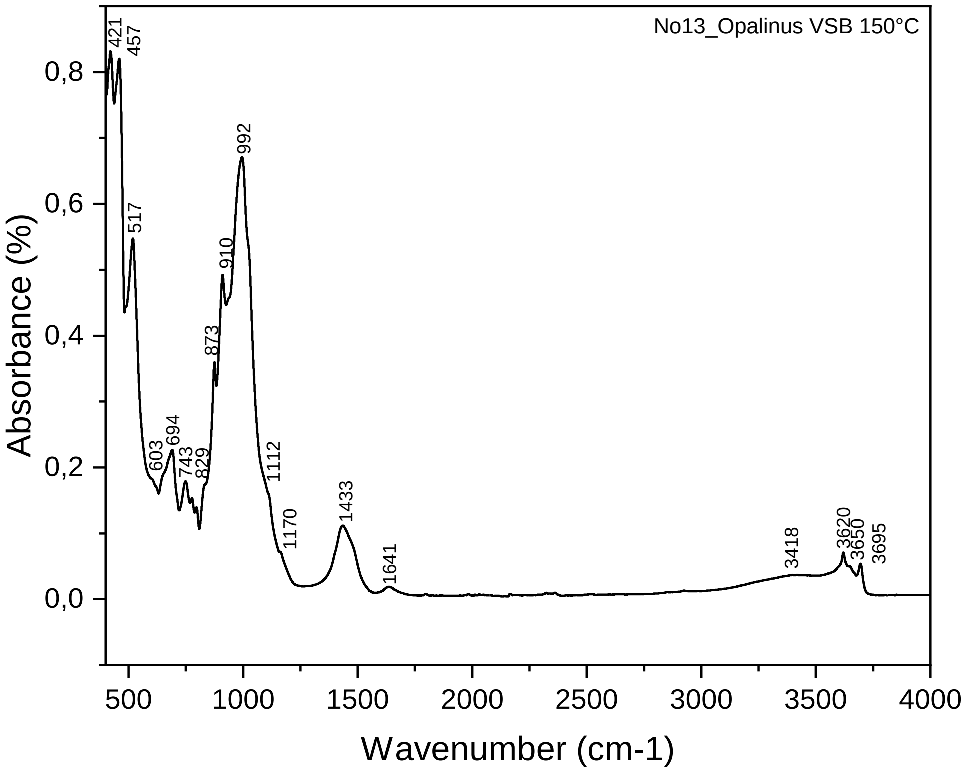

Fig. 16. FTIR-spectrum of OPA + 150 °C – VSB

Tab. 19. Decomposition of FTIR-spectrum of OPA + 150 °C – VSB by Gaussian of Origin 2021

Area Fit	Center Max	Max Height	FWHM	Area Fit	Center Max	Max Height	FWHM
4,06	841,81	0,09	43,87	1,41	828,41	0,05	26,38
4,17	872,25	0,17	23,25	4,57	873,52	0,11	40,44
15,14	909,94	0,32	44,65	0,66	873,52	0,06	10,50
59,75	991,06	0,57	98,74	5,50	908,83	0,19	27,56
0,52	1031,27	0,03	13,95	0,96	933,68	0,05	17,92
3,59	1097,18	0,06	58,11	0,61	963,63	0,02	31,56
11,11	3417,78	0,03	410,30				
1,18	3581,46	0,01	102,40				
0,60	3609,38	0,01	45,49				
0,23	3620,23	0,02	12,51				
1,44	3650,46	0,02	60,40				
0,01	3650,46	0,00	6,56				
0,57	3695,02	0,03	17,34				

Data Sheet – Friedland clay, untreated compacted materials

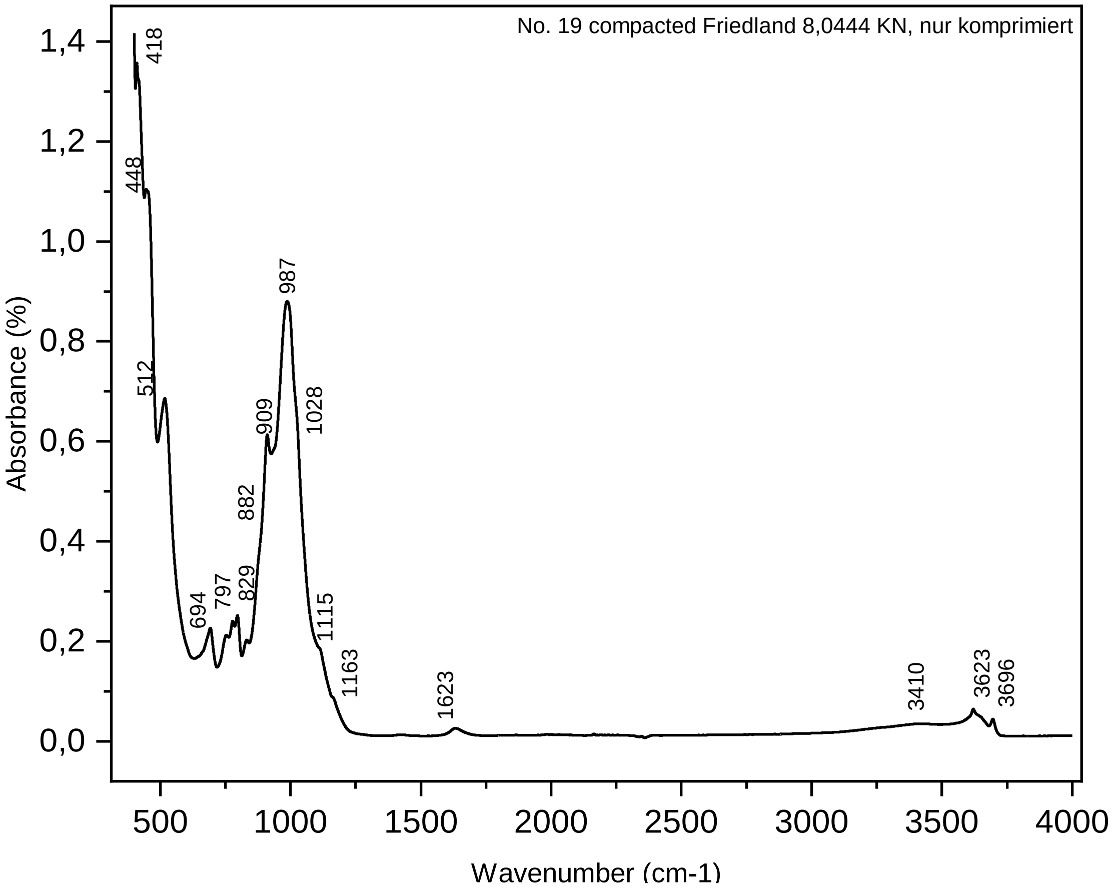

Fig. 17. FTIR-spectrum of compacted Friedland clay

Tab. 20. Decomposition of FTIR-spectrum of compacted FRT clay by Gaussian of Origin 2021

Area Fit	Center Max	Max Height	FWHM	Area Fit	Center Max	Max Height	FWHM
2,80	754,78	0,07	36,38	0,46	828,91	0,02	17,73
1,30	778,77	0,07	16,56	3,97	881,57	0,11	33,69
1,99	796,85	0,11	17,40	5,70	909,07	0,21	25,03
1,41	828,63	0,05	25,89	1,21	931,06	0,06	18,86
15,58	890,82	0,26	56,84	0,29	966,90	0,02	17,19
2,38	907,69	0,12	19,16				
65,14	986,59	0,75	81,96	3,69	3310,96	0,01	285,41
749,00	1027,87	0,05	15,32	2,37	3449,87	0,01	176,47
2,44	1098,10	0,05	47,37	2,06	3582,25	0,02	120,09
6,89	925,59	0,18	36,75	0,97	3620,18	0,02	57,35
5,99	1049,26	0,12	48,03	0,14	3620,18	0,01	11,77
				1,14	3652,40	0,02	59,14
				0,38	3696,30	0,02	15,88

Data Sheet – Friedland clay, treated materials *(OPA, 35 °C, VSC)*

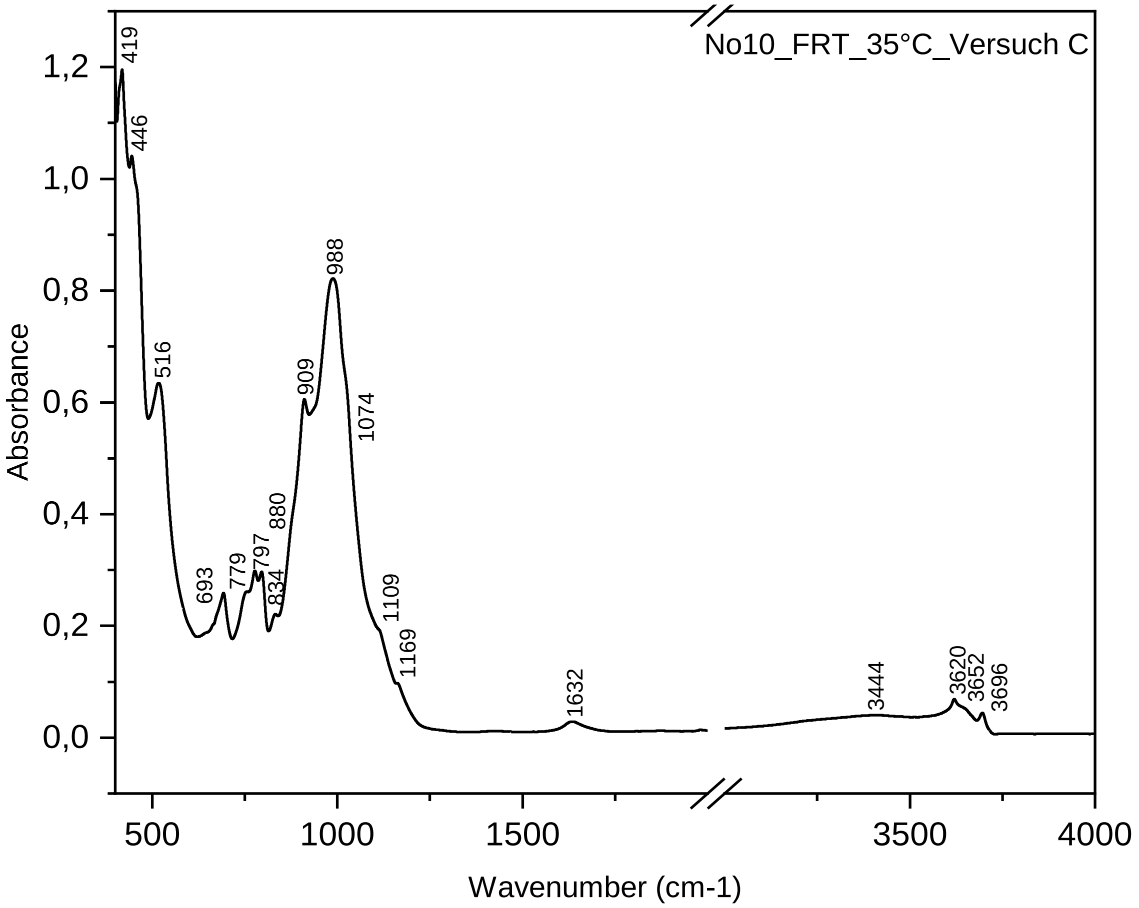

Fig. 18. FTIR-spectrum of compacted FRT+35 °C-VSC

Tab. 21. Decomposition of FTIR-spectrum of FRT+35 °C-VSC by Gaussian of Origin 2021

Area Fit	Center Max	Max Height	FWHM	Area Fit	Center Max	Max Height	FWHM
2,86	753,11	0,08	32,36	0,38	829,26	0,02	16,70
2,33	778,78	0,10	20,98	4,02	880,27	0,11	34,74
1,75	797,10	0,11	15,48	5,26	909,13	0,18	26,76
1,32	833,73	0,04	30,05	0,97	932,22	0,05	18,64
3,67	870,68	0,11	30,10	0,15	964,61	0,01	26,65
14,65	907,17	0,30	45,75				
6,82	987,79	0,06	107,01	4,39	3276,19	0,02	271,33
60,92	987,80	0,58	99,03	3,85	3444,10	0,02	201,80
1,15	1073,51	0,01	109,79	1,79	3577,27	0,02	110,81
				1,18	3619,73	0,02	58,66
				0,17	3619,73	0,01	12,24
				1,27	3651,81	0,02	57,33
				0,38	3695,90	0,02	15,33

Data Sheet – Friedland clay, treated materials *(OPA, 60 °C, VSC)*

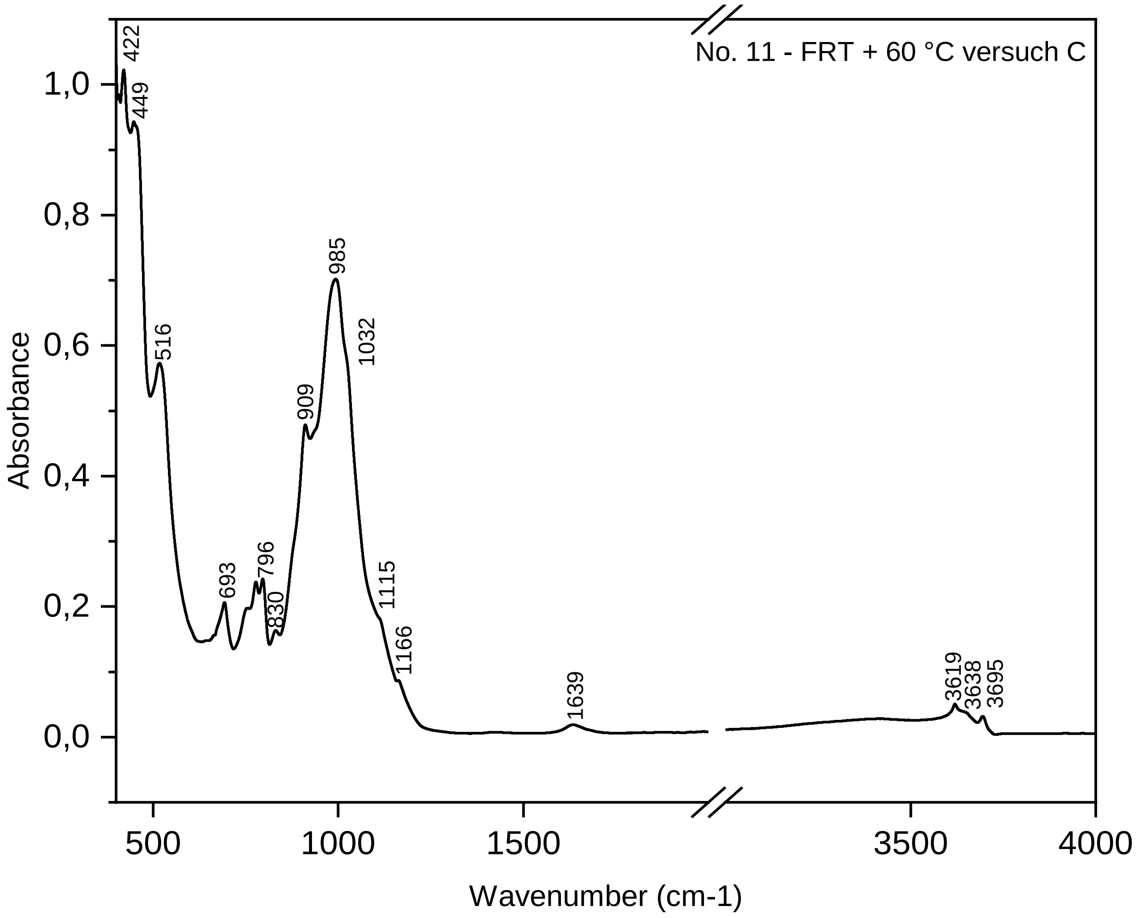

Fig. 19. FTIR-spectrum of compacted FRT+60 °C-VSC

Tab. 22. Decomposition of FTIR-spectrum of FRT+60 °C-VSC by Gaussian of Origin 2021

Area Fit	Center Max	Max Height	FWHM	Area Fit	Center Max	Max Height	FWHM
2,77	755,54	0,07	37,87	0,25	829,76	0,02	13,92
1,41	778,54	0,08	16,71	2,77	880,45	0,08	31,94
1,91	796,75	0,11	16,63	4,75	909,29	0,17	26,95
0,67	829,44	0,03	21,08	0,84	932,57	0,04	17,88
7,83	885,56	0,15	48,67				
1,44	908,04	0,07	18,58	4,12	3314,63	0,01	315,97
10,95	923,73	0,22	47,46	1,69	3448,78	0,01	178,09
34,90	984,65	0,46	70,70	1,35	3576,21	0,01	114,58
4,38	1031,77	0,10	41,86	0,13	3619,24	0,01	11,51
19,64	1031,77	0,16	118,76	1,83	3637,59	0,02	72,22
				0,26	3695,34	0,02	14,78

Data Sheet – Friedland clay, treated materials *(OPA, 100 °C)*

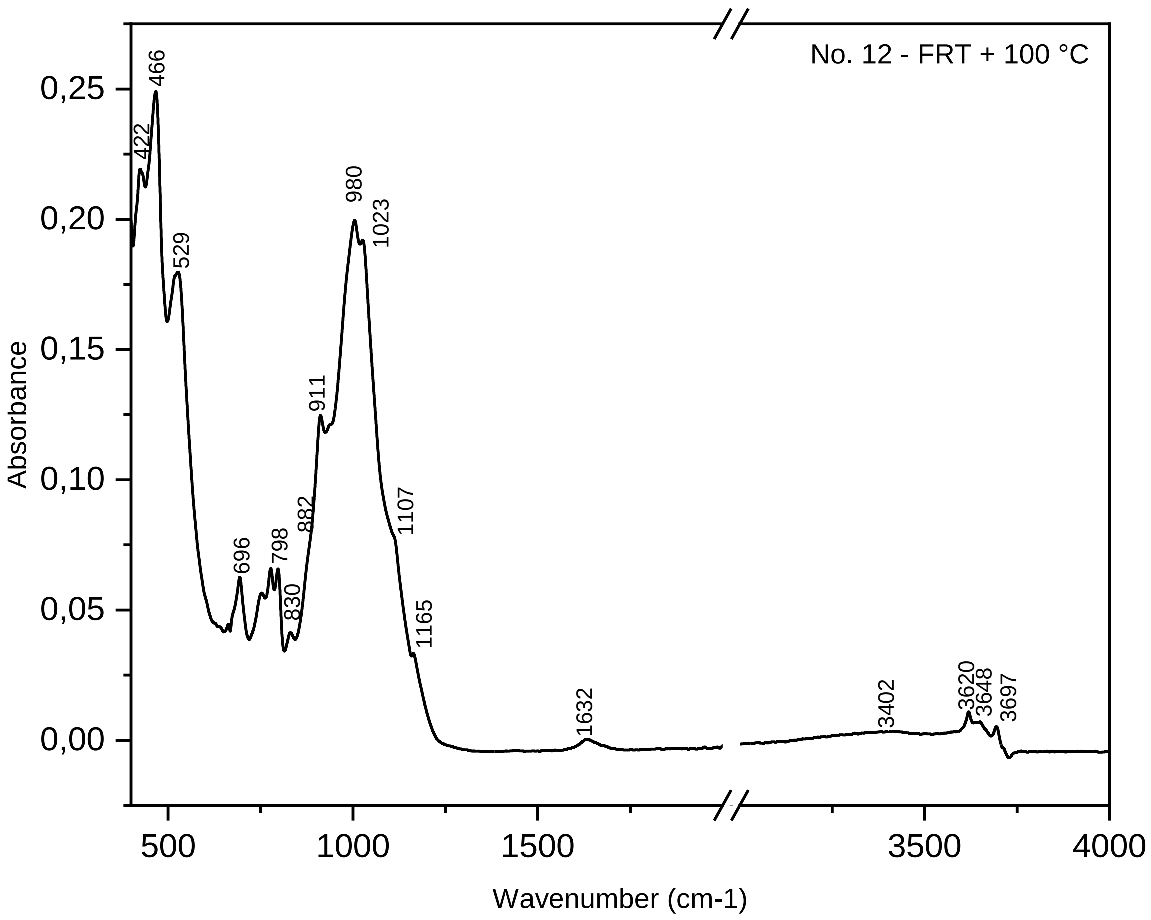

Fig. 20. FTIR-spectrum of compacted FRT+100 °C

Tab. 23. Decomposition of FTIR-spectrum of FRT+100 °C by Gaussian of Origin 2021

Area Fit	Center Max	Max Height	FWHM	Area Fit	Center Max	Max Height	FWHM
1,90	759,27	0,03	64,83	0,14	830,11	0,01	18,32
0,23	779,39	0,02	13,67	0,62	882,87	0,02	34,35
0,40	797,81	0,03	14,01	1,01	910,77	0,04	24,61
0,11	829,82	0,01	14,11	0,21	933,55	0,01	17,88
1,07	829,83	0,00	265,48				
0,24	909,82	0,02	15,05	2,31	3401,86	0,01	426,95
8,52	926,71	0,09	91,80	0,34	3616,20	0,00	95,67
1,67	979,64	0,04	39,22	0,09	3618,44	0,01	14,50
0,18	1001,30	0,01	15,59	0,18	3648,41	0,00	38,69
13,77	1023,27	0,16	81,03	0,04	3691,28	0,00	11,70
3,10	1106,67	0,05	62,56	0,03	3696,90	0,00	9,00

Data Sheet – Friedland clay, treated materials *(OPA, 125 °C, VSD)*

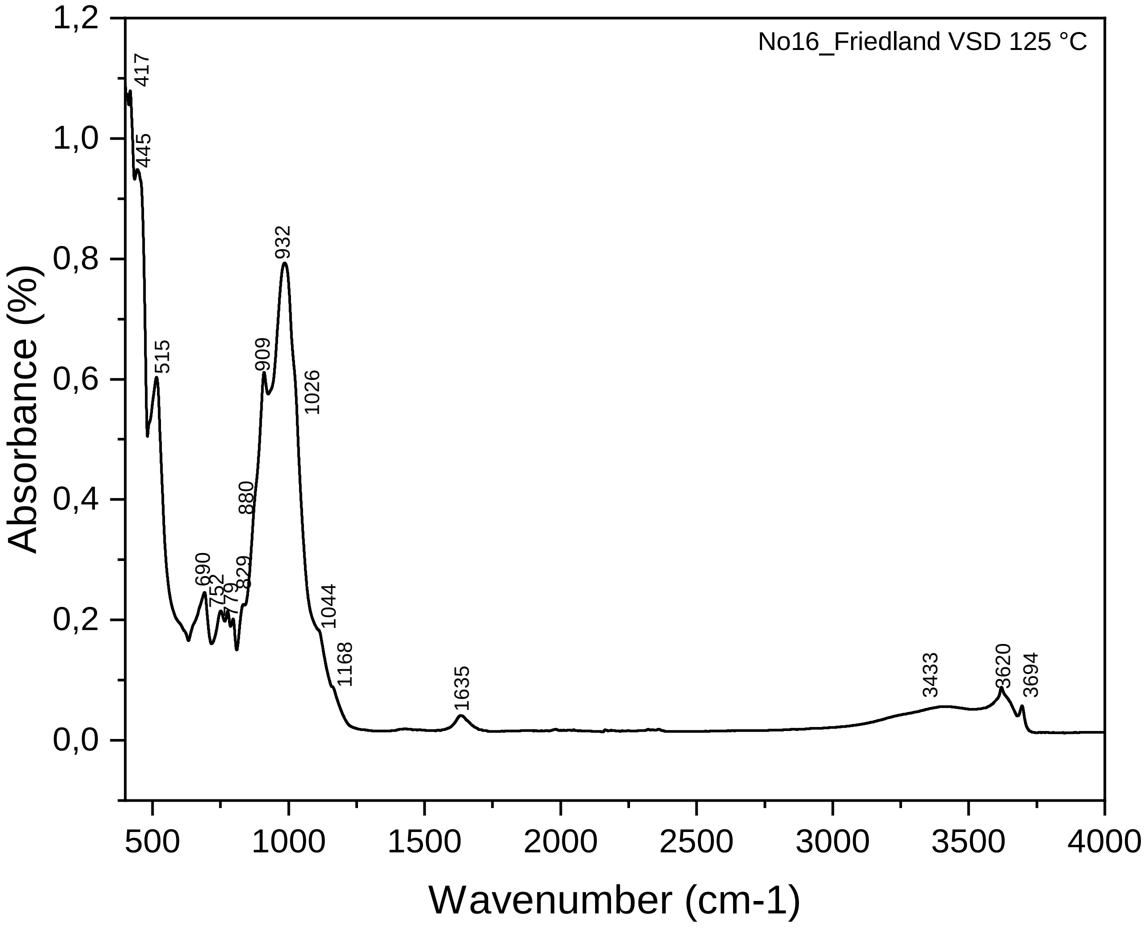

Fig. 21. FTIR-spectrum of compacted FRT+125 °C-VSD

Tab. 24. Decomposition of FTIR-spectrum of FRT+125 °C-VSD by Gaussian of Origin 2021

Area Fit	Center Max	Max Height	FWHM	Area Fit	Center Max	Max Height	FWHM
3,05	751,51	0,07	41,57	0,70	828,98	0,04	18,47
0,78	778,81	0,05	15,51	3,88	879,87	0,10	34,85
0,69	796,05	0,05	12,17	5,03	908,70	0,18	26,31
1,62	832,97	0,06	27,50	0,30	931,49	0,00	99,91
0,67	865,89	0,03	18,55	0,72	931,49	0,04	16,72
30,24	911,12	0,39	72,85				
4,86	911,12	0,04	118,14	3,33	3130,14	0,01	432,57
35,10	981,69	0,54	61,02	3,63	3256,94	0,02	209,31
13,11	1025,98	0,23	52,40	8,03	3433,01	0,04	211,95
10,27	1044,93	0,08	127,01	2,72	3572,24	0,02	121,92
				1,16	3620,31	0,01	80,34
				0,18	3620,31	0,01	12,00
				2,63	3640,38	0,03	75,04
				0,58	3696,36	0,03	17,62

Data Sheet – Friedland clay, treated materials *(OPA, 125 °C, VSC)*

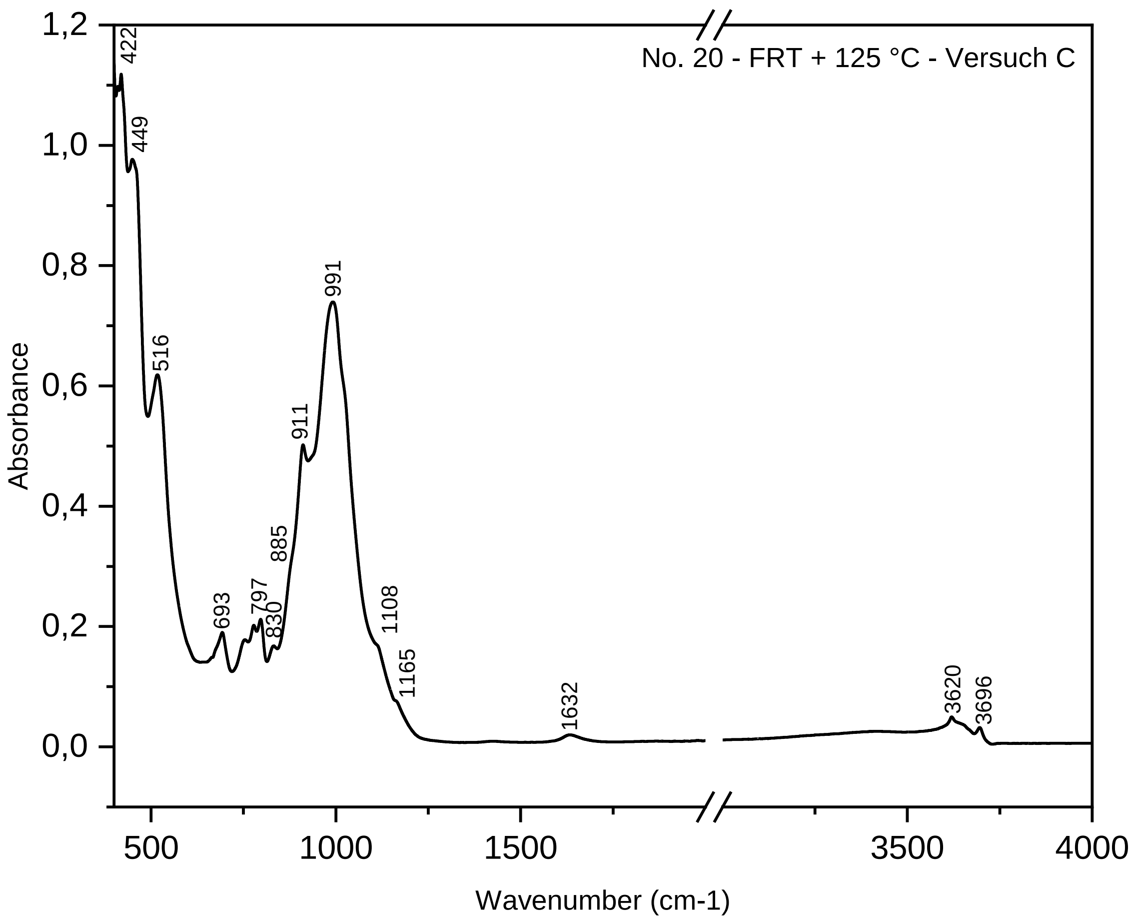

Fig. 22. FTIR-spectrum of compacted FRT+125 °C-VSC

Tab. 25. Decomposition of FTIR-spectrum of FRT+125 °C-VSC by Gaussian of Origin 2021

Area Fit	Center Max	Max Height	FWHM	Area Fit	Center Max	Max Height	FWHM
0,23	829,48	0,02	13,77	2,28	754,99	0,06	36,06
2,76	880,08	0,09	30,34	1,13	779,08	0,06	16,94
5,27	909,23	0,18	27,15	1,59	797,13	0,09	16,71
0,86	932,35	0,05	17,84	1,23	829,53	0,04	27,33
				8,44	884,58	0,16	48,53
5,61	3427,13	0,01	386,20	4,82	910,76	0,18	25,17
0,62	3587,93	0,01	88,63	1,39	931,67	0,07	19,00
0,11	3619,51	0,01	11,32	68,37	991,18	0,60	107,68
1,40	3636,41	0,02	65,47	0,76	991,18	0,03	24,56
0,20	3695,84	0,01	13,17	1,22	1028,12	0,03	36,43

Data Sheet – Friedland clay, treated compacted materials *(OPA, 150 °C, VSC)*

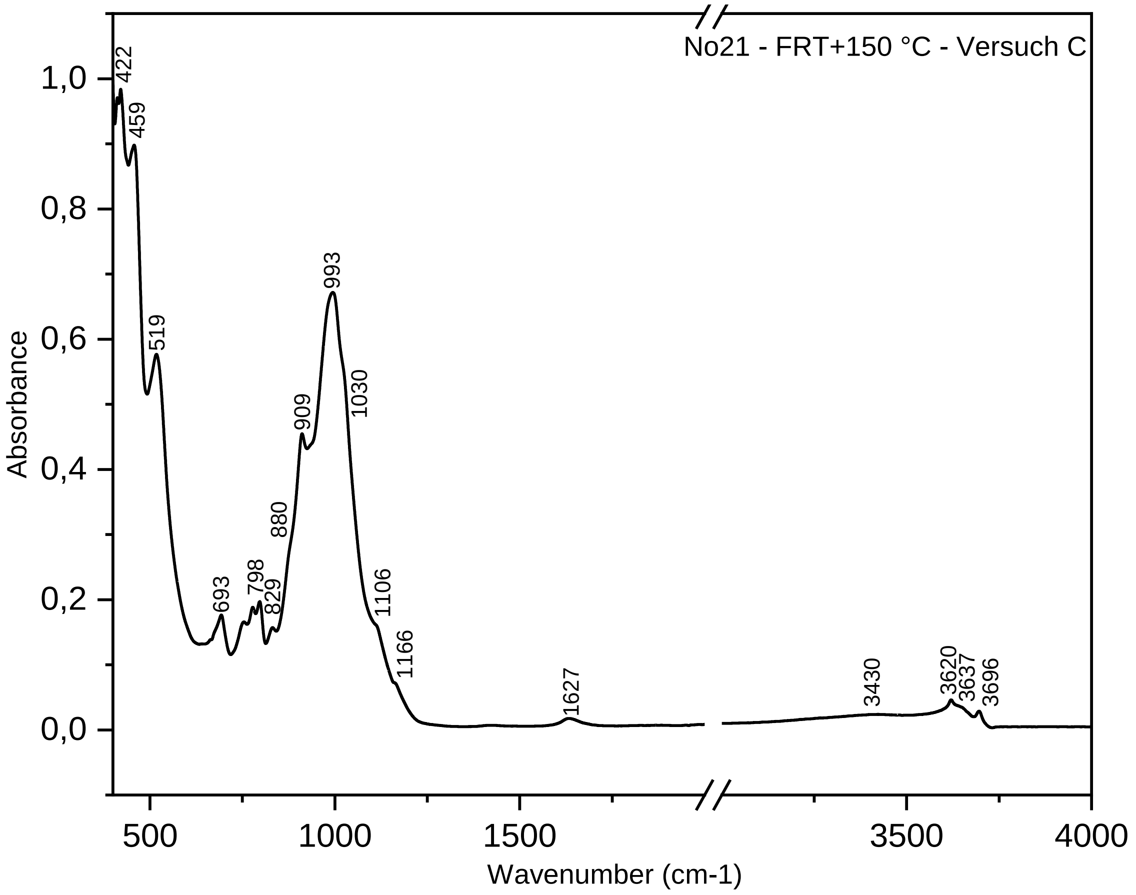

Fig. 23. FTIR-spectrum of compacted FRT+150 °C-VSC

Tab. 26. Decomposition of FTIR-spectrum of FRT+150 °C-VSC by Gaussian of Origin 2021

Area Fit	Center Max	Max Height	FWHM	Area Fit	Center Max	Max Height	FWHM
1,38	753,08	0,05	27,17	0,24	829,23	0,02	14,21
1,38	778,87	0,06	20,04	2,39	879,76	0,07	30,07
1,20	797,63	0,07	15,36	4,54	909,27	0,16	27,38
1,08	831,34	0,04	27,97	0,06	966,79	0,00	12,74
3,38	872,85	0,09	34,12	0,63	932,39	0,04	16,86
10,06	909,03	0,21	44,13				
0,30	909,03	0,03	11,12	5,55	3429,56	0,01	388,11
60,62	993,03	0,55	104,13	0,61	3587,05	0,01	88,95
0,14	1030,07	0,01	9,49	0,11	3619,61	0,01	11,58
1,18	1106,26	0,03	41,84	1,35	3636,46	0,02	65,87
				0,19	3695,86	0,01	13,10

S4. Thermal Analysis (DTA-TG)

SUPPLEMENT - *Thermogravimetry*

Content

Methodology – Thermogravimetry

It is expected a characterization of clay mineral phases in treated B25 bentonite by X-ray diffraction (XRD) of bulk samples also by thermogravimetry. The experiments itself was carried out by GRS gGmbH in Braunschweig. The sample bodies were percolated by adapted Opalinus solution under different temperatures (35 °C, 60 °C, 100 °C, 150 °C) and time intervals.

After the experiment, three samples were investigated from each sample body – material from top position, from central part and from the bottom. The flow direction of percolation was oriented from the top to the bottom of sample body.

For differential thermal analyses, the samples were milled to < 74 µm and dried at 35°C for 1 hour. The measurement was carried out at TU Darmstadt in a NETZSCH STA 449F5 under nitrogen atmosphere (0.08 L/min) and heating of 50 mg of the sample up to 1000°C with a heating rate of 20K/min. The thermogravimetric results were evaluated by software tool ‘Universal V4.5A TA Instruments’.

Data Sheet – Mineral matter in bulk powder of B25-series

Measured mass loss (in %)

Sample	**30 - 300°C**	**300 - 650°C**	**650 - 1 000°C**	*Σ 300 - 1 000°C*
B25 original	10.40%	3.72%	1.47%	*5.19%*
35°C, 285h, 0.7MPa, OPA				
No23	5.88%	3.89%	0.99%	4.88%
35°C, 93.6h, OPA				
No4_T	5.19%	4.19%	0.49%	4.68%
No4_C	5.19%	3.90%	0.72%	4.62%
No4_B	5.60%	3.93%	0.94%	4.87%
60°C, 454h, OPA				
No5_T	4.41%	3.28%	0.89%	4.17%
No5_C	4.42%	3.27%	0.88%	4.15%
No5_B	5.54%	4.07%	0.82%	4.89%
100°C, 110h, OPA				
No0_T	6.98%	3.70%	1.74%	5.44%
No0_C	6.82%	3.26%	1.71%	4.97%
No0_B	6.56%	4.35%	0.91%	5.26%
100°C, 35d, OPA				
No2_T	7.01%	4.28%	1.09%	5.37%
No2_C	7.13%	4.38%	1.18%	5.56%
No2_B	7.19%	4.21%	1.04%	5.25%
100°C, 35d, OPA				
No15	7.07%	3.63%	0.88%	4.51%
150°C, 4d, OPA				
No3_T	6.56%	4.45%	1.42%	5.87%
No3_C	6.39%	3.79%	0.90%	4.69%
No3_B	6.59%	3.96%	0.92%	4.88%

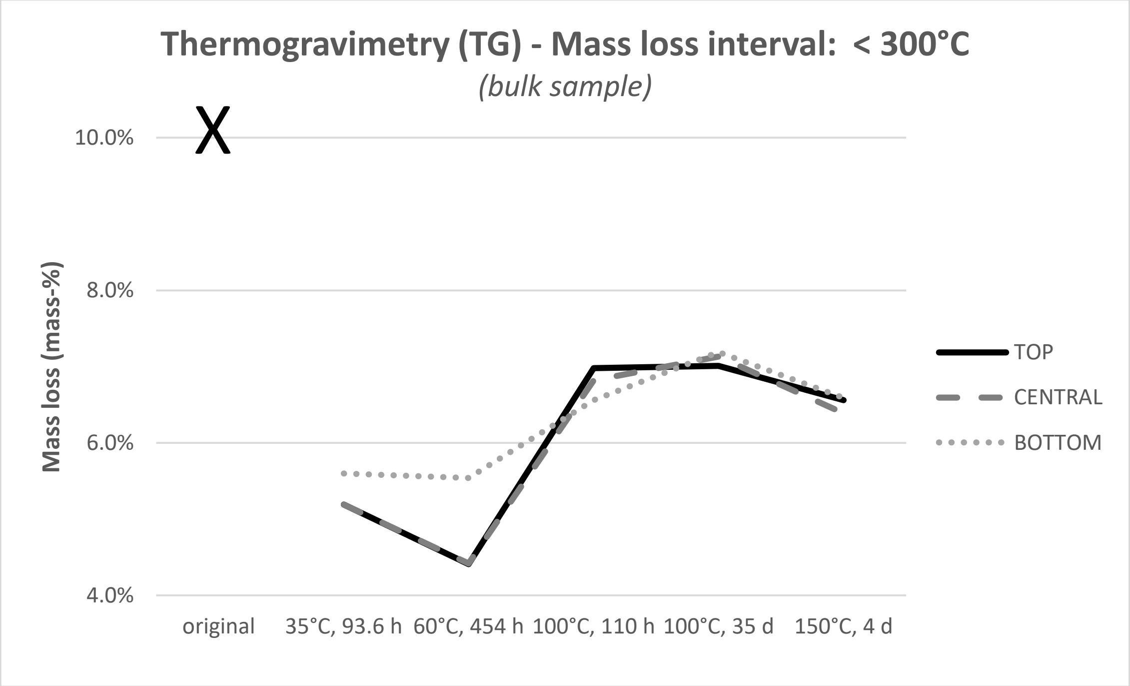

Trend: Interval represents process of dehydration mostly of expandable clay minerals. Water content is lowered by treatment in comparison to original bentonite. Similar behavior in all three parts of sample holder (top, center, bottom).

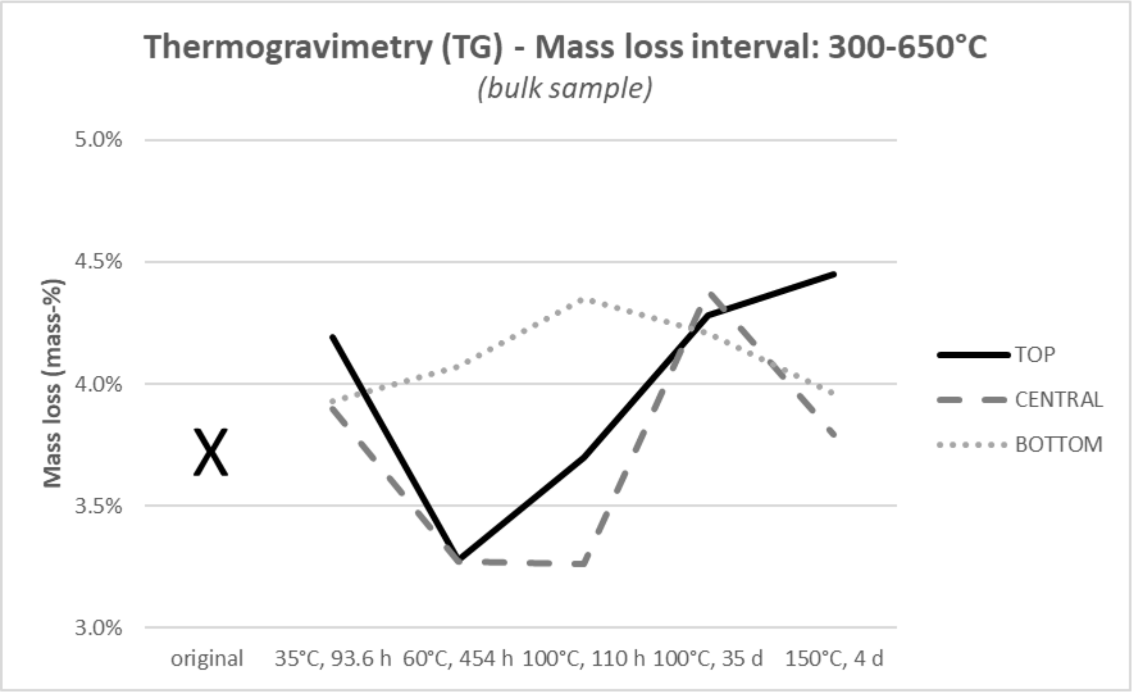

Trend: Dehydroxylation (e.g. kaolinite, beidellite, 1M illite) **-** Similar behavior of samples from top and central positions.

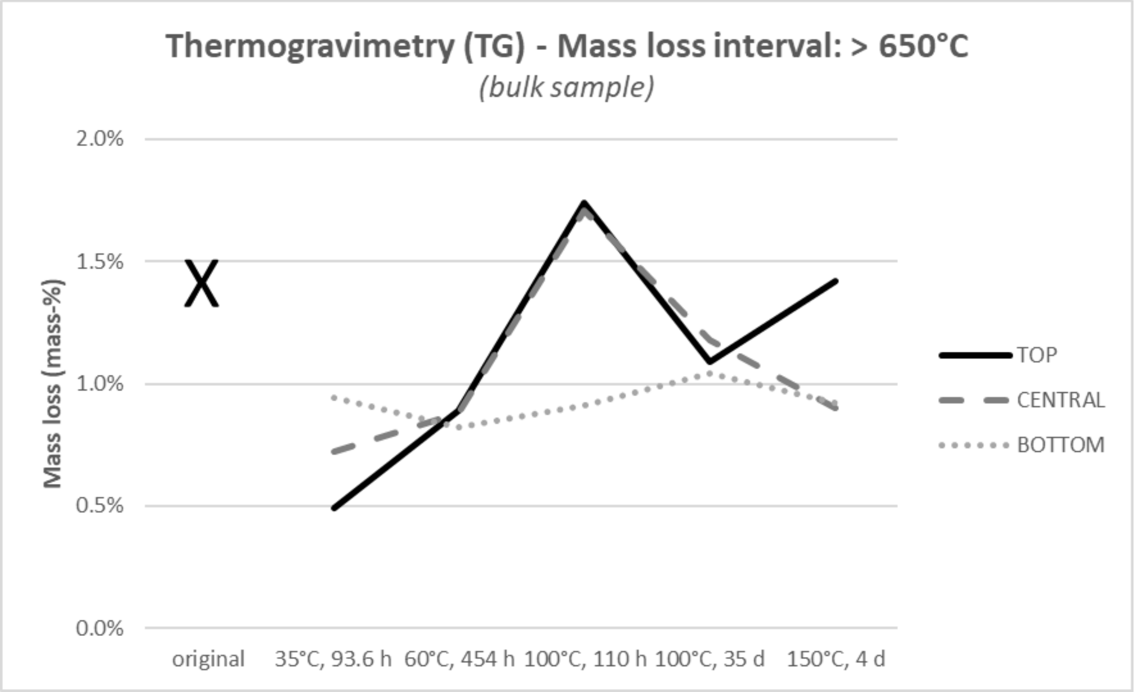

Trend: Dehydroxylation (e.g. montmorillonite, $2M_1$ muscovite) & degradation (e.g. calcite) **-** Similar behavior of samples from top and central positions. Only very low changes for samples from bottom positions.

Data Sheet – Mineral matter in bulk powder of Friedland Clay-series

Measured mass loss (in %)

Sample	30 - 300°C	300 - 650°C	650 - 1 000°C	*Σ 300 - 1 000°C*
orig., compact. **No19**	1.85%	5.10%	1.16%	6.26%
35°C, 46.3h, OPA **No10**	1.53%	4.58%	1.00%	5.58%
60°C, 45.9h, OPA **No11**	1.74%	4.89%	0.95%	5.84%
100°C, 40h, OPA **No16**	3.25%	6.51%	1.58%	8.09%
125°C, 40h, OPA **No20**	1.65%	5.09%	1.14%	6.23%
150°C, 68.3h, OPA **No21**	1.51%	5.03%	1.22%	6.25%
without transport cell				
100°C, OPA **No12**	2.06%	5.16%	1.04%	6.20%

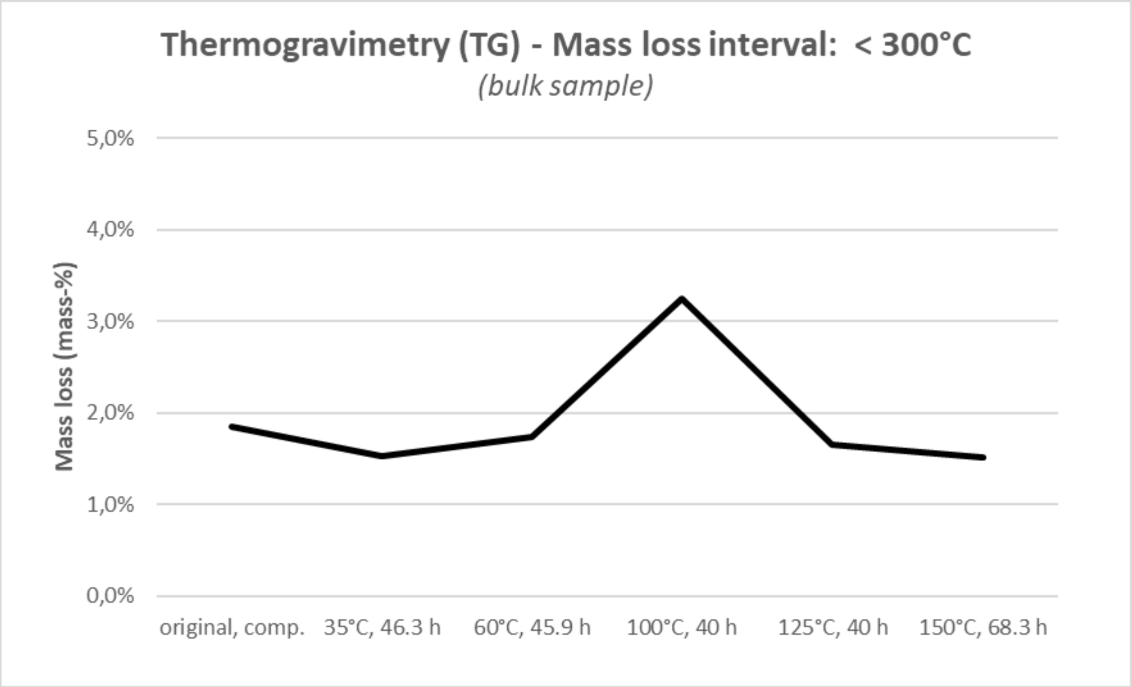

Trend: Interval represents process of dehydration mostly of expandable clay minerals. Water content is comparable. Exception: Sample No16 (100°C) probably by surface activation.

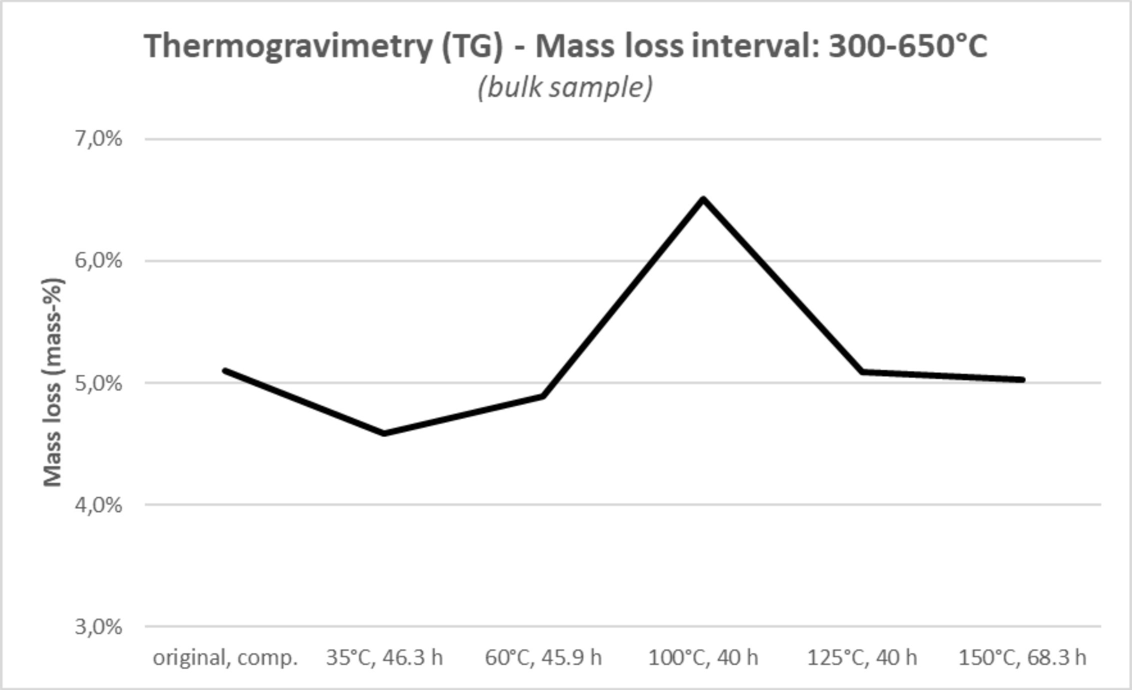

Trend: Dehydroxylation (e.g. kaolinite, beidellite, 1M illite) **-** Similar behavior of samples with special role for sample No16 (100°C).

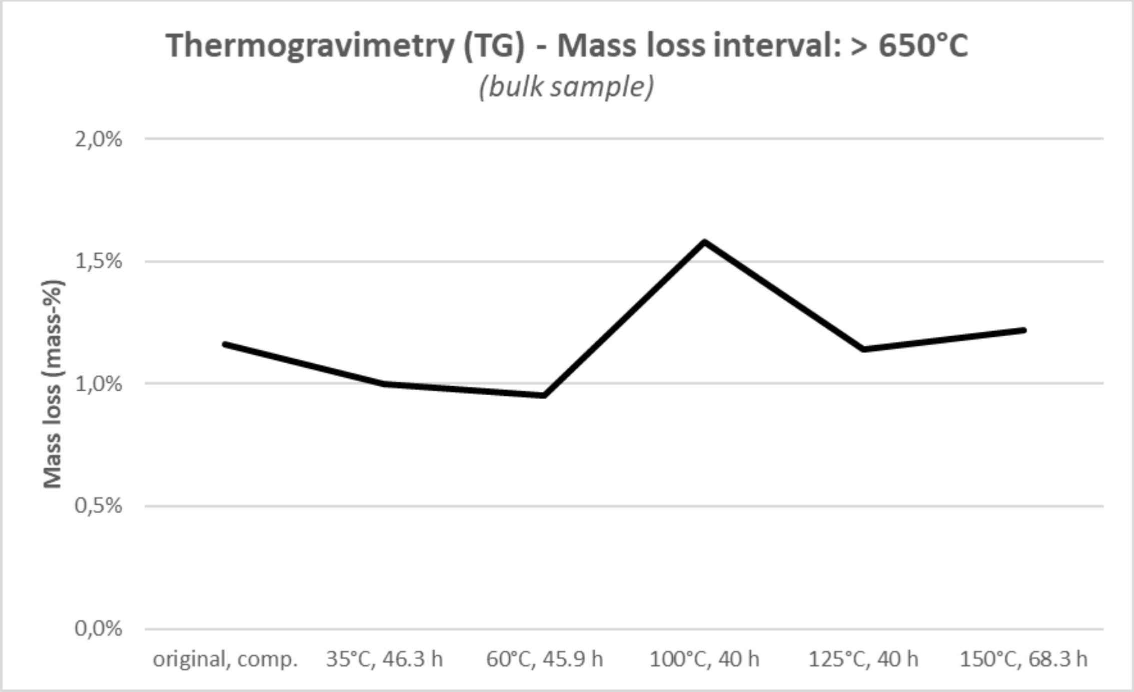

Trend: Dehydroxylation (e.g. montmorillonite, $2M_1$ muscovite) & degradation (e.g. calcite) **-** Similar behavior of samples from with special role for sample No16 (100°C).

Data Sheet – Mineral matter in bulk powder of Opalinus Clay-series

Measured mass loss (in %)

Sample	30 - 300°C	300 - 650°C	650 - 1 000°C	*Σ 300 - 1 000°C*
Opalinus Clay original	1.07%	6.15%	7.75%	*13.90%*
35°C, 144h, OPA **No22**	1.23%	7.39%	5.53%	12.92%
60°C, 45.4h, OPA **No9**	1.06%	7.35%	6.43%	13.78%
60°C, 95.3h, OPA **No7**	0.58%	2.89%	30.29%	33.18%
100°C, 69.3h, OPA **No8**	1.04%	6.45%	7.70%	14.15%
125°C, 48.5h, OPA **No14**	0.88%	7.14%	6.07%	13.21%
150°C, 48.6h, OPA **No13**	0.92%	7.03%	6.24%	13.27%
without transport cell				
35°C, OPA **No9a**	1.06%	6.67%	5.88%	12.55%
125°C, OPA **No9b**	1.20%	6.80%	7.00%	13.80%

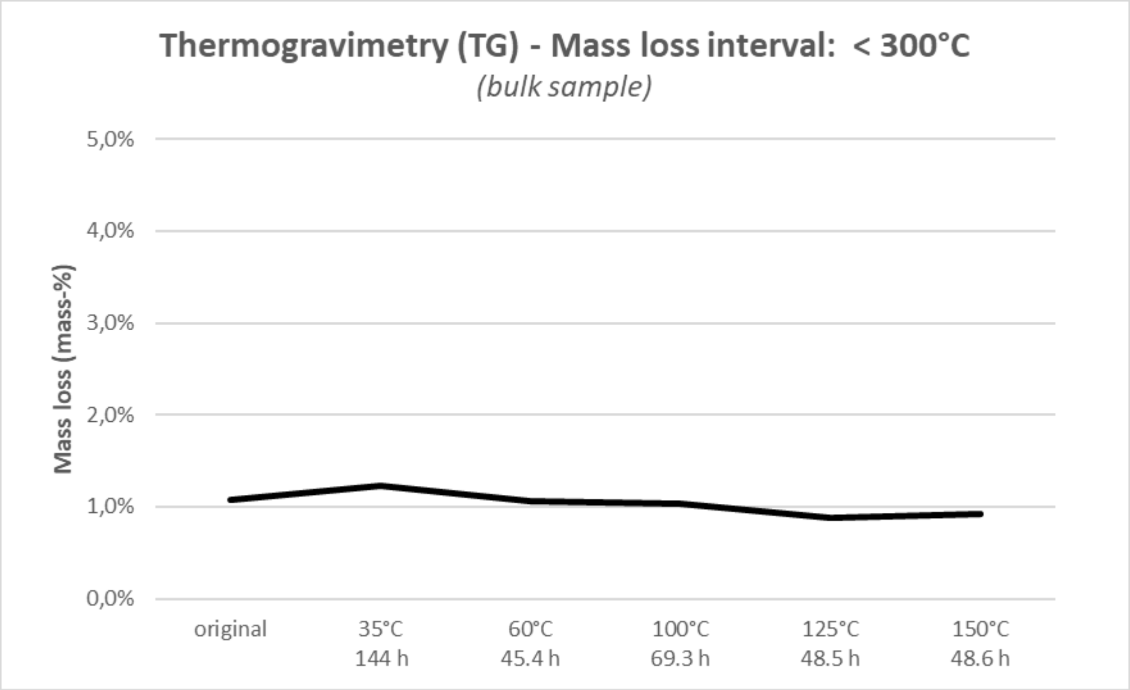

Trend: Interval represents process of dehydration mostly of expandable clay minerals. Water content is comparable low.

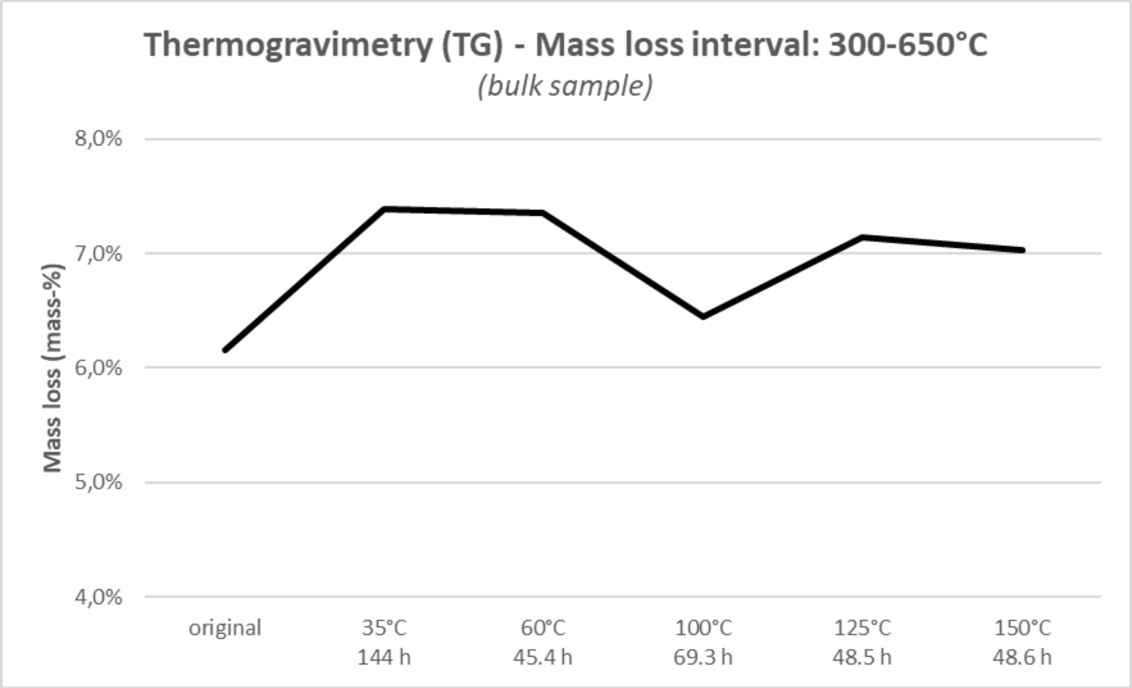

Trend: Dehydroxylation (e.g. kaolinite, beidellite, 1M illite) **-** Similar behavior of all samples.

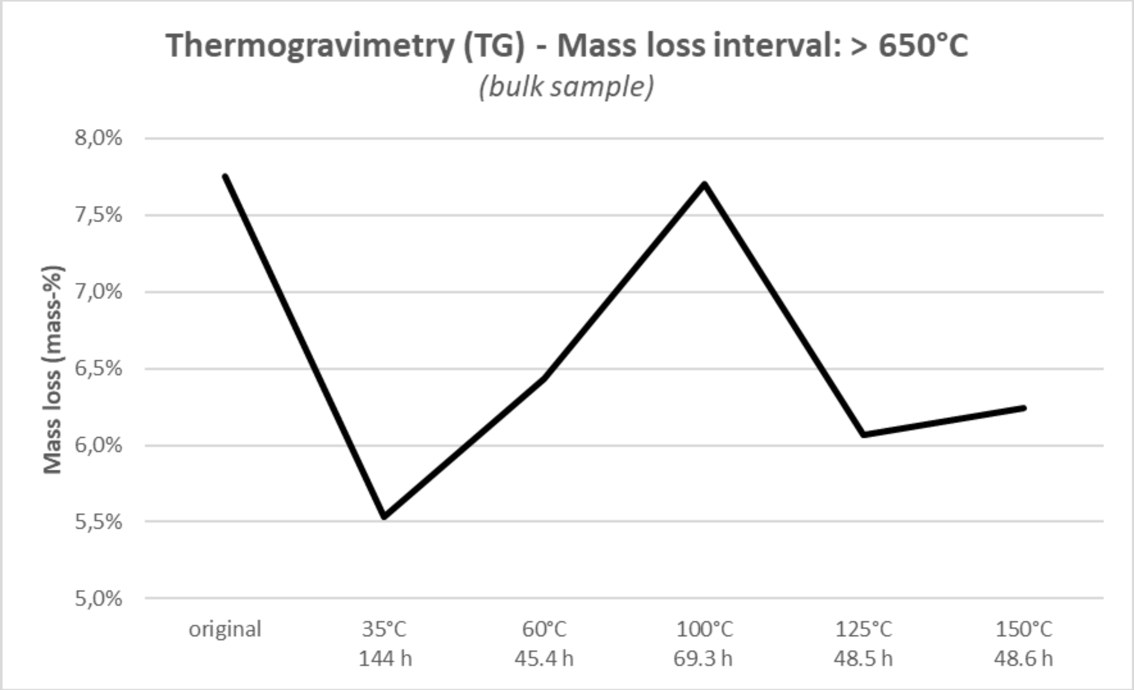

Trend: Dehydroxylation (e.g. montmorillonite, $2M_1$ muscovite) & degradation (e.g. calcite, dolomite) **–** Differences mainly caused by crystalline and amorph carbonates.

Data Sheet – B25 total (powder), original material *(uncompacted)*

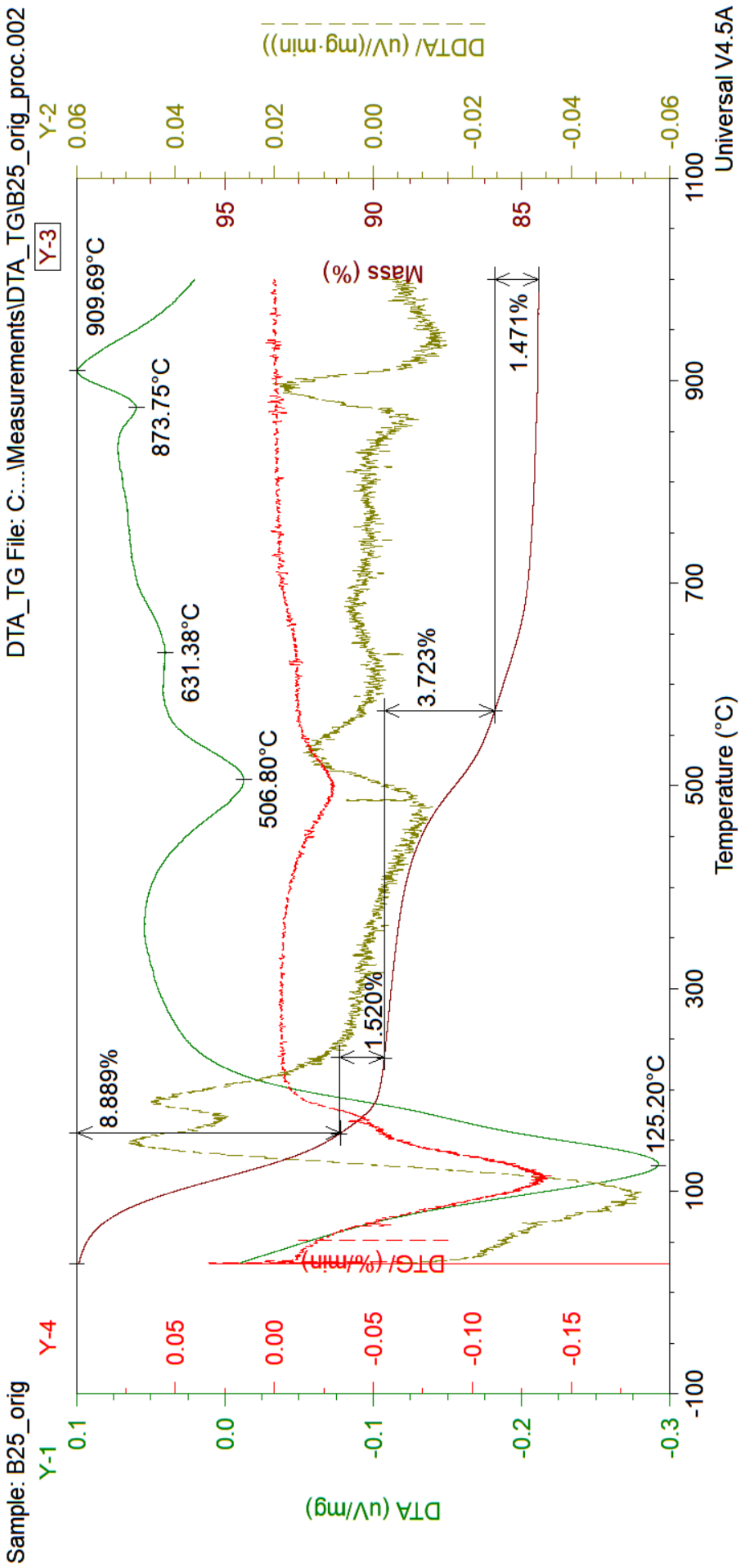

Data Sheet – B25 No4_T (bulk), treated material *(OPA, 35°C, 93.6 hours)*

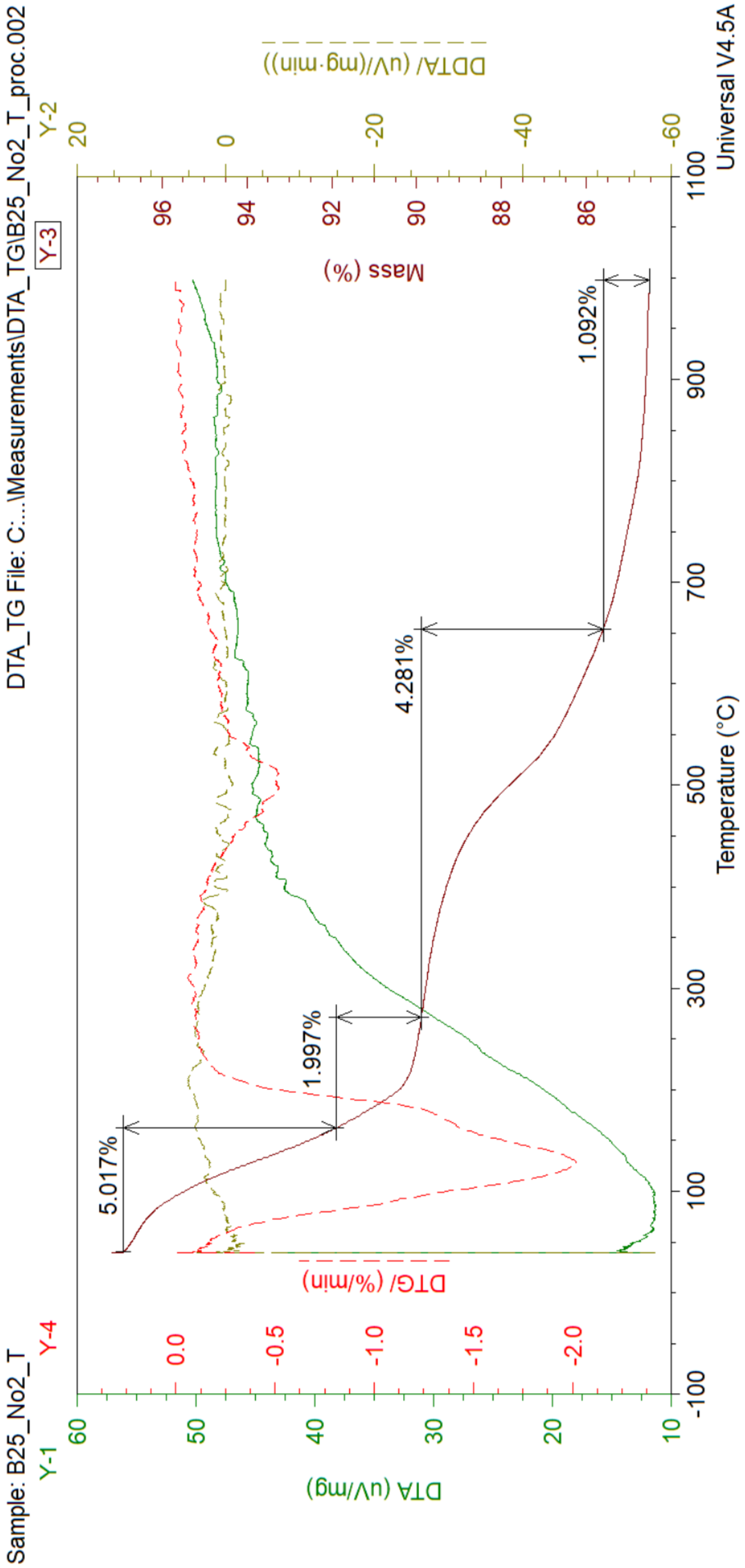

Data Sheet – B25 No4_C (bulk), treated material *(OPA, 35°C, 93.6 hours)*

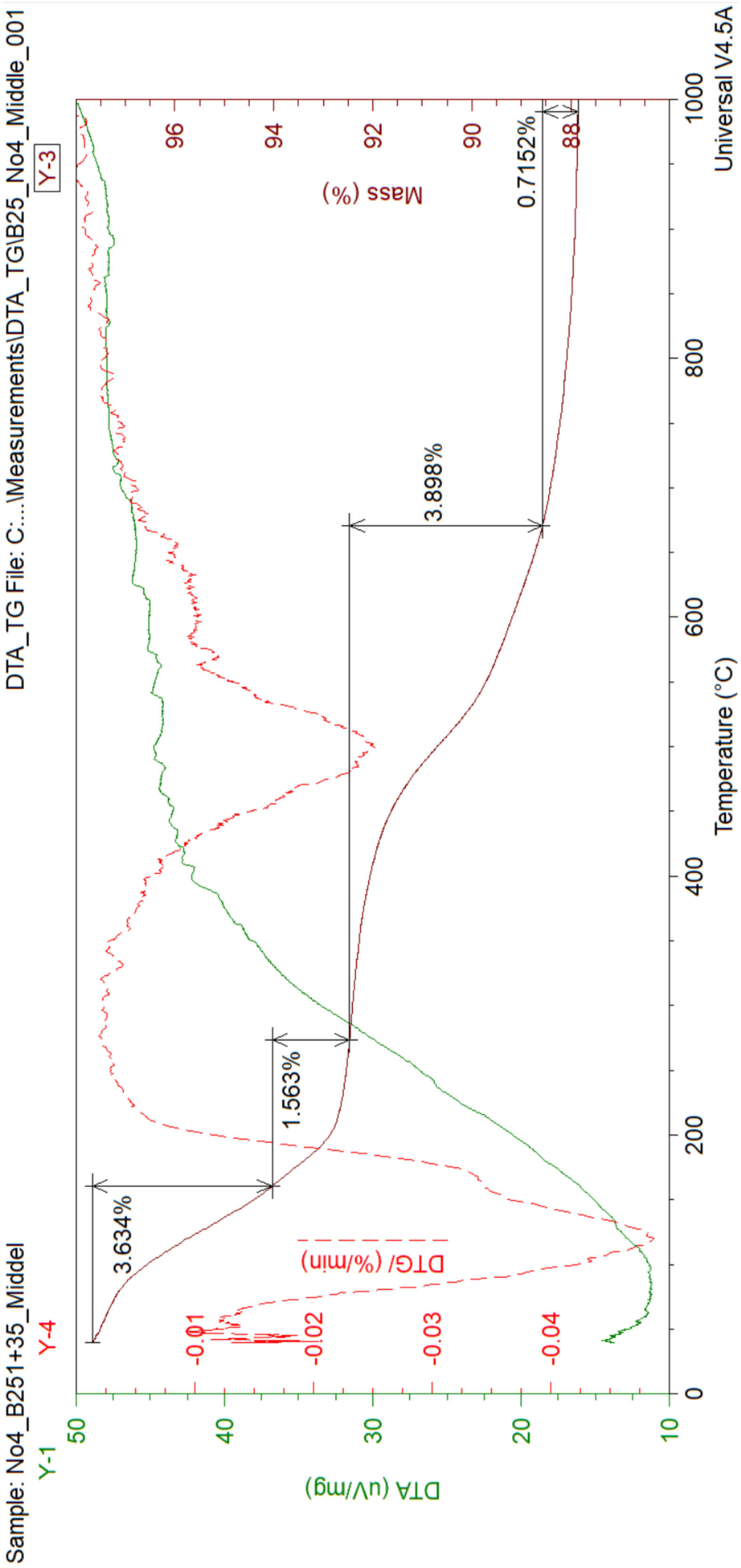

Data Sheet – B25 No4_B (bulk), treated material *(OPA, 35°C, 93.6 hours)*

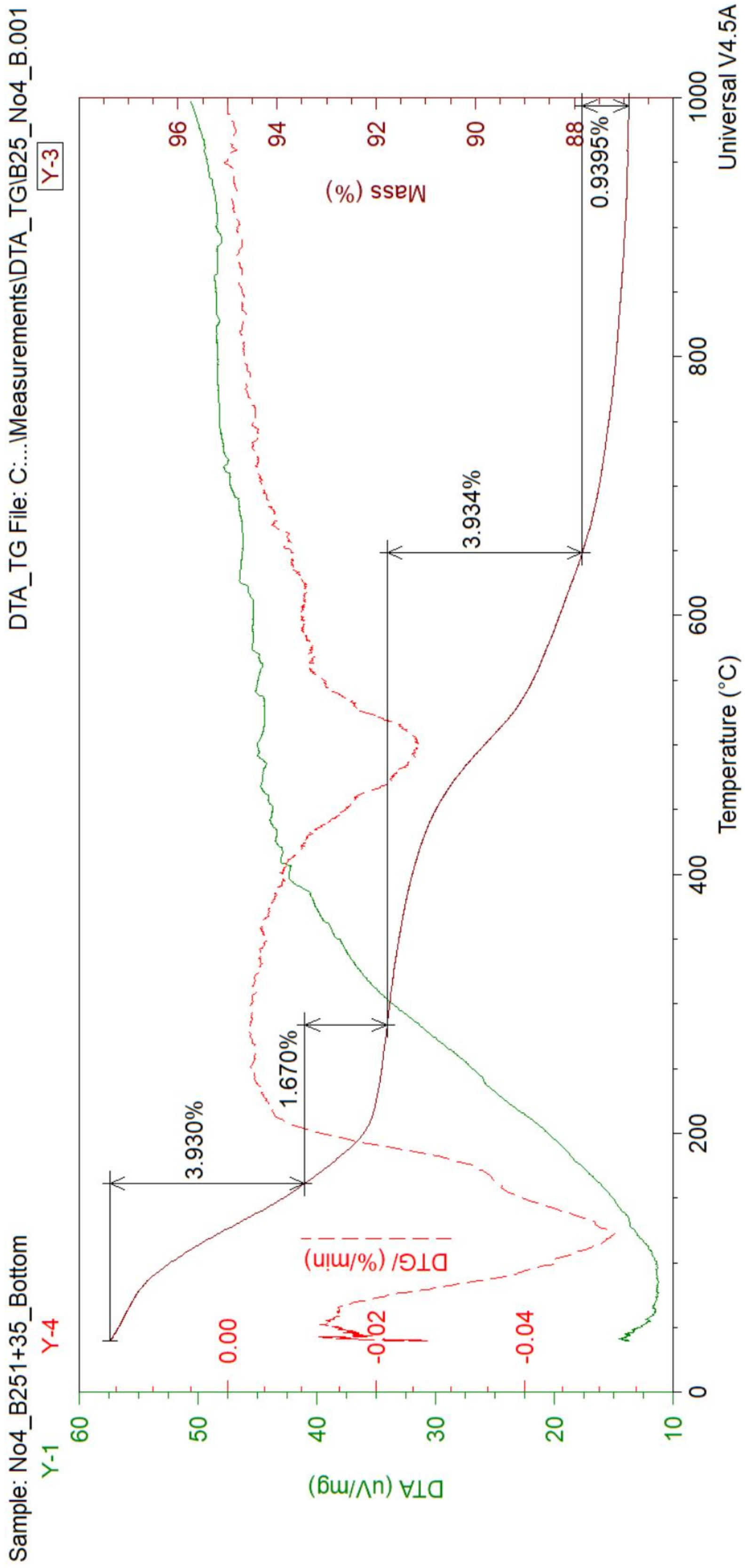

Data Sheet – B25 No23 (bulk), treated material *(OPA, 35°C, 0.7 MPa, 285 h)*

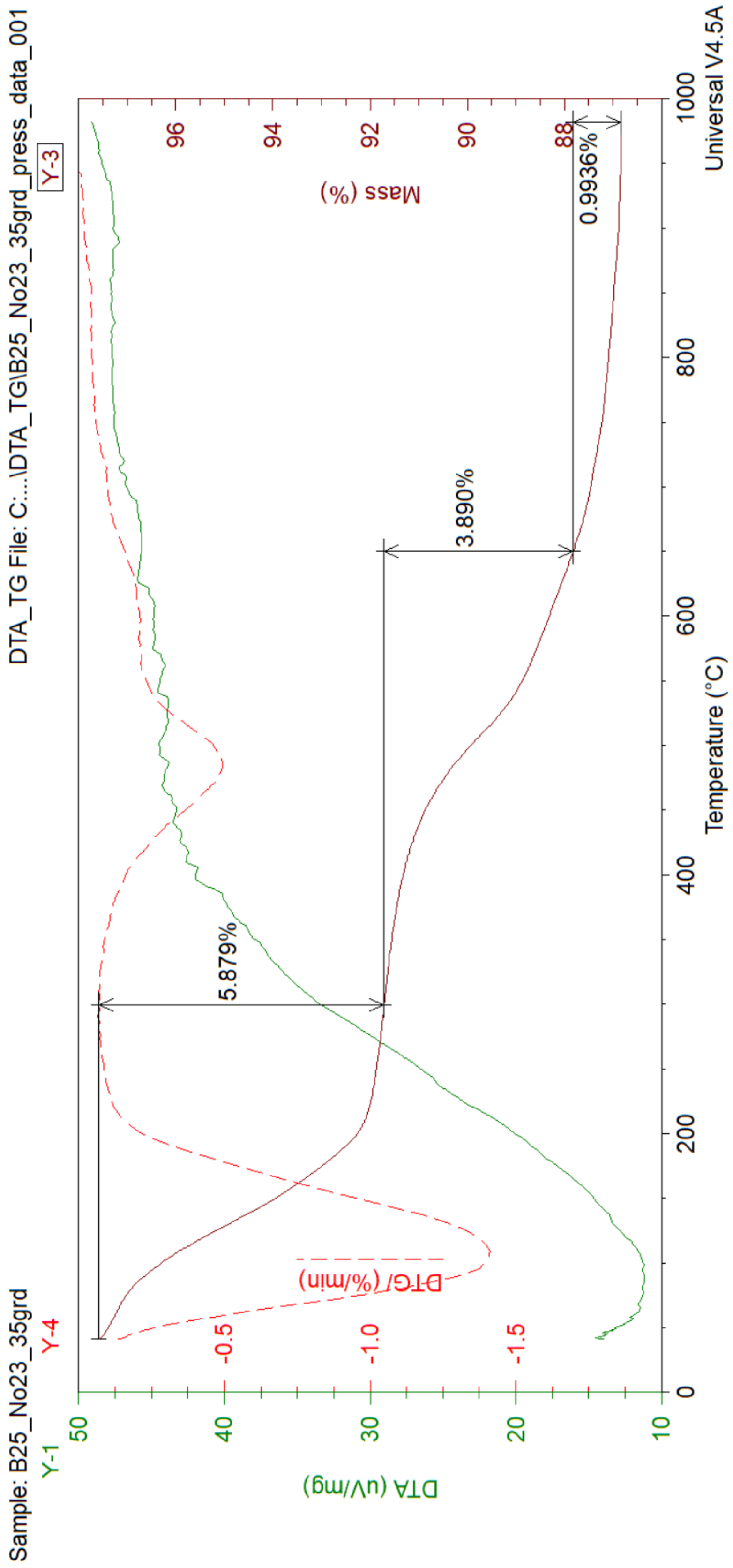

Data Sheet – B25 No5_T (bulk), treated material *(OPA, 60°C, 454 hours)*

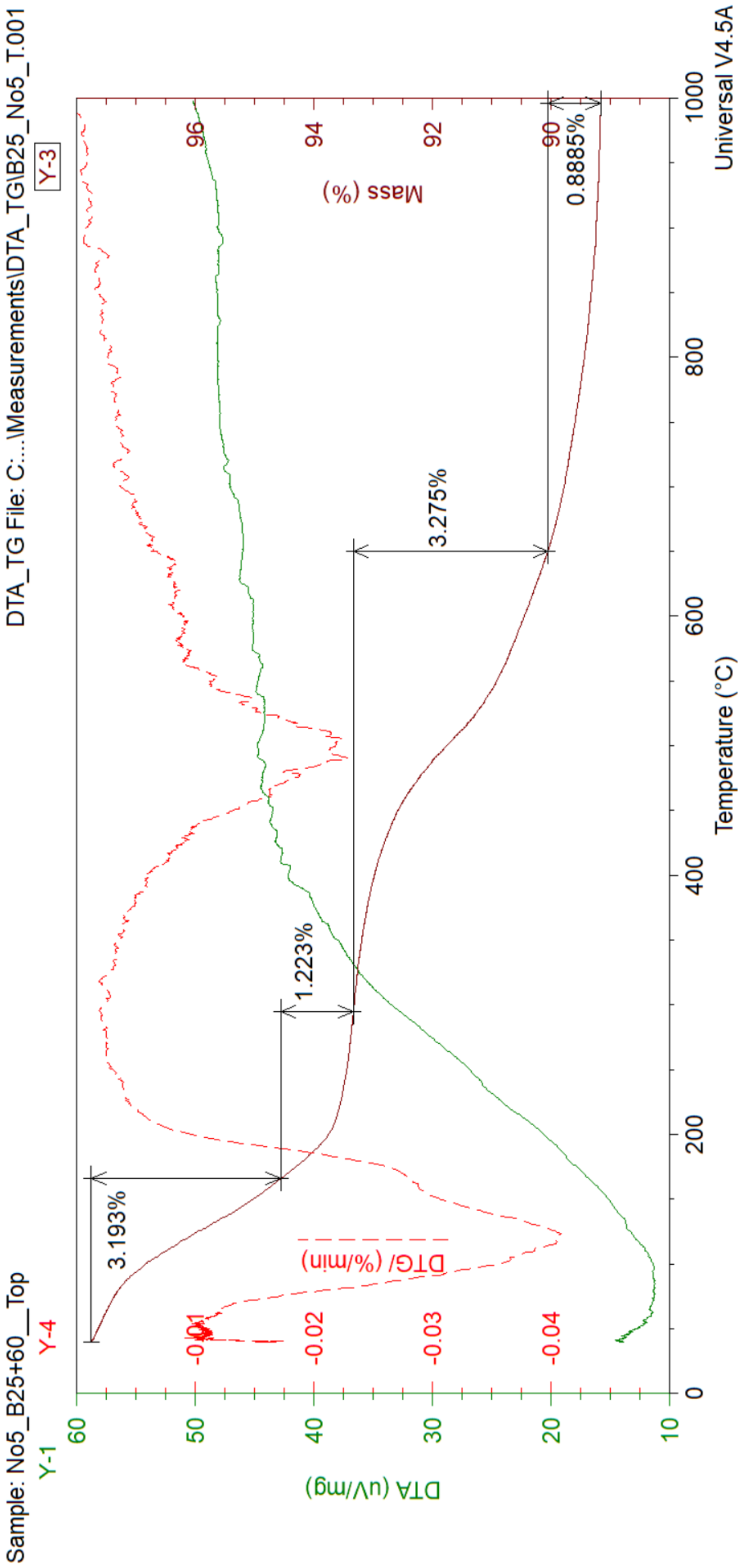

Data Sheet – B25 No5_C (bulk), treated material *(OPA, 60°C, 454 hours)*

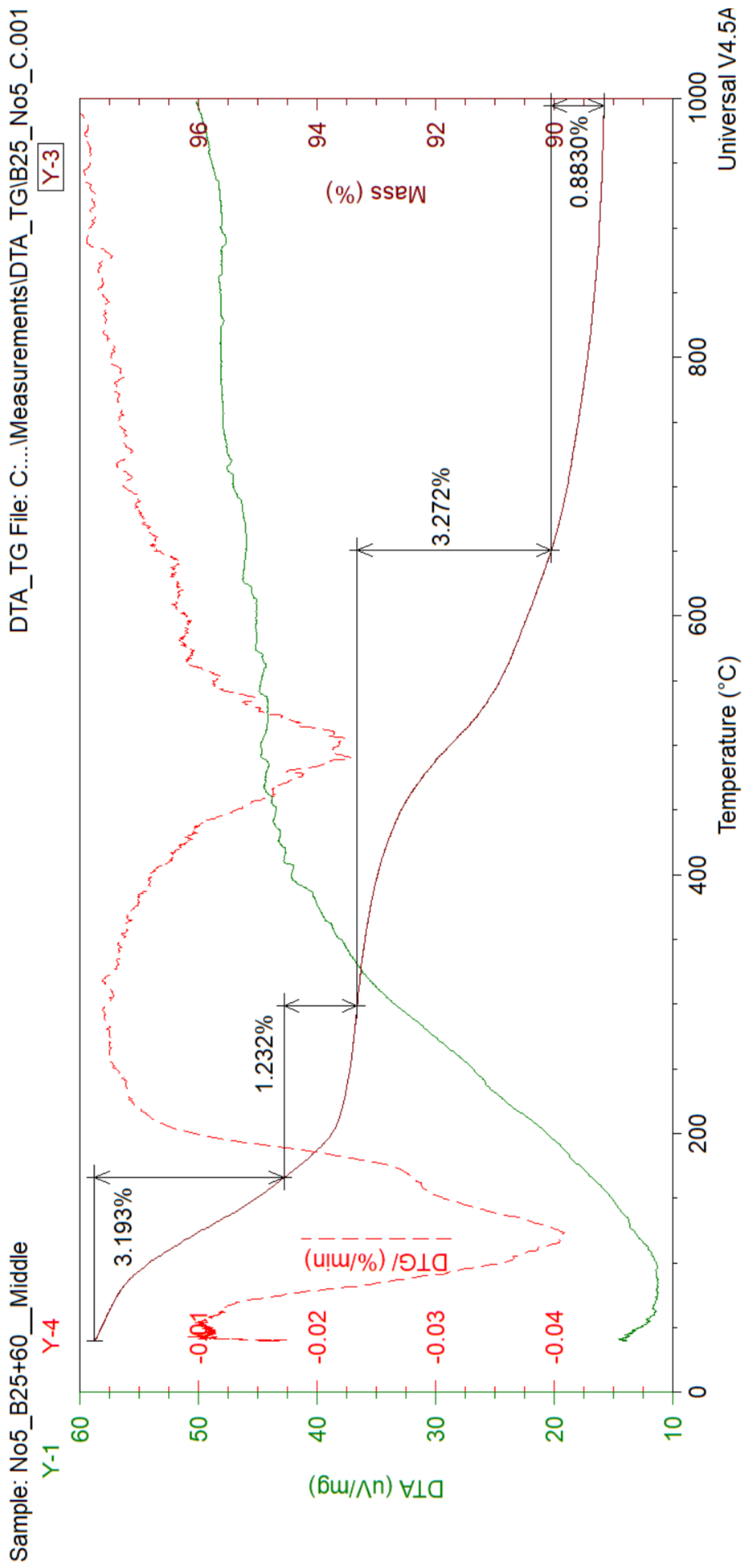

Data Sheet – B25 No5_B (bulk), treated material *(OPA, 60°C, 454 hours)*

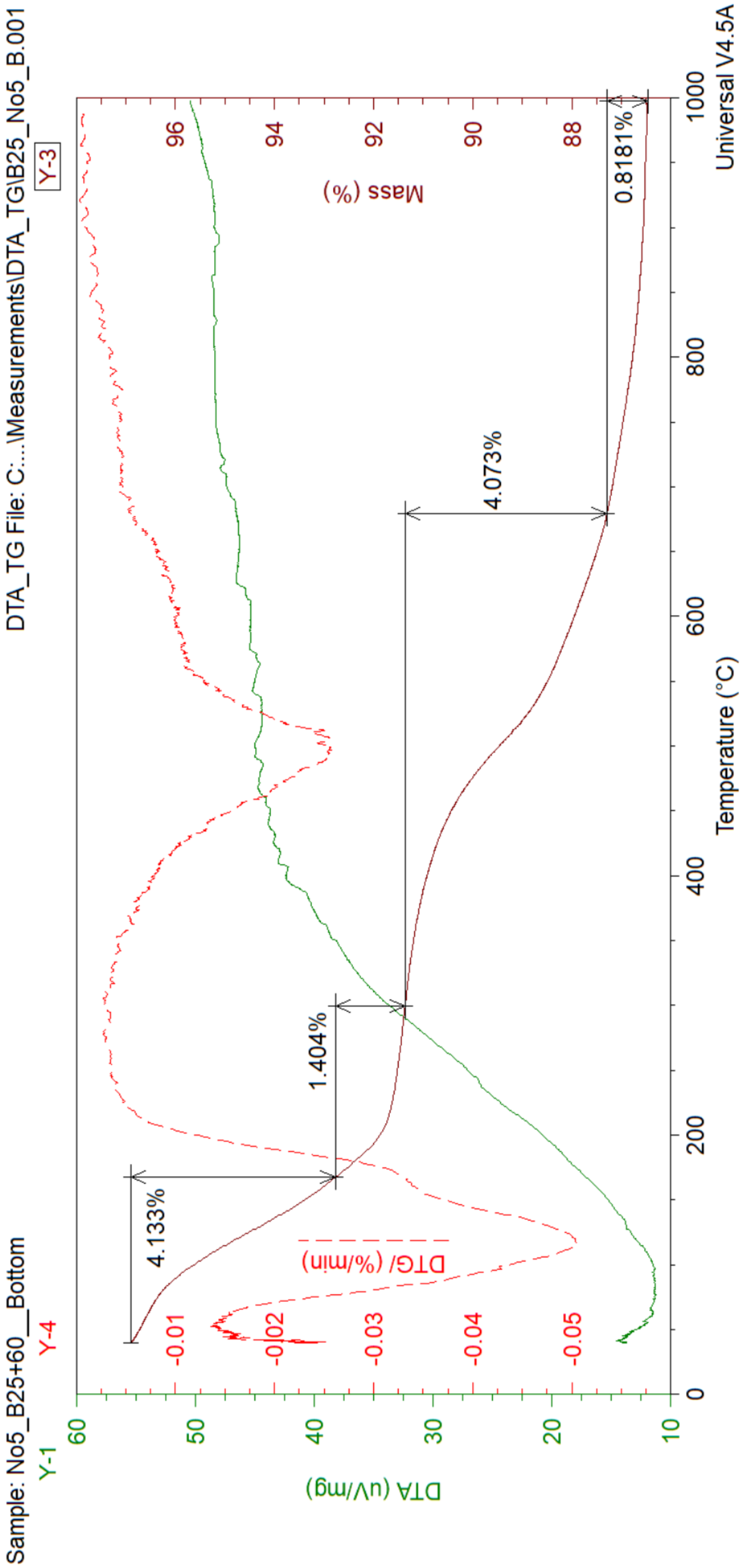

Data Sheet – B25 No0_T (bulk), treated material *(OPA, 100°C, 110 hours)*

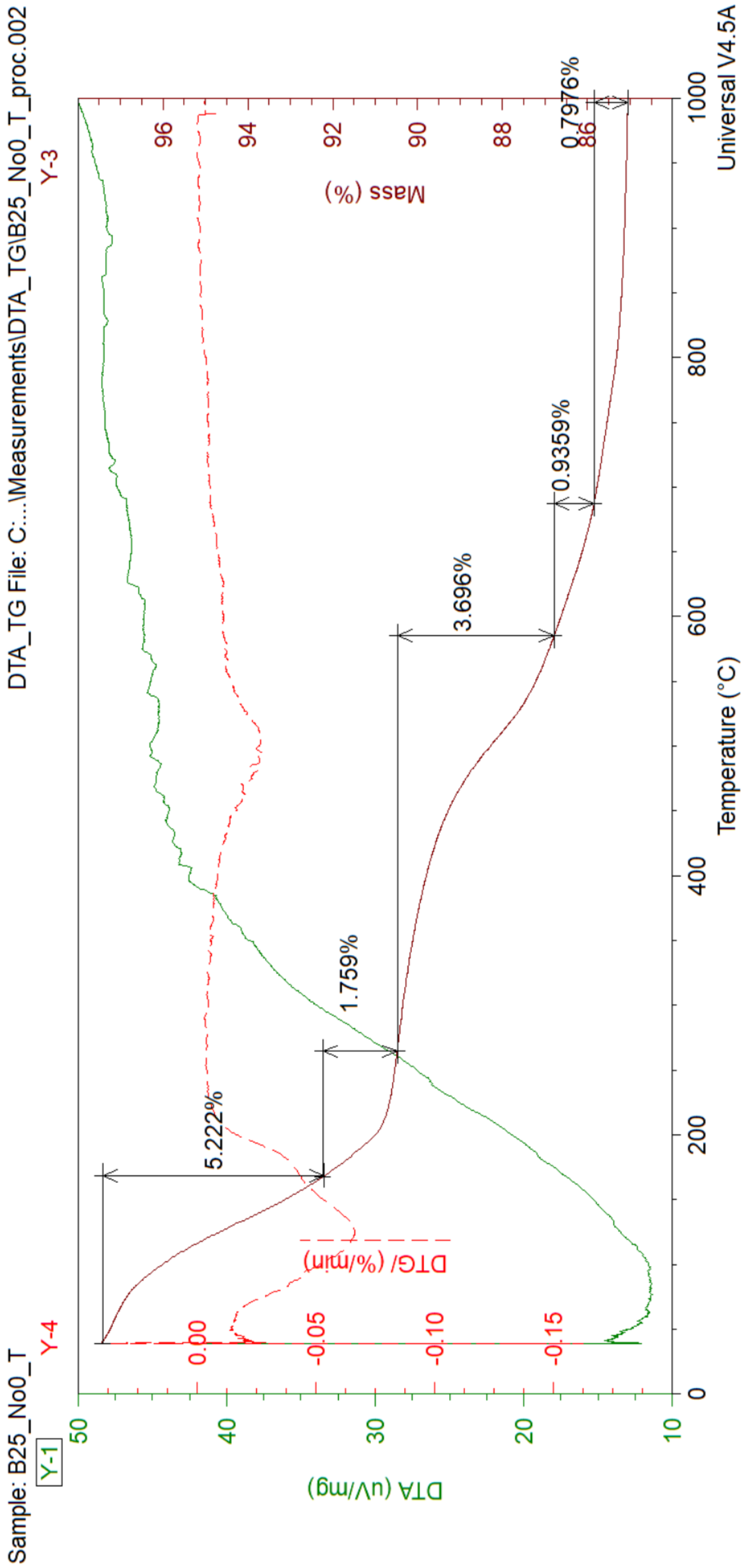

Data Sheet – B25 No0_C (bulk), treated material *(OPA, 100°C, 110 hours)*

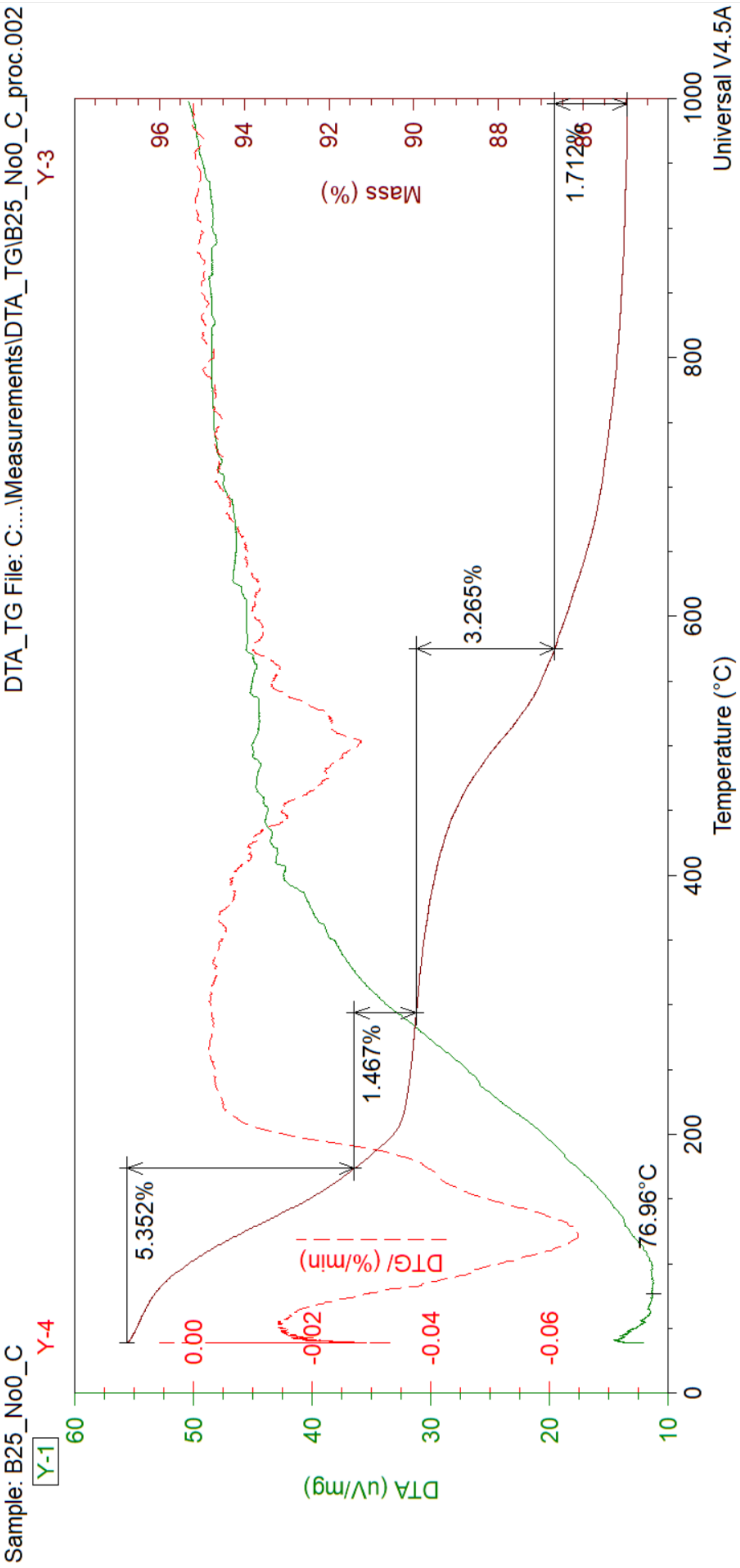

Data Sheet – B25 No0_B (bulk), treated material *(OPA, 100°C, 110 hours)*

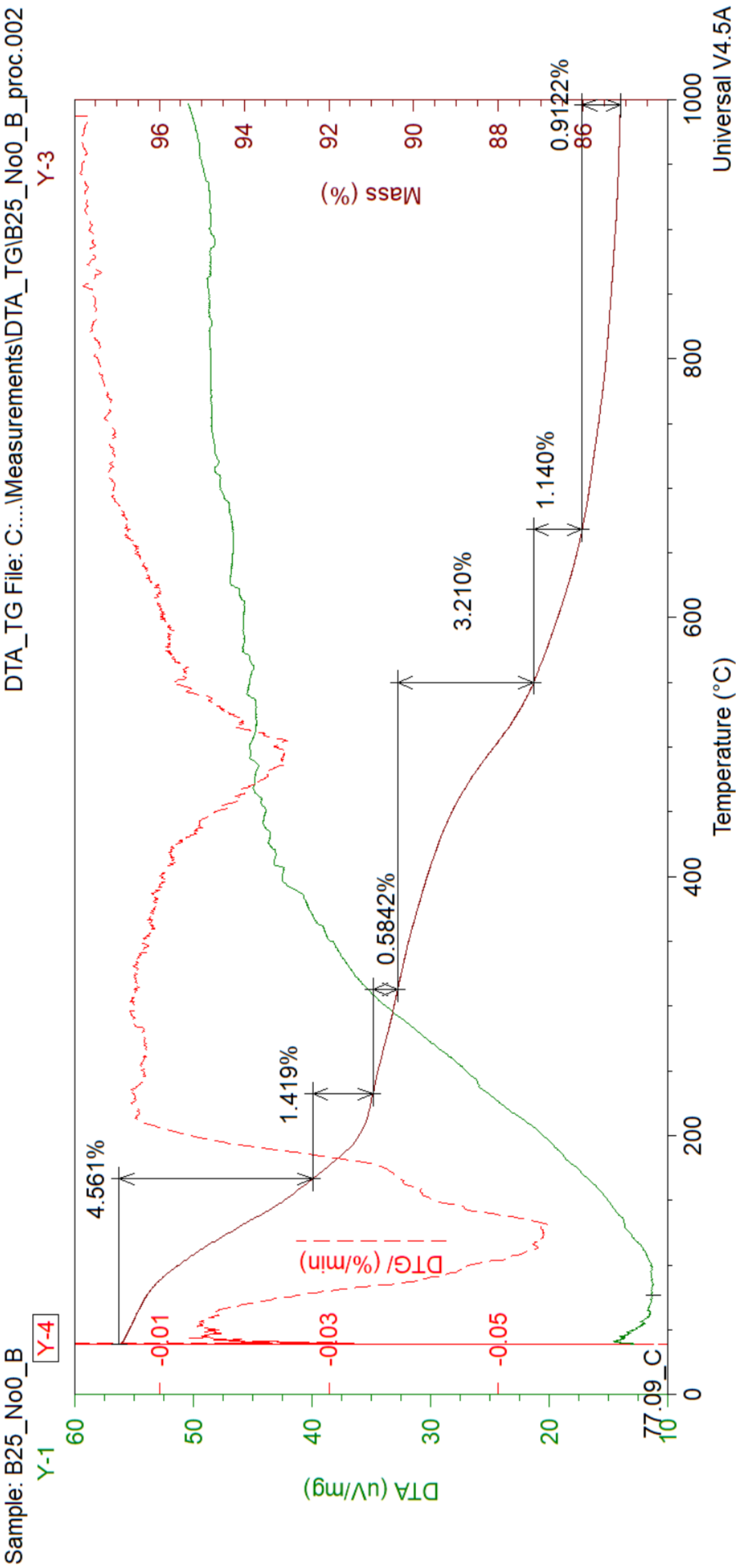

Data Sheet – B25 No2_T (bulk), treated material *(OPA, 100°C, 35 days)*

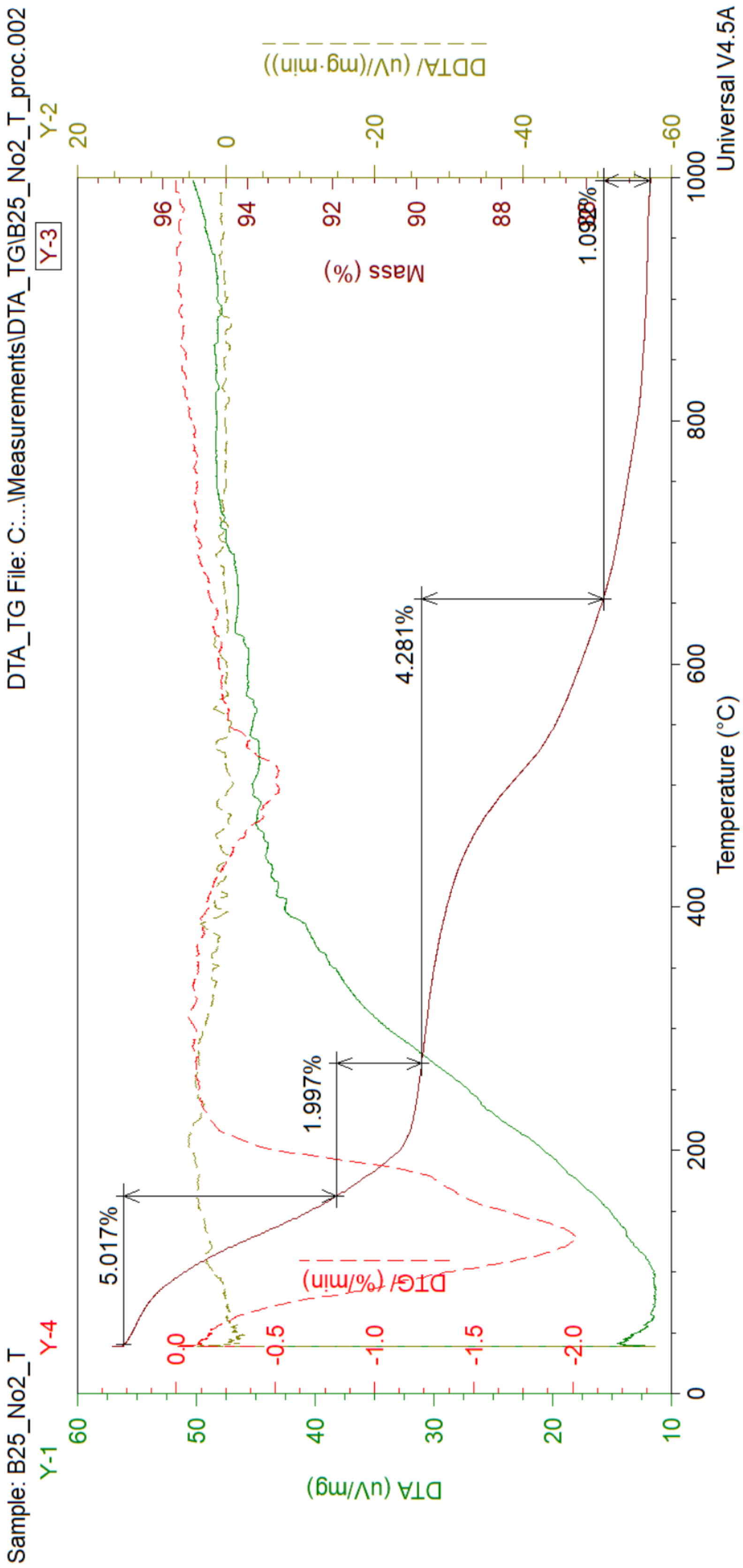

Data Sheet – B25 No2_C (bulk), treated material *(OPA, 100°C, 35 days)*

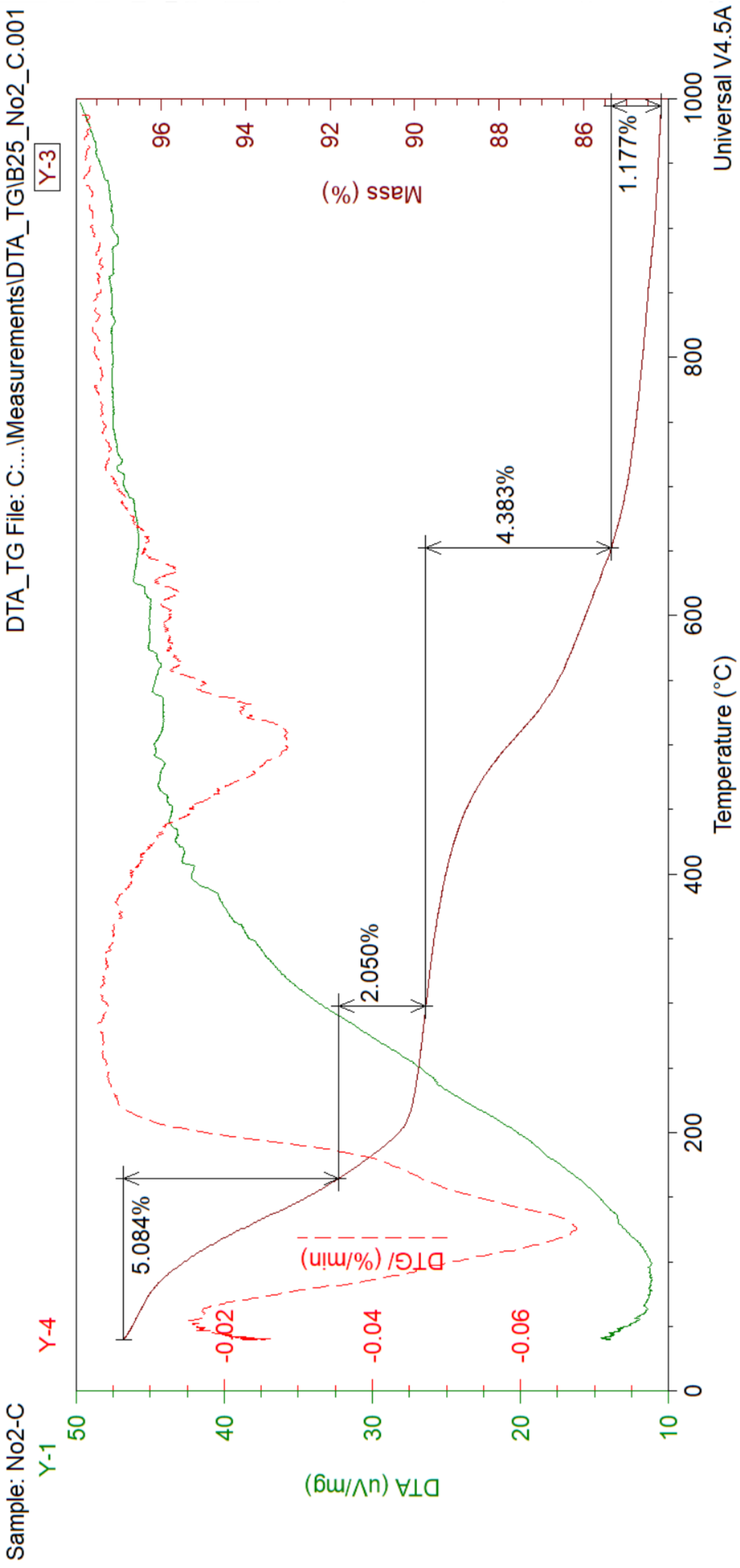

Data Sheet – B25 No2_B (bulk), treated material *(OPA, 100°C, 35 days)*

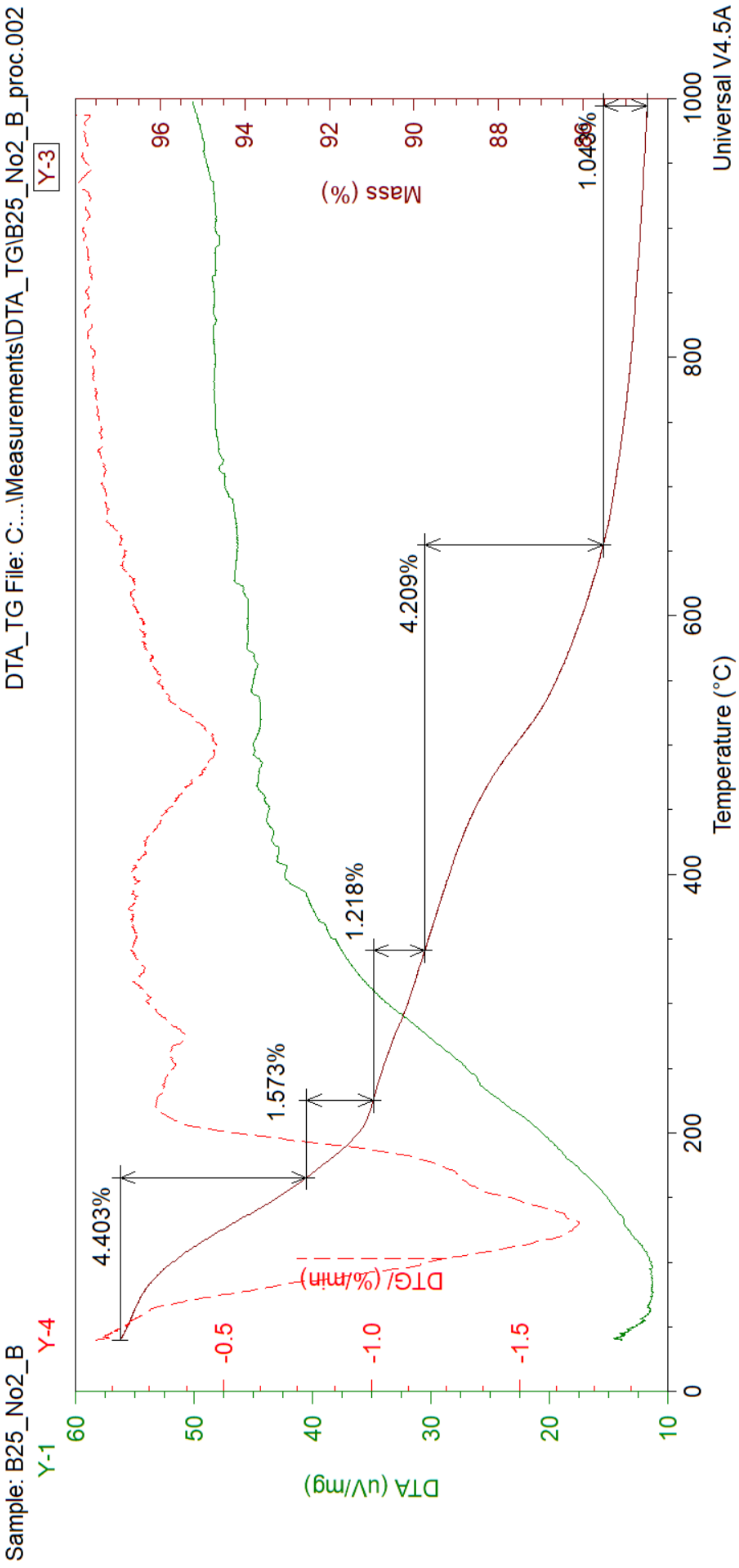

Data Sheet – B25 No15 (bulk), treated material *(OPA, 125°C, 98.6 h)*

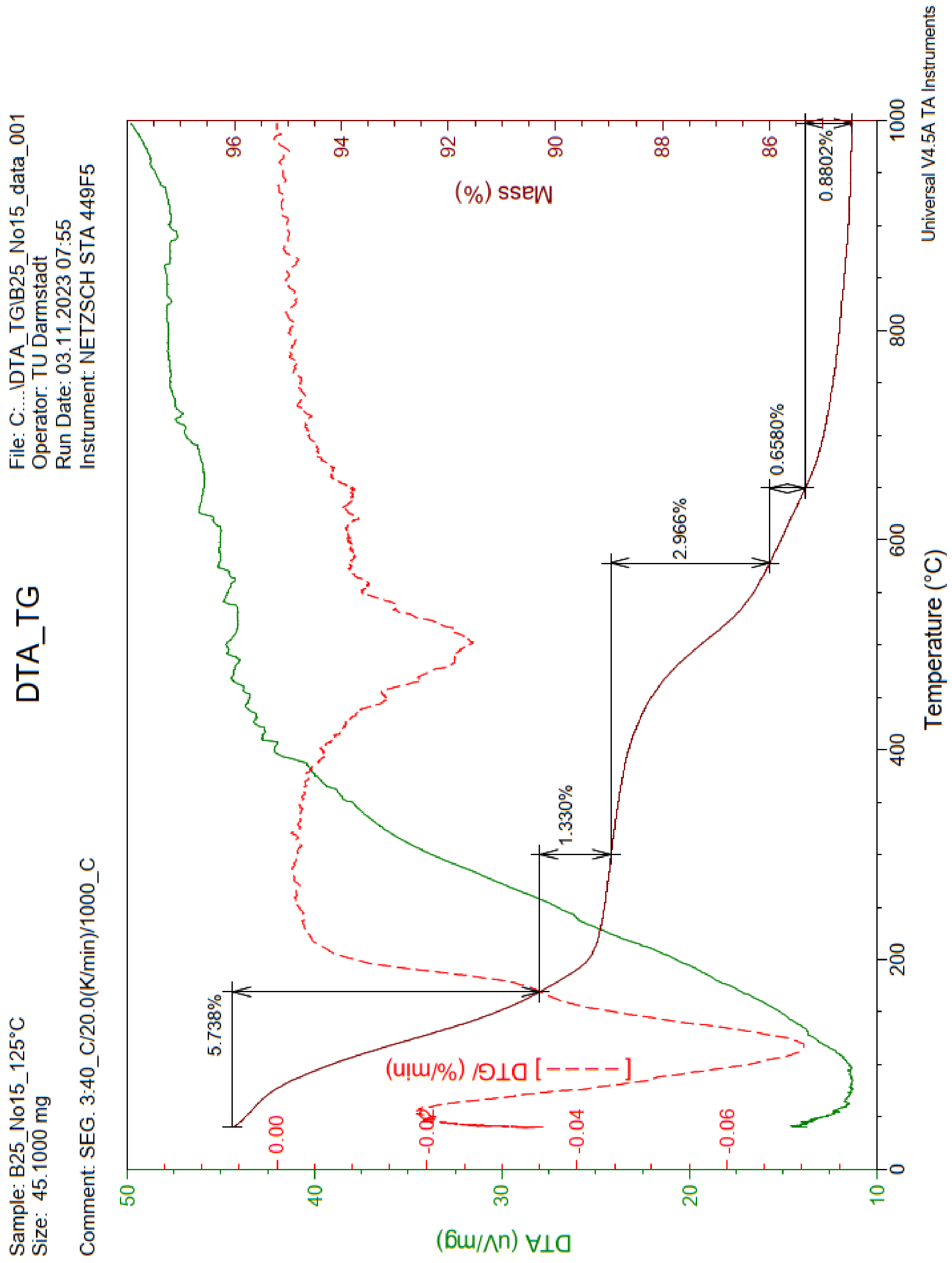

Data Sheet – B25 No3_T (bulk), treated material *(OPA, 150°C, 4 days)*

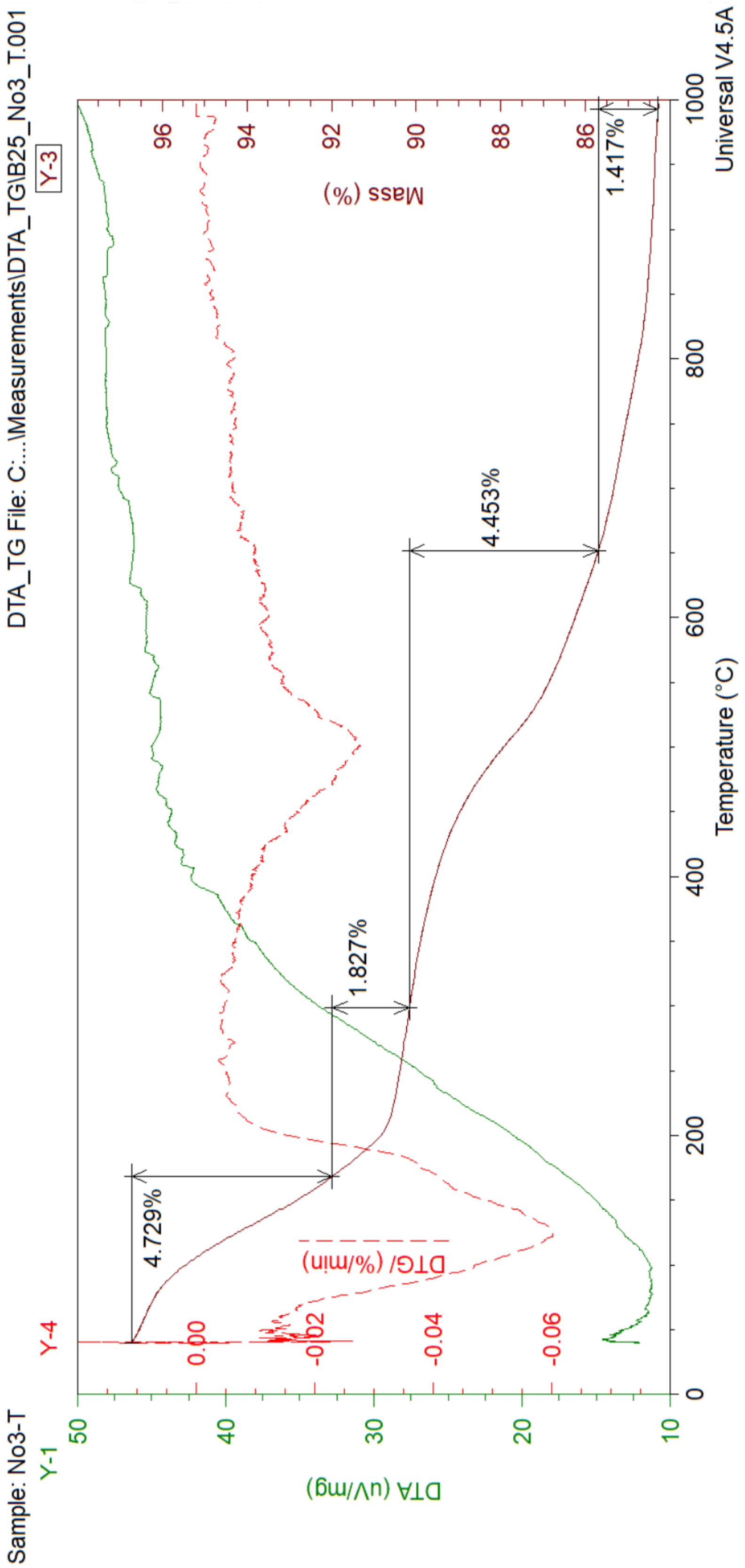

Data Sheet – B25 No3_C (bulk), treated material *(OPA, 150°C, 4 days)*

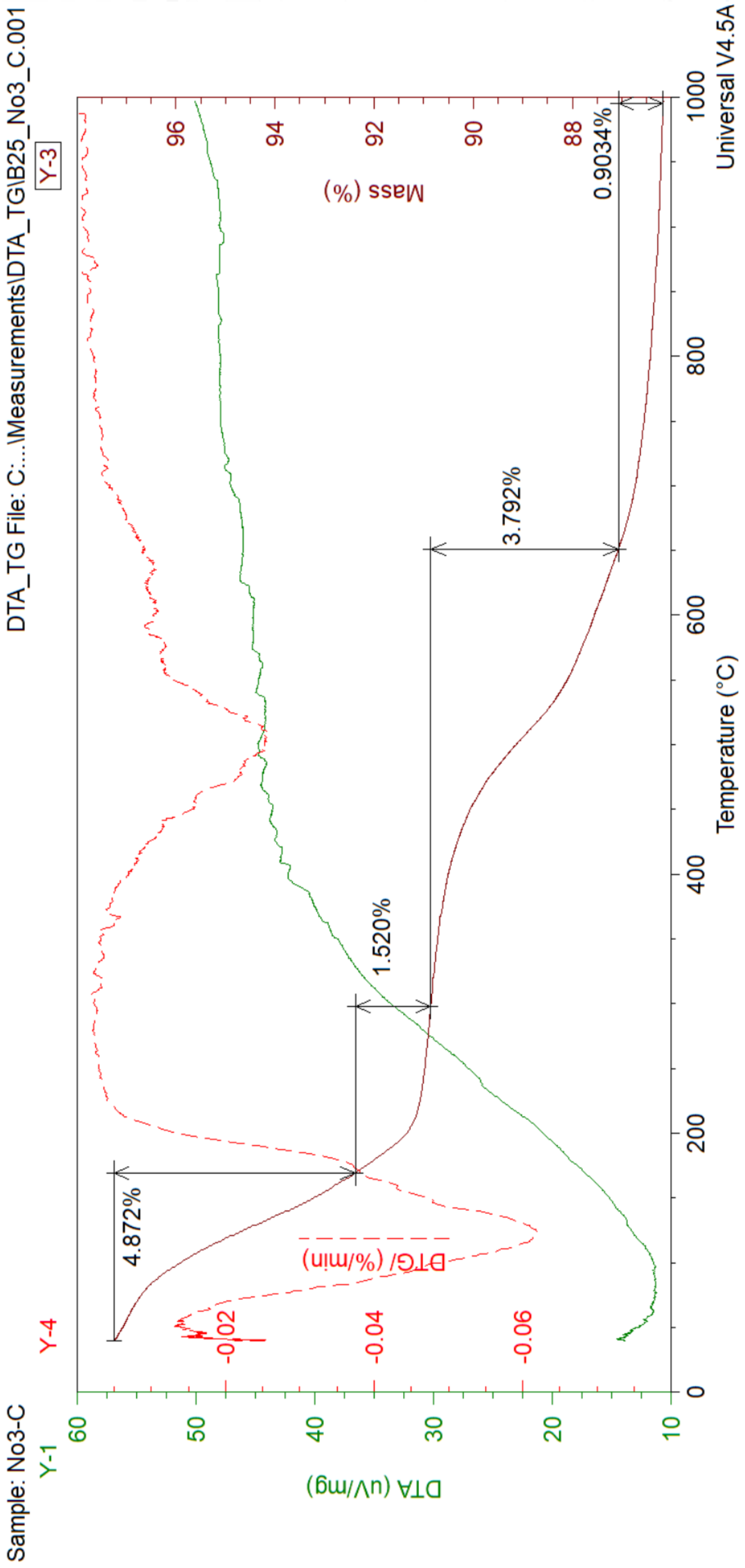

Data Sheet – B25 No3_B (bulk), treated material *(OPA, 150°C, 4 days)*

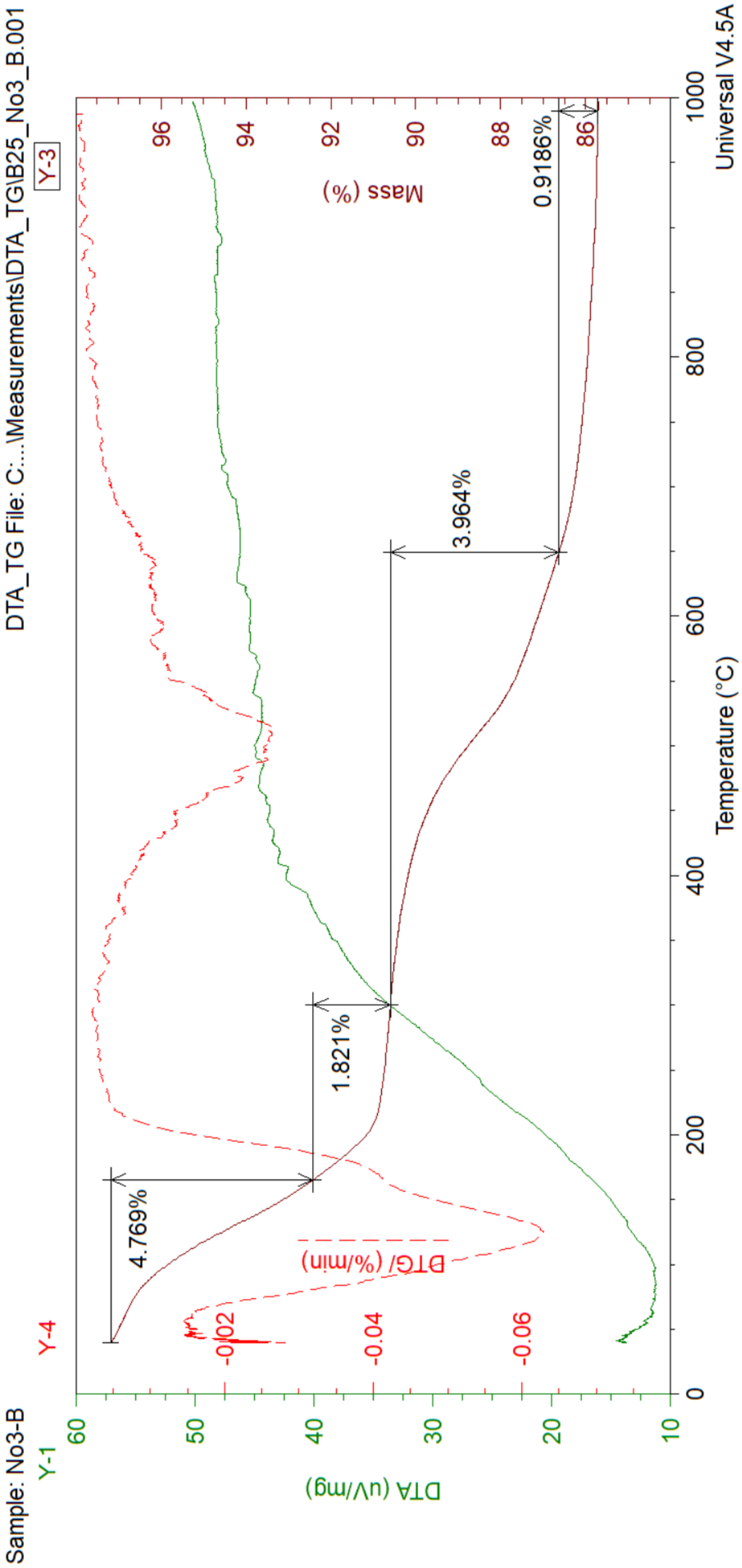

Data Sheet – Friedland No19 (bulk), untreated material *(compacted)*

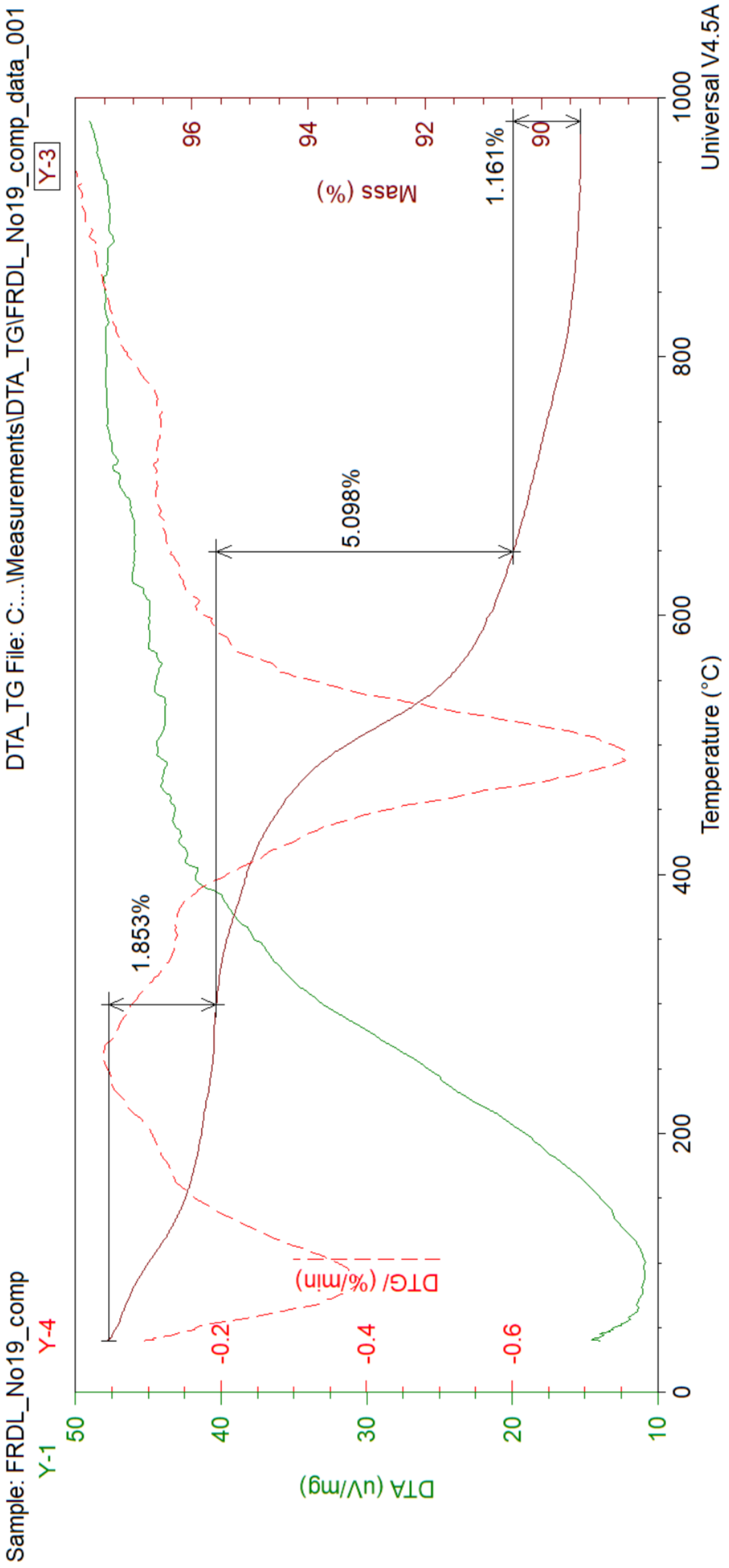

Data Sheet – Friedland No10 (bulk), treated material *(OPA, 35°C, 46.3 h)*

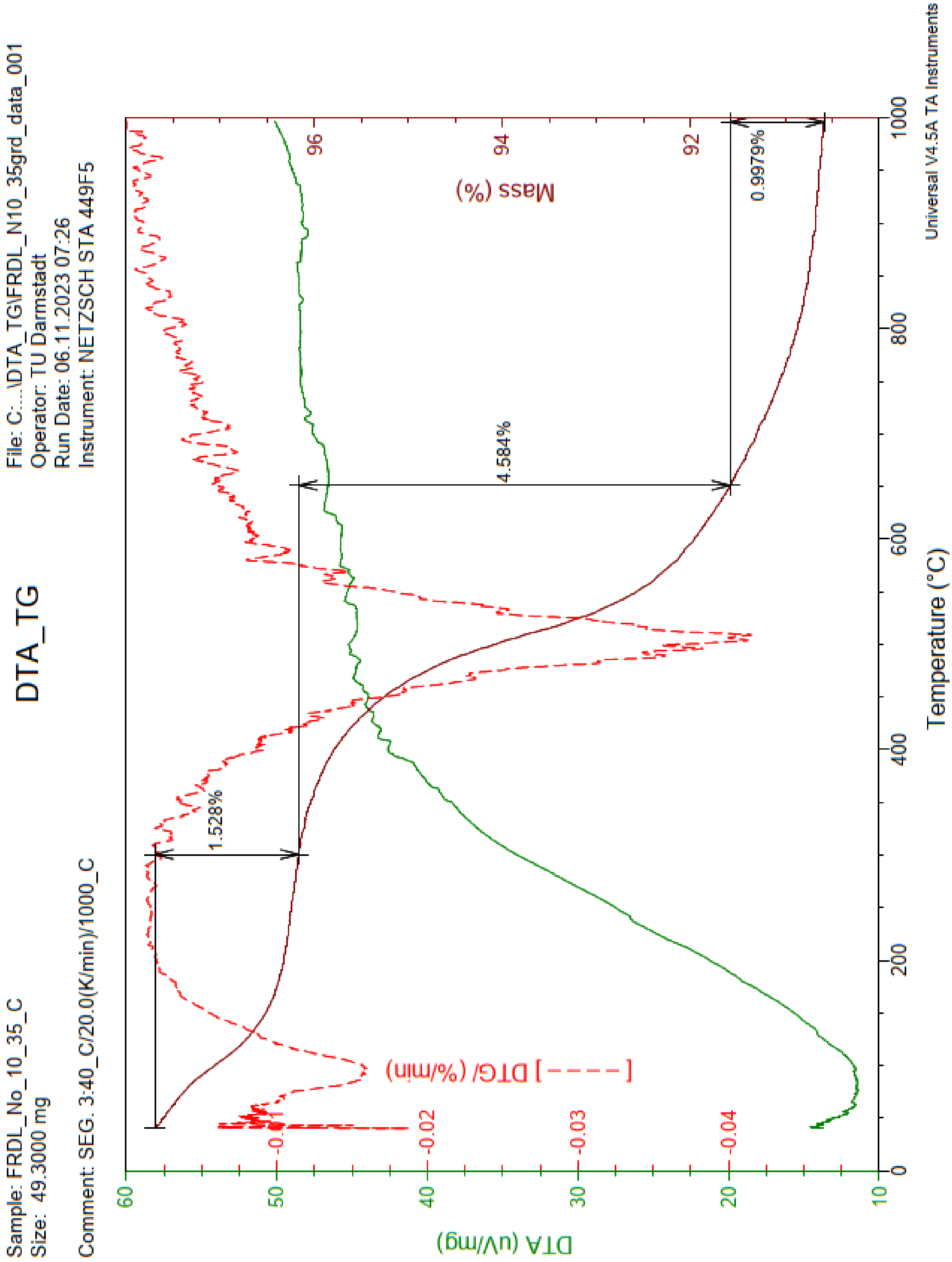

Data Sheet – Friedland No11 (bulk), treated material *(OPA, 60°C, 45.9 h)*

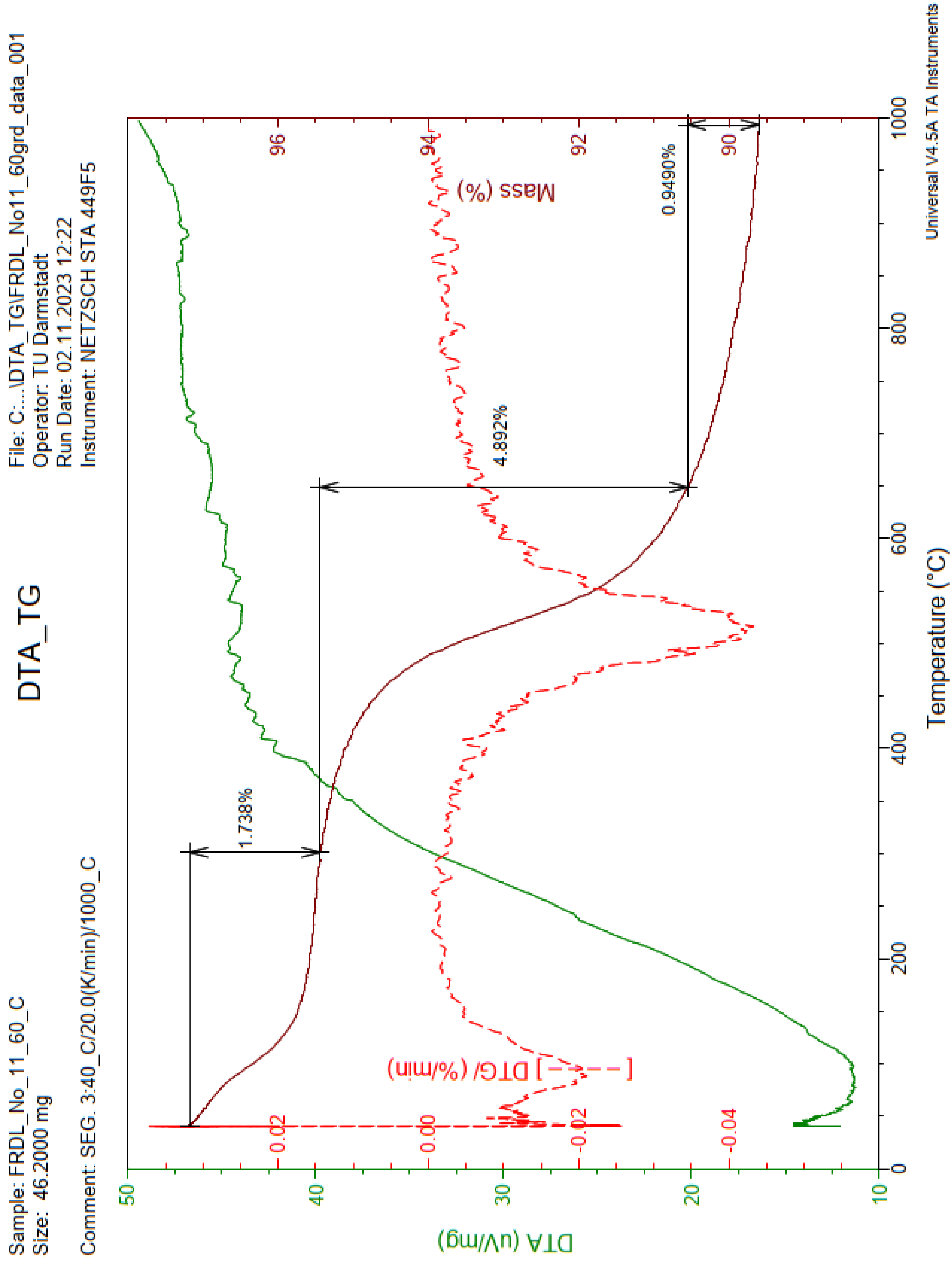

Data Sheet – Friedland No16 (bulk), treated material *(OPA, 100°C, 40 h)*

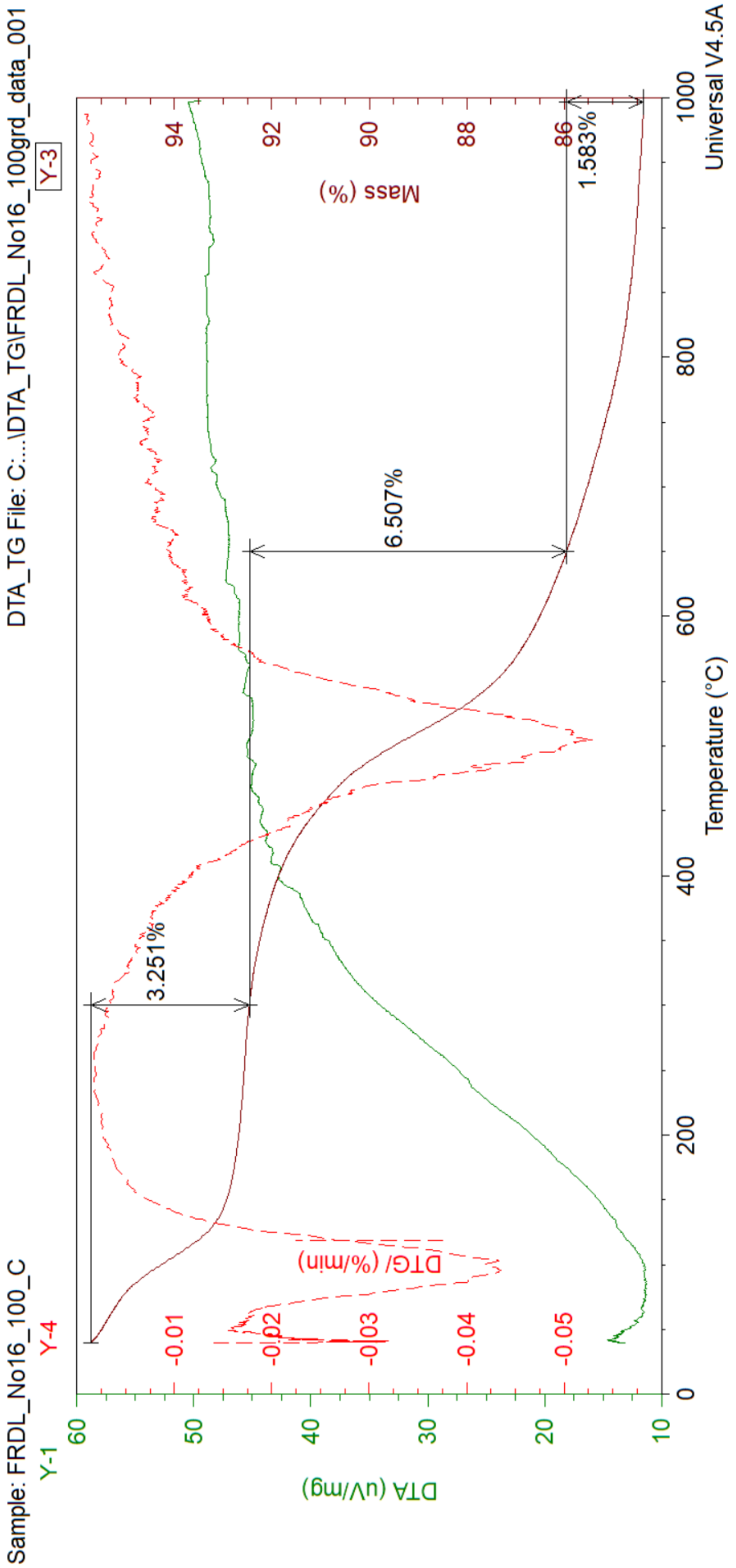

Data Sheet – Friedland No12 (bulk), treated material *(OPA, 100°C)*

[without transport cell]

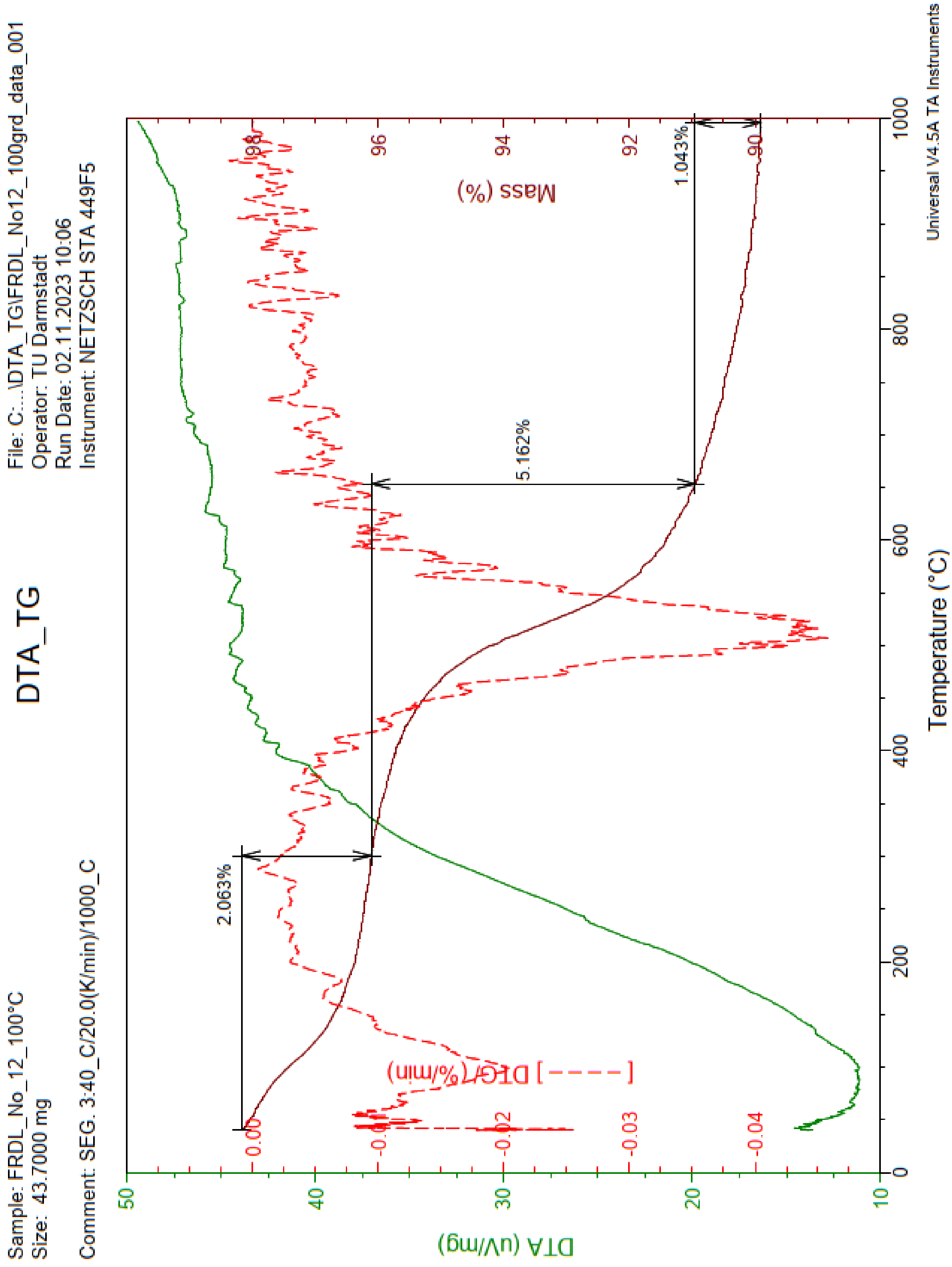

Data Sheet – Friedland No20 (bulk), treated material *(OPA, 125°C, 40 h)*

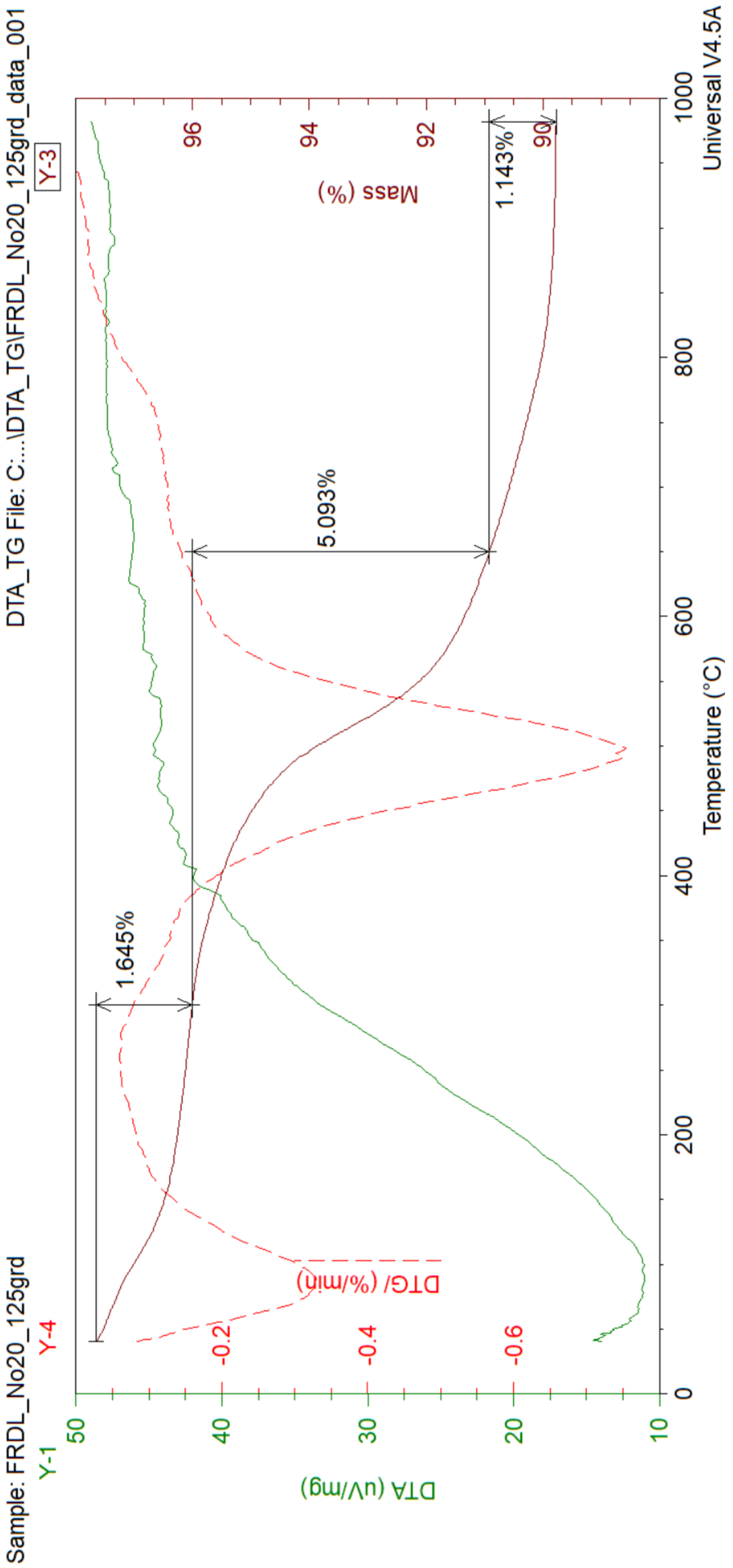

Data Sheet – Friedland No21 (bulk), treated material *(OPA, 150°C, 68.3 h)*

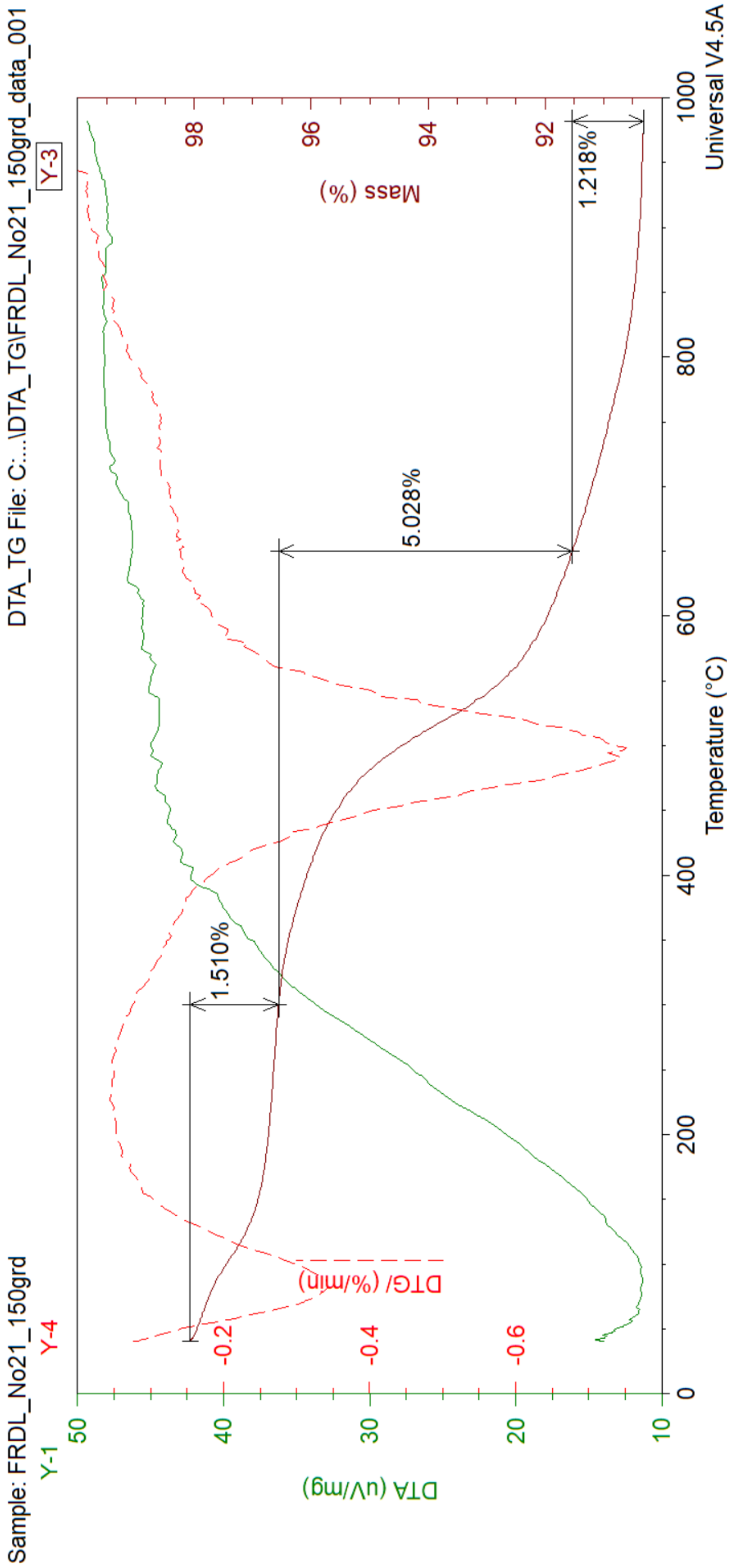

Data Sheet – Opalinus No22 (bulk), treated material *(OPA, 35°C, 144 h)*

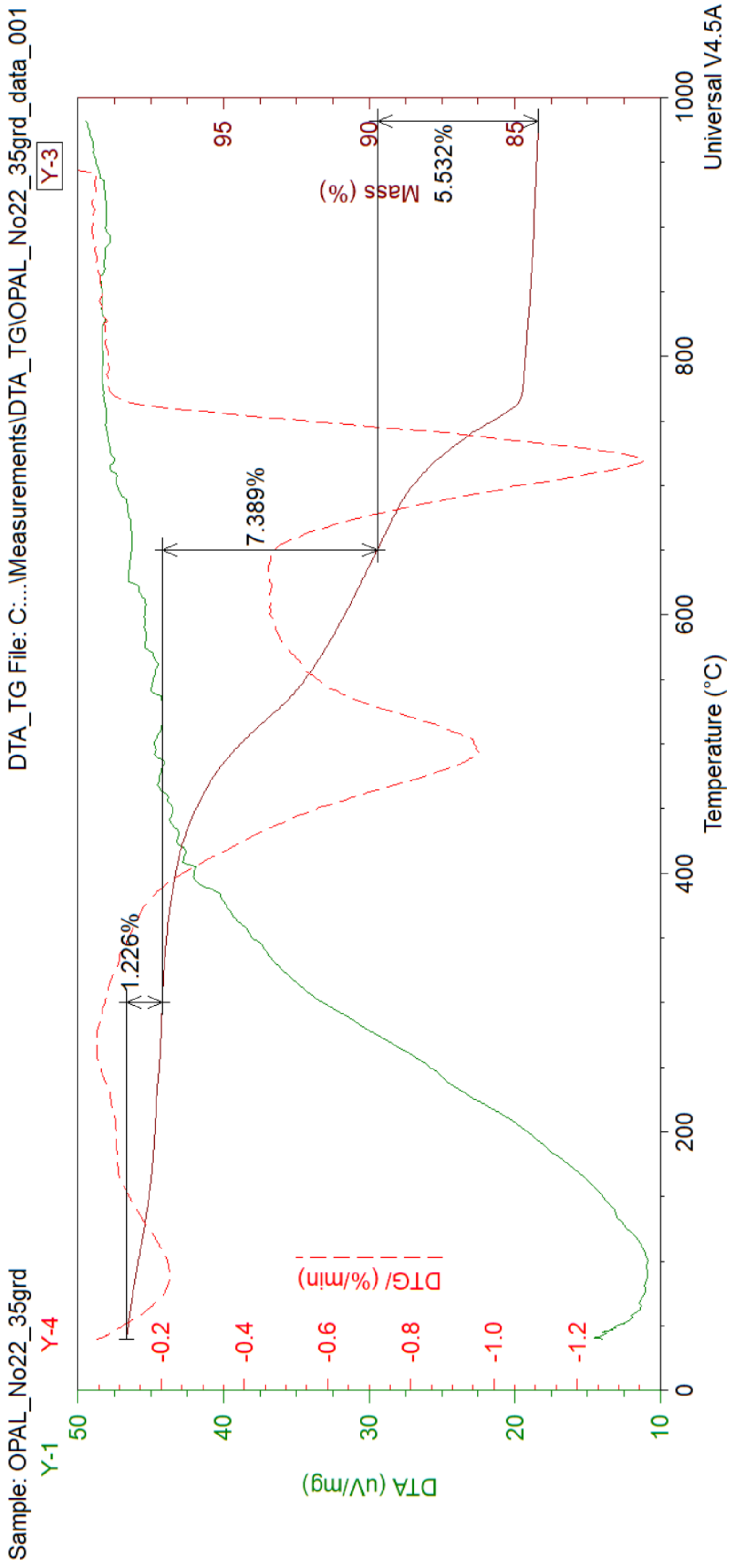

Data Sheet – Opalinus No9 (bulk), treated material *(OPA, 60°C, 45.4 h)*

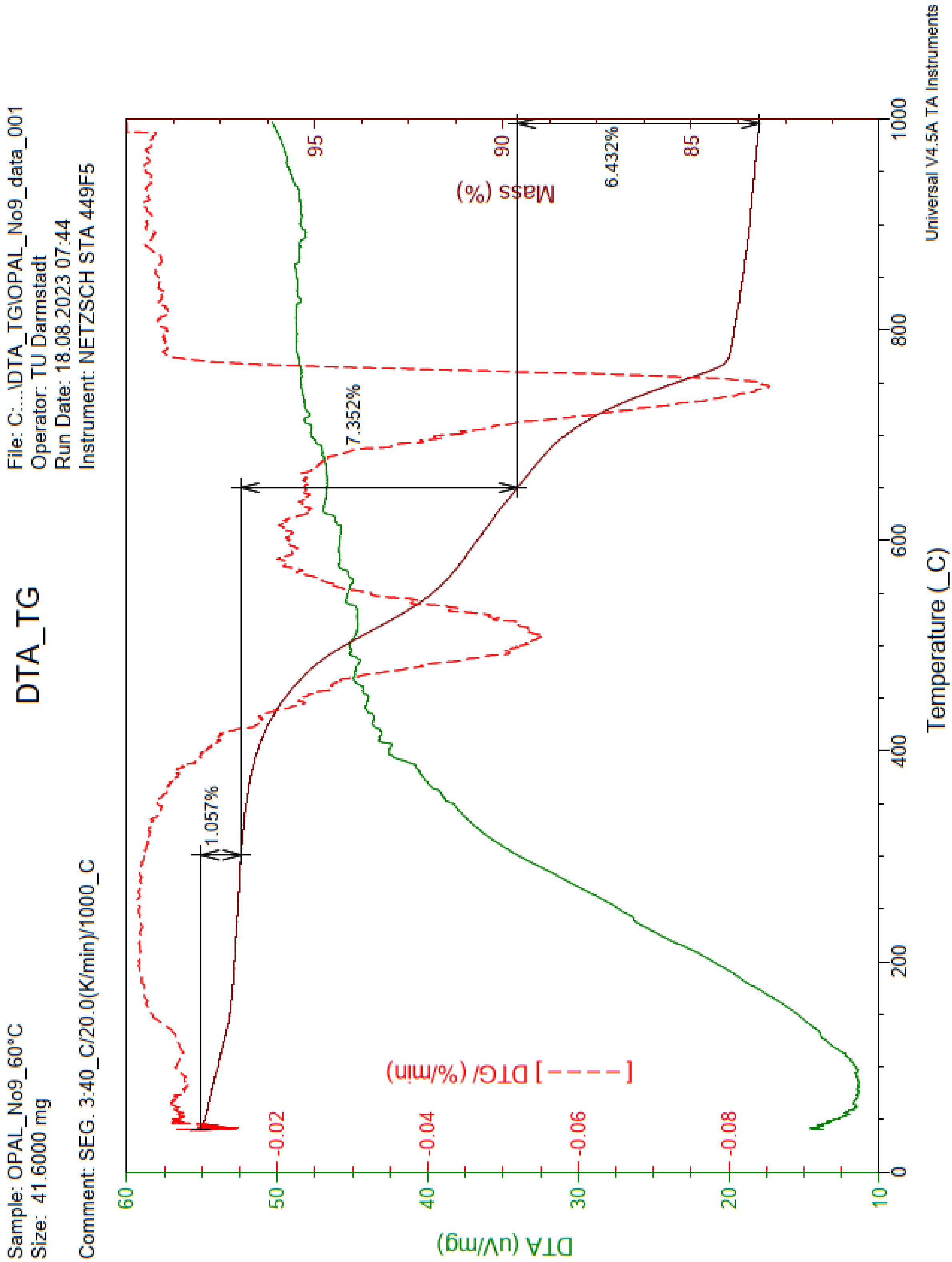

Data Sheet – Opalinus No7 (bulk), treated material *(OPA, 60°C, 95.3 h)*

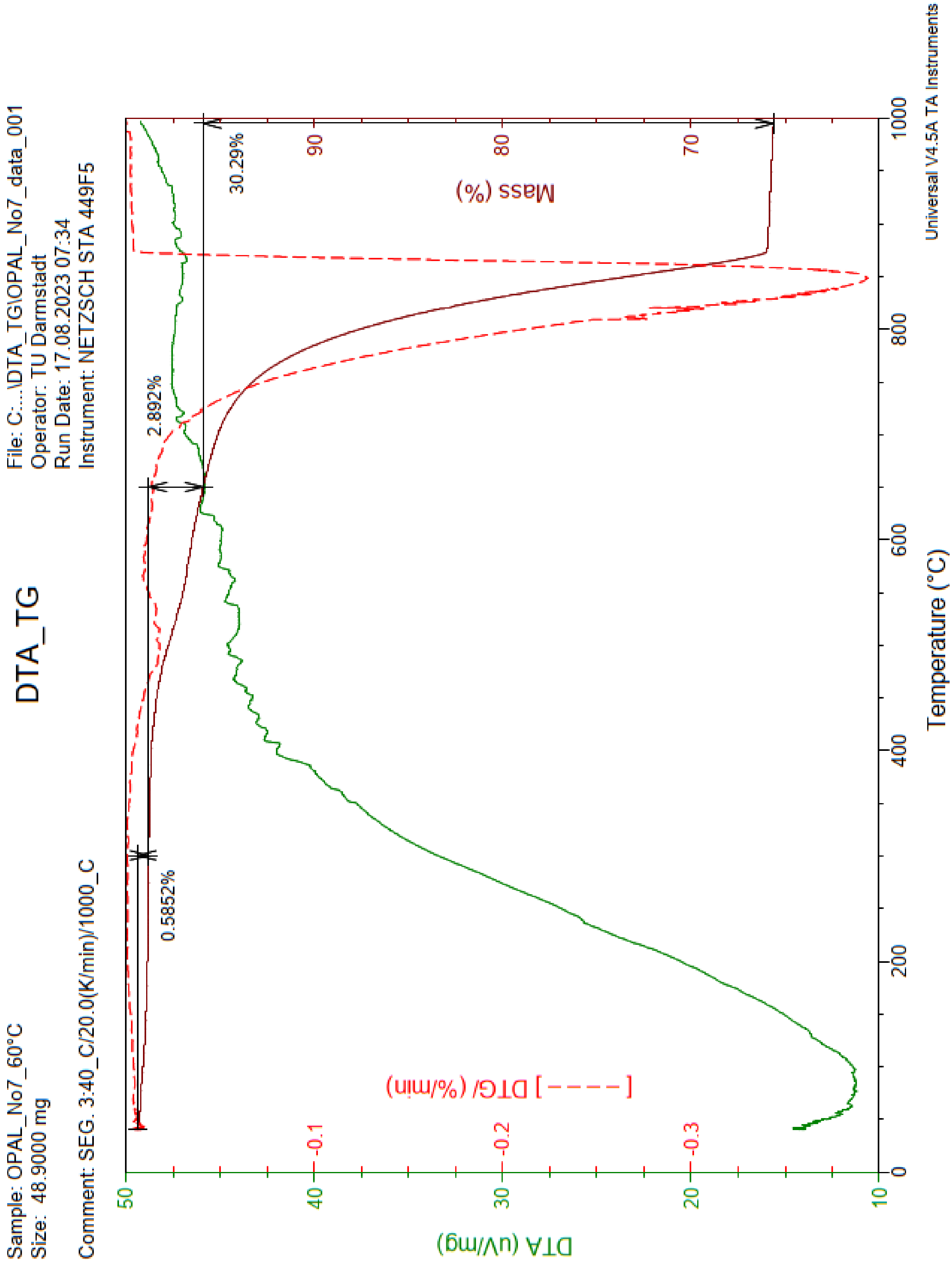

Data Sheet – Opalinus No8 (bulk), treated material *(OPA, 100°C, 69.3 h)*

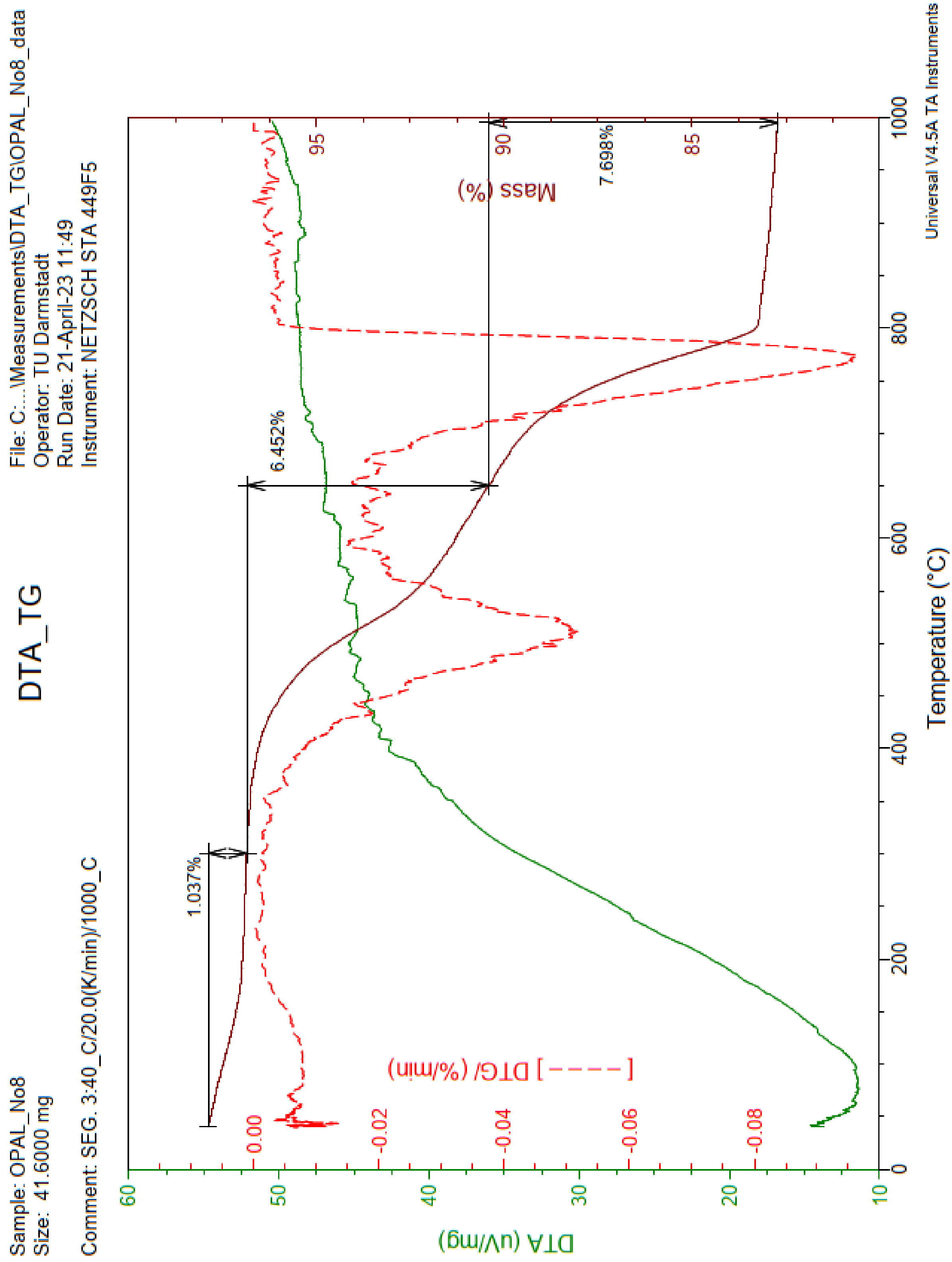

Data Sheet – Opalinus No14 (bulk), treated material *(OPA, 125°C, 48.5 h)*

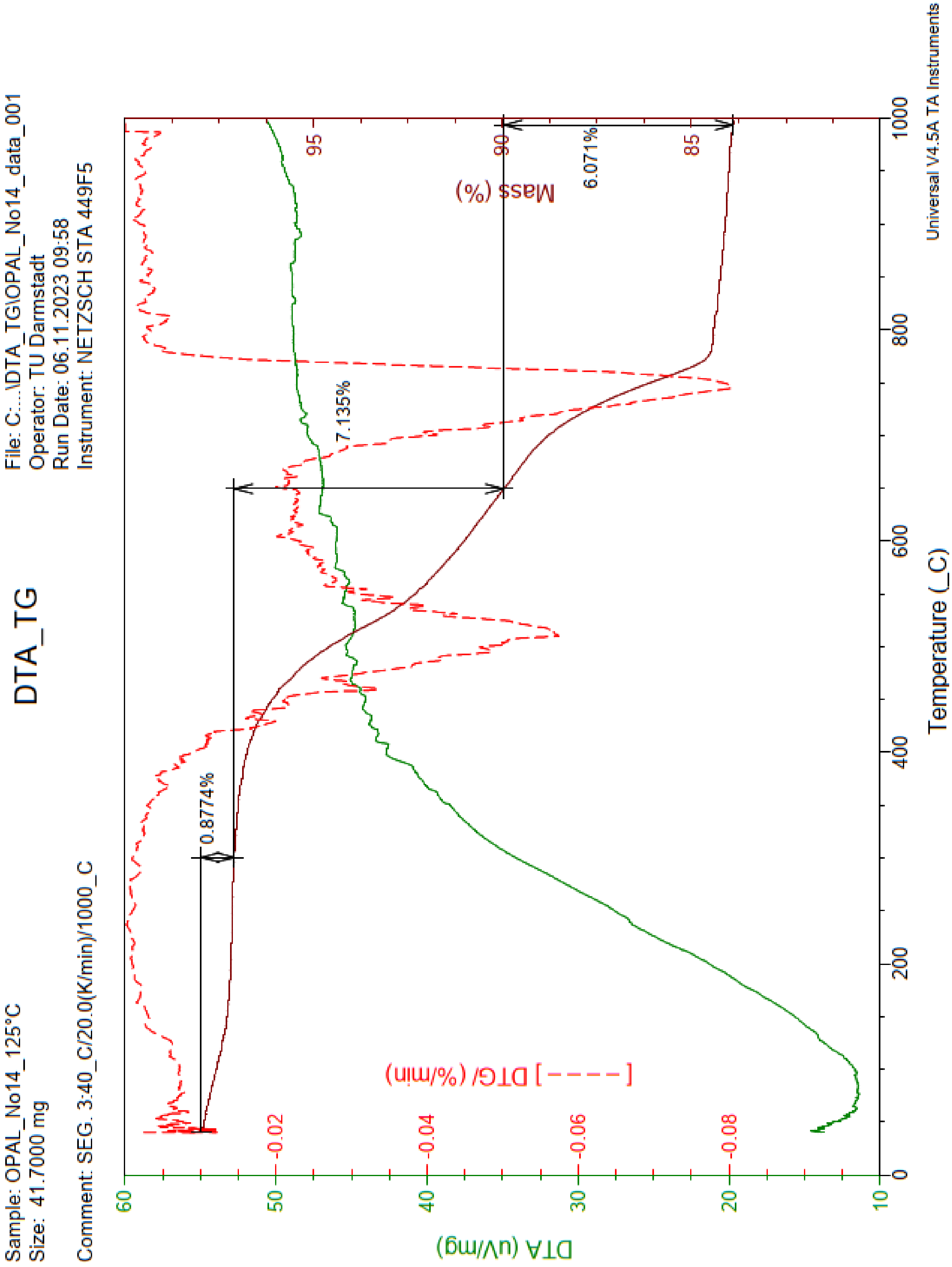

Data Sheet – Opalinus No13 (bulk), treated material *(OPA, 150°C, 48.6 h)*

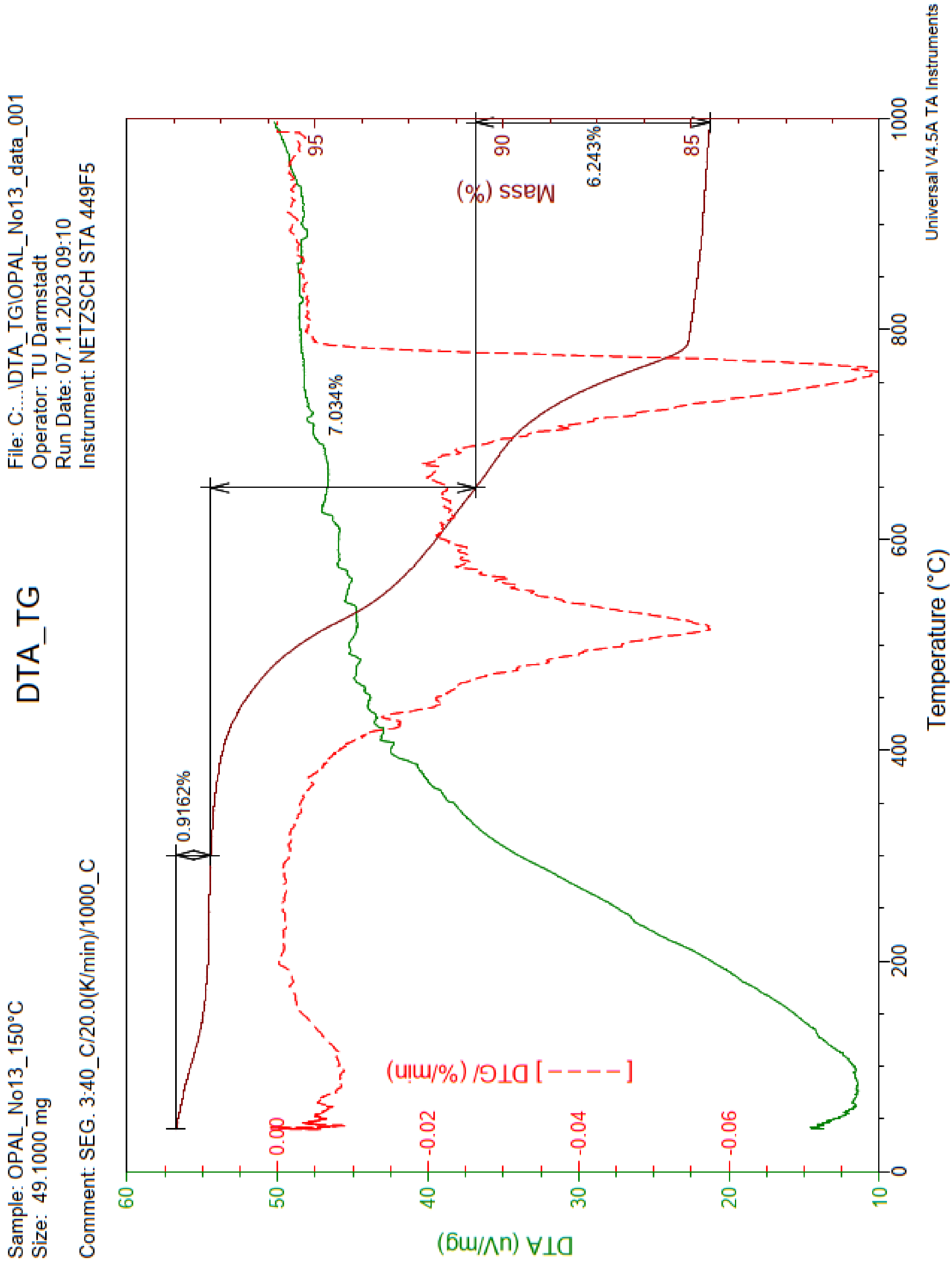

Data Sheet – Opalinus No9a (bulk), treated material *(OPA, 35°C)*

[without transport cell]

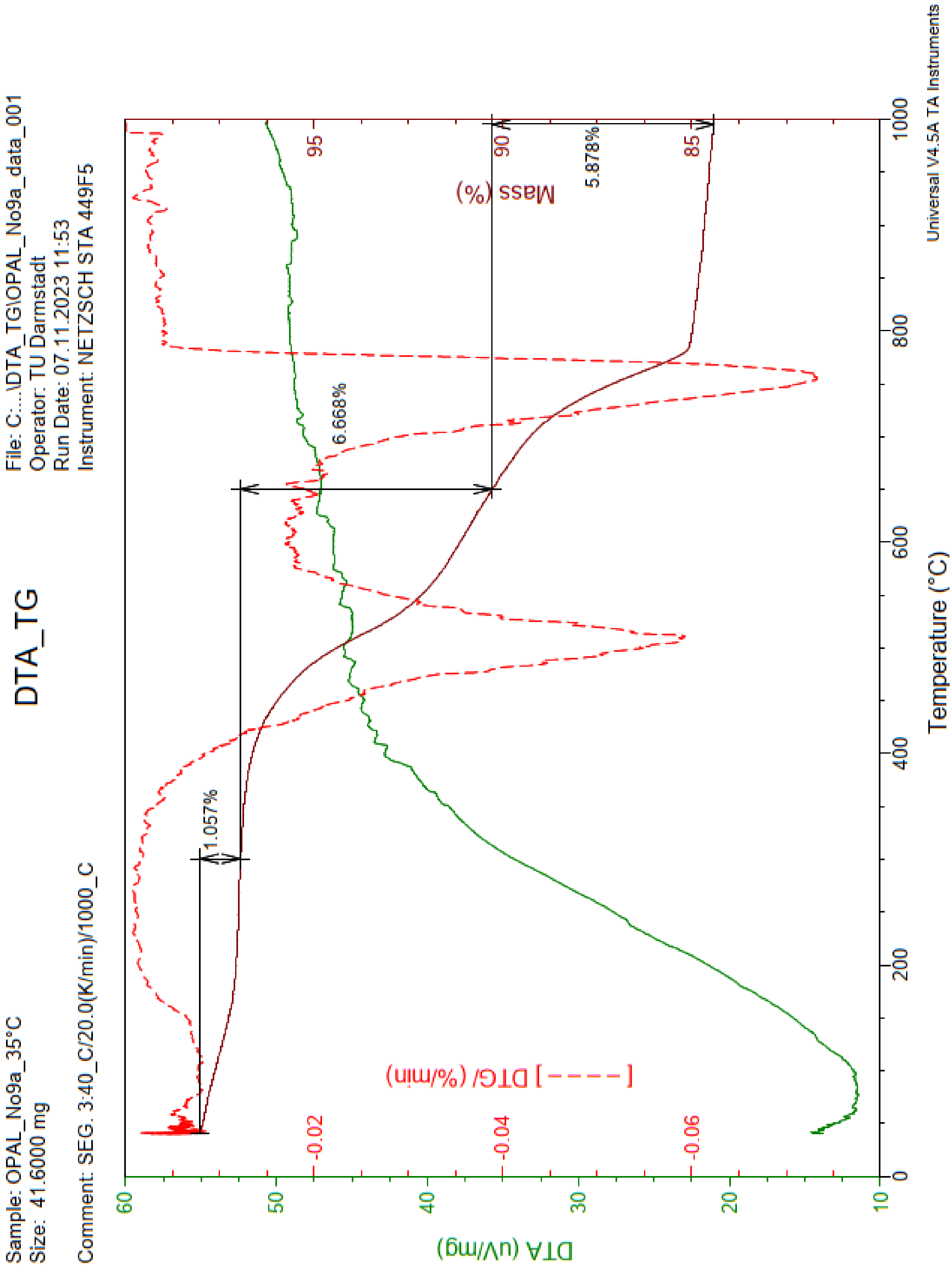

Data Sheet – Opalinus No9b (bulk), treated material *(OPA, 125°C)*

[without transport cell]

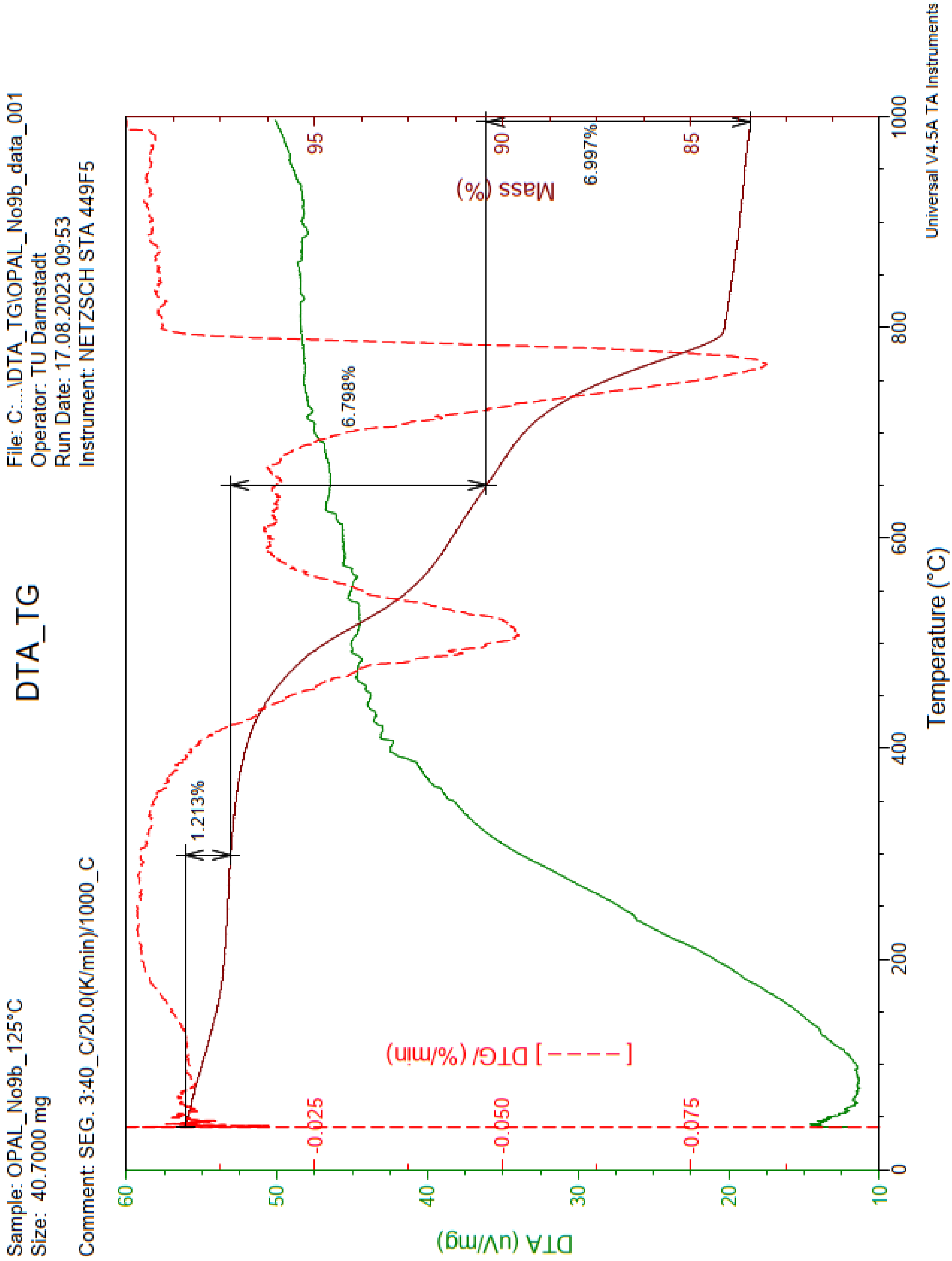

S5. Cation exchange capacity (CEC), Specific surface area (SSA), and surface charges

SUPPLEMENT – cation exchange capacity (CEC), specific surface area (SSA), and surface charge

Methodology

CEC-measurements were implemented according to Hendershot and Duquette, 1986, 0.5 g of air dry clays were mixed with 30 mL 0.1 M aqueous $BaCl_2$ solution and shake slowly on an end-over-end shaker (15 rpm) for 5 h, the supernatant was removed by centrifuge and filter with Whatman No. 41 filter paper. This procedure was repeated 5 times and after each ion exchange, all the liquid fractions were combined and analysed using atomic absortpion spectroscopy (AAS) for Ca, Mg, K, Na, Al, Fe, and Mn. Finally the Ca, Ma, Na and K were used for CEC calculation.

The surface charges of initial and reaction products were determined by polycation titration combined with streaming potential measurements using particle charge detector PCD-06 at Department of Applied Geosciences, TU-Darmstadt.

The Brunauer-Emmett-Teller specific surface area (SSA) was measured by N2 adsorption at 77 K in the relative pressure range of 0.05 to 0.3 (Quantachrome Autosorb-3B, USA) after degassing for 22 h at 80°C at Department of Material Sciences, TU-Darmstadt.

References:

Hendershot, W.H. and M. Duquette, 1986. A Simple Barium Chloride Method for Determining Cation Exchange Capacity and Exchangeable Cations. Soil Science Society of America Journal, 50(3): p. 605-608.

Tab. 1. The CEC, BET specific surface area (SSA) and surface charge of initial and reaction products of THMC-experiments

Sample	SSA (m2/g)	CEC (meq/100g)	Surface charge (µeq/l)
B25			
Initial compacted B25	89,79		-13,7
B25 hand milled	74,01	45,15	
No4_B25+35 °C+93.6h	61,69		-13,3
No23_B25+290h 0.7Ma 35°C	114,1		-16,4
No5_B25 + 60 °C+454h	76,33		-16
No0_B25+OPA+100 °C, 110h	166		-14,7
No2_B25+100oC+35d	96,17		-13,3
No15_B25+125°C+454h	83,04		-15
No3_B25 + 150 °C+4d	80,93		-17,5
Opalinus			
No6_compacted Opalinus	24,55		-8,3
Opalinus Ball milled	38,44	88,23	
Opalinus Hand milled	35,63	82,36	
No9a_Opalinus + 35 °C	43,34		-15,4
No22_Opalinus + 35 °C_VSE	51,81		-15
No9_OPa+60oC_VSE	40,12		-9,7
No8_OP3+100oC	38,54		-8,7
No9b_Opalinus + 125 °C	49,5		-6,3
No14_Opalinus + 125 °C_VSC	43,75		-9
No13_Opalinus + 150 °C	38,32		-11,6
Friedland clay			
No19_compacted Friedland clay	58,35	67,02	-19
No10_Friedland clay + 35 °C_VSC	60,59		-18
No11_Friedland clay + 60 °C_VSC	57,62		-19,1
No12_Friedland clay + 100 °C_VSC	79,18		-16
No16_Friedland clay + 125 °C_VSD	75,71		-24
No20_Friedland clay + 125 °C_VSC	63,82		-17,7
No21_Friedland clay + 150 °C_VSC	62,82		-16,7

S6. Scanning Electron Microscopy (SEM)

SUPPLEMENT – Scanning Electron Microscopy (SEM)

Content

Methodology – Scanning Electron Microscopy of compacted samples

The scanning electron microscopy (SEM) analysis was conducted using an FEI Quanta 400 ESEM FEG instrument (FEI, Eindhoven, the Netherlands) equipped with an energy-dispersive X-ray detector (Oxford, Oxfordshire, UK). The analyses were performed manually, referred to as operator-controlled SEM. An acceleration voltage of 15 kV and a sample chamber pressure of around 1×10^{-5} mbar were used. The Oxford software Aztec was used for single EDX-point and EDX-mapping to control the measurements. Each measurement was conducted with a counting time of 5 to 10 seconds for X-ray microanalysis.

References:

Zandanel, A.; Sauer, K.B; Rock, M.; Caporuscio, F.A.; Telfeyan, K.; Matteo, E.N. Impacts of Crystalline Host Rock on Repository Barrier Materials at 250 °C: Hydrothermal Co-Alteration of Wyoming Bentonite and Steel in the Presence of Grimsel Granodiorite. Minerals *2022,* 12, *1556. https://doi.org/10.3390/min12121556*

Reaction Products

B25 - bentonite

The photomicrographs of Fig 1-8 showed that the typical observed structures of initial B25 bentonite are aggregated structures with very dense surface. They are consisted of small clay platelets and divided by an irregular porous network. The diameter of the aggregates varies from 10 to 20 µm in diameter, some grains of non-clay minerals are embedded between clay aggregations. It is very often to observe some clay platelets are stuck and act as bridges crossing inter-aggregate pores. Basing the morphology and EDX-measurement, it is confirmed the dominance of smectite with impurities of non-clay minerals such as quartz, feldspar, Fe-oxides, rutile.

The observation of B25 bentonite reaction products under SEM-images shows that the typical structures of both the initial and reaction products of B25 bentonite are aggregated structures without any trace of alteration. The aggregated clays consisted of small clay platelets separated by an irregular porous network. The diameter of the clay aggregates is normally larger than 10 µm in diameter, some larger grains of impurities (e.g., quartz, feldspar, Fe-oxides,…) are embedded between the clay aggregates and formed the inter-aggregation pores. It is very common to observe some clay platelets stuck and acting as bridges across inter-aggregate pores. The development of pore systems is mainly characterized by disordered lamellar slits, wedge-shaped, and irregular forms due to properties of the lattice of randomly oriented smectite platelets. The interparticle and intraparticle pores generally distribute irregularly with structures of individual edge-face or edge-edge oriented flakes. Elongate pores in smectite show little preferential orientation (Fig. 2b), and linear intraparticle pores are situated along the (001) faces of clay minerals (smectite, kaolinite, mica). Additionally, the arrangement of intra-granular and inter-crystalline nano-pores is found in framework minerals of impurities (quartz, feldspar, Fe-oxides). An important characteristic of structures and pores in the initial and reaction products at high temperatures of 100, 125, and 150 °C in B25 bentonite is the highly dense clay matrix of compacted aggregated structures with larger size of aggregation (20 -50 µm diameter). The pore system comprised largely of inter-aggregation pores and very limit content of interparticle-pores in clay matrix, some large shrinkage channels/fractures is also observed (100 °C, 35d). Finally, it exhibited later an increase of porosity with traces of fissures or cracks between clay aggregates, and micro-cracks are detected between large crystals of impurities and clays. In contrast, at lower temperatures (35 °C and 60 °C), bentonites are less dense. The pore system is dominated by small to large interparticle pores in irregular form in porous clay matrix. The clay platelets showed a face-to-face and edge-to-face contact types. In some samples (35 °C, 0.7 MPa; 150 °C), the preferential orientation of clay aggregates and smectite particles due to mechanical compaction is clearly detected.

The morphology and chemical composition of some measured points of smectite and impurities particles in reaction products were determined by EDX-analyses. It is not clearly observed the change in composition occurred with the increasing temperature the detection of impurities as rutile, Fe-oxides, quartz, feldspar, and muscovite, kaolinite are found together with smectite.

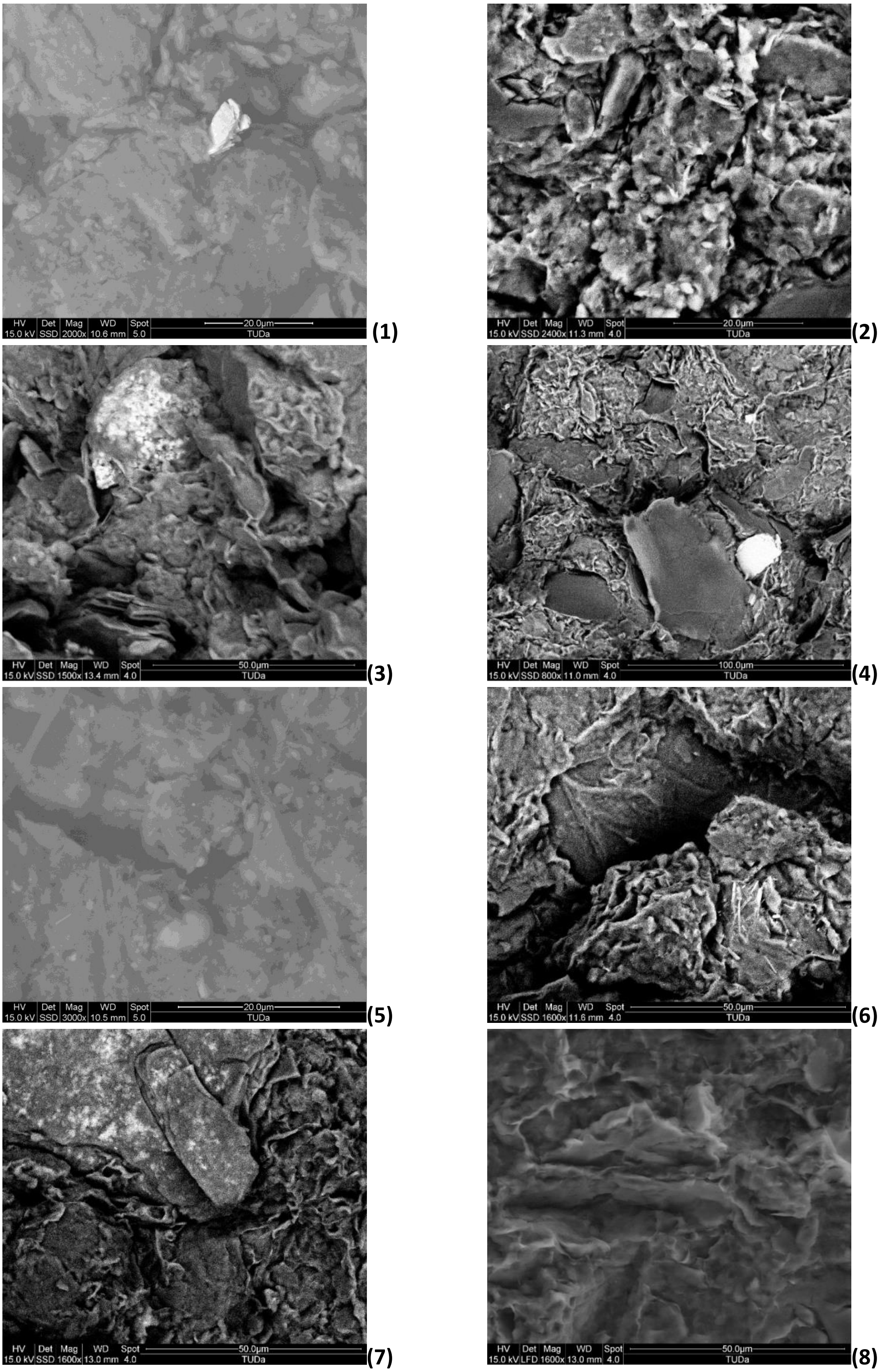

Fig 1. SEM-images of B25 bentonite: (1) compacted bentonite (N01) - magnification of 2000 x, very dense surface with aggregates of >10 – 20 µm diameter; (2) N04, 35 °C – magnification 2400 x, porpus clay matrix on the surface, aggregates of <10 µm diameter; (3) N23, 35 °C, 0.7 MPa – 1500 x magnification, porous clay matrix with large pore spaces (~5 µm) with aggregates <20 µm diameter; (4) N05, 60 °C – 800x magnification with dense surface and aggregates of ~50 µm; (5) No0 100 °C, 110h – 3000x magnification with very dense surface and aggregate

<20 µm diameter; (6) No2, 100 °C, 35d with dense clay matrix on the surface with shrinkage channels and aggreates >20 µm diameter; (7) N15, 125 °C – 1600x magnification, partially very dense but partially porous clay matrix and aggregates >20 µm diameter; (8) No3, 150 °C – 1600x magnification, porous clay matrix and narrow channels on the surface, preferential orientation of clay particles, aggregates <20 µm.

Opalinus clay

Electron micrographs of Opalinus clays (Fig 9-17) show well-developed aggregate and small clay flakes structure, and clay bridges act as connectors in compacted Opalinus clay. The size of clay aggregates is variable ~25 µm but the clay phases (smectite, illite/smectite) are very fine (1 – 2 µm) and widely distributed as clay matrix with foily textures. This structure was changed after the experiment runs to thinner platelets or aggregates mostl associated in a face to face contact /fig. 15/. The non-clay mineral grains of various sizes appear as inclusions and/or embedded in the background of fine-grained clay matrix and consequently formed abundant of inter-particles/aggregates pores. In terms of mineralogical composition, SEM-EDX indicates the presence of all minerals detected by XRD. The clay matrix consists of fine-grained illite/smectite, carbonate fossil (shells, diatoms with main composition of Ca), mica, calcite, quartz, iron-hydro iron-oxides associated with clusters of frameboidal pyrite. No recrystallizaton of smectite to non-swelling clay or conversion processes is observed.

The pore system of Opalinus clays from initial and reaction products are characterized by fractures and inter-particle/granular/crystalline pores with some traces of intraparticle pores in fossils and impurities (e.g, pryrite). They are generally distributed irregularly, the shrinkage fracture system appeared on the background of illite/smectite mixed layer matrix in the experiments of >100 °C /fig. 17, 18, 19). The shapes of interparticle pores in interstratifed illte/smectite are defined by the lattice of randomly oriented clay platelet which promoted the disorder lamellar slit and wedge-shaped pores due to the structure of edges-face or edge-edge oriented smectite flakes. The compaction of clay pellet caused small preferential orientation structure of clay which resulted a development of elongate pores in clay minerals /fig. 15, 17/. In addition, the linear pores are located in the cleavage system of larger grains as mica/kaolinite /fig. 15/. The contact between clay matrix and impurities and/or interaggregate/intercrystalline pores promoted the linear, elongated fractures and irregular pores /fig. 17, 18/. The reaction product at 150 °C – VSB shows the void space between a grain and clay matrix which may related to partial dissolution of grains as mentioned by Zandanel et al., 2022. The intra-agranular/crystalline pores are observed mainly on the surface of impurities as pyrite /fig. 16/ and muscovite /fig. 18/, especially micropores system is widely distributed in the skeleton of fossil. In addition, due to a large amount of non-clay minerals, the intragranular nanopores and intercrystalline pores are distributed widely in framework minerals such as pyrite and carbonate fossils in Opalinus clays.

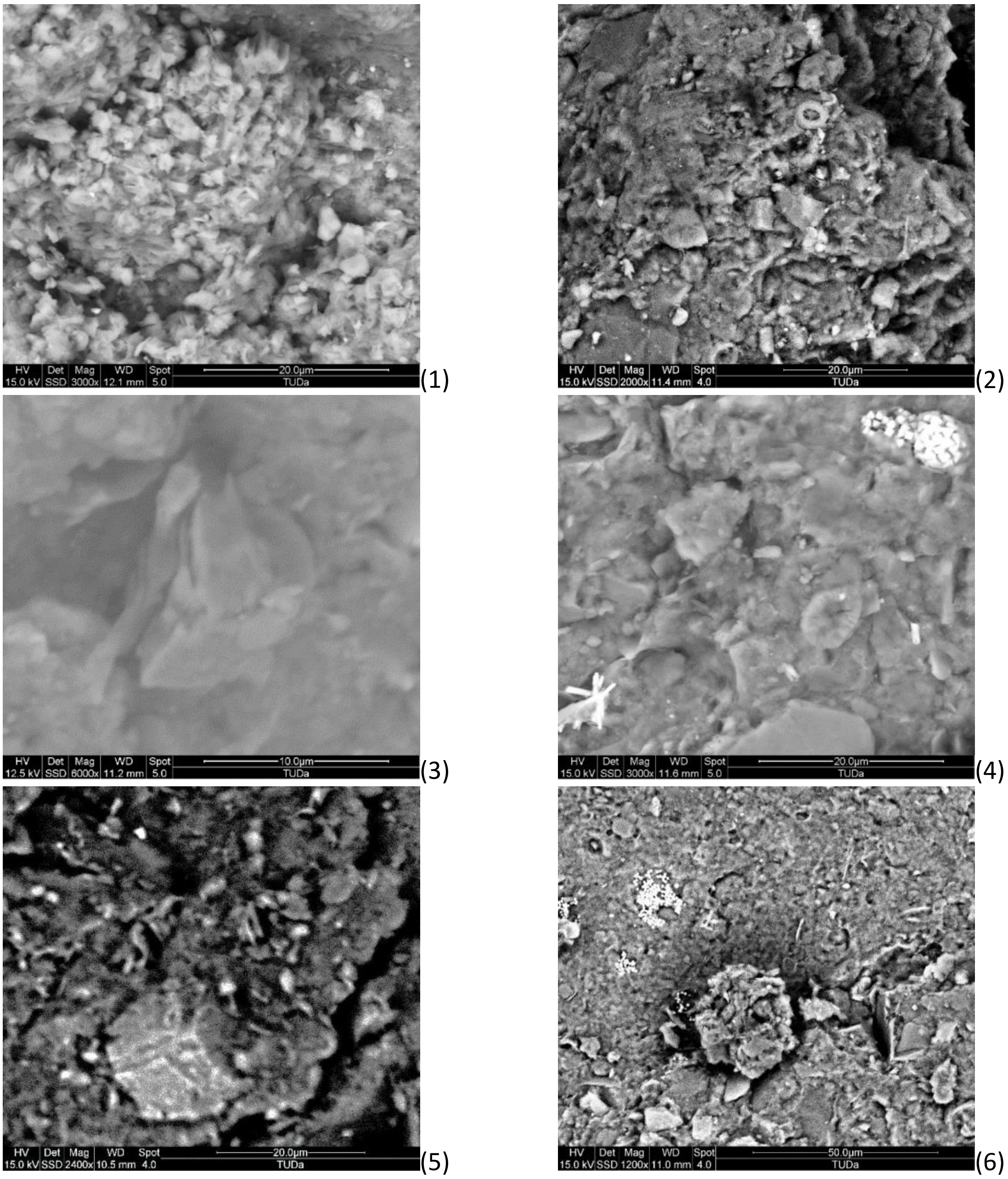

Fig 2. SEM-images of Opalinus clay: (1) compacted Opalinus (N06) - magnification of 3000 x, surface is normally dense but partially porous matrix with aggregates of <25 µm diameter and single particle structure <2 µm; (2) Opalinus at 35 °C (N22) magnification of 2000 x, surface is normally dense but partially porous matrix with aggregates of <25 µm diameter and single particle structure <2 µm; (3) Opalinus at 60 °C (N09), magnification 6000x, dense matrix surface with aggregates of >25 µm diameter and particle structure <2 µm; (4) Opalinus at 100 °C, magnification 3000x, mostly dense matrix surface, aggregates of >25 µm diameter and particle structure <2 µm including fossils, pyrite; (5) Opalinus at 125 °C, magnification 2500x, normally dense but partially porous matrix surface with aggregates of < 25 µm and particle structure <2 µm; Opalinus at 150 °C, magnification 1200x, mostly dense matrix surface, aggregates of >25 µm diameter and particle structure <2 µm including fossils, pyrite.

Friedland clay

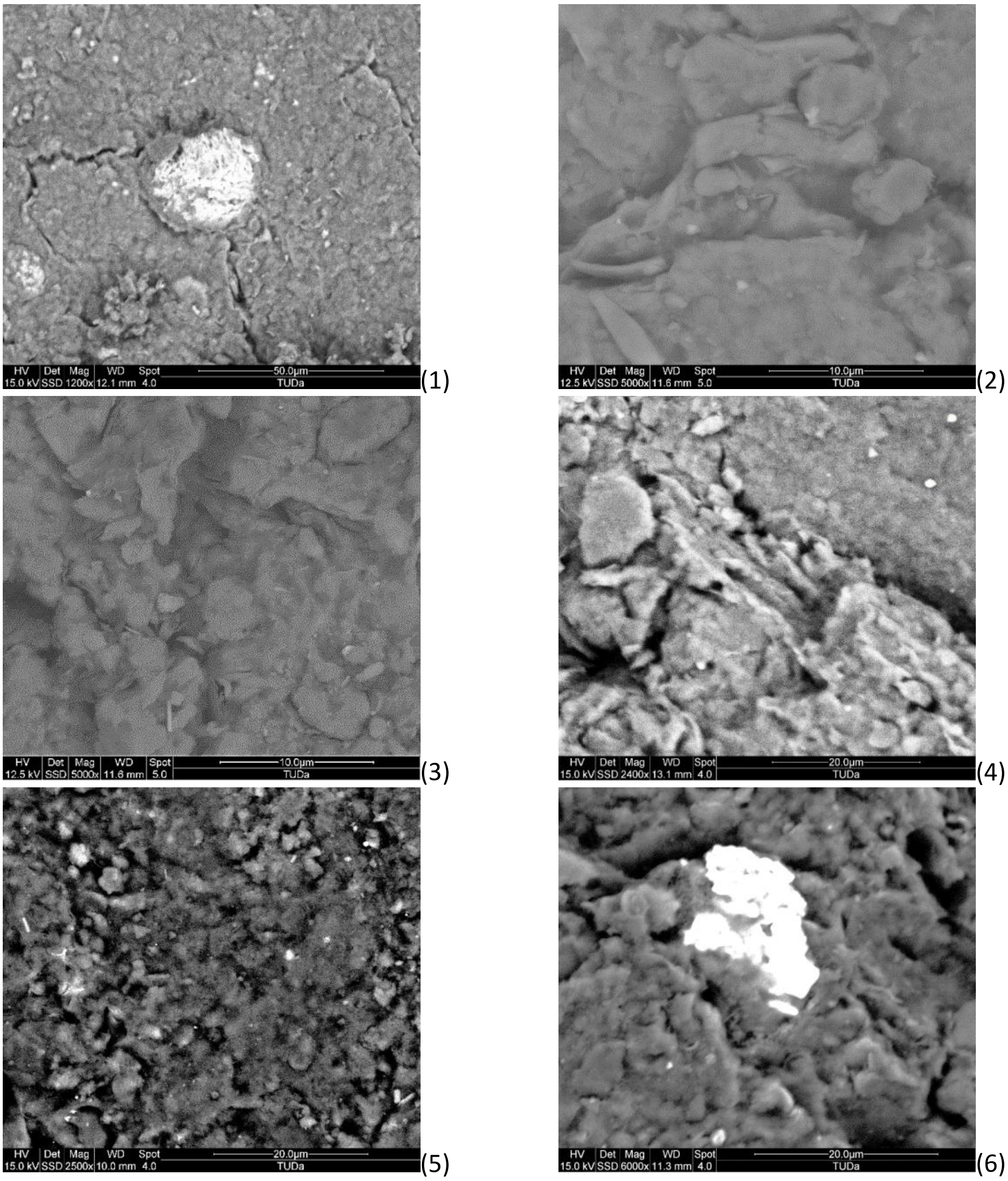

Fig 3. SEM-images of Friedland clay: (1) compacted Friedland (N19) - magnification of 1200x, very dense matrix surface with aggregate >25 mm; Friedland clay at 35 °C (N10), magnification 5000x, dense matrix surface with aggregrate >25 µm diameter and particle structure <5 µm; Friedland clay at 60 °C (N11), magnification 5000x, dense matrix surface with aggregrates >25 µm diameter and particle structure <5 µm; Friedland clay at 100 °C (N16), magnification 800x, mostly dense matrix surface with aggregrates >25 µm diameter and particle structure <5 µm; Friedland clay at 125 °C (N20), magnification 2500x, normally dense but partiall porous matrix surface with aggregrates >25 µm diameter and particle structure <5 µm; Friedland clay at 150 °C (N21), magnification 5000x, normally dense but partiall porous matrix surface with aggregrates >25 µm diameter and particle structure <5 µm.

Under SEM-images observation, the Friedland clays before and after THMC-experiment runs /Tab. 18-22/ are characterized by aggregated structures with a dense clay matrix. The impact of compaction is clearly defined as preferred orientation of small clay platelets (<5 µm) (35 °C, 100 °C). The small clay platelets are associated and formed an large aggregation (>25 µm). No evidence of clay transformation or newly phases are found in Friedland clays after the THMC-experiment runs.

Due to the dominant of illite/smectite mixed layer which is characterized by disorder structure, the pore systems are in lamellar slit and wedge-shaped form. The association of pores and minerals are greatly observed, its combination is designed by micropores between clay minerals and/or interparticle pores between clay minerals and impurities but the most abundant is the development of interparticle pores of illite-smectite mixed layer. The pore widths are concentrated in 2 nm to 10 µm. The shape of pores are mostly controlled by crystal shapes of lamillar of illite-smectite mixed layer and contact between them. The interaggregate pores fractures (shrinkage and contact surface between aggregates-aggregate and clay matrix-aggregate/impurities) are mostly linear and irregular form but voids and interparticle/granular/crystalline are varies from linear to angular, spherical to irregularly polygon. The intraparticles pores in Friedland clay is not clearly observed in clay minerals but non-clay minerals phases (e.g pyrite, Fe-oxides) /fig. 22/. Fracture types are mainly developed illite/smectite mixed layer shrinkage and fractures between clay-clay aggregate, clay-impurities aggregate (clay and pyrite framboid, clay platelets, and interlayer microfractures with size of fractures vary from 3 – 12 µm. In general, the surface matrix of the Friedland clays at lower temperatures (initial material, 35 °C, 60 °C) are very dense but at the higher temperatures of >100 °C they are mostl dense matrix but partially porous matrix due to the interparticle pores.

Data Sheet – B25 bentonite, untreated compacted materials

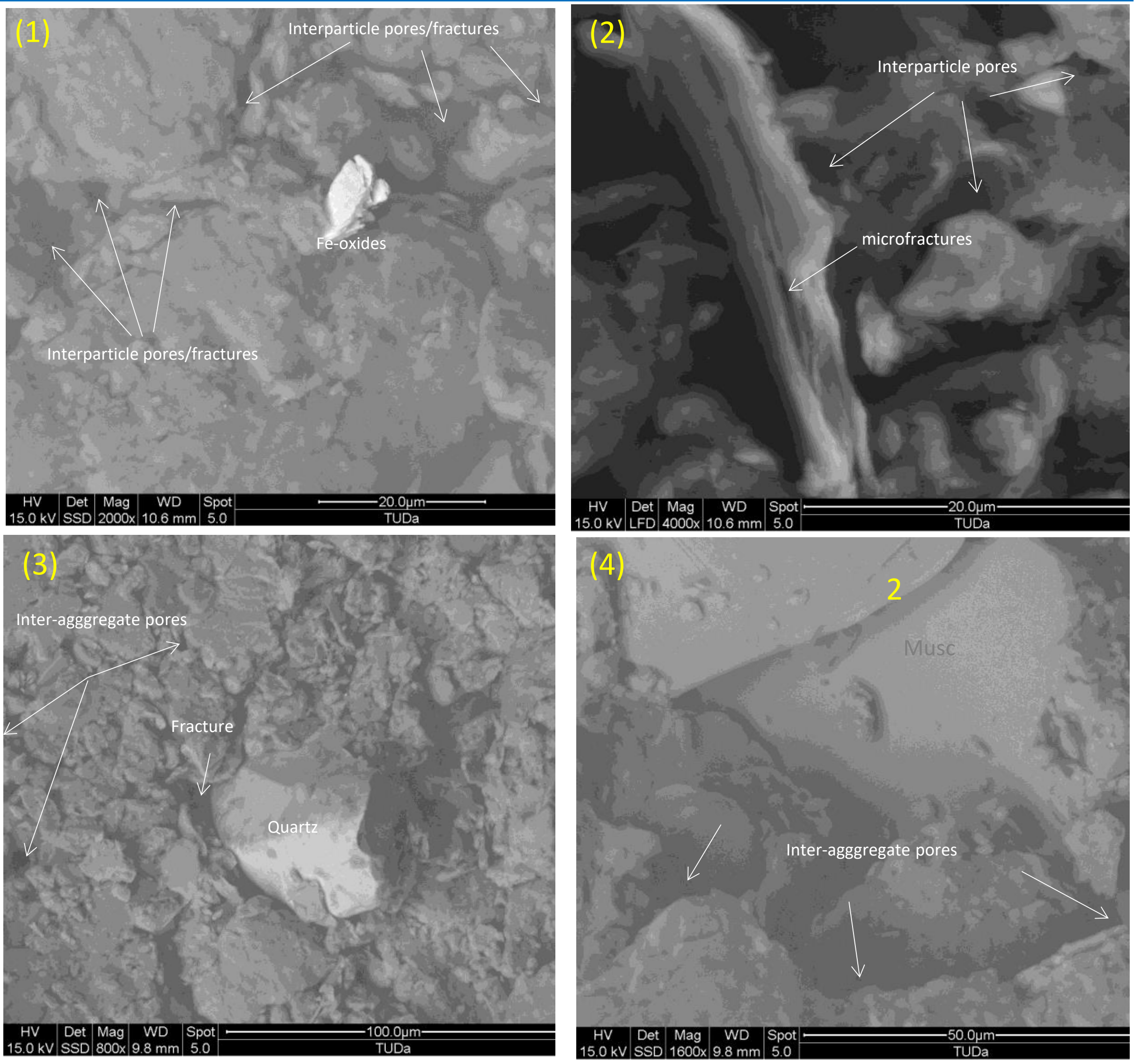

Fig. 4. SEM-images of initial compacted B25-bentonite

(1) Compacted clay with a lot of shrinkage fractures and interparticles pores/fracture on the background of clay

(2) Lossely compacted clay with large portion of smectite cause abundant of interpartice pores/caves, it probably caused by volume decrease when dehydrated from injection of OPA solution (saturated condition) and a large thin and platy mica particles with a system of linear microfractures between laminar sheets. The flocculation structure showed the edge to face and face to face contact style.

(3) Aggregated structure of clay, the large grain of quartz is embbeded in clay matrix and caused a system of fractures between clay matrix and quartz grain. The inter-aggregation pores developed largely in clay background.

(4) Laminar structure of smectite aggregation associated with large, thin muscovite (Musc.) form a system of linear and angular forms of inter-aggregate pores/fractures

Data Sheet – B25 bentonite, treated materials *(OPA, 35 °C, 93.6h)*

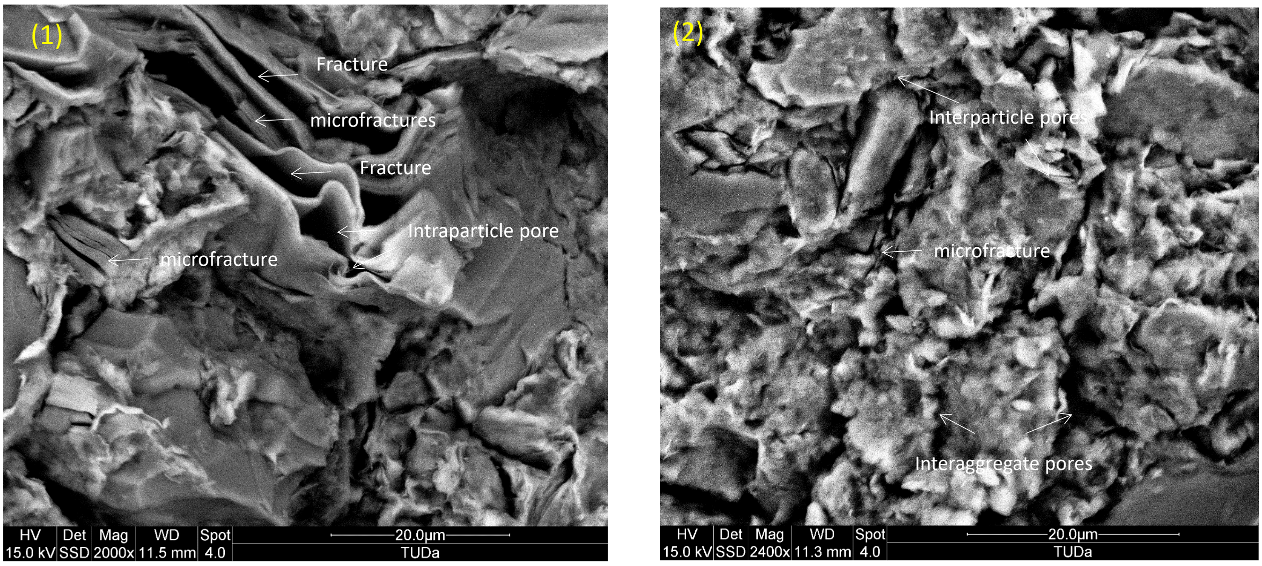

Fig. 5. SEM-images of B25 bentonite, treated materials (OPA, 25 °C, 93.6h)

(1) A system of linear microfractures and angular fractures developed in curly edges of hexagonal form of muscovite, kaolinite platelets. The triangular intraparticle pore and interparticles pores spreaded widely in the rock

(2) Edge-to-face and face-to-face contact of aggregation of smectite/smectite and smectite/impurities promoted the development of interaggregation pores and linear fractures between them

Data Sheet – B25 bentonite, treated materials *(35 °C, 0.7Ma, 290h-VSD)*

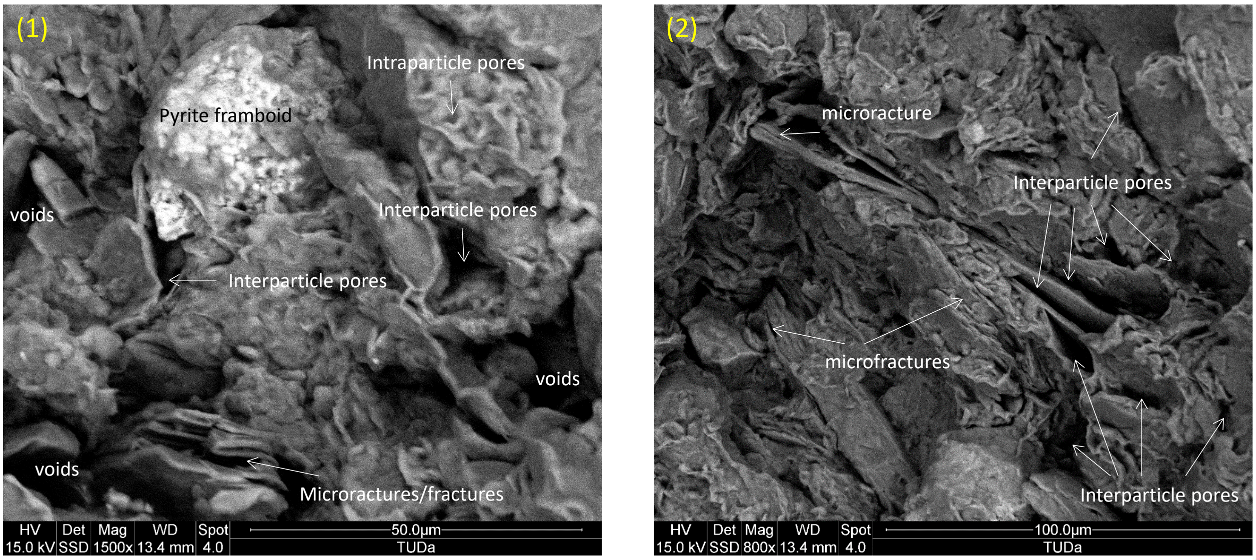

Fig. 6. SEM-images of B25 bentonite, treated material (35 °C, 0.7Ma, 290h-VSD)

(1) The disordered lamellar properties of illite-smectite mixed layer resulted the curly edged flakes morphology and wedge-shaped intra- and interparticle pores (<1 µm). The contact between clay aggregation caused larger interparticle pores /voids (5-8 µm in diameter). The linear microfractures are observed between the platelets of clay minerals.

(2) The angular and wedge-shaped interparticle pores distributed widely, the microfractures developed along the sheet of clay minerals.

Data Sheet – B25 bentonite, treated materials *(OPA, 60 °C, 454h)*

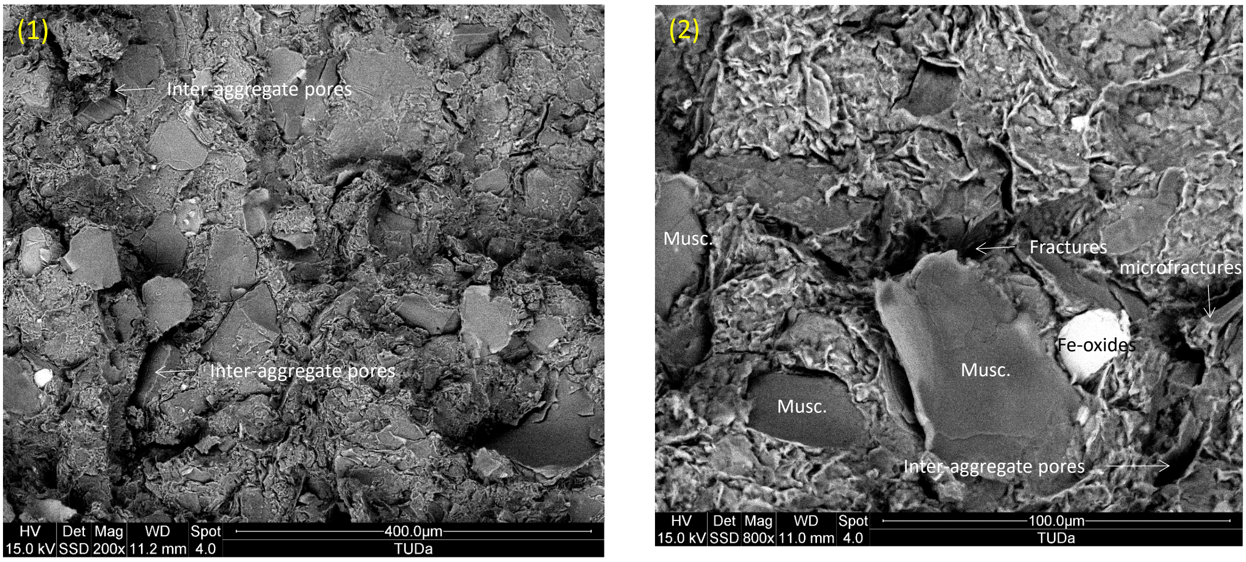

Fig. 7. SEM-images of B25 bentonite, treated materials (OPA, 60 °C, 454h)

(1) Highly compacted clay matrix associated with preferred orientation of lot of platy, thiny but large particles caused a development of inter-aggregate pores

(2) Preferred orientation of clay matrix and large particles of muscovite caused a development of linear fractures around the muscovite, the inter-aggregation pores between clay matrix is observed together with microfractures developed in muscovite platelets.

Data Sheet – B25 bentonite, treated materials *(OPA, 100 °C, 35d)*

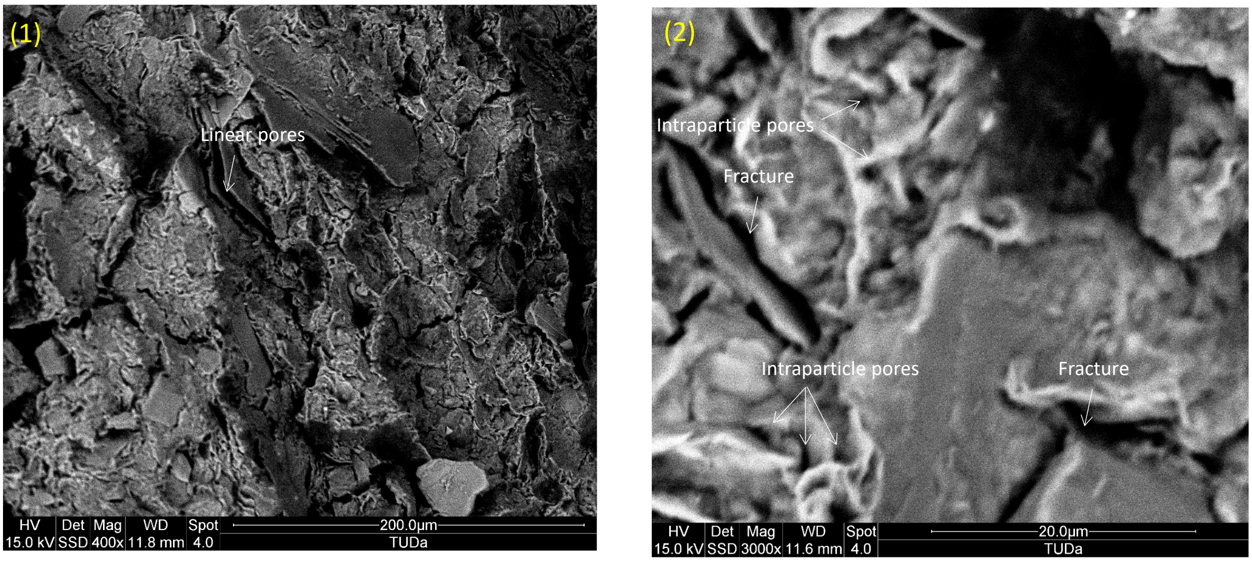

Fig. 8. SEM-images of B25 bentonite, treated material (OPA, 100°C, 35d)

(1) Overview of highly compacted clay matrix associated with impurities and a development of shinkrage fractures as well as linear pores/fracture between mica/kaolinite platelets

(2) Development of linear, angular fractures/pores/caves between clay aggregation and clay platelets

Data Sheet – B25 bentonite, treated materials (OPA, 100 °C, 110h)

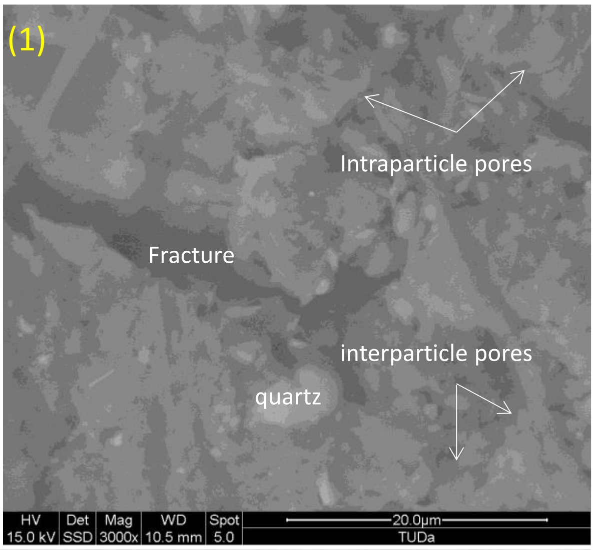

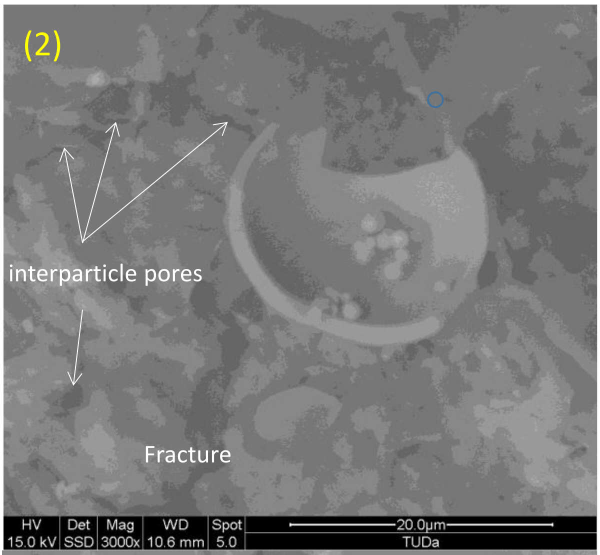

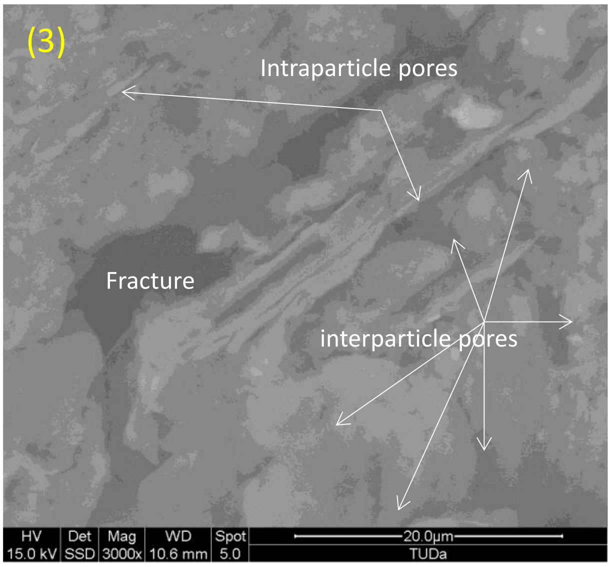

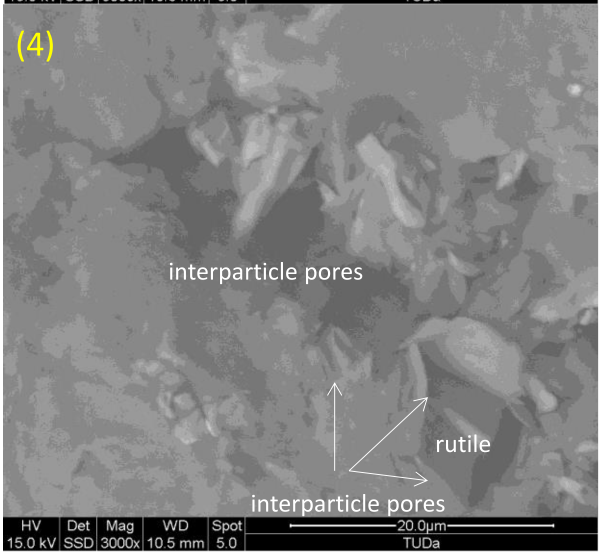

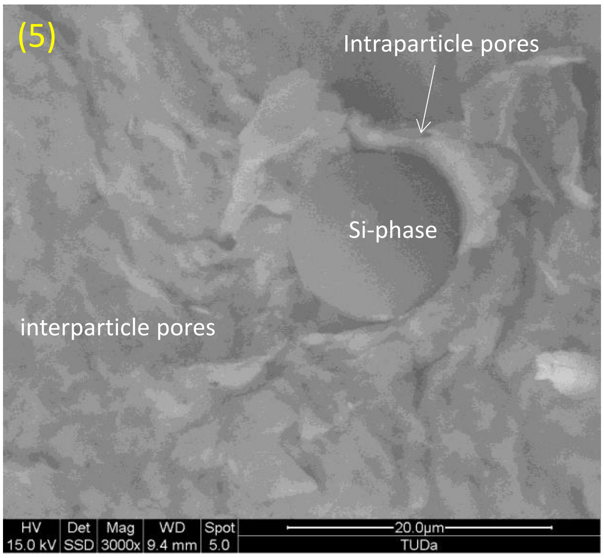

Fig. 9. SEM-images of B25 benonite + OPA + 100 °C + 110h

(1) Development of shrinkage fracture (2-5 µm) and intraparticle pores in aggregation of clay matrix, some small smectite particle flocculated onto the edge of large particles and formed a system of micro interparticle pores.

(2) Fractures and interparticle pores in clay matrix, a presence of Si-shell with granulars of Ca-zeolite.

(3) System of shrinkage fractures/caves in the background of laminar structure of clay with association of thin large clay platelets (muscovite), the interparticles pores between smectite/muscovite, smectite/smectite and linear microfractures developed along the clay sheet. The face-to-face contact style is mostly observed

(4) Laminar aggregation of clay associated with tiny flocculated particles on the edges or surface of large particles and/or aggregation, the interparticle pores developed betweet clay particles/aggregation and clay/impurities . Some curly edge smetite particles are found around the impurites (rutile).

(5) Laminar structure of thin smectite platelets developed round the conical form of Si-phase, the interparticles pores and intraparticles pores between smectite platelets are observed, the intraparticle pores on the edge of clay platelets is typical of nanopore in the rock

Data Sheet – B25 bentonite, treated materials *(OPA, 125 °C, VSD)*

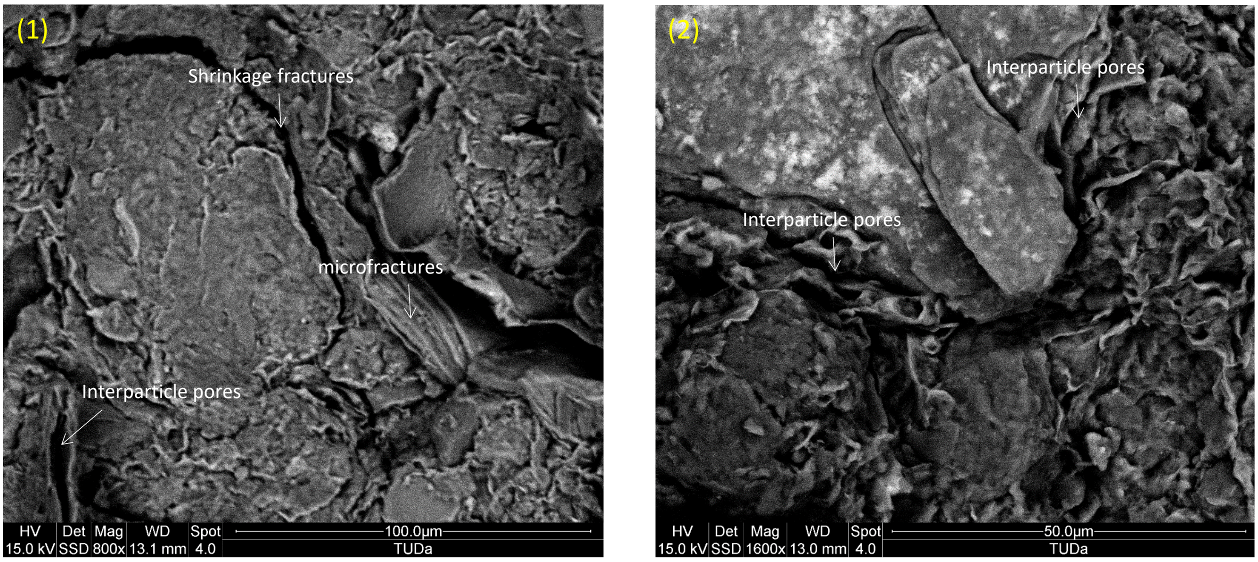

Fig. 10. SEM-images of B25 bentonite, treated materials (OPA, 125 °C, VSD)

(1) The linear shrinkage fractures (5 – 10 µm) developed widely together with interparticle pores (>5 µm) and microfractures developed along the cleavage-sheet of clay minerals. The contact of clay particles are mainly face-to-face contact style.

(2) The linear fractures system grew on the contact point of impurities and clay aggregate but the interparticle pores are mainly angular form, distributed irregularly in mixed layer illite-smectite. They display structures of edge-face and face-face contact.

Data Sheet – B25 bentonite, treated materials *(OPA, 150°C, 4d)*

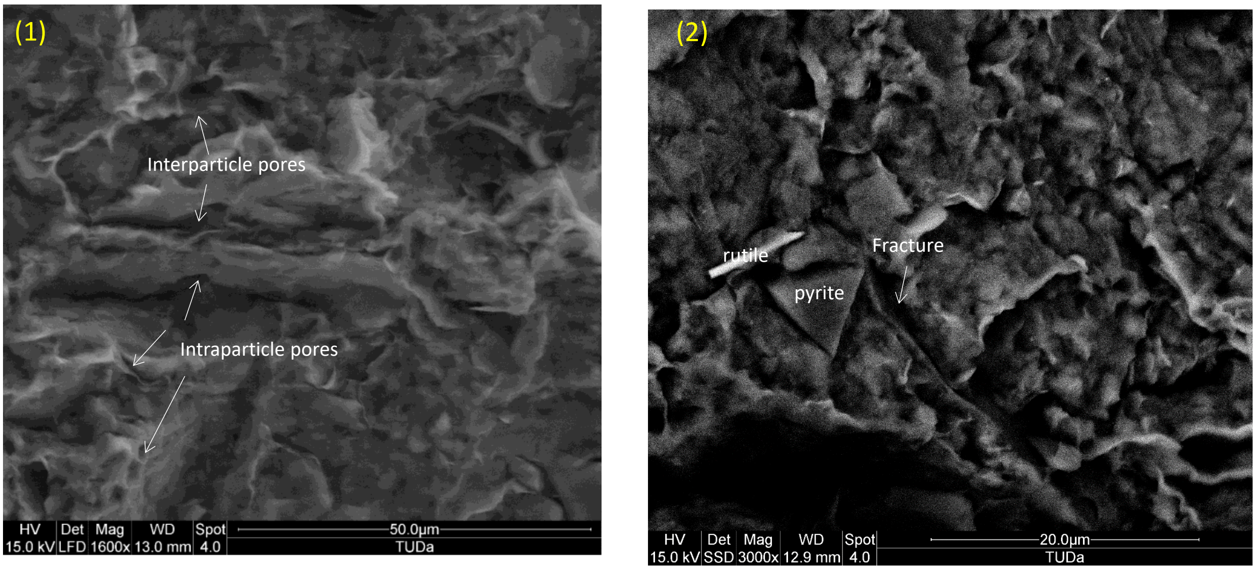

Fig. 11. SEM-images of B25 bentonite, treated materials (OPA, 150 °C, 4d)

(1) Laminar structures with larger, thinner smectite platelets mostly associated in a face to face contact style. The interparticle pores are mostly in linear or angular form. The curly edges of smectite platelet cause a system of intraparticle pores in honeycomb form.

(2) Dominant of platty laminar structure of curly edged smectite particles with a system of interparticle pores in linear and angular form, the interparticles pores between impurities (pyrite, rutile) and smectite are mainly in linear form.

Data Sheet – Opalinus, untreated compacted materials

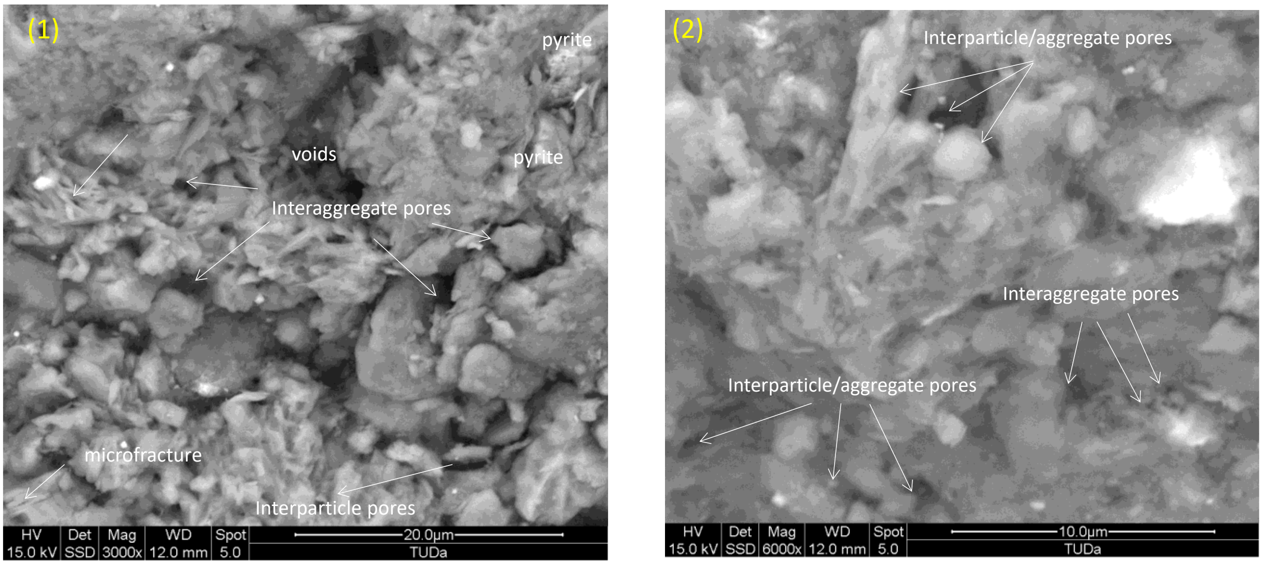

Fig. 12. SEM-images of untreated compacted Opalinus clay

Aggregation of platy illite-smectite mixed layer, interparticles and inter-aggregation pores and voids are observed with different angular form. The microfractures between sheet of illite-smectite mixed layer flakes and/or between aggregation are distributed widely due to the face-to-face and edge-to-face contact.

Data Sheet – Opalinus, treated materials *(OPA, 35°C, without transport cell)*

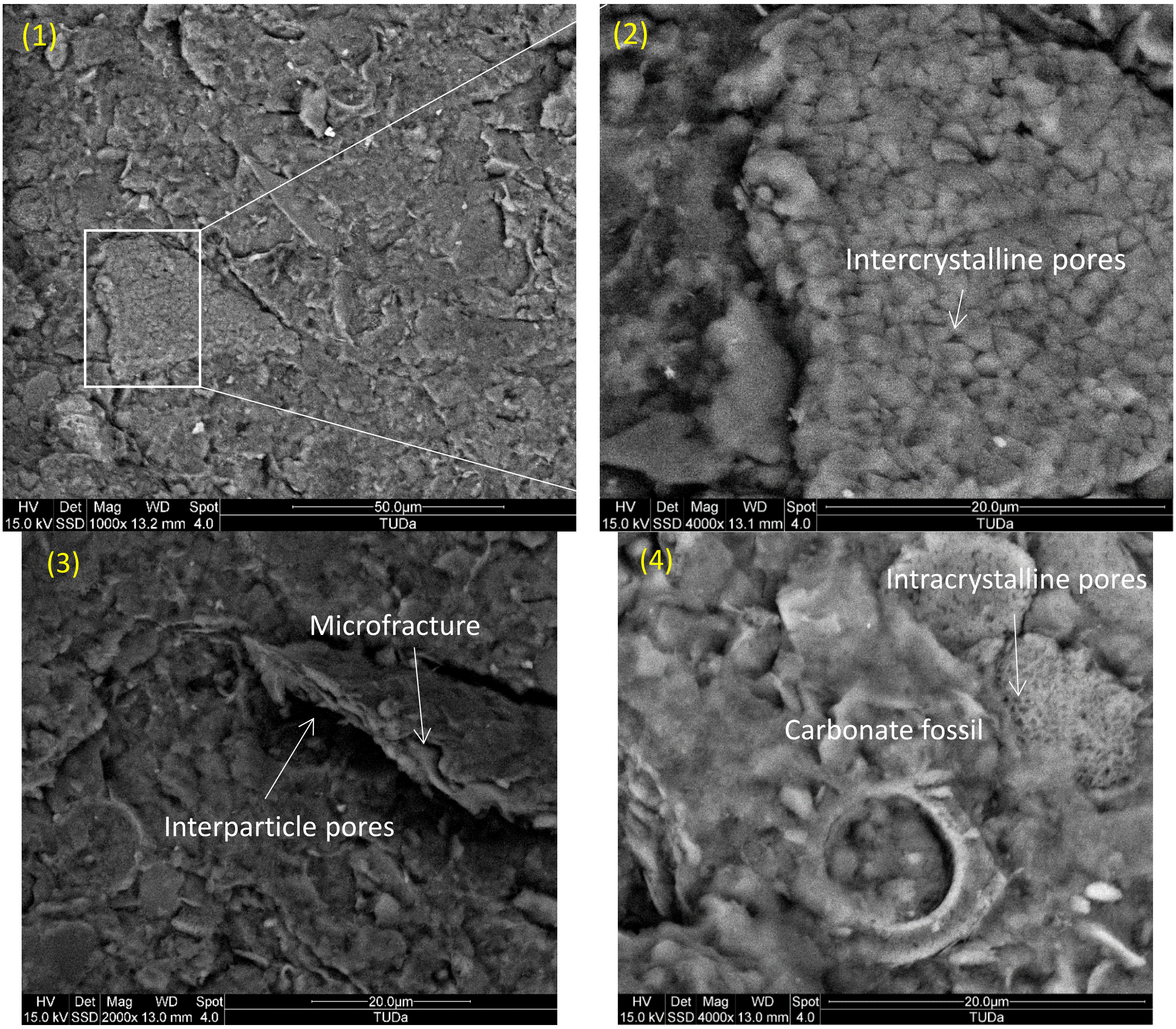

Fig. 13. SEM-images of Opalinus clay, treated materials (OPA, 35°C, without transport cell)

Beside the fratures/pores which develope along the contact faces of impurites and clay, the presence of fossil and pyrite shows different form of intra-crystalline/granular pores. The appearance of some large, thin clay particles showed a system of linear microfractures between sheet of them.

Data Sheet – Opalinus, treated materials *(OPA, 35°C, VSE)*

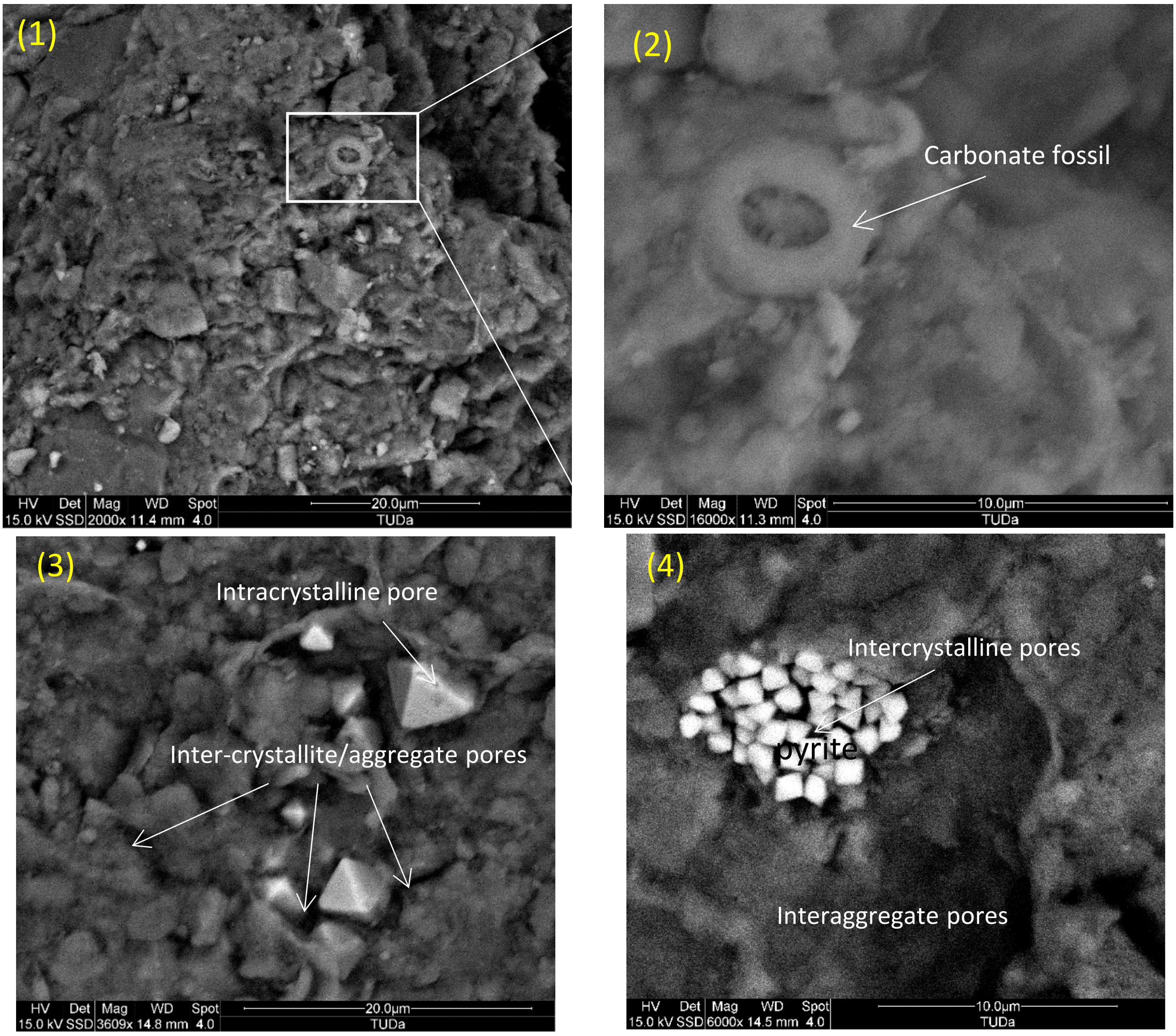

Fig. 14. SEM-images of Opalinus clay, treated materials (OPA, 35 °C, VSE)

The presence of impurities (fossils and pyrite) in illite-smectite mixed layer matrix caused a system of pores between them as well as inter-aggregation/interparticle pores. The intracrystalline pores is observed on the crystal face of pyrite as well as inter-crystalline pores between pyrite granular.

Data Sheet – Opalinus, treated materials *(OPA, 60°C, VSB)*

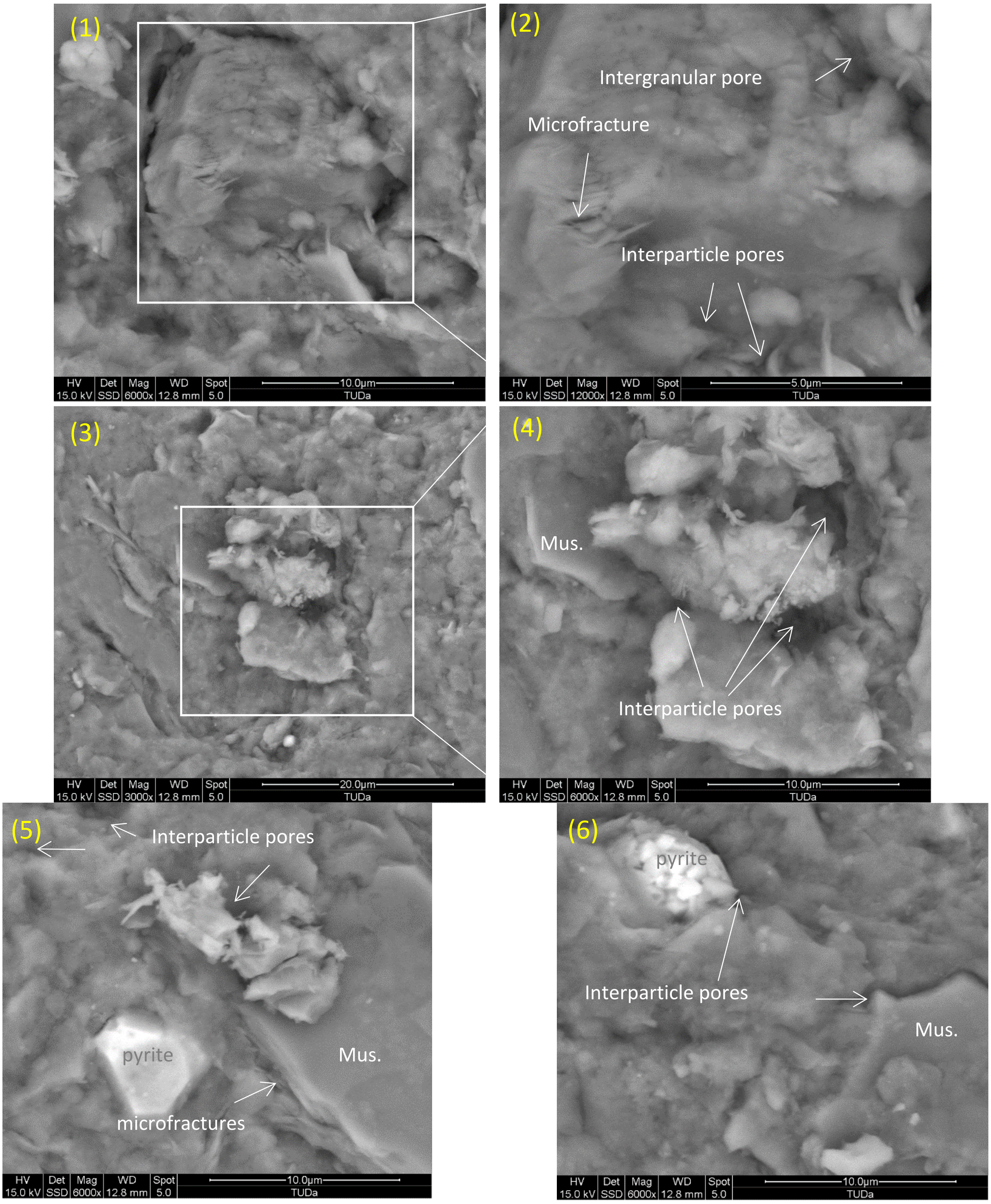

Fig. 15. SEM-images of Opalinus clay, treated materials (OPA, 60 °C, VSB)

The association of impurities (pyrite, muscovite) and dense to partially porous clay matrix aggregates caused a linear fractures and intergranular pores. The interparticle pores and intraparticles pores apparently appeared between clay-clay particles and along the 001-faces of clay minerals.

Data Sheet – Opalinus, treated materials *(OPA, 60°C, VSE)*

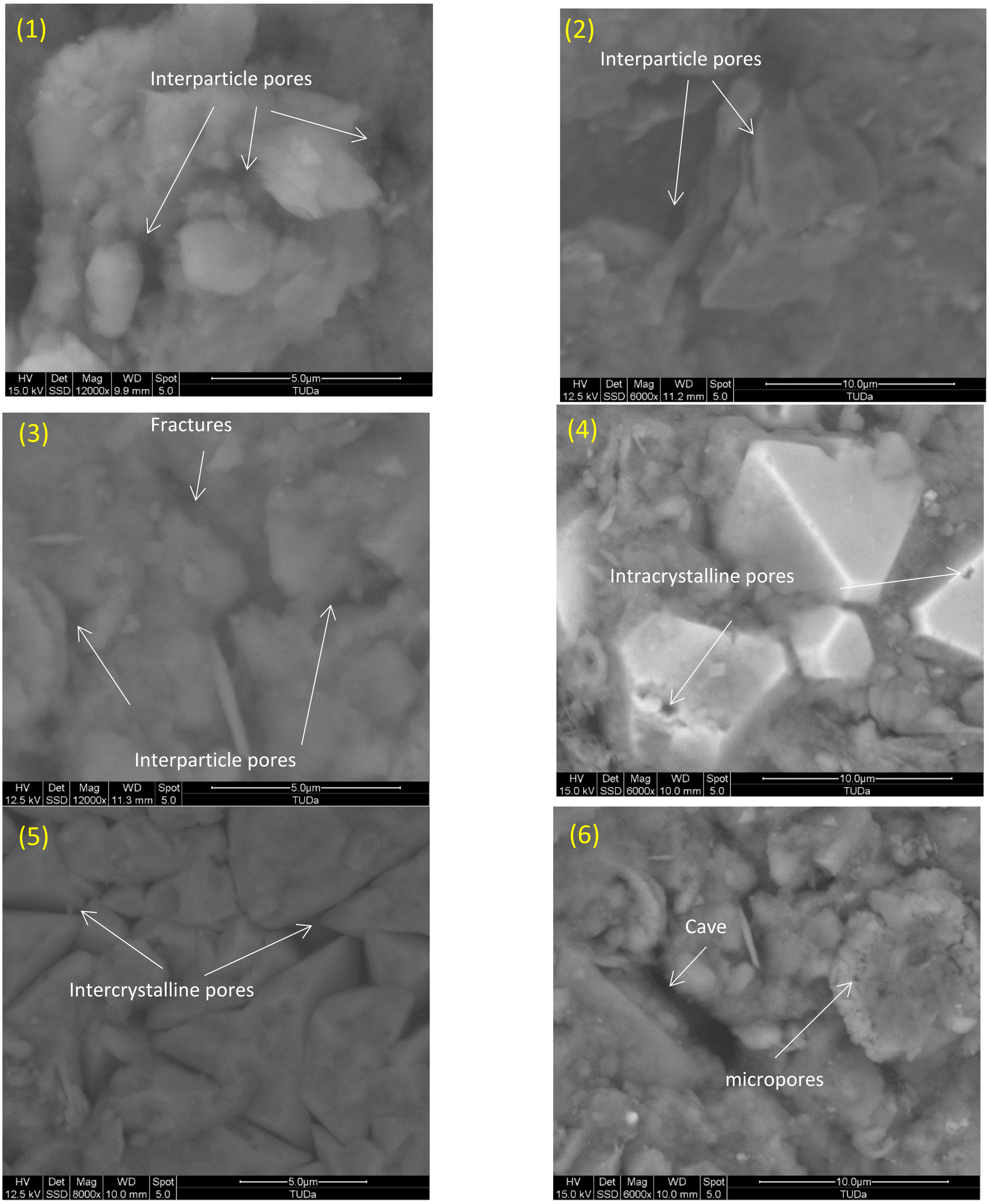

Fig. 16. SEM-images of Opalinus clay, treated materials (OPA, 60 °C, VSE)

The partially porous clay matrix from aggregated structure with fakes and platy particles of illite-smectite mixed layer and impurities (pyrite, carbonate fossils) are distributed widely in the rock. The interparticles pores of illite-smectite mixed layer show variable forms of linear, angurlar but intercrystallite (pyrite) are mainly linear. The intraparticle pores (micropores) are mainly observed on the surface of pyrite grains and carbonate fossils.

Data Sheet – Opalinus, treated materials *(OPA, 100°C, VSD)*

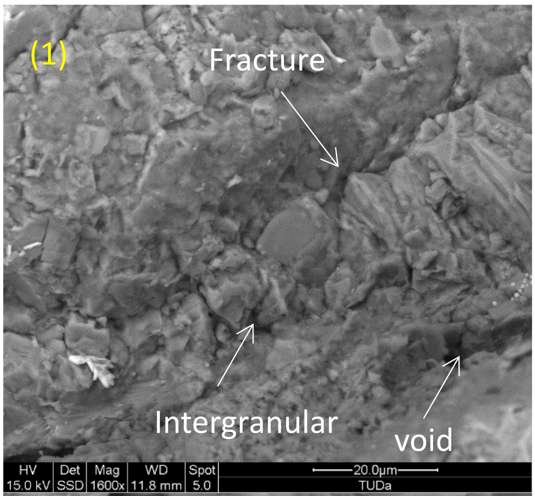

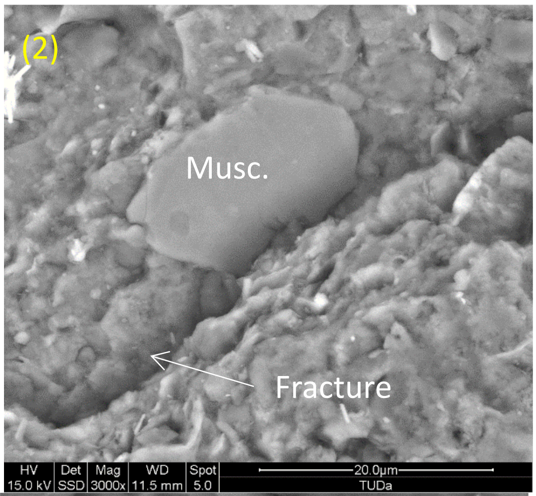

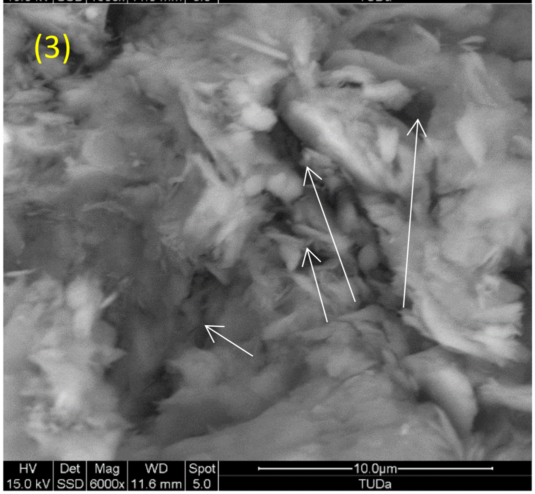

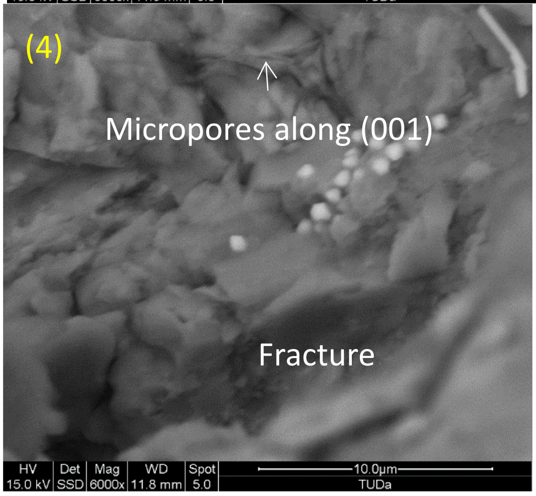

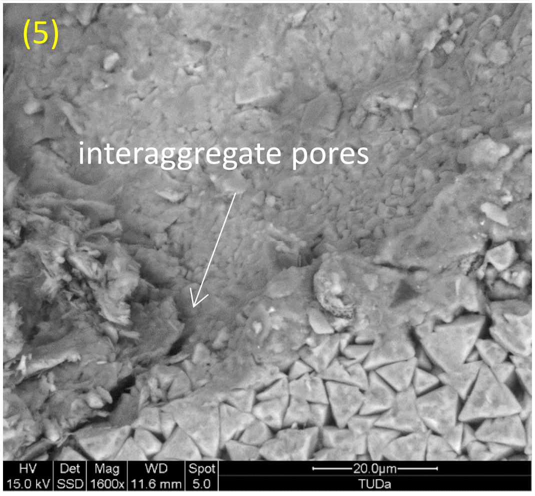

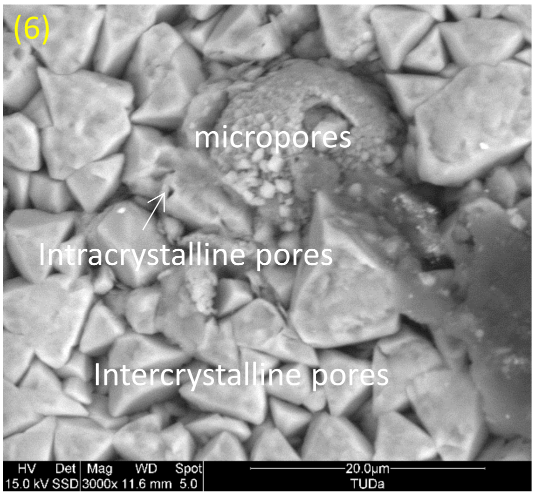

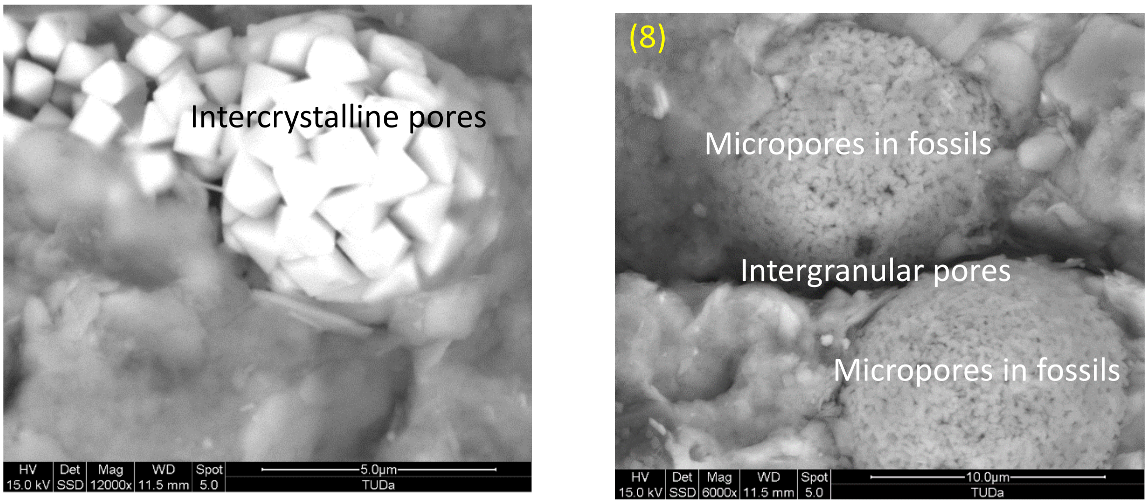

Fig. 17. SEM-images of Opalinus clay, treated materials (OPA, 100 ^C, VSD)

Linear shrinkage fractures between aggregates and/or between fossils/granulars. The interparticles pores developed widely between illte/smectite mixed layer particles (edge-to-face, edge-to-edge contacts) but some micropores are observed along the (001) crystal faces of illite/smectite mixed layer (face-to-face contact). The micropores and intracrystall pores are distributed widely on fossils and pyrite grains.

Data Sheet – Opalinus, treated materials *(OPA, 125°C, VSE)*

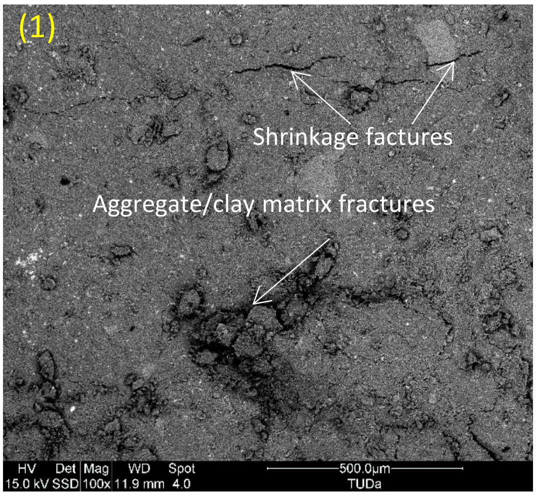

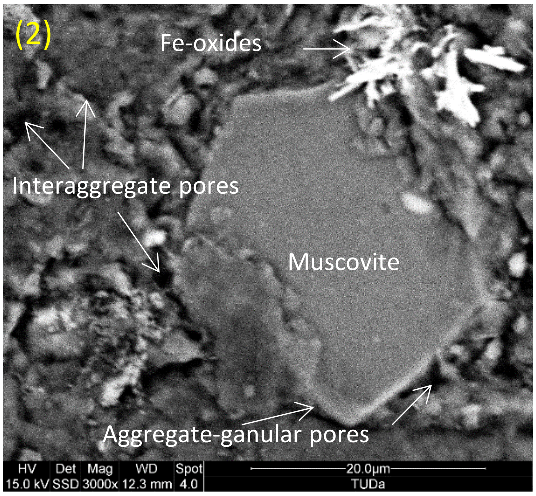

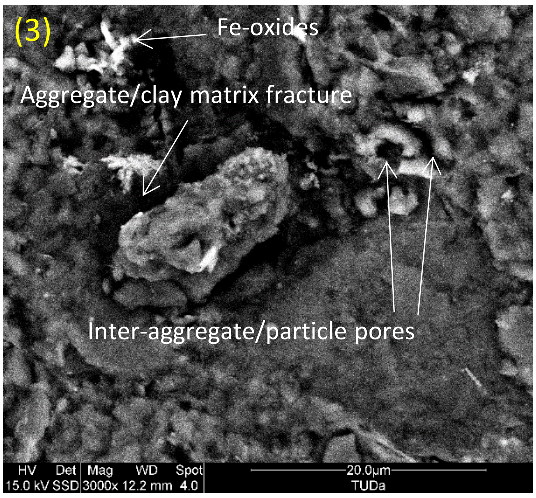

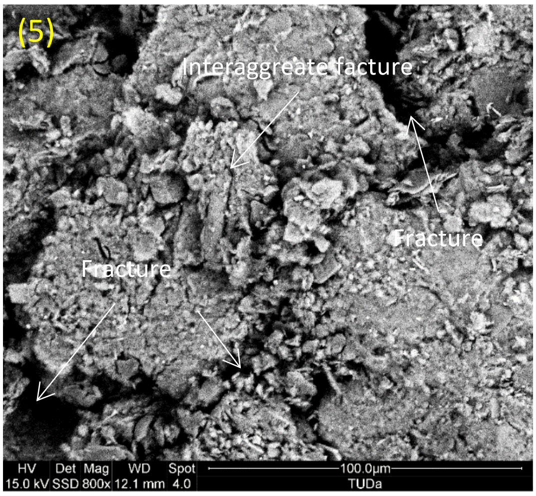

Fig. 18. SEM-images of Opalinus clay, treated materials (OPA, 125 °C, VSE)

Linear shrinkage factures fractures between clay aggregates and cla matrix. The presence of impurities caused the aggregates of clay and impurities fractures, pores in linear and linear, angular form

Data Sheet – Opalinus, treated materials *(OPA, 125°C, VSC)*

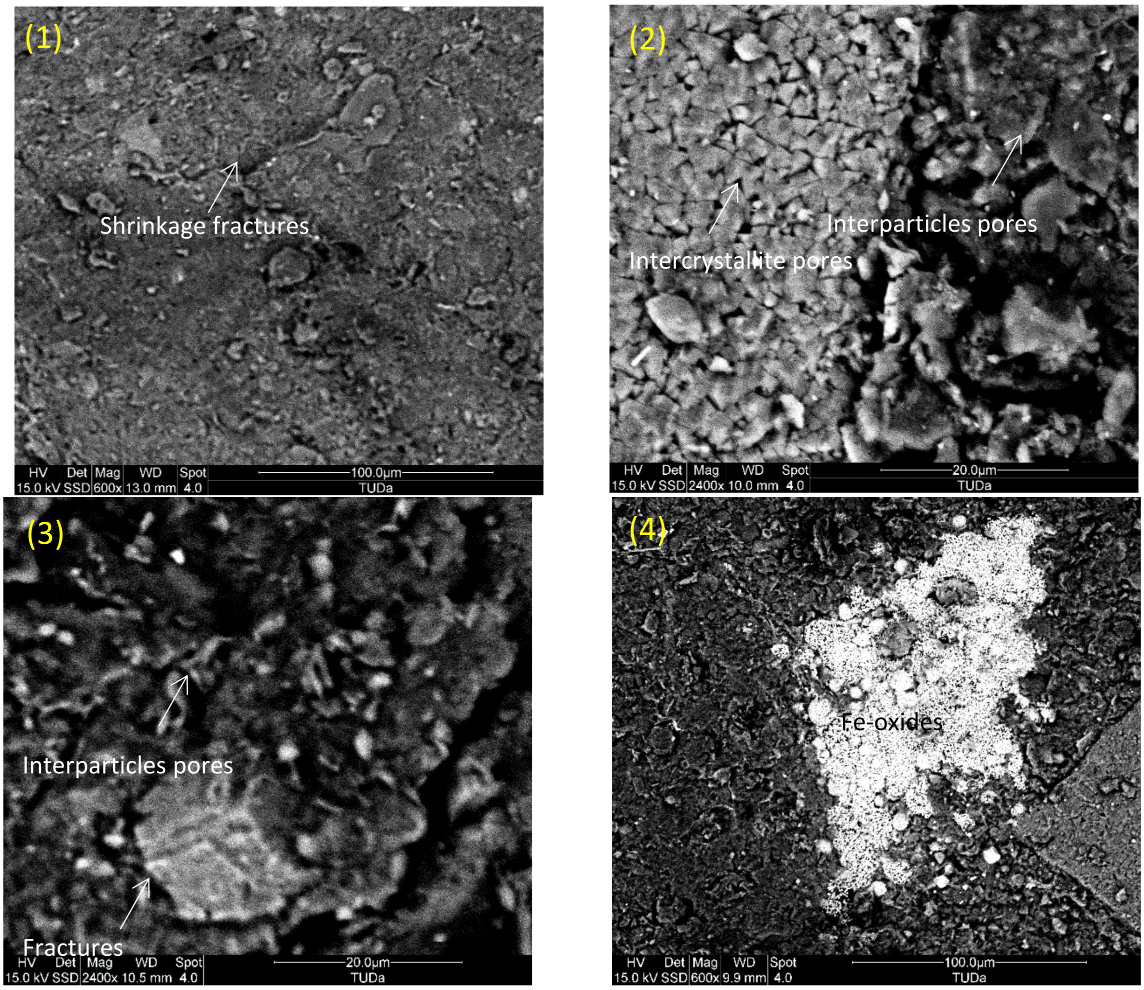

Fig. 19. SEM-images of Opalinus clay, treated materials (OPA, 125°C, VSC)

The surface of clay pellet is normally dense but partially porous matrix. The aggregrates are mostly observed with the diameter <25 µm. Linear fractures system developed around the large aggregrates and impurities as well as aggregates/clay matrix, the intercrystallite pores are well developed between pyrite crystals, the intracrystallite micropores could observed also on the surface of pyrite crystals. The interparticles pores between clay flakes are in irregular form with mostly face-to-edge contact styles

Data Sheet – Opalinus, treated materials *(OPA, 150 °C, VSB)*

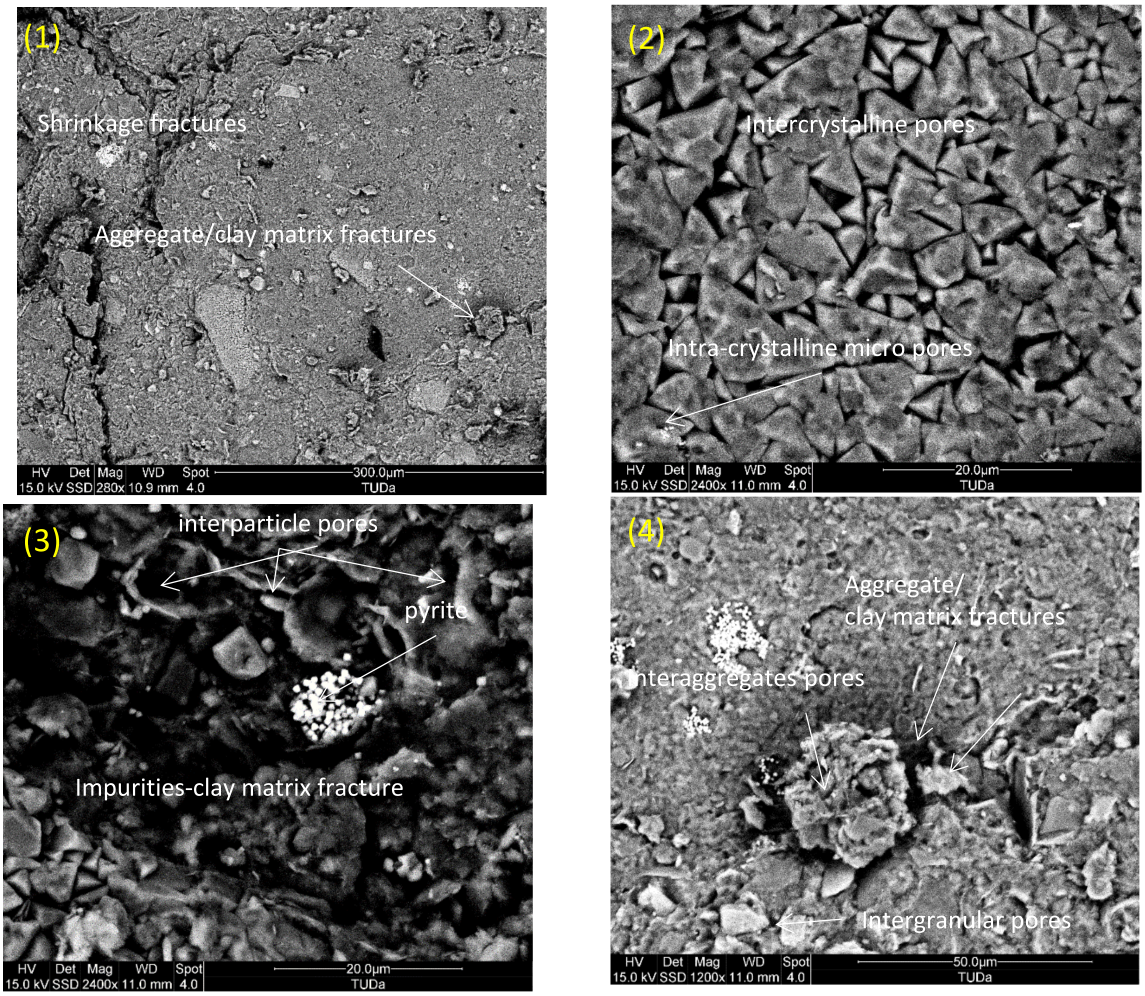

Fig. 20. SEM-images of Opalinus clay, treated materials (OPA, 150 °C, VSB)

Linear shrinkage fractures system developed on the surface of clay pellet together with aggregate/clay matrix fractures, the interparticles pores between flake form of illite-smectite mixed layer and two kind of pyrite are observed which promoted the factures as border between clay matrix and impurities (pyrite). The intercrystalline pores appeared between pyrite crystals and the intra-crystalline micropores are found on the surface of pyrite crystals, too. The aggregates of clay and non-clay granular were embbed on the clay matrix and formed the irregular form of pores and fractures

Data Sheet – Friedland clay, untreated compacted materials

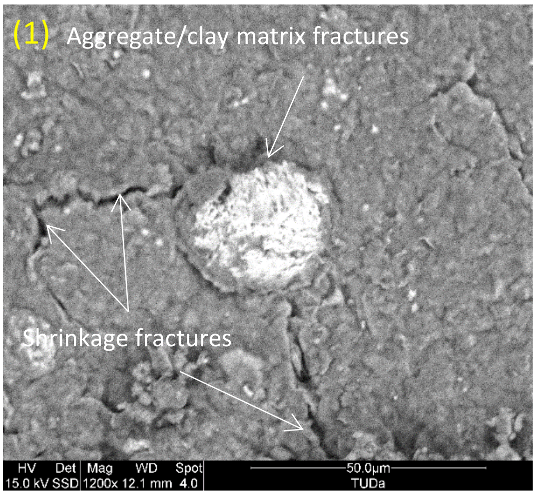

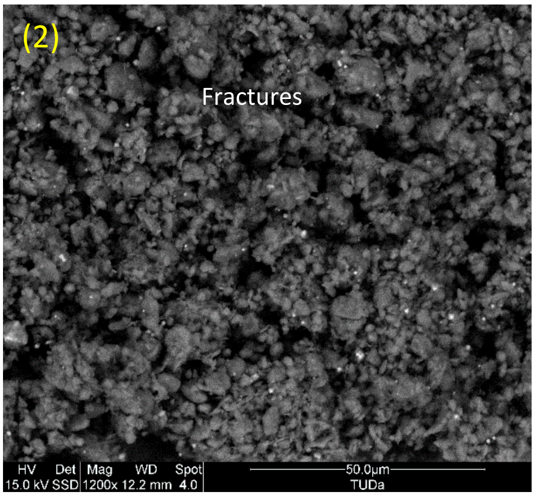

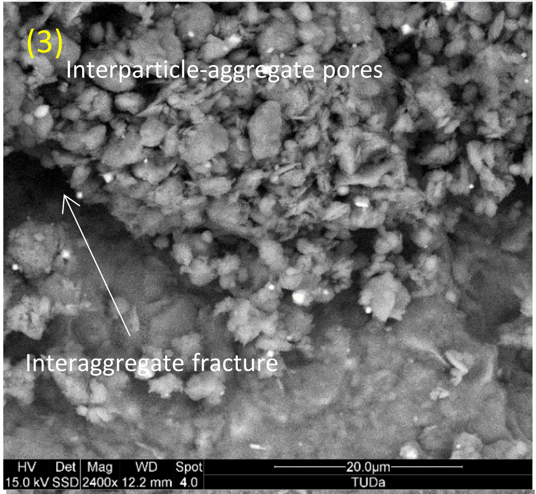

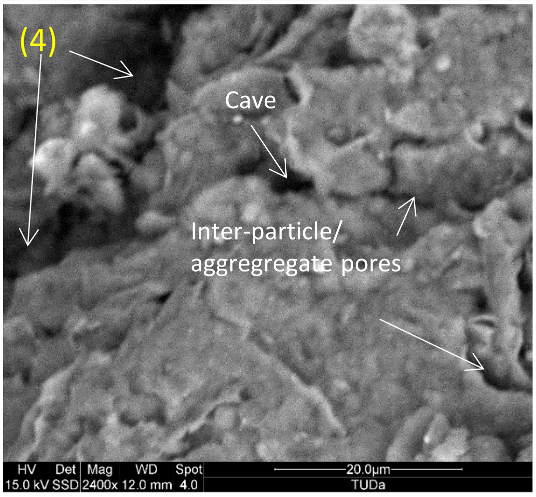

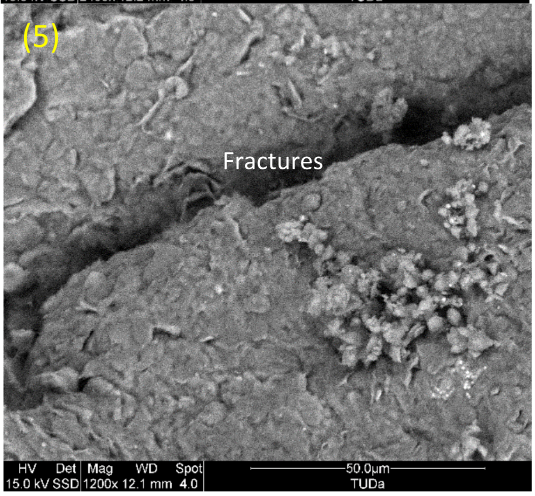

Fig. 21. SEM-images of untread compacated Friedland clay

Large aggregate contains platy illite –smectite mixed layer partiles. The large syste of pores and voids appeared between aggregate of clays but micro interparticle pores are typical observed between illite-smectite platelets. The edge-to-face and face-to-face contact styles are found mainly in the contact between clay particles. (2) large angular factures and caves (8 – 10 µm in diamter) formed between aggregate of clays but the small and linear fractures are found, too.

Data Sheet – Friedland clay, treated materials *(OPA, 35 °C, VSC)*

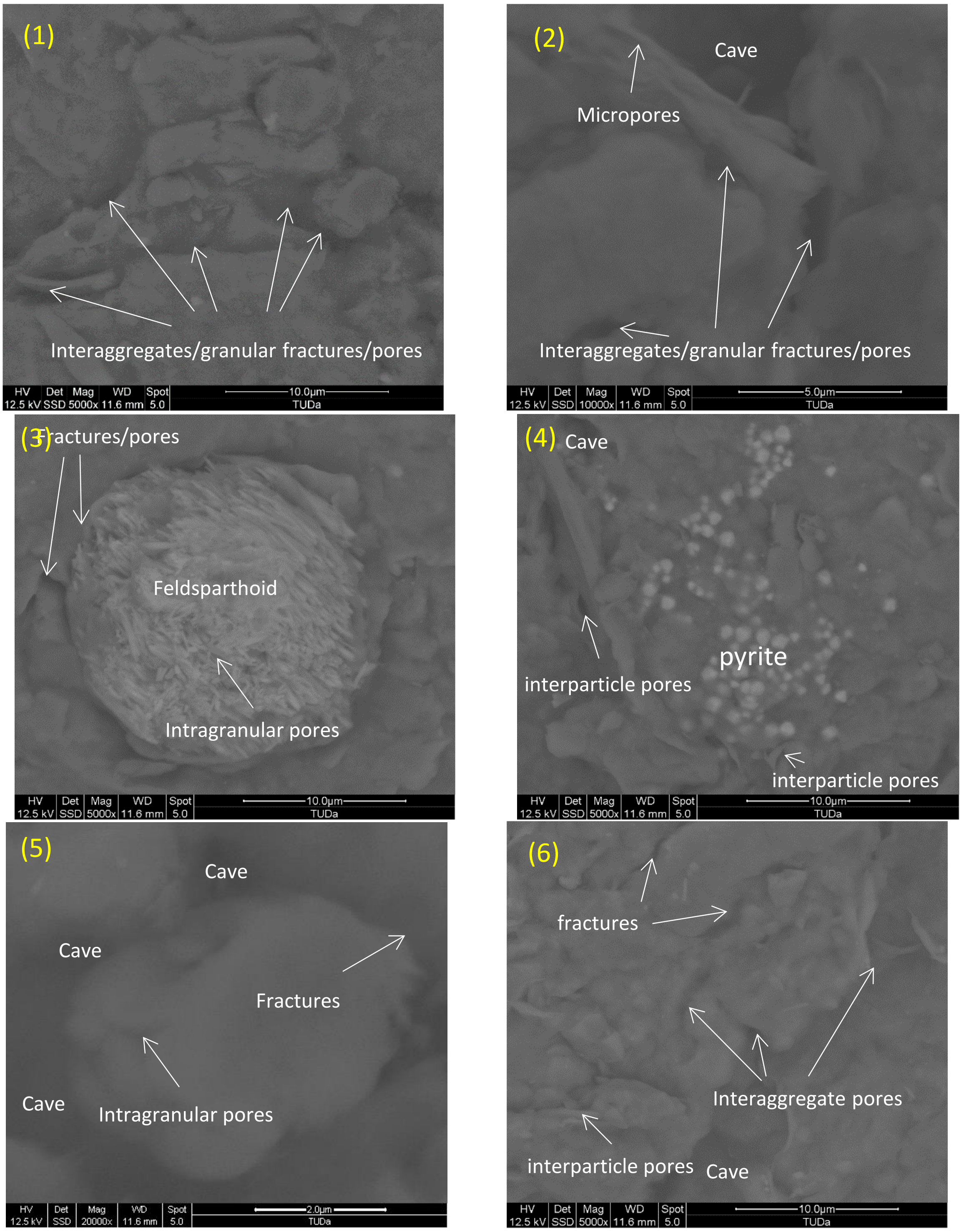

Fig. 22. SEM-images of Friedland clay, treated materials (OPA, 35°C, VSC)

The surface of clay matrix is mostly dense to partially porous matrix with abundant of pores, fractures and caves which were developed between aggregrates, border of aggregates and clay matrix. The intragranular is observed on the surface of feldsparthoid grain.

Data Sheet – Friedland clay, treated materials *(OPA, 60 °C, VSC)*

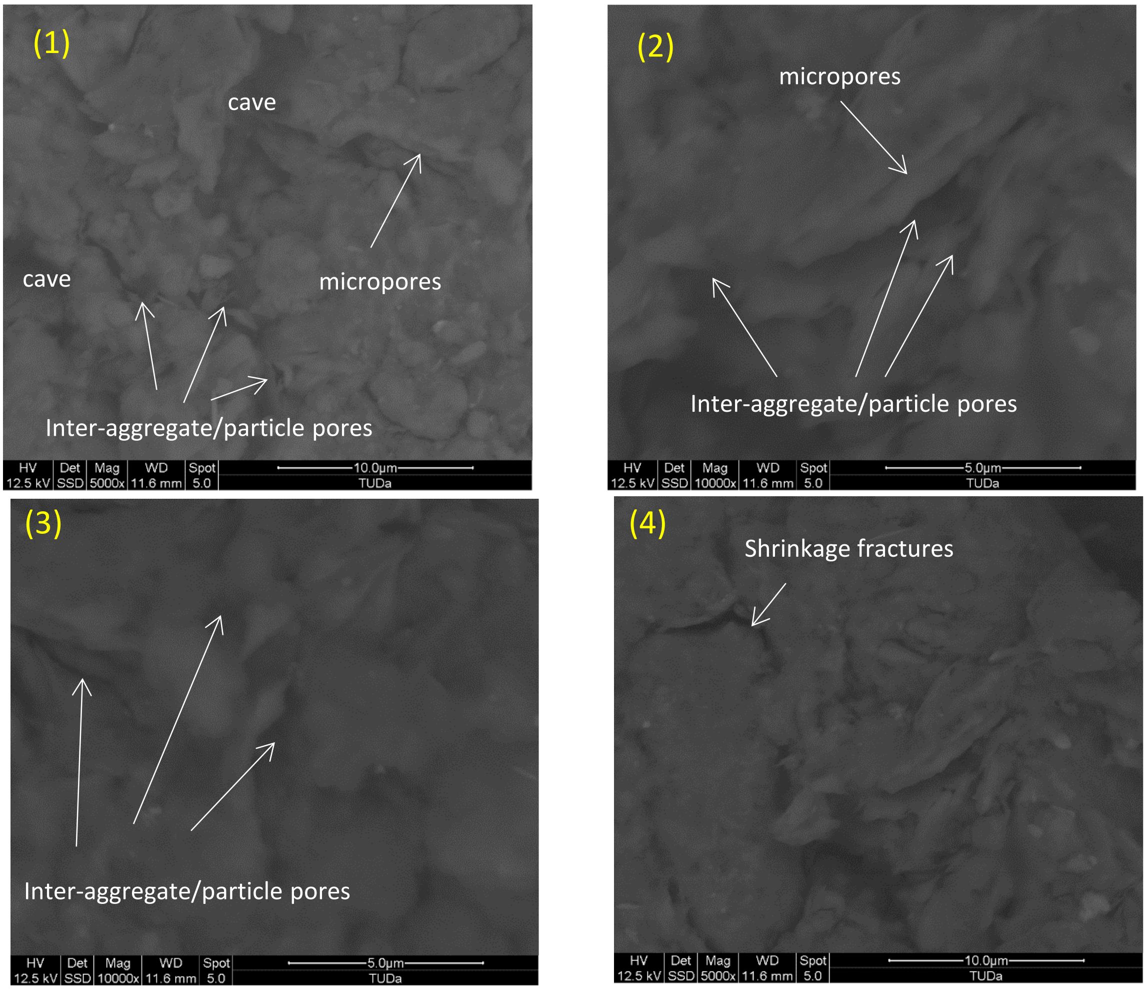

Fig. 23. SEM-images of Friedland clay, treated materials (OPA, 60°C, VSC)

The sample is characterized by dense matrix to partially porous matrix of aggregated structures with the diameter of aggregates >25 mm and particle structure is < 5 µm. A system of inter-particle/aggregate pores and/or aggregates/clay matrix. They are in linear or angurlar form some caves are in elipsoid and oval form but shrinkage linear fractures are found mainly at the border between aggregates/impurities and clay matrix. The micropores was detected between clay layer along (001)-faces. The clay flakes show face-to-face, edge-to-edge and edge-to-face contact style.

Data Sheet – Friedland clay, treated materials *(OPA, 125 °C, VSD)*

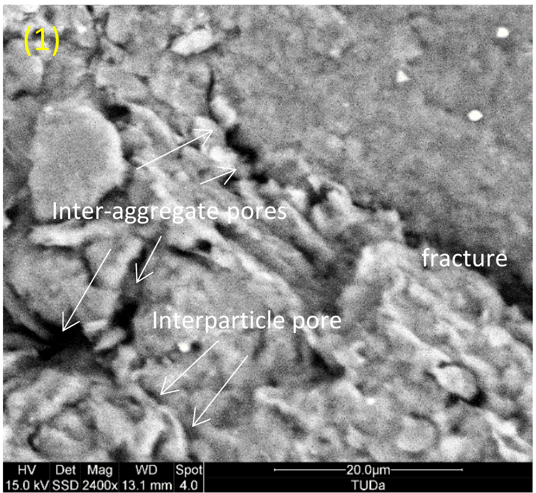

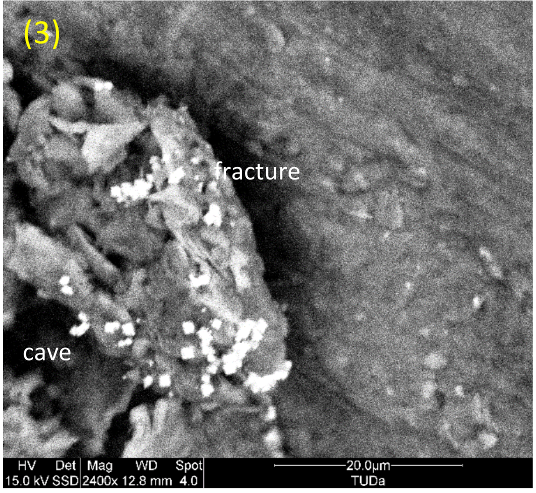

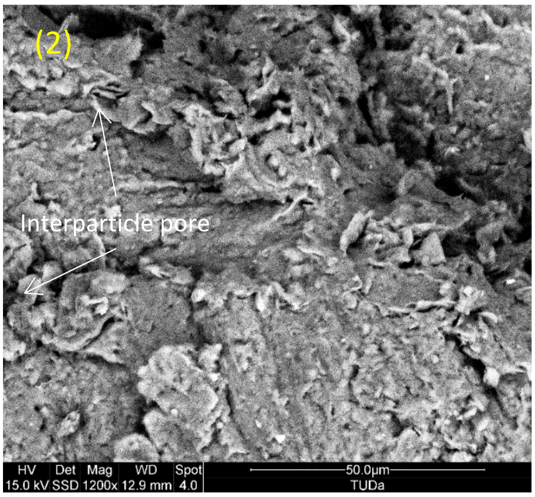

Fig. 24. SEM-images of Friedland clay, treated materials (OPA, 125°C, VSD)

The surface of clay is mostly dense and characterized by aggregated structure with aggregate diameter >25 mm and particle size is <5 µm. The pore system shows angular form of inter-aggregate pores/fractures. The clay flakes show face-to-face contact style.

Data Sheet – Friedland clay, treated materials *(OPA, 125 °C, VSC)*

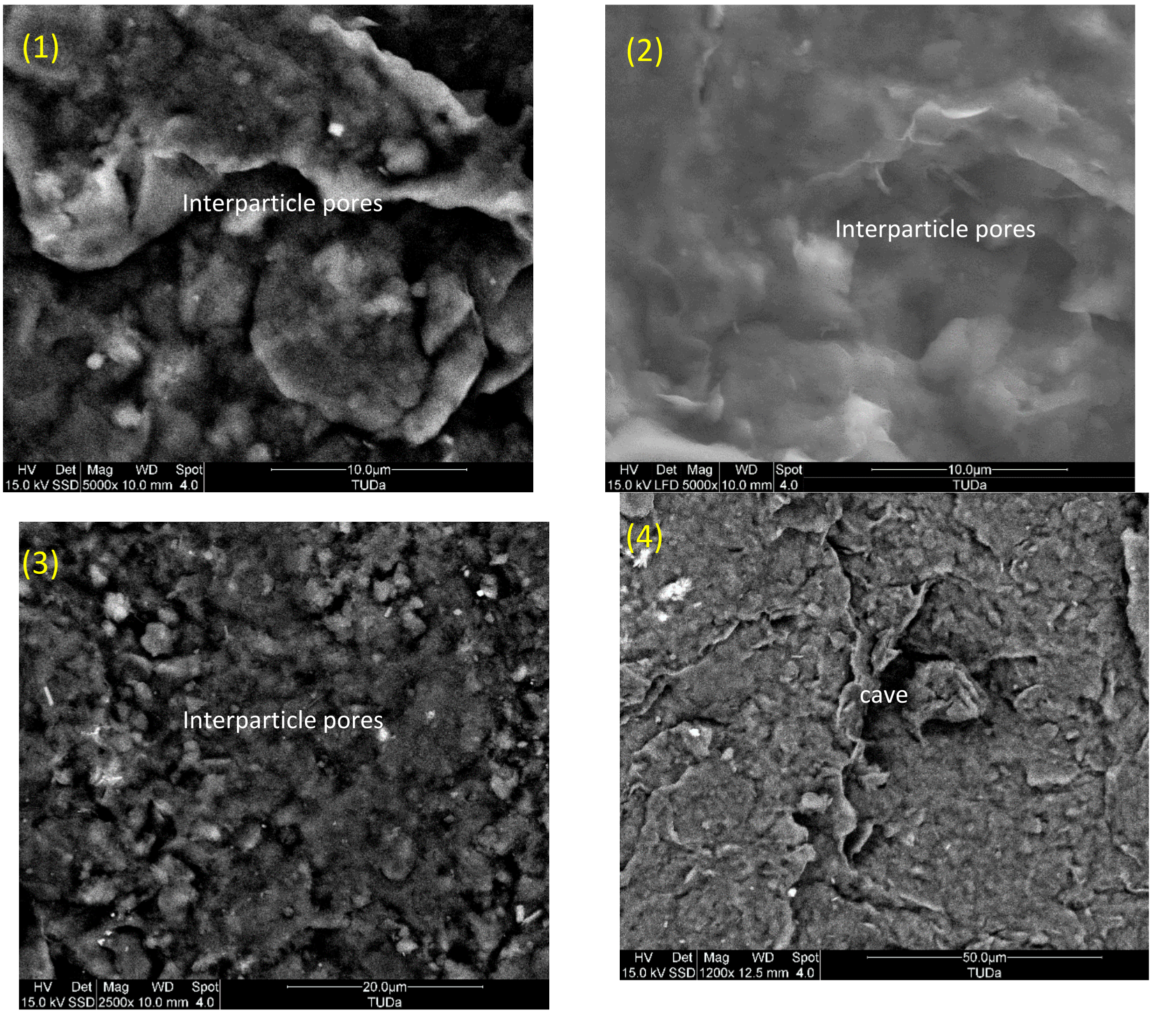

Fig. 25. SEM-images of Friedland clay, treated materials (OPA, 125 °C, VSC)

Dense surface of clay matrix of illite-smectite mixed layer, the clay flakes are thin and showed a face-to-face and face-to-edges, edge-to-edge contact styles but the overall of aggregated structure is dominated. The pores system is composed of interparticle pores (clay-clay contact), interaggregate pores (aggregate-aggregate contact) and impurities-clay matrix contact.

Data Sheet – Friedland clay, treated compacted materials *(OPA, 150 °C, VSC)*

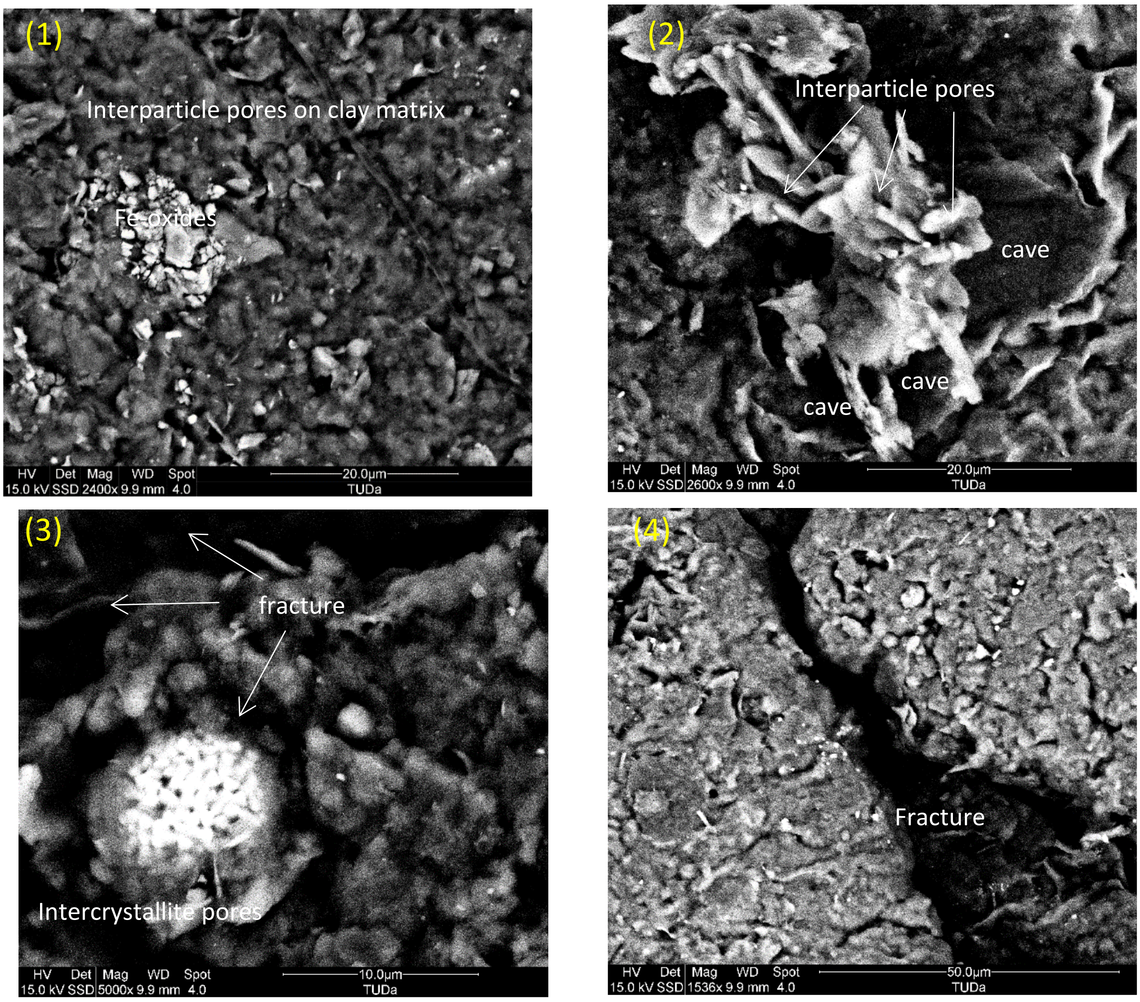

Fig. 23. SEM-images of Friedland clay, treated materials (OPA, 150°C, VSC)

The clay matrix is quite compacted with aggregate structures and some impurities (pyrite, Fe-oxides) are embbed in the clay matrix. The interparticle pores are developed widely in the clay matrix but large fractures are caves are found at the border between aggregates and impurities or between aggregrates. At the small scales, a large shrinkage fractures found between dense matrix of aggregates. The interparticle pores and cave between particles, the clay flakes are thin with wavy border causes angular to irregular forms of cave. The contact style between clay particles are mostly face-to-face and edge-to-face style.

S7. Transmission Electron Microscopy coupled Energy-dispersive X-ray Spectroscopy (TEM-EDX)

Content

SUPPLEMENT – Transmission Electron Microscopy coupled Energy dispersive X-ray Spectroscopy (TEM-EDX) of B25 bentonite

Methodology - Transmission electron microscopy linked with energy-dispersive X-ray spectroscopy (TEM-EDX)

It is expected a characterization of clay mineral phases in original B25 bentonite by transmission electron microscopy. The different clay mineral phases are to identify and to describe by chemical composition and its variability, morphology, the specific dissolution potential, and further parameter.

Such further parameter like distribution of smectite layers probability (%S) and distribution of charges caused by exchangeable cations interlayer space should serve as additional indicators for mineralogical alterations in later treatment experiments with B25 bentonite.

The samples were suspended in deionized water and dispersed by ultrasonic treatment for approximately 20 min. The clay fraction (<2 µm) was separated by sedimentation and diluted with deionized water to get a clear suspension. The suspension was dropped onto carbon-coated Cu grids, air dried and stored under environment-controlled conditions at 45% humidity.

TEM-EDX investigations were carried out on the <2 µm fraction using a FEI TECNAI G^2 20 electron transmission microscope at the VNU University of Science, Vietnam National University, Hanoi. This equipment (operated at 200 kV with LaB_6 cathode) was combined with an S-TWIN objective, a windowless EDAX energy-dispersive X-ray system and a FEI Eagle 2k CCD TEM camera.

About 200 individual clay particles per sample were characterized by TEM-EDX with respect to crystal size, crystal habit, and particle morphology and element distribution. The crystal size, crystal habit and particle morphology were described according to Henning & Störr (1986).

For the quantification of element distribution, a calibration of k factors is mandatory (Cliff & Lorimer, 1975; Lorimer & Cliff, 1976; Mellini & Menichini, 1985). These k values are used to calibrate for the specific behaviour of particles against possible irradiation damage. The elements O, Na, Mg, Al, Si, K, Ca and Fe were quantified by applying the EDAX GENESIS–TEM Quant Materials quantification procedure.

In this procedure, the acquired EDX spectra are corrected by background subtraction, Gaussian deconvolution and k-factor corrections using values previously determined on a phyllosilicate standard (muscovite) and selected non-phyllosilicate standards. The average errors in the analyzed elements using the phyllosilicate standard, expressed as the atomic proportions, are 10 (Na), 5 (Fe, Mg, K, Ti, Ca) and 1 (Si, Al).

The measurement time per particle was lowered to 20 s and the exposed area was limited to a 50 nm diameter, avoiding possible irradiation damage of particles. The stability of particles of the sample series was tested for this measurement time at the beginning of any measurement campaign.

Further methodological details related to TEM-EDX-measurements and the Excel-based mathematical procedure using TEM-EDX data for calculation of mineral formulae are described in Hoang-Minh et al. (2019).

These mathematical procedures described in Hoang-Minh et al. (2019) were extended by k-means clustering method for finding subgroups of observations within a data set. The data were standardized (i.e., scaled) to make variables comparable. Euclidean distances were applied as classical method for distance measures. The optimal clusters were determined by Elbow method and Gap statistics[2].

---

[2] *https://uc-r.github.io/kmeans_clustering*

Data Sheet – B25 bentonite (< 2 µm), original material

Preparation for TEM

- raw material: <40 µm powder of original B25-sample
- suspension on particles < 2 µm on carbon-filmed Cu-grid
- air-dried and humidity-controlled storing

Mineral Matter

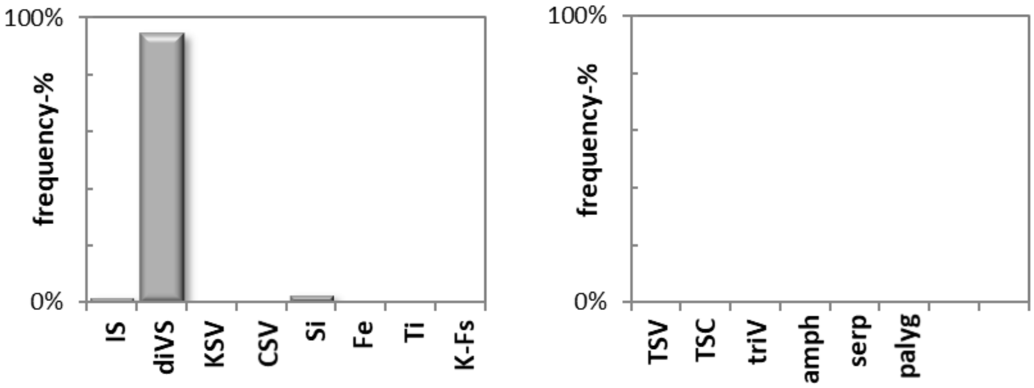

Fig. 1. *Distribution of mineral groups in fraction < 2 µm (in frequency-%)*
Legend: ***IS*** *– illite-smectite-mixed layer series in sense of Środon et al. (1992), diVS – dioctahedral vermiculite-smectite illite-smectite-mixed layer series (= charge- and/or K-deficit),* ***KSV*** *– kaolinite-smectite-dioctahedral vermiculite-mixed layer series,* ***CSV*** *– chlorite-saponite-trioctahedral vermiculite-mixed layer series,* ***Si*** *– quartz or particles with Si-surplus,* ***Fe*** *– Fe-oxide or Fe-oxyhydroxide,* ***Ti*** *– Ti-bearing phases (e.g. rutile, anatase),* ***K-Fs*** *– K-feldspar*

Clay Mineral Composition

All particles of smectite group:

$$Ca_{0.10}\ Mg_{0.08}\ Na_{0.01}\ K_{0.12}\quad Al_{1.27}\ Fe^{3+}_{0.56}\ Mg_{0.17}\ Ti_{0.00}\ (OH)_2\quad Si_{3.70}\ Al_{0.30}\ O_{10}$$

Charge: XII = 0.48 VI = 5.82 IV = 15.70 **Σ = 22.00**
Probability of smectite layers (%S): 54%
Probability of illite layers (%I): 46%

Specific Dissolution Potential (ΔS%)

for H2O, 20 + 60 rpm	-8	(= moderate reacting, interlayer group: Ca+Mg (= type B))
for NaCl, 20 rpm	-9	(= moderate reacting, interlayer group: Ca+Mg (= type B))
for NaCl, 60 rpm	-96	(= fast reacting, ‘illitization’, interlayer group: Na (= type A))
CEC$_{calc}$:	48 meq / 100 g	(literature: 56 meq / 100 g [Matschiavelli et al., 2019: MAT19])

Measured particles: 110

Table 1. *Summarized chemical composition*

SiO_2	TiO_2	Al_2O_3	Fe_2O_3	MnO	MgO	CaO	Na_2O	K_2O	P_2O_5	Σ	
58.6%	0.0%	22.0%	5.9%		3.0%	1.0%	0.1%	1.1%	0.1%	0.92	measured particles
61.5%	0.5%	21.1%	6.4%	0.1%	4.0%	3.8%	0.4%	2.0%	0.1%	1.00	MAT19 (bulk sample)

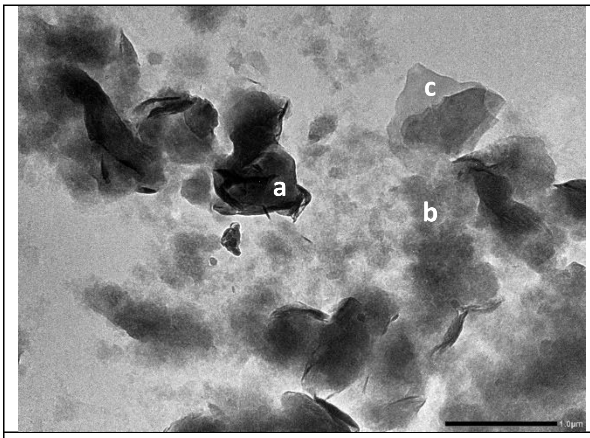	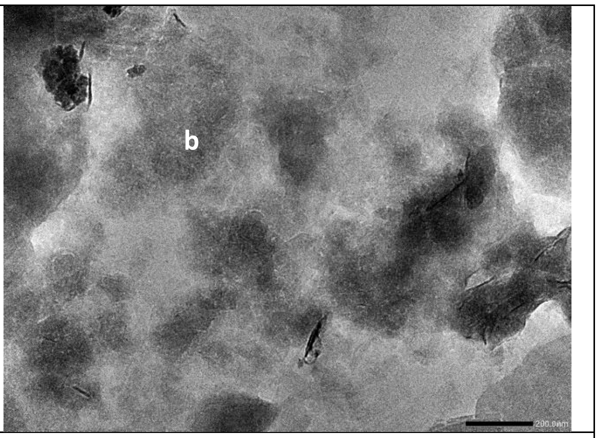
JEM-2100_MAG_X10k_B25-40um_I08.bmp Magnification: 10k (g) large (≤ 1 µm) xenomorph film-like platy crystals with folds; (h) aggregates formed by small (≤ 200 nm) xenomorphous plates; (i) large (≤ 1 µm) xenomorph plates, homogenous thickness	*JEM-2100_MAG_X30k_B25-40um_I10.bmp* Magnification: 30k (b) aggregates formed by small (≤ 200 nm) xenomorphous plates

Fig. 2. *Morphology of particles (TEM-micrographs)*

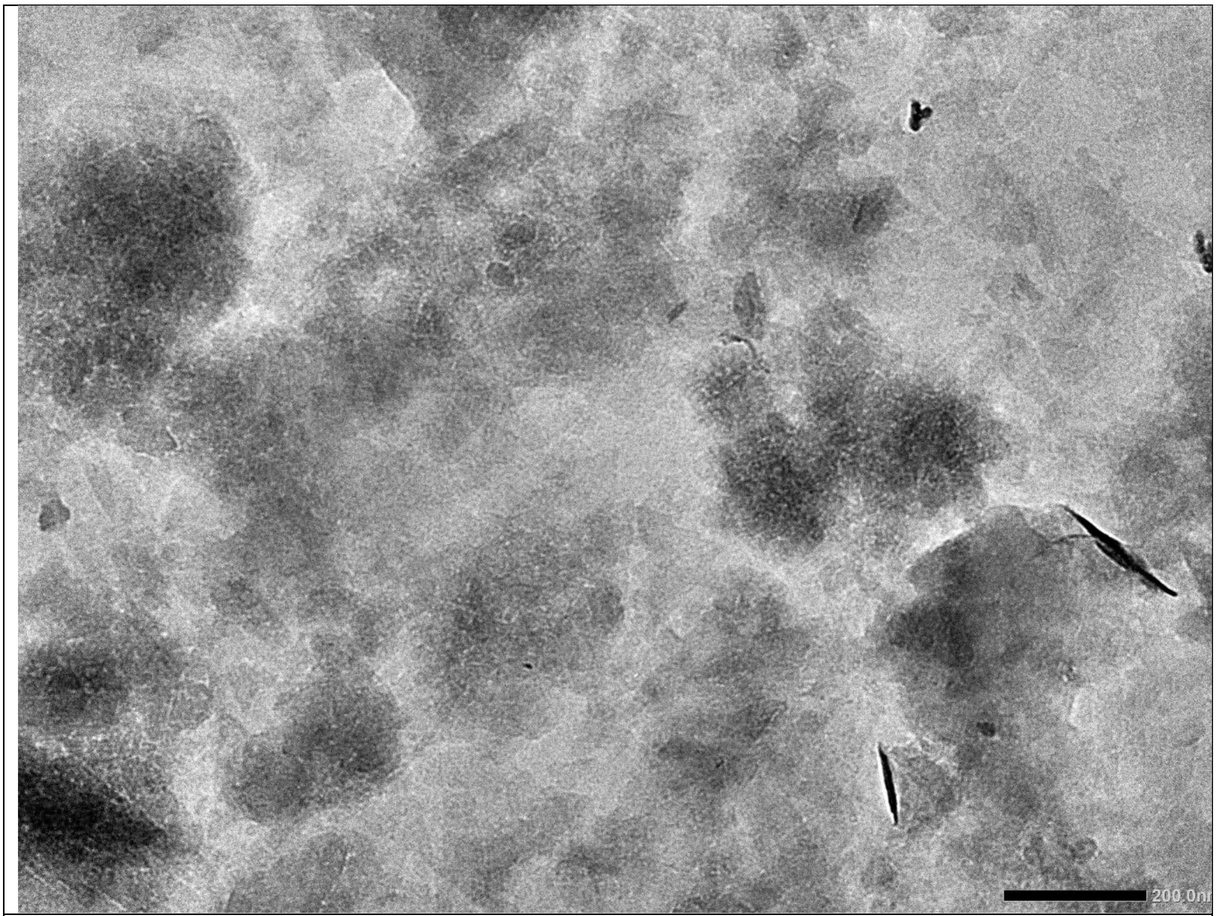

JEM-2100_MAG_X30k_B25-40um-I07.bmp

Magnification: 30k

aggregates formed by small (≤ 200 nm) xenomorphous plates

Fig. 3. *Morphology of particles (TEM-micrographs)*

Distribution of smectite layers probability (%S)

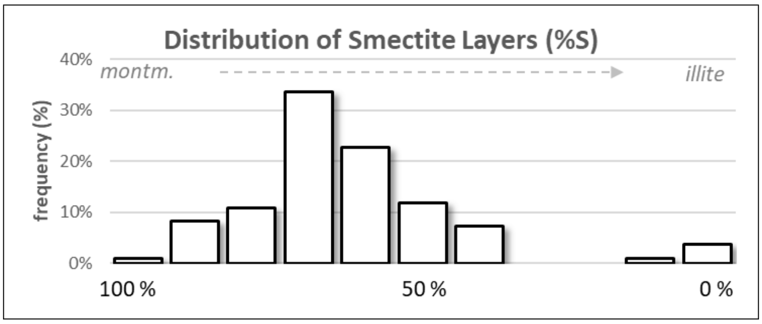

Description: *The distribution of %S-probability indicates the occurrence of three groups: (i) montmorillonite (in traces), (ii) mixture of beidellite-montmorillonite interstratifications (= assumption) with diVS-ml as well as (iii) illite with K-deficiency.*

Fig. 4a. *Distribution of smectite layers probability (%S)*

Differentiation by relation “Octahedral Mg vs. tetrahedral Si”?

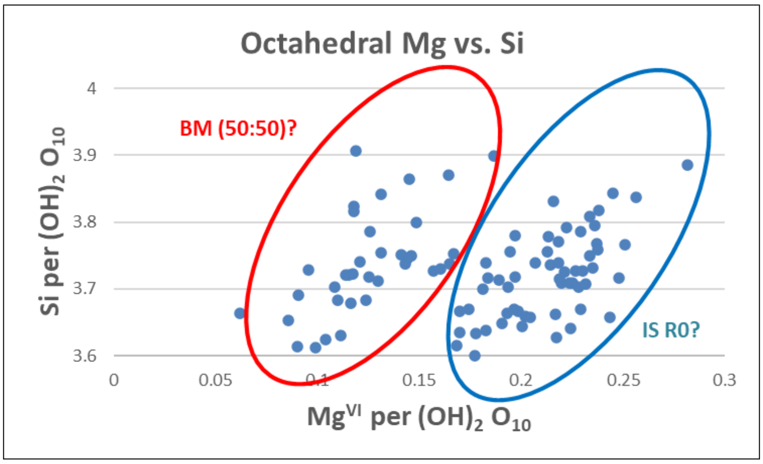

Description: *This diagram indicates the occurrence of two groups of Mg in relation to tetrahedral Si. Probably, this distribution mirrors 2 phases (I) beidellite-montmorillonite interstratifications and (II) diVS-ml (labeled as IS GLY R0 by Sybilla-processing of XRD-traces of EG-solvated fraction < 2 µm, $\%S_{xrd}$=55%)*

Fig. 4b. *Distribution of octahedral Mg vs. tetrahedral Si [all per$(OH)_2$ O_{10}]*

Distribution of K in relation to tetrahedral Si

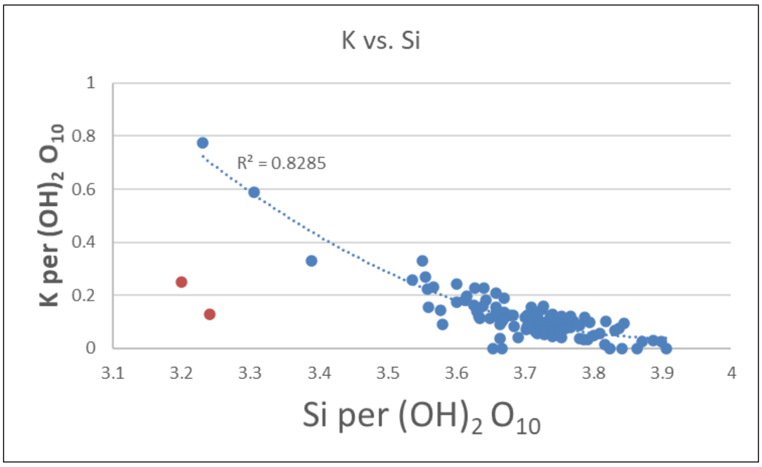

Description: *This diagram visualizes possible particles with a very low K (red dots)*

Fig. 4c. *Distribution of K in interlayer space vs. tetrahedral Si [all per$(OH)_2$ O_{10}]*

Distribution of charges (exchangeable from interlayer space)

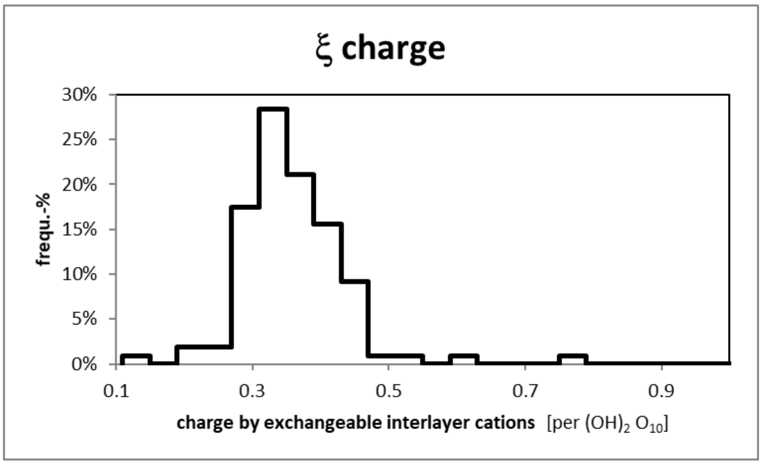

This diagram visualizes the distribution of exchangeable charges in the interlayer space (Ca, Mg, Na) determined and computed by TEM-EDX-data.

Description: *Maximal frequency-% of charge density at 0.35 per* $(OH)_2 O_{10}$.

Fig. 5. *Distribution of charges*

Montmorillonite *(as end member of IS-ml series; confirmed as Cluster3):*

$$Ca_{0.11}\ Mg_{0.09}\ Na_{0.00}\ K_{0.04}\quad Al_{1.31}\ Fe^{3+}_{0.46}\ Mg_{0.17}\ Ti_{0.00}\ (OH)_2\quad Si_{3.92}\ Al_{0.08}\ O_{10}$$

Charge: XII = 0.44 VI = 5.64 IV = 15.92 **Σ = 22.00**

Probability of smectite layers (%S): 92%

Probability of illite layers (%I): 8%

Measured particles: 2

Distribution of smectite layers probability (%S) in IS-ml *(2 particles only)*

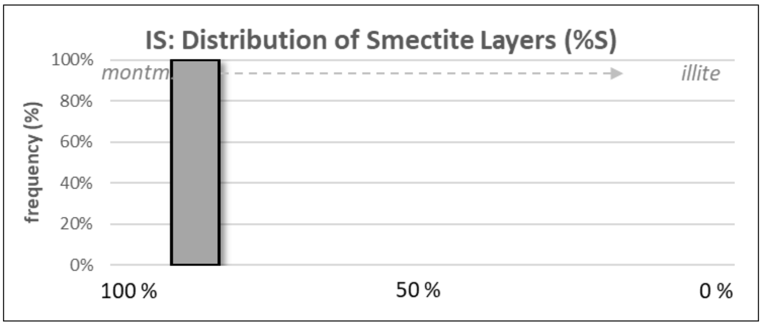

Description: *The distribution of %S-probability indicates also the occurrence of montmorillonite (confirmed as Cluster3).*

Fig. 6. *Distribution of smectite layers probability (%S) in IS-ml*

Beidellite-Montmorillonite interstratification (BM ~ 50%:50%) *(Cluster1 in diVS-ml group):*

$$Ca_{0.04}\ Mg_{0.11}\ Na_{0.00}\ K_{0.09}\quad Al_{1.32}\ Fe^{3+}_{0.56}\ Mg_{0.12}\ Ti_{0.00}\ (OH)_2\quad Si_{3.72}\ Al_{0.28}\ O_{10}$$

Charge: XII = 0.40 VI = 5.88 IV = 15.72 **Σ = 22.00**

Measured particles: 40

Distribution of BM-interstratifications (Cluster1)

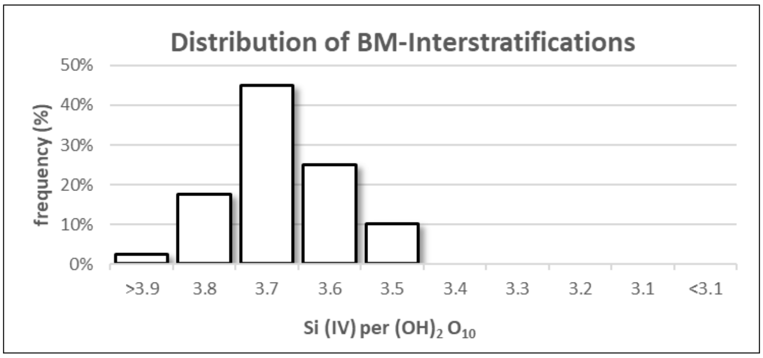

Description: *The distribution of BM-interstratifications (classified as Cluster1) draws a maximum of frequency (%) at tetrahedral Si-value between 3.7 – 3.8 e phuc*

Fig. 7a. *Distribution of assumed beidellite-montmorillonite interstratifications*

BM50:50		*particles (abs)*	Ca (XII)	Mg (XII)	Na (XII)	K (XII)	Cr3+ (VI)	Al (VI)	Fe3+ (VI)	Mg (VI)	Ti (VI)	Al (IV)	Si (IV)	XII	n_VI	%S
Si	>3.9	n = 1	0.00	0.11	0.00	0.00	0.00	1.32	0.56	0.12	0.00	0.09	3.91	0.2	2.0	90
Si	3.9-3.8	n = 7	0.04	0.11	0.00	0.02	0.00	1.34	0.51	0.14	0.00	0.16	3.84	0.3	2.0	79
Si	**3.8-3.7**	**n = 18**	**0.05**	**0.11**	**0.00**	**0.08**	**0.00**	**1.28**	**0.59**	**0.13**	**0.00**	**0.26**	**3.74**	**0.4**	**2.0**	**60**
Si	3.7-3.6	n = 10	0.04	0.12	0.00	0.11	0.00	1.36	0.54	0.10	0.00	0.35	3.65	0.4	2.0	48
Si	3.6-3.5	n = 4	0.05	0.08	0.00	0.26	0.00	1.40	0.51	0.08	0.00	0.44	3.56	0.5	2.0	35
Si	3.5-3.4	n = 0														
Si	3.4-3.3	n = 0														
Si	3.3-3.2	n = 0														
Si	3.2-3.1	n = 0														
Si	<3.1	n = 0														

Fig. 7b. *Computed averaged mineral formulae of phases in the different Si(IV)-classes*

Dioctahedral Vermiculite-Smectite mixed layer phases (diVS-ml) *(Cluster5 in diVS-ml group):*

$$Ca_{0.13}\ Mg_{0.05}\ Na_{0.01}\ K_{0.12}\quad Al_{1.22}\ Fe^{3+}_{0.56}\ Mg_{0.21}\ Ti_{0.00}\ (OH)_2\quad Si_{3.71}\ Al_{0.29}\ O_{10}$$

Charge: XII = 0.50 VI = 5.79 IV = 15.71 **Σ = 22.00**

Probability of smectite layers (%S): 56%

Probability of illite layers (%I): 44%

Measured particles: 63

Distribution of smectite layers probability (%S) in diVS-ml (Cluster5)

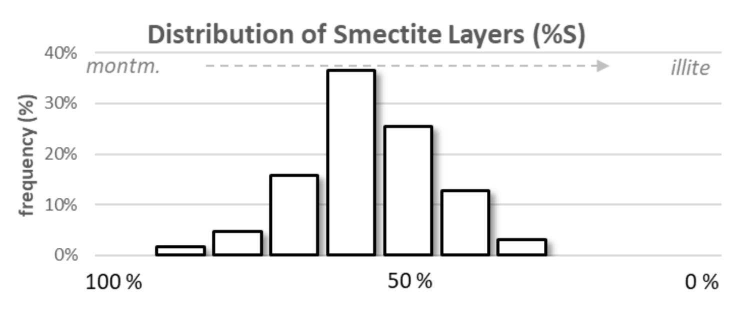

Description: *The distribution of diVS-ml (classified as Cluster5) draws a maximum of frequency (%) for smectite layer probability at 60%*

Fig. 8a. *Distribution of smectite layers probability in diVS-ml*

diVS-ml	*particles (abs)*	Ca (XII)	Mg (XII)	Na (XII)	K (XII)	Cr3+ (VI)	Al (VI)	Fe3+ (VI)	Mg (VI)	Ti (VI)	Al (IV)	Si (IV)	XII	n_VI	%S
%S >95%	n = 0														
%S 95-85%	n = 1	0.16	0.02	0.00	0.03	0.00	1.28	0.44	0.28	0.00	0.11	3.89	0.4	2.0	86
%S 85-75%	n = 3	0.10	0.05	0.02	0.08	0.00	1.33	0.43	0.24	0.00	0.16	3.84	0.4	2.0	77
%S 75-65%	n = 10	0.13	0.04	0.02	0.08	0.00	1.24	0.52	0.23	0.00	0.21	3.79	0.4	2.0	68
%S 65-55%	**n = 23**	**0.14**	**0.05**	**0.01**	**0.10**	**0.00**	**1.22**	**0.57**	**0.21**	**0.00**	**0.27**	**3.73**	**0.5**	**2.0**	**59**
%S 55-45%	n = 16	0.14	0.05	0.01	0.13	0.00	1.21	0.58	0.20	0.00	0.34	3.66	0.5	2.0	49
%S 45-35%	n = 8	0.13	0.06	0.02	0.17	0.00	1.19	0.62	0.18	0.00	0.40	3.60	0.6	2.0	41
%S 35-25%	n = 2	0.10	0.08	0.02	0.19	0.00	1.24	0.61	0.14	0.01	0.44	3.56	0.6	2.0	35
%S 25-15%	n = 0														
%S <15%	n = 0														

Fig. 8b. *Computed averaged mineral formulae of diVS-ml phases in the different smectite layers probability (%S)-classes*

Illite *(as end member of diVS-ml series; confirmed as Cluster2):*

$$\mathrm{Ca_{0.06}\ Mg_{0.03}\ Na_{0.03}\ K_{0.56}\quad Al_{1.55}\ Fe^{3+}_{0.33}\ Mg_{0.11}\ Ti_{0.01}\ (OH)_2\ \ Si_{3.31}\ Al_{0.69}\ O_{10}}$$

Charge:	XII = 0.78	VI = 5.91	IV = 15.31	**Σ = 22.00**
Probability of smectite layers (%S):	10%			
Probability of illite layers (%I):	90%			
Measured particles:	3			

Illite *(as end member of diVS-ml series; confirmed as Cluster4):*

$$\mathrm{Ca_{0.07}\ Mg_{0.28}\ Na_{0.01}\ K_{0.19}\quad Al_{0.99}\ Fe^{3+}_{0.90}\ Mg_{0.11}\ Ti_{0.00}\ (OH)_2\ \ Si_{3.22}\ Al_{0.78}\ O_{10}}$$

Charge:	XII = 0.89	VI = 5.89	IV = 15.22	**Σ = 22.00**
Probability of smectite layers (%S):	4%			
Probability of illite layers (%I):	96%			
Measured particles:	2			

Specific Dissolution Potential

		Specific Dissolution Potential (*)			
B25	**original**	**H2O 20 rpm**	**H2O 60 rpm**	**NaCl 20 rpm**	**NaCl 60 rpm**
Interlayer Type (*)		Ca+Mg	Ca+Mg	Ca+Mg	Na
calculated Δ%S		-8 ± 1	-8 ± 1	-9 ± 1	-96 ± 3
measured $\%S_{initial}$	54				
reaction type by modelling*		*moderate*	*moderate*	*moderate*	*sprinter*

Description: *Overhead-rotation systems like H2O 20 rpm serve as indicator for rate of alteration of selected bentonite. Low grade reduction of smectitic layers (Δ%S) indicate a slow reaction of smectite phases (so-called sleeper).*

An opposite behavior is called as sprinter.

Fig. 9. *Specific Dissolution Potential of B25 bentonite, < 2 µm (* in according to Nguyen-Thanh et al., 2014)*

Description – B25 (< 2 µm), original material

Preparation for TEM

The <40 µm powder of original B25-sample were suspended in deionized water and dispersed by ultrasonic treatment for approximately 20 min. The clay fraction (<2 µm) was separated by sedimentation and diluted with deionized water to get a clear suspension. The suspension was dropped onto carbon-coated Cu grids, air dried and stored under environment-controlled conditions at 45% humidity.

Mineral Matter - Overview

The fraction < 2 µm of original B25 bentonite sample is mainly composed by dioctahedral vermiculite-smectite mixed layer phases (diVS-ml) and assumed beidellite-montmorillonite interstratifications (B:M ~50:50), abbreviated as BM-ml, and accompanied by montmorillonite and two types of illite. Furthermore, Si-surplus particles (Si, e.g. quartz) were identified in traces in this sample [fig. 1].

	frequency-% *(n = 113 measured particles)*
BM-ml (Cluster1)	35%
diVS-ml (Cluster5)	56%
Montmorillonite (Cluster3)	2%
Illite (Cluster2)	3%
Illite (Cluster4)	2%
Si-surplus	3%

All measured clay mineral phases summarized result following mineral formula computed from TEM-EDX-measurement of 110 individual particles:

	$Ca^{2+}_{0.10}$	$Mg^{2+}_{0.08}$	$Na^{+}_{0.01}$	$K^{+}_{0.12}$	$Al^{3+}_{1.27}$	$Fe^{3+}_{0.56}$	$Mg^{2+}_{0.17}$	$Ti^{4+}_{0.00}$	$(OH)_2$	$Si^{4+}_{3.70}$	$Al^{3+}_{0.30}$	O_{10}
SDOM	*± 0.00*	*± 0.00*	*± 0.00*	*± 0.01*	*± 0.01*	*± 0.01*	*± 0.01*	*± 0.00*		*± 0.01*	*± 0.01*	

Legend: SDOM - standard deviation of the mean (= the standard deviation divided by the square root of the number of samples)

The interlayer charge is calculated as 0.48 per $(OH)_2$ O_{10} and the octahedral charge as 5.82 per $(OH)_2$ O_{10}. The particles are characterized by a high octahedral Fe-amount.

The summarized chemical composition of all 110 computed particles is compared with chemical data from literature [tab. 1]. Such comparison is only limited valid because of different origin of samples and the differences in composition for fraction < 2 µm (the measured sample) and the bulk material (the applied literature data). The chemical composition averaged by measured particles show especially a lower amount of CaO, Na_2O and K_2O as the applied literature data, probably an indication for a higher concentration of feldspars in the bulk sample than in fraction < 2 µm.

B25 bentonite is characterized by three morphological groups: (i) large (≤ 1 µm) xenomorph film-like platy crystals with folds, (ii) aggregates formed by small (≤ 200 nm) xenomorphous plates and (iii) large (≤ 1 µm) xenomorph plates with homogenous thickness [fig. 2]. Thin aggregates formed by small (≤ 200 nm) xenomorphous plates dominate the shapes of particles in the micrographs [fig. 2, fig. 3].

The distribution of %S-probability of all measured clay mineral phases [fig. 4a] also indicates the occurrence of three groups: (i) montmorillonite (in traces; %S-class = 100%), (ii) as main group a mixture of beidellite-montmorillonite interstratifications and diVS-ml (%S-max of this mixture at 70%) and (iii) illite with K- and charge deficit (%S-class = 0%).

The numerous measured particles by TEM-EDX allow a visualization of distribution of interlayer charges. Considering the TEM-EDX-determined cations Ca^{++}, Mg^{++} and Na^{+} and then computed their ratio as interlayer cations in the mineral formula, Ca^{++}, Mg^{++} and Na^{+} offer to characterize the degree of exchangeable charges in the interlayer space. This charge density of untreated B25 bentonite (< 2 µm) shows only a narrow interval at the maximal frequency-% of charge density at 0.35 per $(OH)_2\ O_{10}$ [fig. 5]. This narrow interval of interlayer charge density caused by exchangeable cations from 0.27 – 0.47 per $(OH)_2\ O_{10}$ represents mainly the BM- and diVS-ml phases. The few measured montmorillonite particles are part of this interval. Also, the measured illite particles (Cluster2) offer only a low number of exchangeable cations and indicating a lower degree of weathering.

Mineral Matter - Specification

Result of Clustering & Comparison with XRD-data (Sybilla-processing)

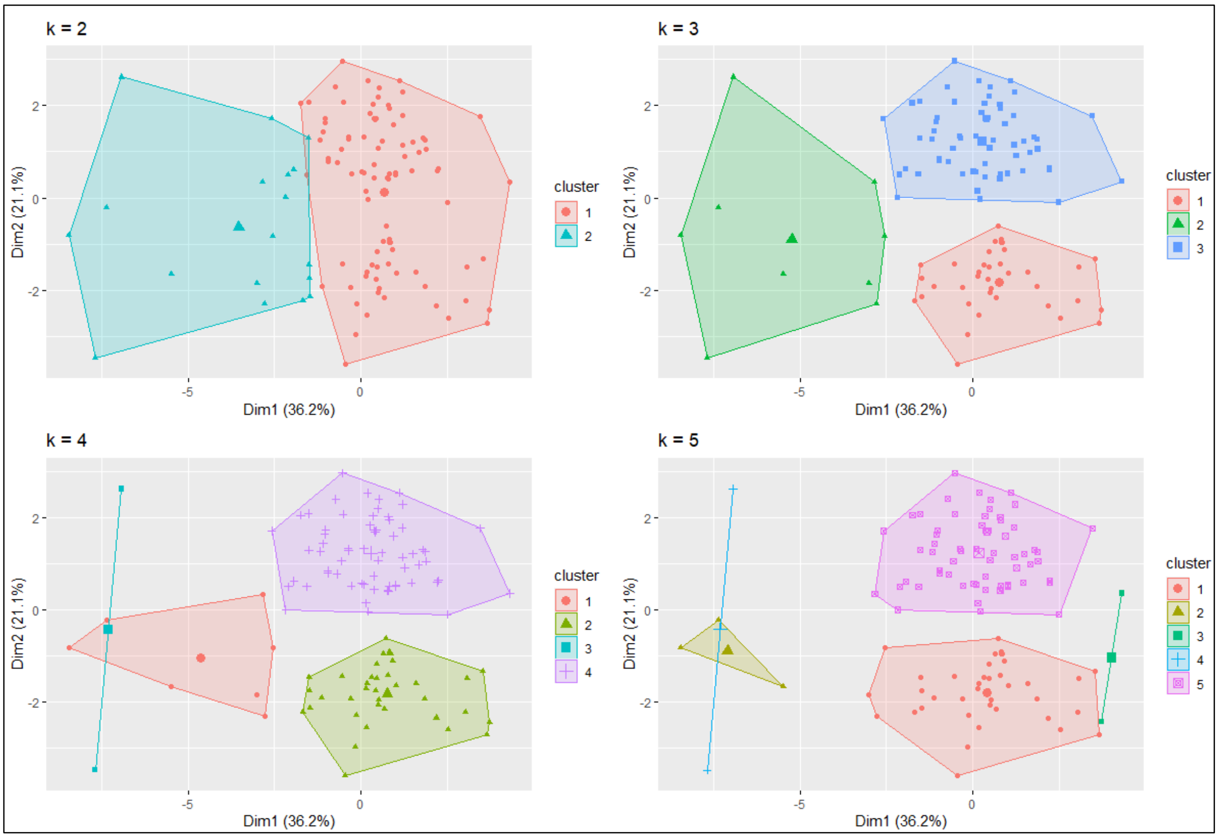

Fig. 9. *Clustering of all measured particles for clusters k = 2, k = 3, k = 4 and k = 5 (source for R-coding: https://uc-r.github.io/kmeans_clustering)*

The optimum of clusters was calculated with k = 5. This number of clusters differentiates also clearly illite particles (Cluster2, Cluster4) from smectite-bearing phases (Cluster1, Cluster3, Cluster5).

		Ca (XII)	Mg (XII)	Na (XII)	K (XII)	Cr3+ (VI)	Al (VI)	Fe3+ (VI)	Mg (VI)	Ti (VI)	Al (IV)	Si (IV)	XII	n_VI	%S
Cluster1	n = 40	0.04	0.11	0.00	0.09	0.00	1.32	0.56	0.12	0.00	0.28	3.72	0.4	2.0	58
Cluster2	n = 3	0.06	0.03	0.03	0.56	0.00	1.55	0.33	0.11	0.01	0.69	3.31	0.8	2.0	10
Cluster3	n = 2	0.11	0.09	0.00	0.04	0.00	1.31	0.46	0.17	0.00	0.08	3.92	0.4	1.9	92
Cluster4	n = 2	0.07	0.28	0.00	0.19	0.00	0.99	0.90	0.11	0.00	0.78	3.22	0.9	2.0	4
Cluster5	n = 63	0.13	0.05	0.01	0.12	0.00	1.22	0.56	0.21	0.00	0.29	3.71	0.5	2.0	56

Fig. 10. *Mineral formulae based on TEM-EDX-data summarized following the result of clustering for k=5*

	Sybilla-results	**TEM-EDX-results**	**Notes**
Cluster1	IS R0 (1) *(%S = 99%)*	BM-ml *(%B ~ 55%)*	*XRD: Montmorillonite and beidellite are only to distinguish by Green-Kelly-test (not available here).*
Cluster2	Illite	Illite	*K-deficit, Al(VI)-rich*
Cluster3	IS R0 (1) *(%S = 99%)*	IS-ml *(%S = 92%)*	*high charged Fe-rich Ca,Mg-montmorillonite*
Cluster4	Illite	Illite	*high K-deficit, nearby a Fe-illite*
Cluster5	IS R0 (2) *(%S = 55%)*	diVS-ml *(%S = 56%)*	*high K-deficit, Fe(VI)-rich*

Tab. 2. *Comparison of results from TEM-EDX- and XRD-measurements with clustering procedure*

The clustering of TEM-EDX-data offers a good agreement with the recent result of Sybilla-processing of XRD-traces from oriented specimen [tab. 2].

IS R0 (1): The X-ray diffraction pattern of the ethylene-glycol saturated oriented specimen shows a full expandability to 1.7 nm and a difference of 5.42°2θ between 2. and 3. order of smectite interferences. This distance is typically for montmorillonite (Moore & Reynolds, 1989). This result of XRD-processing let expect a maximum of particles for %S ~ 90-100% by TEM-EDX-measurements, but the maximum of particles measured by TEM-EDX is to find at %S=70% [fig. 4a].

Montmorillonite and beidellite have the same behavior concerning the expandability and they are only to distinguish by XRD using Li like by Greene-Kelly test (Green-Kelly 1952, 1953). So, combination of XRD- and TEM-results (full expandability by XRD and Si ~ 3.72 by TEM-EDX) led conclude the occurrence of 'beidellite-montmorillonite interstratifications', a beidellite-montmorillonite interstratification with about 50% beidellite and 50% montmorillonite layers (BM-ml 50:50).

The methodical combination of XRD-processing and TEM-EDX- data (incl. clustering) indicates further sub-groups of identified phases by Sybilla-procedure for illite-smectite mixed layer phases (IS R0 (1)): (i) BM-ml (Cluster1) and (ii) IS-ml (Cluster3) [tab. 2].

IS R0 (2): The Sybilla-procedure of XRD-traces (oriented mounts) has shown an occurrence of a second illite-smectite mixed layer phase with a smectite layers probability of %S = 55%. This situation is to find in Cluster5 (%S = 56%) representing a K- and charge deficient and Fe-rich dioctahedral vermiculite-smectite mixed layer phase (diV-ml) [tab. 2].

Illite: The Sybilla-procedure of XRD-traces (oriented mounts) draws the occurrence of illite. The clustering of TEM-EDX-data confirmed the Sybilla-results, but it indicates two sub-groups of illite: (i) illite (Cluster2) as K-deficient and Al(VI)-rich illite and (ii) illite (Cluster5) as very high K-deficient and Fe(VI)-rich illite.

The Sybilla-processing of XRD-traces (oriented mounts) also supports the existence of kaolinite and kaolinite-smectite mixed layer phases in fine fraction of B25 bentonite. Such phases were not to identify in TEM-EDX-database (a grain size effect?).

Specifics to the identified clay mineral groups

Montmorillonite as part of illite-smectite mixed-layer series *(IS-ml in sense of Środon et al., 1992)*

The term 'illite-smectite mixed layer series in sense of Środon et al. (1992)' describes illite-smectite interstratifications with a normal interlayer charge for illite layers of 0.89 (representing fixed K) and a normal interlayer charge for smectite layers of 0.40 per $(OH)_2\ O_{10}$. This series occurs in B25 bentonite (< 2 µm) in traces as end member of this series: montmorillonite. Only 2 of 110 measured particles belong so to this normal charged group IS-ml in sense of Środon et al. (1992).

Montmorillonite:

$$Ca_{0.11}\ Mg_{0.09}\ Na_{0.00}\ K_{0.04}\quad Al_{1.31}\ Fe^{3+}_{0.46}\ Mg_{0.17}\ Ti_{0.00}\ (OH)_2\quad Si_{3.92}\ Al_{0.08}\ O_{10}$$

Charge: XII = 0.44 VI = 5.64 IV = 15.92 **Σ = 22.00**
Probability of smectite layers (%S): 92%
Probability of illite layers (%I): 8%

Measured particles by TEM-EDX: 2
Result of clustering: Cluster3 [tab. 2]

The %S-probability of these particles (%S ~ 92%) indicates the occurrence of montmorillonite. Furthermore, the value for octahedral iron (0.46 per $(OH)_2\ O_{10}$) in the computed mineral formula characterizes this montmorillonite as Fe-rich.

The distribution of %S-probability, specified for normal charged IS-ml, indicates the occurrence only of one group of phases, here with %S mainly at 90% [fig. 6].

Beidellite-montmorillonite interstratifications (B:M ~50:50)

40 of 110 measured particles belong so to this assumed classification. The dioctahedral character of this group is proofed by X-ray diffraction. The position of the large (060)-interference of smectite is in the random oriented powder specimen at 1.497 Å.

The X-ray diffraction pattern of the ethylene-glycol saturated oriented specimen shows a full expandability to 1.7 nm and a difference of 5.42°2θ between 2. and 3. order of smectite interferences. This distance is typically for montmorillonite (Moore & Reynolds, 1989). This result of XRD-processing let expect a maximum of particles for %S ~ 90-100% by TEM-EDX-measurements, but the maximum of particles measured by TEM-EDX is to find at %S=70% [fig. 4a].

Montmorillonite and beidellite have the same behavior concerning the expandability and they are only to distinguish by XRD using Li by means of Greene-Kelly test (Green-Kelly 1952, 1953). So, combination of XRD- and TEM-results (full expandability by XRD and Si ~ 3.69 by TEM-EDX) led conclude the occurrence of 'beidellite-montmorillonite interstratifications', a beidellite-montmorillonite interstratification with about 50% beidellite and 50% montmorillonite layers (BM-ml 50:50).

Beidellite-montmorillonite interstratifications (B:M ~50:50):

$$Ca_{0.04}\ Mg_{0.11}\ Na_{0.00}\ K_{0.09}\quad Al_{1.32}\ Fe^{3+}_{0.56}\ Mg_{0.12}\ Ti_{0.00}\ (OH)_2\quad Si_{3.72}\ Al_{0.28}\ O_{10}$$

Charge: XII = 0.40 VI = 5.88 IV = 15.72 **Σ = 22.00**

Measured particles by TEM-EDX: 40
Result of clustering: Cluster1 [tab. 2]

Beidellitic structures are characterized by a low octahedral Mg-amount (because of high ratio of octahedral, 3-valent cations). A comparison of octahedral Mg vs. tetrahedral Si indicates the occurrence of two groups for octahedral Mg based on TEM-EDX-data [fig. 4b]. The group with a lower Mg-ratio should represent the already mentioned BM-ml (50:50) phases (= IS GLY R0_1 with $\%S_{xrd}$ = 99%; see also Cluster1 in tab. 2) and the other group with a higher Mg-ratio is considered as diVS-ml (= IS GLY R0_2 with $\%S_{xrd}$ = 55%).

Using the results of clustering (see Cluster1 in tab. 2), the maximum of frequency-% is to find for particles in the Si(IV)-class 3.7 – 3.8 e phuc [tab. 7a], representing the mentioned relation 50% montmorillonite and 50% beidellite as ratio of interstratification. The mineral formulae, summarized in classes of tetrahedral Si, draw for the maximum an Fe-rich BM 50:50 phase with low K, but remarkable amount of Mg in the interlayer space [tab. 7b].

Dioctahedral vermiculite-smectite mixed layer phase (diVS-ml)

The processing of XRD-traces (oriented mounts) by Sybilla-software has drawn the occurrence of two types of IS GLY R0-phases: (i) IS GLY R0 (1) with $\%S_{xrd}$ = 99% above discussed as BM-ml (50:50) and (ii) IS GLY R0 (2) with $S\%_{xrd}$ = 55% (see Cluster5 in tab. 2).

Dioctahedral vermiculite-smectite mixed layer phase (diVS-ml):

$$Ca_{0.13}\ Mg_{0.05}\ Na_{0.01}\ K_{0.12}\quad Al_{1.22}\ Fe^{3+}_{0.56}\ Mg_{0.21}\ Ti_{0.00}\ (OH)_2\quad Si_{3.71}\ Al_{0.29}\ O_{10}$$

Charge: XII = 0.50 VI = 5.79 IV = 15.71 **Σ = 22.00**
Probability of smectite layers (%S): 56%
Probability of illite layers (%I): 44%

Measured particles by TEM-EDX: 63
Result of clustering: Cluster5 [tab. 2]

The probability of smectite layers determined by TEM-EDX-data and Sybilla-processing of XRD-traces (oriented mounts) gives similar results: $\%S_{TEM}$ = 56% [tab. 8a] and $\%S_{XRD}$ = 55%.

The Rietveld refinement by Profex software (Döbelin & Kleeberg, 2015) draws for octahedral composition of this mixed layer phase in bulk sample: $Al^{3+}_{1.2}$ $Fe^{3+}_{0.60}$ $Mg^{2+}_{0.20}$ per ($(OH)_2$ O_{10}) as best refinement result. This refinement of X-ray diffraction traces confirms additionally the Fe-rich occupation of octahedral layer as determined also by TEM-EDX [tab. 8b].

Illite

The TEM-EDX-based distribution of %S-probability [fig. 4a] indicates three possible groups: (i) the occurrence of montmorillonite with %S ~ 100%, (ii) BM-ml in mixture with diVS-ml (maximum at $Si_{tetrahedral}$ 3.74 per $(OH)_2$ O_{10} [fig. 7b]) and (iii) illite with K- & charge-deficit. The clustering of TEM-EDX-data shows two illite clusters Cluster2 and Cluster4 [tab. 2].

***Illite** (as end member of diVS-ml series; confirmed as Cluster2)**:*

$$\mathrm{Ca_{0.06}\ Mg_{0.03}\ Na_{0.03}\ K_{0.56}\quad Al_{1.55}\ Fe^{3+}_{0.33}\ Mg_{0.11}\ Ti_{0.01}\ (OH)_2\quad Si_{3.31}\ Al_{0.69}\ O_{10}}$$

Charge: XII = 0.78 VI = 5.91 IV = 15.31 **Σ = 22.00**

Probability of smectite layers (%S): 10%

Probability of illite layers (%I): 90%

Measured particles by TEM-EDX: 3

***Illite** (as end member of diVS-ml series; confirmed as Cluster4)**:*

$$\mathrm{Ca_{0.07}\ Mg_{0.28}\ Na_{0.01}\ K_{0.19}\quad Al_{0.99}\ Fe^{3+}_{0.90}\ Mg_{0.11}\ Ti_{0.00}\ (OH)_2\quad Si_{3.22}\ Al_{0.78}\ O_{10}}$$

Charge: XII = 0.89 VI = 5.89 IV = 15.22 **Σ = 22.00**

Probability of smectite layers (%S): 4%

Probability of illite layers (%I): 96%

Measured particles by TEM-EDX: 2

Illite of Cluster2 is characterized by slight K-deficiency and Al-rich octahedral layer. Few smectite layers are not excluded because of Si(IV) = 3.31 e phuc.

Otherwise, illite particles of Cluster4 show a very high K-deficit and very Fe-rich octahedral layer.

The Rietveld refinement by Profex software (Döbelin & Kleeberg, 2015) indicates the occurrence of two polytypes for illite in B25 bentonite: $2M_1$- and 1M-polytype.

Kaolinite-montmorillonite mixed layer phases

The Excel-based procedure (Hoang-Minh et al., 2019) to identify possible clay mineral groups using the TEM-EDX-measurements also includes algorithms to classify kaolinite and kaolinite-montmorillonite mixed layer phases. These algorithms couldn't identify such phases basing on the measured TEM-EDX-data. Even also the clustering gives no indications for the occurrence of kaolinite-bearing phases.

Otherwise, the processing of XRD-traces (oriented mounts) by Sybilla-Software indicated the occurrence of kaolinite-montmorillonite mixed layer phases (KS GLY R1, $\%S_{xrd}$=45%). Such particles should be characterized by a low potassium (because of missing K in kaolinite structure). A visualization of TEM-EDX-measurements in a relation "K vs. Si" shows only two possible measurements (of 108 particles), which could represent phases with a very low potassium ratio in the structure [fig. 4c]. The mean of particle thickness for KS GLY R1 was computed by Sybilla-software at 11 nm. Probably, this higher thickness is underrepresenting the kaolinite-bearing phases in the TEM-EDX-results in comparison to the finer particles of BM 50:50 in mixture with diVS-ml (T_{mean} ~ 4.4 nm).

Estimation of Specific Dissolution Potential *(in according to Nguyen-Thanh et al., 2014)*

Previous investigations have shown (summarized in Nguyen-Thanh et al., 2014), each bentonite or clay have a specific dissolution potential expressed as loss of smectite layer. The expected specific behavior of smectite layers is classified using the mineral formula as result of TEM-EDX-measurements. The authors developed different experimental overhead rotation setups to determine the maximal possible loss of smectite layers under pre-defined conditions [fig. 8]. These different experimental settings should represent different strength of acting forces in mineralogical alteration of original smectite (with water as low energy-level). The previous results with a large series of bentonites and clays allow to predict the expected rate of alteration of smectite layers distinguishing slow-reacting smectite layers (= sleepers), moderate-reacting smectite layers and fast-reacting smectite layers (= sprinters). The limits between these free classes are postulated only: sleepers are smectites with loss of smectite layers lower than $\Delta\%S = 5\%$ and are a sprinter with loss of smectite layers larger than $\Delta\%S = 20\%$. Negative values for $\Delta\%S$ mirroring a 'illitization'-like process and positive values represent a smectitization potential.

The modelled values for B25 bentonite [fig. 9] let expect mainly a moderate-reacting smectite with a change from the original $Si_{tetrahedral}$ 3.69 in direction to $Si_{tetrahedral}$ 3.60 per $(OH)_2 O_{10}$ for the run products ($\Delta\%S = -8\%$). Otherwise under strong conditions (e.g. higher temperature, high ionic strength, high saline solution), the modelling let assume for B25 bentonite a very fast and nearby complete loss of smectite layers ($\Delta\%S = -96\%$).

The type of cations in the interlayer space (here type B with Ca + Mg) and the Fe-rich composition of octahedral layer are the driving forces for these estimations.

Following aspect could influence the expected behavior for B25 bentonite: The alteration mechanisms and the rate of alteration of beidellite are unknown until now.

Finally, only further experiments with the selected bentonite can validate these estimations.

References

Cliff, G. & Lorimer, G. W. (1975). *J. Microsc.* **103**, 203–207.

Döbelin, N., Kleeberg, R. (2015). *Journal of Applied Crystallography* **48**, 1573-1580. DOI: 10.1107/S1600576715014685

Henning, K.-H. & Störr, M. (1986). Electron Micrographs (TEM, SEM) of Clays and Clay Minerals, p. 325. Akademie-Verlag Berlin.

Hoang-Minh, T., Kasbohm, J., Nguyen-Thanh, L., Nga, P. T., Lai, L. T., Duong, N. T., Thanh, N. D., Thuyet, N. T. M., Anh, D. D., Pusch, R., Knutsson, S. & Ferreiro Mahlmann, R. (2019). *J. Appl. Cryst.* **52**, 133-147. DOI: 10.1107/S1600576718018162

Lorimer, G. W. & Cliff, G. (1976). *Electron Microscopy in Mineralogy*, edited by H. R. Wenk, pp. 506–519. Berlin: Springer Verlag.

Matschiavelli, N., Kluge, S., Podlech, C., Standhaft, D., Grathoff, G., Ikeda-Ohno, A., Warr, L.N., Chukharkina, A., Arnold, T. & Cherkouk, A. (2019). *Environmental Science & Technology.* **53** (17), 10514-10524, DOI: 10.1021/acs.est.9b02670

Mellini, M. & Menichini, R. (1985). *R. Soc. Ital. Miner. Petrol.* **40**, 261–266.

Moore, D.M., Reynolds, R.C. (1989). X-ray Diffraction and the Identification and Analysis of Clay Minerals, Oxford University Press, New York, 332 + xvi pp.

Nguyen-Thanh, L., Herbert, H.-J., Kasbohm, J., Hoang-Minh, T. & Mählmann, R. F. (2014). *Clays Clay Miner.* **62**, 425–446.

Środoń, J., Elsass, F., McHardy, W. J. & Morgan, D. J. (1992). *Clay Miner.* **27**, 137–158.

Data Sheet – B25 bentonite, treated materials *(OPA, 100^C, 110h)* - TOP

Methodology - Transmission electron microscopy linked with energy-dispersive X-ray spectroscopy (TEM-EDX)

It is expected a characterization of clay mineral phases in treated B25 bentonite by transmission electron microscopy. The sample series No4 represents a percolation of B25 bentonite by Opalinus Clay solution at 35°C for 93.6 hours. The sample No4_T is the label for the material at the top of sample cylinder.

The different clay mineral phases are to identify and to describe by chemical composition and its variability, morphology, the specific dissolution potential, and further parameter.

Such further parameter like distribution of smectite layers probability (%S) and distribution of charges caused by exchangeable cations interlayer space should serve as additional indicators for mineralogical alterations in treatment experiments with B25 bentonite.

The sample were suspended for TEM-measurement in deionized water and dispersed by ultrasonic treatment for approximately 20 min. The clay fraction (<2 µm) was separated by sedimentation and diluted with deionized water to get a clear suspension. The suspension was dropped onto carbon-coated Cu grids, air dried and stored under environment-controlled conditions at 45% humidity.

TEM-EDX investigations were carried out on the <2 µm fraction using a FEI TECNAI G^2 20 electron transmission microscope at the VNU University of Science, Vietnam National University, Hanoi. This equipment (operated at 200 kV with LaB_6 cathode) was combined with an S-TWIN objective, a windowless EDAX energy-dispersive X-ray system and a FEI Eagle 2k CCD TEM camera.

About 100 individual clay particles per sample were characterized by TEM-EDX with respect to crystal size, crystal habit, and particle morphology and element distribution. The crystal size, crystal habit and particle morphology were described according to Henning & Störr (1986).

For the quantification of element distribution, a calibration of k factors is mandatory (Cliff & Lorimer, 1975; Lorimer & Cliff, 1976; Mellini & Menichini, 1985). These k values are used to calibrate for the specific behaviour of particles against possible irradiation damage. The elements O, Na, Mg, Al, Si, K, Ca and Fe were quantified by applying the EDAX GENESIS–TEM Quant Materials quantification procedure.

In this procedure, the acquired EDX spectra are corrected by background subtraction, Gaussian deconvolution and k-factor corrections using values previously determined on a phyllosilicate standard (muscovite) and selected non-phyllosilicate standards. The average errors in the analyzed elements using the phyllosilicate standard, expressed as the atomic proportions, are 10 (Na), 5 (Fe, Mg, K, Ti, Ca) and 1 (Si, Al).

The measurement time per particle was lowered to 20 s and the exposed area was limited to a 50 nm diameter, avoiding possible irradiation damage of particles. The stability of particles of the sample series was tested for this measurement time at the beginning of any measurement campaign.

Further methodological details related to TEM-EDX-measurements and the Excel-based mathematical procedure using TEM-EDX data for calculation of mineral formulae are described in Hoang-Minh et al. (2019).

These mathematical procedures described in Hoang-Minh et al. (2019) were extended by k-means clustering method for finding subgroups of observations within a data set. The data were standardized (i.e., scaled) to make variables comparable. Euclidean distances were applied as classical method for distance measures. The optimal clusters were determined by Elbow method and Gap statistics[3].

---

[3] *https://uc-r.github.io/kmeans_clustering*

Data Sheet – B25 No4_T (< 2 µm), treated material *(OPA, 35°C, 93.6 hrs)*

Preparation for TEM

- raw material: compacted material (1.6 g/cm³) of treated B25-sample (OPA, 35°C, 93.6 hrs)
- suspension on particles < 2 µm on carbon-filmed Cu-grid
- air-dried and humidity-controlled storing

Mineral Matter

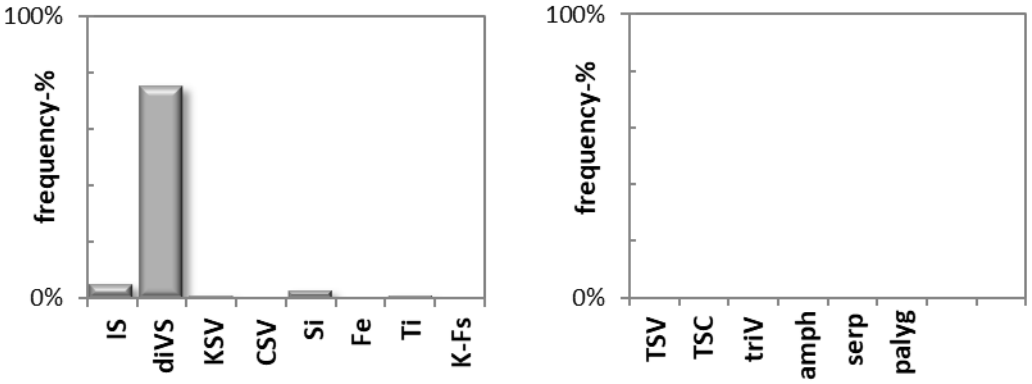

Fig. 1. *Distribution of mineral groups in fraction < 2 µm (in frequency-%)*
Legend: ***IS*** *– illite-smectite-mixed layer series in sense of Środon et al. (1992), diVS – dioctahedral vermiculite-smectite illite-smectite-mixed layer series (= charge- and/or K-deficit),* ***KSV*** *– kaolinite-smectite-dioctahedral vermiculite-mixed layer series,* ***CSV*** *– chlorite-saponite-trioctahedral vermiculite-mixed layer series,* ***Si*** *– quartz or particles with Si-surplus,* ***Fe*** *– Fe-oxide or Fe-oxyhydroxide,* ***Ti*** *– Ti-bearing phases (e.g. rutile, anatase),* ***K-Fs*** *– K-feldspar*

Clay Mineral Composition

All particles of smectite group:

$$Ca_{0.08}\ Mg_{0.11}\ Na_{0.01}\ K_{0.20}\quad Al_{1.01}\ Fe^{3+}_{0.89}\ Mg_{0.09}\ Ti_{0.01}\ (OH)_2\quad Si_{3.48}\ Al_{0.52}\ O_{10}$$

Charge: XII = 0.59 VI = 5.93 IV = 15.48 **Σ = 22.00**

Probability of smectite layers (%S): 26%

Probability of illite layers (%I): 74%

Specific Dissolution Potential (ΔS%)

for H2O, 20 + 60 rpm	-17	(= slow reacting, interlayer group: Ca+Mg (= type B))
for NaCl, 20 rpm	-18	(= slow reacting, interlayer group: Ca+Mg (= type B))
for NaCl, 60 rpm	-92	(= fast reacting, 'illitization', interlayer group: Na (= type A))
CEC$_{calc}$:	71 meq / 100 g	(literature: 56 meq / 100 g [Matschiavelli et al., 2019: MAT19])

Measured particles: 142

Table 1. *Summarized chemical composition*

SiO_2	TiO_2	Al_2O_3	Fe_2O_3	MnO	MgO	CaO	Na_2O	K_2O	P_2O_5	Σ	
65.8%	0.2%	25.6%	11.2%		2.9%	1.3%	0.6%	2.1%	0.1%	1.10	measured particles
58.6%	0.0%	22.0%	5.9%		3.0%	1.0%	0.1%	1.1%	0.1%	0.92	measured particles of original B25

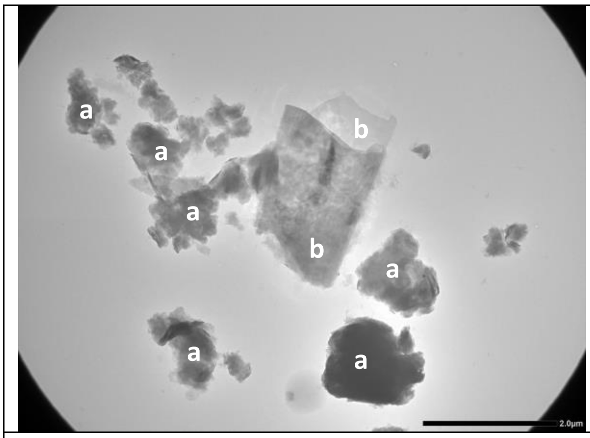	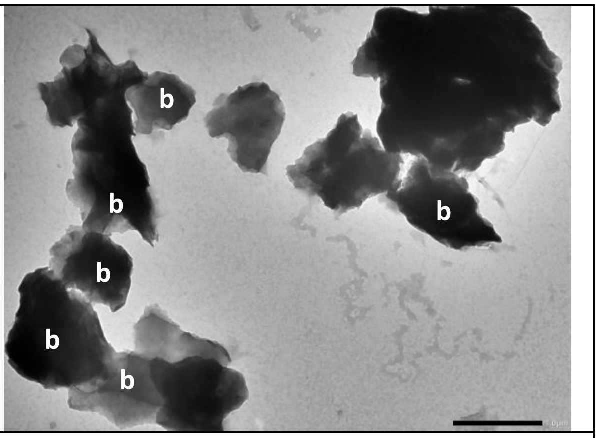
JEM-2100_MAG_X6000_005_AISZ_5ML.bmp Magnification: 6k (j) aggregates formed by small (≤ 200 nm) xenomorphous plates; (k) large (≤ 1 µm) xenomorph film-like platy crystals	*JEM-2100_MAG_X8000_003_AISZ_5ML.bmp* Magnification: 8k (a) (b) large (≤ 1 µm) xenomorph film-like platy crystals partially with folds

Fig. 2. *Morphology of particles (TEM-micrographs)*

Distribution of smectite layers probability (%S)

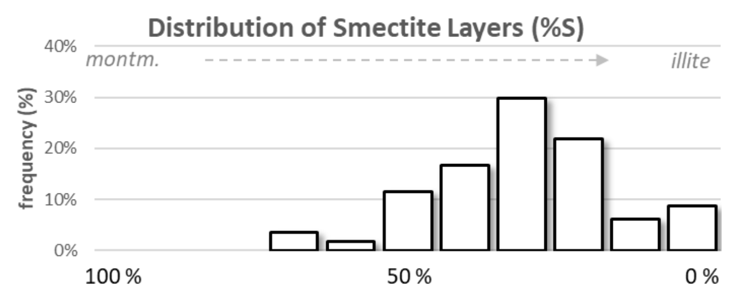

Description: *The distribution of %S-probability indicates the occurrence of two groups: (i) mixture of beidellite-montmorillonite interstratifications (= assumption) with diVS-ml as well as (ii) illite with K-deficiency.*

Fig. 3a. *Distribution of smectite layers probability (%S)*

Differentiation by relation "Octahedral Mg vs. tetrahedral Si"?

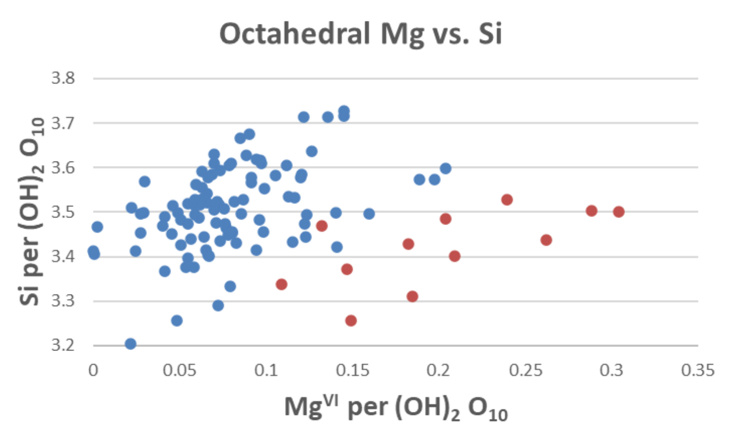

Description: *This diagram indicates the occurrence of two groups of Mg in relation to tetrahedral Si. Probably, this distribution mirrors 2 phases (I) beidellite-montmorillonite interstratifications (blue) and (II) diVS-ml (red)*

Fig. 3b. *Distribution of octahedral Mg vs. tetrahedral Si [all per(OH)$_2$ O$_{10}$]*

Distribution of K in relation to tetrahedral Si

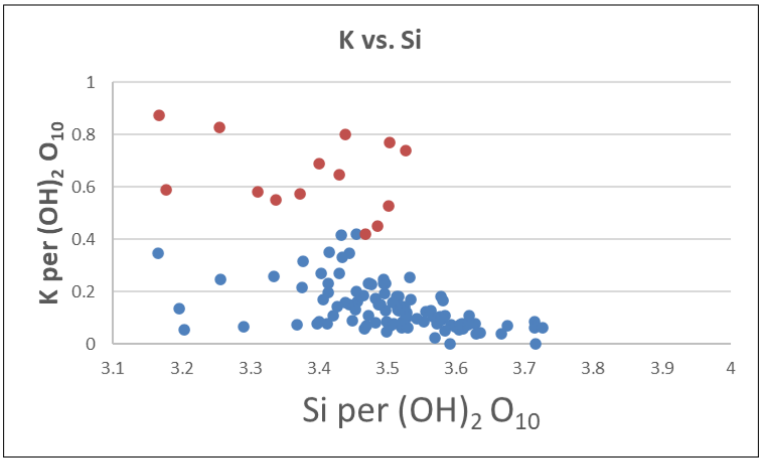

***Description:** This diagram visualizes possible particles (beidellite-montmorillonite interstratification?) with a very low K (blue dots)*

***Fig. 4.** Distribution of K in interlayer space vs. tetrahedral Si [all per$(OH)_2$ O_{10}]*

Distribution of charges (exchangeable from interlayer space)

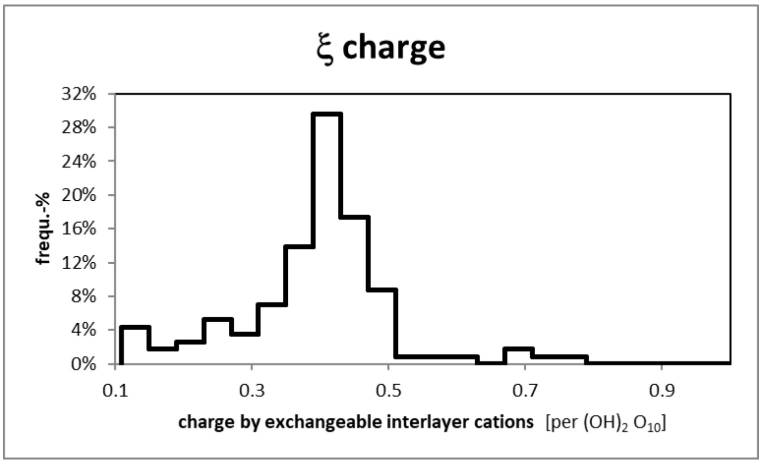

This diagram visualizes the distribution of exchangeable charges in the interlayer space (Ca, Mg, Na) determined and computed by TEM-EDX-data.

***Description:** Maximal frequency-% of charge density at 0.39 per $(OH)_2$ O_{10}. Generally, dominated by low exchangeable charges.*

***Fig. 5.** Distribution of charges*

***Beidellite** (Cluster1):*

$$Ca_{0.08}\,Mg_{0.12}\,Na_{0.01}\,K_{0.14}\quad Al_{1.00}\,Fe^{3+}_{0.92}\,Mg_{0.08}\,Ti_{0.01}\,(OH)_2\quad Si_{3.50}\,Al_{0.0}\,O_{10}$$

Charge: XII = 0.56 VI = 5.94 IV = 15.50 **Σ = 22.00**

Measured particles: 102

Distribution of BM-interstratifications (Cluster1)

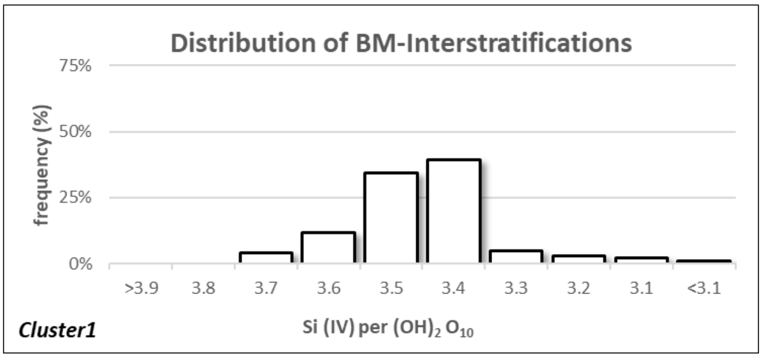

***Description:** The distribution of BM-interstratifications (classified as Cluster1) draws a maximum of frequency (%) at tetrahedral Si-value between 3.4 – 3.5 e phuc*

***Fig. 6a.** Distribution of assumed beidellite-montmorillonite interstratifications*

Beidellite?	*particles (abs)*	Ca (XII)	Mg (XII)	Na (XII)	K (XII)	Cr3+ (VI)	Al (VI)	Fe3+ (VI)	Mg (VI)	Ti (VI)	Al (IV)	Si (IV)	XII	n_VI	%S
Si >3.9	n = 0														
Si 3.9-3.8	n = 0														
Si 3.8-3.7	n = 4	0.09	0.10	0.00	0.05	0.00	1.15	0.72	0.14	0.00	0.28	3.72	0.42	2.0	57
Si 3.7-3.6	n = 12	0.08	0.11	0.00	0.06	0.00	1.04	0.86	0.09	0.01	0.37	3.63	0.46	2.0	44
Si 3.6-3.5	n = 35	0.08	0.11	0.01	0.11	0.00	1.01	0.91	0.08	0.01	0.45	3.55	0.51	2.0	33
Si 3.5-3.4	**n = 40**	**0.08**	**0.12**	**0.01**	**0.19**	**0.00**	**1.02**	**0.90**	**0.07**	**0.01**	**0.54**	**3.46**	**0.60**	**2.0**	**23**
Si 3.4-3.3	n = 5	0.08	0.13	0.01	0.19	0.00	0.91	0.97	0.06	0.06	0.63	3.37	0.63	2.0	15
Si 3.3-3.2	n = 3	0.10	0.23	0.00	0.12	0.00	0.68	1.25	0.05	0.03	0.75	3.25	0.77	2.0	6
Si 3.2-3.1	n = 2	0.09	0.21	0.00	0.24	0.00	0.57	1.33	0.06	0.04	0.82	3.18	0.84	2.0	2
Si <3.1	n = 1	0.05	0.33	0.00	0.23	0.00	0.43	1.48	0.08	0.00	0.91	3.09	0.99	2.0	-1

Fig. 6b. *Computed averaged mineral formulae of phases in the different Si(IV)-classes*

Dioctahedral Vermiculite-Smectite mixed layer phases (diVS-ml) *(Cluster2):*

$$Ca_{0.02}\ Mg_{0.02}\ Na_{0.06}\ K_{0.66}\quad Al_{1.17}\ Fe^{3+}_{0.64}\ Mg_{0.17}\ Ti_{0.02}\ (OH)_2\quad Si_{3.36}\ Al_{0.64}\ O_{10}$$

Charge: XII = 0.80 VI = 5.84 IV = 15.36 **Σ = 22.00**

Probability of smectite layers (%S): 15%

Probability of illite layers (%I): 85%

Measured particles: 15

Distribution of smectite layers probability (%S) in diVS-ml (Cluster2)

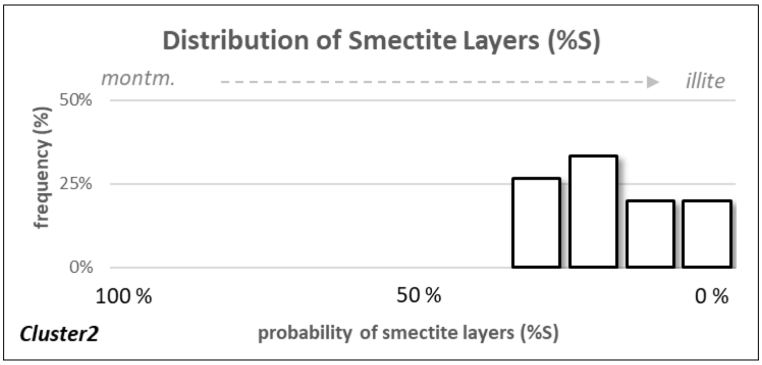

Description: *The distribution of diVS-ml (classified as Cluster2) draws a maximum of frequency (%) for smectite layer probability at 20%*

Fig. 7a. *Distribution of smectite layers probability in diVS-ml*

diVS-ml	*particles (abs)*	Ca (XII)	Mg (XII)	Na (XII)	K (XII)	Cr3+ (VI)	Al (VI)	Fe3+ (VI)	Mg (VI)	Ti (VI)	Al (IV)	Si (IV)	XII	n_VI	%S
%S >95%	n = 0														
%S 95-85%	n = 0														
%S 85-75%	n = 0														
%S 75-65%	n = 0														
%S 65-55%	n = 0														
%S 55-45%	n = 0														
%S 45-35%	n = 0														
%S 35-25%	n = 4	0.02	0.00	0.07	0.62	0.00	0.96	0.74	0.26	0.03	0.50	3.50	0.74	2.0	29
%S 25-15%	n = 5	0.04	0.01	0.03	0.63	0.00	1.22	0.59	0.19	0.01	0.58	3.42	0.76	2.0	20
%S <15%	n = 6	0.01	0.03	0.08	0.71	0.00	1.28	0.60	0.10	0.01	0.78	3.22	0.87	2.0	4

Fig. 7b. *Computed averaged mineral formulae of diVS-ml phases in the different smectite layers probability (%S)-classes*

Description – B25 No4_T (< 2 µm), treated material *(OPA, 35°C, 93.6 hrs)*

Preparation for TEM

The powder of compacted and treated B25-No4_T-sample was suspended in deionized water and dispersed by ultrasonic treatment for approximately 20 min. The clay fraction (<2 µm) was separated by sedimentation and diluted with deionized water to get a clear suspension. The suspension was dropped onto carbon-coated Cu grids, air dried and stored under environment-controlled conditions at 45% humidity.

Mineral Matter - Overview

The fraction < 2 µm of treated B25 bentonite sample (Opalinus Clay solution, at 35°C, for 93.6 hours) is mainly composed by beidellite (beid) and dioctahedral vermiculite-smectite mixed layer phases (diVS-ml) and accompanied by two types of illite. Furthermore, kaolinite and Si-surplus particles (Si, e.g. quartz) were identified in traces in this sample [fig. 1].

	frequency-% *(n = 142 measured particles)*
Beidellite (Cluster1)	72%
diVS-ml (Cluster2)	11%
Kaolinite & KSV-ml	1%
Si-surplus	3%
Ti-phases	1%
Unknown	15%

All measured clay mineral phases summarized result following mineral formula computed from TEM-EDX-measurement of 117 individual particles:

	$Ca^{2+}_{0.08}$	$Mg^{2+}_{0.11}$	$Na^{+}_{0.01}$	$K^{+}_{0.20}$	$Al^{3+}_{1.01}$	$Fe^{3+}_{0.89}$	$Mg^{2+}_{0.09}$	$Ti^{4+}_{0.01}$	$(OH)_2$	$Si^{4+}_{3.48}$	$Al^{3+}_{0.52}$	O_{10}
SDOM	*± 0.00*	*± 0.01*	*± 0.00*	*± 0.02*	*± 0.02*	*± 0.02*	*± 0.00*	*± 0.01*		*± 0.01*	*± 0.01*	

Legend: SDOM - standard deviation of the mean (= the standard deviation divided by the square root of the number of samples)

The interlayer charge is calculated as 0.59 per $(OH)_2$ O_{10} and the octahedral charge as 5.93 per $(OH)_2$ O_{10}. The particles are characterized by a high octahedral Fe-amount.

The summarized chemical composition of all 117 computed particles is compared with measured data of original B25-bentonite sample [tab. 1]. The chemical composition averaged by measured particles show especially a higher amount of SiO_2, Al_2O_3, Fe_2O_3 and K_2O in comparison to the measured data of original untreated B25-bentonite.

B25-No4_T sample is characterized by two morphological groups: (i) aggregates formed by small (≤ 200 nm) xenomorphous plates and (ii) large (≤ 1 µm) xenomorph film-like platy crystals partially with folds [fig. 2]. Thin aggregates formed by small (≤ 200 nm) xenomorphous plates dominate the shapes of particles in the micrographs [fig. 2].

The distribution of %S-probability of all measured clay mineral phases [fig. 3a] also indicates the occurrence of two groups: (i) as main group a mixture of beidellite-montmorillonite interstratifications and diVS-ml (%S-max of this mixture for %S at 30%) and (ii) illite with K- and charge deficit (%S-class = 0%).

The numerous measured particles by TEM-EDX allow a visualization of distribution of interlayer charges. Considering the TEM-EDX-determined cations Ca^{++}, Mg^{++} and Na^{+} and then computed their ratio as interlayer cations in the mineral formula, Ca^{++}, Mg^{++} and Na^{+} offer to characterize the degree of exchangeable charges in the interlayer space. This charge density of treated B25 bentonite (< 2 µm) shows only a narrow interval at the maximal frequency-% of charge density at 0.43 per $(OH)_2$ O_{10} [fig. 5]. This narrow interval of interlayer charge density caused by exchangeable cations from 0.35 - 0.50 per $(OH)_2$ O_{10} represents mainly the BM-phases. The measured diVS-ml phases offer only a strong reduced number of exchangeable cations at 0.10 – 0.30 per $(OH)_2$ O_{10} caused by the higher part of K.

Mineral Matter - Specification

Result of Clustering

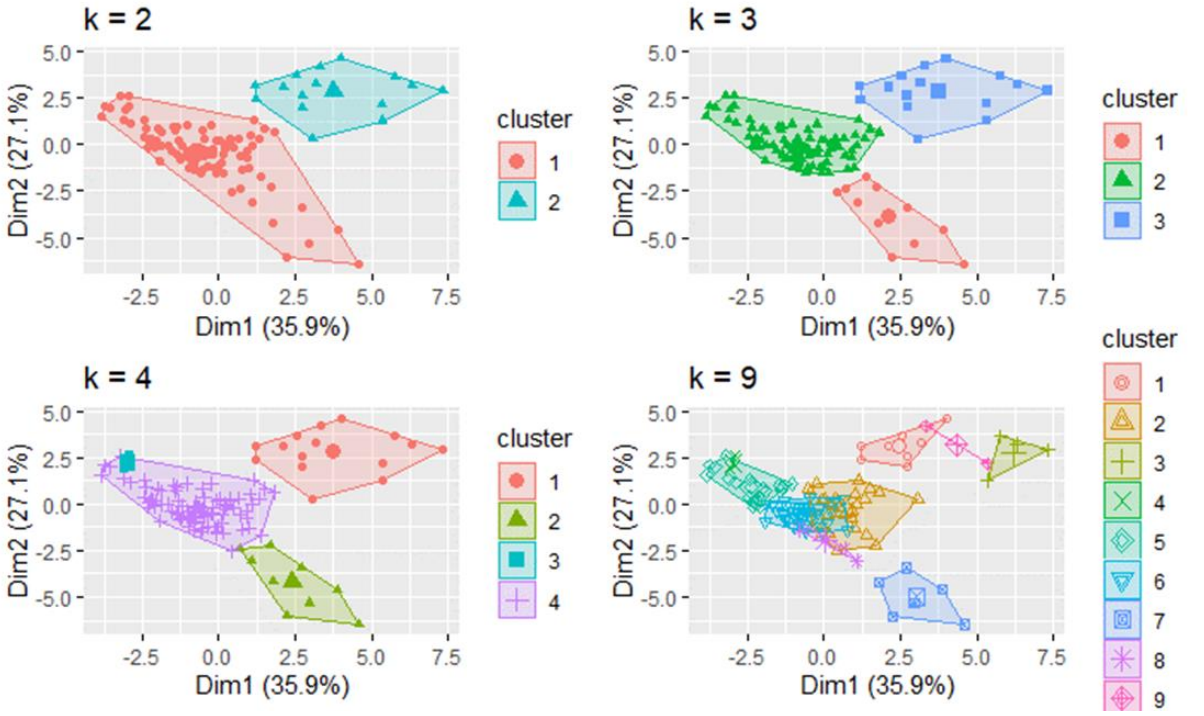

Fig. 8. *Clustering of all measured particles for clusters k = 2, k = 3, k = 4 and k = 5 (source for R-coding: https://uc-r.github.io/kmeans_clustering)*

The optimum of clusters was calculated with k = 2.

		Ca (XII)	Mg (XII)	Na (XII)	K (XII)	Cr3+ (VI)	Al (VI)	Fe3+ (VI)	Mg (VI)	Ti (VI)	Al (IV)	Si (IV)	XII	n_VI	%S
Cluster1	n = 102	0.08	0.12	0.01	0.14	0.00	1.00	0.92	0.08	0.01	0.50	3.50	0.56	2.0	28
Cluster2	n = 15	0.02	0.02	0.06	0.66	0.00	1.17	0.64	0.17	0.02	0.64	3.36	0.80	2.0	15

Fig. 9. *Mineral formulae based on TEM-EDX-data summarized following the result of clustering for k=2*

	Sybilla-results	**TEM-EDX-results**	**Notes**
Cluster1	IS R0(1) *(%S = 100%)*	Beidellite	*XRD: Montmorillonite and beidellite is only to distinguish by Green-Kelly-test (not available here).*
Cluster2	IS R0(2) *(%S = 30%)*	diVS-ml *(%S ~ 15%)*	*high K-deficit, Fe(VI)-rich*

Tab. 2. *Comparison of results from TEM-EDX- and XRD-measurements with clustering procedure*

The clustering of TEM-EDX-data offers a good agreement with the recent result of Sybilla-processing of XRD-traces from oriented specimen [tab. 2]. The higher part of illite particles is increasing the difference in %S between determined by Sybilla (XRD) and calculated by TEM-EDX-data.

IS R0 (1): The X-ray diffraction pattern of the ethylene-glycol saturated oriented specimen shows a full expandability to 1.71 nm and a difference of 5.40°2θ between 2. and 3. order of smectite interferences. This distance is typically for montmorillonite (Moore & Reynolds, 1989). This result of XRD-processing let expect a maximum of particles for %S ~ 100% by TEM-EDX-measurements, but the maximum of particles measured by TEM-EDX is to find at %S=30% [fig. 3a].

Montmorillonite and beidellite have the same behavior concerning the expandability and they are only to distinguish by XRD using Li like by Greene-Kelly test (Green-Kelly 1952, 1953). So, combination of XRD- and TEM-results (full expandability by XRD and Si ~ 3.50 by TEM-EDX) led conclude the occurrence of beidellite.

IS R0 (2): The Sybilla-procedure of XRD-traces (oriented mounts) has shown an occurrence of a second illite-smectite mixed layer phase with a smectite layers probability of %S = 30%. This situation is to find in Cluster2 ($\%S_{TEM}$ = 15%) representing a high K-amount and low charge deficient and very Fe-rich dioctahedral vermiculite-smectite mixed layer phase (diV-ml) [tab. 2]. The higher amount on illite particles [tab. 7b] is responsible for the difference in %S computed by Sybilla and by TEM-EDX-data.

The Sybilla-processing of XRD-traces (oriented mounts) also supports the existence of kaolinite and kaolinite-smectite mixed layer phases in fine fraction of sample. Such phases were not to identify or to calculate in TEM-EDX-database (a grain size effect?).

Specifics to the identified clay mineral groups

Beidellite

102 of 117 measured particles belong so to this assumed classification. The dioctahedral character of this group is proofed by X-ray diffraction. The position of the large (060)-interference of smectite is in the random oriented powder specimen at 1.497 Å.

Montmorillonite and beidellite have the same behavior concerning the expandability and they are only to distinguish by XRD using Li by means of Greene-Kelly test (Greene-Kelly 1952, 1953). So, combination of XRD- and TEM-results (full expandability by XRD and Si ~ 3.50 by TEM-EDX) led conclude the occurrence of beidellite.

Beidellite

$$Ca_{0.08}\,Mg_{0.12}\,Na_{0.01}\,K_{0.14}\quad Al_{1.00}\,Fe^{3+}_{0.92}\,Mg_{0.08}\,Ti_{0.01}\,(OH)_2\quad Si_{3.50}\,Al_{0.50}\,O_{10}$$

Charge:	XII = 0.56	VI = 5.94	IV = 15.50	**Σ = 22.00**
Measured particles by TEM-EDX:	102			
Result of clustering:	Cluster1 [tab. 2]			

In this sample, beidellite is characterized by a typical low octahedral Mg-amount (because of high ratio of octahedral, 3-valent cations). A comparison of octahedral Mg vs. tetrahedral Si indicates the occurrence of two groups for octahedral Mg based on TEM-EDX-data [fig. 3b].

Using the results of clustering (see Cluster1 in tab. 2), the maximum of frequency-% is to find for particles in the Si(IV)-class ~ 3.5 e phuc [tab. 6a], representing a beidellite. The mineral formulae, summarized in classes of tetrahedral Si, draw for the maximum an Fe-rich beidellite with low Mg(VI), but remarkable amount of K in the interlayer space [tab. 6b].

Dioctahedral vermiculite-smectite mixed layer phase (diVS-ml):

$$Ca_{0.02}\ Mg_{0.02}\ Na_{0.06}\ K_{0.66}\quad Al_{1.17}\ Fe^{3+}_{0.64}\ Mg_{0.17}\ Ti_{0.02}\ (OH)_2\quad Si_{3.36}\ Al_{0.64}\ O_{10}$$

Charge: XII = 0.80 VI = 5.84 IV = 15.36 **Σ = 22.00**

Probability of smectite layers (%S):	15%
Probability of illite layers (%I):	85%
Measured particles by TEM-EDX:	15
Result of clustering:	Cluster2 [tab. 2]

Illite as part of diVS-ml series

The Rietveld refinement by Profex software (Döbelin & Kleeberg, 2015) indicates the occurrence of two polytypes for illite in treated B25 bentonite: $2M_1$- and 1M-polytype.

Kaolinite-montmorillonite mixed layer phases

The Excel-based procedure (Hoang-Minh et al., 2019) to identify possible clay mineral groups using the TEM-EDX-measurements also includes algorithms to classify kaolinite and kaolinite-montmorillonite mixed layer phases. These algorithms couldn't identify such phases basing on the measured TEM-EDX-data. Otherwise, few particles, which were not to compute, have shown small hexagonal plates typically for kaolinite-bearing phases.

References

Cliff, G. & Lorimer, G. W. (1975). *J. Microsc.* **103**, 203–207.

Döbelin, N., Kleeberg, R. (2015). *Journal of Applied Crystallography* **48**, 1573-1580. DOI: 10.1107/S1600576715014685

Greene-Kelly, R., *Clay Minerals Bull.*, **1**, 221 (1952).

Greene-Kelly, R. 1953. The identification of montmorillonoids in clays. *Journal of Soil Science*. **4** (2), pp. 232-237. https://doi.org/10.1111/j.1365-2389.1953.tb00657.x

Greene-Kelly, R. (1955). Dehydration of the montmorillonite minerals. *Mineralogical Magazine and Journal of the Mineralogical Society*, **30**(228), 604-615. doi:10.1180/minmag.1955.030.228.06

Henning, K.-H. & Störr, M. (1986). Electron Micrographs (TEM, SEM) of Clays and Clay Minerals, p. 325. Akademie-Verlag Berlin.

Hoang-Minh, T., Kasbohm, J., Nguyen-Thanh, L., Nga, P. T., Lai, L. T., Duong, N. T., Thanh, N. D., Thuyet, N. T. M., Anh, D. D., Pusch, R., Knutsson, S. & Ferreiro Mahlmann, R. (2019). *J. Appl. Cryst.* **52**, 133-147. DOI: 10.1107/S1600576718018162

Lorimer, G. W. & Cliff, G. (1976). *Electron Microscopy in Mineralogy*, edited by H. R. Wenk, pp. 506–519. Berlin: Springer Verlag.

Matschiavelli, N., Kluge, S., Podlech, C., Standhaft, D., Grathoff, G., Ikeda-Ohno, A., Warr, L.N., Chukharkina, A., Arnold, T. & Cherkouk, A. (2019). *Environmental Science & Technology.* **53** (17), 10514-10524, DOI: 10.1021/acs.est.9b02670

Mellini, M. & Menichini, R. (1985). *R. Soc. Ital. Miner. Petrol.* **40**, 261–266.

Moore, D.M., Reynolds, R.C. (1989). X-ray Diffraction and the Identification and Analysis of Clay Minerals, Oxford University Press, New York, 332 + xvi pp.

Nguyen-Thanh, L., Herbert, H.-J., Kasbohm, J., Hoang-Minh, T. & Mählmann, R. F. (2014). *Clays Clay Miner.* **62**, 425–446.

Środoń, J., Elsass, F., McHardy, W. J. & Morgan, D. J. (1992). *Clay Miner.* **27**, 137–158.

Data Sheet – B25 bentonite, treated materials *(OPA, 100^C, 110h)* - CENTER

Methodology - Transmission electron microscopy linked with energy-dispersive X-ray spectroscopy (TEM-EDX)

It is expected a characterization of clay mineral phases in treated B25 bentonite by transmission electron microscopy. The sample series No4 represents a percolation of B25 bentonite by Opalinus Clay solution at 35°C for 93.6 hours. The sample No4_C is the label for the material at the center of sample cylinder.

The different clay mineral phases are to identify and to describe by chemical composition and its variability, morphology, the specific dissolution potential, and further parameter.

Such further parameter like distribution of smectite layers probability (%S) and distribution of charges caused by exchangeable cations interlayer space should serve as additional indicators for mineralogical alterations in treatment experiments with B25 bentonite.

The sample were suspended for TEM-measurement in deionized water and dispersed by ultrasonic treatment for approximately 20 min. The clay fraction (<2 µm) was separated by sedimentation and diluted with deionized water to get a clear suspension. The suspension was dropped onto carbon-coated Cu grids, air dried and stored under environment-controlled conditions at 45% humidity.

TEM-EDX investigations were carried out on the <2 µm fraction using a FEI TECNAI G^2 20 electron transmission microscope at the VNU University of Science, Vietnam National University, Hanoi. This equipment (operated at 200 kV with LaB_6 cathode) was combined with an S-TWIN objective, a windowless EDAX energy-dispersive X-ray system and a FEI Eagle 2k CCD TEM camera.

About 100 individual clay particles per sample were characterized by TEM-EDX with respect to crystal size, crystal habit, particle morphology and element distribution. The crystal size, crystal habit and particle morphology were described according to Henning & Störr (1986).

For the quantification of element distribution, a calibration of k factors is mandatory (Cliff & Lorimer, 1975; Lorimer & Cliff, 1976; Mellini & Menichini, 1985). These k values are used to calibrate for the specific behaviour of particles against possible irradiation damage. The elements O, Na, Mg, Al, Si, K, Ca and Fe were quantified by applying the EDAX GENESIS–TEM Quant Materials quantification procedure.

In this procedure, the acquired EDX spectra are corrected by background subtraction, Gaussian deconvolution and k-factor corrections using values previously determined on a phyllosilicate standard (muscovite) and selected non-phyllosilicate standards. The average errors in the analyzed elements using the phyllosilicate standard, expressed as the atomic proportions, are 10 (Na), 5 (Fe, Mg, K, Ti, Ca) and 1 (Si, Al).

The measurement time per particle was lowered to 20 s and the exposed area was limited to a 50 nm diameter, avoiding possible irradiation damage of particles. The stability of particles of the sample series was tested for this measurement time at the beginning of any measurement campaign.

Further methodological details related to TEM-EDX-measurements and the Excel-based mathematical procedure using TEM-EDX data for calculation of mineral formulae are described in Hoang-Minh et al. (2019).

These mathematical procedures described in Hoang-Minh et al. (2019) were extended by k-means clustering method for finding subgroups of observations within a data set. The data were standardized (i.e., scaled) to make variables comparable. Euclidean distances were applied as classical method for distance measures. The optimal clusters were determined by Elbow method and Gap statistics[4].

---

[4] *https://uc-r.github.io/kmeans_clustering*

Data Sheet – B25 No4_C (< 2 µm), treated material *(OPA, 35°C, 93.6 hrs)*

Preparation for TEM

- raw material: compacted material (1.6 g/cm³) of treated B25-sample (OPA, 35°C, 93.6 hrs)
- suspension on particles < 2 µm on carbon-filmed Cu-grid
- air-dried and humidity-controlled storing

Mineral Matter

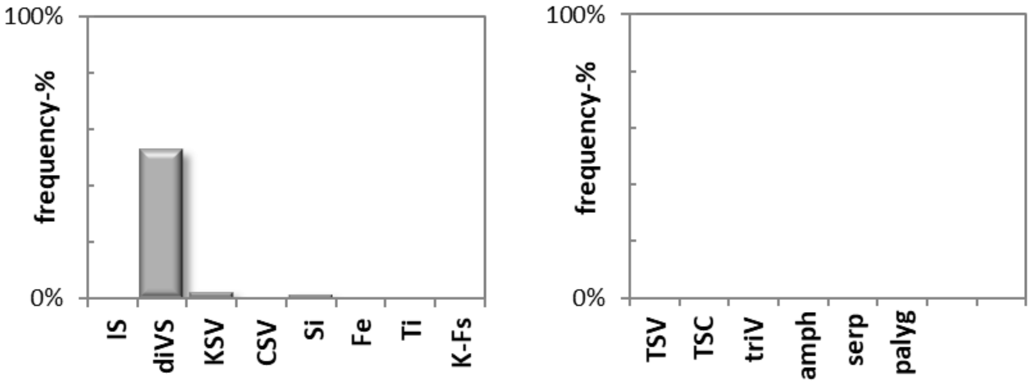

Fig. 1. *Distribution of mineral groups in fraction < 2 µm (in frequency-%)*
*Legend: **IS** – illite-smectite-mixed layer series in sense of Środon et al. (1992), diVS – dioctahedral vermiculite-smectite illite-smectite-mixed layer series (= charge- and/or K-deficit), **KSV** – kaolinite-smectite-dioctahedral vermiculite-mixed layer series, **CSV** – chlorite-saponite-trioctahedral vermiculite-mixed layer series, **Si** – quartz or particles with Si-surplus, **Fe** – Fe-oxide or Fe-oxyhydroxide, **Ti** – Ti-bearing phases (e.g. rutile, anatase), **K-Fs** – K-feldspar*

Clay Mineral Composition

All particles of smectite group:

$$Ca_{0.14}\ Mg_{0.06}\ Na_{0.18}\ K_{0.32}\quad Al_{0.84}\ Fe^{3+}_{0.82}\ Mg_{0.33}\ Ti_{0.01}\ (OH)_2\quad Si_{3.43}\ Al_{0.57}\ O_{10}$$

Charge: XII = 0.89 VI = 5.68 IV = 15.43 **Σ = 22.00**
Probability of smectite layers (%S): 21%
Probability of illite layers (%I): 79%

Specific Dissolution Potential (ΔS%)

for H2O, 20 + 60 rpm -61 (= fast reacting, interlayer group: Ca+Mg (= type B))
for NaCl, 20 rpm -68 (= fast reacting, interlayer group: Ca+Mg (= type B))
for NaCl, 60 rpm -24 (= fast reacting, 'illitization', interlayer group: Na (= type A))
CEC$_{calc}$: 297 meq / 100 g (literature: 56 meq / 100 g [Matschiavelli et al., 2019: MAT19])

Measured particles: 142

Table 1. *Summarized chemical composition*

SiO_2	TiO_2	Al_2O_3	Fe_2O_3	MnO	MgO	CaO	Na_2O	K_2O	P_2O_5	Σ	
54.9%	0.2%	20.0%	8.9%		4.6%	9.3%	1.8%	2.9%	0.8%	1.03	measured particles
58.6%	0.0%	22.0%	5.9%		3.0%	1.0%	0.1%	1.1%	0.1%	0.92	measured particles of original B25

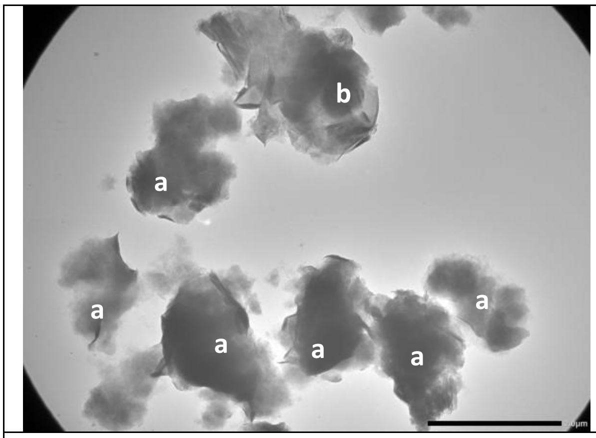	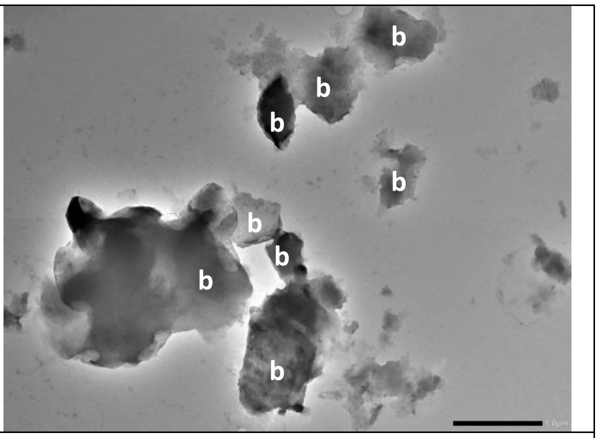
JEM-2100_MAG_X6000_017_AISZ_5ML.bmp Magnification: 6k (l) Aggregates, partially with folds, formed by small (≤ 200 nm) xenomorphous plates; (m) large (≤ 1 µm) xenomorph film-like platy crystals	*JEM-2100_MAG_X8000_001_AISZ_5ML.bmp* Magnification: 8k (c) (d) large (≤ 1 µm) xenomorph film-like platy crystals

Fig. 2. *Morphology of particles (TEM-micrographs)*

Distribution of smectite layers probability (%S)

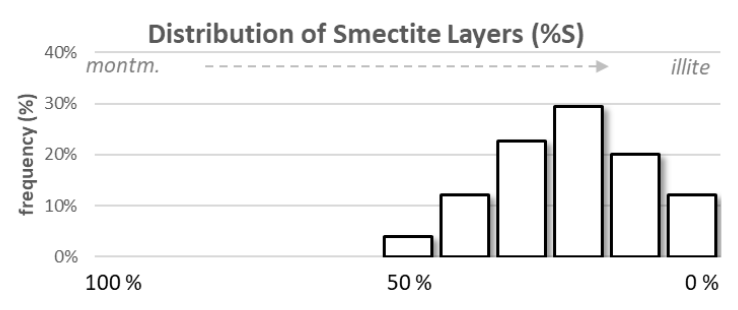

Description: *The distribution of %S-probability indicates the occurrence of two groups: (i) mixture of beidellite-montmorillonite interstratifications (= assumption) with diVS-ml as well as (ii) illite with K-deficiency.*

Fig. 3a. *Distribution of smectite layers probability (%S)*

Differentiation by relation “Octahedral Mg vs. tetrahedral Si”?

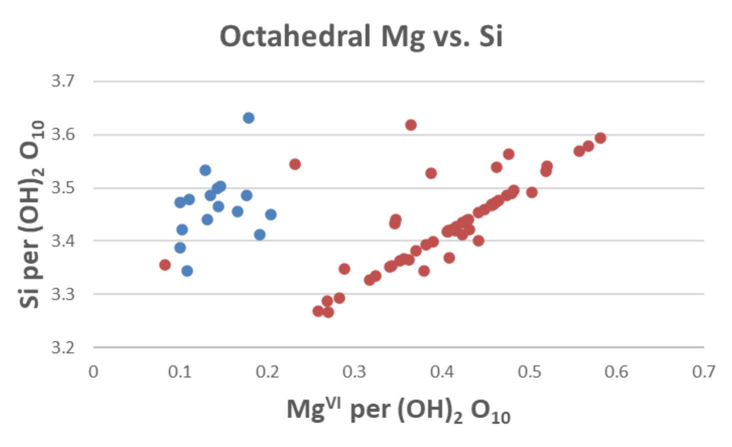

Description: *This diagram indicates the occurrence of two groups of Mg in relation to tetrahedral Si. Probably, this distribution mirrors 2 phases (I) beidellite-montmorillonite interstratifications (blue) and (II) diVS-ml (red)*

Fig. 3b. *Distribution of octahedral Mg vs. tetrahedral Si [all per(OH)$_2$ O$_{10}$]*

Distribution of K in relation to tetrahedral Si

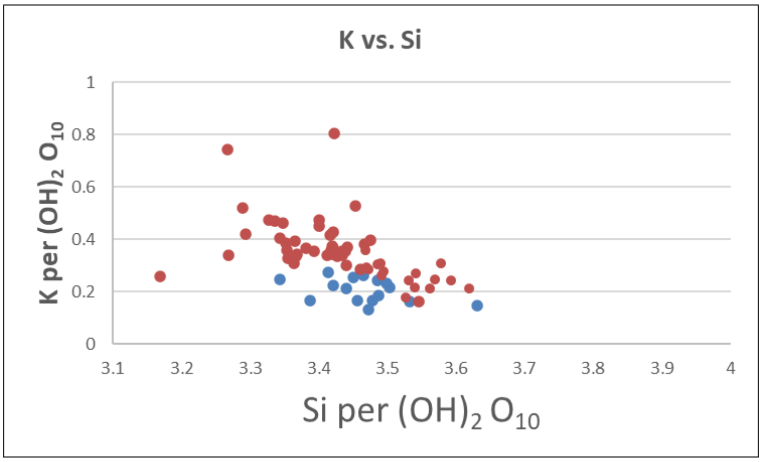

***Description:** This diagram visualizes possible particles (beidellite-montmorillonite interstratification?) with low K (blue dots)*

***Fig. 4.** Distribution of K in interlayer space vs. tetrahedral Si [all per $(OH)_2\ O_{10}$]*

Distribution of charges (exchangeable from interlayer space)

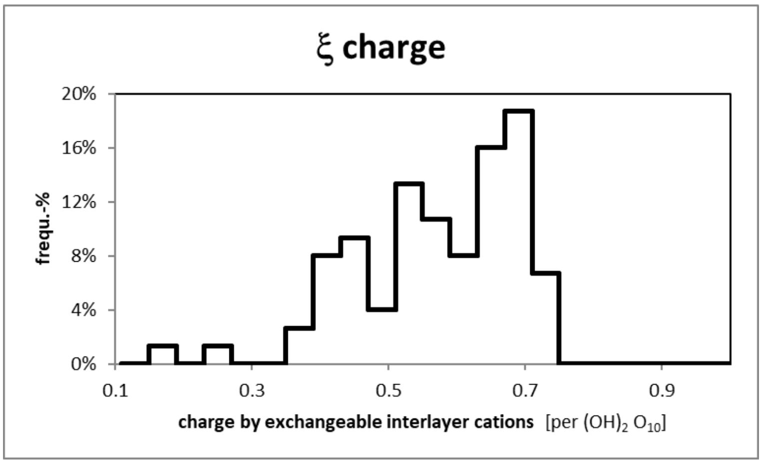

***Fig. 5.** Distribution of charges*

This diagram visualizes the distribution of exchangeable charges in the interlayer space (Ca, Mg, Na) determined and computed by TEM-EDX-data.

***Description:** Maximal frequency-% of broad charge density at 0.71 per $(OH)_2\ O_{10}$. Generally, dominated by high exchangeable charges.*

***Beidellite** (Cluster2):*

$$Ca_{0.14}\ Mg_{0.06}\ Na_{0.05}\ K_{0.21}\quad Al_{0.94}\ Fe^{3+}_{0.91}\ Mg_{0.14}\ Ti_{0.01}\ (OH)_2\quad Si_{3.47}\ Al_{0.53}\ O_{10}$$

Charge: XII = 0.66 VI = 5.87 IV = 15.47 **Σ = 22.00**

Measured particles: 16

Distribution of BM-interstratifications (Cluster2)

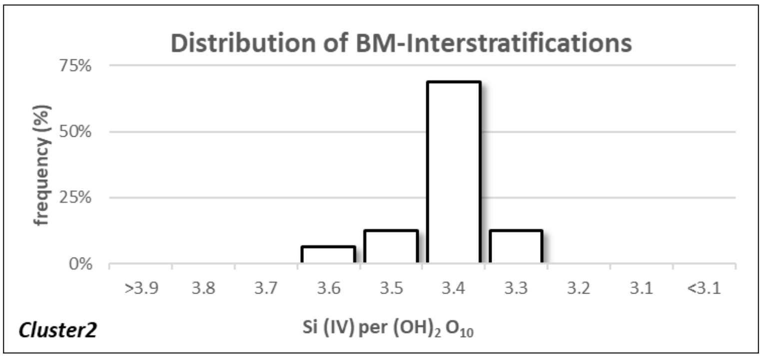

Description: *The distribution of BM-interstratifications (classified as Cluster2) draws a maximum of frequency (%) at tetrahedral Si-value between 3.4 – 3.5 e phuc*

Fig. 6a. *Distribution of assumed beidellite-montmorillonite interstratifications*

Beidellite?	*particles (abs)*	**Ca (XII)**	**Mg (XII)**	**Na (XII)**	**K (XII)**	**Cr3+ (VI)**	**Al (VI)**	**Fe3+ (VI)**	**Mg (VI)**	**Ti (VI)**	**Al (IV)**	**Si (IV)**	**XII**	**n_VI**	**%S**
Si >3.9	n = 0														
Si 3.9-3.8	n = 0														
Si 3.8-3.7	n = 0														
Si 3.7-3.6	n = 1	0.12	0.06	0.04	0.15	0.00	1.01	0.81	0.18	0.00	0.37	3.63	0.55	2.0	44
Si 3.6-3.5	n = 2	0.11	0.07	0.05	0.19	0.00	0.91	0.92	0.14	0.03	0.48	3.52	0.59	2.0	30
Si 3.5-3.4	**n = 11**	**0.15**	**0.06**	**0.05**	**0.21**	**0.00**	**0.92**	**0.92**	**0.15**	**0.01**	**0.54**	**3.46**	**0.67**	**2.0**	**24**
Si 3.4-3.3	n = 2	0.13	0.11	0.05	0.21	0.00	1.02	0.87	0.10	0.01	0.63	3.37	0.73	2.0	15
Si 3.3-3.2	n = 0														
Si 3.2-3.1	n = 0														
Si <3.1	n = 0														

Fig. 6b. *Computed averaged mineral formulae of phases in the different Si(IV)-classes*

Dioctahedral Vermiculite-Smectite mixed layer phases (diVS-ml) *(Cluster1,3,4,6,7,8):*

$$Ca_{0.13}\ Mg_{0.05}\ Na_{0.23}\ K_{0.36}\quad Al_{0.81}\ Fe^{3+}_{0.79}\ Mg_{0.39}\ Ti_{0.01}\ (OH)_2\ \ Si_{3.42}\ Al_{0.58}\ O_{10}$$

Charge: XII = 0.96 VI = 5.62 IV = 15.42 **Σ = 22.00**

Probability of smectite layers (%S): 19%

Probability of illite layers (%I): 81%

Measured particles: 58

Distribution of smectite layers probability (%S) in diVS-ml (Cluster1,3,4,6,7,8)

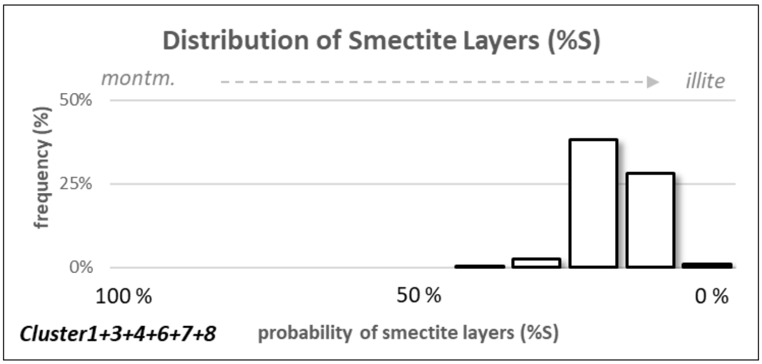

Description: *The distribution of diVS-ml (classified as Clusters 1,3,4,6,7,8) draws a maximum of frequency (%) for smectite layer probability at 20%*

Fig. 7a. *Distribution of smectite layers probability in diVS-ml*

diVS-ml	*particles (abs)*	**Ca (XII)**	**Mg (XII)**	**Na (XII)**	**K (XII)**	**Cr3+ (VI)**	**Al (VI)**	**Fe3+ (VI)**	**Mg (VI)**	**Ti (VI)**	**Al (IV)**	**Si (IV)**	**XII**	**n_VI**	**%S**
%S >95%	n = 0														
%S 95-85%	n = 0														
%S 85-75%	n = 0														
%S 75-65%	n = 0														
%S 65-55%	n = 0														
%S 55-45%	n = 0														
%S 45-35%	n = 4	0.17	0.03	0.31	0.25	0.00	0.84	0.61	0.55	0.00	0.42	3.58	0.97	2.0	37
%S 35-25%	n = 9	0.15	0.05	0.29	0.27	0.00	0.79	0.73	0.48	0.00	0.49	3.51	0.97	2.0	29
%S 25-15%	n = 25	0.11	0.06	0.24	0.39	0.00	0.76	0.82	0.41	0.01	0.57	3.43	0.97	2.0	20
%S <15%	n = 18	0.14	0.06	0.18	0.39	0.00	0.84	0.85	0.30	0.02	0.69	3.31	0.97	2.0	10

Fig. 7b. *Computed averaged mineral formulae of diVS-ml phases in the different smectite layers probability (%S)-classes*

Description – B25 No4_C (< 2 µm), treated material *(OPA, 35°C, 93.6 hrs)*

Preparation for TEM

The powder of compacted and treated B25-No4_C-sample was suspended in deionized water and dispersed by ultrasonic treatment for approximately 20 min. The clay fraction (<2 µm) was separated by sedimentation and diluted with deionized water to get a clear suspension. The suspension was dropped onto carbon-coated Cu grids, air dried and stored under environment-controlled conditions at 45% humidity.

Mineral Matter - Overview

The fraction < 2 µm of treated B25 bentonite sample (Opalinus Clay solution, at 35°C, for 93.6 hours) is mainly composed by beidellite (beid) and dioctahedral vermiculite-smectite mixed layer phases (diVS-ml) and accompanied by two types of illite. Furthermore, kaolinite and Si-surplus particles (Si, e.g. quartz) were identified in traces in this sample [fig. 1].

The mineral formula couldn't be computed for nearby the half of measured particles. These particles have shown an overload of adsorbed Ca and Na mirrored also by a very high calculated CEC-value for all computed particles (297 meq / 100 g located at surface and in the interlayer space).

	frequency-% *(n = 142 measured particles)*
Beidellite (Cluster2)	12%
diVS-ml (Cluster1,3,4,6,7,8)	41%
Kaolinite & KSV-ml	2%
Si-surplus	1%
Unknown	44%

All measured clay mineral phases summarized result following mineral formula computed from TEM-EDX-measurement of 76 individual particles:

	$Ca^{2+}_{0.14}$	$Mg^{2+}_{0.06}$	$Na^{+}_{0.18}$	$K^{+}_{0.32}$	$Al^{3+}_{0.84}$	$Fe^{3+}_{0.82}$	$Mg^{2+}_{0.33}$	$Ti^{4+}_{0.01}$	$(OH)_2$	$Si^{4+}_{3.43}$	$Al^{3+}_{0.57}$	O_{10}
SDOM	*± 0.01*	*± 0.01*	*± 0.01*	*± 0.01*	*± 0.02*	*± 0.02*	*± 0.02*	*± 0.00*		*± 0.01*	*± 0.01*	

Legend: SDOM - standard deviation of the mean (= the standard deviation divided by the square root of the number of samples)

The interlayer charge is calculated as 0.88 per $(OH)_2$ O_{10} and the octahedral charge as 5.68 per $(OH)_2$ O_{10}. The particles are characterized by a high octahedral Fe-amount.

The summarized chemical composition of all 76 computed particles is compared with measured data of original B25-bentonite sample [tab. 1]. The chemical composition averaged by measured particles show a lower amount of SiO_2 and Al_2O_3, a higher amount for Fe_2O_3, MgO and K_2O as well as a remarkable higher amount for CaO and Na_2O in comparison to the measured data of original untreated B25-bentonite.

B25-No4_C sample is characterized by two morphological groups: (i) aggregates formed by small (≤ 200 nm) xenomorphous plates (partially with folds) and (ii) large (≤ 1 µm) xenomorph film-like platy crystals [fig. 2]. Aggregates formed by large (≤ 1 µm) xenomorphous plates dominate the shapes of particles in the micrographs [fig. 2].

The distribution of %S-probability of all measured clay mineral phases [fig. 3a] also indicates the occurrence of two groups: (i) as main group a mixture of beidellite-montmorillonite interstratifications and diVS-ml (%S-max of this mixture for %S at 20%) and (ii) illite with K- and charge deficit (%S-class = 0%).

The numerous measured particles by TEM-EDX allow a visualization of distribution of interlayer charges. Considering the TEM-EDX-determined cations Ca^{++}, Mg^{++} and Na^{+} and then computed their ratio as interlayer cations in the mineral formula, Ca^{++}, Mg^{++} and Na^{+} offer to characterize the degree of exchangeable charges in the interlayer space. This charge density of treated B25 bentonite (< 2 µm) shows in this sample a very broad interval with three maximal frequency-% of charge density at 0.47, 0.55 and 0.71 per $(OH)_2$ O_{10} [fig. 5]. This broad interval of interlayer charge density caused by exchangeable cations from 0.35 - 0.75 per $(OH)_2$ O_{10} represents mainly beidellite (lowest peak at 0.47 per $(OH)_2$ O_{10}) and the diVS-ml phases with the other two higher peaks. The measured diVS-ml phases offer two groups of higher non-exchangeable K in the interlayer space.

Mineral Matter - Specification

Result of Clustering

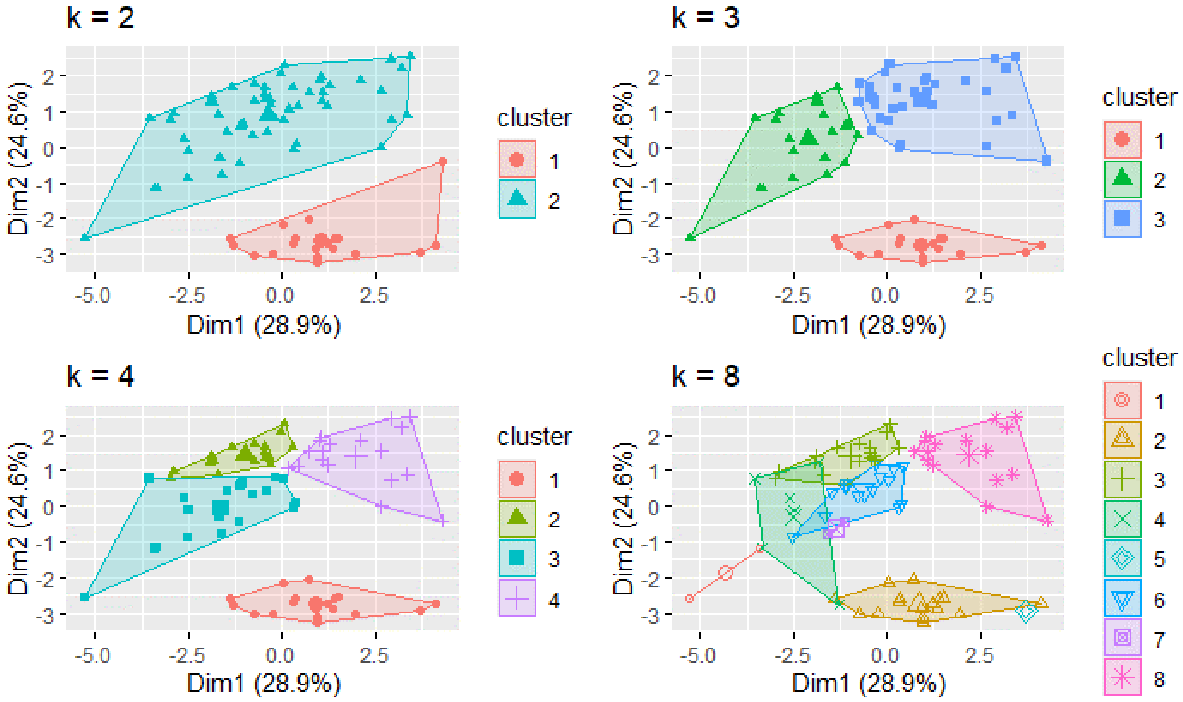

Fig. 8. *Clustering of all measured particles for clusters k = 2, k = 3, k = 4 and k = 5 (source for R-coding: https://uc-r.github.io/kmeans_clustering)*

The optimum of clusters was calculated with k = 8.

		Ca (XII)	Mg (XII)	Na (XII)	K (XII)	Cr3+ (VI)	Al (VI)	Fe3+ (VI)	Mg (VI)	Ti (VI)	Al (IV)	Si (IV)	XII	n_VI	%S
Cluster1	n = 2	0.15	0.14	0.07	0.28	0.00	0.56	1.30	0.14	0.00	0.79	3.21	0.94	2.0	4
Cluster2	n = 16	0.14	0.06	0.05	0.21	0.00	0.94	0.91	0.14	0.01	0.53	3.47	0.66	2.0	24
Cluster3	n = 17	0.06	0.10	0.27	0.39	0.00	0.76	0.83	0.40	0.00	0.59	3.41	0.99	2.0	19
Cluster4	n = 6	0.09	0.06	0.12	0.51	0.00	1.18	0.56	0.25	0.02	0.70	3.30	0.93	2.0	9
Cluster5	n = 1	0.26	0.00	0.05	0.16	0.00	0.84	0.88	0.23	0.02	0.45	3.55	0.73	2.0	33
Cluster6	n = 15	0.19	0.02	0.19	0.36	0.00	0.75	0.86	0.37	0.01	0.61	3.39	0.97	2.0	17
Cluster7	n = 2	0.16	0.00	0.17	0.35	0.00	0.70	0.78	0.35	0.16	0.65	3.35	0.84	2.0	13
Cluster8	n = 16	0.17	0.03	0.28	0.26	0.00	0.81	0.71	0.48	0.00	0.47	3.53	0.95	2.0	31

Fig. 9. *Mineral formulae based on TEM-EDX-data summarized following the result of clustering for k=8*

	Sybilla-results	**TEM-EDX-results**	**Notes**
Clusters 1, 4 & 7	Illite	diVS-ml (illite)	*K-deficit, low Al(VI), Fe(VI)-rich, Mg(VI) variable*
Clusters 2 & 5	IS R0(1) *(%S = 100%)*	Beidellite	*XRD: Montmorillonite and beidellite is only to distinguish by Green-Kelly-test (not available here).*
Clusters 3, 6 & 8	IS R0(2) *(%S = 38%)*	diVS-ml *(%S ~ 25%)*	*K-deficit, Fe(VI)-rich, Mg(VI)-rich*

Tab. 2. *Comparison of results from TEM-EDX- and XRD-measurements with clustering procedure*

The clustering of TEM-EDX-data offers an relative agreement with the recent result of Sybilla-processing of XRD-traces from oriented specimen [tab. 2]. The higher part of unknown particles (because of overload of Ca and Na) is increasing the difference in %S between determined by Sybilla (XRD) and calculated by TEM-EDX-data.

IS R0 (1): The X-ray diffraction pattern of the ethylene-glycol saturated oriented specimen shows a full expandability to 1.75 nm and a difference of 5.36°2θ between 2. and 3. order of smectite interferences. This distance is typically for montmorillonite (Moore & Reynolds, 1989). This result of XRD-processing let expect a maximum of particles for %S ~ 100% by TEM-EDX-measurements, but the maximum of particles measured by TEM-EDX is to find at %S=20% [fig. 3a].

Montmorillonite and beidellite have the same behavior concerning the expandability and they are only to distinguish by XRD using Li like by Greene-Kelly test (Green-Kelly 1952, 1953). So, combination of XRD- and TEM-results (full expandability by XRD and Si ~ 3.47 by TEM-EDX) led conclude the occurrence of beidellite.

IS R0 (2): The Sybilla-procedure of XRD-traces (oriented mounts) has shown an occurrence of a second illite-smectite mixed layer phase with a smectite layers probability of %S = 38%. This situation is to find in Clusters 3,6 & 8 ($\%S_{TEM}$ = 25%) representing high K- & Na amounts and low charge deficient and very Fe-rich dioctahedral vermiculite-smectite mixed layer phase (diV-ml) [tab. 2]. The higher amount on unknown particles is responsible for the difference in %S computed by Sybilla and by TEM-EDX-data.

The Sybilla-processing of XRD-traces (oriented mounts) also supports the existence of kaolinite and kaolinite-smectite mixed layer phases in fine fraction of sample. Such phases were not to identify or to calculate in TEM-EDX-database (a grain size effect?).

Specifics to the identified clay mineral groups

Beidellite

17 of 58 computed particles belong so to this assumed classification. The dioctahedral character of this group is proofed by X-ray diffraction. The position of the large (060)-interference of smectite is in the random oriented powder specimen at 1.497 Å.

Montmorillonite and beidellite have the same behavior concerning the expandability and they are only to distinguish by XRD using Li by means of Greene-Kelly test (Greene-Kelly 1952, 1953). So, combination of XRD- and TEM-results (full expandability by XRD and Si ~ 3.47 by TEM-EDX) led conclude the occurrence of beidellite.

Beidellite

$$Ca_{0.14}\ Mg_{0.06}\ Na_{0.05}\ K_{0.21}\quad Al_{0.94}\ Fe^{3+}_{0.91}\ Mg_{0.14}\ Ti_{0.01}\ (OH)_2\quad Si_{3.47}\ Al_{0.53}\ O_{10}$$

Charge: XII = 0.66 VI = 5.87 IV = 15.47 **Σ = 22.00**
Measured particles by TEM-EDX: 16
Result of clustering: Cluster2 [tab. 2]

In this sample, beidellite is characterized by a typical low octahedral Mg-amount (because of high ratio of octahedral, 3-valent cations). A comparison of octahedral Mg vs. tetrahedral Si indicates the occurrence of two groups for octahedral Mg based on TEM-EDX-data [fig. 3b].

Using the results of clustering (see Cluster2 in tab. 2), the maximum of frequency-% is to find for particles in the Si(IV)-class ~ 3.5 - 3.5 e phuc [tab. 6a], representing a beidellite. The mineral formulae, summarized in classes of tetrahedral Si, draw for the maximum an Fe-rich beidellite with low Mg(VI), but remarkable amount of K in the interlayer space [tab. 6b].

Dioctahedral vermiculite-smectite mixed layer phase (diVS-ml):

$$Ca_{0.13}\ Mg_{0.05}\ Na_{0.23}\ K_{0.36}\quad Al_{0.81}\ Fe^{3+}_{0.79}\ Mg_{0.39}\ Ti_{0.01}\ (OH)_2\quad Si_{3.42}\ Al_{0.58}\ O_{10}$$

Charge: XII = 0.96 VI = 5.62 IV = 15.42 **Σ = 22.00**
Probability of smectite layers (%S): 19%
Probability of illite layers (%I): 81%
Measured particles by TEM-EDX: 58
Result of clustering: Cluster 1, 3, 4, 6, 7, 8 [tab. 2]

Illite as part of diVS-ml series

The Rietveld refinement by Profex software (Döbelin & Kleeberg, 2015) indicates the occurrence of two polytypes for illite in treated B25 bentonite: $2M_1$- and 1M-polytype.

Kaolinite-montmorillonite mixed layer phases

The Excel-based procedure (Hoang-Minh et al., 2019) to identify possible clay mineral groups using the TEM-EDX-measurements also includes algorithms to classify kaolinite and kaolinite-montmorillonite mixed layer phases. These algorithms couldn't identify such phases basing on the measured TEM-EDX-data. Otherwise, few particles, which were not to compute, have shown small hexagonal plates typically for kaolinite-bearing phases.

References

Cliff, G. & Lorimer, G. W. (1975). *J. Microsc.* **103**, 203–207.

Döbelin, N., Kleeberg, R. (2015). *Journal of Applied Crystallography* **48**, 1573-1580. DOI: 10.1107/S1600576715014685

Greene-Kelly, R., *Clay Minerals Bull.*, **1**, 221 (1952).

Greene-Kelly, R. 1953. The identification of montmorillonoids in clays. *Journal of Soil Science*. **4** (2), pp. 232-237. https://doi.org/10.1111/j.1365-2389.1953.tb00657.x

Greene-Kelly, R. (1955). Dehydration of the montmorillonite minerals. *Mineralogical Magazine and Journal of the Mineralogical Society*, **30**(228), 604-615. doi:10.1180/minmag.1955.030.228.06

Henning, K.-H. & Störr, M. (1986). Electron Micrographs (TEM, SEM) of Clays and Clay Minerals, p. 325. Akademie-Verlag Berlin.

Hoang-Minh, T., Kasbohm, J., Nguyen-Thanh, L., Nga, P. T., Lai, L. T., Duong, N. T., Thanh, N. D., Thuyet, N. T. M., Anh, D. D., Pusch, R., Knutsson, S. & Ferreiro Mahlmann, R. (2019). *J. Appl. Cryst.* **52**, 133-147. DOI: 10.1107/S1600576718018162

Lorimer, G. W. & Cliff, G. (1976). *Electron Microscopy in Mineralogy*, edited by H. R. Wenk, pp. 506–519. Berlin: Springer Verlag.

Matschiavelli, N., Kluge, S., Podlech, C., Standhaft, D., Grathoff, G., Ikeda-Ohno, A., Warr, L.N., Chukharkina, A., Arnold, T. & Cherkouk, A. (2019). *Environmental Science & Technology.* **53** (17), 10514-10524, DOI: 10.1021/acs.est.9b02670

Mellini, M. & Menichini, R. (1985). *R. Soc. Ital. Miner. Petrol.* **40**, 261–266.

Moore, D.M., Reynolds, R.C. (1989). X-ray Diffraction and the Identification and Analysis of Clay Minerals, Oxford University Press, New York, 332 + xvi pp.

Nguyen-Thanh, L., Herbert, H.-J., Kasbohm, J., Hoang-Minh, T. & Mählmann, R. F. (2014). *Clays Clay Miner.* **62**, 425–446.

Środoń, J., Elsass, F., McHardy, W. J. & Morgan, D. J. (1992). *Clay Miner.* **27**, 137–158.

Data Sheet – B25 bentonite, treated materials *(OPA, 100^C, 110h)* - BOTTOM

Methodology - Transmission electron microscopy linked with energy-dispersive X-ray spectroscopy (TEM-EDX)

It is expected a characterization of clay mineral phases in treated B25 bentonite by transmission electron microscopy. The sample series No4 represents a percolation of B25 bentonite by Opalinus Clay solution at 35°C for 93.6 hours. The sample No4_B is the label for the material at the bottom of sample cylinder.

The different clay mineral phases are to identify and to describe by chemical composition and its variability, morphology, the specific dissolution potential, and further parameter.

Such further parameter like distribution of smectite layers probability (%S) and distribution of charges caused by exchangeable cations interlayer space should serve as additional indicators for mineralogical alterations in treatment experiments with B25 bentonite.

The sample were suspended for TEM-measurement in deionized water and dispersed by ultrasonic treatment for approximately 20 min. The clay fraction (<2 µm) was separated by sedimentation and diluted with deionized water to get a clear suspension. The suspension was dropped onto carbon-coated Cu grids, air dried and stored under environment-controlled conditions at 45% humidity.

TEM-EDX investigations were carried out on the <2 µm fraction using a FEI TECNAI G^2 20 electron transmission microscope at the VNU University of Science, Vietnam National University, Hanoi. This equipment (operated at 200 kV with LaB_6 cathode) was combined with an S-TWIN objective, a windowless EDAX energy-dispersive X-ray system and a FEI Eagle 2k CCD TEM camera.

About 100 individual clay particles per sample were characterized by TEM-EDX with respect to crystal size, crystal habit, particle morphology and element distribution. The crystal size, crystal habit and particle morphology were described according to Henning & Störr (1986).

For the quantification of element distribution, a calibration of k factors is mandatory (Cliff & Lorimer, 1975; Lorimer & Cliff, 1976; Mellini & Menichini, 1985). These k values are used to calibrate for the specific behaviour of particles against possible irradiation damage. The elements O, Na, Mg, Al, Si, K, Ca and Fe were quantified by applying the EDAX GENESIS–TEM Quant Materials quantification procedure.

In this procedure, the acquired EDX spectra are corrected by background subtraction, Gaussian deconvolution and k-factor corrections using values previously determined on a phyllosilicate standard (muscovite) and selected non-phyllosilicate standards. The average errors in the analyzed elements using the phyllosilicate standard, expressed as the atomic proportions, are 10 (Na), 5 (Fe, Mg, K, Ti, Ca) and 1 (Si, Al).

The measurement time per particle was lowered to 20 s and the exposed area was limited to a 50 nm diameter, avoiding possible irradiation damage of particles. The stability of particles of the sample series was tested for this measurement time at the beginning of any measurement campaign.

Further methodological details related to TEM-EDX-measurements and the Excel-based mathematical procedure using TEM-EDX data for calculation of mineral formulae are described in Hoang-Minh et al. (2019).

These mathematical procedures described in Hoang-Minh et al. (2019) were extended by k-means clustering method for finding subgroups of observations within a data set. The data were standardized (i.e., scaled) to make variables comparable. Euclidean distances were applied as classical method for distance measures. The optimal clusters were determined by Elbow method and Gap statistics[5].

---

[5] *https://uc-r.github.io/kmeans_clustering*

Data Sheet – B25 No4_B (< 2 µm), treated material *(OPA, 35°C, 93.6 hrs)*

Preparation for TEM

- raw material: compacted material (1.6 g/cm³) of treated B25-sample (OPA, 35°C, 93.6 hrs)
- suspension on particles < 2 µm on carbon-filmed Cu-grid
- air-dried and humidity-controlled storing

Mineral Matter

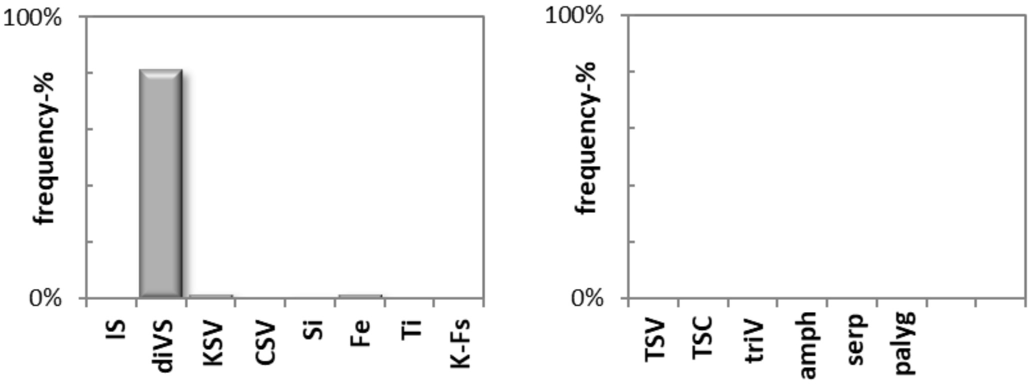

Fig. 1. *Distribution of mineral groups in fraction < 2 µm (in frequency-%)*
Legend: ***IS*** *– illite-smectite-mixed layer series in sense of Środon et al. (1992), diVS – dioctahedral vermiculite-smectite illite-smectite-mixed layer series (= charge- and/or K-deficit),* ***KSV*** *– kaolinite-smectite-dioctahedral vermiculite-mixed layer series,* ***CSV*** *– chlorite-saponite-trioctahedral vermiculite-mixed layer series,* ***Si*** *– quartz or particles with Si-surplus,* ***Fe*** *– Fe-oxide or Fe-oxyhydroxide,* ***Ti*** *– Ti-bearing phases (e.g. rutile, anatase),* ***K-Fs*** *– K-feldspar*

Clay Mineral Composition

All particles of smectite group:

$$Ca_{0.15}\,Mg_{0.08}\,Na_{0.00}\,K_{0.19}\quad Al_{0.95}\,Fe^{3+}_{0.91}\,Mg_{0.11}\,Ti_{0.01}\,(OH)_2\quad Si_{3.42}\,Al_{0.58}\,O_{10}$$

Charge: XII = 0.65 VI = 5.93 IV = 15.42 **Σ = 22.00**
Probability of smectite layers (%S): 21%
Probability of illite layers (%I): 79%

Specific Dissolution Potential (ΔS%)

for H2O, 20 + 60 rpm	-11	(= medium reacting, interlayer group: Ca+Mg (= type B))
for NaCl, 20 rpm	-16	(= medium reacting, interlayer group: Ca+Mg (= type B))
for NaCl, 60 rpm	-109	(= fast reacting, 'illitization', interlayer group: Na (= type A))
CEC_{calc}:	58 meq / 100 g	(literature: 56 meq / 100 g [Matschiavelli et al., 2019: MAT19])

Measured particles: 108

Table 1. *Summarized chemical composition*

SiO_2	**TiO_2**	**Al_2O_3**	**Fe_2O_3**	**MnO**	**MgO**	**CaO**	**Na_2O**	**K_2O**	**P_2O_5**	**Σ**	
59.5%	0.3%	23.3%	10.6%		2.8%	1.8%	0.0%	1.7%	0.0%	1.00	measured particles
58.6%	0.0%	22.0%	5.9%		3.0%	1.0%	0.1%	1.1%	0.1%	0.92	measured particles of original B25

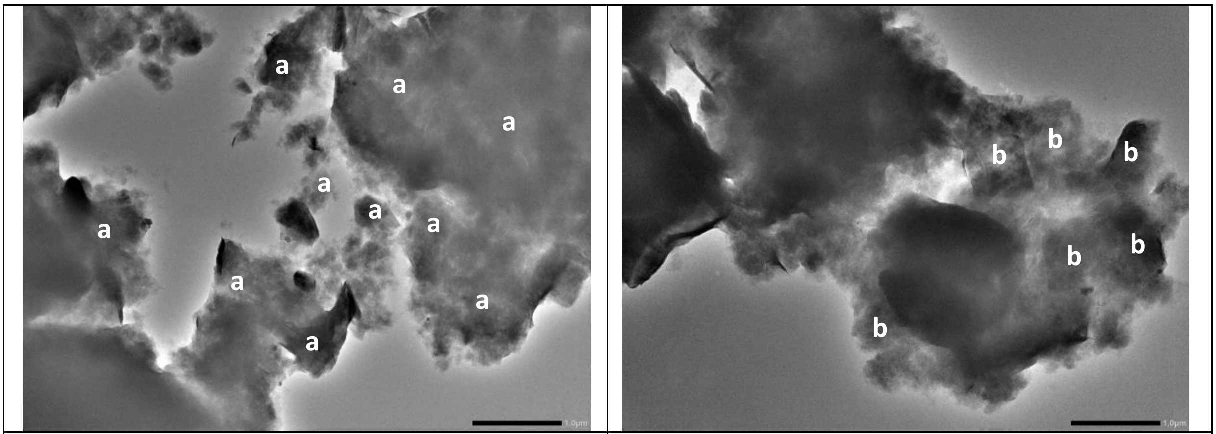

JEM-2100_MAG_X8000_006_B25+35B.bmp

Magnification: 8k

(n) Aggregates formed by small (≤ 200 nm) xenomorphous plates

JEM-2100_MAG_X8000_004_B25+35B.bmp

Magnification: 8k

(e)

(f) large (≤ 1 µm) xenomorph film-like platy crystals

Fig. 2. *Morphology of particles (TEM-micrographs)*

Distribution of smectite layers probability (%S)

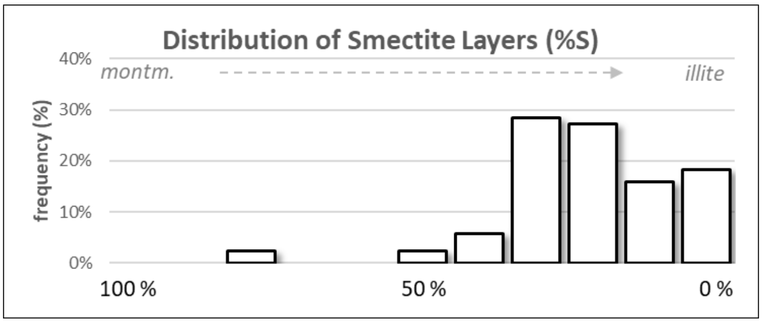

Fig. 3a. *Distribution of smectite layers probability (%S)*

Description: *The distribution of %S-probability indicates the occurrence of two groups: (i) mixture of beidellite-montmorillonite interstratifications (= assumption) with diVS-ml as well as (ii) illite with K-deficiency.*

Differentiation by relation "Octahedral Mg vs. tetrahedral Si"?

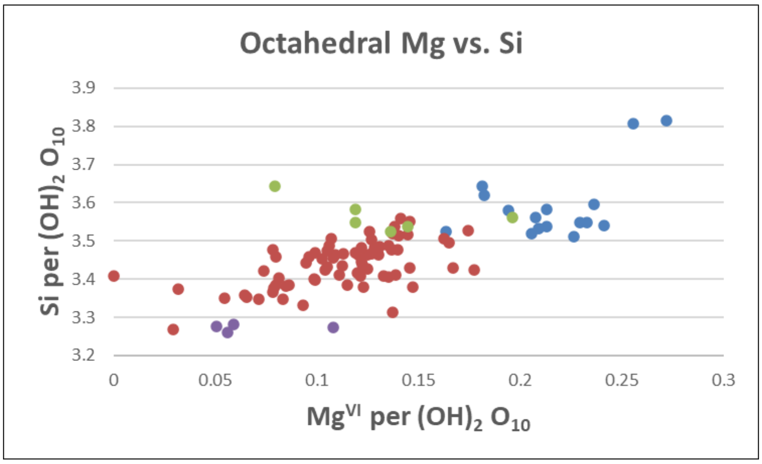

Description: *This diagram indicates the occurrence of two groups of Mg in relation to tetrahedral Si. Probably, this distribution mirrors 2 phases (I) beidellite-montmorillonite interstratifications (red) and (II) diVS-ml (blue, green, magenta)*

Fig. 3b. *Distribution of octahedral Mg vs. tetrahedral Si [all per(OH)$_2$ O$_{10}$]*

Distribution of K in relation to tetrahedral Si

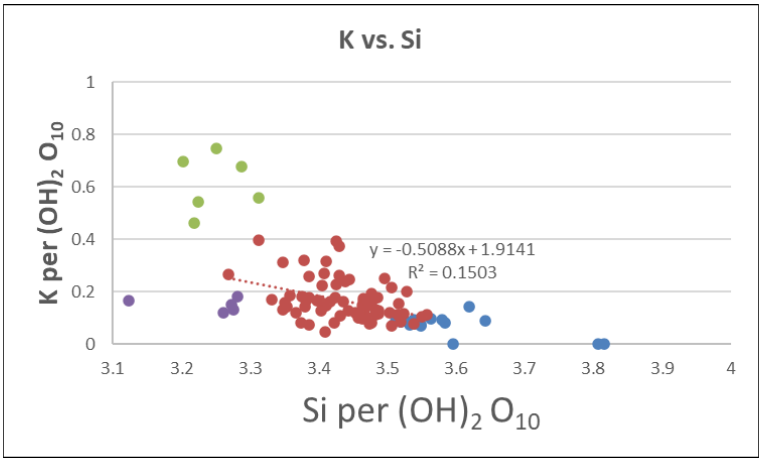

Description: *This diagram visualizes possible particles (beidellite-montmorillonite interstratification?) with low K (red dots)*

Fig. 4. *Distribution of K in interlayer space vs. tetrahedral Si [all per(OH)$_2$ O$_{10}$]*

Distribution of charges (exchangeable from interlayer space)

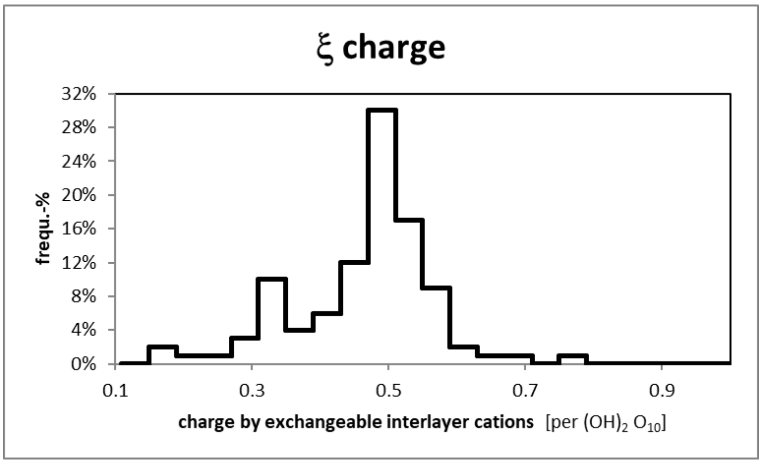

This diagram visualizes the distribution of exchangeable charges in the interlayer space (Ca, Mg, Na) determined and computed by TEM-EDX-data.

Description: *Bimodal distribution of charge density at 0.35 (for mica-near diVS-ml, Cluster 1) and 0.51 per (OH)$_2$ O$_{10}$.*

Fig. 5. *Distribution of charges*

Beidellite *(Cluster4):*

$Ca_{0.15}\ Mg_{0.09}\ Na_{0.00}\ K_{0.17}\quad Al_{0.95}\ Fe^{3+}_{0.92}\ Mg_{0.11}\ Ti_{0.01}\ (OH)_2\quad Si_{3.44}\ Al_{0.55}\ O_{10}$

Charge:	XII = 0.66	VI = 5.90	IV = 15.44	**Σ = 22.00**

Measured particles: 71

Distribution of BM-interstratifications (Cluster4)

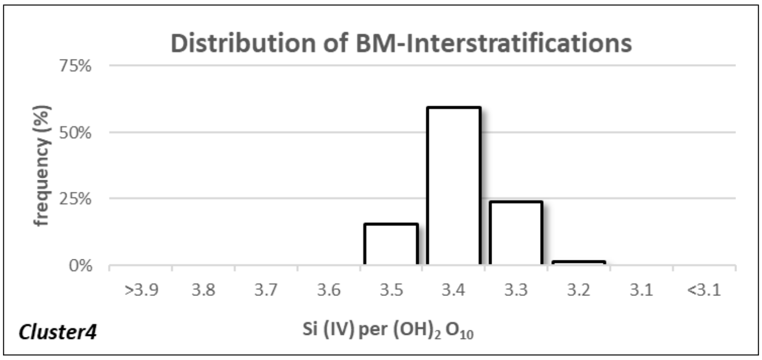

Description: *The distribution of BM-interstratifications (classified as Cluster4) draws a maximum of frequency (%) at tetrahedral Si-value between 3.4 – 3.5 e phuc*

Fig. 6a. *Distribution of assumed beidellite-montmorillonite interstratifications*

Beidellite?	*particles (abs)*	**Ca (XII)**	**Mg (XII)**	**Na (XII)**	**K (XII)**	**Cr3+ (VI)**	**Al (VI)**	**Fe3+ (VI)**	**Mg (VI)**	**Ti (VI)**	**Al (IV)**	**Si (IV)**	**XII**	**n_VI**	**%S**
Si >3.9	n = 0														
Si 3.9-3.8	n = 0														
Si 3.8-3.7	n = 0														
Si 3.7-3.6	n = 0														
Si 3.6-3.5	n = 11	0.16	0.08	0.00	0.12	0.00	0.96	0.89	0.14	0.01	0.48	3.52	0.60	2.0	31
Si 3.5-3.4	**n = 42**	**0.15**	**0.09**	**0.00**	**0.16**	**0.00**	**0.95**	**0.92**	**0.12**	**0.01**	**0.55**	**3.45**	**0.65**	**2.0**	**22**
Si 3.4-3.3	n = 17	0.15	0.10	0.00	0.19	0.00	0.94	0.95	0.09	0.03	0.63	3.37	0.70	2.0	15
Si 3.3-3.2	n = 1	0.12	0.12	0.00	0.27	0.00	1.22	0.73	0.03	0.02	0.73	3.27	0.74	2.0	7
Si 3.2-3.1	n = 0														
Si <3.1	n = 0														

Fig. 6b. *Computed averaged mineral formulae of phases in the different Si(IV)-classes*

Dioctahedral Vermiculite-Smectite mixed layer phases (diVS-ml) *(Cluster1, 2 & 3):*

$$Ca_{0.15}\ Mg_{0.05}\ Na_{0.01}\ K_{0.21}\quad Al_{0.96}\ Fe^{3+}_{0.89}\ Mg_{0.16}\ Ti_{0.02}\ (OH)_2\ \ Si_{3.43}\ Al_{0.57}\ O_{10}$$

Charge: XII = 0.61 VI = 5.96 IV = 15.43 **Σ = 22.00**

Probability of smectite layers (%S): 20%

Probability of illite layers (%I): 80%

Measured particles: 29

Distribution of smectite layers probability (%S) in diVS-ml (Cluster1, 2 & 3)

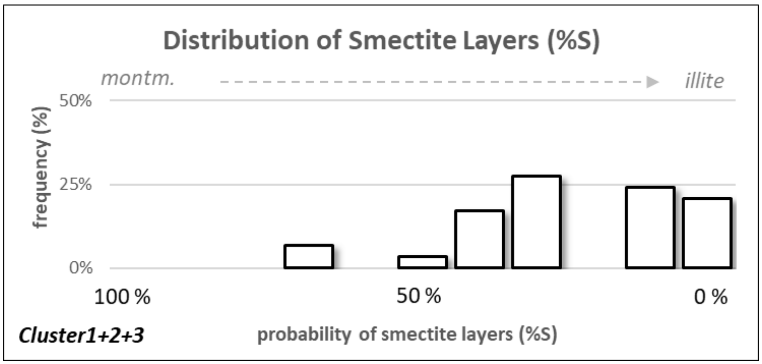

Description: *The distribution of diVS-ml (classified as Clusters 1, 2 & 3) draws a maximum of frequency (%) for smectite layer probability at 30%*

Fig. 7a. *Distribution of smectite layers probability in diVS-ml*

diVS-ml	*particles (abs)*	**Ca (XII)**	**Mg (XII)**	**Na (XII)**	**K (XII)**	**Cr3+ (VI)**	**Al (VI)**	**Fe3+ (VI)**	**Mg (VI)**	**Ti (VI)**	**Al (IV)**	**Si (IV)**	**XII**	**n_VI**	**%S**
%S >95%	n = 0														
%S 95-85%	n = 0														
%S 85-75%	n = 0														
%S 75-65%	n = 2	0.19	0.03	0.00	0.00	0.00	1.19	0.55	0.26	0.00	0.19	3.81	0.5	2.0	73
%S 65-55%	n = 0														
%S 55-45%	n = 1	0.15	0.08	0.00	0.09	0.00	1.04	0.78	0.18	0.00	0.36	3.64	0.5	2.0	46
%S 45-35%	n = 5	0.15	0.01	0.00	0.08	0.00	1.06	0.80	0.21	0.01	0.41	3.59	0.41	2.1	39
%S 35-25%	n = 8	0.17	0.00	0.00	0.08	0.00	0.94	0.92	0.22	0.00	0.47	3.53	0.42	2.1	32
%S 25-15%	n = 0														
%S <15%	**n = 13**	**0.13**	**0.09**	**0.01**	**0.38**	**0.00**	**0.89**	**0.97**	**0.10**	**0.05**	**0.78**	**3.22**	**0.83**	**2.0**	**4**

Fig. 7b. *Computed averaged mineral formulae of diVS-ml phases in the different smectite layers probability (%S)-classes*

Description – B25 No4_B (< 2 µm), treated material *(OPA, 35°C, 93.6 hrs)*

Preparation for TEM

The powder of compacted and treated B25-No4_B-sample was suspended in deionized water and dispersed by ultrasonic treatment for approximately 20 min. The clay fraction (<2 µm) was separated by sedimentation and diluted with deionized water to get a clear suspension. The suspension was dropped onto carbon-coated Cu grids, air dried and stored under environment-controlled conditions at 45% humidity.

Mineral Matter - Overview

The fraction < 2 µm of treated B25 bentonite sample (Opalinus Clay solution, at 35°C, for 93.6 hours) is mainly composed by beidellite (beid) and dioctahedral vermiculite-smectite mixed layer phases (diVS-ml) and accompanied by two types of illite. Furthermore, kaolinite and Si-surplus particles (Si, e.g. quartz) were identified in traces in this sample [fig. 1].

	frequency-% *(n = 108 measured particles)*
Beidellite (Cluster4)	66%
diVS-ml (Cluster1, 2 & 3)	27%
Kaolinite & KSV-ml	2%
Si-surplus	1%
Unknown	3%

All measured clay mineral phases summarized result following mineral formula computed from TEM-EDX-measurement of 100 individual particles:

$$Ca^{2+}_{0.15}\ Mg^{2+}_{0.08}\ Na^{+}_{0.00}\ K^{+}_{0.19}\quad Al^{3+}_{0.97}\ Fe^{3+}_{0.90}\ Mg^{2+}_{0.13}\ Ti^{4+}_{0.02}\ (OH)_2\quad Si^{4+}_{3.44}\ Al^{3+}_{0.56}\ O_{10}$$

SDOM *± 0.00 ± 0.00 ± 0.00 ± 0.02 ± 0.02 ± 0.02 ± 0.01 ± 0.00 ± 0.01 ± 0.01*

Legend: SDOM - standard deviation of the mean (= the standard deviation divided by the square root of the number of samples)

The interlayer charge is calculated as 0.64 per $(OH)_2\ O_{10}$ and the octahedral charge as 5.92 per $(OH)_2\ O_{10}$. The particles are characterized by a high octahedral Fe-amount.

The summarized chemical composition of all 100 computed particles is compared with measured data of original B25-bentonite sample [tab. 1]. The chemical composition averaged by measured particles show a slight increased amount of SiO_2 and Al_2O_3 and a remarkable higher amount for Fe_2O_3, CaO and K_2O in comparison to the measured data of original untreated B25-bentonite.

B25-No4_B sample is characterized by two morphological groups: (i) aggregates formed by small (≤ 200 nm) xenomorphous plates and (ii) large (≤ 1 µm) xenomorph film-like platy crystals [fig. 2]. Aggregates formed by small (≤ 200 nm) xenomorphous plates dominate the shapes of particles in the micrographs [fig. 2].

The distribution of %S-probability of all measured clay mineral phases [fig. 3a] also indicates the occurrence of two groups: (i) as main group a mixture of beidellite and diVS-ml (%S-max of this mixture for %S at 30%) and (ii) illite with K- and charge deficit (%S-class = 0-10%).

The numerous measured particles by TEM-EDX allow a visualization of distribution of interlayer charges. Considering the TEM-EDX-determined cations Ca^{++}, Mg^{++} and Na^{+} and then computed their ratio as interlayer cations in the mineral formula, Ca^{++}, Mg^{++} and Na^{+} offer to characterize the degree of exchangeable charges in the interlayer space. This charge density of treated B25 bentonite (< 2 µm) shows in this sample a bimodal distribution with maximal frequency-% of charge density at 0.35 and 0.51 per (OH)$_2$ O$_{10}$ [fig. 5]. This interval of interlayer charge density caused by exchangeable cations from 0.3 - 0.63 per (OH)$_2$ O$_{10}$ represents mainly mica-near diVS-ml (lowest peak at 0.35 per (OH)$_2$ O$_{10}$) and beidellite and the other diVS-ml phases with the higher peak. The measured diVS-ml phases offer two groups of non-exchangeable K in the interlayer space (cluster 1 vs. cluster 2, 3).

Mineral Matter - Specification

Result of Clustering

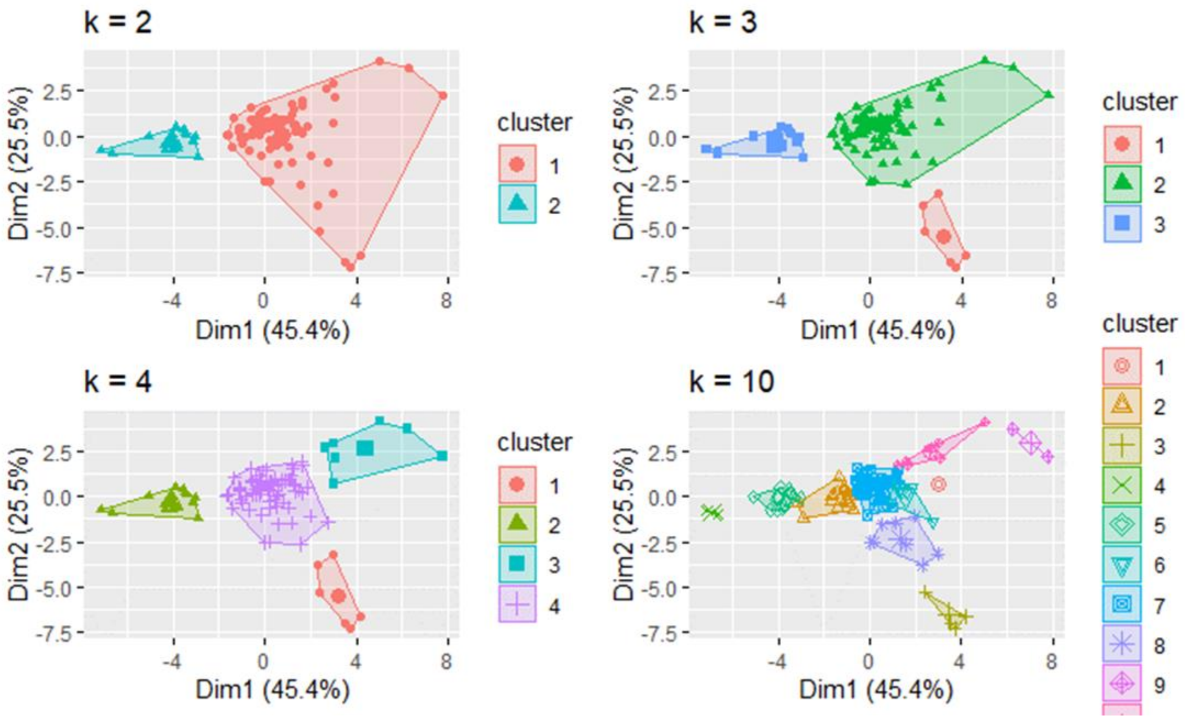

Fig. 8. *Clustering of all measured particles for clusters k = 2, k = 3, k = 4 and k = 5 (source for R-coding: https://uc-r.github.io/kmeans_clustering)*

The optimum of clusters was calculated with k = 4.

		Ca (XII)	Mg (XII)	Na (XII)	K (XII)	Cr3+ (VI)	Al (VI)	Fe3+ (VI)	Mg (VI)	Ti (VI)	Al (IV)	Si (IV)	XII	n_VI	%S
Cluster1	n = 6	0.10	0.02	0.03	0.61	0.00	1.24	0.60	0.13	0.03	0.75	3.25	0.87	2.0	6
Cluster2	n = 16	0.17	0.01	0.00	0.07	0.00	1.02	0.83	0.22	0.00	0.41	3.59	0.43	2.1	39
Cluster3	n = 7	0.15	0.16	0.00	0.18	0.00	0.59	1.28	0.06	0.06	0.80	3.20	0.80	2.0	3
Cluster4	n = 71	0.15	0.09	0.00	0.17	0.00	0.95	0.92	0.11	0.02	0.56	3.44	0.66	2.0	21

Fig. 9. *Mineral formulae based on TEM-EDX-data summarized following the result of clustering for k=4*

	Sybilla-results	**TEM-EDX-results**	**Notes**
Cluster 1	Illite	diVS-ml (illite)	*Low K-deficit, no charge deficit, Fe(VI)-rich*
Cluster 3		diVS-ml (illite)	*High K-deficit, low Al(VI), very high Fe(VI)*
Cluster 2	IS R0(2) *(%S = 38%)*	diVS-ml *(%S ~ 39%)*	*High K-deficit, low Al(VI), high Fe(VI)*
Cluster 4	IS R0(1) *(%S = 100%)*	Beidellite	*XRD: Montmorillonite and beidellite is only to distinguish by Green-Kelly-test (not available here).*

Tab. 2. *Comparison of results from TEM-EDX- and XRD-measurements with clustering procedure*

The clustering of TEM-EDX-data offers a good agreement with the recent result of Sybilla-processing of XRD-traces from oriented specimen [tab. 2].

IS R0 (1): The X-ray diffraction pattern of the ethylene-glycol saturated oriented specimen shows a full expandability to 1.76 nm and a difference of 5.36°2θ between 2. and 3. order of smectite interferences. This distance is typically for montmorillonite (Moore & Reynolds, 1989). This result of XRD-processing let expect a maximum of particles for %S ~ 100% by TEM-EDX-measurements, but the maximum of particles measured by TEM-EDX is to find at %S=21% [fig. 3a].

Montmorillonite and beidellite have the same behavior concerning the expandability and they are only to distinguish by XRD using Li like by Greene-Kelly test (Green-Kelly 1952, 1953). So, combination of XRD- and TEM-results (full expandability by XRD and Si ~ 3.44 by TEM-EDX) led conclude the occurrence of beidellite.

IS R0 (2): The Sybilla-procedure of XRD-traces (oriented mounts) has shown an occurrence of a second illite-smectite mixed layer phase with a smectite layers probability of %S = 38%. This situation is to find in Clusters 2 ($\%S_{TEM}$ = 39%) representing high K- and low charge deficient and Fe-rich dioctahedral vermiculite-smectite mixed layer phase (diV-ml) [tab. 2].

The Sybilla-processing of XRD-traces (oriented mounts) also supports the existence of kaolinite and kaolinite-smectite mixed layer phases in fine fraction of sample. Such phases were not to identify or to calculate in TEM-EDX-database (a grain size effect?).

Specifics to the identified clay mineral groups

Beidellite

71 of 100 computed particles belong so to this assumed classification. The dioctahedral character of this group is proofed by X-ray diffraction. The position of the large (060)-interference of smectite is in the random oriented powder specimen at 1.497 Å.

Montmorillonite and beidellite have the same behavior concerning the expandability and they are only to distinguish by XRD using Li by means of Greene-Kelly test (Greene-Kelly 1952, 1953). So, combination of XRD- and TEM-results (full expandability by XRD and Si ~ 3.44 by TEM-EDX) led conclude the occurrence of beidellite.

Beidellite

$$Ca_{0.15}\,Mg_{0.09}\,Na_{0.00}\,K_{0.17}\quad Al_{0.95}\,Fe^{3+}_{0.92}\,Mg_{0.11}\,Ti_{0.02}\,(OH)_2\quad Si_{3.44}\,Al_{0.56}\,O_{10}$$

Charge: XII = 0.66 VI = 5.90 IV = 15.44 **Σ = 22.00**
Measured particles by TEM-EDX: 71
Result of clustering: Cluster4 [tab. 2]

In this sample, beidellite is characterized by a typical low octahedral Mg-amount (because of high ratio of octahedral, 3-valent cations). A comparison of octahedral Mg vs. tetrahedral Si indicates the occurrence of two groups for octahedral Mg based on TEM-EDX-data [fig. 3b].

Using the results of clustering (see Cluster4 in tab. 2), the maximum of frequency-% is to find for particles in the Si(IV)-class ~ 3.4 - 3.5 e phuc [tab. 6a], representing a beidellite. The mineral formulae, summarized in classes of tetrahedral Si, draw for the maximum an Fe-rich beidellite with low Mg(VI), but remarkable amount of K in the interlayer space [tab. 6b].

Dioctahedral vermiculite-smectite mixed layer phase (diVS-ml):

$$\boxed{Ca_{0.15}\ Mg_{0.05}\ Na_{0.01}\ K_{0.21}\quad Al_{0.96}\ Fe^{3+}_{0.89}\ Mg_{0.16}\ Ti_{0.02}\ (OH)_2\ \ Si_{3.43}\ Al_{0.57}\ O_{10}}$$

Charge: XII = 0.61 VI = 5.96 IV = 15.43 **Σ = 22.00**
Probability of smectite layers (%S): 20%
Probability of illite layers (%I): 80%
Measured particles by TEM-EDX: 29
Result of clustering: Cluster 1, 2, 3 [tab. 2]

Illite as part of diVS-ml series

The Rietveld refinement by Profex software (Döbelin & Kleeberg, 2015) indicates the occurrence of two polytypes for illite in treated B25 bentonite: $2M_1$- and 1M-polytype.

Kaolinite-montmorillonite mixed layer phases

The Excel-based procedure (Hoang-Minh et al., 2019) to identify possible clay mineral groups using the TEM-EDX-measurements also includes algorithms to classify kaolinite and kaolinite-montmorillonite mixed layer phases. These algorithms couldn’t identify such phases basing on the measured TEM-EDX-data. Otherwise, few particles, which were not to compute, have shown small hexagonal plates typically for kaolinite-bearing phases.

References

Cliff, G. & Lorimer, G. W. (1975). *J. Microsc.* **103**, 203–207.

Döbelin, N., Kleeberg, R. (2015). *Journal of Applied Crystallography* **48**, 1573-1580. DOI: 10.1107/S1600576715014685

Greene-Kelly, R., *Clay Minerals Bull.*, **1**, 221 (1952).

Greene-Kelly, R. 1953. The identification of montmorillonoids in clays. *Journal of Soil Science*. **4** (2), pp. 232-237. https://doi.org/10.1111/j.1365-2389.1953.tb00657.x

Greene-Kelly, R. (1955). Dehydration of the montmorillonite minerals. *Mineralogical Magazine and Journal of the Mineralogical Society*, **30**(228), 604-615. doi:10.1180/minmag.1955.030.228.06

Henning, K.-H. & Störr, M. (1986). Electron Micrographs (TEM, SEM) of Clays and Clay Minerals, p. 325. Akademie-Verlag Berlin.

Hoang-Minh, T., Kasbohm, J., Nguyen-Thanh, L., Nga, P. T., Lai, L. T., Duong, N. T., Thanh, N. D., Thuyet, N. T. M., Anh, D. D., Pusch, R., Knutsson, S. & Ferreiro Mahlmann, R. (2019). *J. Appl. Cryst.* **52**, 133-147. DOI: 10.1107/S1600576718018162

Lorimer, G. W. & Cliff, G. (1976). *Electron Microscopy in Mineralogy*, edited by H. R. Wenk, pp. 506–519. Berlin: Springer Verlag.

Matschiavelli, N., Kluge, S., Podlech, C., Standhaft, D., Grathoff, G., Ikeda-Ohno, A., Warr, L.N., Chukharkina, A., Arnold, T. & Cherkouk, A. (2019). *Environmental Science & Technology.* **53** (17), 10514-10524, DOI: 10.1021/acs.est.9b02670

Mellini, M. & Menichini, R. (1985). *R. Soc. Ital. Miner. Petrol.* **40**, 261–266.

Moore, D.M., Reynolds, R.C. (1989). X-ray Diffraction and the Identification and Analysis of Clay Minerals, Oxford University Press, New York, 332 + xvi pp.

Nguyen-Thanh, L., Herbert, H.-J., Kasbohm, J., Hoang-Minh, T. & Mählmann, R. F. (2014). *Clays Clay Miner.* **62**, 425–446.

Środoń, J., Elsass, F., McHardy, W. J. & Morgan, D. J. (1992). *Clay Miner.* **27**, 137–158.

Data Sheet – B25 bentonite, treated materials *(35 °C, 0.7Ma, 290h-VSD)*

Methodology - Transmission electron microscopy linked with energy-dispersive X-ray spectroscopy (TEM-EDX)

It is expected a characterization of clay mineral phases in treated B25 bentonite by transmission electron microscopy. The sample No23 represents a percolation of B25 bentonite by Opalinus Clay solution at 35°C and 0.7 MPa for 285 hours.

The different clay mineral phases are to identify and to describe by chemical composition and its variability, morphology, the specific dissolution potential, and further parameter.

Such further parameter like distribution of smectite layers probability (%S) and distribution of charges caused by exchangeable cations interlayer space should serve as additional indicators for mineralogical alterations in treatment experiments with B25 bentonite.

The sample were suspended for TEM-measurement in deionized water and dispersed by ultrasonic treatment for approximately 20 min. The clay fraction (<2 µm) was separated by sedimentation and diluted with deionized water to get a clear suspension. The suspension was dropped onto carbon-coated Cu grids, air dried and stored under environment-controlled conditions at 45% humidity.

TEM-EDX investigations were carried out on the <2 µm fraction using a FEI TECNAI G^2 20 electron transmission microscope at the VNU University of Science, Vietnam National University, Hanoi. This equipment (operated at 200 kV with LaB_6 cathode) was combined with an S-TWIN objective, a windowless EDAX energy-dispersive X-ray system and a FEI Eagle 2k CCD TEM camera.

About 100 individual clay particles per sample were characterized by TEM-EDX with respect to crystal size, crystal habit, and particle morphology and element distribution. The crystal size, crystal habit and particle morphology were described according to Henning & Störr (1986).

For the quantification of element distribution, a calibration of k factors is mandatory (Cliff & Lorimer, 1975; Lorimer & Cliff, 1976; Mellini & Menichini, 1985). These k values are used to calibrate for the specific behaviour of particles against possible irradiation damage. The elements O, Na, Mg, Al, Si, K, Ca and Fe were quantified by applying the EDAX GENESIS–TEM Quant Materials quantification procedure.

In this procedure, the acquired EDX spectra are corrected by background subtraction, Gaussian deconvolution and k-factor corrections using values previously determined on a phyllosilicate standard (muscovite) and selected non-phyllosilicate standards. The average errors in the analyzed elements using the phyllosilicate standard, expressed as the atomic proportions, are 10 (Na), 5 (Fe, Mg, K, Ti, Ca) and 1 (Si, Al).

The measurement time per particle was lowered to 20 s and the exposed area was limited to a 50 nm diameter, avoiding possible irradiation damage of particles. The stability of particles of the sample series was tested for this measurement time at the beginning of any measurement campaign.

Further methodological details related to TEM-EDX-measurements and the Excel-based mathematical procedure using TEM-EDX data for calculation of mineral formulae are described in Hoang-Minh et al. (2019).

These mathematical procedures described in Hoang-Minh et al. (2019) were extended by k-means clustering method for finding subgroups of observations within a data set. The data were standardized

(i.e., scaled) to make variables comparable. Euclidean distances were applied as classical method for distance measures. The optimal clusters were determined by Elbow method and Gap statistics[6].

---

[6] *https://uc-r.github.io/kmeans_clustering*

Data Sheet – B25 No23 (< 2 µm), treated material *(OPA, 35°C, 0.7 MPa, 285 hrs)*

Preparation for TEM

- raw material: compacted material (1.6 g/cm³) of treated B25-sample (OPA, 35°C, 0.7 MPa, 285 hrs)
- suspension on particles < 2 µm on carbon-filmed Cu-grid
- air-dried and humidity-controlled storing

Mineral Matter

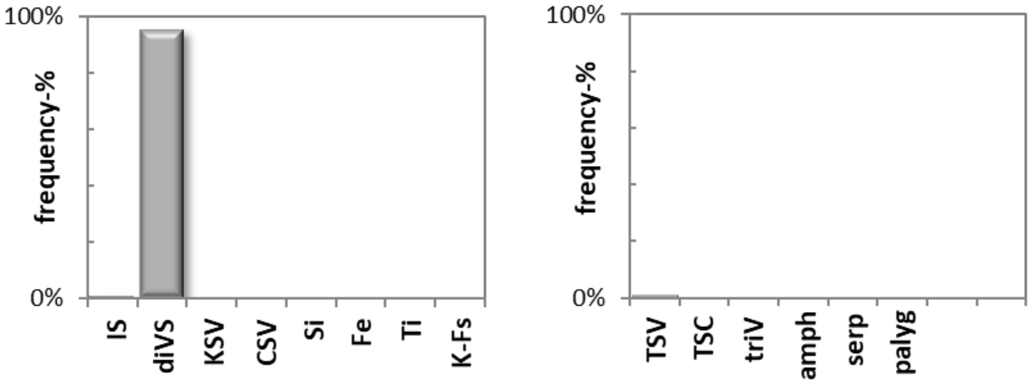

Fig. 1. *Distribution of mineral groups in fraction < 2 µm (in frequency-%)*
Legend: ***IS*** *– illite-smectite-mixed layer series in sense of Środon et al. (1992), diVS – dioctahedral vermiculite-smectite illite-smectite-mixed layer series (= charge- and/or K-deficit),* ***KSV*** *– kaolinite-smectite-dioctahedral vermiculite-mixed layer series,* ***CSV*** *– chlorite-saponite-trioctahedral vermiculite-mixed layer series,* ***Si*** *– quartz or particles with Si-surplus,* ***Fe*** *– Fe-oxide or Fe-oxyhydroxide,* ***Ti*** *– Ti-bearing phases (e.g. rutile, anatase),* ***K-Fs*** *– K-feldspar*

Clay Mineral Composition

All particles of smectite group:

$$Ca_{0.19}\,Mg_{0.05}\,Na_{0.00}\,K_{0.14}\quad Al_{1.18}\,Fe^{3+}_{0.56}\,Mg_{0.26}\,Ti_{0.01}\,(OH)_2\quad Si_{3.62}\,Al_{0.38}\,O_{10}$$

Charge: XII = 0.63 VI = 5.75 IV = 15.62 **Σ = 22.00**

Probability of smectite layers (%S): 43%
Probability of illite layers (%I): 57%

Specific Dissolution Potential (ΔS%)

for H2O, 20 + 60 rpm	-6	(= medium reacting, interlayer group: Ca+Mg (= type B))
for NaCl, 20 rpm	-7	(= medium reacting, interlayer group: Ca+Mg (= type B))
for NaCl, 60 rpm	-110	(= fast reacting, 'illitization', interlayer group: Na (= type A))
CEC$_{calc}$:	97 meq / 100 g	(literature: 56 meq / 100 g [Matschiavelli et al., 2019: MAT19])

Measured particles: 130

Table 1. *Summarized chemical composition*

SiO_2	TiO_2	Al_2O_3	Fe_2O_3	MnO	MgO	CaO	Na_2O	K_2O	P_2O_5	Σ	
61.2%	0.1%	23.1%	6.4%		4.0%	3.6%	0.0%	1.3%	0.2%	1.00	measured particles
63.8%	0.0%	23.9%	6.5%		3.3%	1.1%	0.1%	1.2%	0.1%	1.00	measured particles of original B25

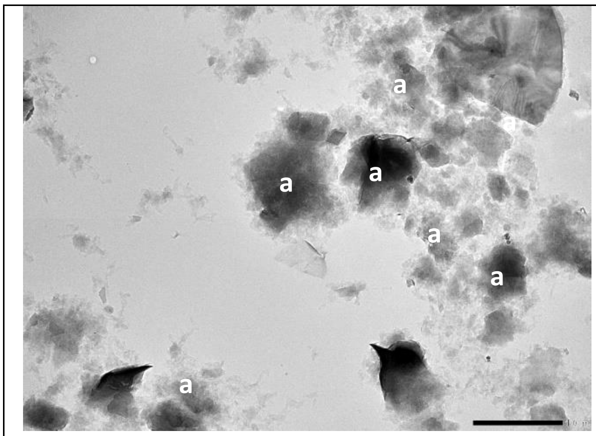	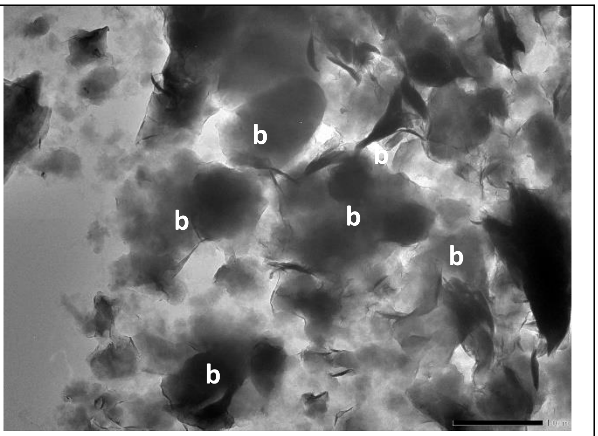
JEM-2100_MAG_X8000_053_No23.bmp Magnification: 8k (o) Aggregates formed by small (≤ 200 nm) xenomorphous plates	*JEM-2100_MAG_X8000_049_No23.bmp* Magnification: 8k (g) (h) large (≤ 1 µm) xenomorph film-like platy crystals, partially with folds

***Fig. 2.** Morphology of particles (TEM-micrographs)*

Distribution of smectite layers probability (%S)

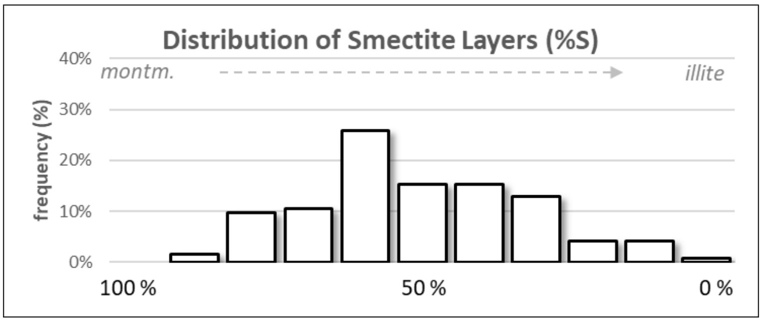

***Description:** The distribution of %S-probability indicates the occurrence of two groups: (i) beidellite-montmorillonite interstratifications (= assumption) as well as (ii) diVS-ml.*

***Fig. 3a.** Distribution of smectite layers probability (%S)*

Differentiation by relation “Octahedral Mg vs. tetrahedral Si”?

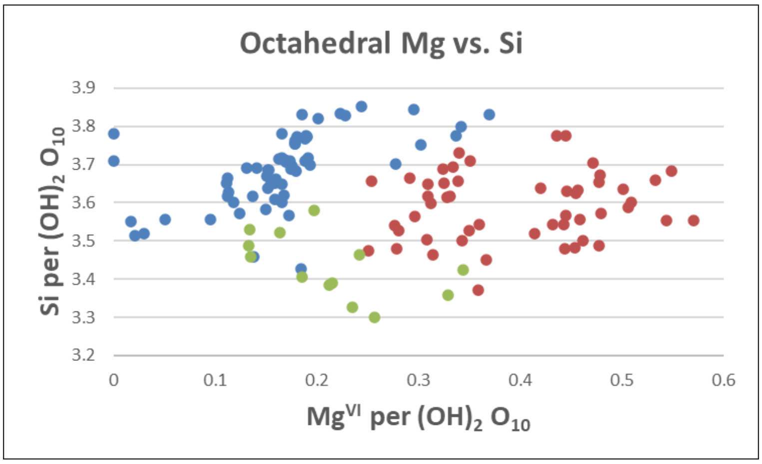

***Description:** This diagram indicates the occurrence of two groups of Mg in relation to tetrahedral Si. Probably, this distribution mirrors 2 phases (I) beidellite-montmorillonite interstratifications (blue) and (II) diVS-ml (red); a third group is free of any Mg-trend (green)*

***Fig. 3b.** Distribution of octahedral Mg vs. tetrahedral Si [all per$(OH)_2 O_{10}$]*

Distribution of K in relation to tetrahedral Si

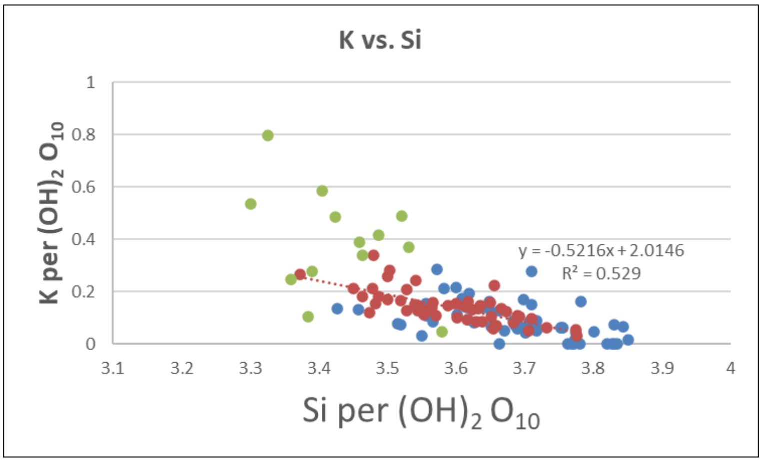

***Description:** This diagram visualizes possible particles (beidellite-montmorillonite interstratification?) with low K (red & blue dots)*

***Fig. 4.** Distribution of K in interlayer space vs. tetrahedral Si [all per$(OH)_2$ O_{10}]*

Distribution of charges (exchangeable from interlayer space)

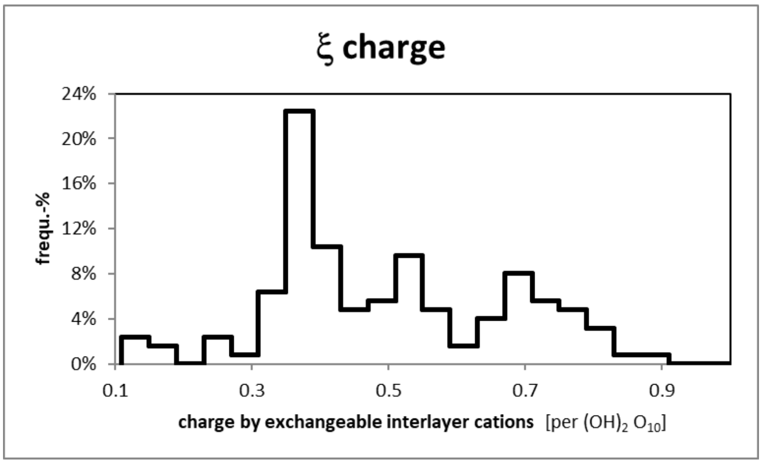

This diagram visualizes the distribution of exchangeable charges in the interlayer space (Ca, Mg, Na) determined and computed by TEM-EDX-data.

***Description:** Trimodal distribution of charge density at 0.39 (Cluster 1) and 0.55 and 0.71 (Cluster2) per $(OH)_2$ O_{10}.*

***Fig. 5.** Distribution of charges*

***Beidellite-Montmorillonite-Illite ml phases BMI 35:45:20** (Cluster1):*

$Ca_{0.11}$ $Mg_{0.08}$ $Na_{0.00}$ $K_{0.09}$ $Al_{1.24}$ $Fe^{3+}_{0.59}$ $Mg_{0.17}$ $Ti_{0.01}$ $(OH)_2$ $Si_{3.69}$ $Al_{0.31}$ O_{10}

Charge: XII = 0.47 VI = 5.84 IV = 15.69 **Σ = 22.00**

Measured particles: 61

Distribution of BM-interstratifications (Cluster1)

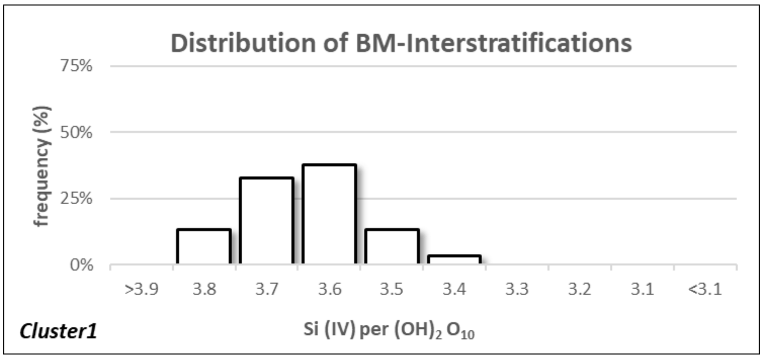

***Description:** The distribution of BM-interstratifications (classified as Cluster1) draws a maximum of frequency (%) at tetrahedral Si-value between 3.6 – 3.7 e phuc*

***Fig. 6a.** Distribution of assumed beidellite-montmorillonite-illite ml phases*

BMI 35:45:20		particles (abs)	Ca (XII)	Mg (XII)	Na (XII)	K (XII)	Cr3+ (VI)	Al (VI)	Fe3+ (VI)	Mg (VI)	Ti (VI)	Al (IV)	Si (IV)	XII	n_VI	%S
Si	>3.9	n = 0														
Si	3.9-3.8	n = 8	0.17	0.04	0.00	0.03	0.00	1.23	0.50	0.26	0.00	0.17	3.83	0.4	2.0	76
Si	3.8-3.7	n = 20	0.12	0.06	0.00	0.07	0.00	1.26	0.56	0.18	0.01	0.26	3.74	0.4	2.0	61
Si	**3.7-3.6**	**n = 23**	**0.10**	**0.09**	**0.00**	**0.11**	**0.00**	**1.22**	**0.63**	**0.15**	**0.01**	**0.35**	**3.65**	**0.5**	**2.0**	**48**
Si	3.6-3.5	n = 8	0.08	0.12	0.00	0.13	0.00	1.35	0.57	0.08	0.00	0.45	3.55	0.5	2.0	34
Si	3.5-3.4	n = 2	0.08	0.20	0.00	0.13	0.00	0.91	0.91	0.16	0.02	0.56	3.44	0.7	2.0	22
Si	3.4-3.3	n = 0														
Si	3.3-3.2	n = 0														
Si	3.2-3.1	n = 0														
Si	<3.1	n = 0														

Fig. 6b. *Computed averaged mineral formulae of phases in the different Si(IV)-classes*

Dioctahedral Vermiculite-Smectite mixed layer phases (diVS-ml) *(Cluster2):*

$$\mathrm{Ca_{0.32}\ Mg_{0.00}\ Na_{0.00}\ K_{0.14}\quad Al_{1.03}\ Fe^{3+}_{0.56}\ Mg_{0.40}\ Ti_{0.01}\ (OH)_2\ \ Si_{3.59}\ Al_{0.41}\ O_{10}}$$

Charge: XII = 0.80 VI = 5.61 IV = 15.59 **Σ = 22.00**

Probability of smectite layers (%S):	39%
Probability of illite layers (%I):	61%
Measured particles:	51

Distribution of smectite layers probability (%S) in diVS-ml (Cluster2)

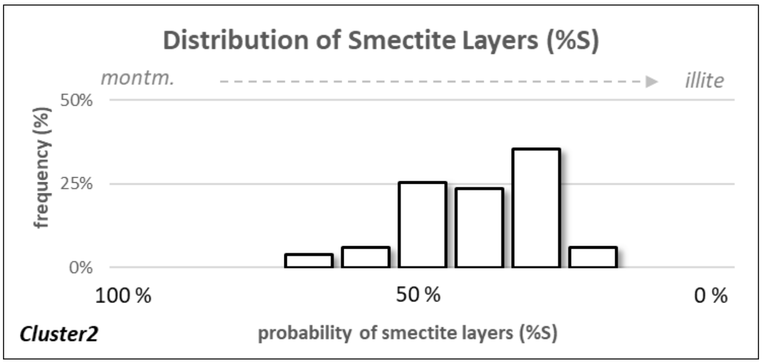

Description: *The distribution of diVS-ml (classified as Cluster2) draws a maximum of frequency (%) for smectite layer probability at 30%*

Fig. 7a. *Distribution of smectite layers probability in diVS-ml*

diVSml		particles (abs)	Ca (XII)	Mg (XII)	Na (XII)	K (XII)	Cr3+ (VI)	Al (VI)	Fe3+ (VI)	Mg (VI)	Ti (VI)	Al (IV)	Si (IV)	XII	n_VI	%S
Si	>3.9	n = 0														
Si	3.9-3.8	n = 0														
Si	3.8-3.7	n = 5	0.30	0.00	0.00	0.06	0.00	1.13	0.46	0.41	0.00	0.26	3.74	0.67	2.0	61
Si	**3.7-3.6**	**n = 20**	**0.32**	**0.00**	**0.00**	**0.12**	**0.00**	**1.04**	**0.56**	**0.40**	**0.00**	**0.35**	**3.65**	**0.75**	**2.0**	**47**
Si	**3.6-3.5**	**n = 18**	**0.34**	**0.01**	**0.00**	**0.16**	**0.00**	**1.01**	**0.57**	**0.40**	**0.01**	**0.46**	**3.54**	**0.85**	**2.0**	**33**
Si	3.5-3.4	n = 7	0.34	0.01	0.00	0.20	0.00	1.01	0.61	0.37	0.02	0.53	3.47	0.89	2.0	25
Si	3.4-3.3	n = 1	0.34	0.00	0.00	0.26	0.00	1.07	0.53	0.36	0.05	0.63	3.37	0.94	2.0	15
Si	3.3-3.2	n = 0														
Si	3.2-3.1	n = 0														
Si	<3.1	n = 0														

Fig. 7b. *Computed averaged mineral formulae of diVS-ml phases in the different smectite layers probability (%S)-classes*

Beidellite-Montmorillonite-Illite ml phases BMI 20:25:55 *(Cluster3):*

$$\mathrm{Ca_{0.15}\ Mg_{0.02}\ Na_{0.03}\ K_{0.39}\quad Al_{1.36}\ Fe^{3+}_{0.43}\ Mg_{0.21}\ Ti_{0.01}\ (OH)_2\ \ Si_{3.43}\ Al_{0.57}\ O_{10}}$$

Charge: XII = 0.76 VI = 5.81 IV = 15.43 **Σ = 22.00**

Measured particles: 13

Distribution of BM-interstratifications (Cluster3)

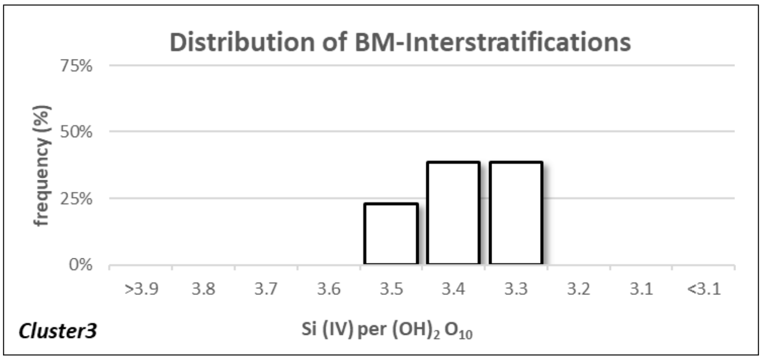

Description: *The distribution of BM-interstratifications (classified as Cluster3) draws a maximum of frequency (%) at tetrahedral Si-value between 3.3 – 3.5 e phuc*

Fig. 7c. *Distribution of assumed beidellite-montmorillonite-illite ml phases*

BMI 20:25:55?	*particles (abs)*	**Ca (XII)**	**Mg (XII)**	**Na (XII)**	**K (XII)**	**Cr3+ (VI)**	**Al (VI)**	**Fe3+ (VI)**	**Mg (VI)**	**Ti (VI)**	**Al (IV)**	**Si (IV)**	**XII**	**n_VI**	**%S**
Si >3.9	n = 0														
Si 3.9-3.8	n = 0														
Si 3.8-3.7	n = 0														
Si 3.7-3.6	n = 0														
Si 3.6-3.5	n = 3	0.05	0.04	0.05	0.30	0.00	1.40	0.46	0.16	0.00	0.46	3.54	0.54	2.0	33
Si 3.5-3.4	**n = 5**	**0.12**	**0.03**	**0.02**	**0.44**	**0.00**	**1.33**	**0.46**	**0.21**	**0.01**	**0.55**	**3.45**	**0.76**	**2.0**	**22**
Si 3.4-3.3	**n = 5**	**0.23**	**0.00**	**0.03**	**0.39**	**0.00**	**1.37**	**0.37**	**0.25**	**0.01**	**0.65**	**3.35**	**0.87**	**2.0**	**14**
Si 3.3-3.2	n = 0														
Si 3.2-3.1	n = 0														
Si <3.1	n = 0														

Fig. 7d. *Computed averaged mineral formulae of phases in the different Si(IV)-classes*

Description – B25 No23 (< 2 µm), treated material *(OPA, 35°C, 0.7 MPa, 285 hrs)*

Preparation for TEM

The powder of compacted and treated B25-No23-sample was suspended in deionized water and dispersed by ultrasonic treatment for approximately 20 min. The clay fraction (<2 µm) was separated by sedimentation and diluted with deionized water to get a clear suspension. The suspension was dropped onto carbon-coated Cu grids, air dried and stored under environment-controlled conditions at 45% humidity.

Mineral Matter - Overview

The fraction < 2 µm of treated B25 bentonite sample (Opalinus Clay solution, at 35°C and 0.7 MPa, for 285 hours) is mainly composed by beidellite-montmorillonite-illite mixed layer phases (BMI-ml) and dioctahedral vermiculite-smectite mixed layer phases (diVS-ml) and accompanied by illite in traces [fig. 1].

	frequency-% *(n = 130 measured particles)*
BMI-ml (Cluster1)	47%
diVS-ml (Cluster2)	39%
BMI-ml (Cluster3)	10%
Unknown	4%

All measured clay mineral phases summarized result following mineral formula computed from TEM-EDX-measurement of 124 individual particles:

$$Ca^{2+}_{0.19}\ Mg^{2+}_{0.05}\ Na^{+}_{0.00}\ K^{+}_{0.14}\quad Al^{3+}_{1.18}\ Fe^{3+}_{0.56}\ Mg^{2+}_{0.26}\ Ti^{4+}_{0.01}\ (OH)_2\quad Si^{4+}_{3.62}\ Al^{3+}_{0.38}\ O_{10}$$

SDOM *± 0.01 ± 0.00 ± 0.00 ± 0.01 ± 0.01 ± 0.01 ± 0.01 ± 0.00 ± 0.01 ± 0.01*

Legend: SDOM - standard deviation of the mean (= the standard deviation divided by the square root of the number of samples)

The interlayer charge is calculated as 0.63 per $(OH)_2\ O_{10}$ and the octahedral charge as 5.74 per $(OH)_2\ O_{10}$. The particles are characterized by a high octahedral Fe-amount.

The summarized chemical composition of all 124 computed particles is compared with measured data of original B25-bentonite sample [tab. 1]. The chemical composition averaged by measured particles show a slight decreased amount of SiO_2 and Al_2O_3 and a remarkable higher amount for MgO and CaO in comparison to the measured data of original untreated B25-bentonite.

B25-No23 sample is characterized by two morphological groups: (i) aggregates formed by small (≤ 200 nm) xenomorphous plates and (ii) large (≤ 1 µm) xenomorph film-like platy crystals [fig. 2]. Aggregates formed by small (≤ 200 nm) xenomorphous plates dominate the shapes of particles in the micrographs [fig. 2].

The distribution of %S-probability of all measured clay mineral phases [fig. 3a] also indicates the occurrence of two groups: (i) as main group beidellite-montmorillonite-illite ml phases and (ii) diVS-ml (%S-max of this mixture for %S at 30%).

The numerous measured particles by TEM-EDX allow a visualization of distribution of interlayer charges. Considering the TEM-EDX-determined cations Ca^{++}, Mg^{++} and Na^{+} and then computed their ratio as interlayer cations in the mineral formula, Ca^{++}, Mg^{++} and Na^{+} offer to characterize the degree of exchangeable charges in the interlayer space. This charge density of treated B25 bentonite (< 2 µm) shows in this sample a trimodal distribution with maximal frequency-% of charge density at 0.39 (Cluster 1) and 0.55 and 0.71 (Cluster2) per $(OH)_2\ O_{10}$ [fig. 5].

Mineral Matter - Specification

Result of Clustering

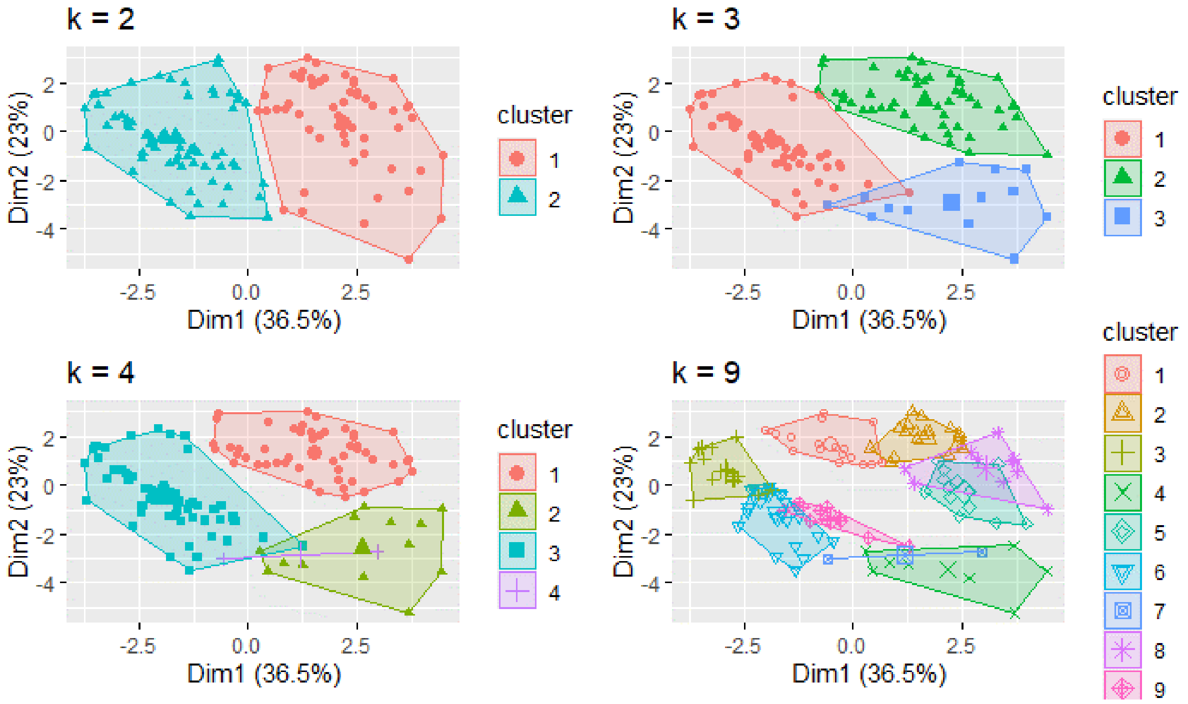

Fig. 8. *Clustering of all measured particles for clusters k = 2, k = 3, k = 4 and k = 9 (source for R-coding: https://uc-r.github.io/kmeans_clustering)*

The optimum of clusters was calculated with k = 3.

		Ca (XII)	Mg (XII)	Na (XII)	K (XII)	Cr3+ (VI)	Al (VI)	Fe3+ (VI)	Mg (VI)	Ti (VI)	Al (IV)	Si (IV)	XII	n_VI	%S
Cluster1	n = 61	0.11	0.08	0.00	0.09	0.00	1.24	0.59	0.17	0.01	0.31	3.69	0.47	2.0	52
Cluster2	n = 51	0.32	0.00	0.00	0.14	0.00	1.03	0.56	0.40	0.01	0.41	3.59	0.80	2.0	39
Cluster3	n = 13	0.15	0.02	0.03	0.39	0.00	1.36	0.43	0.21	0.01	0.57	3.43	0.75	2.0	21

Fig. 9. *Mineral formulae based on TEM-EDX-data summarized following the result of clustering for k=3*

	Sybilla-results	**TEM-EDX-results**	**Notes**
	Illite	diVS-ml (illite)	
Cluster 1	ISS R0	BMI-ml *(BMI 35:45:20)*	*XRD: Montmorillonite and beidellite is only to distinguish by Green-Kelly-test (not available here).*
Cluster 2	IS R0(2) *(%S = 45%)*	diVS-ml *(%S ~ 39%)*	*High K-deficit, low Al(VI), high Fe(VI), high Mg(VI)*
Cluster 3	IS R0(2) *(%S = 45%)*	BMI-ml *(BMI 20:35:45)*	*XRD: Montmorillonite and beidellite is only to distinguish by Green-Kelly-test (not available here).*
Cluster 3	Illite	diVS-ml (illite)	*High K-deficit, no charge deficit, Fe(VI)-rich*

Tab. 2. *Comparison of results from TEM-EDX- and XRD-measurements with clustering procedure*

The clustering of TEM-EDX-data offers a good agreement with the recent result of Sybilla-processing of XRD-traces from oriented specimen [tab. 2].

ISS R0: The X-ray diffraction pattern of the ethylene-glycol saturated oriented specimen shows a limited expandability to 1.47 nm and a difference of 5.60°2θ between 2. and 3. order of smectite interferences. This distance is typically for montmorillonite (Moore & Reynolds, 1989). This result of XRD-processing let expect a maximum of particles for %S ~ 80% by TEM-EDX-measurements, but the maximum of particles measured by TEM-EDX is to find at %S=52% [fig. 3a].

Montmorillonite and beidellite have the same behavior concerning the expandability and they are only to distinguish by XRD using Li like by Greene-Kelly test (Green-Kelly 1952, 1953). So, combination of XRD- and TEM-results (full expandability by XRD and Si ~ 3.69 by TEM-EDX) led conclude the occurrence of beidellite.

IS R0 (2): The Sybilla-procedure of XRD-traces (oriented mounts) has shown an occurrence of a second illite-smectite mixed layer phase with a smectite layers probability of %S = 45%. This situation is to find in Clusters 2 ($\%S_{TEM}$ = 39%) representing high K- and low charge deficient and Fe-rich dioctahedral vermiculite-smectite mixed layer phase (diV-ml) [tab. 2].

The Sybilla-processing of XRD-traces (oriented mounts) also supports the existence of kaolinite and kaolinite-smectite mixed layer phases in fine fraction of sample. Such phases were not to identify or to calculate in TEM-EDX-database (a grain size effect?).

Specifics to the identified clay mineral groups

Beidellite-Montmorillonite-Illite mixed layers (BMI 35:45:20)

61 of 130 computed particles belong so to this assumed classification. The dioctahedral character of this group is proofed by X-ray diffraction. The position of the large (060)-interference of smectite is in the random oriented powder specimen at 1.497 Å.

Montmorillonite and beidellite have the same behavior concerning the expandability and they are only to distinguish by XRD using Li by means of Greene-Kelly test (Greene-Kelly 1952, 1953). So, combination of XRD- and TEM-results (limited expandability by XRD and Si ~ 3.69 by TEM-EDX) led conclude the partial occurrence of beidellite.

Beidellite-Montmorillonite-Illite mixed layers (BMI 35:45:20)

$$Ca_{0.11}\ Mg_{0.08}\ Na_{0.00}\ K_{0.09}\quad Al_{1.24}\ Fe^{3+}_{0.59}\ Mg_{0.17}\ Ti_{0.01}\ (OH)_2\quad Si_{3.69}\ Al_{0.31}\ O_{10}$$

Charge: XII = 0.47 VI = 5.84 IV = 15.69 **Σ = 22.00**
Measured particles by TEM-EDX: 61
Result of clustering: Cluster1 [tab. 2]

In this sample, beidellite is characterized by a typical low octahedral Mg-amount (because of high ratio of octahedral, 3-valent cations). A comparison of octahedral Mg vs. tetrahedral Si indicates the occurrence of two groups for octahedral Mg based on TEM-EDX-data [fig. 3b].

Using the results of clustering (see Cluster1 in tab. 2), the maximum of frequency-% is to find for particles in the Si(IV)-class ~ 3.6 - 3.7 e phuc [tab. 6a]. The mineral formulae, summarized in classes of tetrahedral Si, draw for the maximum an Fe-rich beidellite with low Mg(VI), but remarkable amount of K in the interlayer space [tab. 6b].

Dioctahedral vermiculite-smectite mixed layer phase (diVS-ml):

$$Ca_{0.32}\ Mg_{0.00}\ Na_{0.00}\ K_{0.14}\quad Al_{1.03}\ Fe^{3+}_{0.56}\ Mg_{0.40}\ Ti_{0.01}\ (OH)_2\quad Si_{3.59}\ Al_{0.41}\ O_{10}$$

Charge:	XII = 0.80	VI = 5.61	IV = 15.59	**Σ = 22.00**

Probability of smectite layers (%S): 39%
Probability of illite layers (%I): 61%
Measured particles by TEM-EDX: 51
Result of clustering: Cluster2 [tab. 2]

Illite as part of diVS-ml series

The Rietveld refinement by Profex software (Döbelin & Kleeberg, 2015) indicates the occurrence of two polytypes for illite in treated B25 bentonite: $2M_1$- and 1M-polytype.

Kaolinite-montmorillonite mixed layer phases

The Excel-based procedure (Hoang-Minh et al., 2019) to identify possible clay mineral groups using the TEM-EDX-measurements also includes algorithms to classify kaolinite and kaolinite-montmorillonite mixed layer phases. These algorithms couldn't identify such phases basing on the measured TEM-EDX-data. Otherwise, few particles, which were not to compute, have shown small hexagonal plates typically for kaolinite-bearing phases.

References

Cliff, G. & Lorimer, G. W. (1975). *J. Microsc.* **103**, 203–207.

Döbelin, N., Kleeberg, R. (2015). *Journal of Applied Crystallography* **48**, 1573-1580. DOI: 10.1107/S1600576715014685

Greene-Kelly, R., *Clay Minerals Bull.*, **1**, 221 (1952).

Greene-Kelly, R. 1953. The identification of montmorillonoids in clays. *Journal of Soil Science*. **4** (2), pp. 232-237. https://doi.org/10.1111/j.1365-2389.1953.tb00657.x

Greene-Kelly, R. (1955). Dehydration of the montmorillonite minerals. *Mineralogical Magazine and Journal of the Mineralogical Society*, **30**(228), 604-615. doi:10.1180/minmag.1955.030.228.06

Henning, K.-H. & Störr, M. (1986). Electron Micrographs (TEM, SEM) of Clays and Clay Minerals, p. 325. Akademie-Verlag Berlin.

Hoang-Minh, T., Kasbohm, J., Nguyen-Thanh, L., Nga, P. T., Lai, L. T., Duong, N. T., Thanh, N. D., Thuyet, N. T. M., Anh, D. D., Pusch, R., Knutsson, S. & Ferreiro Mahlmann, R. (2019). *J. Appl. Cryst.* **52**, 133-147. DOI: 10.1107/S1600576718018162

Lorimer, G. W. & Cliff, G. (1976). *Electron Microscopy in Mineralogy*, edited by H. R. Wenk, pp. 506–519. Berlin: Springer Verlag.

Matschiavelli, N., Kluge, S., Podlech, C., Standhaft, D., Grathoff, G., Ikeda-Ohno, A., Warr, L.N., Chukharkina, A., Arnold, T. & Cherkouk, A. (2019). *Environmental Science & Technology.* **53** (17), 10514-10524, DOI: 10.1021/acs.est.9b02670

Mellini, M. & Menichini, R. (1985). *R. Soc. Ital. Miner. Petrol.* **40**, 261–266.

Moore, D.M., Reynolds, R.C. (1989). X-ray Diffraction and the Identification and Analysis of Clay Minerals, Oxford University Press, New York, 332 + xvi pp.

Nguyen-Thanh, L., Herbert, H.-J., Kasbohm, J., Hoang-Minh, T. & Mählmann, R. F. (2014). *Clays Clay Miner.* **62**, 425–446.

Środoń, J., Elsass, F., McHardy, W. J. & Morgan, D. J. (1992). *Clay Miner.* **27**, 137–158.

Data Sheet – B25 bentonite, treated materials *(OPA, 60 °C, 454h)* – TOP

Methodology - Transmission electron microscopy linked with energy-dispersive X-ray spectroscopy (TEM-EDX)

It is expected a characterization of clay mineral phases in treated B25 bentonite by transmission electron microscopy. The sample series No5 represents a percolation of B25 bentonite by Opalinus Clay solution at 60°C for 454 hours. The sample No5_T is the label for the material at the top of sample cylinder.

The different clay mineral phases are to identify and to describe by chemical composition and its variability, morphology, the specific dissolution potential, and further parameter.

Such further parameter like distribution of smectite layers probability (%S) and distribution of charges caused by exchangeable cations interlayer space should serve as additional indicators for mineralogical alterations in treatment experiments with B25 bentonite.

The sample were suspended for TEM-measurement in deionized water and dispersed by ultrasonic treatment for approximately 20 min. The clay fraction (<2 µm) was separated by sedimentation and diluted with deionized water to get a clear suspension. The suspension was dropped onto carbon-coated Cu grids, air dried and stored under environment-controlled conditions at 45% humidity.

TEM-EDX investigations were carried out on the <2 µm fraction using a FEI TECNAI G^2 20 electron transmission microscope at the VNU University of Science, Vietnam National University, Hanoi. This equipment (operated at 200 kV with LaB_6 cathode) was combined with an S-TWIN objective, a windowless EDAX energy-dispersive X-ray system and a FEI Eagle 2k CCD TEM camera.

About 100 individual clay particles per sample were characterized by TEM-EDX with respect to crystal size, crystal habit, and particle morphology and element distribution. The crystal size, crystal habit and particle morphology were described according to Henning & Störr (1986).

For the quantification of element distribution, a calibration of k factors is mandatory (Cliff & Lorimer, 1975; Lorimer & Cliff, 1976; Mellini & Menichini, 1985). These k values are used to calibrate for the specific behaviour of particles against possible irradiation damage. The elements O, Na, Mg, Al, Si, K, Ca and Fe were quantified by applying the EDAX GENESIS–TEM Quant Materials quantification procedure.

In this procedure, the acquired EDX spectra are corrected by background subtraction, Gaussian deconvolution and k-factor corrections using values previously determined on a phyllosilicate standard (muscovite) and selected non-phyllosilicate standards. The average errors in the analyzed elements using the phyllosilicate standard, expressed as the atomic proportions, are 10 (Na), 5 (Fe, Mg, K, Ti, Ca) and 1 (Si, Al).

The measurement time per particle was lowered to 20 s and the exposed area was limited to a 50 nm diameter, avoiding possible irradiation damage of particles. The stability of particles of the sample series was tested for this measurement time at the beginning of any measurement campaign.

Further methodological details related to TEM-EDX-measurements and the Excel-based mathematical procedure using TEM-EDX data for calculation of mineral formulae are described in Hoang-Minh et al. (2019).

These mathematical procedures described in Hoang-Minh et al. (2019) were extended by k-means clustering method for finding subgroups of observations within a data set. The data were standardized (i.e., scaled) to make variables comparable. Euclidean distances were applied as classical method for distance measures. The optimal clusters were determined by Elbow method and Gap statistics[7].

---

[7] *https://uc-r.github.io/kmeans_clustering*

Data Sheet – B25 No5_T (< 2 µm), treated material *(OPA, 60°C, 454 hrs)*

Preparation for TEM

- raw material: compacted material (1.6 g/cm³) of treated B25-sample (OPA, 60°C, 454 hrs)
- suspension on particles < 2 µm on carbon-filmed Cu-grid
- air-dried and humidity-controlled storing

Mineral Matter

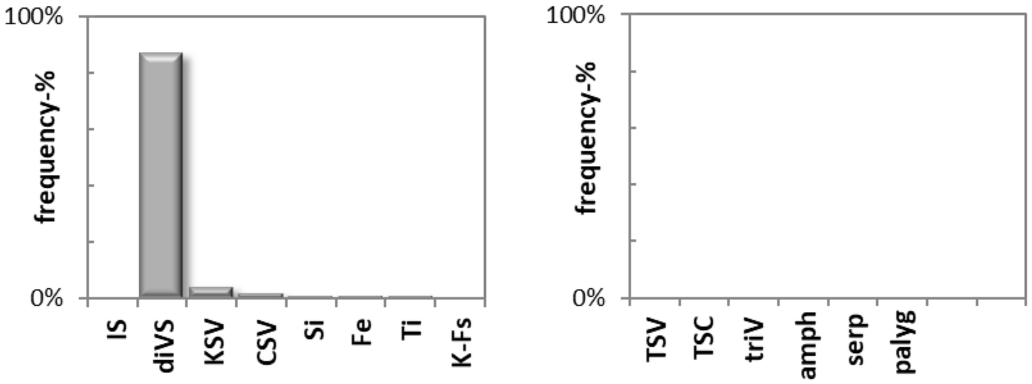

Fig. 1. *Distribution of mineral groups in fraction < 2 µm (in frequency-%)*
Legend: ***IS*** *– illite-smectite-mixed layer series in sense of Środon et al. (1992), diVS – dioctahedral vermiculite-smectite illite-smectite-mixed layer series (= charge- and/or K-deficit),* ***KSV*** *– kaolinite-smectite-dioctahedral vermiculite-mixed layer series,* ***CSV*** *– chlorite-saponite-trioctahedral vermiculite-mixed layer series,* ***Si*** *– quartz or particles with Si-surplus,* ***Fe*** *– Fe-oxide or Fe-oxyhydroxide,* ***Ti*** *– Ti-bearing phases (e.g. rutile, anatase),* ***K-Fs*** *– K-feldspar*

Clay Mineral Composition

All particles of smectite group:

$$Ca_{0.05}\ Mg_{0.13}\ Na_{0.00}\ K_{0.13}\quad Al_{1.26}\ Fe^{3+}_{0.61}\ Mg_{0.11}\ Ti_{0.01}\ (OH)_2\quad Si_{3.62}\ Al_{0.38}\ O_{10}$$

Charge: XII = 0.48 VI = 5.90 IV = 15.62 **Σ = 22.00**

Probability of smectite layers (%S): 42%
Probability of illite layers (%I): 58%

Specific Dissolution Potential (ΔS%)

for H2O, 20 + 60 rpm	-4	(= slow reacting, interlayer group: Ca+Mg (= type B))
for NaCl, 20 rpm	-4	(= slow reacting, interlayer group: Ca+Mg (= type B))
for NaCl, 60 rpm	-109	(= fast reacting, ‘illitization’, interlayer group: Na (= type A))
CEC$_{calc}$:	46 meq / 100 g	(literature: 56 meq / 100 g [Matschiavelli et al., 2019: MAT19])

Measured particles: 120

Table 1. *Summarized chemical composition*

SiO_2	TiO_2	Al_2O_3	Fe_2O_3	MnO	MgO	CaO	Na_2O	K_2O	P_2O_5	Σ	
62.0%	0.1%	24.7%	7.0%		3.1%	0.6%	0.0%	1.2%	0.0%	0.99	measured particles
58.6%	0.0%	22.0%	5.9%		3.0%	1.0%	0.1%	1.1%	0.1%	0.92	measured particles of original B25

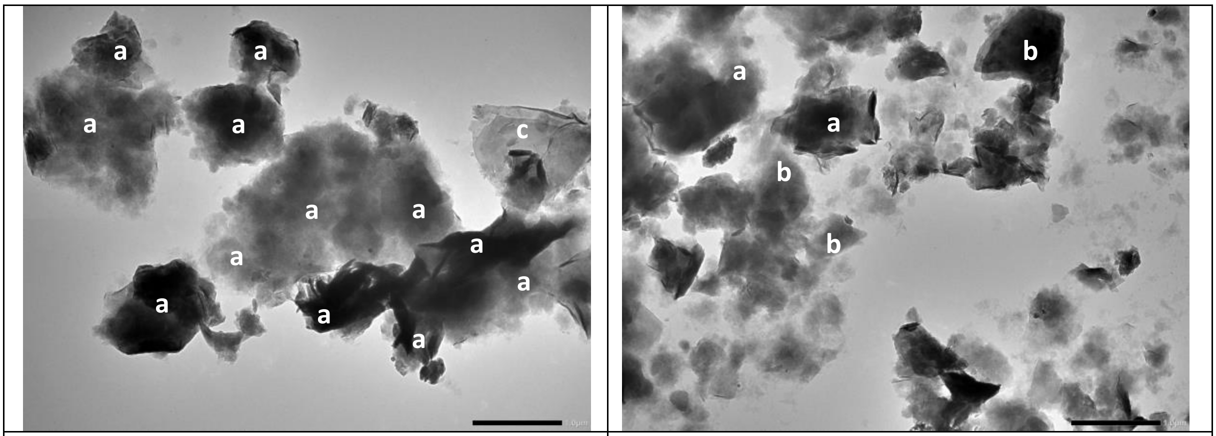

JEM-2100_MAG_X8000_003_AlSZ-5ML.bmp

Magnification: 8k

(p) Aggregates formed by small (≤ 200 nm) xenomorphous plates

(c) Aggregates formed by film-like hypidiomorphous plates

JEM-2100_MAG_X8000_007_AlSZ-5ML.bmp

Magnification: 8k

(i) Aggregates formed by small (≤ 200 nm) xenomorphous plates, partially with folds

(j) large (≤ 1 µm) xenomorph film-like platy crystals

Fig. 2. *Morphology of particles (TEM-micrographs)*

Distribution of smectite layers probability (%S)

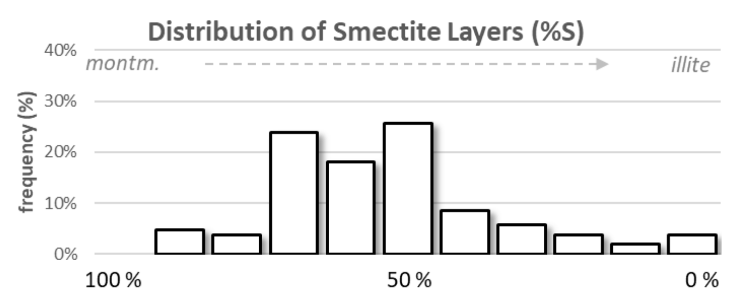

Description: *The distribution of %S-probability indicates the occurrence of two groups: (i) mixture of beidellite-montmorillonite interstratifications (= assumption) with diVS-ml as well as (ii) illite with K-deficiency.*

Fig. 3a. *Distribution of smectite layers probability (%S)*

Differentiation by relation “Octahedral Mg vs. tetrahedral Si”?

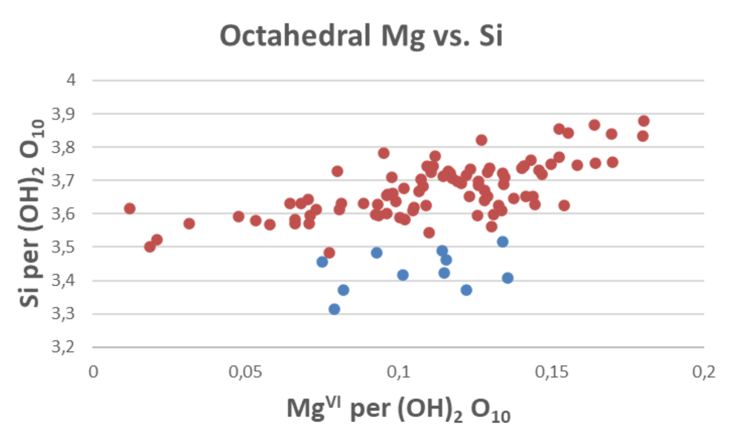

Description: *This diagram indicates the occurrence of two groups of Mg in relation to tetrahedral Si. Probably, this distribution mirrors 2 phases (I) beidellite-montmorillonite interstratifications (red) and (II) diVS-ml (blue)*

Fig. 3b. *Distribution of octahedral Mg vs. tetrahedral Si [all per(OH)$_2$ O$_{10}$]*

Distribution of K in relation to tetrahedral Si

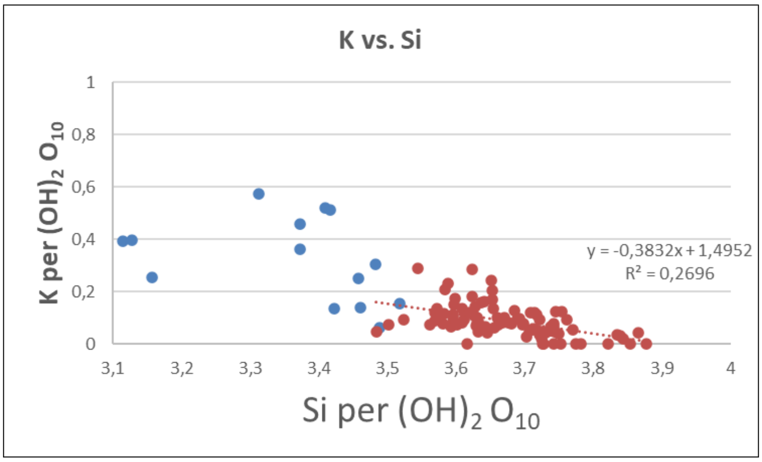

Description: *This diagram visualizes possible particles (beidellite-montmorillonite interstratification?) with low K (red dots) and diVS-ml phases (blue dots)*

Fig. 4. *Distribution of K in interlayer space vs. tetrahedral Si [all per$(OH)_2$ O_{10}]*

Distribution of charges (exchangeable from interlayer space)

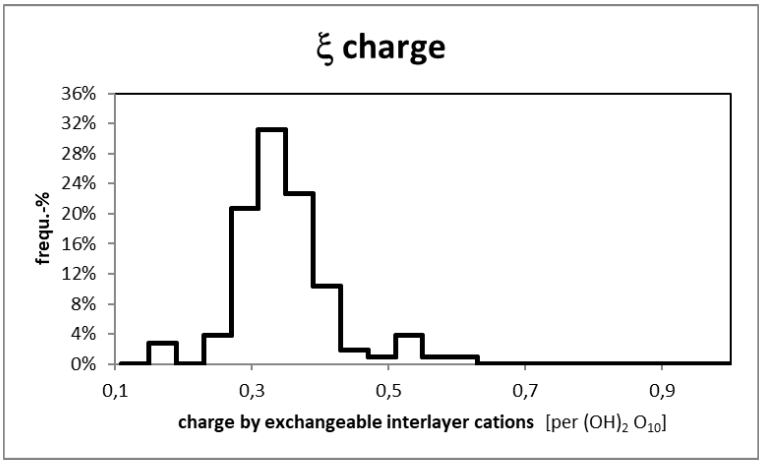

This diagram visualizes the distribution of exchangeable charges in the interlayer space (Ca, Mg, Na) determined and computed by TEM-EDX-data.

Description: *Distribution of charge density at 0.31 per $(OH)_2$ O_{10}.*

Fig. 5. *Distribution of charges*

Beidellite-montmorillonite interstratification BM 65:35 *(Cluster2):*

$$Ca_{0.05}\ Mg_{0.12}\ Na_{0.00}\ K_{0.09}\quad Al_{1.28}\ Fe^{3+}_{0.60}\ Mg_{0.11}\ Ti_{0.01}\ (OH)_2\ \ Si_{3.67}\ Al_{0.33}\ O_{10}$$

Charge: XII = 0.43 VI = 5.90 IV = 15.67 **Σ = 22.00**

Measured particles: 92

Distribution of BM-interstratifications (Cluster2)

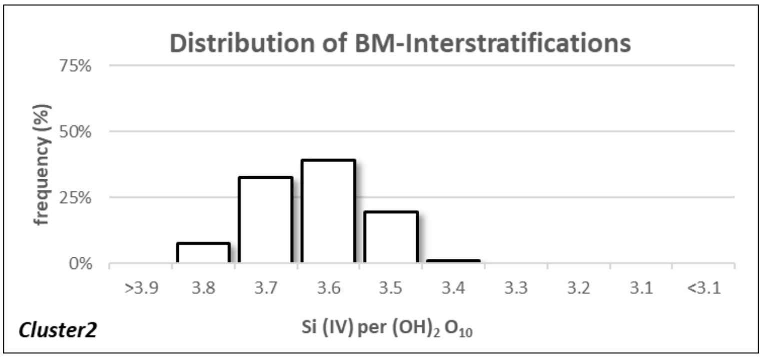

Description: *The distribution of BM-interstratifications (classified as Cluster2) draws a maximum of frequency (%) at tetrahedral Si-value between 3.6 – 3.7 e phuc*

Fig. 6a. *Distribution of assumed beidellite-montmorillonite interstratifications*

BM65:35?	particles (abs)	Ca (XII)	Mg (XII)	Na (XII)	K (XII)	Cr3+ (VI)	Al (VI)	Fe3+ (VI)	Mg (VI)	Ti (VI)	Al (IV)	Si (IV)	XII	n_VI	%S
Si >3.9	n = 0														
Si 3.9-3.8	n = 7	0.04	0.10	0.00	0.02	0.00	1.38	0.46	0.16	0.00	0.15	3.85	0.3	2.0	79
Si 3.8-3.7	n = 30	0.05	0.12	0.00	0.05	0.00	1.27	0.59	0.13	0.01	0.27	3.73	0.4	2.0	60
Si 3.7-3.6	**n = 36**	**0.05**	**0.12**	**0.00**	**0.11**	**0.00**	**1.27**	**0.62**	**0.11**	**0.01**	**0.35**	**3.65**	**0.5**	**2.0**	**47**
Si 3.6-3.5	n = 18	0.05	0.13	0.00	0.13	0.00	1.30	0.62	0.08	0.01	0.43	3.57	0.5	2.0	37
Si 3.5-3.4	n = 1	0.06	0.21	0.00	0.05	0.00	1.34	0.58	0.08	0.00	0.52	3.48	0.6	2.0	26
Si 3.4-3.3	n = 0														
Si 3.3-3.2	n = 0														
Si 3.2-3.1	n = 0														
Si <3.1	n = 0														

Fig. 6b. *Computed averaged mineral formulae of phases in the different Si(IV)-classes*

Dioctahedral Vermiculite-Smectite mixed layer phases (diVS-ml) *(Cluster1):*

$$Ca_{0.04}\ Mg_{0.15}\ Na_{0.01}\ K_{0.32}\quad Al_{1.19}\ Fe^{3+}_{0.68}\ Mg_{0.11}\ Ti_{0.03}\ (OH)_2\ \ Si_{3.37}\ Al_{0.63}\ O_{10}$$

Charge: XII = 0.71 VI = 5.92 IV = 15.37 **Σ = 22.00**

Probability of smectite layers (%S):	15%
Probability of illite layers (%I):	85%
Measured particles:	14

Distribution of smectite layers probability (%S) in diVS-ml (Cluster1)

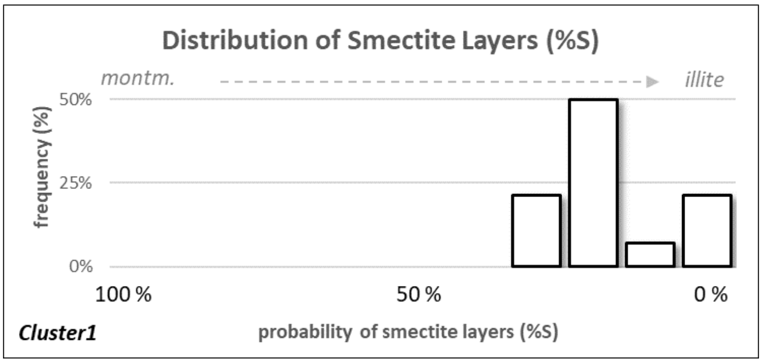

Description: *The distribution of diVS-ml (classified as Cluster 1) draws a maximum of frequency (%) for smectite layer probability at 20%*

Fig. 7a. *Distribution of smectite layers probability in diVS-ml*

diVS-ml?	particles (abs)	Ca (XII)	Mg (XII)	Na (XII)	K (XII)	Cr3+ (VI)	Al (VI)	Fe3+ (VI)	Mg (VI)	Ti (VI)	Al (IV)	Si (IV)	XII	n_VI	%S
%S >95%	n = 0														
%S 95-85%	n = 0														
%S 85-75%	n = 0														
%S 75-65%	n = 0														
%S 65-55%	n = 0														
%S 55-45%	n = 0														
%S 45-35%	n = 0														
%S 35-25%	n = 3	0.04	0.16	0.00	0.17	0.00	1.14	0.71	0.11	0.04	0.50	3.50	0.6	2.0	28
%S 25-15%	**n = 7**	**0.05**	**0.12**	**0.01**	**0.34**	**0.00**	**1.28**	**0.60**	**0.11**	**0.01**	**0.58**	**3.42**	**0.7**	**2.0**	**19**
%S <15%	n = 4	0.03	0.19	0.01	0.41	0.00	1.06	0.79	0.10	0.05	0.82	3.18	0.9	2.0	2

Fig. 7b. *Computed averaged mineral formulae of diVS-ml phases in the different smectite layers probability (%S)-classes*

Description – B25 No5_T (< 2 µm), treated material *(OPA, 60°C, 454 hrs)*

Preparation for TEM

The powder of compacted and treated B25-No5_T-sample was suspended in deionized water and dispersed by ultrasonic treatment for approximately 20 min. The clay fraction (<2 µm) was separated by sedimentation and diluted with deionized water to get a clear suspension. The suspension was dropped onto carbon-coated Cu grids, air dried and stored under environment-controlled conditions at 45% humidity.

Mineral Matter - Overview

The fraction < 2 µm of treated B25 bentonite sample (Opalinus Clay solution, at 60°C, for 454 hours) is mainly composed by beidellite-montmorillonite interstratification (BM) and dioctahedral vermiculite-smectite mixed layer phases (diVS-ml) and accompanied by two types of illite. Furthermore, kaolinite, Si-surplus particles (Si, e.g. quartz) and chlorite-bearing phases were identified in traces in this sample [fig. 1].

	frequency-% *(n = 120 measured particles)*
BM (Cluster2)	77%
diVS-ml (Cluster1)	11%
Kaolinite & KSV-ml	4%
Chlorite & CSV-ml	2%
Si-surplus	1%
Unknown	4%

All measured clay mineral phases summarized result following mineral formula computed from TEM-EDX-measurement of 106 individual particles:

$$Ca^{2+}_{0.05}\ Mg^{2+}_{0.13}\ Na^{+}_{0.00}\ K^{+}_{0.13}\quad Al^{3+}_{1.27}\ Fe^{3+}_{0.61}\ Mg^{2+}_{0.11}\ Ti^{4+}_{0.01}\ (OH)_2\quad Si^{4+}_{3.62}\ Al^{3+}_{0.38}\ O_{10}$$

SDOM *± 0.00 ± 0.00 ± 0.00 ± 0.01 ± 0.01 ± 0.01 ± 0.00 ± 0.00 ± 0.01 ± 0.01*

Legend: SDOM - standard deviation of the mean (= the standard deviation divided by the square root of the number of samples)

The interlayer charge is calculated as 0.48 per $(OH)_2$ O_{10} and the octahedral charge as 5.90 per $(OH)_2$ O_{10}. The particles are characterized by a high octahedral Fe-amount.

The summarized chemical composition of all 106 computed particles is compared with measured data of original B25-bentonite sample [tab. 1]. The chemical composition averaged by measured particles show a slight increased amount of Al_2O_3 and Fe_2O_3 and reduced amount for SiO_2 and CaO in comparison to the measured data of original untreated B25-bentonite.

B25-No5_T sample is characterized by two morphological groups: (i) aggregates formed by small (≤ 200 nm) xenomorphous plates and (ii) large (≤ 1 µm) xenomorph film-like platy crystals [fig. 2].

Aggregates formed by small (≤ 200 nm) xenomorphous plates dominate the shapes of particles in the micrographs [fig. 2].

The distribution of %S-probability of all measured clay mineral phases [fig. 3a] also indicates the occurrence of two groups: (i) as main group a mixture of beidellite-montmorillonite interstratifications (%S-max of this part at %S ~ 70%) and diVS-ml (%S-max of this part of mixture for %S at 40-50%) and (ii) illite with K- and charge deficit (%S-class = 0-10%).

The numerous measured particles by TEM-EDX allow a visualization of distribution of interlayer charges. Considering the TEM-EDX-determined cations Ca^{++}, Mg^{++} and Na^{+} and then computed their ratio as interlayer cations in the mineral formula, Ca^{++}, Mg^{++} and Na^{+} offer to characterize the degree of exchangeable charges in the interlayer space. This charge density of treated B25 bentonite (< 2 µm) shows in this sample a distribution with maximal frequency-% of charge density at 0.31 per $(OH)_2$ O_{10} [fig. 5]. This interval of interlayer charge density caused by exchangeable cations from 0.23 - 0.43 per $(OH)_2$ O_{10} represents diVS-ml and beidellite-montmorillonite interstratifications.

Mineral Matter - Specification

Result of Clustering

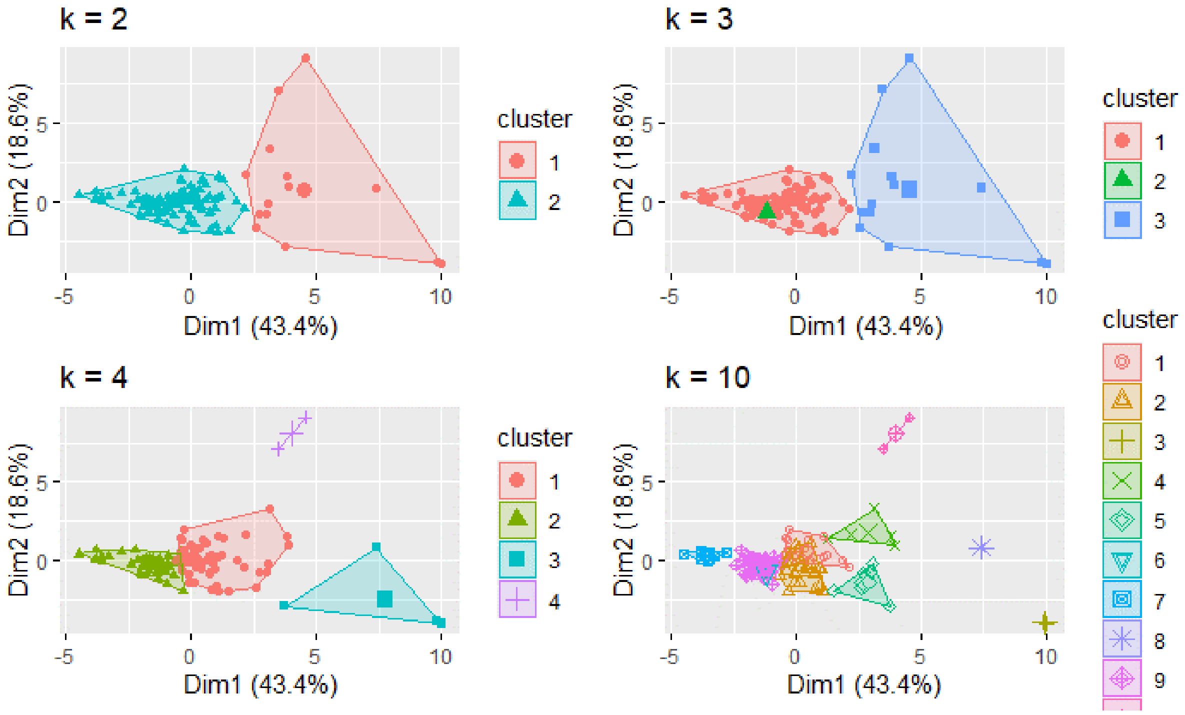

Fig. 8. *Clustering of all measured particles for clusters k = 2, k = 3, k = 4 and k = 5 (source for R-coding: https://uc-r.github.io/kmeans_clustering)*

The optimum of clusters was calculated with k = 2.

		Ca (XII)	Mg (XII)	Na (XII)	K (XII)	Cr3+ (VI)	Al (VI)	Fe3+ (VI)	Mg (VI)	Ti (VI)	Al (IV)	Si (IV)	XII	n_VI	%S
Cluster1	n = 14	0.04	0.15	0.01	0.32	0.00	1.19	0.68	0.11	0.03	0.63	3.37	0.71	2.0	15
Cluster2	n = 92	0.05	0.12	0.00	0.09	0.00	1.28	0.60	0.11	0.01	0.33	3.67	0.43	2.0	51

Fig. 9. *Mineral formulae based on TEM-EDX-data summarized following the result of clustering for k=2*

	Sybilla-results	TEM-EDX-results	Notes

Cluster 1	IS R0(2) *(%S = 33%)*	diVS-ml *(%S ~ 15%)*	*High K-deficit, low Al(VI), high Fe(VI)*
Cluster 2	IS R0(1) *(%S = 100%)*	BM 65:35	*XRD: Montmorillonite and beidellite is only to distinguish by Green-Kelly-test (not available here).*

Tab. 2. *Comparison of results from TEM-EDX- and XRD-measurements with clustering procedure*

The clustering of TEM-EDX-data indicates a comparable agreement with the recent result of Sybilla-processing of XRD-traces from oriented specimen [tab. 2]. The clustering of diVS-ml includes also mica-near, non-swelling diVS-ml phases that is reducing the %S-value by TEM-EDX-data in comparison to Sybilla-results.

IS R0 (1): The X-ray diffraction pattern of the ethylene-glycol saturated oriented specimen shows a full expandability to 1.75 nm and a difference of 5.34°2θ between 2. and 3. order of smectite interferences. This distance is typically for montmorillonite (Moore & Reynolds, 1989). This result of XRD-processing let expect a maximum of particles for %S ~ 100% by TEM-EDX-measurements, but the maximum of particles measured by TEM-EDX is to find at %S=51% [fig. 3a].

Montmorillonite and beidellite have the same behavior concerning the expandability and they are only to distinguish by XRD using Li like by Greene-Kelly test (Green-Kelly 1952, 1953). So, combination of XRD- and TEM-results (full expandability by XRD and Si ~ 3.67 by TEM-EDX) led conclude the occurrence of beidellite.

IS R0 (2): The Sybilla-procedure of XRD-traces (oriented mounts) has shown an occurrence of a second illite-smectite mixed layer phase with a smectite layers probability of %S = 33%. This situation is to find in Cluster 1 ($\%S_{TEM}$ = 15%) representing high K- and low charge deficient and Fe-rich dioctahedral vermiculite-smectite mixed layer phase (diV-ml) [tab. 2].

The Sybilla-processing of XRD-traces (oriented mounts) also supports the existence of kaolinite and kaolinite-smectite mixed layer phases in fine fraction of sample. Such phases were not to calculate in TEM-EDX-database (a grain size effect?).

Specifics to the identified clay mineral groups

Beidellite-montmorillonite-interstratification (BM 65:35)

92 of 106 computed particles belong so to this assumed classification. The dioctahedral character of this group is proofed by X-ray diffraction. The position of the large (060)-interference of smectite is in the random oriented powder specimen at 1.497 Å.

Montmorillonite and beidellite have the same behavior concerning the expandability and they are only to distinguish by XRD using Li by means of Greene-Kelly test (Greene-Kelly 1952, 1953). So, combination of XRD- and TEM-results (full expandability by XRD and Si ~ 3.67 by TEM-EDX) led conclude the occurrence of beidellite.

Beidellite-Montmorillonite Interstratification *(BM 65:35)*

$$Ca_{0.05}\,Mg_{0.12}\,Na_{0.00}\,K_{0.09}\quad Al_{1.28}\,Fe^{3+}_{0.60}\,Mg_{0.11}\,Ti_{0.01}\,(OH)_2\quad Si_{3.67}\,Al_{0.33}\,O_{10}$$

Charge: XII = 0.43 VI = 5.90 IV = 15.67 **Σ = 22.00**

Measured particles by TEM-EDX: 92

Result of clustering: Cluster2 [tab. 2]

In this sample, beidellite is characterized by a typical low octahedral Mg-amount (because of high ratio of octahedral, 3-valent cations). A comparison of octahedral Mg vs. tetrahedral Si based on TEM-EDX-data indicates the growing occurrence of octahedral Mg with rising ratio of montmorillonite in this beidellite-montmorillonite interstratification [fig. 3b].

Using the results of clustering (see Cluster2 in tab. 2), the maximum of frequency-% is to find for particles in the Si(IV)-class ~ 3.6 - 3.7 e phuc [tab. 6a], representing a beidellite-montmorillonite interstratification in a ratio BM ~ 65:35. The mineral formulae, summarized in classes of tetrahedral Si, draw for the maximum an Fe-rich beidellite with low Mg(VI), but remarkable amount of K in the interlayer space [tab. 6b].

Dioctahedral vermiculite-smectite mixed layer phase (diVS-ml):

$$Ca_{0.04}\ Mg_{0.15}\ Na_{0.01}\ K_{0.32}\quad Al_{1.19}\ Fe^{3+}_{0.68}\ Mg_{0.11}\ Ti_{0.03}\ (OH)_2\quad Si_{3.37}\ Al_{0.63}\ O_{10}$$

Charge:	XII = 0.71	VI = 5.92	IV = 15.37	**Σ = 22.00**
Probability of smectite layers (%S):	15%			
Probability of illite layers (%I):	85%			
Measured particles by TEM-EDX:	14			
Result of clustering:	Cluster 1 [tab. 2]			

Illite as part of diVS-ml series

The Rietveld refinement by Profex software (Döbelin & Kleeberg, 2015) indicates the occurrence of two polytypes for illite in treated B25 bentonite: $2M_1$- and 1M-polytype.

Kaolinite-montmorillonite mixed layer phases

The Excel-based procedure (Hoang-Minh et al., 2019) to identify possible clay mineral groups using the TEM-EDX-measurements also includes algorithms to classify kaolinite and kaolinite-montmorillonite mixed layer phases. These algorithms couldn't identify such phases basing on the measured TEM-EDX-data. Otherwise, few particles, which were not to compute, have shown small hexagonal plates typically for kaolinite-bearing phases.

References

Cliff, G. & Lorimer, G. W. (1975). *J. Microsc.* **103**, 203–207.

Döbelin, N., Kleeberg, R. (2015). *Journal of Applied Crystallography* **48**, 1573-1580. DOI: 10.1107/S1600576715014685

Greene-Kelly, R., *Clay Minerals Bull.*, **1**, 221 (1952).

Greene-Kelly, R. 1953. The identification of montmorillonoids in clays. *Journal of Soil Science*. **4** (2), pp. 232-237. https://doi.org/10.1111/j.1365-2389.1953.tb00657.x

Greene-Kelly, R. (1955). Dehydration of the montmorillonite minerals. *Mineralogical Magazine and Journal of the Mineralogical Society*, **30**(228), 604-615. doi:10.1180/minmag.1955.030.228.06

Henning, K.-H. & Störr, M. (1986). Electron Micrographs (TEM, SEM) of Clays and Clay Minerals, p. 325. Akademie-Verlag Berlin.

Hoang-Minh, T., Kasbohm, J., Nguyen-Thanh, L., Nga, P. T., Lai, L. T., Duong, N. T., Thanh, N. D., Thuyet, N. T. M., Anh, D. D., Pusch, R., Knutsson, S. & Ferreiro Mahlmann, R. (2019). *J. Appl. Cryst.* **52**, 133-147. DOI: 10.1107/S1600576718018162

Lorimer, G. W. & Cliff, G. (1976). *Electron Microscopy in Mineralogy*, edited by H. R. Wenk, pp. 506–519. Berlin: Springer Verlag.

Matschiavelli, N., Kluge, S., Podlech, C., Standhaft, D., Grathoff, G., Ikeda-Ohno, A., Warr, L.N., Chukharkina, A., Arnold, T. & Cherkouk, A. (2019). *Environmental Science & Technology.* **53** (17), 10514-10524, DOI: 10.1021/acs.est.9b02670

Mellini, M. & Menichini, R. (1985). *R. Soc. Ital. Miner. Petrol.* **40**, 261–266.

Moore, D.M., Reynolds, R.C. (1989). X-ray Diffraction and the Identification and Analysis of Clay Minerals, Oxford University Press, New York, 332 + xvi pp.

Nguyen-Thanh, L., Herbert, H.-J., Kasbohm, J., Hoang-Minh, T. & Mählmann, R. F. (2014). *Clays Clay Miner.* **62**, 425–446.

Środoń, J., Elsass, F., McHardy, W. J. & Morgan, D. J. (1992). *Clay Miner.* **27**, 137–158.

Data Sheet – B25 bentonite, treated materials *(OPA, 60 °C, 454h)* - CENTER

Methodology - Transmission electron microscopy linked with energy-dispersive X-ray spectroscopy (TEM-EDX)

It is expected a characterization of clay mineral phases in treated B25 bentonite by transmission electron microscopy. The sample series No5 represents a percolation of B25 bentonite by Opalinus Clay solution at 60°C for 454 hours. The sample No5_M is the label for the material at the center of sample cylinder.

The different clay mineral phases are to identify and to describe by chemical composition and its variability, morphology, the specific dissolution potential, and further parameter.

Such further parameter like distribution of smectite layers probability (%S) and distribution of charges caused by exchangeable cations interlayer space should serve as additional indicators for mineralogical alterations in treatment experiments with B25 bentonite.

The sample were suspended for TEM-measurement in deionized water and dispersed by ultrasonic treatment for approximately 20 min. The clay fraction (<2 µm) was separated by sedimentation and diluted with deionized water to get a clear suspension. The suspension was dropped onto carbon-coated Cu grids, air dried and stored under environment-controlled conditions at 45% humidity.

TEM-EDX investigations were carried out on the <2 µm fraction using a FEI TECNAI G^2 20 electron transmission microscope at the VNU University of Science, Vietnam National University, Hanoi. This equipment (operated at 200 kV with LaB_6 cathode) was combined with an S-TWIN objective, a windowless EDAX energy-dispersive X-ray system and a FEI Eagle 2k CCD TEM camera.

About 100 individual clay particles per sample were characterized by TEM-EDX with respect to crystal size, crystal habit, and particle morphology and element distribution. The crystal size, crystal habit and particle morphology were described according to Henning & Störr (1986).

For the quantification of element distribution, a calibration of k factors is mandatory (Cliff & Lorimer, 1975; Lorimer & Cliff, 1976; Mellini & Menichini, 1985). These k values are used to calibrate for the specific behaviour of particles against possible irradiation damage. The elements O, Na, Mg, Al, Si, K, Ca and Fe were quantified by applying the EDAX GENESIS–TEM Quant Materials quantification procedure.

In this procedure, the acquired EDX spectra are corrected by background subtraction, Gaussian deconvolution and k-factor corrections using values previously determined on a phyllosilicate standard (muscovite) and selected non-phyllosilicate standards. The average errors in the analyzed elements using the phyllosilicate standard, expressed as the atomic proportions, are 10 (Na), 5 (Fe, Mg, K, Ti, Ca) and 1 (Si, Al).

The measurement time per particle was lowered to 20 s and the exposed area was limited to a 50 nm diameter, avoiding possible irradiation damage of particles. The stability of particles of the sample series was tested for this measurement time at the beginning of any measurement campaign.

Further methodological details related to TEM-EDX-measurements and the Excel-based mathematical procedure using TEM-EDX data for calculation of mineral formulae are described in Hoang-Minh et al. (2019).

These mathematical procedures described in Hoang-Minh et al. (2019) were extended by k-means clustering method for finding subgroups of observations within a data set. The data were standardized (i.e., scaled) to make variables comparable. Euclidean distances were applied as classical method for distance measures. The optimal clusters were determined by Elbow method and Gap statistics[8].

---

[8] *https://uc-r.github.io/kmeans_clustering*

Data Sheet – B25 No5_M (< 2 µm), treated material *(OPA, 60°C, 454 hrs)*

Preparation for TEM

- raw material: compacted material (1.6 g/cm³) of treated B25-sample (OPA, 60°C, 454 hrs)
- suspension on particles < 2 µm on carbon-filmed Cu-grid
- air-dried and humidity-controlled storing

Mineral Matter

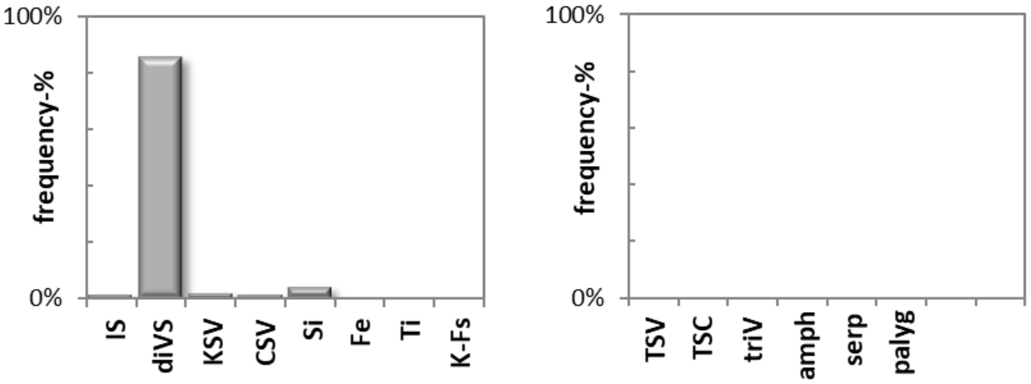

Fig. 1. *Distribution of mineral groups in fraction < 2 µm (in frequency-%)*
Legend: ***IS*** *– illite-smectite-mixed layer series in sense of Środon et al. (1992), diVS – dioctahedral vermiculite-smectite illite-smectite-mixed layer series (= charge- and/or K-deficit),* ***KSV*** *– kaolinite-smectite-dioctahedral vermiculite-mixed layer series,* ***CSV*** *– chlorite-saponite-trioctahedral vermiculite-mixed layer series,* ***Si*** *– quartz or particles with Si-surplus,* ***Fe*** *– Fe-oxide or Fe-oxyhydroxide,* ***Ti*** *– Ti-bearing phases (e.g. rutile, anatase),* ***K-Fs*** *– K-feldspar*

Clay Mineral Composition

All particles of smectite group:

$$Ca_{0.07}\ Mg_{0.13}\ Na_{0.00}\ K_{0.14}\quad Al_{1.02}\ Fe^{3+}_{0.88}\ Mg_{0.08}\ Ti_{0.01}\ (OH)_2\quad Si_{3.53}\ Al_{0.47}\ O_{10}$$

Charge:	XII = 0.54	VI = 5.93	IV = 15.53	**Σ = 22.00**
Probability of smectite layers (%S):	32%			
Probability of illite layers (%I):	68%			

Specific Dissolution Potential (ΔS%)

for H2O, 20 + 60 rpm	-9	(= slow reacting, interlayer group: Ca+Mg (= type B))
for NaCl, 20 rpm	-10	(= slow reacting, interlayer group: Ca+Mg (= type B))
for NaCl, 60 rpm	-112	(= fast reacting, 'illitization', interlayer group: Na (= type A))
CEC$_{calc}$:	50 meq / 100 g	(literature: 56 meq / 100 g [Matschiavelli et al., 2019: MAT19])

Measured particles: 155

Table 1. *Summarized chemical composition*

SiO_2	TiO_2	Al_2O_3	Fe_2O_3	MnO	MgO	CaO	Na_2O	K_2O	P_2O_5	Σ	
61.3%	0.2%	23.0%	10.5%		2.8%	0.8%	0.0%	1.4%	0.0%	1.00	measured particles
63.7%	0.0%	23.9%	6.4%		3.3%	1.1%	0.0%	1.2%	0.0%	1.00	measured particles of original B25

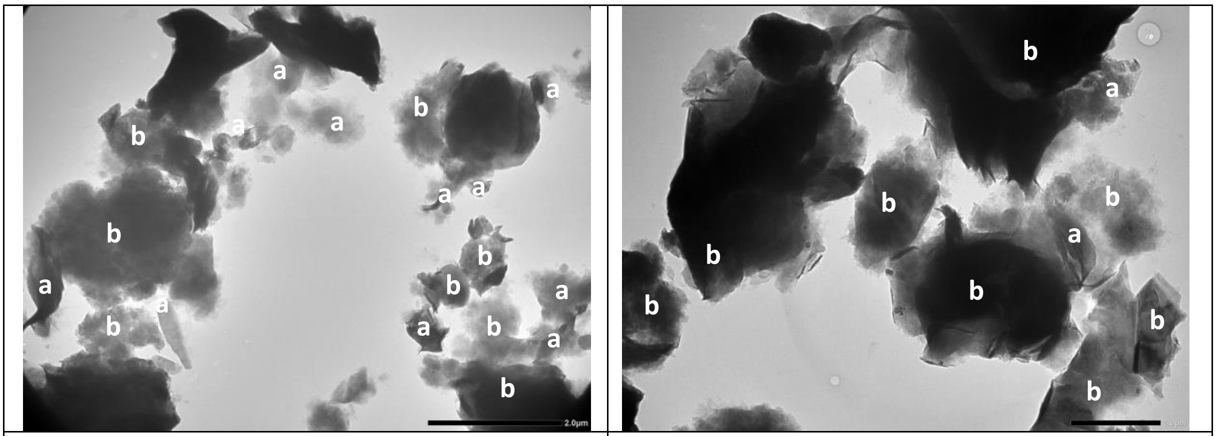

JEM-2100_MAG_X6000_010_AISZ-5ML.bmp

Magnification: 6k

(q) Aggregates formed by small (≤ 200 nm) xenomorphous plates
(r) mostly large (≤ 1 µm) xenomorph film-like platy crystals

JEM-2100_MAG_X8000_001_AISZ-5ML.bmp

Magnification: 8k

(k) Aggregates formed by small (≤ 200 nm) xenomorphous plates
(l) large (≤ 1 µm) xenomorph film-like platy crystals

Fig. 2. *Morphology of particles (TEM-micrographs)*

Distribution of smectite layers probability (%S)

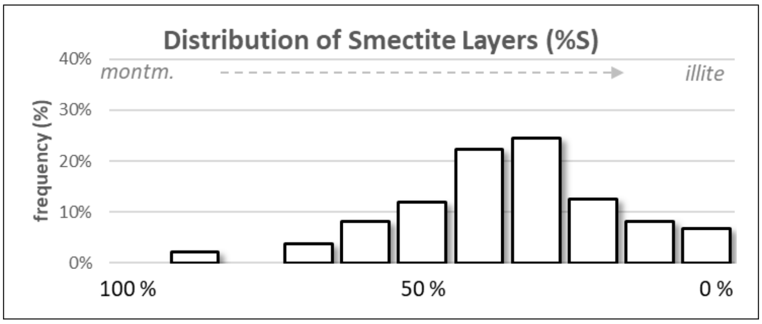

Fig. 3a. *Distribution of smectite layers probability (%S)*

Description: *The distribution of %S-probability indicates the occurrence of two groups: (i) mixture of beidellite-montmorillonite interstratifications (= assumption) with diVS-ml as well as (ii) illite with K-deficiency.*

Differentiation by relation “Octahedral Mg vs. tetrahedral Si”?

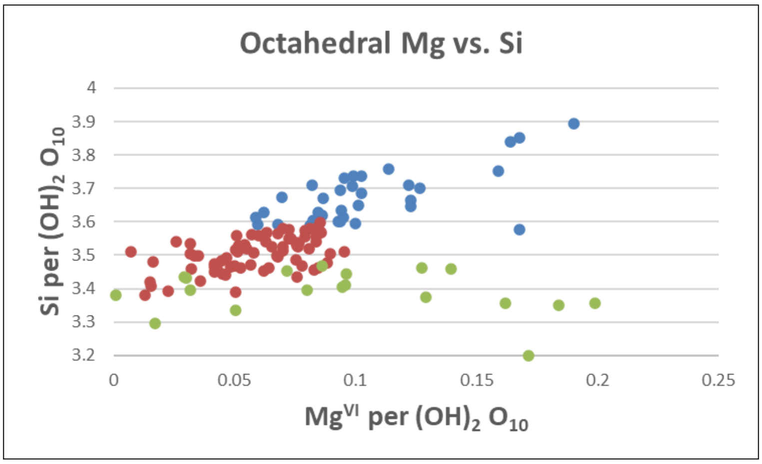

Description: *This diagram indicates the occurrence of groups of Mg in relation to tetrahedral Si. Probably, this distribution mirrors 2 phases (I) beidellite-montmorillonite interstratifications (blue) and (II) diVS-ml (red, green)*

Fig. 3b. *Distribution of octahedral Mg vs. tetrahedral Si [all per$(OH)_2$ O_{10}]*

Distribution of K in relation to tetrahedral Si

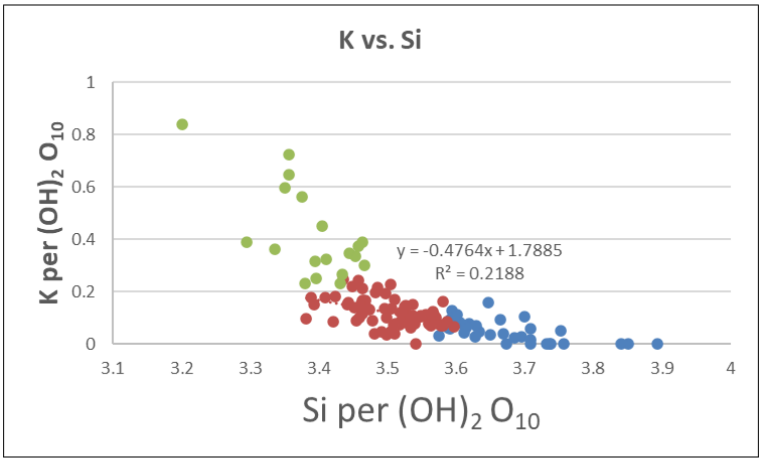

Description: *This diagram visualizes possible particles (beidellite-montmorillonite interstratification?) with low K (blue dots) and two groups of diVS-ml phases (red dots; green dots = mica-near)*

Fig. 4. *Distribution of K in interlayer space vs. tetrahedral Si [all per$(OH)_2\ O_{10}$]*

Distribution of charges (exchangeable from interlayer space)

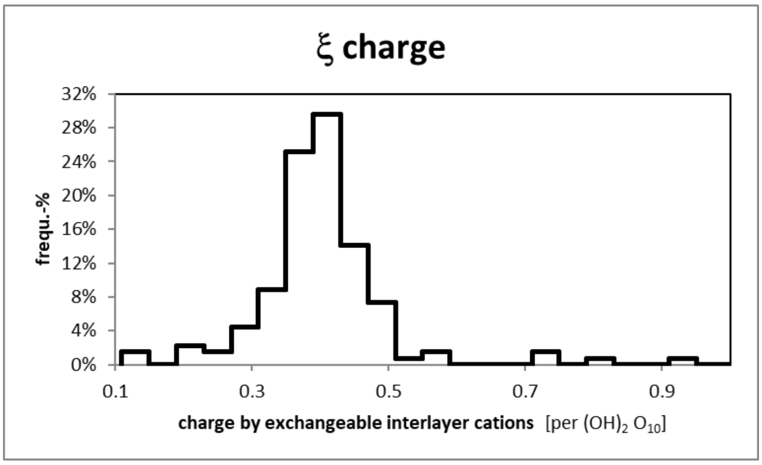

This diagram visualizes the distribution of exchangeable charges in the interlayer space (Ca, Mg, Na) determined and computed by TEM-EDX-data.

Description: *Distribution with maximum of charge density at 0.39 per $(OH)_2\ O_{10}$.*

Fig. 5. *Distribution of charges*

Beidellite-montmorillonite interstratification BM 65:35 *(Cluster1):*

$$Ca_{0.07}\ Mg_{0.11}\ Na_{0.00}\ K_{0.05}\quad Al_{1.12}\ Fe^{3+}_{0.77}\ Mg_{0.10}\ Ti_{0.01}\ (OH)_2\quad Si_{3.67}\ Al_{0.33}\ O_{10}$$

Charge: XII = 0.42 VI = 5.91 IV = 15.67 **Σ = 22.00**

Measured particles: 34

Distribution of BM-interstratifications (Cluster1)

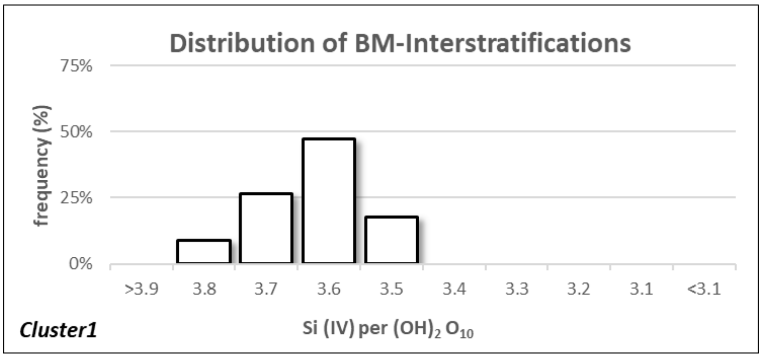

Description: *The distribution of BM-interstratifications (classified as Cluster1) draws a maximum of frequency (%) at tetrahedral Si-value between 3.6 – 3.7 e phuc*

Fig. 6a. *Distribution of assumed beidellite-montmorillonite interstratifications*

BM 65:35?	*particles (abs)*	**Ca (XII)**	**Mg (XII)**	**Na (XII)**	**K (XII)**	**Cr3+ (VI)**	**Al (VI)**	**Fe3+ (VI)**	**Mg (VI)**	**Ti (VI)**	**Al (IV)**	**Si (IV)**	**XII**	**n_VI**	**%S**
Si >3.9	n = 0														
Si 3.9-3.8	n = 3	0.06	0.09	0.00	0.00	0.00	1.30	0.52	0.17	0.00	0.14	3.86	0.31	2.0	82
Si 3.8-3.7	n = 9	0.06	0.11	0.00	0.03	0.00	1.17	0.70	0.11	0.01	0.27	3.73	0.37	2.0	59
Si 3.7-3.6	**n = 16**	**0.08**	**0.12**	**0.00**	**0.06**	**0.00**	**1.07**	**0.83**	**0.09**	**0.01**	**0.36**	**3.64**	**0.44**	**2.0**	**46**
Si 3.6-3.5	n = 6	0.10	0.12	0.00	0.08	0.00	1.07	0.83	0.09	0.00	0.41	3.59	0.50	2.0	39
Si 3.5-3.4	n = 0														
Si 3.4-3.3	n = 0														
Si 3.3-3.2	n = 0														
Si 3.2-3.1	n = 0														
Si <3.1	n = 0														

Fig. 6b. *Computed averaged mineral formulae of phases in the different Si(IV)-classes*

Dioctahedral Vermiculite-Smectite mixed layer phases (diVS-ml) *(Cluster3):*

$$Ca_{0.08}\ Mg_{0.23}\ Na_{0.00}\ K_{0.18}\quad Al_{0.57}\ Fe^{3+}_{1.29}\ Mg_{0.10}\ Ti_{0.04}\ (OH)_2\quad Si_{3.25}\ Al_{0.75}\ O_{10}$$

Charge: XII = 0.81 VI = 5.94 IV = 15.25 **Σ = 22.00**

Probability of smectite layers (%S): 6%

Probability of illite layers (%I): 94%

Measured particles: 8

Distribution of smectite layers probability (%S) in diVS-ml (Cluster2,3,4,5)

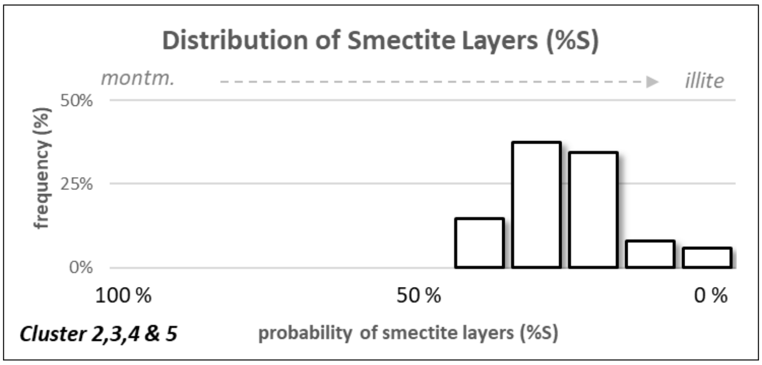

Description: *The distribution of diVS-ml (classified as Cluster 2,3,4 & 5) draws a maximum of frequency (%) for smectite layer probability at 20-30%*

Fig. 7a. *Distribution of smectite layers probability in diVS-ml*

diVS-ml?	*particles (abs)*	**Ca (XII)**	**Mg (XII)**	**Na (XII)**	**K (XII)**	**Cr3+ (VI)**	**Al (VI)**	**Fe3+ (VI)**	**Mg (VI)**	**Ti (VI)**	**Al (IV)**	**Si (IV)**	**XII**	**n_VI**	**%S**
%S >95%	n = 0														
%S 95-85%	n = 0														
%S 85-75%	n = 0														
%S 75-65%	n = 0														
%S 65-55%	n = 0														
%S 55-45%	n = 0														
%S 45-35%	n = 15	0.08	0.12	0.00	0.09	0.00	1.02	0.90	0.08	0.01	0.43	3.57	0.5	2.0	37
%S 35-25%	**n = 38**	**0.08**	**0.14**	**0.00**	**0.11**	**0.00**	**0.97**	**0.95**	**0.06**	**0.01**	**0.48**	**3.52**	**0.5**	**2.0**	**30**
%S 25-15%	**n = 35**	**0.07**	**0.12**	**0.00**	**0.22**	**0.00**	**1.02**	**0.91**	**0.06**	**0.02**	**0.56**	**3.44**	**0.6**	**2.0**	**21**
%S <15%	n = 14	0.06	0.16	0.00	0.35	0.00	0.81	1.05	0.11	0.03	0.72	3.28	0.8	2.0	8

Fig. 7b. *Computed averaged mineral formulae of diVS-ml phases in the different smectite layers probability (%S)-classes*

Description – B25 No5_M (< 2 µm), treated material *(OPA, 60°C, 454 hrs)*

Preparation for TEM

The powder of compacted and treated B25-No5_M-sample was suspended in deionized water and dispersed by ultrasonic treatment for approximately 20 min. The clay fraction (<2 µm) was separated by sedimentation and diluted with deionized water to get a clear suspension. The suspension was dropped onto carbon-coated Cu grids, air dried and stored under environment-controlled conditions at 45% humidity.

Mineral Matter - Overview

The fraction < 2 µm of treated B25 bentonite sample (Opalinus Clay solution, at 60°C, for 454 hours) is mainly composed by beidellite-montmorillonite interstratification (BM) and dioctahedral vermiculite-smectite mixed layer phases (diVS-ml) and accompanied by two types of illite. Furthermore, kaolinite, Si-surplus particles (Si, e.g. quartz) and chlorite-bearing phases were identified in traces in this sample [fig. 1].

	frequency-% *(n = 155 measured particles)*
BM (Cluster1)	22%
diVS-ml (Cluster2-5)	66%
Kaolinite & KSV-ml	2%
Chlorite & CSV-ml	1%
Si-surplus	4%
Unknown	6%

All measured clay mineral phases summarized result following mineral formula computed from TEM-EDX-measurement of 136 individual particles:

	$Ca^{2+}_{0.07}$	$Mg^{2+}_{0.13}$	$Na^{+}_{0.00}$	$K^{+}_{0.14}$	$Al^{3+}_{1.02}$	$Fe^{3+}_{0.88}$	$Mg^{2+}_{0.08}$	$Ti^{4+}_{0.01}$	$(OH)_2$	$Si^{4+}_{3.53}$	$Al^{3+}_{0.47}$	O_{10}
SDOM	*± 0.00*	*± 0.00*	*± 0.00*	*± 0.01*	*± 0.02*	*± 0.02*	*± 0.00*	*± 0.00*		*± 0.01*	*± 0.01*	

Legend: SDOM - standard deviation of the mean (= the standard deviation divided by the square root of the number of samples)

The interlayer charge is calculated as 0.53 per $(OH)_2$ O_{10} and the octahedral charge as 5.94 per $(OH)_2$ O_{10}. The particles are characterized by a high octahedral Fe-amount.

The summarized chemical composition of all 136 computed particles is compared with measured data of original B25-bentonite sample [tab. 1]. The chemical composition averaged by measured particles show an increased amount of Fe_2O_3 and slight reduced amount for SiO_2, Al_2O_3, MgO and CaO in comparison to the measured data of original untreated B25-bentonite.

B25-No5_M sample is characterized by two morphological groups: (i) aggregates formed by small (≤ 200 nm) xenomorphous plates and (ii) large (≤ 1 µm) xenomorph film-like platy crystals [fig. 2].

Aggregates formed by large (≤ 1 µm) xenomorph film-like platy crystals dominate the shapes of particles in the micrographs [fig. 2].

The distribution of %S-probability of all measured clay mineral phases [fig. 3a] also indicates the occurrence of two groups: (i) as main group a mixture of beidellite-montmorillonite interstratifications (%S-max of this part at %S ~ 45%) and diVS-ml (%S-max of this part of mixture for %S at 15-35%) and (ii) illite with K- and charge deficit (%S-class = 0-10%).

The numerous measured particles by TEM-EDX allow a visualization of distribution of interlayer charges. Considering the TEM-EDX-determined cations Ca^{++}, Mg^{++} and Na^{+} and then computed their ratio as interlayer cations in the mineral formula, Ca^{++}, Mg^{++} and Na^{+} offer to characterize the degree of exchangeable charges in the interlayer space. This charge density of treated B25 bentonite (< 2 µm) shows in this sample a distribution with maximal frequency-% of charge density at 0.43 per $(OH)_2\ O_{10}$ [fig. 5]. This interval of interlayer charge density caused by exchangeable cations from 0.27 - 0.51 per $(OH)_2\ O_{10}$ represents diVS-ml and beidellite-montmorillonite interstratifications.

Mineral Matter - Specification

Result of Clustering

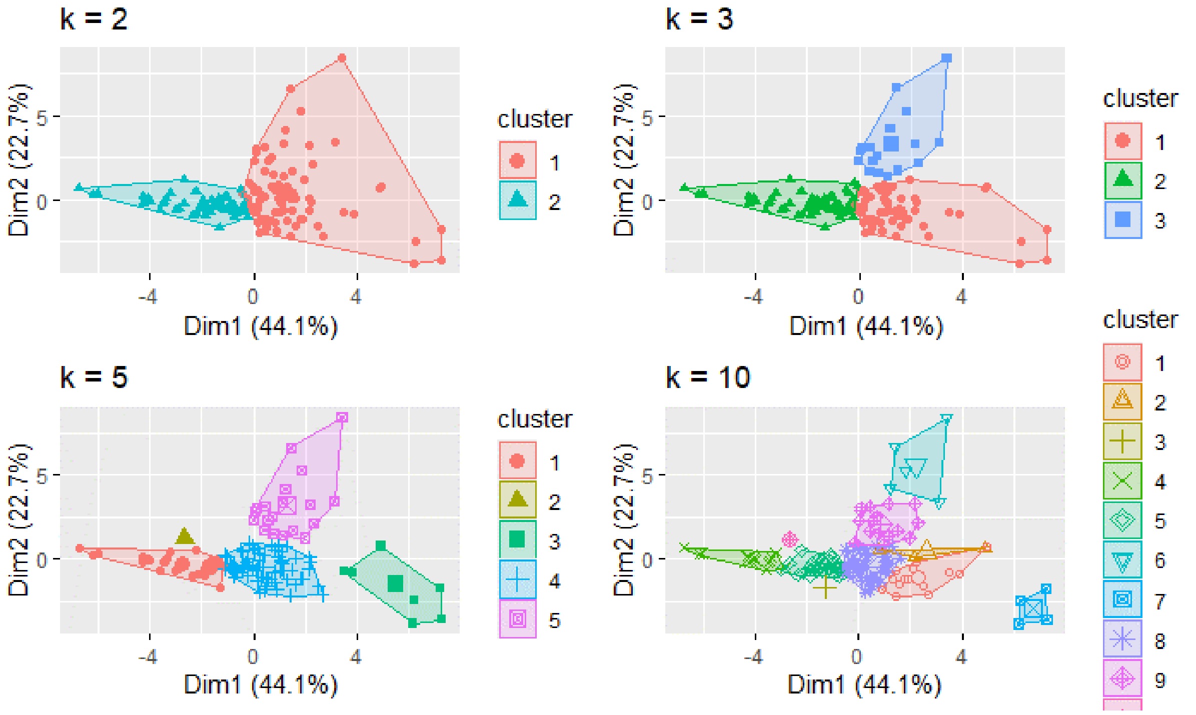

Fig. 8. *Clustering of all measured particles for clusters k = 2, k = 3, k = 5 and k = 10 (source for R-coding: https://uc-r.github.io/kmeans_clustering)*

The optimum of clusters was calculated with k = 5.

		Ca (XII)	Mg (XII)	Na (XII)	K (XII)	Cr3+ (VI)	Al (VI)	Fe3+ (VI)	Mg (VI)	Ti (VI)	Al (IV)	Si (IV)	XII	n_VI	%S
Cluster1	n = 34	0.07	0.11	0.00	0.05	0.00	1.12	0.77	0.10	0.01	0.33	3.67	0.42	2.0	51
Cluster2	n = 1	0.14	0.00	0.00	0.05	0.00	0.96	0.93	0.21	0.00	0.43	3.57	0.34	2.1	37
Cluster3	n = 8	0.08	0.23	0.00	0.18	0.00	0.57	1.29	0.10	0.04	0.75	3.25	0.81	2.0	6
Cluster4	n = 74	0.07	0.14	0.00	0.12	0.00	0.97	0.96	0.06	0.01	0.49	3.51	0.54	2.0	29
Cluster5	n = 19	0.05	0.08	0.00	0.42	0.00	1.17	0.72	0.09	0.02	0.61	3.39	0.68	2.0	17

Fig. 9. *Mineral formulae based on TEM-EDX-data summarized following the result of clustering for k=5*

	Sybilla-results	**TEM-EDX-results**	**Notes**
Cluster 1	IS R0(1) *(%S = 100%)*	BM 65:35	*XRD: Montmorillonite and beidellite is only to distinguish by Green-Kelly-test (not available here).*
Cluster 2			*Only one member in this cluster*
Cluster 3	Illite	diVS-ml *(%S ~ 6%)*	*High K-deficit, low Al(VI), VERY high Fe(VI)*
Cluster 4	IS R0(2) *(%S = 39%)*	diVS-ml *(%S ~ 29%)*	*High K-deficit, low Al(VI), very high Fe(VI)*
Cluster 5	???	diVS-ml *(%S ~ 17%)*	*Low K-deficit, low Al(VI), high Fe(VI)*

Tab. 2. *Comparison of results from TEM-EDX- and XRD-measurements with clustering procedure*

The clustering of TEM-EDX-data indicates a comparable agreement with the recent result of Sybilla-processing of XRD-traces from oriented specimen [tab. 2].

IS R0 (1): The X-ray diffraction pattern of the ethylene-glycol saturated oriented specimen shows a full expandability to 1.76 nm and a difference of 5.34°2θ between 2. and 3. order of smectite interferences. This distance is typically for montmorillonite (Moore & Reynolds, 1989). This result of XRD-processing let expect a maximum of particles for %S ~ 100% by TEM-EDX-measurements, but the maximum of particles measured by TEM-EDX is to find at %S = 30% [fig. 3a].

Montmorillonite and beidellite have the same behavior concerning the expandability and they are only to distinguish by XRD using Li like by Greene-Kelly test (Green-Kelly 1952, 1953). So, combination of XRD- and TEM-results (full expandability by XRD and Si ~ 3.67 by TEM-EDX) led conclude the occurrence of beidellite.

IS R0 (2): The Sybilla-procedure of XRD-traces (oriented mounts) has shown an occurrence of a second illite-smectite mixed layer phase with a smectite layers probability of %S = 39%. This situation is to find in Cluster 4 ($\%S_{TEM}$ = 29%) representing high K- and low charge deficient and Fe-rich dioctahedral vermiculite-smectite mixed layer phase (diV-ml) [tab. 2].

The Sybilla-processing of XRD-traces (oriented mounts) also supports the existence of kaolinite and kaolinite-smectite mixed layer phases in fine fraction of sample. Such phases were not to calculate in TEM-EDX-database (a grain size effect?).

Specifics to the identified clay mineral groups

Beidellite-montmorillonite-interstratification (BM 65:35)

34 of 136 computed particles belong so to this assumed classification. The dioctahedral character of this group is proofed by X-ray diffraction. The position of the large (060)-interference of smectite is in the random oriented powder specimen at 1.497 Å.

Montmorillonite and beidellite have the same behavior concerning the expandability and they are only to distinguish by XRD using Li by means of Greene-Kelly test (Greene-Kelly 1952, 1953). So, combination of XRD- and TEM-results (full expandability by XRD and Si ~ 3.67 by TEM-EDX) led conclude the occurrence of beidellite.

Beidellite-Montmorillonite Interstratification *(BM 65:35)*

$$\mathrm{Ca_{0.07}\,Mg_{0.11}\,Na_{0.00}\,K_{0.05}\quad Al_{1.12}\,Fe^{3+}_{0.77}\,Mg_{0.10}\,Ti_{0.01}\,(OH)_2\;\;Si_{3.67}\,Al_{0.33}\,O_{10}}$$

Charge: XII = 0.42 VI = 5.91 IV = 15.67 **Σ = 22.00**
Measured particles by TEM-EDX: 34
Result of clustering: Cluster1 [tab. 2]

In this sample, beidellite is characterized by a typical low octahedral Mg-amount (because of high ratio of octahedral, 3-valent cations). A comparison of octahedral Mg vs. tetrahedral Si based on TEM-EDX-data indicates the growing occurrence of octahedral Mg with rising ratio of montmorillonite in this beidellite-montmorillonite interstratification [fig. 3b].

Using the results of clustering (see Cluster1 in tab. 2), the maximum of frequency-% is to find for particles in the Si(IV)-class ~ 3.6 - 3.7 e phuc [tab. 6a], representing a beidellite-montmorillonite interstratification in a ratio BM ~ 65:35. The mineral formulae, summarized in classes of tetrahedral Si, draw for the maximum an Fe-rich beidellite with low Mg(VI), but remarkable amount of K in the interlayer space [tab. 6b].

Dioctahedral vermiculite-smectite mixed layer phase (diVS-ml):

$$Ca_{0.07}\ Mg_{0.13}\ Na_{0.00}\ K_{0.18}\quad Al_{0.97}\ Fe^{3+}_{0.94}\ Mg_{0.07}\ Ti_{0.02}\ (OH)_2\quad Si_{3.46}\ Al_{0.54}\ O_{10}$$

Charge: XII = 0.59 VI = 5.95 IV = 15.46 **Σ = 22.00**
Probability of smectite layers (%S): 24%
Probability of illite layers (%I): 76%
Measured particles by TEM-EDX: 102
Result of clustering: Cluster 2,3,4 & 5 [tab. 2]

Illite as part of diVS-ml series

The Rietveld refinement by Profex software (Döbelin & Kleeberg, 2015) indicates the occurrence of two polytypes for illite in treated B25 bentonite: $2M_1$- and 1M-polytype.

Kaolinite-montmorillonite mixed layer phases

The Excel-based procedure (Hoang-Minh et al., 2019) to identify possible clay mineral groups using the TEM-EDX-measurements also includes algorithms to classify kaolinite and kaolinite-montmorillonite mixed layer phases. These algorithms couldn’t identify such phases basing on the measured TEM-EDX-data. Otherwise, few particles, which were not to compute, have shown small hexagonal plates typically for kaolinite-bearing phases.

References

Cliff, G. & Lorimer, G. W. (1975). *J. Microsc.* **103**, 203–207.

Döbelin, N., Kleeberg, R. (2015). *Journal of Applied Crystallography* **48**, 1573-1580. DOI: 10.1107/S1600576715014685

Greene-Kelly, R., *Clay Minerals Bull.*, **1**, 221 (1952).

Greene-Kelly, R. 1953. The identification of montmorillonoids in clays. *Journal of Soil Science*. **4** (2), pp. 232-237. https://doi.org/10.1111/j.1365-2389.1953.tb00657.x

Greene-Kelly, R. (1955). Dehydration of the montmorillonite minerals. *Mineralogical Magazine and Journal of the Mineralogical Society*, **30**(228), 604-615. doi:10.1180/minmag.1955.030.228.06

Henning, K.-H. & Störr, M. (1986). Electron Micrographs (TEM, SEM) of Clays and Clay Minerals, p. 325. Akademie-Verlag Berlin.

Hoang-Minh, T., Kasbohm, J., Nguyen-Thanh, L., Nga, P. T., Lai, L. T., Duong, N. T., Thanh, N. D., Thuyet, N. T. M., Anh, D. D., Pusch, R., Knutsson, S. & Ferreiro Mahlmann, R. (2019). *J. Appl. Cryst.* **52**, 133-147. DOI: 10.1107/S1600576718018162

Lorimer, G. W. & Cliff, G. (1976). *Electron Microscopy in Mineralogy*, edited by H. R. Wenk, pp. 506–519. Berlin: Springer Verlag.

Matschiavelli, N., Kluge, S., Podlech, C., Standhaft, D., Grathoff, G., Ikeda-Ohno, A., Warr, L.N., Chukharkina, A., Arnold, T. & Cherkouk, A. (2019). *Environmental Science & Technology.* **53** (17), 10514-10524, DOI: 10.1021/acs.est.9b02670

Mellini, M. & Menichini, R. (1985). *R. Soc. Ital. Miner. Petrol.* **40**, 261–266.

Moore, D.M., Reynolds, R.C. (1989). X-ray Diffraction and the Identification and Analysis of Clay Minerals, Oxford University Press, New York, 332 + xvi pp.

Nguyen-Thanh, L., Herbert, H.-J., Kasbohm, J., Hoang-Minh, T. & Mählmann, R. F. (2014). *Clays Clay Miner.* **62**, 425–446.

Środoń, J., Elsass, F., McHardy, W. J. & Morgan, D. J. (1992). *Clay Miner.* **27**, 137–158.

Data Sheet – B25 bentonite, treated materials *(OPA, 60 °C, 454h)* - BOTTOM

Methodology - Transmission electron microscopy linked with energy-dispersive X-ray spectroscopy (TEM-EDX)

It is expected a characterization of clay mineral phases in treated B25 bentonite by transmission electron microscopy. The sample series No5 represents a percolation of B25 bentonite by Opalinus Clay solution at 60°C for 454 hours. The sample No5_B is the label for the material at the bottom of sample cylinder.

The different clay mineral phases are to identify and to describe by chemical composition and its variability, morphology, the specific dissolution potential, and further parameter.

Such further parameter like distribution of smectite layers probability (%S) and distribution of charges caused by exchangeable cations interlayer space should serve as additional indicators for mineralogical alterations in treatment experiments with B25 bentonite.

The sample were suspended for TEM-measurement in deionized water and dispersed by ultrasonic treatment for approximately 20 min. The clay fraction (<2 µm) was separated by sedimentation and diluted with deionized water to get a clear suspension. The suspension was dropped onto carbon-coated Cu grids, air dried and stored under environment-controlled conditions at 45% humidity.

TEM-EDX investigations were carried out on the <2 µm fraction using a FEI TECNAI G^2 20 electron transmission microscope at the VNU University of Science, Vietnam National University, Hanoi. This equipment (operated at 200 kV with LaB_6 cathode) was combined with an S-TWIN objective, a windowless EDAX energy-dispersive X-ray system and a FEI Eagle 2k CCD TEM camera.

About 100 individual clay particles per sample were characterized by TEM-EDX with respect to crystal size, crystal habit, and particle morphology and element distribution. The crystal size, crystal habit and particle morphology were described according to Henning & Störr (1986).

For the quantification of element distribution, a calibration of k factors is mandatory (Cliff & Lorimer, 1975; Lorimer & Cliff, 1976; Mellini & Menichini, 1985). These k values are used to calibrate for the specific behaviour of particles against possible irradiation damage. The elements O, Na, Mg, Al, Si, K, Ca and Fe were quantified by applying the EDAX GENESIS–TEM Quant Materials quantification procedure.

In this procedure, the acquired EDX spectra are corrected by background subtraction, Gaussian deconvolution and k-factor corrections using values previously determined on a phyllosilicate standard (muscovite) and selected non-phyllosilicate standards. The average errors in the analyzed elements using the phyllosilicate standard, expressed as the atomic proportions, are 10 (Na), 5 (Fe, Mg, K, Ti, Ca) and 1 (Si, Al).

The measurement time per particle was lowered to 20 s and the exposed area was limited to a 50 nm diameter, avoiding possible irradiation damage of particles. The stability of particles of the sample series was tested for this measurement time at the beginning of any measurement campaign.

Further methodological details related to TEM-EDX-measurements and the Excel-based mathematical procedure using TEM-EDX data for calculation of mineral formulae are described in Hoang-Minh et al. (2019).

These mathematical procedures described in Hoang-Minh et al. (2019) were extended by k-means clustering method for finding subgroups of observations within a data set. The data were standardized (i.e., scaled) to make variables comparable. Euclidean distances were applied as classical method for distance measures. The optimal clusters were determined by Elbow method and Gap statistics[9].

---

[9] *https://uc-r.github.io/kmeans_clustering*

Data Sheet – B25 No5_B (< 2 µm), treated material *(OPA, 60°C, 454 hrs)*

Preparation for TEM

- raw material: compacted material (1.6 g/cm³) of treated B25-sample (OPA, 60°C, 454 hrs)
- suspension on particles < 2 µm on carbon-filmed Cu-grid
- air-dried and humidity-controlled storing

Mineral Matter

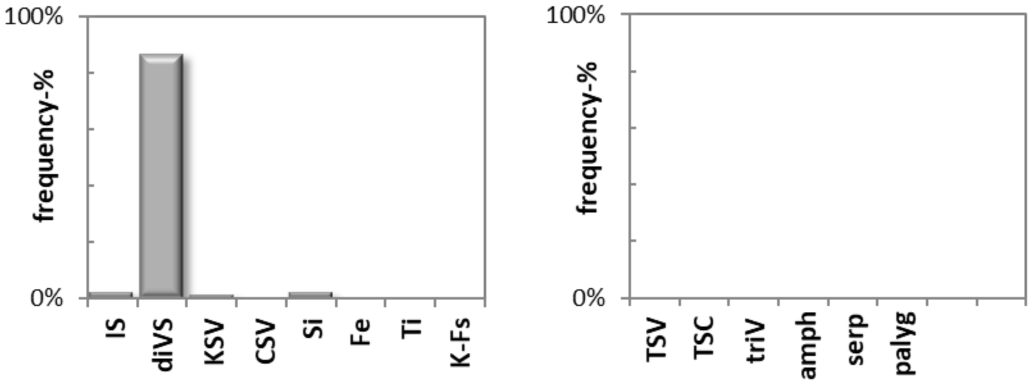

Fig. 1. *Distribution of mineral groups in fraction < 2 µm (in frequency-%)*
Legend: ***IS*** *– illite-smectite-mixed layer series in sense of Środon et al. (1992), diVS – dioctahedral vermiculite-smectite illite-smectite-mixed layer series (= charge- and/or K-deficit),* ***KSV*** *– kaolinite-smectite-dioctahedral vermiculite-mixed layer series,* ***CSV*** *– chlorite-saponite-trioctahedral vermiculite-mixed layer series,* ***Si*** *– quartz or particles with Si-surplus,* ***Fe*** *– Fe-oxide or Fe-oxyhydroxide,* ***Ti*** *– Ti-bearing phases (e.g. rutile, anatase),* ***K-Fs*** *– K-feldspar*

Clay Mineral Composition

All particles of smectite group:

$$Ca_{0.12}\ Mg_{0.00}\ Na_{0.21}\ K_{0.38}\quad Al_{0.89}\ Fe^{3+}_{0.82}\ Mg_{0.29}\ Ti_{0.01}\ (OH)_2\quad Si_{3.44}\ Al_{0.56}\ O_{10}$$

Charge: XII = 0.84 VI = 5.72 IV = 15.44 **Σ = 22.00**
Probability of smectite layers (%S): 22%
Probability of illite layers (%I): 78%

Specific Dissolution Potential (ΔS%)
for H2O, 20 + 60 rpm -62 (= fast reacting, interlayer group: Ca+Mg (= type B))
for NaCl, 20 rpm -70 (= fast reacting, interlayer group: Ca+Mg (= type B))
for NaCl, 60 rpm -16 (= medium reacting, ‘illitization’, interlayer group: Na (= type A))
CEC_{calc}: 157 meq / 100 g (literature: 56 meq / 100 g [Matschiavelli et al., 2019: MAT19])

Measured particles: 142

Table 1. *Summarized chemical composition*

SiO_2	TiO_2	Al_2O_3	Fe_2O_3	MnO	MgO	CaO	Na_2O	K_2O	P_2O_5	Σ	
55.2%	0.1%	20.5%	8.9%		3.6%	4.4%	2.1%	3.5%	1.8%	1.00	measured particles
63.7%	0.0%	23.9%	6.4%		3.3%	1.1%	0.0%	1.2%	0.0%	1.00	measured particles of original B25

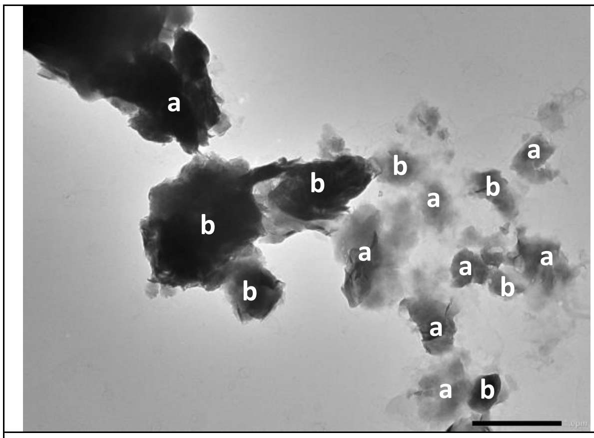

JEM-2100_MAG_X8000_004_AlSZ-5ML.bmp

Magnification: 8k

(a) Aggregates commonly formed by small (≤ 200 nm) xenomorphous plates

(b) mostly large (≤ 1 µm) xenomorph film-like platy crystals

Fig. 2. *Morphology of particles (TEM-micrographs)*

Distribution of smectite layers probability (%S)

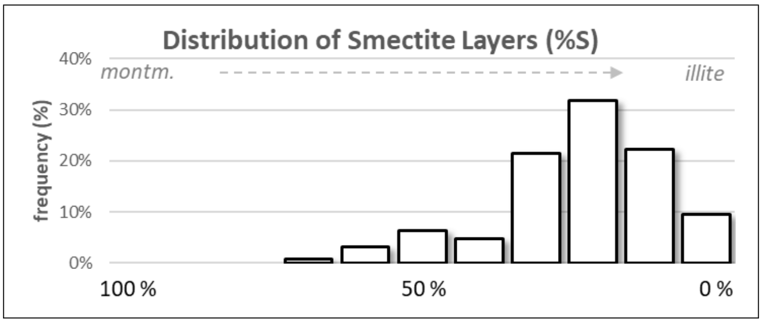

Description: *The distribution of %S-probability indicates the occurrence of two groups: (i) mixture of beidellite-montmorillonite interstratifications (= assumption) with diVS-ml as well as (ii) illite with K-deficiency.*

Fig. 3a. *Distribution of smectite layers probability (%S)*

Differentiation by relation “Octahedral Mg vs. tetrahedral Si”?

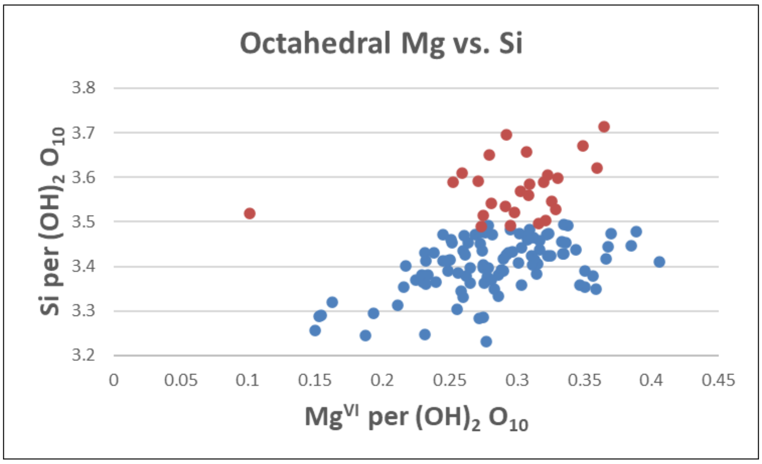

Description: *This diagram indicates the occurrence of groups of Mg in relation to tetrahedral Si. Probably, this distribution mirrors 2 phases (I) beidellite-montmorillonite inter-stratifications (red) and (II) diVS-ml (blue)*

Fig. 3b. *Distribution of octahedral Mg vs. tetrahedral Si [all per(OH)$_2$ O$_{10}$]*

Distribution of K in relation to tetrahedral Si

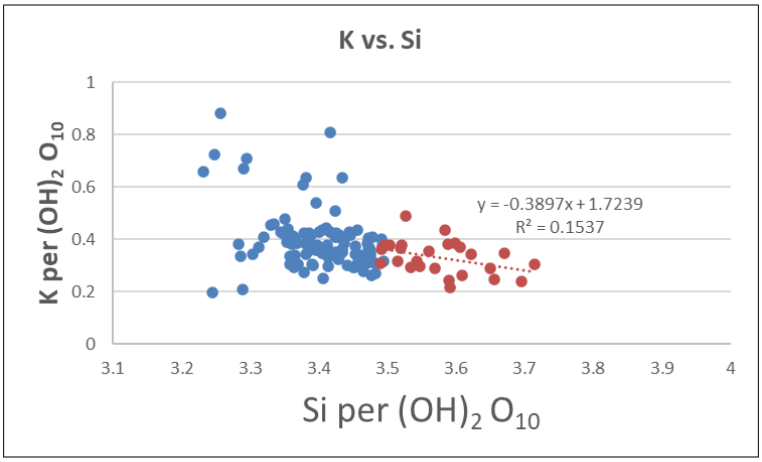

Description: *This diagram visualizes possible particles (beidellite-montmorillonite interstratification?) with low K (red dots) and diVS-ml phases (blue dots)*

Fig. 4. *Distribution of K in interlayer space vs. tetrahedral Si [all per*$(OH)_2\ O_{10}$*]*

Distribution of charges (exchangeable from interlayer space)

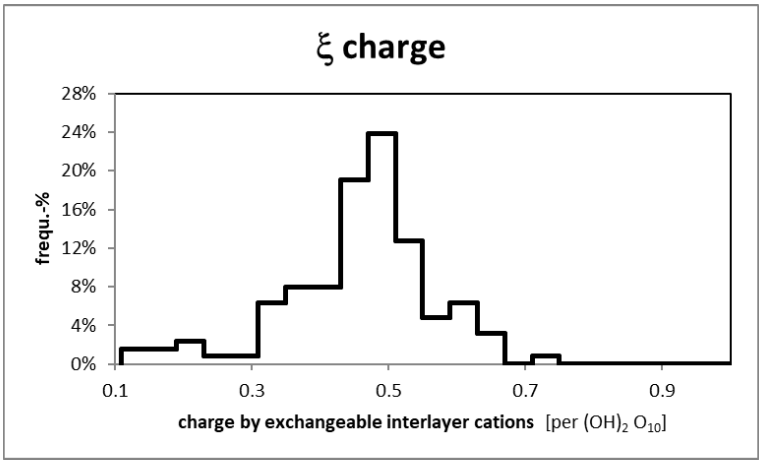

This diagram visualizes the distribution of exchangeable charges in the interlayer space (Ca, Mg, Na) determined and computed by TEM-EDX-data.

Description: *Distribution with maximum of charge density at 0.51 per* $(OH)_2\ O_{10}$.

Fig. 5. *Distribution of exchangeable charges*

Beidellite-montmorillonite interstratification BM 85:15 *(Cluster2):*

$Ca_{0.08}\ Mg_{0.00}\ Na_{0.22}\ K_{0.33}\quad Al_{0.96}\ Fe^{3+}_{0.74}\ Mg_{0.30}\ Ti_{0.01}\ (OH)_2\quad Si_{3.58}\ Al_{0.42}\ O_{10}$

Charge: XII = 0.71 VI = 5.71 IV = 15.58 **Σ = 22.00**

Measured particles: 26

Distribution of BM-interstratifications (Cluster2)

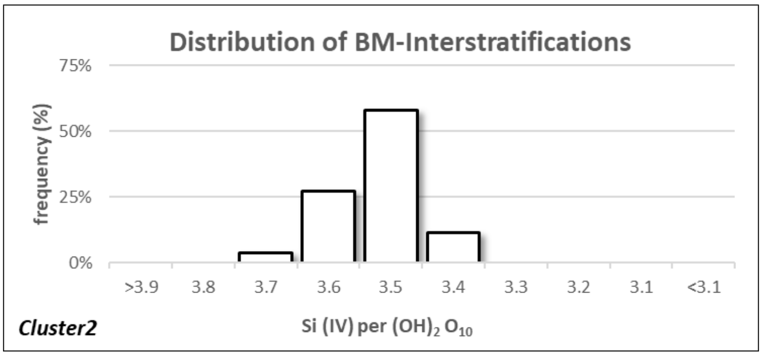

Description: *The distribution of BM-interstratifications (classified as Cluster2) draws a maximum of frequency (%) at tetrahedral Si-value between 3.5 – 3.6 e phuc*

Fig. 6a. *Distribution of assumed beidellite-montmorillonite interstratifications*

BM85:15?	particles (abs)	Ca (XII)	Mg (XII)	Na (XII)	K (XII)	Cr3+ (VI)	Al (VI)	Fe3+ (VI)	Mg (VI)	Ti (VI)	Al (IV)	Si (IV)	XII	n_VI	%S
Si >3.9	n = 0														
Si 3.9-3.8	n = 0														
Si 3.8-3.7	n = 1	0.07	0.00	0.20	0.30	0.00	1.11	0.53	0.36	0.00	0.29	3.71	0.6	2.0	57
Si 3.7-3.6	n = 7	0.08	0.00	0.21	0.30	0.00	0.99	0.70	0.31	0.01	0.36	3.64	0.7	2.0	46
Si 3.6-3.5	**n = 15**	**0.09**	**0.00**	**0.21**	**0.34**	**0.00**	**0.94**	**0.76**	**0.29**	**0.01**	**0.45**	**3.55**	**0.7**	**2.0**	**34**
Si 3.5-3.4	n = 3	0.08	0.00	0.28	0.35	0.00	0.93	0.78	0.29	0.00	0.51	3.49	0.8	2.0	27
Si 3.4-3.3	n = 0														
Si 3.3-3.2	n = 0														
Si 3.2-3.1	n = 0														
Si <3.1	n = 0														

Fig. 6b. *Computed averaged mineral formulae of phases in the different Si(IV)-classes*

Dioctahedral Vermiculite-Smectite mixed layer phases (diVS-ml) *(Cluster1):*

$$Ca_{0.13}\,Mg_{0.00}\,Na_{0.21}\,K_{0.39}\quad Al_{0.87}\,Fe^{3+}_{0.84}\,Mg_{0.28}\,Ti_{0.01}\,(OH)_2\quad Si_{3.40}\,Al_{0.60}\,O_{10}$$

Charge: XII = 0.87 VI = 5.73 IV = 15.40 **Σ = 22.00**

Probability of smectite layers (%S): 18%

Probability of illite layers (%I): 82%

Measured particles: 100

Distribution of smectite layers probability (%S) in diVS-ml (Cluster1)

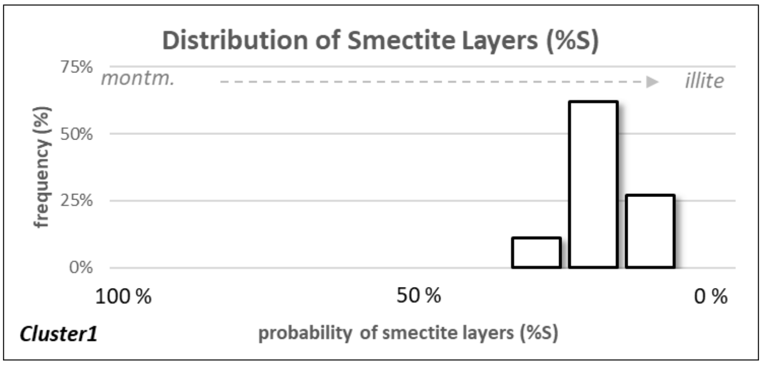

Description: *The distribution of diVS-ml (classified as Cluster1) draws a maximum of frequency (%) for smectite layer probability at 20%*

Fig. 7a. *Distribution of smectite layers probability in diVS-ml*

diVS-ml?	particles (abs)	Ca (XII)	Mg (XII)	Na (XII)	K (XII)	Cr3+ (VI)	Al (VI)	Fe3+ (VI)	Mg (VI)	Ti (VI)	Al (IV)	Si (IV)	XII	n_VI	%S
%S >95%	n = 0														
%S 95-85%	n = 0														
%S 85-75%	n = 0														
%S 75-65%	n = 0														
%S 65-55%	n = 0														
%S 55-45%	n = 0														
%S 45-35%	n = 0														
%S 35-25%	n = 11	0.12	0.00	0.25	0.34	0.00	0.83	0.85	0.32	0.00	0.52	3.48	0.8	2.0	26
%S 25-15%	**n = 62**	**0.13**	**0.00**	**0.21**	**0.39**	**0.00**	**0.84**	**0.85**	**0.29**	**0.01**	**0.58**	**3.42**	**0.9**	**2.0**	**20**
%S <15%	n = 27	0.13	0.01	0.19	0.44	0.00	0.93	0.81	0.25	0.01	0.68	3.32	0.9	2.0	11

Fig. 7b. *Computed averaged mineral formulae of diVS-ml phases in the different smectite layers probability (%S)-classes*

Description – B25 No5_B (< 2 µm), treated material *(OPA, 60°C, 454 hrs)*

Preparation for TEM

The powder of compacted and treated B25-No5_B-sample was suspended in deionized water and dispersed by ultrasonic treatment for approximately 20 min. The clay fraction (<2 µm) was separated by sedimentation and diluted with deionized water to get a clear suspension. The suspension was dropped onto carbon-coated Cu grids, air dried and stored under environment-controlled conditions at 45% humidity.

Mineral Matter - Overview

The fraction < 2 µm of treated B25 bentonite sample (Opalinus Clay solution, at 60°C, for 454 hours) is mainly composed by beidellite-montmorillonite interstratification (BM) and dioctahedral vermiculite-smectite mixed layer phases (diVS-ml) and accompanied by two types of illite. Furthermore, kaolinite, Si-surplus particles (Si, e.g. quartz) and chlorite-bearing phases were identified in traces in this sample [fig. 1].

	frequency-% *(n = 155 measured particles)*
BM (Cluster2)	18%
diVS-ml (Cluster1)	70%
Kaolinite & KSV-ml	1%
Si-surplus	2%
Unknown	8%

All measured clay mineral phases summarized result following mineral formula computed from TEM-EDX-measurement of 126 individual particles:

	$Ca^{2+}_{0.12}$	$Mg^{2+}_{0.00}$	$Na^{+}_{0.21}$	$K^{+}_{0.38}$	$Al^{3+}_{0.89}$	$Fe^{3+}_{0.82}$	$Mg^{2+}_{0.29}$	$Ti^{4+}_{0.01}$	$(OH)_2$	$Si^{4+}_{3.44}$	$Al^{3+}_{0.56}$	O_{10}
SDOM	*± 0.00*	*± 0.00*	*± 0.01*	*± 0.01*	*± 0.01*	*± 0.01*	*± 0.00*	*± 0.00*		*± 0.01*	*± 0.01*	

Legend: SDOM - standard deviation of the mean (= the standard deviation divided by the square root of the number of samples)

The interlayer charge is calculated as 0.84 per $(OH)_2$ O_{10} and the octahedral charge as 5.73 per $(OH)_2$ O_{10}. The particles are characterized by a high octahedral Fe-amount.

The summarized chemical composition of all 126 computed particles is compared with measured data of original B25-bentonite sample [tab. 1]. The chemical composition averaged by measured particles show an increased amount of Fe_2O_3, Na_2O, K_2O and CaO and remarkable reduced amount for SiO_2 and Al_2O_3 in comparison to the measured data of original untreated B25-bentonite.

B25-No5_B sample is characterized by two morphological groups: (i) aggregates mostly formed by small (≤ 200 nm) xenomorphous plates and (ii) large (≤ 1 µm) xenomorph film-like platy crystals [fig. 2]. Aggregates formed by large (≤ 1 µm) xenomorph film-like platy crystals dominate the shapes of particles in the micrographs [fig. 2].

The distribution of %S-probability of all measured clay mineral phases [fig. 3a] also indicates the occurrence of two groups: (i) as main group a mixture of beidellite-montmorillonite interstratifications (%S-max of this part at %S ~ 50%) and diVS-ml (%S-max of this part of mixture for %S at 15-25%) and (ii) illite with K- and charge deficit (%S-class = 0-10%).

The numerous measured particles by TEM-EDX allow a visualization of distribution of interlayer charges. Considering the TEM-EDX-determined cations Ca^{++}, Mg^{++} and Na^{+} and then computed their ratio as interlayer cations in the mineral formula, Ca^{++}, Mg^{++} and Na^{+} offer to characterize the degree of exchangeable charges in the interlayer space. This charge density of treated B25 bentonite (< 2 µm) shows in this sample a distribution with maximal frequency-% of charge density at 0.51 per $(OH)_2\ O_{10}$ [fig. 5]. This interval of interlayer charge density caused by exchangeable cations from 0.31 - 0.67 per $(OH)_2\ O_{10}$ represents diVS-ml and beidellite-montmorillonite interstratifications.

Mineral Matter - Specification

Result of Clustering

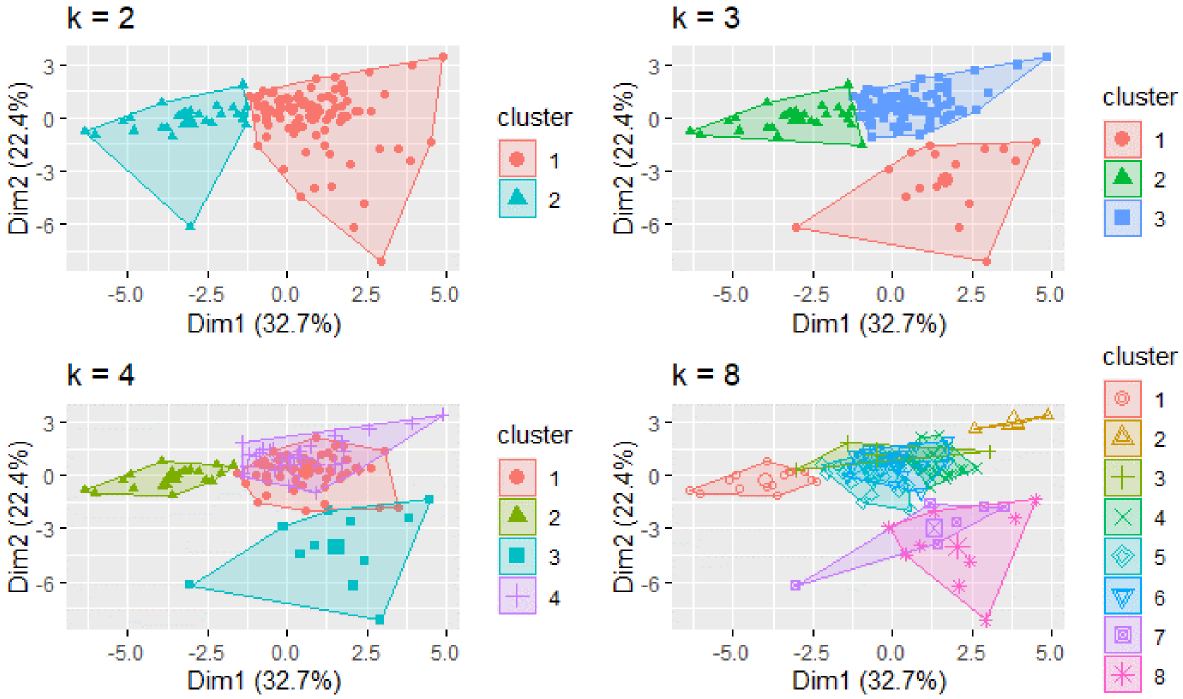

Fig. 8. *Clustering of all measured particles for clusters k = 2, k = 3, k = 4 and k = 8 (source for R-coding: https://uc-r.github.io/kmeans_clustering)*

The optimum of clusters was calculated with k = 2.

		Ca (XII)	Mg (XII)	Na (XII)	K (XII)	Cr3+ (VI)	Al (VI)	Fe3+ (VI)	Mg (VI)	Ti (VI)	Al (IV)	Si (IV)	XII	n_VI	%S
Cluster1	n = 100	0.13	0.00	0.21	0.39	0.00	0.87	0.84	0.28	0.01	0.60	3.40	0.87	2.0	18
Cluster2	n = 26	0.08	0.00	0.22	0.33	0.00	0.96	0.74	0.30	0.01	0.42	3.58	0.72	2.0	37

Fig. 9. *Mineral formulae based on TEM-EDX-data summarized following the result of clustering for k=2*

	Sybilla-results	**TEM-EDX-results**	**Notes**
Cluster 1	IS R0(2) *(%S = 55%)*	diVS-ml *(%S = 18%)*	*K- deficit, low Al(VI) and high Fe(VI)*
Cluster 2	IS R0(1) *(%S = 100%)*	BM 85:15	*XRD: Montmorillonite and beidellite is only to distinguish by Green-Kelly-test (not available here).*

Tab. 2. *Comparison of results from TEM-EDX- and XRD-measurements with clustering procedure*

The clustering of TEM-EDX-data shows for diVS-ml phases only a limited agreement with the recent result of Sybilla-processing of XRD-traces from oriented specimen [tab. 2].

IS R0 (1): The X-ray diffraction pattern of the ethylene-glycol saturated oriented specimen shows a full expandability to 1.75 nm and a difference of 5.34°2θ between 2. and 3. order of smectite interferences. This distance is typically for montmorillonite (Moore & Reynolds, 1989). This result of XRD-pattern processing let expect a maximum of particles for %S ~ 100% by TEM-EDX-measurements, but the maximum of particles measured by TEM-EDX is to find at %S = 20% [fig. 3a].

Montmorillonite and beidellite have the same behavior concerning the expandability and they are only to distinguish by XRD using Li like by Greene-Kelly test (Green-Kelly 1952, 1953). So, combination of XRD- and TEM-results (full expandability by XRD and Si ~ 3.58 by TEM-EDX) led conclude the occurrence of beidellite.

IS R0 (2): The Sybilla-procedure of XRD-traces (oriented mounts) has shown an occurrence of a second illite-smectite mixed layer phase with a smectite layers probability of %S = 55%. This situation is not mirrored in Cluster 1 ($\%S_{TEM}$ = 18%) representing K- and low charge deficient and Fe-rich dioctahedral vermiculite-smectite mixed layer phase (diV-ml) [tab. 2].

The Sybilla-processing of XRD-traces (oriented mounts) also supports the existence of kaolinite and kaolinite-smectite mixed layer phases in fine fraction of sample. Such phases were not to calculate in TEM-EDX-database (a grain size effect?).

Specifics to the identified clay mineral groups

Beidellite-montmorillonite-interstratification (BM 85:15)

26 of 106 computed particles belong so to this assumed classification. The dioctahedral character of this group is proofed by X-ray diffraction. The position of the large (060)-interference of smectite is in the random oriented powder specimen at 1.497 Å.

Montmorillonite and beidellite have the same behavior concerning the expandability and they are only to distinguish by XRD using Li by means of Greene-Kelly test (Greene-Kelly 1952, 1953). So, combination of XRD- and TEM-results (full expandability by XRD and Si ~ 3.58 by TEM-EDX) led conclude the occurrence of beidellite.

Beidellite-Montmorillonite Interstratification *(BM 85:15)*

$$\boxed{Ca_{0.08}\ Mg_{0.00}\ Na_{0.22}\ K_{0.33}\quad Al_{0.96}\ Fe^{3+}_{0.74}\ Mg_{0.30}\ Ti_{0.01}\ (OH)_2\ \ Si_{3.58}\ Al_{0.42}\ O_{10}}$$

Charge: XII = 0.72 VI = 5.70 IV = 15.58 **Σ = 22.00**
Measured particles by TEM-EDX: 26
Result of clustering: Cluster2 [tab. 2]

In this sample, beidellite is characterized by a typical low octahedral Mg-amount (because of high ratio of octahedral, 3-valent cations). A comparison of octahedral Mg vs. tetrahedral Si based on TEM-EDX-data indicates the growing occurrence of octahedral Mg with rising ratio of montmorillonite in this beidellite-montmorillonite interstratification [fig. 3b].

Using the results of clustering (see Cluster1 in tab. 2), the maximum of frequency-% is to find for particles in the Si(IV)-class ~ 3.5 - 3.6 e phuc [tab. 6a], representing a beidellite-montmorillonite interstratification in a ratio BM ~ 85:15. The mineral formulae, summarized in classes of tetrahedral Si, draw for the maximum an Fe-rich beidellite with high Mg(VI), but remarkable amount of K in the interlayer space [tab. 6b].

Dioctahedral vermiculite-smectite mixed layer phase (diVS-ml):

$$Ca_{0.13}\ Mg_{0.00}\ Na_{0.21}\ K_{0.39}\quad Al_{0.87}\ Fe^{3+}_{0.84}\ Mg_{0.28}\ Ti_{0.01}\ (OH)_2\ \ Si_{3.40}\ Al_{0.60}\ O_{10}$$

Charge: XII = 0.87 VI = 5.73 IV = 15.40 **Σ = 22.00**

Probability of smectite layers (%S):	18%
Probability of illite layers (%I):	82%
Measured particles by TEM-EDX:	100
Result of clustering:	Cluster 1 [tab. 2]

Illite as part of diVS-ml series

The Rietveld refinement by Profex software (Döbelin & Kleeberg, 2015) indicates the occurrence of two polytypes for illite in treated B25 bentonite: $2M_1$- and 1M-polytype.

Kaolinite-montmorillonite mixed layer phases

The Excel-based procedure (Hoang-Minh et al., 2019) to identify possible clay mineral groups using the TEM-EDX-measurements also includes algorithms to classify kaolinite and kaolinite-montmorillonite mixed layer phases. These algorithms couldn't identify such phases basing on the measured TEM-EDX-data. Otherwise, few particles, which were not to compute, have shown small hexagonal plates typically for kaolinite-bearing phases.

References

Cliff, G. & Lorimer, G. W. (1975). *J. Microsc.* **103**, 203–207.

Döbelin, N., Kleeberg, R. (2015). *Journal of Applied Crystallography* **48**, 1573-1580. DOI: 10.1107/S1600576715014685

Greene-Kelly, R., *Clay Minerals Bull.*, **1**, 221 (1952).

Greene-Kelly, R. 1953. The identification of montmorillonoids in clays. *Journal of Soil Science*. **4** (2), pp. 232-237. https://doi.org/10.1111/j.1365-2389.1953.tb00657.x

Greene-Kelly, R. (1955). Dehydration of the montmorillonite minerals. *Mineralogical Magazine and Journal of the Mineralogical Society*, **30**(228), 604-615. doi:10.1180/minmag.1955.030.228.06

Henning, K.-H. & Störr, M. (1986). Electron Micrographs (TEM, SEM) of Clays and Clay Minerals, p. 325. Akademie-Verlag Berlin.

Hoang-Minh, T., Kasbohm, J., Nguyen-Thanh, L., Nga, P. T., Lai, L. T., Duong, N. T., Thanh, N. D., Thuyet, N. T. M., Anh, D. D., Pusch, R., Knutsson, S. & Ferreiro Mahlmann, R. (2019). *J. Appl. Cryst.* **52**, 133-147. DOI: 10.1107/S1600576718018162

Lorimer, G. W. & Cliff, G. (1976). *Electron Microscopy in Mineralogy*, edited by H. R. Wenk, pp. 506–519. Berlin: Springer Verlag.

Matschiavelli, N., Kluge, S., Podlech, C., Standhaft, D., Grathoff, G., Ikeda-Ohno, A., Warr, L.N., Chukharkina, A., Arnold, T. & Cherkouk, A. (2019). *Environmental Science & Technology.* **53** (17), 10514-10524, DOI: 10.1021/acs.est.9b02670

Mellini, M. & Menichini, R. (1985). *R. Soc. Ital. Miner. Petrol.* **40**, 261–266.

Moore, D.M., Reynolds, R.C. (1989). X-ray Diffraction and the Identification and Analysis of Clay Minerals, Oxford University Press, New York, 332 + xvi pp.

Nguyen-Thanh, L., Herbert, H.-J., Kasbohm, J., Hoang-Minh, T. & Mählmann, R. F. (2014). *Clays Clay Miner.* **62**, 425–446.

Środoń, J., Elsass, F., McHardy, W. J. & Morgan, D. J. (1992). *Clay Miner.* **27**, 137–158.

Data Sheet – B25 bentonite, treated materials *(OPA, 100 °C, 35d)* - TOP

Methodology - Transmission electron microscopy linked with energy-dispersive X-ray spectroscopy (TEM-EDX)

It is expected a characterization of clay mineral phases in treated B25 bentonite by transmission electron microscopy. The sample series No2 represents a percolation of B25 bentonite by Opalinus Clay solution at 100°C for 35 days. The sample No2_T is the label for the material at the top of sample cylinder.

The different clay mineral phases are to identify and to describe by chemical composition and its variability, morphology, the specific dissolution potential, and further parameter.

Such further parameter like distribution of smectite layers probability (%S) and distribution of charges caused by exchangeable cations interlayer space should serve as additional indicators for mineralogical alterations in treatment experiments with B25 bentonite.

The sample were suspended for TEM-measurement in deionized water and dispersed by ultrasonic treatment for approximately 20 min. The clay fraction (<2 µm) was separated by sedimentation and diluted with deionized water to get a clear suspension. The suspension was dropped onto carbon-coated Cu grids, air dried and stored under environment-controlled conditions at 45% humidity.

TEM-EDX investigations were carried out on the <2 µm fraction using a FEI TECNAI G^2 20 electron transmission microscope at the VNU University of Science, Vietnam National University, Hanoi. This equipment (operated at 200 kV with LaB_6 cathode) was combined with an S-TWIN objective, a windowless EDAX energy-dispersive X-ray system and a FEI Eagle 2k CCD TEM camera.

About 100 individual clay particles per sample were characterized by TEM-EDX with respect to crystal size, crystal habit, and particle morphology and element distribution. The crystal size, crystal habit and particle morphology were described according to Henning & Störr (1986).

For the quantification of element distribution, a calibration of k factors is mandatory (Cliff & Lorimer, 1975; Lorimer & Cliff, 1976; Mellini & Menichini, 1985). These k values are used to calibrate for the specific behaviour of particles against possible irradiation damage. The elements O, Na, Mg, Al, Si, K, Ca and Fe were quantified by applying the EDAX GENESIS–TEM Quant Materials quantification procedure.

In this procedure, the acquired EDX spectra are corrected by background subtraction, Gaussian deconvolution and k-factor corrections using values previously determined on a phyllosilicate standard (muscovite) and selected non-phyllosilicate standards. The average errors in the analyzed elements using the phyllosilicate standard, expressed as the atomic proportions, are 10 (Na), 5 (Fe, Mg, K, Ti, Ca) and 1 (Si, Al).

The measurement time per particle was lowered to 20 s and the exposed area was limited to a 50 nm diameter, avoiding possible irradiation damage of particles. The stability of particles of the sample series was tested for this measurement time at the beginning of any measurement campaign.

Further methodological details related to TEM-EDX-measurements and the Excel-based mathematical procedure using TEM-EDX data for calculation of mineral formulae are described in Hoang-Minh et al. (2019).

These mathematical procedures described in Hoang-Minh et al. (2019) were extended by k-means clustering method for finding subgroups of observations within a data set. The data were standardized (i.e., scaled) to make variables comparable. Euclidean distances were applied as classical method for distance measures. The optimal clusters were determined by Elbow method and Gap statistics[10].

---

[10] *https://uc-r.github.io/kmeans_clustering*

Data Sheet – B25 No2_T (< 2 µm), treated material *(OPA, 100°C, 35 days)*

Preparation for TEM

- raw material: compacted material (1.6 g/cm³) of treated B25-sample (OPA, 100°C, 35 days)
- suspension on particles < 2 µm on carbon-filmed Cu-grid
- air-dried and humidity-controlled storing

Mineral Matter

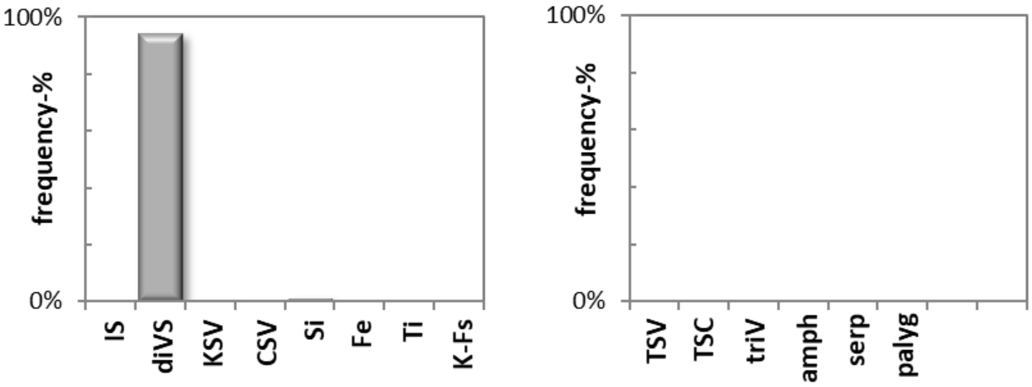

Fig. 1. *Distribution of mineral groups in fraction < 2 µm (in frequency-%)*
*Legend: **IS** – illite-smectite-mixed layer series in sense of Środon et al. (1992), diVS – dioctahedral vermiculite-smectite illite-smectite-mixed layer series (= charge- and/or K-deficit), **KSV** – kaolinite-smectite-dioctahedral vermiculite-mixed layer series, **CSV** – chlorite-saponite-trioctahedral vermiculite-mixed layer series, **Si** – quartz or particles with Si-surplus, **Fe** – Fe-oxide or Fe-oxyhydroxide, **Ti** – Ti-bearing phases (e.g. rutile, anatase), **K-Fs** – K-feldspar*

Clay Mineral Composition

All particles of smectite group:

$$\mathrm{Ca_{0.15}\,Mg_{0.06}\,Na_{0.01}\,K_{0.14}\quad Al_{1.22}\,Fe^{3+}_{0.57}\,Mg_{0.19}\,Ti_{0.01}\,(OH)_2\quad Si_{3.62}\,Al_{0.38}\,O_{10}}$$

Charge: XII = 0.58 VI = 5.80 IV = 15.62 **Σ = 22.00**

Probability of smectite layers (%S): 43%
Probability of illite layers (%I): 57%

Specific Dissolution Potential (ΔS%)

for H2O, 20 + 60 rpm - 9 (= medium reacting, interlayer group: Ca+Mg (= type B))
for NaCl, 20 rpm - 9 (= medium reacting, interlayer group: Ca+Mg (= type B))
for NaCl, 60 rpm -100 (= fast reacting, 'illitization', interlayer group: Na (= type A))
$\mathrm{CEC_{calc}}$: 58 meq / 100 g (literature: 56 meq / 100 g [Matschiavelli et al., 2019: MAT19])

Measured particles: 122

Table 1. *Summarized chemical composition*

SiO_2	TiO_2	Al_2O_3	Fe_2O_3	MnO	MgO	CaO	Na_2O	K_2O	P_2O_5	Σ	
58.6%	0.1%	22.6%	6.3%		3.2%	1.7%	0.1%	1.2%		0.94	measured particles
58.6%	0.0%	22.0%	5.9%		3.0%	1.0%	0.1%	1.1%	0.1%	0.92	measured particles of original B25

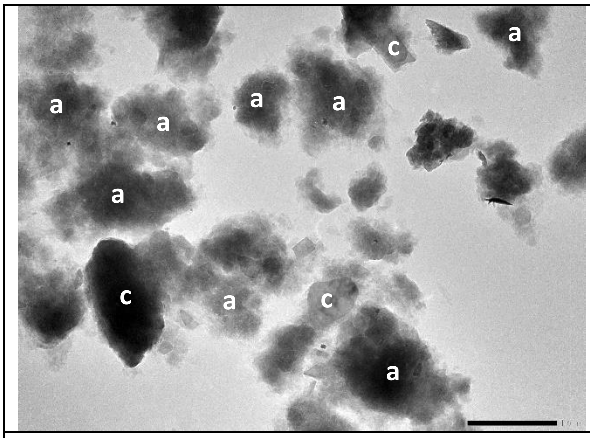

JEM-2100_No2_T_A3_X8000.bmp

Magnification: 8k

- (s) aggregates formed by small (≤ 200 nm) xenomorphous plates *(BM 70:30)*;
- (c) large (≤ 1 µm) xenomorph film-like platy crystals partially with folds *(K-rich diVS-ml: illite)*

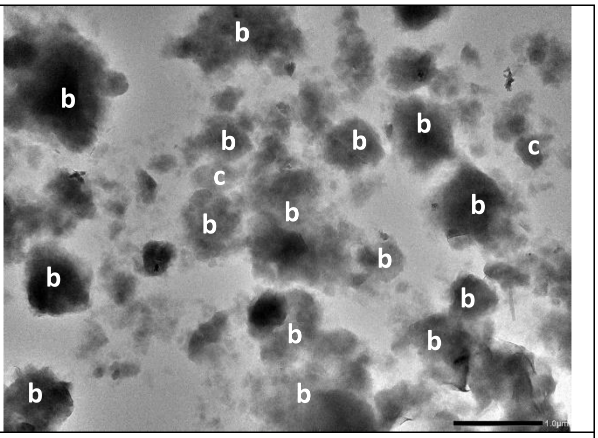

JEM-2100_No2-T_A2_X8000.bmp

Magnification: 8k

- (b) xenomorph film-like platy crystals partially with folds *(low K diVS-ml)*;
- (c) xenomorph film-like platy crystals partially with folds *(K-rich diVS-ml)*

Fig. 2. *Morphology of particles (TEM-micrographs)*

Distribution of smectite layers probability (%S)

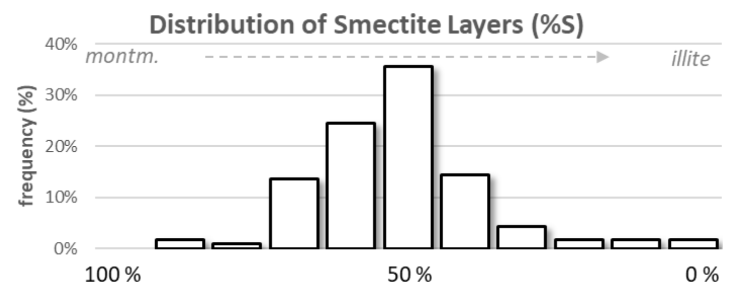

Description: *The distribution of %S-probability indicates the occurrence of two groups: (i) mixture of beidellite-montmorillonite interstratifications (= assumption) with diVS-ml as well as (ii) illite with K-deficiency (%S-class = 0%).*

Fig. 3a. *Distribution of smectite layers probability (%S)*

Differentiation by relation “Octahedral Mg vs. tetrahedral Si”?

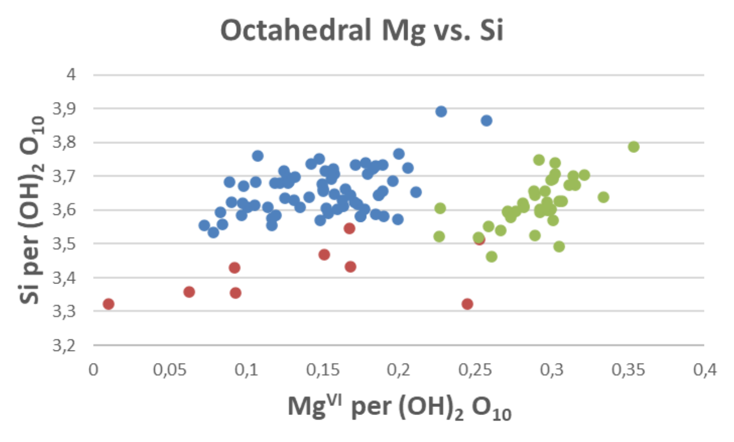

Description: *This diagram indicates the occurrence of three groups of Mg in relation to tetrahedral Si. Probably, this distribution mirrors (I) beidellite-montmorillonite inter-stratifications (BM) with typical amount of Ca in interlayer (blue), (II) even BM with high amount of Ca in interlayer (green) and (III) K-rich diVS-ml incl. illite (red)*

Fig. 3b. *Distribution of octahedral Mg vs. tetrahedral Si [all per$(OH)_2 O_{10}$]*

Distribution of K in relation to tetrahedral Si

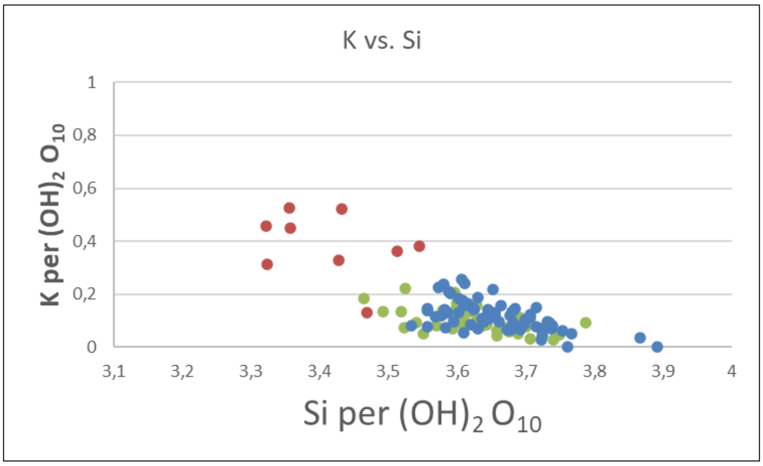

Description: *This diagram visualizes possible particles of beidellite-montmorillonite interstratification (blue and green dots) and K-rich diVS-ml phases (red dots)*

Fig. 4. *Distribution of K in interlayer space vs. tetrahedral Si [all per(OH)$_2$ O$_{10}$]*

Distribution of charges (exchangeable from interlayer space)

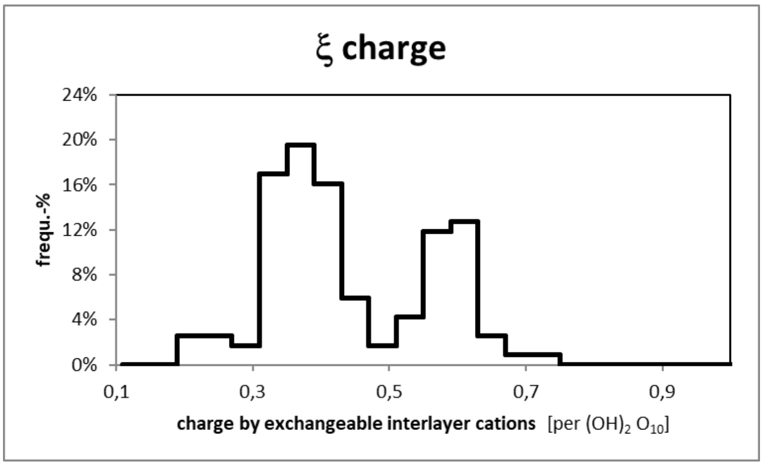

This diagram visualizes the distribution of exchangeable charges in the interlayer space (Ca, Mg, Na) determined and computed by TEM-EDX-data.

Description: *Bimodal maximal frequency-% of charge density at 0.39 and 0.59-0.63 per (OH)$_2$ O$_{10}$.*

Fig. 5. *Distribution of charges*

Beidellite-Montmorillonite interstratification (BM ~ 70%:30%) *(Cluster3):*

$$Ca_{0.09}\ Mg_{0.10}\ Na_{0.00}\ K_{0.11}\quad Al_{1.24}\ Fe^{3+}_{0.61}\ Mg_{0.15}\ Ti_{0.00}\ (OH)_2\quad Si_{3.66}\ Al_{0.34}\ O_{10}$$

Charge: XII = 0.49 VI = 5.85 IV = 15.66 **Σ = 22.00**

Measured particles: 70

Beidellite-Montmorillonite interstratification (BM ~ 75%:25%) *(Cluster2):*

$$Ca_{0.28}\ Mg_{0.00}\ Na_{0.02}\ K_{0.10}\quad Al_{1.13}\ Fe^{3+}_{0.56}\ Mg_{0.29}\ Ti_{0.01}\ (OH)_2\quad Si_{3.62}\ Al_{0.38}\ O_{10}$$

Charge: XII = 0.69 VI = 5.69 IV = 15.62 **Σ = 22.00**

Measured particles: 39

Distribution of BM-interstratifications (Cluster3)

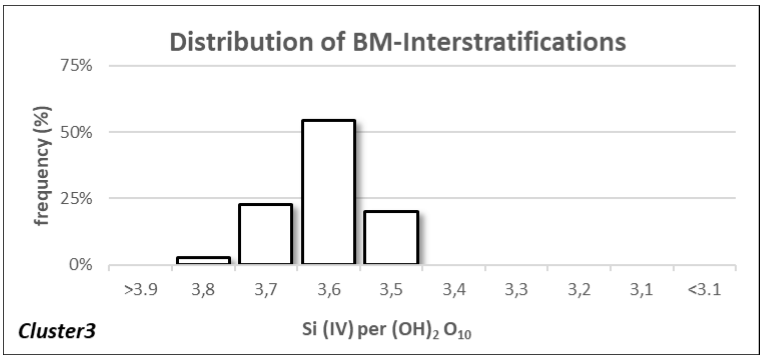

Description: *The distribution of BM-interstratifications (classified as Cluster3) draws a maximum of frequency (%) at tetrahedral Si-value between 3.6 – 3.7 e phuc*

Fig. 6a. *Distribution of assumed beidellite-montmorillonite interstratifications*

BM 70:30 ?	*particles (abs)*	Ca (XII)	Mg (XII)	Na (XII)	K (XII)	Cr3+ (VI)	Al (VI)	Fe3+ (VI)	Mg (VI)	Ti (VI)	Al (IV)	Si (IV)	XII	n_VI	%S
Si >3.9	n = 0														
Si 3.9-3.8	n = 2	0,09	0,09	0,00	0,02	0,00	1,34	0,42	0,24	0,00	0,12	3,88	0,4	2,0	85
Si 3.8-3.7	n = 16	0,09	0,09	0,00	0,08	0,00	1,24	0,59	0,17	0,00	0,27	3,73	0,4	2,0	59
Si 3.7-3.6	**n = 38**	**0,08**	**0,10**	**0,00**	**0,13**	**0,00**	**1,23**	**0,63**	**0,14**	**0,00**	**0,35**	**3,65**	**0,5**	**2,0**	**47**
Si 3.6-3.5	n = 14	0,10	0,10	0,00	0,14	0,00	1,26	0,61	0,13	0,01	0,43	3,57	0,6	2,0	37
Si 3.5-3.4	n = 0														
Si 3.4-3.3	n = 0														
Si 3.3-3.2	n = 0														
Si 3.2-3.1	n = 0														
Si <3.1	n = 0														

Fig. 6b. *Computed averaged mineral formulae of phases in the different Si(IV)-classes*

Distribution of smectite layers probability (%S) in diVS-ml (Cluster2)

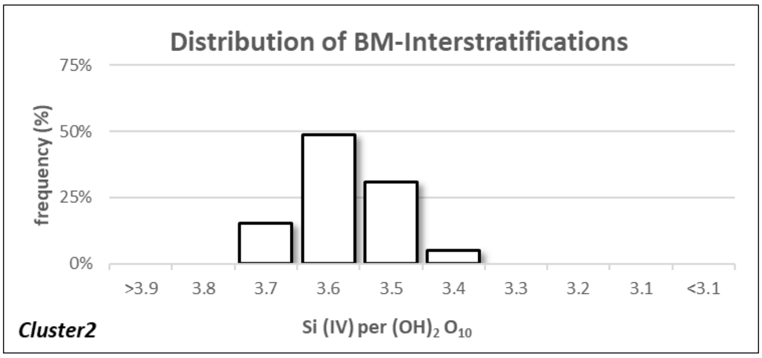

Description: *The distribution of BM-interstratifications (classified as Cluster2) draws a maximum of frequency (%) at tetrahedral Si-value at 3.6 e phuc.*

Fig. 7a. *Distribution of assumed beidellite-montmorillonite interstratifications*

Cluster 2

BM 70:30 ?	*particles (abs)*	Ca (XII)	Mg (XII)	Na (XII)	K (XII)	Cr3+ (VI)	Al (VI)	Fe3+ (VI)	Mg (VI)	Ti (VI)	Al (IV)	Si (IV)	XII	n_VI	%S
Si >3.9	n = 0														
Si 3.9-3.8	n = 0														
Si 3.8-3.7	n = 6	0.27	0.00	0.01	0.07	0.00	1.22	0.45	0.31	0.00	0.27	3.73	0.6	2.0	60
Si 3.7-3.6	**n = 19**	**0.29**	**0.00**	**0.02**	**0.10**	**0.00**	**1.11**	**0.58**	**0.29**	**0.00**	**0.36**	**3.64**	**0.7**	**2.0**	**45**
Si 3.6-3.5	n = 12	0.28	0.01	0.02	0.12	0.00	1.14	0.56	0.27	0.01	0.43	3.57	0.7	2.0	36
Si 3.5-3.4	n = 2	0.29	0.02	0.00	0.16	0.00	0.99	0.66	0.28	0.06	0.52	3.48	0.8	2.0	26
Si 3.4-3.3	n = 0														
Si 3.3-3.2	n = 0														
Si 3.2-3.1	n = 0														
Si <3.1	n = 0														

Fig. 7b. *Computed averaged mineral formulae of phases in the different Si(IV)-classes*

Dioctahedral Vermiculite-Smectite mixed layer phases (diVS-ml) *(Cluster1):*

$Ca_{0.08}\ Mg_{0.07}\ Na_{0.01}\ K_{0.39}\quad Al_{1.37}\ Fe^{3+}_{0.48}\ Mg_{0.14}\ Ti_{0.01}\ (OH)_2\quad Si_{3.42}\ Al_{0.58}\ O_{10}$

Charge:	XII = 0.71	VI = 5.87	IV = 15.42	**Σ = 22.00**
Probability of smectite layers (%S):	19%			
Probability of illite layers (%I):	81%			
Measured particles:	9			

Distribution of smectite layers probability (%S) in diVS-ml (Cluster1)

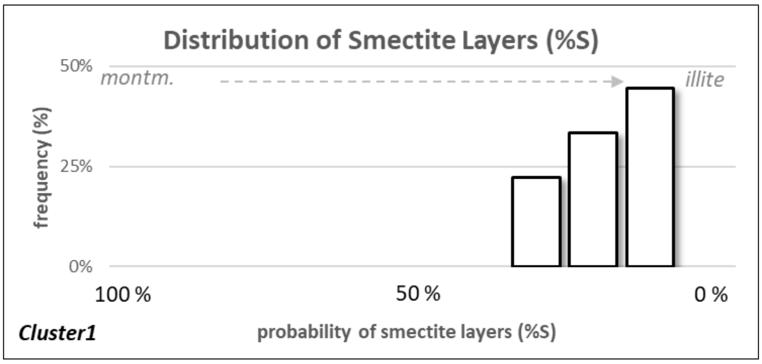

Description: *The distribution of diVS-ml (classified as Cluster1) draws a maximum of frequency (%) for smectite layer probability at <15%.*

Fig. 8a. *Distribution of smectite layers probability in diVS-ml*

Cluster 1

diVS-ml	particles (abs)	Ca (XII)	Mg (XII)	Na (XII)	K (XII)	Cr3+ (VI)	Al (VI)	Fe3+ (VI)	Mg (VI)	Ti (VI)	Al (IV)	Si (IV)	XII	n_VI	%S
%S >95%	n = 0														
%S 95-85%	n = 0														
%S 85-75%	n = 0														
%S 75-65%	n = 0														
%S 65-55%	n = 0														
%S 55-45%	n = 0														
%S 45-35%	n = 0														
%S 35-25%	n = 2	0.13	0.03	0.00	0.37	0.00	1.30	0.49	0.21	0.00	0.47	3.53	0.7	2.0	31
%S 25-15%	n = 3	0.12	0.06	0.01	0.33	0.00	1.44	0.42	0.14	0.01	0.56	3.44	0.7	2.0	22
%S <15%	n = 4	0.04	0.11	0.01	0.44	0.00	1.36	0.53	0.10	0.02	0.66	3.34	0.7	2.0	13

Fig. 8b. *Computed averaged mineral formulae of diVS-ml phases in the different smectite layers probability (%S)-classes*

Description – B25 No2_T (< 2 µm), treated material *(OPA, 100°C, 35 days)*

Preparation for TEM

The powder of compacted and treated B25-No2_T-sample was suspended in deionized water and dispersed by ultrasonic treatment for approximately 20 min. The clay fraction (<2 µm) was separated by sedimentation and diluted with deionized water to get a clear suspension. The suspension was dropped onto carbon-coated Cu grids, air dried and stored under environment-controlled conditions at 45% humidity.

Mineral Matter - Overview

The fraction < 2 µm of treated B25 bentonite sample (Opalinus Clay solution, at 100°C, for 35 days) is mainly composed by assumed beidellite-montmorillonite interstratifications (B:M ~70:30), abbreviated as BM-ml, and dioctahedral vermiculite-smectite mixed layer phases (diVS-ml) and accompanied by two types of illite. Furthermore, kaolinite, Si-surplus particles (Si, e.g. quartz) and chlorite-bearing mixed layer phases were identified in traces in this sample [fig. 1].

	frequency-% *(n = 125 measured particles)*
BM-ml (Clusters 2+3)	87%
diVS-ml (Cluster1)	7%
Kaolinite & KSV-ml	1%
Si-surplus	2%
CSV-ml	1%
others	2%

All measured dioctahedral clay mineral phases summarized result following mineral formula computed from TEM-EDX-measurement of 118 individual particles:

$$\boxed{Ca^{2+}_{0.15}\ Mg^{2+}_{0.06}\ Na^{+}_{0.01}\ K^{+}_{0.14}\quad Al^{3+}_{1.22}\ Fe^{3+}_{0.57}\ Mg^{2+}_{0.19}\ Ti^{4+}_{0.01}\ (OH)_2\quad Si^{4+}_{3.62}\ Al^{3+}_{0.38}\ O_{10}}$$

SDOM	*± 0.01*	*± 0.00*	*± 0.00*	*± 0.01*	*± 0.01*	*± 0.01*	*± 0.01*	*± 0.00*		*± 0.01*	*± 0.01*

Legend: SDOM - standard deviation of the mean (= the standard deviation divided by the square root of the number of samples)

The interlayer charge is calculated as 0.58 per $(OH)_2\ O_{10}$ and the octahedral charge as 5.80 per $(OH)_2\ O_{10}$. The particles are characterized by a high octahedral Fe-amount.

The summarized chemical composition of all 118 computed particles is compared with measured data of original B25-bentonite sample [tab. 1]. The chemical composition averaged by measured particles show especially a slight higher amount of Al_2O_3, Fe_2O_3 and CaO in comparison to the measured data of original untreated B25-bentonite.

B25-No2_T sample is characterized by two morphological groups: (i) aggregates formed by small (≤ 200 nm) xenomorphous plates [fig. 2 left] and (ii) xenomorph film-like platy crystals partially with folds [fig. 2 right]. Thin aggregates formed by small (≤ 200 nm) xenomorphous plates dominate the shapes of particles in the micrographs [fig. 2 left].

The distribution of %S-probability of all measured clay mineral phases [fig. 3a] also indicates the occurrence of two groups: (i) as main group a mixture of beidellite-montmorillonite interstratifications and (ii) diVS-ml with K- and charge deficit (%S-classes = 0% & 10%).

The numerous measured particles by TEM-EDX allow a visualization of distribution of interlayer charges. Considering the TEM-EDX-determined cations Ca^{++}, Mg^{++} and Na^{+} and then computed their ratio as interlayer cations in the mineral formula, Ca^{++}, Mg^{++} and Na^{+} offer to characterize the degree of exchangeable charges in the interlayer space. This charge density of treated B25 bentonite (< 2 µm) shows a broad and bimodal distribution of charge density at 0.35 - 0.43 and 0.59 – 0.63 per $(OH)_2$ O_{10} [fig. 5]. This bimodal interval of interlayer charge density is caused by exchangeable cations from 0.17 – 0.20 per $(OH)_2$ O_{10} representing mainly the BM-phases and from 0.24 – 0.31 per $(OH)_2$ O_{10} represented mainly by diVS-ml phases.

Mineral Matter - Specification

Result of Clustering

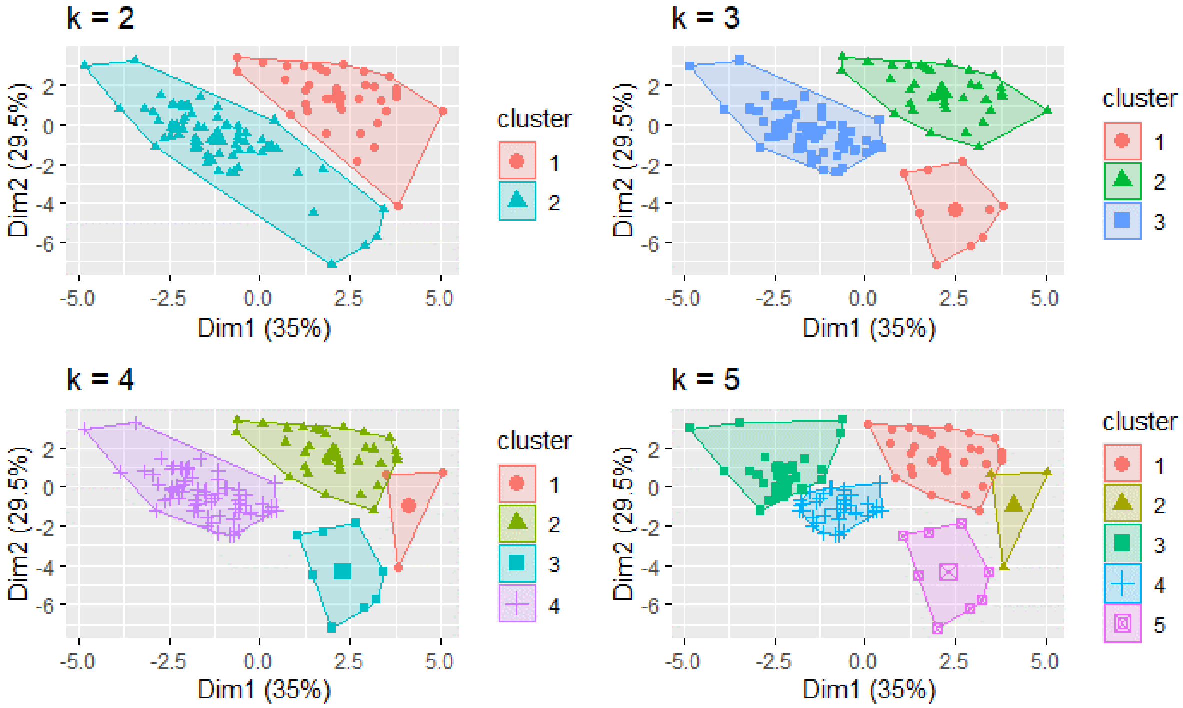

***Fig. 9.** Clustering of all measured particles for clusters k = 2, k = 3, k = 4 and k = 5 (source for R-coding: https://uc-r.github.io/kmeans_clustering)*

The optimum of clusters was calculated with k = 3.

		Ca (XII)	Mg (XII)	Na (XII)	K (XII)	Cr3+ (VI)	Al (VI)	Fe3+ (VI)	Mg (VI)	Ti (VI)	Al (IV)	Si (IV)	XII	n_VI	%S
Cluster1	n = 9	0,08	0,07	0,01	0,39	0,00	1,37	0,48	0,14	0,01	0,58	3,42	0,71	2,0	19
Cluster2	n = 39	0,28	0,00	0,02	0,10	0,00	1,13	0,56	0,29	0,01	0,38	3,62	0,69	2,0	43
Cluster3	n = 70	0,09	0,10	0,00	0,11	0,00	1,24	0,61	0,15	0,00	0,34	3,66	0,49	2,0	48

***Fig. 10.** Mineral formulae based on TEM-EDX-data summarized following the result of clustering for k=3*

	Sybilla-results	TEM-EDX-results	Notes
Cluster3	IS R0(1) *(%S = 100%)*	BM-ml *(BM 70:30?)*	*XRD: Montmorillonite and beidellite is only to distinguish by Green-Kelly-test (not available here).*
Cluster2	IS R0(1) *(%S = 100%)*	BM-ml *(BM 75:25?)*	*See XRD-note above; high Ca(XII), Fe(VI)- & Mg(VI)-rich*
Cluster1	IS R0(2) *(%S = 20%)*	diVS-ml *(%S = 19%)*	*Low K-deficit, slight Al(VI)-rich*

Tab. 2. *Comparison of results from TEM-EDX- and XRD-measurements with clustering procedure*

The clustering of TEM-EDX-data offers a good agreement with the recent result of Sybilla-processing of XRD-traces from oriented specimen [tab. 2].

IS R0 (1): The X-ray diffraction pattern of the ethylene-glycol saturated oriented specimen shows a full expandability to 1.7 nm and a difference of 5.40°2θ between 2. and 3. order of smectite interferences. This distance is typically for montmorillonite (Moore & Reynolds, 1989). This result of XRD-processing let expect a maximum of particles for %S ~ 100% by TEM-EDX-measurements, but the maximum of particles measured by TEM-EDX is to find at %S=70% [fig. 3a].

Montmorillonite and beidellite have the same behavior concerning the expandability and they are only to distinguish by XRD using Li like by Greene-Kelly test (Green-Kelly 1952, 1953). So, combination of XRD- and TEM-results (full expandability by XRD and Si ~ 3.62 and 3.66 by TEM-EDX) led conclude the occurrence of 'beidellite-montmorillonite interstratifications', a beidellite-montmorillonite inter-stratification with about 75% beidellite and 25% montmorillonite layers (BM-ml 75:25) for Cluster 2 and with about 70% beidellite and 30% montmorillonite layers (BM-ml 70:30) for Cluster 3.

IS R0 (2): The Sybilla-procedure of XRD-traces (oriented mounts) has shown an occurrence of a second illite-smectite mixed layer phase with a smectite layers probability of %S = 20%. This situation is to find in Cluster1 (%S_{TEM} = 19%) representing a K- and only low charge deficient dioctahedral vermiculite-smectite mixed layer phase (diV-ml) [tab. 2].

The Sybilla-processing of XRD-traces (oriented mounts) also supports the existence of kaolinite and kaolinite-smectite mixed layer phases in fine fraction of sample. Such phases were not to identify or to calculate in TEM-EDX-database (a grain size effect?).

Specifics to the identified clay mineral groups

Beidellite-montmorillonite interstratifications (B:M ~70:30?)

109 of 118 measured particles belong so to this assumed classification. The dioctahedral character of this group is proofed by X-ray diffraction. The position of the large (060)-interference of smectite is in the random oriented powder specimen at 1.497 Å.

Montmorillonite and beidellite have the same behavior concerning the expandability and they are only to distinguish by XRD using Li by means of Greene-Kelly test (Green-Kelly 1952, 1953). So, combination of XRD- and TEM-results (full expandability by XRD and Si ~ 3.62 and 3.66 by TEM-EDX) led conclude the occurrence of 'beidellite-montmorillonite interstratifications', a beidellite-montmorillonite inter-stratification with about 70% beidellite and 30% montmorillonite layers (BM-ml 70:30) and with about 75% beidellite and 25% montmorillonite layers (BM-ml 75:25).

Beidellite-montmorillonite interstratifications (B:M ~70:30?):

$$Ca_{0.09}\ Mg_{0.10}\ Na_{0.00}\ K_{0.11}\quad Al_{1.24}\ Fe^{3+}_{0.61}\ Mg_{0.15}\ Ti_{0.00}\ (OH)_2\quad Si_{3.66}\ Al_{0.34}\ O_{10}$$

Charge: XII = 0.49 VI = 5.85 IV = 15.66 **Σ = 22.00**

Measured particles by TEM-EDX: 70
Result of clustering: Cluster3 [tab. 2]

Beidellite-montmorillonite interstratifications (B:M ~75:25?):

$$Ca_{0.28}\ Mg_{0.00}\ Na_{0.02}\ K_{0.10}\quad Al_{1.13}\ Fe^{3+}_{0.56}\ Mg_{0.29}\ Ti_{0.01}\ (OH)_2\quad Si_{3.62}\ Al_{0.38}\ O_{10}$$

Charge: XII = 0.69 VI = 5.69 IV = 15.62 **Σ = 22.00**
Measured particles by TEM-EDX: 39
Result of clustering: Cluster2 [tab. 2]

Beidellitic structures are characterized by a low octahedral Mg-amount (because of high ratio of octahedral, 3-valent cations). A comparison of octahedral Mg vs. tetrahedral Si indicates the occurrence of two groups for octahedral Mg based on TEM-EDX-data, separated by tetrahedral Si [fig. 3b]. The core of BM-ml shows an octahedral Mg-amount between 0.13 – 0.24 e phuc, probably pronounced by a higher Mg^{VI} in montmorillonite compound in this type interstratification.

Using the results of clustering (see Clusters 2+3 in tab. 2), the maximum of frequency-% is to find for particles in the Si(IV)-class 3.6 – 3.7 e phuc [tab. 6a], representing the mentioned relation 30% montmorillonite and 70% beidellite as ratio of interstratification. The mineral formulae of cluster 3, summarized in classes of tetrahedral Si, draw for the maximum an Fe-rich BM 70:30 phase with K and remarkable amount of Mg in the interlayer space [tab. 6b] and cluster 2 is characterized as Fe-rich BM 75:25 phase with high Ca-amount in interlayer space [tab. 7b].

A further hypothesis is to verify: The increasing K by lower tetrahedral Si [tab. 6b] could be an indication that it's not a change of 50:50 ratio of BM-ml into a 70:30 ratio of BM-ml, but an alteration of montmorillonite into diVS-ml phases resulting into an interstratification by beidellite – montmorillonite – dioctahedral vermiculite.

Dioctahedral vermiculite-smectite mixed layer phase

The Rietveld refinement by Profex software (Döbelin & Kleeberg, 2015) indicates the occurrence of two polytypes for illite in treated B25 bentonite: $2M_1$- and 1M-polytype. Also, the clustering of TEM-data indicates the occurrence of illite-pronounced and K-rich diVS-ml phases (cluster 1).

$$Ca_{0.08}\ Mg_{0.07}\ Na_{0.01}\ K_{0.39}\quad Al_{1.37}\ Fe^{3+}_{0.48}\ Mg_{0.14}\ Ti_{0.01}\ (OH)_2\quad Si_{3.42}\ Al_{0.58}\ O_{10}$$

Charge: XII = 0.71 VI = 5.87 IV = 15.42 **Σ = 22.00**
Probability of smectite layers (%S): 19%
Probability of illite layers (%I): 81%

Measured particles by TEM-EDX: 9
Result of clustering: Cluster1 [tab. 2]

Kaolinite-montmorillonite mixed layer phases

The Excel-based procedure (Hoang-Minh et al., 2019) to identify possible clay mineral groups using the TEM-EDX-measurements also includes algorithms to classify kaolinite and kaolinite-montmorillonite mixed layer phases. These algorithms couldn't identify such phases basing on the measured TEM-EDX-data. Otherwise, very few particles, which were not to compute, have shown small hexagonal plates typically for kaolinite-bearing phases.

References

Cliff, G. & Lorimer, G. W. (1975). *J. Microsc.* **103**, 203–207.

Döbelin, N., Kleeberg, R. (2015). *Journal of Applied Crystallography* **48**, 1573-1580. DOI: 10.1107/S1600576715014685

Henning, K.-H. & Störr, M. (1986). Electron Micrographs (TEM, SEM) of Clays and Clay Minerals, p. 325. Akademie-Verlag Berlin.

Hoang-Minh, T., Kasbohm, J., Nguyen-Thanh, L., Nga, P. T., Lai, L. T., Duong, N. T., Thanh, N. D., Thuyet, N. T. M., Anh, D. D., Pusch, R., Knutsson, S. & Ferreiro Mahlmann, R. (2019). *J. Appl. Cryst.* **52**, 133-147. DOI: 10.1107/S1600576718018162

Lorimer, G. W. & Cliff, G. (1976). *Electron Microscopy in Mineralogy*, edited by H. R. Wenk, pp. 506–519. Berlin: Springer Verlag.

Matschiavelli, N., Kluge, S., Podlech, C., Standhaft, D., Grathoff, G., Ikeda-Ohno, A., Warr, L.N., Chukharkina, A., Arnold, T. & Cherkouk, A. (2019). *Environmental Science & Technology.* **53** (17), 10514-10524, DOI: 10.1021/acs.est.9b02670

Mellini, M. & Menichini, R. (1985). *R. Soc. Ital. Miner. Petrol.* **40**, 261–266.

Moore, D.M., Reynolds, R.C. (1989). X-ray Diffraction and the Identification and Analysis of Clay Minerals, Oxford University Press, New York, 332 + xvi pp.

Nguyen-Thanh, L., Herbert, H.-J., Kasbohm, J., Hoang-Minh, T. & Mählmann, R. F. (2014). *Clays Clay Miner.* **62**, 425–446.

Środoń, J., Elsass, F., McHardy, W. J. & Morgan, D. J. (1992). *Clay Miner.* **27**, 137–158.

Data Sheet – B25 bentonite, treated materials *(OPA, 100 °C, 35d)* – CENTER

Methodology - Transmission electron microscopy linked with energy-dispersive X-ray spectroscopy (TEM-EDX)

It is expected a characterization of clay mineral phases in treated B25 bentonite by transmission electron microscopy. The sample series No2 represents a percolation of B25 bentonite by Opalinus Clay solution at 100°C for 35 days. The sample No2_C is the label for the material at the middle of sample cylinder.

The different clay mineral phases are to identify and to describe by chemical composition and its variability, morphology, the specific dissolution potential, and further parameter.

Such further parameter like distribution of smectite layers probability (%S) and distribution of charges caused by exchangeable cations interlayer space should serve as additional indicators for mineralogical alterations in treatment experiments with B25 bentonite.

The sample were suspended for TEM-measurement in deionized water and dispersed by ultrasonic treatment for approximately 20 min. The clay fraction (<2 µm) was separated by sedimentation and diluted with deionized water to get a clear suspension. The suspension was dropped onto carbon-coated Cu grids, air dried and stored under environment-controlled conditions at 45% humidity.

TEM-EDX investigations were carried out on the <2 µm fraction using a FEI TECNAI G^2 20 electron transmission microscope at the VNU University of Science, Vietnam National University, Hanoi. This equipment (operated at 200 kV with LaB_6 cathode) was combined with an S-TWIN objective, a windowless EDAX energy-dispersive X-ray system and a FEI Eagle 2k CCD TEM camera.

About 100 individual clay particles per sample were characterized by TEM-EDX with respect to crystal size, crystal habit, and particle morphology and element distribution. The crystal size, crystal habit and particle morphology were described according to Henning & Störr (1986).

For the quantification of element distribution, a calibration of k factors is mandatory (Cliff & Lorimer, 1975; Lorimer & Cliff, 1976; Mellini & Menichini, 1985). These k values are used to calibrate for the specific behaviour of particles against possible irradiation damage. The elements O, Na, Mg, Al, Si, K, Ca and Fe were quantified by applying the EDAX GENESIS–TEM Quant Materials quantification procedure.

In this procedure, the acquired EDX spectra are corrected by background subtraction, Gaussian deconvolution and k-factor corrections using values previously determined on a phyllosilicate standard (muscovite) and selected non-phyllosilicate standards. The average errors in the analyzed elements using the phyllosilicate standard, expressed as the atomic proportions, are 10 (Na), 5 (Fe, Mg, K, Ti, Ca) and 1 (Si, Al).

The measurement time per particle was lowered to 20 s and the exposed area was limited to a 50 nm diameter, avoiding possible irradiation damage of particles. The stability of particles of the sample series was tested for this measurement time at the beginning of any measurement campaign.

Further methodological details related to TEM-EDX-measurements and the Excel-based mathematical procedure using TEM-EDX data for calculation of mineral formulae are described in Hoang-Minh et al. (2019).

These mathematical procedures described in Hoang-Minh et al. (2019) were extended by k-means clustering method for finding subgroups of observations within a data set. The data were standardized (i.e., scaled) to make variables comparable. Euclidean distances were applied as classical method for distance measures. The optimal clusters were determined by Elbow method and Gap statistics[11].

---

[11] *https://uc-r.github.io/kmeans_clustering*

Data Sheet – B25 No2_C (< 2 µm), treated material *(OPA, 100°C, 35 days)*

Preparation for TEM

- raw material: compacted material (1.6 g/cm³) of treated B25-sample (OPA, 100°C, 35 days)
- suspension on particles < 2 µm on carbon-filmed Cu-grid
- air-dried and humidity-controlled storing

Mineral Matter

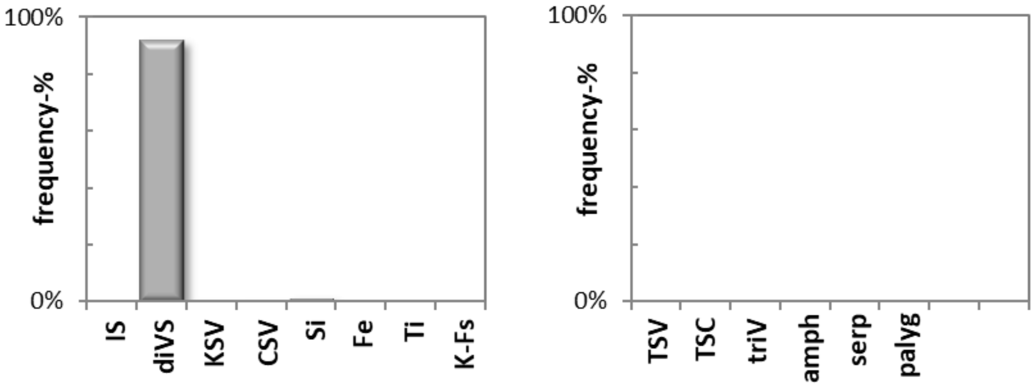

Fig. 1. *Distribution of mineral groups in fraction < 2 µm (in frequency-%)*
Legend: ***IS*** *– illite-smectite-mixed layer series in sense of Środon et al. (1992), diVS – dioctahedral vermiculite-smectite illite-smectite-mixed layer series (= charge- and/or K-deficit),* ***KSV*** *– kaolinite-smectite-dioctahedral vermiculite-mixed layer series,* ***CSV*** *– chlorite-saponite-trioctahedral vermiculite-mixed layer series,* ***Si*** *– quartz or particles with Si-surplus,* ***Fe*** *– Fe-oxide or Fe-oxyhydroxide,* ***Ti*** *– Ti-bearing phases (e.g. rutile, anatase),* ***K-Fs*** *– K-feldspar*

Clay Mineral Composition

All particles of smectite group:

$$Ca_{0.10}\,Mg_{0.09}\,Na_{0.01}\,K_{0.15}\quad Al_{1.22}\,Fe^{3+}_{0.60}\,Mg_{0.16}\,Ti_{0.01}\,(OH)_2\quad Si_{3.61}\,Al_{0.39}\,O_{10}$$

Charge: XII = 0.54 VI = 5.85 IV = 15.61 **Σ = 22.00**
Probability of smectite layers (%S): 42%
Probability of illite layers (%I): 58%

Specific Dissolution Potential (ΔS%)

for H2O, 20 + 60 rpm	-11	(= slow reacting, interlayer group: Ca+Mg (= type B))
for NaCl, 20 rpm	-12	(= slow reacting, interlayer group: Ca+Mg (= type B))
for NaCl, 60 rpm	-87	(= fast reacting, 'illitization', interlayer group: Na (= type A))
CEC_{calc}:	51 meq / 100 g	(literature: 56 meq / 100 g [Matschiavelli et al., 2019: MAT19])

Measured particles: 129

Table 1. *Summarized chemical composition*

SiO_2	TiO_2	Al_2O_3	Fe_2O_3	MnO	MgO	CaO	Na_2O	K_2O	P_2O_5	Σ	
59.1%	0.1%	23.2%	6.5%		3.1%	1.1%	0.1%	1.4%		0.95	measured particles
58.6%	0.0%	22.0%	5.9%		3.0%	1.0%	0.1%	1.1%	0.1%	0.92	measured particles of original B25

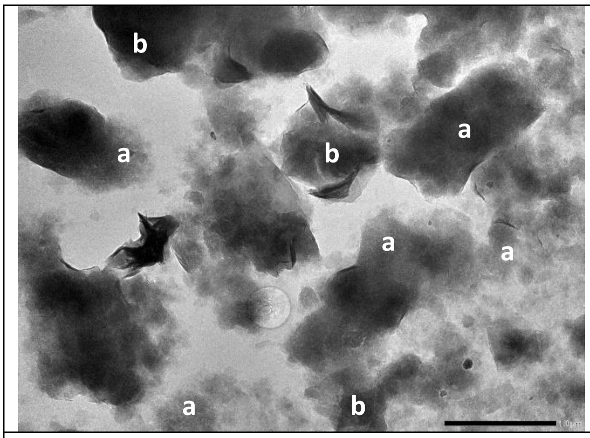	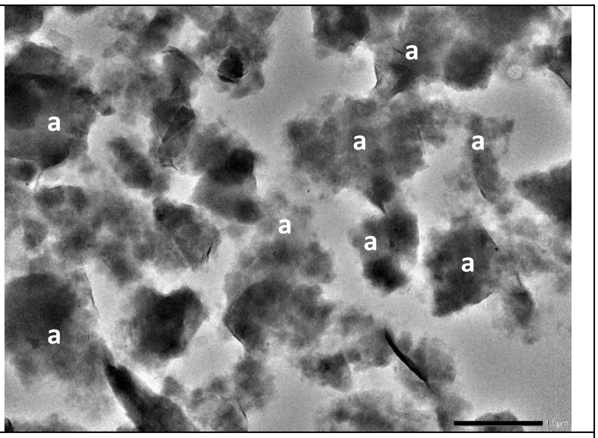
JEM-2100_No2-C_A2_X10k.bmp	*JEM-2100_No2-C_A4_X10k.bmp*
Magnification: 10k (t) aggregates formed by small (≤ 200 nm) xenomorphous plates; (u) large (≤ 1 µm) xenomorph film-like platy crystals partially with folds	Magnification: 10k (a) aggregates formed by small (≤ 200 nm) xenomorphous plates;

Fig. 2. *Morphology of particles (TEM-micrographs)*

Distribution of smectite layers probability (%S)

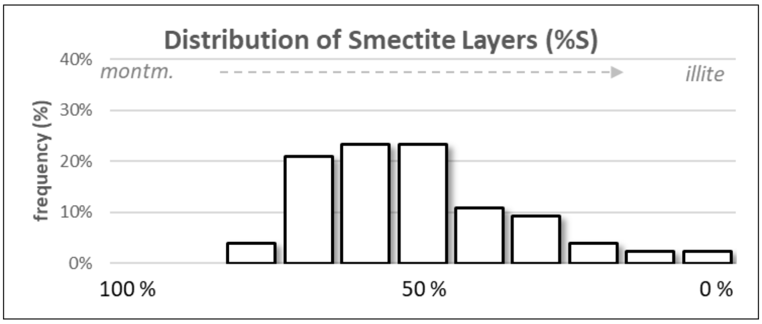

Fig. 3a. *Distribution of smectite layers probability (%S)*

Description: *The distribution of %S-probability indicates the occurrence of two groups: (i) mixture of beidellite-montmorillonite interstratifications (= assumption) with diVS-ml as well as (ii) illite with K-deficiency (%S-class = 0%).*

Differentiation by relation “Octahedral Mg vs. tetrahedral Si”?

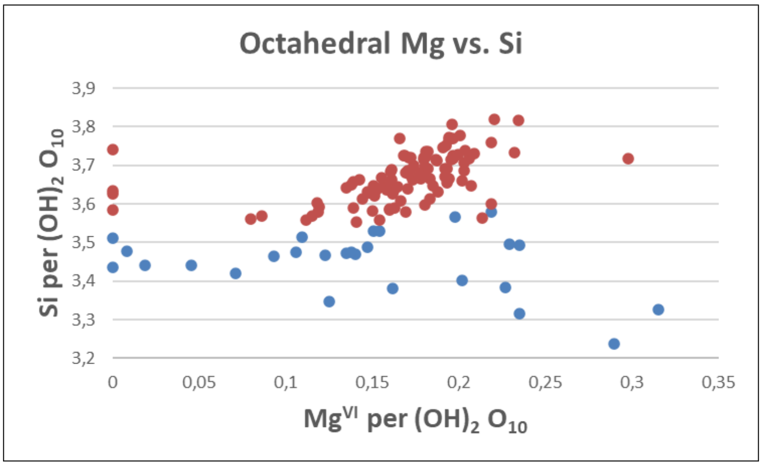

Description: *This diagram indicates the occurrence of two groups of Mg in relation to tetrahedral Si. Probably, this distribution mirrors 2 phases (I) beidellite-montmorillonite interstratifications (red) and (II) diVS-ml (blue)*

Fig. 3b. *Distribution of octahedral Mg vs. tetrahedral Si [all per* $(OH)_2\ O_{10}$*]*

Distribution of K in relation to tetrahedral Si

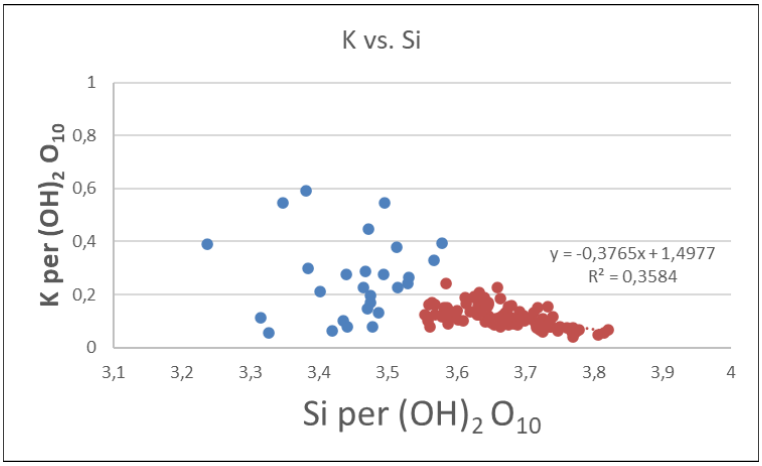

***Description:** This diagram visualizes possible particles (beidellite-montmorillonite interstratification?) with a very low K (red dots) and particles with a broad interval of K (blue dots = diVS-ml?)*

***Fig. 4.** Distribution of K in interlayer space vs. tetrahedral Si [all per$(OH)_2O_{10}$]*

Distribution of charges (exchangeable from interlayer space)

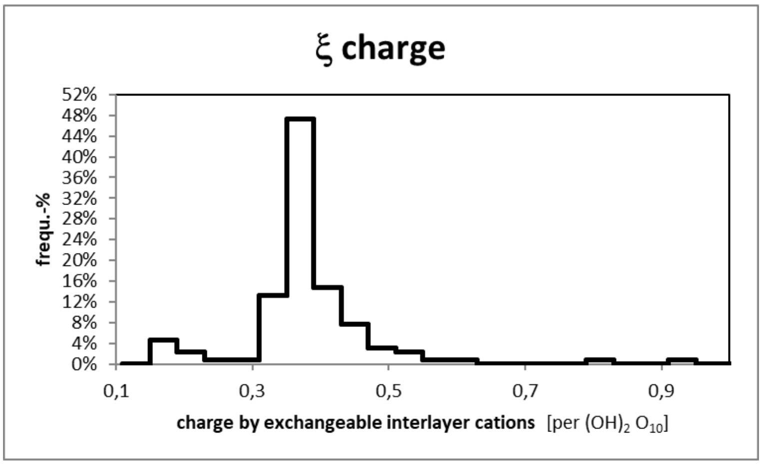

This diagram visualizes the distribution of exchangeable charges in the interlayer space (Ca, Mg, Na) determined and computed by TEM-EDX-data.

***Description:** Maximal frequency-% of charge density at 0.39 per $(OH)_2O_{10}$.*

***Fig. 5.** Distribution of charges*

***Beidellite-Montmorillonite interstratification (BM ~ 70%:30%)** (Cluster2):*

$$Ca_{0.10}\ Mg_{0.07}\ Na_{0.01}\ K_{0.12}\quad Al_{1.23}\ Fe^{3+}_{0.59}\ Mg_{0.17}\ Ti_{0.01}\ (OH)_2\quad Si_{3.67}\ Al_{0.33}\ O_{10}$$

Charge:	XII = 0.49	VI = 5.84	IV = 15.67	**Σ = 22.00**

Measured particles: 102

Distribution of BM-interstratifications (Cluster2)

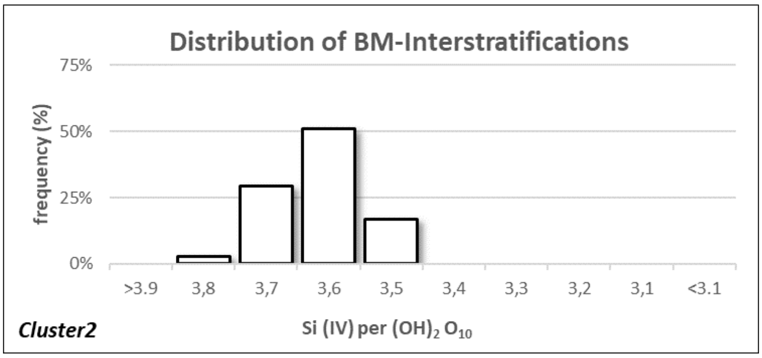

***Description:** The distribution of BM-interstratifications (classified as Cluster2) draws a maximum of frequency (%) at tetrahedral Si-value between 3.6 – 3.7 e phuc*

***Fig. 6a.** Distribution of assumed beidellite-montmorillonite interstratifications*

Cluster 2

BM70:30??	*particles (abs)*	**Ca (XII)**	**Mg (XII)**	**Na (XII)**	**K (XII)**	**Cr3+ (VI)**	**Al (VI)**	**Fe3+ (VI)**	**Mg (VI)**	**Ti (VI)**	**Al (IV)**	**Si (IV)**	**XII**	**n_VI**	**%S**
Si >3.9	n = 0														
Si 3.9-3.8	n = 3	0.10	0.07	0.02	0.06	0.00	1.31	0.47	0.22	0.00	0.19	3.81	0.4	2.0	73
Si 3.8-3.7	n = 30	0.11	0.07	0.01	0.09	0.00	1.23	0.58	0.19	0.00	0.27	3.73	0.5	2.0	60
Si 3.7-3.6	**n = 52**	**0.10**	**0.07**	**0.01**	**0.13**	**0.00**	**1.23**	**0.60**	**0.16**	**0.01**	**0.35**	**3.65**	**0.5**	**2.0**	**48**
Si 3.6-3.5	n = 17	0.10	0.09	0.02	0.14	0.00	1.24	0.62	0.13	0.01	0.42	3.58	0.5	2.0	37
Si 3.5-3.4	n = 0														
Si 3.4-3.3	n = 0														
Si 3.3-3.2	n = 0														
Si 3.2-3.1	n = 0														
Si <3.1	n = 0														

Fig. 6b. *Computed averaged mineral formulae of phases in the different Si(IV)-classes*

Dioctahedral Vermiculite-Smectite mixed layer phases (diVS-ml) *(Cluster1):*

$$Ca_{0.08}\ Mg_{0.12}\ Na_{0.01}\ K_{0.26}\quad Al_{1.22}\ Fe^{3+}_{0.62}\ Mg_{0.14}\ Ti_{0.02}\ (OH)_2\ \ Si_{3.45}\ Al_{0.55}\ O_{10}$$

Charge:	XII = 0.68	VI = 5.87	IV = 15.45	**Σ = 22.00**

Probability of smectite layers (%S): 23%

Probability of illite layers (%I): 77%

Measured particles: 27

Distribution of smectite layers probability (%S) in diVS-ml (Cluster2)

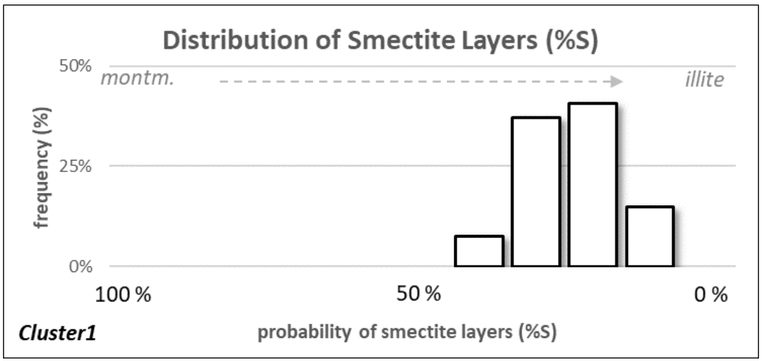

Description: *The distribution of diVS-ml (classified as Cluster1) draws a maximum of frequency (%) for smectite layer probability at 15-35%.*

Fig. 7a. *Distribution of smectite layers probability in diVS-ml*

diVS-ml	*particles (abs)*	**Ca (XII)**	**Mg (XII)**	**Na (XII)**	**K (XII)**	**Cr3+ (VI)**	**Al (VI)**	**Fe3+ (VI)**	**Mg (VI)**	**Ti (VI)**	**Al (IV)**	**Si (IV)**	**XII**	**n_VI**	**%S**
%S >95%	n = 0														
%S 95-85%	n = 0														
%S 85-75%	n = 0														
%S 75-65%	n = 0														
%S 65-55%	n = 0														
%S 55-45%	n = 0														
%S 45-35%	n = 2	0,08	0,04	0,02	0,36	0,00	1,30	0,47	0,21	0,01	0,43	3,57	0,6	2,0	37
%S 35-25%	**n = 10**	**0,09**	**0,10**	**0,00**	**0,25**	**0,00**	**1,26**	**0,59**	**0,13**	**0,02**	**0,50**	**3,50**	**0,6**	**2,0**	**28**
%S 25-15%	**n = 11**	**0,08**	**0,11**	**0,01**	**0,25**	**0,00**	**1,26**	**0,61**	**0,11**	**0,02**	**0,57**	**3,43**	**0,7**	**2,0**	**21**
%S <15%	n = 4	0,07	0,24	0,02	0,28	0,00	0,92	0,82	0,24	0,02	0,69	3,31	0,9	2,0	10

Fig. 7b. *Computed averaged mineral formulae of diVS-ml phases in the different smectite layers probability (%S)-classes*

Description – B25 No2_C (< 2 µm), treated material *(OPA, 100°C, 35 days)*

Preparation for TEM

The powder of compacted and treated B25-No2_C-sample was suspended in deionized water and dispersed by ultrasonic treatment for approximately 20 min. The clay fraction (<2 µm) was separated by sedimentation and diluted with deionized water to get a clear suspension. The suspension was dropped onto carbon-coated Cu grids, air dried and stored under environment-controlled conditions at 45% humidity.

Mineral Matter - Overview

The fraction < 2 µm of treated B25 bentonite sample (Opalinus Clay solution, at 100°C, for 35 days) is mainly composed by assumed beidellite-montmorillonite interstratifications (B:M ~50:50), abbreviated as BM-ml, and dioctahedral vermiculite-smectite mixed layer phases (diVS-ml) and accompanied by two types of illite. Furthermore, kaolinite, Si-surplus particles (Si, e.g. quartz) and chlorite-bearing mixed layer phases were identified in traces in this sample [fig. 1].

	frequency-% *(n = 140 measured particles)*
BM-ml (Cluster1)	73%
diVS-ml (Cluster2)	19%
Kaolinite & KSV-ml	1%
Si-surplus	1%
CSV-ml	1%

All measured dioctahedral clay mineral phases summarized result following mineral formula computed from TEM-EDX-measurement of 129 individual particles:

	$Ca^{2+}_{0.10}$	$Mg^{2+}_{0.09}$	$Na^{+}_{0.01}$	$K^{+}_{0.15}$	$Al^{3+}_{1.22}$	$Fe^{3+}_{0.60}$	$Mg^{2+}_{0.16}$	$Ti^{4+}_{0.01}$	$(OH)_2$	$Si^{4+}_{3.61}$	$Al^{3+}_{0.39}$	O_{10}
SDOM	*± 0.00*	*± 0.00*	*± 0.00*	*± 0.01*	*± 0.01*	*± 0.01*	*± 0.00*	*± 0.00*		*± 0.01*	*± 0.01*	

Legend: SDOM - standard deviation of the mean (= the standard deviation divided by the square root of the number of samples)

The interlayer charge is calculated as 0.54 per $(OH)_2$ O_{10} and the octahedral charge as 5.85 per $(OH)_2$ O_{10}. The particles are characterized by a high octahedral Fe-amount.

The summarized chemical composition of all 129 computed particles is compared with measured data of original B25-bentonite sample [tab. 1]. The chemical composition averaged by measured particles show especially a higher amount of Al_2O_3, Fe_2O_3 and K_2O in comparison to the measured data of original untreated B25-bentonite.

B25-No2_C sample is characterized by two morphological groups: (i) aggregates formed by small (≤ 200 nm) xenomorphous plates and (ii) large (≤ 1 µm) xenomorph film-like platy crystals partially with folds [fig. 2 left]. Thin aggregates formed by small (≤ 200 nm) xenomorphous plates dominate the shapes of particles in the micrographs [fig. 2 right].

The distribution of %S-probability of all measured clay mineral phases [fig. 3a] also indicates the occurrence of two groups: (i) as main group a mixture of beidellite-montmorillonite interstratifications and diVS-ml (%S-max of this mixture for %S at 50-70%) and (ii) illite with K- and charge deficit (%S-classes = 0% & 10%).

The numerous measured particles by TEM-EDX allow a visualization of distribution of interlayer charges. Considering the TEM-EDX-determined cations Ca^{++}, Mg^{++} and Na^{+} and then computed their ratio as interlayer cations in the mineral formula, Ca^{++}, Mg^{++} and Na^{+} offer to characterize the degree of exchangeable charges in the interlayer space. This charge density of treated B25 bentonite (< 2 µm) shows only a sharp and narrow interval at the maximal frequency-% of charge density at 0.39 per $(OH)_2$ O_{10} [fig. 5]. This narrow interval of interlayer charge density caused by exchangeable cations from 0.18 – 0.21 per $(OH)_2$ O_{10} represents mainly the BM-phases. Also, the measured diVS-ml phases offer only a reduced number of exchangeable cations at 0.14 – 0.33 per $(OH)_2$ O_{10}.

Mineral Matter - Specification

Result of Clustering

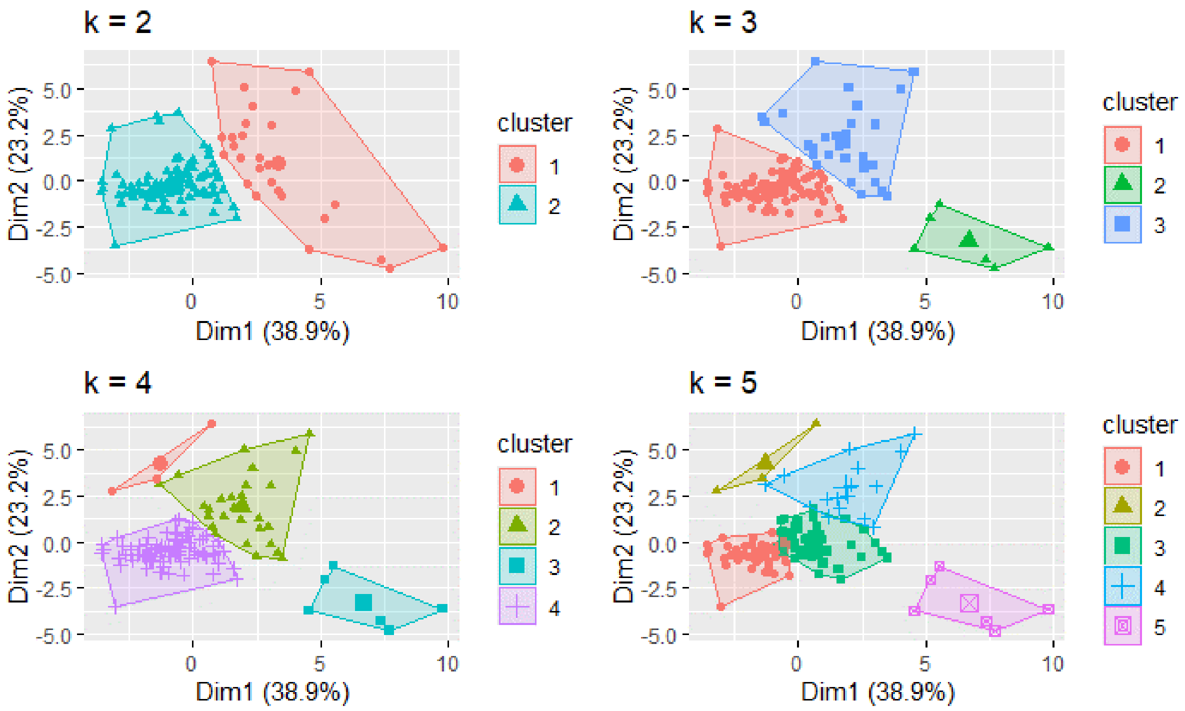

Fig. 8. *Clustering of all measured particles for clusters k = 2, k = 3, k = 4 and k = 5 (source for R-coding: https://uc-r.github.io/kmeans_clustering)*

The optimum of clusters was calculated with k = 2.

		Ca (XII)	Mg (XII)	Na (XII)	K (XII)	Cr3+ (VI)	Al (VI)	Fe3+ (VI)	Mg (VI)	Ti (VI)	Al (IV)	Si (IV)	XII	n_VI	%S
Cluster1	n = 27	0,08	0,12	0,01	0,26	0,00	1,22	0,62	0,14	0,02	0,55	3,45	0,68	2,0	23
Cluster2	n = 102	0,10	0,07	0,01	0,12	0,00	1,23	0,59	0,17	0,01	0,33	3,67	0,49	2,0	50

Fig. 9. *Mineral formulae based on TEM-EDX-data summarized following the result of clustering for k=2*

	Sybilla-results	**TEM-EDX-results**	**Notes**
Cluster2	IS R0(1) *(%S = 100%)*	BM-ml *(BM 70:30?)*	*XRD: Montmorillonite and beidellite is only to distinguish by Green-Kelly-test (not available here).*
Cluster1	IS R0(2) *(%S = 23%)*	diVS-ml *(%S = 23%)*	*high K-deficit, Fe(VI)-rich*

Tab. 2. *Comparison of results from TEM-EDX- and XRD-measurements with clustering procedure*

The clustering of TEM-EDX-data offers a good agreement with the recent result of Sybilla-processing of XRD-traces from oriented specimen [tab. 2].

IS R0 (1): The X-ray diffraction pattern of the ethylene-glycol saturated oriented specimen shows a full expandability to 1.71 nm and a difference of 5.40°2θ between 2. and 3. order of smectite interferences. This distance is typically for montmorillonite (Moore & Reynolds, 1989). This result of XRD-processing let expect a maximum of particles for %S ~ 100% by TEM-EDX-measurements, but the maximum of particles measured by TEM-EDX is to find at %S=50-60% [fig. 3a].

Montmorillonite and beidellite have the same behavior concerning the expandability and they are only to distinguish by XRD using Li like by Greene-Kelly test (Green-Kelly 1952, 1953). So, combination of XRD- and TEM-results (full expandability by XRD and Si ~ 3.67 by TEM-EDX) led conclude the occurrence of 'beidellite-montmorillonite interstratifications', a beidellite-montmorillonite interstratification with about 70% beidellite and 30% montmorillonite layers (BM-ml 70:30).

IS R0 (2): The Sybilla-procedure of XRD-traces (oriented mounts) has shown an occurrence of a second illite-smectite mixed layer phase with a smectite layers probability of %S = 23%. This situation is to find in Cluster1 ($\%S_{TEM}$ = 23%) representing a high K-. but low charge deficient and very Fe-rich dioctahedral vermiculite-smectite mixed layer phase (diV-ml) [tab. 2].

The Sybilla-processing of XRD-traces (oriented mounts) also supports the existence of kaolinite and kaolinite-smectite mixed layer phases in fine fraction of sample. Such phases were not to identify or to calculate in TEM-EDX-database (a grain size effect?).

Specifics to the identified clay mineral groups

Beidellite-montmorillonite interstratifications (B:M ~70:30?)

102 of 129 measured particles belong so to this assumed classification. The dioctahedral character of this group is proofed by X-ray diffraction. The position of the large (060)-interference of smectite is in the random oriented powder specimen at 1.497 Å.

Montmorillonite and beidellite have the same behavior concerning the expandability and they are only to distinguish by XRD using Li by means of Greene-Kelly test (Green-Kelly 1952, 1953). So, combination of XRD- and TEM-results (full expandability by XRD and Si ~ 3.67 by TEM-EDX) led conclude the occurrence of 'beidellite-montmorillonite interstratifications', a beidellite-montmorillonite interstratification with about 70% beidellite and 30% montmorillonite layers (BM-ml 70:30).

Beidellite-montmorillonite interstratifications (B:M ~70:30):

$$Ca_{0.12}\ Mg_{0.08}\ Na_{0.00}\ K_{0.07}\quad Al_{1.24}\ Fe^{3+}_{0.57}\ Mg_{0.18}\ Ti_{0.01}\ (OH)_2\ \ Si_{3.67}\ Al_{0.33}\ O_{10}$$

Charge:	XII = 0.49	VI = 5.84	IV = 15.67	**Σ = 22.00**

Measured particles by TEM-EDX: 102
Result of clustering: Cluster2 [tab. 2]

Beidellitic structures are characterized by a low octahedral Mg-amount (because of high ratio of octahedral, 3-valent cations). A comparison of octahedral Mg vs. tetrahedral Si indicates the occurrence of two groups for octahedral Mg based on TEM-EDX-data, separated by tetrahedral Si [fig. 3b]. The core of BM-ml shows an octahedral Mg-amount between 0.1 – 0.23 e phuc, probably pronounced by a higher Mg^{VI} in montmorillonite compound in this type interstratification.

Using the results of clustering (see Cluster2 in tab. 2), the maximum of frequency-% is to find for particles in the Si(IV)-class 3.6 – 3.7 e phuc [tab. 6a], representing the mentioned relation 30% montmorillonite and 70% beidellite as ratio of interstratification. The mineral formulae, summarized in classes of tetrahedral Si, draw for the maximum an Fe-rich BM 70:30 phase with K and remarkable amount of Mg in the interlayer space [tab. 6b].

A further hypothesis is to verify: The increasing K by lower tetrahedral Si [tab. 6b] could be an indication that it’s not a change of 50:50 ratio of BM-ml, but an alteration of montmorillonite into diVS-ml phases resulting an interstratification by beidellite – montmorillonite – dioctahedral vermiculite.

Dioctahedral vermiculite-smectite mixed layer phase (diVS-ml):

$$Ca_{0.08}\ Mg_{0.12}\ Na_{0.01}\ K_{0.26}\quad Al_{1.22}\ Fe^{3+}_{0.62}\ Mg_{0.14}\ Ti_{0.02}\ (OH)_2\quad Si_{3.45}\ Al_{0.55}\ O_{10}$$

Charge: XII = 0.68 VI = 5.87 IV = 15.55 **Σ = 22.00**
Probability of smectite layers (%S): 23%
Probability of illite layers (%I): 77%

Measured particles by TEM-EDX: 27
Result of clustering: Cluster1 [tab. 2]

Illite as part of diVS-ml series

The Rietveld refinement by Profex software (Döbelin & Kleeberg, 2015) indicates the occurrence of two polytypes for illite in treated B25 bentonite: $2M_1$- and 1M-polytype.

Kaolinite-montmorillonite mixed layer phases

The Excel-based procedure (Hoang-Minh et al., 2019) to identify possible clay mineral groups using the TEM-EDX-measurements also includes algorithms to classify kaolinite and kaolinite-montmorillonite mixed layer phases. These algorithms couldn’t identify such phases basing on the measured TEM-EDX-data. Otherwise, very few particles, which were not to compute, have shown small hexagonal plates typically for kaolinite-bearing phases.

References

Cliff, G. & Lorimer, G. W. (1975). *J. Microsc.* **103**, 203–207.

Döbelin, N., Kleeberg, R. (2015). *Journal of Applied Crystallography* **48**, 1573-1580. DOI: 10.1107/S1600576715014685

Henning, K.-H. & Störr, M. (1986). Electron Micrographs (TEM, SEM) of Clays and Clay Minerals, p. 325. Akademie-Verlag Berlin.

Hoang-Minh, T., Kasbohm, J., Nguyen-Thanh, L., Nga, P. T., Lai, L. T., Duong, N. T., Thanh, N. D., Thuyet, N. T. M., Anh, D. D., Pusch, R., Knutsson, S. & Ferreiro Mahlmann, R. (2019). *J. Appl. Cryst.* **52**, 133-147. DOI: 10.1107/S1600576718018162

Lorimer, G. W. & Cliff, G. (1976). *Electron Microscopy in Mineralogy*, edited by H. R. Wenk, pp. 506–519. Berlin: Springer Verlag.

Matschiavelli, N., Kluge, S., Podlech, C., Standhaft, D., Grathoff, G., Ikeda-Ohno, A., Warr, L.N., Chukharkina, A., Arnold, T. & Cherkouk, A. (2019). *Environmental Science & Technology.* **53** (17), 10514-10524, DOI: 10.1021/acs.est.9b02670

Mellini, M. & Menichini, R. (1985). *R. Soc. Ital. Miner. Petrol.* **40**, 261–266.

Moore, D.M., Reynolds, R.C. (1989). X-ray Diffraction and the Identification and Analysis of Clay Minerals, Oxford University Press, New York, 332 + xvi pp.

Nguyen-Thanh, L., Herbert, H.-J., Kasbohm, J., Hoang-Minh, T. & Mählmann, R. F. (2014). *Clays Clay Miner.* **62**, 425–446.

Środoń, J., Elsass, F., McHardy, W. J. & Morgan, D. J. (1992). *Clay Miner.* **27**, 137–158.

Data Sheet – B25 bentonite, treated materials *(OPA, 100 °C, 35d)* - BOTTOM

Methodology - Transmission electron microscopy linked with energy-dispersive X-ray spectroscopy (TEM-EDX)

It is expected a characterization of clay mineral phases in treated B25 bentonite by transmission electron microscopy. The sample series No2 represents a percolation of B25 bentonite by Opalinus Clay solution at 100°C for 35 days. The sample No2_B is the label for the material at the bottom of sample cylinder.

The different clay mineral phases are to identify and to describe by chemical composition and its variability, morphology, the specific dissolution potential, and further parameter.

Such further parameter like distribution of smectite layers probability (%S) and distribution of charges caused by exchangeable cations interlayer space should serve as additional indicators for mineralogical alterations in treatment experiments with B25 bentonite.

The sample were suspended for TEM-measurement in deionized water and dispersed by ultrasonic treatment for approximately 20 min. The clay fraction (<2 µm) was separated by sedimentation and diluted with deionized water to get a clear suspension. The suspension was dropped onto carbon-coated Cu grids, air dried and stored under environment-controlled conditions at 45% humidity.

TEM-EDX investigations were carried out on the <2 µm fraction using a FEI TECNAI G^2 20 electron transmission microscope at the VNU University of Science, Vietnam National University, Hanoi. This equipment (operated at 200 kV with LaB_6 cathode) was combined with an S-TWIN objective, a windowless EDAX energy-dispersive X-ray system and a FEI Eagle 2k CCD TEM camera.

About 100 individual clay particles per sample were characterized by TEM-EDX with respect to crystal size, crystal habit, and particle morphology and element distribution. The crystal size, crystal habit and particle morphology were described according to Henning & Störr (1986).

For the quantification of element distribution, a calibration of k factors is mandatory (Cliff & Lorimer, 1975; Lorimer & Cliff, 1976; Mellini & Menichini, 1985). These k values are used to calibrate for the specific behavior of particles against possible irradiation damage. The elements O, Na, Mg, Al, Si, K, Ca and Fe were quantified by applying the EDAX GENESIS–TEM Quant Materials quantification procedure.

In this procedure, the acquired EDX spectra are corrected by background subtraction, Gaussian deconvolution and k-factor corrections using values previously determined on a phyllosilicate standard (muscovite) and selected non-phyllosilicate standards. The average errors in the analyzed elements using the phyllosilicate standard, expressed as the atomic proportions, are 10 (Na), 5 (Fe, Mg, K, Ti, Ca) and 1 (Si, Al).

The measurement time per particle was lowered to 20 s and the exposed area was limited to a 50 nm diameter, avoiding possible irradiation damage of particles. The stability of particles of the sample series was tested for this measurement time at the beginning of any measurement campaign.

Further methodological details related to TEM-EDX-measurements and the Excel-based mathematical procedure using TEM-EDX data for calculation of mineral formulae are described in Hoang-Minh et al. (2019).

These mathematical procedures described in Hoang-Minh et al. (2019) were extended by k-means clustering method for finding subgroups of observations within a data set. The data were standardized (i.e., scaled) to make variables comparable. Euclidean distances were applied as classical method for distance measures. The optimal clusters were determined by Elbow method and Gap statistics[12].

---

[12] *https://uc-r.github.io/kmeans_clustering*

Data Sheet – B25 No2_B (< 2 µm), treated material *(OPA, 100°C, 35 days)*

Preparation for TEM

- raw material: compacted material (1.6 g/cm³) of treated B25-sample (OPA, 100°C, 35 days)
- suspension on particles < 2 µm on carbon-filmed Cu-grid
- air-dried and humidity-controlled storing

Mineral Matter

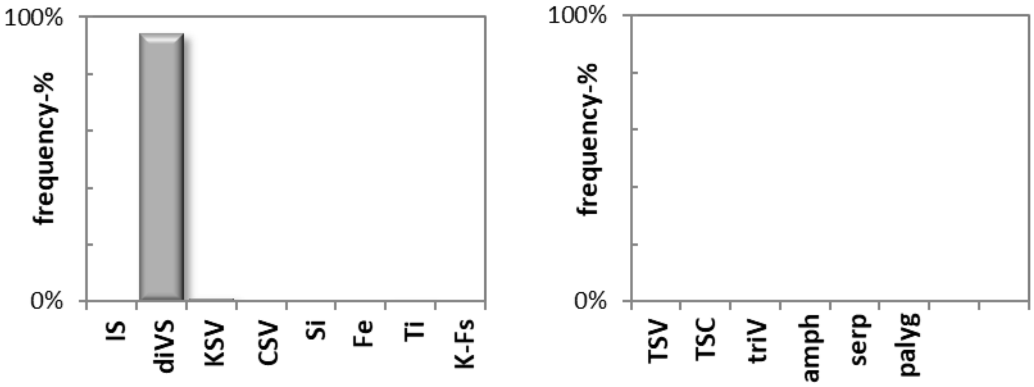

Fig. 1. *Distribution of mineral groups in fraction < 2 µm (in frequency-%)*
Legend: ***IS*** *– illite-smectite-mixed layer series in sense of Środon et al. (1992), diVS – dioctahedral vermiculite-smectite illite-smectite-mixed layer series (= charge- and/or K-deficit),* ***KSV*** *– kaolinite-smectite-dioctahedral vermiculite-mixed layer series,* ***CSV*** *– chlorite-saponite-trioctahedral vermiculite-mixed layer series,* ***Si*** *– quartz or particles with Si-surplus,* ***Fe*** *– Fe-oxide or Fe-oxyhydroxide,* ***Ti*** *– Ti-bearing phases (e.g. rutile, anatase),* ***K-Fs*** *– K-feldspar*

Clay Mineral Composition

All particles of smectite group:

$$\mathrm{Ca_{0.14}\,Mg_{0.06}\,Na_{0.01}\,K_{0.11}\quad Al_{1.24}\,Fe^{3+}_{0.57}\,Mg_{0.18}\,Ti_{0.01}\,(OH)_2\quad Si_{3.64}\,Al_{0.36}\,O_{10}}$$

Charge: XII = 0.52 VI = 5.84 IV = 15.64 **Σ = 22.00**

Probability of smectite layers (%S): 46%

Probability of illite layers (%I): 54%

Specific Dissolution Potential (ΔS%)

for H2O, 20 + 60 rpm	- 8	(= medium reacting, interlayer group: Ca+Mg (= type B))
for NaCl, 20 rpm	- 9	(= medium reacting, interlayer group: Ca+Mg (= type B))
for NaCl, 60 rpm	-100	(= fast reacting, 'illitization', interlayer group: Na (= type A))
$\mathrm{CEC_{calc}}$:	58 meq / 100 g	(literature: 56 meq / 100 g [Matschiavelli et al., 2019: MAT19])

Measured particles: 123

Table 1. *Summarized chemical composition*

SiO_2	TiO_2	Al_2O_3	Fe_2O_3	MnO	MgO	CaO	Na_2O	K_2O	P_2O_5	Σ	
58.7%	0.1%	22.6%	6.2%		3.0%	1.5%	0.1%	1.0%		0.93	measured particles
58.6%	0.0%	22.0%	5.9%		3.0%	1.0%	0.1%	1.1%	0.1%	0.92	measured particles of original B25

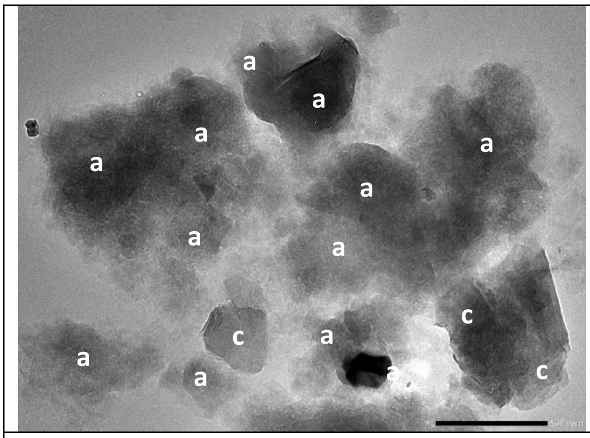	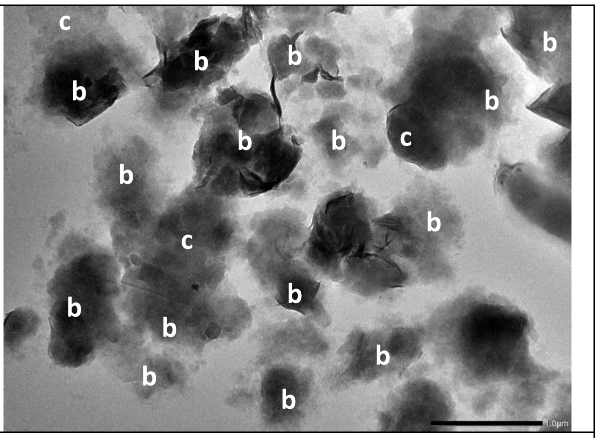
JEM-2100_No2_B_A2_X20k.bmp	*JEM-2100_No2-B_A5_X10k.bmp*
Magnification: 20k (v) aggregates formed by small (≤ 200 nm) xenomorphous plates *(BM-ml?)*; (d) large (≤ 1 µm) xenomorph film-like platy crystals (diVS-ml?)	Magnification: 10k (d) xenomorph film-like platy crystals partially with folds *(diVS-ml?)*; (e) xenomorph film-like platy crystals *(diVS-ml?)*

Fig. 2. *Morphology of particles (TEM-micrographs)*

Distribution of smectite layers probability (%S)

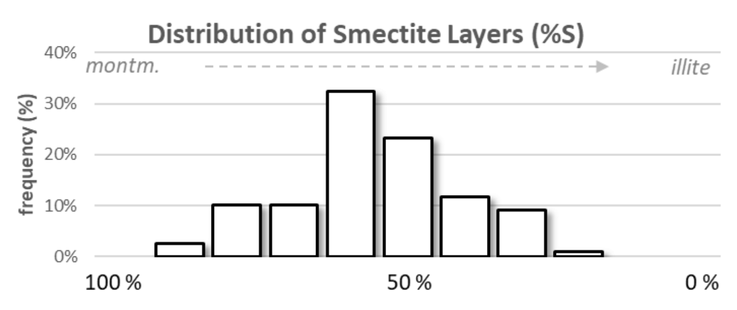

Description: *The distribution of %S-probability indicates the occurrence of mixture of beidellite-montmorillonite interstratifications with diVS-ml.*

Fig. 3a. *Distribution of smectite layers probability (%S)*

Differentiation by relation “Octahedral Mg vs. tetrahedral Si”?

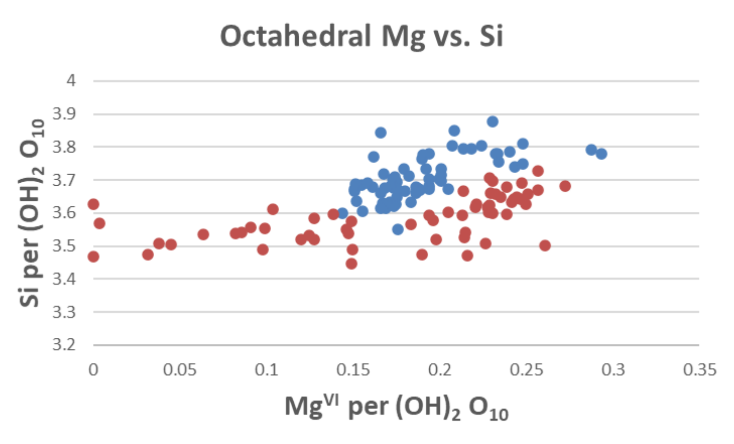

Description: *This diagram indicates the occurrence of two groups of Mg in relation to tetrahedral Si. Probably, this distribution mirrors (I) beidellite-montmorillonite interstratifications (blue) and (II) diVS-ml (red)*

Fig. 3b. *Distribution of octahedral Mg vs. tetrahedral Si [all per(OH)$_2$ O$_{10}$]*

Distribution of K in relation to tetrahedral Si

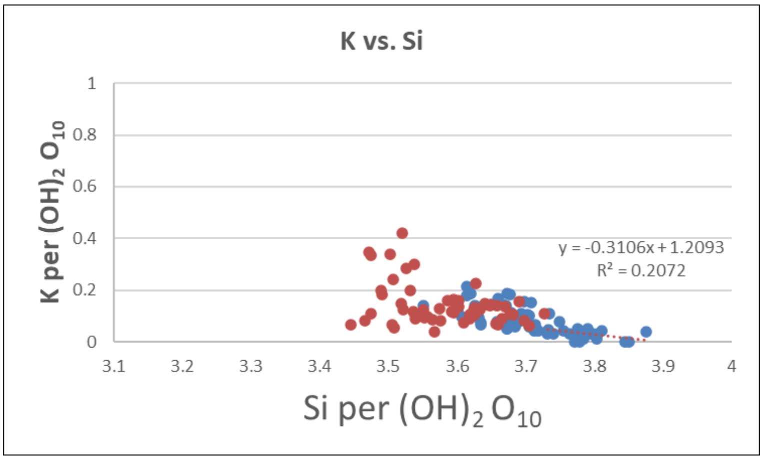

Description: *This diagram visualizes possible particles of beidellite-montmorillonite interstratification (blue dots) and diVS-ml phases (red dots)*

Fig. 4. *Distribution of K in interlayer space vs. tetrahedral Si [all per(OH)$_2$ O$_{10}$]*

Distribution of charges (exchangeable from interlayer space)

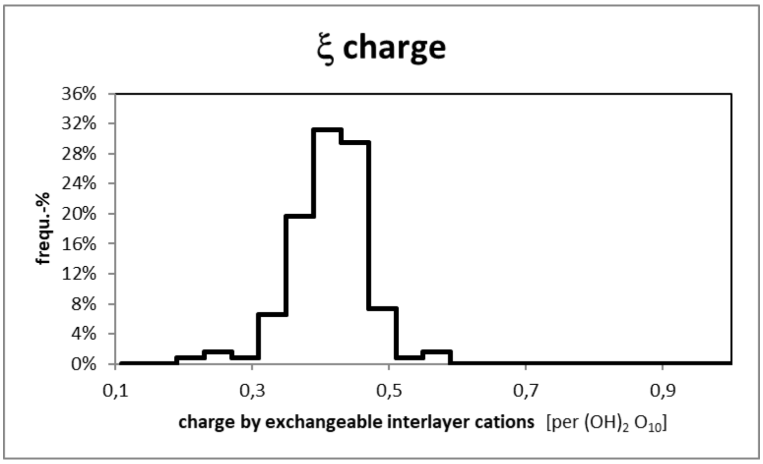

This diagram visualizes the distribution of exchangeable charges in the interlayer space (Ca, Mg, Na) determined and computed by TEM-EDX-data.

Description: *Broad maximal frequency-% of charge density at 0.39 - 0.47 per (OH)$_2$ O$_{10}$.*

Fig. 5. *Distribution of charges*

Beidellite-Montmorillonite interstratification (BM ~ 70%:30%) *(Cluster1):*

$Ca_{0.12}\ Mg_{0.08}\ Na_{0.00}\ K_{0.11}\quad Al_{1.21}\ Fe^{3+}_{0.61}\ Mg_{0.17}\ Ti_{0.01}\ (OH)_2\ \ Si_{3.66}\ Al_{0.34}\ O_{10}$

Charge: XII = 0.50 VI = 5.84 IV = 15.66 **Σ = 22.00**
Measured particles: 41

Beidellite-Montmorillonite interstratification (BM ~ 70%:30%) *(Cluster6):*

$Ca_{0.19}\ Mg_{0.03}\ Na_{0.02}\ K_{0.12}\quad Al_{1.16}\ Fe^{3+}_{0.60}\ Mg_{0.23}\ Ti_{0.01}\ (OH)_2\ \ Si_{3.64}\ Al_{0.36}\ O_{10}$

Charge: XII = 0.58 VI = 5.78 IV = 15.64 **Σ = 22.00**
Measured particles: 27

Beidellite-Montmorillonite interstratification (BM ~ 50%:50%) *(Cluster2):*

$Ca_{0.15}\ Mg_{0.05}\ Na_{0.00}\ K_{0.03}\quad Al_{1.26}\ Fe^{3+}_{0.52}\ Mg_{0.22}\ Ti_{0.00}\ (OH)_2\ \ Si_{3.78}\ Al_{0.22}\ O_{10}$

Charge: XII = 0.43 VI = 5.79 IV = 15.78 **Σ = 22.00**
Measured particles: 23

Distribution of BM-interstratifications (Cluster 1 + 2 + 6)

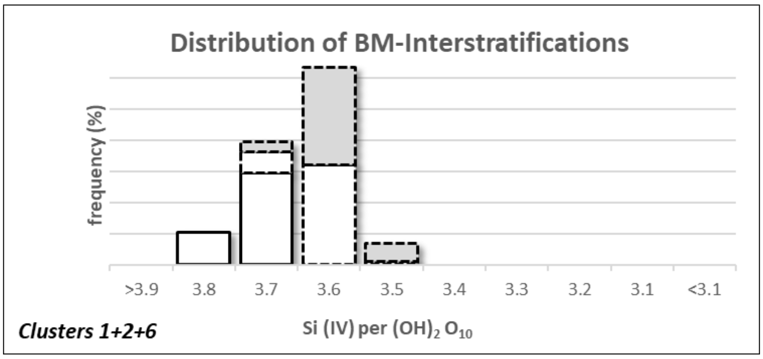

***Description:** The distribution of BM-interstratifications (classified as cluster1+2+6) draws a maximum of frequency (%) at tetrahedral Si-value between 3.6 – 3.7 e phuc*

***Fig. 6a.** Distribution of assumed beidellite-montmorillonite interstratifications*
Legend: solid – BM 50:50; dashed – BM 70:30

Cluster 2

BM 50:50?	particles (abs)	Ca (XII)	Mg (XII)	Na (XII)	K (XII)	Cr3+ (VI)	Al (VI)	Fe3+ (VI)	Mg (VI)	Ti (VI)	Al (IV)	Si (IV)	XII	n_VI	%S
Si >3.9	n = 0														
Si 3.9-3.8	n = 6	0,13	0,05	0,00	0,02	0,00	1,29	0,49	0,21	0,00	0,17	3,83	0,4	2,0	76
Si 3.8-3.7	**n = 17**	**0,15**	**0,05**	**0,01**	**0,04**	**0,00**	**1,24**	**0,53**	**0,22**	**0,00**	**0,23**	**3,77**	**0,4**	**2,0**	**65**
Si 3.7-3.6	n = 0														
Si 3.6-3.5	n = 0														
Si 3.5-3.4	n = 0														
Si 3.4-3.3	n = 0														
Si 3.3-3.2	n = 0														
Si 3.2-3.1	n = 0														
Si <3.1	n = 0														

Cluster 1

BM 70:30?	particles (abs)	Ca (XII)	Mg (XII)	Na (XII)	K (XII)	Cr3+ (VI)	Al (VI)	Fe3+ (VI)	Mg (VI)	Ti (VI)	Al (IV)	Si (IV)	XII	n_VI	%S
Si >3.9	n = 0														
Si 3.9-3.8	n = 0														
Si 3.8-3.7	n = 7	0,12	0,07	0,00	0,08	0,00	1,19	0,62	0,18	0,00	0,29	3,71	0,5	2,0	56
Si 3.7-3.6	**n = 33**	**0,12**	**0,08**	**0,00**	**0,11**	**0,00**	**1,22**	**0,60**	**0,17**	**0,01**	**0,34**	**3,66**	**0,5**	**2,0**	**48**
Si 3.6-3.5	n = 1	0,11	0,13	0,00	0,14	0,00	1,04	0,79	0,18	0,00	0,45	3,55	0,6	2,0	34
Si 3.5-3.4	n = 0														
Si 3.4-3.3	n = 0														
Si 3.3-3.2	n = 0														
Si 3.2-3.1	n = 0														
Si <3.1	n = 0														

Cluster 6

BM 70:30?	particles (abs)	Ca (XII)	Mg (XII)	Na (XII)	K (XII)	Cr3+ (VI)	Al (VI)	Fe3+ (VI)	Mg (VI)	Ti (VI)	Al (IV)	Si (IV)	XII	n_VI	%S
Si >3.9	n = 0														
Si 3.9-3.8	n = 0														
Si 3.8-3.7	n = 2	0.19	0.02	0.02	0.09	0.00	1.20	0.56	0.24	0.00	0.28	3.72	0.5	2.0	57
Si 3.7-3.6	**n = 21**	**0.19**	**0.03**	**0.02**	**0.12**	**0.00**	**1.16**	**0.60**	**0.24**	**0.01**	**0.35**	**3.65**	**0.6**	**2.0**	**47**
Si 3.6-3.5	n = 4	0.18	0.05	0.01	0.14	0.00	1.13	0.65	0.21	0.01	0.41	3.59	0.6	2.0	39
Si 3.5-3.4	n = 0														
Si 3.4-3.3	n = 0														
Si 3.3-3.2	n = 0														
Si 3.2-3.1	n = 0														
Si <3.1	n = 0														

***Fig. 6b.** Computed averaged mineral formulae of phases in the different Si(IV)-classes*

Dioctahedral Vermiculite-Smectite mixed layer phases (K-rich diVS-ml) *(Cluster 3):*

$$Ca_{0.18}\ Mg_{0.02}\ Na_{0.01}\ K_{0.27}\quad Al_{1.23}\ Fe^{3+}_{0.53}\ Mg_{0.21}\ Ti_{0.03}\ (OH)_2\ \ Si_{3.51}\ Al_{0.49}\ O_{10}$$

Charge:	XII = 0.68	VI = 5.81	IV = 15.51	**Σ = 22.00**
Probability of smectite layers (%S):	29%			
Probability of illite layers (%I):	71%			
Measured particles:	8			

Distribution of smectite layers probability (%S) in diVS-ml (Clusters 3+4+5)

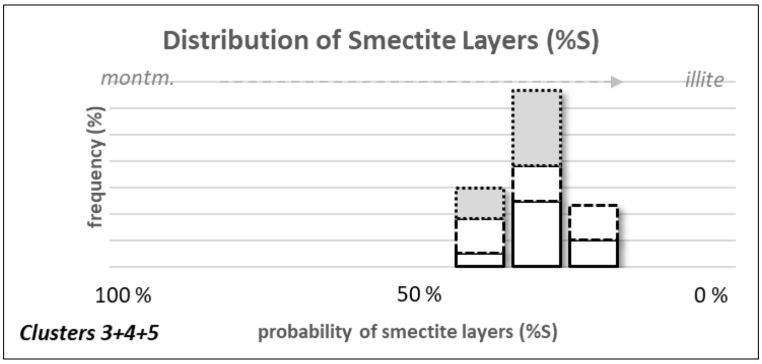

Description: *The distribution of diVS-ml (classified as clusters 3+4+ 5) draws a maximum of frequency (%) for smectite layer probability at 25 - 35%.*

Fig. 7a. *Distribution of smectite layers probability in diVS-ml*
Legend: solid – K-rich diVS-ml; dashed & dotted – low K diVS-ml (Clusters 4+5)

Cluster 3

K-rich diVS-ml	*particles (abs)*	Ca (XII)	Mg (XII)	Na (XII)	K (XII)	Cr3+ (VI)	Al (VI)	Fe3+ (VI)	Mg (VI)	Ti (VI)	Al (IV)	Si (IV)	XII	n_VI	%S
%S >95%	n = 0														
%S 95-85%	n = 0														
%S 85-75%	n = 0														
%S 75-65%	n = 0														
%S 65-55%	n = 0														
%S 55-45%	n = 0														
%S 45-35%	n = 1	0,20	0,03	0,00	0,12	0,00	1,15	0,58	0,21	0,05	0,41	3,59	0,6	2,0	39
%S 35-25%	**n = 5**	**0,16**	**0,02**	**0,01**	**0,32**	**0,00**	**1,24**	**0,53**	**0,22**	**0,02**	**0,49**	**3,51**	**0,7**	**2,0**	**29**
%S 25-15%	n = 2	0,22	0,02	0,00	0,21	0,00	1,25	0,50	0,18	0,06	0,54	3,46	0,7	2,0	24
%S <15%	n = 0														

Cluster 4

diVS-ml?	*particles (abs)*	Ca (XII)	Mg (XII)	Na (XII)	K (XII)	Cr3+ (VI)	Al (VI)	Fe3+ (VI)	Mg (VI)	Ti (VI)	Al (IV)	Si (IV)	XII	n_VI	%S
%S >95%	n = 0														
%S 95-85%	n = 0														
%S 85-75%	n = 0														
%S 75-65%	n = 0														
%S 65-55%	n = 0														
%S 55-45%	n = 0														
%S 45-35%	n = 1	0.11	0.00	0.00	0.08	0.00	1.37	0.51	0.20	0.02	0.42	3.58	0.3	2.1	37
%S 35-25%	n = 1	0.15	0.00	0.00	0.09	0.00	1.39	0.50	0.21	0.00	0.46	3.54	0.4	2.1	33
%S 25-15%	n = 1	0.12	0.00	0.00	0.08	0.00	1.32	0.72	0.00	0.02	0.53	3.47	0.3	2.1	24
%S <15%	n = 0														

Cluster 5

diVS-ml?	*particles (abs)*	Ca (XII)	Mg (XII)	Na (XII)	K (XII)	Cr3+ (VI)	Al (VI)	Fe3+ (VI)	Mg (VI)	Ti (VI)	Al (IV)	Si (IV)	XII	n_VI	%S
%S >95%	n = 0														
%S 95-85%	n = 0														
%S 85-75%	n = 0														
%S 75-65%	n = 0														
%S 65-55%	n = 0														
%S 55-45%	n = 0														
%S 45-35%	n = 6	0.10	0.08	0.01	0.12	0.00	1.40	0.51	0.09	0.00	0.41	3.59	0.5	2.0	39
%S 35-25%	**n = 15**	**0.11**	**0.10**	**0.00**	**0.13**	**0.00**	**1.35**	**0.54**	**0.10**	**0.01**	**0.48**	**3.52**	**0.6**	**2.0**	**31**
%S 25-15%	n = 0														
%S <15%	n = 0														

Fig. 7b. *Computed averaged mineral formulae of diVS-ml phases in the different smectite layers probability (%S)-classes*

Description – B25 No2_B (< 2 µm), treated material *(OPA, 100°C, 35 days)*

Preparation for TEM

The powder of compacted and treated B25-No2_B-sample was suspended in deionized water and dispersed by ultrasonic treatment for approximately 20 min. The clay fraction (<2 µm) was separated by sedimentation and diluted with deionized water to get a clear suspension. The suspension was dropped onto carbon-coated Cu grids, air dried and stored under environment-controlled conditions at 45% humidity.

Mineral Matter - Overview

The fraction < 2 µm of treated B25 bentonite sample (Opalinus Clay solution, at 100°C, for 35 days) is mainly composed by assumed two groups of beidellite-montmorillonite interstratifications (B:M ~70:30 and ~50:50), abbreviated as BM-ml, two groups of dioctahedral vermiculite-smectite mixed layer phases (K-rich and low K diVS-ml) and accompanied by two types of beidellite (beidellite and K-beidellite). Furthermore, kaolinite and Ti phases were identified in traces in this sample [fig. 1].

	frequency-% *(n = 127 measured particles)*
BM-ml (Cluster 1+2+6)	72%
diVS-ml (Cluster 3+4+5)	25%
Kaolinite & KSV-ml	2%
Ti phases	1%

All measured dioctahedral clay mineral phases summarized result following mineral formula computed from TEM-EDX-measurement of 118 individual particles:

$$Ca^{2+}_{0.14}\ Mg^{2+}_{0.06}\ Na^{+}_{0.01}\ K^{+}_{0.11}\quad Al^{3+}_{1.24}\ Fe^{3+}_{0.57}\ Mg^{2+}_{0.18}\ Ti^{4+}_{0.01}\ (OH)_2\quad Si^{4+}_{3.64}\ Al^{3+}_{0.36}\ O_{10}$$

SDOM *± 0.00 ± 0.00 ± 0.00 ± 0.01 ± 0.01 ± 0.01 ± 0.01 ± 0.00 ± 0.01 ± 0.01*

Legend: SDOM - standard deviation of the mean (= the standard deviation divided by the square root of the number of samples)

The interlayer charge is calculated as 0.52 per $(OH)_2\ O_{10}$ and the octahedral charge as 5.83 per $(OH)_2\ O_{10}$. The particles are characterized by a high octahedral Fe-amount.

The summarized chemical composition of all 127 computed particles is compared with measured data of original B25-bentonite sample [tab. 1]. The chemical composition averaged by measured particles show especially a slight higher amount of Al_2O_3 and CaO in comparison to the measured data of original untreated B25-bentonite.

B25-No2_B sample is characterized by three morphological groups: (i) aggregates formed by small (≤ 200 nm) xenomorphous plates [fig. 2 left], (ii) xenomorph film-like platy crystals partially with folds [fig. 2 right] and (iii) xenomorph film-like platy crystals [fig. 2 left]. Thin aggregates formed by small (≤ 200 nm) xenomorphous plates dominate the shapes of particles in the micrographs [fig. 2 left].

The distribution of %S-probability of all measured clay mineral phases [fig. 3a] also indicates the occurrence of two groups: (i) as main group a mixture of beidellite-montmorillonite interstratifications

and diVS-ml (%S-max of this mixture for %S at 55-65%) and (ii) illite with K- and charge deficit (%S-classes = 0% & 10%).

The numerous measured particles by TEM-EDX allow a visualization of distribution of interlayer charges. Considering the TEM-EDX-determined cations Ca^{++}, Mg^{++} and Na^{+} and then computed their ratio as interlayer cations in the mineral formula, Ca^{++}, Mg^{++} and Na^{+} offer to characterize the degree of exchangeable charges in the interlayer space. This charge density of treated B25 bentonite (< 2 µm) shows a broad distribution of charge density at 0.39 - 0.47 per $(OH)_2\ O_{10}$ [fig. 5]. This broad interval of interlayer charge density is caused by exchangeable cations from 0.17 – 0.24 per $(OH)_2\ O_{10}$ representing mainly the BM-phases and diVS-ml phases.

Mineral Matter - Specification

Result of Clustering

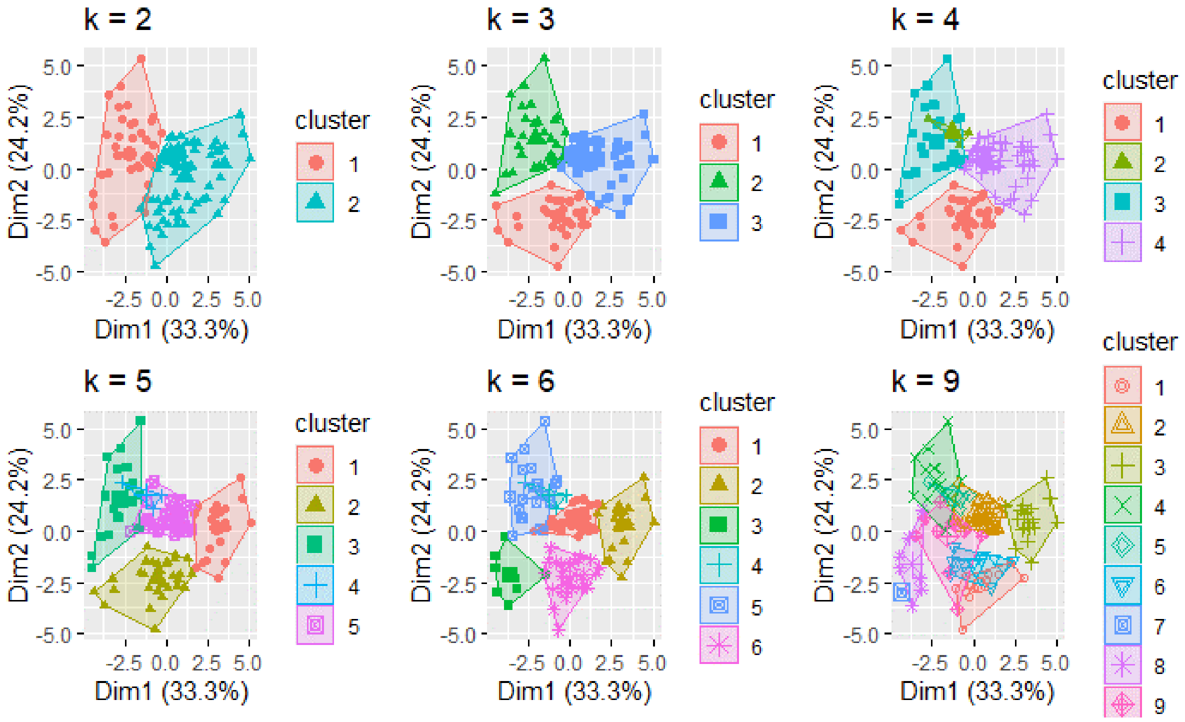

Fig. 8. *Clustering of all measured particles for clusters k = 2, k = 3, k = 4, k = 5, k = 6 and k = 9 (source for R-coding: https://uc-r.github.io/kmeans_clustering)*

The optimum of clusters was calculated with k = 6.

		Ca (XII)	Mg (XII)	Na (XII)	K (XII)	Cr3+ (VI)	Al (VI)	Fe3+ (VI)	Mg (VI)	Ti (VI)	Al (IV)	Si (IV)	XII	n_VI	%S
Cluster1	n = 41	0,12	0,08	0,00	0,11	0,00	1,21	0,61	0,17	0,01	0,34	3,66	0,50	2,0	49
Cluster2	n = 23	0,15	0,05	0,00	0,03	0,00	1,26	0,52	0,22	0,00	0,22	3,78	0,43	2,0	68
Cluster3	n = 8	0,18	0,02	0,01	0,27	0,00	1,23	0,53	0,21	0,03	0,49	3,51	0,68	2,0	29
Cluster4	n = 3	0,13	0,00	0,00	0,09	0,00	1,36	0,58	0,14	0,01	0,47	3,53	0,34	2,1	31
Cluster5	n = 21	0,11	0,10	0,00	0,13	0,00	1,37	0,53	0,09	0,01	0,46	3,54	0,54	2,0	33
Cluster6	n = 27	0,19	0,03	0,02	0,12	0,00	1,16	0,60	0,23	0,01	0,36	3,64	0,58	2,0	46

Fig. 9. *Mineral formulae based on TEM-EDX-data summarized following the result of clustering for k=6*

	Sybilla-results	**TEM-EDX-results**	**Notes**
Cluster 1	IS R0(1) *(%S = 100%)*	BM-ml *(BM 70:30?)*	*XRD: Montmorillonite and beidellite is only to distinguish by Green-Kelly-test (not available here).*
Cluster 2	IS R0(1) *(%S = 100%)*	BM-ml *(BM 50:50?)*	

Cluster 3	IS R0(2) *(%S = 23%)*	diVS-ml *(%S = 29%)*	*K-rich, Fe(VI)-rich*
Cluster 4	IS R0(2) *(%S = 23%)*	diVS-ml *(%S = 31%)*	*Fe(VI)-rich, reduced Mg(VI)*
Cluster 5	IS R0(2) *(%S = 23%)*	diVS-ml *(%S = 33%)*	*Fe(VI)-rich, reduced Mg(VI)*
Cluster 6	IS R0(1) *(%S = 100%)*	BM-ml *(BM 70:30?)*	*see above concerning XRD*

Tab. 2. *Comparison of results from TEM-EDX- and XRD-measurements with clustering procedure*

The clustering of TEM-EDX-data offers similar situation compared with the recent results of Sybilla-processing of XRD-traces from oriented specimen [tab. 2].

Specifics to the identified clay mineral groups

Beidellite-montmorillonite interstratifications (B:M ~70:30? & ~50:50?)

91 of 127 measured particles belong so to this assumed classification. The dioctahedral character of this group is proofed by X-ray diffraction. The position of the large (060)-interference of smectite is in the random oriented powder specimen at 1.497 Å.

Montmorillonite and beidellite have the same behavior concerning the expandability and they are only to distinguish by XRD using Li by means of Greene-Kelly test (Green-Kelly 1952, 1953). So, combination of XRD- and TEM-results (full expandability by XRD and Si ~ ≥ 3.64 and ≤ 3.78 by TEM-EDX) led conclude the occurrence of 'beidellite-montmorillonite interstratifications', a beidellite-montmorillonite interstratification. The differences in the chemistry indicate two groups: (i) with about 70% beidellite and 30% montmorillonite layers (BM-ml 70:30) and (ii) with about 50% beidellite and 50% montmorillonite layers (BM-ml 50:50).

Beidellite-montmorillonite interstratifications (B:M ~70:30?):

$$\mathrm{Ca_{0.12}\ Mg_{0.08}\ Na_{0.00}\ K_{0.11}\quad Al_{1.21}\ Fe^{3+}_{0.61}\ Mg_{0.17}\ Ti_{0.01}\ (OH)_2\quad Si_{3.66}\ Al_{0.34}\ O_{10}}$$

Charge: XII = 0.50 VI = 5.84 IV = 15.66 **Σ = 22.00**
Measured particles by TEM-EDX: 41
Result of clustering: Cluster1 [tab. 2]

$$\mathrm{Ca_{0.19}\ Mg_{0.03}\ Na_{0.02}\ K_{0.12}\quad Al_{1.16}\ Fe^{3+}_{0.60}\ Mg_{0.23}\ Ti_{0.01}\ (OH)_2\quad Si_{3.64}\ Al_{0.36}\ O_{10}}$$

Charge: XII = 0.58 VI = 5.78 IV = 15.64 **Σ = 22.00**
Measured particles by TEM-EDX: 27
Result of clustering: Cluster 6 [tab. 2]

Beidellite-montmorillonite interstratifications (B:M ~50:50?):

$$\mathrm{Ca_{0.15}\ Mg_{0.05}\ Na_{0.00}\ K_{0.03}\quad Al_{1.26}\ Fe^{3+}_{0.52}\ Mg_{0.22}\ Ti_{0.00}\ (OH)_2\quad Si_{3.78}\ Al_{0.22}\ O_{10}}$$

Charge: XII = 0.43 VI = 5.79 IV = 15.78 **Σ = 22.00**
Measured particles by TEM-EDX: 23
Result of clustering: Cluster2 [tab. 2]

Beidellitic structures are characterized by a low octahedral Mg-amount (because of high ratio of octahedral, 3-valent cations). A comparison of octahedral Mg vs. tetrahedral Si indicates the occurrence of two groups for octahedral Mg based on TEM-EDX-data, separated by tetrahedral Si [fig. 3b].

The core of BM-ml (blue dots) shows an octahedral Mg-amount between 0.21 – 0.24 e phuc, probably pronounced by a higher Mg^{VI} in montmorillonite compound in this type of interstratification.

Using the results of clustering (see Clusters 1+2+6 in tab. 2), the maximum of frequency-% is to find for particles in the Si(IV)-class 3.6 – 3.7 e phuc [tab. 6a], representing the mentioned relation 30% montmorillonite and 70% beidellite as ratio of interstratification and in the Si(IV)-class 3.7 – 3.8 e phuc [tab. 6a], representing the other mentioned relation 50% montmorillonite and 50% beidellite as ratio of interstratification. The mineral formulae, summarized in classes of tetrahedral Si, draw for the maximum an Fe-rich BM 70:30 with K and remarkable amount of Mg in the interlayer space and an Fe-rich BM 50:50 with low K and lowered amount of Mg in the interlayer space [tab. 6b].

A further hypothesis is to verify: The increasing K by lower tetrahedral Si [tab. 6b] in BM 70:30 could be an indication that it's not a change of 50:50 ratio of BM-ml into a 70:30 ratio of BM-ml, but an alteration of montmorillonite into diVS-ml phases resulting into an interstratification by beidellite – montmorillonite – dioctahedral vermiculite.

Dioctahedral vermiculite-smectite mixed layer phase (high K diVS-ml):

The Rietveld refinement by Profex software (Döbelin & Kleeberg, 2015) indicates the occurrence of two polytypes for illite in bulk powder of treated B25 bentonite: $2M_1$- and 1M-polytype. The clustering of TEM-data indicates the occurrence of K-rich diVS-ml phases (cluster 3), but illite was not identified by TEM-EDX.

$$Ca_{0.18}\ Mg_{0.02}\ Na_{0.01}\ K_{0.27}\quad Al_{1.23}\ Fe^{3+}_{0.53}\ Mg_{0.21}\ Ti_{0.03}\ (OH)_2\quad Si_{3.51}\ Al_{0.49}\ O_{10}$$

Charge:	XII = 0.68	VI = 5.81	IV = 15.51	**Σ = 22.00**
Probability of smectite layers (%S):	29%			
Probability of illite layers (%I):	71%			

Measured particles by TEM-EDX: 8
Result of clustering: Cluster 3 [tab. 2]

Dioctahedral vermiculite-smectite mixed layer phase (low K diVS-ml):

$$Ca_{0.13}\ Mg_{0.00}\ Na_{0.00}\ K_{0.09}\quad Al_{1.36}\ Fe^{3+}_{0.58}\ Mg_{0.14}\ Ti_{0.01}\ (OH)_2\quad Si_{3.53}\ Al_{0.47}\ O_{10}$$

Charge:	XII = 0.34	VI = 6.13	IV = 15.53	**Σ = 22.00**

Measured particles by TEM-EDX: 3
Result of clustering: Cluster 4 [tab. 2]

$$Ca_{0.13}\ Mg_{0.10}\ Na_{0.00}\ K_{0.13}\quad Al_{1.37}\ Fe^{3+}_{0.53}\ Mg_{0.09}\ Ti_{0.01}\ (OH)_2\quad Si_{3.54}\ Al_{0.46}\ O_{10}$$

Charge:	XII = 0.54	VI = 5.92	IV = 15.54	**Σ = 22.00**

Measured particles by TEM-EDX: 21
Result of clustering: Cluster 5 [tab. 2]

Kaolinite-montmorillonite mixed layer phases

The Excel-based procedure (Hoang-Minh et al., 2019) to identify possible clay mineral groups using the TEM-EDX-measurements also includes algorithms to classify kaolinite and kaolinite-montmorillonite mixed layer phases. These algorithms couldn't identify such phases basing on the measured TEM-EDX-data. Otherwise, very few particles, which were not to compute, have shown small hexagonal plates typically for kaolinite-bearing phases.

References

Cliff, G. & Lorimer, G. W. (1975). *J. Microsc.* **103**, 203–207.

Döbelin, N., Kleeberg, R. (2015). *Journal of Applied Crystallography* **48**, 1573-1580. DOI: 10.1107/S1600576715014685

Henning, K.-H. & Störr, M. (1986). Electron Micrographs (TEM, SEM) of Clays and Clay Minerals, p. 325. Akademie-Verlag Berlin.

Hoang-Minh, T., Kasbohm, J., Nguyen-Thanh, L., Nga, P. T., Lai, L. T., Duong, N. T., Thanh, N. D., Thuyet, N. T. M., Anh, D. D., Pusch, R., Knutsson, S. & Ferreiro Mahlmann, R. (2019). *J. Appl. Cryst.* **52**, 133-147. DOI: 10.1107/S1600576718018162

Lorimer, G. W. & Cliff, G. (1976). *Electron Microscopy in Mineralogy*, edited by H. R. Wenk, pp. 506–519. Berlin: Springer Verlag.

Matschiavelli, N., Kluge, S., Podlech, C., Standhaft, D., Grathoff, G., Ikeda-Ohno, A., Warr, L.N., Chukharkina, A., Arnold, T. & Cherkouk, A. (2019). *Environmental Science & Technology.* **53** (17), 10514-10524, DOI: 10.1021/acs.est.9b02670

Mellini, M. & Menichini, R. (1985). *R. Soc. Ital. Miner. Petrol.* **40**, 261–266.

Moore, D.M., Reynolds, R.C. (1989). X-ray Diffraction and the Identification and Analysis of Clay Minerals, Oxford University Press, New York, 332 + xvi pp.

Nguyen-Thanh, L., Herbert, H.-J., Kasbohm, J., Hoang-Minh, T. & Mählmann, R. F. (2014). *Clays Clay Miner.* **62**, 425–446.

Środoń, J., Elsass, F., McHardy, W. J. & Morgan, D. J. (1992). *Clay Miner.* **27**, 137–158.

Data Sheet – B25 bentonite, treated materials *(OPA, 100 °C, 110h)* - TOP

Methodology - Transmission electron microscopy linked with energy-dispersive X-ray spectroscopy (TEM-EDX)

It is expected a characterization of clay mineral phases in treated B25 bentonite by transmission electron microscopy. The sample series No0 represents a percolation of B25 bentonite by Opalinus Clay solution at 100°C for 110 hours. The sample No0_T is the label for the material at the top sample cylinder.

The different clay mineral phases are to identify and to describe by chemical composition and its variability, morphology, the specific dissolution potential, and further parameter.

Such further parameter like distribution of smectite layers probability (%S) and distribution of charges caused by exchangeable cations interlayer space should serve as additional indicators for mineralogical alterations in treatment experiments with B25 bentonite.

The sample were suspended for TEM-measurement in deionized water and dispersed by ultrasonic treatment for approximately 20 min. The clay fraction (<2 µm) was separated by sedimentation and diluted with deionized water to get a clear suspension. The suspension was dropped onto carbon-coated Cu grids, air dried and stored under environment-controlled conditions at 45% humidity.

TEM-EDX investigations were carried out on the <2 µm fraction using a FEI TECNAI G^2 20 electron transmission microscope at the VNU University of Science, Vietnam National University, Hanoi. This equipment (operated at 200 kV with LaB_6 cathode) was combined with an S-TWIN objective, a windowless EDAX energy-dispersive X-ray system and a FEI Eagle 2k CCD TEM camera.

About 100 individual clay particles per sample were characterized by TEM-EDX with respect to crystal size, crystal habit, particle morphology and element distribution. The crystal size, crystal habit and particle morphology were described according to Henning & Störr (1986).

For the quantification of element distribution, a calibration of k factors is mandatory (Cliff & Lorimer, 1975; Lorimer & Cliff, 1976; Mellini & Menichini, 1985). These k values are used to calibrate for the specific behaviour of particles against possible irradiation damage. The elements O, Na, Mg, Al, Si, K, Ca and Fe were quantified by applying the EDAX GENESIS–TEM Quant Materials quantification procedure.

In this procedure, the acquired EDX spectra are corrected by background subtraction, Gaussian deconvolution and k-factor corrections using values previously determined on a phyllosilicate standard (muscovite) and selected non-phyllosilicate standards. The average errors in the analyzed elements using the phyllosilicate standard, expressed as the atomic proportions, are 10 (Na), 5 (Fe, Mg, K, Ti, Ca) and 1 (Si, Al).

The measurement time per particle was lowered to 20 s and the exposed area was limited to a 50 nm diameter, avoiding possible irradiation damage of particles. The stability of particles of the sample series was tested for this measurement time at the beginning of any measurement campaign.

Further methodological details related to TEM-EDX-measurements and the Excel-based mathematical procedure using TEM-EDX data for calculation of mineral formulae are described in Hoang-Minh et al. (2019).

These mathematical procedures described in Hoang-Minh et al. (2019) were extended by k-means clustering method for finding subgroups of observations within a data set. The data were standardized (i.e., scaled) to make variables comparable. Euclidean distances were applied as classical method for distance measures. The optimal clusters were determined by Elbow method and Gap statistics[13].

---

[13] *https://uc-r.github.io/kmeans_clustering*

Data Sheet – B25 No0_T (< 2 µm), treated material *(OPA, 100°C, 110 hrs)*

Preparation for TEM

- raw material: compacted material (1.6 g/cm³) of treated B25-sample (OPA, 100°C, 110 hrs)
- suspension on particles < 2 µm on carbon-filmed Cu-grid
- air-dried and humidity-controlled storing

Mineral Matter

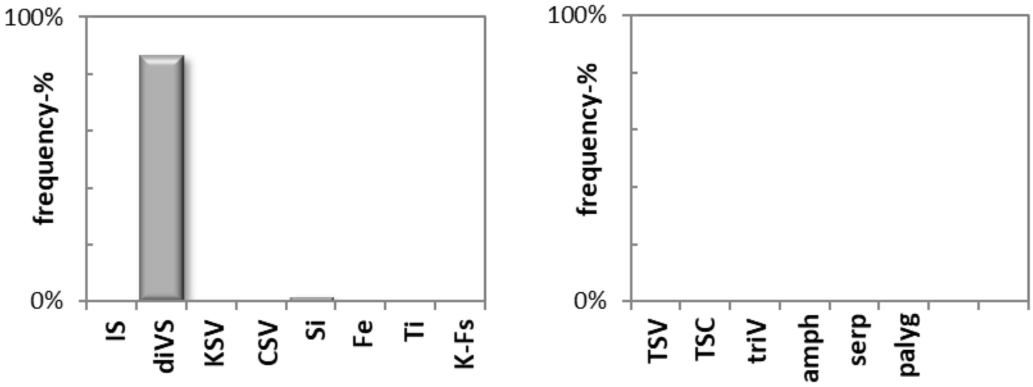

Fig. 1. *Distribution of mineral groups in fraction < 2 µm (in frequency-%)*
*Legend: **IS** – illite-smectite-mixed layer series in sense of Środon et al. (1992), diVS – dioctahedral vermiculite-smectite illite-smectite-mixed layer series (= charge- and/or K-deficit), **KSV** – kaolinite-smectite-dioctahedral vermiculite-mixed layer series, **CSV** – chlorite-saponite-trioctahedral vermiculite-mixed layer series, **Si** – quartz or particles with Si-surplus, **Fe** – Fe-oxide or Fe-oxyhydroxide, **Ti** – Ti-bearing phases (e.g. rutile, anatase), **K-Fs** – K-feldspar*

Clay Mineral Composition

All particles of smectite group:

$$Ca_{0.09}\ Mg_{0.10}\ Na_{0.00}\ K_{0.10}\quad Al_{1.24}\ Fe^{3+}_{0.61}\ Mg_{0.14}\ Ti_{0.01}\ (OH)_2\quad Si_{3.65}\ Al_{0.35}\ O_{10}$$

Charge: XII = 0.48 VI = 5.87 IV = 15.65 **Σ = 22.00**
Probability of smectite layers (%S): 47%
Probability of illite layers (%I): 53%

Specific Dissolution Potential (ΔS%)

for H2O, 20 + 60 rpm -4 (= slow reacting, interlayer group: Ca+Mg (= type B))
for NaCl, 20 rpm -5 (= slow reacting, interlayer group: Ca+Mg (= type B))
for NaCl, 60 rpm -110 (= fast reacting, 'illitization', interlayer group: Na (= type A))
CEC$_{calc}$: 49 meq / 100 g (literature: 56 meq / 100 g [Matschiavelli et al., 2019: MAT19])

Measured particles: 90

Table 1. *Summarized chemical composition*

SiO_2	TiO_2	Al_2O_3	Fe_2O_3	MnO	MgO	CaO	Na_2O	K_2O	P_2O_5	Σ	
61.6%	0.2%	23.5%	6.9%		3.2%	0.9%	0.0%	0.9%	0.0%	0.97	measured particles
58.6%	0.0%	22.0%	5.9%		3.0%	1.0%	0.1%	1.1%	0.1%	0.92	measured particles of original B25

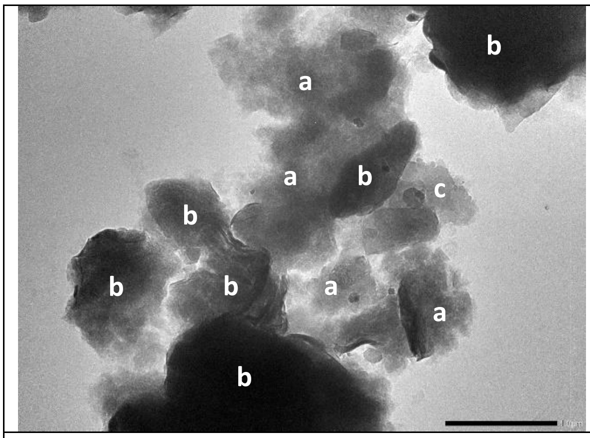

JEM-2100_No0-T_A3_X10k.bmp

Magnification: 10k

- (w) aggregates formed by small (≤ 200 nm) xenomorphous plates *(interstratification by beidellite & montmorillonite)*;
- (x) large (≤ 1 µm) xenomorph film-like platy crystals partially with folds (*diVS-ml*);
- (y) aggregates formed by idiomorph hexagonal plates (≤ 200 nm) (*kaolinite*)

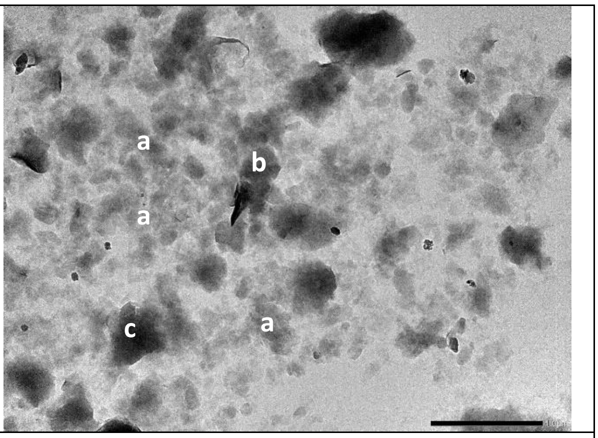

JEM-2100_No0-T_A6_X10k.bmp

Magnification: 10k

- (a) aggregates formed by small (≤ 200 nm) xenomorphous plates *(interstratification by beidellite & montmorillonite)*;
- (b) large (≤ 1 µm) xenomorph film-like platy crystals with folds (*diVS-ml*);
- (c) aggregates formed by idiomorph hexagonal plates (≤ 200 nm) (*kaolinite/montmorillonite interstratification*)

Fig. 2. *Morphology of particles (TEM-micrographs)*

Distribution of smectite layers probability (%S)

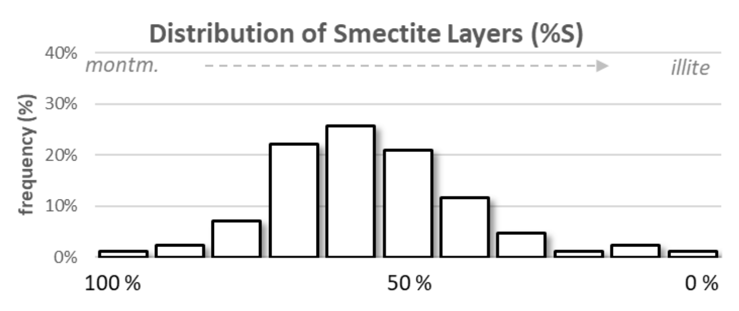

Description: *The distribution of %S-probability indicates the occurrence of three groups: (i) montmorillonite (in traces), (ii) mixture of beidellite-montmorillonite interstratifications (= assumption) with diVS-ml as well as (iii) illite with K-deficiency.*

Fig. 3a. *Distribution of smectite layers probability (%S)*

Differentiation by relation “Octahedral Mg vs. tetrahedral Si”?

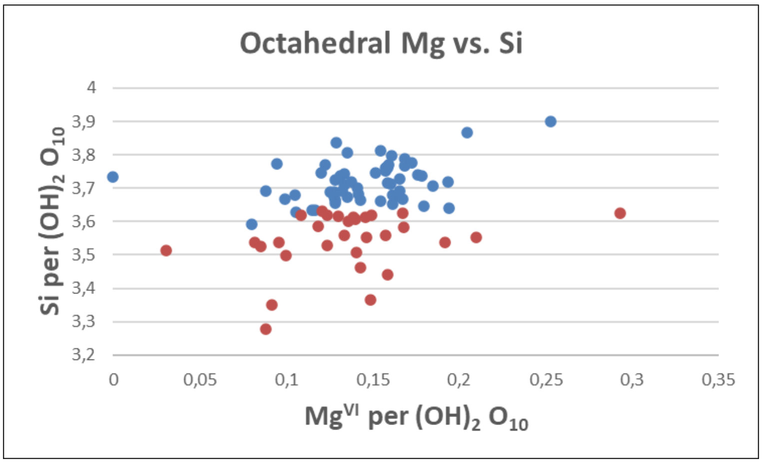

Description: *This diagram indicates the occurrence of two groups of Mg in relation to tetrahedral Si. Probably, this distribution mirrors 2 phases (I) beidellite-montmorillonite interstratifications and (II) diVS-ml*

Fig. 3b. *Distribution of octahedral Mg vs. tetrahedral Si [all per(OH)$_2$ O$_{10}$]*

Distribution of K in relation to tetrahedral Si

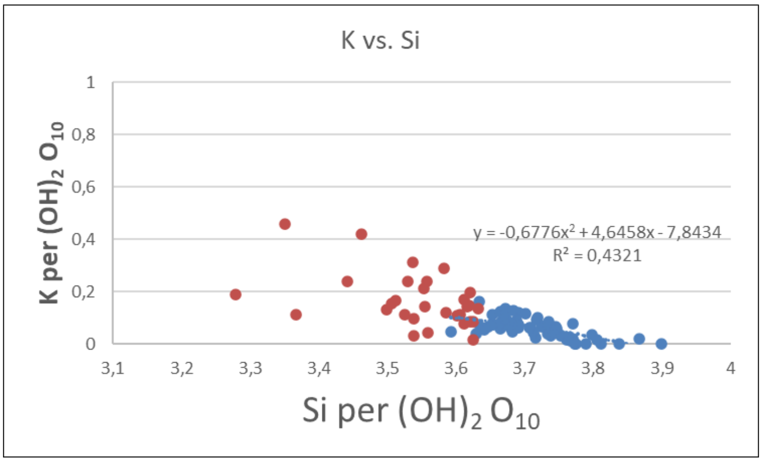

Description: *This diagram visualizes possible particles (beidellite-montmorillonite interstratification?) with a very low K (blue dots)*

Fig. 4. *Distribution of K in interlayer space vs. tetrahedral Si [all per* $(OH)_2\ O_{10}$*]*

Distribution of charges (exchangeable from interlayer space)

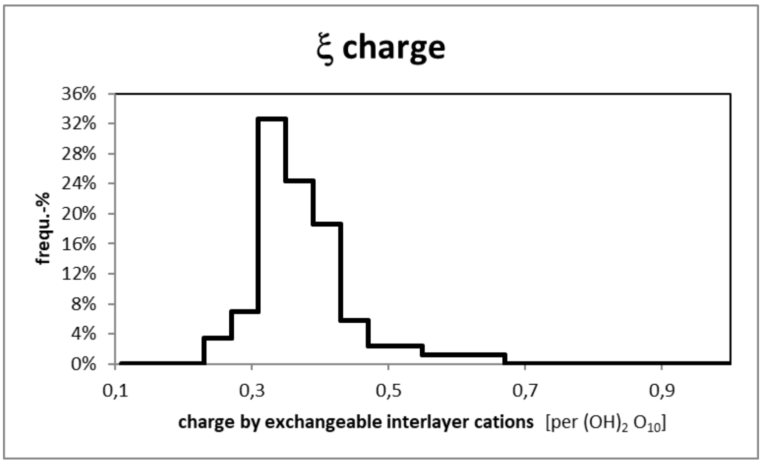

This diagram visualizes the distribution of exchangeable charges in the interlayer space (Ca, Mg, Na) determined and computed by TEM-EDX-data.

Description: *Maximal frequency-% of charge density at 0.35 per* $(OH)_2\ O_{10}$*.*

Fig. 5. *Distribution of charges*

Beidellite-Montmorillonite interstratification (BM ~ 50%:50%) *(Cluster1):*

$Ca_{0.08}\ Mg_{0.09}\ Na_{0.00}\ K_{0.06}\quad Al_{1.27}\ Fe^{3+}_{0.58}\ Mg_{0.14}\ Ti_{0.01}\ (OH)_2\ \ Si_{3.72}\ Al_{0.28}\ O_{10}$

Charge: XII = 0.40 VI = 5.88 IV = 15.72 **Σ = 22.00**

Measured particles: 56

Distribution of BM-interstratifications (Cluster1)

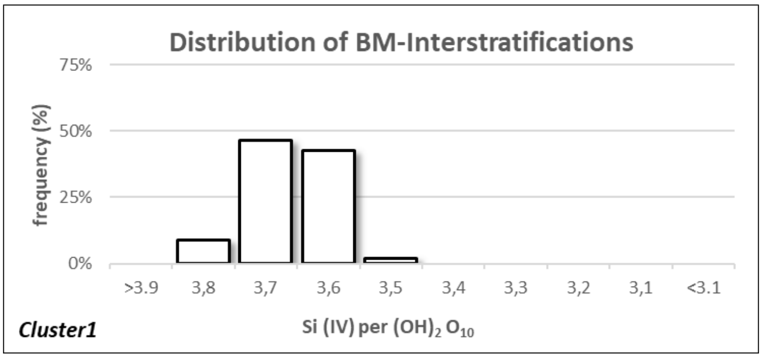

Description: *The distribution of BM-interstratifications (classified as Cluster1) draws a maximum of frequency (%) at tetrahedral Si-value between 3.6 – 3.8 e phuc*

Fig. 6a. *Distribution of assumed beidellite-montmorillonite interstratifications*

BM50:50	*particles (abs)*	Ca (XII)	Mg (XII)	Na (XII)	K (XII)	Cr3+ (VI)	Al (VI)	Fe3+ (VI)	Mg (VI)	Ti (VI)	Al (IV)	Si (IV)	XII	n_VI	%S
Si >3.9	n = 0														
Si 3.9-3.8	n = 5	0,07	0,09	0,00	0,01	0,00	1,38	0,44	0,18	0,01	0,16	3,84	0,3	2,0	79
Si 3.8-3.7	**n = 26**	**0,09**	**0,09**	**0,00**	**0,05**	**0,00**	**1,27**	**0,58**	**0,15**	**0,00**	**0,26**	**3,74**	**0,4**	**2,0**	**61**
Si 3.7-3.6	n = 24	0,08	0,10	0,00	0,09	0,00	1,23	0,61	0,14	0,02	0,33	3,67	0,5	2,0	50
Si 3.6-3.5	n = 1	0,10	0,12	0,00	0,05	0,00	1,40	0,50	0,08	0,01	0,41	3,59	0,5	2,0	39
Si 3.5-3.4	n = 0														
Si 3.4-3.3	n = 0														
Si 3.3-3.2	n = 0														
Si 3.2-3.1	n = 0														
Si <3.1	n = 0														

Fig. 6b. *Computed averaged mineral formulae of phases in the different Si(IV)-classes*

Dioctahedral Vermiculite-Smectite mixed layer phases (diVS-ml) *(Cluster2):*

$$Ca_{0.09}\,Mg_{0.12}\,Na_{0.00}\,K_{0.17}\quad Al_{1.17}\,Fe^{3+}_{0.67}\,Mg_{0.14}\,Ti_{0.02}\,(OH)_2\quad Si_{3.54}\,Al_{0.46}\,O_{10}$$

Charge: XII = 0.58 VI = 5.98 IV = 15.54 **Σ = 22.00**

Probability of smectite layers (%S): 33%

Probability of illite layers (%I): 67%

Measured particles: 30

Distribution of smectite layers probability (%S) in diVS-ml (Cluster2)

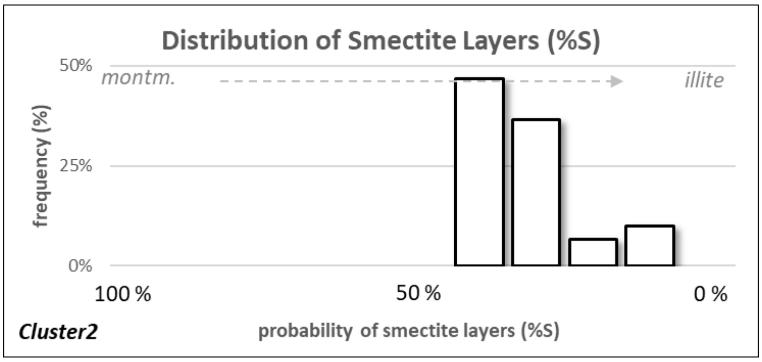

Description: *The distribution of diVS-ml (classified as Cluster2) draws a maximum of frequency (%) for smectite layer probability at 40%*

Fig. 7a. *Distribution of smectite layers probability in diVS-ml*

diVS-ml	*particles (abs)*	Ca (XII)	Mg (XII)	Na (XII)	K (XII)	Cr3+ (VI)	Al (VI)	Fe3+ (VI)	Mg (VI)	Ti (VI)	Al (IV)	Si (IV)	XII	n_VI	%S
%S >95%	n = 0														
%S 95-85%	n = 0														
%S 85-75%	n = 0														
%S 75-65%	n = 0														
%S 65-55%	n = 0														
%S 55-45%	n = 0														
%S 45-35%	**n = 14**	**0,09**	**0,11**	**0,00**	**0,12**	**0,00**	**1,18**	**0,66**	**0,15**	**0,01**	**0,39**	**3,61**	**0,5**	**2,0**	**41**
%S 35-25%	n = 11	0,09	0,12	0,00	0,17	0,00	1,18	0,69	0,12	0,02	0,47	3,53	0,6	2,0	32
%S 25-15%	n = 2	0,09	0,08	0,00	0,33	0,00	1,16	0,67	0,15	0,02	0,55	3,45	0,7	2,0	23
%S <15%	n = 3	0,07	0,17	0,02	0,25	0,00	1,15	0,72	0,11	0,02	0,67	3,33	0,8	2,0	12

Fig. 7b. *Computed averaged mineral formulae of diVS-ml phases in the different smectite layers probability (%S)-classes*

Description – B25 No0_T (< 2 µm), treated material *(OPA, 100°C, 110 hrs)*

Preparation for TEM

The powder of compacted and treated B25-No0_T-sample was suspended in deionized water and dispersed by ultrasonic treatment for approximately 20 min. The clay fraction (<2 µm) was separated by sedimentation and diluted with deionized water to get a clear suspension. The suspension was dropped onto carbon-coated Cu grids, air dried and stored under environment-controlled conditions at 45% humidity.

Mineral Matter - Overview

The fraction < 2 µm of treated B25 bentonite sample (Opalinus Clay solution, at 100°C, for 110 hours) is mainly composed by assumed beidellite-montmorillonite interstratifications (B:M ~50:50), abbreviated as BM-ml, and dioctahedral vermiculite-smectite mixed layer phases (diVS-ml) and accompanied by two types of illite. Furthermore, kaolinite and Si-surplus particles (Si, e.g. quartz) were identified in traces in this sample [fig. 1].

	frequency-% *(n = 90 measured particles)*
BM-ml (Cluster1)	62%
diVS-ml (Cluster2)	33%
Kaolinite & KSV-ml	4%
Si-surplus	1%

All measured clay mineral phases summarized result following mineral formula computed from TEM-EDX-measurement of 90 individual particles:

$$Ca^{2+}_{0.09}\ Mg^{2+}_{0.10}\ Na^{+}_{0.00}\ K^{+}_{0.10}\quad Al^{3+}_{1.24}\ Fe^{3+}_{0.61}\ Mg^{2+}_{0.14}\ Ti^{4+}_{0.01}\ (OH)_2\quad Si^{4+}_{3.65}\ Al^{3+}_{0.35}\ O_{10}$$

SDOM *± 0.00 ± 0.00 ± 0.00 ± 0.01 ± 0.01 ± 0.01 ± 0.00 ± 0.00 ± 0.01 ± 0.01*

Legend: SDOM - standard deviation of the mean (= the standard deviation divided by the square root of the number of samples)

The interlayer charge is calculated as 0.48 per $(OH)_2\ O_{10}$ and the octahedral charge as 5.87 per $(OH)_2\ O_{10}$. The particles are characterized by a high octahedral Fe-amount.

The summarized chemical composition of all 90 computed particles is compared with measured data of original B25-bentonite sample [tab. 1]. The chemical composition averaged by measured particles show especially a higher amount of SiO_2, Al_2O_3, Fe_2O_3 and TiO_2 as well as a lower amount of K_2O in comparison to the measured data of original untreated B25-bentonite.

B25-No0_T sample is characterized by three morphological groups: (i) aggregates formed by small (≤ 200 nm) xenomorphous plates, (ii) large (≤ 1 µm) xenomorph film-like platy crystals partially with folds, (iii) aggregates formed by idiomorph hexagonal plates (≤ 200 nm) [fig. 2]. Thin aggregates formed by small (≤ 200 nm) xenomorphous plates dominate the shapes of particles in the micrographs [see fig. 2 right].

The distribution of %S-probability of all measured clay mineral phases [fig. 3a] also indicates the occurrence of three groups: (i) montmorillonite (in traces; %S-class = 100%), (ii) as main group a mixture of beidellite-montmorillonite interstratifications and diVS-ml (%S-max of this mixture at 60%) and (iii) illite with K- and charge deficit (%S-class = 0%).

The numerous measured particles by TEM-EDX allow a visualization of distribution of interlayer charges. Considering the TEM-EDX-determined cations Ca^{++}, Mg^{++} and Na^{+} and then computed their ratio as interlayer cations in the mineral formula, Ca^{++}, Mg^{++} and Na^{+} offer to characterize the degree of exchangeable charges in the interlayer space. This charge density of treated B25 bentonite (< 2 µm) shows only a narrow interval at the maximal frequency-% of charge density at 0.35 per $(OH)_2\ O_{10}$ [fig. 5]. This narrow interval of interlayer charge density caused by exchangeable cations from 0.32 – 0.47 per $(OH)_2\ O_{10}$ represents mainly the BM-phases. Also, the measured diVS-ml phases offer only a reduced number of exchangeable cations at 0.53 – 0.76 per $(OH)_2\ O_{10}$.

Mineral Matter - Specification

Result of Clustering

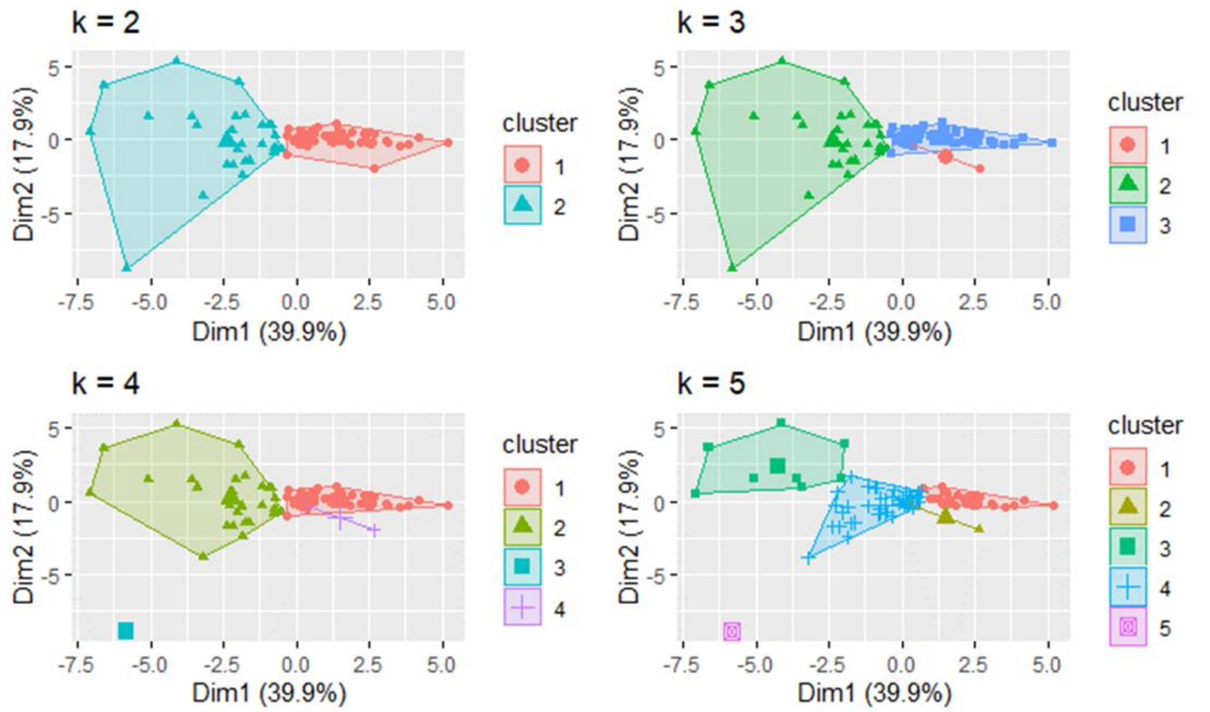

Fig. 8. *Clustering of all measured particles for clusters k = 2, k = 3, k = 4 and k = 5 (source for R-coding: https://uc-r.github.io/kmeans_clustering)*

The optimum of clusters was calculated with k = 2.

		Ca (XII)	Mg (XII)	Na (XII)	K (XII)	Cr3+ (VI)	Al (VI)	Fe3+ (VI)	Mg (VI)	Ti (VI)	Al (IV)	Si (IV)	XII	n_VI	%S
Cluster1	n = 56	0,08	0,09	0,00	0,06	0,00	1,27	0,58	0,14	0,01	0,28	3,72	0,4	2,0	57
Cluster2	n = 30	0,09	0,12	0,00	0,17	0,00	1,17	0,67	0,14	0,02	0,46	3,54	0,6	2,0	33

Fig. 9. *Mineral formulae based on TEM-EDX-data summarized following the result of clustering for k=2*

	Sybilla-results	TEM-EDX-results	Notes
Cluster1	IS R0(1) *(%S = 99%)*	BM-ml *(%B = 55%)*	*XRD: Montmorillonite and beidellite is only to distinguish by Green-Kelly-test (not available here).*
Cluster2	IS R0(2) *(%S = 30%)*	diVS-ml *(%S = 33%)*	*high K-deficit, Fe(VI)-rich*

Tab. 2. *Comparison of results from TEM-EDX- and XRD-measurements with clustering procedure*

The clustering of TEM-EDX-data offers a good agreement with the recent result of Sybilla-processing of XRD-traces from oriented specimen [tab. 2].

IS R0 (1): The X-ray diffraction pattern of the ethylene-glycol saturated oriented specimen shows a full expandability to 1.71 nm and a difference of 5.44°2θ between 2. and 3. order of smectite interferences. This distance is typically for montmorillonite (Moore & Reynolds, 1989). This result of XRD-processing let expect a maximum of particles for %S ~ 99% by TEM-EDX-measurements, but the maximum of particles measured by TEM-EDX is to find at %S=60% [fig. 3a].

Montmorillonite and beidellite have the same behavior concerning the expandability and they are only to distinguish by XRD using Li like by Greene-Kelly test (Green-Kelly 1952, 1953). So, combination of XRD- and TEM-results (full expandability by XRD and Si ~ 3.72 by TEM-EDX) led conclude the occurrence of 'beidellite-montmorillonite interstratifications', a beidellite-montmorillonite interstratification with about 55% beidellite and 45% montmorillonite layers (BM-ml 55:45).

IS R0 (2): The Sybilla-procedure of XRD-traces (oriented mounts) has shown an occurrence of a second illite-smectite mixed layer phase with a smectite layers probability of %S = 30%. This situation is to find in Cluster2 ($\%S_{TEM}$ = 33%) representing a high K-, but low charge deficient and very Fe-rich dioctahedral vermiculite-smectite mixed layer phase (diV-ml) [tab. 2].

The Sybilla-processing of XRD-traces (oriented mounts) also supports the existence of kaolinite and kaolinite-smectite mixed layer phases in fine fraction of sample. Such phases were not to identify or to calculate in TEM-EDX-database (a grain size effect?).

Specifics to the identified clay mineral groups

Beidellite-montmorillonite interstratifications (B:M ~55:45)

56 of 90 measured particles belong so to this assumed classification. The dioctahedral character of this group is proofed by X-ray diffraction. The position of the large (060)-interference of smectite is in the random oriented powder specimen at 1.497 Å.

Montmorillonite and beidellite have the same behavior concerning the expandability and they are only to distinguish by XRD using Li by means of Greene-Kelly test (Green-Kelly 1952, 1953). So, combination of XRD- and TEM-results (full expandability by XRD and Si ~ 3.72 by TEM-EDX) led conclude the occurrence of 'beidellite-montmorillonite interstratifications', a beidellite-montmorillonite interstratification with about 55% beidellite and 45% montmorillonite layers (BM-ml 55:45).

Beidellite-montmorillonite interstratifications (B:M ~55:45):

$$Ca_{0.08}\,Mg_{0.09}\,Na_{0.00}\,K_{0.06}\quad Al_{1.27}\,Fe^{3+}_{0.58}\,Mg_{0.14}\,Ti_{0.01}\,(OH)_2\quad Si_{3.72}\,Al_{0.28}\,O_{10}$$

Charge: XII = 0.40 VI = 5.88 IV = 15.72 **Σ = 22.00**

Measured particles by TEM-EDX: 56
Result of clustering: Cluster1 [tab. 2]

Beidellitic structures are characterized by a low octahedral Mg-amount (because of high ratio of octahedral, 3-valent cations). A comparison of octahedral Mg vs. tetrahedral Si indicates the occurrence of two groups for octahedral Mg based on TEM-EDX-data [fig. 3b]. The group with a lower Mg-ratio should represent the already mentioned BM-ml (55:45) phases (Cluster1 in tab. 2) and the other group with a higher Mg-ratio is considered as diVS-ml.

Using the results of clustering (see Cluster1 in tab. 2), the maximum of frequency-% is to find for particles in the Si(IV)-class 3.6 – 3.8 e phuc [tab. 6a], representing the mentioned relation 50% montmorillonite and 50% beidellite as ratio of interstratification. The mineral formulae, summarized in classes of tetrahedral Si, draw for the maximum an Fe-rich BM 55:45 phase with low K, but remarkable amount of Mg in the interlayer space [tab. 6b].

Dioctahedral vermiculite-smectite mixed layer phase (diVS-ml):

$$\mathrm{Ca_{0.09}\ Mg_{0.12}\ Na_{0.01}\ K_{0.17}\quad Al_{1.17}\ Fe^{3+}_{0.67}\ Mg_{0.14}\ Ti_{0.02}\ (OH)_2\ \ Si_{3.54}\ Al_{0.46}\ O_{10}}$$

Charge: XII = 0.58 VI = 5.88 IV = 15.54 **Σ = 22.00**
Probability of smectite layers (%S): 33%
Probability of illite layers (%I): 67%

Measured particles by TEM-EDX: 30
Result of clustering: Cluster2 [tab. 2]

Illite as part of diVS-ml series

The Rietveld refinement by Profex software (Döbelin & Kleeberg, 2015) indicates the occurrence of two polytypes for illite in treated B25 bentonite: $2M_1$- and 1M-polytype.

Kaolinite-montmorillonite mixed layer phases

The Excel-based procedure (Hoang-Minh et al., 2019) to identify possible clay mineral groups using the TEM-EDX-measurements also includes algorithms to classify kaolinite and kaolinite-montmorillonite mixed layer phases. These algorithms couldn't identify such phases basing on the measured TEM-EDX-data. Otherwise, few particles, which were not to compute, have shown small hexagonal plates typically for kaolinite-bearing phases [fig. 2].

References

Cliff, G. & Lorimer, G. W. (1975). *J. Microsc.* **103**, 203–207.

Döbelin, N., Kleeberg, R. (2015). *Journal of Applied Crystallography* **48**, 1573-1580. DOI: 10.1107/S1600576715014685

Greene-Kelly, R., *Clay Minerals Bull.*, **1**, 221 (1952).

Greene-Kelly, R. 1953. The identification of montmorillonoids in clays. *Journal of Soil Science*. **4** (2), pp. 232-237. https://doi.org/10.1111/j.1365-2389.1953.tb00657.x

Henning, K.-H. & Störr, M. (1986). Electron Micrographs (TEM, SEM) of Clays and Clay Minerals, p. 325. Akademie-Verlag Berlin.

Hoang-Minh, T., Kasbohm, J., Nguyen-Thanh, L., Nga, P. T., Lai, L. T., Duong, N. T., Thanh, N. D., Thuyet, N. T. M., Anh, D. D., Pusch, R., Knutsson, S. & Ferreiro Mahlmann, R. (2019). *J. Appl. Cryst.* **52**, 133-147. DOI: 10.1107/S1600576718018162

Lorimer, G. W. & Cliff, G. (1976). *Electron Microscopy in Mineralogy*, edited by H. R. Wenk, pp. 506–519. Berlin: Springer Verlag.

Matschiavelli, N., Kluge, S., Podlech, C., Standhaft, D., Grathoff, G., Ikeda-Ohno, A., Warr, L.N., Chukharkina, A., Arnold, T. & Cherkouk, A. (2019). *Environmental Science & Technology.* **53** (17), 10514-10524, DOI: 10.1021/acs.est.9b02670

Mellini, M. & Menichini, R. (1985). *R. Soc. Ital. Miner. Petrol.* **40**, 261–266.

Moore, D.M., Reynolds, R.C. (1989). X-ray Diffraction and the Identification and Analysis of Clay Minerals, Oxford University Press, New York, 332 + xvi pp.

Nguyen-Thanh, L., Herbert, H.-J., Kasbohm, J., Hoang-Minh, T. & Mählmann, R. F. (2014). *Clays Clay Miner.* **62**, 425–446.

Środoń, J., Elsass, F., McHardy, W. J. & Morgan, D. J. (1992). *Clay Miner.* **27**, 137–158.

Data Sheet – B25 bentonite, treated materials *(OPA, 100 °C, 110h)* - CENTER

Methodology - Transmission electron microscopy linked with energy-dispersive X-ray spectroscopy (TEM-EDX)

It is expected a characterization of clay mineral phases in treated B25 bentonite by transmission electron microscopy. The sample series No0 represents a percolation of B25 bentonite by Opalinus Clay solution at 100°C for 110 hours. The sample No0_C is the label for the material at the middle of sample cylinder.

The different clay mineral phases are to identify and to describe by chemical composition and its variability, morphology, the specific dissolution potential, and further parameter.

Such further parameter like distribution of smectite layers probability (%S) and distribution of charges caused by exchangeable cations interlayer space should serve as additional indicators for mineralogical alterations in treatment experiments with B25 bentonite.

The sample were suspended for TEM-measurement in deionized water and dispersed by ultrasonic treatment for approximately 20 min. The clay fraction (<2 µm) was separated by sedimentation and diluted with deionized water to get a clear suspension. The suspension was dropped onto carbon-coated Cu grids, air dried and stored under environment-controlled conditions at 45% humidity.

TEM-EDX investigations were carried out on the <2 µm fraction using a FEI TECNAI G^2 20 electron transmission microscope at the VNU University of Science, Vietnam National University, Hanoi. This equipment (operated at 200 kV with LaB_6 cathode) was combined with an S-TWIN objective, a windowless EDAX energy-dispersive X-ray system and a FEI Eagle 2k CCD TEM camera.

About 100 individual clay particles per sample were characterized by TEM-EDX with respect to crystal size, crystal habit, and particle morphology and element distribution. The crystal size, crystal habit and particle morphology were described according to Henning & Störr (1986).

For the quantification of element distribution, a calibration of k factors is mandatory (Cliff & Lorimer, 1975; Lorimer & Cliff, 1976; Mellini & Menichini, 1985). These k values are used to calibrate for the specific behaviour of particles against possible irradiation damage. The elements O, Na, Mg, Al, Si, K, Ca and Fe were quantified by applying the EDAX GENESIS–TEM Quant Materials quantification procedure.

In this procedure, the acquired EDX spectra are corrected by background subtraction, Gaussian deconvolution and k-factor corrections using values previously determined on a phyllosilicate standard (muscovite) and selected non-phyllosilicate standards. The average errors in the analyzed elements using the phyllosilicate standard, expressed as the atomic proportions, are 10 (Na), 5 (Fe, Mg, K, Ti, Ca) and 1 (Si, Al).

The measurement time per particle was lowered to 20 s and the exposed area was limited to a 50 nm diameter, avoiding possible irradiation damage of particles. The stability of particles of the sample series was tested for this measurement time at the beginning of any measurement campaign.

Further methodological details related to TEM-EDX-measurements and the Excel-based mathematical procedure using TEM-EDX data for calculation of mineral formulae are described in Hoang-Minh et al. (2019).

These mathematical procedures described in Hoang-Minh et al. (2019) were extended by k-means clustering method for finding subgroups of observations within a data set. The data were standardized (i.e., scaled) to make variables comparable. Euclidean distances were applied as classical method for distance measures. The optimal clusters were determined by Elbow method and Gap statistics[14].

---

[14] *https://uc-r.github.io/kmeans_clustering*

Data Sheet – B25 No0_C (< 2 µm), treated material *(OPA, 100°C, 110 hrs)*

Preparation for TEM

- raw material: compacted material (1.6 g/cm³) of treated B25-sample (OPA, 100°C, 110 hrs)
- suspension on particles < 2 µm on carbon-filmed Cu-grid
- air-dried and humidity-controlled storing

Mineral Matter

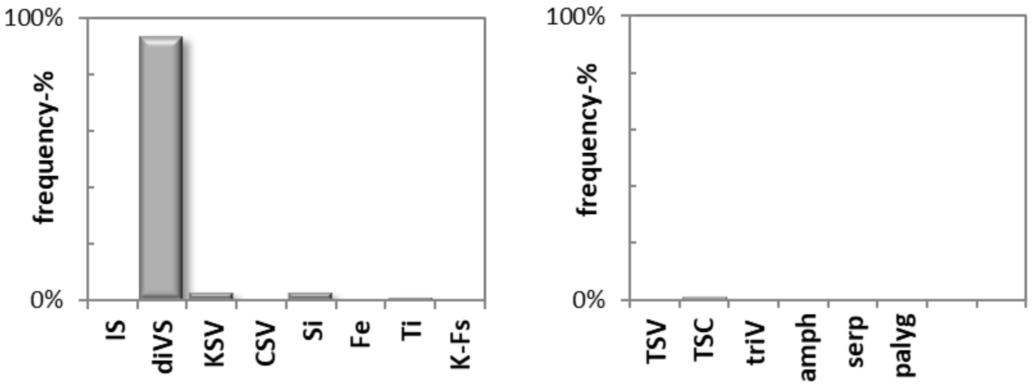

Fig. 1. *Distribution of mineral groups in fraction < 2 µm (in frequency-%)*
Legend: ***IS*** *– illite-smectite-mixed layer series in sense of Środon et al. (1992), diVS – dioctahedral vermiculite-smectite illite-smectite-mixed layer series (= charge- and/or K-deficit),* ***KSV*** *– kaolinite-smectite-dioctahedral vermiculite-mixed layer series,* ***CSV*** *– chlorite-saponite-trioctahedral vermiculite-mixed layer series,* ***Si*** *– quartz or particles with Si-surplus,* ***Fe*** *– Fe-oxide or Fe-oxyhydroxide,* ***Ti*** *– Ti-bearing phases (e.g. rutile, anatase),* ***K-Fs*** *– K-feldspar*

Clay Mineral Composition

All particles of smectite group:

$$Ca_{0.11}\ Mg_{0.08}\ Na_{0.00}\ K_{0.10}\quad Al_{1.27}\ Fe^{3+}_{0.57}\ Mg_{0.16}\ Ti_{0.01}\ (OH)_2\quad Si_{3.65}\ Al_{0.35}\ O_{10}$$

Charge: XII = 0.50 VI = 5.85 IV = 15.65 **Σ = 22.00**
Probability of smectite layers (%S): 48%
Probability of illite layers (%I): 52%

Specific Dissolution Potential (ΔS%)

for H2O, 20 + 60 rpm -4 (= slow reacting, interlayer group: Ca+Mg (= type B))
for NaCl, 20 rpm -4 (= slow reacting, interlayer group: Ca+Mg (= type B))
for NaCl, 60 rpm -111 (= fast reacting, 'illitization', interlayer group: Na (= type A))
CEC_{calc}: 52 meq / 100 g (literature: 56 meq / 100 g [Matschiavelli et al., 2019: MAT19])

Measured particles: 114

Table 1. *Summarized chemical composition*

SiO_2	**TiO_2**	**Al_2O_3**	**Fe_2O_3**	**MnO**	**MgO**	**CaO**	**Na_2O**	**K_2O**	**P_2O_5**	**Σ**	
60.5%	0.1%	23.5%	6.3%		3.1%	1.3%	0.0%	0.9%	0.2%	0.96	measured particles
58.6%	0.0%	22.0%	5.9%		3.0%	1.0%	0.1%	1.1%	0.1%	0.92	measured particles of original B25

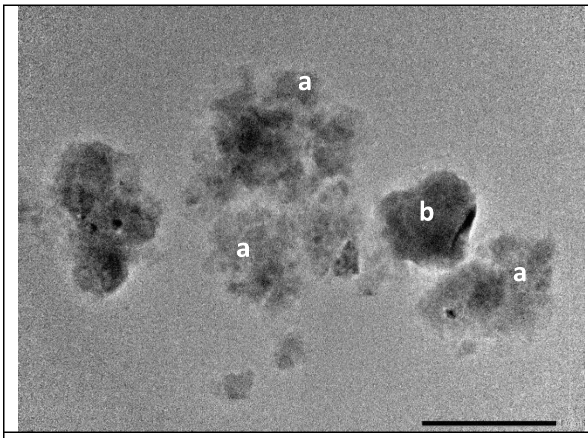	
JEM-2100_No0-C_A1_X12k.bmp Magnification: 12k (a) aggregates formed by small (≤ 200 nm) xenomorphous plates; (b) large (≤ 1 µm) xenomorph film-like platy crystals partially with folds	

Fig. 2. *Morphology of particles (TEM-micrographs)*

Distribution of smectite layers probability (%S)

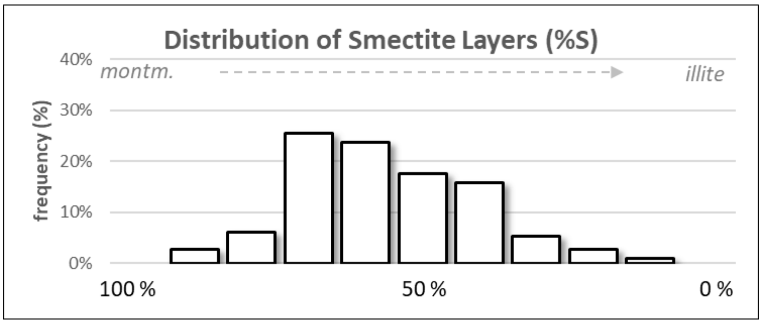

***Description:** The distribution of %S-probability indicates the occurrence of two groups: (i) mixture of beidellite-montmorillonite interstratifications (= assumption) with diVS-ml as well as (ii) illite with K-deficiency.*

Fig. 3a. *Distribution of smectite layers probability (%S)*

Differentiation by relation "Octahedral Mg vs. tetrahedral Si"?

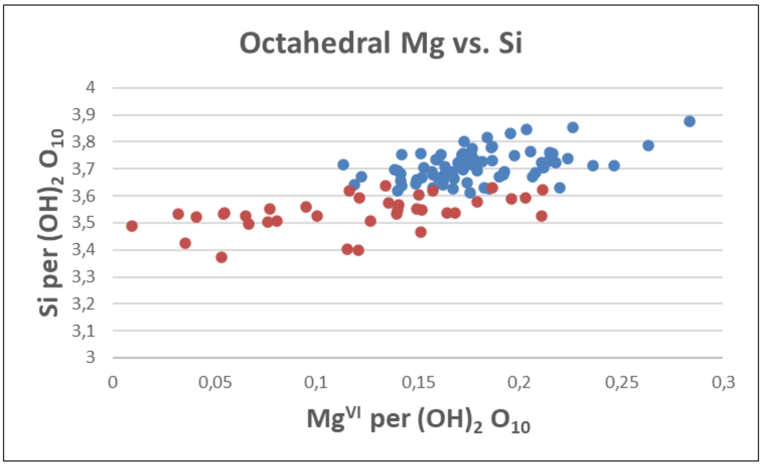

***Description:** This diagram indicates the occurrence of two groups of Mg in relation to tetrahedral Si. Probably, this distribution mirrors 2 phases (I) beidellite-montmorillonite interstratifications (blue) and (II) diVS-ml (red)*

Fig. 3b. *Distribution of octahedral Mg vs. tetrahedral Si [all per$(OH)_2\ O_{10}$]*

Distribution of K in relation to tetrahedral Si

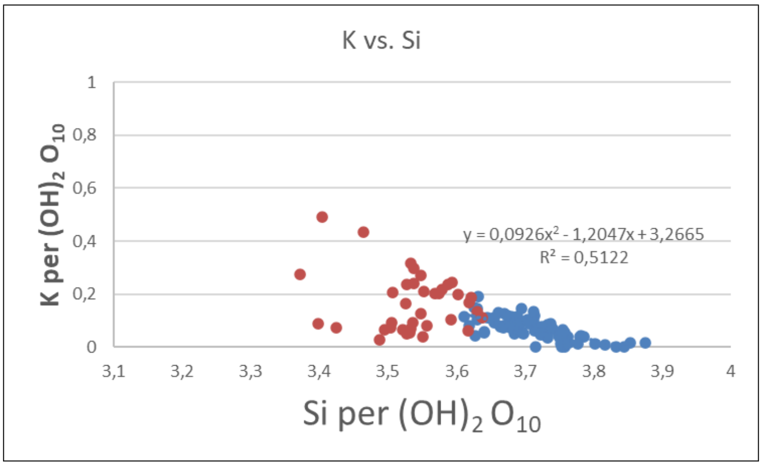

Description: *This diagram visualizes possible particles (beidellite-montmorillonite interstratification?) with a very low K (blue dots)*

Fig. 4. *Distribution of K in interlayer space vs. tetrahedral Si [all per$(OH)_2$ O_{10}]*

Distribution of charges (exchangeable from interlayer space)

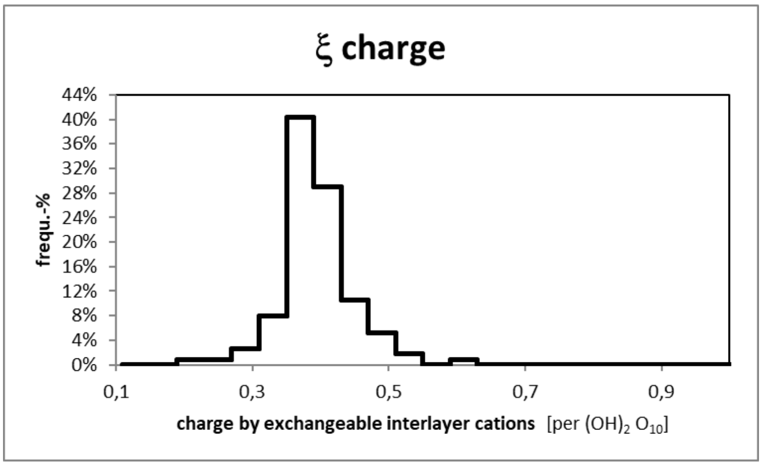

This diagram visualizes the distribution of exchangeable charges in the interlayer space (Ca, Mg, Na) determined and computed by TEM-EDX-data.

Description: *Maximal frequency-% of charge density at 0.39 per $(OH)_2$ O_{10}.*

Fig. 5. *Distribution of charges*

Beidellite-Montmorillonite interstratification (BM ~ 60%:40%) *(Cluster1):*

$$Ca_{0.12}\ Mg_{0.08}\ Na_{0.00}\ K_{0.07}\quad Al_{1.24}\ Fe^{3+}_{0.57}\ Mg_{0.18}\ Ti_{0.01}\ (OH)_2\quad Si_{3.71}\ Al_{0.29}\ O_{10}$$

Charge: XII = 0.46 VI = 5.83 IV = 15.71 **Σ = 22.00**

Measured particles: 77

Distribution of BM-interstratifications (Cluster1)

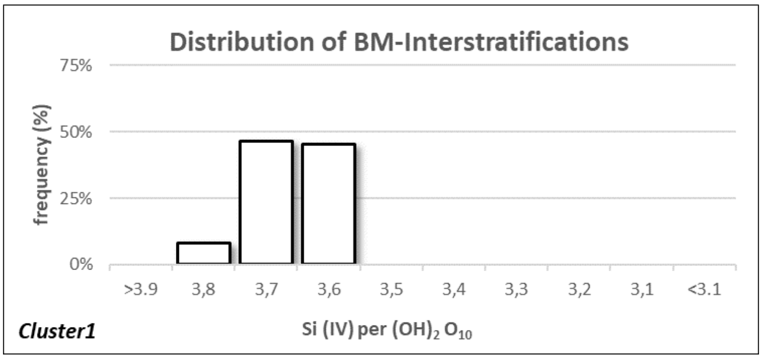

Description: *The distribution of BM-interstratifications (classified as Cluster1) draws a maximum of frequency (%) at tetrahedral Si-value between 3.6 – 3.8 e phuc*

Fig. 6a. *Distribution of assumed beidellite-montmorillonite interstratifications*

BM50:50	particles (abs)	Ca (XII)	Mg (XII)	Na (XII)	K (XII)	Cr3+ (VI)	Al (VI)	Fe3+ (VI)	Mg (VI)	Ti (VI)	Al (IV)	Si (IV)	XII	n_VI	%S
Si >3.9	n = 0														
Si 3.9-3.8	n = 6	0,11	0,07	0,00	0,01	0,00	1,34	0,44	0,21	0,00	0,16	3,84	0,4	2,0	77
Si 3.8-3.7	**n = 36**	**0,12**	**0,07**	**0,00**	**0,06**	**0,00**	**1,25**	**0,56**	**0,19**	**0,01**	**0,26**	**3,74**	**0,4**	**2,0**	**61**
Si 3.7-3.6	n = 35	0,12	0,08	0,00	0,10	0,00	1,22	0,61	0,17	0,01	0,34	3,66	0,5	2,0	49
Si 3.6-3.5	n = 0														
Si 3.5-3.4	n = 0														
Si 3.4-3.3	n = 0														
Si 3.3-3.2	n = 0														
Si 3.2-3.1	n = 0														
Si <3.1	n = 0														

Fig. 6b. *Computed averaged mineral formulae of phases in the different Si(IV)-classes*

Dioctahedral Vermiculite-Smectite mixed layer phases (diVS-ml) *(Cluster2):*

$$Ca_{0.09}\ Mg_{0.10}\ Na_{0.00}\ K_{0.17}\quad Al_{1.30}\ Fe^{3+}_{0.57}\ Mg_{0.12}\ Ti_{0.01}\ (OH)_2\ \ Si_{3.54}\ Al_{0.46}\ O_{10}$$

Charge: XII = 0.57 VI = 5.89 IV = 15.54 **Σ = 22.00**

Probability of smectite layers (%S): 32%

Probability of illite layers (%I): 68%

Measured particles: 37

Distribution of smectite layers probability (%S) in diVS-ml (Cluster2)

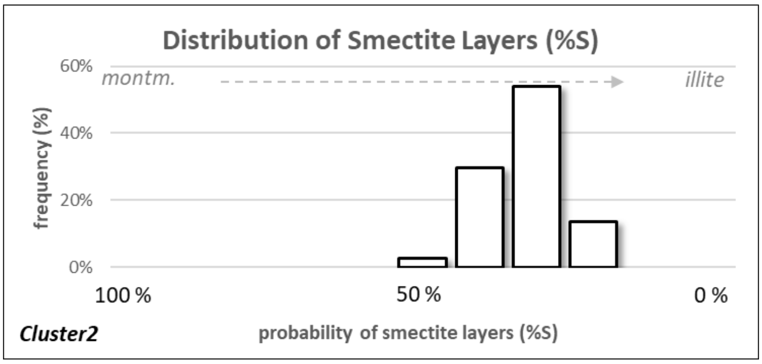

Description: *The distribution of diVS-ml (classified as Cluster2) draws a maximum of frequency (%) for smectite layer probability at 30%*

Fig. 7a. *Distribution of smectite layers probability in diVS-ml*

diVS-ml	particles (abs)	Ca (XII)	Mg (XII)	Na (XII)	K (XII)	Cr3+ (VI)	Al (VI)	Fe3+ (VI)	Mg (VI)	Ti (VI)	Al (IV)	Si (IV)	XII	n_VI	%S
%S >95%	n = 0														
%S 95-85%	n = 0														
%S 85-75%	n = 0														
%S 75-65%	n = 0														
%S 65-55%	n = 0														
%S 55-45%	n = 1	0,09	0,10	0,00	0,11	0,00	1,35	0,52	0,13	0,00	0,36	3,64	0,5	2,0	45
%S 45-35%	n = 11	0,11	0,08	0,00	0,18	0,00	1,26	0,57	0,16	0,01	0,40	3,60	0,6	2,0	40
%S 35-25%	**n = 20**	**0,10**	**0,11**	**0,00**	**0,14**	**0,00**	**1,32**	**0,57**	**0,10**	**0,01**	**0,47**	**3,53**	**0,6**	**2,0**	**31**
%S 25-15%	n = 5	0,10	0,10	0,00	0,27	0,00	1,32	0,57	0,10	0,01	0,59	3,41	0,7	2,0	19
%S <15%	n = 0														

Fig. 7b. *Computed averaged mineral formulae of diVS-ml phases in the different smectite layers probability (%S)-classes*

Description – B25 No0_C (< 2 µm), treated material *(OPA, 100°C, 110 hrs)*

Preparation for TEM

The powder of compacted and treated B25-No0_C-sample was suspended in deionized water and dispersed by ultrasonic treatment for approximately 20 min. The clay fraction (<2 µm) was separated by sedimentation and diluted with deionized water to get a clear suspension. The suspension was dropped onto carbon-coated Cu grids, air dried and stored under environment-controlled conditions at 45% humidity.

Mineral Matter - Overview

The fraction < 2 µm of treated B25 bentonite sample (Opalinus Clay solution, at 100°C, for 110 hours) is mainly composed by assumed beidellite-montmorillonite interstratifications (B:M ~50:50), abbreviated as BM-ml, and dioctahedral vermiculite-smectite mixed layer phases (diVS-ml) and accompanied by two types of illite. Furthermore, kaolinite and Si-surplus particles (Si, e.g. quartz) were identified in traces in this sample [fig. 1].

	frequency-% *(n = 90 measured particles)*
BM-ml (Cluster1)	63%
diVS-ml (Cluster2)	30%
Kaolinite & KSV-ml	2%
Si-surplus	2%
Ti-phases	1%

All measured clay mineral phases summarized result following mineral formula computed from TEM-EDX-measurement of 114 individual particles:

	$Ca^{2+}_{0.11}$	$Mg^{2+}_{0.08}$	$Na^{+}_{0.00}$	$K^{+}_{0.10}$	$Al^{3+}_{1.27}$	$Fe^{3+}_{0.57}$	$Mg^{2+}_{0.16}$	$Ti^{4+}_{0.01}$	$(OH)_2$	$Si^{4+}_{3.65}$	$Al^{3+}_{0.35}$	O_{10}
SDOM	*± 0.00*	*± 0.00*	*± 0.00*	*± 0.01*	*± 0.01*	*± 0.01*	*± 0.00*	*± 0.00*		*± 0.01*	*± 0.01*	

Legend: SDOM - standard deviation of the mean (= the standard deviation divided by the square root of the number of samples)

The interlayer charge is calculated as 0.50 per $(OH)_2$ O_{10} and the octahedral charge as 5.85 per $(OH)_2$ O_{10}. The particles are characterized by a high octahedral Fe-amount.

The summarized chemical composition of all 114 computed particles is compared with measured data of original B25-bentonite sample [tab. 1]. The chemical composition averaged by measured particles show especially a higher amount of SiO_2, Al_2O_3 and Fe_2O_3 as well as a slight lower amount of K_2O in comparison to the measured data of original untreated B25-bentonite.

B25-No0_C sample is characterized by three morphological groups: (i) aggregates formed by small (≤ 200 nm) xenomorphous plates, (ii) large (≤ 1 µm) xenomorph film-like platy crystals partially with folds, (iii) aggregates formed by idiomorph hexagonal plates (≤ 200 nm) [fig. 2]. Thin aggregates formed by small (≤ 200 nm) xenomorphous plates dominate the shapes of particles in the micrographs [fig. 2].

The distribution of %S-probability of all measured clay mineral phases [fig. 3a] also indicates the occurrence of two groups: (i) as main group a mixture of beidellite-montmorillonite interstratifications and diVS-ml (%S-max of this mixture for %S at 70%) and (ii) illite with K- and charge deficit (%S-class = 10%).

The numerous measured particles by TEM-EDX allow a visualization of distribution of interlayer charges. Considering the TEM-EDX-determined cations Ca^{++}, Mg^{++} and Na^{+} and then computed their ratio as interlayer cations in the mineral formula, Ca^{++}, Mg^{++} and Na^{+} offer to characterize the degree of exchangeable charges in the interlayer space. This charge density of treated B25 bentonite (< 2 µm) shows only a narrow interval at the maximal frequency-% of charge density at 0.39 per $(OH)_2$ O_{10} [fig. 5]. This narrow interval of interlayer charge density caused by exchangeable cations from 0.37 – 0.50 per $(OH)_2$ O_{10} represents mainly the BM-phases. Also, the measured diVS-ml phases offer only a reduced number of exchangeable cations at 0.50 – 0.67 per $(OH)_2$ O_{10}.

Mineral Matter - Specification

Result of Clustering

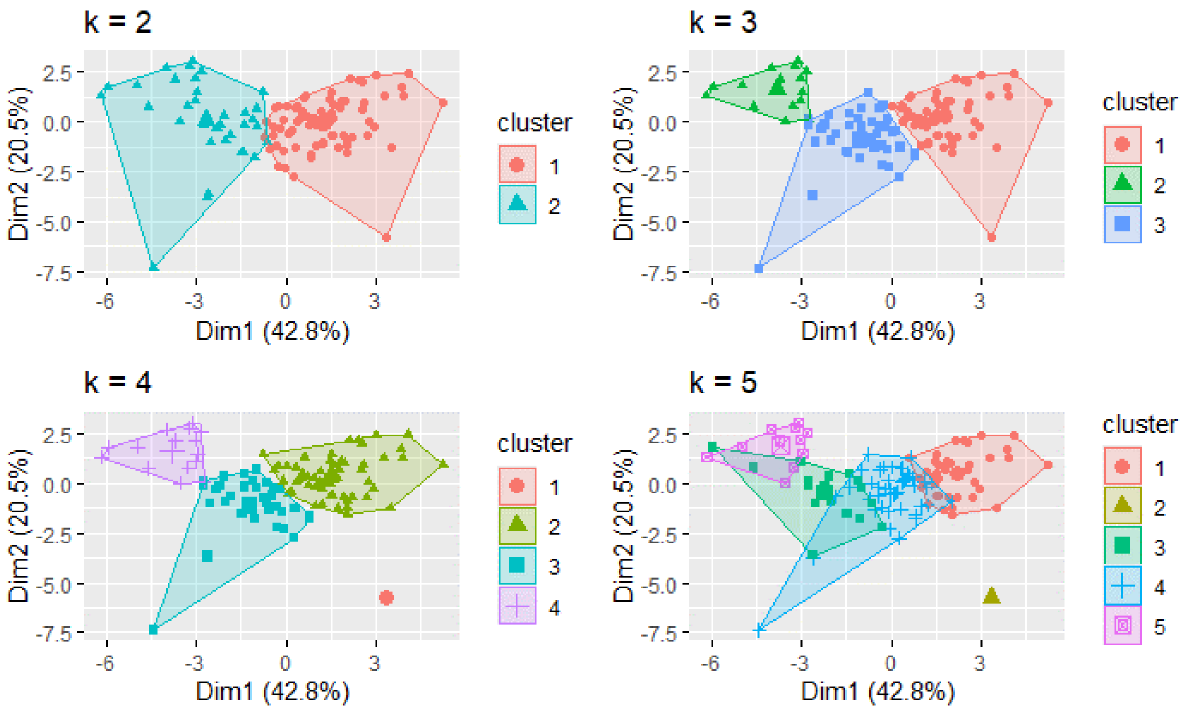

Fig. 8. *Clustering of all measured particles for clusters k = 2, k = 3, k = 4 and k = 5 (source for R-coding: https://uc-r.github.io/kmeans_clustering)*

The optimum of clusters was calculated with k = 2.

		Ca (XII)	Mg (XII)	Na (XII)	K (XII)	Cr3+ (VI)	Al (VI)	Fe3+ (VI)	Mg (VI)	Ti (VI)	Al (IV)	Si (IV)	XII	n_VI	%S
Cluster1	n = 77	0,12	0,08	0,00	0,07	0,00	1,24	0,57	0,18	0,01	0,29	3,71	0,5	2,0	56
Cluster2	n = 37	0,10	0,10	0,00	0,17	0,00	1,30	0,57	0,12	0,01	0,46	3,54	0,6	2,0	32

Fig. 9. *Mineral formulae based on TEM-EDX-data summarized following the result of clustering for k=2*

	Sybilla-results	TEM-EDX-results	Notes
Cluster1	IS R0(1) *(%S = 94%)*	BM-ml *(%B ~ 60%)*	*XRD: Montmorillonite and beidellite is only to distinguish by Green-Kelly-test (not available here).*
Cluster2	IS R0(2) *(%S = 30%)*	diVS-ml *(%S ~ 32%)*	*high K-deficit, Fe(VI)-rich*

Tab. 2. *Comparison of results from TEM-EDX- and XRD-measurements with clustering procedure*

The clustering of TEM-EDX-data offers a good agreement with the recent result of Sybilla-processing of XRD-traces from oriented specimen [tab. 2].

IS R0 (1): The X-ray diffraction pattern of the ethylene-glycol saturated oriented specimen shows a full expandability to 1.71 nm and a difference of 5.46°2θ between 2. and 3. order of smectite interferences. This distance is typically for montmorillonite (Moore & Reynolds, 1989). This result of XRD-processing let expect a maximum of particles for %S ~ 94% by TEM-EDX-measurements, but the maximum of particles measured by TEM-EDX is to find at %S=60-70% [fig. 3a].

Montmorillonite and beidellite have the same behavior concerning the expandability and they are only to distinguish by XRD using Li like by Greene-Kelly test (Green-Kelly 1952, 1953). So, combination of XRD- and TEM-results (full expandability by XRD and Si ~ 3.71 by TEM-EDX) led conclude the occurrence of 'beidellite-montmorillonite interstratifications', a beidellite-montmorillonite interstratification with about 60% beidellite and 40% montmorillonite layers (BM-ml 60:40).

IS R0 (2): The Sybilla-procedure of XRD-traces (oriented mounts) has shown an occurrence of a second illite-smectite mixed layer phase with a smectite layers probability of %S = 30%. This situation is to find in Cluster1 ($\%S_{TEM}$ = 32%) representing a high K-, but low charge deficient and very Fe-rich dioctahedral vermiculite-smectite mixed layer phase (diV-ml) [tab. 2].

The Sybilla-processing of XRD-traces (oriented mounts) also supports the existence of kaolinite and kaolinite-smectite mixed layer phases in fine fraction of sample. Such phases were not to identify or to calculate in TEM-EDX-database (a grain size effect?).

Specifics to the identified clay mineral groups

Beidellite-montmorillonite interstratifications (B:M ~60:40)

77 of 114 measured particles belong so to this assumed classification. The dioctahedral character of this group is proofed by X-ray diffraction. The position of the large (060)-interference of smectite is in the random oriented powder specimen at 1.497 Å.

Montmorillonite and beidellite have the same behavior concerning the expandability and they are only to distinguish by XRD using Li by means of Greene-Kelly test (Greene-Kelly 1952, 1953). So, combination of XRD- and TEM-results (full expandability by XRD and Si ~ 3.71 by TEM-EDX) led conclude the occurrence of 'beidellite-montmorillonite interstratifications', a beidellite-montmorillonite interstratification with about 60% beidellite and 40% montmorillonite layers (BM-ml 60:40).

Beidellite-montmorillonite interstratifications (B:M ~60:40):

$$Ca_{0.12}\ Mg_{0.08}\ Na_{0.00}\ K_{0.07}\quad Al_{1.24}\ Fe^{3+}_{0.57}\ Mg_{0.18}\ Ti_{0.01}\ (OH)_2\ \ Si_{3.71}\ Al_{0.29}\ O_{10}$$

Charge: XII = 0.46 VI = 5.83 IV = 15.71 **Σ = 22.00**

Measured particles by TEM-EDX: 77

Result of clustering: Cluster1 [tab. 2]

Beidellitic structures are characterized by a low octahedral Mg-amount (because of high ratio of octahedral, 3-valent cations). A comparison of octahedral Mg vs. tetrahedral Si indicates the occurrence of two groups for octahedral Mg based on TEM-EDX-data [fig. 3b].

Using the results of clustering (see Cluster1 in tab. 2), the maximum of frequency-% is to find for particles in the Si(IV)-class 3.6 – 3.8 e phuc [tab. 6a], representing the mentioned relation 60% montmorillonite and 40% beidellite as ratio of interstratification. The mineral formulae, summarized in classes of tetrahedral Si, draw for the maximum an Fe-rich BM 60:40 phase with low K, but remarkable amount of Mg in the interlayer space [tab. 6b].

Dioctahedral vermiculite-smectite mixed layer phase (diVS-ml):

$$\boxed{Ca_{0.10}\,Mg_{0.10}\,Na_{0.00}\,K_{0.17}\quad Al_{1.30}\,Fe^{3+}_{0.57}\,Mg_{0.12}\,Ti_{0.01}\,(OH)_2\quad Si_{3.54}\,Al_{0.46}\,O_{10}}$$

Charge: XII = 0.57 VI = 5.89 IV = 15.54 **Σ = 22.00**
Probability of smectite layers (%S): 32%
Probability of illite layers (%I): 68%
Measured particles by TEM-EDX: 37
Result of clustering: Cluster2 [tab. 2]

Illite as part of diVS-ml series

The Rietveld refinement by Profex software (Döbelin & Kleeberg, 2015) indicates the occurrence of two polytypes for illite in treated B25 bentonite: $2M_1$- and 1M-polytype.

Kaolinite-montmorillonite mixed layer phases

The Excel-based procedure (Hoang-Minh et al., 2019) to identify possible clay mineral groups using the TEM-EDX-measurements also includes algorithms to classify kaolinite and kaolinite-montmorillonite mixed layer phases. These algorithms couldn't identify such phases basing on the measured TEM-EDX-data. Otherwise, few particles, which were not to compute, have shown small hexagonal plates typically for kaolinite-bearing phases.

References

Cliff, G. & Lorimer, G. W. (1975). *J. Microsc.* **103**, 203–207.

Döbelin, N., Kleeberg, R. (2015). *Journal of Applied Crystallography* **48**, 1573-1580. DOI: 10.1107/S1600576715014685

Greene-Kelly, R., *Clay Minerals Bull.*, **1**, 221 (1952).

Greene-Kelly, R. 1953. The identification of montmorillonoids in clays. *Journal of Soil Science*. **4** (2), pp. 232-237. https://doi.org/10.1111/j.1365-2389.1953.tb00657.x

Greene-Kelly, R. (1955). Dehydration of the montmorillonite minerals. *Mineralogical Magazine and Journal of the Mineralogical Society*, **30**(228), 604-615. doi:10.1180/minmag.1955.030.228.06

Henning, K.-H. & Störr, M. (1986). Electron Micrographs (TEM, SEM) of Clays and Clay Minerals, p. 325. Akademie-Verlag Berlin.

Hoang-Minh, T., Kasbohm, J., Nguyen-Thanh, L., Nga, P. T., Lai, L. T., Duong, N. T., Thanh, N. D., Thuyet, N. T. M., Anh, D. D., Pusch, R., Knutsson, S. & Ferreiro Mahlmann, R. (2019). *J. Appl. Cryst.* **52**, 133-147. DOI: 10.1107/S1600576718018162

Lorimer, G. W. & Cliff, G. (1976). *Electron Microscopy in Mineralogy*, edited by H. R. Wenk, pp. 506–519. Berlin: Springer Verlag.

Matschiavelli, N., Kluge, S., Podlech, C., Standhaft, D., Grathoff, G., Ikeda-Ohno, A., Warr, L.N., Chukharkina, A., Arnold, T. & Cherkouk, A. (2019). *Environmental Science & Technology.* **53** (17), 10514-10524, DOI: 10.1021/acs.est.9b02670

Mellini, M. & Menichini, R. (1985). *R. Soc. Ital. Miner. Petrol.* **40**, 261–266.

Moore, D.M., Reynolds, R.C. (1989). X-ray Diffraction and the Identification and Analysis of Clay Minerals, Oxford University Press, New York, 332 + xvi pp.

Nguyen-Thanh, L., Herbert, H.-J., Kasbohm, J., Hoang-Minh, T. & Mählmann, R. F. (2014). *Clays Clay Miner.* **62**, 425–446.

Środoń, J., Elsass, F., McHardy, W. J. & Morgan, D. J. (1992). *Clay Miner.* **27**, 137–158.

Data Sheet – B25 bentonite, treated materials *(OPA, 100 °C, 110h)* - BOTTOM

Methodology - Transmission electron microscopy linked with energy-dispersive X-ray spectroscopy (TEM-EDX)

It is expected a characterization of clay mineral phases in treated B25 bentonite by transmission electron microscopy. The sample series No0 represents a percolation of B25 bentonite by Opalinus Clay solution at 100°C for 110 hours. The sample No0_B is the label for the material at the bottom of sample cylinder.

The different clay mineral phases are to identify and to describe by chemical composition and its variability, morphology, the specific dissolution potential, and further parameter.

Such further parameter like distribution of smectite layers probability (%S) and distribution of charges caused by exchangeable cations interlayer space should serve as additional indicators for mineralogical alterations in treatment experiments with B25 bentonite.

The sample were suspended for TEM-measurement in deionized water and dispersed by ultrasonic treatment for approximately 20 min. The clay fraction (<2 µm) was separated by sedimentation and diluted with deionized water to get a clear suspension. The suspension was dropped onto carbon-coated Cu grids, air dried and stored under environment-controlled conditions at 45% humidity.

TEM-EDX investigations were carried out on the <2 µm fraction using a FEI TECNAI G^2 20 electron transmission microscope at the VNU University of Science, Vietnam National University, Hanoi. This equipment (operated at 200 kV with LaB_6 cathode) was combined with an S-TWIN objective, a windowless EDAX energy-dispersive X-ray system and a FEI Eagle 2k CCD TEM camera.

About 100 individual clay particles per sample were characterized by TEM-EDX with respect to crystal size, crystal habit, and particle morphology and element distribution. The crystal size, crystal habit and particle morphology were described according to Henning & Störr (1986).

For the quantification of element distribution, a calibration of k factors is mandatory (Cliff & Lorimer, 1975; Lorimer & Cliff, 1976; Mellini & Menichini, 1985). These k values are used to calibrate for the specific behaviour of particles against possible irradiation damage. The elements O, Na, Mg, Al, Si, K, Ca and Fe were quantified by applying the EDAX GENESIS–TEM Quant Materials quantification procedure.

In this procedure, the acquired EDX spectra are corrected by background subtraction, Gaussian deconvolution and k-factor corrections using values previously determined on a phyllosilicate standard (muscovite) and selected non-phyllosilicate standards. The average errors in the analyzed elements using the phyllosilicate standard, expressed as the atomic proportions, are 10 (Na), 5 (Fe, Mg, K, Ti, Ca) and 1 (Si, Al).

The measurement time per particle was lowered to 20 s and the exposed area was limited to a 50 nm diameter, avoiding possible irradiation damage of particles. The stability of particles of the sample series was tested for this measurement time at the beginning of any measurement campaign.

Further methodological details related to TEM-EDX-measurements and the Excel-based mathematical procedure using TEM-EDX data for calculation of mineral formulae are described in Hoang-Minh et al. (2019).

These mathematical procedures described in Hoang-Minh et al. (2019) were extended by k-means clustering method for finding subgroups of observations within a data set. The data were standardized (i.e., scaled) to make variables comparable. Euclidean distances were applied as classical method for distance measures. The optimal clusters were determined by Elbow method and Gap statistics[15].

---

[15] *https://uc-r.github.io/kmeans_clustering*

Data Sheet – B25 No0_B (< 2 µm), treated material *(OPA, 100°C, 110 hrs)*

Preparation for TEM

- raw material: compacted material (1.6 g/cm³) of treated B25-sample (OPA, 100°C, 110 hrs)
- suspension on particles < 2 µm on carbon-filmed Cu-grid
- air-dried and humidity-controlled storing

Mineral Matter

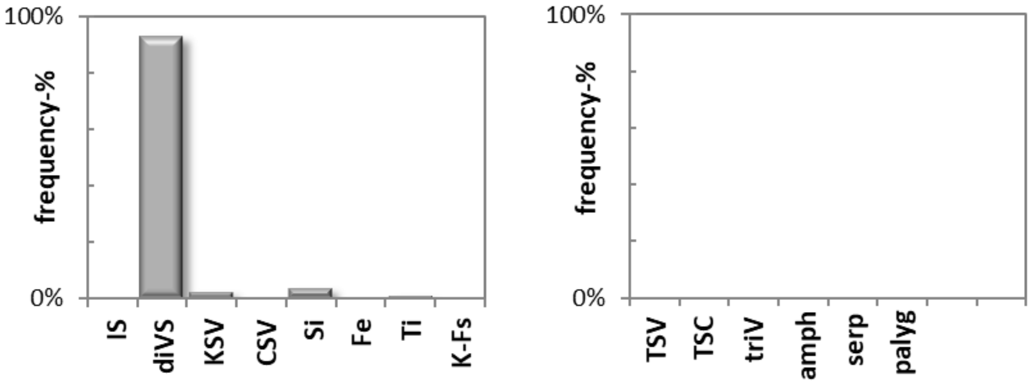

Fig. 1. *Distribution of mineral groups in fraction < 2 µm (in frequency-%)*
Legend: ***IS*** *– illite-smectite-mixed layer series in sense of Środon et al. (1992), diVS – dioctahedral vermiculite-smectite illite-smectite-mixed layer series (= charge- and/or K-deficit),* ***KSV*** *– kaolinite-smectite-dioctahedral vermiculite-mixed layer series,* ***CSV*** *– chlorite-saponite-trioctahedral vermiculite-mixed layer series,* ***Si*** *– quartz or particles with Si-surplus,* ***Fe*** *– Fe-oxide or Fe-oxyhydroxide,* ***Ti*** *– Ti-bearing phases (e.g. rutile, anatase),* ***K-Fs*** *– K-feldspar*

Clay Mineral Composition

All particles of smectite group:

$$Ca_{0.21}\ Mg_{0.04}\ Na_{0.02}\ K_{0.15}\quad Al_{1.14}\ Fe^{3+}_{0.61}\ Mg_{0.23}\ Ti_{0.01}\ (OH)_2\quad Si_{3.56}\ Al_{0.44}\ O_{10}$$

Charge: XII = 0.67 VI = 5.77 IV = 15.56 **Σ = 22.00**

Probability of smectite layers (%S): 35%

Probability of illite layers (%I): 65%

Specific Dissolution Potential (ΔS%)

for H2O, 20 + 60 rpm	-16	(= medium reacting, interlayer group: Ca+Mg (= type B))
for NaCl, 20 rpm	-18	(= medium reacting, interlayer group: Ca+Mg (= type B))
for NaCl, 60 rpm	-85	(= fast reacting, 'illitization', interlayer group: Na (= type A))
CEC$_{calc}$:	68 meq / 100 g	(literature: 56 meq / 100 g [Matschiavelli et al., 2019: MAT19])

Measured particles: 136

Table 1. *Summarized chemical composition*

SiO_2	TiO_2	Al_2O_3	Fe_2O_3	MnO	MgO	CaO	Na_2O	K_2O	P_2O_5	Σ	
58.7%	0.1%	23.2%	6.9%		3.5%	2.9%	0.2%	1.5%		0.97	measured particles
58.6%	0.0%	22.0%	5.9%		3.0%	1.0%	0.1%	1.1%	0.1%	0.92	measured particles of original B25

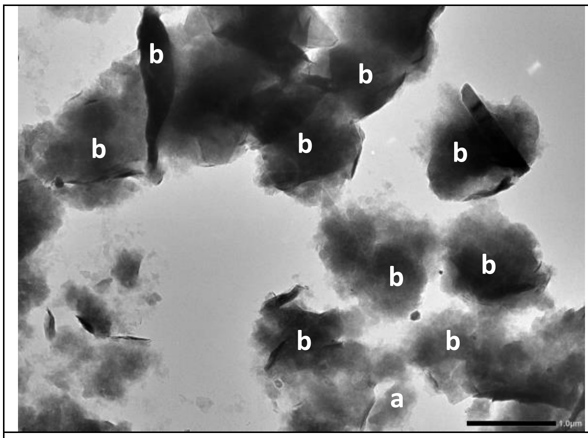	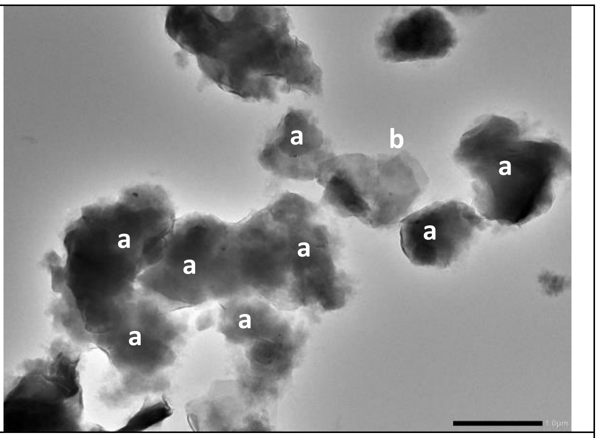
JEM-2100_No0-B_A6_X8000.bmp Magnification: 8k (z) aggregates formed by small (≤ 200 nm) xenomorphous plates; (aa) large (≤ 1 µm) xenomorph film-like platy crystals partially with folds	*JEM-2100_No0-B_A4_X8000.bmp* Magnification: 8k (a) aggregates formed by small (≤ 200 nm) xenomorphous plates partially with folds; (b) large (≤ 1 µm) xenomorph film-like platy crystals

Fig. 2. *Morphology of particles (TEM-micrographs)*

Distribution of smectite layers probability (%S)

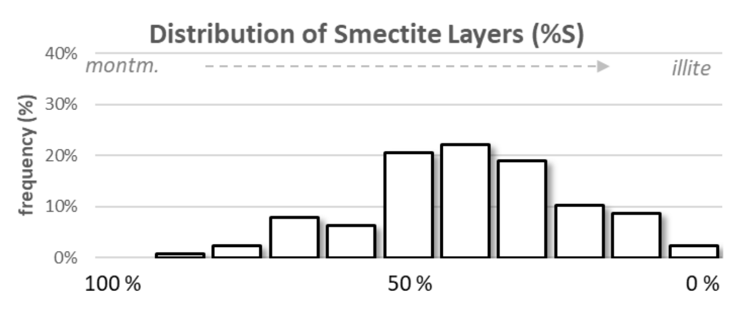

Description: *The distribution of %S-probability indicates the occurrence of two groups: (i) mixture of beidellite-montmorillonite interstratifications (= assumption) with diVS-ml as well as (ii) illite with K-deficiency.*

Fig. 3a. *Distribution of smectite layers probability (%S)*

Differentiation by relation "Octahedral Mg vs. tetrahedral Si"?

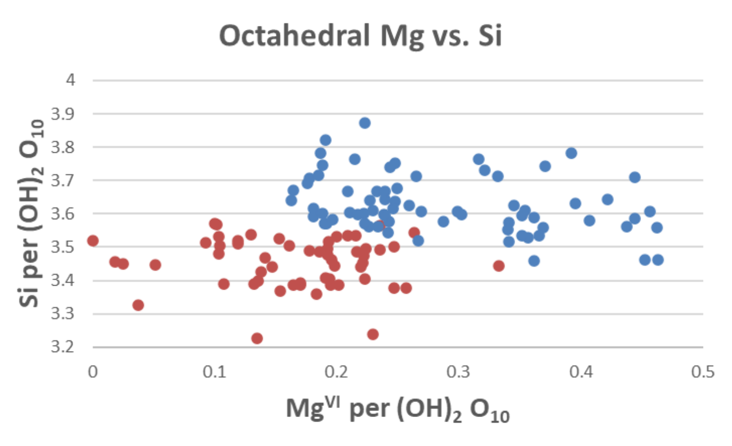

Description: *This diagram indicates the occurrence of two groups of Mg in relation to tetrahedral Si. Probably, this distribution mirrors 2 phases (I) beidellite-montmorillonite interstratifications (blue) and (II) diVS-ml (red)*

Fig. 3b. *Distribution of octahedral Mg vs. tetrahedral Si [all per$(OH)_2 O_{10}$]*

Distribution of K in relation to tetrahedral Si

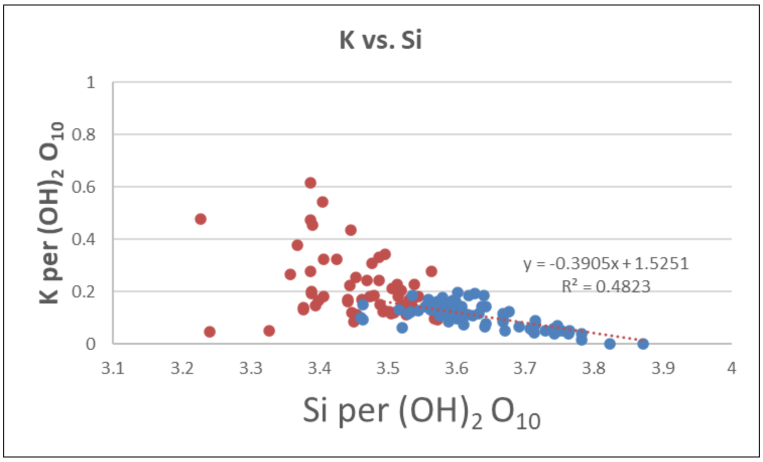

Description: *This diagram visualizes possible particles (beidellite-montmorillonite interstratification?) with a very low K (blue dots) and particles (diVS-ml ?) with an increased K-amount (red dots)*

Fig. 4. *Distribution of K in interlayer space vs. tetrahedral Si [all per(OH)$_2$ O$_{10}$]*

Distribution of charges (exchangeable from interlayer space)

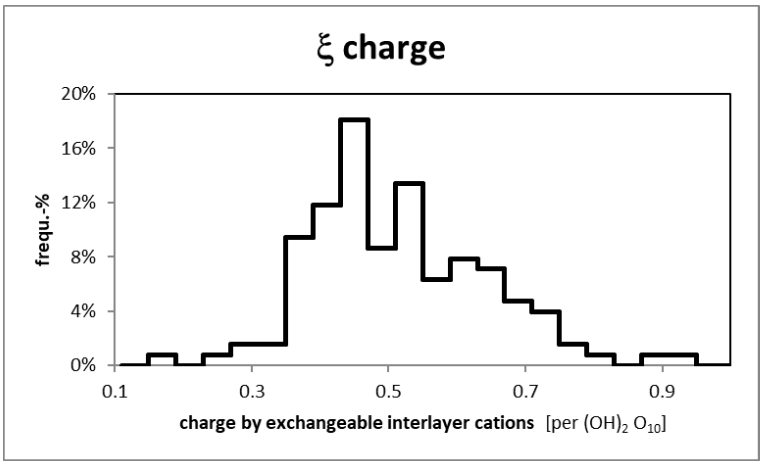

This diagram visualizes the distribution of exchangeable charges in the interlayer space (Ca, Mg, Na) determined and computed by TEM-EDX-data.

Description: *Broad charge density distribution with a maximal frequency-% of charge density at 0.45 per (OH)$_2$ O$_{10}$.*

Fig. 5. *Distribution of charges*

Beidellite-Montmorillonite interstratification (BM ~ 50%:50%) *(Cluster2):*

$$Ca_{0.24}\ Mg_{0.03}\ Na_{0.01}\ K_{0.11}\quad Al_{1.12}\ Fe^{3+}_{0.59}\ Mg_{0.28}\ Ti_{0.01}\ (OH)_2\quad Si_{3.63}\ Al_{0.37}\ O_{10}$$

Charge: XII = 0.65 VI = 5.72 IV = 15.63 **Σ = 22.00**

Measured particles: 71

Distribution of BM-interstratifications (Cluster2)

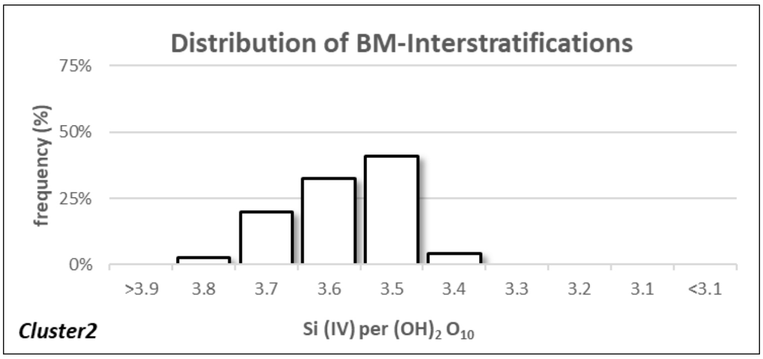

Description: *The distribution of BM-interstratifications (classified as Cluster2) draws a maximum of frequency (%) at tetrahedral Si-value between 3.5 – 3.7 e phuc*

Fig. 6a. *Distribution of assumed beidellite-montmorillonite interstratifications*

BM	particles (abs)	Ca (XII)	Mg (XII)	Na (XII)	K (XII)	Cr3+ (VI)	Al (VI)	Fe3+ (VI)	Mg (VI)	Ti (VI)	Al (IV)	Si (IV)	XII	n_VI	%S
Si >3.9	n = 0														
Si 3.9-3.8	n = 2	0.11	0.07	0.00	0.00	0.00	1.36	0.42	0.21	0.01	0.15	3.85	0.4	2.0	79
Si 3.8-3.7	n = 14	0.22	0.02	0.00	0.05	0.00	1.20	0.52	0.28	0.01	0.26	3.74	0.5	2.0	61
Si 3.7-3.6	**n = 23**	**0.22**	**0.03**	**0.01**	**0.12**	**0.00**	**1.11**	**0.62**	**0.26**	**0.00**	**0.36**	**3.64**	**0.6**	**2.0**	**45**
Si 3.6-3.5	**n = 29**	**0.26**	**0.02**	**0.01**	**0.14**	**0.00**	**1.08**	**0.62**	**0.30**	**0.01**	**0.43**	**3.57**	**0.7**	**2.0**	**36**
Si 3.5-3.4	n = 3	0.40	0.02	0.00	0.11	0.00	0.96	0.60	0.43	0.01	0.54	3.46	0.9	2.0	24
Si 3.4-3.3	n = 0														
Si 3.3-3.2	n = 0														
Si 3.2-3.1	n = 0														
Si <3.1	n = 0														

Fig. 6b. *Computed averaged mineral formulae of phases in the different Si(IV)-classes*

Dioctahedral Vermiculite-Smectite mixed layer phases (diVS-ml) *(Cluster1):*

$$Ca_{0.17}\,Mg_{0.06}\,Na_{0.03}\,K_{0.22}\quad Al_{1.17}\,Fe^{3+}_{0.65}\,Mg_{0.17}\,Ti_{0.01}\,(OH)_2\quad Si_{3.45}\,Al_{0.55}\,O_{10}$$

Charge: XII = 0.71 VI = 5.84 IV = 15.45 **Σ = 22.00**

Probability of smectite layers (%S): 23%

Probability of illite layers (%I): 77%

Measured particles: 56

Distribution of smectite layers probability (%S) in diVS-ml (Cluster1)

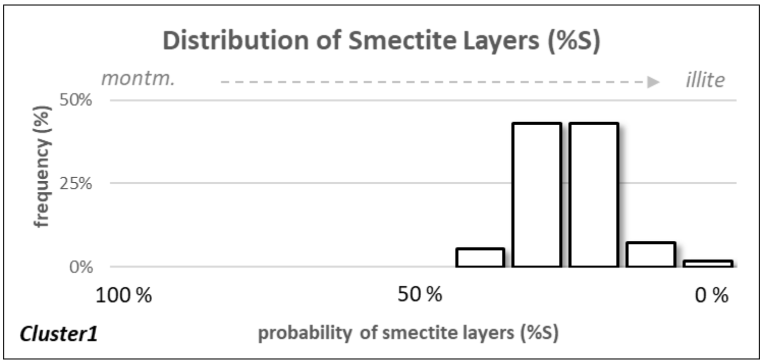

Description: *The distribution of diVS-ml (classified as Cluster1) draws a maximum of frequency (%) for smectite layer probability at 20-30%*

Fig. 7a. *Distribution of smectite layers probability in diVS-ml*

diVS-ml	particles (abs)	Ca (XII)	Mg (XII)	Na (XII)	K (XII)	Cr3+ (VI)	Al (VI)	Fe3+ (VI)	Mg (VI)	Ti (VI)	Al (IV)	Si (IV)	XII	n_VI	%S
%S >95%	n = 0														
%S 95-85%	n = 0														
%S 85-75%	n = 0														
%S 75-65%	n = 0														
%S 65-55%	n = 0														
%S 55-45%	n = 0														
%S 45-35%	n = 3	0.12	0.07	0.02	0.16	0.00	1.22	0.62	0.15	0.01	0.43	3.57	0.6	2.0	36
%S 35-25%	**n = 24**	**0.17**	**0.05**	**0.02**	**0.19**	**0.00**	**1.11**	**0.71**	**0.17**	**0.01**	**0.49**	**3.51**	**0.6**	**2.0**	**29**
%S 25-15%	**n = 24**	**0.17**	**0.05**	**0.04**	**0.26**	**0.00**	**1.22**	**0.60**	**0.17**	**0.01**	**0.58**	**3.42**	**0.7**	**2.0**	**19**
%S <15%	n = 5	0.16	0.13	0.02	0.24	0.00	1.22	0.63	0.15	0.00	0.70	3.30	0.8	2.0	10

Fig. 7b. *Computed averaged mineral formulae of diVS-ml phases in the different smectite layers probability (%S)-classes*

Description – B25 No0_B (< 2 µm), treated material *(OPA, 100°C, 110 hrs)*

Preparation for TEM

The powder of compacted and treated B25-No0_B-sample was suspended in deionized water and dispersed by ultrasonic treatment for approximately 20 min. The clay fraction (<2 µm) was separated by sedimentation and diluted with deionized water to get a clear suspension. The suspension was dropped onto carbon-coated Cu grids, air dried and stored under environment-controlled conditions at 45% humidity.

Mineral Matter - Overview

The fraction < 2 µm of treated B25 bentonite sample (Opalinus Clay solution, at 100°C, for 110 hours) is mainly composed by assumed beidellite-montmorillonite interstratifications dominated by beidellite layers, abbreviated as BM-ml, and dioctahedral vermiculite-smectite mixed layer phases (diVS-ml) and accompanied by two types of illite. Furthermore, kaolinite and Si-surplus particles (Si, e.g. quartz) were identified in traces in this sample [fig. 1].

	frequency-% *(n = 136 measured particles)*
BM-ml (Cluster2)	52%
diVS-ml (Cluster1)	41%
Kaolinite & KSV-ml	2%
Si-surplus	4%
Ti-phases	1%

All measured clay mineral phases summarized result following mineral formula computed from TEM-EDX-measurement of 127 individual particles (BM, diVS-ml):

$$\mathrm{Ca^{2+}_{0.21}\ Mg^{2+}_{0.04}\ Na^{+}_{0.02}\ K^{+}_{0.15}\ \ Al^{3+}_{1.15}\ Fe^{3+}_{0.61}\ Mg^{2+}_{0.23}\ Ti^{4+}_{0.01}\ (OH)_2\ \ Si^{4+}_{3.56}\ Al^{3+}_{0.44}\ O_{10}}$$

SDOM *± 0.00 ± 0.00 ± 0.00 ± 0.00 ± 0.00 ± 0.00 ± 0.00 ± 0.00 ± 0.00 ± 0.00*

Legend: SDOM - standard deviation of the mean (= the standard deviation divided by the square root of the number of samples)

The interlayer charge is calculated as 0.67 per $(OH)_2\ O_{10}$ and the octahedral charge as 5.77 per $(OH)_2\ O_{10}$. The particles are characterized by a high octahedral Fe-amount.

The summarized chemical composition of all 127 computed particles is compared with measured data of original B25-bentonite sample [tab. 1]. The chemical composition averaged by measured particles show especially a higher amount of Fe_2O_3, MgO, CaO and K_2O in comparison to the measured data of original untreated B25-bentonite.

B25-No0_B sample is characterized by three morphological groups: (i) aggregates formed by small (≤ 200 nm) xenomorphous plates, (ii) large (≤ 1 µm) xenomorph film-like platy crystals partially with folds [fig. 2], (iii) aggregates formed by idiomorph hexagonal plates (≤ 200 nm). Thin aggregates formed by small (≤ 200 nm) xenomorphous plates dominate the shapes of particles in the micrographs [fig. 2].

The distribution of %S-probability of all measured clay mineral phases [fig. 3a] also indicates the occurrence of two groups: (i) as main group a mixture of beidellite-montmorillonite interstratifications and diVS-ml and (ii) illite with K- and charge deficit (%S-class = 10%).

The numerous measured particles by TEM-EDX allow a visualization of distribution of interlayer charges. Considering the TEM-EDX-determined cations Ca^{++}, Mg^{++} and Na^{+} and then computed their ratio as interlayer cations in the mineral formula, Ca^{++}, Mg^{++} and Na^{+} offer to characterize the degree of exchangeable charges in the interlayer space. This charge density of treated B25 bentonite (< 2 µm) shows a broad interval at the maximal frequency-% of charge density at 0.45 per $(OH)_2$ O_{10} [fig. 5]. This broad interval of interlayer charge density caused by exchangeable cations from 0.37 – 0.50 per $(OH)_2$ O_{10} represents mainly the BM-phases. Also, the measured diVS-ml phases offer only a reduced number of exchangeable cations at 0.30 – 0.87 per $(OH)_2$ O_{10}.

Mineral Matter - Specification

Result of Clustering

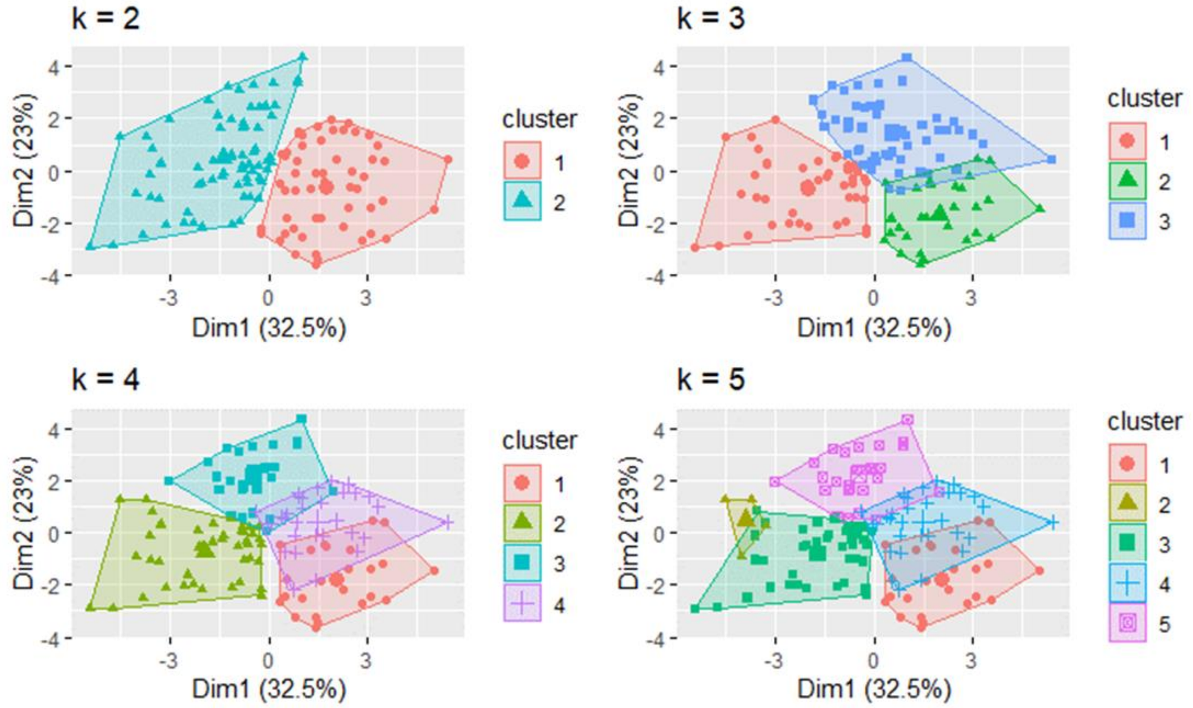

Fig. 8. *Clustering of all measured particles for clusters k = 2, k = 3, k = 4 and k = 5 (source for R-coding: https://uc-r.github.io/kmeans_clustering)*

		Ca (XII)	Mg (XII)	Na (XII)	K (XII)	Cr3+ (VI)	Al (VI)	Fe3+ (VI)	Mg (VI)	Ti (VI)	Al (IV)	Si (IV)	XII	n_VI	%S
Cluster1	n = 56	0.17	0.06	0.03	0.22	0.00	1.17	0.65	0.17	0.01	0.55	3.45	0.70	2.0	23
Cluster2	n = 71	0.24	0.03	0.01	0.11	0.00	1.12	0.59	0.28	0.01	0.37	3.63	0.65	2.0	44

Fig. 9a. *Mineral formulae based on TEM-EDX-data summarized following the result of clustering for k=2*

	Sybilla-results	**TEM-EDX-results**	**Notes**
Cluster2	IS R0(1) *(%S = 100%)*	BM-ml *(%B = 74%)*	*XRD: Montmorillonite and beidellite are only to distinguish by Green-Kelly-test (not available here).*
Cluster1	IS R0(2) *(%S = 25%)*	diVS-ml *(%S = 23%)*	*high K-deficit, Fe(VI)-rich*

Tab. 2a. *Comparison of results from TEM-EDX- and XRD-measurements with clustering procedure*

The clustering of TEM-EDX-data offers a good agreement with the recent result of Sybilla-processing of XRD-traces from oriented specimen [tab. 2].

IS R0 (1): The X-ray diffraction pattern of the ethylene-glycol saturated oriented specimen shows a full expandability to 1.7 nm and a difference of 5.42°2θ between 2. and 3. order of smectite interferences. This distance is typically for montmorillonite (Moore & Reynolds, 1989). This result of XRD-processing let expect a maximum of particles for %S ~ 100% by TEM-EDX-measurements, but the maximum of particles measured by TEM-EDX is to find at %S=70% [fig. 3a].

Montmorillonite and beidellite have the same behavior concerning the expandability and they are only to distinguish by XRD using Li like by Greene-Kelly test (Green-Kelly 1952, 1953). So, combination of XRD- and TEM-results (full expandability by XRD and Si ~ 3.63 by TEM-EDX) led conclude the occurrence of ‘beidellite-montmorillonite interstratifications’, a beidellite-montmorillonite interstratification with about 75% beidellite and 25% montmorillonite layers (BM-ml 75:25).

IS R0 (2): The Sybilla-procedure of XRD-traces (oriented mounts) has shown an occurrence of a second illite-smectite mixed layer phase with a smectite layers probability of %S = 25%. This situation is to find in Cluster1 (%S_{TEM} = 23%) representing a high K-. but low charge deficient and very Fe-rich dioctahedral vermiculite-smectite mixed layer phase (diV-ml) [tab. 2].

The Sybilla-processing of XRD-traces (oriented mounts) also supports the existence of kaolinite and kaolinite-smectite mixed layer phases in fine fraction of sample. Such phases were not to identify or to calculate in TEM-EDX-database (a grain size effect?).

Additional Notes:

The Average Silhouette Method calculated k = 5 as optimum of clusters. These five clusters are not to recognize or to differentiate by Sybilla procedure of XRD-data.

		Ca (XII)	Mg (XII)	Na (XII)	K (XII)	Cr3+ (VI)	Al (VI)	Fe3+ (VI)	Mg (VI)	Ti (VI)	Al (IV)	Si (IV)	XII	n_VI	%S
Cluster1	n = 24	0.13	0.06	0.03	0.28	0.00	1.40	0.46	0.14	0.00	0.56	3.44	0.7	2.0	22
Cluster2	n = 4	0.28	0.00	0.01	0.04	0.00	1.18	0.50	0.30	0.00	0.26	3.74	0.6	2.0	61
Cluster3	n = 40	0.18	0.04	0.01	0.10	0.00	1.18	0.60	0.22	0.01	0.34	3.66	0.6	2.0	48
Cluster4	n = 32	0.19	0.06	0.03	0.17	0.00	0.98	0.81	0.19	0.01	0.53	3.47	0.7	2.0	25
Cluster5	n = 27	0.33	0.01	0.00	0.12	0.00	1.04	0.58	0.37	0.01	0.44	3.56	0.8	2.0	35

Fig. 9b. *Mineral formulae based on TEM-EDX-data summarized following the result of clustering for k=5*

	Sybilla-results	TEM-EDX-results	Notes
Cluster1	IS R0(2) *(%S = 25%)*	diVS-ml *(%S = 22%)*	*K-deficit, Al(VI)- & Fe(VI)-rich*
Cluster4		diVS-ml *(%S = 25%)*	*high K-deficit, low Al(VI), very Fe(VI)-rich*
Cluster5		diVS-ml *(%S = 35%)*	*high K-deficit, low Al(VI), highest Mg(VI), high Fe(VI)*
Cluster2	IS R0(1) *(%S=100%)*	BM ~50:50	*XRD: Montmorillonite and beidellite is only to distinguish by Green-Kelly-test (not available here).*
Cluster3		BM ~70:30	

Tab. 2b. *Comparison of results from TEM-EDX- and XRD-measurements with clustering procedure in case k = 5*

Specifics to the identified clay mineral groups

Beidellite-montmorillonite interstratifications (B:M ~70:30)

44 of 127 measured particles belong so to this assumed classification. The dioctahedral character of this group is proofed by X-ray diffraction. The position of the large (060)-interference of smectite is in the random oriented powder specimen at 1.497 Å.

Montmorillonite and beidellite have the same behavior concerning the expandability and they are only to distinguish by XRD using Li by means of Greene-Kelly test (Green-Kelly 1952, 1953). So, combination of XRD- and TEM-results (full expandability by XRD and Si ~ 3.66 by TEM-EDX) led conclude the occurrence of 'beidellite-montmorillonite interstratifications', a beidellite-montmorillonite interstratification with about 70% beidellite and 30% montmorillonite layers (BM-ml 70:30).

Beidellite-montmorillonite interstratifications (B:M ~70:30):

$$Ca_{0.19}\ Mg_{0.04}\ Na_{0.01}\ K_{0.10}\quad Al_{1.18}\ Fe^{3+}_{0.59}\ Mg_{0.23}\ Ti_{0.01}\ (OH)_2\quad Si_{3.66}\ Al_{0.34}\ O_{10}$$

Charge: XII = 0.56 VI = 5.78 IV = 15.66 **Σ = 22.00**

Measured particles by TEM-EDX: 71
Result of clustering: Clustera 2+3 [tab. 2a]

Beidellitic structures are characterized by a low octahedral Mg-amount (because of high ratio of octahedral, 3-valent cations). A comparison of octahedral Mg vs. tetrahedral Si indicates the occurrence of two groups for octahedral Mg based on TEM-EDX-data [fig. 3b].

Using the results of clustering (see Cluster 2+3 in tab. 2a), the maximum of frequency-% is to find for particles in the Si(IV)-class 3.5 – 3.7 e phuc [tab. 6a], representing the mentioned relation 50% montmorillonite and 50% beidellite as ratio of interstratification. The mineral formulae, summarized in classes of tetrahedral Si, draw for the maximum an Fe-rich BM 70:20 phase with low K, but remarkable amount of Mg in the interlayer space [tab. 6b].

Dioctahedral vermiculite-smectite mixed layer phase (diVS-ml):

$$Ca_{0.22}\ Mg_{0.04}\ Na_{0.02}\ K_{0.19}\quad Al_{1.12}\ Fe^{3+}_{0.63}\ Mg_{0.24}\ Ti_{0.01}\ (OH)_2\quad Si_{3.49}\ Al_{0.51}\ O_{10}$$

Charge: XII = 0.74 VI = 5.77 IV = 15.49 **Σ = 22.00**
Probability of smectite layers (%S): 27%
Probability of illite layers (%I): 73%

Measured particles by TEM-EDX: 83
Result of clustering: Clusters 1, 4 + 5 [tab. 2a]

Illite as part of diVS-ml series

The Rietveld refinement by Profex software (Döbelin & Kleeberg, 2015) indicates the occurrence of two polytypes for illite in treated B25 bentonite: $2M_1$- and 1M-polytype.

Kaolinite-montmorillonite mixed layer phases

The Excel-based procedure (Hoang-Minh et al., 2019) to identify possible clay mineral groups using the TEM-EDX-measurements also includes algorithms to classify kaolinite and kaolinite-montmorillonite mixed layer phases. These algorithms couldn't identify such phases basing on the measured TEM-EDX-data. Otherwise, few particles, which were not to compute, have shown small hexagonal plates typically for kaolinite-bearing phases.

References

Cliff, G. & Lorimer, G. W. (1975). *J. Microsc.* **103**, 203–207.

Döbelin, N., Kleeberg, R. (2015). *Journal of Applied Crystallography* **48**, 1573-1580. DOI: 10.1107/S1600576715014685

Henning, K.-H. & Störr, M. (1986). Electron Micrographs (TEM, SEM) of Clays and Clay Minerals, p. 325. Akademie-Verlag Berlin.

Hoang-Minh, T., Kasbohm, J., Nguyen-Thanh, L., Nga, P. T., Lai, L. T., Duong, N. T., Thanh, N. D., Thuyet, N. T. M., Anh, D. D., Pusch, R., Knutsson, S. & Ferreiro Mahlmann, R. (2019). *J. Appl. Cryst.* **52**, 133-147. DOI: 10.1107/S1600576718018162

Lorimer, G. W. & Cliff, G. (1976). *Electron Microscopy in Mineralogy*, edited by H. R. Wenk, pp. 506–519. Berlin: Springer Verlag.

Matschiavelli, N., Kluge, S., Podlech, C., Standhaft, D., Grathoff, G., Ikeda-Ohno, A., Warr, L.N., Chukharkina, A., Arnold, T. & Cherkouk, A. (2019). *Environmental Science & Technology.* **53** (17), 10514-10524, DOI: 10.1021/acs.est.9b02670

Mellini, M. & Menichini, R. (1985). *R. Soc. Ital. Miner. Petrol.* **40**, 261–266.

Moore, D.M., Reynolds, R.C. (1989). X-ray Diffraction and the Identification and Analysis of Clay Minerals, Oxford University Press, New York, 332 + xvi pp.

Nguyen-Thanh, L., Herbert, H.-J., Kasbohm, J., Hoang-Minh, T. & Mählmann, R. F. (2014). *Clays Clay Miner.* **62**, 425–446.

Środoń, J., Elsass, F., McHardy, W. J. & Morgan, D. J. (1992). *Clay Miner.* **27**, 137–158.

Data Sheet – B25 bentonite, treated materials *(OPA, 125 °C, VSD)*

Methodology - Transmission electron microscopy linked with energy-dispersive X-ray spectroscopy (TEM-EDX)

It is expected a characterization of clay mineral phases in treated B25 bentonite by transmission electron microscopy. The sample No15 represents a percolation of B25 bentonite by Opalinus Clay solution at 125°C for 285 hours.

The different clay mineral phases are to identify and to describe by chemical composition and its variability, morphology, the specific dissolution potential, and further parameter.

Such further parameter like distribution of smectite layers probability (%S) and distribution of charges caused by exchangeable cations interlayer space should serve as additional indicators for mineralogical alterations in treatment experiments with B25 bentonite.

The sample were suspended for TEM-measurement in deionized water and dispersed by ultrasonic treatment for approximately 20 min. The clay fraction (<2 µm) was separated by sedimentation and diluted with deionized water to get a clear suspension. The suspension was dropped onto carbon-coated Cu grids, air dried and stored under environment-controlled conditions at 45% humidity.

TEM-EDX investigations were carried out on the <2 µm fraction using a FEI TECNAI G^2 20 electron transmission microscope at the VNU University of Science, Vietnam National University, Hanoi. This equipment (operated at 200 kV with LaB_6 cathode) was combined with an S-TWIN objective, a windowless EDAX energy-dispersive X-ray system and a FEI Eagle 2k CCD TEM camera.

About 100 individual clay particles per sample were characterized by TEM-EDX with respect to crystal size, crystal habit, and particle morphology and element distribution. The crystal size, crystal habit and particle morphology were described according to Henning & Störr (1986).

For the quantification of element distribution, a calibration of k factors is mandatory (Cliff & Lorimer, 1975; Lorimer & Cliff, 1976; Mellini & Menichini, 1985). These k values are used to calibrate for the specific behavior of particles against possible irradiation damage. The elements O, Na, Mg, Al, Si, K, Ca and Fe were quantified by applying the EDAX GENESIS–TEM Quant Materials quantification procedure.

In this procedure, the acquired EDX spectra are corrected by background subtraction, Gaussian deconvolution and k-factor corrections using values previously determined on a phyllosilicate standard (muscovite) and selected non-phyllosilicate standards. The average errors in the analyzed elements using the phyllosilicate standard, expressed as the atomic proportions, are 10 (Na), 5 (Fe, Mg, K, Ti, Ca) and 1 (Si, Al).

The measurement time per particle was lowered to 20 s and the exposed area was limited to a 50 nm diameter, avoiding possible irradiation damage of particles. The stability of particles of the sample series was tested for this measurement time at the beginning of any measurement campaign.

Further methodological details related to TEM-EDX-measurements and the Excel-based mathematical procedure using TEM-EDX data for calculation of mineral formulae are described in Hoang-Minh et al. (2019).

These mathematical procedures described in Hoang-Minh et al. (2019) were extended by k-means clustering method for finding subgroups of observations within a data set. The data were standardized

(i.e., scaled) to make variables comparable. Euclidean distances were applied as classical method for distance measures. The optimal clusters were determined by Elbow method and Gap statistics[16].

---

[16] *https://uc-r.github.io/kmeans_clustering*

Data Sheet – B25 No15 (< 2 µm), treated material *(OPA, 125°C, 98.6 hrs)*

Preparation for TEM

- raw material: compacted material (1.6 g/cm³) of treated B25-sample (OPA, 125°C, 98.6 hrs)
- suspension on particles < 2 µm on carbon-filmed Cu-grid
- air-dried and humidity-controlled storing

Mineral Matter

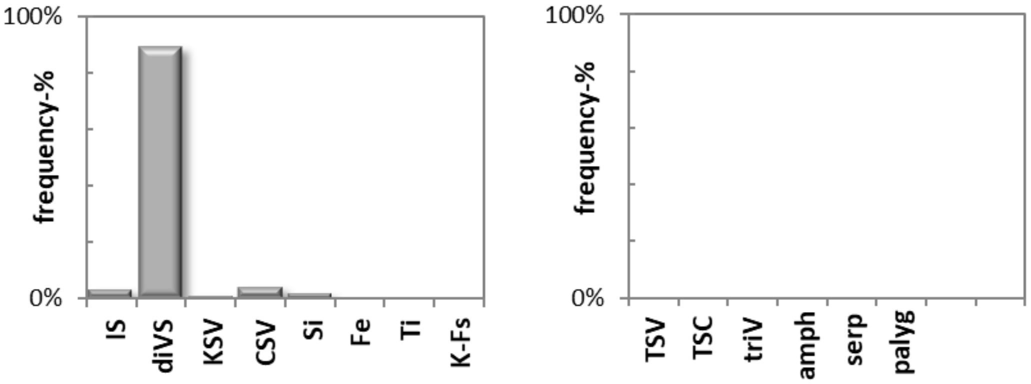

Fig. 1. *Distribution of mineral groups in fraction < 2 µm (in frequency-%)*
Legend: ***IS*** *– illite-smectite-mixed layer series in sense of Środon et al. (1992),* *diVS – dioctahedral vermiculite-smectite illite-smectite-mixed layer series (= charge- and/or K-deficit),* ***KSV*** *– kaolinite-smectite-dioctahedral vermiculite-mixed layer series,* ***CSV*** *– chlorite-saponite-trioctahedral vermiculite-mixed layer series,* ***Si*** *– quartz or particles with Si-surplus,* ***Fe*** *– Fe-oxide or Fe-oxyhydroxide,* ***Ti*** *– Ti-bearing phases (e.g. rutile, anatase),* ***K-Fs*** *– K-feldspar*

Clay Mineral Composition

All particles of smectite group:

$$Ca_{0.14}\,Mg_{0.05}\,Na_{0.03}\,K_{0.17}\quad Al_{1.21}\,Fe^{3+}_{0.58}\,Mg_{0.20}\,Ti_{0.01}\,(OH)_2\quad Si_{3.59}\,Al_{0.41}\,O_{10}$$

Charge:	XII = 0.57	VI = 5.84	IV = 15.59	**Σ = 22.00**
Probability of smectite layers (%S):	39%			
Probability of illite layers (%I):	61%			

Specific Dissolution Potential (ΔS%)

for H2O, 20 + 60 rpm	-19	(= fast reacting, interlayer group: Ca+Mg (= type B))
for NaCl, 20 rpm	-21	(= fast reacting, interlayer group: Ca+Mg (= type B))
for NaCl, 60 rpm	-67	(= fast reacting, ‘illitization’, interlayer group: Na (= type A))
CEC_{calc}:	56 meq / 100 g	(literature: 56 meq / 100 g [Matschiavelli et al., 2019: MAT19])

Measured particles: 152

Table 1. *Summarized chemical composition*

SiO_2	TiO_2	Al_2O_3	Fe_2O_3	MnO	MgO	CaO	Na_2O	K_2O	P_2O_5	Σ	
61.6%	0.2%	24.6%	6.7%		3.3%	1.6%	0.3%	1.6%	0.1%	1.00	measured particles
63.8%	0.0%	23.9%	6.5%		3.3%	1.1%	0.1%	1.2%	0.1%	1.00	measured particles of original B25

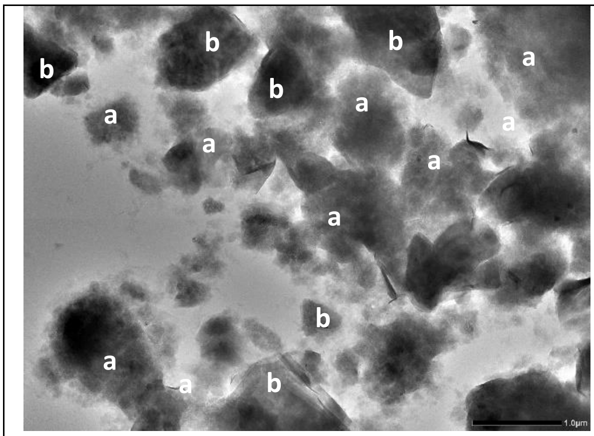	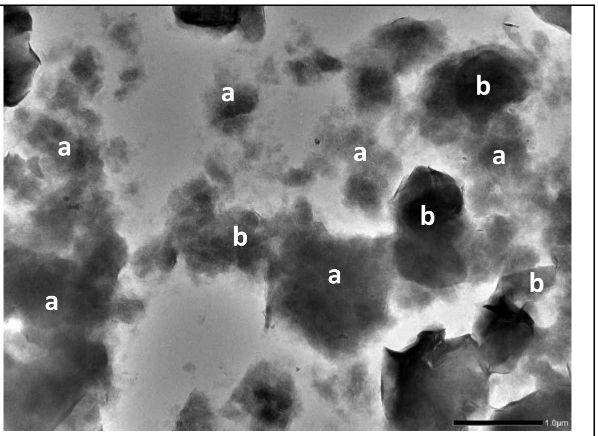
JEM-2100_MAG_X8000_027_No15.bmp Magnification: 8k (bb) aggregates formed by small (≤ 200 nm) xenomorphous plates; (cc) large (≤ 1 µm) xenomorph film-like platy crystals	*JEM-2100_MAG_X8000_031_No15.bmp* Magnification: 8k (m) aggregates formed by small (≤ 200 nm) xenomorphous plates; (n) large (≤ 1 µm) xenomorph film-like platy crystals, partially with folds

***Fig. 2.** Morphology of particles (TEM-micrographs)*

Distribution of smectite layers probability (%S)

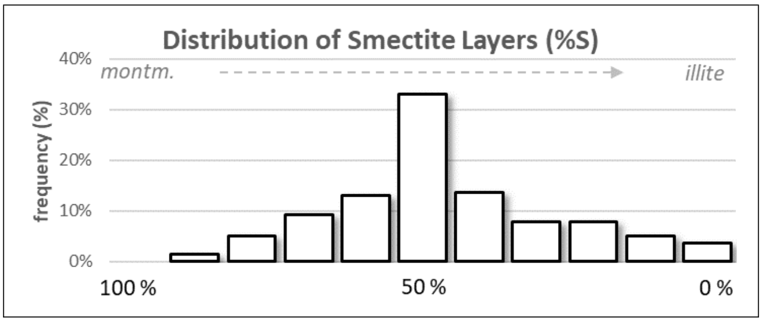

***Description:** The distribution of %S-probability indicates the occurrence of two groups: (i) diVS-ml as well as (ii) illite with K-and charge deficiency.*

***Fig. 3a.** Distribution of smectite layers probability (%S)*

Differentiation by relation “Octahedral Mg vs. tetrahedral Si”?

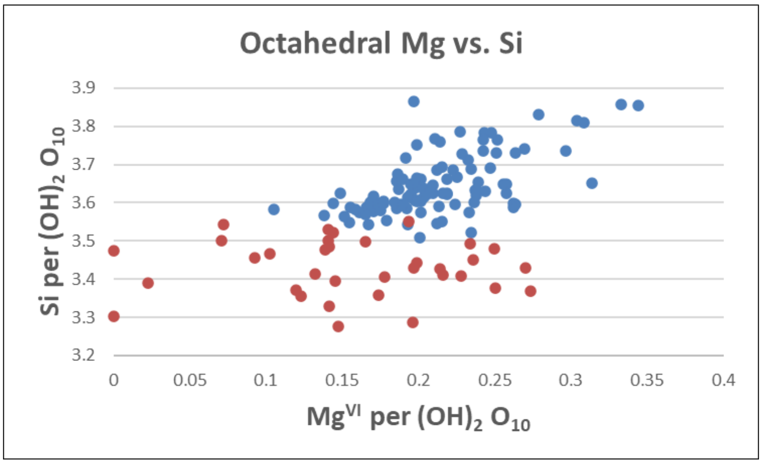

***Description:** This diagram indicates the occurrence of two groups of Mg in relation to tetrahedral Si. Probably, this distribution mirrors 2 phases (I) beidellitic diVS-ml with Mg(VI) > 0.15 per $(OH)_2$ O_{10} (blue) and (II) diVS-ml (red)*

***Fig. 3b.** Distribution of octahedral Mg vs. tetrahedral Si [all per$(OH)_2$ O_{10}]*

Distribution of K in relation to tetrahedral Si

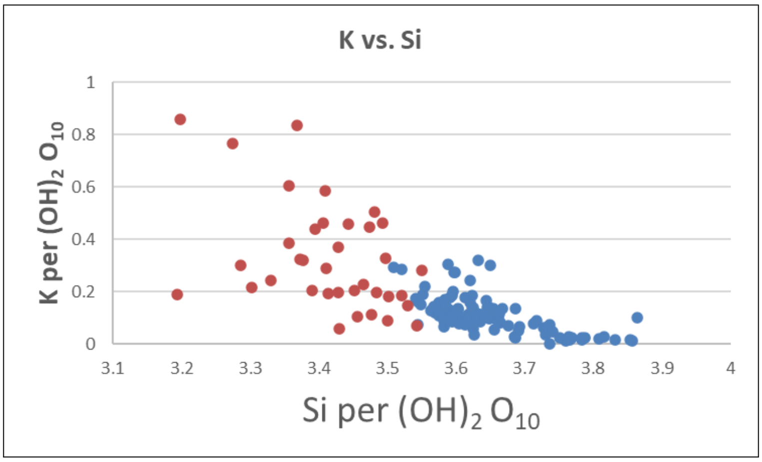

Description: *This diagram visualizes possible particles (beidellitic diVS-ml) with low K (blue dots) and diVS-ml with a broad interval of K (red dots)*

Fig. 4. *Distribution of K in interlayer space vs. tetrahedral Si [all per(OH)$_2$ O$_{10}$]*

Distribution of charges (exchangeable from interlayer space)

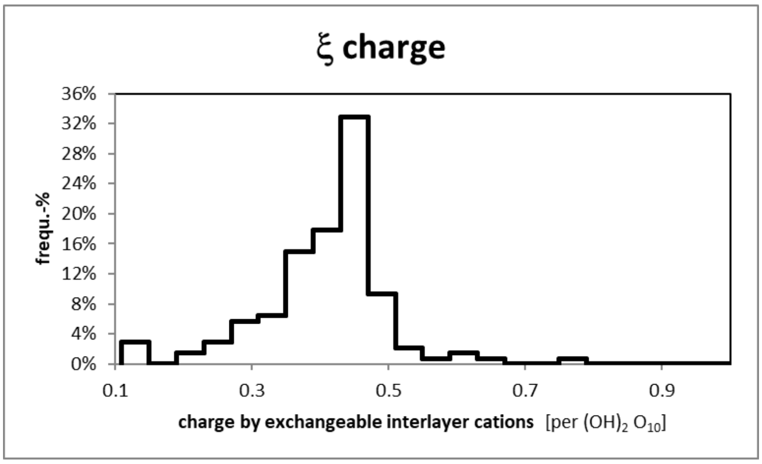

This diagram visualizes the distribution of exchangeable charges in the interlayer space (Ca, Mg, Na) determined and computed by TEM-EDX-data.

Description: *Maximal distribution of charge density at 0.47 per (OH)$_2$ O$_{10}$ for both Clusters*

Fig. 5. *Distribution of charges*

Beidellitic dioctahedral Vermiculite-Smectite mixed layer phases (beid. diVS-ml** BMI 05:55:40**) (Cluster1):

$Ca_{0.15}\ Mg_{0.05}\ Na_{0.03}\ K_{0.11}\quad Al_{1.19}\ Fe^{3+}_{0.60}\ Mg_{0.21}\ Ti_{0.01}\ (OH)_2\quad Si_{3.65}\ Al_{0.35}\ O_{10}$

Charge: XII = 0.53 VI = 5.82 IV = 15.65 **Σ = 22.00**

Measured particles: 104

Distribution of beid. diVS-ml (Cluster1)

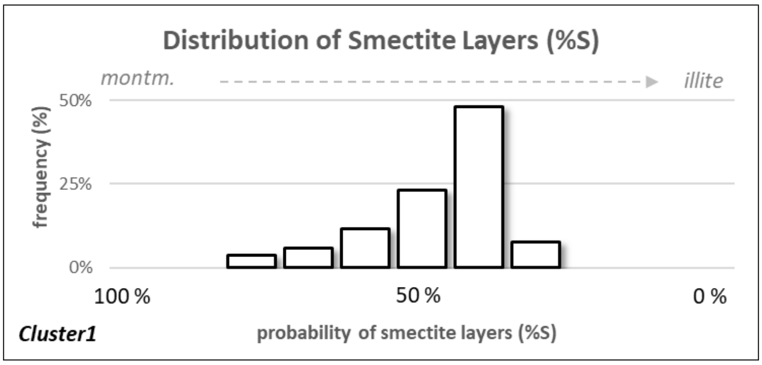

Description: *The distribution of beidellitic diVS-ml (classified as Cluster1) draws a maximum of frequency (%) for smectite layer probability at 40%*

Fig. 6a. *Distribution of assumed beidellitic diVS ml phases*

BMI 05:55:40	particles (abs)	Ca (XII)	Mg (XII)	Na (XII)	K (XII)	Cr3+ (VI)	Al (VI)	Fe3+ (VI)	Mg (VI)	Ti (VI)	Al (IV)	Si (IV)	XII	n_VI	%S
%S >95%	n = 0														
%S 95-85%	n = 0														
%S 85-75%	n = 4	0.16	0.01	0.01	0.04	0.00	1.24	0.48	0.29	0.01	0.15	3.85	0.39	2.0	80
%S 75-65%	n = 6	0.17	0.03	0.03	0.02	0.00	1.28	0.46	0.26	0.01	0.21	3.79	0.45	2.0	69
%S 65-55%	n = 12	0.16	0.02	0.03	0.04	0.00	1.23	0.54	0.24	0.00	0.26	3.74	0.44	2.0	61
%S 55-45%	n = 24	0.15	0.04	0.03	0.11	0.00	1.16	0.62	0.22	0.01	0.34	3.66	0.53	2.0	49
%S 45-35%	**n = 50**	**0.14**	**0.06**	**0.03**	**0.14**	**0.00**	**1.17**	**0.62**	**0.19**	**0.01**	**0.40**	**3.60**	**0.57**	**2.0**	**40**
%S 35-25%	n = 8	0.13	0.04	0.05	0.19	0.00	1.20	0.61	0.19	0.02	0.46	3.54	0.58	2.0	33
%S 25-15%	n = 0														
%S <15%	n = 0														

Fig. 6b. *Computed averaged mineral formulae of beid. diVS-ml phases in the different smectite layers probability (%S)-classes*

Dioctahedral Vermiculite-Smectite mixed layer phases (diVS-ml) *(Cluster2):*

$$Ca_{0.10}\ Mg_{0.07}\ Na_{0.03}\ K_{0.33}\quad Al_{1.28}\ Fe^{3+}_{0.54}\ Mg_{0.15}\ Ti_{0.03}\ (OH)_2\quad Si_{3.42}\ Al_{0.58}\ O_{10}$$

Charge: XII = 0.70 VI = 5.88 IV = 15.42 **Σ = 22.00**
Probability of smectite layers (%S): 19%
Probability of illite layers (%I): 81%
Measured particles: 36

Distribution of smectite layers probability (%S) in diVS-ml (Cluster2)

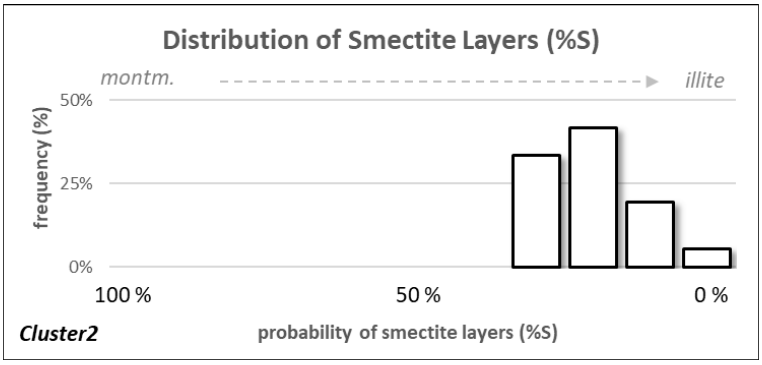

Description: *The distribution of diVS-ml (classified as Cluster2) draws a maximum of frequency (%) for smectite layer probability at 20%*

Fig. 7a. *Distribution of smectite layers probability in diVS-ml*

diVS-ml	particles (abs)	Ca (XII)	Mg (XII)	Na (XII)	K (XII)	Cr3+ (VI)	Al (VI)	Fe3+ (VI)	Mg (VI)	Ti (VI)	Al (IV)	Si (IV)	XII	n_VI	%S
%S >95%	n = 0														
%S 95-85%	n = 0														
%S 85-75%	n = 0														
%S 75-65%	n = 0														
%S 65-55%	n = 0														
%S 55-45%	n = 0														
%S 45-35%	n = 0														
%S 35-25%	**n = 12**	**0.11**	**0.07**	**0.02**	**0.25**	**0.00**	**1.32**	**0.52**	**0.14**	**0.02**	**0.50**	**3.50**	**0.6**	**2.0**	**28**
%S 25-15%	**n = 15**	**0.11**	**0.07**	**0.04**	**0.30**	**0.00**	**1.21**	**0.57**	**0.17**	**0.04**	**0.58**	**3.42**	**0.7**	**2.0**	**19**
%S <15%	n = 9	0.07	0.08	0.02	0.49	0.00	1.35	0.51	0.13	0.01	0.70	3.30	0.8	2.0	9

Fig. 7b. *Computed averaged mineral formulae of diVS-ml phases in the different smectite layers probability (%S)-classes*

Description – B25 No15 (< 2 µm), treated material *(OPA, 125°C, 98.6 hrs)*

Preparation for TEM

The powder of compacted and treated B25-No15-sample was suspended in deionized water and dispersed by ultrasonic treatment for approximately 20 min. The clay fraction (<2 µm) was separated by sedimentation and diluted with deionized water to get a clear suspension. The suspension was dropped onto carbon-coated Cu grids, air dried and stored under environment-controlled conditions at 45% humidity.

Mineral Matter - Overview

The fraction < 2 µm of treated B25 bentonite sample (Opalinus Clay solution, at 125°C, for 285 hours) is mainly composed by beidellitic dioctahedral vermiculite-smectite mixed layer phases (beid. diVS-ml) and dioctahedral vermiculite-smectite mixed layer phases (diVS-ml) and accompanied by illite, CSV-ml, KSV-ml and quartz in traces [fig. 1].

	frequency-% *(n = 152 measured particles)*
beid. diVS-ml (Cluster1)	68%
diVS-ml (Cluster2)	24%
CSV-ml	4%
KSV-ml	1%
Quartz	2%
Unknown	1%

All measured clay mineral phases summarized result following mineral formula computed from TEM-EDX-measurement of 140 individual particles:

	$Ca^{2+}_{0.14}$	$Mg^{2+}_{0.05}$	$Na^{+}_{0.03}$	$K^{+}_{0.17}$	$Al^{3+}_{1.21}$	$Fe^{3+}_{0.58}$	$Mg^{2+}_{0.20}$	$Ti^{4+}_{0.01}$	$(OH)_2$	$Si^{4+}_{3.59}$	$Al^{3+}_{0.41}$	O_{10}
SDOM	*± 0.00*	*± 0.00*	*± 0.00*	*± 0.01*	*± 0.01*	*± 0.01*	*± 0.00*	*± 0.00*		*± 0.01*	*± 0.01*	

Legend: SDOM - standard deviation of the mean (= the standard deviation divided by the square root of the number of samples)

The interlayer charge is calculated as 0.57 per $(OH)_2$ O_{10} and the octahedral charge as 5.84 per $(OH)_2$ O_{10}. The particles are characterized by a high octahedral Fe-amount.

The summarized chemical composition of all 140 computed particles is compared with measured data of original B25-bentonite sample [tab. 1]. The chemical composition averaged by measured particles show a slight decreased amount of SiO_2 and a slight higher amount for Al_2O_3 and K_2O in comparison to the measured data of original untreated B25-bentonite.

B25-No15 sample is characterized by two morphological groups: (i) aggregates formed by small (≤ 200 nm) xenomorphous plates and (ii) large (≤ 1 µm) xenomorph film-like platy crystals [fig. 2]. Aggregates formed by small (≤ 200 nm) xenomorphous plates dominate the shapes of particles in the micrographs [fig. 2].

The distribution of %S-probability of all measured clay mineral phases [fig. 3a] also indicates the occurrence of two groups: (i) as main group diVS-ml (%S-max of this mixture for %S at 50%) and (ii) illite with K- and charge deficiency.

The numerous measured particles by TEM-EDX allow a visualization of distribution of interlayer charges. Considering the TEM-EDX-determined cations Ca^{++}, Mg^{++} and Na^{+} and then computed their ratio as interlayer cations in the mineral formula, Ca^{++}, Mg^{++} and Na^{+} offer to characterize the degree of exchangeable charges in the interlayer space. This charge density of treated B25 bentonite (< 2 µm) shows in this sample a distribution with maximal frequency-% of charge density at 0.47 per $(OH)_2\ O_{10}$ [fig. 5].

Mineral Matter - Specification

Result of Clustering

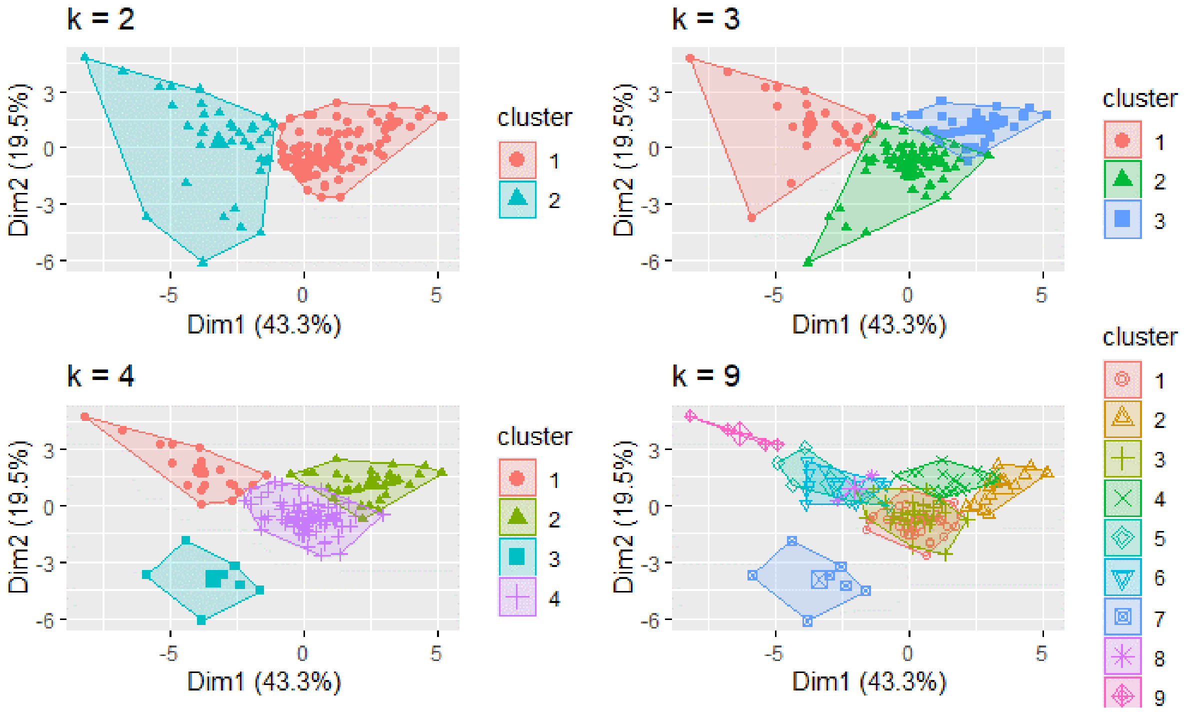

Fig. 8. *Clustering of all measured particles for clusters k = 2, k = 3, k = 4 and k = 9 (source for R-coding: https://uc-r.github.io/kmeans_clustering)*

The optimum of clusters was calculated with k = 2.

		Ca (XII)	Mg (XII)	Na (XII)	K (XII)	Cr3+ (VI)	Al (VI)	Fe3+ (VI)	Mg (VI)	Ti (VI)	Al (IV)	Si (IV)	XII	n_VI	%S
Cluster1	n = 104	0.15	0.05	0.03	0.11	0.00	1.19	0.60	0.21	0.01	0.35	3.65	0.53	2.0	47
Cluster2	n = 36	0.10	0.07	0.03	0.33	0.00	1.28	0.54	0.15	0.03	0.58	3.42	0.70	2.0	19

Fig. 9. *Mineral formulae based on TEM-EDX-data summarized following the result of clustering for k=2*

	Sybilla-results	**TEM-EDX-results**	**Notes**
	Illite	diVS-ml (illite)	
Cluster 1	IS R0(1) *(%S = 60%)*	beid. diVS-ml *(BMI 05:55:40)*	*High K-deficit, low Al(VI), high Fe(VI), high Mg(VI)*
Cluster 2	IS R0(2) *(%S = 28%)*	diVS-ml *(%S ~ 19%)*	*High K-deficit, high Fe(VI)*

Tab. 2. *Comparison of results from TEM-EDX- and XRD-measurements with clustering procedure*

The clustering of TEM-EDX-data offers a good agreement with the recent result of Sybilla-processing of XRD-traces from oriented specimen [tab. 2].

IS R0(1): The X-ray diffraction pattern of the ethylene-glycol saturated oriented specimen shows a expandability to 1.69 nm and a difference of 6.34°2θ between 2. and 3. order of smectite interferences. This distance is typically for montmorillonite (Moore & Reynolds, 1989). This result of XRD-processing let expect a maximum of particles for %S ~ 60% by TEM-EDX-measurements, but the maximum of particles measured by TEM-EDX is to find at %S=47% [fig. 3a].

Montmorillonite and beidellite have the same behavior concerning the expandability and they are only to distinguish by XRD using Li like by Greene-Kelly test (Green-Kelly 1952, 1953). So, combination of XRD- and TEM-results (expandability by XRD and Si ~ 3.65 by TEM-EDX) led conclude the occurrence of beidellite.

IS R0 (2): The Sybilla-procedure of XRD-traces (oriented mounts) has shown an occurrence of a second illite-smectite mixed layer phase with a smectite layers probability of %S = 28%. This situation is to find in Cluster 2 ($\%S_{TEM}$ = 19%) representing high K- and low charge deficient and Fe-rich dioctahedral vermiculite-smectite mixed layer phase (diV-ml) [tab. 2].

The Sybilla-processing of XRD-traces (oriented mounts) also supports the existence of kaolinite and kaolinite-smectite mixed layer phases in fine fraction of sample. Such phases were not to calculate in TEM-EDX-database (a grain size effect?).

Specifics to the identified clay mineral groups

***Beidellitic dioctahedral vermiculite-smectite mixed layer phase (beid. diVS-ml** BMI 05:55:40)*

104 of 140 computed particles belong so to this assumed classification. The dioctahedral character of this group is proofed by X-ray diffraction. The position of the large (060)-interference of smectite is in the random oriented powder specimen at 1.497 Å.

Montmorillonite and beidellite have the same behavior concerning the expandability and they are only to distinguish by XRD using Li by means of Greene-Kelly test (Greene-Kelly 1952, 1953). So, combination of XRD- and TEM-results (limited expandability by XRD and Si ~ 3.65 by TEM-EDX) led conclude the partial occurrence of beidellite.

***Beidellitic dioctahedral vermiculite-smectite mixed layer phase (beid. diVS-ml** BMI 05:55:40)*

$$\boxed{Ca_{0.15}\ Mg_{0.05}\ Na_{0.03}\ K_{0.11}\quad Al_{1.19}\ Fe^{3+}_{0.60}\ Mg_{0.21}\ Ti_{0.01}\ (OH)_2\ \ Si_{3.65}\ Al_{0.35}\ O_{10}}$$

Charge:	XII = 0.53	VI = 5.82	IV = 15.65	**Σ = 22.00**
Measured particles by TEM-EDX:	104			
Result of clustering:	Cluster1 [tab. 2]			

In this sample, beidellite is characterized by a typical low octahedral Mg-amount (because of high ratio of octahedral, 3-valent cations). A comparison of octahedral Mg vs. tetrahedral Si indicates the occurrence of two groups for octahedral Mg based on TEM-EDX-data [fig. 3b].

Using the results of clustering (see Cluster1 in tab. 2), the maximum of frequency-% is to find for particles in the %S-class ~ 40% [tab. 6a]. The mineral formulae, summarized in classes of tetrahedral Si, draw for the maximum an Fe-rich beidellite with low Mg(VI), but remarkable amount of K in the interlayer space [tab. 6b].

Dioctahedral vermiculite-smectite mixed layer phase (diVS-ml):

$$\mathrm{Ca_{0.10}\,Mg_{0.07}\,Na_{0.03}\,K_{0.33}\quad Al_{1.28}\,Fe^{3+}_{0.54}\,Mg_{0.15}\,Ti_{0.01}\,(OH)_2\;\;Si_{3.42}\,Al_{0.58}\,O_{10}}$$

Charge: XII = 0.70 VI = 5.88 IV = 15.42 **Σ = 22.00**
Probability of smectite layers (%S): 19%
Probability of illite layers (%I): 81%
Measured particles by TEM-EDX: 36
Result of clustering: Cluster2 [tab. 2]

Illite as part of diVS-ml series

The Rietveld refinement by Profex software (Döbelin & Kleeberg, 2015) indicates the occurrence of two polytypes for illite in treated B25 bentonite: $2M_1$- and 1M-polytype.

Kaolinite-montmorillonite mixed layer phases

The Excel-based procedure (Hoang-Minh et al., 2019) to identify possible clay mineral groups using the TEM-EDX-measurements also includes algorithms to classify kaolinite and kaolinite-montmorillonite mixed layer phases. These algorithms couldn’t identify such phases basing on the measured TEM-EDX-data. Otherwise, few particles, which were not to compute, have shown small hexagonal plates typically for kaolinite-bearing phases.

References

Cliff, G. & Lorimer, G. W. (1975). *J. Microsc.* **103**, 203–207.

Döbelin, N., Kleeberg, R. (2015). *Journal of Applied Crystallography* **48**, 1573-1580. DOI: 10.1107/S1600576715014685

Greene-Kelly, R., *Clay Minerals Bull.*, **1**, 221 (1952).

Greene-Kelly, R. 1953. The identification of montmorillonoids in clays. *Journal of Soil Science*. **4** (2), pp. 232-237. https://doi.org/10.1111/j.1365-2389.1953.tb00657.x

Greene-Kelly, R. (1955). Dehydration of the montmorillonite minerals. *Mineralogical Magazine and Journal of the Mineralogical Society*, **30**(228), 604-615. doi:10.1180/minmag.1955.030.228.06

Henning, K.-H. & Störr, M. (1986). Electron Micrographs (TEM, SEM) of Clays and Clay Minerals, p. 325. Akademie-Verlag Berlin.

Hoang-Minh, T., Kasbohm, J., Nguyen-Thanh, L., Nga, P. T., Lai, L. T., Duong, N. T., Thanh, N. D., Thuyet, N. T. M., Anh, D. D., Pusch, R., Knutsson, S. & Ferreiro Mahlmann, R. (2019). *J. Appl. Cryst.* **52**, 133-147. DOI: 10.1107/S1600576718018162

Lorimer, G. W. & Cliff, G. (1976). *Electron Microscopy in Mineralogy*, edited by H. R. Wenk, pp. 506–519. Berlin: Springer Verlag.

Matschiavelli, N., Kluge, S., Podlech, C., Standhaft, D., Grathoff, G., Ikeda-Ohno, A., Warr, L.N., Chukharkina, A., Arnold, T. & Cherkouk, A. (2019). *Environmental Science & Technology.* **53** (17), 10514-10524, DOI: 10.1021/acs.est.9b02670

Mellini, M. & Menichini, R. (1985). *R. Soc. Ital. Miner. Petrol.* **40**, 261–266.

Moore, D.M., Reynolds, R.C. (1989). X-ray Diffraction and the Identification and Analysis of Clay Minerals, Oxford University Press, New York, 332 + xvi pp.

Nguyen-Thanh, L., Herbert, H.-J., Kasbohm, J., Hoang-Minh, T. & Mählmann, R. F. (2014). *Clays Clay Miner.* **62**, 425–446.

Środoń, J., Elsass, F., McHardy, W. J. & Morgan, D. J. (1992). *Clay Miner.* **27**, 137–158.

Data Sheet – B25 bentonite, treated materials *(OPA, 150°C, 4d)* - TOP

Methodology - Transmission electron microscopy linked with energy-dispersive X-ray spectroscopy (TEM-EDX)

It is expected a characterization of clay mineral phases in treated B25 bentonite by transmission electron microscopy. The sample series No3 represents a percolation of B25 bentonite by Opalinus Clay solution at 150°C for 4 days. The sample No3_T is the label for the material at the top of sample cylinder.

The different clay mineral phases are to identify and to describe by chemical composition and its variability, morphology, the specific dissolution potential, and further parameter.

Such further parameter like distribution of smectite layers probability (%S) and distribution of charges caused by exchangeable cations interlayer space should serve as additional indicators for mineralogical alterations in treatment experiments with B25 bentonite.

The sample were suspended for TEM-measurement in deionized water and dispersed by ultrasonic treatment for approximately 20 min. The clay fraction (<2 µm) was separated by sedimentation and diluted with deionized water to get a clear suspension. The suspension was dropped onto carbon-coated Cu grids, air dried and stored under environment-controlled conditions at 45% humidity.

TEM-EDX investigations were carried out on the <2 µm fraction using a FEI TECNAI G^2 20 electron transmission microscope at the VNU University of Science, Vietnam National University, Hanoi. This equipment (operated at 200 kV with LaB_6 cathode) was combined with an S-TWIN objective, a windowless EDAX energy-dispersive X-ray system and a FEI Eagle 2k CCD TEM camera.

About 100 individual clay particles per sample were characterized by TEM-EDX with respect to crystal size, crystal habit, and particle morphology and element distribution. The crystal size, crystal habit and particle morphology were described according to Henning & Störr (1986).

For the quantification of element distribution, a calibration of k factors is mandatory (Cliff & Lorimer, 1975; Lorimer & Cliff, 1976; Mellini & Menichini, 1985). These k values are used to calibrate for the specific behaviour of particles against possible irradiation damage. The elements O, Na, Mg, Al, Si, K, Ca and Fe were quantified by applying the EDAX GENESIS–TEM Quant Materials quantification procedure.

In this procedure, the acquired EDX spectra are corrected by background subtraction, Gaussian deconvolution and k-factor corrections using values previously determined on a phyllosilicate standard (muscovite) and selected non-phyllosilicate standards. The average errors in the analyzed elements using the phyllosilicate standard, expressed as the atomic proportions, are 10 (Na), 5 (Fe, Mg, K, Ti, Ca) and 1 (Si, Al).

The measurement time per particle was lowered to 20 s and the exposed area was limited to a 50 nm diameter, avoiding possible irradiation damage of particles. The stability of particles of the sample series was tested for this measurement time at the beginning of any measurement campaign.

Further methodological details related to TEM-EDX-measurements and the Excel-based mathematical procedure using TEM-EDX data for calculation of mineral formulae are described in Hoang-Minh et al. (2019).

These mathematical procedures described in Hoang-Minh et al. (2019) were extended by k-means clustering method for finding subgroups of observations within a data set. The data were standardized (i.e., scaled) to make variables comparable. Euclidean distances were applied as classical method for distance measures. The optimal clusters were determined by Elbow method and Gap statistics[17].

---

[17] *https://uc-r.github.io/kmeans_clustering*

Data Sheet – B25 No3_T (< 2 µm), treated material *(OPA, 150°C, 4 days)*

Preparation for TEM

- raw material: compacted material (1.6 g/cm³) of treated B25-sample (OPA, 150°C, 4 days)
- suspension on particles < 2 µm on carbon-filmed Cu-grid
- air-dried and humidity-controlled storing

Mineral Matter

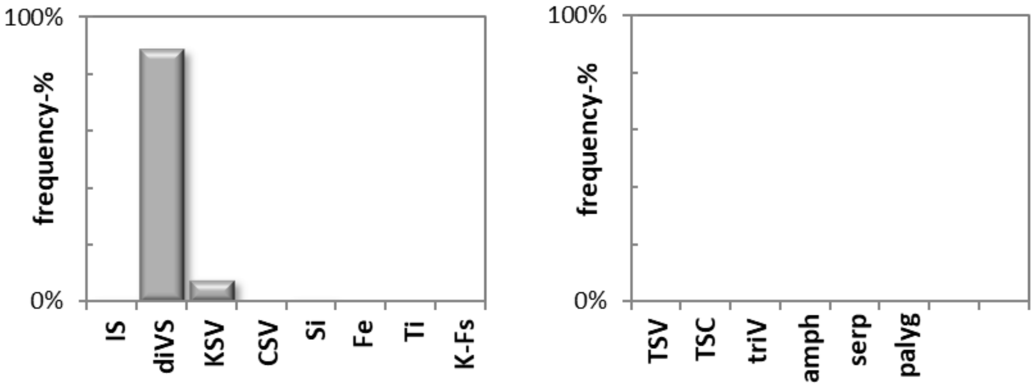

Fig. 1. *Distribution of mineral groups in fraction < 2 µm (in frequency-%)*
Legend: ***IS*** *– illite-smectite-mixed layer series in sense of Środon et al. (1992), diVS – dioctahedral vermiculite-smectite illite-smectite-mixed layer series (= charge- and/or K-deficit),* ***KSV*** *– kaolinite-smectite-dioctahedral vermiculite-mixed layer series,* ***CSV*** *– chlorite-saponite-trioctahedral vermiculite-mixed layer series,* ***Si*** *– quartz or particles with Si-surplus,* ***Fe*** *– Fe-oxide or Fe-oxyhydroxide,* ***Ti*** *– Ti-bearing phases (e.g. rutile, anatase),* ***K-Fs*** *– K-feldspar*

Clay Mineral Composition

All particles of smectite group:

$$Ca_{0.10}\ Mg_{0.11}\ Na_{0.00}\ K_{0.12}\quad Al_{1.18}\ Fe^{3+}_{0.68}\ Mg_{0.14}\ Ti_{0.00}\ (OH)_2\quad Si_{3.59}\ Al_{0.41}\ O_{10}$$

Charge: XII = 0.54 VI = 5.86 IV = 15.59 **Σ = 22.00**
Probability of smectite layers (%S): 39%
Probability of illite layers (%I): 61%

Specific Dissolution Potential (ΔS%)

for H2O, 20 + 60 rpm	- 6	(= medium reacting, interlayer group: Ca+Mg (= type B))
for NaCl, 20 rpm	- 6	(= medium reacting, interlayer group: Ca+Mg (= type B))
for NaCl, 60 rpm	-111	(= fast reacting, ‘illitization’, interlayer group: Na (= type A))
CEC_{calc}:	54 meq / 100 g	(literature: 56 meq / 100 g [Matschiavelli et al., 2019: MAT19])

Measured particles: 90

Table 1. *Summarized chemical composition*

SiO_2	TiO_2	Al_2O_3	Fe_2O_3	MnO	MgO	CaO	Na_2O	K_2O	P_2O_5	Σ	
59.5%	0.1%	23.2%	7.4%		3.2%	1.1%	0.1%	1.1%		0.96	measured particles
58.6%	0.0%	22.0%	5.9%		3.0%	1.0%	0.1%	1.1%	0.1%	0.92	measured particles of original B25

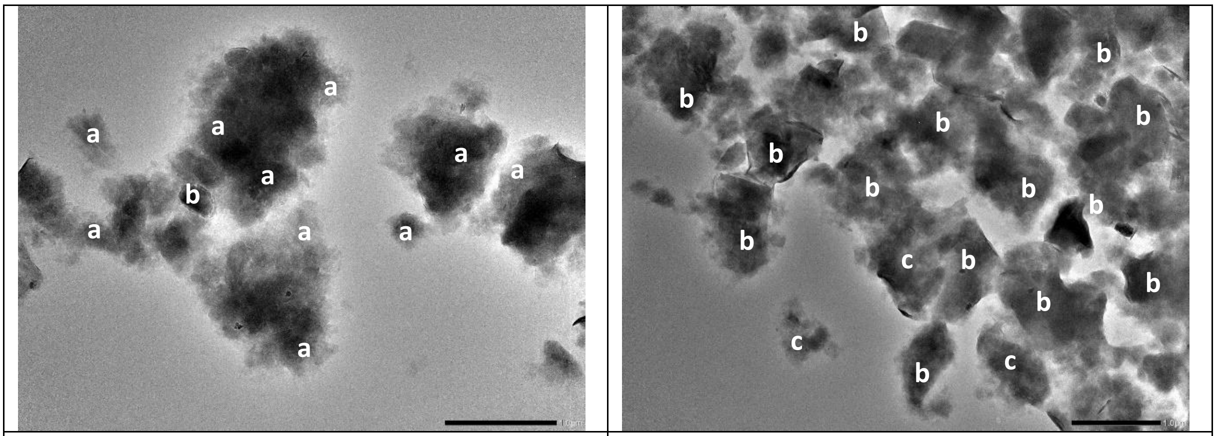

JEM-2100_No3_T_A2_X10k.bmp

Magnification: 10k

- (dd) aggregates formed by small (≤ 200 nm) xenomorphous plates *(BM 70:30)*;
- (ee) xenomorph film-like platy crystals partially with folds *(diVS-ml)*

JEM-2100_No3_T_A4_X10k.bmp

Magnification: 10k

- (f) xenomorph film-like platy crystals partially with folds *(diVS-ml)*;
- (g) partially idiomorph plates (≤ 200 nm) *(KSV-ml)*

Fig. 2. *Morphology of particles (TEM-micrographs)*

Distribution of smectite layers probability (%S)

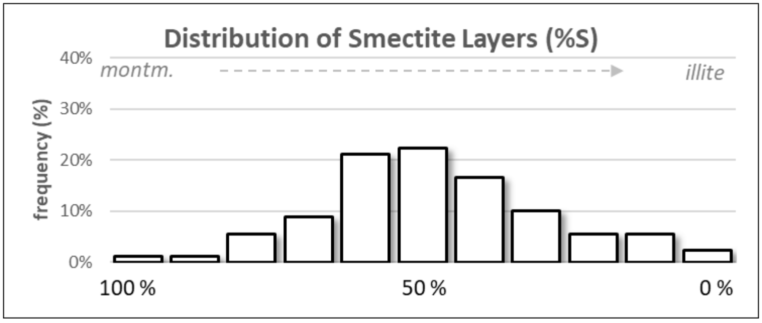

Fig. 3a. *Distribution of smectite layers probability (%S)*

Description: *The distribution of %S-probability indicates the occurrence of two groups: (i) mixture of beidellite-montmorillonite interstratifications (= assumption) with diVS-ml as well as (ii) illite with K-deficiency (%S-class = 0%).*

Differentiation by relation “Octahedral Mg vs. tetrahedral Si”?

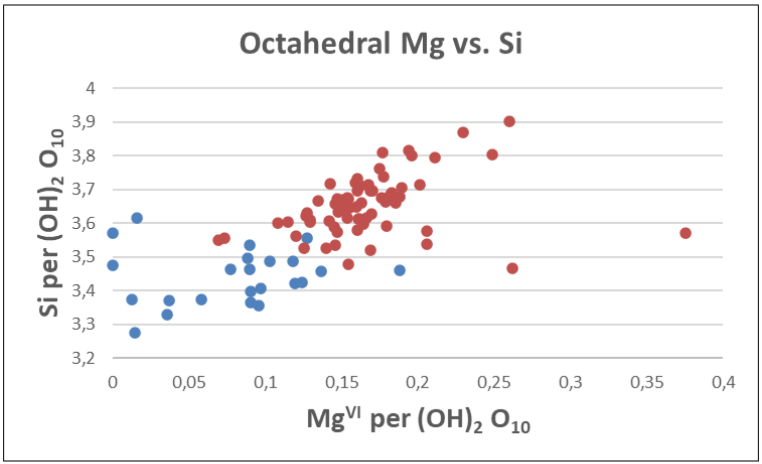

Description: *This diagram indicates the occurrence of two groups of Mg in relation to tetrahedral Si. Probably, this distribution mirrors (I) beidellite-montmorillonite interstratifications (red) and (II) diVS-ml incl. illite (blue)*

Fig. 3b. *Distribution of octahedral Mg vs. tetrahedral Si [all per$(OH)_2$ O_{10}]*

Distribution of K in relation to tetrahedral Si

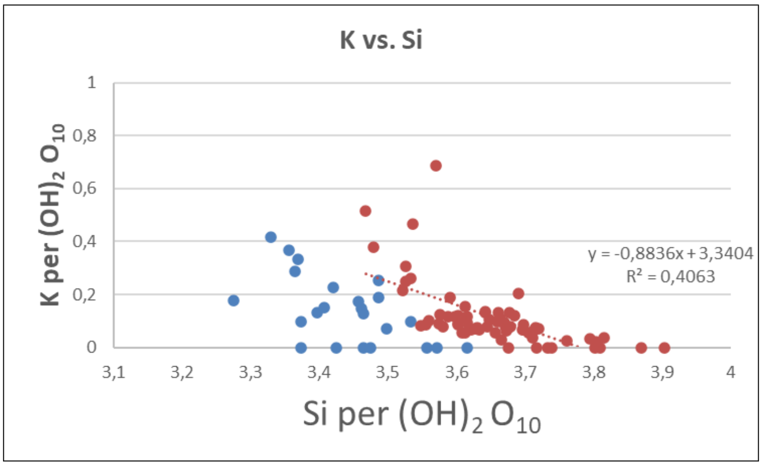

__Description:__ This diagram visualizes possible particles of beidellite-montmorillonite interstratification (red dots) and diVS-ml phases (blue dots)

Fig. 4. *Distribution of K in interlayer space vs. tetrahedral Si [all per(OH)$_2$ O$_{10}$]*

Distribution of charges (exchangeable from interlayer space)

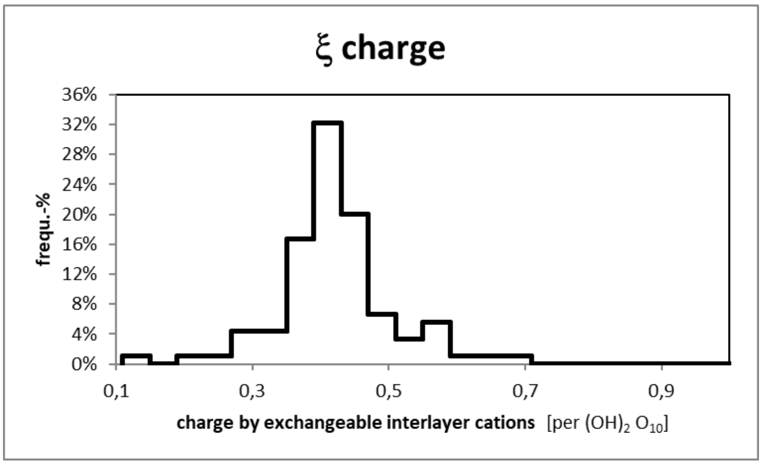

This diagram visualizes the distribution of exchangeable charges in the interlayer space (Ca, Mg, Na) determined and computed by TEM-EDX-data.

__Description:__ Maximal frequency-% of charge density at 0.43 per (OH)$_2$ O$_{10}$.

Fig. 5. *Distribution of charges*

Beidellite-Montmorillonite interstratification (BM ~ 70%:30%) *(Cluster2):*

$$Ca_{0.11}\ Mg_{0.09}\ Na_{0.00}\ K_{0.11}\quad Al_{1.22}\ Fe^{3+}{}_{0.60}\ Mg_{0.17}\ Ti_{0.01}\ (OH)_2\quad Si_{3.65}\ Al_{0.35}\ O_{10}$$

Charge: XII = 0.51 VI = 5.84 IV = 15.65 **Σ = 22.00**

Measured particles: 67

Distribution of BM-interstratifications (Cluster2)

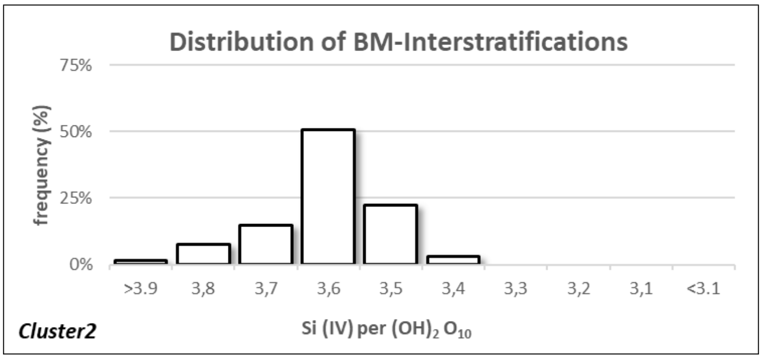

__Description:__ The distribution of BM-interstratifications (classified as Cluster2) draws a maximum of frequency (%) at tetrahedral Si-value between 3.6 – 3.7 e phuc

Fig. 6a. *Distribution of assumed beidellite-montmorillonite interstratifications*

BM70:30??	particles (abs)	Ca (XII)	Mg (XII)	Na (XII)	K (XII)	Cr3+ (VI)	Al (VI)	Fe3+ (VI)	Mg (VI)	Ti (VI)	Al (IV)	Si (IV)	XII	n_VI	%S
Si >3.9	n = 1	0,10	0,07	0,00	0,00	0,00	1,36	0,38	0,26	0,00	0,10	3,90	0,4	2,0	90
Si 3.9-3.8	n = 5	0,11	0,08	0,00	0,01	0,00	1,30	0,49	0,21	0,00	0,18	3,82	0,4	2,0	74
Si 3.8-3.7	n = 10	0,11	0,09	0,00	0,04	0,00	1,24	0,59	0,17	0,00	0,27	3,73	0,4	2,0	59
Si 3.7-3.6	**n = 34**	**0,11**	**0,09**	**0,00**	**0,09**	**0,00**	**1,19**	**0,65**	**0,16**	**0,00**	**0,35**	**3,65**	**0,5**	**2,0**	**47**
Si 3.6-3.5	n = 15	0,09	0,09	0,00	0,21	0,00	1,24	0,59	0,16	0,01	0,44	3,56	0,6	2,0	35
Si 3.5-3.4	n = 2	0,07	0,06	0,02	0,45	0,00	1,33	0,45	0,21	0,02	0,53	3,47	0,7	2,0	25
Si 3.4-3.3	n = 0														
Si 3.3-3.2	n = 0														
Si 3.2-3.1	n = 0														
Si <3.1	n = 0														

Fig. 6b. *Computed averaged mineral formulae of phases in the different Si(IV)-classes*

Dioctahedral Vermiculite-Smectite mixed layer phases (diVS-ml) *(Cluster1):*

$$Ca_{0.09}\ Mg_{0.15}\ Na_{0.00}\ K_{0.14}\quad Al_{1.08}\ Fe^{3+}_{0.85}\ Mg_{0.08}\ Ti_{0.00}\ (OH)_2\quad Si_{3.44}\ Al_{0.56}\ O_{10}$$

Charge: XII = 0.64 VI = 5.92 IV = 15.44 **Σ = 22.00**

Probability of smectite layers (%S): 22%

Probability of illite layers (%I): 78%

Measured particles: 23

Distribution of smectite layers probability (%S) in diVS-ml (Cluster1)

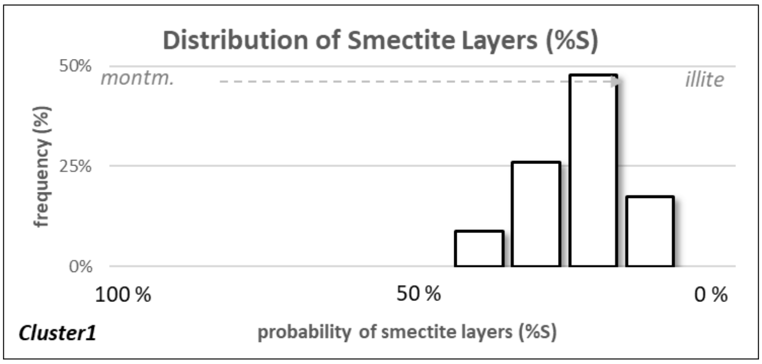

Description: *The distribution of diVS-ml (classified as Cluster1) draws a maximum of frequency (%) for smectite layer probability at 15-25%.*

Fig. 7a. *Distribution of smectite layers probability in diVS-ml*

diVS-ml	particles (abs)	Ca (XII)	Mg (XII)	Na (XII)	K (XII)	Cr3+ (VI)	Al (VI)	Fe3+ (VI)	Mg (VI)	Ti (VI)	Al (IV)	Si (IV)	XII	n_VI	%S
%S >95%	n = 0														
%S 95-85%	n = 0														
%S 85-75%	n = 0														
%S 75-65%	n = 0														
%S 65-55%	n = 0														
%S 55-45%	n = 0														
%S 45-35%	n = 2	0,00	0,20	0,00	0,00	0,00	1,06	0,93	0,01	0,00	0,41	3,59	0,4	2,0	39
%S 35-25%	n = 6	0,09	0,15	0,00	0,10	0,00	1,14	0,77	0,09	0,00	0,49	3,51	0,6	2,0	29
%S 25-15%	**n = 11**	**0,11**	**0,16**	**0,00**	**0,13**	**0,00**	**1,02**	**0,88**	**0,09**	**0,00**	**0,58**	**3,42**	**0,7**	**2,0**	**20**
%S <15%	n = 4	0,08	0,12	0,00	0,31	0,00	1,13	0,81	0,06	0,00	0,67	3,33	0,7	2,0	12

Fig. 7b. *Computed averaged mineral formulae of diVS-ml phases in the different smectite layers probability (%S)-classes*

Description – B25 No3_T (< 2 µm), treated material *(OPA, 150°C, 4 days)*

Preparation for TEM

The powder of compacted and treated B25-No3_T-sample was suspended in deionized water and dispersed by ultrasonic treatment for approximately 20 min. The clay fraction (<2 µm) was separated by sedimentation and diluted with deionized water to get a clear suspension. The suspension was dropped onto carbon-coated Cu grids, air dried and stored under environment-controlled conditions at 45% humidity.

Mineral Matter - Overview

The fraction < 2 µm of treated B25 bentonite sample (Opalinus Clay solution, at 150°C, for 4 days) is mainly composed by assumed beidellite-montmorillonite interstratifications (B:M ~70:30), abbreviated as BM-ml, and dioctahedral vermiculite-smectite mixed layer phases (diVS-ml) and accompanied by two types of illite. Furthermore, kaolinite and Si surplus (e.g. quartz) were identified in traces in this sample [fig. 1].

	frequency-% *(n = 100 measured particles)*
BM-ml (Cluster2)	67%
diVS-ml (Cluster1)	23%
Si surplus (e.g. quartz)	1%
Kaolinite & KSV-ml	8%

All measured dioctahedral clay mineral phases summarized result following mineral formula computed from TEM-EDX-measurement of 100 individual particles:

	$Ca^{2+}_{0.10}$	$Mg^{2+}_{0.11}$	$Na^{+}_{0.00}$	$K^{+}_{0.12}$	$Al^{3+}_{1.18}$	$Fe^{3+}_{0.68}$	$Mg^{2+}_{0.14}$	$Ti^{4+}_{0.001}$	$(OH)_2$	$Si^{4+}_{3.59}$	$Al^{3+}_{0.41}$	O_{10}
SDOM	*± 0.00*	*± 0.00*	*± 0.00*	*± 0.01*	*± 0.01*	*± 0.02*	*± 0.01*	*± 0.00*		*± 0.01*	*± 0.01*	

Legend: SDOM - standard deviation of the mean (= the standard deviation divided by the square root of the number of samples)

The interlayer charge is calculated as 0.54 per $(OH)_2$ O_{10} and the octahedral charge as 5.86 per $(OH)_2$ O_{10}. The particles are characterized by a high octahedral Fe-amount.

The summarized chemical composition of all 90 computed particles is compared with measured data of original B25-bentonite sample [tab. 1]. The chemical composition averaged by measured particles show especially a slight higher amount of SiO_2, Al_2O_3 and Fe_2O_3 in comparison to the measured data of original untreated B25-bentonite.

B25-No3_T sample is characterized by two morphological groups: (i) aggregates formed by small (≤ 200 nm) xenomorphous plates [fig. 2 left] and (ii) xenomorph film-like platy crystals partially with folds [fig. 2 right]. Thin aggregates formed by small (≤ 200 nm) xenomorphous plates dominate the shapes of particles in the micrographs [fig. 2 left].

The distribution of %S-probability of all measured clay mineral phases [fig. 3a] also indicates the occurrence of two groups: (i) as main group a mixture of beidellite-montmorillonite interstratifications

and diVS-ml (%S-max of this mixture for %S at 45-55%) and (ii) illite with K- and charge deficit (%S-classes = 0% & 10%).

The numerous measured particles by TEM-EDX allow a visualization of distribution of interlayer charges. Considering the TEM-EDX-determined cations Ca^{++}, Mg^{++} and Na^{+} and then computed their ratio as interlayer cations in the mineral formula, Ca^{++}, Mg^{++} and Na^{+} offer to characterize the degree of exchangeable charges in the interlayer space. This charge density of treated B25 bentonite (< 2 µm) shows a narrow maximal distribution of charge density at 0.43 per $(OH)_2\ O_{10}$ [fig. 5]. This interval of interlayer charge density is caused by exchangeable cations from 0.19 – 0.21 per $(OH)_2\ O_{10}$ representing mainly the BM-phases and from 0.20 – 0.27 per $(OH)_2\ O_{10}$ represented mainly by diVS-ml phases.

Mineral Matter - Specification

Result of Clustering

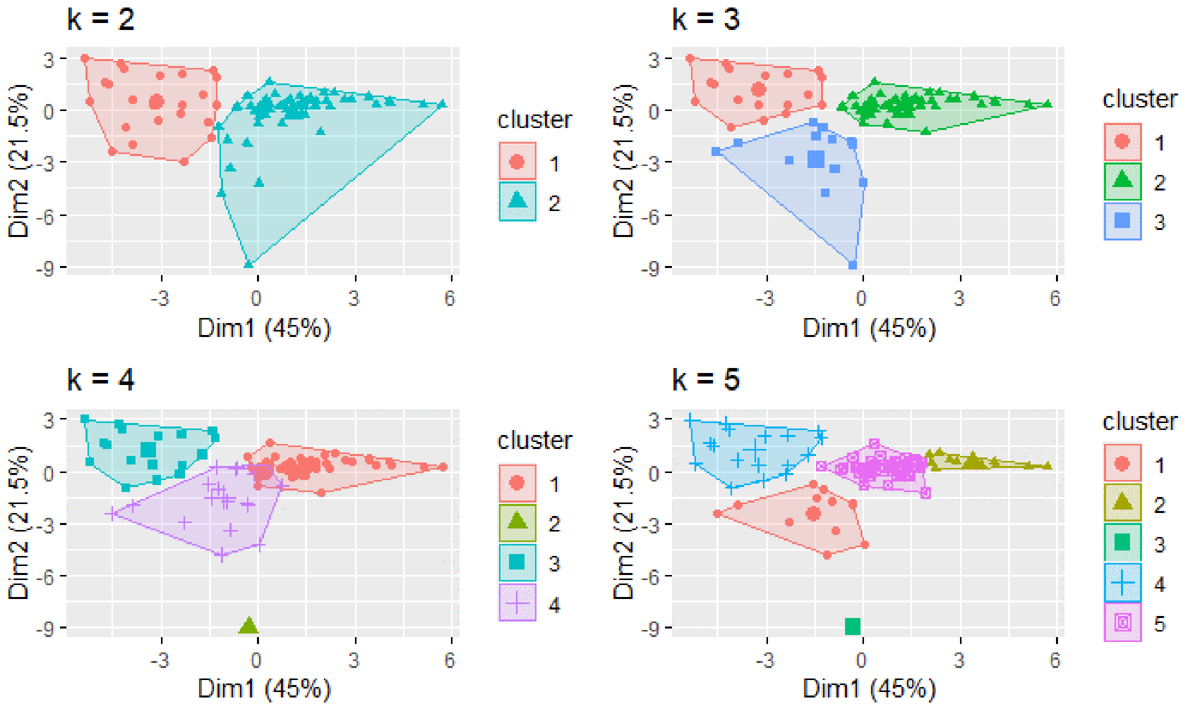

Fig. 8. *Clustering of all measured particles for clusters k = 2, k = 3, k = 4 and k = 5 (source for R-coding: https://uc-r.github.io/kmeans_clustering)*

The optimum of clusters was calculated with k = 2.

		Ca (XII)	Mg (XII)	Na (XII)	K (XII)	Cr3+ (VI)	Al (VI)	Fe3+ (VI)	Mg (VI)	Ti (VI)	Al (IV)	Si (IV)	XII	n_VI	%S
Cluster1	n = 23	0,09	0,15	0,00	0,14	0,00	1,08	0,85	0,08	0,00	0,56	3,44	0,64	2,0	22
Cluster2	n = 67	0,11	0,09	0,00	0,11	0,00	1,22	0,60	0,17	0,01	0,35	3,65	0,51	2,0	47

Fig. 9. *Mineral formulae based on TEM-EDX-data summarized following the result of clustering for k=2*

	Sybilla-results	TEM-EDX-results	Notes
Cluster2	IS R0(1) *(%S = 100%)*	BM-ml *(BM 70:30?)*	*XRD: Montmorillonite and beidellite is only to distinguish by Green-Kelly-test (not available here).*
Cluster1	IS R0(2) *(%S = 22%)*	diVS-ml *(%S = 22%)*	*High K-deficit, very Fe(VI)-rich*

Tab. 2. *Comparison of results from TEM-EDX- and XRD-measurements with clustering procedure*

The clustering of TEM-EDX-data offers a good agreement with the recent result of Sybilla-processing of XRD-traces from oriented specimen [tab. 2].

IS R0 (1): The X-ray diffraction pattern of the ethylene-glycol saturated oriented specimen shows a full expandability to 1.69 nm and a difference of 5.46°2θ between 2. and 3. order of smectite interferences. This distance is typically for montmorillonite (Moore & Reynolds, 1989). This result of XRD-processing let expect a maximum of particles for %S ~ 100% by TEM-EDX-measurements, but the maximum of particles measured by TEM-EDX is to find at %S=50% [fig. 3a].

Montmorillonite and beidellite have the same behavior concerning the expandability and they are only to distinguish by XRD using Li like by Greene-Kelly test (Green-Kelly 1952, 1953). So, combination of XRD- and TEM-results (full expandability by XRD and Si ~ 3.65 by TEM-EDX) led conclude the occurrence of 'beidellite-montmorillonite interstratifications', a beidellite-montmorillonite interstratification with about 70% beidellite and 30% montmorillonite layers (BM-ml 70:30).

IS R0 (2): The Sybilla-procedure of XRD-traces (oriented mounts) has shown an occurrence of a second illite-smectite mixed layer phase with a smectite layers probability of %S = 22%. This situation is even to find in Cluster1 ($\%S_{TEM}$ = 22%) representing a high K-, but low charge deficient and very Fe-rich dioctahedral vermiculite-smectite mixed layer phase (diV-ml) [tab. 2].

The Sybilla-processing of XRD-traces (oriented mounts) also supports the existence of kaolinite and kaolinite-smectite mixed layer phases in fine fraction of sample. Such phases were not to identify or to calculate in TEM-EDX-database (a grain size effect?).

Specifics to the identified clay mineral groups

Beidellite-montmorillonite interstratifications (B:M ~70:30?)

67 of 100 measured particles belong so to this assumed classification. The dioctahedral character of this group is proofed by X-ray diffraction. The position of the large (060)-interference of smectite is in the random oriented powder specimen at 1.497 Å.

Montmorillonite and beidellite have the same behavior concerning the expandability and they are only to distinguish by XRD using Li by means of Greene-Kelly test (Green-Kelly 1952, 1953). So, combination of XRD- and TEM-results (full expandability by XRD and Si ~ 3.65 by TEM-EDX) led conclude the occurrence of 'beidellite-montmorillonite interstratifications', a beidellite-montmorillonite interstratification with about 70% beidellite and 30% montmorillonite layers (BM-ml 70:30).

Beidellite-montmorillonite interstratifications (B:M ~70:30?):

$$\mathrm{Ca_{0.11}\ Mg_{0.09}\ Na_{0.00}\ K_{0.11}\quad Al_{1.22}\ Fe^{3+}_{0.60}\ Mg_{0.17}\ Ti_{0.00}\ (OH)_2\quad Si_{3.65}\ Al_{0.35}\ O_{10}}$$

Charge: XII = 0.51 VI = 5.84 IV = 15.65 **Σ = 22.00**

Measured particles by TEM-EDX: 67
Result of clustering: Cluster2 [tab. 2]

Beidellitic structures are characterized by a low octahedral Mg-amount (because of high ratio of octahedral, 3-valent cations). A comparison of octahedral Mg vs. tetrahedral Si indicates the occurrence of two groups for octahedral Mg based on TEM-EDX-data, separated by tetrahedral Si [fig. 3b]. The core of BM-ml shows an octahedral Mg-amount between 0.16 – 0.21 e phuc, probably pronounced by a higher Mg^{VI} in montmorillonite compound in this type interstratification.

Using the results of clustering (see Cluster2 in tab. 2), the maximum of frequency-% is to find for particles in the Si(IV)-class 3.6 – 3.7 e phuc [tab. 6a], representing the mentioned relation 30% montmorillonite and 70% beidellite as ratio of interstratification. The mineral formulae, summarized in classes of tetrahedral Si, draw for the maximum an Fe-rich BM 70:30 phase with K and remarkable amount of Mg in the interlayer space [tab. 6b].

A further hypothesis is to verify: The increasing K by lower tetrahedral Si [tab. 6b] could be an indication that it's not a change of 50:50 ratio of BM-ml into a 70:30 ratio of BM-ml, but an alteration of montmorillonite into diVS-ml phases resulting into an interstratification by beidellite – montmorillonite – dioctahedral vermiculite.

Dioctahedral vermiculite-smectite mixed layer phase (low K diVS-ml):

$$\boxed{\mathrm{Ca_{0.09}\,Mg_{0.15}\,Na_{0.00}\,K_{0.14}\quad Al_{1.08}\,Fe^{3+}_{0.85}\,Mg_{0.08}\,Ti_{0.00}\,(OH)_{2}\quad Si_{3.44}\,Al_{0.56}\,O_{10}}}$$

Charge: XII = 0.64 VI = 5.92 IV = 15.44 **Σ = 22.00**
Probability of smectite layers (%S): 22%
Probability of illite layers (%I): 78%

Measured particles by TEM-EDX: 23
Result of clustering: Cluster1 [tab. 2]

Illite as part of diVS-ml series (high K diVS-ml):

The Rietveld refinement by Profex software (Döbelin & Kleeberg, 2015) indicates the occurrence of two polytypes for illite in treated B25 bentonite: $2M_1$- and 1M-polytype.

Kaolinite-montmorillonite-dioctahedral vermiculite mixed layer phases

$$\boxed{\mathrm{Ca_{0.00}\,Mg_{0.17}\,Na_{0.00}\,K_{0.00}\quad Al_{1.42}\,Fe^{3+}_{1.16}\,Mg_{0.02}\,Ti_{0.00}\,(OH)_{3.76}\quad Si_{3.64}\,Al_{0.36}\,O_{10}}}$$

Charge: XII = 0.33 n_VI = 2.60 VI = 7.79 IV = 15.64 **Σ = 23.76**
Probability of kaolinite layers (%K): 29%
Probability of smectite layers (%S): 20%
Probability of vermiculite layers (%V): 51%

Measured particles by TEM-EDX: 4

The Excel-based procedure (Hoang-Minh et al., 2019) to identify possible clay mineral groups using the TEM-EDX-measurements also includes algorithms to classify kaolinite and kaolinite-montmorillonite mixed layer phases. These algorithms could identify four such phases basing on the measured TEM-EDX-data. Otherwise, very few particles, which were not to compute, have shown small hexagonal plates typically for kaolinite-bearing phases.

References

Cliff, G. & Lorimer, G. W. (1975). *J. Microsc.* **103**, 203–207.

Döbelin, N., Kleeberg, R. (2015). *Journal of Applied Crystallography* **48**, 1573-1580. DOI: 10.1107/S1600576715014685

Henning, K.-H. & Störr, M. (1986). Electron Micrographs (TEM, SEM) of Clays and Clay Minerals, p. 325. Akademie-Verlag Berlin.

Hoang-Minh, T., Kasbohm, J., Nguyen-Thanh, L., Nga, P. T., Lai, L. T., Duong, N. T., Thanh, N. D., Thuyet, N. T. M., Anh, D. D., Pusch, R., Knutsson, S. & Ferreiro Mahlmann, R. (2019). *J. Appl. Cryst.* **52**, 133-147. DOI: 10.1107/S1600576718018162

Lorimer, G. W. & Cliff, G. (1976). *Electron Microscopy in Mineralogy*, edited by H. R. Wenk, pp. 506–519. Berlin: Springer Verlag.

Matschiavelli, N., Kluge, S., Podlech, C., Standhaft, D., Grathoff, G., Ikeda-Ohno, A., Warr, L.N., Chukharkina, A., Arnold, T. & Cherkouk, A. (2019). *Environmental Science & Technology.* **53** (17), 10514-10524, DOI: 10.1021/acs.est.9b02670

Mellini, M. & Menichini, R. (1985). *R. Soc. Ital. Miner. Petrol.* **40**, 261–266.

Moore, D.M., Reynolds, R.C. (1989). X-ray Diffraction and the Identification and Analysis of Clay Minerals, Oxford University Press, New York, 332 + xvi pp.

Nguyen-Thanh, L., Herbert, H.-J., Kasbohm, J., Hoang-Minh, T. & Mählmann, R. F. (2014). *Clays Clay Miner.* **62**, 425–446.

Środoń, J., Elsass, F., McHardy, W. J. & Morgan, D. J. (1992). *Clay Miner.* **27**, 137–158.

Data Sheet – B25 bentonite, treated materials *(OPA, 150°C, 4d)* - CENTER

Methodology - Transmission electron microscopy linked with energy-dispersive X-ray spectroscopy (TEM-EDX)

It is expected a characterization of clay mineral phases in treated B25 bentonite by transmission electron microscopy. The sample series No3 represents a percolation of B25 bentonite by Opalinus Clay solution at 150°C for 4 days. The sample No3_C is the label for the material at the middle of sample cylinder.

The different clay mineral phases are to identify and to describe by chemical composition and its variability, morphology, the specific dissolution potential, and further parameter.

Such further parameter like distribution of smectite layers probability (%S) and distribution of charges caused by exchangeable cations interlayer space should serve as additional indicators for mineralogical alterations in treatment experiments with B25 bentonite.

The sample were suspended for TEM-measurement in deionized water and dispersed by ultrasonic treatment for approximately 20 min. The clay fraction (<2 µm) was separated by sedimentation and diluted with deionized water to get a clear suspension. The suspension was dropped onto carbon-coated Cu grids, air dried and stored under environment-controlled conditions at 45% humidity.

TEM-EDX investigations were carried out on the <2 µm fraction using a FEI TECNAI G^2 20 electron transmission microscope at the VNU University of Science, Vietnam National University, Hanoi. This equipment (operated at 200 kV with LaB_6 cathode) was combined with an S-TWIN objective, a windowless EDAX energy-dispersive X-ray system and a FEI Eagle 2k CCD TEM camera.

About 100 individual clay particles per sample were characterized by TEM-EDX with respect to crystal size, crystal habit, and particle morphology and element distribution. The crystal size, crystal habit and particle morphology were described according to Henning & Störr (1986).

For the quantification of element distribution, a calibration of k factors is mandatory (Cliff & Lorimer, 1975; Lorimer & Cliff, 1976; Mellini & Menichini, 1985). These k values are used to calibrate for the specific behaviour of particles against possible irradiation damage. The elements O, Na, Mg, Al, Si, K, Ca and Fe were quantified by applying the EDAX GENESIS–TEM Quant Materials quantification procedure.

In this procedure, the acquired EDX spectra are corrected by background subtraction, Gaussian deconvolution and k-factor corrections using values previously determined on a phyllosilicate standard (muscovite) and selected non-phyllosilicate standards. The average errors in the analyzed elements using the phyllosilicate standard, expressed as the atomic proportions, are 10 (Na), 5 (Fe, Mg, K, Ti, Ca) and 1 (Si, Al).

The measurement time per particle was lowered to 20 s and the exposed area was limited to a 50 nm diameter, avoiding possible irradiation damage of particles. The stability of particles of the sample series was tested for this measurement time at the beginning of any measurement campaign.

Further methodological details related to TEM-EDX-measurements and the Excel-based mathematical procedure using TEM-EDX data for calculation of mineral formulae are described in Hoang-Minh et al. (2019).

These mathematical procedures described in Hoang-Minh et al. (2019) were extended by k-means clustering method for finding subgroups of observations within a data set. The data were standardized (i.e., scaled) to make variables comparable. Euclidean distances were applied as classical method for distance measures. The optimal clusters were determined by Elbow method and Gap statistics[18].

---

[18] *https://uc-r.github.io/kmeans_clustering*

Data Sheet – B25 No3_C (< 2 µm), treated material *(OPA, 150°C, 4 days)*

Preparation for TEM

- raw material: compacted material (1.6 g/cm³) of treated B25-sample (OPA, 150°C, 4 days)
- suspension on particles < 2 µm on carbon-filmed Cu-grid
- air-dried and humidity-controlled storing

Mineral Matter

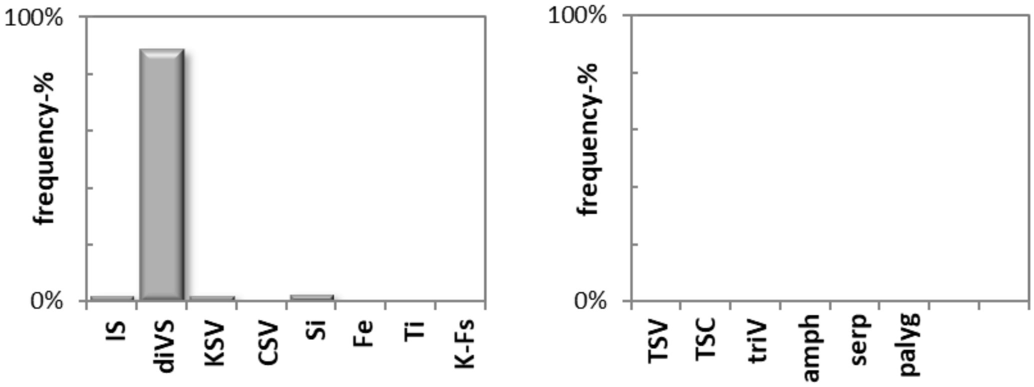

Fig. 1. *Distribution of mineral groups in fraction < 2 µm (in frequency-%)*
Legend: ***IS*** *– illite-smectite-mixed layer series in sense of Środon et al. (1992), diVS – dioctahedral vermiculite-smectite illite-smectite-mixed layer series (= charge- and/or K-deficit),* ***KSV*** *– kaolinite-smectite-dioctahedral vermiculite-mixed layer series,* ***CSV*** *– chlorite-saponite-trioctahedral vermiculite-mixed layer series,* ***Si*** *– quartz or particles with Si-surplus,* ***Fe*** *– Fe-oxide or Fe-oxyhydroxide,* ***Ti*** *– Ti-bearing phases (e.g. rutile, anatase),* ***K-Fs*** *– K-feldspar*

Clay Mineral Composition

All particles of smectite group:

$$Ca_{0.14}\ Mg_{0.06}\ Na_{0.00}\ K_{0.14}\quad Al_{1.23}\ Fe^{3+}_{0.58}\ Mg_{0.19}\ Ti_{0.01}\ (OH)_2\quad Si_{3.62}\ Al_{0.38}\ O_{10}$$

Charge: XII = 0.56 VI = 5.82 IV = 15.62 **Σ = 22.00**
Probability of smectite layers (%S): 42%
Probability of illite layers (%I): 58%

Specific Dissolution Potential (ΔS%)
for H2O, 20 + 60 rpm - 4 (= slow reacting, interlayer group: Ca+Mg (= type B))
for NaCl, 20 rpm - 5 (= slow reacting, interlayer group: Ca+Mg (= type B))
for NaCl, 60 rpm -109 (= fast reacting, 'illitization', interlayer group: Na (= type A))
CEC$_{calc}$: 54 meq / 100 g (literature: 56 meq / 100 g [Matschiavelli et al., 2019: MAT19])

Measured particles: 125

Table 1. *Summarized chemical composition*

SiO_2	TiO_2	Al_2O_3	Fe_2O_3	MnO	MgO	CaO	Na_2O	K_2O	P_2O_5	Σ	
60.7%	0.2%	23.9%	6.5%		3.2%	1.6%	0.0%	1.4%		0.97	measured particles
58.6%	0.0%	22.0%	5.9%		3.0%	1.0%	0.1%	1.1%	0.1%	0.92	measured particles of original B25

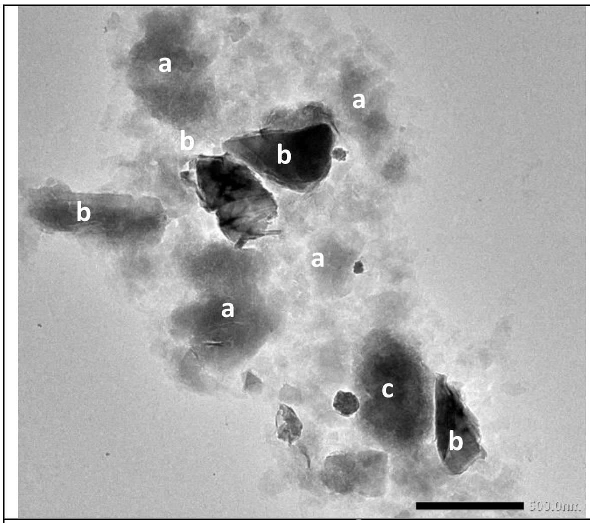	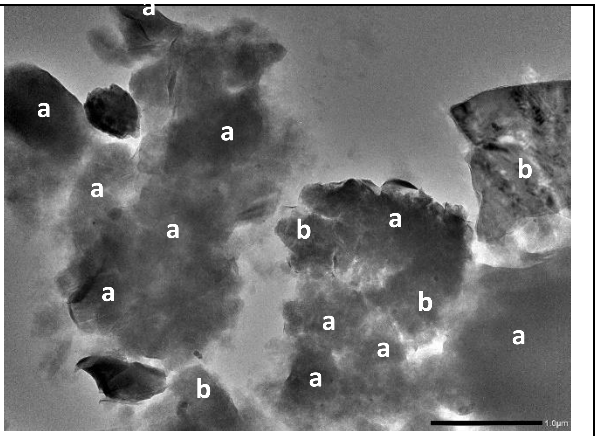
JEM-2100_No3_C_A1_X12k.bmp Magnification: 12k (ff) aggregates formed by small (≤ 200 nm) xenomorphous plates *(BM 70:30)*; (h) xenomorph film-like platy crystals partially with folds *(diVS-ml)*; (i) partially idiomorph plates (≤ 200 nm) *(KSV-ml)*	*JEM-2100_No3_C_A6_X10k.bmp* Magnification: 10k (a) aggregates formed by small (≤ 200 nm) xenomorphous plates *(BM 70:30)*; (b) xenomorph film-like platy crystals partially with folds *(diVS-ml)*

Fig. 2. *Morphology of particles (TEM-micrographs)*

Distribution of smectite layers probability (%S)

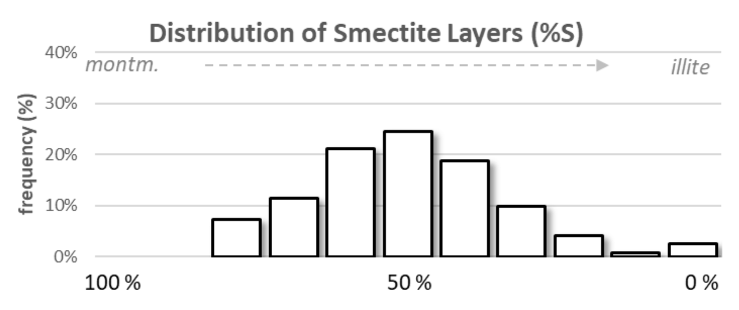

Fig. 3a. *Distribution of smectite layers probability (%S)*

Description: *The distribution of %S-probability indicates the occurrence of two groups: (i) mixture of beidellite-montmorillonite interstratifications (= assumption) with diVS-ml as well as (ii) illite with K-deficiency (%S-class = 0%).*

Differentiation by relation “Octahedral Mg vs. tetrahedral Si”?

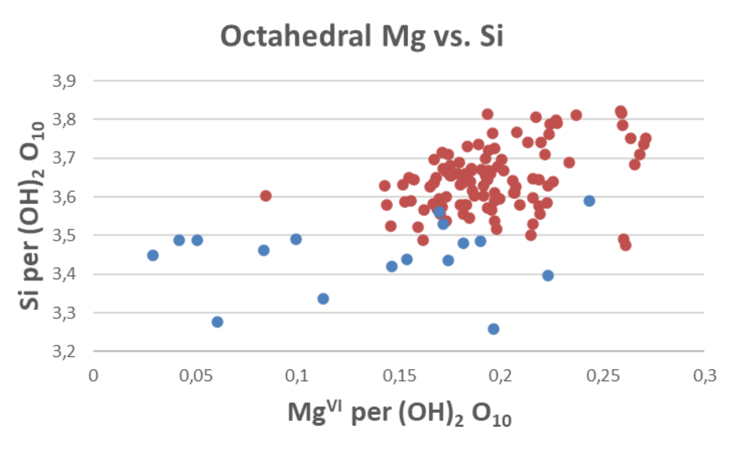

Description: *This diagram indicates the occurrence of two groups of Mg in relation to tetrahedral Si. Probably, this distribution mirrors (I) beidellite-montmorillonite interstratifications (red) and (II) diVS-ml incl. illite (blue)*

Fig. 3b. *Distribution of octahedral Mg vs. tetrahedral Si [all per(OH)$_2$ O$_{10}$]*

Distribution of K in relation to tetrahedral Si

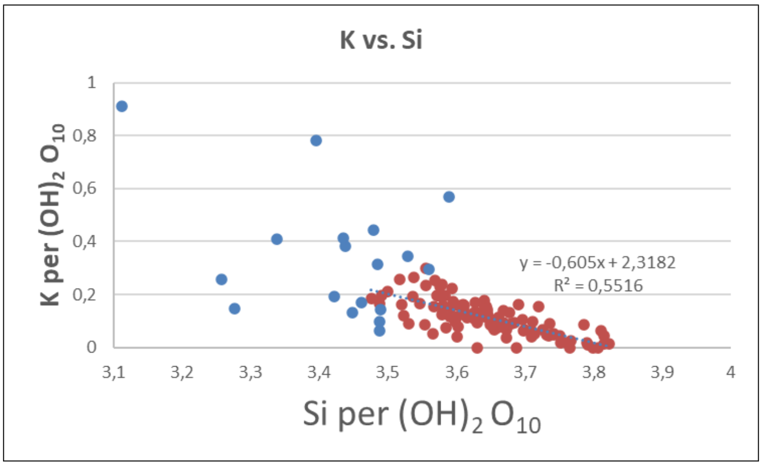

Description: This diagram visualizes possible particles of beidellite-montmorillonite interstratification (red dots) and diVS-ml phases (blue dots)

Fig. 4. *Distribution of K in interlayer space vs. tetrahedral Si [all per$(OH)_2$ O_{10}]*

Distribution of charges (exchangeable from interlayer space)

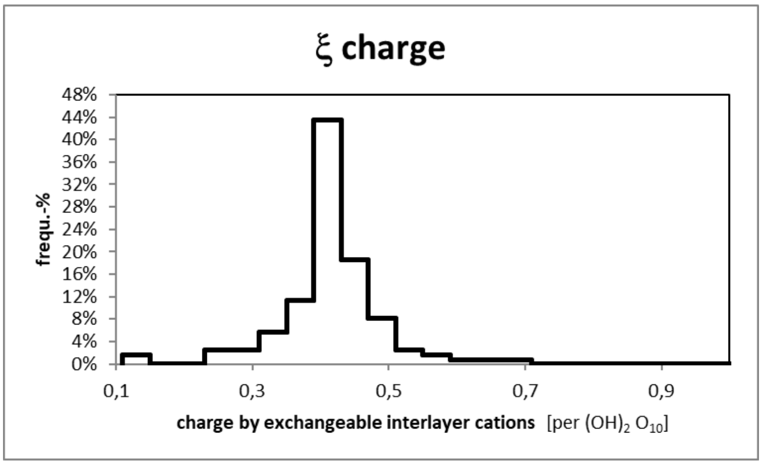

This diagram visualizes the distribution of exchangeable charges in the interlayer space (Ca, Mg, Na) determined and computed by TEM-EDX-data.

Description: *Maximal frequency-% of charge density at 0.43 per $(OH)_2$ O_{10}.*

Fig. 5. *Distribution of charges*

Beidellite-Montmorillonite interstratification (BM ~ 70%:30%) *(Cluster1):*

$Ca_{0.15}\ Mg_{0.06}\ Na_{0.00}\ K_{0.11}\quad Al_{1.20}\ Fe^{3+}_{0.60}\ Mg_{0.20}\ Ti_{0.01}\ (OH)_2\quad Si_{3.65}\ Al_{0.35}\ O_{10}$

Charge:	XII = 0.53	VI = 5.82	IV = 15.65	**Σ = 22.00**

Measured particles: 107

Distribution of BM-interstratifications (Cluster1)

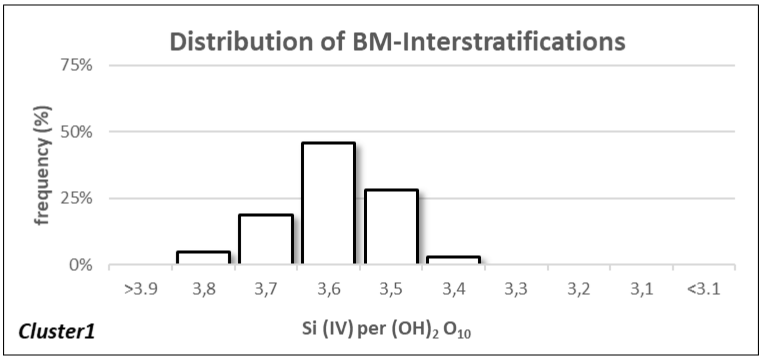

Description: *The distribution of BM-interstratifications (classified as Cluster1) draws a maximum of frequency (%) at tetrahedral Si-value between 3.6 – 3.7 e phuc*

Fig. 6a. *Distribution of assumed beidellite-montmorillonite interstratifications*

BM70:30??	particles (abs)	Ca (XII)	Mg (XII)	Na (XII)	K (XII)	Cr3+ (VI)	Al (VI)	Fe3+ (VI)	Mg (VI)	Ti (VI)	Al (IV)	Si (IV)	XII	n_VI	%S
Si >3.9	n = 0														
Si 3.9-3.8	n = 5	0,16	0,03	0,00	0,03	0,00	1,27	0,49	0,23	0,01	0,19	3,81	0,4	2,0	73
Si 3.8-3.7	n = 20	0,16	0,05	0,00	0,05	0,00	1,23	0,54	0,22	0,00	0,25	3,75	0,5	2,0	62
Si 3.7-3.6	**n = 49**	**0,14**	**0,07**	**0,00**	**0,11**	**0,00**	**1,21**	**0,60**	**0,19**	**0,01**	**0,35**	**3,65**	**0,5**	**2,0**	**47**
Si 3.6-3.5	n = 30	0,15	0,06	0,00	0,17	0,00	1,17	0,64	0,18	0,01	0,44	3,56	0,6	2,0	36
Si 3.5-3.4	n = 3	0,16	0,10	0,00	0,18	0,00	1,04	0,70	0,23	0,04	0,52	3,48	0,7	2,0	26
Si 3.4-3.3	n = 0														
Si 3.3-3.2	n = 0														
Si 3.2-3.1	n = 0														
Si <3.1	n = 0														

Fig. 6b. *Computed averaged mineral formulae of phases in the different Si(IV)-classes*

Dioctahedral Vermiculite-Smectite mixed layer phases (diVS-ml) *(Cluster2):*

$$Ca_{0.10}\ Mg_{0.07}\ Na_{0.02}\ K_{0.34}\quad Al_{1.38}\ Fe^{3+}_{0.47}\ Mg_{0.13}\ Ti_{0.02}\ (OH)_2\quad Si_{3.43}\ Al_{0.57}\ O_{10}$$

Charge: XII = 0.70 VI = 5.87 IV = 15.43 **Σ = 22.00**

Probability of smectite layers (%S): 20%

Probability of illite layers (%I): 80%

Measured particles: 18

Distribution of smectite layers probability (%S) in diVS-ml (Cluster1)

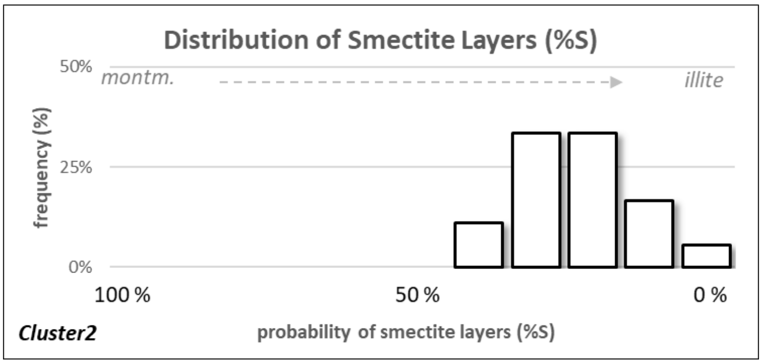

Description: *The distribution of diVS-ml (classified as Cluster1) draws a maximum of frequency (%) for smectite layer probability at 15-35%.*

Fig. 7a. *Distribution of smectite layers probability in diVS-ml*

diVS-ml??	particles (abs)	Ca (XII)	Mg (XII)	Na (XII)	K (XII)	Cr3+ (VI)	Al (VI)	Fe3+ (VI)	Mg (VI)	Ti (VI)	Al (IV)	Si (IV)	XII	n_VI	%S
%S >95%	n = 0														
%S 95-85%	n = 0														
%S 85-75%	n = 0														
%S 75-65%	n = 0														
%S 65-55%	n = 0														
%S 55-45%	n = 0														
%S 45-35%	n = 2	0,09	0,02	0,00	0,43	0,00	1,27	0,48	0,21	0,03	0,42	3,58	0,7	2,0	37
%S 35-25%	**n = 6**	**0,12**	**0,08**	**0,00**	**0,23**	**0,00**	**1,34**	**0,53**	**0,12**	**0,01**	**0,51**	**3,49**	**0,6**	**2,0**	**27**
%S 25-15%	**n = 6**	**0,10**	**0,07**	**0,00**	**0,35**	**0,00**	**1,44**	**0,40**	**0,14**	**0,02**	**0,57**	**3,43**	**0,7**	**2,0**	**21**
%S <15%	n = 4	0,07	0,10	0,09	0,43	0,00	1,39	0,49	0,11	0,01	0,75	3,25	0,8	2,0	6

Fig. 7b. *Computed averaged mineral formulae of diVS-ml phases in the different smectite layers probability (%S)-classes*

Description – B25 No3_C (< 2 µm), treated material *(OPA, 150°C, 4 days)*

Preparation for TEM

The powder of compacted and treated B25_No3_C-sample was suspended in deionized water and dispersed by ultrasonic treatment for approximately 20 min. The clay fraction (<2 µm) was separated by sedimentation and diluted with deionized water to get a clear suspension. The suspension was dropped onto carbon-coated Cu grids, air dried and stored under environment-controlled conditions at 45% humidity.

Mineral Matter - Overview

The fraction < 2 µm of treated B25 bentonite sample (Opalinus Clay solution, at 150°C, for 4 days) is mainly composed by assumed beidellite-montmorillonite interstratifications (B:M ~70:30), abbreviated as BM-ml, and dioctahedral vermiculite-smectite mixed layer phases (diVS-ml) and accompanied by two types of illite. Furthermore, kaolinite and Si surplus (e.g. quartz) were identified in traces in this sample [fig. 1].

	frequency-% *(n = 135 measured particles)*
BM-ml (Cluster1)	79%
diVS-ml (Cluster2)	13%
Si surplus (e.g. quartz)	3%
Kaolinite & KSV-ml	2%

All measured dioctahedral clay mineral phases summarized result following mineral formula computed from TEM-EDX-measurement of 125 individual particles:

	$Ca^{2+}_{0.14}$	$Mg^{2+}_{0.06}$	$Na^{+}_{0.00}$	$K^{+}_{0.14}$	$Al^{3+}_{1.23}$	$Fe^{3+}_{0.58}$	$Mg^{2+}_{0.19}$	$Ti^{4+}_{0.01}$	$(OH)_2$	$Si^{4+}_{3.62}$	$Al^{3+}_{0.38}$	O_{10}
SDOM	*± 0.00*	*± 0.00*	*± 0.00*	*± 0.01*	*± 0.01*	*± 0.01*	*± 0.00*	*± 0.00*		*± 0.01*	*± 0.01*	

Legend: SDOM - standard deviation of the mean (= the standard deviation divided by the square root of the number of samples)

The interlayer charge is calculated as 0.56 per $(OH)_2$ O_{10} and the octahedral charge as 5.83 per $(OH)_2$ O_{10}. The particles are characterized by a high octahedral Fe-amount.

The summarized chemical composition of all 125 computed particles is compared with measured data of original B25-bentonite sample [tab. 1]. The chemical composition averaged by measured particles show especially a slight higher amount of SiO_2, Al_2O_3, Fe_2O_3, CaO and K_2O in comparison to the measured data of original untreated B25-bentonite.

B25-No3_C sample is characterized by two morphological groups: (i) aggregates formed by small (≤ 200 nm) xenomorphous plates [fig. 2] and (ii) xenomorph film-like platy crystals partially with folds [fig. 2]. Thin aggregates formed by small (≤ 200 nm) xenomorphous plates dominate the shapes of particles in the micrographs [fig. 2].

The distribution of %S-probability of all measured clay mineral phases [fig. 3a] also indicates the occurrence of two groups: (i) as main group a mixture of beidellite-montmorillonite interstratifications

and diVS-ml (%S-max of this mixture for %S at 15-35%) and (ii) illite with K- and charge deficit (%S-classes = 0% & 10%).

The numerous measured particles by TEM-EDX allow a visualization of distribution of interlayer charges. Considering the TEM-EDX-determined cations Ca^{++}, Mg^{++} and Na^{+} and then computed their ratio as interlayer cations in the mineral formula, Ca^{++}, Mg^{++} and Na^{+} offer to characterize the degree of exchangeable charges in the interlayer space. This charge density of treated B25 bentonite (< 2 µm) shows a narrow maximal distribution of charge density at 0.43 per $(OH)_2\ O_{10}$ [fig. 5]. This interval of interlayer charge density is caused by exchangeable cations from 0.19 – 0.26 per $(OH)_2\ O_{10}$ representing mainly the BM-phases and from 0.11 – 0.25 per $(OH)_2\ O_{10}$ represented mainly by diVS-ml phases.

Mineral Matter - Specification

Result of Clustering

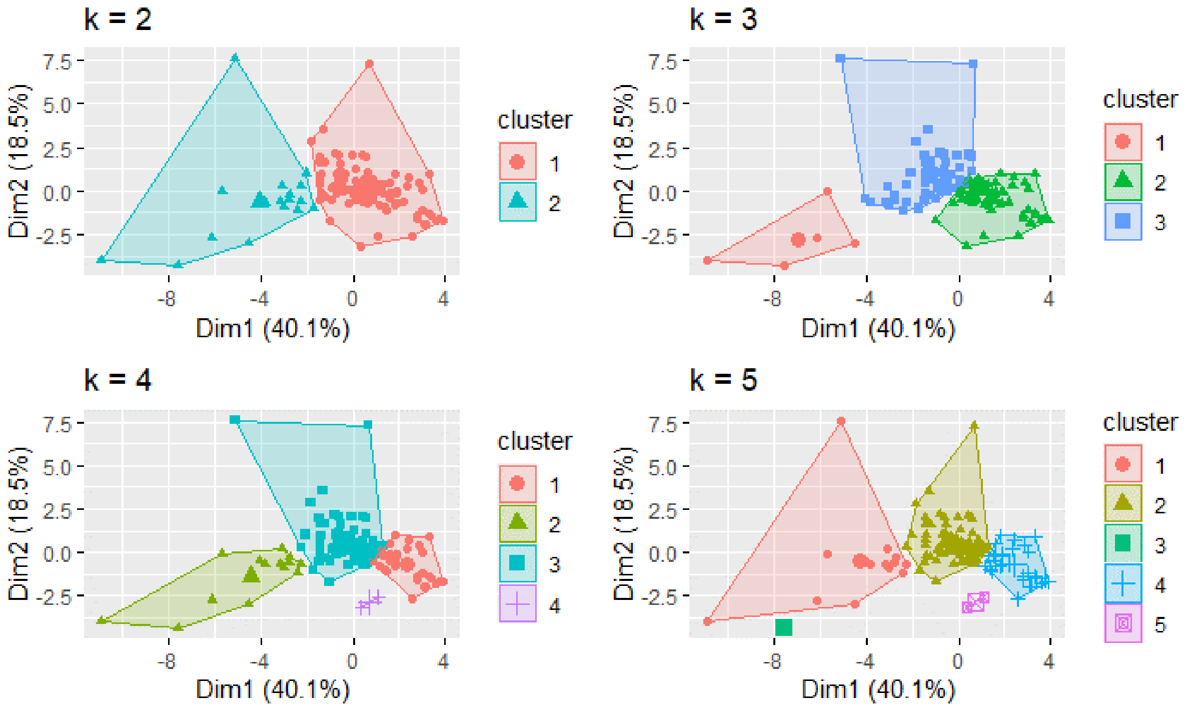

Fig. 8. *Clustering of all measured particles for clusters k = 2, k = 3, k = 4 and k = 5 (source for R-coding: https://uc-r.github.io/kmeans_clustering)*

The optimum of clusters was calculated with k = 2.

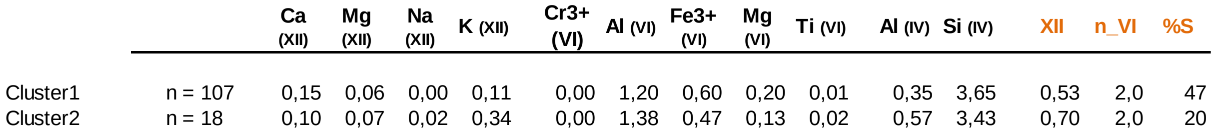

		Ca (XII)	Mg (XII)	Na (XII)	K (XII)	Cr3+ (VI)	Al (VI)	Fe3+ (VI)	Mg (VI)	Ti (VI)	Al (IV)	Si (IV)	XII	n_VI	%S
Cluster1	n = 107	0,15	0,06	0,00	0,11	0,00	1,20	0,60	0,20	0,01	0,35	3,65	0,53	2,0	47
Cluster2	n = 18	0,10	0,07	0,02	0,34	0,00	1,38	0,47	0,13	0,02	0,57	3,43	0,70	2,0	20

Fig. 9. *Mineral formulae based on TEM-EDX-data summarized following the result of clustering for k=2*

	Sybilla-results	TEM-EDX-results	Notes
Cluster1	IS R0(1) *(%S = 100%)*	BM-ml *(BM 70:30?)*	*XRD: Montmorillonite and beidellite is only to distinguish by Green-Kelly-test (not available here).*
Cluster2	IS R0(2) *(%S = 22%)*	diVS-ml *(%S = 20%)*	*Low K, Fe(VI)-rich*

Tab. 2. *Comparison of results from TEM-EDX- and XRD-measurements with clustering procedure*

The clustering of TEM-EDX-data offers a good agreement with the recent result of Sybilla-processing of XRD-traces from oriented specimen [tab. 2].

IS R0 (1): The X-ray diffraction pattern of the ethylene-glycol saturated oriented specimen shows a full expandability to 1.7 nm and a difference of 5.44°2θ between 2. and 3. order of smectite interferences. This distance is typically for montmorillonite (Moore & Reynolds, 1989). This result of XRD-processing let expect a maximum of particles for %S ~ 100% by TEM-EDX-measurements, but the maximum of particles measured by TEM-EDX is to find at %S=50% [fig. 3a].

Montmorillonite and beidellite have the same behavior concerning the expandability and they are only to distinguish by XRD using Li like by Greene-Kelly test (Green-Kelly 1952, 1953). So, combination of XRD- and TEM-results (full expandability by XRD and Si ~ 3.65 by TEM-EDX) led conclude the occurrence of 'beidellite-montmorillonite interstratifications', a beidellite-montmorillonite interstratification with about 70% beidellite and 30% montmorillonite layers (BM-ml 70:30).

IS R0 (2): The Sybilla-procedure of XRD-traces (oriented mounts) has shown an occurrence of a second illite-smectite mixed layer phase with a smectite layers probability of %S = 22%. This situation is to find in Cluster1 ($\%S_{TEM}$ = 20%) representing a high K-, but low charge deficient and very Fe-rich dioctahedral vermiculite-smectite mixed layer phase (diV-ml) [tab. 2].

The Sybilla-processing of XRD-traces (oriented mounts) also supports the existence of kaolinite and kaolinite-smectite mixed layer phases in fine fraction of sample. Such phases were not to identify or to calculate in TEM-EDX-database (a grain size effect?).

Specifics to the identified clay mineral groups

Beidellite-montmorillonite interstratifications (B:M ~70:30?)

107 of 125 measured particles belong so to this assumed classification. The dioctahedral character of this group is proofed by X-ray diffraction. The position of the large (060)-interference of smectite is in the random oriented powder specimen at 1.497 Å.

Montmorillonite and beidellite have the same behavior concerning the expandability and they are only to distinguish by XRD using Li by means of Greene-Kelly test (Green-Kelly 1952, 1953). So, combination of XRD- and TEM-results (full expandability by XRD and Si ~ 3.65 by TEM-EDX) led conclude the occurrence of 'beidellite-montmorillonite interstratifications', a beidellite-montmorillonite interstratification with about 70% beidellite and 30% montmorillonite layers (BM-ml 70:30).

Beidellite-montmorillonite interstratifications (B:M ~70:30?):

$$Ca_{0.15}\ Mg_{0.06}\ Na_{0.00}\ K_{0.11}\quad Al_{1.20}\ Fe^{3+}_{0.60}\ Mg_{0.20}\ Ti_{0.01}\ (OH)_2\ \ Si_{3.65}\ Al_{0.35}\ O_{10}$$

Charge: XII = 0.53 VI = 5.82 IV = 15.65 **Σ = 22.00**

Measured particles by TEM-EDX: 107
Result of clustering: Cluster1 [tab. 2]

Beidellitic structures are characterized by a low octahedral Mg-amount (because of high ratio of octahedral, 3-valent cations). A comparison of octahedral Mg vs. tetrahedral Si indicates the occurrence of two groups for octahedral Mg based on TEM-EDX-data, separated by tetrahedral Si [fig. 3b].

The core of BM-ml shows an octahedral Mg-amount between 0.18 – 0.23 e phuc, probably pronounced by a higher Mg^{VI} in montmorillonite compound in this type of interstratification.

Using the results of clustering (see Cluster1 in tab. 2), the maximum of frequency-% is to find for particles in the Si(IV)-class 3.6 – 3.7 e phuc [tab. 6a], representing the mentioned relation 30% montmorillonite and 70% beidellite as ratio of interstratification. The mineral formulae, summarized in classes of tetrahedral Si, draw for the maximum an Fe-rich BM 70:30 phase with K and remarkable amount of Mg in the interlayer space [tab. 6b].

A further hypothesis is to verify: The increasing K by lower tetrahedral Si [tab. 6b] could be an indication that it's not a change of 50:50 ratio of BM-ml into a 70:30 ratio of BM-ml, but an alteration of montmorillonite into diVS-ml phases resulting into an interstratification by beidellite – montmorillonite – dioctahedral vermiculite.

Dioctahedral vermiculite-smectite mixed layer phase (low K diVS-ml):

$$Ca_{0.10}\,Mg_{0.07}\,Na_{0.02}\,K_{0.34}\quad Al_{1.38}\,Fe^{3+}_{0.47}\,Mg_{0.13}\,Ti_{0.02}\,(OH)_2\quad Si_{3.43}\,Al_{0.70}\,O_{10}$$

Charge: XII = 0.70 VI = 5.87 IV = 15.43 **Σ = 22.00**
Probability of smectite layers (%S): 20%
Probability of illite layers (%I): 80%

Measured particles by TEM-EDX: 18
Result of clustering: Cluster1 [tab. 2]

Illite as part of diVS-ml series (high K diVS-ml):

The Rietveld refinement by Profex software (Döbelin & Kleeberg, 2015) indicates the occurrence of two polytypes for illite in treated B25 bentonite: $2M_1$- and 1M-polytype.

Kaolinite-montmorillonite-dioctahedral vermiculite mixed layer phases

The Excel-based procedure (Hoang-Minh et al., 2019) to identify possible clay mineral groups using the TEM-EDX-measurements also includes algorithms to classify kaolinite and kaolinite-montmorillonite mixed layer phases. These algorithms could identify four such phases basing on the measured TEM-EDX-data. Otherwise, very few particles, which were not to compute, have shown small hexagonal plates typically for kaolinite-bearing phases.

References

Cliff, G. & Lorimer, G. W. (1975). *J. Microsc.* **103**, 203–207.

Döbelin, N., Kleeberg, R. (2015). *Journal of Applied Crystallography* **48**, 1573-1580. DOI: 10.1107/S1600576715014685

Henning, K.-H. & Störr, M. (1986). Electron Micrographs (TEM, SEM) of Clays and Clay Minerals, p. 325. Akademie-Verlag Berlin.

Hoang-Minh, T., Kasbohm, J., Nguyen-Thanh, L., Nga, P. T., Lai, L. T., Duong, N. T., Thanh, N. D., Thuyet, N. T. M., Anh, D. D., Pusch, R., Knutsson, S. & Ferreiro Mahlmann, R. (2019). *J. Appl. Cryst.* **52**, 133-147. DOI: 10.1107/S1600576718018162

Lorimer, G. W. & Cliff, G. (1976). *Electron Microscopy in Mineralogy*, edited by H. R. Wenk, pp. 506–519. Berlin: Springer Verlag.

Matschiavelli, N., Kluge, S., Podlech, C., Standhaft, D., Grathoff, G., Ikeda-Ohno, A., Warr, L.N., Chukharkina, A., Arnold, T. & Cherkouk, A. (2019). *Environmental Science & Technology.* **53** (17), 10514-10524, DOI: 10.1021/acs.est.9b02670

Mellini, M. & Menichini, R. (1985). *R. Soc. Ital. Miner. Petrol.* **40**, 261–266.

Moore, D.M., Reynolds, R.C. (1989). X-ray Diffraction and the Identification and Analysis of Clay Minerals, Oxford University Press, New York, 332 + xvi pp.

Nguyen-Thanh, L., Herbert, H.-J., Kasbohm, J., Hoang-Minh, T. & Mählmann, R. F. (2014). *Clays Clay Miner.* **62**, 425–446.

Środoń, J., Elsass, F., McHardy, W. J. & Morgan, D. J. (1992). *Clay Miner.* **27**, 137–158.

Data Sheet – B25 bentonite, treated materials *(OPA, 150°C, 4d)* - BOTTOM

Methodology - Transmission electron microscopy linked with energy-dispersive X-ray spectroscopy (TEM-EDX)

It is expected a characterization of clay mineral phases in treated B25 bentonite by transmission electron microscopy. The sample series No3 represents a percolation of B25 bentonite by Opalinus Clay solution at 150°C for 4 days. The sample No3_B is the label for the material at the bottom of sample cylinder.

The different clay mineral phases are to identify and to describe by chemical composition and its variability, morphology, the specific dissolution potential, and further parameter.

Such further parameter like distribution of smectite layers probability (%S) and distribution of charges caused by exchangeable cations interlayer space should serve as additional indicators for mineralogical alterations in treatment experiments with B25 bentonite.

The sample were suspended for TEM-measurement in deionized water and dispersed by ultrasonic treatment for approximately 20 min. The clay fraction (<2 µm) was separated by sedimentation and diluted with deionized water to get a clear suspension. The suspension was dropped onto carbon-coated Cu grids, air dried and stored under environment-controlled conditions at 45% humidity.

TEM-EDX investigations were carried out on the <2 µm fraction using a FEI TECNAI G^2 20 electron transmission microscope at the VNU University of Science, Vietnam National University, Hanoi. This equipment (operated at 200 kV with LaB_6 cathode) was combined with an S-TWIN objective, a windowless EDAX energy-dispersive X-ray system and a FEI Eagle 2k CCD TEM camera.

About 100 individual clay particles per sample were characterized by TEM-EDX with respect to crystal size, crystal habit, and particle morphology and element distribution. The crystal size, crystal habit and particle morphology were described according to Henning & Störr (1986).

For the quantification of element distribution, a calibration of k factors is mandatory (Cliff & Lorimer, 1975; Lorimer & Cliff, 1976; Mellini & Menichini, 1985). These k values are used to calibrate for the specific behaviour of particles against possible irradiation damage. The elements O, Na, Mg, Al, Si, K, Ca and Fe were quantified by applying the EDAX GENESIS–TEM Quant Materials quantification procedure.

In this procedure, the acquired EDX spectra are corrected by background subtraction, Gaussian deconvolution and k-factor corrections using values previously determined on a phyllosilicate standard (muscovite) and selected non-phyllosilicate standards. The average errors in the analyzed elements using the phyllosilicate standard, expressed as the atomic proportions, are 10 (Na), 5 (Fe, Mg, K, Ti, Ca) and 1 (Si, Al).

The measurement time per particle was lowered to 20 s and the exposed area was limited to a 50 nm diameter, avoiding possible irradiation damage of particles. The stability of particles of the sample series was tested for this measurement time at the beginning of any measurement campaign.

Further methodological details related to TEM-EDX-measurements and the Excel-based mathematical procedure using TEM-EDX data for calculation of mineral formulae are described in Hoang-Minh et al. (2019).

These mathematical procedures described in Hoang-Minh et al. (2019) were extended by k-means clustering method for finding subgroups of observations within a data set. The data were standardized (i.e., scaled) to make variables comparable. Euclidean distances were applied as classical method for distance measures. The optimal clusters were determined by Elbow method and Gap statistics[19].

---

[19] *https://uc-r.github.io/kmeans_clustering*

Data Sheet – B25 No3_B (< 2 µm), treated material *(OPA, 150°C, 4 days)*

Preparation for TEM

- raw material: compacted material (1.6 g/cm³) of treated B25-sample (OPA, 150°C, 4 days)
- suspension on particles < 2 µm on carbon-filmed Cu-grid
- air-dried and humidity-controlled storing

Mineral Matter

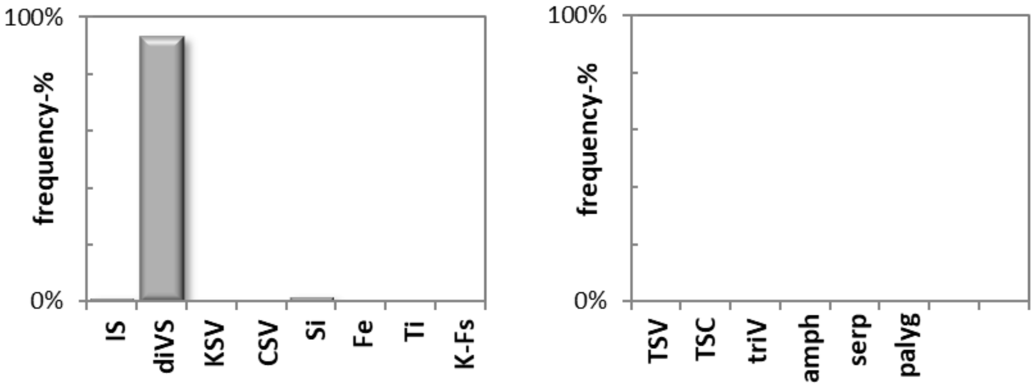

Fig. 1. *Distribution of mineral groups in fraction < 2 µm (in frequency-%)*
*Legend: **IS** – illite-smectite-mixed layer series in sense of Środon et al. (1992), diVS – dioctahedral vermiculite-smectite illite-smectite-mixed layer series (= charge- and/or K-deficit), **KSV** – kaolinite-smectite-dioctahedral vermiculite-mixed layer series, **CSV** – chlorite-saponite-trioctahedral vermiculite-mixed layer series, **Si** – quartz or particles with Si-surplus, **Fe** – Fe-oxide or Fe-oxyhydroxide, **Ti** – Ti-bearing phases (e.g. rutile, anatase), **K-Fs** – K-feldspar*

Clay Mineral Composition

All particles of smectite group:

$$Ca_{0.20}\,Mg_{0.04}\,Na_{0.00}\,K_{0.14}\quad Al_{1.19}\,Fe^{3+}_{0.58}\,Mg_{0.22}\,Ti_{0.01}\,(OH)_2\quad Si_{3.59}\,Al_{0.41}\,O_{10}$$

Charge: XII = 0.62 VI = 5.79 IV = 15.59 **Σ = 22.00**

Probability of smectite layers (%S): 38%

Probability of illite layers (%I): 62%

Specific Dissolution Potential (ΔS%)

for H2O, 20 + 60 rpm - 6 (= medium reacting, interlayer group: Ca+Mg (= type B))

for NaCl, 20 rpm - 6 (= medium reacting, interlayer group: Ca+Mg (= type B))

for NaCl, 60 rpm -109 (= fast reacting, 'illitization', interlayer group: Na (= type A))

CEC$_{calc}$: 68 meq / 100 g (literature: 56 meq / 100 g [Matschiavelli et al., 2019: MAT19])

Measured particles: 142

Table 1. *Summarized chemical composition*

SiO_2	TiO_2	Al_2O_3	Fe_2O_3	MnO	MgO	CaO	Na_2O	K_2O	P_2O_5	Σ	
61.2%	0.2%	24.0%	6.7%		3.5%	2.4%	0.0%	1.2%		0.99	measured particles
58.6%	0.0%	22.0%	5.9%		3.0%	1.0%	0.1%	1.1%	0.1%	0.92	measured particles of original B25

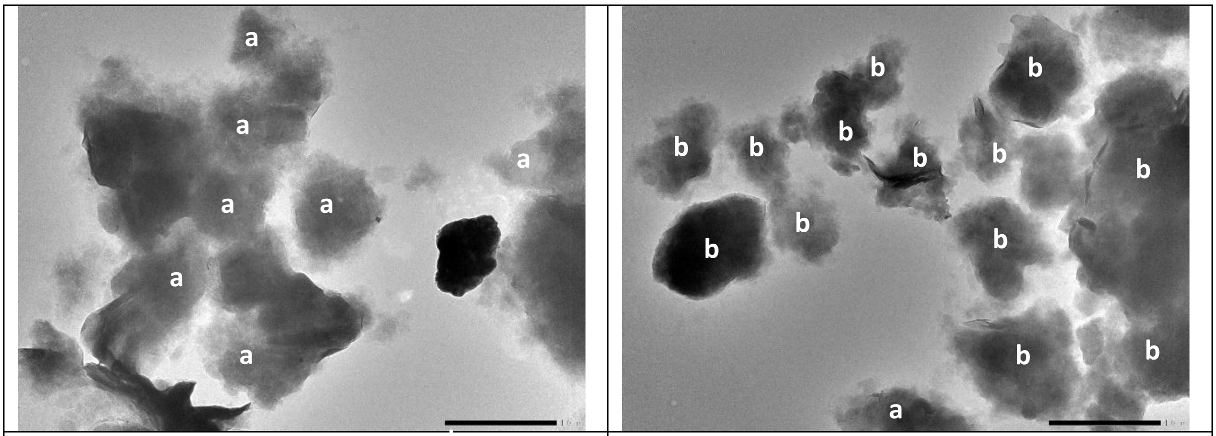

JEM-2100_No3_B_A3_X10k.bmp Magnification: 10k (gg) aggregates formed by small (≤ 200 nm) xenomorphous plates *(BM 70:30)*	*JEM-2100_No3_B_A5_X10k.bmp* Magnification: 10k (a) aggregates formed by small (≤ 200 nm) xenomorphous plates *(BM 70:30)* (b) xenomorph film-like platy crystals partially with folds *(diVS-ml)*

Fig. 2. *Morphology of particles (TEM-micrographs)*

Distribution of smectite layers probability (%S)

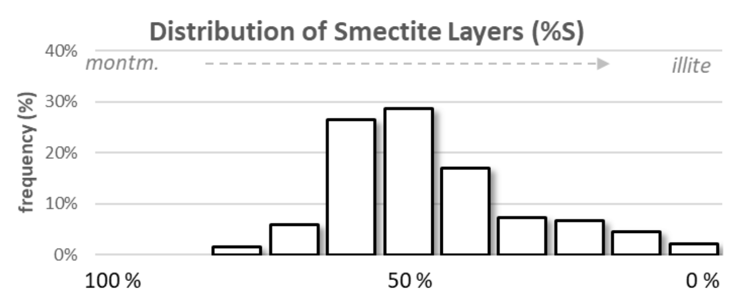

Description: *The distribution of %S-probability indicates the occurrence of two groups: (i) mixture of beidellite-montmorillonite interstratifications (= assumption) with diVS-ml as well as (ii) illite with K-deficiency (%S-class = 0%).*

Fig. 3a. *Distribution of smectite layers probability (%S)*

Differentiation by relation "Octahedral Mg vs. tetrahedral Si"?

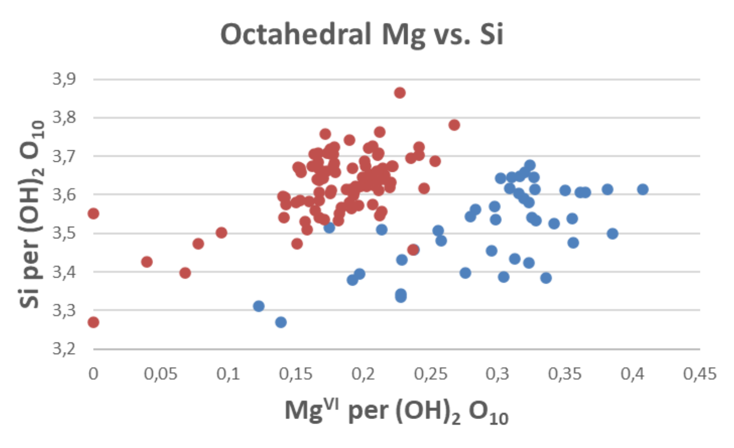

Description: *This diagram indicates the occurrence of two groups of Mg in relation to tetrahedral Si. Probably, this distribution mirrors (I) beidellite-montmorillonite interstratifications (red) and (II) diVS-ml incl. illite (blue)*

Fig. 3b. *Distribution of octahedral Mg vs. tetrahedral Si [all per $(OH)_2$ O_{10}]*

Distribution of K in relation to tetrahedral Si

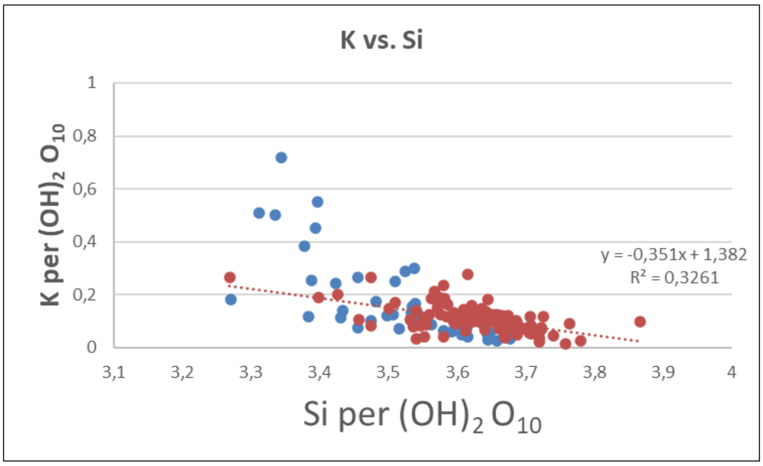

Description: *This diagram visualizes possible particles of beidellite-montmorillonite interstratification (red dots) and diVS-ml phases (blue dots)*

Fig. 4. *Distribution of K in interlayer space vs. tetrahedral Si [all per$(OH)_2$ O_{10}]*

Distribution of charges (exchangeable from interlayer space)

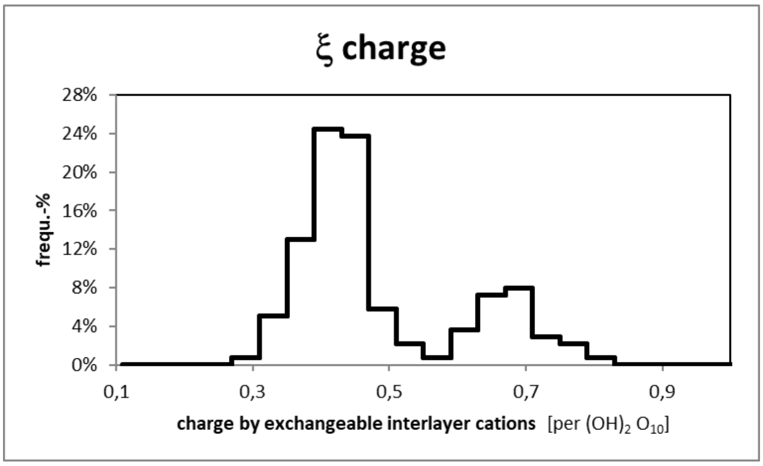

Fig. 5. *Distribution of charges*

This diagram visualizes the distribution of exchangeable charges in the interlayer space (Ca, Mg, Na) determined and computed by TEM-EDX-data.

Description: *Maximal frequency-% of charge density in a bimodal distribution at 0.43-0.47 and at 0.67-0.71 per $(OH)_2$ O_{10}.*

Beidellite-Montmorillonite interstratification (BM ~ 70%:30%) *(Cluster2):*

$$Ca_{0.15}\ Mg_{0.06}\ Na_{0.00}\ K_{0.11}\quad Al_{1.22}\ Fe^{3+}_{0.59}\ Mg_{0.18}\ Ti_{0.01}\ (OH)_2\quad Si_{3.63}\ Al_{0.37}\ O_{10}$$

Charge: XII = 0.53 VI = 5.84 IV = 15.63 **Σ = 22.00**

Measured particles: 96

Distribution of BM-interstratifications (Cluster2)

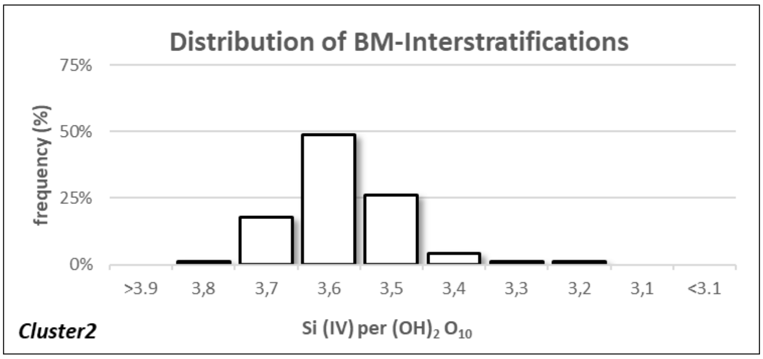

Description: *The distribution of BM-interstratifications (classified as Cluster2) draws a maximum of frequency (%) at tetrahedral Si-value between 3.6 – 3.7 e phuc*

Fig. 6a. *Distribution of assumed beidellite-montmorillonite interstratifications*

BM70:30??	particles (abs)	Ca (XII)	Mg (XII)	Na (XII)	K (XII)	Cr3+ (VI)	Al (VI)	Fe3+ (VI)	Mg (VI)	Ti (VI)	Al (IV)	Si (IV)	XII	n_VI	%S
Si >3.9	n = 0														
Si 3.9-3.8	n = 1	0,12	0,07	0,00	0,10	0,00	1,14	0,58	0,23	0,01	0,13	3,87	0,5	2,0	83
Si 3.8-3.7	n = 17	0,14	0,06	0,00	0,06	0,00	1,24	0,56	0,20	0,01	0,28	3,72	0,5	2,0	58
Si 3.7-3.6	**n = 47**	**0,15**	**0,06**	**0,00**	**0,11**	**0,00**	**1,18**	**0,61**	**0,19**	**0,01**	**0,35**	**3,65**	**0,5**	**2,0**	**47**
Si 3.6-3.5	n = 25	0,15	0,06	0,00	0,13	0,00	1,22	0,61	0,16	0,02	0,44	3,56	0,5	2,0	35
Si 3.5-3.4	n = 4	0,12	0,12	0,00	0,16	0,00	1,30	0,56	0,13	0,02	0,54	3,46	0,7	2,0	23
Si 3.4-3.3	n = 1	0,11	0,12	0,00	0,19	0,00	1,61	0,30	0,07	0,03	0,60	3,40	0,6	2,0	18
Si 3.3-3.2	n = 1	0,08	0,13	0,00	0,27	0,00	1,74	0,25	0,00	0,01	0,73	3,27	0,7	2,0	7
Si 3.2-3.1	n = 0														
Si <3.1	n = 0														

Fig. 6b. *Computed averaged mineral formulae of phases in the different Si(IV)-classes*

Dioctahedral Vermiculite-Smectite mixed layer phases (diVS-ml) *(Cluster1):*

$Ca_{0.29}\ Mg_{0.0}\ Na_{0.01}\ K_{0.18}\quad Al_{1.12}\ Fe^{3+}_{0.58}\ Mg_{0.29}\ Ti_{0.01}\ (OH)_2\ \ Si_{3.52}\ Al_{0.48}\ O_{10}$

Charge: XII = 0.79 VI = 5.69 IV = 15.52 **Σ = 22.00**

Probability of smectite layers (%S):	30%
Probability of illite layers (%I):	70%
Measured particles:	44

Distribution of smectite layers probability (%S) in diVS-ml (Cluster1)

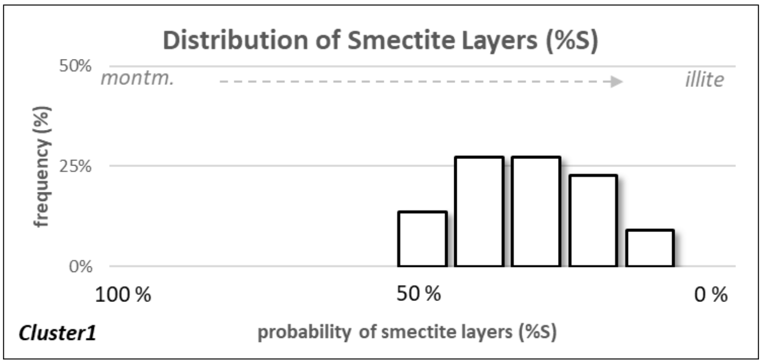

Description: *The distribution of diVS-ml (classified as Cluster1) draws a maximum of frequency (%) for smectite layer probability at 25-45%.*

Fig. 7a. *Distribution of smectite layers probability in diVS-ml*

diVS-ml	particles (abs)	Ca (XII)	Mg (XII)	Na (XII)	K (XII)	Cr3+ (VI)	Al (VI)	Fe3+ (VI)	Mg (VI)	Ti (VI)	Al (IV)	Si (IV)	XII	n_VI	%S
%S >95%	n = 0														
%S 95-85%	n = 0														
%S 85-75%	n = 0														
%S 75-65%	n = 0														
%S 65-55%	n = 0														
%S 55-45%	n = 6	0,33	0,00	0,00	0,04	0,00	1,11	0,55	0,32	0,00	0,35	3,65	0,7	2,0	48
%S 45-35%	**n = 12**	**0,34**	**0,00**	**0,00**	**0,08**	**0,00**	**1,04**	**0,61**	**0,34**	**0,00**	**0,40**	**3,60**	**0,8**	**2,0**	**40**
%S 35-25%	**n = 12**	**0,29**	**0,02**	**0,00**	**0,17**	**0,00**	**1,07**	**0,62**	**0,30**	**0,01**	**0,48**	**3,52**	**0,8**	**2,0**	**30**
%S 25-15%	n = 10	0,28	0,01	0,01	0,26	0,00	1,12	0,60	0,27	0,01	0,59	3,41	0,9	2,0	19
%S <15%	n = 4	0,15	0,02	0,05	0,48	0,00	1,46	0,35	0,18	0,01	0,68	3,32	0,8	2,0	11

Fig. 7b. *Computed averaged mineral formulae of diVS-ml phases in the different smectite layers probability (%S)-classes*

Description – B25 No3_B (< 2 µm), treated material *(OPA, 150°C, 4 days)*

Preparation for TEM

The powder of compacted and treated B25_No3_B-sample was suspended in deionized water and dispersed by ultrasonic treatment for approximately 20 min. The clay fraction (<2 µm) was separated by sedimentation and diluted with deionized water to get a clear suspension. The suspension was dropped onto carbon-coated Cu grids, air dried and stored under environment-controlled conditions at 45% humidity.

Mineral Matter - Overview

The fraction < 2 µm of treated B25 bentonite sample (Opalinus Clay solution, at 150°C, for 4 days) is mainly composed by assumed beidellite-montmorillonite interstratifications (B:M ~70:30), abbreviated as BM-ml, and dioctahedral vermiculite-smectite mixed layer phases (diVS-ml) and accompanied by two types of illite. Furthermore, kaolinite and Si surplus (e.g. quartz) were identified in traces in this sample [fig. 1].

	frequency-% *(n = 150 measured particles)*
BM-ml (Cluster2)	64%
diVS-ml (Cluster1)	29%
Si surplus (e.g. quartz)	2%
Kaolinite & KSV-ml	1%

All measured dioctahedral clay mineral phases summarized result following mineral formula computed from TEM-EDX-measurement of 140 individual particles:

	$Ca^{2+}_{0.20}$	$Mg^{2+}_{0.04}$	$Na^{+}_{0.00}$	$K^{+}_{0.14}$	$Al^{3+}_{1.19}$	$Fe^{3+}_{0.58}$	$Mg^{2+}_{0.22}$	$Ti^{4+}_{0.01}$	$(OH)_2$	$Si^{4+}_{3.59}$	$Al^{3+}_{0.41}$	O_{10}
SDOM	*± 0.01*	*± 0.00*	*± 0.00*	*± 0.01*	*± 0.01*	*± 0.01*	*± 0.01*	*± 0.00*		*± 0.01*	*± 0.01*	

Legend: SDOM - standard deviation of the mean (= the standard deviation divided by the square root of the number of samples)

The interlayer charge is calculated as 0.62 per $(OH)_2$ O_{10} and the octahedral charge as 5.80 per $(OH)_2$ O_{10}. The particles are characterized by a high octahedral Fe-amount.

The summarized chemical composition of all 140 computed particles is compared with measured data of original B25-bentonite sample [tab. 1]. The chemical composition averaged by measured particles show especially a higher amount of SiO_2, Al_2O_3, Fe_2O_3, MgO and CaO in comparison to the measured data of original untreated B25-bentonite.

B25-No3_B sample is characterized by two morphological groups: (i) aggregates formed by small (≤ 200 nm) xenomorphous plates [fig. 2 left] and (ii) xenomorph film-like platy crystals partially with folds [fig. 2 right]. Thin aggregates formed by small (≤ 200 nm) xenomorphous plates dominate the shapes of particles in the micrographs [fig. 2 left].

The distribution of %S-probability of all measured clay mineral phases [fig. 3a] also indicates the occurrence of two groups: (i) as main group a mixture of beidellite-montmorillonite interstratifications

and diVS-ml (%S-max of this mixture for %S at 45-65%) and (ii) illite with K- and charge deficit (%S-classes = 0% & 10%).

The numerous measured particles by TEM-EDX allow a visualization of distribution of interlayer charges. Considering the TEM-EDX-determined cations Ca^{++}, Mg^{++} and Na^{+} and then computed their ratio as interlayer cations in the mineral formula, Ca^{++}, Mg^{++} and Na^{+} offer to characterize the degree of exchangeable charges in the interlayer space. This charge density of treated B25 bentonite (< 2 µm) shows a broader, bimodal maximal distribution of charge density at 0.43 – 0.47 and 0.67 – 0.71 per $(OH)_2\ O_{10}$ [fig. 5]. This interval of interlayer charge density is caused by exchangeable cations from 0.19 – 0.21 per $(OH)_2\ O_{10}$ representing mainly the BM-phases and from 0.21 – 0.34 per $(OH)_2\ O_{10}$ represented mainly by diVS-ml phases.

Mineral Matter - Specification

Result of Clustering

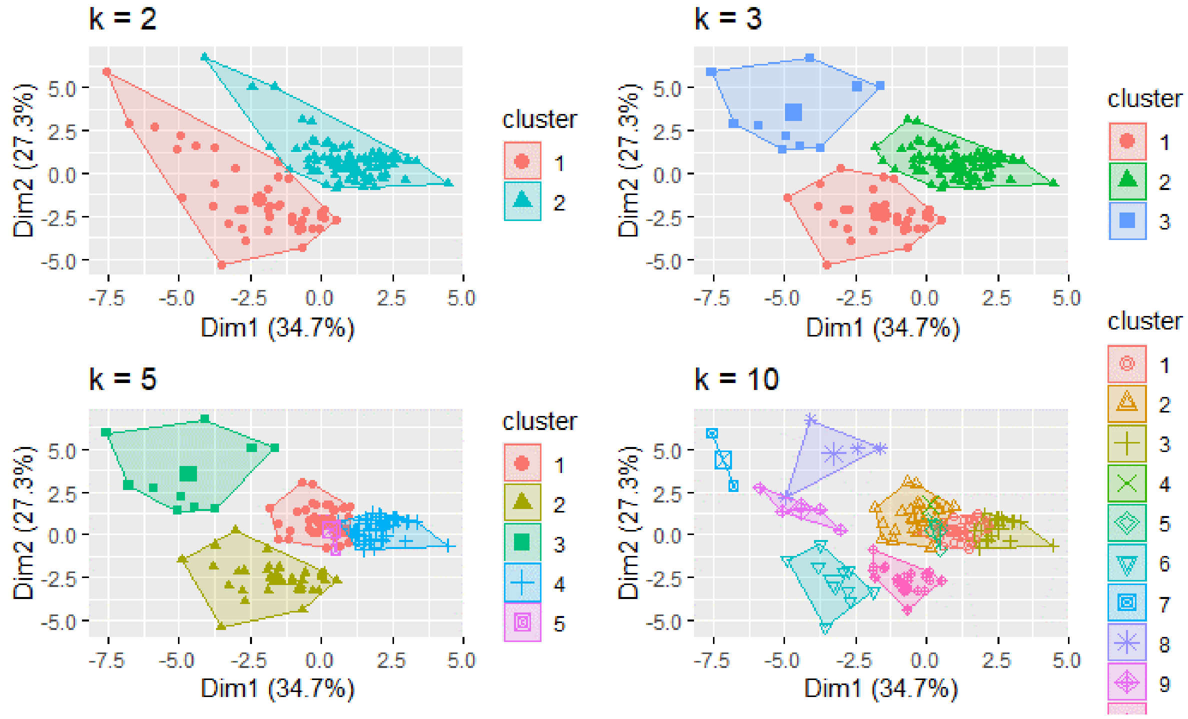

Fig. 8. Clustering of all measured particles for clusters k = 2, k = 3, k = 4 and k = 5 (source for R-coding: https://uc-r.github.io/kmeans_clustering)

The optimum of clusters was calculated with k = 2.

		Ca (XII)	Mg (XII)	Na (XII)	K (XII)	Cr3+ (VI)	Al (VI)	Fe3+ (VI)	Mg (VI)	Ti (VI)	Al (IV)	Si (IV)	XII	n_VI	%S
Cluster1	n = 44	0,29	0,01	0,01	0,18	0,00	1,12	0,58	0,29	0,01	0,48	3,52	0,79	2,0	30
Cluster2	n = 96	0,15	0,06	0,00	0,11	0,00	1,22	0,59	0,18	0,01	0,37	3,63	0,53	2,0	44

***Fig. 9.** Mineral formulae based on TEM-EDX-data summarized following the result of clustering for k=2*

	Sybilla-results	**TEM-EDX-results**	**Notes**
Cluster2	IS R0(1) *(%S = 100%)*	BM-ml *(%B ~ 75%)*	*XRD: Montmorillonite and beidellite is only to distinguish by Green-Kelly-test (not available here).*
Cluster1	IS R0(2) *(%S = 27%)*	diVS-ml *(%S = 30%)*	*Low K, Fe(VI)-rich*

***Tab. 2.** Comparison of results from TEM-EDX- and XRD-measurements with clustering procedure*

The clustering of TEM-EDX-data offers a good agreement with the recent result of Sybilla-processing of XRD-traces from oriented specimen [tab. 2].

IS R0 (1): The X-ray diffraction pattern of the ethylene-glycol saturated oriented specimen shows a full expandability to 1.7 nm and a difference of 5.38°2θ between 2. and 3. order of smectite interferences. This distance is typically for montmorillonite (Moore & Reynolds, 1989). This result of XRD-processing let expect a maximum of particles for %S ~ 100% by TEM-EDX-measurements, but the maximum of particles measured by TEM-EDX is to find at %S=50% [fig. 3a].

Montmorillonite and beidellite have the same behavior concerning the expandability and they are only to distinguish by XRD using Li like by Greene-Kelly test (Green-Kelly 1952, 1953). So, combination of XRD- and TEM-results (full expandability by XRD and Si ~ 3.63 by TEM-EDX) led conclude the occurrence of 'beidellite-montmorillonite interstratifications', a beidellite-montmorillonite interstratification with about 75% beidellite and 25% montmorillonite layers (BM-ml 75:25).

IS R0 (2): The Sybilla-procedure of XRD-traces (oriented mounts) has shown an occurrence of a second illite-smectite mixed layer phase with a smectite layers probability of %S = 27%. This situation is to find in Cluster1 ($\%S_{TEM}$ = 30%) representing a high K-deficient, a normal interlayer charge and very Fe-rich dioctahedral vermiculite-smectite mixed layer phase (diV-ml) [tab. 2].

The Sybilla-processing of XRD-traces (oriented mounts) also supports the existence of kaolinite and kaolinite-smectite mixed layer phases in fine fraction of sample. Such phases were not to identify or to calculate in TEM-EDX-database (a grain size effect?).

Specifics to the identified clay mineral groups

Beidellite-montmorillonite interstratifications (B:M ~75:25?)

96 of 140 measured particles belong so to this assumed classification. The dioctahedral character of this group is proofed by X-ray diffraction. The position of the large (060)-interference of smectite is in the random oriented powder specimen at 1.497 Å.

Montmorillonite and beidellite have the same behavior concerning the expandability and they are only to distinguish by XRD using Li by means of Greene-Kelly test (Green-Kelly 1952, 1953). So, combination of XRD- and TEM-results (full expandability by XRD and Si ~ 3.63 by TEM-EDX) led conclude the occurrence of 'beidellite-montmorillonite interstratifications', a beidellite-montmorillonite interstratification with about 75% beidellite and 25% montmorillonite layers (BM-ml 75:25).

Beidellite-montmorillonite interstratifications (B:M ~75:25?):

$$Ca_{0.15}\,Mg_{0.06}\,Na_{0.00}\,K_{0.11}\quad Al_{1.22}\,Fe^{3+}_{0.59}\,Mg_{0.18}\,Ti_{0.01}\,(OH)_2\quad Si_{3.63}\,Al_{0.37}\,O_{10}$$

Charge: XII = 0.53 VI = 5.84 IV = 15.63 **Σ = 22.00**

Measured particles by TEM-EDX: 96
Result of clustering: Cluster2 [tab. 2]

Beidellitic structures are characterized by a low octahedral Mg-amount (because of high ratio of octahedral, 3-valent cations). A comparison of octahedral Mg vs. tetrahedral Si indicates the occurrence of two groups for octahedral Mg based on TEM-EDX-data, separated by tetrahedral Si [fig. 3b]. The core of BM-ml shows an octahedral Mg-amount between 0.16 – 0.20 e phuc, probably pronounced by a higher Mg^{VI} in montmorillonite compound in this type interstratification.

Using the results of clustering (see Cluster2 in tab. 2), the maximum of frequency-% is to find for particles in the Si(IV)-class 3.6 – 3.7 e phuc [tab. 6a], representing the mentioned relation 30% montmorillonite and 70% beidellite as ratio of interstratification. The mineral formulae, summarized in classes of tetrahedral Si, draw for the maximum an Fe-rich BM 70:30 phase with K and remarkable amount of Mg in the interlayer space [tab. 6b].

A further hypothesis is to verify: The increasing K by lower tetrahedral Si [tab. 6b] could be an indication that it's not a change of 50:50 ratio of BM-ml into a 70:30 ratio of BM-ml, but an alteration of montmorillonite into diVS-ml phases resulting into an interstratification by beidellite – montmorillonite – dioctahedral vermiculite.

Dioctahedral vermiculite-smectite mixed layer phase (low K diVS-ml):

$$\boxed{Ca_{0.29}\ Mg_{0.01}\ Na_{0.01}\ K_{0.18}\quad Al_{1.12}\ Fe^{3+}_{0.58}\ Mg_{0.29}\ Ti_{0.01}\ (OH)_2\ \ Si_{3.52}\ Al_{0.48}\ O_{10}}$$

Charge:	XII = 0.79	VI = 5.69	IV = 15.52	**Σ = 22.00**
Probability of smectite layers (%S):	30%			
Probability of illite layers (%I):	70%			

Measured particles by TEM-EDX: 44

Result of clustering: Cluster1 [tab. 2]

Illite as part of diVS-ml series (high K diVS-ml):

The Rietveld refinement by Profex software (Döbelin & Kleeberg, 2015) indicates the occurrence of two polytypes for illite in treated B25 bentonite: $2M_1$- and 1M-polytype.

Kaolinite-montmorillonite-dioctahedral vermiculite mixed layer phases

The Excel-based procedure (Hoang-Minh et al., 2019) to identify possible clay mineral groups using the TEM-EDX-measurements also includes algorithms to classify kaolinite and kaolinite-montmorillonite mixed layer phases. These algorithms could identify few such phases basing on the measured TEM-EDX-data. Otherwise, very few particles, which were not to compute, have shown small hexagonal plates typically for kaolinite-bearing phases.

References

Cliff, G. & Lorimer, G. W. (1975). *J. Microsc.* **103**, 203–207.

Döbelin, N., Kleeberg, R. (2015). *Journal of Applied Crystallography* **48**, 1573-1580. DOI: 10.1107/S1600576715014685

Henning, K.-H. & Störr, M. (1986). Electron Micrographs (TEM, SEM) of Clays and Clay Minerals, p. 325. Akademie-Verlag Berlin.

Hoang-Minh, T., Kasbohm, J., Nguyen-Thanh, L., Nga, P. T., Lai, L. T., Duong, N. T., Thanh, N. D., Thuyet, N. T. M., Anh, D. D., Pusch, R., Knutsson, S. & Ferreiro Mahlmann, R. (2019). *J. Appl. Cryst.* **52**, 133-147. DOI: 10.1107/S1600576718018162

Lorimer, G. W. & Cliff, G. (1976). *Electron Microscopy in Mineralogy*, edited by H. R. Wenk, pp. 506–519. Berlin: Springer Verlag.

Matschiavelli, N., Kluge, S., Podlech, C., Standhaft, D., Grathoff, G., Ikeda-Ohno, A., Warr, L.N., Chukharkina, A., Arnold, T. & Cherkouk, A. (2019). *Environmental Science & Technology.* **53** (17), 10514-10524, DOI: 10.1021/acs.est.9b02670

Mellini, M. & Menichini, R. (1985). *R. Soc. Ital. Miner. Petrol.* **40**, 261–266.

Moore, D.M., Reynolds, R.C. (1989). X-ray Diffraction and the Identification and Analysis of Clay Minerals, Oxford University Press, New York, 332 + xvi pp.

Nguyen-Thanh, L., Herbert, H.-J., Kasbohm, J., Hoang-Minh, T. & Mählmann, R. F. (2014). *Clays Clay Miner.* **62**, 425–446.

Środoń, J., Elsass, F., McHardy, W. J. & Morgan, D. J. (1992). *Clay Miner.* **27**, 137–158.

SUPPLEMENT – Transmission Electron Microscopy coupled Energy dispersive X-ray Spectroscopy (TEM-EDX) of Opalinus clay

Data Sheet – Opalinus, untreated materials

Methodology - Transmission electron microscopy linked with energy-dispersive X-ray spectroscopy (TEM-EDX)

It is expected a characterization of clay mineral phases in treated Opalinus Clay by transmission electron microscopy. This report describes the results of untreated, original material from Opalinus Clay.

The different clay mineral phases are to identify and to describe by chemical composition and its variability, morphology, the specific dissolution potential, and further parameter.

Such further parameter like distribution of smectite layers probability (%S) and distribution of charges caused by exchangeable cations interlayer space should serve as additional indicators for mineralogical alterations in treatment experiments with Friedland Clay.

The sample were suspended for TEM-measurement in deionized water and dispersed by ultrasonic treatment for approximately 20 min. The clay fraction (<2 µm) was separated by sedimentation and diluted with deionized water to get a clear suspension. The suspension was dropped onto carbon-coated Cu grids, air dried and stored under environment-controlled conditions at 45% humidity.

TEM-EDX investigations were carried out on the <2 µm fraction using a FEI TECNAI G^2 20 electron transmission microscope at the VNU University of Science, Vietnam National University, Hanoi. This equipment (operated at 200 kV with LaB_6 cathode) was combined with an S-TWIN objective, a windowless EDAX energy-dispersive X-ray system and a FEI Eagle 2k CCD TEM camera.

About 100 individual clay particles per sample were characterized by TEM-EDX with respect to crystal size, crystal habit, and particle morphology and element distribution. The crystal size, crystal habit and particle morphology were described according to Henning & Störr (1986).

For the quantification of element distribution, a calibration of k factors is mandatory (Cliff & Lorimer, 1975; Lorimer & Cliff, 1976; Mellini & Menichini, 1985). These k values are used to calibrate for the specific behaviour of particles against possible irradiation damage. The elements O, Na, Mg, Al, Si, K, Ca and Fe were quantified by applying the EDAX GENESIS–TEM Quant Materials quantification procedure.

In this procedure, the acquired EDX spectra are corrected by background subtraction, Gaussian deconvolution and k-factor corrections using values previously determined on a phyllosilicate standard (muscovite) and selected non-phyllosilicate standards. The average errors in the analyzed elements using the phyllosilicate standard, expressed as the atomic proportions, are 10 (Na), 5 (Fe, Mg, K, Ti, Ca) and 1 (Si, Al).

The measurement time per particle was lowered to 20 s and the exposed area was limited to a 50 nm diameter, avoiding possible irradiation damage of particles. The stability of particles of the sample series was tested for this measurement time at the beginning of any measurement campaign.

Further methodological details related to TEM-EDX-measurements and the Excel-based mathematical procedure using TEM-EDX data for calculation of mineral formulae are described in Hoang-Minh et al. (2019).

These mathematical procedures described in Hoang-Minh et al. (2019) were extended by k-means clustering method for finding subgroups of observations within a data set. The data were standardized (i.e., scaled) to make variables comparable. Euclidean distances were applied as classical method for distance measures. The optimal clusters were determined by Elbow method and Gap statistics[20].

---

[20] *https://uc-r.github.io/kmeans_clustering*

Data Sheet – Opalinus Clay original (< 2 µm), untreated material

Preparation for TEM

- raw material: <40 µm powder of original Opalinus-sample
- suspension on particles < 2 µm on carbon-filmed Cu-grid
- air-dried and humidity-controlled storing

Mineral Matter

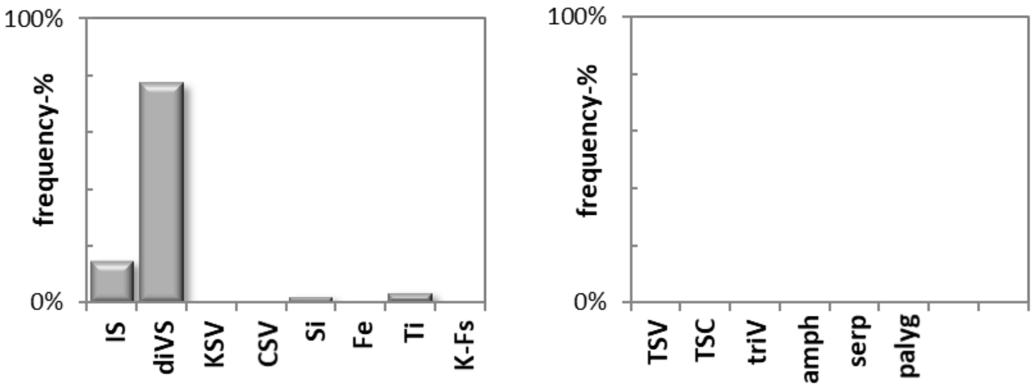

Fig. 1. *Distribution of mineral groups in fraction < 2 µm (in frequency-%)*
Legend: ***IS*** *– illite-smectite-mixed layer series in sense of Środon et al. (1992), diVS – dioctahedral vermiculite-smectite illite-smectite-mixed layer series (= charge- and/or K-deficit),* ***KSV*** *– kaolinite-smectite-dioctahedral vermiculite-mixed layer series,* ***CSV*** *– chlorite-saponite-trioctahedral vermiculite-mixed layer series,* ***Si*** *– quartz or particles with Si-surplus,* ***Fe*** *– Fe-oxide or Fe-oxyhydroxide,* ***Ti*** *– Ti-bearing phases (e.g. rutile, anatase),* ***K-Fs*** *– K-feldspar*

Clay Mineral Composition

All measured dioctahedral particles:

$$Ca_{0.09}\,Mg_{0.06}\,Na_{0.01}\,K_{0.39}\quad Al_{1.40}\,Fe^{3+}_{0.42}\,Mg_{0.17}\,Ti_{0.01}\,(OH)_2\quad Si_{3.46}\,Al_{0.54}\,O_{10}$$

Charge: XII = 0.7 VI = 5.83 IV = 15.46 **Σ = 21.99**

Probability of smectite layers (%S): 24%

Probability of illite layers (%I): 76%

Specific Dissolution Potential (ΔS%)

for H2O, 20 + 60 rpm 1 (= slow reacting, interlayer group: Ca+Mg (= type B))

for NaCl, 20 rpm 1 (= slow reacting, interlayer group: Ca+Mg (= type B))

for NaCl, 60 rpm -103 (= fast reacting, 'illitization', interlayer group: Na (= type A))

CEC$_{calc}$: 52 meq / 100 g

Measured particles: 70

Table 1. *Summarized chemical composition*

SiO_2	**TiO_2**	**Al_2O_3**	**Fe_2O_3**	**MnO**	**MgO**	**CaO**	**Na_2O**	**K_2O**	**P_2O_5**	**Σ**	
52.7%	0.1%	26.1%	4.3%		2.7%	1.3%	0.0%	3.4%	0.3%	0.91	measured particles
53.1%	1.0%	19.7%	6.2%	<0.1%	2.3%	3.0%	0.6%	2.6%		0.91	GAU03 (SHGN - bulk)

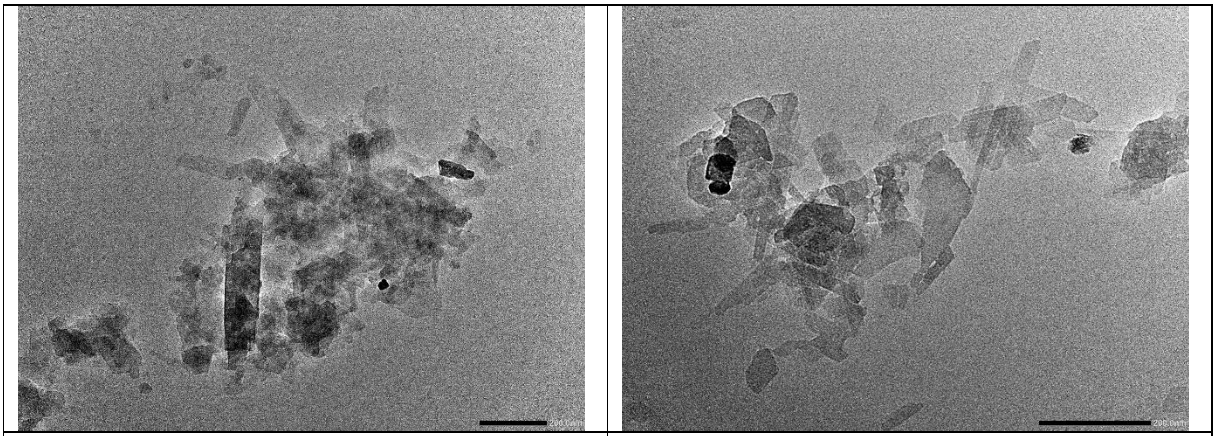

JEM-2100_MAG_X30k_Opalinus-40um-16.9_008.bmp

Magnification: 30k

JEM-2100_MAG_X50k_Opalinus-40um-16.9_011.bmp

Magnification: 50k

aggregates composed by slat-shaped crystals (length ~ 200 nm) with idiomorphic ends, commonly parallel or hexagonal intergrowths *(IS-ml and diVS-ml, not to distinguish by morphology of particles)*

Fig. 2a. *Morphology of particles (TEM-micrographs)*

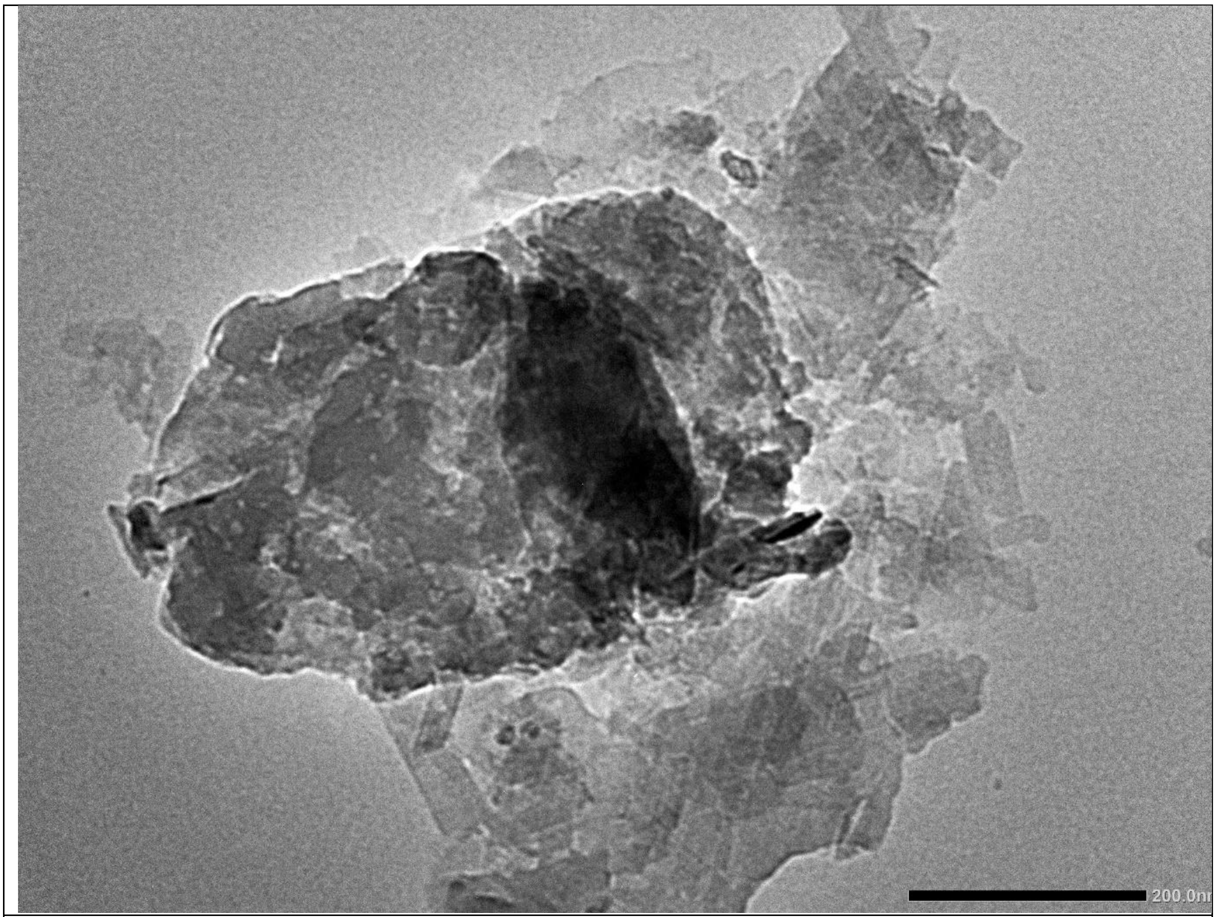

JEM-2100_MAG_X50k_Opalinus-40um-16.9_015.bmp
Magnification: 50k

former idiomorphic platy muscovite weathered into high charged dioctahedral vermiculite-smectite mixed layer phases with K-deficit (%S ~10%, %I ~ 90%)

Fig. 2b. *Morphology of particles (TEM-micrographs)*

Distribution of smectite layers probability (%S)

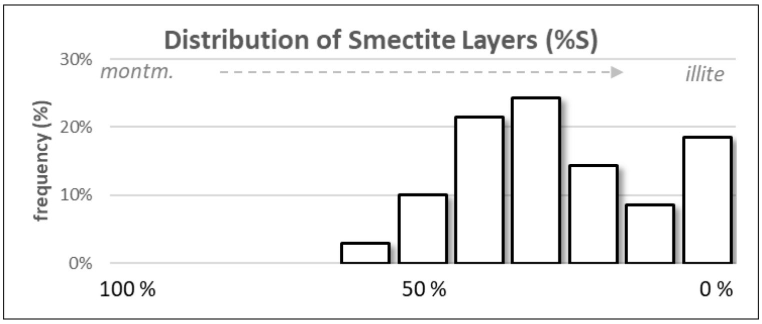

Description: *The distribution of %S-probability indicates two groups: (i) the occurrence of diVS-ml + IS-ml with %S mainly at 30-40% and (ii) illite with K- & charge-deficit.*

Fig. 3a. *Distribution of smectite layers probability (%S)*

Differentiation by relation “Octahedral Mg vs. tetrahedral Si”?

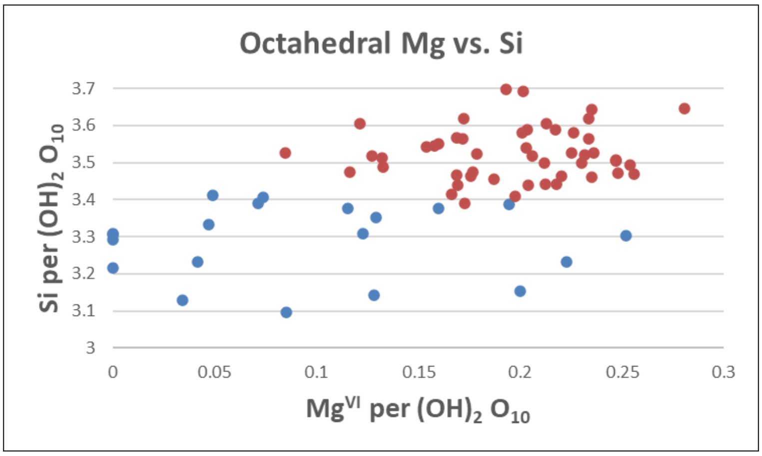

Description: *This diagram doesn’t indicate any separation on low and high ratio of Mg in relation to tetrahedral Si (blue dots – Cluster1; red dots – Cluster2). Phases of Cluster2 are mostly characterized by Mg(VI) > 0.1 per* $(OH)_2 O_{10}$.

Fig. 3b. *Distribution of octahedral Mg vs. tetrahedral Si [all per* $(OH)_2 O_{10}$*]*

Distribution of K in relation to tetrahedral Si

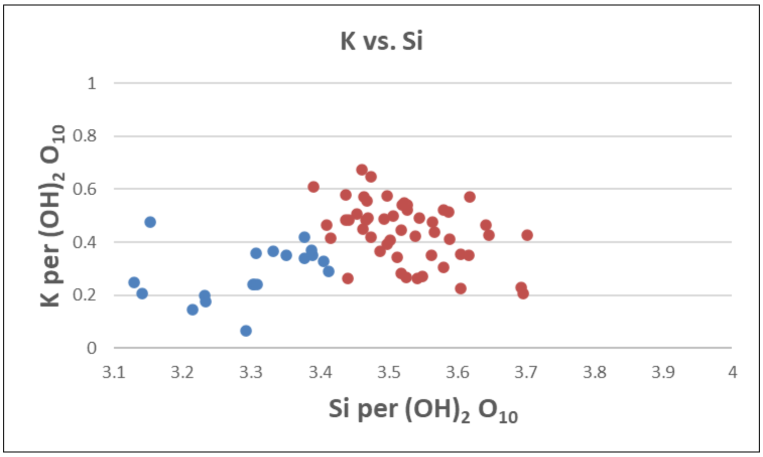

Description: *This diagram indicates a weak separation on low and high ratio of K in relation to tetrahedral Si (blue dots – Cluster1; red dots – Cluster2). Phases of Cluster1 are mostly characterized by K < 0.45 per* $(OH)_2 O_{10}$.

Fig. 4. *Distribution of K in interlayer space vs. tetrahedral Si [all per* $(OH)_2 O_{10}$*]*

Distribution of charges (exchangeable from interlayer space)

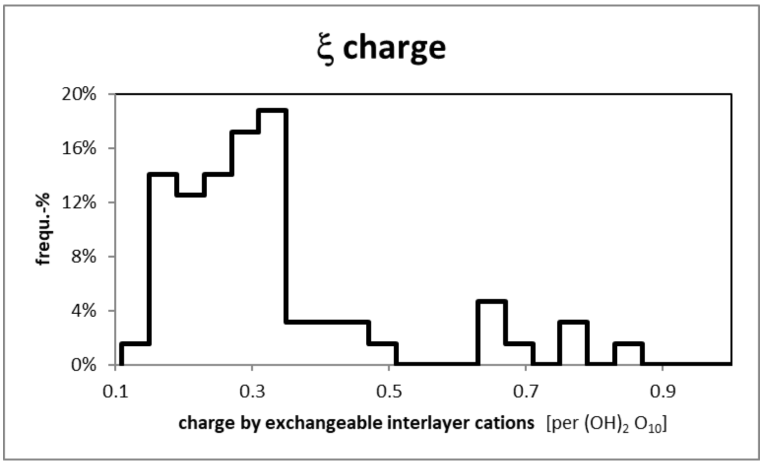

This diagram visualizes the distribution of exchangeable charges in the interlayer space (Ca, Mg, Na) determined and computed by TEM-EDX-data.

Description: *The charge density indicates a broad distribution of exchangeable interlayer cations lower than 0.35 per $(OH)_2\ O_{10}$.*

Fig. 5. *Distribution of charges*

Dioctahedral Vermiculite-Smectite mixed layer phases (diVS-ml) *(Cluster1):*

$Ca_{0.11}\ Mg_{0.12}\ Na_{0.01}\ K_{0.28}\ \ Al_{1.42}\ Fe^{3+}_{0.45}\ Mg_{0.10}\ Ti_{0.03}\ (OH)_2\ \ Si_{3.29}\ Al_{0.71}\ O_{10}$

Charge: XII = 0.74 VI = 5.97 IV = 15.29 **Σ = 22.00**
Probability of smectite layers (%S): 9%
Probability of illite layers (%I): 91%
Measured particles: 20

Distribution of smectite layers probability (%S) in diVS-ml (Cluster1)

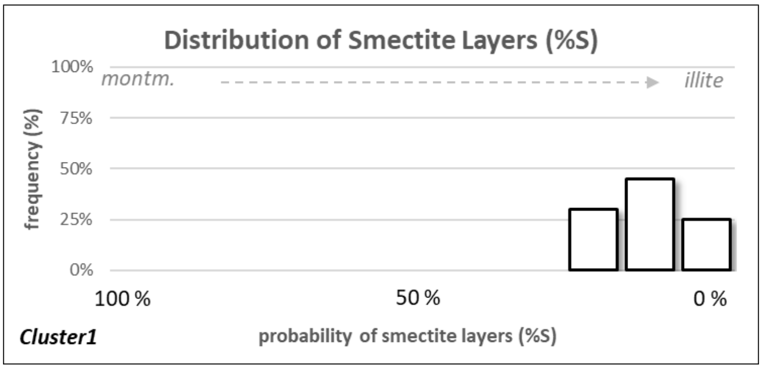

Description: *The distribution of diVS-ml (classified as Cluster1) draws a maximum of frequency (%) for smectite layer probability at 10%*

Fig. 6a. *Distribution of smectite layers probability in diVS-ml*

diVS-ml	*particles (abs)*	Ca (XII)	Mg (XII)	Na (XII)	K (XII)	Cr3+ (VI)	Al (VI)	Fe3+ (VI)	Mg (VI)	Ti (VI)	Al (IV)	Si (IV)	XII	n_VI	%S
%S >95%	n = 0														
%S 95-85%	n = 0														
%S 85-75%	n = 0														
%S 75-65%	n = 0														
%S 65-55%	n = 0														
%S 55-45%	n = 0														
%S 45-35%	n = 0														
%S 35-25%	n = 0														
%S 25-15%	n = 6	0.09	0.09	0.01	0.35	0.00	1.49	0.40	0.11	0.00	0.61	3.39	0.72	2.0	17
%S <15%	**n = 14**	**0.13**	**0.13**	**0.01**	**0.25**	**0.00**	**1.39**	**0.48**	**0.09**	**0.04**	**0.76**	**3.24**	**0.76**	**2.0**	**6**

Fig. 6b. *Computed averaged mineral formulae of diVS-ml phases in the different smectite layers probability (%S)-classes*

Beidellitic dioctahedral Vermiculite-Smectite mixed layer phases (beid. diVS-ml) *(Cluster2):*

$Ca_{0.08}\ Mg_{0.04}\ Na_{0.00}\ K_{0.44}\quad Al_{1.39}\ Fe^{3+}_{0.41}\ Mg_{0.20}\ Ti_{0.00}\ (OH)_2\quad Si_{3.53}\ Al_{0.47}\ O_{10}$

Charge:	XII = 0.68	VI = 5.79	IV = 15.53	**Σ = 22.00**

Probability of smectite layers (%S): 31%
Probability of illite layers (%I): 69%
Measured particles: 50

Distribution of smectite layers probability (%S) in diVS-ml (Cluster2)

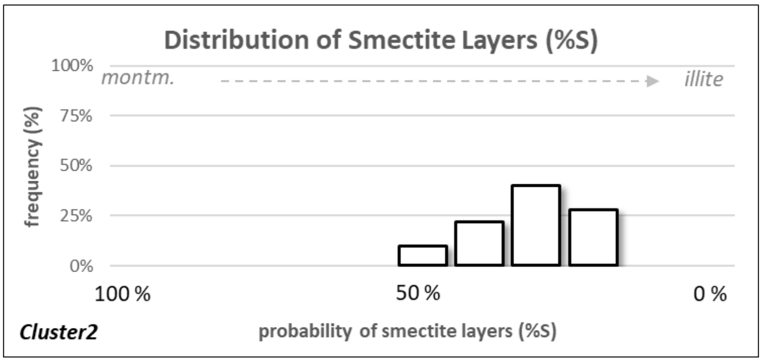

Description: *The distribution of diVS-ml (classified as Cluster2) draws a maximum of frequency (%) for smectite layer probability at 30%*

Fig. 7a. *Distribution of smectite layers probability in diVS-ml*

beid. diVS-ml *particles (abs)*		**Ca** **(XII)**	**Mg** **(XII)**	**Na** **(XII)**	**K (XII)**	**Cr3+** **(VI)**	**Al (VI)**	**Fe3+** **(VI)**	**Mg** **(VI)**	**Ti (VI)**	**Al (IV)**	**Si (IV)**	**XII**	**n_VI**	**%S**
%S >95%	n = 0														
%S 95-85%	n = 0														
%S 85-75%	n = 0														
%S 75-65%	n = 0														
%S 65-55%	n = 0														
%S 55-45%	n = 5	0.10	0.02	0.00	0.35	0.00	1.35	0.41	0.23	0.00	0.32	3.68	0.58	2.0	51
%S 45-35%	n = 11	0.07	0.04	0.01	0.41	0.00	1.39	0.40	0.20	0.00	0.41	3.59	0.64	2.0	39
%S 35-25%	**n = 20**	**0.08**	**0.04**	**0.01**	**0.44**	**0.00**	**1.44**	**0.37**	**0.19**	**0.00**	**0.49**	**3.51**	**0.68**	**2.0**	**30**
%S 25-15%	n = 14	0.08	0.05	0.00	0.50	0.00	1.32	0.47	0.20	0.00	0.56	3.44	0.76	2.0	22
%S <15%	n = 0														

Fig. 7b. *Computed averaged mineral formulae of diVS-ml phases in the different smectite layers probability (%S)-classes*

Description – Opalinus Clay original (< 2 µm), untreated material

Preparation for TEM

The powder of Opalinus Clay-sample was suspended in deionized water and dispersed by ultrasonic treatment for approximately 20 min. The clay fraction (<2 µm) was separated by sedimentation and diluted with deionized water to get a clear suspension. The suspension was dropped onto carbon-coated Cu grids, air dried and stored under environment-controlled conditions at 45% humidity.

Mineral Matter - Overview

The fraction < 2 µm of Opalinus Clay original sample is mainly composed by two different types of dioctahedral vermiculite-smectite mixed layer phases (diVS-ml). Rarely, rutile and quartz were identified in traces in this sample [fig. 1].

The measured and computed particles have shown a calculated CEC-value of 52 meq / 100 g located at surface and in the interlayer space.

	frequency-% *(n = 75 measured particles)*
diVS-ml	92%
Ti-phases	4%
Quartz	3%
Unknown phases	1%

All measured dioctahedral 2:1 clay mineral phases summarized result following mineral formula computed from TEM-EDX-measurement of 70 individual particles:

$$Ca^{2+}_{0.09}\ Mg^{2+}_{0.06}\ Na^{+}_{0.01}\ K^{+}_{0.39}\quad Al^{3+}_{1.40}\ Fe^{3+}_{0.42}\ Mg^{2+}_{0.17}\ Ti^{4+}_{0.01}\ (OH)_2\quad Si^{4+}_{3.46}\ Al^{3+}_{0.54}\ O_{10}$$

SDOM *± 0.01 ± 0.01 ± 0.0 ± 0.02 ± 0.02 ± 0.02 ± 0.01 ± 0.01 ± 0.02 ± 0.02*

Legend: SDOM - standard deviation of the mean (= the standard deviation divided by the square root of the number of samples)

The interlayer charge is calculated as 0.70 per $(OH)_2\ O_{10}$ and the octahedral charge as 5.83 per $(OH)_2\ O_{10}$. The particles are characterized by a high octahedral Fe-amount.

The summarized chemical composition of all 70 computed particles is listed [tab. 1].

Opalinus Clay original sample is also characterized by two morphological groups: (i) large (≤ 1 µm) xenomorph platy crystals and (ii) aggregates, formed by small (≤ 200 nm) laths with idiomorph ends [fig. 2]. Aggregates formed by small (≤ 200 nm) laths with idiomorph ends dominate the shapes of particles in the micrographs [fig. 2].

The distribution of %S-probability of all measured clay mineral phases [fig. 3a] also indicates the occurrence of two groups: (i) diVS-ml with $\%S_{max}$=30-40% and (ii) illite with K-deficiency.

The numerous measured particles by TEM-EDX allow a visualization of distribution of interlayer charges. Considering the TEM-EDX-determined cations Ca^{++}, Mg^{++} and Na^{+} and then computed their ratio as interlayer cations in the mineral formula, Ca^{++}, Mg^{++} and Na^{+} offer to characterize the degree of exchangeable charges in the interlayer space. This charge density of Opalinus Clay original (< 2 µm) shows in this sample a maximal frequency-% of charge density at 0.35 per $(OH)_2\ O_{10}$ [fig. 5]. This interval of interlayer charge density caused by exchangeable cations from 0.15 - 0.51 per $(OH)_2 O_{10}$ represents mentioned two groups of diVS-ml.

Mineral Matter - Specification

Result of Clustering

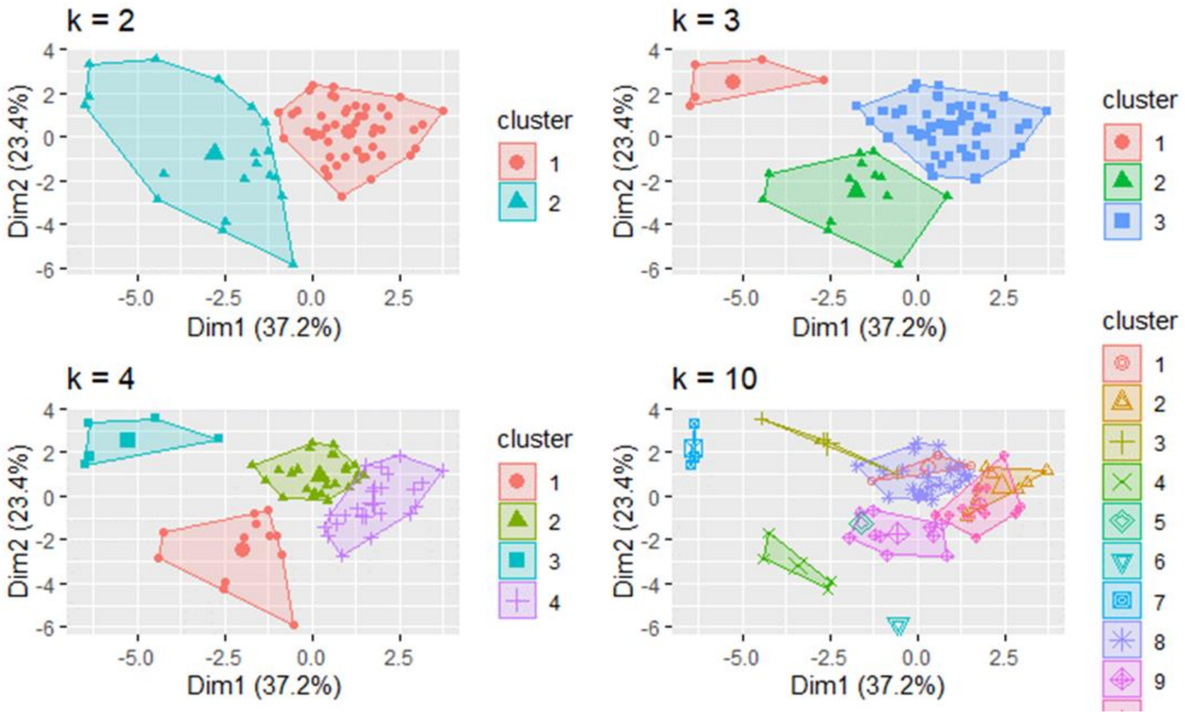

Fig. 8. *Clustering of all measured particles for clusters k = 2, k = 3, k = 4 and k = 10 (source for R-coding: https://uc-r.github.io/kmeans_clustering)*

The optimum of clusters was calculated with k = 2.

		Ca (XII)	Mg (XII)	Na (XII)	K (XII)	Cr3+ (VI)	Al (VI)	Fe3+ (VI)	Mg (VI)	Ti (VI)	Al (IV)	Si (IV)	XII	n_VI	%S
Cluster1	n = 20	0.11	0.12	0.01	0.28	0.00	1.42	0.45	0.10	0.03	0.71	3.29	0.74	2.0	9
Cluster2	n = 50	0.08	0.04	0.00	0.44	0.00	1.39	0.41	0.20	0.00	0.47	3.53	0.68	2.0	31

Fig. 9a. *Mineral formulae based on TEM-EDX-data summarized following the result of clustering for k=2*

	Sybilla-results	**TEM-EDX-results**	**Notes**
	Illite	diVS-ml (illite)	*very high K-deficit, low XII-charge deficit, Fe(VI)-rich, low Mg(VI)*
Cluster1	IS R0(1) *(%S = 11%)*	diVS-ml *(%S = 9%)*	*high K-deficit, low XII-charge deficit, Al(VI)- & Fe(VI)-rich*
Cluster2	ISS R0 *(%S = 48%)*	beid. diVS-ml *BMI 10:40:50*	*K-deficit, no XII-charge deficit, Fe(VI)-rich*

Tab. 2. *Comparison of results from TEM-EDX- and XRD-measurements*

The TEM-EDX-data offers a good agreement with the result of Sybilla-processing of XRD-traces from oriented specimen [tab. 2] considering traces of beidellite as further smectite component.

ISS R0: The X-ray diffraction pattern of the ethylene-glycol saturated oriented specimen shows a limited expandability to 1.46 nm. This result of XRD-pattern processing let expect a maximum of particles for %S ~ 50% by TEM-EDX-measurements, but the maximum of particles measured by TEM-EDX is to find at %S = 31%. Using a model for beidellite-montmorillonite-illite-mixed layer phases (BMI-ml) with 3.50, 4.00 and 3.20 as tetrahedral Si-value per $(OH)_2$ O_{10} the calculation of member ratios offers a solution for 10% layer probability for %B and 40% for %S, if %I is given with 50% [see Cluster2 in tab. 2].

IS R0 (1): The Sybilla-procedure of XRD-traces (oriented mounts) has shown an occurrence of an illite-smectite mixed layer phase with a smectite layers probability of %S = 11%. This result of XRD-pattern processing is in good agreement with founded maximum of particles for %S ~ 9% by TEM-EDX-measurements [tab. 2].

The Sybilla-processing of XRD-traces (oriented mounts) also supports low amount of kaolinite and kaolinite-smectite mixed layer phases in fine fraction of sample.

Specifics to the identified clay mineral groups

Dioctahedral vermiculite-smectite mixed layer phase *(Cluster1)*

20 of 70 computed particles belong so to this assumed classification. The dioctahedral character of this group is proofed by X-ray diffraction. The position of the large (060)-interference of smectite is in the random oriented powder specimen at 1.497 Å.

Dioctahedral vermiculite-smectite mixed layer phase *(Cluster1)*

$$\mathrm{Ca_{0.11}\ Mg_{0.12}\ Na_{0.01}\ K_{0.28}\quad Al_{1.42}\ Fe^{3+}_{0.45}\ Mg_{0.10}\ Ti_{0.03}\ (OH)_2\quad Si_{3.29}\ Al_{0.71}\ O_{10}}$$

Charge: XII = 0.74 VI = 5.97 IV = 15.29 **Σ = 22.00**
Measured particles by TEM-EDX: 20
Probability of smectite layers (%S): 9%
Probability of illite layers (%I): 91%
Result of clustering: Cluster1 [tab. 2]

A comparison of octahedral Mg vs. tetrahedral Si doesn't indicate any differentiation for octahedral Mg in comparison to Cluster2 based on TEM-EDX-data [fig. 3b]. Particles of Cluster1 contain commonly Mg(VI) < 0.25 per $(OH)_2\ O_{10}$ in octahedral layer.

The mineral formulae, summarized in classes of %S, draws for the maximum an Al- & Fe-rich diVS-ml with a low Mg(VI) as well as low amount of K in the interlayer space [tab. 6b].

Dioctahedral vermiculite-smectite mixed layer phase *(beid. diVS-ml, Cluster2)*

$$\mathrm{Ca_{0.08}\ Mg_{0.04}\ Na_{0.00}\ K_{0.44}\quad Al_{1.39}\ Fe^{3+}_{0.41}\ Mg_{0.20}\ Ti_{0.00}\ (OH)_2\quad Si_{3.53}\ Al_{0.47}\ O_{10}}$$

Charge: XII = 0.68 VI = 5.79 IV = 15.53 **Σ = 22.00**
Probability of smectite layers (%S): 50%
Probability of illite layers (%I): 50%
Measured particles by TEM-EDX: 50
Result of clustering: Cluster2 [tab. 2]

A comparison of octahedral Mg vs. tetrahedral Si doesn't indicate any differentiation for octahedral Mg in comparison to Cluster1 based on TEM-EDX-data [fig. 3b]. Particles of Cluster2 contain commonly Mg(VI) > 0.1 per $(OH)_2\ O_{10}$ in octahedral layer.

The mineral formulae, summarized in classes of %S, draws for the maximum an Al- & Fe-rich diVS-ml as well as reduced amount of K in the interlayer space [tab. 7b].

Kaolinite-montmorillonite mixed layer phases

The Excel-based procedure (Hoang-Minh et al., 2019) to identify possible clay mineral groups using the TEM-EDX-measurements also includes algorithms to classify kaolinite and kaolinite-montmorillonite mixed layer phases. These algorithms couldn't compute no such phases basing on the measured TEM-EDX-data. Such particles have shown small hexagonal plates typically for kaolinite-bearing phases.

References

Cliff, G. & Lorimer, G. W. (1975). *J. Microsc.* **103**, 203–207.

Döbelin, N., Kleeberg, R. (2015). *Journal of Applied Crystallography* **48**, 1573-1580. DOI: 10.1107/S1600576715014685

Henning, K.-H. & Störr, M. (1986). Electron Micrographs (TEM, SEM) of Clays and Clay Minerals, p. 325. Akademie-Verlag Berlin.

Hoang-Minh, T., Kasbohm, J., Nguyen-Thanh, L., Nga, P. T., Lai, L. T., Duong, N. T., Thanh, N. D., Thuyet, N. T. M., Anh, D. D., Pusch, R., Knutsson, S. & Ferreiro Mahlmann, R. (2019). *J. Appl. Cryst.* **52**, 133-147. DOI: 10.1107/S1600576718018162

Lorimer, G. W. & Cliff, G. (1976). *Electron Microscopy in Mineralogy*, edited by H. R. Wenk, pp. 506–519. Berlin: Springer Verlag.

Mellini, M. & Menichini, R. (1985). *R. Soc. Ital. Miner. Petrol.* **40**, 261–266.

Moore, D.M., Reynolds, R.C. (1989). X-ray Diffraction and the Identification and Analysis of Clay Minerals, Oxford University Press, New York, 332 + xvi pp.

Nguyen-Thanh, L., Herbert, H.-J., Kasbohm, J., Hoang-Minh, T. & Mählmann, R. F. (2014). *Clays Clay Miner.* **62**, 425–446.

Środoń, J., Elsass, F., McHardy, W. J. & Morgan, D. J. (1992). *Clay Miner.* **27**, 137–158.

Methodology - Transmission electron microscopy linked with energy-dispersive X-ray spectroscopy (TEM-EDX)

It is expected a characterization of clay mineral phases in treated Opalinus Clay by transmission electron microscopy. This report describes the results of treated material from Opalinus Clay percolated at a temperature of 35°C.

The different clay mineral phases are to identify and to describe by chemical composition and its variability, morphology, the specific dissolution potential, and further parameter.

Such further parameter like distribution of smectite layers probability (%S) and distribution of charges caused by exchangeable cations interlayer space should serve as additional indicators for mineralogical alterations in treatment experiments with Friedland Clay.

The sample were suspended for TEM-measurement in deionized water and dispersed by ultrasonic treatment for approximately 20 min. The clay fraction (<2 µm) was separated by sedimentation and diluted with deionized water to get a clear suspension. The suspension was dropped onto carbon-coated Cu grids, air dried and stored under environment-controlled conditions at 45% humidity.

TEM-EDX investigations were carried out on the <2 µm fraction using a FEI TECNAI G^2 20 electron transmission microscope at the VNU University of Science, Vietnam National University, Hanoi. This equipment (operated at 200 kV with LaB_6 cathode) was combined with an S-TWIN objective, a windowless EDAX energy-dispersive X-ray system and a FEI Eagle 2k CCD TEM camera.

About 100 individual clay particles per sample were characterized by TEM-EDX with respect to crystal size, crystal habit, and particle morphology and element distribution. The crystal size, crystal habit and particle morphology were described according to Henning & Störr (1986).

For the quantification of element distribution, a calibration of k factors is mandatory (Cliff & Lorimer, 1975; Lorimer & Cliff, 1976; Mellini & Menichini, 1985). These k values are used to calibrate for the specific behaviour of particles against possible irradiation damage. The elements O, Na, Mg, Al, Si, K, Ca and Fe were quantified by applying the EDAX GENESIS–TEM Quant Materials quantification procedure.

In this procedure, the acquired EDX spectra are corrected by background subtraction, Gaussian deconvolution and k-factor corrections using values previously determined on a phyllosilicate standard (muscovite) and selected non-phyllosilicate standards. The average errors in the analyzed elements using the phyllosilicate standard, expressed as the atomic proportions, are 10 (Na), 5 (Fe, Mg, K, Ti, Ca) and 1 (Si, Al).

The measurement time per particle was lowered to 20 s and the exposed area was limited to a 50 nm diameter, avoiding possible irradiation damage of particles. The stability of particles of the sample series was tested for this measurement time at the beginning of any measurement campaign.

Further methodological details related to TEM-EDX-measurements and the Excel-based mathematical procedure using TEM-EDX data for calculation of mineral formulae are described in Hoang-Minh et al. (2019).

These mathematical procedures described in Hoang-Minh et al. (2019) were extended by k-means clustering method for finding subgroups of observations within a data set. The data were standardized (i.e., scaled) to make variables comparable. Euclidean distances were applied as classical method for distance measures. The optimal clusters were determined by Elbow method and Gap statistics[21].

---

[21] *https://uc-r.github.io/kmeans_clustering*

Data Sheet – Opalinus Clay N22 (< 2 µm), treated material *(35°C, 144 h)*

Preparation for TEM

- raw material: compacted material (1.6 g/cm³) of treated Opalinus Clay-sample
- suspension on particles < 2 µm on carbon-filmed Cu-grid
- air-dried and humidity-controlled storing

Mineral Matter

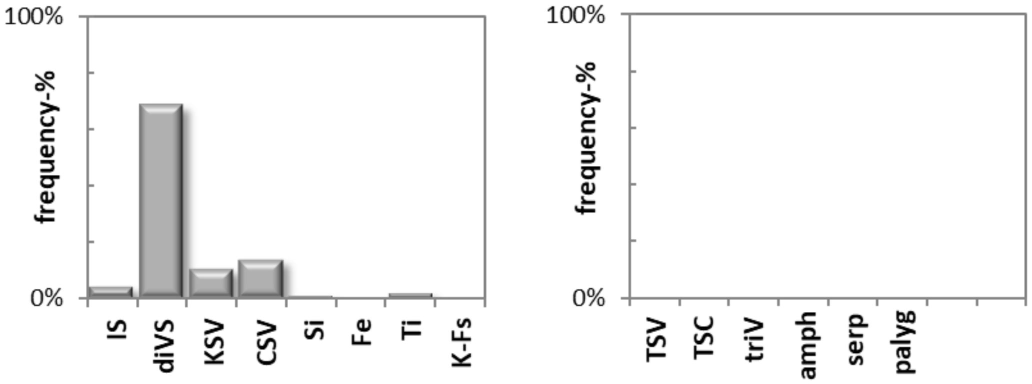

Fig. 1. *Distribution of mineral groups in fraction < 2 µm (in frequency-%)*
Legend: ***IS*** *– illite-smectite-mixed layer series in sense of Środon et al. (1992), diVS – dioctahedral vermiculite-smectite illite-smectite-mixed layer series (= charge- and/or K-deficit),* ***KSV*** *– kaolinite-smectite-dioctahedral vermiculite-mixed layer series,* ***CSV*** *– chlorite-saponite-trioctahedral vermiculite-mixed layer series,* ***Si*** *– quartz or particles with Si-surplus,* ***Fe*** *– Fe-oxide or Fe-oxyhydroxide,* ***Ti*** *– Ti-bearing phases (e.g. rutile, anatase),* ***K-Fs*** *– K-feldspar*

Clay Mineral Composition

All measured dioctahedral particles:

$$\mathrm{Ca_{0.10}\,Mg_{0.08}\,Na_{0.02}\,K_{0.48}\quad Al_{1.40}\,Fe^{3+}_{0.45}\,Mg_{0.14}\,Ti_{0.02}\,(OH)_2\quad Si_{3.24}\,Al_{0.76}\,O_{10}}$$

Charge: XII = 0.88 VI = 5.88 IV = 15.24 **Σ = 22.00**
Probability of smectite layers (%S): 6%
Probability of illite layers (%I): 94%

Specific Dissolution Potential (ΔS%)

for H2O, 20 + 60 rpm -3 (= slow reacting, interlayer group: Ca+Mg (= type B))
for NaCl, 20 rpm -3 (= slow reacting, interlayer group: Ca+Mg (= type B))
for NaCl, 60 rpm -79 (= fast reacting, 'illitization', interlayer group: Na (= type A))
CEC$_{calc}$: 57 meq / 100 g

Measured particles: 125

Table 1. *Summarized chemical composition*

SiO₂	**TiO₂**	**Al₂O₃**	**Fe₂O₃**	**MnO**	**MgO**	**CaO**	**Na₂O**	**K₂O**	**P₂O₅**	**Σ**	
54.1%	0.2%	31.2%	5.0%		2.9%	1.3%	0.3%	4.6%	0.1%	1.00	measured particles of treated sample
59.4%	0.3%	28.1%	5.9%		2.5%	0.3%	0.1%	3.3%	0.1%	1.00	measured particles of original Opalinus Clay

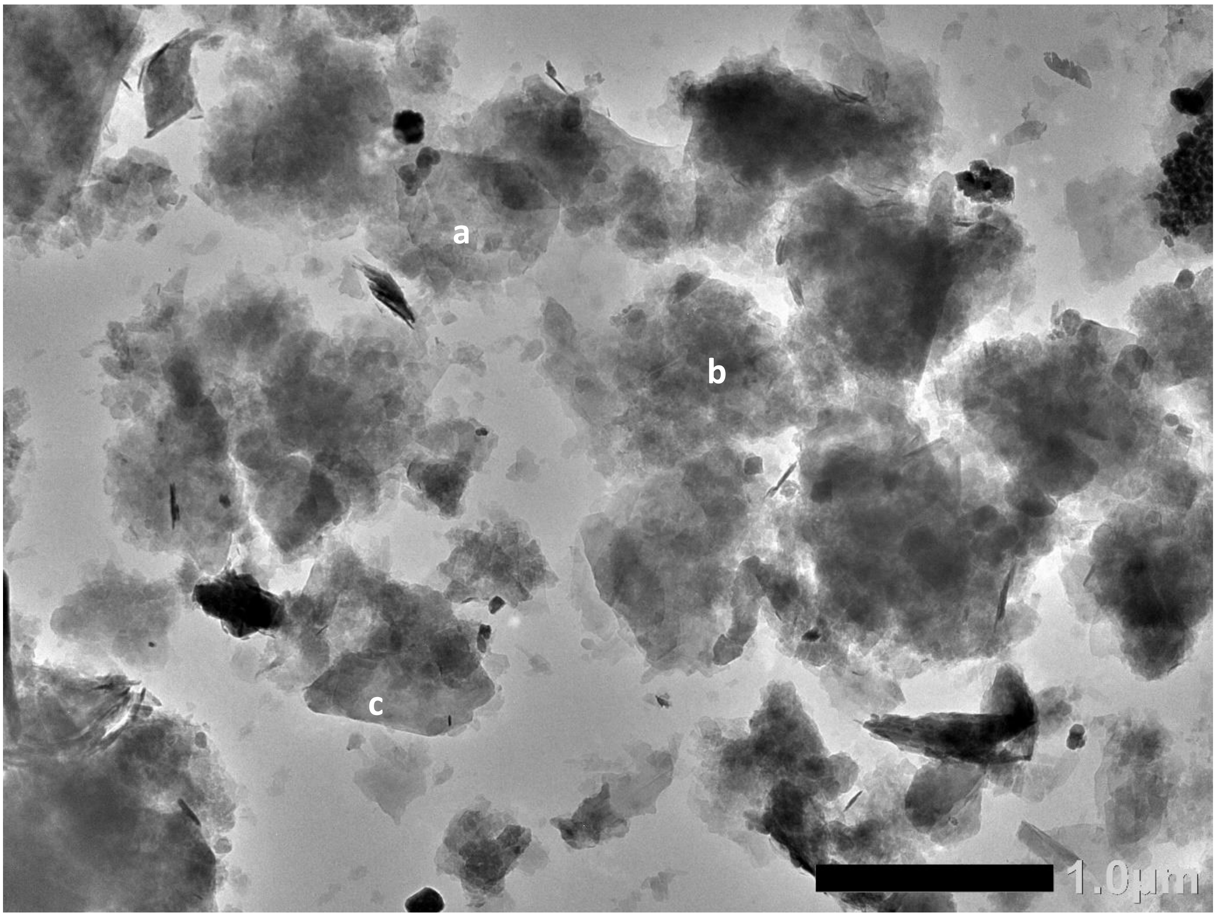

JEM-2100_MAG_X10k_No22_009.bmp

Magnification: 10k

- (a) large (≤ 1 µm) xenomorph platy crystals;
- (b) aggregates formed by small (≤ 100 nm) xenomorphous plates;
- (c) hypidiomorph, hexagonal plates

Fig. 2. *Morphology of particles (TEM-micrographs)*

Distribution of smectite layers probability (%S)

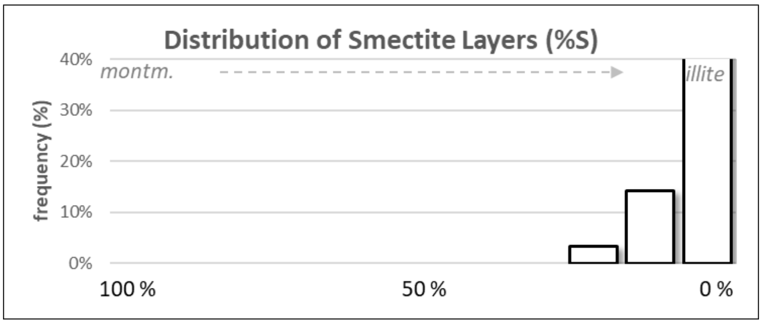

Description: *The distribution of %S-probability indicates the occurrence of two groups: (i) low number of diVS-ml phases as well as (ii) dominating illite with K-deficiency.*

Fig. 3a. *Distribution of smectite layers probability (%S)*

Differentiation by relation “Octahedral Mg vs. tetrahedral Si”?

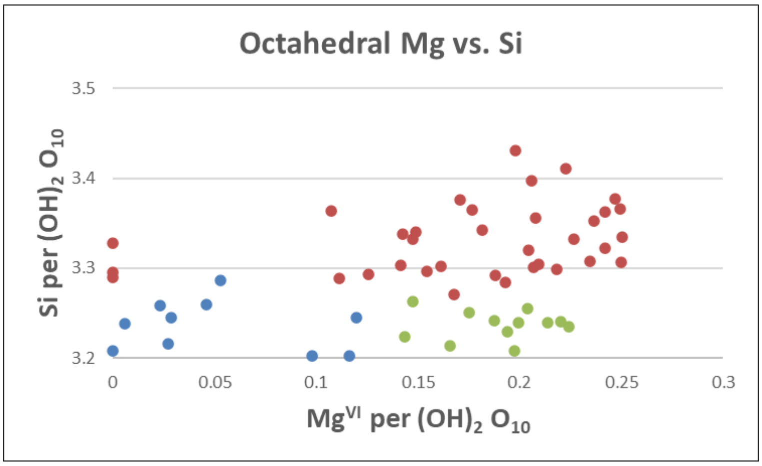

***Description:** This diagram indicates a separation on low and high ratio of Mg in relation to tetrahedral Si (blue dots – Cluster1: illite; green dots – Cluster3: illite). DiVS-ml phases are mostly characterized by Mg(VI) > 0.1 per $(OH)_2$ O_{10}.*

***Fig. 3b.** Distribution of octahedral Mg vs. tetrahedral Si [all per$(OH)_2$ O_{10}]*

Distribution of K in relation to tetrahedral Si

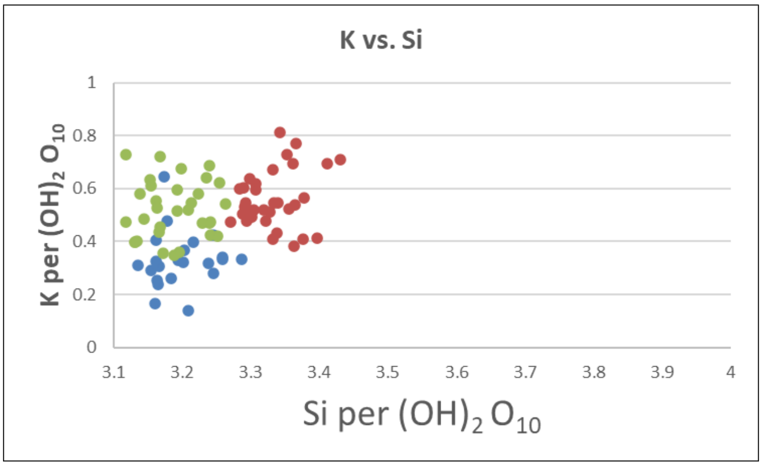

***Description:** This diagram indicates a separation on low and high ratio of K in relation to tetrahedral Si (blue dots – Cluster1: illite; green dots – Cluster3: illite). DiVS-ml phases (red dots – Cluster2) are mostly characterized by K > 0.4 per $(OH)_2$ O_{10}.*

***Fig. 4.** Distribution of K in interlayer space vs. tetrahedral Si [all per$(OH)_2$ O_{10}]*

Distribution of charges (exchangeable from interlayer space)

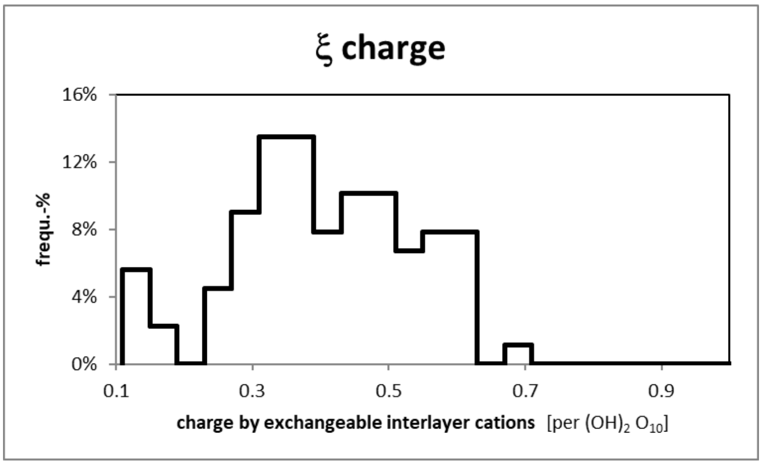

This diagram visualizes the distribution of exchangeable charges in the interlayer space (Ca, Mg, Na) determined and computed by TEM-EDX-data.

***Description:** Very broad distribution of charge density with maximal frequency-% at 0.35 per $(OH)_2$ O_{10}*

***Fig. 5.** Distribution of charges*

Dioctahedral Vermiculite-Smectite mixed layer phases (diVS-ml) *(Cluster1):*

$$Ca_{0.10}\ Mg_{0.14}\ Na_{0.03}\ K_{0.33}\quad Al_{1.58}\ Fe^{3+}_{0.37}\ Mg_{0.05}\ Ti_{0.01}\ (OH)_2\quad Si_{3.20}\ Al_{0.80}\ O_{10}$$

Charge: XII = 0.83 VI = 5.97 IV = 15.20 **Σ = 22.00**

Probability of smectite layers (%S): 3%

Probability of illite layers (%I): 97%

Measured particles: 22

Distribution of smectite layers probability (%S) in diVS-ml (Cluster1)

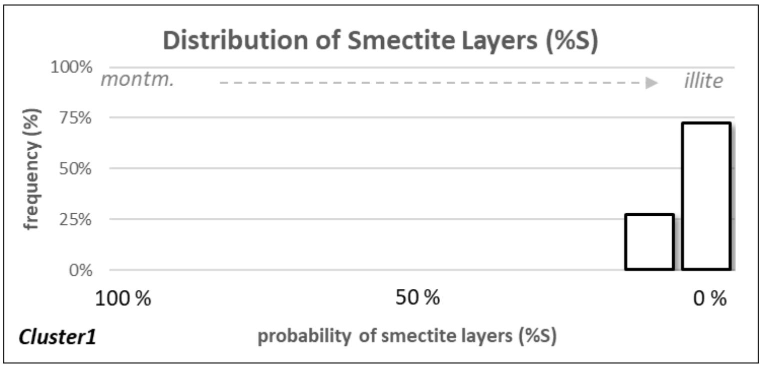

Description: *The distribution of diVS-ml (classified as Cluster1) draws a maximum of frequency (%) for smectite layer probability at 0%*

Fig. 6a. *Distribution of smectite layers probability in diVS-ml*

diVS-ml	*particles (abs)*	Ca (XII)	Mg (XII)	Na (XII)	K (XII)	Cr3+ (VI)	Al (VI)	Fe3+ (VI)	Mg (VI)	Ti (VI)	Al (IV)	Si (IV)	XII	n_VI	%S
%S >95%	n = 0														
%S 95-85%	n = 0														
%S 85-75%	n = 0														
%S 75-65%	n = 0														
%S 65-55%	n = 0														
%S 55-45%	n = 0														
%S 45-35%	n = 0														
%S 35-25%	n = 0														
%S 25-15%	n = 0														
%S <15%	**n = 22**	**0.10**	**0.14**	**0.03**	**0.33**	**0.00**	**1.58**	**0.37**	**0.05**	**0.01**	**0.80**	**3.20**	**0.83**	**2.0**	**3**

Fig. 6b. *Computed averaged mineral formulae of diVS-ml phases in the different smectite layers probability (%S)-classes*

Dioctahedral Vermiculite-Smectite mixed layer phases (diVS-ml) *(Cluster2):*

$$Ca_{0.10}\ Mg_{0.03}\ Na_{0.03}\ K_{0.56}\quad Al_{1.42}\ Fe^{3+}_{0.39}\ Mg_{0.18}\ Ti_{0.01}\ (OH)_2\quad Si_{3.33}\ Al_{0.67}\ O_{10}$$

Charge: XII = 0.84 VI = 5.83 IV = 15.33 **Σ = 22.00**

Probability of smectite layers (%S): 12%

Probability of illite layers (%I): 88%

Measured particles: 35

Distribution of smectite layers probability (%S) in diVS-ml (Cluster2)

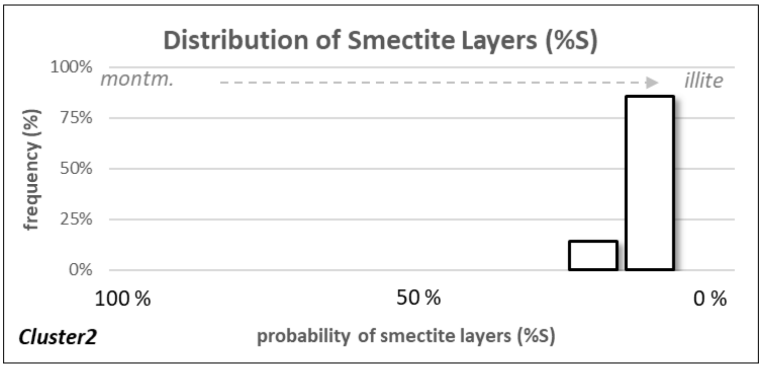

Description: *The distribution of diVS-ml (classified as Cluster2) draws a maximum of frequency (%) for smectite layer probability at 10%*

Fig. 7a. *Distribution of smectite layers probability in diVS-ml*

diVS-ml	particles (abs)	Ca (XII)	Mg (XII)	Na (XII)	K (XII)	Cr3+ (VI)	Al (VI)	Fe3+ (VI)	Mg (VI)	Ti (VI)	Al (IV)	Si (IV)	XII	n_VI	%S
%S >95%	n = 0														
%S 95-85%	n = 0														
%S 85-75%	n = 0														
%S 75-65%	n = 0														
%S 65-55%	n = 0														
%S 55-45%	n = 0														
%S 45-35%	n = 0														
%S 35-25%	n = 0														
%S 25-15%	n = 5	0.10	0.02	0.02	0.56	0.00	1.38	0.38	0.21	0.02	0.60	3.40	0.8	2.0	18
%S <15%	**n = 30**	**0.10**	**0.03**	**0.03**	**0.56**	**0.00**	**1.43**	**0.39**	**0.17**	**0.01**	**0.68**	**3.32**	**0.8**	**2.0**	**11**

Fig. 7b. *Computed averaged mineral formulae of diVS-ml phases in the different smectite layers probability (%S)-classes*

Cluster2		Ca (XII)	Mg (XII)	Na (XII)	K (XII)	Cr3+ (VI)	Al (VI)	Fe3+ (VI)	Mg (VI)	Ti (VI)	Al (IV)	Si (IV)	XII	n_VI	%S
without illite	n = 5	0.10	0.02	0.02	0.56	0.00	1.38	0.38	0.21	0.02	0.60	3.40	0.82	2.0	18
only illite	n = 30	0.10	0.03	0.03	0.56	0.00	1.43	0.39	0.17	0.01	0.68	3.32	0.84	2.0	11

Fig. 7c. *Computed averaged mineral formulae of diVS-ml phases differentiated by illite*

Dioctahedral Vermiculite-Smectite mixed layer phases (diVS-ml) *(Cluster3):*

$$Ca_{0.10}\ Mg_{0.10}\ Na_{0.02}\ K_{0.51}\quad Al_{1.26}\ Fe^{3+}_{0.55}\ Mg_{0.16}\ Ti_{0.03}\ (OH)_2\ \ Si_{3.18}\ Al_{0.82}\ O_{10}$$

Charge:	XII = 0.95	VI = 5.87	IV = 15.18	**Σ = 22.00**

Probability of smectite layers (%S): 2%

Probability of illite layers (%I): 98%

Measured particles: 34

Distribution of smectite layers probability (%S) in diVS-ml (Cluster3)

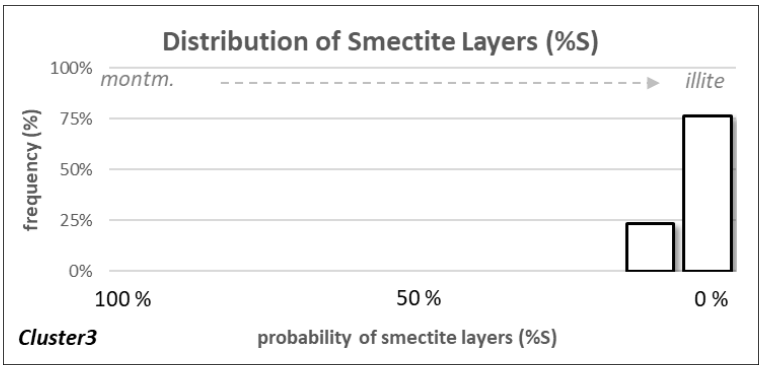

Description: *The distribution of diVS-ml (classified as Cluster3) draws a maximum of frequency (%) for smectite layer probability at 0%*

Fig. 7d. *Distribution of smectite layers probability in diVS-ml*

diVS-ml	particles (abs)	Ca (XII)	Mg (XII)	Na (XII)	K (XII)	Cr3+ (VI)	Al (VI)	Fe3+ (VI)	Mg (VI)	Ti (VI)	Al (IV)	Si (IV)	XII	n_VI	%S
%S >95%	n = 0														
%S 95-85%	n = 0														
%S 85-75%	n = 0														
%S 75-65%	n = 0														
%S 65-55%	n = 0														
%S 55-45%	n = 0														
%S 45-35%	n = 0														
%S 35-25%	n = 0														
%S 25-15%	n = 0														
%S <15%	**n = 34**	**0.10**	**0.10**	**0.02**	**0.51**	**0.00**	**1.26**	**0.55**	**0.16**	**0.03**	**0.82**	**3.18**	**1.0**	**2.0**	**2**

Fig. 7e. *Computed averaged mineral formulae of diVS-ml phases in the different smectite layers probability (%S)-classes*

Description – Opalinus Clay N22 (< 2 µm), treated material *(35°C)*

Preparation for TEM

The powder of Opalinus Clay-sample was suspended in deionized water and dispersed by ultrasonic treatment for approximately 20 min. The clay fraction (<2 µm) was separated by sedimentation and diluted with deionized water to get a clear suspension. The suspension was dropped onto carbon-coated Cu grids, air dried and stored under environment-controlled conditions at 45% humidity.

Mineral Matter - Overview

The fraction < 2 µm of Opalinus Clay N22 sample is mainly composed by three different types of dioctahedral vermiculite-smectite mixed layer phases (diVS-ml). Rarely, kaolinite and kaolinite-smectite-ml phases as well as chlorite-smectite-ml phases, rutile and quartz were identified in traces in this sample [fig. 1].

The measured and computed particles have shown a calculated CEC-value of 57 meq / 100 g located at surface and in the interlayer space.

	frequency-% *(n = 125 measured particles)*
diVS-ml	73%
Kaolinite & KSV-ml	10%
CSV-ml	14%
Ti-phases	2%
Quartz	1%
Unknown phases	1%

All measured dioctahedral 2:1 clay mineral phases summarized result following mineral formula computed from TEM-EDX-measurement of 91 individual particles:

	$Ca^{2+}_{0.10}$	$Mg^{2+}_{0.08}$	$Na^{+}_{0.02}$	$K^{+}_{0.48}$	$Al^{3+}_{1.40}$	$Fe^{3+}_{0.45}$	$Mg^{2+}_{0.14}$	$Ti^{4+}_{0.02}$	$(OH)_2$	$Si^{4+}_{3.24}$	$Al^{3+}_{0.76}$	O_{10}
SDOM	*± 0.00*	*± 0.01*	*± 0.00*	*± 0.01*	*± 0.02*	*± 0.01*	*± 0.01*	*± 0.00*		*± 0.01*	*± 0.01*	

Legend: SDOM - standard deviation of the mean (= the standard deviation divided by the square root of the number of samples)

The interlayer charge is calculated as 0.88 per $(OH)_2$ O_{10} and the octahedral charge as 5.88 per $(OH)_2$ O_{10}. The particles are characterized by a high octahedral Fe-amount.

The summarized chemical composition of all 91 computed particles is listed [tab. 1].

Opalinus Clay N22 sample is also characterized by two morphological groups: (i) large (≤ 1 µm) xenomorph platy crystals and (ii) aggregates, partially with folds, formed by small (≤ 100 nm) xenomorphous plates [fig. 2]. Aggregates formed by small (≤ 100 nm) xenomorphous plates dominate the shapes of particles in the micrographs [fig. 2].

The distribution of %S-probability of all measured clay mineral phases [fig. 3a] also indicates the occurrence of two groups: (i) diVS-ml and dominating (ii) illite with K-deficiency.

The numerous measured particles by TEM-EDX allow a visualization of distribution of interlayer charges. Considering the TEM-EDX-determined cations Ca^{++}, Mg^{++} and Na^{+} and then computed their ratio as interlayer cations in the mineral formula, Ca^{++}, Mg^{++} and Na^{+} offer to characterize the degree of exchangeable charges in the interlayer space. This charge density of Opalinus Clay N22 (< 2 µm) shows in this sample a maximal frequency-% of charge density at 0.35 per $(OH)_2\,O_{10}$ [fig. 5]. This interval of interlayer charge density caused by exchangeable cations from 0.23 - 0.59 per $(OH)_2\,O_{10}$ represents mentioned diVS-ml.

Mineral Matter - Specification

Result of Clustering

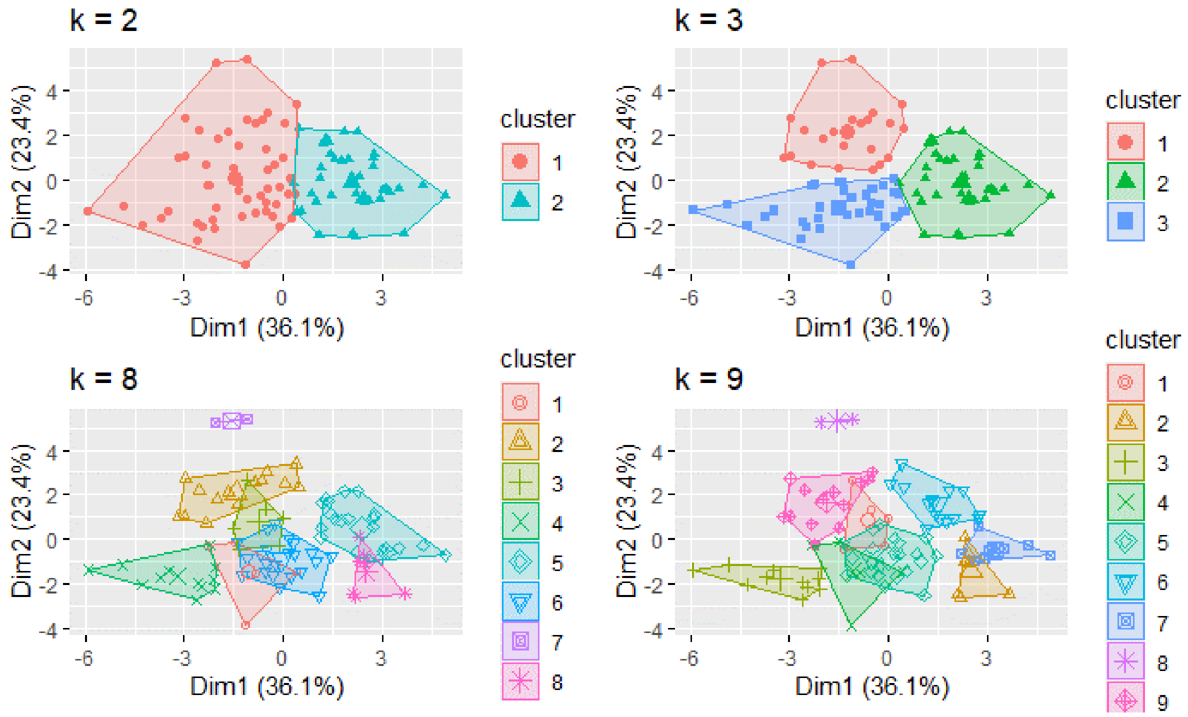

Fig. 8. *Clustering of all measured particles for clusters k = 2, k = 3, k = 8 and k = 9 (source for R-coding: https://uc-r.github.io/kmeans_clustering)*

The optimum of clusters was calculated with k = 3.

		Ca (XII)	Mg (XII)	Na (XII)	K (XII)	Cr3+ (VI)	Al (VI)	Fe3+ (VI)	Mg (VI)	Ti (VI)	Al (IV)	Si (IV)	XII	n_VI	%S
Cluster1	n = 22	0.10	0.14	0.03	0.33	0.00	1.58	0.37	0.05	0.01	0.80	3.20	0.83	2.0	3
Cluster2	n = 35	0.10	0.03	0.03	0.56	0.00	1.42	0.39	0.18	0.01	0.67	3.33	0.84	2.0	12
Cluster3	n = 34	0.10	0.10	0.02	0.51	0.00	1.26	0.55	0.16	0.03	0.82	3.18	0.95	2.0	2

Fig. 9a. *Mineral formulae based on TEM-EDX-data summarized following the result of clustering for k=3*

	Sybilla-results	**TEM-EDX-results**	**Notes**
Cluster1	Illite	diVS-ml (illite)	*very high K-deficit, low XII-charge deficit, Al(VI)-rich, Fe(VI)-rich, low Mg(VI)*
Cluster3		diVS-ml (illite)	*high K-deficit, no XII-charge deficit, Fe(VI)-rich*
Cluster2	IS R0(1) *(%S = 16%)*	diVS-ml *(%S = 12%)*	*high K-deficit, XII-charge deficit, Al(VI)-rich, Fe(VI)-rich*
	Kaolinite + KS GL R0		*in traces only*

Tab. 2. *Comparison of results from TEM-EDX- and XRD-measurements*

The TEM-EDX-data offers a good agreement with the result of Sybilla-processing of XRD-traces from oriented specimen [tab. 2].

IS R0 (1): The Sybilla-procedure of XRD-traces (oriented mounts) has shown an occurrence of a illite-smectite mixed layer phase with a smectite layers probability of %S = 16%. This result of XRD-pattern processing is in good agreement with founded maximum of particles for %S ~ 12% by TEM-EDX-measurements [tab. 2].

The Sybilla-processing of XRD-traces (oriented mounts) also supports low amount of kaolinite and kaolinite-smectite mixed layer phases in fine fraction of sample.

Specifics to the identified clay mineral groups

Dioctahedral vermiculite-smectite mixed layer phase *(Cluster1)*

22 of 91 computed particles belong so to this assumed classification. The dioctahedral character of this group is proofed by X-ray diffraction. The position of the large (060)-interference of smectite is in the random oriented powder specimen at 1.497 Å.

Dioctahedral vermiculite-smectite mixed layer phase *(Cluster1)*

$$Ca_{0.10}\,Mg_{0.14}\,Na_{0.03}\,K_{0.33}\quad Al_{1.58}\,Fe^{3+}_{0.37}\,Mg_{0.05}\,Ti_{0.01}\,(OH)_2\quad Si_{3.20}\,Al_{0.80}\,O_{10}$$

Charge:	XII = 0.83	VI = 5.97	IV = 15.20	**Σ = 22.00**
Measured particles by TEM-EDX:	22			
Probability of smectite layers (%S):	3%			
Probability of illite layers (%I):	97%			
Result of clustering:	Cluster1 [tab. 2]			

A comparison of octahedral Mg vs. tetrahedral Si indicates a differentiation for octahedral Mg based on TEM-EDX-data [fig. 3b]. Particles of Cluster1 contain commonly Mg(VI) < 0.12 per $(OH)_2\ O_{10}$ in octahedral layer.

The mineral formulae, summarized in classes of %S, draws for the maximum an Al- & Fe-rich diVS-ml with low Mg(VI) as well as low amount of K in the interlayer space [tab. 6b].

Dioctahedral vermiculite-smectite mixed layer phase *(diVS-ml, Cluster2)*

$$Ca_{0.10}\,Mg_{0.03}\,Na_{0.03}\,K_{0.56}\quad Al_{1.42}\,Fe^{3+}_{0.39}\,Mg_{0.18}\,Ti_{0.01}\,(OH)_2\quad Si_{3.33}\,Al_{0.67}\,O_{10}$$

Charge:	XII = 0.84	VI = 5.83	IV = 15.33	**Σ = 22.00**
Probability of smectite layers (%S):	12%			
Probability of illite layers (%I):	88%			
Measured particles by TEM-EDX:	35			
Result of clustering:	Cluster1 [tab. 2]			

A comparison of octahedral Mg vs. tetrahedral Si indicates a missing differentiation for octahedral Mg based on TEM-EDX-data of Cluster2 [fig. 3b].

The mineral formulae, summarized in classes of %S, draws for the maximum an Fe-rich diVS-ml with remarkable Mg(VI)-amount as well as reduced amount of K in the interlayer space [tab. 6b].

Dioctahedral vermiculite-smectite mixed layer phase *(Cluster3)*

$$\mathrm{Ca_{0.10}\ Mg_{0.10}\ Na_{0.02}\ K_{0.51}\quad Al_{1.26}\ Fe^{3+}_{0.55}\ Mg_{0.16}\ Ti_{0.03}\ (OH)_2\ \ Si_{3.18}\ Al_{0.82}\ O_{10}}$$

Charge: XII = 0.95 VI = 5.87 IV = 15.18 **Σ = 22.00**

Measured particles by TEM-EDX: 34

Probability of smectite layers (%S): 2%

Probability of illite layers (%I): 98%

Result of clustering: Cluster3 [tab. 2]

A comparison of octahedral Mg vs. tetrahedral Si indicates a differentiation for octahedral Mg based on TEM-EDX-data [fig. 3b]. Particles of Cluster3 contain commonly Mg(VI) > 0.13 per $(OH)_2\ O_{10}$ in octahedral layer.

The mineral formulae, summarized in classes of %S, draws for the maximum an Fe-rich diVS-ml with remarkable amount of Mg(VI) as well as low amount of K in the interlayer space [tab. 6b].

Kaolinite-montmorillonite mixed layer phases

The Excel-based procedure (Hoang-Minh et al., 2019) to identify possible clay mineral groups using the TEM-EDX-measurements also includes algorithms to classify kaolinite and kaolinite-montmorillonite mixed layer phases. These algorithms couldn’t compute no such phases basing on the measured TEM-EDX-data. Such particles have shown small hexagonal plates typically for kaolinite-bearing phases.

References

Cliff, G. & Lorimer, G. W. (1975). *J. Microsc.* **103**, 203–207.

Döbelin, N., Kleeberg, R. (2015). *Journal of Applied Crystallography* **48**, 1573-1580. DOI: 10.1107/S1600576715014685

Henning, K.-H. & Störr, M. (1986). Electron Micrographs (TEM, SEM) of Clays and Clay Minerals, p. 325. Akademie-Verlag Berlin.

Hoang-Minh, T., Kasbohm, J., Nguyen-Thanh, L., Nga, P. T., Lai, L. T., Duong, N. T., Thanh, N. D., Thuyet, N. T. M., Anh, D. D., Pusch, R., Knutsson, S. & Ferreiro Mahlmann, R. (2019). *J. Appl. Cryst.* **52**, 133-147. DOI: 10.1107/S1600576718018162

Lorimer, G. W. & Cliff, G. (1976). *Electron Microscopy in Mineralogy*, edited by H. R. Wenk, pp. 506–519. Berlin: Springer Verlag.

Mellini, M. & Menichini, R. (1985). *R. Soc. Ital. Miner. Petrol.* **40**, 261–266.

Moore, D.M., Reynolds, R.C. (1989). X-ray Diffraction and the Identification and Analysis of Clay Minerals, Oxford University Press, New York, 332 + xvi pp.

Nguyen-Thanh, L., Herbert, H.-J., Kasbohm, J., Hoang-Minh, T. & Mählmann, R. F. (2014). *Clays Clay Miner.* **62**, 425–446.

Środoń, J., Elsass, F., McHardy, W. J. & Morgan, D. J. (1992). *Clay Miner.* **27**, 137–158.

Data Sheet – Opalinus, treated materials *(OPA, 60°C, VSE)*

Methodology - Transmission electron microscopy linked with energy-dispersive X-ray spectroscopy (TEM-EDX)

It is expected a characterization of clay mineral phases in treated Opalinus Clay by transmission electron microscopy. This report describes the results of treated material from Opalinus Clay percolated at a temperature of 60°C.

The different clay mineral phases are to identify and to describe by chemical composition and its variability, morphology, the specific dissolution potential, and further parameter.

Such further parameter like distribution of smectite layers probability (%S) and distribution of charges caused by exchangeable cations interlayer space should serve as additional indicators for mineralogical alterations in treatment experiments with Friedland Clay.

The sample were suspended for TEM-measurement in deionized water and dispersed by ultrasonic treatment for approximately 20 min. The clay fraction (<2 µm) was separated by sedimentation and diluted with deionized water to get a clear suspension. The suspension was dropped onto carbon-coated Cu grids, air dried and stored under environment-controlled conditions at 45% humidity.

TEM-EDX investigations were carried out on the <2 µm fraction using a FEI TECNAI G^2 20 electron transmission microscope at the VNU University of Science, Vietnam National University, Hanoi. This equipment (operated at 200 kV with LaB_6 cathode) was combined with an S-TWIN objective, a windowless EDAX energy-dispersive X-ray system and a FEI Eagle 2k CCD TEM camera.

About 100 individual clay particles per sample were characterized by TEM-EDX with respect to crystal size, crystal habit, and particle morphology and element distribution. The crystal size, crystal habit and particle morphology were described according to Henning & Störr (1986).

For the quantification of element distribution, a calibration of k factors is mandatory (Cliff & Lorimer, 1975; Lorimer & Cliff, 1976; Mellini & Menichini, 1985). These k values are used to calibrate for the specific behaviour of particles against possible irradiation damage. The elements O, Na, Mg, Al, Si, K, Ca and Fe were quantified by applying the EDAX GENESIS–TEM Quant Materials quantification procedure.

In this procedure, the acquired EDX spectra are corrected by background subtraction, Gaussian deconvolution and k-factor corrections using values previously determined on a phyllosilicate standard (muscovite) and selected non-phyllosilicate standards. The average errors in the analyzed elements using the phyllosilicate standard, expressed as the atomic proportions, are 10 (Na), 5 (Fe, Mg, K, Ti, Ca) and 1 (Si, Al).

The measurement time per particle was lowered to 20 s and the exposed area was limited to a 50 nm diameter, avoiding possible irradiation damage of particles. The stability of particles of the sample series was tested for this measurement time at the beginning of any measurement campaign.

Further methodological details related to TEM-EDX-measurements and the Excel-based mathematical procedure using TEM-EDX data for calculation of mineral formulae are described in Hoang-Minh et al. (2019).

These mathematical procedures described in Hoang-Minh et al. (2019) were extended by k-means clustering method for finding subgroups of observations within a data set. The data were standardized

(i.e., scaled) to make variables comparable. Euclidean distances were applied as classical method for distance measures. The optimal clusters were determined by Elbow method and Gap statistics[22].

---

[22] *https://uc-r.github.io/kmeans_clustering*

Data Sheet – Opalinus Clay N09 (< 2 µm), treated material *(60°C, 45.4 h)*

Preparation for TEM

- raw material: compacted material (1.6 g/cm³) of treated Opalinus Clay-sample
- suspension on particles < 2 µm on carbon-filmed Cu-grid
- air-dried and humidity-controlled storing

Mineral Matter

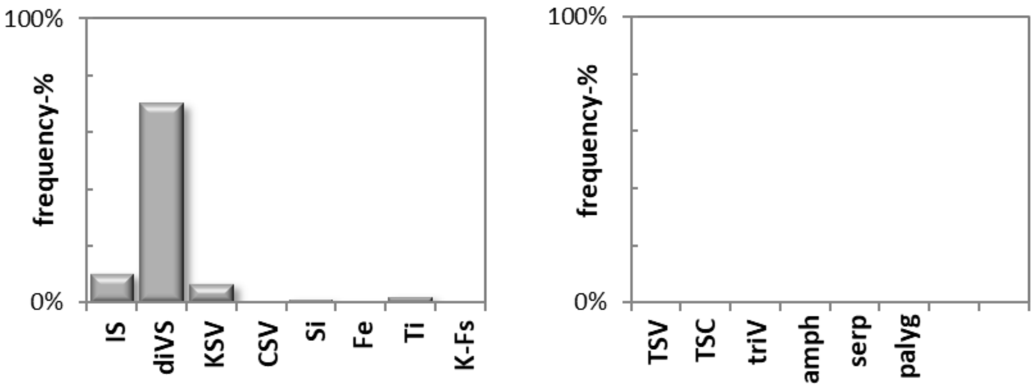

Fig. 1. *Distribution of mineral groups in fraction < 2 µm (in frequency-%)*
Legend: ***IS*** *– illite-smectite-mixed layer series in sense of Środon et al. (1992), diVS – dioctahedral vermiculite-smectite illite-smectite-mixed layer series (= charge- and/or K-deficit),* ***KSV*** *– kaolinite-smectite-dioctahedral vermiculite-mixed layer series,* ***CSV*** *– chlorite-saponite-trioctahedral vermiculite-mixed layer series,* ***Si*** *– quartz or particles with Si-surplus,* ***Fe*** *– Fe-oxide or Fe-oxyhydroxide,* ***Ti*** *– Ti-bearing phases (e.g. rutile, anatase),* ***K-Fs*** *– K-feldspar*

Clay Mineral Composition

All measured dioctahedral particles:

$$Ca_{0.13}\ Mg_{0.04}\ Na_{0.04}\ K_{0.50}\quad Al_{1.39}\ Fe^{3+}_{0.42}\ Mg_{0.18}\ Ti_{0.02}\ (OH)_2\quad Si_{3.27}\ Al_{0.73}\ O_{10}$$

Charge: XII = 0.89 VI = 5.84 IV = 15.27 **Σ = 22.00**
Probability of smectite layers (%S): 7%
Probability of illite layers (%I): 93%

Specific Dissolution Potential (ΔS%)

for H2O, 20 + 60 rpm -7 (= medium reacting, interlayer group: Ca+Mg (= type B))
for NaCl, 20 rpm -8 (= medium reacting, interlayer group: Ca+Mg (= type B))
for NaCl, 60 rpm -54 (= fast reacting, 'illitization', interlayer group: Na (= type A))
CEC_{calc}: 78 meq / 100 g

Measured particles: 132

Table 1. *Summarized chemical composition*

SiO_2	TiO_2	Al_2O_3	Fe_2O_3	MnO	MgO	CaO	Na_2O	K_2O	P_2O_5	Σ	
53.9%	0.2%	30.9%	4.7%		2.8%	2.4%	0.4%	4.6%	0.1%	1.00	measured particles of treated sample
59.4%	0.3%	28.1%	5.9%		2.5%	0.3%	0.1%	3.3%	0.1%	1.00	measured particles of original Opalinus Clay

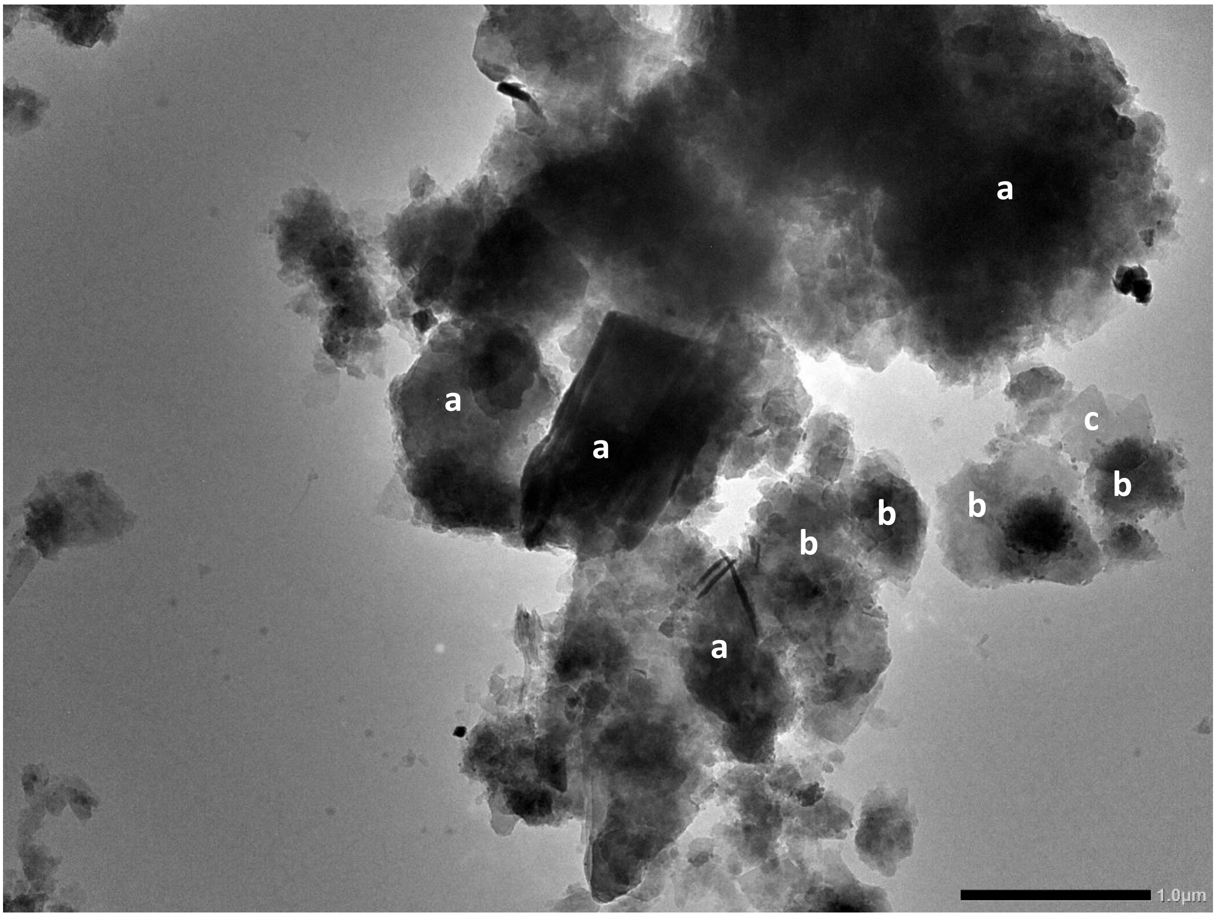

JEM-2100_MAG_X8000_003.bmp

Magnification: 8k

- (a) large (≤ 1 µm) xenomorph platy crystals;
- (b) aggregates formed by small (≤ 100 nm) xenomorphous plates;
- (c) hypidiomorph, hexagonal plates

Fig. 2. *Morphology of particles (TEM-micrographs)*

Distribution of smectite layers probability (%S)

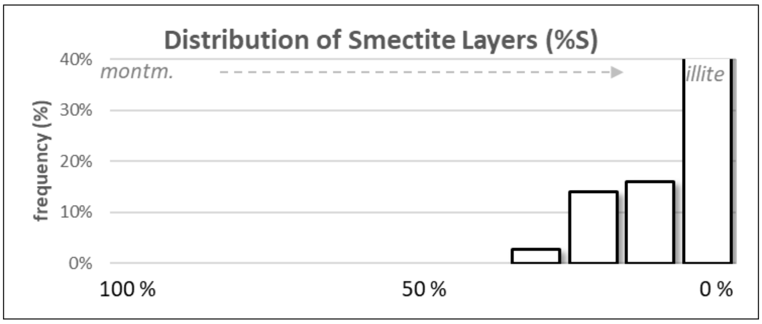

Description: *The distribution of %S-probability indicates the occurrence of two groups: (i) low number of diVS-ml phases as well as (ii) dominating illite with K-deficiency.*

Fig. 3a. *Distribution of smectite layers probability (%S)*

Differentiation by relation “Octahedral Mg vs. tetrahedral Si”?

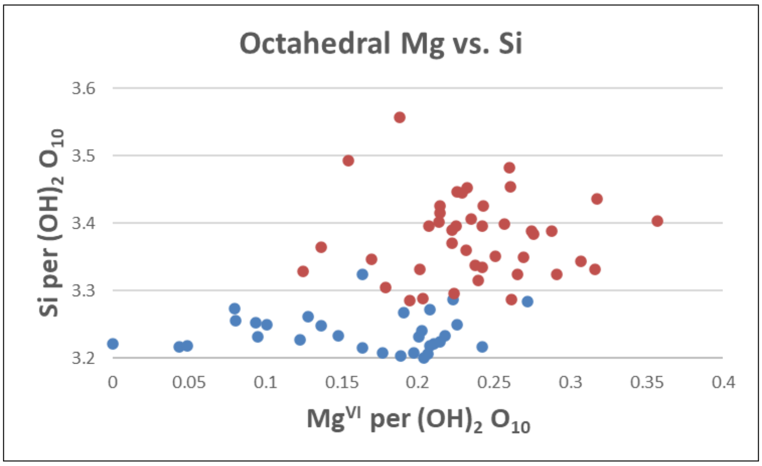

Description: This diagram indicates a separation on low and high ratio of Mg in relation to tetrahedral Si (blue dots – Cluster1: illite; red dots – Cluster2: diVS-ml). DiVS-ml phases are mostly characterized by Mg(VI) > 0.1 per (OH)$_2$ O$_{10}$.

***Fig. 3b.** Distribution of octahedral Mg vs. tetrahedral Si [all per(OH)$_2$ O$_{10}$]*

Distribution of K in relation to tetrahedral Si

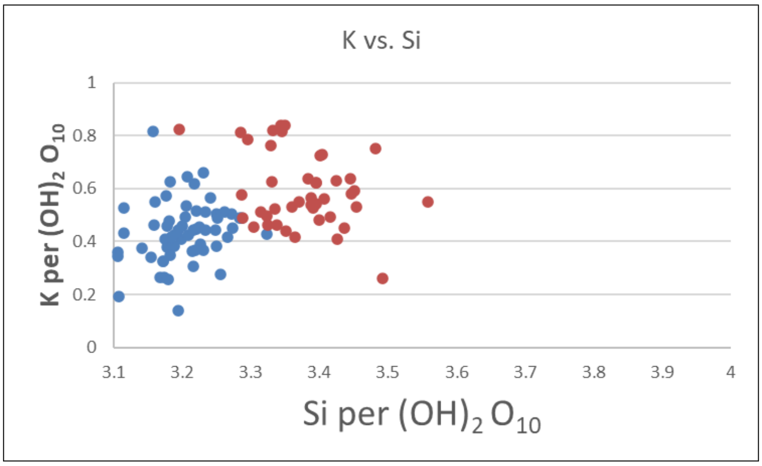

Description: This diagram doesn’t indicate any separation on low and high ratio of K in relation to tetrahedral Si (blue dots – Cluster1: illite; red dots – Cluster2: diVS-ml). DiVS-ml phases (red dots – Cluster2) are mostly characterized by K > 0.4 per (OH)$_2$ O$_{10}$.

***Fig. 4.** Distribution of K in interlayer space vs. tetrahedral Si [all per(OH)$_2$ O$_{10}$]*

Distribution of charges (exchangeable from interlayer space)

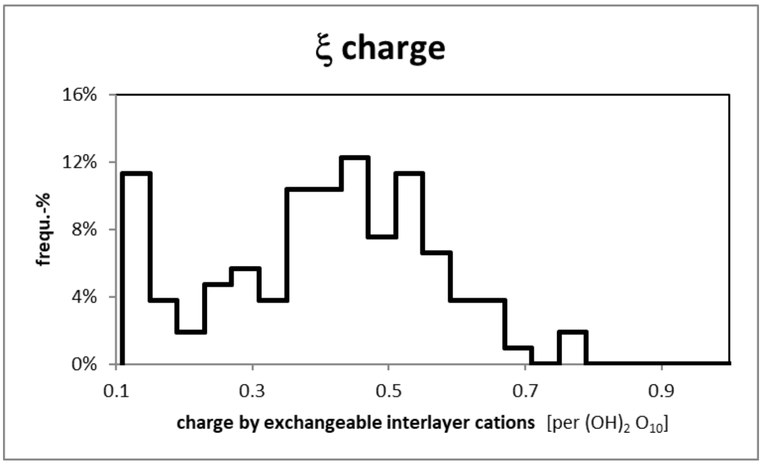

This diagram visualizes the distribution of exchangeable charges in the interlayer space (Ca, Mg, Na) determined and computed by TEM-EDX-data.

***Description:** Very broad distribution of charge density with maximal frequency-% at 0.43 per (OH)$_2$ O$_{10}$*

***Fig. 5.** Distribution of charges*

Dioctahedral Vermiculite-Smectite mixed layer phases (diVS-ml - illite) *(Cluster1):*

$$\mathrm{Ca_{0.15}\ Mg_{0.07}\ Na_{0.04}\ K_{0.43}\quad Al_{1.41}\ Fe^{3+}_{0.43}\ Mg_{0.14}\ Ti_{0.02}\ (OH)_2\ \ Si_{3.19}\ Al_{0.81}\ O_{10}}$$

Charge: XII = 0.93 VI = 5.88 IV = 15.19 **Σ = 22.00**

Probability of smectite layers (%S): 3%

Probability of illite layers (%I): 97%

Measured particles: 64

Distribution of smectite layers probability (%S) in diVS-ml (Cluster1)

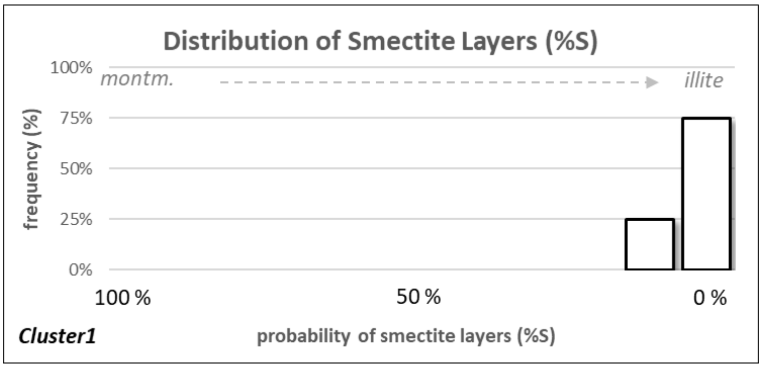

Description: *The distribution of diVS-ml (classified as Cluster1) draws a maximum of frequency (%) for smectite layer probability at 0%*

Fig. 6a. *Distribution of smectite layers probability in diVS-ml*

diVS-ml	*particles (abs)*	Ca (XII)	Mg (XII)	Na (XII)	K (XII)	Cr3+ (VI)	Al (VI)	Fe3+ (VI)	Mg (VI)	Ti (VI)	Al (IV)	Si (IV)	XII	n_VI	%S
%S >95%	n = 0														
%S 95-85%	n = 0														
%S 85-75%	n = 0														
%S 75-65%	n = 0														
%S 65-55%	n = 0														
%S 55-45%	n = 0														
%S 45-35%	n = 0														
%S 35-25%	n = 0														
%S 25-15%	n = 0														
%S <15%	**n = 64**	**0.15**	**0.07**	**0.04**	**0.43**	**0.00**	**1.41**	**0.43**	**0.14**	**0.02**	**0.81**	**3.19**	**0.93**	**2.0**	**3**

Fig. 6b. *Computed averaged mineral formulae of diVS-ml phases in the different smectite layers probability (%S)-classes*

Dioctahedral Vermiculite-Smectite mixed layer phases (diVS-ml) *(Cluster2):*

$$\mathrm{Ca_{0.10}\ Mg_{0.00}\ Na_{0.04}\ K_{0.59}\quad Al_{1.36}\ Fe^{3+}_{0.41}\ Mg_{0.24}\ Ti_{0.01}\ (OH)_2\ \ Si_{3.38}\ Al_{0.62}\ O_{10}}$$

Charge: XII = 0.84 VI = 5.78 IV = 15.38 **Σ = 22.00**

Probability of smectite layers (%S): 16%

Probability of illite layers (%I): 84%

Measured particles: 43

Distribution of smectite layers probability (%S) in diVS-ml (Cluster2)

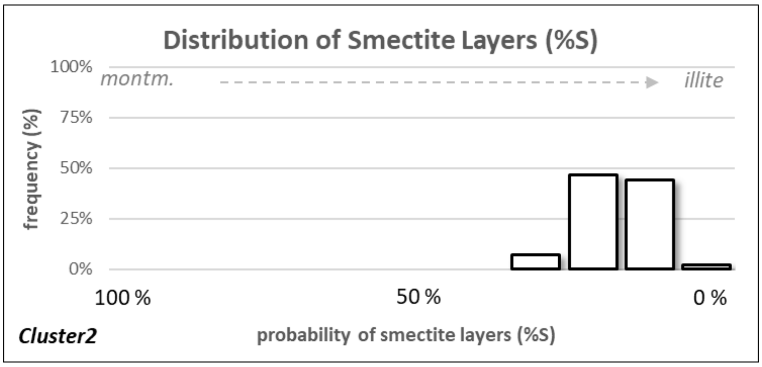

Description: *The distribution of diVS-ml (classified as Cluster2) draws a maximum of frequency (%) for smectite layer probability at 20%*

Fig. 7a. *Distribution of smectite layers probability in diVS-ml*

diVS-ml	particles (abs)	Ca (XII)	Mg (XII)	Na (XII)	K (XII)	Cr3+ (VI)	Al (VI)	Fe3+ (VI)	Mg (VI)	Ti (VI)	Al (IV)	Si (IV)	XII	n_VI	%S
%S >95%	n = 0														
%S 95-85%	n = 0														
%S 85-75%	n = 0														
%S 75-65%	n = 0														
%S 65-55%	n = 0														
%S 55-45%	n = 0														
%S 45-35%	n = 0														
%S 35-25%	n = 3	0.07	0.01	0.04	0.52	0.00	1.38	0.40	0.20	0.00	0.49	3.51	0.7	2.0	29
%S 25-15%	**n = 20**	**0.11**	**0.00**	**0.05**	**0.57**	**0.00**	**1.33**	**0.42**	**0.25**	**0.00**	**0.59**	**3.41**	**0.8**	**2.0**	**19**
%S <15%	**n = 20**	**0.10**	**0.01**	**0.03**	**0.62**	**0.00**	**1.37**	**0.39**	**0.23**	**0.01**	**0.68**	**3.32**	**0.9**	**2.0**	**11**

Fig. 7b. *Computed averaged mineral formulae of diVS-ml phases in the different smectite layers probability (%S)-classes*

Cluster2		Ca (XII)	Mg (XII)	Na (XII)	K (XII)	Cr3+ (VI)	Al (VI)	Fe3+ (VI)	Mg (VI)	Ti (VI)	Al (IV)	Si (IV)	XII	n_VI	%S
without illite	**n = 23**	**0.10**	**0.00**	**0.04**	**0.56**	**0.00**	**1.34**	**0.42**	**0.24**	**0.00**	**0.58**	**3.42**	**0.82**	**2.0**	**20**
only illite	n = 20	0.10	0.01	0.03	0.62	0.00	1.37	0.39	0.23	0.01	0.68	3.32	0.88	2.0	11

Fig. 7c. *Computed averaged mineral formulae of diVS-ml phases differentiated by illite*

Description – Opalinus Clay N09 (< 2 µm), treated material *(60°C)*

Preparation for TEM

The powder of Opalinus Clay-sample was suspended in deionized water and dispersed by ultrasonic treatment for approximately 20 min. The clay fraction (<2 µm) was separated by sedimentation and diluted with deionized water to get a clear suspension. The suspension was dropped onto carbon-coated Cu grids, air dried and stored under environment-controlled conditions at 45% humidity.

Mineral Matter - Overview

The fraction < 2 µm of Opalinus Clay N09 sample is mainly composed by two different types of dioctahedral vermiculite-smectite mixed layer phases (diVS-ml). Rarely, kaolinite and kaolinite-smectite-ml phases as well as chlorite-smectite-ml phases, rutile and quartz were identified in traces in this sample [fig. 1].

The measured and computed particles have shown a calculated CEC-value of 78 meq / 100 g located at surface and in the interlayer space.

	frequency-% *(n = 132 measured particles)*
diVS-ml	81%
Kaolinite & KSV-ml	7%
CSV-ml	7%
Ti-phases	2%
Quartz	2%
Fe-phases	1%
Unknown phases	1%

All measured dioctahedral 2:1 clay mineral phases summarized result following mineral formula computed from TEM-EDX-measurement of 107 individual particles:

	$Ca^{2+}_{0.13}$	$Mg^{2+}_{0.04}$	$Na^{+}_{0.04}$	$K^{+}_{0.50}$	$Al^{3+}_{1.39}$	$Fe^{3+}_{0.42}$	$Mg^{2+}_{0.18}$	$Ti^{4+}_{0.02}$	$(OH)_2$	$Si^{4+}_{3.27}$	$Al^{3+}_{0.73}$	O_{10}
SDOM	*± 0.01*	*± 0.01*	*± 0.00*	*± 0.01*	*± 0.02*	*± 0.01*	*± 0.01*	*± 0.00*		*± 0.01*	*± 0.01*	

Legend: SDOM - standard deviation of the mean (= the standard deviation divided by the square root of the number of samples)

The interlayer charge is calculated as 0.89 per $(OH)_2$ O_{10} and the octahedral charge as 5.84 per $(OH)_2$ O_{10}. The particles are characterized by a high octahedral Fe-amount.

The summarized chemical composition of all 107 computed particles is listed [tab. 1].

Opalinus Clay N09 sample is also characterized by two morphological groups: (i) large (≤ 1 µm) xenomorph platy crystals and (ii) aggregates, partially with folds, formed by small (≤ 100 nm) xenomorphous plates [fig. 2]. Aggregates formed by large (≤ 1 µm) xenomorph platy crystals dominate the shapes of particles in the micrographs [fig. 2].

The distribution of %S-probability of all measured clay mineral phases [fig. 3a] also indicates the occurrence of two groups: (i) diVS-ml and dominating (ii) illite with K-deficiency.

The numerous measured particles by TEM-EDX allow a visualization of distribution of interlayer charges. Considering the TEM-EDX-determined cations Ca^{++}, Mg^{++} and Na^{+} and then computed their ratio as interlayer cations in the mineral formula, Ca^{++}, Mg^{++} and Na^{+} offer to characterize the degree of exchangeable charges in the interlayer space. This charge density of Opalinus Clay N09 (< 2 µm) shows in this sample a maximal frequency-% of charge density at 0.47 per $(OH)_2\,O_{10}$ [fig. 5]. This interval of interlayer charge density caused by exchangeable cations from 0.23 - 0.71 per $(OH)_2\,O_{10}$ represents mentioned diVS-ml.

Mineral Matter - Specification

Result of Clustering

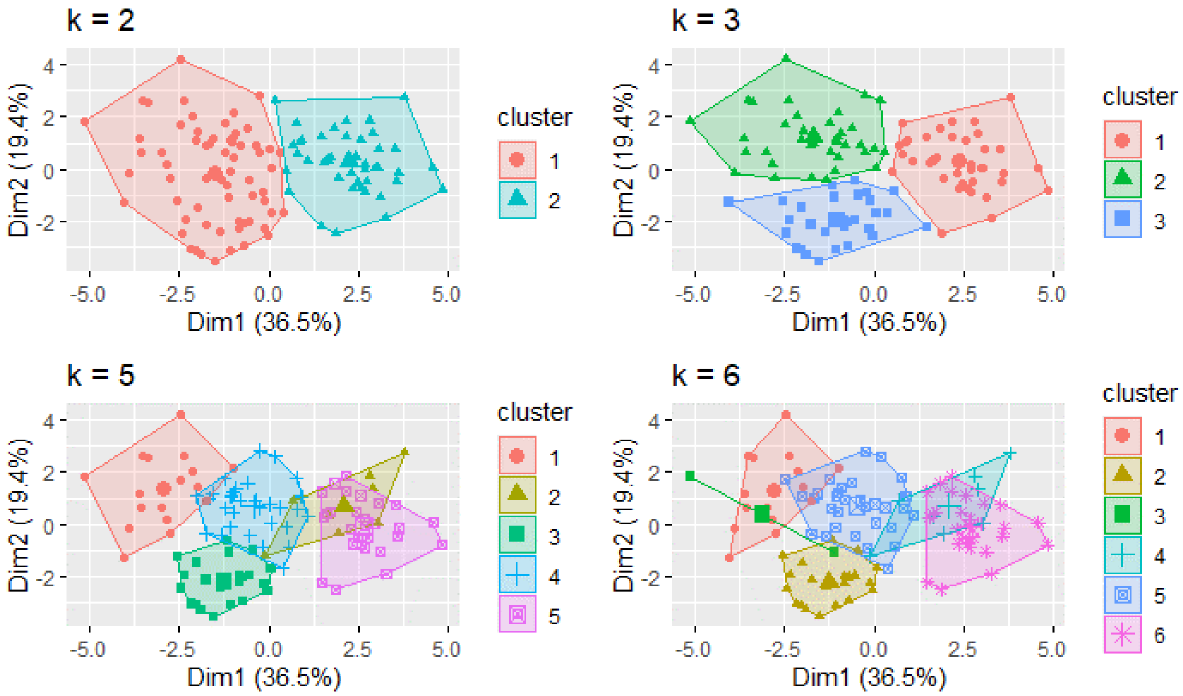

Fig. 8. *Clustering of all measured particles for clusters k = 2, k = 3, k = 5 and k = 6 (source for R-coding: https://uc-r.github.io/kmeans_clustering)*

The optimum of clusters was calculated with k = 2 and k = 6.

		Ca (XII)	Mg (XII)	Na (XII)	K (XII)	Cr3+ (VI)	Al (VI)	Fe3+ (VI)	Mg (VI)	Ti (VI)	Al (IV)	Si (IV)	XII	n_VI	%S
Cluster1	n = 64	0.15	0.07	0.04	0.43	0.00	1.41	0.43	0.14	0.02	0.81	3.19	0.93	2.0	3
Cluster2	n = 43	0.10	0.00	0.04	0.59	0.00	1.36	0.41	0.24	0.01	0.62	3.38	0.85	2.0	16

Fig. 9a. *Mineral formulae based on TEM-EDX-data summarized following the result of clustering for k=2*

	Sybilla-results	**TEM-EDX-results**	**Notes**
Cluster1	Illite	diVS-ml (illite)	*very high K-deficit, no XII-charge deficit, Al(VI)-rich, Fe(VI)-rich, low Mg(VI)*
Cluster2	IS R0(1) *(%S = 23%)*	diVS-ml *(%S = 16%)*	*high K-deficit, no XII-charge deficit, Fe(VI)-rich*
	Kaolinite + KS GL R0		*in traces only*

Tab. 2. *Comparison of results from TEM-EDX- and XRD-measurements*

The TEM-EDX-data offers a good agreement with the result of Sybilla-processing of XRD-traces from oriented specimen [tab. 2].

IS R0 (1): The Sybilla-procedure of XRD-traces (oriented mounts) has shown an occurrence of a illite-smectite mixed layer phase with a smectite layers probability of %S = 23%. This result of XRD-pattern processing is in good agreement with founded maximum of particles for %S ~ 16% by TEM-EDX-measurements [tab. 2].

The Sybilla-processing of XRD-traces (oriented mounts) also supports low amount of kaolinite and kaolinite-smectite mixed layer phases in fine fraction of sample.

Specifics to the identified clay mineral groups

Dioctahedral vermiculite-smectite mixed layer phase *(Cluster1)*

64 of 107 computed particles belong so to this assumed classification. The dioctahedral character of this group is proofed by X-ray diffraction. The position of the large (060)-interference of smectite is in the random oriented powder specimen at 1.497 Å.

Dioctahedral vermiculite-smectite mixed layer phase *(Cluster1)*

$$Ca_{0.15}\,Mg_{0.07}\,Na_{0.04}\,K_{0.43}\quad Al_{1.41}\,Fe^{3+}_{0.43}\,Mg_{0.14}\,Ti_{0.02}\,(OH)_2\quad Si_{3.19}\,Al_{0.81}\,O_{10}$$

Charge: XII = 0.93 VI = 5.88 IV = 15.19 **Σ = 22.00**
Measured particles by TEM-EDX: 64
Probability of smectite layers (%S): 3%
Probability of illite layers (%I): 97%
Result of clustering: Cluster1 [tab. 2]

A comparison of octahedral Mg vs. tetrahedral Si indicates a differentiation for octahedral Mg based on TEM-EDX-data [fig. 3b]. Particles of Cluster1 contain commonly Mg(VI) < 0.25 per $(OH)_2\ O_{10}$ in octahedral layer.

The mineral formulae, summarized in classes of %S, draws for the maximum an Al- & Fe-rich diVS-ml with low Mg(VI) as well as low amount of K in the interlayer space [tab. 6b].

Dioctahedral vermiculite-smectite mixed layer phase *(diVS-ml, Cluster2)*

$$Ca_{0.10}\,Mg_{0.00}\,Na_{0.04}\,K_{0.59}\quad Al_{1.36}\,Fe^{3+}_{0.41}\,Mg_{0.24}\,Ti_{0.01}\,(OH)_2\quad Si_{3.38}\,Al_{0.62}\,O_{10}$$

Charge: XII = 0.84 VI = 5.78 IV = 15.38 **Σ = 22.00**
Probability of smectite layers (%S): 16%
Probability of illite layers (%I): 84%
Measured particles by TEM-EDX: 43
Result of clustering: Cluster2 [tab. 2]

A comparison of octahedral Mg vs. tetrahedral Si indicates a missing differentiation for octahedral Mg based on TEM-EDX-data of Cluster2 [fig. 3b].

The mineral formulae, summarized in classes of %S, draws for the maximum an Fe-rich diVS-ml with remarkable Mg(VI)-amount as well as reduced amount of K in the interlayer space [tab. 7b].

Kaolinite-montmorillonite mixed layer phases

The Excel-based procedure (Hoang-Minh et al., 2019) to identify possible clay mineral groups using the TEM-EDX-measurements also includes algorithms to classify kaolinite and kaolinite-montmorillonite mixed layer phases. These algorithms couldn’t compute no such phases basing on the measured TEM-EDX-data. Such particles have shown small hexagonal plates typically for kaolinite-bearing phases.

References

Cliff, G. & Lorimer, G. W. (1975). *J. Microsc.* **103**, 203–207.

Döbelin, N., Kleeberg, R. (2015). *Journal of Applied Crystallography* **48**, 1573-1580. DOI: 10.1107/S1600576715014685

Henning, K.-H. & Störr, M. (1986). Electron Micrographs (TEM, SEM) of Clays and Clay Minerals, p. 325. Akademie-Verlag Berlin.

Hoang-Minh, T., Kasbohm, J., Nguyen-Thanh, L., Nga, P. T., Lai, L. T., Duong, N. T., Thanh, N. D., Thuyet, N. T. M., Anh, D. D., Pusch, R., Knutsson, S. & Ferreiro Mahlmann, R. (2019). *J. Appl. Cryst.* **52**, 133-147. DOI: 10.1107/S1600576718018162

Lorimer, G. W. & Cliff, G. (1976). *Electron Microscopy in Mineralogy*, edited by H. R. Wenk, pp. 506–519. Berlin: Springer Verlag.

Mellini, M. & Menichini, R. (1985). *R. Soc. Ital. Miner. Petrol.* **40**, 261–266.

Moore, D.M., Reynolds, R.C. (1989). X-ray Diffraction and the Identification and Analysis of Clay Minerals, Oxford University Press, New York, 332 + xvi pp.

Nguyen-Thanh, L., Herbert, H.-J., Kasbohm, J., Hoang-Minh, T. & Mählmann, R. F. (2014). *Clays Clay Miner.* **62**, 425–446.

Środoń, J., Elsass, F., McHardy, W. J. & Morgan, D. J. (1992). *Clay Miner.* **27**, 137–158.

Data Sheet – Opalinus, treated materials *(OPA, 100°C, VSD)*

Methodology - Transmission electron microscopy linked with energy-dispersive X-ray spectroscopy (TEM-EDX)

It is expected a characterization of clay mineral phases in treated Opalinus Clay by transmission electron microscopy. This report describes the results of treated material from Opalinus Clay percolated at a temperature of 100°C.

The different clay mineral phases are to identify and to describe by chemical composition and its variability, morphology, the specific dissolution potential, and further parameter.

Such further parameter like distribution of smectite layers probability (%S) and distribution of charges caused by exchangeable cations interlayer space should serve as additional indicators for mineralogical alterations in treatment experiments with Friedland Clay.

The sample were suspended for TEM-measurement in deionized water and dispersed by ultrasonic treatment for approximately 20 min. The clay fraction (<2 µm) was separated by sedimentation and diluted with deionized water to get a clear suspension. The suspension was dropped onto carbon-coated Cu grids, air dried and stored under environment-controlled conditions at 45% humidity.

TEM-EDX investigations were carried out on the <2 µm fraction using a FEI TECNAI G^2 20 electron transmission microscope at the VNU University of Science, Vietnam National University, Hanoi. This equipment (operated at 200 kV with LaB_6 cathode) was combined with an S-TWIN objective, a windowless EDAX energy-dispersive X-ray system and a FEI Eagle 2k CCD TEM camera.

About 100 individual clay particles per sample were characterized by TEM-EDX with respect to crystal size, crystal habit, and particle morphology and element distribution. The crystal size, crystal habit and particle morphology were described according to Henning & Störr (1986).

For the quantification of element distribution, a calibration of k factors is mandatory (Cliff & Lorimer, 1975; Lorimer & Cliff, 1976; Mellini & Menichini, 1985). These k values are used to calibrate for the specific behaviour of particles against possible irradiation damage. The elements O, Na, Mg, Al, Si, K, Ca and Fe were quantified by applying the EDAX GENESIS–TEM Quant Materials quantification procedure.

In this procedure, the acquired EDX spectra are corrected by background subtraction, Gaussian deconvolution and k-factor corrections using values previously determined on a phyllosilicate standard (muscovite) and selected non-phyllosilicate standards. The average errors in the analyzed elements using the phyllosilicate standard, expressed as the atomic proportions, are 10 (Na), 5 (Fe, Mg, K, Ti, Ca) and 1 (Si, Al).

The measurement time per particle was lowered to 20 s and the exposed area was limited to a 50 nm diameter, avoiding possible irradiation damage of particles. The stability of particles of the sample series was tested for this measurement time at the beginning of any measurement campaign.

Further methodological details related to TEM-EDX-measurements and the Excel-based mathematical procedure using TEM-EDX data for calculation of mineral formulae are described in Hoang-Minh et al. (2019).

These mathematical procedures described in Hoang-Minh et al. (2019) were extended by k-means clustering method for finding subgroups of observations within a data set. The data were standardized

(i.e., scaled) to make variables comparable. Euclidean distances were applied as classical method for distance measures. The optimal clusters were determined by Elbow method and Gap statistics[23].

---

[23] *https://uc-r.github.io/kmeans_clustering*

Data Sheet – Opalinus Clay N08 (< 2 µm), treated material *(100°C, 69.3 h)*

Preparation for TEM

- raw material: compacted material (1.6 g/cm³) of treated Opalinus Clay-sample
- suspension on particles < 2 µm on carbon-filmed Cu-grid
- air-dried and humidity-controlled storing

Mineral Matter

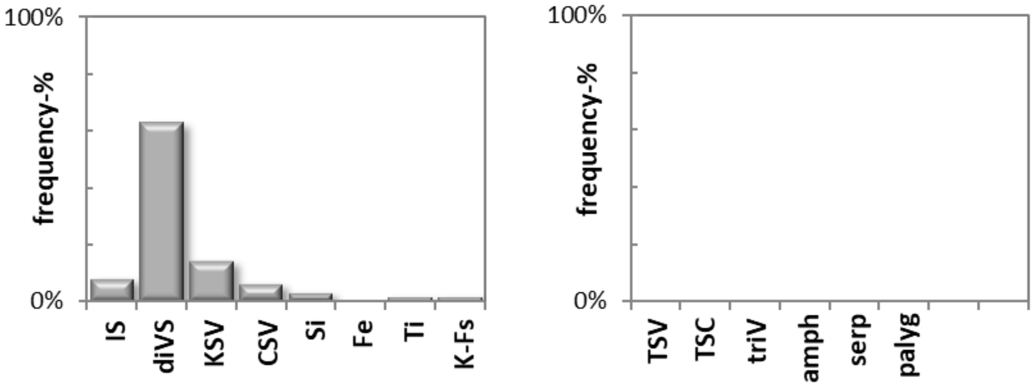

Fig. 1. *Distribution of mineral groups in fraction < 2 µm (in frequency-%)*
Legend: ***IS*** *– illite-smectite-mixed layer series in sense of Środon et al. (1992), diVS – dioctahedral vermiculite-smectite illite-smectite-mixed layer series (= charge- and/or K-deficit),* ***KSV*** *– kaolinite-smectite-dioctahedral vermiculite-mixed layer series,* ***CSV*** *– chlorite-saponite-trioctahedral vermiculite-mixed layer series,* ***Si*** *– quartz or particles with Si-surplus,* ***Fe*** *– Fe-oxide or Fe-oxyhydroxide,* ***Ti*** *– Ti-bearing phases (e.g. rutile, anatase),* ***K-Fs*** *– K-feldspar*

Clay Mineral Composition

All measured dioctahedral particles:

$$\mathrm{Ca_{0.07}\,Mg_{0.10}\,Na_{0.00}\,K_{0.47}\quad Al_{1.40}\,Fe^{3+}_{0.45}\,Mg_{0.13}\,Ti_{0.01}\,(OH)_2\quad Si_{3.30}\,Al_{0.70}\,O_{10}}$$

Charge: XII = 0.83 VI = 5.87 IV = 15.30 **Σ = 22.00**
Probability of smectite layers (%S): 10%
Probability of illite layers (%I): 90%

Specific Dissolution Potential (ΔS%)

for H2O, 20 + 60 rpm -53 (= fast reacting, 'illitization', interlayer group: Ca+Mg (= type B))
for NaCl, 20 rpm -53 (= fast reacting, 'illitization', interlayer group: Ca+Mg (= type B))
for NaCl, 60 rpm -102 (= fast reacting, 'illitization', interlayer group: Na (= type A))
CEC_{calc}: 42 meq / 100 g

Measured particles: 160

Table 1. *Summarized chemical composition*

SiO_2	TiO_2	Al_2O_3	Fe_2O_3	MnO	MgO	CaO	Na_2O	K_2O	P_2O_5	Σ	
55.2%	0.1%	31.2%	4.9%		3.0%	0.8%	0.0%	4.8%	0.1%	1.00	measured particles of treated sample
59.4%	0.3%	28.1%	5.9%		2.5%	0.3%	0.1%	3.3%	0.1%	1.00	measured particles of original Opalinus Clay

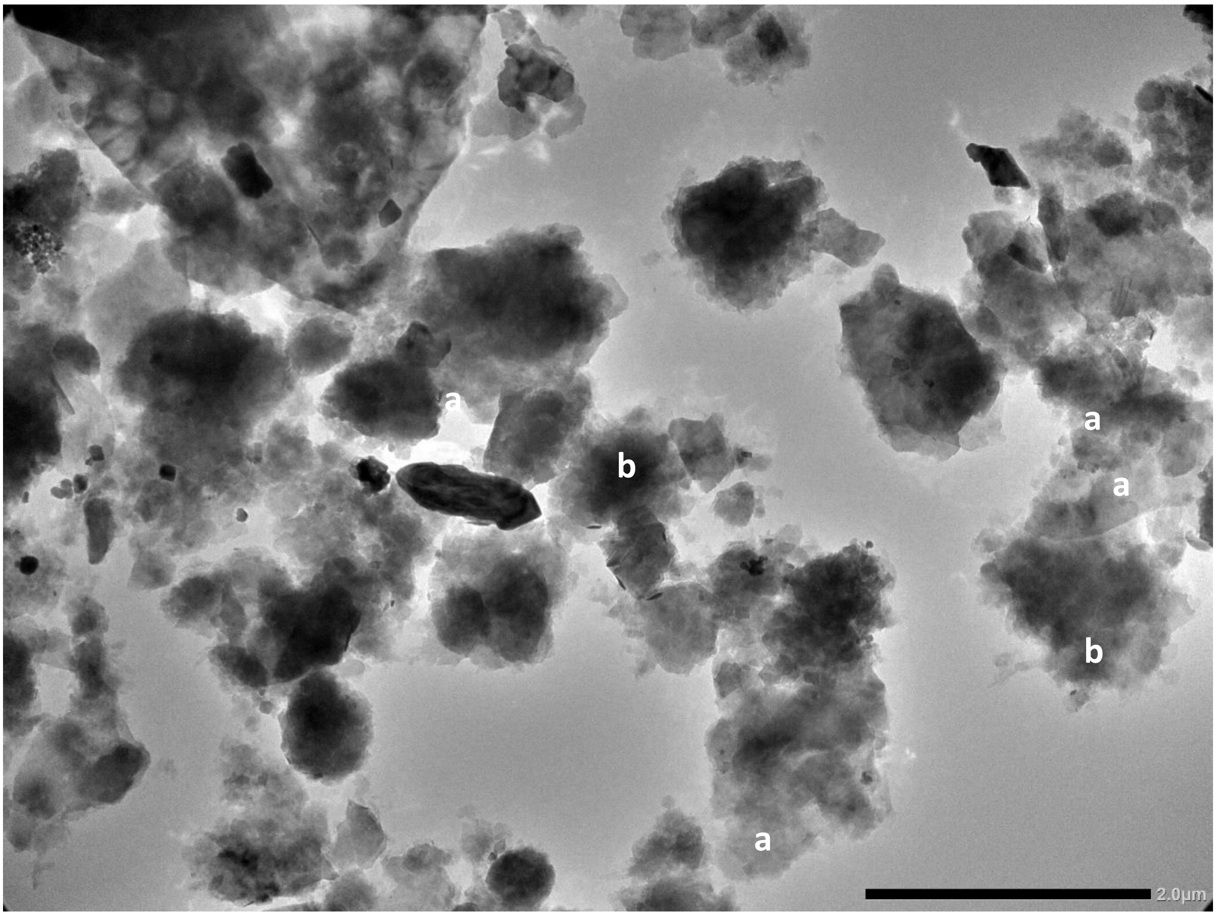

JEM-2100_MAG_X6000_028.bmp

Magnification: 6k

(a) large (≤ 1 µm) xenomorph platy crystals;
(b) aggregates formed by small (≤ 100 nm) xenomorphous plates

Fig. 2. *Morphology of particles (TEM-micrographs)*

Distribution of smectite layers probability (%S)

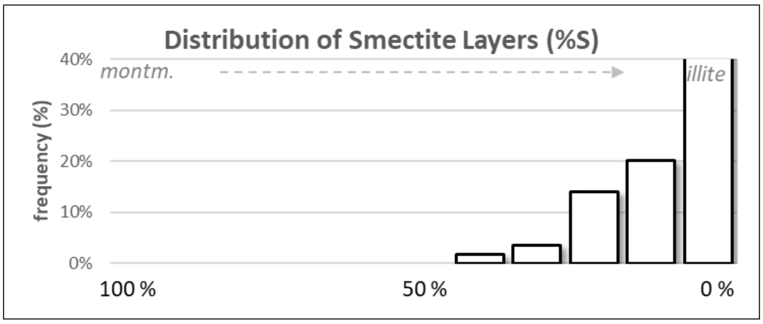

Description: *The distribution of %S-probability indicates the occurrence of two groups: (i) low number of diVS-ml phases as well as (ii) dominating illite with K-deficiency.*

Fig. 3a. *Distribution of smectite layers probability (%S)*

Differentiation by relation "Octahedral Mg vs. tetrahedral Si"?

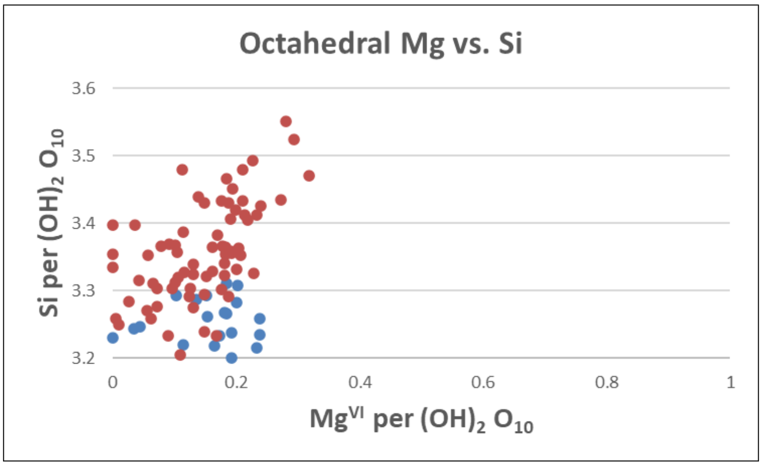

***Description:** This diagram doesn't indicate any separation on low and high ratio of Mg in relation to tetrahedral Si (blue dots – Cluster1: illite; red dots – Cluster2: diVS-ml). All phases are mostly characterized by Mg(VI) < 0.25 per $(OH)_2 O_{10}$.*

***Fig. 3b.** Distribution of octahedral Mg vs. tetrahedral Si [all per$(OH)_2 O_{10}$]*

Distribution of K in relation to tetrahedral Si

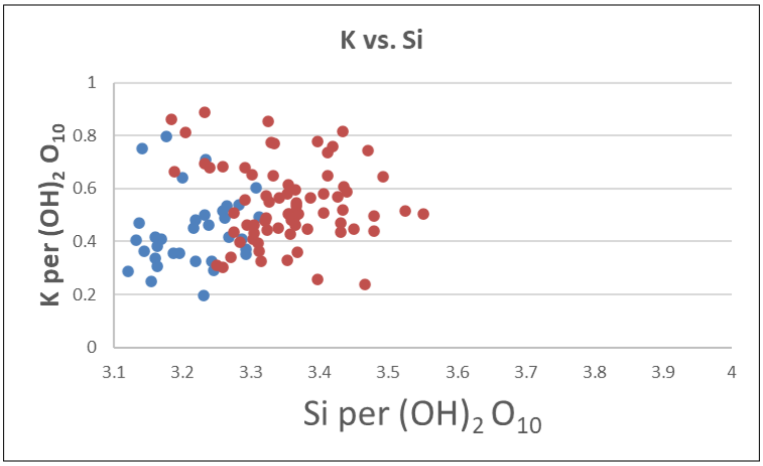

***Description:** This diagram doesn't indicate any separation on low and high ratio of K in relation to tetrahedral Si (blue dots – Cluster1: illite; red dots – Cluster2: diVS-ml).*

***Fig. 4.** Distribution of K in interlayer space vs. tetrahedral Si [all per$(OH)_2 O_{10}$]*

Distribution of charges (exchangeable from interlayer space)

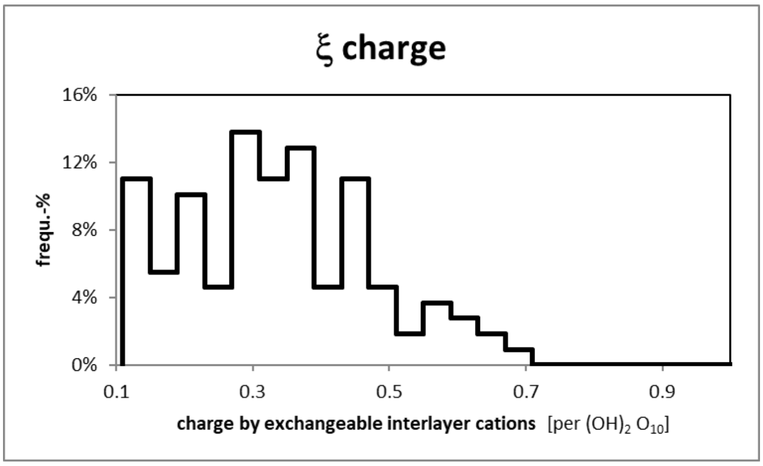

This diagram visualizes the distribution of exchangeable charges in the interlayer space (Ca, Mg, Na) determined and computed by TEM-EDX-data.

***Description:** Very broad distribution of charge density with a weak maximal frequency-% at 0.31 per $(OH)_2 O_{10}$*

***Fig. 5.** Distribution of charges*

Dioctahedral Vermiculite-Smectite mixed layer phases (diVS-ml - illite) *(Cluster1):*

$$Ca_{0.08}\ Mg_{0.15}\ Na_{0.00}\ K_{0.44}\quad Al_{1.28}\ Fe^{3+}_{0.57}\ Mg_{0.13}\ Ti_{0.02}\ (OH)_2\ \ Si_{3.21}\ Al_{0.79}\ O_{10}$$

Charge:	XII = 0.90	VI = 5.89	IV = 15.21	**Σ = 22.00**
Probability of smectite layers (%S):	4%			
Probability of illite layers (%I):	96%			
Measured particles:	38			

Distribution of smectite layers probability (%S) in diVS-ml (Cluster1)

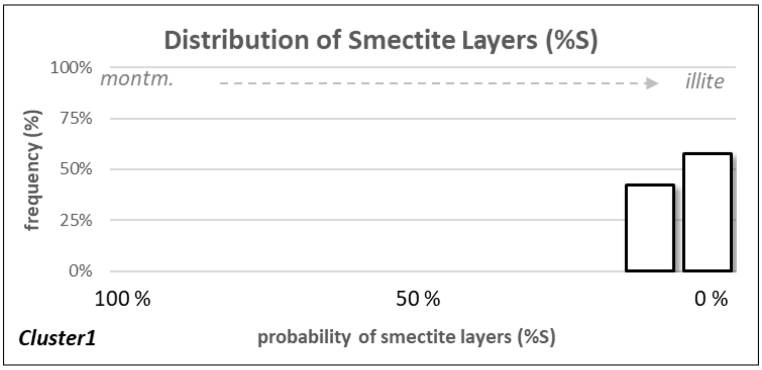

Description: *The distribution of diVS-ml (classified as Cluster1) draws a maximum of frequency (%) for smectite layer probability at 0%*

Fig. 6a. *Distribution of smectite layers probability in diVS-ml*

diVS-ml	*particles (abs)*	Ca (XII)	Mg (XII)	Na (XII)	K (XII)	Cr3+ (VI)	Al (VI)	Fe3+ (VI)	Mg (VI)	Ti (VI)	Al (IV)	Si (IV)	XII	n_VI	%S
%S >95%	n = 0														
%S 95-85%	n = 0														
%S 85-75%	n = 0														
%S 75-65%	n = 0														
%S 65-55%	n = 0														
%S 55-45%	n = 0														
%S 45-35%	n = 0														
%S 35-25%	n = 0														
%S 25-15%	n = 0														
%S <15%	**n = 38**	**0.08**	**0.15**	**0.00**	**0.44**	**0.00**	**1.28**	**0.57**	**0.13**	**0.02**	**0.79**	**3.21**	**0.90**	**2.0**	**4**

Fig. 6b. *Computed averaged mineral formulae of diVS-ml phases in the different smectite layers probability (%S)-classes*

Dioctahedral Vermiculite-Smectite mixed layer phases (diVS-ml) *(Cluster2):*

$$Ca_{0.06}\ Mg_{0.06}\ Na_{0.00}\ K_{0.54}\quad Al_{1.49}\ Fe^{3+}_{0.37}\ Mg_{0.14}\ Ti_{0.01}\ (OH)_2\ \ Si_{3.35}\ Al_{0.65}\ O_{10}$$

Charge:	XII = 0.79	VI = 5.86	IV = 15.35	**Σ = 22.00**
Probability of smectite layers (%S):	13%			
Probability of illite layers (%I):	87%			
Measured particles:	76			

Distribution of smectite layers probability (%S) in diVS-ml (Cluster2)

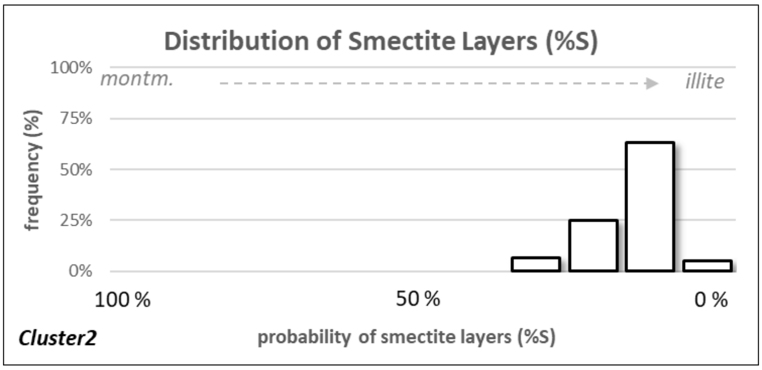

Description: *The distribution of diVS-ml (classified as Cluster2) draws a maximum of frequency (%) for smectite layer probability at 10%*

Fig. 7a. *Distribution of smectite layers probability in diVS-ml*

diVS-ml	particles (abs)	Ca (XII)	Mg (XII)	Na (XII)	K (XII)	Cr3+ (VI)	Al (VI)	Fe3+ (VI)	Mg (VI)	Ti (VI)	Al (IV)	Si (IV)	XII	n_VI	%S
%S >95%	n = 0														
%S 95-85%	n = 0														
%S 85-75%	n = 0														
%S 75-65%	n = 0														
%S 65-55%	n = 0														
%S 55-45%	n = 0														
%S 45-35%	n = 0														
%S 35-25%	n = 5	0.06	0.04	0.00	0.52	0.00	1.36	0.42	0.22	0.00	0.49	3.51	0.7	2.0	29
%S 25-15%	n = 19	0.06	0.04	0.01	0.56	0.00	1.42	0.39	0.18	0.01	0.58	3.42	0.8	2.0	20
%S <15%	**n = 52**	**0.06**	**0.08**	**0.00**	**0.54**	**0.00**	**1.52**	**0.35**	**0.12**	**0.01**	**0.69**	**3.31**	**0.8**	**2.0**	**10**

Fig. 7b. *Computed averaged mineral formulae of diVS-ml phases in the different smectite layers probability (%S)-classes*

Cluster2		Ca (XII)	Mg (XII)	Na (XII)	K (XII)	Cr3+ (VI)	Al (VI)	Fe3+ (VI)	Mg (VI)	Ti (VI)	Al (IV)	Si (IV)	XII	n_VI	%S
without illite	**n = 24**	**0.06**	**0.04**	**0.00**	**0.55**	**0.00**	**1.40**	**0.40**	**0.19**	**0.00**	**0.56**	**3.44**	**0.75**	**2.0**	**22**
only illite	n = 52	0.06	0.08	0.00	0.54	0.00	1.52	0.35	0.12	0.01	0.69	3.31	0.81	2.0	10

Fig. 7c. *Computed averaged mineral formulae of diVS-ml phases differentiated by illite*

Description – Opalinus Clay N08 (< 2 µm), treated material *(100°C)*

Preparation for TEM

The powder of Opalinus Clay-sample was suspended in deionized water and dispersed by ultrasonic treatment for approximately 20 min. The clay fraction (<2 µm) was separated by sedimentation and diluted with deionized water to get a clear suspension. The suspension was dropped onto carbon-coated Cu grids, air dried and stored under environment-controlled conditions at 45% humidity.

Mineral Matter - Overview

The fraction < 2 µm of Opalinus Clay N08 sample is mainly composed by two different types of dioctahedral vermiculite-smectite mixed layer phases (diVS-ml). Rarely, kaolinite and kaolinite-smectite-ml phases as well as chlorite-smectite-ml phases, rutile and quartz were identified in traces in this sample [fig. 1].

The measured and computed particles have shown a calculated CEC-value of 42 meq / 100 g located at surface and in the interlayer space.

	frequency-% *(n = 160 measured particles)*
diVS-ml	71%
Kaolinite & KSV-ml	14%
CSV-ml	6%
Ti-phases	2%
Quartz	3%
K-feldspar	2%
Unknown phases	1%

All measured dioctahedral 2:1 clay mineral phases summarized result following mineral formula computed from TEM-EDX-measurement of 114 individual particles:

$$Ca^{2+}_{0.06}\ Mg^{2+}_{0.10}\ Na^{+}_{0.00}\ K^{+}_{0.51}\quad Al^{3+}_{1.41}\ Fe^{3+}_{0.44}\ Mg^{2+}_{0.14}\ Ti^{4+}_{0.01}\ (OH)_2\quad Si^{4+}_{3.30}\ Al^{3+}_{0.70}\ O_{10}$$

SDOM *± 0.00 ± 0.01 ± 0.00 ± 0.01 ± 0.02 ± 0.01 ± 0.01 ± 0.00 ± 0.01 ± 0.01*

Legend: SDOM - standard deviation of the mean (= the standard deviation divided by the square root of the number of samples)

The interlayer charge is calculated as 0.83 per $(OH)_2\ O_{10}$ and the octahedral charge as 5.87 per $(OH)_2\ O_{10}$. The particles are characterized by a high octahedral Fe-amount.

The summarized chemical composition of all 114 computed particles is listed [tab. 1].

Opalinus Clay N08 sample is also characterized by two morphological groups: (i) large (≤ 1 µm) xenomorph platy crystals and (ii) aggregates, partially with folds, formed by small (≤ 100 nm) xenomorphous plates [fig. 2]. Aggregates formed by large (≤ 1 µm) xenomorph platy crystals dominate the shapes of particles in the micrographs [fig. 2].

The distribution of %S-probability of all measured clay mineral phases [fig. 3a] also indicates the occurrence of two groups: (i) diVS-ml and dominating (ii) illite with K-deficiency.

The numerous measured particles by TEM-EDX allow a visualization of distribution of interlayer charges. Considering the TEM-EDX-determined cations Ca^{++}, Mg^{++} and Na^{+} and then computed their ratio as interlayer cations in the mineral formula, Ca^{++}, Mg^{++} and Na^{+} offer to characterize the degree of exchangeable charges in the interlayer space. This charge density of Opalinus Clay N08 (< 2 µm) shows in this sample a weak maximal frequency-% of charge density at 0.31 per $(OH)_2$ O_{10} [fig. 5]. This interval of interlayer charge density caused by exchangeable cations from 0.00 - 0.71 per $(OH)_2$ O_{10} represents mentioned diVS-ml.

Mineral Matter - Specification

Result of Clustering

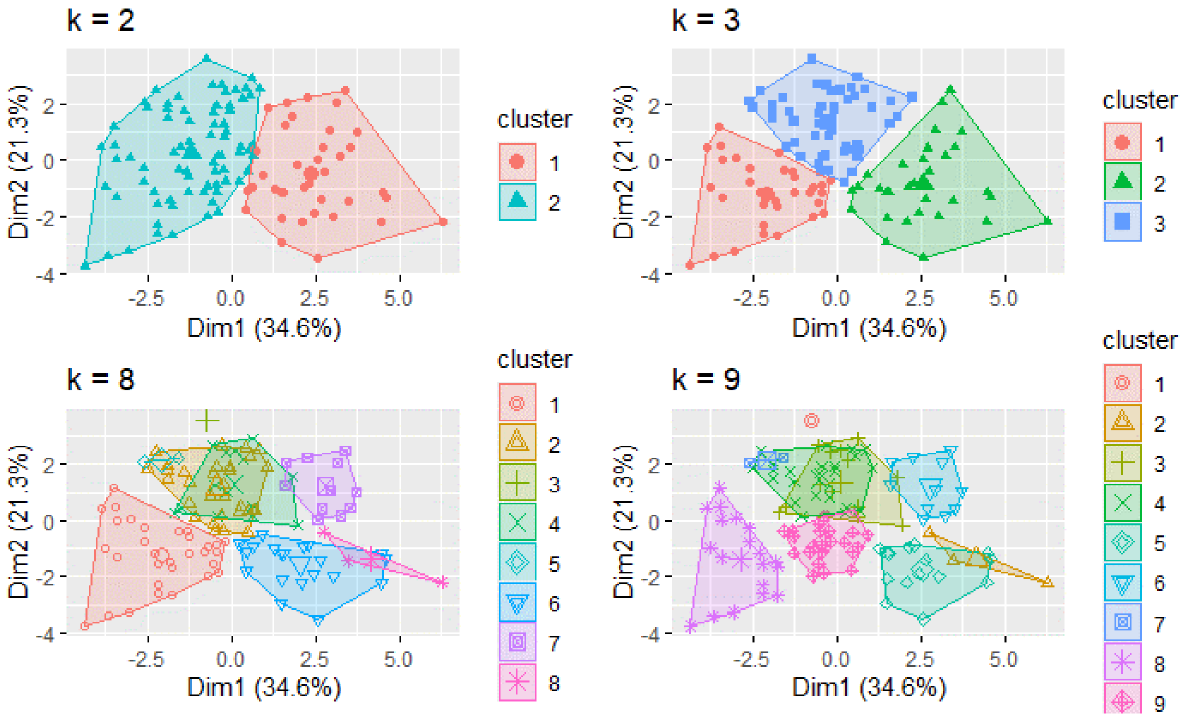

Fig. 8. *Clustering of all measured particles for clusters k = 2, k = 3, k = 8 and k = 9 (source for R-coding: https://uc-r.github.io/kmeans_clustering)*

The optimum of clusters was calculated with k = 2.

		Ca (XII)	Mg (XII)	Na (XII)	K (XII)	Cr3+ (VI)	Al (VI)	Fe3+ (VI)	Mg (VI)	Ti (VI)	Al (IV)	Si (IV)	XII	n_VI	%S
Cluster1	n = 38	0.08	0.15	0.00	0.44	0.00	1.28	0.57	0.13	0.02	0.79	3.21	0.90	2.0	4
Cluster2	n = 76	0.06	0.06	0.00	0.54	0.00	1.49	0.37	0.14	0.01	0.65	3.35	0.79	2.0	13

Fig. 9a. *Mineral formulae based on TEM-EDX-data summarized following the result of clustering for k=2*

	Sybilla-results	**TEM-EDX-results**	**Notes**
Cluster1	Illite	diVS-ml (illite)	*very high K-deficit, no XII-charge deficit, Fe(VI)-rich, low Mg(VI)*
Cluster2	IS R0(1) *(%S = 26%)*	diVS-ml *(%S = 13%)*	*high K-deficit, low XII-charge deficit, Fe(VI)-rich*
	Kaolinite + KS GL R0		*in traces only*

Tab. 2. *Comparison of results from TEM-EDX- and XRD-measurements*

The TEM-EDX-data offers a good agreement with the result of Sybilla-processing of XRD-traces from oriented specimen [tab. 2].

IS R0 (1): The Sybilla-procedure of XRD-traces (oriented mounts) has shown an occurrence of an illite-smectite mixed layer phase with a smectite layers probability of %S = 26%. This result of XRD-pattern processing is in good agreement with founded maximum of particles for %S ~ 13% by TEM-EDX-measurements [tab. 2].

The Sybilla-processing of XRD-traces (oriented mounts) also supports low amount of kaolinite and kaolinite-smectite mixed layer phases in fine fraction of sample.

Specifics to the identified clay mineral groups

Dioctahedral vermiculite-smectite mixed layer phase *(Cluster1)*

38 of 114 computed particles belong so to this assumed classification. The dioctahedral character of this group is proofed by X-ray diffraction. The position of the large (060)-interference of smectite is in the random oriented powder specimen at 1.497 Å.

Dioctahedral vermiculite-smectite mixed layer phase *(Cluster1)*

$$Ca_{0.08}\ Mg_{0.15}\ Na_{0.00}\ K_{0.44}\quad Al_{1.28}\ Fe^{3+}_{0.57}\ Mg_{0.13}\ Ti_{0.02}\ (OH)_2\ \ Si_{3.21}\ Al_{0.79}\ O_{10}$$

Charge: XII = 0.90 VI = 5.89 IV = 15.21 **Σ = 22.00**

Measured particles by TEM-EDX: 38

Probability of smectite layers (%S): 4%

Probability of illite layers (%I): 96%

Result of clustering: Cluster1 [tab. 2]

A comparison of octahedral Mg vs. tetrahedral Si doesn't indicate any differentiation for octahedral Mg based on TEM-EDX-data [fig. 3b]. Particles of Cluster1 contain commonly Mg(VI) < 0.25 per $(OH)_2$ O_{10} in octahedral layer.

The mineral formulae, summarized in classes of %S, draws for the maximum an Fe-rich diVS-ml with low Mg(VI) as well as low amount of K in the interlayer space [tab. 6b].

Dioctahedral vermiculite-smectite mixed layer phase *(diVS-ml, Cluster2)*

$$Ca_{0.06}\ Mg_{0.08}\ Na_{0.00}\ K_{0.54}\quad Al_{1.49}\ Fe^{3+}_{0.37}\ Mg_{0.14}\ Ti_{0.01}\ (OH)_2\ \ Si_{3.35}\ Al_{0.65}\ O_{10}$$

Charge: XII = 0.79 VI = 5.86 IV = 15.35 **Σ = 22.00**

Probability of smectite layers (%S): 13%

Probability of illite layers (%I): 87%

Measured particles by TEM-EDX: 76

Result of clustering: Cluster2 [tab. 2]

A comparison of octahedral Mg vs. tetrahedral Si indicates a missing differentiation for octahedral Mg based on TEM-EDX-data of Cluster2 [fig. 3b].

The mineral formulae, summarized in classes of %S, draws for the maximum an Al- & Fe-rich diVS-ml with low Mg(VI)-amount as well as reduced amount of K in the interlayer space [tab. 7b].

Kaolinite-montmorillonite mixed layer phases

The Excel-based procedure (Hoang-Minh et al., 2019) to identify possible clay mineral groups using the TEM-EDX-measurements also includes algorithms to classify kaolinite and kaolinite-montmorillonite mixed layer phases. These algorithms couldn't compute no such phases basing on the measured TEM-EDX-data. Such particles have shown small hexagonal plates typically for kaolinite-bearing phases.

References

Cliff, G. & Lorimer, G. W. (1975). *J. Microsc.* **103**, 203–207.

Döbelin, N., Kleeberg, R. (2015). *Journal of Applied Crystallography* **48**, 1573-1580. DOI: 10.1107/S1600576715014685

Henning, K.-H. & Störr, M. (1986). Electron Micrographs (TEM, SEM) of Clays and Clay Minerals, p. 325. Akademie-Verlag Berlin.

Hoang-Minh, T., Kasbohm, J., Nguyen-Thanh, L., Nga, P. T., Lai, L. T., Duong, N. T., Thanh, N. D., Thuyet, N. T. M., Anh, D. D., Pusch, R., Knutsson, S. & Ferreiro Mahlmann, R. (2019). *J. Appl. Cryst.* **52**, 133-147. DOI: 10.1107/S1600576718018162

Lorimer, G. W. & Cliff, G. (1976). *Electron Microscopy in Mineralogy*, edited by H. R. Wenk, pp. 506–519. Berlin: Springer Verlag.

Mellini, M. & Menichini, R. (1985). *R. Soc. Ital. Miner. Petrol.* **40**, 261–266.

Moore, D.M., Reynolds, R.C. (1989). X-ray Diffraction and the Identification and Analysis of Clay Minerals, Oxford University Press, New York, 332 + xvi pp.

Nguyen-Thanh, L., Herbert, H.-J., Kasbohm, J., Hoang-Minh, T. & Mählmann, R. F. (2014). *Clays Clay Miner.* **62**, 425–446.

Środoń, J., Elsass, F., McHardy, W. J. & Morgan, D. J. (1992). *Clay Miner.* **27**, 137–158.

Data Sheet – Opalinus, treated materials *(OPA, 125°C, VSC)*

Methodology - Transmission electron microscopy linked with energy-dispersive X-ray spectroscopy (TEM-EDX)

It is expected a characterization of clay mineral phases in treated Opalinus Clay by transmission electron microscopy. This report describes the results of treated material from Opalinus Clay percolated at a temperature of 125°C.

The different clay mineral phases are to identify and to describe by chemical composition and its variability, morphology, the specific dissolution potential, and further parameter.

Such further parameter like distribution of smectite layers probability (%S) and distribution of charges caused by exchangeable cations interlayer space should serve as additional indicators for mineralogical alterations in treatment experiments with Friedland Clay.

The sample were suspended for TEM-measurement in deionized water and dispersed by ultrasonic treatment for approximately 20 min. The clay fraction (<2 µm) was separated by sedimentation and diluted with deionized water to get a clear suspension. The suspension was dropped onto carbon-coated Cu grids, air dried and stored under environment-controlled conditions at 45% humidity.

TEM-EDX investigations were carried out on the <2 µm fraction using a FEI TECNAI G^2 20 electron transmission microscope at the VNU University of Science, Vietnam National University, Hanoi. This equipment (operated at 200 kV with LaB_6 cathode) was combined with an S-TWIN objective, a windowless EDAX energy-dispersive X-ray system and a FEI Eagle 2k CCD TEM camera.

About 100 individual clay particles per sample were characterized by TEM-EDX with respect to crystal size, crystal habit, particle morphology and element distribution. The crystal size, crystal habit and particle morphology were described according to Henning & Störr (1986).

For the quantification of element distribution, a calibration of k factors is mandatory (Cliff & Lorimer, 1975; Lorimer & Cliff, 1976; Mellini & Menichini, 1985). These k values are used to calibrate for the specific behaviour of particles against possible irradiation damage. The elements O, Na, Mg, Al, Si, K, Ca and Fe were quantified by applying the EDAX GENESIS–TEM Quant Materials quantification procedure.

In this procedure, the acquired EDX spectra are corrected by background subtraction, Gaussian deconvolution and k-factor corrections using values previously determined on a phyllosilicate standard (muscovite) and selected non-phyllosilicate standards. The average errors in the analyzed elements using the phyllosilicate standard, expressed as the atomic proportions, are 10 (Na), 5 (Fe, Mg, K, Ti, Ca) and 1 (Si, Al).

The measurement time per particle was lowered to 20 s and the exposed area was limited to a 50 nm diameter, avoiding possible irradiation damage of particles. The stability of particles of the sample series was tested for this measurement time at the beginning of any measurement campaign.

Further methodological details related to TEM-EDX-measurements and the Excel-based mathematical procedure using TEM-EDX data for calculation of mineral formulae are described in Hoang-Minh et al. (2019).

These mathematical procedures described in Hoang-Minh et al. (2019) were extended by k-means clustering method for finding subgroups of observations within a data set. The data were standardized (i.e., scaled) to make variables comparable. Euclidean distances were applied as classical method for distance measures. The optimal clusters were determined by Elbow method and Gap statistics[24].

---

[24] *https://uc-r.github.io/kmeans_clustering*

Data Sheet – Opalinus Clay N14 (< 2 µm), treated material *(125°C, 48.5 h)*

Preparation for TEM

- raw material: compacted material (1.6 g/cm³) of treated Opalinus Clay-sample
- suspension on particles < 2 µm on carbon-filmed Cu-grid
- air-dried and humidity-controlled storing

Mineral Matter

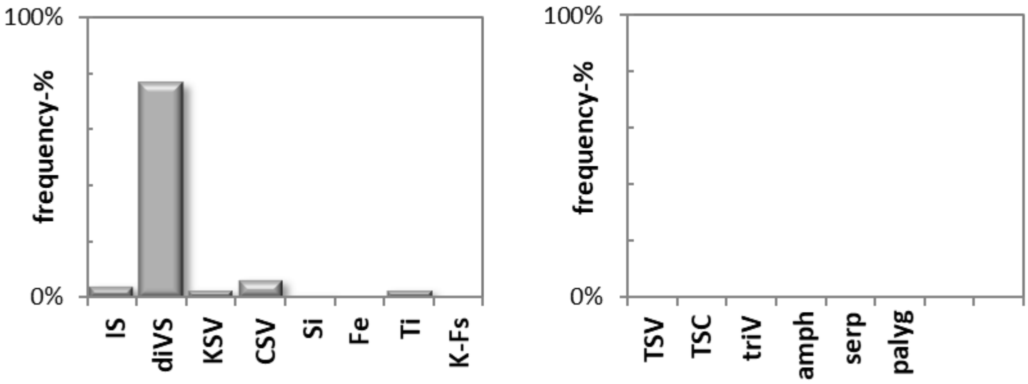

***Fig. 1.** Distribution of mineral groups in fraction < 2 µm (in frequency-%)*
*Legend: **IS** – illite-smectite-mixed layer series in sense of Środon et al. (1992), diVS – dioctahedral vermiculite-smectite illite-smectite-mixed layer series (= charge- and/or K-deficit), **KSV** – kaolinite-smectite-dioctahedral vermiculite-mixed layer series, **CSV** – chlorite-saponite-trioctahedral vermiculite-mixed layer series, **Si** – quartz or particles with Si-surplus, **Fe** – Fe-oxide or Fe-oxyhydroxide, **Ti** – Ti-bearing phases (e.g. rutile, anatase), **K-Fs** – K-feldspar*

Clay Mineral Composition

All measured dioctahedral particles:

$$\mathrm{Ca_{0.11}\,Mg_{0.07}\,Na_{0.06}\,K_{0.48}\quad Al_{1.36}\,Fe^{3+}_{0.45}\,Mg_{0.18}\,Ti_{0.01}\,(OH)_2\quad Si_{3.26}\,Al_{0.74}\,O_{10}}$$

Charge: XII = 0.90 VI = 5.84 IV = 15.26 **Σ = 22.00**
Probability of smectite layers (%S): 6%
Probability of illite layers (%I): 94%

Specific Dissolution Potential (ΔS%)

for H2O, 20 + 60 rpm -13 (= medium reacting, 'illitization', interlayer group: Ca+Mg (= type B))
for NaCl, 20 rpm -14 (= medium reacting, 'illitization', interlayer group: Ca+Mg (= type B))
for NaCl, 60 rpm -46 (= fast reacting, 'illitization', interlayer group: Na (= type A))
CEC_{calc}: 72 meq / 100 g

Measured particles: 165

***Table 1.** Summarized chemical composition*

SiO_2	TiO_2	Al_2O_3	Fe_2O_3	MnO	MgO	CaO	Na_2O	K_2O	P_2O_5	Σ	
53.8%	0.2%	30.9%	5.0%		3.2%	1.7%	0.6%	4.5%	0.1%	1.00	measured particles of treated sample
59.4%	0.3%	28.1%	5.9%		2.5%	0.3%	0.1%	3.3%	0.1%	1.00	measured particles of original Opalinus Clay

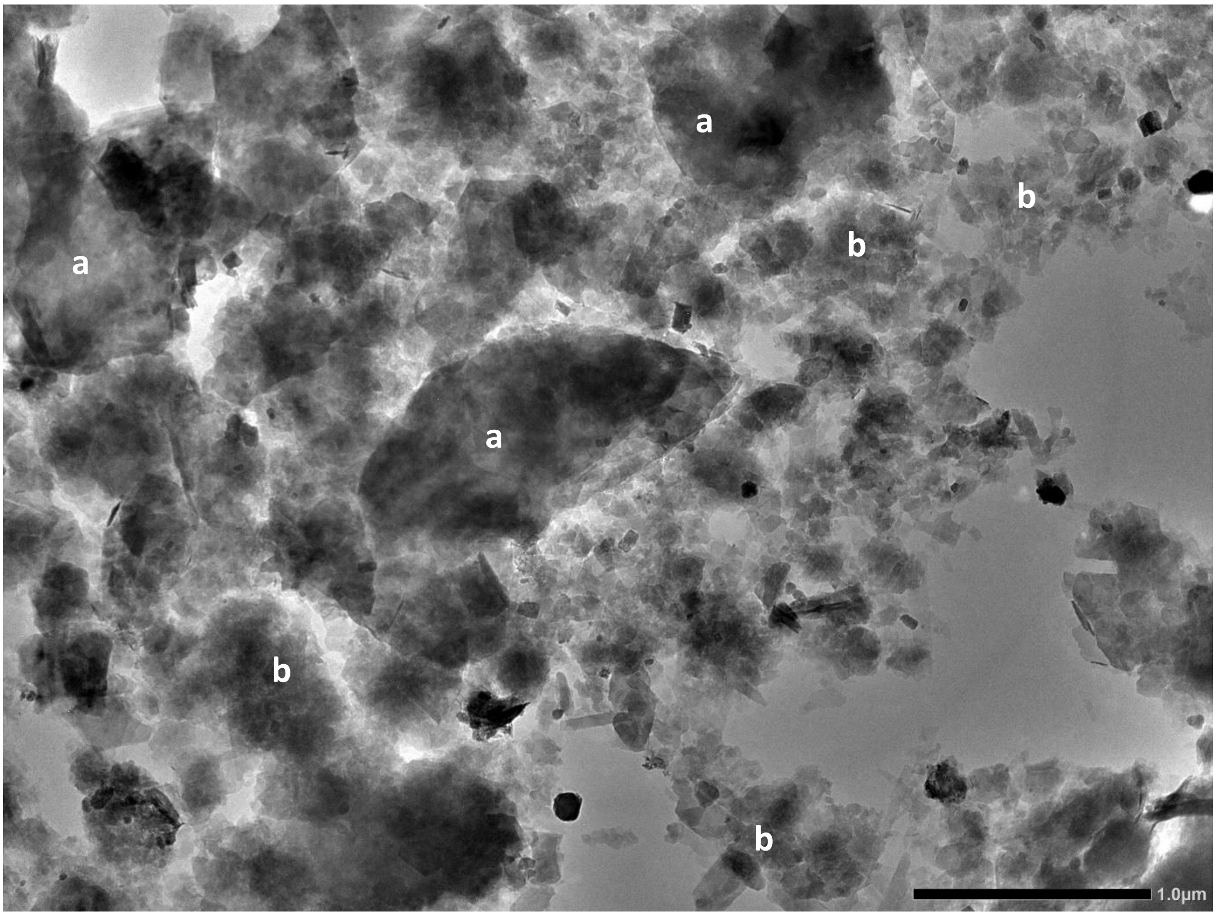

JEM-2100_MAG_X10k_016_No14.bmp

Magnification: 10k

(a) large (≤ 1 µm) xenomorph platy crystals;

(b) aggregates formed by small (≤ 100 nm) xenomorphous plates

Fig. 2. *Morphology of particles (TEM-micrographs)*

Distribution of smectite layers probability (%S)

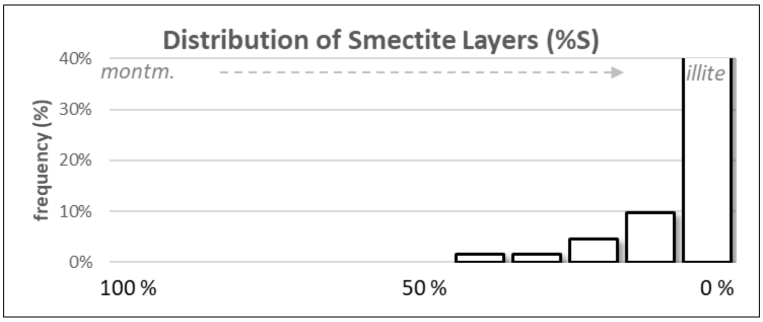

Description: *The distribution of %S-probability indicates the occurrence of two groups: (i) low number of diVS-ml phases as well as (ii) dominating illite with K-deficiency.*

Fig. 3a. *Distribution of smectite layers probability (%S)*

Differentiation by relation “Octahedral Mg vs. tetrahedral Si”?

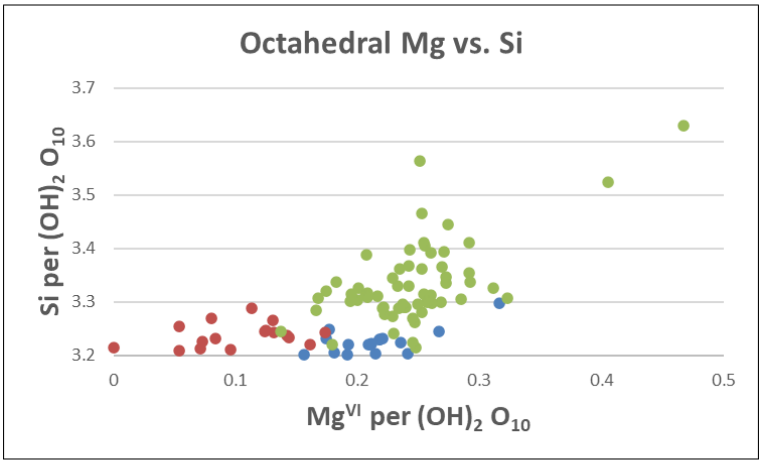

Description: *This diagram indicates a separation on low and high ratio of Mg in relation to tetrahedral Si (blue dots – Cluster1: illite; green dots – Cluster3: diVS-ml vs. red dots – Cluster2: illite). Phases of Cluster2 are mostly characterized by Mg(VI) < 0.2 per* $(OH)_2\ O_{10}$*.*

Fig. 3b. *Distribution of octahedral Mg vs. tetrahedral Si [all per* $(OH)_2\ O_{10}$*]*

Distribution of K in relation to tetrahedral Si

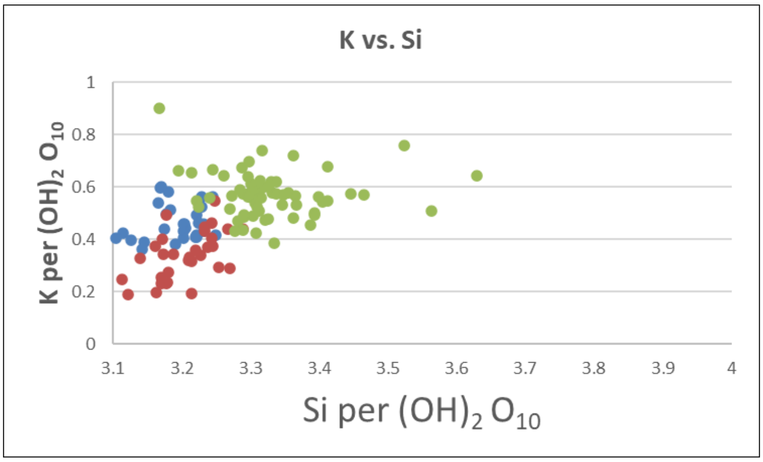

Description: *This diagram indicates a weak separation on low and high ratio of K in relation to tetrahedral Si (blue dots – Cluster1: illite; green dots – Cluster3: diVS-ml vs. red dots – Cluster2: illite). Phases of Cluster1+3 are mostly characterized by K > 0.4 per* $(OH)_2\ O_{10}$*.*

Fig. 4. *Distribution of K in interlayer space vs. tetrahedral Si [all per* $(OH)_2\ O_{10}$*]*

Distribution of charges (exchangeable from interlayer space)

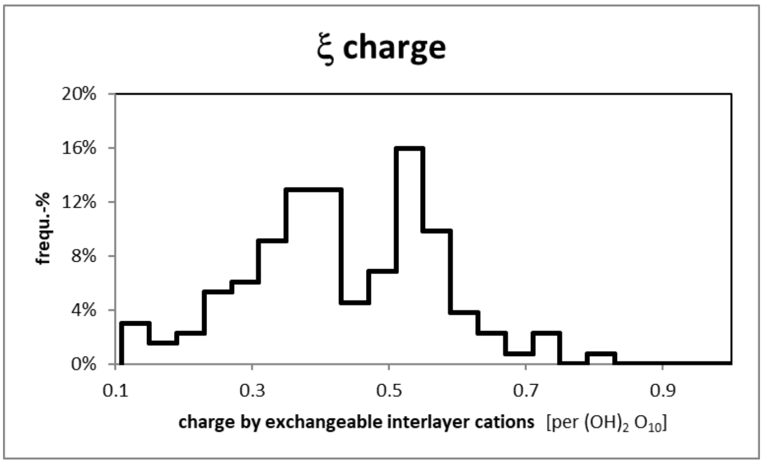

This diagram visualizes the distribution of exchangeable charges in the interlayer space (Ca, Mg, Na) determined and computed by TEM-EDX-data.

Description: *Very broad distribution of charge density with a bimodal maximal frequency-% at 0.39 (diVS-ml) and 0.55 (illite) per* $(OH)_2\ O_{10}$*.*

Fig. 5. *Distribution of charges*

Dioctahedral Vermiculite-Smectite mixed layer phases (diVS-ml - illite) *(Cluster1):*

$$Ca_{0.11}\ Mg_{0.10}\ Na_{0.06}\ K_{0.47}\quad Al_{1.18}\ Fe^{3+}_{0.59}\ Mg_{0.19}\ Ti_{0.04}\ (OH)_2\quad Si_{3.18}\ Al_{0.82}\ O_{10}$$

Charge:	XII = 0.96	VI = 5.86	IV = 15.18	**Σ = 22.00**
Probability of smectite layers (%S):	2%			
Probability of illite layers (%I):	98%			
Measured particles:	33			

Distribution of smectite layers probability (%S) in diVS-ml (Cluster1)

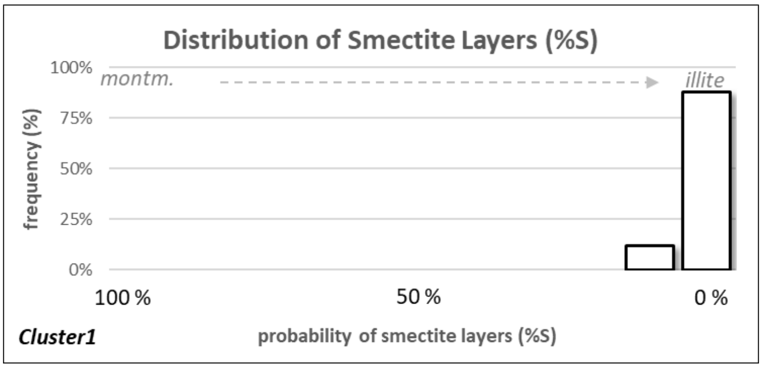

Description: *The distribution of diVS-ml (classified as Cluster1) draws a maximum of frequency (%) for smectite layer probability at 0%*

Fig. 6a. *Distribution of smectite layers probability in diVS-ml*

diVS-ml?	*particles (abs)*	Ca (XII)	Mg (XII)	Na (XII)	K (XII)	Cr3+ (VI)	Al (VI)	Fe3+ (VI)	Mg (VI)	Ti (VI)	Al (IV)	Si (IV)	XII	n_VI	%S
%S >95%	n = 0														
%S 95-85%	n = 0														
%S 85-75%	n = 0														
%S 75-65%	n = 0														
%S 65-55%	n = 0														
%S 55-45%	n = 0														
%S 45-35%	n = 0														
%S 35-25%	n = 0														
%S 25-15%	n = 0														
%S <15%	**n = 33**	**0.11**	**0.10**	**0.06**	**0.47**	**0.00**	**1.18**	**0.59**	**0.19**	**0.04**	**0.82**	**3.18**	**0.96**	**2.0**	**2**

Fig. 6b. *Computed averaged mineral formulae of diVS-ml phases in the different smectite layers probability (%S)-classes*

Dioctahedral Vermiculite-Smectite mixed layer phases (diVS-ml) *(Cluster2):*

$$Ca_{0.12}\ Mg_{0.13}\ Na_{0.04}\ K_{0.32}\quad Al_{1.56}\ Fe^{3+}_{0.38}\ Mg_{0.07}\ Ti_{0.00}\ (OH)_2\quad Si_{3.18}\ Al_{0.82}\ O_{10}$$

Charge:	XII = 0.87	VI = 5.95	IV = 15.18	**Σ = 22.00**
Probability of smectite layers (%S):	2%			
Probability of illite layers (%I):	88%			
Measured particles:	38			

Distribution of smectite layers probability (%S) in diVS-ml (Cluster2)

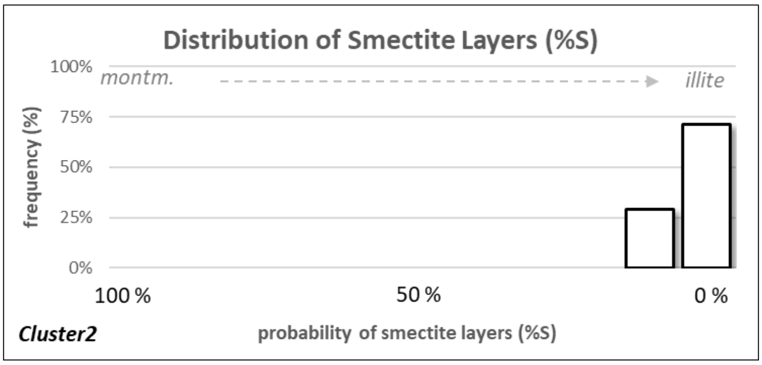

Description: *The distribution of diVS-ml (classified as Cluster2) draws a maximum of frequency (%) for smectite layer probability at 0%*

Fig. 7a. *Distribution of smectite layers probability in diVS-ml*

diVS-ml	particles (abs)	Ca (XII)	Mg (XII)	Na (XII)	K (XII)	Cr3+ (VI)	Al (VI)	Fe3+ (VI)	Mg (VI)	Ti (VI)	Al (IV)	Si (IV)	XII	n_VI	%S
%S >95%	n = 0														
%S 95-85%	n = 0														
%S 85-75%	n = 0														
%S 75-65%	n = 0														
%S 65-55%	n = 0														
%S 55-45%	n = 0														
%S 45-35%	n = 0														
%S 35-25%	n = 0														
%S 25-15%	n = 0														
%S <15%	**n = 38**	**0.12**	**0.13**	**0.04**	**0.32**	**0.00**	**1.56**	**0.38**	**0.07**	**0.00**	**0.82**	**3.18**	**0.9**	**2.0**	**2**

Fig. 7b. *Computed averaged mineral formulae of diVS-ml phases in the different smectite layers probability (%S)-classes*

Dioctahedral Vermiculite-Smectite mixed layer phases (diVS-ml) *(Cluster3):*

$$Ca_{0.11}\ Mg_{0.01}\ Na_{0.06}\ K_{0.57}\quad Al_{1.34}\ Fe^{3+}_{0.41}\ Mg_{0.24}\ Ti_{0.01}\ (OH)_2\quad Si_{3.33}\ Al_{0.67}\ O_{10}$$

Charge: XII = 0.89 VI = 5.78 IV = 15.33 **Σ = 22.00**

Probability of smectite layers (%S): 12%

Probability of illite layers (%I): 88%

Measured particles: 63

Distribution of smectite layers probability (%S) in diVS-ml (Cluster3)

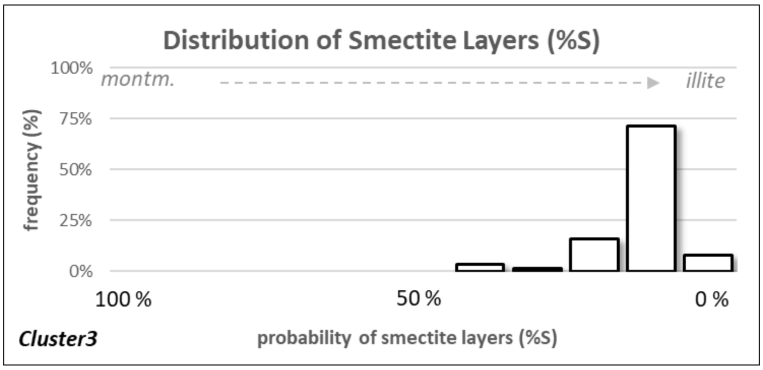

Description: *The distribution of diVS-ml (classified as Cluster3) draws a maximum of frequency (%) for smectite layer probability at 10%*

Fig. 7c. *Distribution of smectite layers probability in diVS-ml*

diVS-ml	particles (abs)	Ca (XII)	Mg (XII)	Na (XII)	K (XII)	Cr3+ (VI)	Al (VI)	Fe3+ (VI)	Mg (VI)	Ti (VI)	Al (IV)	Si (IV)	XII	n_VI	%S
%S >95%	n = 0														
%S 95-85%	n = 0														
%S 85-75%	n = 0														
%S 75-65%	n = 0														
%S 65-55%	n = 0														
%S 55-45%	n = 0														
%S 45-35%	n = 2	0.02	0.00	0.05	0.58	0.00	1.01	0.65	0.36	0.00	0.40	3.60	0.7	2.0	40
%S 35-25%	n = 1	0.00	0.00	0.00	0.76	0.00	0.92	0.72	0.41	0.00	0.48	3.52	0.8	2.0	31
%S 25-15%	n = 10	0.11	0.00	0.06	0.57	0.00	1.35	0.39	0.26	0.00	0.59	3.41	0.8	2.0	19
%S <15%	**n = 50**	**0.12**	**0.02**	**0.06**	**0.57**	**0.00**	**1.36**	**0.40**	**0.23**	**0.01**	**0.70**	**3.30**	**0.9**	**2.0**	**9**

Fig. 7d. *Computed averaged mineral formulae of diVS-ml phases in the different smectite layers probability (%S)-classes*

Cluster3		Ca (XII)	Mg (XII)	Na (XII)	K (XII)	Cr3+ (VI)	Al (VI)	Fe3+ (VI)	Mg (VI)	Ti (VI)	Al (IV)	Si (IV)	XII	n_VI	%S
without illite	n = 13	0.08	0.00	0.05	0.59	0.00	1.27	0.46	0.28	0.00	0.55	3.45	0.81	2.0	22
only illite	n = 50	0.12	0.02	0.06	0.57	0.00	1.36	0.40	0.23	0.01	0.70	3.30	0.91	2.0	9

Fig. 7e. *Computed averaged mineral formulae of diVS-ml phases differentiated by illite*

Description – Opalinus Clay N14 (< 2 µm), treated material *(125°C)*

Preparation for TEM

The powder of Opalinus Clay-sample was suspended in deionized water and dispersed by ultrasonic treatment for approximately 20 min. The clay fraction (<2 µm) was separated by sedimentation and diluted with deionized water to get a clear suspension. The suspension was dropped onto carbon-coated Cu grids, air dried and stored under environment-controlled conditions at 45% humidity.

Mineral Matter - Overview

The fraction < 2 µm of Opalinus Clay N14 sample is mainly composed by three different types of dioctahedral vermiculite-smectite mixed layer phases (diVS-ml). Rarely, kaolinite and kaolinite-smectite-ml phases as well as chlorite-smectite-ml phases, rutile and quartz were identified in traces in this sample [fig. 1].

The measured and computed particles have shown a calculated CEC-value of 72 meq / 100 g located at surface and in the interlayer space.

	frequency-% *(n = 165 measured particles)*
diVS-ml	81%
Kaolinite & KSV-ml	3%
CSV-ml	7%
Ti-phases	3%
Quartz	1%
K-feldspar	1%
Unknown phases	4%

All measured dioctahedral 2:1 clay mineral phases summarized result following mineral formula computed from TEM-EDX-measurement of 134 individual particles:

	$Ca^{2+}_{0.11}$	$Mg^{2+}_{0.07}$	$Na^{+}_{0.06}$	$K^{+}_{0.48}$	$Al^{3+}_{1.36}$	$Fe^{3+}_{0.45}$	$Mg^{2+}_{0.18}$	$Ti^{4+}_{0.01}$	$(OH)_2$	$Si^{4+}_{3.26}$	$Al^{3+}_{0.74}$	O_{10}
SDOM	*± 0.00*	*± 0.01*	*± 0.00*	*± 0.01*	*± 0.02*	*± 0.01*	*± 0.01*	*± 0.00*		*± 0.01*	*± 0.01*	

Legend: SDOM - standard deviation of the mean (= the standard deviation divided by the square root of the number of samples)

The interlayer charge is calculated as 0.90 per $(OH)_2$ O_{10} and the octahedral charge as 5.85 per $(OH)_2$ O_{10}. The particles are characterized by a high octahedral Fe-amount.

The summarized chemical composition of all 134 computed particles is listed [tab. 1].

Opalinus Clay N14 sample is also characterized by two morphological groups: (i) large (≤ 1 µm) xenomorph platy crystals and (ii) aggregates, partially with folds, formed by small (≤ 100 nm) xenomorphous plates [fig. 2]. Aggregates formed by large (≤ 1 µm) xenomorph platy crystals dominate the shapes of particles in the micrographs [fig. 2].

The distribution of %S-probability of all measured clay mineral phases [fig. 3a] also indicates the occurrence of two groups: (i) diVS-ml and dominating (ii) illite with K-deficiency.

The numerous measured particles by TEM-EDX allow a visualization of distribution of interlayer charges. Considering the TEM-EDX-determined cations Ca^{++}, Mg^{++} and Na^{+} and then computed their ratio as interlayer cations in the mineral formula, Ca^{++}, Mg^{++} and Na^{+} offer to characterize the degree of exchangeable charges in the interlayer space. This charge density of Opalinus Clay N14 (< 2 µm) shows in this sample a bimodal maximal frequency-% of charge density at 0.39 (caused by diVS-ml) and 0.55 (caused by illite) per $(OH)_2\ O_{10}$ [fig. 5]. This interval of interlayer charge density caused by exchangeable cations from 0.19 - 0.75 per $(OH)_2\ O_{10}$ represents mentioned three groups of diVS-ml.

Mineral Matter - Specification

Result of Clustering

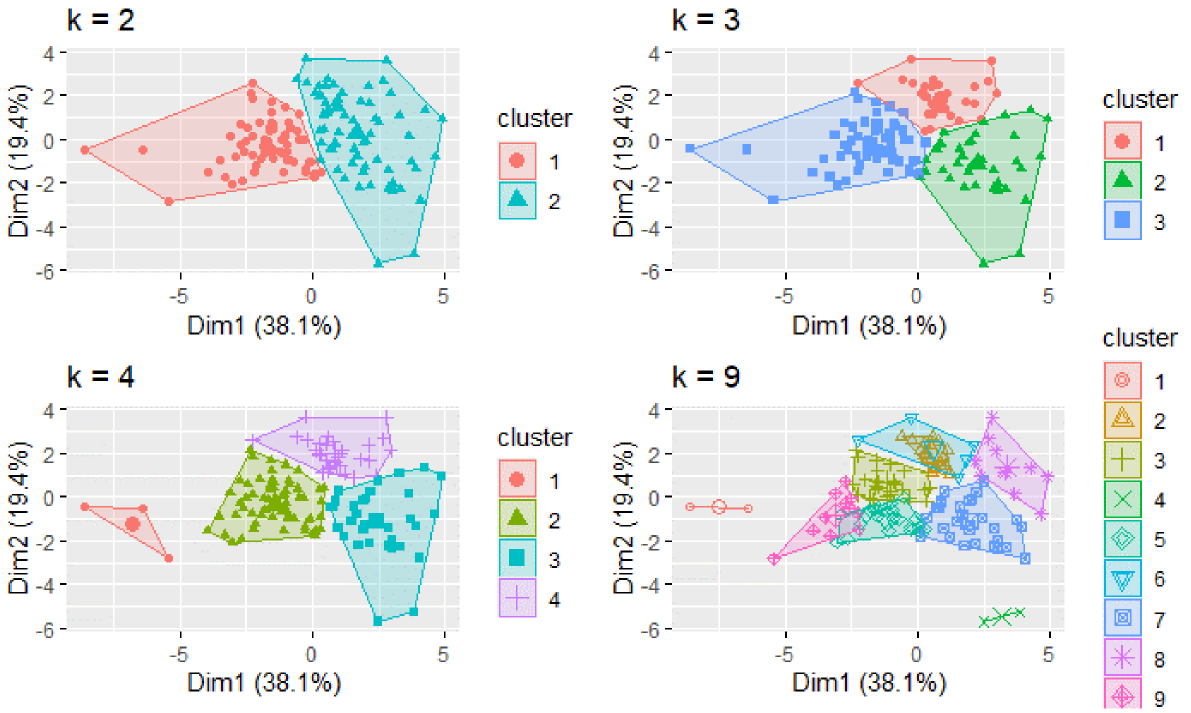

Fig. 8. *Clustering of all measured particles for clusters k = 2, k = 3, k = 4 and k = 9 (source for R-coding: https://uc-r.github.io/kmeans_clustering)*

The optimum of clusters was calculated with k = 3.

		Ca (XII)	Mg (XII)	Na (XII)	K (XII)	Cr3+ (VI)	Al (VI)	Fe3+ (VI)	Mg (VI)	Ti (VI)	Al (IV)	Si (IV)	XII	n_VI	%S
Cluster1	n = 33	0.11	0.10	0.06	0.47	0.00	1.18	0.59	0.19	0.04	0.82	3.18	0.96	2.0	2
Cluster2	n = 38	0.12	0.13	0.04	0.32	0.00	1.56	0.38	0.07	0.00	0.82	3.18	0.87	2.0	2
Cluster3	n = 63	0.11	0.01	0.06	0.57	0.00	1.34	0.41	0.24	0.01	0.67	3.33	0.89	2.0	12

Fig. 9a. *Mineral formulae based on TEM-EDX-data summarized following the result of clustering for k=3*

	Sybilla-results	**TEM-EDX-results**	**Notes**
Cluster1	Illite	diVS-ml (illite)	*very high K-deficit, no XII-charge deficit, lowered Al(VI), Fe(VI)-rich, low Mg(VI)*
Cluster2		diVS-ml (illite)	*very high K-deficit, no XII-charge deficit, high Al(VI), Fe(VI)-rich, low Mg(VI)*
Cluster2	IS R0(1) *(%S = 24%)*	diVS-ml *(%S = 12%)*	*K-deficit, no XII-charge deficit, Fe(VI)-rich*
	Kaolinite + KS GL R0		*in traces only*

Tab. 2. *Comparison of results from TEM-EDX- and XRD-measurements*

The TEM-EDX-data offers a good agreement with the result of Sybilla-processing of XRD-traces from oriented specimen [tab. 2, tab. 7d].

IS R0 (1): The Sybilla-procedure of XRD-traces (oriented mounts) has shown an occurrence of an illite-smectite mixed layer phase with a smectite layers probability of %S = 24%. This result of XRD-pattern processing is in good agreement with founded maximum of particles for %S ~ 12% by TEM-EDX-measurements [tab. 2].

The Sybilla-processing of XRD-traces (oriented mounts) also supports low amount of kaolinite and kaolinite-smectite mixed layer phases in fine fraction of sample.

Specifics to the identified clay mineral groups

Dioctahedral vermiculite-smectite mixed layer phase *(Cluster1)*

33 of 134 computed particles belong so to this assumed classification. The dioctahedral character of this group is proofed by X-ray diffraction. The position of the large (060)-interference of smectite is in the random oriented powder specimen at 1.497 Å.

Dioctahedral vermiculite-smectite mixed layer phase *(Cluster1)*

$$\mathrm{Ca_{0.11}\ Mg_{0.10}\ Na_{0.06}\ K_{0.47}\quad Al_{1.18}\ Fe^{3+}_{0.59}\ Mg_{0.19}\ Ti_{0.04}\ (OH)_2\quad Si_{3.18}\ Al_{0.82}\ O_{10}}$$

Charge: XII = 0.96 VI = 5.86 IV = 15.18 **Σ = 22.00**
Measured particles by TEM-EDX: 33
Probability of smectite layers (%S): 2%
Probability of illite layers (%I): 98%
Result of clustering: Cluster1 [tab. 2]

A comparison of octahedral Mg vs. tetrahedral Si indicates a differentiation for octahedral Mg in comparison to Cluster2 based on TEM-EDX-data [fig. 3b]. Particles of Cluster1 contain commonly Mg(VI) > 0.15 per $(OH)_2\ O_{10}$ in octahedral layer.

The mineral formulae, summarized in classes of %S, draws for the maximum an Fe-rich diVS-ml with a remarkable Mg(VI) as well as low amount of K in the interlayer space [tab. 6b].

Dioctahedral vermiculite-smectite mixed layer phase *(diVS-ml, Cluster2)*

$$\mathrm{Ca_{0.12}\ Mg_{0.13}\ Na_{0.04}\ K_{0.32}\quad Al_{1.56}\ Fe^{3+}_{0.38}\ Mg_{0.07}\ Ti_{0.00}\ (OH)_2\quad Si_{3.18}\ Al_{0.82}\ O_{10}}$$

Charge: XII = 0.87 VI = 5.95 IV = 15.18 **Σ = 22.00**
Probability of smectite layers (%S): 2%
Probability of illite layers (%I): 98%
Measured particles by TEM-EDX: 38
Result of clustering: Cluster2 [tab. 2]

A comparison of octahedral Mg vs. tetrahedral Si indicates a differentiation for octahedral Mg in comparison to Cluster1+Cluster3 based on TEM-EDX-data [fig. 3b]. Particles of Cluster2 contain commonly Mg(VI) < 0.2 per $(OH)_2\ O_{10}$ in octahedral layer.

The mineral formulae, summarized in classes of %S, draws for the maximum an Al- & Fe-rich diVS-ml with low Mg(VI)-amount as well as reduced amount of K in the interlayer space [tab. 7b].

Dioctahedral vermiculite-smectite mixed layer phase *(diVS-ml, Cluster3)*

$$\mathrm{Ca_{0.11}\ Mg_{0.01}\ Na_{0.06}\ K_{0.57}\quad Al_{1.34}\ Fe^{3+}_{0.41}\ Mg_{0.24}\ Ti_{0.01}\ (OH)_2\quad Si_{3.33}\ Al_{0.67}\ O_{10}}$$

Charge: XII = 0.89 VI = 5.78 IV = 15.33 **Σ = 22.00**
Probability of smectite layers (%S): 12%
Probability of illite layers (%I): 88%
Measured particles by TEM-EDX: 63
Result of clustering: Cluster3 [tab. 2]

A comparison of octahedral Mg vs. tetrahedral Si indicates a differentiation for octahedral Mg in comparison only to Cluster2 based on TEM-EDX-data [fig. 3b]. Particles of Cluster3 contain commonly Mg(VI) > 0.15 per $(OH)_2\ O_{10}$ in octahedral layer.

The mineral formulae, summarized in classes of %S, draws for the maximum an Al- & Fe-rich diVS-ml with remarkable Mg(VI)-amount as well as reduced amount of K in the interlayer space [tab. 7b].

Kaolinite-montmorillonite mixed layer phases

The Excel-based procedure (Hoang-Minh et al., 2019) to identify possible clay mineral groups using the TEM-EDX-measurements also includes algorithms to classify kaolinite and kaolinite-montmorillonite mixed layer phases. These algorithms couldn't compute no such phases basing on the measured TEM-EDX-data. Such particles have shown small hexagonal plates typically for kaolinite-bearing phases.

References

Cliff, G. & Lorimer, G. W. (1975). *J. Microsc.* **103**, 203–207.

Döbelin, N., Kleeberg, R. (2015). *Journal of Applied Crystallography* **48**, 1573-1580. DOI: 10.1107/S1600576715014685

Henning, K.-H. & Störr, M. (1986). Electron Micrographs (TEM, SEM) of Clays and Clay Minerals, p. 325. Akademie-Verlag Berlin.

Hoang-Minh, T., Kasbohm, J., Nguyen-Thanh, L., Nga, P. T., Lai, L. T., Duong, N. T., Thanh, N. D., Thuyet, N. T. M., Anh, D. D., Pusch, R., Knutsson, S. & Ferreiro Mahlmann, R. (2019). *J. Appl. Cryst.* **52**, 133-147. DOI: 10.1107/S1600576718018162

Lorimer, G. W. & Cliff, G. (1976). *Electron Microscopy in Mineralogy*, edited by H. R. Wenk, pp. 506–519. Berlin: Springer Verlag.

Mellini, M. & Menichini, R. (1985). *R. Soc. Ital. Miner. Petrol.* **40**, 261–266.

Moore, D.M., Reynolds, R.C. (1989). X-ray Diffraction and the Identification and Analysis of Clay Minerals, Oxford University Press, New York, 332 + xvi pp.

Nguyen-Thanh, L., Herbert, H.-J., Kasbohm, J., Hoang-Minh, T. & Mählmann, R. F. (2014). *Clays Clay Miner.* **62**, 425–446.

Środoń, J., Elsass, F., McHardy, W. J. & Morgan, D. J. (1992). *Clay Miner.* **27**, 137–158.

Methodology - Transmission electron microscopy linked with energy-dispersive X-ray spectroscopy (TEM-EDX)

It is expected a characterization of clay mineral phases in treated Opalinus Clay by transmission electron microscopy. This report describes the results of treated material from Opalinus Clay percolated at a temperature of 150°C.

The different clay mineral phases are to identify and to describe by chemical composition and its variability, morphology, the specific dissolution potential, and further parameter.

Such further parameter like distribution of smectite layers probability (%S) and distribution of charges caused by exchangeable cations interlayer space should serve as additional indicators for mineralogical alterations in treatment experiments with Friedland Clay.

The sample were suspended for TEM-measurement in deionized water and dispersed by ultrasonic treatment for approximately 20 min. The clay fraction (<2 µm) was separated by sedimentation and diluted with deionized water to get a clear suspension. The suspension was dropped onto carbon-coated Cu grids, air dried and stored under environment-controlled conditions at 45% humidity.

TEM-EDX investigations were carried out on the <2 µm fraction using a FEI TECNAI G^2 20 electron transmission microscope at the VNU University of Science, Vietnam National University, Hanoi. This equipment (operated at 200 kV with LaB_6 cathode) was combined with an S-TWIN objective, a windowless EDAX energy-dispersive X-ray system and a FEI Eagle 2k CCD TEM camera.

About 100 individual clay particles per sample were characterized by TEM-EDX with respect to crystal size, crystal habit, particle morphology and element distribution. The crystal size, crystal habit and particle morphology were described according to Henning & Störr (1986).

For the quantification of element distribution, a calibration of k factors is mandatory (Cliff & Lorimer, 1975; Lorimer & Cliff, 1976; Mellini & Menichini, 1985). These k values are used to calibrate for the specific behaviour of particles against possible irradiation damage. The elements O, Na, Mg, Al, Si, K, Ca and Fe were quantified by applying the EDAX GENESIS–TEM Quant Materials quantification procedure.

In this procedure, the acquired EDX spectra are corrected by background subtraction, Gaussian deconvolution and k-factor corrections using values previously determined on a phyllosilicate standard (muscovite) and selected non-phyllosilicate standards. The average errors in the analyzed elements using the phyllosilicate standard, expressed as the atomic proportions, are 10 (Na), 5 (Fe, Mg, K, Ti, Ca) and 1 (Si, Al).

The measurement time per particle was lowered to 20 s and the exposed area was limited to a 50 nm diameter, avoiding possible irradiation damage of particles. The stability of particles of the sample series was tested for this measurement time at the beginning of any measurement campaign.

Further methodological details related to TEM-EDX-measurements and the Excel-based mathematical procedure using TEM-EDX data for calculation of mineral formulae are described in Hoang-Minh et al. (2019).

These mathematical procedures described in Hoang-Minh et al. (2019) were extended by k-means clustering method for finding subgroups of observations within a data set. The data were standardized (i.e., scaled) to make variables comparable. Euclidean distances were applied as classical method for distance measures. The optimal clusters were determined by Elbow method and Gap statistics[25].

---

[25] *https://uc-r.github.io/kmeans_clustering*

Data Sheet – Opalinus Clay N13 (< 2 µm), treated material *(150°C, 48.6 h)*

Preparation for TEM

- raw material: compacted material (1.6 g/cm³) of treated Opalinus Clay-sample
- suspension on particles < 2 µm on carbon-filmed Cu-grid
- air-dried and humidity-controlled storing

Mineral Matter

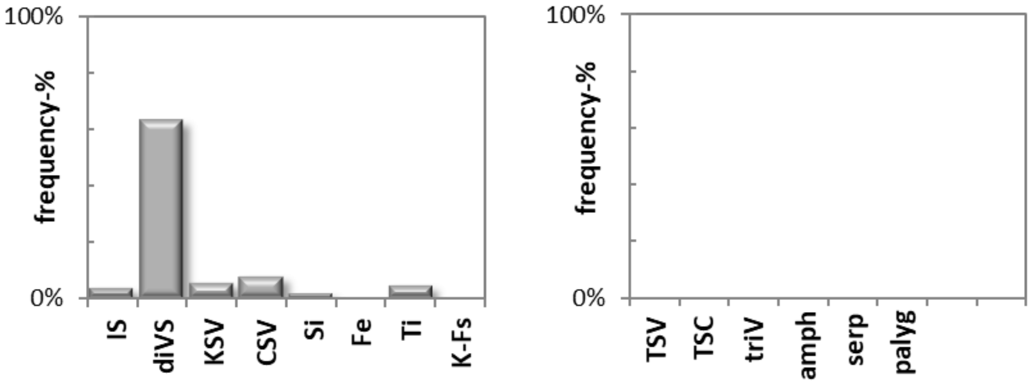

Fig. 1. *Distribution of mineral groups in fraction < 2 µm (in frequency-%)*
Legend: ***IS*** *– illite-smectite-mixed layer series in sense of Środon et al. (1992), diVS – dioctahedral vermiculite-smectite illite-smectite-mixed layer series (= charge- and/or K-deficit),* ***KSV*** *– kaolinite-smectite-dioctahedral vermiculite-mixed layer series,* ***CSV*** *– chlorite-saponite-trioctahedral vermiculite-mixed layer series,* ***Si*** *– quartz or particles with Si-surplus,* ***Fe*** *– Fe-oxide or Fe-oxyhydroxide,* ***Ti*** *– Ti-bearing phases (e.g. rutile, anatase),* ***K-Fs*** *– K-feldspar*

Clay Mineral Composition

All measured dioctahedral particles:

$$\mathrm{Ca_{0.11}\,Mg_{0.05}\,Na_{0.12}\,K_{0.53}\quad Al_{1.38}\,Fe^{3+}_{0.43}\,Mg_{0.18}\,Ti_{0.01}\,(OH)_2\quad Si_{3.21}\,Al_{0.79}\,O_{10}}$$

Charge: XII = 0.95 VI = 5.84 IV = 15.21 **Σ = 22.00**

Probability of smectite layers (%S): 4%

Probability of illite layers (%I): 96%

Specific Dissolution Potential (ΔS%)

for H2O, 20 + 60 rpm	-14	(= medium reacting, 'illitization', interlayer group: Ca+Mg (= type B))
for NaCl, 20 rpm	-17	(= medium reacting, 'illitization', interlayer group: Ca+Mg (= type B))
for NaCl, 60 rpm	-21	(= fast reacting, 'illitization', interlayer group: Na (= type A))

$\mathrm{CEC_{calc}}$: 133 meq / 100 g

Measured particles: 114

Table 1. *Summarized chemical composition*

SiO_2	TiO_2	Al_2O_3	Fe_2O_3	MnO	MgO	CaO	Na_2O	K_2O	P_2O_5	Σ	
51.4%	0.2%	30.8%	4.6%		2.8%	3.5%	1.4%	4.8%	0.5%	1.00	measured particles of treated sample
59.4%	0.3%	28.1%	5.9%		2.5%	0.3%	0.1%	3.3%	0.1%	1.00	measured particles of original Opalinus Clay

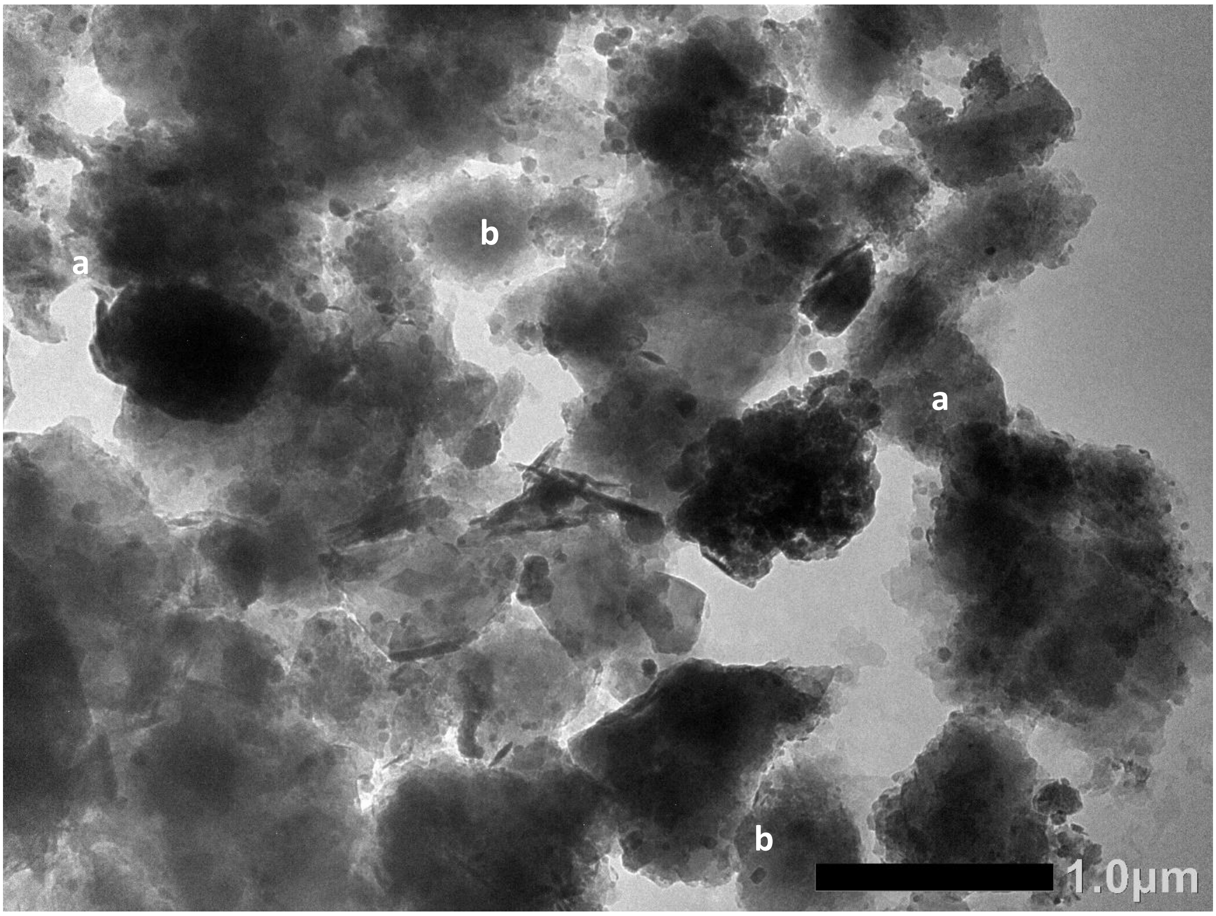

JEM-2100_MAG_X10k_No13_017.bmp

Magnification: 10k

(a) large (≤ 1 µm) xenomorph platy crystals;
(b) aggregates formed by small (≤ 100 nm) xenomorphous plates

Fig. 2. *Morphology of particles (TEM-micrographs)*

Distribution of smectite layers probability (%S)

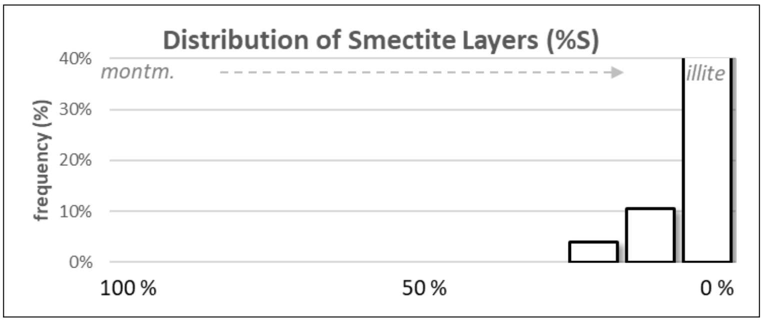

Description: *The distribution of %S-probability indicates the occurrence of two groups: (i) low number of diVS-ml phases as well as (ii) dominating illite with K-deficiency.*

Fig. 3a. *Distribution of smectite layers probability (%S)*

Differentiation by relation “Octahedral Mg vs. tetrahedral Si”?

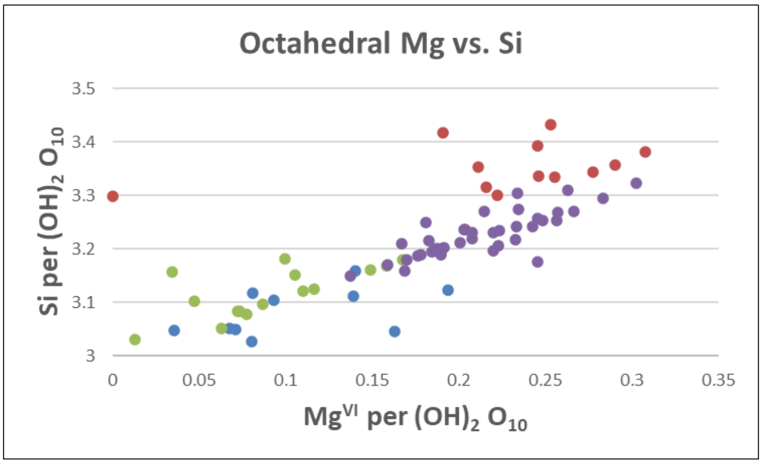

Description: *This diagram indicates a separation on low and high ratio of Mg in relation to tetrahedral Si (blue dots – Cluster1: illite; green dots – Cluster3: illite vs. red dots – Cluster2: diVS-ml; violet dots – Cluster4: illite). Phases of Cluster2 are mostly characterized by Mg(VI) > 0.2 per* $(OH)_2\ O_{10}$.

Fig. 3b. *Distribution of octahedral Mg vs. tetrahedral Si [all per* $(OH)_2\ O_{10}$*]*

Distribution of K in relation to tetrahedral Si

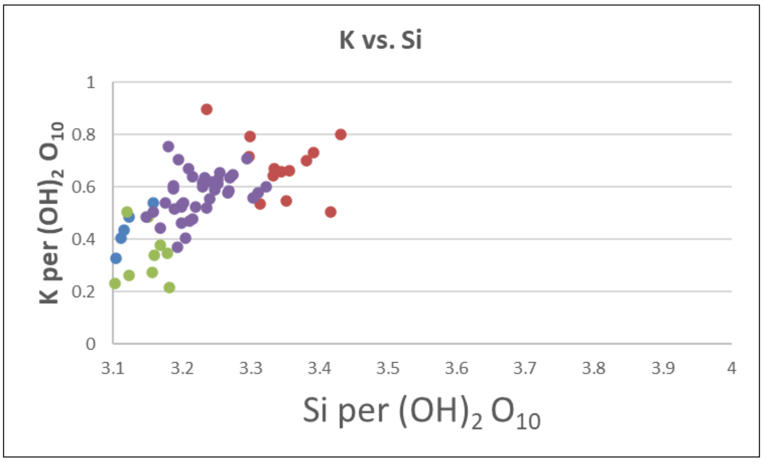

Description: *This diagram indicates a weak separation on low and high ratio of K in relation to tetrahedral Si (blue dots – Cluster1: illite; green dots – Cluster3: illite vs. red dots – Cluster2: diVS-ml; violet dots – Cluster4: illite). Phases of Cluster1+3 are mostly characterized by K < 0.45 per* $(OH)_2\ O_{10}$.

Fig. 4. *Distribution of K in interlayer space vs. tetrahedral Si [all per* $(OH)_2\ O_{10}$*]*

Distribution of charges (exchangeable from interlayer space)

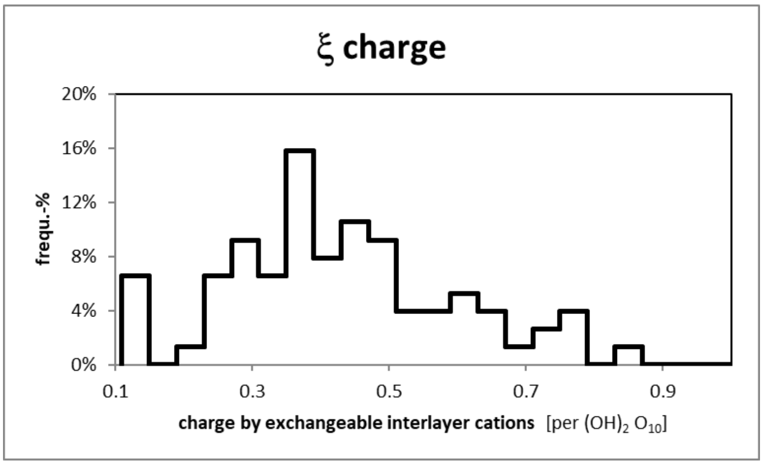

This diagram visualizes the distribution of exchangeable charges in the interlayer space (Ca, Mg, Na) determined and computed by TEM-EDX-data.

Description: *Very broad distribution of charge density with a maximal frequency-% at 0.39 per* $(OH)_2\ O_{10}$.

Fig. 5. *Distribution of charges*

Dioctahedral Vermiculite-Smectite mixed layer phases (diVS-ml - illite) *(Cluster1):*

$$\mathrm{Ca_{0.06}\ Mg_{0.16}\ Na_{0.06}\ K_{0.45}\quad Al_{1.21}\ Fe^{3+}_{0.64}\ Mg_{0.11}\ Ti_{0.05}\ (OH)_2\quad Si_{3.08}\ Al_{0.92}\ O_{10}}$$

Charge:	XII = 0.97	VI = 5.94	IV = 15.08	**Σ = 22.00**
Probability of smectite layers (%S):	0%			
Probability of illite layers (%I):	100%			
Measured particles:	10			

Distribution of smectite layers probability (%S) in diVS-ml (Cluster1)

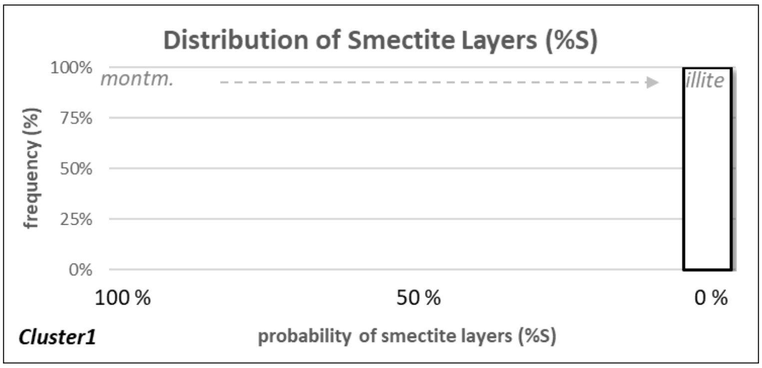

Description: *The distribution of diVS-ml (classified as Cluster1) draws a maximum of frequency (%) for smectite layer probability at 0%*

Fig. 6a. *Distribution of smectite layers probability in diVS-ml*

diVS-ml	*particles (abs)*	Ca (XII)	Mg (XII)	Na (XII)	K (XII)	Cr3+ (VI)	Al (VI)	Fe3+ (VI)	Mg (VI)	Ti (VI)	Al (IV)	Si (IV)	XII	n_VI	%S
%S >95%	n = 0														
%S 95-85%	n = 0														
%S 85-75%	n = 0														
%S 75-65%	n = 0														
%S 65-55%	n = 0														
%S 55-45%	n = 0														
%S 45-35%	n = 0														
%S 35-25%	n = 0														
%S 25-15%	n = 0														
%S <15%	**n = 10**	**0.06**	**0.16**	**0.06**	**0.45**	**0.00**	**1.21**	**0.64**	**0.11**	**0.05**	**0.92**	**3.08**	**0.97**	**2.0**	**-2**

Fig. 6b. *Computed averaged mineral formulae of diVS-ml phases in the different smectite layers probability (%S)-classes*

Dioctahedral Vermiculite-Smectite mixed layer phases (diVS-ml) *(Cluster2):*

$$\mathrm{Ca_{0.05}\ Mg_{0.00}\ Na_{0.09}\ K_{0.68}\quad Al_{1.36}\ Fe^{3+}_{0.46}\ Mg_{0.22}\ Ti_{0.00}\ (OH)_2\quad Si_{3.35}\ Al_{0.65}\ O_{10}}$$

Charge:	XII = 0.87	VI = 5.78	IV = 15.35	**Σ = 22.00**
Probability of smectite layers (%S):	13%			
Probability of illite layers (%I):	87%			
Measured particles:	13			

Distribution of smectite layers probability (%S) in diVS-ml (Cluster2)

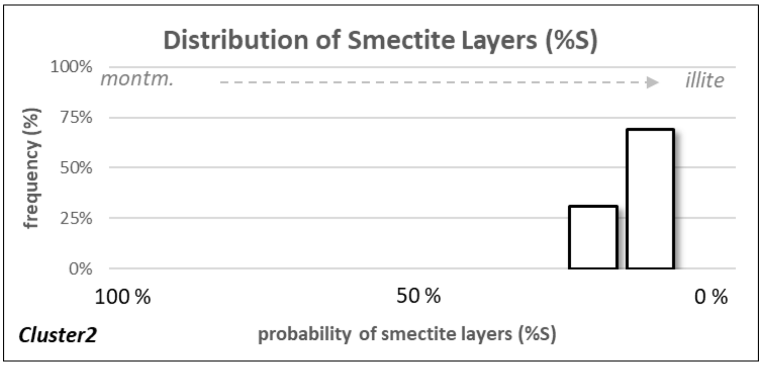

Description: *The distribution of diVS-ml (classified as Cluster2) draws a maximum of frequency (%) for smectite layer probability at 10%*

Fig. 7a. *Distribution of smectite layers probability in diVS-ml*

diVS-ml	particles (abs)	Ca (XII)	Mg (XII)	Na (XII)	K (XII)	Cr3+ (VI)	Al (VI)	Fe3+ (VI)	Mg (VI)	Ti (VI)	Al (IV)	Si (IV)	XII	n_VI	%S
%S >95%	n = 0														
%S 95-85%	n = 0														
%S 85-75%	n = 0														
%S 75-65%	n = 0														
%S 65-55%	n = 0														
%S 55-45%	n = 0														
%S 45-35%	n = 0														
%S 35-25%	n = 0														
%S 25-15%	n = 4	0.03	0.00	0.08	0.68	0.00	1.29	0.46	0.25	0.00	0.59	3.41	0.8	2.0	18
%S <15%	**n = 9**	**0.05**	**0.00**	**0.09**	**0.68**	**0.00**	**1.39**	**0.40**	**0.21**	**0.00**	**0.68**	**3.32**	**0.9**	**2.0**	**11**

Fig. 7b. *Computed averaged mineral formulae of diVS-ml phases in the different smectite layers probability (%S)-classes*

Cluster2		Ca (XII)	Mg (XII)	Na (XII)	K (XII)	Cr3+ (VI)	Al (VI)	Fe3+ (VI)	Mg (VI)	Ti (VI)	Al (IV)	Si (IV)	XII	n_VI	%S
without illite	n = 4	0.03	0.00	0.08	0.68	0.00	1.29	0.46	0.25	0.00	0.59	3.41	0.83	2.0	18
only illite	n = 9	0.05	0.00	0.09	0.68	0.00	1.39	0.40	0.21	0.00	0.68	3.32	0.88	2.0	11

Fig. 7b2. *Computed averaged mineral formulae of diVS-ml phases differentiated by illite*

Dioctahedral Vermiculite-Smectite mixed layer phases (diVS-ml) *(Cluster3):*

$$Ca_{0.20}\ Mg_{0.05}\ Na_{0.13}\ K_{0.34}\quad Al_{1.67}\ Fe^{3+}_{0.24}\ Mg_{0.09}\ Ti_{0.00}\ (OH)_2\quad Si_{3.12}\ Al_{0.88}\ O_{10}$$

Charge: XII = 0.97 VI = 5.91 IV = 15.12 **Σ = 22.00**

Probability of smectite layers (%S):	0%
Probability of illite layers (%I):	100%
Measured particles:	15

Distribution of smectite layers probability (%S) in diVS-ml (Cluster3)

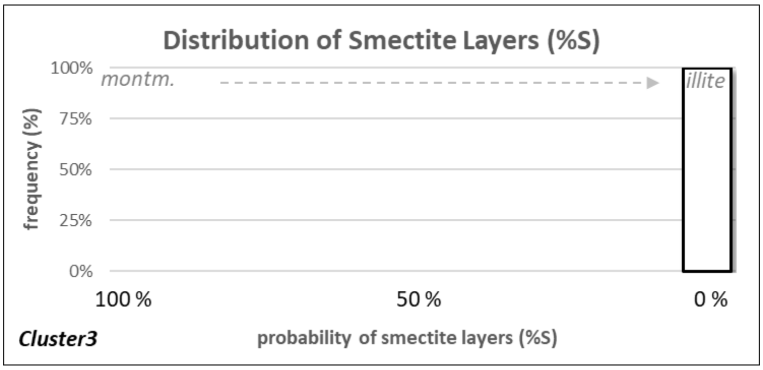

Description: *The distribution of diVS-ml (classified as Cluster3) draws a maximum of frequency (%) for smectite layer probability at 0%*

Fig. 7c. *Distribution of smectite layers probability in diVS-ml*

diVS-ml	particles (abs)	Ca (XII)	Mg (XII)	Na (XII)	K (XII)	Cr3+ (VI)	Al (VI)	Fe3+ (VI)	Mg (VI)	Ti (VI)	Al (IV)	Si (IV)	XII	n_VI	%S
%S >95%	n = 0														
%S 95-85%	n = 0														
%S 85-75%	n = 0														
%S 75-65%	n = 0														
%S 65-55%	n = 0														
%S 55-45%	n = 0														
%S 45-35%	n = 0														
%S 35-25%	n = 0														
%S 25-15%	n = 0														
%S <15%	**n = 15**	**0.20**	**0.05**	**0.13**	**0.34**	**0.00**	**1.67**	**0.24**	**0.09**	**0.00**	**0.88**	**3.12**	**1.0**	**2.0**	**0**

Fig. 7d. *Computed averaged mineral formulae of diVS-ml phases in the different smectite layers probability (%S)-classes*

Dioctahedral Vermiculite-Smectite mixed layer phases (diVS-ml) *(Cluster4):*

$$Ca_{0.10}\ Mg_{0.03}\ Na_{0.14}\ K_{0.57}\quad Al_{1.33}\ Fe^{3+}_{0.45}\ Mg_{0.21}\ Ti_{0.01}\ (OH)_2\ \ Si_{3.23}\ Al_{0.77}\ O_{10}$$

Charge: XII = 0.97 VI = 5.80 IV = 15.23 **Σ = 22.00**

Probability of smectite layers (%S): 5%

Probability of illite layers (%I): 95%

Measured particles: 38

Distribution of smectite layers probability (%S) in diVS-ml (Cluster4)

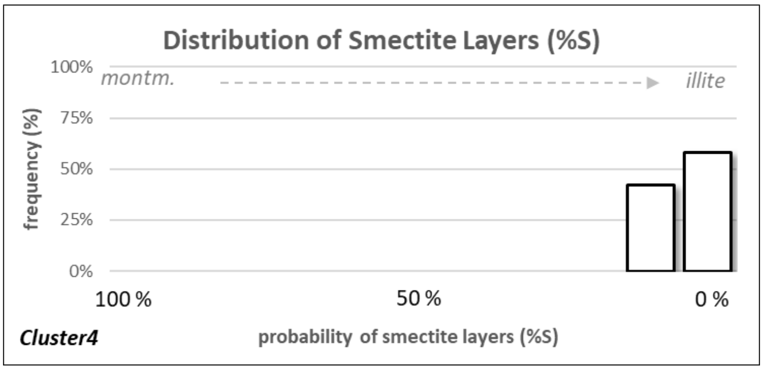

Description: *The distribution of diVS-ml (classified as Cluster4) draws a maximum of frequency (%) for smectite layer probability at 0%*

Fig. 7c. *Distribution of smectite layers probability in diVS-ml*

diVS-ml	particles (abs)	Ca (XII)	Mg (XII)	Na (XII)	K (XII)	Cr3+ (VI)	Al (VI)	Fe3+ (VI)	Mg (VI)	Ti (VI)	Al (IV)	Si (IV)	XII	n_VI	%S
%S >95%	n = 0														
%S 95-85%	n = 0														
%S 85-75%	n = 0														
%S 75-65%	n = 0														
%S 65-55%	n = 0														
%S 55-45%	n = 0														
%S 45-35%	n = 0														
%S 35-25%	n = 0														
%S 25-15%	n = 0														
%S <15%	**n = 38**	**0.10**	**0.03**	**0.14**	**0.57**	**0.00**	**1.33**	**0.45**	**0.21**	**0.01**	**0.77**	**3.23**	**1.0**	**2.0**	**5**

Fig. 7d. *Computed averaged mineral formulae of diVS-ml phases in the different smectite layers probability (%S)-classes*

Description – Opalinus Clay N13 (< 2 µm), treated material *(150°C)*

Preparation for TEM

The powder of Opalinus Clay-sample was suspended in deionized water and dispersed by ultrasonic treatment for approximately 20 min. The clay fraction (<2 µm) was separated by sedimentation and diluted with deionized water to get a clear suspension. The suspension was dropped onto carbon-coated Cu grids, air dried and stored under environment-controlled conditions at 45% humidity.

Mineral Matter - Overview

The fraction < 2 µm of Opalinus Clay N13 sample is mainly composed by four different types of dioctahedral vermiculite-smectite mixed layer phases (diVS-ml). Rarely, kaolinite and kaolinite-smectite-ml phases as well as chlorite-smectite-ml phases, rutile and quartz were identified in traces in this sample [fig. 1].

The measured and computed particles have shown a calculated CEC-value of 133 meq / 100 g located at surface and in the interlayer space.

	frequency-% *(n = 114 measured particles)*
diVS-ml	67%
Kaolinite & KSV-ml	5%
CSV-ml	8%
Ti-phases	4%
Quartz	2%
Unknown phases	14%

All measured dioctahedral 2:1 clay mineral phases summarized result following mineral formula computed from TEM-EDX-measurement of 114 individual particles:

$$Ca^{2+}_{0.11}\ Mg^{2+}_{0.05}\ Na^{+}_{0.12}\ K^{+}_{0.53}\quad Al^{3+}_{1.38}\ Fe^{3+}_{0.43}\ Mg^{2+}_{0.18}\ Ti^{4+}_{0.01}\ (OH)_2\quad Si^{4+}_{3.21}\ Al^{3+}_{0.79}\ O_{10}$$

SDOM *± 0.01 ± 0.01 ± 0.01 ± 0.02 ± 0.02 ± 0.02 ± 0.01 ± 0.00 ± 0.01 ± 0.01*

Legend: SDOM - standard deviation of the mean (= the standard deviation divided by the square root of the number of samples)

The interlayer charge is calculated as 0.95 per $(OH)_2\ O_{10}$ and the octahedral charge as 5.84 per $(OH)_2\ O_{10}$. The particles are characterized by a high octahedral Fe-amount.

The summarized chemical composition of all 114 computed particles is listed [tab. 1].

Opalinus Clay N13 sample is also characterized by two morphological groups: (i) large (≤ 1 µm) xenomorph platy crystals and (ii) aggregates, partially with folds, formed by small (≤ 100 nm) xenomorphous plates [fig. 2]. Aggregates formed by large (≤ 1 µm) xenomorph platy crystals dominate the shapes of particles in the micrographs [fig. 2].

The distribution of %S-probability of all measured clay mineral phases [fig. 3a] also indicates the occurrence of two groups: (i) diVS-ml and dominating (ii) illite with K-deficiency.

The numerous measured particles by TEM-EDX allow a visualization of distribution of interlayer charges. Considering the TEM-EDX-determined cations Ca^{++}, Mg^{++} and Na^{+} and then computed their ratio as interlayer cations in the mineral formula, Ca^{++}, Mg^{++} and Na^{+} offer to characterize the degree of exchangeable charges in the interlayer space. This charge density of Opalinus Clay N13 (< 2 µm) shows in this sample a maximal frequency-% of charge density at 0.39 per $(OH)_2 O_{10}$ [fig. 5]. This interval of interlayer charge density caused by exchangeable cations from 0.23 - 0.79 per $(OH)_2 O_{10}$ represents mentioned four groups of diVS-ml.

Mineral Matter - Specification

Result of Clustering

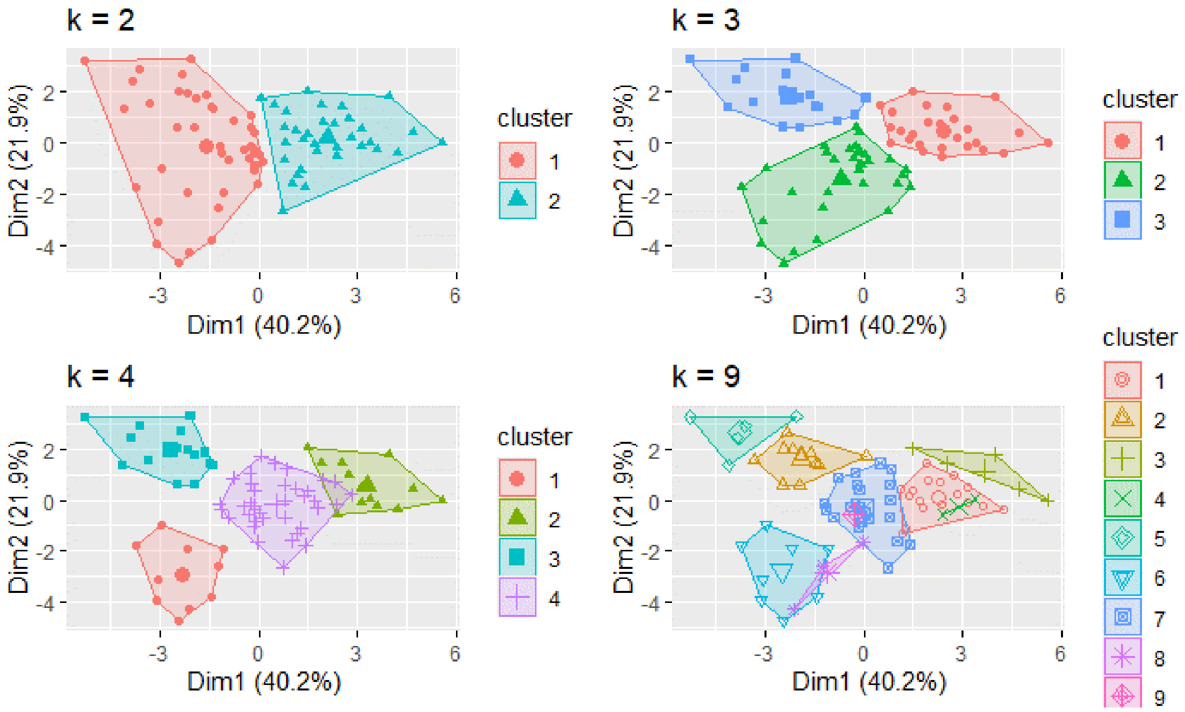

Fig. 8. *Clustering of all measured particles for clusters k = 2, k = 3, k = 4 and k = 9 (source for R-coding: https://uc-r.github.io/kmeans_clustering)*

The optimum of clusters was calculated with k = 4.

		Ca (XII)	Mg (XII)	Na (XII)	K (XII)	Cr3+ (VI)	Al (VI)	Fe3+ (VI)	Mg (VI)	Ti (VI)	Al (IV)	Si (IV)	XII	n_VI	%S
Cluster1	n = 10	0.06	0.16	0.06	0.45	0.00	1.21	0.64	0.11	0.05	0.92	3.08	0.97	2.0	-2
Cluster2	n = 13	0.05	0.00	0.09	0.68	0.00	1.36	0.42	0.22	0.00	0.65	3.35	0.87	2.0	13
Cluster3	n = 15	0.20	0.05	0.13	0.34	0.00	1.67	0.24	0.09	0.00	0.88	3.12	0.97	2.0	0
Cluster4	n = 38	0.10	0.03	0.14	0.57	0.00	1.33	0.45	0.21	0.01	0.77	3.23	0.98	2.0	5

Fig. 9a. *Mineral formulae based on TEM-EDX-data summarized following the result of clustering for k=4*

	Sybilla-results	TEM-EDX-results	Notes
Cluster1	Illite	diVS-ml (illite)	*very high K-deficit, no XII-charge deficit, Fe(VI)-rich, low Mg(VI)*
Cluster3		diVS-ml (illite)	*very high K-deficit, no XII-charge deficit, high Al(VI), low Mg(VI)*
Cluster4		diVS-ml (illite)	*high K-deficit, no XII-charge deficit, Fe(VI)-rich*
Cluster2	IS R0(1) *(%S = 16%)*	diVS-ml *(%S = 13%)*	*K-deficit, no XII-charge deficit, Fe(VI)-rich*
	Kaolinite + KS GL R0		*in traces only*

Tab. 2. *Comparison of results from TEM-EDX- and XRD-measurements*

The TEM-EDX-data offers a good agreement with the result of Sybilla-processing of XRD-traces from oriented specimen [tab. 2].

IS R0 (1): The Sybilla-procedure of XRD-traces (oriented mounts) has shown an occurrence of an illite-smectite mixed layer phase with a smectite layers probability of %S = 16%. This result of XRD-pattern processing is in good agreement with founded maximum of particles for %S ~ 13% by TEM-EDX-measurements [tab. 2].

The Sybilla-processing of XRD-traces (oriented mounts) also supports low amount of kaolinite and kaolinite-smectite mixed layer phases in fine fraction of sample.

Specifics to the identified clay mineral groups

Dioctahedral vermiculite-smectite mixed layer phase *(Cluster1)*

10 of 76 computed particles belong so to this assumed classification. The dioctahedral character of this group is proofed by X-ray diffraction. The position of the large (060)-interference of smectite is in the random oriented powder specimen at 1.497 Å.

Dioctahedral vermiculite-smectite mixed layer phase *(Cluster1)*

$$\mathrm{Ca_{0.06}\ Mg_{0.16}\ Na_{0.06}\ K_{0.45}\quad Al_{1.21}\ Fe^{3+}_{0.64}\ Mg_{0.11}\ Ti_{0.05}\ (OH)_2\ \ Si_{3.08}\ Al_{0.92}\ O_{10}}$$

Charge: XII = 0.97 VI = 5.95 IV = 15.08 **Σ = 22.00**
Measured particles by TEM-EDX: 10
Probability of smectite layers (%S): 0%
Probability of illite layers (%I): 100%
Result of clustering: Cluster1 [tab. 2]

A comparison of octahedral Mg vs. tetrahedral Si indicates a differentiation for octahedral Mg in comparison to Cluster2+4 based on TEM-EDX-data [fig. 3b]. Particles of Cluster1 contain commonly Mg(VI) < 0.15 per $(OH)_2\ O_{10}$ in octahedral layer.

The mineral formulae, summarized in classes of %S, draws for the maximum an Fe-rich diVS-ml with a low Mg(VI) as well as low amount of K in the interlayer space [tab. 6b].

Dioctahedral vermiculite-smectite mixed layer phase *(diVS-ml, Cluster2)*

$$\mathrm{Ca_{0.05}\ Mg_{0.00}\ Na_{0.09}\ K_{0.68}\quad Al_{1.36}\ Fe^{3+}_{0.42}\ Mg_{0.22}\ Ti_{0.00}\ (OH)_2\ \ Si_{3.35}\ Al_{0.65}\ O_{10}}$$

Charge: XII = 0.87 VI = 5.78 IV = 15.35 **Σ = 22.00**
Probability of smectite layers (%S): 13%
Probability of illite layers (%I): 87%
Measured particles by TEM-EDX: 13
Result of clustering: Cluster2 [tab. 2]

A comparison of octahedral Mg vs. tetrahedral Si indicates a differentiation for octahedral Mg in comparison to Cluster1+Cluster3 based on TEM-EDX-data [fig. 3b]. Particles of Cluster2 contain commonly Mg(VI) > 0.15 per $(OH)_2\ O_{10}$ in octahedral layer.

The mineral formulae, summarized in classes of %S, draws for the maximum an Al- & Fe-rich diVS-ml as well as reduced amount of K in the interlayer space [tab. 7b].

Dioctahedral vermiculite-smectite mixed layer phase *(diVS-ml, Cluster3)*

$$Ca_{0.20}\ Mg_{0.05}\ Na_{0.13}\ K_{0.34}\quad Al_{1.67}\ Fe^{3+}_{0.24}\ Mg_{0.09}\ Ti_{0.00}\ (OH)_2\quad Si_{3.12}\ Al_{0.88}\ O_{10}$$

Charge: XII = 0.97 VI = 5.91 IV = 15.12 **Σ = 22.00**
Probability of smectite layers (%S): 0%
Probability of illite layers (%I): 100%
Measured particles by TEM-EDX: 15
Result of clustering: Cluster3 [tab. 2]

A comparison of octahedral Mg vs. tetrahedral Si indicates a differentiation for octahedral Mg in comparison to Cluster2+4 based on TEM-EDX-data [fig. 3b]. Particles of Cluster3 contain commonly Mg(VI) < 0.15 per $(OH)_2\ O_{10}$ in octahedral layer.

The mineral formulae, summarized in classes of %S, draws for the maximum an Al-rich diVS-ml with low Mg(VI)-amount as well as reduced amount of K in the interlayer space [tab. 7b].

Dioctahedral vermiculite-smectite mixed layer phase *(diVS-ml, Cluster4)*

$$Ca_{0.10}\ Mg_{0.03}\ Na_{0.14}\ K_{0.57}\quad Al_{1.33}\ Fe^{3+}_{0.45}\ Mg_{0.21}\ Ti_{0.01}\ (OH)_2\quad Si_{3.23}\ Al_{0.77}\ O_{10}$$

Charge: XII = 0.98 VI = 5.79 IV = 15.23 **Σ = 22.00**
Probability of smectite layers (%S): 5%
Probability of illite layers (%I): 95%
Measured particles by TEM-EDX: 38
Result of clustering: Cluster4 [tab. 2]

A comparison of octahedral Mg vs. tetrahedral Si indicates a differentiation for octahedral Mg in comparison to Cluster1+3 based on TEM-EDX-data [fig. 3b]. Particles of Cluster4 contain commonly Mg(VI) > 0.15 per $(OH)_2\ O_{10}$ in octahedral layer.

The mineral formulae, summarized in classes of %S, draws for the maximum an Fe-rich diVS-ml with remarkable Mg(VI)-amount as well as reduced amount of K in the interlayer space [tab. 7b].

Kaolinite-montmorillonite mixed layer phases

The Excel-based procedure (Hoang-Minh et al., 2019) to identify possible clay mineral groups using the TEM-EDX-measurements also includes algorithms to classify kaolinite and kaolinite-montmorillonite mixed layer phases. These algorithms couldn’t compute no such phases basing on the measured TEM-EDX-data. Such particles have shown small hexagonal plates typically for kaolinite-bearing phases.

References

Cliff, G. & Lorimer, G. W. (1975). *J. Microsc.* **103**, 203–207.

Döbelin, N., Kleeberg, R. (2015). *Journal of Applied Crystallography* **48**, 1573-1580. DOI: 10.1107/S1600576715014685

Henning, K.-H. & Störr, M. (1986). Electron Micrographs (TEM, SEM) of Clays and Clay Minerals, p. 325. Akademie-Verlag Berlin.

Hoang-Minh, T., Kasbohm, J., Nguyen-Thanh, L., Nga, P. T., Lai, L. T., Duong, N. T., Thanh, N. D., Thuyet, N. T. M., Anh, D. D., Pusch, R., Knutsson, S. & Ferreiro Mahlmann, R. (2019). *J. Appl. Cryst.* **52**, 133-147. DOI: 10.1107/S1600576718018162

Lorimer, G. W. & Cliff, G. (1976). *Electron Microscopy in Mineralogy*, edited by H. R. Wenk, pp. 506–519. Berlin: Springer Verlag.

Mellini, M. & Menichini, R. (1985). *R. Soc. Ital. Miner. Petrol.* **40**, 261–266.

Moore, D.M., Reynolds, R.C. (1989). X-ray Diffraction and the Identification and Analysis of Clay Minerals, Oxford University Press, New York, 332 + xvi pp.

Nguyen-Thanh, L., Herbert, H.-J., Kasbohm, J., Hoang-Minh, T. & Mählmann, R. F. (2014). *Clays Clay Miner.* **62**, 425–446.

Środoń, J., Elsass, F., McHardy, W. J. & Morgan, D. J. (1992). *Clay Miner.* **27**, 137–158.

SUPPLEMENT – Transmission Electron Microscopy coupled Energy dispersive X-ray Spectroscopy (TEM-EDX) of Friedland clay

Data Sheet – Friedland clay, untreated compacted materials

Methodology - Transmission electron microscopy linked with energy-dispersive X-ray spectroscopy (TEM-EDX)

It is expected a characterization of clay mineral phases in treated Friedland Clay by transmission electron microscopy. This report describes the results of original material from Friedland Clay sampled in January 2023.

The different clay mineral phases are to identify and to describe by chemical composition and its variability, morphology, the specific dissolution potential, and further parameter.

Such further parameter like distribution of smectite layers probability (%S) and distribution of charges caused by exchangeable cations interlayer space should serve as additional indicators for mineralogical alterations in treatment experiments with Friedland Clay.

The sample were suspended for TEM-measurement in deionized water and dispersed by ultrasonic treatment for approximately 20 min. The clay fraction (<2 µm) was separated by sedimentation and diluted with deionized water to get a clear suspension. The suspension was dropped onto carbon-coated Cu grids, air dried and stored under environment-controlled conditions at 45% humidity.

TEM-EDX investigations were carried out on the <2 µm fraction using a FEI TECNAI G^2 20 electron transmission microscope at the VNU University of Science, Vietnam National University, Hanoi. This equipment (operated at 200 kV with LaB_6 cathode) was combined with an S-TWIN objective, a windowless EDAX energy-dispersive X-ray system and a FEI Eagle 2k CCD TEM camera.

About 100 individual clay particles per sample were characterized by TEM-EDX with respect to crystal size, crystal habit, and particle morphology and element distribution. The crystal size, crystal habit and particle morphology were described according to Henning & Störr (1986).

For the quantification of element distribution, a calibration of k factors is mandatory (Cliff & Lorimer, 1975; Lorimer & Cliff, 1976; Mellini & Menichini, 1985). These k values are used to calibrate for the specific behaviour of particles against possible irradiation damage. The elements O, Na, Mg, Al, Si, K, Ca and Fe were quantified by applying the EDAX GENESIS–TEM Quant Materials quantification procedure.

In this procedure, the acquired EDX spectra are corrected by background subtraction, Gaussian deconvolution and k-factor corrections using values previously determined on a phyllosilicate standard (muscovite) and selected non-phyllosilicate standards. The average errors in the analyzed elements using the phyllosilicate standard, expressed as the atomic proportions, are 10 (Na), 5 (Fe, Mg, K, Ti, Ca) and 1 (Si, Al).

The measurement time per particle was lowered to 20 s and the exposed area was limited to a 50 nm diameter, avoiding possible irradiation damage of particles. The stability of particles of the sample series was tested for this measurement time at the beginning of any measurement campaign.

Further methodological details related to TEM-EDX-measurements and the Excel-based mathematical procedure using TEM-EDX data for calculation of mineral formulae are described in Hoang-Minh et al. (2019).

These mathematical procedures described in Hoang-Minh et al. (2019) were extended by k-means clustering method for finding subgroups of observations within a data set. The data were standardized (i.e., scaled) to make variables comparable. Euclidean distances were applied as classical method for distance measures. The optimal clusters were determined by Elbow method and Gap statistics[26].

---

[26] *https://uc-r.github.io/kmeans_clustering*

Data Sheet – Friedland Clay (< 2 µm), untreated material

Preparation for TEM

- raw material: compacted material (1.6 g/cm³) of untreated Friedland Clay-sample
- suspension on particles < 2 µm on carbon-filmed Cu-grid
- air-dried and humidity-controlled storing

Mineral Matter

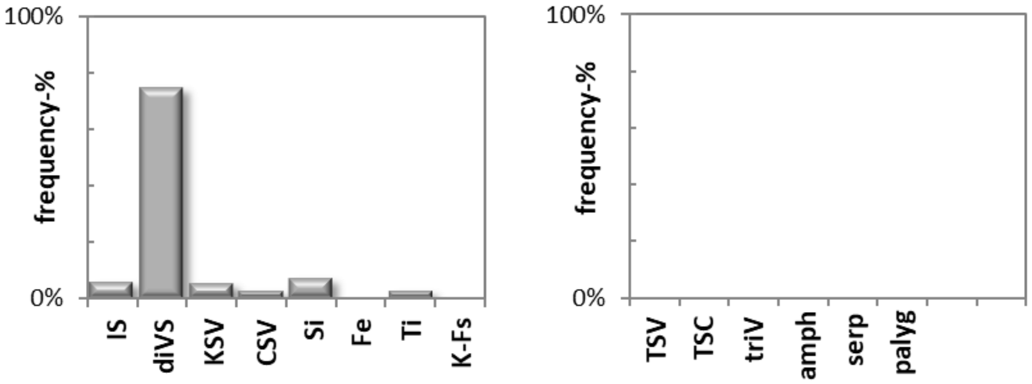

Fig. 1. *Distribution of mineral groups in fraction < 2 µm (in frequency-%)*
Legend: ***IS*** *– illite-smectite-mixed layer series in sense of Środon et al. (1992), diVS – dioctahedral vermiculite-smectite illite-smectite-mixed layer series (= charge- and/or K-deficit),* ***KSV*** *– kaolinite-smectite-dioctahedral vermiculite-mixed layer series,* ***CSV*** *– chlorite-saponite-trioctahedral vermiculite-mixed layer series,* ***Si*** *– quartz or particles with Si-surplus,* ***Fe*** *– Fe-oxide or Fe-oxyhydroxide,* ***Ti*** *– Ti-bearing phases (e.g. rutile, anatase),* ***K-Fs*** *– K-feldspar*

Clay Mineral Composition

All particles of smectite group:

$$\mathrm{Ca_{0.02}\,Mg_{0.09}\,Na_{0.01}\,K_{0.35}\quad Al_{1.36}\,Fe^{3+}_{0.52}\,Mg_{0.10}\,Ti_{0.02}\,(OH)_2\quad Si_{3.49}\,Al_{0.51}\,O_{10}}$$

Charge: XII = 0.58 VI = 5.93 IV = 15.49 **Σ = 22.00**
Probability of smectite layers (%S): 27%
Probability of illite layers (%I): 73%

Specific Dissolution Potential (ΔS%)

for H2O, 20 + 60 rpm - 2 (= slow reacting, interlayer group: Ca+Mg (= type B))
for NaCl, 20 rpm - 2 (= slow reacting, interlayer group: Ca+Mg (= type B))
for NaCl, 60 rpm -98 (= fast reacting, 'illitization', interlayer group: Na (= type A))
CEC$_{calc}$: 32 meq / 100 g

Measured particles: 152

Table 1. *Summarized chemical composition*

SiO_2	**TiO_2**	**Al_2O_3**	**Fe_2O_3**	**MnO**	**MgO**	**CaO**	**Na_2O**	**K_2O**	**P_2O_5**	**Σ**	
59.4%	0.3%	28.1%	5.9%		2.5%	0.3%	0.1%	3.3%	0.1%	1.00	measured particles of original Friedland Clay

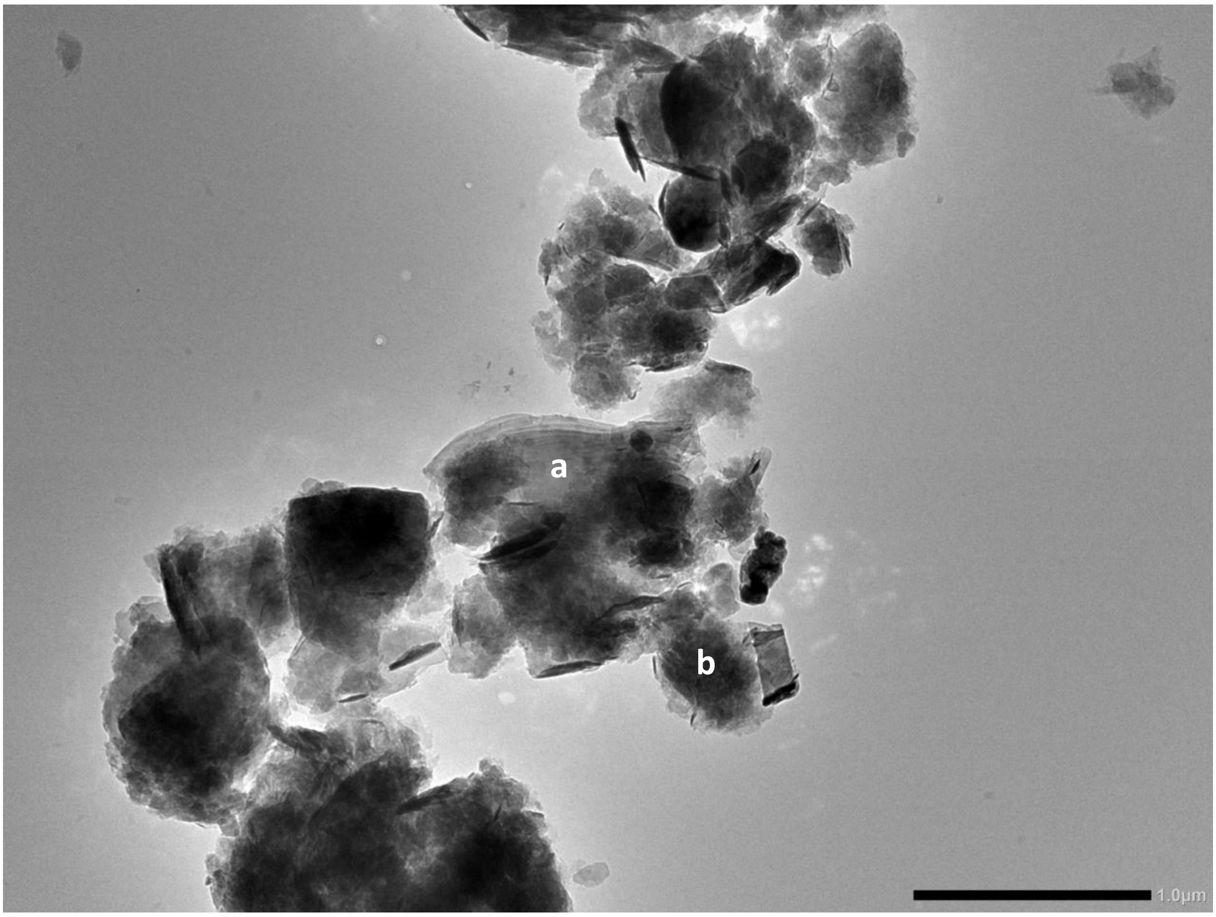

JEM-2100_MAG_X10k_007_AISZ-5ML.bmp

Magnification: 10k

(a) large (≤ 1 µm) xenomorph platy crystals;
(b) aggregates, partially with folds, formed by small (≤ 100 nm) xenomorph plates

Fig. 2. *Morphology of particles (TEM-micrographs)*

Distribution of smectite layers probability (%S)

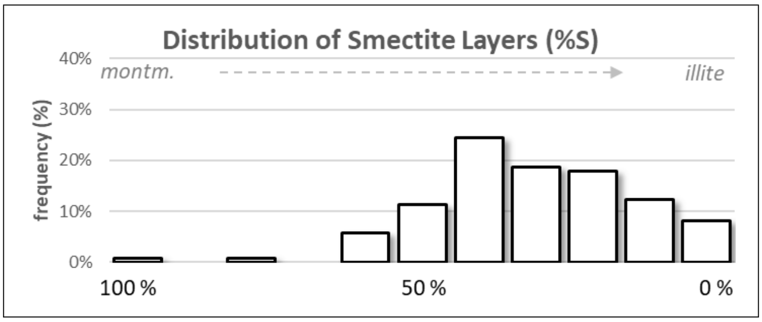

Description: *The distribution of %S-probability indicates the occurrence of two groups: (i) BMI- and beidellitic diVS-ml phases incl. illite with K-deficiency as well as (ii) montmorillonite (rare).*

Fig. 3a. *Distribution of smectite layers probability (%S)*

Differentiation by relation “Octahedral Mg vs. tetrahedral Si”?

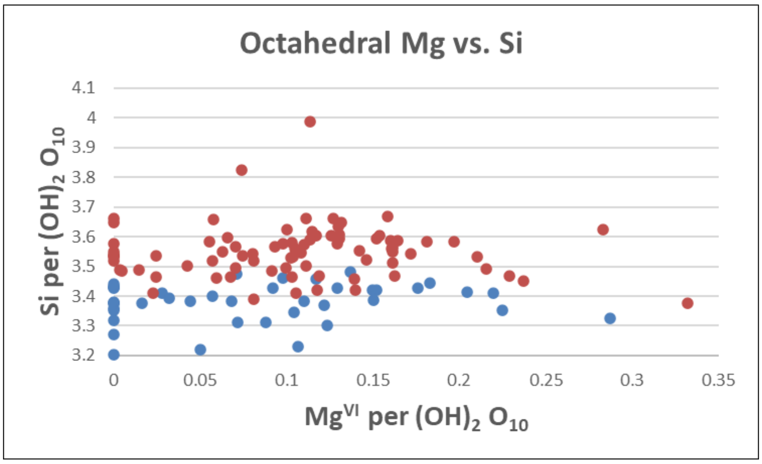

__Description:__ This diagram doesn’t indicate any trend of Mg in relation to tetrahedral Si, also not between BMI-ml phases of cluster2 (red dots) and beidellitic diVS-ml phases of cluster1 (blue dots).

Fig. 3b. *Distribution of octahedral Mg vs. tetrahedral Si [all per$(OH)_2$ O_{10}]*

Distribution of K in relation to tetrahedral Si

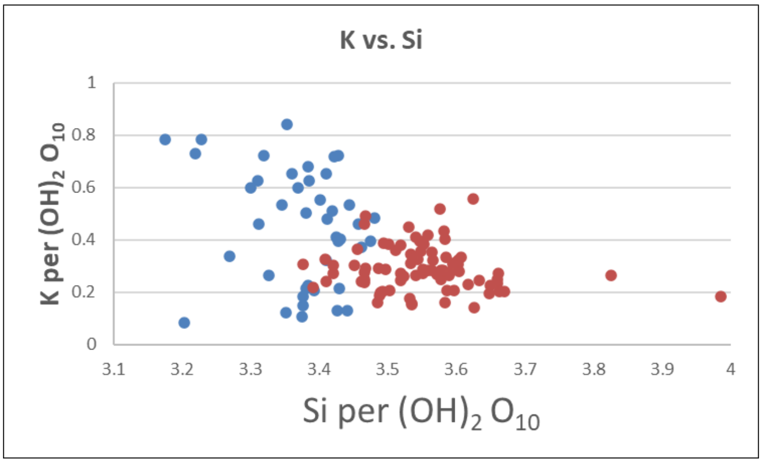

__Description:__ This diagram visualizes a trend to higher K-values in beidellitic diVS-ml / cluster1 (blue dots) than in beidellite-montmorillonite-illite-ml phases / cluster2 (red dots).

Fig. 4. *Distribution of K in interlayer space vs. tetrahedral Si [all per$(OH)_2$ O_{10}]*

Distribution of charges (exchangeable from interlayer space)

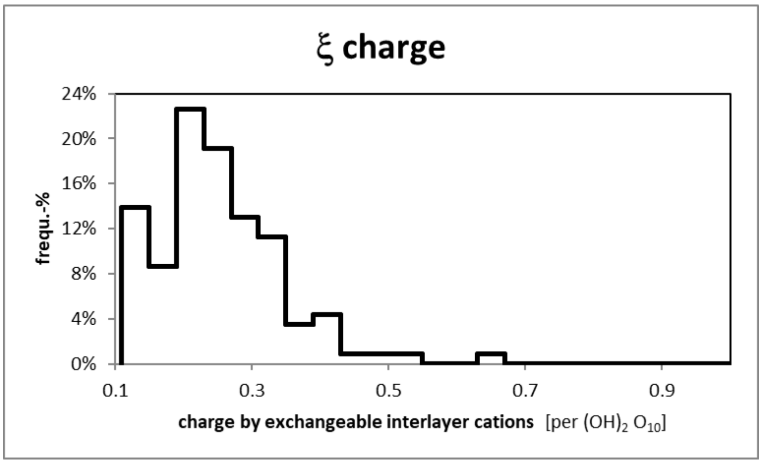

This diagram visualizes the distribution of exchangeable charges in the interlayer space (Ca, Mg, Na) determined and computed by TEM-EDX-data.

__Description:__ Bimodal distribution of charge density with (i) first maximal frequency-% at 0.15 per $(OH)_2$ O_{10} (mica) as well as (ii) at 0.23 per $(OH)_2$ O_{10} as second maximal frequency-%

Fig. 5. *Distribution of charges*

Beidellite-montmorillonite-illite-ml BMI ~60:20:20 *(Cluster2)*

$$Ca_{0.02}\ Mg_{0.10}\ Na_{0.00}\ K_{0.29}\quad Al_{1.30}\ Fe^{3+}_{0.58}\ Mg_{0.11}\ Ti_{0.02}\ (OH)_2\ \ Si_{3.55}\ Al_{0.45}\ O_{10}$$

Charge: XII = 0.54 VI = 5.91 IV = 15.55 **Σ = 22.00**
Measured particles: 81

Distribution of beidellite-montmorillonite-illite-ml phases (BMI-ml)

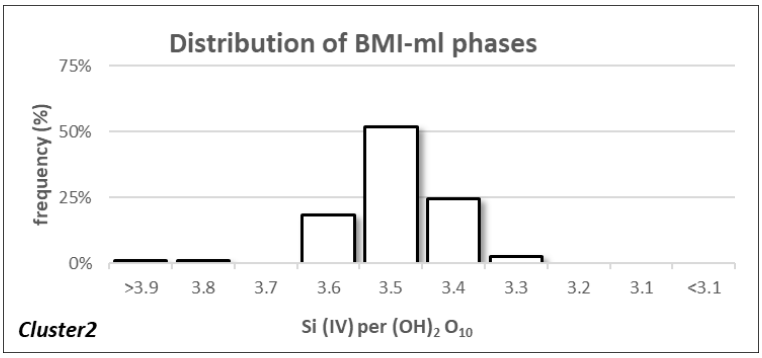

Description: *The distribution of BMI-ml phases (cluster2) draws a maximum of frequency (%) at tetrahedral Si-value between 3.5 – 3.6 e phuc.*

Fig. 6a. *Distribution of smectite layer probability (%S) in diVS-ml*

BMI 60:20:20?		*particles (abs)*	Ca (XII)	Mg (XII)	Na (XII)	K (XII)	Cr3+ (VI)	Al (VI)	Fe3+ (VI)	Mg (VI)	Ti (VI)	Al (IV)	Si (IV)	XII	n_VI	%S
Si	>3.9	n = 1	0.03	0.06	0.00	0.18	0.00	1.32	0.48	0.11	0.00	0.01	3.99	0.37	1.9	106
Si	3.9-3.8	n = 1	0.02	0.10	0.00	0.27	0.00	1.32	0.52	0.07	0.00	0.17	3.83	0.52	1.9	75
Si	3.8-3.7	n = 0														
Si	3.7-3.6	n = 15	0.02	0.08	0.00	0.27	0.00	1.28	0.60	0.12	0.00	0.36	3.64	0.47	2.0	45
Si	**3.6-3.5**	**n = 42**	**0.02**	**0.08**	**0.01**	**0.31**	**0.00**	**1.32**	**0.57**	**0.10**	**0.02**	**0.45**	**3.55**	**0.52**	**2.0**	**34**
Si	3.5-3.4	n = 20	0.03	0.13	0.00	0.29	0.00	1.28	0.60	0.10	0.02	0.54	3.46	0.62	2.0	24
Si	3.4-3.3	n = 2	0.03	0.20	0.00	0.26	0.00	1.00	0.69	0.21	0.10	0.62	3.38	0.72	2.0	16
Si	3.3-3.2	n = 0														
Si	3.2-3.1	n = 0														
Si	<3.1	n = 0														

Fig. 6b. *Computed averaged mineral formulae of phases in the different Si(IV)-classes*

Beidellitic dioctahedral Vermiculite-Smectite mixed layer phases *(beid. diVS-ml: BMI 05:20:75) (Cluster1)*

$$Ca_{0.01}\ Mg_{0.08}\ Na_{0.01}\ K_{0.45}\quad Al_{1.50}\ Fe^{3+}_{0.40}\ Mg_{0.08}\ Ti_{0.03}\ (OH)_2\ \ Si_{3.37}\ Al_{0.63}\ O_{10}$$

Charge: XII = 0.65 VI = 5.98 IV = 15.37 **Σ = 22.00**
Probability of smectite layers (%S): 25%
Probability of illite layers (%I): 75%
Measured particles: 42

Distribution of smectite layers probability (%S) in beidellitic diVS-ml

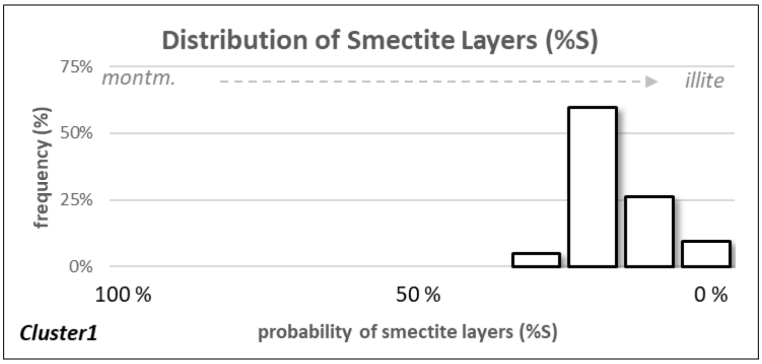

Description: *The distribution of beidellitic diVS-ml (classified as Cluster1) draws a maximum of frequency (%) for smectite layer probability at 20%*

Fig. 7a. *Distribution of smectite layers probability in diVS-ml*

beid. diVS-ml?	*particles (abs)*	Ca (XII)	Mg (XII)	Na (XII)	K (XII)	Cr3+ (VI)	Al (VI)	Fe3+ (VI)	Mg (VI)	Ti (VI)	Al (IV)	Si (IV)	XII	n_VI	%S
%S >95%	n = 0														
%S 95-85%	n = 0														
%S 85-75%	n = 0														
%S 75-65%	n = 0														
%S 65-55%	n = 0														
%S 55-45%	n = 0														
%S 45-35%	n = 0														
%S 35-25%	n = 2	0.01	0.07	0.02	0.44	0.00	1.50	0.39	0.10	0.01	0.52	3.48	0.62	2.0	26
%S 25-15%	**n = 25**	**0.02**	**0.09**	**0.01**	**0.40**	**0.00**	**1.50**	**0.41**	**0.08**	**0.02**	**0.59**	**3.41**	**0.62**	**2.0**	**19**
%S <15%	n = 15	0.01	0.07	0.01	0.54	0.00	1.49	0.39	0.08	0.05	0.70	3.30	0.72	2.0	9

Fig. 7b. *Computed averaged mineral formulae of beidellitic diVS-ml phases in the different smectite layers probability (%S)-classes*

Cluster1		Ca (XII)	Mg (XII)	Na (XII)	K (XII)	Cr3+ (VI)	Al (VI)	Fe3+ (VI)	Mg (VI)	Ti (VI)	Al (IV)	Si (IV)	XII	n_VI	%S
without illite	n = 27	0.02	0.09	0.01	0.40	0.00	1.50	0.41	0.08	0.02	0.58	3.42	0.62	2.0	19
only illite	n = 15	0.01	0.07	0.01	0.54	0.00	1.49	0.39	0.08	0.05	0.70	3.30	0.72	2.0	9

Fig. 7c. *Computed averaged mineral formulae of beidellitic diVS-ml phases differentiated by illite*

Description – Friedland Clay (< 2 µm), untreated material

Preparation for TEM

The powder of Friedland Clay-sample was suspended in deionized water and dispersed by ultrasonic treatment for approximately 20 min. The clay fraction (<2 µm) was separated by sedimentation and diluted with deionized water to get a clear suspension. The suspension was dropped onto carbon-coated Cu grids, air dried and stored under environment-controlled conditions at 45% humidity.

Mineral Matter - Overview

The fraction < 2 µm of Friedland Clay N10 sample is mainly composed by beidellite-montmorillonite-illite mixed layer phases (BMI-ml) and beidellitic dioctahedral vermiculite-smectite mixed layer phases (beid. diVS-ml). Furthermore, kaolinite and kaolinite-smectite-ml phases (with computed KSV = 60:25:15), chlorite-smectite-vermiculite mixed layer phases, Si-surplus particles (Si, e.g. quartz) and rutile were identified in traces in this sample [fig. 1].

The measured and computed particles have shown a calculated CEC-value of 32 meq / 100 g located at surface and in the interlayer space.

	frequency-% *(n = 152 measured particles)*
BMI-ml	53%
beid. diVS-ml	28%
Kaolinite & KSV-ml	5%
CSV-ml	3%
Si-surplus	7%
Ti-phases	3%
Unknown	1%

All measured dioctahedral 2:1 clay mineral phases summarized result following mineral formula computed from TEM-EDX-measurement of 123 individual particles:

	$Ca^{2+}_{0.02}$	$Mg^{2+}_{0.09}$	$Na^{+}_{0.01}$	$K^{+}_{0.35}$	$Al^{3+}_{1.36}$	$Fe^{3+}_{0.52}$	$Mg^{2+}_{0.10}$	$Ti^{4+}_{0.02}$	$(OH)_2$	$Si^{4+}_{3.49}$	$Al^{3+}_{0.51}$	O_{10}
SDOM	*± 0.00*	*± 0.00*	*± 0.00*	*± 0.01*	*± 0.02*	*± 0.01*	*± 0.01*	*± 0.00*		*± 0.01*	*± 0.01*	

Legend: SDOM - standard deviation of the mean (= the standard deviation divided by the square root of the number of samples)

The interlayer charge is calculated as 0.58 per $(OH)_2$ O_{10} and the octahedral charge as 5.93 per $(OH)_2$ O_{10}. The particles are characterized by a high octahedral Fe-amount.

The summarized chemical composition of all 123 computed particles is listed [tab. 1].

Friedland Clay, Siedlungsscholle, East-field is characterized by two morphological groups: (i) large (≤ 1 µm) xenomorph platy crystals and (ii) aggregates, partially with folds, formed by small (≤ 100 nm) xenomorphous plates [fig. 2]. Aggregates formed by small (≤ 100 nm) xenomorphous plates dominate the shapes of particles in the micrographs [fig. 2].

The distribution of %S-probability of all measured clay mineral phases [fig. 3a] also indicates the occurrence of two groups: (i) BMI- and beidellitic diVS-ml phases incl. illite with K-deficiency as well as (ii) montmorillonite (rare).

The numerous measured particles by TEM-EDX allow a visualization of distribution of interlayer charges. Considering the TEM-EDX-determined cations Ca^{++}, Mg^{++} and Na^{+} and then computed their ratio as interlayer cations in the mineral formula, Ca^{++}, Mg^{++} and Na^{+} offer to characterize the degree of exchangeable charges in the interlayer space. This charge density of Friedland Clay (< 2 µm) shows in this sample a broad interval with two maximal frequency-% of charge density at 0.15 and 0.23 per $(OH)_2\ O_{10}$ [fig. 5]. This broad interval of interlayer charge density caused by exchangeable cations from 0.10 - 0.43 per $(OH)_2\ O_{10}$ represents mainly IS-ml (lowest peak at 0.15 per $(OH)_2\ O_{10}$) and the diVS-ml phases with the other higher peak at 0.23 per $(OH)_2\ O_{10}$.

Mineral Matter - Specification

Result of Clustering

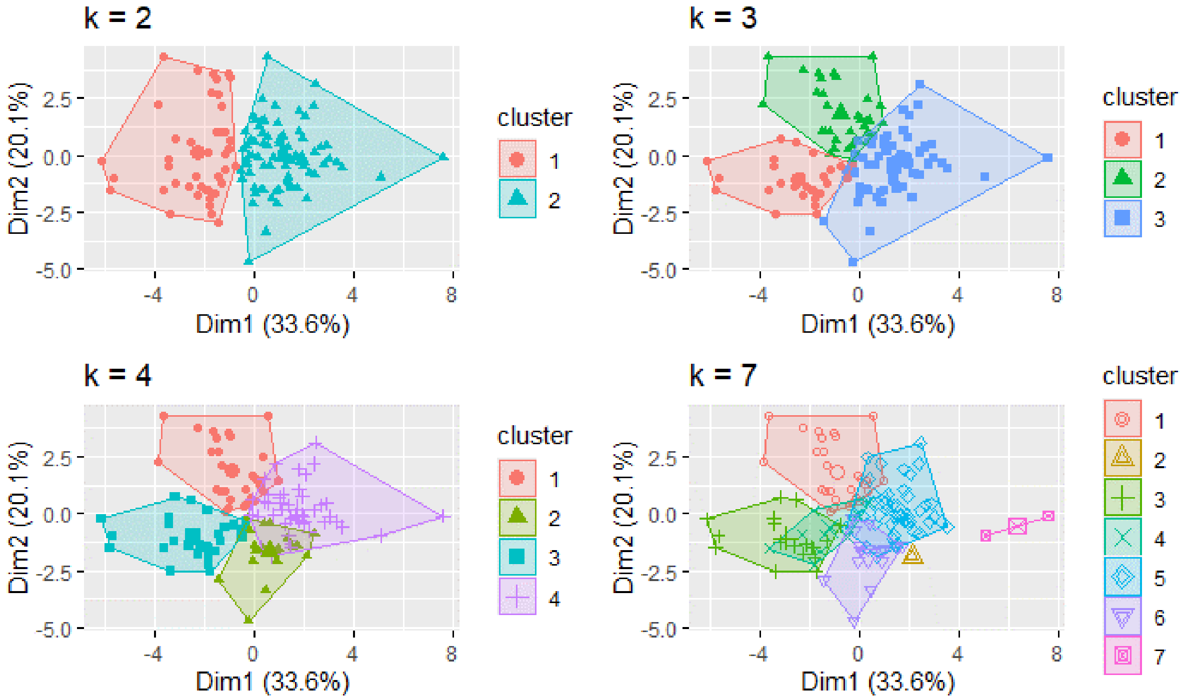

Fig. 8. *Clustering of all measured particles for clusters k = 2, k = 3, k = 4 and k = 7 (source for R-coding: https://uc-r.github.io/kmeans_clustering)*

The optimum of clusters was calculated with k = 2 and k=7.

		Ca (XII)	Mg (XII)	Na (XII)	K (XII)	Cr3+ (VI)	Al (VI)	Fe3+ (VI)	Mg (VI)	Ti (VI)	Al (IV)	Si (IV)	XII	n_VI	%S
Cluster1	n = 42	0.01	0.08	0.01	0.45	0.00	1.50	0.40	0.08	0.03	0.63	3.37	0.65	2.0	15
Cluster2	n = 81	0.02	0.10	0.00	0.29	0.00	1.30	0.58	0.11	0.02	0.45	3.55	0.54	2.0	34

Fig. 9a. *Mineral formulae based on TEM-EDX-data summarized following the result of clustering for k=2*

	Sybilla-results	**TEM-EDX-results**	**Notes**
	Illite	beid. diVS-ml (illite)	*high K-deficit, low XII-charge deficit, Al(VI)-rich, Fe(VI)-rich*
Cluster1	IS R0(2) *(%S = 25%)*	beid. diVS-ml, without illite *(BMI 05:15:75)*	*high K-deficit, charge deficit, Al(VI)-rich, Fe(VI)-rich*
Cluster2	IS R0(1) *(%S = 82%)*	BMI ~60:20:20	*XRD: Montmorillonite and beidellite is only to distinguish by Green-Kelly-test (not available here).*
	Kaolinite + KS GL R0		*in traces only*

Tab. 2. *Comparison of results from TEM-EDX- and XRD-measurements*

The TEM-EDX-data offers a good agreement with the result of Sybilla-processing of XRD-traces from oriented specimen, but only under consideration of the option beidellite [tab. 2].

IS R0 (1): The X-ray diffraction pattern of the ethylene-glycol saturated oriented specimen shows a nearby full expandability to 1.67 nm and a difference of 5.68°2θ between 2. and 3. order of smectite interferences. This distance is typically for a probability of smectite layers (%S) of 80% (Moore & Reynolds, 1989). This result of XRD-processing let expect a maximum of particles for %S ~ 80% by TEM-EDX-measurements, but the maximum of particles measured by TEM-EDX is to find at %S=40% [fig. 3a]. Using a model for beidellite-montmorillonite-illite-mixed layer phases (BMI-ml) with 3.50, 4.00 and 3.20 as tetrahedral Si-value per $(OH)_2\ O_{10}$ the calculation of member ratios offers a solution for 60% layer probability for %B and 20% for %S, if %I is given with 20% [see Cluster2 in tab. 2].

IS R0 (2): The Sybilla-procedure of XRD-traces (oriented mounts) has shown an occurrence of a second illite-smectite mixed layer phase with a smectite layers probability of %S = 25%. This situation is to find also by TEM-EDX ($\%S_{TEM}$ = 15%). Using a model for beidellite-montmorillonite-illite-mixed layer phases (BMI-ml) with 3.50, 4.00 and 3.20 as tetrahedral Si-value per $(OH)_2\ O_{10}$ the calculation of member ratios offers a solution for 5% layer probability for %B and 20% for %S, if %I is given with 75% [see Cluster2 in tab. 2]. That means, few parts of smectite layers are formed as beidellite in these phases. These phases represent remarkable K-amounts and slight charge deficit and Al- & Fe-rich, beidellitic dioctahedral vermiculite-smectite mixed layer phase (beid. diVS-ml) [tab. 2].

The Sybilla-processing of XRD-traces (oriented mounts) also supports the existence of kaolinite and kaolinite-smectite mixed layer phases in fine fraction of sample. The mineral formula was to compute for only 3 particles of KSV-ml phases (average: %K 60%, %S 26%, %V 14%).

Specifics to the identified clay mineral groups

Beidellite-montmorillonite-illite-ml (BMI-ml 60:20:20) *(Cluster2)*

81 of 123 computed particles belong so to this assumed classification. The dioctahedral character of this group is proofed by X-ray diffraction. The position of the large (060)-interference of smectite is in the random oriented powder specimen at 1.497 Å.

Montmorillonite and beidellite have the same behavior concerning the expandability and they are only to distinguish by XRD using Li by means of Greene-Kelly test (Greene-Kelly 1952, 1953). So, combination of XRD- and TEM-results (full expandability by XRD and Si ~ 3.55 by TEM-EDX) led conclude the occurrence of beidellite.

Beidellite-montmorillonite-illite-ml *(BMI 60:20:20)*

$$Ca_{0.02}\ Mg_{0.10}\ Na_{0.00}\ K_{0.29}\quad Al_{1.30}\ Fe^{3+}_{0.58}\ Mg_{0.11}\ Ti_{0.02}\ (OH)_2\quad Si_{3.55}\ Al_{0.45}\ O_{10}$$

Charge: XII = 0.54 VI = 5.91 IV = 15.45 **Σ = 22.00**
Measured particles by TEM-EDX: 81
Result of clustering: Cluster2 [tab. 2]

In this sample, beidellite is characterized by a low octahedral Mg-amount (because of high ratio of octahedral, 3-valent cations). A comparison of octahedral Mg vs. tetrahedral Si doesn't indicate any differentiation for octahedral Mg based on TEM-EDX-data [fig. 3b]. Particles of Cluster2 contain full interval of Mg(VI) from 0.0 to 0.3 per $(OH)_2\ O_{10}$ in octahedral layer.

Using the results of TEM-EDX data processing (see cluster2 in tab. 2), the maximum of frequency-% is to find for particles at 3.5-3.6e phuc [tab. 6a]. The mineral formulae, summarized in classes of %S, draws for the maximum an Fe-rich BMI-ml with low Mg(VI), but remarkable amount of K in the interlayer space [tab. 6b].

Beidellitic dioctahedral vermiculite-smectite mixed layer phase (Cluster1)

(beid. diVS-ml, %S = 25%, without illite)

$$Ca_{0.02}\ Mg_{0.09}\ Na_{0.01}\ K_{0.40}\quad Al_{1.50}\ Fe^{3+}_{0.40}\ Mg_{0.08}\ Ti_{0.02}\ (OH)_2\quad Si_{3.42}\ Al_{0.58}\ O_{10}$$

Charge: XII = 0.62 VI = 5.96 IV = 15.42 **Σ = 22.00**

Probability of smectite layers (%S): 25%

Probability of illite layers (%I): 75%

Measured particles by TEM-EDX: 27

Illite as part of beid. diVS-ml series

$$Ca_{0.01}\ Mg_{0.07}\ Na_{0.01}\ K_{0.54}\quad Al_{1.49}\ Fe^{3+}_{0.39}\ Mg_{0.08}\ Ti_{0.05}\ (OH)_2\quad Si_{3.30}\ Al_{0.70}\ O_{10}$$

Charge: XII = 0.72 VI = 5.99 IV = 15.30 **Σ = 22.00**

Probability of smectite layers (%S): 9%

Probability of illite layers (%I): 91%

Measured particles by TEM-EDX: 15

Kaolinite-montmorillonite mixed layer phases

The Excel-based procedure (Hoang-Minh et al., 2019) to identify possible clay mineral groups using the TEM-EDX-measurements also includes algorithms to classify kaolinite and kaolinite-montmorillonite mixed layer phases. These algorithms could identify such phases basing on the measured TEM-EDX-data for only 3 particles. Such particles have shown small hexagonal plates typically for kaolinite-bearing phases.

References

Cliff, G. & Lorimer, G. W. (1975). *J. Microsc.* **103**, 203–207.

Döbelin, N., Kleeberg, R. (2015). *Journal of Applied Crystallography* **48**, 1573-1580. DOI: 10.1107/S1600576715014685

Henning, K.-H. & Störr, M. (1986). Electron Micrographs (TEM, SEM) of Clays and Clay Minerals, p. 325. Akademie-Verlag Berlin.

Hoang-Minh, T., Kasbohm, J., Nguyen-Thanh, L., Nga, P. T., Lai, L. T., Duong, N. T., Thanh, N. D., Thuyet, N. T. M., Anh, D. D., Pusch, R., Knutsson, S. & Ferreiro Mahlmann, R. (2019). *J. Appl. Cryst.* **52**, 133-147. DOI: 10.1107/S1600576718018162

Lorimer, G. W. & Cliff, G. (1976). *Electron Microscopy in Mineralogy*, edited by H. R. Wenk, pp. 506–519. Berlin: Springer Verlag.

Matschiavelli, N., Kluge, S., Podlech, C., Standhaft, D., Grathoff, G., Ikeda-Ohno, A., Warr, L.N., Chukharkina, A., Arnold, T. & Cherkouk, A. (2019). *Environmental Science & Technology.* **53** (17), 10514-10524, DOI: 10.1021/acs.est.9b02670

Mellini, M. & Menichini, R. (1985). *R. Soc. Ital. Miner. Petrol.* **40**, 261–266.

Moore, D.M., Reynolds, R.C. (1989). X-ray Diffraction and the Identification and Analysis of Clay Minerals, Oxford University Press, New York, 332 + xvi pp.

Nguyen-Thanh, L., Herbert, H.-J., Kasbohm, J., Hoang-Minh, T. & Mählmann, R. F. (2014). *Clays Clay Miner.* **62**, 425–446.

Środoń, J., Elsass, F., McHardy, W. J. & Morgan, D. J. (1992). *Clay Miner.* **27**, 137–158.

Data Sheet – Friedland clay, treated materials *(OPA, 35 °C, VSC)*

Methodology - Transmission electron microscopy linked with energy-dispersive X-ray spectroscopy (TEM-EDX)

It is expected a characterization of clay mineral phases in treated Friedland Clay by transmission electron microscopy. This report describes the results of treated material from Friedland Clay percolated at a temperature of 35°C.

The different clay mineral phases are to identify and to describe by chemical composition and its variability, morphology, the specific dissolution potential, and further parameter.

Such further parameter like distribution of smectite layers probability (%S) and distribution of charges caused by exchangeable cations interlayer space should serve as additional indicators for mineralogical alterations in treatment experiments with Friedland Clay.

The sample were suspended for TEM-measurement in deionized water and dispersed by ultrasonic treatment for approximately 20 min. The clay fraction (<2 µm) was separated by sedimentation and diluted with deionized water to get a clear suspension. The suspension was dropped onto carbon-coated Cu grids, air dried and stored under environment-controlled conditions at 45% humidity.

TEM-EDX investigations were carried out on the <2 µm fraction using a FEI TECNAI G^2 20 electron transmission microscope at the VNU University of Science, Vietnam National University, Hanoi. This equipment (operated at 200 kV with LaB_6 cathode) was combined with an S-TWIN objective, a windowless EDAX energy-dispersive X-ray system and a FEI Eagle 2k CCD TEM camera.

About 100 individual clay particles per sample were characterized by TEM-EDX with respect to crystal size, crystal habit, and particle morphology and element distribution. The crystal size, crystal habit and particle morphology were described according to Henning & Störr (1986).

For the quantification of element distribution, a calibration of k factors is mandatory (Cliff & Lorimer, 1975; Lorimer & Cliff, 1976; Mellini & Menichini, 1985). These k values are used to calibrate for the specific behaviour of particles against possible irradiation damage. The elements O, Na, Mg, Al, Si, K, Ca and Fe were quantified by applying the EDAX GENESIS–TEM Quant Materials quantification procedure.

In this procedure, the acquired EDX spectra are corrected by background subtraction, Gaussian deconvolution and k-factor corrections using values previously determined on a phyllosilicate standard (muscovite) and selected non-phyllosilicate standards. The average errors in the analyzed elements using the phyllosilicate standard, expressed as the atomic proportions, are 10 (Na), 5 (Fe, Mg, K, Ti, Ca) and 1 (Si, Al).

The measurement time per particle was lowered to 20 s and the exposed area was limited to a 50 nm diameter, avoiding possible irradiation damage of particles. The stability of particles of the sample series was tested for this measurement time at the beginning of any measurement campaign.

Further methodological details related to TEM-EDX-measurements and the Excel-based mathematical procedure using TEM-EDX data for calculation of mineral formulae are described in Hoang-Minh et al. (2019).

These mathematical procedures described in Hoang-Minh et al. (2019) were extended by k-means clustering method for finding subgroups of observations within a data set. The data were standardized

(i.e., scaled) to make variables comparable. Euclidean distances were applied as classical method for distance measures. The optimal clusters were determined by Elbow method and Gap statistics[27].

---

[27] *https://uc-r.github.io/kmeans_clustering*

Data Sheet – Friedland Clay N10 (< 2 µm), treated material *(35°C)*

Preparation for TEM

- raw material: compacted material (1.6 g/cm³) of treated Friedland Clay-sample
- suspension on particles < 2 µm on carbon-filmed Cu-grid
- air-dried and humidity-controlled storing

Mineral Matter

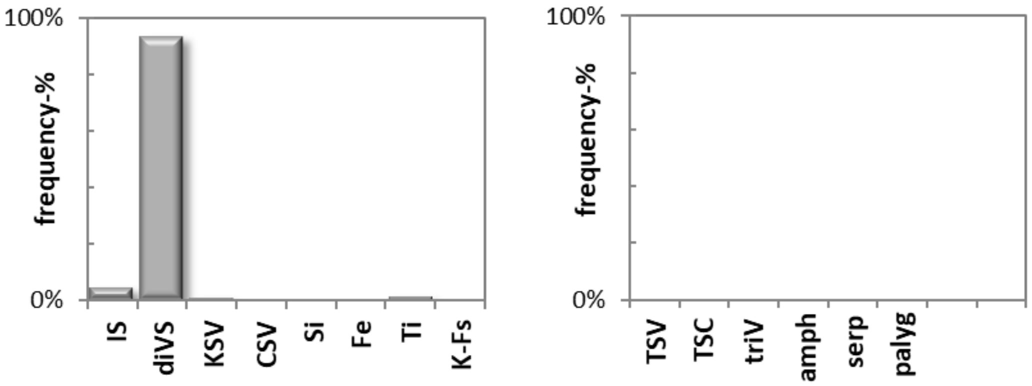

Fig. 1. *Distribution of mineral groups in fraction < 2 µm (in frequency-%)*
Legend: ***IS*** *– illite-smectite-mixed layer series in sense of Środon et al. (1992), diVS – dioctahedral vermiculite-smectite illite-smectite-mixed layer series (= charge- and/or K-deficit),* ***KSV*** *– kaolinite-smectite-dioctahedral vermiculite-mixed layer series,* ***CSV*** *– chlorite-saponite-trioctahedral vermiculite-mixed layer series,* ***Si*** *– quartz or particles with Si-surplus,* ***Fe*** *– Fe-oxide or Fe-oxyhydroxide,* ***Ti*** *– Ti-bearing phases (e.g. rutile, anatase),* ***K-Fs*** *– K-feldspar*

Clay Mineral Composition

All particles of smectite group:

$$Ca_{0.04}\ Mg_{0.04}\ Na_{0.13}\ K_{0.35}\quad Al_{1.25}\ Fe^{3+}_{0.56}\ Mg_{0.17}\ Ti_{0.02}\ (OH)_2\quad Si_{3.50}\ Al_{0.50}\ O_{10}$$

Charge: XII = 0.65 VI = 5.85 IV = 15.50 **Σ = 22.00**
Probability of smectite layers (%S): 29%
Probability of illite layers (%I): 71%

Specific Dissolution Potential (ΔS%)

for H2O, 20 + 60 rpm -33 (= fast reacting, interlayer group: Ca+Mg (= type B))
for NaCl, 20 rpm -38 (= fast reacting, interlayer group: Ca+Mg (= type B))
for NaCl, 60 rpm -15 (= moderate reacting, ‘illitization’, interlayer group: Na (= type A))
CEC$_{calc}$: 56 meq / 100 g

Measured particles: 137

Table 1. *Summarized chemical composition*

SiO_2	**TiO_2**	**Al_2O_3**	**Fe_2O_3**	**MnO**	**MgO**	**CaO**	**Na_2O**	**K_2O**	**P_2O_5**	**Σ**	
59.3%	0.3%	26.1%	6.3%		2.8%	0.5%	1.4%	3.3%	0.0%	1.00	measured particles of treated sample
59.4%	0.3%	28.1%	5.9%		2.5%	0.3%	0.1%	3.3%	0.1%	1.00	measured particles of original Friedland Clay

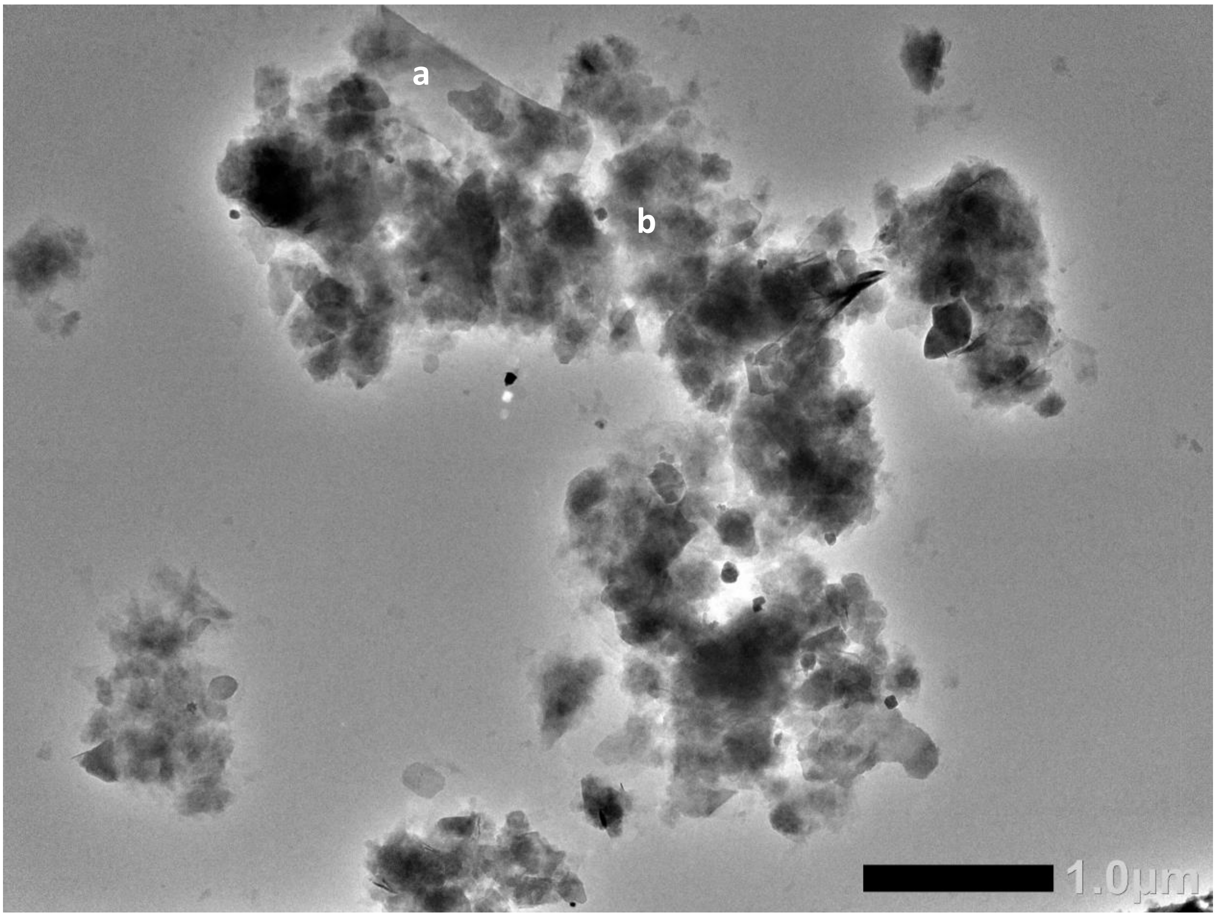

JEM-2100_JEOL_007_MAG_X8000.bmp

Magnification: 8k

(a) large (≤ 1 µm) xenomorph platy crystals;
(b) Aggregates formed by small (≤ 100 nm) xenomorphous plates

Fig. 2. *Morphology of particles (TEM-micrographs)*

Distribution of smectite layers probability (%S)

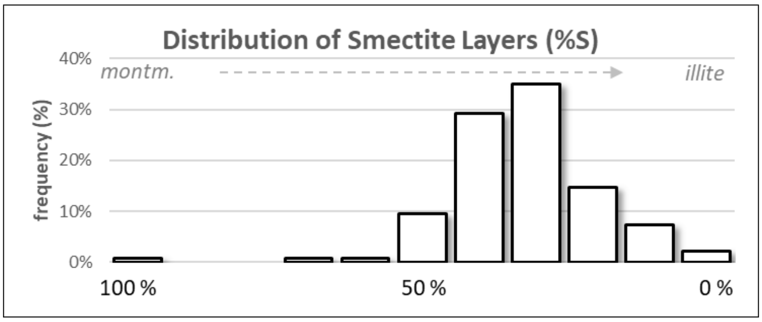

Description: *The distribution of %S-probability indicates the occurrence of two groups: (i) diVS-ml and beidellite-montmorillonite-illite-ml phases as well as (ii) illite with K-deficiency.*

Fig. 3a. *Distribution of smectite layers probability (%S)*

Differentiation by relation “Octahedral Mg vs. tetrahedral Si”?

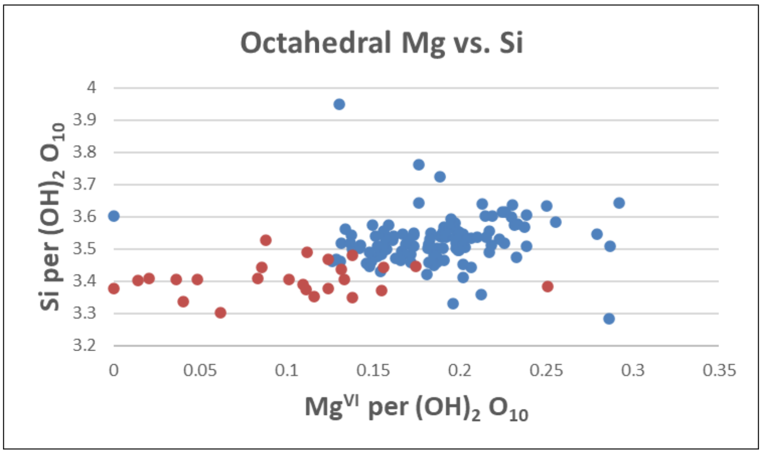

Description: *This diagram indicates a separation on low and high ratio of Mg in relation to tetrahedral Si (red dots – Cluster1: diVS-ml only; blue dots – Cluster2: BMI-ml).*

Fig. 3b. *Distribution of octahedral Mg vs. tetrahedral Si [all per(OH)$_2$ O$_{10}$]*

Distribution of K in relation to tetrahedral Si

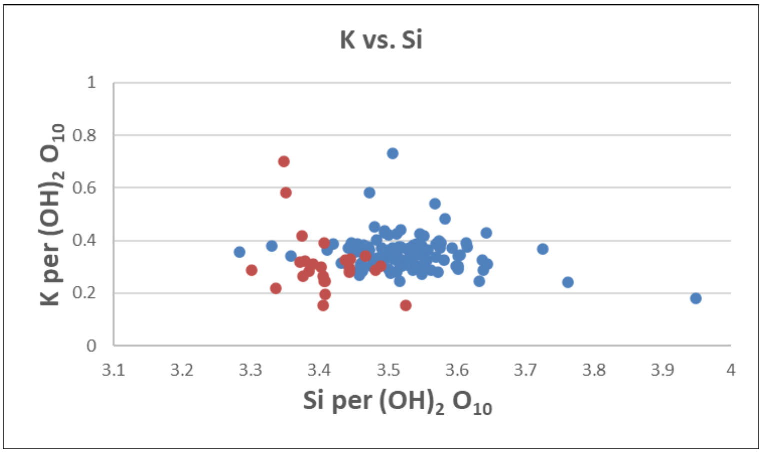

Description: *This diagram visualizes a similar K-distribution in beidellite-montmorillonite-illite-ml phases (blue dots) and in diVS-ml phases (red dots).*

Fig. 4. *Distribution of K in interlayer space vs. tetrahedral Si [all per(OH)$_2$ O$_{10}$]*

Distribution of charges (exchangeable from interlayer space)

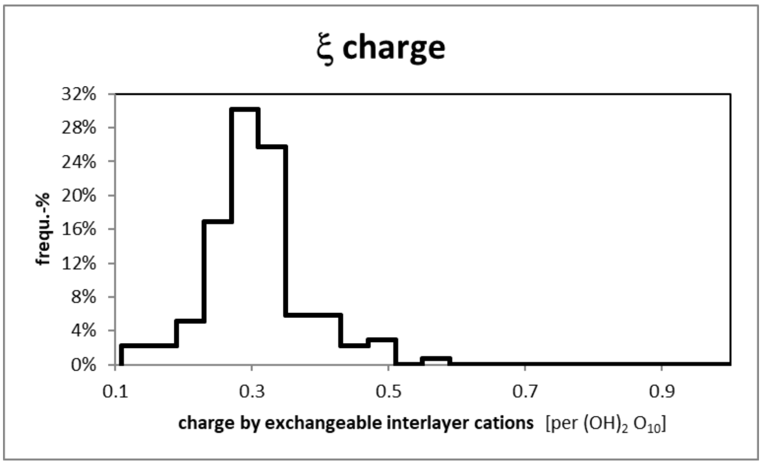

This diagram visualizes the distribution of exchangeable charges in the interlayer space (Ca, Mg, Na) determined and computed by TEM-EDX-data.

Description: *Distribution of charge density with maximal frequency-% at 0.31 per (OH)$_2$ O$_{10}$*

Fig. 5. *Distribution of charges*

Beidellite-montmorillonite-illite-ml BMI ~65:15:20 *(Cluster2):*

$$Ca_{0.04}\ Mg_{0.03}\ Na_{0.14}\ K_{0.35}\quad Al_{1.21}\ Fe^{3+}_{0.58}\ Mg_{0.19}\ Ti_{0.02}\ (OH)_2\quad Si_{3.53}\ Al_{0.47}\ O_{10}$$

Charge: XII = 0.64 VI = 5.83 IV = 15.53 **Σ = 22.00**

Measured particles: 112

Distribution of beidellite-montmorillonite-illite-ml phases (BMI-ml)

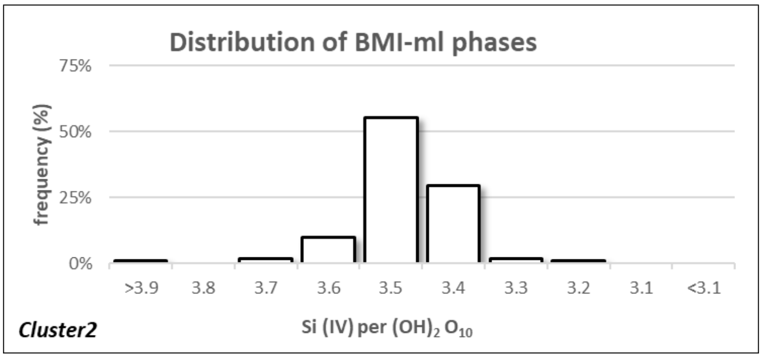

Description: *The distribution of BMI-ml phases (cluster2) draws a maximum of frequency (%) at tetrahedral Si-value between 3.5 – 3.6 e phuc.*

Fig. 6a. *Distribution of assumed beidellite-montmorillonite-illite-ml phases*

BMI 65:15:20?		particles (abs)	Ca (XII)	Mg (XII)	Na (XII)	K (XII)	Cr3+ (VI)	Al (VI)	Fe3+ (VI)	Mg (VI)	Ti (VI)	Al (IV)	Si (IV)	XII	n_VI	%S
Si	>3.9	n = 1	0.04	0.04	0.07	0.18	0.00	1.42	0.38	0.13	0.00	0.05	3.95	0.41	1.9	99
Si	3.9-3.8	n = 0														
Si	3.8-3.7	n = 2	0.04	0.04	0.05	0.30	0.00	1.18	0.60	0.18	0.01	0.26	3.74	0.51	2.0	61
Si	3.7-3.6	n = 11	0.04	0.02	0.13	0.33	0.00	1.14	0.65	0.21	0.00	0.38	3.62	0.59	2.0	43
Si	**3.6-3.5**	**n = 62**	**0.04**	**0.03**	**0.14**	**0.36**	**0.00**	**1.23**	**0.57**	**0.19**	**0.01**	**0.46**	**3.54**	**0.64**	**2.0**	**32**
Si	3.5-3.4	n = 33	0.04	0.04	0.13	0.36	0.00	1.21	0.57	0.17	0.04	0.53	3.47	0.66	2.0	24
Si	3.4-3.3	n = 2	0.04	0.02	0.15	0.36	0.00	0.93	0.64	0.20	0.23	0.66	3.34	0.63	2.0	13
Si	3.3-3.2	n = 1	0.11	0.00	0.25	0.36	0.00	0.92	0.62	0.29	0.17	0.72	3.28	0.83	2.0	8
Si	3.2-3.1	n = 0														
Si	<3.1	n = 0														

Fig. 6b. *Computed averaged mineral formulae of phases in the different Si(IV)-classes*

Dioctahedral Vermiculite-Smectite mixed layer phases (diVS-ml) *(Cluster1):*

$$Ca_{0.04}\ Mg_{0.09}\ Na_{0.13}\ K_{0.31}\quad Al_{1.43}\ Fe^{3+}_{0.46}\ Mg_{0.10}\ Ti_{0.01}\ (OH)_2\quad Si_{3.41}\ Al_{0.59}\ O_{10}$$

Charge: XII = 0.69 VI = 5.90 IV = 15.41 **Σ = 22.00**

Probability of smectite layers (%S): 18%

Probability of illite layers (%I): 82%

Measured particles: 25

Distribution of smectite layers probability (%S) in diVS-ml (Cluster1)

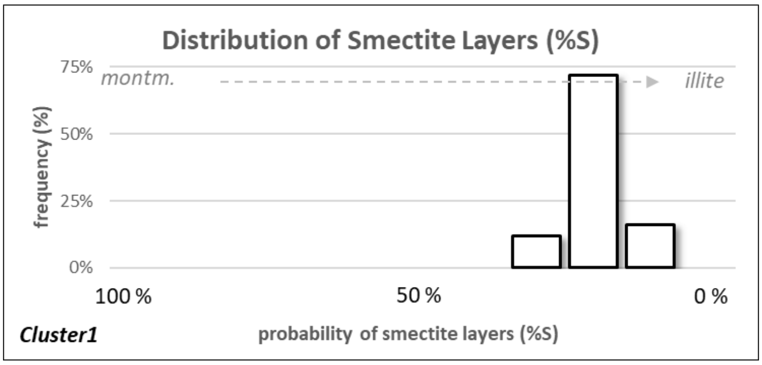

Description: *The distribution of diVS-ml (classified as Cluster1) draws a maximum of frequency (%) for smectite layer probability at 20%*

Fig. 7a. *Distribution of smectite layers probability in diVS-ml*

diVS-ml?	particles (abs)	Ca (XII)	Mg (XII)	Na (XII)	K (XII)	Cr3+ (VI)	Al (VI)	Fe3+ (VI)	Mg (VI)	Ti (VI)	Al (IV)	Si (IV)	XII	n_VI	%S
%S >95%	n = 0														
%S 95-85%	n = 0														
%S 85-75%	n = 0														
%S 75-65%	n = 0														
%S 65-55%	n = 0														
%S 55-45%	n = 0														
%S 45-35%	n = 0														
%S 35-25%	n = 3	0.05	0.06	0.14	0.25	0.00	1.43	0.45	0.11	0.00	0.50	3.50	0.61	2.0	28
%S 25-15%	**n = 18**	**0.04**	**0.09**	**0.13**	**0.29**	**0.00**	**1.41**	**0.47**	**0.10**	**0.01**	**0.59**	**3.41**	**0.68**	**2.0**	**19**
%S <15%	n = 4	0.02	0.07	0.14	0.45	0.00	1.49	0.41	0.09	0.00	0.67	3.33	0.76	2.0	12

Fig. 7b. *Computed averaged mineral formulae of diVS-ml phases in the different smectite layers probability (%S)-classes*

Cluster1		Ca (XII)	Mg (XII)	Na (XII)	K (XII)	Cr3+ (VI)	Al (VI)	Fe3+ (VI)	Mg (VI)	Ti (VI)	Al (IV)	Si (IV)	XII	n_VI	%S
without illite	n = 21	0.04	0.09	0.13	0.29	0.00	1.42	0.47	0.10	0.01	0.58	3.42	0.67	2.0	20
only illite	n = 4	0.02	0.07	0.14	0.45	0.00	1.49	0.41	0.09	0.00	0.67	3.33	0.76	2.0	12

Fig. 7c. *Computed averaged mineral formulae of diVS-ml phases differentiated by illite*

Description – Friedland Clay N10 (< 2 µm), treated material *(35°C)*

Preparation for TEM

The powder of Friedland Clay-sample was suspended in deionized water and dispersed by ultrasonic treatment for approximately 20 min. The clay fraction (<2 µm) was separated by sedimentation and diluted with deionized water to get a clear suspension. The suspension was dropped onto carbon-coated Cu grids, air dried and stored under environment-controlled conditions at 45% humidity.

Mineral Matter - Overview

The fraction < 2 µm of Friedland Clay N10 sample is mainly composed by beidellite-montmorillonite-illite mixed layer phases (BMI-ml) and beidellitic dioctahedral vermiculite-smectite mixed layer phases (beid. diVS-ml). Rarely, kaolinite and kaolinite-smectite-ml phases and rutile were identified in traces in this sample [fig. 1].

The measured and computed particles have shown a calculated CEC-value of 56 meq / 100 g located at surface and in the interlayer space.

	frequency-% *(n = 140 measured particles)*
BMI-ml	80%
beid. diVS-ml	18%
Kaolinite & KSV-ml	1%
Ti-phases	1%

All measured dioctahedral 2:1 clay mineral phases summarized result following mineral formula computed from TEM-EDX-measurement of 137 individual particles:

$$Ca^{2+}_{0.04}\ Mg^{2+}_{0.04}\ Na^{+}_{0.13}\ K^{+}_{0.35}\quad Al^{3+}_{1.25}\ Fe^{3+}_{0.56}\ Mg^{2+}_{0.17}\ Ti^{4+}_{0.02}\ (OH)_2\quad Si^{4+}_{3.50}\ Al^{3+}_{0.50}\ O_{10}$$

SDOM *± 0.00 ± 0.00 ± 0.00 ± 0.01 ± 0.01 ± 0.01 ± 0.00 ± 0.00 ± 0.01 ± 0.01*

Legend: SDOM - standard deviation of the mean (= the standard deviation divided by the square root of the number of samples)

The interlayer charge is calculated as 0.65 per $(OH)_2\ O_{10}$ and the octahedral charge as 5.85 per $(OH)_2\ O_{10}$. The particles are characterized by a high octahedral Fe-amount.

The summarized chemical composition of all 137 computed particles is listed [tab. 1].

Friedland Clay N10 sample is also characterized by two morphological groups: (i) large (≤ 1 µm) xenomorph platy crystals and (ii) aggregates, partially with folds, formed by small (≤ 100 nm) xenomorphous plates [fig. 2]. Aggregates formed by small (≤ 100 nm) xenomorphous plates dominate the shapes of particles in the micrographs [fig. 2].

The distribution of %S-probability of all measured clay mineral phases [fig. 3a] also indicates the occurrence of two groups: (i) beid. diVS-ml and beidellite-montmorillonite-illite-ml phases as well as (ii) illite with K-deficiency.

The numerous measured particles by TEM-EDX allow a visualization of distribution of interlayer charges. Considering the TEM-EDX-determined cations Ca^{++}, Mg^{++} and Na^{+} and then computed their ratio as interlayer cations in the mineral formula, Ca^{++}, Mg^{++} and Na^{+} offer to characterize the degree of exchangeable charges in the interlayer space. This charge density of Friedland Clay N10 (< 2 µm) shows in this sample a maximal frequency-% of charge density at 0.31 per $(OH)_2$ O_{10} [fig. 5]. This interval of interlayer charge density caused by exchangeable cations from 0.23 - 0.35 per $(OH)_2$ O_{10} represents beid. diVS-ml and beidellite-montmorillonite-illite-ml.

Mineral Matter - Specification

Result of Clustering

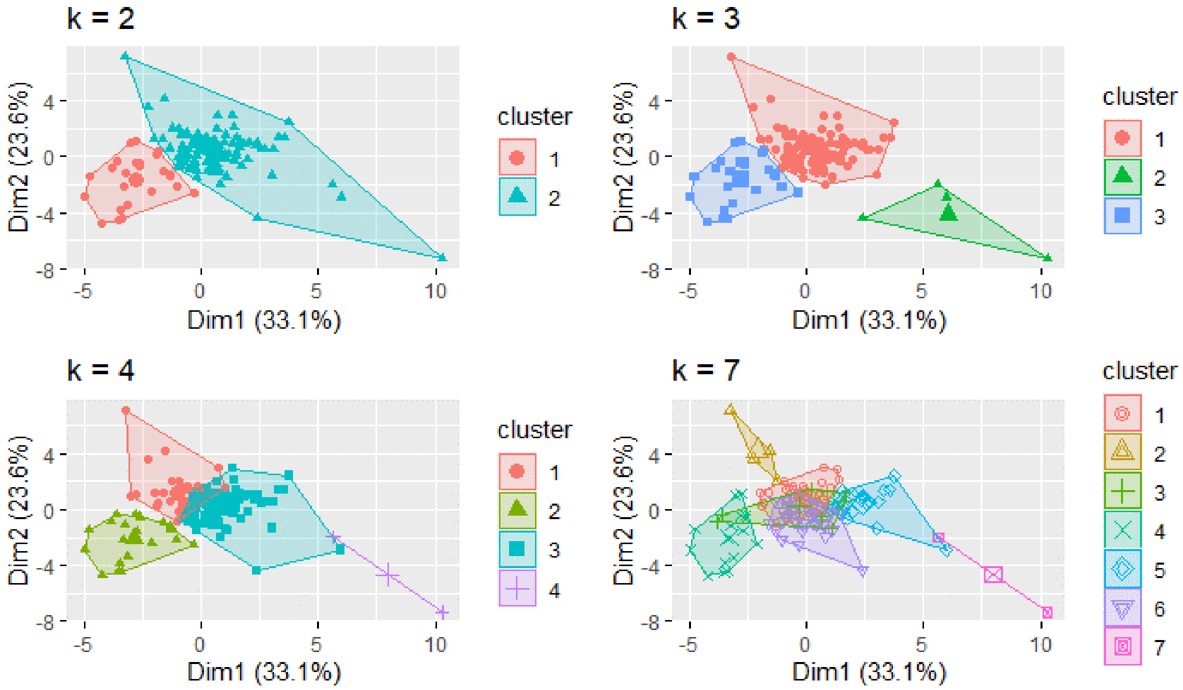

Fig. 8. *Clustering of all measured particles for clusters k = 2, k = 3, k = 4 and k = 7 (source for R-coding: https://uc-r.github.io/kmeans_clustering)*

The optimum of clusters was calculated with k = 2.

		Ca (XII)	Mg (XII)	Na (XII)	K (XII)	Cr3+ (VI)	Al (VI)	Fe3+ (VI)	Mg (VI)	Ti (VI)	Al (IV)	Si (IV)	XII	n_VI	%S
Cluster1	n = 25	0.04	0.09	0.13	0.31	0.00	1.43	0.46	0.10	0.01	0.59	3.41	0.69	2.0	18
Cluster2	n = 112	0.04	0.03	0.14	0.35	0.00	1.21	0.58	0.19	0.02	0.47	3.53	0.64	2.0	31

Fig. 9a. *Mineral formulae based on TEM-EDX-data summarized following the result of clustering for k=2*

	Sybilla-results	TEM-EDX-results	Notes
	Illite	diVS-ml (illite)	*strong K-deficit, low XII-charge deficit, Fe(VI)-rich*
Cluster1	ISS R1 *(%S = 34%)*	BMI ~15:20:65	*high K-deficit, XII-charge deficit, Al(VI)-rich, Fe(VI)-rich*
Cluster2	IS R0(1) *(%S = 100%)*	BMI ~65:15:20	*XRD: Montmorillonite and beidellite is only to distinguish by Green-Kelly-test (not available here).*
	Kaolinite + KS GL R0		*in traces only*

Tab. 2. *Comparison of results from TEM-EDX- and XRD-measurements*

The TEM-EDX-data offers a good agreement with the result of Sybilla-processing of XRD-traces from oriented specimen, but only under consideration of the option beidellite [tab. 2].

IS R0 (1): The X-ray diffraction pattern of the ethylene-glycol saturated oriented specimen shows a full expandability to 1.77 nm and a difference of 5.42°2θ between 2. and 3. order of smectite interferences. This distance is typically for a probability of smectite layers (%S) of 100% (Moore & Reynolds, 1989). This result of XRD-pattern processing let expect a maximum of particles for %S ~ 100% by TEM-EDX-measurements, but the maximum of particles measured by TEM-EDX is to find at %S = 30% [fig. 3a]. Using a model for beidellite-montmorillonite-illite-mixed layer phases (BMI-ml) with 3.50, 4.00 and 3.20 as tetrahedral Si-value per $(OH)_2\,O_{10}$ the calculation of member ratios offers a solution for 95% layer probability for %B and 5% for %S, if %I is given with 0% [see Cluster2 in tab. 2], close to a pure beidellite.

IS R0 (2): The Sybilla-procedure of XRD-traces (oriented mounts) has shown an occurrence of a second illite-smectite mixed layer phase with a smectite layers probability of %S = 34%. This result of XRD-pattern processing let expect a maximum of particles for %S ~ 34% by TEM-EDX-measurements, but the maximum of particles measured by TEM-EDX is to find at %S = 18% [tab. 2]. Using a model for beidellite-montmorillonite-illite-mixed layer phases (BMI-ml) with 3.50, 4.00 and 3.20 as tetrahedral Si-value per $(OH)_2\,O_{10}$ the calculation of member ratios offers a solution for 15% layer probability for %B and 20% for %S, if %I is given with 65% [see Cluster1 in tab. 2].

The Sybilla-processing of XRD-traces (oriented mounts) also supports low amount of kaolinite and kaolinite-smectite mixed layer phases in fine fraction of sample.

Specifics to the identified clay mineral groups

Beidellite-montmorillonite-illite-ml (BMI-ml 95:05:00) *(Cluster2)*

112 of 137 computed particles belong so to this assumed classification. The dioctahedral character of this group is proofed by X-ray diffraction. The position of the large (060)-interference of smectite is in the random oriented powder specimen at 1.497 Å.

Montmorillonite and beidellite have the same behavior concerning the expandability and they are only to distinguish by XRD using Li by means of Greene-Kelly test (Greene-Kelly 1952, 1953). So, combination of XRD- and TEM-results (full expandability by XRD and Si ~ 3.53 by TEM-EDX) led conclude the occurrence of beidellite.

Beidellite-montmorillonite-illite-ml *(BMI 95:05:00)*

$$Ca_{0.04}\,Mg_{0.03}\,Na_{0.14}\,K_{0.35}\quad Al_{1.21}\,Fe^{3+}_{0.58}\,Mg_{0.19}\,Ti_{0.02}\,(OH)_2\quad Si_{3.53}\,Al_{0.47}\,O_{10}$$

Charge:	XII = 0.64	VI = 5.83	IV = 15.53	**Σ = 22.00**

Measured particles by TEM-EDX: 112
Result of clustering: Cluster2 [tab. 2]

In this sample, beidellite is characterized by a low octahedral Mg-amount (because of high ratio of octahedral, 3-valent cations). A comparison of octahedral Mg vs. tetrahedral Si indicates a differentiation for octahedral Mg based on TEM-EDX-data [fig. 3b]. Particles of Cluster2 contain commonly Mg(VI) > 0.15 per $(OH)_2\ O_{10}$ in octahedral layer.

The mineral formulae, summarized in classes of %S, draws for the maximum an Fe-rich BMI-ml with low Mg(VI), but remarkable amount of K in the interlayer space [tab. 6b].

Beidellitic dioctahedral vermiculite-smectite mixed layer phase

(beid. diVS-ml, BMI 15:20:65, Cluster1)

$$\boxed{Ca_{0.04}\ Mg_{0.09}\ Na_{0.13}\ K_{0.31}\quad Al_{1.43}\ Fe^{3+}_{0.46}\ Mg_{0.10}\ Ti_{0.01}\ (OH)_2\ \ Si_{3.41}\ Al_{0.59}\ O_{10}}$$

Charge: XII = 0.69 VI = 5.90 IV = 15.41 **Σ = 22.00**
Probability of smectite layers (%S): 18%
Probability of illite layers (%I): 82%
Measured particles by TEM-EDX: 25

Kaolinite-montmorillonite mixed layer phases

The Excel-based procedure (Hoang-Minh et al., 2019) to identify possible clay mineral groups using the TEM-EDX-measurements also includes algorithms to classify kaolinite and kaolinite-montmorillonite mixed layer phases. These algorithms couldn’t compute no such phases basing on the measured TEM-EDX-data. Such particles have shown small hexagonal plates typically for kaolinite-bearing phases.

References

Cliff, G. & Lorimer, G. W. (1975). *J. Microsc.* **103**, 203–207.

Döbelin, N., Kleeberg, R. (2015). *Journal of Applied Crystallography* **48**, 1573-1580. DOI: 10.1107/S1600576715014685

Henning, K.-H. & Störr, M. (1986). Electron Micrographs (TEM, SEM) of Clays and Clay Minerals, p. 325. Akademie-Verlag Berlin.

Hoang-Minh, T., Kasbohm, J., Nguyen-Thanh, L., Nga, P. T., Lai, L. T., Duong, N. T., Thanh, N. D., Thuyet, N. T. M., Anh, D. D., Pusch, R., Knutsson, S. & Ferreiro Mahlmann, R. (2019). *J. Appl. Cryst.* **52**, 133-147. DOI: 10.1107/S1600576718018162

Lorimer, G. W. & Cliff, G. (1976). *Electron Microscopy in Mineralogy*, edited by H. R. Wenk, pp. 506–519. Berlin: Springer Verlag.

Mellini, M. & Menichini, R. (1985). *R. Soc. Ital. Miner. Petrol.* **40**, 261–266.

Moore, D.M., Reynolds, R.C. (1989). X-ray Diffraction and the Identification and Analysis of Clay Minerals, Oxford University Press, New York, 332 + xvi pp.

Nguyen-Thanh, L., Herbert, H.-J., Kasbohm, J., Hoang-Minh, T. & Mählmann, R. F. (2014). *Clays Clay Miner.* **62**, 425–446.

Środoń, J., Elsass, F., McHardy, W. J. & Morgan, D. J. (1992). *Clay Miner.* **27**, 137–158.

Methodology - Transmission electron microscopy linked with energy-dispersive X-ray spectroscopy (TEM-EDX)

It is expected a characterization of clay mineral phases in treated Friedland Clay by transmission electron microscopy. This report describes the results of treated material from Friedland Clay percolated at a temperature of 60°C.

The different clay mineral phases are to identify and to describe by chemical composition and its variability, morphology, the specific dissolution potential, and further parameter.

Such further parameter like distribution of smectite layers probability (%S) and distribution of charges caused by exchangeable cations interlayer space should serve as additional indicators for mineralogical alterations in treatment experiments with Friedland Clay.

The sample were suspended for TEM-measurement in deionized water and dispersed by ultrasonic treatment for approximately 20 min. The clay fraction (<2 µm) was separated by sedimentation and diluted with deionized water to get a clear suspension. The suspension was dropped onto carbon-coated Cu grids, air dried and stored under environment-controlled conditions at 45% humidity.

TEM-EDX investigations were carried out on the <2 µm fraction using a FEI TECNAI G^2 20 electron transmission microscope at the VNU University of Science, Vietnam National University, Hanoi. This equipment (operated at 200 kV with LaB_6 cathode) was combined with an S-TWIN objective, a windowless EDAX energy-dispersive X-ray system and a FEI Eagle 2k CCD TEM camera.

About 100 individual clay particles per sample were characterized by TEM-EDX with respect to crystal size, crystal habit, particle morphology and element distribution. The crystal size, crystal habit and particle morphology were described according to Henning & Störr (1986).

For the quantification of element distribution, a calibration of k factors is mandatory (Cliff & Lorimer, 1975; Lorimer & Cliff, 1976; Mellini & Menichini, 1985). These k values are used to calibrate for the specific behaviour of particles against possible irradiation damage. The elements O, Na, Mg, Al, Si, K, Ca and Fe were quantified by applying the EDAX GENESIS–TEM Quant Materials quantification procedure.

In this procedure, the acquired EDX spectra are corrected by background subtraction, Gaussian deconvolution and k-factor corrections using values previously determined on a phyllosilicate standard (muscovite) and selected non-phyllosilicate standards. The average errors in the analyzed elements using the phyllosilicate standard, expressed as the atomic proportions, are 10 (Na), 5 (Fe, Mg, K, Ti, Ca) and 1 (Si, Al).

The measurement time per particle was lowered to 20 s and the exposed area was limited to a 50 nm diameter, avoiding possible irradiation damage of particles. The stability of particles of the sample series was tested for this measurement time at the beginning of any measurement campaign.

Further methodological details related to TEM-EDX-measurements and the Excel-based mathematical procedure using TEM-EDX data for calculation of mineral formulae are described in Hoang-Minh et al. (2019).

These mathematical procedures described in Hoang-Minh et al. (2019) were extended by k-means clustering method for finding subgroups of observations within a data set. The data were standardized (i.e., scaled) to make variables comparable. Euclidean distances were applied as classical method for distance measures. The optimal clusters were determined by Elbow method and Gap statistics[28].

---

[28] *https://uc-r.github.io/kmeans_clustering*

Data Sheet – Friedland Clay N11 (< 2 µm), treated material *(60°C)*

Preparation for TEM

- raw material: compacted material (1.6 g/cm³) of treated Friedland Clay-sample
- suspension on particles < 2 µm on carbon-filmed Cu-grid
- air-dried and humidity-controlled storing

Mineral Matter

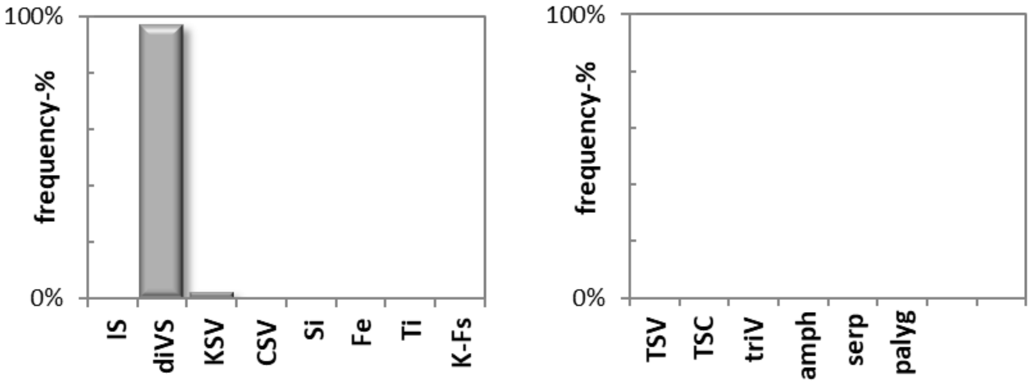

Fig. 1. *Distribution of mineral groups in fraction < 2 µm (in frequency-%)*
Legend: ***IS*** *– illite-smectite-mixed layer series in sense of Środon et al. (1992), diVS – dioctahedral vermiculite-smectite illite-smectite-mixed layer series (= charge- and/or K-deficit),* ***KSV*** *– kaolinite-smectite-dioctahedral vermiculite-mixed layer series,* ***CSV*** *– chlorite-saponite-trioctahedral vermiculite-mixed layer series,* ***Si*** *– quartz or particles with Si-surplus,* ***Fe*** *– Fe-oxide or Fe-oxyhydroxide,* ***Ti*** *– Ti-bearing phases (e.g. rutile, anatase),* ***K-Fs*** *– K-feldspar*

Clay Mineral Composition

All particles of smectite group:

$$\mathrm{Ca_{0.09}\,Mg_{0.03}\,Na_{0.03}\,K_{0.32}\quad Al_{1.21}\,Fe^{3+}_{0.60}\,Mg_{0.18}\,Ti_{0.02}\,(OH)_2\quad Si_{3.53}\,Al_{0.47}\,O_{10}}$$

Charge: XII = 0.60 VI = 5.87 IV = 15.53 **Σ = 22.00**
Probability of smectite layers (%S): 32%
Probability of illite layers (%I): 68%

Specific Dissolution Potential (ΔS%)

for H2O, 20 + 60 rpm -23 (= fast reacting, interlayer group: Ca+Mg (= type B))
for NaCl, 20 rpm -26 (= fast reacting, interlayer group: Ca+Mg (= type B))
for NaCl, 60 rpm -56 (= fast reacting, 'illitization', interlayer group: Na (= type A))
$\mathrm{CEC_{calc}}$: 41 meq / 100 g

Measured particles: 137

Table 1. *Summarized chemical composition*

SiO_2	TiO_2	Al_2O_3	Fe_2O_3	MnO	MgO	CaO	Na_2O	K_2O	P_2O_5	Σ	
60.3%	0.3%	25.4%	6.8%		2.7%	1.1%	0.3%	3.0%	0.0%	1.00	measured particles of treated sample
59.4%	0.3%	28.1%	5.9%		2.5%	0.3%	0.1%	3.3%	0.1%	1.00	measured particles of original Friedland Clay

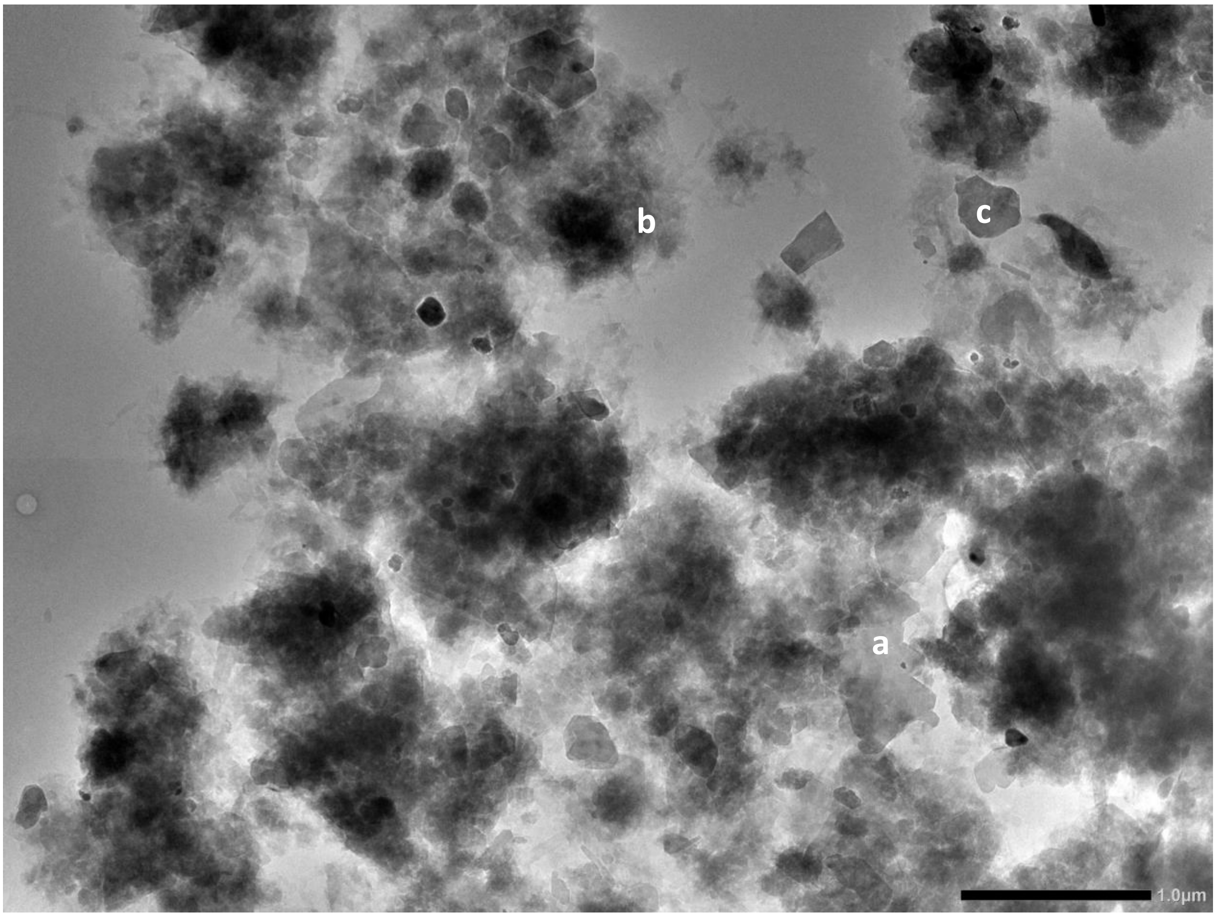

JEM-2100_JEOL_014_MAG_X8000.bmp

Magnification: 8k

(a) large (≤ 1 μm) xenomorph platy crystals;
(b) aggregates formed by small (≤ 100 nm) xenomorphous plates;
(c) hypidiomorph hexagonal plates

Fig. 2. *Morphology of particles (TEM-micrographs)*

Distribution of smectite layers probability (%S)

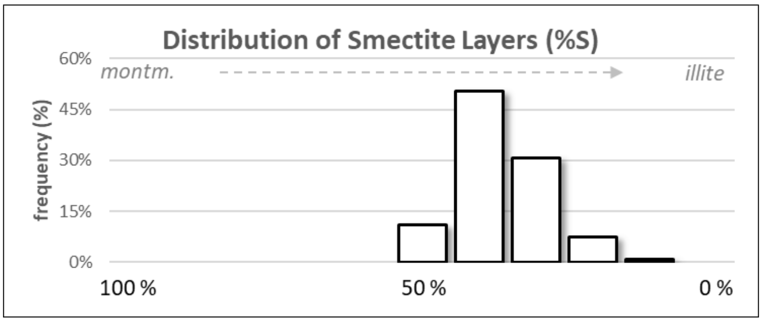

Description: *The distribution of %S-probability indicates the occurrence of only one group?*

Fig. 3a. *Distribution of smectite layers probability (%S)*

Differentiation by relation “Octahedral Mg vs. tetrahedral Si”?

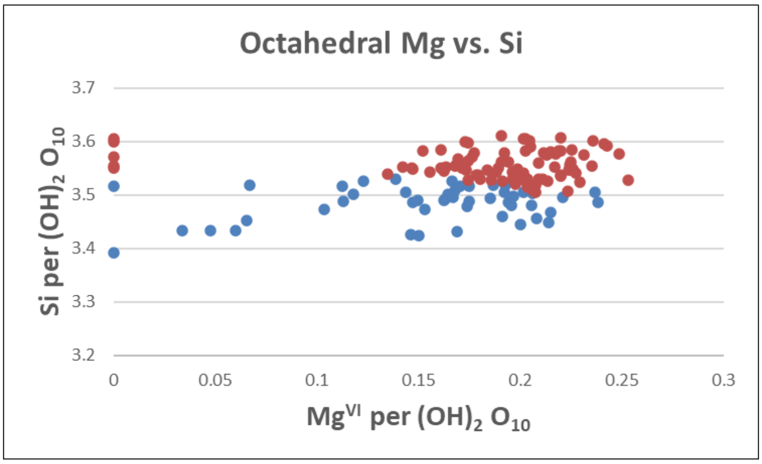

Fig. 3b. *Distribution of octahedral Mg vs. tetrahedral Si [all per$(OH)_2$ O_{10}]*

Description: *This diagram indicates for the most particles a missing relation of Mg in comparison to tetrahedral Si (blue dots – Cluster1: diVS-ml; red dots – Cluster2: BMI-ml).*

Distribution of K in relation to tetrahedral Si

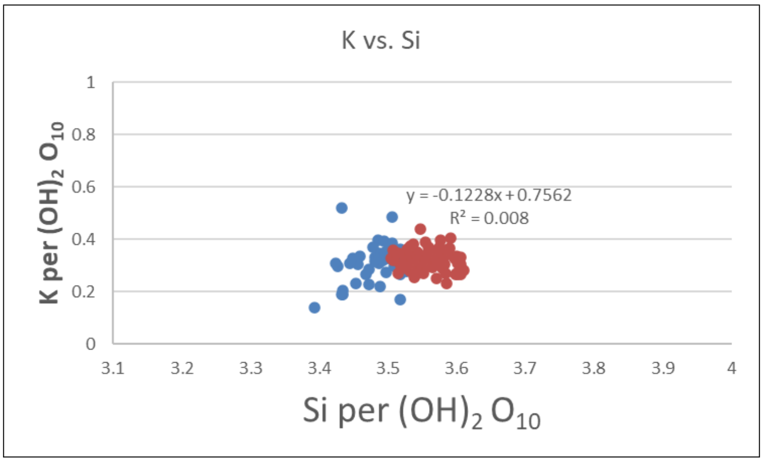

Description: *This diagram visualizes for the most particles a missing relation of K in comparison to tetrahedral Si (blue dots – Cluster1: diVS-ml; red dots – Cluster2: BMI-ml).*

Fig. 4. *Distribution of K in interlayer space vs. tetrahedral Si [all per$(OH)_2$ O_{10}]*

Distribution of charges (exchangeable from interlayer space)

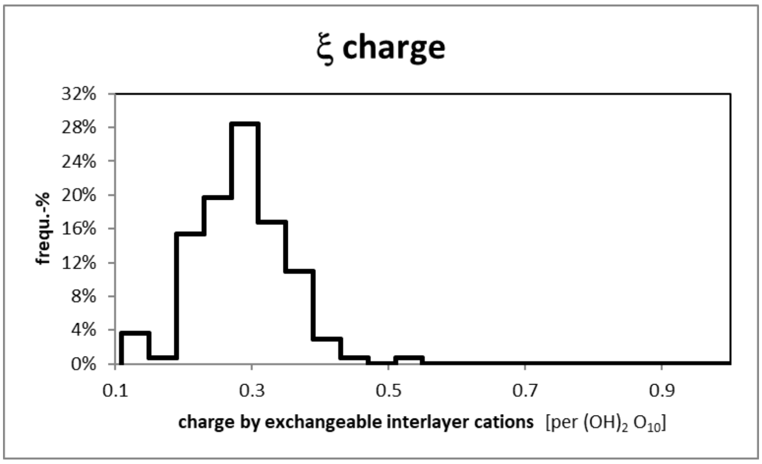

This diagram visualizes the distribution of exchangeable charges in the interlayer space (Ca, Mg, Na) determined and computed by TEM-EDX-data.

Description: *Distribution of charge density with maximal frequency-% at 0.27 per $(OH)_2$ O_{10}*

Fig. 5. *Distribution of charges*

Dioctahedral Vermiculite-Smectite mixed layer phases (diVS-ml) *(Cluster1)*

$$\mathrm{Ca_{0.10}\ Mg_{0.05}\ Na_{0.03}\ K_{0.31}\quad Al_{1.24}\ Fe^{3+}_{0.58}\ Mg_{0.15}\ Ti_{0.03}\ (OH)_2\ \ Si_{3.48}\ Al_{0.52}\ O_{10}}$$

Charge: XII = 0.64 VI = 5.88 IV = 15.48 **Σ = 22.00**

Probability of smectite layers (%S):	26%
Probability of illite layers (%I):	74%
Measured particles:	49

Distribution of smectite layers probability (%S) in diVS-ml (Cluster1)

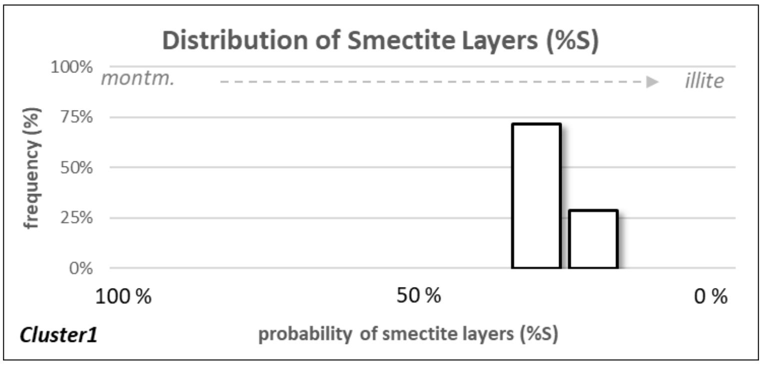

Description: *The distribution of diVS-ml phases draws a maximum of frequency (%) at 30% of smectite layer probability (%S).*

Fig. 6a. *Distribution of smectite layer probability (%S) in diVS-ml*

diVS-ml?	*particles (abs)*	Ca (XII)	Mg (XII)	Na (XII)	K (XII)	Cr3+ (VI)	Al (VI)	Fe3+ (VI)	Mg (VI)	Ti (VI)	Al (IV)	Si (IV)	XII	n_VI	%S
%S >95%	n = 0														
%S 95-85%	n = 0														
%S 85-75%	n = 0														
%S 75-65%	n = 0														
%S 65-55%	n = 0														
%S 55-45%	n = 0														
%S 45-35%	n = 0														
%S 35-25%	**n = 35**	**0.09**	**0.04**	**0.04**	**0.32**	**0.00**	**1.22**	**0.59**	**0.17**	**0.02**	**0.50**	**3.50**	**0.64**	**2.0**	**28**
%S 25-15%	n = 14	0.10	0.06	0.03	0.27	0.00	1.29	0.54	0.13	0.05	0.56	3.44	0.63	2.0	22
%S <15%	n = 0														

Fig. 6b. *Computed averaged mineral formulae of phases in the different Si(IV)-classes*

Beidellite-montmorillonite-illite-ml BMI ~80:15:05 *(Cluster2):*

$$\mathrm{Ca_{0.09}\ Mg_{0.02}\ Na_{0.03}\ K_{0.32}\quad Al_{1.20}\ Fe^{3+}_{0.61}\ Mg_{0.19}\ Ti_{0.02}\ (OH)_2\ \ Si_{3.56}\ Al_{0.44}\ O_{10}}$$

Charge: XII = 0.58 VI = 5.86 IV = 15.56 **Σ = 22.00**

Measured particles: 88

Distribution of beidellite-montmorillonite-illite-ml phases (BMI-ml)

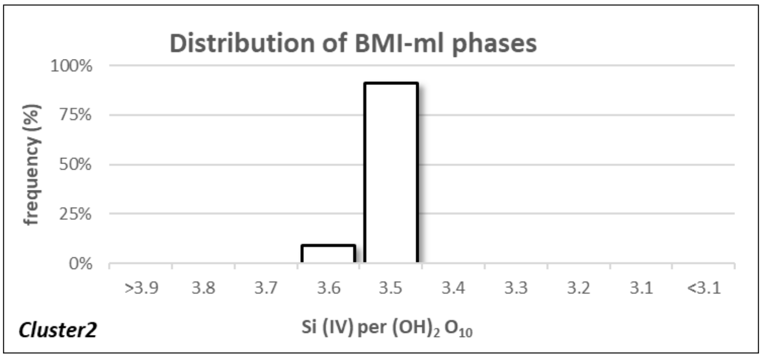

Description: *The distribution of BMI-ml phases (cluster2) draws a maximum of frequency (%) at tetrahedral Si-value between 3.5 – 3.6 e phuc.*

Fig. 7a. *Distribution of assumed beidellite-montmorillonite-illite-ml phases*

BMI 55:25:20?	particles (abs)	Ca (XII)	Mg (XII)	Na (XII)	K (XII)	Cr3+ (VI)	Al (VI)	Fe3+ (VI)	Mg (VI)	Ti (VI)	Al (IV)	Si (IV)	XII	n_VI	%S
Si >3.9	n = 0														
Si 3.9-3.8	n = 0														
Si 3.8-3.7	n = 0														
Si 3.7-3.6	n = 8	0.09	0.02	0.03	0.29	0.00	1.20	0.62	0.18	0.01	0.40	3.60	0.53	2.0	41
Si 3.6-3.5	**n = 80**	**0.09**	**0.02**	**0.03**	**0.32**	**0.00**	**1.20**	**0.61**	**0.19**	**0.02**	**0.45**	**3.55**	**0.58**	**2.0**	**34**
Si 3.5-3.4	n = 0														
Si 3.4-3.3	n = 0														
Si 3.3-3.2	n = 0														
Si 3.2-3.1	n = 0														
Si <3.1	n = 0														

Fig. 7b. *Computed averaged mineral formulae of phases in the different Si(IV)-classes*

Description – Friedland Clay N11 (< 2 µm), treated material *(60°C)*

Preparation for TEM

The powder of Friedland Clay-sample was suspended in deionized water and dispersed by ultrasonic treatment for approximately 20 min. The clay fraction (<2 µm) was separated by sedimentation and diluted with deionized water to get a clear suspension. The suspension was dropped onto carbon-coated Cu grids, air dried and stored under environment-controlled conditions at 45% humidity.

Mineral Matter - Overview

The fraction < 2 µm of Friedland Clay N11 sample is mainly composed by beidellite-montmorillonite-illite mixed layer phases (BMI-ml) and dioctahedral vermiculite-smectite mixed layer phases (diVS-ml). Rarely, kaolinite and kaolinite-smectite-ml phases and rutile were identified in traces in this sample [fig. 1].

The measured and computed particles have shown an calculated CEC-value of 56 meq / 100 g located at surface and in the interlayer space.

	frequency-% *(n = 141 measured particles)*
BMI-ml	62%
diVS-ml	35%
Kaolinite & KSV-ml	1%
Ti-phases	1%

All measured dioctahedral 2:1 clay mineral phases summarized result following mineral formula computed from TEM-EDX-measurement of 137 individual particles:

$$Ca^{2+}_{0.09}\ Mg^{2+}_{0.03}\ Na^{+}_{0.03}\ K^{+}_{0.31}\quad Al^{3+}_{1.22}\ Fe^{3+}_{0.59}\ Mg^{2+}_{0.17}\ Ti^{4+}_{0.02}\ (OH)_2\quad Si^{4+}_{3.53}\ Al^{3+}_{0.47}\ O_{10}$$

SDOM *± 0.00 ± 0.00 ± 0.00 ± 0.00 ± 0.01 ± 0.01 ± 0.00 ± 0.00 ± 0.00 ± 0.00*

Legend: SDOM - standard deviation of the mean (= the standard deviation divided by the square root of the number of samples)

The interlayer charge is calculated as 0.60 per $(OH)_2\ O_{10}$ and the octahedral charge as 5.87 per $(OH)_2\ O_{10}$. The particles are characterized by a high octahedral Fe-amount.

The summarized chemical composition of all 137 computed particles is listed [tab. 1].

Friedland Clay N11 sample is also characterized by two morphological groups: (i) large (≤ 1 µm) xenomorph platy crystals and (ii) aggregates formed by small (≤ 100 nm) xenomorphous plates [fig. 2]. Aggregates formed by small (≤ 100 nm) xenomorphous plates dominate the shapes of particles in the micrographs [fig. 2]. Furthermore, in few rare cases, there are also to identify particles formed by hypidiomorph hexagonal plates [fig. 2].

The distribution of %S-probability of all measured clay mineral phases [fig. 3a] also indicates the occurrence of one group of phases?

The numerous measured particles by TEM-EDX allow a visualization of distribution of interlayer charges. Considering the TEM-EDX-determined cations Ca^{++}, Mg^{++} and Na^{+} and then computed their ratio as interlayer cations in the mineral formula, Ca^{++}, Mg^{++} and Na^{+} offer to characterize the degree of exchangeable charges in the interlayer space. This charge density of Friedland Clay N11 (< 2 µm) shows in this sample a maximal frequency-% of charge density at 0.27 per $(OH)_2 O_{10}$ [fig. 5] embedded in a broader interval of interlayer charge density caused by exchangeable cations from 0.19 - 0.43 per $(OH)_2 O_{10}$.

Mineral Matter - Specification

Result of Clustering

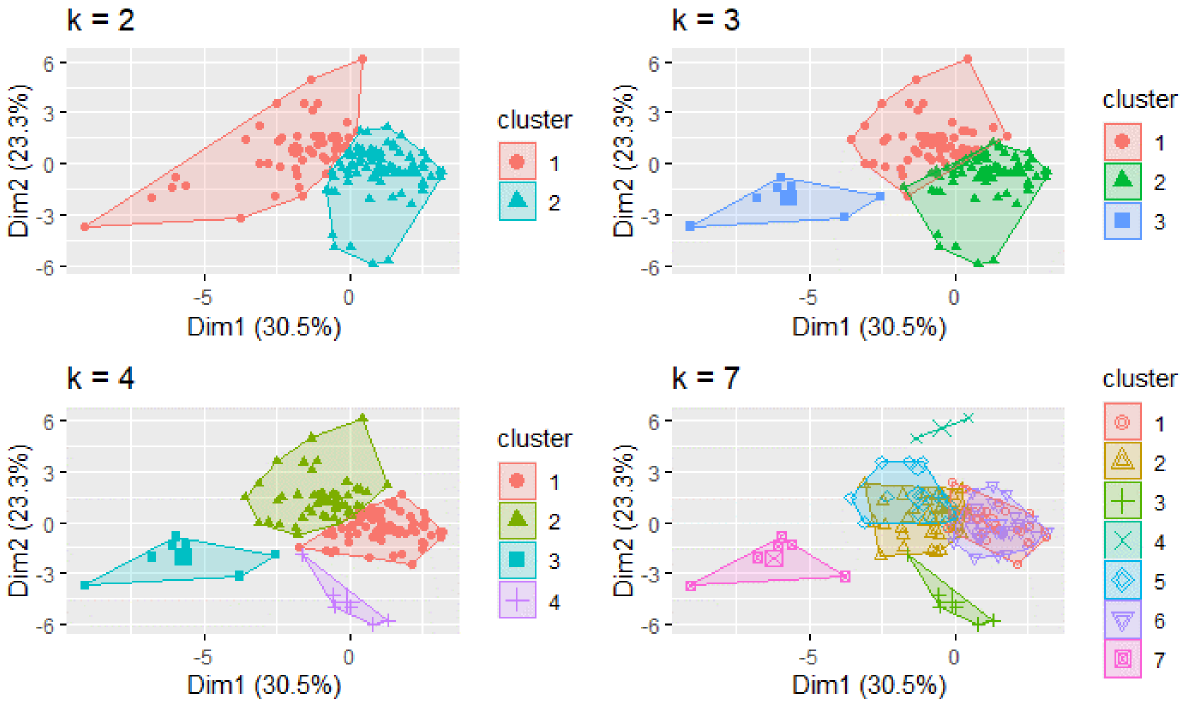

Fig. 8. *Clustering of all measured particles for clusters k = 2, k = 3, k = 4 and k = 7 (source for R-coding: https://uc-r.github.io/kmeans_clustering)*

The optimum of clusters was calculated at k = 1, 2, 4 and 9.

		Ca (XII)	Mg (XII)	Na (XII)	K (XII)	Cr3+ (VI)	Al (VI)	Fe3+ (VI)	Mg (VI)	Ti (VI)	Al (IV)	Si (IV)	XII	n_VI	%S
Cluster1	n = 49	0.10	0.05	0.03	0.31	0.00	1.24	0.58	0.15	0.03	0.52	3.48	0.63	2.0	26
Cluster2	n = 88	0.09	0.02	0.03	0.32	0.00	1.20	0.61	0.19	0.02	0.44	3.56	0.58	2.0	35

Fig. 9a. *Mineral formulae based on TEM-EDX-data summarized following the result of clustering for k=2*

	Sybilla-results	**TEM-EDX-results**	**Notes**
	Illite	not to identify	
Cluster 2	IS R0(1) *(%S = 94%)*	BMI ~80:15:05	*XRD: Montmorillonite and beidellite are only to distinguish by Green-Kelly-test (not available here).*
Cluster 1	ISS R1 *(%S = 34%)*	diVS-ml *(%S ~ 26%)*	*high K-deficit, XII-charge deficit, Al(VI)-rich, Fe(VI)-rich*
	Kaolinite + KS GL R0		*in traces only*

Tab. 2. *Comparison of results from TEM-EDX- and XRD-measurements*

The TEM-EDX-data offers a sufficient agreement with the result of Sybilla-processing of XRD-traces from oriented specimen, but only under consideration of the option beidellite [tab. 2].

IS R0 (1): The X-ray diffraction pattern of the ethylene-glycol saturated oriented specimen shows a full expandability to 1.75 nm and a difference of $5.62^\circ 2\theta$ between 2. and 3. order of smectite interferences. This distance is typically for a probability of smectite layers (%S) of 94% (Moore & Reynolds, 1989). This result of XRD-processing let expect a maximum of particles for %S ~ 94% by TEM-EDX-measurements, but the maximum of particles measured by TEM-EDX is to find at %S=40% [fig. 3a]. Using a model for beidellite-montmorillonite-illite-mixed layer phases (BMI-ml) with 3.50, 4.00 and 3.20 as tetrahedral Si-value per $(OH)_2\ O_{10}$ the calculation of member ratios offers a solution for 80% layer probability for %B and 15% for %S, if %I is given with 5% [see Cluster2 in tab. 2].

IS R0 (2): The Sybilla-procedure of XRD-traces (oriented mounts) has shown an occurrence of a second illite-smectite mixed layer phase with a smectite layers probability of %S = 34%. A similar situation is to find by TEM-EDX ($\%S_{TEM}$ = 26 %), representing remarkable K- and charge deficit and Fe-rich dioctahedral vermiculite-smectite mixed layer phase (diVS-ml) [see Cluster1 in tab. 2].

The Sybilla-processing of XRD-traces (oriented mounts) also supports low amount of illite, kaolinite and kaolinite-smectite mixed layer phases in fine fraction of sample.

Specifics to the identified clay mineral groups

Beidellite-montmorillonite-illite-ml (BMI-ml 80:15:05) *(Cluster2)*

88 of 137 computed particles belong so to this assumed classification. The dioctahedral character of this group is proofed by X-ray diffraction. The position of the large (060)-interference of smectite is in the random oriented powder specimen at 1.497 Å.

Montmorillonite and beidellite have the same behavior concerning the expandability and they are only to distinguish by XRD using Li by means of Greene-Kelly test (Greene-Kelly 1952, 1953). So, combination of XRD- and TEM-results (full expandability by XRD and Si ~ 3.56 by TEM-EDX) led conclude the occurrence of beidellite.

Beidellite-montmorillonite-illite-ml *(BMI 80:15:05)*

$$Ca_{0.09}\,Mg_{0.02}\,Na_{0.03}\,K_{0.32}\quad Al_{1.20}\,Fe^{3+}_{0.61}\,Mg_{0.19}\,Ti_{0.02}\,(OH)_2\quad Si_{3.56}\,Al_{0.44}\,O_{10}$$

Charge: XII = 0.58 VI = 5.86 IV = 15.56 **Σ = 22.00**
Measured particles by TEM-EDX: 88
Result of clustering: Cluster2 [tab. 2]

In this sample, beidellite is characterized by a low octahedral Mg-amount (because of high ratio of octahedral, 3-valent cations). A comparison of octahedral Mg vs. tetrahedral Si indicates a differentiation for octahedral Mg based on TEM-EDX-data [fig. 3b]. Particles of Cluster2 contain commonly Mg(VI) > 0.15 per $(OH)_2\ O_{10}$ in octahedral layer.

Using the results of TEM-EDX data processing (see cluster2 in tab. 2), the maximum of frequency-% is to find for particles at 3.5 -3.6e phuc [tab. 6a]. The mineral formulae, summarized in classes of %S, draws for the maximum an Fe-rich BMI-ml with low Mg(VI), but remarkable amount of K in the interlayer space [tab. 6b].

Dioctahedral vermiculite-smectite mixed layer phase *(diVS-ml, %S = 26%, Cluster1)*

$$Ca_{0.10}\ Mg_{0.05}\ Na_{0.03}\ K_{0.31}\quad Al_{1.24}\ Fe^{3+}_{0.58}\ Mg_{0.15}\ Ti_{0.03}\ (OH)_2\quad Si_{3.48}\ Al_{0.52}\ O_{10}$$

Charge:	XII = 0.64	VI = 5.88	IV = 15.48	**Σ = 22.00**
Probability of smectite layers (%S):	26%			
Probability of illite layers (%I):	74%			
Measured particles by TEM-EDX:	49			

Kaolinite-montmorillonite mixed layer phases

The Excel-based procedure (Hoang-Minh et al., 2019) to identify possible clay mineral groups using the TEM-EDX-measurements also includes algorithms to classify kaolinite and kaolinite-montmorillonite mixed layer phases. These algorithms couldn’t compute no such phases basing on the measured TEM-EDX-data. Such particles have shown small hypidiomorph hexagonal plates typically for kaolinite-bearing phases.

References

Cliff, G. & Lorimer, G. W. (1975). *J. Microsc.* **103**, 203–207.

Döbelin, N., Kleeberg, R. (2015). *Journal of Applied Crystallography* **48**, 1573-1580. DOI: 10.1107/S1600576715014685

Henning, K.-H. & Störr, M. (1986). Electron Micrographs (TEM, SEM) of Clays and Clay Minerals, p. 325. Akademie-Verlag Berlin.

Hoang-Minh, T., Kasbohm, J., Nguyen-Thanh, L., Nga, P. T., Lai, L. T., Duong, N. T., Thanh, N. D., Thuyet, N. T. M., Anh, D. D., Pusch, R., Knutsson, S. & Ferreiro Mahlmann, R. (2019). *J. Appl. Cryst.* **52**, 133-147. DOI: 10.1107/S1600576718018162

Lorimer, G. W. & Cliff, G. (1976). *Electron Microscopy in Mineralogy*, edited by H. R. Wenk, pp. 506–519. Berlin: Springer Verlag.

Mellini, M. & Menichini, R. (1985). *R. Soc. Ital. Miner. Petrol.* **40**, 261–266.

Moore, D.M., Reynolds, R.C. (1989). X-ray Diffraction and the Identification and Analysis of Clay Minerals, Oxford University Press, New York, 332 + xvi pp.

Nguyen-Thanh, L., Herbert, H.-J., Kasbohm, J., Hoang-Minh, T. & Mählmann, R. F. (2014). *Clays Clay Miner.* **62**, 425–446.

Środoń, J., Elsass, F., McHardy, W. J. & Morgan, D. J. (1992). *Clay Miner.* **27**, 137–158.

Methodology - Transmission electron microscopy linked with energy-dispersive X-ray spectroscopy (TEM-EDX)

It is expected a characterization of clay mineral phases in treated Friedland Clay by transmission electron microscopy. This report describes the results of treated material from Friedland Clay percolated at a temperature of 100°C.

The different clay mineral phases are to identify and to describe by chemical composition and its variability, morphology, the specific dissolution potential, and further parameter.

Such further parameter like distribution of smectite layers probability (%S) and distribution of charges caused by exchangeable cations interlayer space should serve as additional indicators for mineralogical alterations in treatment experiments with Friedland Clay.

The sample were suspended for TEM-measurement in deionized water and dispersed by ultrasonic treatment for approximately 20 min. The clay fraction (<2 µm) was separated by sedimentation and diluted with deionized water to get a clear suspension. The suspension was dropped onto carbon-coated Cu grids, air dried and stored under environment-controlled conditions at 45% humidity.

TEM-EDX investigations were carried out on the <2 µm fraction using a FEI TECNAI G^2 20 electron transmission microscope at the VNU University of Science, Vietnam National University, Hanoi. This equipment (operated at 200 kV with LaB_6 cathode) was combined with an S-TWIN objective, a windowless EDAX energy-dispersive X-ray system and a FEI Eagle 2k CCD TEM camera.

About 100 individual clay particles per sample were characterized by TEM-EDX with respect to crystal size, crystal habit, particle morphology and element distribution. The crystal size, crystal habit and particle morphology were described according to Henning & Störr (1986).

For the quantification of element distribution, a calibration of k factors is mandatory (Cliff & Lorimer, 1975; Lorimer & Cliff, 1976; Mellini & Menichini, 1985). These k values are used to calibrate for the specific behaviour of particles against possible irradiation damage. The elements O, Na, Mg, Al, Si, K, Ca and Fe were quantified by applying the EDAX GENESIS–TEM Quant Materials quantification procedure.

In this procedure, the acquired EDX spectra are corrected by background subtraction, Gaussian deconvolution and k-factor corrections using values previously determined on a phyllosilicate standard (muscovite) and selected non-phyllosilicate standards. The average errors in the analyzed elements using the phyllosilicate standard, expressed as the atomic proportions, are 10 (Na), 5 (Fe, Mg, K, Ti, Ca) and 1 (Si, Al).

The measurement time per particle was lowered to 20 s and the exposed area was limited to a 50 nm diameter, avoiding possible irradiation damage of particles. The stability of particles of the sample series was tested for this measurement time at the beginning of any measurement campaign.

Further methodological details related to TEM-EDX-measurements and the Excel-based mathematical procedure using TEM-EDX data for calculation of mineral formulae are described in Hoang-Minh et al. (2019).

These mathematical procedures described in Hoang-Minh et al. (2019) were extended by k-means clustering method for finding subgroups of observations within a data set. The data were standardized (i.e., scaled) to make variables comparable. Euclidean distances were applied as classical method for distance measures. The optimal clusters were determined by Elbow method and Gap statistics[29].

---

[29] *https://uc-r.github.io/kmeans_clustering*

Data Sheet – Friedland Clay N16 (< 2 µm), treated material *(100°C)*

Preparation for TEM

- raw material: compacted material (1.6 g/cm³) of treated Friedland Clay-sample
- suspension on particles < 2 µm on carbon-filmed Cu-grid
- air-dried and humidity-controlled storing

Mineral Matter

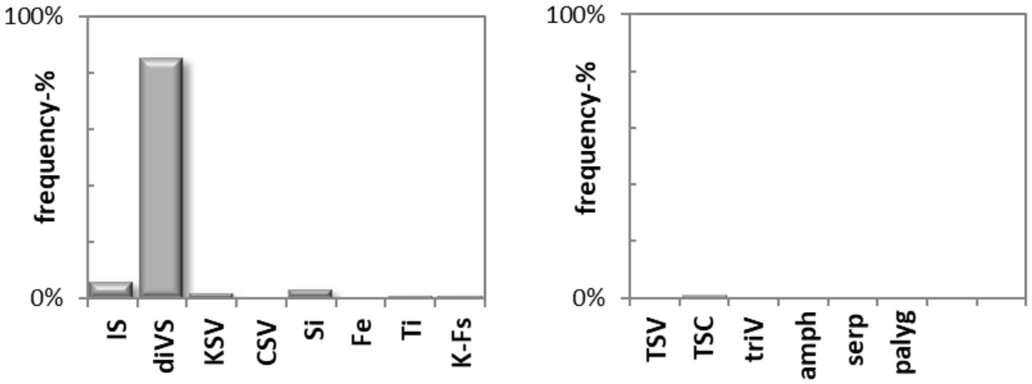

Fig. 1. *Distribution of mineral groups in fraction < 2 µm (in frequency-%)*
*Legend: **IS** – illite-smectite-mixed layer series in sense of Środon et al. (1992), diVS – dioctahedral vermiculite-smectite illite-smectite-mixed layer series (= charge- and/or K-deficit), **KSV** – kaolinite-smectite-dioctahedral vermiculite-mixed layer series, **CSV** – chlorite-saponite-trioctahedral vermiculite-mixed layer series, **Si** – quartz or particles with Si-surplus, **Fe** – Fe-oxide or Fe-oxyhydroxide, **Ti** – Ti-bearing phases (e.g. rutile, anatase), **K-Fs** – K-feldspar*

Clay Mineral Composition

All particles of smectite group:

$$Ca_{0.02}\,Mg_{0.03}\,Na_{0.12}\,K_{0.45}\quad Al_{1.28}\,Fe^{3+}_{0.55}\,Mg_{0.15}\,Ti_{0.02}\,(OH)_2\quad Si_{3.45}\,Al_{0.55}\,O_{10}$$

Charge: XII = 0.68 VI = 5.87 IV = 15.45 **Σ = 22.00**
Probability of smectite layers (%S): 23%
Probability of illite layers (%I): 77%

Specific Dissolution Potential (ΔS%)

for H2O, 20 + 60 rpm	-29	(= fast reacting, interlayer group: Ca+Mg (= type B))
for NaCl, 20 rpm	-33	(= fast reacting, interlayer group: Ca+Mg (= type B))
for NaCl, 60 rpm	-27	(= fast reacting, 'illitization', interlayer group: Na (= type A))

CEC_{calc}: 47 meq / 100 g

Measured particles: 125

Table 1. *Summarized chemical composition*

SiO_2	TiO_2	Al_2O_3	Fe_2O_3	MnO	MgO	CaO	Na_2O	K_2O	P_2O_5	Σ	
58.3%	0.2%	26.9%	6.3%		2.4%	0.4%	1.3%	4.2%	0.0%	1.00	measured particles of treated sample
59.4%	0.3%	28.1%	5.9%		2.5%	0.3%	0.1%	3.3%	0.1%	1.00	measured particles of original Friedland Clay

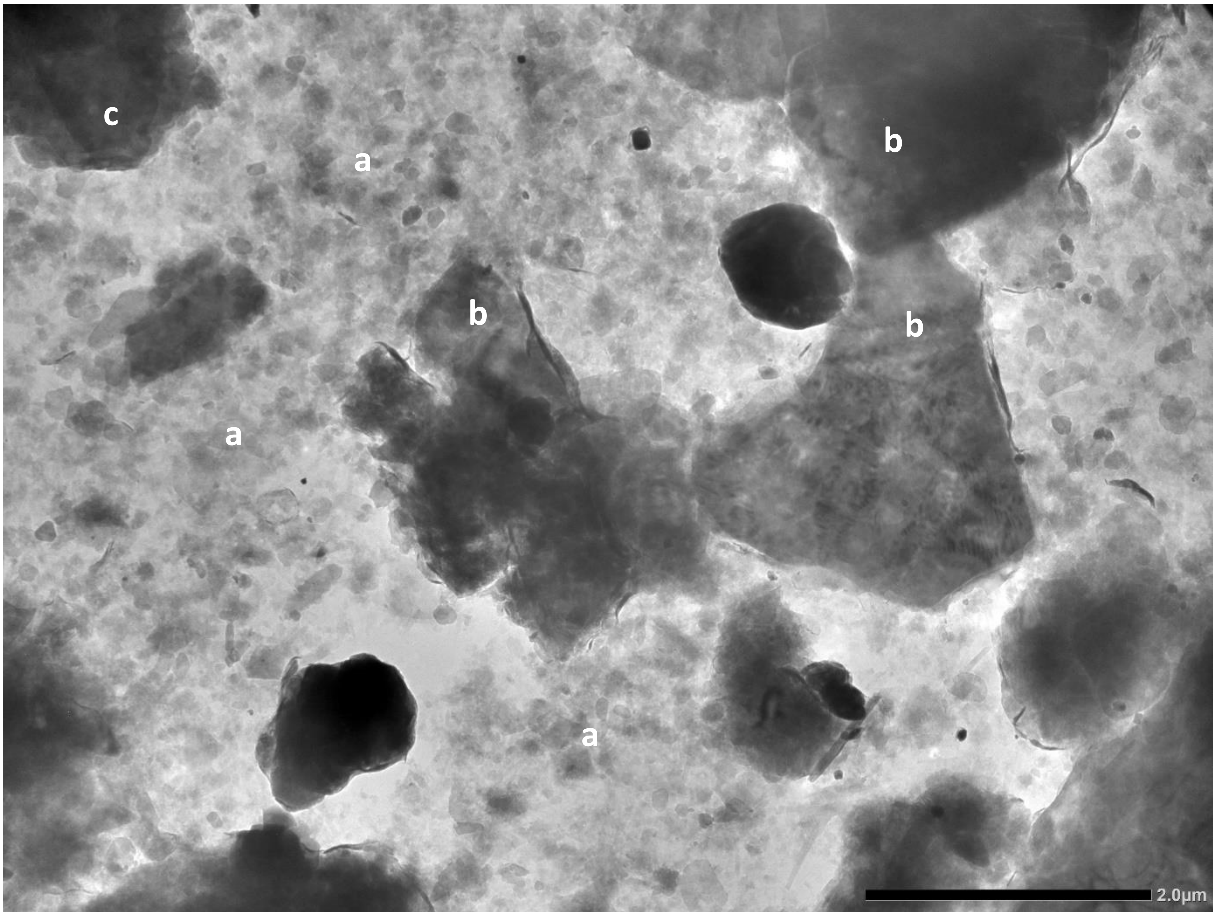

JEM-2100_MAG_X6000_074_No16.bmp

Magnification: 6k

(a) Aggregates formed by small (≤ 100 nm) xenomorphous plates;
(b) large (≤ 1 µm) xenomorph platy crystals;
(c) large hypidiomorph crystals

Fig. 2. *Morphology of particles (TEM-micrographs)*

Distribution of smectite layers probability (%S)

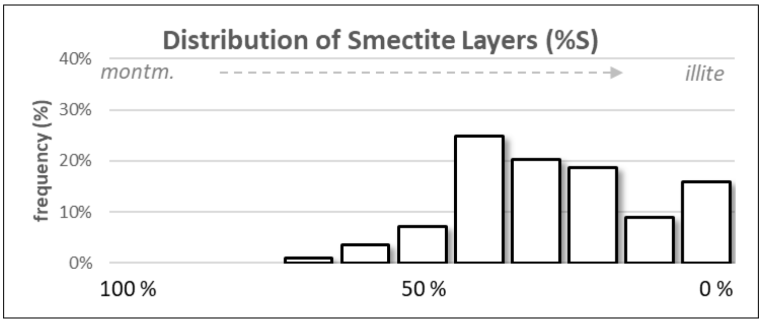

Description: *The distribution of %S-probability indicates the occurrence of two groups: (i) diVS-ml and beidellite-montmorillonite-illite-ml phases as well as (ii) illite with K-deficiency.*

Fig. 3a. *Distribution of smectite layers probability (%S)*

Differentiation by relation “Octahedral Mg vs. tetrahedral Si”?

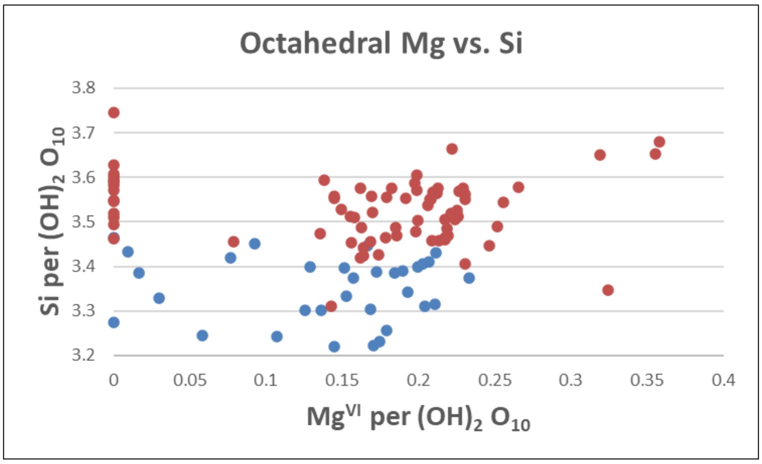

__Description:__ This diagram doesn’t indicate any separation on low and high ratio of Mg in relation to tetrahedral Si (red dots – Cluster2: BMI-ml; blue dots – Cluster1: BMI-ml with dominating illite layers).

Fig. 3b. *Distribution of octahedral Mg vs. tetrahedral Si [all per$(OH)_2$ O_{10}]*

Distribution of K in relation to tetrahedral Si

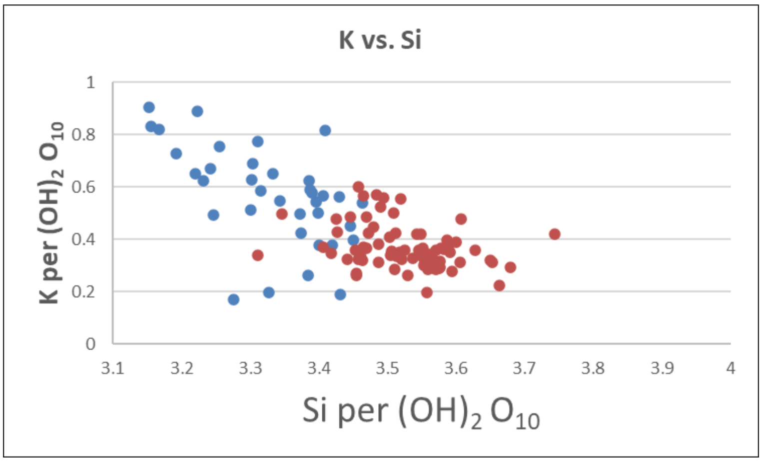

__Description:__ This diagram visualizes a K-separation of both beidellite-montmorillonite-illite-ml phases (blue dots – Cluster1; red dots – Cluster2).

Fig. 4. *Distribution of K in interlayer space vs. tetrahedral Si [all per$(OH)_2$ O_{10}]*

Distribution of charges (exchangeable from interlayer space)

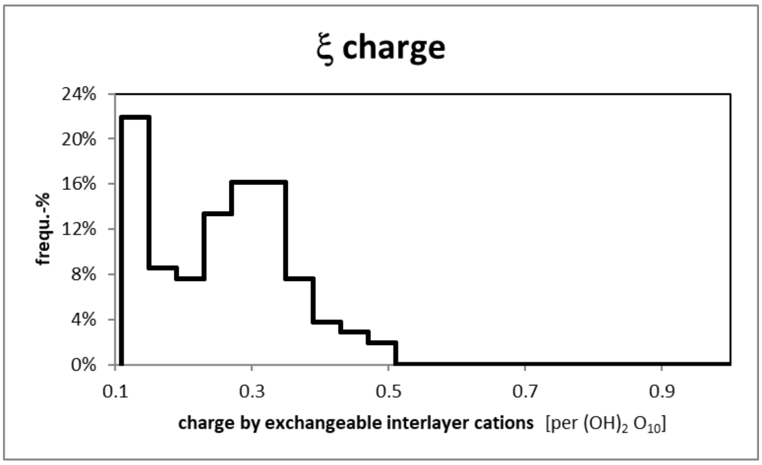

This diagram visualizes the distribution of exchangeable charges in the interlayer space (Ca, Mg, Na) determined and computed by TEM-EDX-data.

__Description:__ Distribution of charge density with bimodal maximal frequency-% at 0.11 and 0.35 per $(OH)_2$ O_{10}

Fig. 5. *Distribution of charges*

Beidellite-montmorillonite-illite-ml BMI ~10:40:50 *(Cluster2):*

$$\mathrm{Ca_{0.03}\ Mg_{0.03}\ Na_{0.13}\ K_{0.37}\quad Al_{1.19}\ Fe^{3+}{}_{0.63}\ Mg_{0.17}\ Ti_{0.01}\ (OH)_2\quad Si_{3.53}\ Al_{0.47}\ O_{10}}$$

Charge:	XII = 0.62	VI = 5.85	IV = 15.53	**Σ = 22.00**
Measured particles:	76			

Distribution of beidellite-montmorillonite-illite-ml phases (BMI-ml)

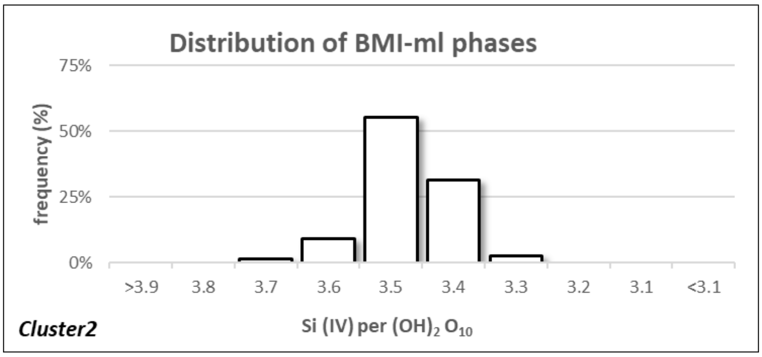

***Description:** The distribution of BMI-ml phases (cluster2) draws a maximum of frequency (%) at tetrahedral Si-value between 3.5 – 3.6 e phuc.*

Fig. 6a. *Distribution of assumed beidellite-montmorillonite-illite-ml phases*

BMI 10:40:50?	*particles (abs)*	Ca (XII)	Mg (XII)	Na (XII)	K (XII)	Cr3+ (VI)	Al (VI)	Fe3+ (VI)	Mg (VI)	Ti (VI)	Al (IV)	Si (IV)	XII	n_VI	%S
Si >3.9	n = 0														
Si 3.9-3.8	n = 0														
Si 3.8-3.7	n = 1	0.00	0.00	0.00	0.42	0.00	1.46	0.49	0.00	0.00	0.26	3.74	0.42	1.9	62
Si 3.7-3.6	n = 7	0.03	0.00	0.14	0.33	0.00	1.12	0.67	0.21	0.01	0.36	3.64	0.54	2.0	46
Si 3.6-3.5	**n = 42**	**0.03**	**0.03**	**0.13**	**0.34**	**0.00**	**1.19**	**0.64**	**0.16**	**0.01**	**0.45**	**3.55**	**0.59**	**2.0**	**34**
Si 3.5-3.4	n = 24	0.04	0.03	0.13	0.41	0.00	1.23	0.58	0.17	0.02	0.54	3.46	0.68	2.0	24
Si 3.4-3.3	n = 2	0.02	0.13	0.13	0.42	0.00	0.82	0.89	0.23	0.06	0.67	3.33	0.84	2.0	12
Si 3.3-3.2	n = 0														
Si 3.2-3.1	n = 0														
Si <3.1	n = 0														

Fig. 6b. *Computed averaged mineral formulae of phases in the different Si(IV)-classes*

Beidellitic dioctahedral vermiculite-smectite-ml BMI ~15:20:65 (beid. diVS-ml) *(Cluster1):*

$$\mathrm{Ca_{0.01}\ Mg_{0.04}\ Na_{0.11}\ K_{0.58}\quad Al_{1.43}\ Fe^{3+}{}_{0.42}\ Mg_{0.13}\ Ti_{0.02}\ (OH)_2\quad Si_{3.32}\ Al_{0.68}\ O_{10}}$$

Charge:	XII = 0.78	VI = 5.90	IV = 15.32	**Σ = 22.00**
Probability of smectite layers (%S):	11%			
Probability of illite layers (%I):	89%			
Measured particles:	37			

Distribution of smectite layers probability (%S) in beidellitic diVS-ml (Cluster1)

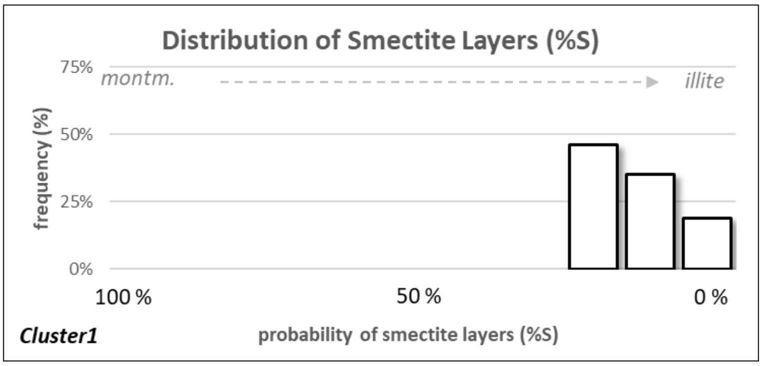

***Description:** The distribution of beidellitic diVS-ml (classified as Cluster1) draws a maximum of frequency (%) for smectite layer probability at 20%*

Fig. 7a. *Distribution of smectite layers probability in diVS-ml*

	particles (abs)	Ca (XII)	Mg (XII)	Na (XII)	K (XII)	Cr3+ (VI)	Al (VI)	Fe3+ (VI)	Mg (VI)	Ti (VI)	Al (IV)	Si (IV)	XII	n_VI	%S
%S >95%	n = 0														
%S 95-85%	n = 0														
%S 85-75%	n = 0														
%S 75-65%	n = 0														
%S 65-55%	n = 0														
%S 55-45%	n = 0														
%S 45-35%	n = 0														
%S 35-25%	n = 0														
%S 25-15%	**n = 17**	**0.01**	**0.04**	**0.12**	**0.49**	**0.00**	**1.40**	**0.45**	**0.14**	**0.01**	**0.59**	**3.41**	**0.71**	**2.0**	**19**
%S <15%	**n = 20**	**0.01**	**0.03**	**0.10**	**0.65**	**0.00**	**1.46**	**0.40**	**0.12**	**0.02**	**0.75**	**3.25**	**0.84**	**2.0**	**6**

Fig. 7b. *Computed averaged mineral formulae of beidellitic diVS -ml phases in the different smectite layers probability (%S)-classes*

Cluster1		Ca (XII)	Mg (XII)	Na (XII)	K (XII)	Cr3+ (VI)	Al (VI)	Fe3+ (VI)	Mg (VI)	Ti (VI)	Al (IV)	Si (IV)	XII	n_VI	%S
without illite	n = 17	0.01	0.04	0.12	0.49	0.00	1.40	0.45	0.14	0.01	0.59	3.41	0.71	2.0	19
only illite	n = 20	0.01	0.03	0.10	0.65	0.00	1.46	0.40	0.12	0.02	0.75	3.25	0.84	2.0	6

Fig. 7c. *Computed averaged mineral formulae of beidellitic diVS-ml phases differentiated by illite*

Description – Friedland Clay N16 (< 2 µm), treated material *(100°C)*

Preparation for TEM

The powder of Friedland Clay-sample was suspended in deionized water and dispersed by ultrasonic treatment for approximately 20 min. The clay fraction (<2 µm) was separated by sedimentation and diluted with deionized water to get a clear suspension. The suspension was dropped onto carbon-coated Cu grids, air dried and stored under environment-controlled conditions at 45% humidity.

Mineral Matter - Overview

The fraction < 2 µm of Friedland Clay N16 sample is mainly composed by beidellite-montmorillonite-illite mixed layer phases (BMI-ml) and beidellitic dioctahedral vermiculite-smectite mixed layer phases (beid. diVS-ml). Rarely, quartz, K-feldspar, kaolinite and kaolinite-smectite-ml phases as well as rutile were identified in traces in this sample [fig. 1].

The measured and computed particles have shown a calculated CEC-value of 47 meq / 100 g located at surface and in the interlayer space.

	frequency-% *(n = 125 measured particles)*
BMI-ml	61%
beid. diVS-ml	30%
Kaolinite & KSV-ml	2%
Quartz	3%
K-feldspar	1%
Ti-phases	1%

All measured dioctahedral 2:1 clay mineral phases summarized result following mineral formula computed from TEM-EDX-measurement of 113 individual particles:

	$Ca^{2+}_{0.02}$	$Mg^{2+}_{0.03}$	$Na^{+}_{0.12}$	$K^{+}_{0.45}$	$Al^{3+}_{1.28}$	$Fe^{3+}_{0.55}$	$Mg^{2+}_{0.15}$	$Ti^{4+}_{0.02}$	$(OH)_2$	$Si^{4+}_{3.45}$	$Al^{3+}_{0.55}$	O_{10}
SDOM	*± 0.00*	*± 0.00*	*± 0.01*	*± 0.02*	*± 0.02*	*± 0.01*	*± 0.01*	*± 0.00*		*± 0.01*	*± 0.01*	

Legend: SDOM - standard deviation of the mean (= the standard deviation divided by the square root of the number of samples)

The interlayer charge is calculated as 0.68 per $(OH)_2$ O_{10} and the octahedral charge as 5.87 per $(OH)_2$ O_{10}. The particles are characterized by a high octahedral Fe-amount.

The summarized chemical composition of all 113 computed particles is listed [tab. 1].

Friedland Clay N16 sample is also characterized by two morphological groups: (i) large (≤ 1 µm) xenomorph platy crystals and (ii) aggregates, partially with folds, formed by small (≤ 100 nm) xenomorphous plates [fig. 2]. Aggregates formed by small (≤ 100 nm) xenomorphous plates dominate the shapes of particles in the micrographs [fig. 2].

The distribution of %S-probability of all measured clay mineral phases [fig. 3a] also indicates the occurrence of two groups: (i) beid. diVS-ml and beidellite-montmorillonite-illite-ml phases as well as (ii) illite with K-deficiency.

The numerous measured particles by TEM-EDX allow a visualization of distribution of interlayer charges. Considering the TEM-EDX-determined cations Ca^{++}, Mg^{++} and Na^{+} and then computed their ratio as interlayer cations in the mineral formula, Ca^{++}, Mg^{++} and Na^{+} offer to characterize the degree of exchangeable charges in the interlayer space. This charge density of Friedland Clay N16 (< 2 µm) shows in this sample a bimodal maximal frequency-% at 0.11 and 0.35 per $(OH)_2\ O_{10}$ [fig. 5]. This interval of interlayer charge density caused by exchangeable cations from 0.23 - 0.43 per $(OH)_2\ O_{10}$ represents beid. diVS-ml and beidellite-montmorillonite-illite-ml.

Mineral Matter - Specification

Result of Clustering

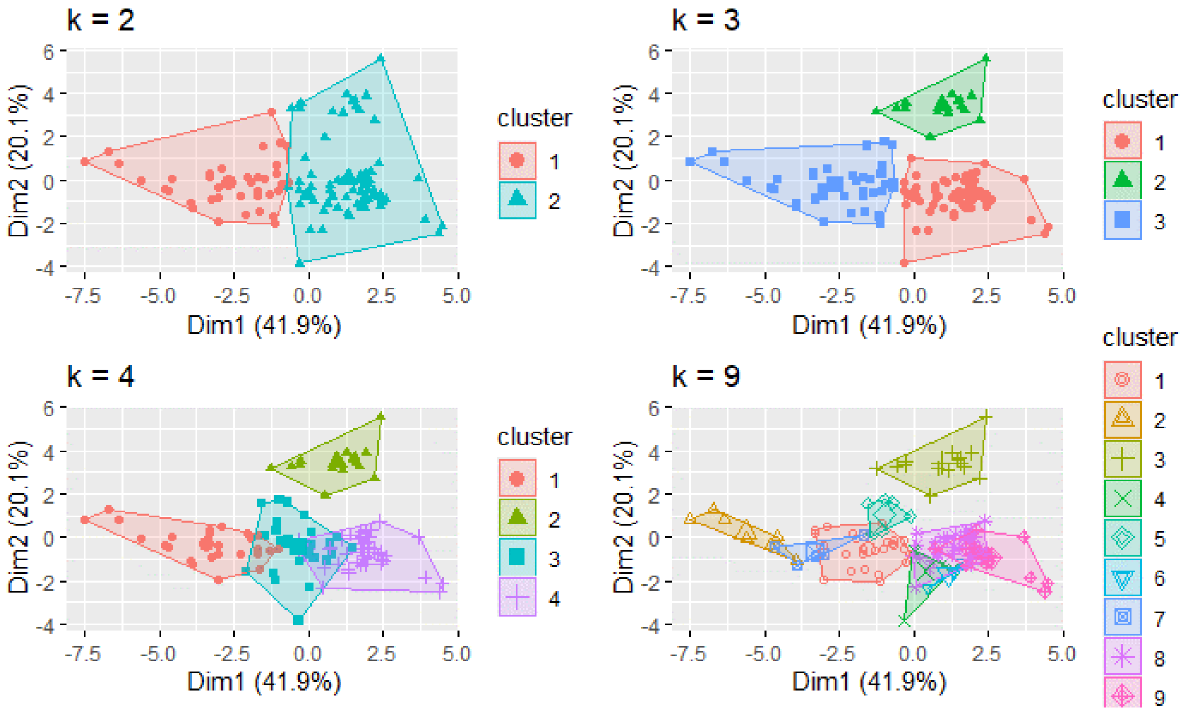

Fig. 8. *Clustering of all measured particles for clusters k = 2, k = 3, k = 4 and k = 9 (source for R-coding: https://uc-r.github.io/kmeans_clustering)*

The optimum of clusters was calculated with k = 2.

		Ca (XII)	Mg (XII)	Na (XII)	K (XII)	Cr3+ (VI)	Al (VI)	Fe3+ (VI)	Mg (VI)	Ti (VI)	Al (IV)	Si (IV)	XII	n_VI	%S
Cluster1	n = 37	0.01	0.04	0.11	0.58	0.00	1.43	0.42	0.13	0.02	0.68	3.32	0.78	2.0	11
Cluster2	n = 76	0.03	0.03	0.13	0.37	0.00	1.19	0.63	0.17	0.01	0.47	3.53	0.62	2.0	31

Fig. 9a. *Mineral formulae based on TEM-EDX-data summarized following the result of clustering for k=2*

	Sybilla-results	**TEM-EDX-results**	**Notes**
	Illite	diVS-ml (illite)	*K-deficit, low XII-charge deficit, Fe(VI)-rich*
Cluster1	IS R0 *(%S = 36%)*	beid. diVS-ml *(BMI ~15:20:65)*	*K-deficit, XII-charge deficit, Al(VI)-rich, Fe(VI)-rich*
Cluster2	ISS R0 *(%S = 47%)*	BMI-ml *(BMI ~10:40:50)*	*high K-deficit, XII-charge deficit, very Fe(VI)-rich*
	Kaolinite + KS GL R0		*in traces only*

Tab. 2. *Comparison of results from TEM-EDX- and XRD-measurements*

The TEM-EDX-data offers a good agreement with the result of Sybilla-processing of XRD-traces from oriented specimen, but only under consideration of the option beidellite [tab. 2].

ISS R0: The X-ray diffraction pattern of the ethylene-glycol saturated oriented specimen shows a full expandability to 1.78 nm and a difference of 7.27°2θ between 2. and 3. order of smectite interferences. This distance is typically for a probability of smectite layers (%S) of 50% (Moore & Reynolds, 1989). This result of XRD-pattern processing let expect a maximum of particles for %S ~ 50% by TEM-EDX-measurements, but the maximum of particles measured by TEM-EDX is to find at %S = 32% [fig. 3a]. Using a model for beidellite-montmorillonite-illite-mixed layer phases (BMI-ml) with 3.50, 4.00 and 3.20 as tetrahedral Si-value per $(OH)_2\ O_{10}$ the calculation of member ratios offers a solution for 10% layer probability for %B and 40% for %S, if %I is given with 50% [see Cluster2 in tab. 2].

IS R0: The Sybilla-procedure of XRD-traces (oriented mounts) has shown an occurrence of a second illite-smectite mixed layer phase with a smectite layers probability of %S = 36%. This result of XRD-pattern processing let expect a maximum of particles for %S ~ 36% by TEM-EDX-measurements, but the maximum of particles measured by TEM-EDX is to find at %S = 19% [tab. 2]. Using a model for beidellite-montmorillonite-illite-mixed layer phases (BMI-ml) with 3.50, 4.00 and 3.20 as tetrahedral Si-value per $(OH)_2\ O_{10}$ the calculation of member ratios offers a solution for 15% layer probability for %B and 20% for %S, if %I is given with 65% [see Cluster1 in tab. 2].

The Sybilla-processing of XRD-traces (oriented mounts) also supports low amount of kaolinite and kaolinite-smectite mixed layer phases in fine fraction of sample.

Specifics to the identified clay mineral groups

Beidellite-montmorillonite-illite-ml (BMI-ml 10:40:50) *(Cluster2)*

76 of 113 computed particles belong so to this assumed classification. The dioctahedral character of this group is proofed by X-ray diffraction. The position of the large (060)-interference of smectite is in the random oriented powder specimen at 1.497 Å.

Montmorillonite and beidellite have the same behavior concerning the expandability and they are only to distinguish by XRD using Li by means of Greene-Kelly test (Greene-Kelly 1952, 1953). So, combination of XRD- and TEM-results (high expandability by XRD and Si ~ 3.53 by TEM-EDX) led conclude the occurrence of beidellite.

Beidellite-montmorillonite-illite-ml *(BMI 10:40:50)*

$$Ca_{0.03}\ Mg_{0.03}\ Na_{0.13}\ K_{0.37}\quad Al_{1.19}\ Fe^{3+}_{0.63}\ Mg_{0.17}\ Ti_{0.01}\ (OH)_2\ \ Si_{3.53}\ Al_{0.47}\ O_{10}$$

Charge: XII = 0.62 VI = 5.85 IV = 15.53 **Σ = 22.00**
Measured particles by TEM-EDX: 76
Result of clustering: Cluster2 [tab. 2]

In this sample, beidellite is characterized by a low octahedral Mg-amount (because of high ratio of octahedral, 3-valent cations). A comparison of octahedral Mg vs. tetrahedral Si doesn't indicate any differentiation for octahedral Mg based on TEM-EDX-data [fig. 3b]. Particles of Cluster2 contain Mg(VI) from 0 … 0.37 per $(OH)_2\ O_{10}$ in octahedral layer.

The mineral formulae, summarized in classes of %S, draws for the maximum an Fe-rich BMI-ml with low Mg(VI), but remarkable amount of K in the interlayer space [tab. 6b].

Beidellitic dioctahedral vermiculite-smectite mixed layer phase

(beid. diVS-ml, BMI 15:20:65, Cluster1)

$$Ca_{0.01}\ Mg_{0.04}\ Na_{0.11}\ K_{0.58}\quad Al_{1.43}\ Fe^{3+}_{0.42}\ Mg_{0.13}\ Ti_{0.02}\ (OH)_2\ \ Si_{3.32}\ Al_{0.68}\ O_{10}$$

Charge: XII = 0.78 VI = 5.90 IV = 15.32 **Σ = 22.00**
Probability of smectite layers (%S): 35%
Probability of illite layers (%I): 65%
Measured particles by TEM-EDX: 37

Kaolinite-montmorillonite mixed layer phases

The Excel-based procedure (Hoang-Minh et al., 2019) to identify possible clay mineral groups using the TEM-EDX-measurements also includes algorithms to classify kaolinite and kaolinite-montmorillonite mixed layer phases. These algorithms couldn't compute no such phases basing on the measured TEM-EDX-data. Such particles have shown small hexagonal plates typically for kaolinite-bearing phases.

References

Cliff, G. & Lorimer, G. W. (1975). *J. Microsc.* **103**, 203–207.

Döbelin, N., Kleeberg, R. (2015). *Journal of Applied Crystallography* **48**, 1573-1580. DOI: 10.1107/S1600576715014685

Henning, K.-H. & Störr, M. (1986). Electron Micrographs (TEM, SEM) of Clays and Clay Minerals, p. 325. Akademie-Verlag Berlin.

Hoang-Minh, T., Kasbohm, J., Nguyen-Thanh, L., Nga, P. T., Lai, L. T., Duong, N. T., Thanh, N. D., Thuyet, N. T. M., Anh, D. D., Pusch, R., Knutsson, S. & Ferreiro Mahlmann, R. (2019). *J. Appl. Cryst.* **52**, 133-147. DOI: 10.1107/S1600576718018162

Lorimer, G. W. & Cliff, G. (1976). *Electron Microscopy in Mineralogy*, edited by H. R. Wenk, pp. 506–519. Berlin: Springer Verlag.

Mellini, M. & Menichini, R. (1985). *R. Soc. Ital. Miner. Petrol.* **40**, 261–266.

Moore, D.M., Reynolds, R.C. (1989). X-ray Diffraction and the Identification and Analysis of Clay Minerals, Oxford University Press, New York, 332 + xvi pp.

Nguyen-Thanh, L., Herbert, H.-J., Kasbohm, J., Hoang-Minh, T. & Mählmann, R. F. (2014). *Clays Clay Miner.* **62**, 425–446.

Środoń, J., Elsass, F., McHardy, W. J. & Morgan, D. J. (1992). *Clay Miner.* **27**, 137–158.

Methodology - Transmission electron microscopy linked with energy-dispersive X-ray spectroscopy (TEM-EDX)

It is expected a characterization of clay mineral phases in treated Friedland Clay by transmission electron microscopy. This report describes the results of treated material from Friedland Clay percolated at a temperature of 125°C.

The different clay mineral phases are to identify and to describe by chemical composition and its variability, morphology, the specific dissolution potential, and further parameter.

Such further parameter like distribution of smectite layers probability (%S) and distribution of charges caused by exchangeable cations interlayer space should serve as additional indicators for mineralogical alterations in treatment experiments with Friedland Clay.

The sample were suspended for TEM-measurement in deionized water and dispersed by ultrasonic treatment for approximately 20 min. The clay fraction (<2 µm) was separated by sedimentation and diluted with deionized water to get a clear suspension. The suspension was dropped onto carbon-coated Cu grids, air dried and stored under environment-controlled conditions at 45% humidity.

TEM-EDX investigations were carried out on the <2 µm fraction using a FEI TECNAI G^2 20 electron transmission microscope at the VNU University of Science, Vietnam National University, Hanoi. This equipment (operated at 200 kV with LaB_6 cathode) was combined with an S-TWIN objective, a windowless EDAX energy-dispersive X-ray system and a FEI Eagle 2k CCD TEM camera.

About 100 individual clay particles per sample were characterized by TEM-EDX with respect to crystal size, crystal habit, and particle morphology and element distribution. The crystal size, crystal habit and particle morphology were described according to Henning & Störr (1986).

For the quantification of element distribution, a calibration of k factors is mandatory (Cliff & Lorimer, 1975; Lorimer & Cliff, 1976; Mellini & Menichini, 1985). These k values are used to calibrate for the specific behaviour of particles against possible irradiation damage. The elements O, Na, Mg, Al, Si, K, Ca and Fe were quantified by applying the EDAX GENESIS–TEM Quant Materials quantification procedure.

In this procedure, the acquired EDX spectra are corrected by background subtraction, Gaussian deconvolution and k-factor corrections using values previously determined on a phyllosilicate standard (muscovite) and selected non-phyllosilicate standards. The average errors in the analyzed elements using the phyllosilicate standard, expressed as the atomic proportions, are 10 (Na), 5 (Fe, Mg, K, Ti, Ca) and 1 (Si, Al).

The measurement time per particle was lowered to 20 s and the exposed area was limited to a 50 nm diameter, avoiding possible irradiation damage of particles. The stability of particles of the sample series was tested for this measurement time at the beginning of any measurement campaign.

Further methodological details related to TEM-EDX-measurements and the Excel-based mathematical procedure using TEM-EDX data for calculation of mineral formulae are described in Hoang-Minh et al. (2019).

These mathematical procedures described in Hoang-Minh et al. (2019) were extended by k-means clustering method for finding subgroups of observations within a data set. The data were standardized (i.e., scaled) to make variables comparable. Euclidean distances were applied as classical method for distance measures. The optimal clusters were determined by Elbow method and Gap statistics[30].

---

[30] *https://uc-r.github.io/kmeans_clustering*

Data Sheet – Friedland Clay N20 (< 2 µm), treated material *(125°C)*

Preparation for TEM

- raw material: compacted material (1.6 g/cm³) of treated Friedland Clay-sample
- suspension on particles < 2 µm on carbon-filmed Cu-grid
- air-dried and humidity-controlled storing

Mineral Matter

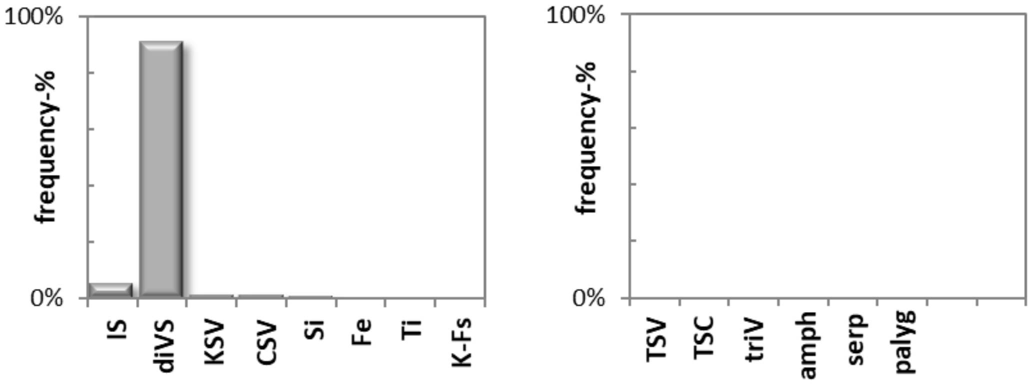

Fig. 1. *Distribution of mineral groups in fraction < 2 µm (in frequency-%)*
Legend: ***IS*** *– illite-smectite-mixed layer series in sense of Środon et al. (1992), diVS – dioctahedral vermiculite-smectite illite-smectite-mixed layer series (= charge- and/orS K-deficit),* ***KSV*** *– kaolinite-smectite-dioctahedral vermiculite-mixed layer series,* ***CSV*** *– chlorite-saponite-trioctahedral vermiculite-mixed layer series,* ***Si*** *– quartz or particles with Si-surplus,* ***Fe*** *– Fe-oxide or Fe-oxyhydroxide,* ***Ti*** *– Ti-bearing phases (e.g. rutile, anatase),* ***K-Fs*** *– K-feldspar*

Clay Mineral Composition

All particles of smectite group:

$$\mathrm{Ca_{0.05}\,Mg_{0.03}\,Na_{0.20}\,K_{0.37}\quad Al_{1.26}\,Fe^{3+}_{0.54}\,Mg_{0.19}\,Ti_{0.01}\,(OH)_2\quad Si_{3.45}\,Al_{0.55}\,O_{10}}$$

Charge: XII = 0.74 VI = 5.82 IV = 15.45 **Σ = 22.00**

Probability of smectite layers (%S): 22%

Probability of illite layers (%I): 78%

Specific Dissolution Potential (ΔS%)

for H2O, 20 + 60 rpm	-32	(= fast reacting, interlayer group: Ca+Mg (= type B))
for NaCl, 20 rpm	-36	(= fast reacting, interlayer group: Ca+Mg (= type B))
for NaCl, 60 rpm	-12	(= fast reacting, 'illitization', interlayer group: Na (= type A))

CEC$_{calc}$: 76 meq / 100 g

Measured particles: 125

Table 1. *Summarized chemical composition*

SiO_2	TiO_2	Al_2O_3	Fe_2O_3	MnO	MgO	CaO	Na_2O	K_2O	P_2O_5	Σ	
57.4%	0.1%	26.4%	6.0%		2.9%	0.7%	2.2%	3.5%	0.8%	1.00	measured particles of treated sample
59.4%	0.3%	28.1%	5.9%		2.5%	0.3%	0.1%	3.3%	0.1%	1.00	measured particles of original Friedland Clay

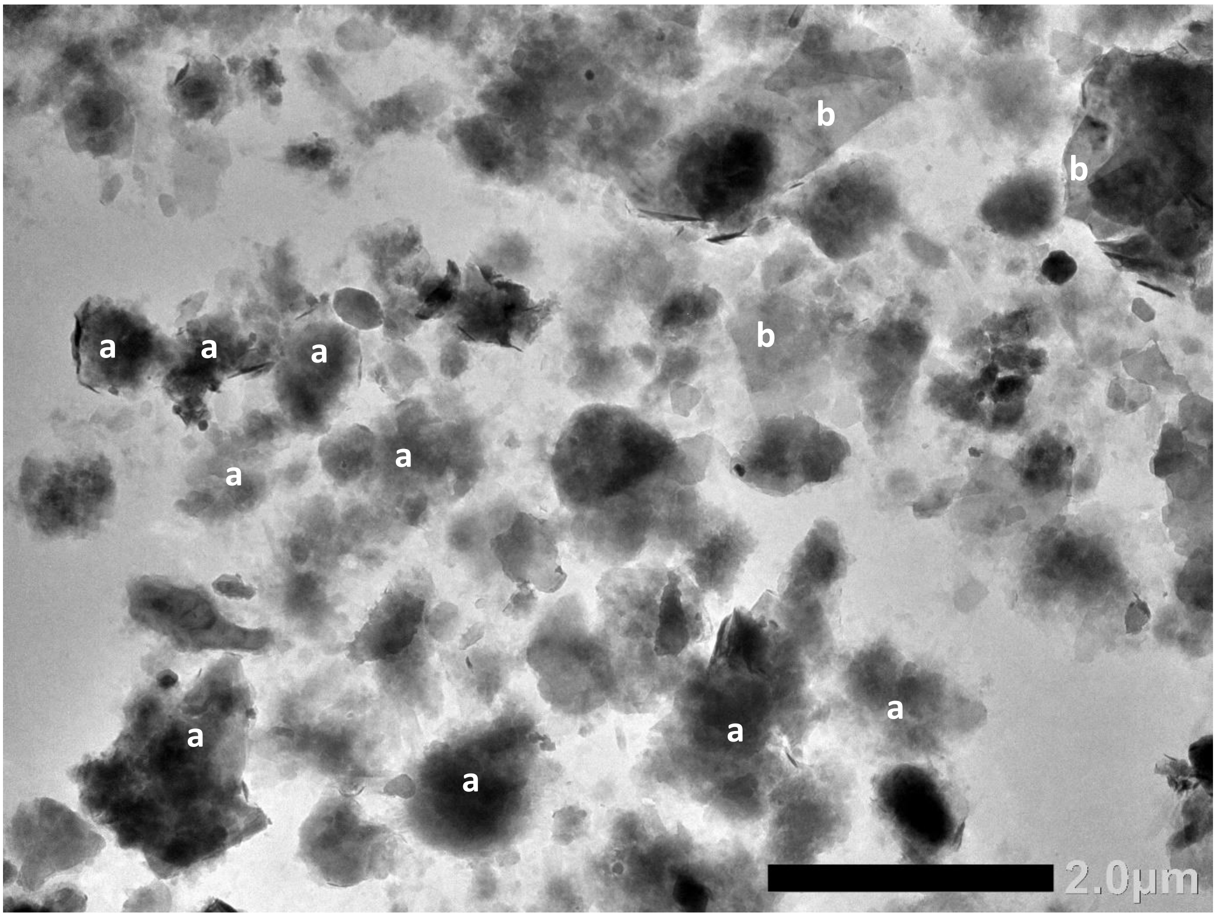

JEM-2100_MAG_X6000_No20_003.bmp

Magnification: 6k

(a) Aggregates formed by small (≤ 100 nm) xenomorphous plates;
(b) large (≤ 1 µm) xenomorph platy crystals

Fig. 2. *Morphology of particles (TEM-micrographs)*

Distribution of smectite layers probability (%S)

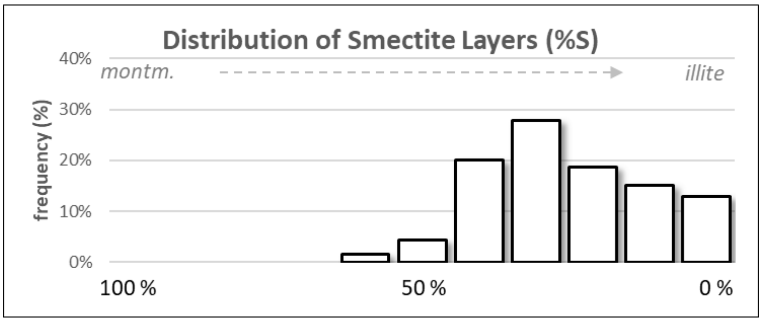

Description: *The distribution of %S-probability indicates the occurrence of two groups: (i) diVS-ml and beidellite-montmorillonite-illite-ml phases as well as (ii) illite with K-deficiency.*

Fig. 3a. *Distribution of smectite layers probability (%S)*

Differentiation by relation “Octahedral Mg vs. tetrahedral Si”?

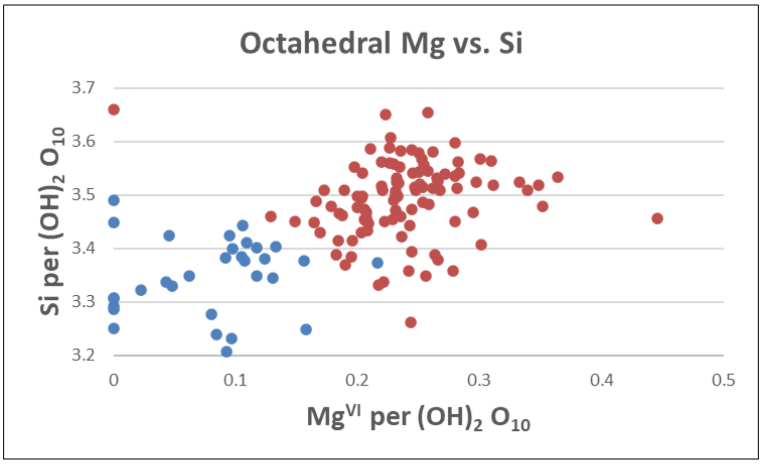

Description: *This diagram indicates a separation on low and high ratio of Mg in relation to tetrahedral Si (red dots – Cluster2: BMI-ml; blue dots – Cluster1: diVS-ml).*

Fig. 3b. *Distribution of octahedral Mg vs. tetrahedral Si [all per(OH)$_2$ O$_{10}$]*

Distribution of K in relation to tetrahedral Si

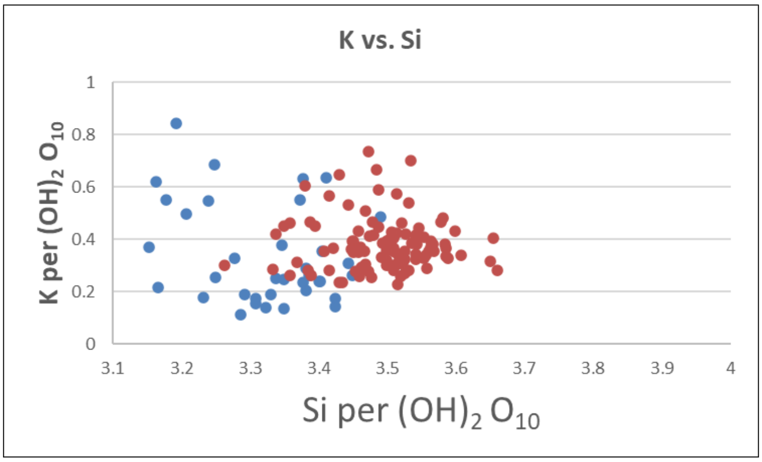

Description: *This diagram doesn’t visualize any K-separation between beidellite-montmorillonite-illite-ml and diVS-ml phases (blue dots – Cluster1: diVS-ml; red dots – Cluster2: BMI-ml).*

Fig. 4. *Distribution of K in interlayer space vs. tetrahedral Si [all per(OH)$_2$ O$_{10}$]*

Distribution of charges (exchangeable from interlayer space)

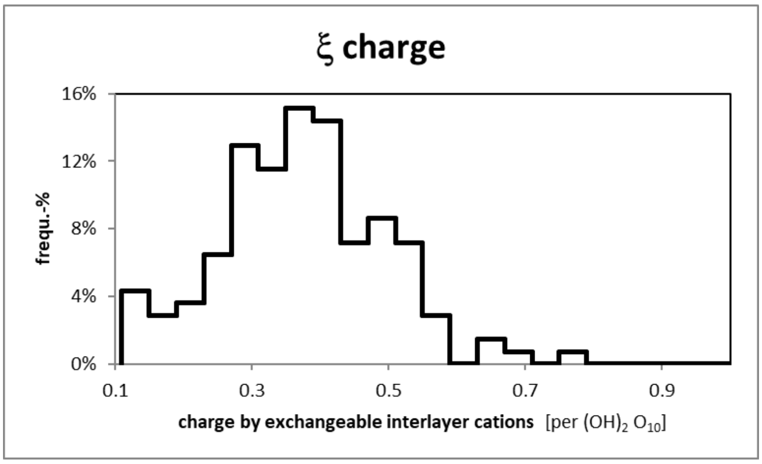

This diagram visualizes the distribution of exchangeable charges in the interlayer space (Ca, Mg, Na) determined and computed by TEM-EDX-data.

Description: *Distribution of charge density with trimodal maximal frequency-% at 0.15, 0.39 and 0.51 per (OH)$_2$ O$_{10}$*

Fig. 5. *Distribution of charges*

Beidellite-montmorillonite-illite-ml BMI ~15:30:55 *(Cluster2):*

$$Ca_{0.05}\ Mg_{0.01}\ Na_{0.23}\ K_{0.38}\quad Al_{1.15}\ Fe^{3+}_{0.60}\ Mg_{0.24}\ Ti_{0.01}\ (OH)_2\quad Si_{3.49}\ Al_{0.51}\ O_{10}$$

Charge: XII = 0.74 VI = 5.77 IV = 15.49 **Σ = 22.00**

Measured particles: 104

Distribution of beidellite-montmorillonite-illite-ml phases (BMI-ml)

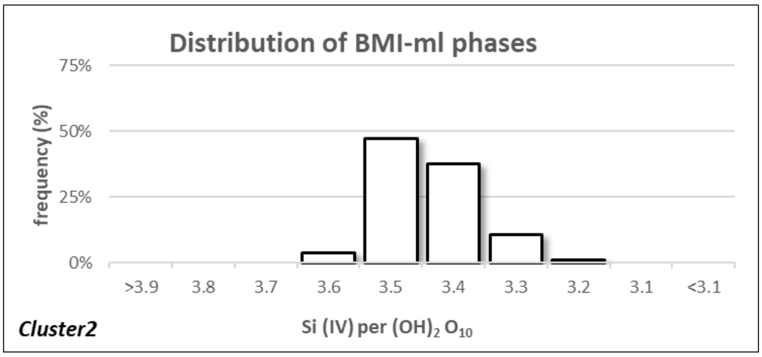

Description: *The distribution of BMI-ml phases (cluster2) draws a maximum of frequency (%) at tetrahedral Si-value between 3.5 – 3.6 e phuc.*

Fig. 6a. *Distribution of assumed beidellite-montmorillonite-illite-ml phases*

BMI 15:30:55?	*particles (abs)*	**Ca (XII)**	**Mg (XII)**	**Na (XII)**	**K (XII)**	**Cr3+ (VI)**	**Al (VI)**	**Fe3+ (VI)**	**Mg (VI)**	**Ti (VI)**	**Al (IV)**	**Si (IV)**	**XII**	**n_VI**	**%S**
Si >3.9	n = 0														
Si 3.9-3.8	n = 0														
Si 3.8-3.7	n = 0														
Si 3.7-3.6	n = 4	0.03	0.01	0.14	0.34	0.00	1.23	0.59	0.18	0.00	0.36	3.64	0.55	2.0	46
Si 3.6-3.5	**n = 49**	**0.05**	**0.01**	**0.24**	**0.37**	**0.00**	**1.12**	**0.61**	**0.26**	**0.01**	**0.46**	**3.54**	**0.72**	**2.0**	**33**
Si 3.5-3.4	n = 39	0.06	0.01	0.21	0.39	0.00	1.20	0.57	0.22	0.01	0.54	3.46	0.75	2.0	24
Si 3.4-3.3	n = 11	0.08	0.02	0.25	0.39	0.00	1.13	0.60	0.23	0.04	0.63	3.37	0.82	2.0	15
Si 3.3-3.2	n = 1	0.00	0.20	0.28	0.30	0.00	0.59	1.17	0.24	0.00	0.74	3.26	0.98	2.0	7
Si 3.2-3.1	n = 0														
Si <3.1	n = 0														

Fig. 6b. *Computed averaged mineral formulae of phases in the different Si(IV)-classes*

Dioctahedral vermiculite-smectite-ml (diVS-ml) *(Cluster1):*

$$Ca_{0.05}\ Mg_{0.07}\ Na_{0.16}\ K_{0.34}\quad Al_{1.54}\ Fe^{3+}_{0.37}\ Mg_{0.08}\ Ti_{0.01}\ (OH)_2\quad Si_{3.32}\ Al_{0.68}\ O_{10}$$

Charge: XII = 0.74 VI = 5.94 IV = 15.32 **Σ = 22.00**

Probability of smectite layers (%S): 11%

Probability of illite layers (%I): 89%

Measured particles: 36

Distribution of smectite layers probability (%S) in beidellitic diVS-ml (Cluster1)

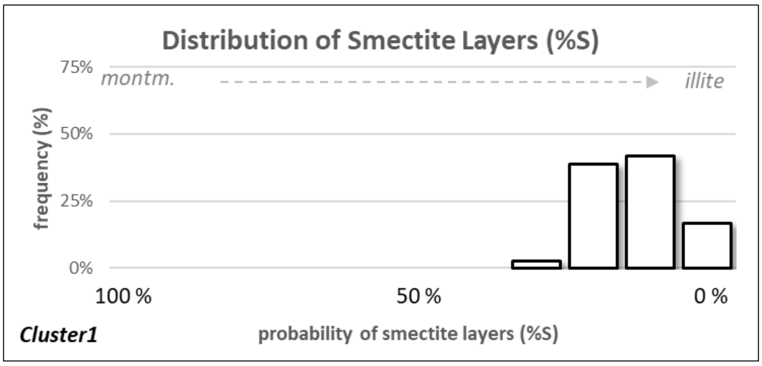

Description: *The distribution of diVS-ml (classified as Cluster1) draws a maximum of frequency (%) for smectite layer probability at 5-25%*

Fig. 7a. *Distribution of smectite layers probability in diVS-ml*

	particles (abs)	**Ca (XII)**	**Mg (XII)**	**Na (XII)**	**K (XII)**	**Cr3+ (VI)**	**Al (VI)**	**Fe3+ (VI)**	**Mg (VI)**	**Ti (VI)**	**Al (IV)**	**Si (IV)**	**XII**	**n_VI**	**%S**
%S >95%	n = 0														
%S 95-85%	n = 0														
%S 85-75%	n = 0														
%S 75-65%	n = 0														
%S 65-55%	n = 0														
%S 55-45%	n = 0														
%S 45-35%	n = 0														
%S 35-25%	n = 1	0.01	0.00	0.00	0.49	0.00	1.52	0.48	0.00	0.00	0.51	3.49	0.51	2.0	27
%S 25-15%	n = 14	0.06	0.05	0.15	0.32	0.00	1.45	0.44	0.11	0.00	0.60	3.40	0.71	2.0	18
%S <15%	**n = 21**	**0.05**	**0.08**	**0.17**	**0.34**	**0.00**	**1.61**	**0.33**	**0.07**	**0.01**	**0.74**	**3.26**	**0.77**	**2.0**	**7**

Fig. 7b. *Computed averaged mineral formulae of diVS -ml phases in the different smectite layers probability (%S)-classes*

Cluster1		**Ca (XII)**	**Mg (XII)**	**Na (XII)**	**K (XII)**	**Cr3+ (VI)**	**Al (VI)**	**Fe3+ (VI)**	**Mg (VI)**	**Ti (VI)**	**Al (IV)**	**Si (IV)**	**XII**	**n_VI**	**%S**
without illite	n = 15	0.06	0.05	0.14	0.33	0.00	1.46	0.44	0.10	0.00	0.59	3.41	0.69	2.0	18
only illite	n = 21	0.05	0.08	0.17	0.34	0.00	1.61	0.33	0.07	0.01	0.74	3.26	0.77	2.0	7

Fig. 7c. *Computed averaged mineral formulae of diVS-ml phases differentiated by illite*

Description – Friedland Clay N20 (< 2 µm), treated material *(125°C)*

Preparation for TEM

The powder of Friedland Clay-sample was suspended in deionized water and dispersed by ultrasonic treatment for approximately 20 min. The clay fraction (<2 µm) was separated by sedimentation and diluted with deionized water to get a clear suspension. The suspension was dropped onto carbon-coated Cu grids, air dried and stored under environment-controlled conditions at 45% humidity.

Mineral Matter - Overview

The fraction < 2 µm of Friedland Clay N20 sample is mainly composed by beidellite-montmorillonite-illite mixed layer phases (BMI-ml) and dioctahedral vermiculite-smectite mixed layer phases (diVS-ml). Rarely, quartz, kaolinite and kaolinite-smectite-ml phases as well as chlorite-smectite-ml phases were identified in traces in this sample [fig. 1].

The measured and computed particles have shown a calculated CEC-value of 76 meq / 100 g located at surface and in the interlayer space.

	frequency-% *(n = 150 measured particles)*
BMI-ml	69%
diVS-ml	24%
Kaolinite & KSV-ml	2%
CSV-ml	2%
Quartz	1%

All measured dioctahedral 2:1 clay mineral phases summarized result following mineral formula computed from TEM-EDX-measurement of 140 individual particles:

$$\boxed{Ca^{2+}_{0.05}\ Mg^{2+}_{0.03}\ Na^{+}_{0.20}\ K^{+}_{0.37}\quad Al^{3+}_{1.26}\ Fe^{3+}_{0.54}\ Mg^{2+}_{0.19}\ Ti^{4+}_{0.01}\ (OH)_2\quad Si^{4+}_{3.45}\ Al^{3+}_{0.55}\ O_{10}}$$

SDOM *± 0.00 ± 0.00 ± 0.01 ± 0.01 ± 0.02 ± 0.01 ± 0.01 ± 0.00 ± 0.01 ± 0.01*

Legend: SDOM - standard deviation of the mean (= the standard deviation divided by the square root of the number of samples)

The interlayer charge is calculated as 0.74 per $(OH)_2\ O_{10}$ and the octahedral charge as 5.81 per $(OH)_2\ O_{10}$. The particles are characterized by a high octahedral Fe-amount.

The summarized chemical composition of all 140 computed particles is listed [tab. 1].

Friedland Clay N20 sample is also characterized by two morphological groups: (i) large (≤ 1 µm) xenomorph platy crystals and (ii) aggregates, partially with folds, formed by small (≤ 100 nm) xenomorphous plates [fig. 2]. Aggregates formed by small (≤ 100 nm) xenomorphous plates dominate the shapes of particles in the micrographs [fig. 2].

The distribution of %S-probability of all measured clay mineral phases [fig. 3a] also indicates the occurrence of two groups: (i) diVS-ml and beidellite-montmorillonite-illite-ml phases as well as (ii) illite with K-deficiency.

The numerous measured particles by TEM-EDX allow a visualization of distribution of interlayer charges. Considering the TEM-EDX-determined cations Ca^{++}, Mg^{++} and Na^{+} and then computed their ratio as interlayer cations in the mineral formula, Ca^{++}, Mg^{++} and Na^{+} offer to characterize the degree of exchangeable charges in the interlayer space. This charge density of Friedland Clay N20 (< 2 µm) shows in this sample a trimodal maximal frequency-% at 0.15, 039 and 0.51 per (OH)$_2$ O$_{10}$ [fig. 5]. This interval of interlayer charge density caused by exchangeable cations from 0.23 - 0.59 per (OH)$_2$ O$_{10}$ represents diVS-ml and beidellite-montmorillonite-illite-ml.

Mineral Matter - Specification

Result of Clustering

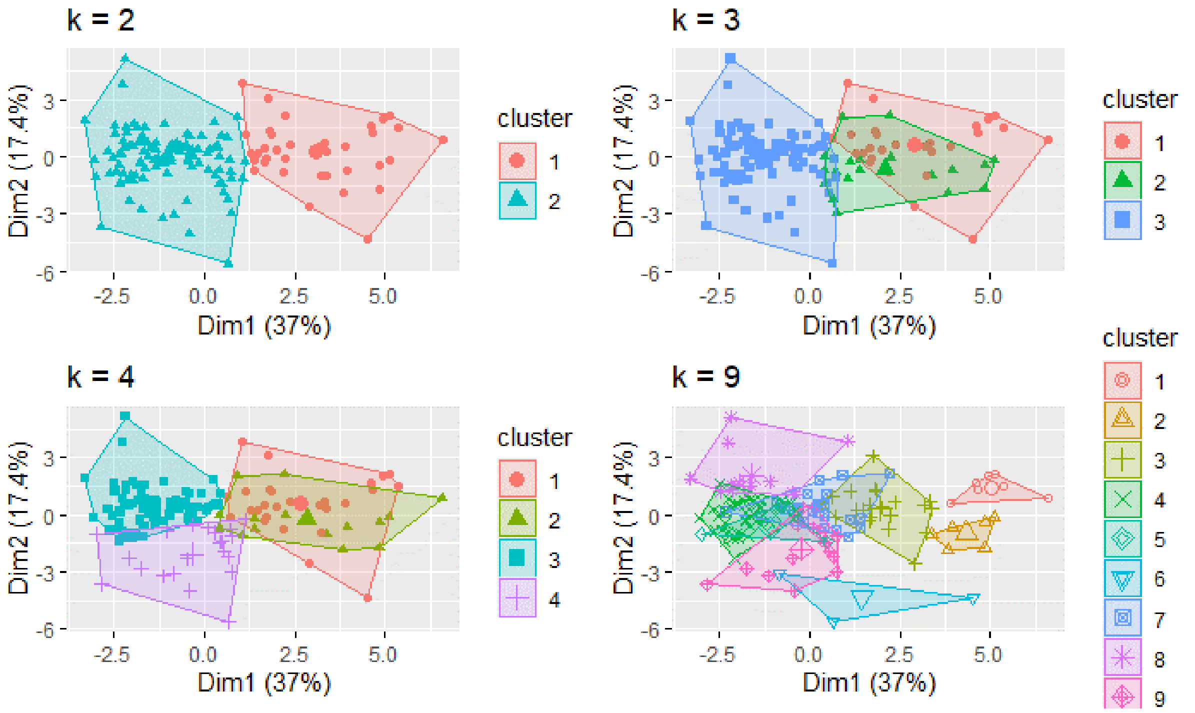

Fig. 8. *Clustering of all measured particles for clusters k = 2, k = 3, k = 4 and k = 9 (source for R-coding: https://uc-r.github.io/kmeans_clustering)*

The optimum of clusters was calculated with k = 2.

		Ca (XII)	Mg (XII)	Na (XII)	K (XII)	Cr3+ (VI)	Al (VI)	Fe3+ (VI)	Mg (VI)	Ti (VI)	Al (IV)	Si (IV)	XII	n_VI	%S
Cluster1	n = 36	0.05	0.07	0.16	0.34	0.00	1.54	0.37	0.08	0.01	0.68	3.32	0.74	2.0	11
Cluster2	n = 104	0.05	0.01	0.23	0.38	0.00	1.15	0.60	0.24	0.01	0.51	3.49	0.74	2.0	27

Fig. 9a. *Mineral formulae based on TEM-EDX-data summarized following the result of clustering for k=2*

	Sybilla-results	**TEM-EDX-results**	**Notes**
	Illite	diVS-ml (illite)	*high K-deficit, low XII-charge deficit, Fe(VI)-rich*
Cluster1	IS R0 *(%S = 10%)*	diVS-ml *(BMI ~00:10:90)*	*high K-deficit, XII-charge deficit, Al(VI)-rich, Fe(VI)-rich*
Cluster2	ISS R0 *(%S = 47%)*	BMI-ml *(BMI ~15:30:55)*	*high K-deficit, no XII-charge deficit, very Fe(VI)-rich*
	Kaolinite + KS GL R0		*in traces only*

Tab. 2. *Comparison of results from TEM-EDX- and XRD-measurements*

The TEM-EDX-data offers a good agreement with the result of Sybilla-processing of XRD-traces from oriented specimen, but for cluster2 only under consideration of the option beidellite [tab. 2].

ISS R0: The X-ray diffraction pattern of the ethylene-glycol saturated oriented specimen shows a limited expandability to 1.45 nm. This result of XRD-pattern processing let expect a maximum of particles for %S ~ 50% by TEM-EDX-measurements, but the maximum of particles measured by TEM-EDX is to find at %S = 27% [fig. 3a]. Using a model for beidellite-montmorillonite-illite-mixed layer phases (BMI-ml) with 3.50, 4.00 and 3.20 as tetrahedral Si-value per $(OH)_2\ O_{10}$ the calculation of member ratios offers a solution for 15% layer probability for %B and 30% for %S, if %I is given with 55% [see Cluster2 in tab. 2].

IS R0: The Sybilla-procedure of XRD-traces (oriented mounts) has shown an occurrence of a second illite-smectite mixed layer phase with a smectite layers probability of %S = 10%. This result of XRD-pattern processing is in a agreement with a maximum of particles for %S ~ 10% by TEM-EDX-measurements [Cluster1 in tab. 2].

The Sybilla-processing of XRD-traces (oriented mounts) also supports low amount of kaolinite, kaolinite-smectite mixed layer and chlorite-smectite-ml phases in fine fraction of sample.

Specifics to the identified clay mineral groups

Beidellite-montmorillonite-illite-ml (BMI-ml 15:30:55) *(Cluster2)*

104 of 140 computed particles belong so to this assumed classification. The dioctahedral character of this group is proofed by X-ray diffraction. The position of the large (060)-interference of smectite is in the random oriented powder specimen at 1.497 Å.

Montmorillonite and beidellite have the same behavior concerning the expandability and they are only to distinguish by XRD using Li by means of Greene-Kelly test (Greene-Kelly 1952, 1953). So, combination of XRD- and TEM-results (high expandability by XRD and Si ~ 3.49 by TEM-EDX) led conclude the occurrence of beidellite.

Beidellite-montmorillonite-illite-ml *(BMI 15:30:55)*

$$Ca_{0.05}\ Mg_{0.01}\ Na_{0.23}\ K_{0.38}\quad Al_{1.15}\ Fe^{3+}_{0.60}\ Mg_{0.24}\ Ti_{0.01}\ (OH)_2\quad Si_{3.49}\ Al_{0.51}\ O_{10}$$

Charge:	XII = 0.74	VI = 5.77	IV = 15.49	**Σ = 22.00**
Measured particles by TEM-EDX:	104			
Result of clustering:	Cluster2 [tab. 2]			

In this sample, beidellite is normally characterized by a low octahedral Mg-amount (because of high ratio of octahedral, 3-valent cations). A comparison of octahedral Mg vs. tetrahedral Si indicates a differentiation for octahedral Mg based on TEM-EDX-data [fig. 3b]. Particles of Cluster2 contain Mg(VI) mainly > 0.17 per $(OH)_2\ O_{10}$ in octahedral layer.

The mineral formulae, summarized in classes of %S, draws for the maximum a very Fe-rich BMI-ml and remarkable reduced amount of K in the interlayer space [tab. 6b].

Dioctahedral vermiculite-smectite mixed layer phase

(diVS-ml, BMI 00:10:90, Cluster1)

$$Ca_{0.05}\ Mg_{0.07}\ Na_{0.16}\ K_{0.34}\quad Al_{1.54}\ Fe^{3+}_{0.37}\ Mg_{0.08}\ Ti_{0.01}\ (OH)_2\quad Si_{3.32}\ Al_{0.68}\ O_{10}$$

Charge: XII = 0.74 VI = 5.94 IV = 15.32 **Σ = 22.00**

Probability of smectite layers (%S): 10%

Probability of illite layers (%I): 90%

Measured particles by TEM-EDX: 36

Kaolinite-montmorillonite mixed layer phases

The Excel-based procedure (Hoang-Minh et al., 2019) to identify possible clay mineral groups using the TEM-EDX-measurements also includes algorithms to classify kaolinite and kaolinite-montmorillonite mixed layer phases. These algorithms couldn’t compute no such phases basing on the measured TEM-EDX-data. Such particles have shown small hexagonal plates typically for kaolinite-bearing phases.

References

Cliff, G. & Lorimer, G. W. (1975). *J. Microsc.* **103**, 203–207.

Döbelin, N., Kleeberg, R. (2015). *Journal of Applied Crystallography* **48**, 1573-1580. DOI: 10.1107/S1600576715014685

Henning, K.-H. & Störr, M. (1986). Electron Micrographs (TEM, SEM) of Clays and Clay Minerals, p. 325. Akademie-Verlag Berlin.

Hoang-Minh, T., Kasbohm, J., Nguyen-Thanh, L., Nga, P. T., Lai, L. T., Duong, N. T., Thanh, N. D., Thuyet, N. T. M., Anh, D. D., Pusch, R., Knutsson, S. & Ferreiro Mahlmann, R. (2019). *J. Appl. Cryst.* **52**, 133-147. DOI: 10.1107/S1600576718018162

Lorimer, G. W. & Cliff, G. (1976). *Electron Microscopy in Mineralogy*, edited by H. R. Wenk, pp. 506–519. Berlin: Springer Verlag.

Mellini, M. & Menichini, R. (1985). *R. Soc. Ital. Miner. Petrol.* **40**, 261–266.

Moore, D.M., Reynolds, R.C. (1989). X-ray Diffraction and the Identification and Analysis of Clay Minerals, Oxford University Press, New York, 332 + xvi pp.

Nguyen-Thanh, L., Herbert, H.-J., Kasbohm, J., Hoang-Minh, T. & Mählmann, R. F. (2014). *Clays Clay Miner.* **62**, 425–446.

Środoń, J., Elsass, F., McHardy, W. J. & Morgan, D. J. (1992). *Clay Miner.* **27**, 137–158.

Methodology - Transmission electron microscopy linked with energy-dispersive X-ray spectroscopy (TEM-EDX)

It is expected a characterization of clay mineral phases in treated Friedland Clay by transmission electron microscopy. This report describes the results of treated material from Friedland Clay percolated at a temperature of 150°C.

The different clay mineral phases are to identify and to describe by chemical composition and its variability, morphology, the specific dissolution potential, and further parameter.

Such further parameter like distribution of smectite layers probability (%S) and distribution of charges caused by exchangeable cations interlayer space should serve as additional indicators for mineralogical alterations in treatment experiments with Friedland Clay.

The sample were suspended for TEM-measurement in deionized water and dispersed by ultrasonic treatment for approximately 20 min. The clay fraction (<2 µm) was separated by sedimentation and diluted with deionized water to get a clear suspension. The suspension was dropped onto carbon-coated Cu grids, air dried and stored under environment-controlled conditions at 45% humidity.

TEM-EDX investigations were carried out on the <2 µm fraction using a FEI TECNAI G^2 20 electron transmission microscope at the VNU University of Science, Vietnam National University, Hanoi. This equipment (operated at 200 kV with LaB_6 cathode) was combined with an S-TWIN objective, a windowless EDAX energy-dispersive X-ray system and a FEI Eagle 2k CCD TEM camera.

About 100 individual clay particles per sample were characterized by TEM-EDX with respect to crystal size, crystal habit, and particle morphology and element distribution. The crystal size, crystal habit and particle morphology were described according to Henning & Störr (1986).

For the quantification of element distribution, a calibration of k factors is mandatory (Cliff & Lorimer, 1975; Lorimer & Cliff, 1976; Mellini & Menichini, 1985). These k values are used to calibrate for the specific behaviour of particles against possible irradiation damage. The elements O, Na, Mg, Al, Si, K, Ca and Fe were quantified by applying the EDAX GENESIS–TEM Quant Materials quantification procedure.

In this procedure, the acquired EDX spectra are corrected by background subtraction, Gaussian deconvolution and k-factor corrections using values previously determined on a phyllosilicate standard (muscovite) and selected non-phyllosilicate standards. The average errors in the analyzed elements using the phyllosilicate standard, expressed as the atomic proportions, are 10 (Na), 5 (Fe, Mg, K, Ti, Ca) and 1 (Si, Al).

The measurement time per particle was lowered to 20 s and the exposed area was limited to a 50 nm diameter, avoiding possible irradiation damage of particles. The stability of particles of the sample series was tested for this measurement time at the beginning of any measurement campaign.

Further methodological details related to TEM-EDX-measurements and the Excel-based mathematical procedure using TEM-EDX data for calculation of mineral formulae are described in Hoang-Minh et al. (2019).

These mathematical procedures described in Hoang-Minh et al. (2019) were extended by k-means clustering method for finding subgroups of observations within a data set. The data were standardized (i.e., scaled) to make variables comparable. Euclidean distances were applied as classical method for distance measures. The optimal clusters were determined by Elbow method and Gap statistics[31].

---

[31] *https://uc-r.github.io/kmeans_clustering*

Data Sheet – Friedland Clay N21 (< 2 µm), treated material *(150°C)*

Preparation for TEM

- raw material: compacted material (1.6 g/cm³) of treated Friedland Clay-sample
- suspension on particles < 2 µm on carbon-filmed Cu-grid
- air-dried and humidity-controlled storing

Mineral Matter

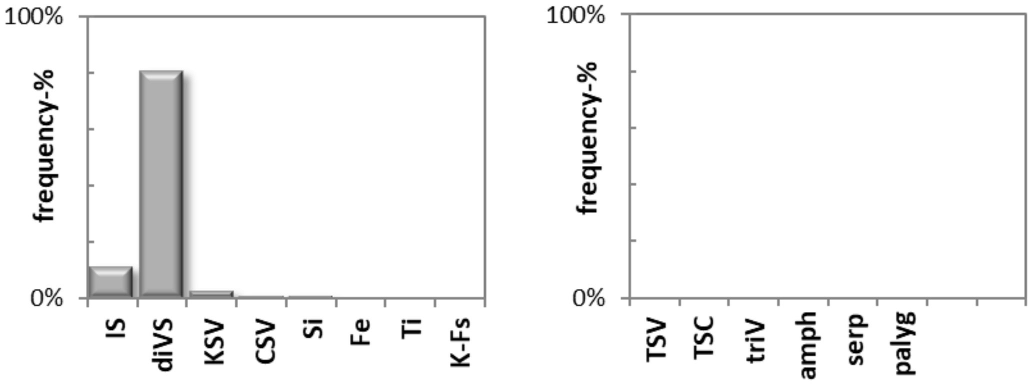

Fig. 1. *Distribution of mineral groups in fraction < 2 µm (in frequency-%)*
Legend: ***IS*** *– illite-smectite-mixed layer series in sense of Środon et al. (1992), diVS – dioctahedral vermiculite-smectite illite-smectite-mixed layer series (= charge- and/or K-deficit),* ***KSV*** *– kaolinite-smectite-dioctahedral vermiculite-mixed layer series,* ***CSV*** *– chlorite-saponite-trioctahedral vermiculite-mixed layer series,* ***Si*** *– quartz or particles with Si-surplus,* ***Fe*** *– Fe-oxide or Fe-oxyhydroxide,* ***Ti*** *– Ti-bearing phases (e.g. rutile, anatase),* ***K-Fs*** *– K-feldspar*

Clay Mineral Composition

All particles of smectite group:

$$Ca_{0.03}\ Mg_{0.04}\ Na_{0.11}\ K_{0.37}\quad Al_{1.29}\ Fe^{3+}_{0.55}\ Mg_{0.15}\ Ti_{0.01}\ (OH)_2\quad Si_{3.51}\ Al_{0.49}\ O_{10}$$

Charge: XII = 0.62 VI = 5.87 IV = 15.51 **Σ = 22.00**
Probability of smectite layers (%S): 29%
Probability of illite layers (%I): 71%

Specific Dissolution Potential (ΔS%)

for H2O, 20 + 60 rpm -25 (= fast reacting, interlayer group: Ca+Mg (= type B))
for NaCl, 20 rpm -29 (= fast reacting, interlayer group: Ca+Mg (= type B))
for NaCl, 60 rpm -26 (= fast reacting, ‘illitization’, interlayer group: Na (= type A))
CEC_{calc}: 59 meq / 100 g

Measured particles: 132

Table 1. *Summarized chemical composition*

SiO_2	TiO_2	Al_2O_3	Fe_2O_3	MnO	MgO	CaO	Na_2O	K_2O	P_2O_5	Σ	
58.9%	0.2%	26.5%	6.2%		2.4%	0.5%	1.2%	3.6%	0.0%	1.00	measured particles of treated sample
59.4%	0.3%	28.1%	5.9%		2.5%	0.3%	0.1%	3.3%	0.1%	1.00	measured particles of original Friedland Clay

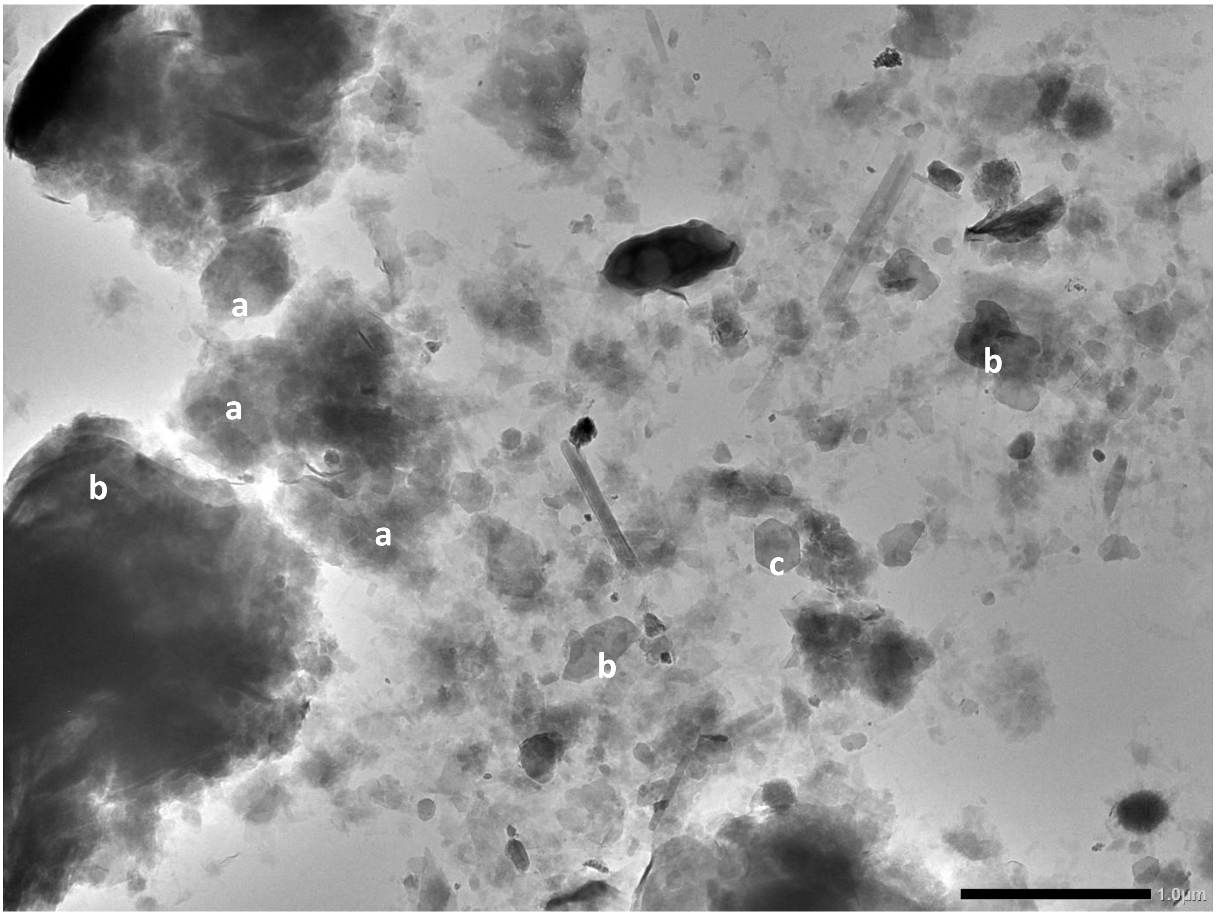

JEM-2100_MAG_X8000_057_No21.bmp

Magnification: 8k

- (a) Aggregates formed by small (≤ 100 nm) xenomorphous plates;
- (b) large (≤ 1 µm) xenomorph platy crystals;
- (c) small idiomorph crystals

Fig. 2. *Morphology of particles (TEM-micrographs)*

Distribution of smectite layers probability (%S)

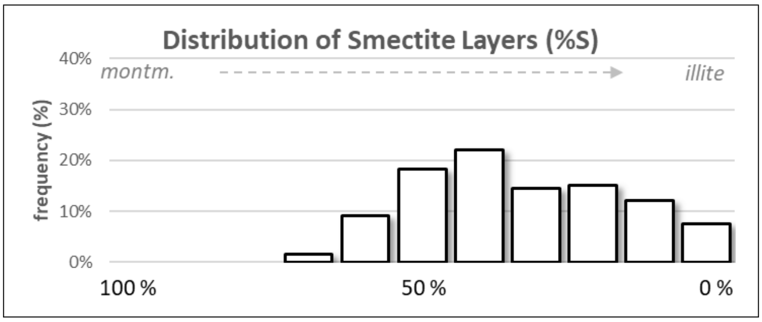

Description: *The distribution of %S-probability indicates the occurrence of two groups: (i) beidellitic diVS-ml as well as (ii) illite with K-deficiency.*

Fig. 3a. *Distribution of smectite layers probability (%S)*

Differentiation by relation “Octahedral Mg vs. tetrahedral Si”?

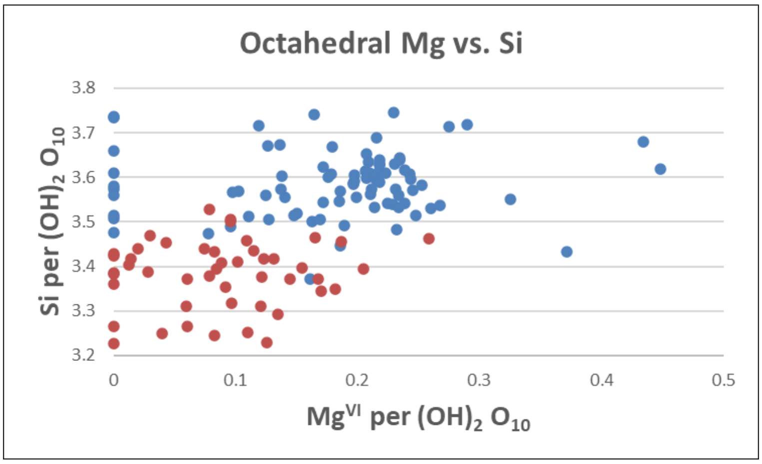

Description: *This diagram indicates only a very weak separation on low and high ratio of Mg in relation to tetrahedral Si (red dots – Cluster2 with lower Mg and with dominating illite layers: BMI-ml; blue dots – Cluster1 with higher Mg: BMI-ml).*

Fig. 3b. *Distribution of octahedral Mg vs. tetrahedral Si [all per(OH)$_2$ O$_{10}$]*

Distribution of K in relation to tetrahedral Si

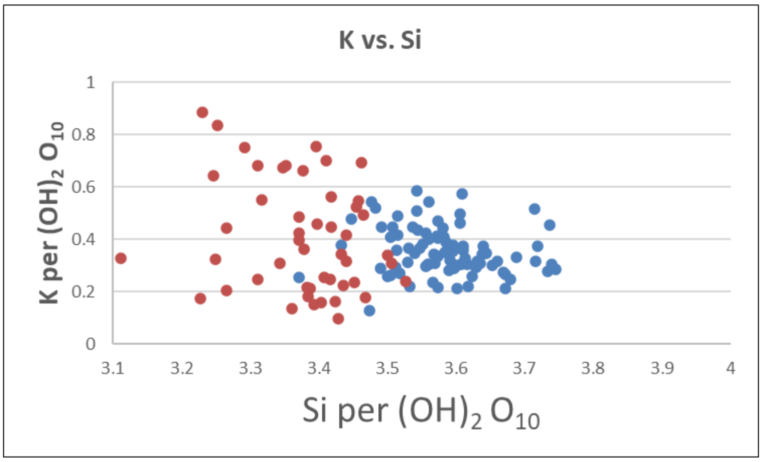

Description: *This diagram doesn’t visualize any K-separation of both beidellite-montmorillonite-illite-ml phases (blue dots – Cluster1; red dots – Cluster2).*

Fig. 4. *Distribution of K in interlayer space vs. tetrahedral Si [all per(OH)$_2$ O$_{10}$]*

Distribution of charges (exchangeable from interlayer space)

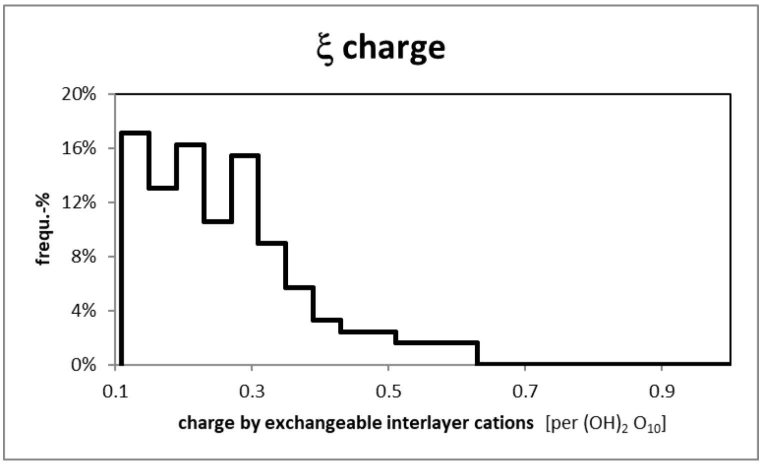

This diagram visualizes the distribution of exchangeable charges in the interlayer space (Ca, Mg, Na) determined and computed by TEM-EDX-data.

Description: *Broad, asymmetric distribution of charge density*

Fig. 5. *Distribution of charges*

Beidellite-montmorillonite-illite-ml BMI ~05:45:50 *(Cluster1):*

$Ca_{0.03}\ Mg_{0.02}\ Na_{0.12}\ K_{0.35}\quad Al_{1.20}\ Fe^{3+}_{0.61}\ Mg_{0.18}\ Ti_{0.01}\ (OH)_2\quad Si_{3.58}\ Al_{0.42}\ O_{10}$

Charge: XII = 0.58 VI = 5.84 IV = 15.58 **Σ = 22.00**

Measured particles: 84

Distribution of beidellite-montmorillonite-illite-ml phases (BMI-ml)

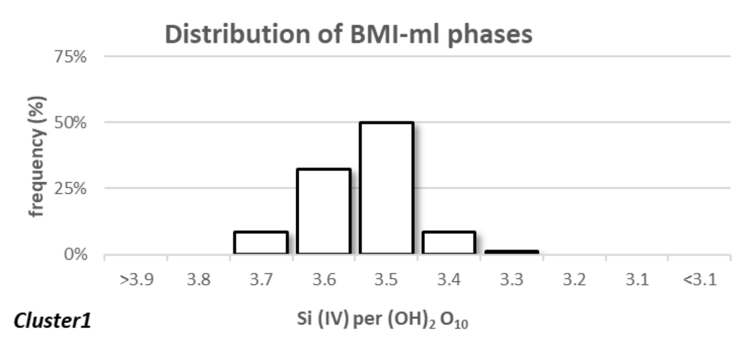

Description: *The distribution of BMI-ml phases (cluster1) draws a maximum of frequency (%) at tetrahedral Si-value between 3.5 – 3.6 e phuc.*

Fig. 6a. *Distribution of assumed beidellite-montmorillonite-illite-ml phases*

BMI 05:45:50?	*particles (abs)*	Ca (XII)	Mg (XII)	Na (XII)	K (XII)	Cr3+ (VI)	Al (VI)	Fe3+ (VI)	Mg (VI)	Ti (VI)	Al (IV)	Si (IV)	XII	n_VI	%S
Si >3.9	n = 0														
Si 3.9-3.8	n = 0														
Si 3.8-3.7	n = 7	0.01	0.03	0.10	0.36	0.00	1.21	0.60	0.15	0.00	0.27	3.73	0.5	2.0	59
Si 3.7-3.6	n = 27	0.02	0.02	0.14	0.33	0.00	1.22	0.58	0.20	0.00	0.37	3.63	0.5	2.0	45
Si 3.6-3.5	**n = 42**	**0.03**	**0.02**	**0.11**	**0.37**	**0.00**	**1.21**	**0.61**	**0.17**	**0.01**	**0.45**	**3.55**	**0.6**	**2.0**	**34**
Si 3.5-3.4	n = 7	0.03	0.04	0.14	0.40	0.00	1.07	0.76	0.16	0.00	0.53	3.47	0.7	2.0	25
Si 3.4-3.3	n = 1	0.06	0.00	0.17	0.25	0.00	0.88	0.67	0.16	0.27	0.63	3.37	0.6	2.0	15
Si 3.3-3.2	n = 0														
Si 3.2-3.1	n = 0														
Si <3.1	n = 0														

Fig. 6b. *Computed averaged mineral formulae of phases in the different Si(IV)-classes*

Beidellitic dioctahedral vermiculite-smectite-ml BMI ~10:20:70 (beid. diVS-ml) *(Cluster2):*

$Ca_{0.02}\ Mg_{0.07}\ Na_{0.09}\ K_{0.41}\quad Al_{1.46}\ Fe^{3+}_{0.43}\ Mg_{0.09}\ Ti_{0.02}\ (OH)_2\quad Si_{3.38}\ Al_{0.62}\ O_{10}$

Charge: XII = 0.68 VI = 5.94 IV = 15.38 **Σ = 22.00**

Probability of smectite layers (%S): 30%

Probability of illite layers (%I): 70%

Measured particles: 48

Distribution of smectite layers probability (%S) in beidellitic diVS-ml (Cluster2)

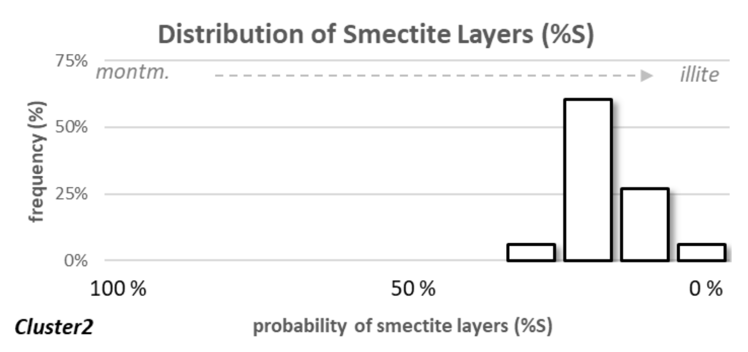

Description: *The distribution of beidellitic diVS-ml (classified as Cluster2) draws a maximum of frequency (%) for smectite layer probability at 20%*

Fig. 7a. *Distribution of smectite layers probability in diVS-ml*

	particles (abs)	**Ca** (XII)	**Mg** (XII)	**Na** (XII)	**K** (XII)	**Cr3+** (VI)	**Al** (VI)	**Fe3+** (VI)	**Mg** (VI)	**Ti** (VI)	**Al** (IV)	**Si** (IV)	**XII**	**n_VI**	**%S**
%S >95%	n = 0														
%S 95-85%	n = 0														
%S 85-75%	n = 0														
%S 75-65%	n = 0														
%S 65-55%	n = 0														
%S 55-45%	n = 0														
%S 45-35%	n = 0														
%S 35-25%	n = 3	0.02	0.08	0.10	0.30	0.00	1.48	0.43	0.09	0.00	0.49	3.51	0.6	2.0	29
%S 25-15%	**n = 29**	**0.02**	**0.08**	**0.10**	**0.38**	**0.00**	**1.46**	**0.45**	**0.09**	**0.01**	**0.58**	**3.42**	**0.7**	**2.0**	**19**
%S <15%	n = 16	0.02	0.07	0.09	0.49	0.00	1.48	0.40	0.09	0.04	0.72	3.28	0.7	2.0	8

Fig. 7b. *Computed averaged mineral formulae of beidellitic diVS -ml phases in the different smectite layers probability (%S)-classes*

Cluster2		**Ca** (XII)	**Mg** (XII)	**Na** (XII)	**K** (XII)	**Cr3+** (VI)	**Al** (VI)	**Fe3+** (VI)	**Mg** (VI)	**Ti** (VI)	**Al** (IV)	**Si** (IV)	**XII**	**n_VI**	**%S**
without illite	n = 32	0.02	0.08	0.10	0.37	0.00	1.46	0.45	0.09	0.01	0.58	3.42	0.65	2.0	20
only illite	n = 16	0.02	0.07	0.09	0.49	0.00	1.48	0.40	0.09	0.04	0.72	3.28	0.75	2.0	8

Fig. 7c. *Computed averaged mineral formulae of beidellitic diVS-ml phases differentiated by illite*

Description – Friedland Clay N21 (< 2 µm), treated material *(150°C)*

Preparation for TEM

The powder of Friedland Clay-sample was suspended in deionized water and dispersed by ultrasonic treatment for approximately 20 min. The clay fraction (<2 µm) was separated by sedimentation and diluted with deionized water to get a clear suspension. The suspension was dropped onto carbon-coated Cu grids, air dried and stored under environment-controlled conditions at 45% humidity.

Mineral Matter - Overview

The fraction < 2 µm of Friedland Clay N21 sample is mainly composed by beidellite-montmorillonite-illite mixed layer phases (BMI-ml) and beidellitic dioctahedral vermiculite-smectite mixed layer phases (beid. diVS-ml). Rarely, quartz, kaolinite and kaolinite-smectite-ml phases as well as chlorite-smectite-ml phases were identified in traces in this sample [fig. 1].

The measured and computed particles have shown a calculated CEC-value of 59 meq / 100 g located at surface and in the interlayer space.

	frequency-% *(n = 143 measured particles)*
BMI-ml	59%
beid. diVS-ml	34%
Kaolinite & KSV-ml	4%
CSV-ml	1%
Quartz	1%
unknown	3%

All measured dioctahedral 2:1 clay mineral phases summarized result following mineral formula computed from TEM-EDX-measurement of 132 individual particles:

$$\boxed{Ca^{2+}_{0.03}\ Mg^{2+}_{0.04}\ Na^{+}_{0.11}\ K^{+}_{0.37}\quad Al^{3+}_{1.29}\ Fe^{3+}_{0.55}\ Mg^{2+}_{0.15}\ Ti^{4+}_{0.01}\ (OH)_2\quad Si^{4+}_{3.51}\ Al^{3+}_{0.49}\ O_{10}}$$

SDOM *± 0.00 ± 0.00 ± 0.01 ± 0.01 ± 0.02 ± 0.01 ± 0.01 ± 0.00 ± 0.01 ± 0.01*

Legend: SDOM - standard deviation of the mean (= the standard deviation divided by the square root of the number of samples)

The interlayer charge is calculated as 0.68 per $(OH)_2\ O_{10}$ and the octahedral charge as 5.87 per $(OH)_2\ O_{10}$. The particles are characterized by a high octahedral Fe-amount.

The summarized chemical composition of all 132 computed particles is listed [tab. 1].

Friedland Clay N21 sample is also characterized by two morphological groups: (i) large (≤ 1 µm) xenomorph platy crystals and (ii) aggregates, partially with folds, formed by small (≤ 100 nm) xenomorphous plates [fig. 2]. Aggregates formed by small (≤ 100 nm) xenomorphous plates dominate the shapes of particles in the micrographs [fig. 2].

The distribution of %S-probability of all measured clay mineral phases [fig. 3a] also indicates the occurrence of two groups: (i) beid. diVS-ml and beidellite-montmorillonite-illite-ml phases as well as (ii) illite with K-deficiency.

The numerous measured particles by TEM-EDX allow a visualization of distribution of interlayer charges. Considering the TEM-EDX-determined cations Ca^{++}, Mg^{++} and Na^{+} and then computed their ratio as interlayer cations in the mineral formula, Ca^{++}, Mg^{++} and Na^{+} offer to characterize the degree of exchangeable charges in the interlayer space. This charge density of Friedland Clay N21 (< 2 µm) shows in this sample a broad, asymmetric distribution [fig. 5]. This interval of interlayer charge density caused by exchangeable cations from 0.11 - 0.59 per $(OH)_2\ O_{10}$ represents beid. diVS-ml and beidellite-montmorillonite-illite-ml.

Mineral Matter - Specification

Result of Clustering

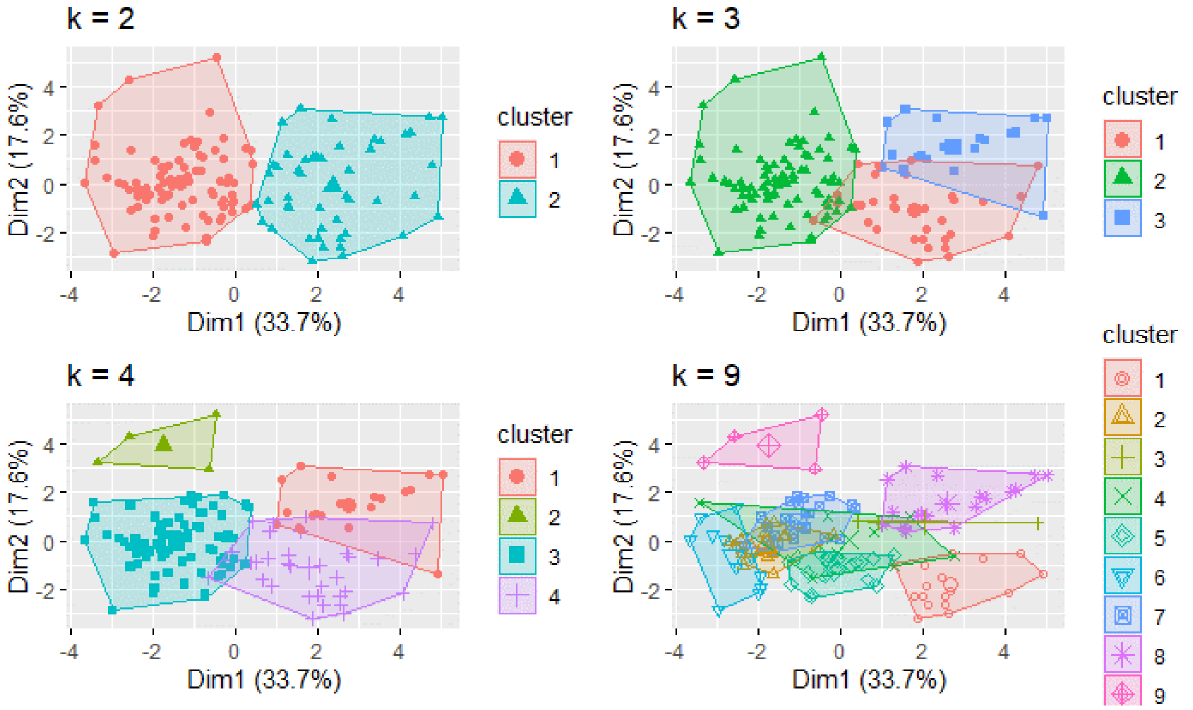

Fig. 8. *Clustering of all measured particles for clusters k = 2, k = 3, k = 4 and k = 9 (source for R-coding: https://uc-r.github.io/kmeans_clustering)*

The optimum of clusters was calculated with k = 2.

		Ca (XII)	Mg (XII)	Na (XII)	K (XII)	Cr3+ (VI)	Al (VI)	Fe3+ (VI)	Mg (VI)	Ti (VI)	Al (IV)	Si (IV)	XII	n_VI	%S
Cluster1	n = 84	0.03	0.02	0.12	0.35	0.00	1.20	0.61	0.18	0.01	0.42	3.58	0.58	2.0	38
Cluster2	n = 48	0.02	0.07	0.09	0.41	0.00	1.46	0.43	0.09	0.02	0.62	3.38	0.68	2.0	16

Fig. 9a. *Mineral formulae based on TEM-EDX-data summarized following the result of clustering for k=2*

	Sybilla-results	**TEM-EDX-results**	**Notes**
	Illite	diVS-ml (illite)	*high K-deficit, low XII-charge deficit, Al(VI)- & Fe(VI)-rich*
Cluster2	IS R0 *(%S = 30%)*	beid. diVS-ml *(BMI ~10:20:70)*	*high K-deficit, XII-charge deficit, Al(VI)-rich, Fe(VI)-rich*
Cluster1	ISS R0 *(%S = 52%)*	BMI-ml *(BMI ~05:45:50)*	*high K-deficit, XII-charge deficit, very Fe(VI)-rich*
	Kaolinite + KS GL R0		*in traces only*

Tab. 2. *Comparison of results from TEM-EDX- and XRD-measurements*

The TEM-EDX-data offers a good agreement with the result of Sybilla-processing of XRD-traces from oriented specimen, but only under consideration of the option beidellite [tab. 2].

ISS R0: The X-ray diffraction pattern of the ethylene-glycol saturated oriented specimen shows a limited expandability to 1.38 nm. This result of XRD-pattern processing let expect a maximum of particles for %S ~ 50% by TEM-EDX-measurements, but the maximum of particles measured by TEM-EDX is to find at %S = 38% [fig. 3a]. Using a model for beidellite-montmorillonite-illite-mixed layer phases (BMI-ml) with 3.50, 4.00 and 3.20 as tetrahedral Si-value per $(OH)_2\ O_{10}$ the calculation of member ratios offers a solution for 5% layer probability for %B and 45% for %S, if %I is given with 50% [see Cluster1 in tab. 2].

IS R0: The Sybilla-procedure of XRD-traces (oriented mounts) has shown an occurrence of a second illite-smectite mixed layer phase with a smectite layers probability of %S = 30%. This result of XRD-pattern processing let expect a maximum of particles for %S ~ 30% by TEM-EDX-measurements, but the maximum of particles measured by TEM-EDX is to find at %S = 16% [tab. 2]. Using a model for beidellite-montmorillonite-illite-mixed layer phases (BMI-ml) with 3.50, 4.00 and 3.20 as tetrahedral Si-value per $(OH)_2\ O_{10}$ the calculation of member ratios offers a solution for 10% layer probability for %B and 20% for %S, if %I is given with 70% [see Cluster2 in tab. 2].

The Sybilla-processing of XRD-traces (oriented mounts) also supports low amount of kaolinite and kaolinite-smectite mixed layer phases in fine fraction of sample.

Specifics to the identified clay mineral groups

Beidellite-montmorillonite-illite-ml (BMI-ml 05:45:50) *(Cluster1)*

84 of 132 computed particles belong so to this assumed classification. The dioctahedral character of this group is proofed by X-ray diffraction. The position of the large (060)-interference of smectite is in the random oriented powder specimen at 1.497 Å.

Montmorillonite and beidellite have the same behavior concerning the expandability and they are only to distinguish by XRD using Li by means of Greene-Kelly test (Greene-Kelly 1952, 1953). So, combination of XRD- and TEM-results (high expandability by XRD and Si ~ 3.58 by TEM-EDX) led conclude the occurrence of beidellite.

Beidellite-montmorillonite-illite-ml *(BMI 05:45:50)*

$$Ca_{0.03}\ Mg_{0.02}\ Na_{0.12}\ K_{0.35}\quad Al_{1.20}\ Fe^{3+}_{0.61}\ Mg_{0.18}\ Ti_{0.01}\ (OH)_2\quad Si_{3.58}\ Al_{0.42}\ O_{10}$$

Charge: XII = 0.58 VI = 5.84 IV = 15.58 **Σ = 22.00**
Measured particles by TEM-EDX: 84
Result of clustering: Cluster1 [tab. 2]

In this sample, beidellite is characterized by a low octahedral Mg-amount (because of high ratio of octahedral, 3-valent cations). A comparison of octahedral Mg vs. tetrahedral Si indicates only a weak differentiation for octahedral Mg based on TEM-EDX-data [fig. 3b]. Particles of Cluster1 contain slight increased Mg(VI) from 0 … 0.46 per $(OH)_2\ O_{10}$ in octahedral layer.

The mineral formulae, summarized in classes of %S, draws for the maximum an Fe-rich BMI-ml with low Mg(VI), but remarkable amount of K in the interlayer space [tab. 6b].

Beidellitic dioctahedral vermiculite-smectite mixed layer phase

(beid. diVS-ml, BMI 10:20:70, Cluster2)

$$Ca_{0.02}\ Mg_{0.07}\ Na_{0.09}\ K_{0.41}\quad Al_{1.46}\ Fe^{3+}_{0.43}\ Mg_{0.09}\ Ti_{0.02}\ (OH)_2\quad Si_{3.38}\ Al_{0.62}\ O_{10}$$

Charge:	XII = 0.68	VI = 5.94	IV = 15.38	**Σ = 22.00**
Probability of smectite layers (%S):	30%			
Probability of illite layers (%I):	70%			
Measured particles by TEM-EDX:	48			

Kaolinite-montmorillonite mixed layer phases

The Excel-based procedure (Hoang-Minh et al., 2019) to identify possible clay mineral groups using the TEM-EDX-measurements also includes algorithms to classify kaolinite and kaolinite-montmorillonite mixed layer phases. These algorithms couldn't compute no such phases basing on the measured TEM-EDX-data. Such particles have shown small hexagonal plates typically for kaolinite-bearing phases.

References

Cliff, G. & Lorimer, G. W. (1975). *J. Microsc.* **103**, 203–207.

Döbelin, N., Kleeberg, R. (2015). *Journal of Applied Crystallography* **48**, 1573-1580. DOI: 10.1107/S1600576715014685

Henning, K.-H. & Störr, M. (1986). Electron Micrographs (TEM, SEM) of Clays and Clay Minerals, p. 325. Akademie-Verlag Berlin.

Hoang-Minh, T., Kasbohm, J., Nguyen-Thanh, L., Nga, P. T., Lai, L. T., Duong, N. T., Thanh, N. D., Thuyet, N. T. M., Anh, D. D., Pusch, R., Knutsson, S. & Ferreiro Mahlmann, R. (2019). *J. Appl. Cryst.* **52**, 133-147. DOI: 10.1107/S1600576718018162

Lorimer, G. W. & Cliff, G. (1976). *Electron Microscopy in Mineralogy*, edited by H. R. Wenk, pp. 506–519. Berlin: Springer Verlag.

Mellini, M. & Menichini, R. (1985). *R. Soc. Ital. Miner. Petrol.* **40**, 261–266.

Moore, D.M., Reynolds, R.C. (1989). X-ray Diffraction and the Identification and Analysis of Clay Minerals, Oxford University Press, New York, 332 + xvi pp.

Nguyen-Thanh, L., Herbert, H.-J., Kasbohm, J., Hoang-Minh, T. & Mählmann, R. F. (2014). *Clays Clay Miner.* **62**, 425–446.

Środoń, J., Elsass, F., McHardy, W. J. & Morgan, D. J. (1992). *Clay Miner.* **27**, 137–158.